

Tokyo Medical and Dental University
Global Center of Excellence (GCOE) Program
International Research Center for Molecular Science in Tooth and Bone Diseases

東京医科歯科大学 グローバルCOEプログラム

歯と骨の分子疾患科学 国際教育研究拠点

～デント・メドミクスのインテリジェンスハブ～



平成21年度 実績報告書

ご挨拶

東京医科歯科大学は大山喬史学長のリーダーシップのもと、「知と癒しの匠を創造する」を理念として掲げ、特色ある教育の1つとして「歯と骨の分子科学の国際研究拠点」を提案し、平成20年からグローバルCOEプログラムとして採択され活動を行って参りました。このプログラムはこれに先行する平成15年からの21世紀COEプログラムにおける活動に対する評価及び検証に基づくものであると共に、特に国際化を目指しより一層の大学院教育研究の充実と強化を目的とする活動拠点です。特に世界最高水準の研究教育基盤を構成し、歯と骨の研究領域における将来のリーダーを養成する創造的な人材育成の場として拠点を形成すること、また国際的に卓越した研究を推進することを目的としてこれを達成するべく国際的な競争力のある大学作りを推進する一環として活動しております。また東京医科歯科大学における歯科臨床・医科臨床また基礎生命科学を合わせた先端的な研究の展開を行うと共にすぐれた若手研究者を採用し、また英語によるインタビューや教育の元に競争的に採用やトレーニングを受けた大学院生に対し重点的な教育プログラムによって本領域の最先端の知見を教授し次世代に向けた飛躍を目指しております。

平成20年度および21年度に至るまでの2年間で4回の国際シンポジウムを開催すると共に、毎週の先進的な歯及び骨に関わる骨と生命科学に関わる総合プレゼンテーションを毎週3名以上の推進担当者の教授の参加のもとに行い、その数は45回を数え参加者総数は1,000名に上っております。また、世界的な研究者の招聘講演は歯科学、医科学及び生命科学の領域から21回を数え、学生並びに若手研究者に対する個別のディスカッションと教育の場として機能しております。さらに東京医科歯科大学を拠点とする国際教育に加え選抜した大学院生に対し積極的に世界のトップ拠点の大学院教育を受けさせるためにすでに毎年ハーバード大学に大学院生を派遣し、カナダのトロント大学における大学院活動並びにカリフォルニア大学サンフランシスコ校の医学系の学生教育に対しても本学の大学院生が派遣され、これらの大学における教員のもとで自らの研究発表をし、また教育を受ける機会を設定しております。これに加え、平成21年度には海外のトップクラスの歯と骨の領域の企業研究所への派遣を行い、メルク等の会社組織の中での研究の実地の場における教育が行われております。特別選抜大学生の選抜試験は年2回行われ英語による選抜のもと選ばれた大学院生に対する教育及び経済的な支援が行われると共に若手の優秀な研究者に対する拠点内での競争的な研究費の申請による訓練、さらには事業推進担当者の教授が新たな分野を開拓するイノベーション研究プログラムを開始し、拠点内部の教授によるピアレビュー並びに若手研究者や大学院生による教授のプレゼンテーションへの評価などの透明性の高い評価システムのもとにこのプログラムの推進を行っております。さらに国際的な外部評価はこれまでに3回を数え、より高度な国際的拠点としての進展を目指していると共に社会への公開の為、ホームページを充実しこれまで5万件を超えるアクセスを頂いております。

このような22年初頭に至るまでの活動は大山学長の御指導のもと教育、研究、国際活動並びに評価をそれぞれ担当する事業推進担当者のご尽力の賜物であり、本プログラムが益々発展することを期待しております。

野田 政樹
Masaki Noda



東京医科歯科大学

平成21年度

グローバルCOEプログラム実績報告書

歯と骨の分子疾患科学の国際教育研究拠点

専攻等名

医歯学総合研究科器官システム制御学系専攻・口腔機能再構築学系専攻・生体支持組織学系専攻
顎顔面顎部機能再建学系専攻・先端医療開発学系専攻・生体環境応答学系専攻・疾病生命科学研究部
生体材料工学研究所・難治疾患研究所

野田 政樹 Masaki Noda

拠点リーダー/医歯学総合研究科・器官システム制御学系専攻・教授
分子薬理学/医学博士・歯学博士

拠点形成統括および先端硬組織分子再建科学の研究



田上 順次 Junji Tagami

医歯学総合研究科・口腔機能再構築学系専攻・教授
齲蝕制御学/歯学博士

先端硬組織分子再建科学



高柳 広 Hiroshi Takayanagi

東京医科歯科大学大学院医歯学総合研究科・教授
分子情報伝達学/医学博士

硬組織分子喪失病態学



森田 育男 Ikuo Morita

医歯学総合研究科・顎顔面顎部機能再建学系専攻・教授
分子細胞機能学/薬学博士

先端硬組織分子再建科学



小村 健 Ken Omura

医歯学総合研究科・口腔機能再構築学系専攻・教授
口腔機能再建学/医学博士

硬組織疾患ゲノム科学



春日井 昇平 Shohei Kasugai

医歯学総合研究科・口腔機能再構築学系専攻・教授
摂食機能制御学/歯学博士

先端硬組織分子再建科学



須田 英明 Hideaki Suda

医歯学総合研究科・口腔機能再構築学系専攻・教授
歯髓生物学/歯学博士

先端硬組織分子再建科学



和泉 雄一 Yuichi Izumi

医歯学総合研究科・生体支持組織学系専攻・教授
歯周病学/歯学博士

硬組織分子喪失病態学



柳下 正樹 Masaki Yanagisita

医歯学総合研究科・生体支持組織学系専攻・教授
硬組織病態制御学/医学士

先端硬組織分子再建科学



山口 朗 Akira Yamaguchi

医歯学総合研究科・口腔機能再構築学系専攻・教授
口腔病理学/医学博士

先端硬組織分子再建科学



森山 啓司 Keiji Moriyama

医歯学総合研究科・顎顔面頸部機能再構築学系専攻・教授
顎顔面矯正学/医学博士

硬組織分子喪失病態学



四宮 謙一 Kenichi Shinomiya

医歯学総合研究科・先端医療開発学系専攻・教授
脊椎・脊髄神経外科学/医学博士

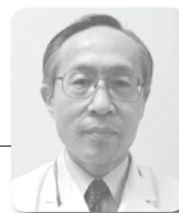
先端硬組織分子再建科学



宮坂 信之 Nobuyuki Miyasaka

医歯学総合研究科・生体環境応答学系専攻・教授
臨床免疫学/医学博士

硬組織分子喪失病態学



宗田 大 Takeshi Muneta

医歯学総合研究科・生体支持組織学系専攻・教授
運動機能再建学/医学博士

先端硬組織分子再建科学



秋吉 一成 Kazunari Akiyoshi

生体材料工学研究所・素材研究部門・教授
有機材料学/工学博士

先端硬組織分子再建科学



稲澤 譲治 Johji Inazawa

難治疾患研究所・遺伝疾患研究部門・教授
分子細胞遺伝学/医学博士

硬組織疾患ゲノム科学



三木 義男 Yoshio Miki

難治疾患研究所・遺伝疾患研究部門・教授
遺伝子応用医学/医学博士

硬組織疾患ゲノム科学



石野 史敏 Fumitoshi Ishino

教授
分子生物学/理学博士

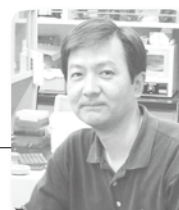
硬組織疾患ゲノム科学



澁谷 浩司 Hiroshi Shibuya

医歯学総合研究科・器官システム制御学系専攻・教授
細胞機能調節学/理学博士

硬組織基礎生命科学



小川 佳宏 Yoshihiro Ogawa

医歯学総合研究科・器官システム制御学系専攻・教授
内分泌学/医学博士

硬組織基礎生命科学



萩原 正敏 Masatoshi Hagiwara

疾患生命科学研究部・高次生命制御研究部門・教授
形質発現制御学/医学博士

硬組織基礎生命科学



国際PIシャペロン、AISS・QAISS

Takuya Notomi, Ph.D.

(納富拓也)

Research Assistant Professor
Department of Molecular Pharmacology



Alireza Sadr, D.D.S., Ph.D.

Research Assistant Professor
Department of Cariology and Operative
Dentistry



Masatsugu Oh-hora, M.D., Ph.D.

(大洞将嗣)

Research Associate Professor
Department of Cell Signaling



Hiroyuki Nakamura, D.D.S., Ph.D.

(中村博幸)

Research Assistant Professor
Department of Hard Tissue Engineering
Biochemistry



Iimura Tadahiro, D.D.S., Ph.D.

(飯村忠浩)

Research Associate Professor
Department of Oral Pathology



Naoto Haruyama, D.D.S., Ph.D.

(春山 直人)

Research Associate Professor
Department of Maxillofacial Orthognathics



Hideyuki Iwai, M.D., Ph.D.

(岩井秀之)

Research Assistant Professor
Department of Medicine & Rheumatology



Kunikazu Tsuji, M.D., Ph.D.

(辻邦和)

Research Assistant Professor
Department of Orthopedic Surgery



Lee Jiyoung, Ph.D.

(李知英)

Research Assistant Professor
Department of Epigenetics



Naoki Sawada, M.D., Ph.D.

(澤田直樹)

Research Assistant Professor
Department of Molecular Medicine and
Metabolism



Paksinee Kamolratanakul

Dept. of Molecular Pharmacology
「ナノゲル scaffold を用いた EP4 アゴニストと
BMP の骨再生能に関する研究」



中川 朋美

Tomomi Nakagawa
Dept. of Molecular Pharmacology
「悪性黒色腫の骨の転移における
転写因子 Ciz の役割の解明」



Patricia Makishi

Dept. of Cariology and Operative Dentistry
「レジセメントと象牙質界面における
ナノリーケージについて」



林 幹人

Mikihito Hayashi
Dept. of Cell Signaling
「破骨細胞の分化ステージ特異的な
NFATc1 標的遺伝子の同定」



青井 陽子

Yoko Aoi
Dept. of Cellular Physiological Chemistry
「低酸素下におけるサイトカイン産生変動機序～
メチル化の関与」



Chalida Nakalekha

Dept. of Cellular Physiological Chemistry
「骨代謝におけるプロスタサイクリンの役割」



Rajib Bhattacharjee

Dept. of Cellular Physiological Chemistry
comment
「骨芽細胞におけるコネキシン43発現の
調節機構の解明」

津川 順一

Junichi Tsugawa
Dept. of Cellular Physiological Chemistry
「印刷技術を用いて羊膜に転写した細胞による
骨再生療法の確立」

**長岡 亮介**

Ryosuke Nagaoka
Dept. of Cellular Physiological Chemistry
「顔面形態形成に対する低酸素の影響」

**Hudieb Malik Ismail**

Dept. of Oral Implantology & Regenerative
Dental Medicine
「インプラントと骨再生との生物物理学的関係」

**MYAT NYAN**

Dept. of Oral Implantology & Regenerative
Dental Medicine
「Simvastatin 含有 α - TCP を用いた骨再生に
関する研究」

**Reena Rodriguez**

Dept. of Oral Implantology & Regenerative
Dental Medicine
「Epigallocatechin-3-gallate 含有
Gelatin Hydrogel を用いた骨再生に関する研究」

**伊達 佑生**

Yuki Date
Dept. of Oral Implantology & Regenerative
Dental Medicine
「歯根発生に関する因子の同定」

**則武 加奈子**

Kanako Noritake
Dept. of Oral Implantology & Regenerative
Dental Medicine
「スーパーGBR膜「ハイドロゲルシート」の開発」

**Gombo Balortuya**

Dept. of Pulp Biology and Endodontics
「インテグリン発現を評価することによる
象牙芽細胞の成熟とシグナル伝達に対する
低出力レーザー療法の効果」

**Aleksic Verica**

Dept. of Periodontology
「歯周疾患は動脈疾患の進行に重要な
リスクファクターとなる」

**Aslam Al Mehdi**

Dept. of Periodontology
「歯周疾患は動脈疾患の進行に重要な
リスクファクターとなる」

**Gamaralalage Amodini Rajakaruna**

Dept. of Periodontology
「歯周病とパーリカー病の関連の解明」



江部 典子

Noriko ebe
Dept. of Periodontology
「歯周疾患において、後期炎症性メディエーター
であるHMGB1放出による炎症の悪化を制御
するための研究」

**新垣 理宣**

Tadanobu Aragaki
口腔病理学分野
角化嚢胞性歯原性腫瘍の生物学的特徴
Biological characteristics of Keratocystic
odontogenic tumors

**Ganburged Ganjargal**

Dept. of Maxillofacial Orthognathics
「マルファン症候群における重篤な歯周炎の
分子機構について」

**鈴木 尋之**

Hiroyuki Suzuki
Dept. of Maxillofacial Orthognathics
「可溶性 fibroblast growth factor receptor2
(FGFR2) の頭蓋冠縫合部早期癒合症に
対する治療効果」

**木村 文子**

Ayako Kimura
Dept. of Orthopaedic and Spinal Surgery
「軟骨細胞の分化調節機構の解明
-軟骨組織特異的 Runx1 マウスを用いた検討-」

**菅田 祐美**

Yumi Sugata
Dept. of Orthopaedic and Spinal Surgery
「HApColとビスフォスフォネート局所徐放による
骨悪性腫瘍の治療法の開発」

**白 樺**

Bai Hua
Dept. of Molecular Cytogenetics
「ヒト癌におけるオートファジー関連遺伝子
LC3A1 遺伝子の機能解析」

**呂 正光**

Lu ZhengGang
Dept. of Molecular Genetics
「転移性骨腫瘍をターゲットとした
NF-kappa B 活性制御機構解明」

**岩舩 浩孝**

Hirotaka Iwafune
Epigenetics
ゲノムインプリンティング
リプログラミング変異体の単離とその解析
Analysis of reprogramming mechanism of
genomic imprinting in mice

**Samir Kumar Pal**

口腔病理学 (Oral Pathology)
口腔扁平上皮癌による骨破壊における
Thrombospondin-1 の役割
The Role of Thrombospondin-1 (TSP-1) in Bone
Destruction by Oral Squamous Cell Carcinoma



下田 麻子

Asako Shimoda

有機材料 (Organic materials)

ナノゲル架橋ハイドロゲルによるタンパク質
デリバリー

Design of Nanogel-assembled hydrogel for protein delivery

**高橋 治子**

Haruko Takahashi

有機材料 (Organic materials)

Polysaccharide nano-ball を用いた

新規ナノキャリアの開発

Design of Functional Polysaccharide nano-ball
as new nanocarrier**木原 翼**

Tasuku Kihara

Oral pathology

骨芽細胞分化と骨再生におけるCCN3の役割
The role of CCN3 in osteoblast differentiation
and bone regeneration**古田 繭子**

Mayuko Furuta

分子細胞遺伝学 (Molecular Cytogenetics)

新たなRNA創薬に寄与する癌制御性

microRNAの機能的スクリーニング

Exploration of novel tumor-suppressive microRNAs using
functional genomics-assisted approach**姫野 彰子**

Akiko Himeno

バイオイメージングを用いた歯周組織幹細胞の
同定Identification of periodontal stem cells by bio-
imaging approaches**辻 香織**

Kaori Tsuji

顎顔面矯正学

Zinc finger 型転写因子POKEMONの

破骨細胞における役割の解明

Investigation of the role of zinc finger
transcription factor, POKEMON in osteoclasts**Amir Nazari**

う蝕制御学

う蝕脱灰象牙質を高度石灰化組織へと変化
させるための再石灰化技術の創造Developing a Dentin Remineralising Method
(DRM) to Transform Carious Demineralised
Dentin into Hypermineralised Substrate**許 レン**

XU Ren

整形外科 (Orthopaedic and Spinal Surgery)

視床下部性神経ペプチドによる

中枢性骨代謝制御機構の解明

Uncovering the molecular mechanism of central control
of bone remodeling by hypothalamic neuropeptides**周 夢宇**

Zhou Mengyu

歯髄生物学 (Pulp Biology and Endodontics)

歯根形成のメカニズム-SCAP (根尖部幹細胞)
からの象牙芽細胞およびセメント芽細胞分化に
関与する因子の解明The mechanisms of root formation- Elucidation of the
signaling molecules on odontoblast and cementoblast
differentiation from SCAP**Smriti Aryal**

分子薬理学 (Molecular Pharmacology)

細胞骨格による骨代謝制御の分子機構 -Nck の
骨の細胞機能調節に於ける役割の解明-Molecular Mechanisms Underlying Cytoskeletal
Regulation of Bone Metabolism-Role of Nck Proteins
in Bone Cell Function-**松本 力**

Tsutomu Matsumoto

口腔病理学

矯正歯の移動における骨細胞の役割

The role of osteocyte in orthodontic tooth movement

**Chokechanachaisakul**

Uraivan

歯髄生物学 (Pulp Biology and Endodontics)

ラットを用いた歯髄生物学

Rat's pulp biology

**Kunawarote Sitthikorn**

う蝕制御学

う蝕象牙質に対する接着性能の改良

Improve Bond strength to Caries-affected
dentin**Ilinaz Hariri**

う蝕制御学

高度に石灰化した接着界面構造の作成と
機械的性質の評価Generation of hyper mineralized adhesive Interface
and study on its mechanical properties**AL-Bari MD. ABDUL**

分子情報伝達学 (Cell Signaling)

破骨細胞分化を制御するphosphatidylinositol-
3,4,5-trisphosphate結合タンパク質の同定と
機能解析Identification and analysis of phosphatidylinositol-3,4,5-
trisphosphatebinding proteins (PIP₃BP) that
regulate osteoclast differentiation**古市 祥子**

Akiko Furuichi

インプラント・口腔再生医学

酸素ナノバブル水の骨組織における

生体活性評価

Evaluation for the biologically activity of oxygen
nano bubbles solution (OXNB)

Hamid Nurrohmam

う蝕制御学

(Cariology and Operative Dentistry)

人口口腔装置を用いたバイオフィルムによる

う蝕形成後の” Super Dentin” のナノ構造解析

The effect of collagenolytic inhibitors on the quality of acid-base resistant zone in dentin



Chui Chanthoeun

歯周病学 (Periodontology)

歯周組織の除菌のための新しい治療様式の開発

:LEDと光感受性色素を用いた抗菌的光線力学

療法の効果に関する基礎的研究

Development of a New Treatment Modality for Periodontal Disinfection: Basic Study on the Effect of Antimicrobial Photodynamic Therapy using the Combination of an LED light Source and a Photosensitizing Dye



Wayakanon Praween

分子細胞機能学

(Cellular Physiological Chemistry)

アニユラーギャップジャンクションの形成機構

The Mechanisms of Annular Gap Junction Formation



村松 智輝

Tomoki Muramatsu

分子細胞遺伝学 (Molecular Cytogenetics)

食道扁平上皮癌の発生・進展におけるYAP増幅・

発現亢進の分子病理学的意義

Significance of YAP amplification/overexpression in the pathogenesis of esophageal squamous cell carcinoma



鈴木 允文

Suzuki Takafumi

歯周病学

骨吸収を引き起こす咬合性外傷の分子機構につ

いて解析する -TRPV4の役割-

Molecular mechanism underlying occlusal trauma, induced-bone loss Role of TRPV4



Bhargava Suhas Srilatha

インプラント・口腔再生医学

表面改良型Y-TZPジルコニア:骨再生に関する

生体外及び生体内の研究

Surface modified Y-TZP Zirconia: an in vitro and in vivo study of bone formation



Atukorallaya Devi Sewvandini

硬組織構造生物学 (インプラント・口腔再生医学)

小型硬骨魚メダカの顎歯と咽頭歯の発生誘導に及ぼ

すエクトディスプラシン情報伝達経路の役割の解析と

歯の進化の検討

Evolutionarily conserved role of ectodysplasin signaling in odontogenesis of ectodermally and endodermally induced teeth in small-sized teleost fish medaka



宮嶋 大輔

Daisuke Miyajima

顎顔面外科 (分子薬理)

骨代謝における負のMCSFシグナルによる新制

御機構の解析-Dok アダプター分子による破骨

細胞制御と骨粗鬆症-

Novel Insights into Negative Molecular Regulation of MCSF Signaling in Bone Metabolism -Function of Dok Adaptor Molecules in Osteoclasts and Osteoporosis -



Rojbani Hisham Khalifa

implantology

異なる骨補填剤 (アルファ TCP, ベータTCP, HA) と

シンバスタチン投与の有無におけるラットでの骨形成に

関する比較研究

A comparative study of the effect of three different Bone substitute materials (α-TCP, β-TCP, and HA) on the formation of new bone with and without the use of Simvastatin



チェン 康

Chen Kang

インプラント・口腔再生医学

(Dental Implantology & Oral Regenerative Medicine)

歯科用インプラント周囲骨における直流電流装

置を用いた骨形成促進作用に関する研究

A direct current device for accelerating bone formation in tissues surrounding a dental implant



Osama Zakaria

インプラント・口腔再生医学

GBRと骨膜ディストラクション法による軟組織の

同時骨再生のための新規開発装置の評価

Evaluation of a new device for bone regeneration by

GBR and periosteal distraction simultaneously with

soft tissue distraction



Khandakar Abu Shameem Md.

Saadat

分子発生学 (分子細胞機能学)

RB/E2F 経路の制御と骨肉腫形成過程に

おけるDRIL1の役割

The Role of DRIL1 in the Regulation of RB/E2F

Pathway and Tumorigenesis of Osteosarcoma



グローバルCOEプログラム概要

1. 目的・必要性

東京医科歯科大学は“歯”と“骨”の疾患科学において世界的な拠点であること特徴とする。日本の研究機関ランキング（出展:Thomson ISI Press Release）の論文の平均被引用数では主要総合大学を含めた我国の大学のなかで、2007年を含めて過去3年度のトップである。本拠点形成の目的は、世界で最も高年齢化の進行する我国にあって、人々が生きるために必須の“歯”と“骨”の分子疾患科学について、21世紀COEの成果を発展的に継承し、世界最先端の研究を展開して、合わせて次世代を担う国際的に活躍する若手研究者を養成する世界でも類のない国際教育研究拠点を形成することである。

2. 人材育成計画

(1) 国際PIシャペロン（PI-Chaperon（PIC））制度

国際PIシャペロン（PIC）制度とは、国際公募により選拔され、国際的に活躍する自立した研究者を目指す（Principal Investigator）、シャペロン型（大学院生を指導し共に研究する）のPostDoc終了後の（PDは採用しない）若手研究者育成制度である。さらに挑戦的な学際領域を開拓して（Prime Innovation）未来の領域を作り上げ、国際的に競争力のある創造性豊かなプロジェクトを遂行する（Project with Imagination）ことの3つのPIをキーワードとする若手研究者を育成するシステムである。英語のインタビューにより、全て外部より採用する。またGrant Write等の指導では米国NIHのGrant査読者やStudy Section担当者による教育を含め国際的視点でのトレーニングを行う。

(2) アドバンスト・I・スーパースチューデント（AI-SS）制度

アドバンスト・I・スーパースチューデントとは選拔され重点的な大学院教育と経済支援を受け、国際的に発展する力をつけるスーパースチューデント（SS）である。21世紀COEにおいては、本拠点は重点教育・経済支援の対象となるSS制度を創出し、優れた大学院生の教育、育成を達成した。本拠点においては、これを発展させ、(i) 国際的に活躍する（International）、(ii) 国際的に大学院生同士で相互に切磋琢磨する（Interactive）、(iii) 個

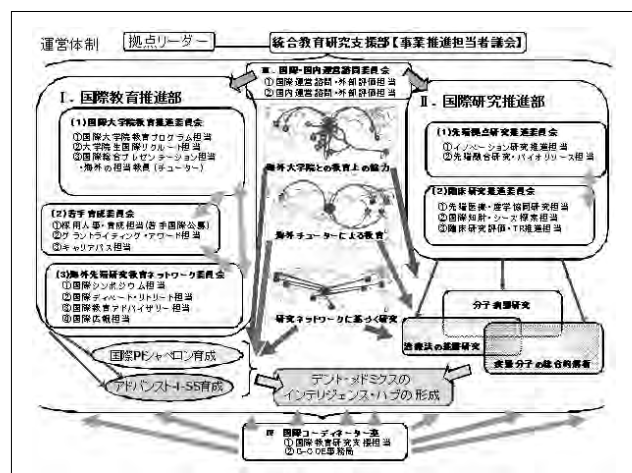
性の輝く（Individual Identity）の“3つのI”をキーワードとする指導的人材の育成を目指す新制度を創設する。新たに、(1) 国際教育としての国際メンター制度、(2) 国際“Interactive”プログラムによる、一流の大学院であるUCSF、ハーバード大（米国）トロント大（カナダ）における大学院の教育（学生発表会）に参加し、海外拠点の大学院生との交流ならびに現地海外教員による教育を受け、(3) 個を伸ばす国際教育プログラムとして国際コンティニューータープログラム（AISS-ICP）などを自ら選択しつつ教育を創造する。医歯学系大学院留学生数は全国一位だが更に海外の若手のリクルート、キャリアパスの担当部を其々設置して強化する。

3. 研究活動計画

拠点の研究においては、歯と骨の疾患領域における世界最高レベルの研究として硬組織の喪失と形成に関わる疾患のメカニズムならびにその診断・治療基盤研究を推進する。具体的研究目的は以下の3点である。即ち、【研究目的1】歯と骨の喪失に至る疾患の分子病態成立のメカニズムの解明、【研究目的2】歯と骨の先進的再建の為の治療法の基盤研究の推進、【研究目的3】歯と骨の疾患の統合的機能ゲノム研究の推進である。これらの有機的融合により新たな歯と骨の疾患分子の統合研究（デントメドミクス）を創成する。この目的のために、歯学部、医学部、難治疾患研究所、生体材料工学研究所、研究部の五つの部局が横断的体制をとり、個々の先進研究をさらに発展させるとともにエピゲノム、ケミカルバイオロジーを合わせた新領域のイノベーションを推進する。

4. 組織構成

研究所、研究部の五つの部局が横断的体制をとり、先進研究をさらに発展させる。



5. 国際外部評価会

2009. 6. 11

第2回 歯と骨のGCOE国際外部評価会 2nd International Advisory Review 2009.6.11

【評価者】

Roland Baron
Professor
Harvard School of Dental Medicine

Roberta Faccio
Assistant Professor
Washington University School of Medicine

Stephen E. Harris
Professor and Director of Research
University of Texas Health Science Center at San Antonio

Jerry Feng
Professor
Baylor College of Dentistry

【Program】

Akira Yamaguchi, Opening Address 15:00
TMDU Education Strategy at Graduate School

Masaki Noda 15:05 – 15:45

Overview and Scope of GCOE program on Tooth and Bone Research in Graduate School

Masatsugu Oh-hora 15:45 – 16:00

Global COE International PI chaperon

Takuya Notomi 16:00 – 16:15

Global COE International PI chaperon

Yoko Aoi 16:15 – 16:30

Global COE Advanced I Super Student AISS

Hiroshi Takayanagi 16:30 – 17:00

Summary and Discussion with the Advisory board members

EVALUATION FORM (4名回答)

A. Overall Evaluation on the Global COE Program

1. Overall evaluation on the Global COE program activities

Excellent	Good	Fair	Poor	N/A
4				

2. Research

2-1. Evaluation on the researches in the Global COE program

Excellent	Good	Fair	Poor	N/A
4				

2-2. Collaboration within the Global COE program

Excellent	Good	Fair	Poor	N/A
3	1			

2-3. Clinical aspects of the Global COE program

Excellent	Good	Fair	Poor	N/A
	2			2

3. Education

3-1. Efforts to promote young scientists in the Global COE program

Excellent	Good	Fair	Poor	N/A
3				1

3-2. International collaborative efforts

Excellent	Good	Fair	Poor	N/A
2	2			

4. Management

4-1. Administrative structure of the Global COE program

Excellent	Good	Fair	Poor	N/A
4				

4-2. Is the budget of the Global COE program spent efficiently?

Excellent	Good	Fair	Poor	N/A
4				

5. Perspective

Will the GCOE program contribute to the future development of the bone and tooth field?

Excellent	Good	Fair	Poor	N/A
4				

B . Evaluation on the Symposium you joined

1. Overall evaluation on this symposium

Excellent	Good	Fair	Poor	N/A
4				

3. Management of this symposium

Excellent	Good	Fair	Poor	N/A
4				

3. Presentations by speakers

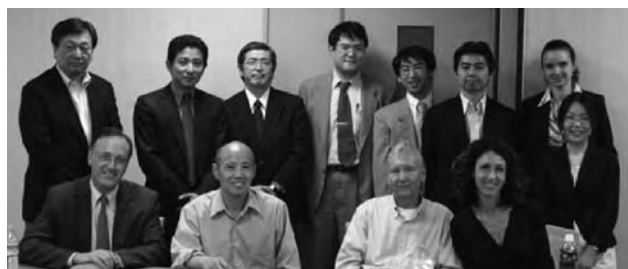
Excellent	Good	Fair	Poor	N/A
4				

4. Floor discussion

Excellent	Good	Fair	Poor	N/A
4				

5. Did this symposium serve as a forum to communicate with other researchers:

Excellent	Good	Fair	Poor	N/A
3	1			



6. 国際教育活動

歯と骨のGCOE 大学院生 (AISS/QAIISS) 海外活動リスト

平成21年8月12-19日 Research Laboratories Merck

参加者:Yoko Aoi



平成21年4月14日 Harvard School of Dental Medicine Student Research Day

参加者:Yoko Aoi、Ganburged Ganjargal、Rajib Bhattacharjee



平成21年2月9-12日

University of Toronto, Research Day

参加者:Christman Neil

Roshan Allexander Alles

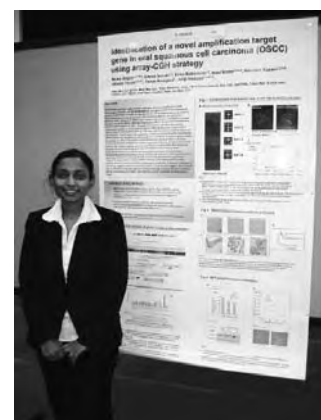


平成20年10月16日 The University of California San Francisco, Research Day

参加者:Begum Asma、

Kanako Noritake、

Chalida Nakalekha


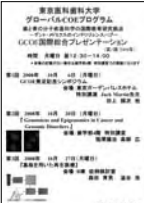


7. 総合プレゼンテーション



ポスター	講義タイトル	日 付
	第45回「う蝕象牙質への接着」	2010年2月8日
	第44回「関節軟骨損傷に対する滑膜由来幹細胞移植」	2010年2月1日
	第43回「口唇裂・口蓋裂患者の歯科矯正治療」	2010年1月25日
	第42回「人工骨を用いた骨再生医療の現状」	2010年1月18日
	第41回「歯の破折」	2009年12月21日
	第40回「脂肪組織と炎症」	2009年12月14日
	第39回「糖鎖生物学(Ⅱ)」	2009年12月7日
	第38回「哺乳類の個体発生の特異性」	2009年11月30日
	第37回「コネクシンとギャップ結合」	2009年11月16日
	第36回「癌と遺伝疾患のゲノム・エピゲノム解析第36回」	2009年11月9日
	「メルク社企業研修報告会」	2009年11月2日
	第35回「骨形成の分子機構」	2009年10月26日
	第34回「血管内皮細胞シグナルによる血管・臓器機能の制御」	2009年10月19日
	第33回「光コヒーレンス・トモグラフィー(OCT): 歯科における非侵襲的診断」	2009年10月5日
	第32回「カルシウムシグナルの生理的な役割」	2009年9月28日
	第31回「骨のホメオスタシスにおける骨形成因子(BMP)の生理機能の解析」	2009年9月14日





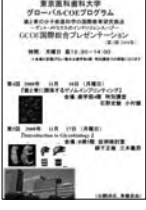
ポスター	講義タイトル	日 付
	第30回「TGF- β による上皮間葉移行の分子機構」	2009年6月29日
	第29回「マウス精子幹細胞における次世代に伝わる エピジェネティック修飾の異常」	2009年6月22日
	第28回「関節症における細胞外マトリックス分解酵素の新たな役割」	2009年6月15日
	第27回「関節リウマチ新規治療法開拓の試み」	2009年5月18日
	第26回「Hox 遺伝子と時計遺伝子による初期骨格形成、バイオイメーキングによるアプローチ」	2009年6月8日
	第25回「エナメル質および象牙質細胞外基質タンパクの シグナル分子としての生物学的機能の解析」	2009年5月25日
	第24回「骨組織におけるペースメーカーチャネル, HCN, の役割」	2009年5月18日
	第23回「歯と骨の分子疾患科学：初期胚発生からのアプローチ」	2009年5月11日
	第22回「歯科インプラント治療の最近の進歩」	2009年4月26日
	第21回「ナノ医療とドラッグデリバリーシステム」	2009年4月20日
	第20回「口腔癌の顎骨浸潤メカニズム」	2009年4月13日
	第19回「関節リウマチ治療において生物学的製剤が もたらしたものは？」	2009年4月6日
	第18回「Periodontal Medicine」	2009年3月30日
	第17回「Deciphering of splicing codes」	2009年3月23日
	第16回「口腔癌の非侵襲的診断に向けて」	2009年3月16日
	第15回「NLKによる頭部形成制御」	2009年3月9日
	第14回「破骨細胞と骨免疫学」	2009年3月2日
	第13回「トランスクリプトーム情報のがん治療への応用」	2009年2月23日
	第12回「口腔バイオフィルム除去技術の未来を探る：歯科病院における除菌外来の設立に向けて」	2009年2月9日
	第11回「Regulation of Bone Function」	2009年1月26日
	第10回「関節液幹細胞からみた関節障害」	2009年1月19日
	第9回「歯科矯正学および生物学的観点からみた顎顔面先天異常」	2008年12月22日
	第8回「骨腫瘍切除後欠損の再建法」	2008年12月15日
	第7回「歯へのレーザー照射 (Laser Irradiation to the Tooth)」	2008年12月8日
	第6回「脂肪組織と炎症」	2008年12月1日

ポスター	講義タイトル	日 付
	第5回「Introduction to Glycobiology」	2008年11月17日
	第4回「歯と骨に関係するゲノムインプリンティング」	2008年11月10日
	第3回「基板を用いた再生医療」	2008年10月27日
	第2回「Genomics and Epigenomics in Cancer and Genomic Disorders」	2008年10月20日
	第1回 GCOE 発足記念講演会	2008年10月6日




8. 国際シンポジウム

ポスター	タイトル	講演者	日 付
	第4回国際シンポジウム “インプラントの表面改変とデザイン”	Peter Schupbach Peter Thomsen 他	2010年2月11日
	第3回歯と骨のGCOE国際シンポジウム (第1回基礎シンポジウム) “Frontiers in bone biology 骨研究の最前線” ※ポスター2枚目に詳細が記載されております	Roland Baron Roberta Faccio 他	2009年6月10 -11日
	第1回国際シンポジウム “Strategies to create super tooth”	Eric Raynolds Hien Chi Ngo 他	2009年1月22日
	【共催】先端ライフ・ワークショップ “骨と軟骨の分子制御” 骨と関節の先端疾患分子医科学	Henry Kronenberg 他	2008年12月2 -5日
	グローバルCOE 発足記念講演会	Jack Martin 他	2008年10月6日




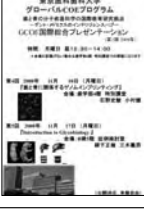
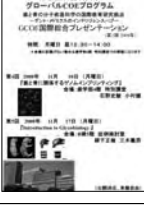
9. 海外研究者招聘講演会

ポスター	タイトル	講演者	日付
 <p>第219回 Bone Biology Seminar 第21回グローバルCOE海外研究者講演会共催 「Molecular Pathology and its Clinical Application in Oncology」</p>	第219回 Bone Biology Seminar 第21回グローバルCOE海外研究者講演会共催 「Molecular Pathology and its Clinical Application in Oncology」	Shuko Harada	2010年1月28日
 <p>第17回 GCOE 講演会 「bHLH 型転写因子 Hand による骨芽細胞分化の負の制御」</p>	第17回 GCOE 講演会 「bHLH 型転写因子 Hand による骨芽細胞分化の負の制御」	Noriko Funato	2009年10月27日
 <p>第16回 GCOE 海外研究者招聘講演会 「IL1BGene Expression Control and IL-1 Signaling : A Molecular Overview and Mapping of Novel Modes of Protein-Protein InteractionIL1BGene Expression Control and IL-1 Signaling : A Molecular Overview and Mapping of Novel Modes of Protein-Protein Interaction」</p>	第16回 GCOE 海外研究者招聘講演会 「IL1BGene Expression Control and IL-1 Signaling : A Molecular Overview and Mapping of Novel Modes of Protein-Protein InteractionIL1BGene Expression Control and IL-1 Signaling : A Molecular Overview and Mapping of Novel Modes of Protein-Protein Interaction」	Nawarat Wara-aswapati Charoen	2009年9月18日
 <p>第15回 GCOE 海外研究者招聘講演会 「1) Mechanisms ofDentine in Man 2) Electrophysiological Evidence on the Properties of Intradental Sensory Receptors」</p>	第15回 GCOE 海外研究者招聘講演会 「1) Mechanisms ofDentine in Man 2) Electrophysiological Evidence on the Properties of Intradental Sensory Receptors」	Bruce Matthews	2009年8月26日
 <p>第14回 GCOE 海外研究者招聘講演会 「The Cervical Vertebral Maturation Method:A Crystal Ball for the Practicing Orthodontist?」</p>	第14回 GCOE 海外研究者招聘講演会 「The Cervical Vertebral Maturation Method:A Crystal Ball for the Practicing Orthodontist?」	James A. McNamara	2009年4月21日
 <p>第13回 GCOE 海外研究者招聘講演会 「Role of thyroid nuclear hormone receptors in normal and tumorigenic development of intestine precursors cells」</p>	第13回 GCOE 海外研究者招聘講演会 「Role of thyroid nuclear hormone receptors in normal and tumorigenic development of intestine precursors cells」	Jacques Samarut	2009年3月17日
 <p>第12回 GCOE 海外研究者招聘講演会 「Mechanisms of NALP3 activation andrelevance for inflammatory diseases」</p>	第12回 GCOE 海外研究者招聘講演会 「Mechanisms of NALP3 activation andrelevance for inflammatory diseases」	Eicke Latz	2009年2月5日

ポスター	タイトル	講演者	日 付
	第11回GCOE 海外研究者招聘講演会 「A major change of understanding bone-titanium integration: Aging and functionalization of TiO ₂ 」	Takahiro Ogawa	2008年11月26日
	第10回GCOE 海外研究者招聘講演会 「自然からの贈り物 - 新薬スタチンの誕生 -」	Akira Endo	2008年11月26日
	第9回GCOE 海外研究者招聘講演会 「Dental Education reform at the University of California 1998-2008: Successes, Setbacks, and Future Challenges」	Mark I. Ryder	2008年11月13日
	第8回GCOE 海外研究者招聘講演会 「New frontiers in Operative Dentistry」	Nairn Wilson	2008年11月4日
	第7回GCOE 海外研究者招聘講演会 「Educational System in Ecole Nomal Superior Lyon」	Vincent Laudet	2008年10月22日
	第6回GCOE 海外研究者招聘講演会 「Dendritic Cells and Osteopontin」	Mari Shinohara	2008年10月3日
	第5回GCOE 海外研究者招聘講演会 「Reciprocal Regulation of Bone and Energy Metabolisms」	Gerard Karsenty	2008年8月20日
	第4回GCOE 海外研究者招聘講演会 「Cathepsin K Inhibitors: from the bench to the clinic」	Le Duong	2008年7月30日

ポスター	タイトル	講演者	日 付
	<p>第3回 GCOE 海外研究者招聘講演会 「Osteoimmunology :roles for osteoclasts, NF-κB and cytokines」</p>	Brendan F. BOYCE	2008年7月28日
	<p>第2回 GCOE 海外研究者招聘講演会 「Dynamic interactions between the nervous and immune systems with the microenvironment, regulate hematopoietic stem cells.」</p>	Tsvee LAPIDOT	2008年6月25日
	<p>第1回 GCOE 海外研究者招聘講演会 「Biology of Bone Metastases: Implications for Therapy」</p>	Theresa A. Guise	2008年6月24日

10. 共催講演会

ポスター	タイトル	講演者	日 付
	大学院特別セミナー 第20回グローバルCOE 講演会共催 「骨から全身へー臓器間ネットワークの内分泌的アプローチー」	竹田 秀	2009年12月3日
	第216回 Bone Biology Seminar 第19回グローバルCOE 講演会共催 「破骨前駆細胞の遊走と位置決めへの制御～ 生体2光子励起顕微鏡を用いた骨組織のライブイメージングより～」	石井 優	2009年12月1日
	第215回 Bone Biology Seminar 第18回グローバルCOE 講演会共催 「BMP（骨形成因子）の骨組織発生とリモデリング、 顔面形成における機能解析」	三品 裕司	2009年11月26日
	(共催) 第16回 癌ゲノムサイエンス研究会		2009年2月27日
	(共催) 第15回 癌ゲノムサイエンス研究会		2008年7月24日

11. イノベーション研究活動推進

異なる分野間のInnovation

歯と骨のグローバルCOE拠点内における異なる分野のInnovationを確立する研究プロジェクト

【2009年度】

実施日:2009年6月29日

審査方法:書類および面接審査

審査結果:

プロジェクト1

研究代表者:う蝕制御学 田上順次

共同研究者:歯周病学 和泉雄一

研究課題名

和文:OCTを用いた口腔軟組織・硬組織の断層画像ならびに3次元画像診断

英文:Cross-sectional and 3D imaging of dental soft and hard tissue using OCT

プロジェクト2

研究代表者:歯周病学 和泉雄一

共同研究者:分子薬理学 野田政樹

研究課題名

和文:歯周炎における硬組織代謝に与える神経性炎症の役割について

英文:Roles of nerve inflammation on the hard tissue metabolism in periodontitis

プロジェクト3

研究代表者:分子細胞生物学 澁谷浩司

共同研究者:口腔病理学 山口朗

研究課題名

和文:原腸陥入組織における細胞運動を制御するWntシグナルの分子動態

英文:Molecular dynamism of Wnt signaling in Xenopus embryos

プロジェクト4

研究代表者:歯髓生物学 須田英明

共同研究者:運動器外科学・軟骨再生学 宗田大

研究課題名

和文:歯の内部および周囲組織の再生に向けた至適幹細胞源を決定するための解析

英文:Characterization of pulpal, periodontal, and gingival stem cells

プロジェクト5

研究代表者:硬組織病態生化学 柳下正樹

共同研究者:歯周病学 和泉雄一

研究課題名

和文:歯周組織炎症部位における酸化ストレスの組織学的・生化学的解析

英文:Histological and biochemical analyses of oxidation stress at the inflammation site of periodontal diseases

プロジェクト6

研究代表者:エピジェネティクス 石野史敏

共同研究者:形質発見 萩原正敏

研究課題名

和文:Non-coding antiPeg11転写産物はどのように肋骨形成制御に関わるのか?—antiPeg11からの組織特異的なmiRNA生成機構の解明—

英文:How does non-coding antiPeg11 transcript regulate rib development? —mechanism of tissue-specific miRNA production from antiPeg11 transcript

プロジェクト7

研究代表者:分子細胞機能学 森田育男

共同研究者:歯周病学 和泉雄一

有機材料 秋吉一成

分子代謝医学 小川佳宏

研究課題名

和文:Drug Delivery System (DDS) 機能を持たせた新規移植材料による新たな歯周組織再生治療法の確立

英文:Establishment of innovative therapy for periodontal tissue regeneration using intelligent nanogel with delivery system

プロジェクト8

研究代表者:口腔病理学 山口朗

共同研究者:分子情報伝達学 高柳広

研究課題名

和文:光イメージングと分子生物学の融合によるオステオネットワークの解明を目指したフロンティア研究拠点

英文:New frontier of osteonetwork research by combinational approaches of optical imaging and molecular biology

プロジェクト9

研究代表者:分子細胞遺伝 稲澤譲治

共同研究者:分子薬理学 野田政樹

顎口腔外科学 小村健

顎顔面矯正学 森山啓司

整形外科 四宮謙一

膠原病・リウマチ内科 宮坂信之

分子遺伝学 三木義男

生体材料工学 秋吉一成

研究課題名

和文:難治性硬組織疾患の病態オミックス先端拠点研究

英文:Advanced omics research for intractable hard tissue diseases

12. プレゼンテーション型 英語クラス

Instructor

Mr. Alexander Paul Gregg, Mr. Richard Wilson, Mr. Kevin Cleary

Presenter

Patricia Makishi
Amir Nazari
Akiko Furuichi
Hideyuki Iwai
Kunikazu Tsuji
Takuya Notomi
Begum Asma
Ayako Kimura
Kanakano Noritake
Myan Nyat
Mayuko Furuta
Amodini Rajakaruna
Ilnaz Hariri
Tomomi Nakagawa
Paksinee Kamolratanakul
Kunawarote Sitthikorn
Rajib Bhattacharjee
Hudieb Malik Ismail
Akiko Oshiro
Aslam Al Mehdi
Mengyu Zhou
Xu Jing
Naoto Haruyama
Takuya Notomi
Hao Jia
Tomomi Nakagawa
Bai Hua

Discussant

Amir Nazari
Akiko Furuichi
Kunikazu Tsuji
Takuya Notomi
Kanakano Noritake
Begum Asma
Amodini Rajakaruna
Myan Nyat
Tomomi Nakagawa
Ilnaz Hariri
Rajib Bhattacharjee
Mengyu Zhou
Akiko Oshiro
Naoto Haruyama
Hao Jia
Kanakano Noritake (abstract guidance)
Xu Jing (abstract guidance)
Takuya Notomi (abstract guidance)

Patricia Makishi
Takuya Notomi
Hideyuki Iwai
Kunikazu Tsuji
Ayako Kimura
Kanakano Noritake
Mayuko Furuta
Amodini Rajakaruna
Paksinee Kamolratanakul
Hudieb Malik Ismail
Kunawarote Sitthikorn
Aslam Al Mehdi
Xu Jing
Bai Hua
Tomomi Nakagawa

PI Chaperon

Alireza Sadr
Naoto Haruyama
Hideyuki Iwai
Kunikazu Tsuji
Alireza Sadr
Takuya Notomi

Students

Patricia Makishi
Amir Nazari
Chalida Nakalekha
Hao Jia, Kanakano Noritake
Amodini Rajakaruna
Bharti Pariksha, Begum Asma
Neil Alles, Bai Hua, Ilnaz Hariri
Aslam Al Mehdi
Kanakano Noritake
Xu Jing, Gombo Balortuya
Tomomi Nakagawa
Smriti Aryal
Takafumi Suzuki
Daisuke Miyajima
Yoshishige Miyabe
Samir Kumar Pal
Akiko Furuichi
Khan Abu Shameem Md. Saadat



13. 歯と骨のGCOE 受賞リスト

- (1) 高柳 広
2009年2月4日
財団法人 井上科学振興財団 井上學術賞,
2009年7月24日 日本骨代謝学会 學術賞
- (2) 森田 育男
2009年7月6-10日 IAIS Poster Award
Therapeutic angiogenesis using ex vivo
formed-capillary networks by human omental
microvascular endothelial cells. The 9th World
Congress on Inflammation, Tokyo
- (3) 小井田 奈美・小村 健
2009年3月17日 平成20年度小林育英会奨学金
Inhibitory role of Plk1 in the regulation of p73-
dependent apoptosis through physical interaction
and phosphorylation.
- (4) 小村 健
2009年10月22-24日 第47回日本癌治療学会総会
優秀演題賞横浜 口腔扁平上皮癌における遠隔転移
発現に関与する因子の検討
- (5) 小村 健
2009年3月27日 Best Clinical Innovation
Presentation, Academy of Osseointegration
- (6) 花田 隆周・須田 英明
日本歯科保存学会デンツプライ賞 受賞 39975
ファイバーポイントが垂直性歯根破折に与える影響
第130回日本歯科保存学会春期大会
- (7) 石村 瞳・須田 英明
日本歯科保存学会奨励賞 受賞 39975 Sealing
Ability of New Adhesive Root Canal Filling
Materials Measured by a New Dye Penetration
Method 第130回日本歯科保存学会春期大会
- (8) 川島 伸之・須田 英明
Endo大賞 40130 Expression of Sp7 in the rat
dental pulp The 11th Joint Meeting between
KACD & JSCD
- (9) 池田 英治・須田 英明
日本歯内療法学会最優秀論文賞 39927 歯内治療に
関連する慢性痛 第30回日本歯内療法学会学術大会
- (10) 和泉 雄一
2009年9月15日 R Earl Robinson Periodontal
Regeneration Award, American Academy of
Periodontology, Boston
- (11) 青木 章・和泉 雄一
日本歯周病学会優秀臨床ポスター賞受賞
侵襲性歯周炎患者の長期治療経過
- (12) 和泉 雄一
2009年5月16日 侵襲性歯周炎患者の長期治療経過
第52回春季日本歯周病学会学術大会, 岡山
2009年10月11日 第52回秋期歯周病学会
- (13) 森山 啓司
2009年11月16-18日 第68回日本矯正歯科学会
優秀発表賞 舌感覚の皮質投影パターンにおける習慣
性咀嚼の関与, 福岡
- (14) 森山 啓司
2009年11月16-18日 第68回日本矯正歯科学会
優秀発表賞 COBRA-DHPLC法によるラッセルシ
ルバー症候群の遺伝子診断システムの開発, 福岡
- (15) 森山 啓司
2009年11月16-18日 第68回日本矯正歯科学会
優秀発表賞 精神的問題が疑われ矯正歯科治療にお
いて対応に苦慮した3症例, 福岡
- (16) 森山 啓司
2009年11月16-18日 第68回日本矯正歯科学会
優秀発表賞 コラーゲン電着固定化Tiの創製と耐久
性評価, 福岡
- (17) 森山 啓司
2009年7月23-25日 第27回日本骨代謝学会
優秀ポスター演題賞 Apert 症候群型変異FGFR2
とその可溶性変異体を過剰発現するトランスジェニ
ックマウス由来芽細胞の分化形質, 大阪

- (18) 森山啓司
2009年5月28-29日 第33回日本口蓋裂学会総会・優秀ポスター賞 歯槽骨延長部への歯の移動に高気圧酸素が与える影響, 東京
- (19) 森山啓司
2009年4月1-4日 International Association for Dental Research/ Unilever Travel Award. International Association for Dental Research, 88th General Session & Exhibition of the International Association for Dental Research Amelogenin is a potent inhibitor of odontoclastic root resorption, Miami
- (20) 堀江雅史・宗田大
Stem Cells. 2009, 27 (4) :878-87 2009年度日本整形外科学会研究奨励賞 Intra-articular Injected synovial stem cells differentiate into meniscal cells directly and promote meniscal regeneration without mobilization to distant organs in rat massive meniscal defect
- (21) 古賀英之・宗田大
2009年11月5-8日 Nycomed Pharma Award (Best paper Award) Idrettsmedisinsk Høstkongress (Norwegian Congress of Sports Medicine) . Trondheim, Norway
- (22) 古賀英之・宗田大
Stem Cells. 2009, 27 (4) :878-87 Reconstruction of the injury mechanisms for anterior cruciate ligament injuries among female basketball and team handball players Intra-articular Injected synovial stem cells differentiate into meniscal cells directly and promote meniscal regeneration without mobilization to distant organs in rat massive meniscal defect
- (23) 神谷厚輝・秋吉一成
2009年3月 日本化学会第88春季年会 学生講演賞
- (24) 高橋治子・秋吉一成
2009年7月 第25回日本DDS学会 ポスター賞
- (25) 澤田直樹・小川佳宏
2009年 First-place winner Young Investigator's Award in Physiology Pharmacology and Pathology The American College of Cardiology
- (26) 菅波孝祥・小川佳宏
2009年 第24回 岡本研究奨励賞
- (27) 田中都・小川佳宏
第30回日本肥満学会 若手研究奨励賞
- (28) 納富拓也・野田政樹
2009年5月30日 ゴールドリボン賞 日本骨形態計測学会
- (29) 納富拓也・野田政樹
2009年9月11日 Plenary Poster アメリカ骨代謝学会
- (30) 長尾雅史・野田政樹
2009年9月11日 Plenary Poster アメリカ骨代謝学会
- (31) 羽生 亮・野田政樹
2009年9月11日 Plenary Poster アメリカ骨代謝学会
- (32) 早田匡芳
2009年9月11日 Plenary Poster アメリカ骨代謝学会

14. リトリート

東京医科歯科大学 グローバル COE

歯と骨の分子疾患科学の国際研究拠点

-デント・メドミクスのインテリジェントハブ-

第1回 リトリート

【日程】3月17日(火)10時~18日(水)3時半頃

【場所】湘南国際村(<http://www.shonan-village.co.jp/>)

神奈川県三浦郡葉山町上山口 1560-39

電話 : 046-855-1810



Tokyo Medical &Dental University
Global Center of Excellence Program
International Research Center for Molecular Science
in Tooth and Bone Diseases
First Retreat Camp

2009.Mar.17-18

At Shonan Village Center (<http://www.shonan-village.co.jp/>)

1560-39 Kamiyamaguchi Hayama Miura-gun Kanagawa

Tel: 046-855-1810

日程 3月17日(火曜日)

10:00 大学集合
10:30 大学出発(バスチャーター)
11:30ごろ 湘南国際村到着

11:30-12:15 昼食
12:30-14:45 セッション1(オーラル)
14:45-15:00 休憩
15:00-16:00 特別講演 Jacques Samarut先生

16:00-16:20 講演 Matas先生
16:20-16:45
Samarut先生、Matas先生 とのディスカッション
16:45-17:00 休憩
17:00-17:30 講演 春日井 昇平先生
17:30-18:30 チェックインおよびポスターセット
18:30-19:30 夕食
19:30-20:30 セッション2(ポスター)
20:45-22:00 シャペロン教官との
ラウンドディスカッション
22:00- ポスター片付け 就寝

日程 3月18日(水曜日)

7:00 起床
7:30-8:30 朝食
8:30-9:30 荷造り チェックアウト
9:30 総研大へ移動
10:00-12:00 総研大での見学
12:00-12:30 湘南国際村へ移動
12:30-13:15 昼食
13:45ごろ 大学へ(バスチャーター)
15:30ごろ 大学到着 解散

Schedule 17 March (Tue.)

10:00 Meeting at the University.
10:30 Departure of the charter bus.
11:30 (approximate time)
Arrival to Shonan village
11:30 - 12:15 Lunch
13:00 - 14:00 Session 1 (Oral)
14:45 - 15:00 Break
15:00 - 16:00 Special lecture by Prof. Jacques Samarut
16:00 - 16:20 Lecture by Prof. Matas.
16:20 - 16:45 Discussion with Prof. Samarut and Prof. Matas.
16:45 - 17:00 Break
17:00 - 17:30 Lecture by Prof. Kasugai
17:30 - 18:30 Check in and poster setup
18:30 - 19:30 Dinner
19:30 - 20:30 Session 2 (Poster).
20:45 - 22:00 Group discussion with Chaperon professors.
22:00 - Poster removal. Free time.

Schedule 18 March (Wed.)

7:00 Wake up
7:30 - 8:30 Breakfast
8:30 - 9:30 Packing & Checkout
9:30 Departure to Soken Univ.
10:00 - 12:00 Soken Univ. Tour
12:00 - 12:30 Go to Shonan Village.
12:30 - 13:15 Lunch
13:45 Departure of the charter bus.
15:30 (approximate time)
- Arrival to TMDU

<Program>

•Session 1 17th(Tue.) 12:30—14:45 Chairman:Chalida Nakalekha, Begum Asma

①シャペロン教官の自己紹介 (Self-introduction of Chaperon professors) Part1.

中元 哲也先生 Dr.Tetsuya Nakamoto (12:30—13:10)

納富 拓也先生 Dr.Takuya Notomi

Dr.Alireza Sadr

大洞 将嗣先生 Dr. Masatsugu Oh-hora

斉藤 正夫先生 Dr. Masao Saito

中村 博幸先生 Dr.Hiroyuki Nakamra

飯村 忠浩先生 Dr.Tadahiro Iimura

② AISS 口演 (Oral Presentation of AISS) (13:10—13:40)

MYAT NYAN

Karine El Feghaly

Hudieb Malik Ismail

13:40-13:50 休憩 Break

③ 春山 直人先生による講演 (Lecture of Dr. Haruyama) (13:50—14:15)

④ シャペロン教官の自己紹介 (Self-introduction of Chaperon professors) Part2.

岩井 秀之先生 Dr.Hideyuki Iwai (14:15—14:45)

辻 邦和先生 Dr.Kunikazu Tsuji

李 知英先生 Dr. Lee Jiyoung

後藤 利保先生 Dr.Toshiyasu Goto

澤田 直樹先生 Dr.Naoki Sawada

Dr. Olga Safronova

• **Special Lectures 17th (Tue.) 15:00—16:45** Chairman: Prof. Shohei Kasugai

① **Prof. Jacques Samarut** Named Interim Director of ENS Lyon



The title of lecture:

Role of thyroid nuclear hormone receptors in normal and tumorigenic development of intestine precursors cells.

(15:00-16:00)

Jacques Samarut has been named Interim Director of the ENS Lyon in a decree issued by the French Ministry of Higher Education and Research. M. Samarut has been Director in charge of Research at the ENS Lyon since 2005 and became the school's interim Director, effective August 1, 2007, following the appointment of the school's director, Philippe Gillet, to the Cabinet Director position under Valerie Pécresse, Minister of Higher Education and Research.

Doctor of science specialized in molecular cell biology, Jacques Samarut is a graduate of the Université Claude Bernard Lyon 1. Following his research on circulatory system development, studying the chicken embryo and the mouse, he then completed a post-doctoral internship at the Rockefeller University in New York, doing research on retroviral oncogenes, before returning to Lyon and joining the Laboratory of Molecular Biology of the Cell, a CNRS-INRA-ENS Lyon joint research unit, which he directed for six years.

Since joining the ENS Lyon, Jacques Samarut has lead a research group working on embryonic stem cells and on signaling by nuclear hormone receptors. In 2002 he was named Professor-hospital practitioner at the *Université Claude Bernard Lyon 1* and *Hospices civils de Lyon*.

Jacques Samarut was director of the life sciences department of the CNRS from 1997 to 1999. He was a founder of the Rhône-Alpes Genopole in 2000 and was its director until the end of 2005. He has been president of the INRA scientific council since 2003.

Jacques Samarut is also director of the Institute of Functional Genomics of Lyon, which was created in January 2007

② **Lecture of Prof. Matas**

(16:00-16:20)

③ **Discussion with Prof. Samarut and Prof. Matas.**

(16:20-16:45)

• Lecture of Prof. Shohei Kasugai	17th (Tue.)	17:00-17:30
--	-------------------------------	--------------------

講演題目：「インプラント治療の過去、現在そして未来」

The title of lecture: Implant Treatment: Past, Present and Future.

• Session 2 Poster presentation	17th (Tue.)	19:30-20:30
--	-------------------------------	--------------------

19:30-19:45 自由にポスター観覧 (See posters freely)

19:45-20:00 No.3n の発表 (#3x should be in front of poster: e.g.#3.6.9~)

20:00-20:15 No.3n+1 の発表 (#3n+1: e.g.#1,4,7,~)

20:15-20:30 No.3n+2 の発表 (#3n+2: e.g.#2,5,8,~)

(各々の名前の前に書かれている番号がポスターナンバーとなります)

<Session A: Cancer>

- 1、 柏森 高 (Koh Kayamori)
- 2、 Begum Asma
- 3、 木村 純子 (Junko Kimura)
- 4、 白 樺 (Bai Hua)
- 5、 呂 正光 (Lu ZhengGang)
- 6、 王 慧峰 (Wang HuiFeng)
- 7、 中西 正一 (Shoichi Nakanishi)
- 8、 中川 朋美 (Tomomi Nakagawa)
- 9、 新垣 理宣 (Tadanobu Aragaki)

<Session B: Biomaterials & Tissue Engineering>

- 10、 来山 修三 (Shuzo Kitayama)
- 11、 Patricia Makishi
- 12、 津川 順一 (Junichi Tsugawa)
- 13、 大島 乃里子 (Noriko Oshima)
- 14、 湯浅 将人 (Masato Yuasa)
- 15、 Paksinee Kamolratanakul
- 16、 菅田 祐美 (Yumi Sugata)
- 17、 郝 佳 (Hao Jia)
- 18、 MYAT NYAN
- 19、 Reena Rodriguez
- 20、 Hudieb Malik Ismail
- 21、 河村 隼 (Jun Kawamura)
- 22、 則武 加奈子 (Kanao Noritake)

<Session C: Inflammation>

- 23、 青井 陽子 (Yoko Aoi)
- 24、 withdrawn
- 25、 Chrisman Neil Roshan Allexander Alles
- 26、 田中 都 (Miyako Tanaka)
- 27、 Aleksic Verica
- 28、 江部 典子 (Noriko Ebe)
- 29、 Aslam Al Mehdi
- 30、 Karine El Feghaly
- 31、 Gamaralalage Amodini Rajakaruna

<Session D: Signal>

- 32、 Chalida Nakalekha
- 33、 Erik Idrus
- 34、 Rajib Bhattacharjee
- 35、 許 婧 (Xu Jing)
- 36、 Ganburged Ganjargal
- 37、 鈴木 尋之 (Hiroyuki Suzuki)
- 38、 長岡 亮介 (Ryosuke Nagaoka)
- 39、 伊達 佑生 (Yuki Date)
- 40、 木村 文子 (Ayako Kimura)
- 41、 Gombo Balortuya
- 42、 岩船 浩孝 (Hirotaka Iwafune)
- 43、 山崎 芳浩 (Yoshihiro Yamazaki)

Round Discussion with Chaperon Professors 17日(Tue.) 20:45-22:00

6つのテーブルに分かれてシャペロンの先生とディスカッションを行います。

10分ごとに AISS はテーブルを移動し、他のグループのシャペロンの先生とディスカッションを行います。また、このグループで翌日の総研大の見学も行っていただきます。

The discussion will be held at 6 tables. Every 10 minutes, AISS will change the table to meet another chaperon professors. These groups will be applied the tour of Soken Univ, too.

Chaperon Professors Groups

GroupA 納富先生 大洞先生

GroupB 斉藤先生 中村先生

GroupC 中元先生 澤田先生
GroupD 飯村先生 春山先生
GroupE 岩井先生、辻先生、後藤先生
GroupF Dr. Olga, Dr. Sadr, 李先生

AISS Groups

Group1 Paksinee Chalida Nyan Gombo Aslam Ganjar Bai
Group2 Patricia Rajib Reena Xu Amodini Neil Wang
Group3 Erik Malik Hao Aleksic Karine Asma Lu
Group4 來山 津川 則武 中西 菅田 岩船
Group5 木村（純） 新垣 長岡 湯浅 田中 江部
Group6 青井 中川 伊達 柏森 鈴木 木村（文） 山崎

・Tour of Soken Univ. 18 日(Wed.) 10:00—12:00



国立大学法人総合研究大学院大学 葉山キャンパス

The Graduate University of Advanced Studies Hayama Center for advanced Studies

<http://www.soken.ac.jp/index.html>

総研大に関する紹介 Pdf です

<http://www.soken.ac.jp/outline/welcome/welcome.pps.html>

What is Soken dai ,please see following Web site...

<http://www.soken.ac.jp/en/about/glance.html>

見学内容 (Contents)

実験室見学(visit Lab.): 蟻川研究室(Arikawa Lab.)

渡辺研究室(Watanabe Lab.)

田辺研究室(Tanabe Lab.)

研究内容のレクチャー(Lecture)

: 田辺 秀之先生 (Hideyuki Tanabe Associate Professor)

東京医科歯科大学 グローバルCOE

歯と骨の分子疾患科学の国際研究拠点 ーデント・メドミクスofインテリジェンスハブー

第2回 リトリート



【日程】

2010年

2月22日(月)9時~23日(火)5時頃

【場所】

ホテルグランド東雲

〒305-0034

茨城県つくば市小野崎涌井488-1

(TEL: 029-856-2212)

Tokyo Medical & Dental University
Global Center of Excellence Program
**International Research Center for
Molecular Science
in Tooth and Bone Diseases
Second Retreat Camp**

Feb.22-23,2010
At Hotel Grand Sinonome
488-1 Onozaki Tsukuba Ibaraki
Tel: 029-856-2212



東京医科歯科大学

日程

1日目

時刻	プログラム
9.00-	東京医科歯科大から出発 バス
11.00-	到着予定 荷物を預ける
11.30-	自己紹介(学生とGCOEスタッフ) 予定より遅れた場合は省略
12.00-	昼食 (ポスターセットアップ)
13.00-	開会の挨拶 野田教授
13.10-14.10	Prof. Jane Aubin (トロント大) 50分 10分ディスカッション
14.10-15.00	辻 孝 先生(東京理科大) 40分 10分ディスカッション
15.00-15.30	Louisa Ho (トロント大院生) 講演
15.30-15.40	休憩
15.40-16.00	前田山紀子先生(ハーバード大)
16.00-17.30	学生によるポスター 投票による優秀賞の選抜
17.30-17.45	Prof. Jane Aubin (Career Pathに関する講演)
17.45-18.20	シャペロンの研究キーワードについての談話
18.20-	チェックイン
18.30-	夕食
19.30-20.45	シャペロンと学生の研究進路などについての 討論会

2日目

7.00-8.50	朝食
9.00-10.00	シャペロンによる口演発表 発表10分、ディスカッション2分
10.00-12.00	学生による口演発表 発表7分、ディスカッション3分
12.00-12.40	チェックアウト・昼食
	宇宙航空研究開発機構訪問 (大森 克徳先生、嶋津 徹先生、大島 博先生による講演)
13.30	集合・守衛室前
13.30-13.45	(バッチ配布) 伏島、斉藤
13.45-14.45	各自展示室、お土産(60分) 個人行動
14.45	ロケット前に再集合 伏島、斉藤
14.45-15.00	(移動・実験棟)
15.00-15.20	嶋津さん講演(20分)
15.20-15.40	大森さん講演(20分)
15.40-16.00	大島さん講演(20分)
16.00-16.15	(移動・守衛室)
16.15	バッチ回収・解散
17.00-	医科歯科大へ到着

Schedule

1st day

time	programme
9.00-	departure from TMDU by bus activities on bus
11.00-	approximate arrival arrange baggage (luggage reception?)
11.30-	self introduction (all students and COE staffs) if schedule becomes late, skip this part briefly
12.00-	lunch (poster setup)
13.00-	opening speech by Prof. Noda
13.10-14.10	Prof. Jane Aubin (University of Toronto) 50 min presentation 10min discussion
14.10-15.00	Prof. Takashi Tsuji (Tokyo University of Science) 40 min presentation 10min discussion
15.00-15.30	Louisa Ho (graduate student, University of Toronto)
15.30-15.40	break
15.40-16.00	Dr. Yukiko Maeda (Harvard Univ.)
16.00-17.30	student poster presentation Selection of Excellent posters
17.30-17.45	Prof. Jane Aubin (University of Toronto) Career Path
17.45-18.20	chaperone key word discussion
18.20-	check in
18.30-	dinner
19.30-20.45	chaperone/prof. activity/ discuss in general topics

2nd day

7.00-8.50	breakfast
9.00-10.00	chaperone oral presentation 10 min. present/ 2 min discussion
10.00-12.00	student oral presentation 7 min. present/ 3 min discussion
12.00-12.40	check out /lunch
13.00-15.30	visiting lab JAXA (Tsukuba, Lectures by Drs. Oshima, Oomori, and Shimazu)
17.00-	back to TMDU

Gja^{Jrt/+} mice are protected from age-related bone loss

Jane E. Aubin

Department of Molecular Genetics, University of Toronto, Toronto, ON



Oculodentodigital dysplasia (ODDD) is an autosomal dominant disorder characterized by pleiotropic developmental anomalies of the limbs, teeth, face and eyes that was shown recently to be caused by mutations in the gap junction protein alpha 1 gene (GJA1), encoding connexin 43 (Cx43). In the course of performing an Nethyl-N-nitrosourea mutagenesis screen, we identified a dominant mouse mutation that exhibits many classic symptoms of ODDD, including syndactyly, enamel hypoplasia, craniofacial anomalies and cardiac dysfunction. Positional cloning revealed that these mice carry a point mutation in Gja1 leading to the substitution of a highly conserved amino acid (G60S) in Cx43. In vivo and in vitro studies revealed that the mutant Cx43 protein acts in a dominant-negative fashion to disrupt gap junction assembly and function. Notably, in addition to the classic features of ODDD, Gja^{Jrt/+} mice exhibit osteopenia throughout life, with delayed ossification of all bones, but the difference in bone mineral density (BMD) compared to wild type littermates becomes less pronounced with age, i.e., Gja^{Jrt/+} mice are protected from the age-related bone loss seen in wild type mice. Cellular assays showed that osteoclast number is normal or even slightly reduced but activity is higher in younger but not older Gja^{Jrt/+} versus wild type mice. On the other hand, osteoblast number in vivo and osteoprogenitor number in stromal cell cultures in vitro display a trend towards being increased in older animals, i.e., in mice at 8 and 12 months of age. In addition, while no differences were seen in osteoblast-associated marker expression at early differentiation times, expression of several mature osteoblast and osteocyte markers was significantly higher at late differentiation time points in bones and stromal cultures of Gja^{Jrt/+} versus wild type mice. Our results indicate that while complete ablation of Cx43 and the presence of a dominant-negative allele of Cx43 both lead to low bone mass phenotypes, the underlying cellular mechanisms are notably different. In particular, our data show that diminution of Cx43 expression and function via the G60S mutation affects bone modeling and remodeling by dysregulation of both osteoclast and osteoblast lineage cells, that the osteopenia seen may reflect primarily increased osteoclast activity in younger mice, but that this is balanced by an increased osteoblast activity, the latter protecting Gja^{Jrt/+} mice from the age-related bone loss seen in wild type mice.

Academic Background

09/1968–06/1972	Bachelor of Science (Honours), Chemistry/Mathematics, Queen's University at Kingston, CANADA
07/1972–02/1977	Doctorate (PhD), Medical Biophysics, University of Toronto, CANADA (Dr. Victor Ling)
07/1977–06/1978	Postdoctorate, Max Planck Institute for Biophysical Chemistry, GERMANY (Dr. Tom Jovin)
07/1978–06/1979	Postdoctorate, Max Planck Institute for Biophysical Chemistry, GERMANY (Dr. Klaus Weber)

Work Experience

07/1979–06/1983	Assistant Professor, Dentistry-Oral Biology / MRC Group in Periodontal Physiology, University of Toronto, CANADA
07/1983–06/1988	Associate Professor, Dentistry-Oral Biology / MRC Group in Periodontal Physiology, Faculty of Dentistry, University of Toronto, CANADA
07/1988–06/1994	Full Professor, Dentistry-Oral Biology / MRC Group in Periodontal Physiology, Faculty of Dentistry, University of Toronto, CANADA
07/1988–06/1994	Director and Chair, Graduate Department of Dentistry / Director Postgraduate Dental Education, Faculty of Dentistry, University of Toronto, CANADA
07/1994–06/2002	Professor and Chair, Anatomy and Cell Biology, Faculty of Medicine, University of Toronto, CANADA
02/2003–12/2005	Scientific Co-Director and CEO, NCE, Networks of Centres of Excellence, Canadian Arthritis Network, CANADA
01/2006–12/2006	Scientific Director and CEO, NCE Network of Centres of Excellence, Canadian Arthritis Network, CANADA
07/1999–	Full Professor, Medical Biophysics, Faculty of Medicine, University of Toronto, CANADA
07/2002–	Full Professor Medical Genetics and Microbiology, Faculty of Medicine, University of Toronto, CANADA
01/2007–	Scientific Director, Institute of Musculoskeletal Health and Arthritis, Canadian Institutes of Health Research, CANADA

Distinctions

06/1970	Canadian Rosebrough Award - Book Prize, Canadian Chemical Society, CANADA
06/1971	Analytical Chemistry Award, Queen's University, CANADA
06/1972	Gold Medal Graduation Award, Queen's University, CANADA
03/1985	Oral Biology Research Award, International Association for Dental Research
10/2004	The William F. Neuman Award, American Society for Bone and Mineral Research, UNITED STATES
09/2005	Louis V. Avioli Memorial Lecture, American Society for Bone and Mineral Research, UNITED STATES

Councils and Leadership Roles (selected):

1997–2000	Board of Directors, Advances in Mineral Metabolism
1998–1999	President, American Society for Bone and Mineral Research (ASBMR)
2000–2002	Chair, Science Policy Committee, ASBMR
1998–2001	Member of Executive, AACBNB Chairpersons (US)
2001–2006	Advisory Board, Institute of Musculoskeletal Health and Arthritis, CIHR; Vice-Chair, 2005–2006
2001–present	Member, Board of Directors, Canadian Arthritis Network NCE
2002–2006	Member, Board of Directors, and Public Affairs Executive Committee, FASEB
2003–2007	Member of the Board, International Bone and Mineral Society
2004–present	Member, Finance Committee, American Society for Cell Biology
2004	Co-Chair, Long range planning advisory committee in research in Bone Biology and Bone Diseases, NIAMS/NIH
2005–2007	President-Elect, International Bone and Mineral Society

Publications (selected)

1. Bonnelye E, Laurin N, Jurdic P, Hart DA, Aubin JE. Estrogen receptor-related receptor- α (ERR- α) is dysregulated in inflammatory arthritis. *Rheumatology* 2008
2. Hasegawa T, Oizumi K, Yoshiko Y, Tanne K, Maeda N, Aubin JE. The PPAR γ -selective ligand BRL-49653 differentially regulates the fate choices of rat calvaria versus rat bone marrow stromal cell populations. *BMC Dev Biol* 2008 ;8:71.

3. Malaval L, Wade-Gu  ye NM, Boudiffa M, Fei J, Zirngibl R, Chen F, Laroche N, Roux JP, Burt-Pichat B, Duboeuf F, Boivin G, Jurdic P, Lafage-Proust MH, Am  d  e J, Vico L, Rossant J, Aubin JE. Bone sialoprotein plays a functional role in bone formation and osteoclastogenesis. *J Exp Med.* 2008; 205(5):1145-53.
4. Zirngibl RA, Chan JS, Aubin JE. Estrogen receptor-related receptor alpha (ERRalpha) regulates osteopontin expression through a non-canonical ERRalpha response element in a cell context-dependent manner. *J Mol Endocrinol.* 2008; 40(2):61-73.
5. Falconi D, Aubin JE. LIF inhibits osteoblast differentiation at least in part by regulation of HAS2 and its product hyaluronan. *J Bone Miner Res.* 2007; 22(8):1289-300.
6. Yoshiko Y, Candelieri GA, Maeda N, Aubin JE. Osteoblast autonomous Pi regulation via Pit1 plays a role in bone mineralization. *Mol Cell Biol.* 2007; 27(12):4465-74.
7. Bonnelye E, Zirngibl RA, Jurdic P, Aubin JE. The orphan nuclear estrogen receptor-related receptor-alpha regulates cartilage formation in vitro: implication of Sox9. *Endocrinology.* 2007; 148(3):1195-205.
8. Zhang S, Chan M, Aubin JE. Pleiotropic effects of the steroid hormone 1,25-dihydroxyvitamin D3 on the recruitment of mesenchymal lineage progenitors in fetal rat calvaria cell populations. *J Mol Endocrinol.* 2006; 36(3):425-33.
9. Liu F, Malaval L, Aubin JE. Global amplification polymerase chain reaction reveals novel transitional stages during osteoprogenitor differentiation. *J Cell Sci.* 2003; 116 (Pt 9):1787-96.

Tooth Regenerative Therapy as a Future Organ Replacement Regenerative Therapy

Takashi Tsuji, PhD

Research Institute for Science and Technology, Tokyo University of Science
Organ Technologies Inc.



To restore the partial loss of organ function, stem cell transplantation therapy has been developed as a cure for various diseases conditions, such as Parkinson's disease, leukemia, spinal injury, cardiac infarction, diabetes and liver diseases. The ultimate goal of regenerative therapy is to develop fully functioning bioengineered organs that can replace lost or damaged organs after disease, injury or aging. The development of three-dimensionally reconstructed bioengineered organs from dissociated single cells in vitro is a goal of this technology. However, no technology yet exists that enables us to create and grow organs through the single cell manipulation.

Almost all organs including tooth arise from the organ germs, which are induced by the reciprocal epithelial-mesenchymal interactions in the developing embryo. It has been proposed a novel concept for a bioengineered organ development that to properly reproduce the developmental process of organogenesis. To demonstrate the possibility of this concept, we attempted to develop a tooth regenerative therapy for lost tooth, which were challenged from the transplantation of a bioengineered tooth germ in adult oral environment as a model of a future organ replacement therapy. In the dental field, the therapy, such as "bridge" and "implant", had been established to prevent the movement of the neighboring teeth and supplement of their functions for the loss of the tooth by injury, caries or diseases. Therefore, "tooth" provides a good feasibility study model for the development of the technologies for a future organ replacement regenerative therapy.

In current research on whole-tooth regenerative therapy, a basic strategy is being pursued in which a bioengineered tooth germ is induced to develop into a fully functional tooth. Previously, we developed a three-dimensional organ-germ culture method for the reconstitution a bioengineered organ germ in the early developmental stages (Nature Methods 2007). The regeneration of tooth and periodontal tissues into a functional tooth unit is a critical issue for achieving proper oral function, including mastication. Recently, we successfully demonstrated that our bioengineered tooth germ could develop a fully functioning tooth, which has hardness for masticatory potential, the functional responsibility against a mechanical stress in maxillofacial region, and perceptive potentials of neural fibers innervated into the periodontal ligament and pulp of the bioengineered tooth to noxious stimulations such as orthodontic treatment and a pulp stimulation (PNAS 2009). These results showed that the bioengineered tooth germ could develop a fully functioning regenerated tooth in vivo after engraftment and an organ replacement regenerative therapy using a bioengineered organ germ might be feasible.

In this presentation, I will talk and discuss about the strategies and recent progress of the research for the establishment of tooth regenerative therapy.

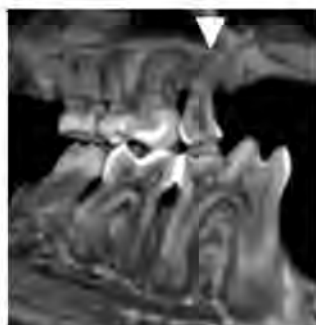


Figure:

Micro-CT analysis of a bioengineered tooth erupted in adult oral environment at 50 days after transplantation. Arrow-head indicates the bioengineered tooth

References:

1. Ikeda, E. et al., Fully functional bioengineered tooth replacement as an organ replacement therapy, *Proc. Natl. Acad. Sci. USA.*, 106 (32), 13475-13480, 2009.
2. Ikeda, E. & Tsuji, T., Growing bioengineered teeth from single cells: potential for dental regenerative medicine., *Expert Opinion on Biological Therapy* 8, 1-10, 2008.
3. Nakao, K., Morita, R., Saji, Y., Ishida, K., Tomita, Y., Ogawa, M., Saitoh, M., Tomooka, Y. & Tsuji, T.: The development of a bioengineered organ germ method, *Nature Methods* 4, 227-230, 2007.

Education

1993	PhD Graduate School of Science and Technology, Niigata University, Japan
1989-1992	Graduate School of Science, Kyushu University, Japan
1986	MSc Graduate School of Science, Niigata University, Japan
1984	BSc Faculty of Science, Niigata University, Japan

Professional Career

2009-Present	Professor, Research Institute for Science and Technology, Tokyo University of Science
2007-2009	Professor, Faculty of Industrial Science and Technology, Tokyo University of Science
2000-2007	Associate Professor, Faculty of Industrial Science and Technology, Tokyo University of Science
1993-2000	Senior Researcher, Pharmaceutical Frontier Research Laboratory, Japan Tobacco Inc.
1986-1989	Researchers, Central Research Laboratories, Yamanouchi Pharmaceutical Co Ltd.

Other Career

2008-Present	Director, Organ Technologies Inc.
2008	Visiting Professor, Louis Pasteur University
2004-Present	Advisor, Otsuka Chemical Co., Ltd.

Academic Activities

2007-Present	Director, the Japanese Association for Regenerative Dentistry
2006-Present	Councilor, the Japan Society for Organ Preservation and Medical Biology

2002-Present Councilor, the Japanese Society for
Regenerative Medicine

Etsuko Ikeda, Ritsuko Morita, Kazuhisa Nakao, Kentaro
Ishida, Takashi Nakamura, Teruko Takano-Yamamoto, Miho
Ogawa, Mitsumasa Mizuno, Shohei Kasugai, and Takashi
Tsuji. Fully functional bioengineered tooth replacement
as an organ replacement therapy, *PNAS* 106, 13475-13480,
2009.

Ryu-ich Fukuda, Kiyohito Tsuchiya, Koji Suzuki, Katsuhiko
Itoh, Jun Fujita, Atae Utsunomiya, and Takashi Tsuji.
HTLV-I Tax downregulates the expression of PIP3 inositol
phosphatases via the NF- κ B pathway, *J. Biol. Chem.* 284,
2680-2689, 2009.

Takashi Tsuji, Pluripotent stem cells developed into
regenerated tooth by organ germ method in combination
with tooth germ-derived epithelium. *Proceeding of
International Symposium on Micro-Nanomechanics and
Human Science* 2007, 342-346, 2007.

Kazuhisa Nakao, Ritsuko Morita, Yasumitsu Saji,
Kentaro Ishida, Miho Ogawa, Masahiro Saitoh, Yasuhiro
Tomooka & Takashi Tsuji. The development and in vivo
transplantation of an artificial tooth germ reconstituted by
the bioengineered organ germ method, *Eur Cell Mater.* 14,
59, 2007

Kazuhisa Nakao, Ritsuko Morita, Yasumitsu Saji, Kentaro
Ishida, Yusuke Tomita, Miho Ogawa, Masahiro Saitoh,
Yasuhiro Tomooka & Takashi Tsuji. The development of a
bioengineered organ germ method, *Nature Methods.* 4, 227-
130, 2007.

Gli2 and p53 interactions in Hedgehog-induced Tumorigenesis

Louisa Ho^{1,3}

Aneta Stojanovski^{1,3}, Heather Whetstone¹, Qing Xia Wei¹, Elaine Mau¹, Jay Wunder², Benjamin Alman^{1,2}

¹ Program in Developmental and Stem Cell Biology, Hospital for Sick Children, University of Toronto, Toronto ON, M5G 1L7.

² Department of Surgery, Mount Sinai Hospital, University of Toronto, Toronto, ON.

³ Department of Laboratory Medicine and Pathobiology, University of Toronto, Toronto, ON



Enchondromas are common benign cartilage tumors that arise in bones that undergo endochondral ossification, and may progress to malignant chondrosarcoma. Development of enchondroma results from abnormal regulation of Indian hedgehog (Ihh) signaling during growth plate development. As well, mutations in p53 have been detected in chondrosarcoma, and are thus suspected to play a role in its progression. Our lab has previously shown that enchondroma develop in transgenic mice in which overexpression of the Ihh activated transcription factor Gli2 is targeted in the growth plate. Furthermore, Gli2 overexpressing mice also carrying a p53 deficiency develop larger more cellular cartilage lesions, but do not develop chondrosarcoma. Embryonic growth plates of Gli2 transgenic and p53 KO mice showed decreased apoptosis compared to WT, with an enhanced effect observed in the double transgenic mice. Furthermore, a microarray screen of C2C12 cells with increased Hh signaling showed a downregulation of IGFBP-3 (insulin-like growth factor binding protein-3), a p53 target gene with known anti-apoptotic effects in other tumor cell models.

To investigate whether IGFBP-3 is regulated by Hh/Gli and p53 signaling pathways in growth plate development and maintenance, murine limb explants were treated with Shh and/or IGFBP-3 peptides. Treatment of these limbs with Shh reduced apoptosis, similar to the effect observed in p53 KO mice, of which addition of IGFBP-3 rescued their apoptotic deficient phenotype. Moreover, ChIP analysis of human CSA samples revealed a Gli2 transcription factor binding site upstream of IGFBP-3, suggesting that Hh signaling directly regulates IGFBP-3 expression within the growth plate. This was confirmed by decreased luciferase activity following activation of the Hh pathway in cell lines transfected with an IGFBP-3 promoter construct, but was not observed when transfected with a mutated construct of the putative Gli binding site. Finally, mice expressing Gli2 developed substantially fewer tumors when they were also deficient for *Igf2*.

Overall our data suggests that the combined effects of Gli2 overexpression and p53 deficiency act to inhibit IGFBP-3, resulting in decreased apoptosis and the development of large cartilage lesions observed in adult murine limbs. Therefore, IGF signaling-mediated apoptosis may play a major role in regulating the progression of benign enchondroma to malignant chondrosarcoma.

CURRICULUM VITAE

Education

- 2005-present Ph.D. University of Toronto
Department of Laboratory Medicine and Pathobiology
Hospital for Sick Children
Department of Developmental and Stem Cell Biology
- 2000-2005 Hon. B.Sc. University of Toronto with Distinction
Major: Biology. Minor: Anthropology

Research Experience

- 2004-2005 Student Research Project on diuretic peptides in *Rhodnius prolixus*
• Dissect adult specimens and observe location of diuretic peptides in the gut and CNS using immunohistochemistry
- 2003 Archaeology Lab Assistant, Volunteer, University of Toronto
• Collected quantitative data on fossil groups
• Sorted fossils and artifacts into categories

Teaching Experience

- 2005-2006 Teaching Assistant, 2nd year undergraduate Physiology, University of Toronto
• Lab based instruction, marking of assignments and tests, exam moderation

Extracurricular Activities

- 2009 Executive committee, Life Science Career Day Seminars
• Graduate student-run initiative at the University of Toronto that aims to help graduate students explore the various career paths that can stem from a life sciences graduate degree
- 2009 Volunteer Coordinator, Heart and Stroke Foundation-University of Toronto
• Recruitment of volunteers and communication of volunteering opportunities for upcoming events
- 2002-2003 Finance Minister, Erindale Math Club, University of Toronto.
• Raised money and communicated balance of funds
- 2002-2004 Intramural team member, Indoor Volleyball

Awards

- 2005-2009 RESTRACOMP, Hospital for Sick Children Foundation
• Awarded to graduate students in biomedical sciences by the SickKids Foundation Graduate Scholarships at the University of Toronto based on academic performance, publication activity, and other research, academic activities to cover their stipend.
- 2009 Gallie Day, The Department of Surgery, University of Toronto
• Awarded second place in oral presentation competition
- 2009 Gordon Research Conference: Cartilage Biology and Pathology
• Poster prize winner
- 2007 Gallie Day, The Department of Surgery, University of Toronto
• Awarded second place in poster prize competition
- 2005,2006 University of Toronto Fellowship Award
- 2000-2004 Volunteer Recognition Award
- 2000 University of Toronto Entrance Scholarship

Publications

- Lin AC, Seejo BL, Bartoszko JM, Khoury MA, Whetstone H, Ho L, Hsu C, Ali AS, Alman BA. Modulating hedgehog signaling can attenuate the severity of osteoarthritis. *Nat Med.* 2009 Dec;15(12):1421-5. Epub 2009 Nov 15.
- Ho L, Alman B. Protecting the Hedgerow: p53 and Hedgehog pathway interactions *Cell Cycle.* 2010 Feb. 1;9(3).
- Ho L, Stojanovski A, Whetstone H, Wei QX, Mau E, Wunder JS, Alman B. Gli2 and p53 cooperate to regulate IGFBP-3 mediated chondrocyte apoptosis in the progression from benign to malignant cartilage tumors. *Cancer Cell.* 2009 Aug 4;16(2):126-36.

Maintenance of bone growth and bone mass requires Hedgehog signaling

Yukiko Maeda Ph.D.

Medical science, Tokyo Medical and Dental University, Tokyo, Japan



Indian hedgehog (Ihh) plays a crucial role during growth plate and endochondral bone formation. Our previous studies with the *col2 α 1-Cre ER⁺Ihhd/d/* animals demonstrated that *Ihh* deletion from all postnatal chondrocytes results in complete loss of the growth plate and subsequently trabecular bone (Maeda et al. 2007).

Since the growth plate is required as a template for trabecular bone direct role of chondrocyte derived Ihh on trabecular bone formation is unknown.

Furthermore, activation of the Ihh downstream target PTH/PTHrP receptor (Jansen) could not rescue the loss of growth plate, suggesting Ihh is essential to maintain the growth plate independent of PTHrP (Maeda et al. 2009).

Therefore to further address the question whether chondrocyte-derived Ihh directly affects trabecular bone formation in postnatal life we generated a new hypomorph mouse model, *colX-Cre:Ihhd/d/*, in which Ihh is only removed from a subset of hypertrophic chondrocytes.

ColX-Cre:Ihhd/d/ mice were born with the expected Mendelian pattern of inheritance and looked indistinguishable from their normal littermates at birth. Deletion of *Ihh* from hypertrophic chondrocytes was confirmed by qRT-PCR and *in situ* hybridization. We analyzed control and mutant mice at 3 weeks and 4 months and could demonstrate that a growth plate as preserved. Micro CT analysis and TRAP staining of bone from *colX-Cre:Ihhd/d/* mice showed reduced bone volume and increased osteoclast number when compared to their control littermates at postnatal 3 weeks and 4 months. These results suggest that chondrocyte-derived Ihh signaling is required for maintenance of postnatal bone.

A. Positions and Honors.

Research Positions:

- 2004-present Research Associate, Department of Developmental Biology, Harvard School of Dental Medicine, Boston, M
- 2004 PhD Student, Center of Excellence Fellow (Super Student) at 21 Century COE Program, Laboratory of M. Noda, Dept. of Molecular Pharmacology, Tokyo Medical and Dental University, Tokyo, Japan
- 2000-2004 PhD Student, Laboratory of M. Noda, Dept. of Molecular Pharmacology, Tokyo Medical and Dental University, Tokyo, Japan

B. Selected Peer-reviewed Publications.

- Correa D, Kiviranta R, Hesse E, Saito H, Yamana K, Neff L, Sitara D, Maeda Y, Warming S, Jenkins NA, Copeland NG, Lanske B, Horne, WC, Baron R. The Transcriptional Co-regulator Zfp521 Regulates Chondrocyte Proliferation and Differentiation, Contributing to the Effects of Parathyroid Hormone-Related Peptide (PTHrP) on the Growth Plate. *Dev Cell* (Under revision)
- Maeda Y, Schipani E, Densmore JM, Lanske B. Partial rescue of postnatal growth plate abnormalities in *Ihh* mutants by expression of a constitutively active PTHrP/PTHrP receptor. *Bone* (In press)
- Ochiai T, Shibukawa Y, Nagayama M, Munday C, Yasuda T, Okabe T, Shimono K, Iwamoto M, Hasegawa T, Maeda Y, Lanske B, Pacifici M, Koyama E. Indian hedgehog roles in postnatal TMJ development and organization. *J Dent Res* (in Press)
- Maeda Y, Nakamura E, Nguyen MT, Suva LJ, Swain FL, Razzaque MS, Mackem S, Lanske B. Indian Hedgehog produced by postnatal chondrocytes is essential for maintaining a growth plate and trabecular bone. *PNAS*. 2007 104 (15) :6382-7.
- Koyama E, Young B, Shibukawa Y, Nagayama M, Enomoto IM, Iwamoto M, Maeda Y, Lanske B, Song B, Serra R, Pacifici M. Conditional Kif3a ablation causes abnormal hedgehog signaling topography, growth plate dysfunction and ectopic cartilage formation in mouse cranial base synchondroses. *Development* 2007 134 (11) :2159-69.
- Matsumoto K, Nishihara S, Kamimura M, Shiraishi T, Ootoguro T, Uehara M, Maeda Y, Ogura K, Lumsden A, Ogura T. The prepattern transcription factor *Irx2*, a target of the FGF8/MAP kinase cascade, is involved in cerebellum formation. *Nat Neurosci*. 2004 7 (6) :605-12.
- Kida Y, Maeda Y, Shiraishi T, Suzuki T, Ogura T, Chick Dachl interacts with the Smad complex and *Sm3a* to control AER formation and limb development along the proximodistal axis. *Development* 2004 131 (17) :4179-87.
- Ohyama Y, Nifuji A, Maeda Y, Amagasa T, Noda M. Spatiotemporal association and bone morphogenetic protein regulation of sclerostin and osterix expression during embryonic osteogenesis. *Endocrinology* 2004 145 (10) :4685-92.
- Maeda Y, Tsuji K, Benezra R, Nifuji A, Noda M. Inhibitory helix-loop-helix transcription factors *Id1/Id3* are required for bone formation in vivo. *J Cell Biochem*. 2004 1:93 (2) :337-44.
- Maeda Y and Noda M. Coordinated development of embryonic long bone on chorioallantoic membrane in ovo prevents perichondrium-derived suppressive signals against cartilage growth. *Bone* 2003 32 (1) :27-34
- Noda M, Kashimada K, Takamoto M, Yumoto K, Maeda Y, Usui M, Ishijima M. The meaning of phosphate in bone formation *Clin Calcium* 2001 Oct;11 (10) :1315-20. Japanese.

C. Meetings and Presentations

- ASBMR Meeting (Poster) Denver, CO (2009)
"Indian hedgehog expressed from hypertrophic chondrocytes is essential for adult trabecular bone formation."
- ASBMR Meeting (Oral) Montreal, QC (2008)
"Chondrocyte-derived *Ihh* Is Required for Osteoblast Differentiation Despite Reconstitution of a Normal Growth Plate"
- ASBMR Meeting (Poster) Honolulu, HI (2007)
"Indian Hedgehog Is Essential for Postnatal Bone"
- ASBMR Meeting (Oral) Philadelphia, PA (2006)
"Indian Hedgehog (*Ihh*) Is Required for Endochondral Bone Formation after Birth"
- Sun Valley Workshop, (Oral) Sun Valley, ID (2006)
"Indian hedgehog is required for endochondral bone formation after birth"
- ASBMR Meeting (Plenary Poster) Nashville, TN (2005)
"Chondrocyte-Specific Deletion of Indian Hedgehog (*Ihh*) in Postnatal Life"
- IBMS Meeting (Oral) Osaka, Japan (2003)
"In vivo bone formation induced by BMP injections onto calvaria and angiogenesis during fracture healing are impaired in *Id1/Id3* double gene knockout mice"
- ASBMR Meeting (Poster) Minneapolis, MN (2003)
"Limbin, a gene required for normal lengthening of limbs, is expressed in chondrocytes in culture and its levels are down-regulated by BMP2"
- ASBMR Meeting (Oral) San Antonio, TX (2002)
"*Id1/Id3* double gene knockout results in defects in angiogenesis in fracture callus and suture development"
- IBMS Meeting (Poster) Okayama, Japan (2002)
"The growth suppression of epiphyseal cartilage by perichondrium is blocked in in ovo organ culture system"

11. ASBMR Meeting (Poster) Phenix, AL (2001)
"Perichondrium acts as an inducer of apoptosis in epiphyseal chondrocytes in in vitro organ cultures but its inhibitory activity is blocked in in ovo organ cultures"
12. JBS Meeting (Poster) Yokohama, Japan (2000)
"The interaction between angiogenesis and perichondrium during endochondral bone formation"
13. MBSJ Meeting (Poster) Hukuoka, Japan (1999)
"The role of chicken Dachshund gene during neural development"

D. Awards and Honors

- 2007 Dean's Scholars Award, Harvard School of Dental Medicine
"Indian Hedgehog produced by postnatal chondrocytes is essential for maintaining a growth plate and trabecular bone"
- 2006 Dean's Scholars Award, Harvard School of Dental Medicine
"The role of Indian hedgehog in endochondral bone formation after birth"
- 2006 ASBMR Harold M. Frost Young Investigator Award, 36th International Sun Valley Workshop on Skeletal Tissue Biology
"Indian hedgehog is required for endochondral bone formation after birth"
- 2006 ASBMR Young Investigator Award, American Society for Bone and Mineral Research (ASBMR), Philadelphia
"Indian Hedgehog (Ihh) Is Required for Endochondral Bone Formation after Birth"
- 2003 Travel Award for International Bone and Mineral Society (IBMS)
"In vivo bone formation induced by BMP injections onto calvaria and angiogenesis during fracture healing are impaired in Id1/Id3 double gene knockout mice"
- 2003 21st Century COE Program, Super Student award, Tokyo Medical and Dental University
"Functional analysis of chondrodysplasia causative gene LIMBIN (LBN)"

E. Teaching

- | | |
|--------------|---|
| 2004-present | Teaching to graduate and undergraduate students, Harvard School of Dental Medicine, Boston, MA |
| 2000-2004 | Teaching assistant of undergraduate students, Tokyo Medical and Dental University, Tokyo, Japan |

15. 拠点内部評価（若手研究者・学生）

Important information.

For each lecture , we would like to evaluate your understanding of the lectures every week as this course would be certified as one of formal lectures of the university. Please express your opinion and submit both the following questionnaire including your short comments on the contents of lecture at the end of each lecture:

Questionnaire

1. The name of the lecturer.
2. Your name and department.
3. Evaluation of the lecture

The quality of the content of the lecture was

(excellent, good, average, relatively poor, poor)

The method of the presentations was

(excellent, good, average, relatively poor, poor)

Overall evaluation of your attitude (effort, motivation and commitment).

(excellent, good, average, relatively poor, poor)

4. Your comments or questions to the lecturer.

Important information.

From the next lecture series we would like to evaluate your understanding of the lectures every week as this course would be certified as one of formal lectures of the university. Please express your opinion and submit both the following questionnaire including your short comments on the contents of lecture at the end of each lecture:

Questionnaire

1. The name of the lecturer.
2. Your name and department.
3. Evaluation of the lecture

The quality of the content of the lecture was

(excellent, good, average, relatively poor, poor)

The method of the presentations was

(excellent, good, average, relatively poor, poor)

Overall evaluation of your attitude (effort, motivation and commitment).

(excellent, good, average, relatively poor, poor)

4. Your comments or questions to the lecturer.

その原因はいろいろある。Fusionという単純で
高効率なエネルギー源である。しかし、その実現には
5.2 高次的・複合的に多くの問題が生じて、組織的に対応し
なければならぬ。そのために、まず、丁寧な説明に
ついては、より詳しく説明してほしい。

また、そのほか、高効率なエネルギー源である。Fusionという単純で
高効率なエネルギー源である。しかし、その実現には
5.2 高次的・複合的に多くの問題が生じて、組織的に対応し
なければならぬ。そのために、まず、丁寧な説明に
ついては、より詳しく説明してほしい。

Prof. F. Ishino, the GCOE Committee on International Education Programs

Prof. I. Morita, the GCOE Committee on Development of Young Scientists

⑧. いよいよ、このところ、Fusionという単純で
高効率なエネルギー源である。しかし、その実現には
5.2 高次的・複合的に多くの問題が生じて、組織的に対応し
なければならぬ。そのために、まず、丁寧な説明に
ついては、より詳しく説明してほしい。

⑨. いよいよ、このところ、Fusionという単純で
高効率なエネルギー源である。しかし、その実現には
5.2 高次的・複合的に多くの問題が生じて、組織的に対応し
なければならぬ。そのために、まず、丁寧な説明に
ついては、より詳しく説明してほしい。

⑩. いよいよ、このところ、Fusionという単純で
高効率なエネルギー源である。しかし、その実現には
5.2 高次的・複合的に多くの問題が生じて、組織的に対応し
なければならぬ。そのために、まず、丁寧な説明に
ついては、より詳しく説明してほしい。

⑪. いよいよ、このところ、Fusionという単純で
高効率なエネルギー源である。しかし、その実現には
5.2 高次的・複合的に多くの問題が生じて、組織的に対応し
なければならぬ。そのために、まず、丁寧な説明に
ついては、より詳しく説明してほしい。

⑫. いよいよ、このところ、Fusionという単純で
高効率なエネルギー源である。しかし、その実現には
5.2 高次的・複合的に多くの問題が生じて、組織的に対応し
なければならぬ。そのために、まず、丁寧な説明に
ついては、より詳しく説明してほしい。

Important information.

From the next lecture series we would like to evaluate your understanding of the lectures every week as this course would be certified as one of formal lectures of the university. Please express your opinion and submit both the following questionnaire including your short comments on the contents of lecture at the end of each lecture:

Questionnaire

1. The name of the lecturer.
2. Your name and department.
3. Evaluation of the lecture

The quality of the content of the lecture was

(excellent) good, average, relatively poor, poor)

The method of the presentations was

(excellent) good, average, relatively poor, poor)

Overall evaluation of your attitude (effort, motivation and commitment).

(excellent) good, average, relatively poor, poor)

4. Your comments or questions to the lecturer.

Thank you for the interesting lecture. There are many points I would like to ask, first what about pulling down the teeth to the site of bone defect (into alveolar bone) without bone graft.
-Second, as we need implant & bone graft in some cases, so why not to place them together instead of placing the bone graft first then wait for several months before the Implant insertion.

Prof. F. Ishino, the GCOE Committee on International Education Programs

Prof. I. Morita, the GCOE Committee on Development of Young Scientists

-Third, is there any Risk regarding the teeth vitality in segmental distraction.

平成21年度 GCOEプログラム 実績報告書

CONTENTS

野田 政樹 (分子薬理学分野)	46
田上 順次 (う蝕制御学分野)	60
高柳 広 (分子情報伝達学分野)	92
森田 育男 (分子細胞機能学)	106
小村 健 (顎口腔外科学分野)	126
春日井 昇平 (インプラント口腔再生学分野)	142
須田 英明 (歯髄生物学分野)	158
和泉 雄一 (歯周病学分野)	180
柳下 正樹 (硬組織病態制御学)	196
山口 朗 (口腔病理学分野)	206
森山 啓司 (顎顔面矯正学分野)	218
四宮 謙一 (整形外科学分野)	250
宮坂 信之 (膠原病・リウマチ内科)	264
宗田 大 (運動器外科分野)	280
秋吉 一成 (有機材料分野)	306
稲澤 譲治 (分子細胞遺伝学分野)	324
三木 義男 (分子遺伝分野)	374
石野 史敏 (分子生物学分野)	388
澁谷 浩司 (分子細胞生物学分野)	410
小川 佳宏 (分子代謝学分野)	428
荻原 正敏 (形質発現分野)	460

分子薬理学

野田 政樹

医歯学総合研究科・器官システム制御学系専攻
分子薬理学・教授



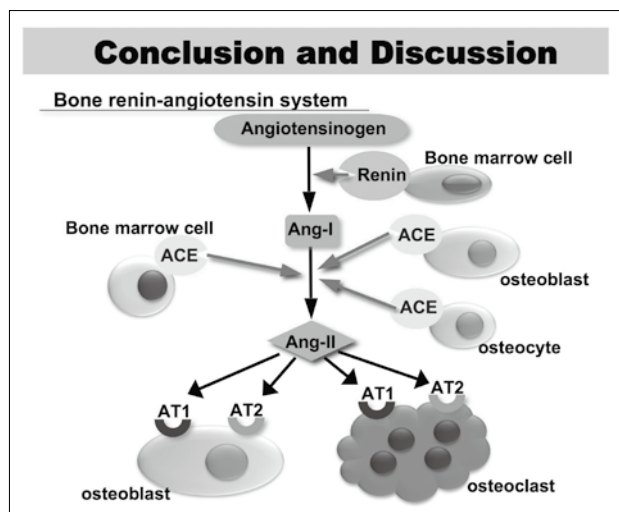
1) 研究の課題名

骨形成制御の分子機構

Molecular Mechanisms of Bone Formation

2)

骨に於ける循環器制御系因子の発現の解析



3) 研究内容の英文要約

Molecular bases of bone formation were studied with respect to bone metabolism being controlled by BMP and its antagonists as well as bone turnover under the influence of mechanical stress and circulation related molecules. Novel roles of microRNA were also identified based on genetic analyses of animals.

J.Biol Chem. 2009 Feb 20;284 (8) :4857-64. Epub 2008 Nov 11.

Angiotensin II type 2 receptor blockade increases bone mass.

Izu Y, Mizoguchi F, Kawamata A, Hayata T, Nakamoto T, Nakashima K, Inagami T, Ezura Y, Noda M.

Department of Molecular Pharmacology, Medical Research Institute, Tokyo Medical and Dental University, Tokyo 101-

0062, Japan.

Renin angiotensin system (RAS) regulates circulating blood volume and blood pressure systemically, whereas RAS also plays a role in the local milieu. Previous in vitro studies suggested that RAS may be involved in the regulation of bone cells. However, it was not known whether molecules involved in RAS are present in bone in vivo. In this study, we examined the presence of RAS components in adult bone and the effects of angiotensin II type 2 (AT2) receptor blocker on bone mass. Immunohistochemistry revealed that AT2 receptor protein was expressed in both osteoblasts and osteoclasts. In addition, renin and angiotensin II-converting enzyme were expressed in bone cells in vivo. Treatment with AT2 receptor blocker significantly enhanced the levels of bone mass, and this effect was based on the enhancement of osteoblastic activity as well as the suppression of osteoclastic activity in vivo. These results indicate that RAS components are present in adult bone and that blockade of AT2 receptor results in alteration in bone mass.

J Biol Chem. 2009 Apr 17;284 (16) :10593-600. Epub 2009 Feb 20.

ANA deficiency enhances bone morphogenetic protein-induced ectopic bone formation via transcriptional events. Miyai K, Yoneda M, Hasegawa U, Toita S, Izu Y, Hemmi H, Hayata T, Ezura Y, Mizutani S, Miyazono K, Akiyoshi K, Yamamoto T, Noda M.

Department of Molecular Pharmacology, Medical Research Institute, Tokyo Medical and Dental University, Japan.

Ectopic bone formation after joint replacement or brain injury in humans is a serious complication that causes immobility of joints and severe pain. However, mechanisms underlying such ectopic bone formation are not fully understood. Bone morphogenetic protein (BMPs) are defined as inducers of ectopic bone formation, and they are regulated by several types of inhibitors. ANA is an antiproliferative molecule that belongs to Tob/BTG family, but its activity in bone metabolism has not been known. Here, we examined the role of ANA on ectopic bone

formation activity of BMP. In ANA-deficient and wild-type mice, BMP2 was implanted to induce ectopic bone formation in muscle. ANA deficiency increased mass of newly formed bone in vivo compared with wild-type based on 3D-muCT analyses. ANA mRNA was expressed in bone in vivo as well as in osteoblastic cells in vitro. Such ANA mRNA levels were increased by BMP2 treatment in MC3T3-E1 osteoblastic cells. Overexpression of ANA suppressed BMP-induced expression of luciferase reporter gene linked to BMP response elements in these cells. Conversely, ANA mRNA knockdown by small interference RNA enhanced the BMP-dependent BMP response element reporter expression. It also enhanced BMP-induced osteoblastic differentiation in muscle-derived C2C12 cells. Immunoprecipitation assay indicated that ANA interacts with Smad8. Thus, ANA is a suppressor of ectopic bone formation induced by BMP, and this inhibitory ANA activity is a part of the negative feedback regulation of BMP function.

Horm Metab Res. 2009 Nov;41 (11) :822-8.

Combinatory effects of androgen receptor deficiency and hind limb unloading on bone.

Saita Y, Nakamura T, Mizoguchi F, Nakashima K, Hemmi H, Hayata T, Ezura Y, Kurosawa H, Kato S, Noda M. Department of Molecular Pharmacology, Medical Research Institute, Tokyo Medical and Dental University, Chiyoda-ku, Tokyo, Japan.

Male sex hormones play a critical role in regulation of bone metabolism. In male mice lacking androgen receptor (AR), osteopenia and high turnover state in bone remodeling have been reported. However, androgen receptor's role in disuse-induced osteopenia is not known. Therefore, we examined the effects of AR deficiency on unloading-induced bone loss. Wild type or androgen receptor deficient mice (ARKO) were subjected to hind limb unloading (HU) or normal housing (Control). The groups of mice were as follows; wild type control mice (Group WT-Cont), ARKO control mice (Group ARKO-Cont), wild type HU mice (Group WT-HU), and ARKO-HU mice (Group ARKO-HU). HU reduced cancellous bone mass in ARKO (ARKO-HU) by about 70% compared to ARKO-Cont and this reduction rate was over two-fold more than that of wild type (WT-HU) (reduction by less than 30% compared to WT-Cont). Combination of ARKO and HU (ARKO-HU) resulted in the least levels of cortical bone mass and bone mineral density among the four groups. ARKO-HU group indicated the highest levels of systemic bone resorption marker, deoxypyridinoline. Osteoclast development levels in the cultures in ARKO-HU derived bone marrow cells were the highest among the four groups. These data suggest that combination of androgen receptor deficiency and hind limb unloading results in exacerbation of disuse-induced

osteopenia due to the enhanced levels of bone resorption.

2008年度においては、破骨細胞における新たな制御系としてマイクロRNAによる意義の解析を行った。この目的でマイクロRNAの産生に必須である酵素、Dicerを破骨細胞と特異的にカテプシンK-Creのプロモーターにてノックアウトしたマウスを作成し検討した。この結果、Dicerが欠失したマウスにおいては破骨細胞数が減少し、また破骨細胞の表面の減少が観察された。Dicerは破骨細胞における酒石酸耐性酸性フォスファターゼの陽性である多核の破骨細胞の形成を抑制した。また、NFATc1の発現を抑制し、遺伝子発現のレベルでの抑制が見られた。一方で破骨細胞の抑制とともに骨芽細胞の機能が抑制され石灰化速度 (MAR) 並びに骨形成速度 (BFR) の抑制が見られ、また遺伝子発現レベルではI型コラーゲン、オステオカルシン、Runx2のレベルの低下が観察された。同時にまたEfnb2の低下も観察され、これらのことからDicerの欠失が骨の低回転性の代謝動態の変化を起し吸収系の抑制が形成の抑制よりも上回ったことから骨量の増加が観察された。これらの観察は骨代謝における破骨細胞の制御に対し、マイクロRNAが関与することを示した点で新たな領域を開くものである。

本年度は更に骨の力学的な刺激への応答の制御と共に体液バランスが、体液のシフトを伴う循環系の動態が骨量の制御と同時に起こることから、循環系の制御分子と骨量の関わりについての検討を行った。この結果、レニン、アンジオテンシンの制御系の構成因子であるアンジオテンシンの受容体の骨芽細胞における発現並びに破骨細胞における発現が観察され、更にレニン並びにアンジオテンシン2の変換酵素が発現することを見出した。またAT2受容体の阻害剤が骨量を増加させ、このことは骨芽細胞の活性を高めることによることが明らかとなった。AT2受容体ノックアウトマウスを用いた検討からも同様の結果が得られ、以上のことからレニン、アンジオテンシン系システムが骨量制御に関わることを明らかにした。これらの研究より、新たな骨芽細胞系ならびに破骨細胞系の制御の分子機構を見出すと共に、骨量制御における循環系調節関連因子の役割が明らかとなった。

4) 本事業に関連して世界的な研究拠点形成に向けて、以下の点で改善・整備等されたこと

A (研究拠点体制)

骨芽細胞の研究に於ける我が国及び国際的な研究協力体制が構築された

B (研究教育環境)

選抜大学院生および 重点育成シャペロンの 育成環境が整備された

C (人材確保)

優れた若手人材を英語面接にもとづく競争的環境で確保した

D (人材育成)

総合プレゼンテーションで活発な討議にもとづく英語の研究発表と教育がなされた

E (国際化)

国際的環境で教育と研究が推進された

5) GCOE 事業を推進するに当たって力を入れた点

世界の先端研究を推進する拠点を形成するとともにグローバルなネットワークを構築した

6) 英文原著論文

1. ©Izu Y, Mizoguchi F, Kawamata A, Hayata T, Nakamoto T, Nakashima K, Inagami T, Ezura Y, Noda M. Angiotensin II type 2 receptor blockade increases bone mass. *Journal of Biological Chemistry*; 284:4857-64, 2009
2. ©Miyai K, Yoneda M, Hasegawa U, Toida S, Izu Y, Hemmi H, Hayata T, Ezura Y, Mizutani S, Miyazono K, Akiyoshi K, Yamamoto T, Noda M. ANA deficiency enhances BMP-induced ectopic bone formation via transcriptional events. *Journal of Biological Chemistry*; 284:10593-600, 2009
3. ©Ezura Y, Koga H, Muneta T, Sekiya I, Noda M. Methylation status of CpG-islands in the promoter regions of signature genes during chondrogenesis of human synovium-derived mesenchymal stem cells. *Arthritis & Rheumatism*; 60:1416-1426, 2009
4. ©Hayashi C, Hasegawa U, Saita Y, Hemmi H, Hayata T, Nakashima K, Ezura Y, Amagasa T, Akiyoshi K, Noda M. Osteoblastic Bone Formation Is Induced by Using Nanogel-Crosslinking Hydrogel as Novel Scaffold for Bone Growth Factor. *Journal of Cellular Physiology*; 220:1-7, 2009

5. ©Mizoguchi F, Izu Y, Hayata T, Hemmi H, Nakashima K, Nakamura T, Kato S, Miyasaka N, Ezura Y, Noda M. Osteoclast-specific Dicer gene deficiency suppresses osteoclastic bone resorption. *Journal of Cellular Biochemistry*; 2009

7) 平成21年度までの自己評価

本年度においては、骨代謝調節機構の新たな分子の探索と骨再生へのナノサイエンスとBMPシグナル制御分子の研究を推進した。

また破骨細胞の新たな制御に関わるマイクロRNA制御系の意義を明らかにした。

その結果、骨のメカニカルストレスにおける制御と連関する循環器系の制御分子群である

アンジオテンシンを始めとする受容体並びにそのブロッカーを用いた解析から骨形成及び骨吸収における循環系との接点を明らかにした。さらに骨の形成に関わる新たなナノゲルを用いた骨再構成システムを構築し、BMPに基づく効率的な骨形成のシステムを開発した。BMPについてはそのシグナルメカニズムの検討を行い、これにより新たなBMPの抑止分子としてのANAの役割を見出し、これが特に単なる骨形成のみならず異所性の骨形成に特異的な働きを持つことを見出した。骨吸収の分子メカニズムにおいてはマイクロRNAの骨吸収及び白骨細胞の機能における意義を見出し、さらに変形性関節症と軟骨の形成に関わる人の遺伝子及び遺伝子発現の解析により、エピジェネティクスに基づく軟骨の分化制御における意義の解明が進展した。以上のことから歯と骨の分子疾患科学に関わる

研究が推進されたと評価する。

8) 和文原著論文

1. 野田政樹、江面陽一. 「骨と軟骨」 炎症・再生医学事典 547-549, 2009. (予定)
2. 野田政樹, 長尾雅史, 羽生亮, 宮井健太郎, 江面陽一. 「分子生物学からみた骨折治癒」 *CLINICAL CALCIUM* 20 (5) :634-40, 2009

9) 学会発表 (英文)

1. Ezura Y, Sekiya I, Muneta T, Noda M. The hypermethylated high-density CpG-region (-1112/-888) of the stromal cell-derived factor 1 (SDF1) is demethylated in the synovium derived mesenchymal stem cells during chondrogenesis. The 31st Annual Meeting of American

- Society for Bone and Mineral Research, Denver, Colorado, USA, September 11-15, 2009
2. Hayata T, Ezura Y, Noda M Dullard, a novel phosphatase, that dephosphorylates and degrades BMP receptors, suppresses signaling in osteoblasts. The 31st Annual Meeting of American Society for Bone and Mineral Research, Denver, Colorado, USA, September 11-15, 2009
 3. Hemmi H, Idoyaga J, Suda K, Noda M, Steinman R. M. The identification and characterization of a new Trem-like molecule. The 31st Annual Meeting of American Society for Bone and Mineral Research, Denver, Colorado, USA, September 11-15, 2009
 4. Nakamoto T, Ono N, Hanyu R, Sakuma T, Hayata T, Ezura Y, Schipani E, Kronenberg HM, Noda M Anabolic Action of PTH/PTHrP Receptor Signaling in Bone is Suppressed by a Nucleocytoplasmic Shuttling Protein CIZ The 31st Annual Meeting of American Society for Bone and Mineral Research, Denver, Colorado, USA, September 11-15, 2009
 5. Notomi T, Tanaka S, Amano H, Nakamura T, Noda M, Skerry TM, Kuno M Pacemaker channel HCN1 affects osteoclast function in vitro and bone remodeling in vivo. The 31st Annual Meeting of American Society for Bone and Mineral Research, Denver, Colorado, USA, September 11-15, 2009
 6. Hanyu R, Takeda S, Notomi T, Hemmi H, Hayata T, Ezura Y, Noda M Sympathetic nervous tone modulates constitutively active parathyroid hormone receptor signaling in vivo The 31st Annual Meeting of American Society for Bone and Mineral Research, Denver, Colorado, USA, September 11-15, 2009
 7. Nagao M, Saita Y, Hanyu R, Hemmi H, Notomi T, Nakamoto T, Hayata T, Ezura Y, Kurosawa H, Noda M Schnurri-2 (SHN-2) deficiency counteracts against bone loss induced by ovariectomy. The 31st Annual Meeting of American Society for Bone and Mineral Research, Denver, Colorado, USA, September 11-15, 2009
 8. Kamolratanakul P, Kawamata A, Yamamoto Y, Hayata T, Ezura Y, Akiyoshi K, Amagasa T, Noda M Nanogel scaffold delivery of Prostaglandin E2 Receptor (EP4) specific agonist in combination with BMP repairs microstructure of bone produced in the defect via potentiation of transcription activity of smad response element. The 31st Annual Meeting of American Society for Bone and Mineral Research, Denver, Colorado, USA, September 11-15, 2009
 9. Sakuma T, Nakamoto T, Hayata T, Miyai K, Amagasa T, Ezura Y, Noda M Deficiency of Ciz, Cas Interactive Zinc Finger Protein, suppresses tumor invasion into bone. The 31st Annual Meeting of American Society for Bone and Mineral Research, Denver, Colorado, USA, September 11-15, 2009
 10. Morishita M, Ono N, Hanyu R, Kamolratanakul P, Nagao M, Hemmi H, Hayata T, Noda M PTH signaling and Osteopontin deficiency coordinately enhance progenitor niche for the cells to support tooth development. The 31st Annual Meeting of American Society for Bone and Mineral Research, Denver, Colorado, USA, September 11-15, 2009
 11. Ampornaramveth, R, Pavasant, Noda, M Cbl-b enhanced Runx2 function on osteocalcin promoter activity in osteoblastic cell line The 31st Annual Meeting of American Society for Bone and Mineral Research, Denver, Colorado, USA, September 11-15, 2009
- ## 10) 学会発表 (和文)
1. 納富拓也、田中伸哉、天野均、中村利孝、野田政樹、久野みゆき ペースメーカーチャネル (HCN1) の欠損は高代謝回転による骨量減少を引き起こす 第29回日本骨形態計測学会 5月28日-30日, 2009
 2. 羽生亮、斎田良知、長尾雅史、伊豆弥生、竹田秀、江面陽一、黒澤尚、野田政樹 若令マウスにおけるアドレナリン β 2受容体遺伝子欠損はPTHの高回転型骨量増加作用を抑制する 第31回日本整形外科学会基礎学術集会 11月5日-6日, 2009
 3. 長尾雅史、斎田良知、羽生亮、辺見弘明、納富拓也、早田匡芳、江面陽一、黒澤尚、野田政樹 Schnurri-2欠損マウスでは卵巣摘出後も野生型の骨量を維持する 11月5日-6日, 2009
 4. 納富拓也、田中伸哉、天野均、中村利孝、野田政樹、久野みゆき ペースメーカーチャネル (HCN1) の破骨細胞機能と骨代謝機構への関与 第27回日本骨代謝学会 7月23日-25日, 2009
 5. 江面陽一、関矢一郎、宗田大、野田政樹 ヒト滑膜由来間葉系幹細胞におけるSDF1遺伝子上流の高密度CpG部位 (-1115/-888) の高メチル化状態は軟骨細胞分化過程において脱メチル化される 7月23日-25日, 2009

6. 早田匡芳、江面陽一、野田政樹 BMP受容体を脱リン酸化し分解する新規脱リン酸化酵素 Dullard は、骨芽細胞において BMP シグナルを抑制する 7月23日-25日,2009

11) 外部資金の獲得状況

グローバルCOEプログラム（拠点リーダー）	369,356万円（2009年）
硬組織疾患プロジェクト（拠点リーダー）	2,600万円（2009年）
日本学術振興会研究費補助金（基盤S）	1,690万円（2009年）
日本学術振興会研究費補助金（特定・がん）	430万円（2009年）
日本宇宙フォーラム	420万円（2009年）

12) 特別講演、招待講演

- 野田政樹:第20回栃木県骨・カルシウム代謝研究会
2009年6月19日
演題:骨形成の制御機構
- 野田政樹:第29回日本骨形態計測学会
2009年5月29日
演題:骨の形成とその調節機構
- 野田政樹:第63回日本口腔科学会 2009年4月17日
- 野田政樹:第61回関西カルシウム懇話会
2009年3月28日
演題:骨芽細胞制御の分子機構
- 野田政樹:第12回超音波骨折治療研究会
2009年1月17日
演題:メカニカルストレスと骨代謝
- 野田政樹:宇宙医学生物学ワークショップ
「微小重力と骨代謝」
(財団法人日本宇宙フォーラム)
2009年1月16日
演題:メカニカルストレスと骨

13) 教室、分野や講座の准教授、講師、助教、特別研究員、ポスドク、指導を受けた大学院生の名前（AISSには○印）のリスト

助 教 授	江面陽一
准 教 授	早田匡芳
特任教員	中元哲也、辺見弘明
国際PIシャペロン	納富拓也、
大学院生	羽生亮、長尾雅史、
	AISS ○Paksinee Kamolratanakul、
	○中川朋美、○Smriti Aryal、
	○鈴木允文
	QAISS 宮嶋大輔

14) GCOE 活動についての感想、コメント、改善を望む点など

GCOEの拠点として大学院教育の上で部局を超えた教育研究体制が整備されるとともに海外の研究者の招聘や海外への若手の派遣による国際的拠点としての整備が推進された。

Angiotensin II Type 2 Receptor Blockade Increases Bone Mass*

Received for publication, October 1, 2008, and in revised form, November 10, 2008. Published, JBC Papers in Press, November 11, 2008. DOI: 10.1074/jbc.M807610200.

Yayoi Izu[†], Fumitaka Mizoguchi^{‡§¶}, Aya Kawamata^{||}, Tadayoshi Hayata[¶], Testuya Nakamoto^{‡§¶}, Kazuhisa Nakashima[¶], Tadashi Inagami^{‡¶}, Yoichi Ezura^{||}, and Masaki Noda^{¶¶}

From the [†]Department of Molecular Pharmacology, Medical Research Institute, Tokyo Medical and Dental University, Tokyo 101-0062, Japan, the [‡]Department of Medicine and Rheumatology and ^{||}Maxillofacial Surgery, Tokyo Medical and Dental University, Tokyo 113-8510, Japan, [¶]Global Center of Excellence Program for International Research Center for Molecular Science in Tooth and Bone Diseases, Tokyo Medical and Dental University, Tokyo 101-0062, Japan, and the ^{¶¶}Department of Biochemistry, Vanderbilt University School of Medicine, Nashville, Tennessee 37232

Renin angiotensin system (RAS) regulates circulating blood volume and blood pressure systemically, whereas RAS also plays a role in the local milieu. Previous *in vitro* studies suggested that RAS may be involved in the regulation of bone cells. However, it was not known whether molecules involved in RAS are present in bone *in vivo*. In this study, we examined the presence of RAS components in adult bone and the effects of angiotensin II type 2 (AT2) receptor blocker on bone mass. Immunohistochemistry revealed that AT2 receptor protein was expressed in both osteoblasts and osteoclasts. In addition, renin and angiotensin II-converting enzyme were expressed in bone cells *in vivo*. Treatment with AT2 receptor blocker significantly enhanced the levels of bone mass, and this effect was based on the enhancement of osteoblastic activity as well as the suppression of osteoclastic activity *in vivo*. These results indicate that RAS components are present in adult bone and that blockade of AT2 receptor results in alteration in bone mass.

Osteoporosis is one of the major diseases associated with aging. This disease is based on the imbalance between the two major activities, *i.e.* bone formation and bone resorption. Systemic signals such as parathyroid hormone (PTH)³ and vitamin D are the major regulators of the maintenance of bone mass and

blood calcium (1–3). In addition, bone mass levels are also determined by a central nervous control through the activities of sympathetic tone on both bone formation and resorption sides (4–7). In the local milieu of bone, two major types of cells, osteoblasts and osteoclasts, are located in close proximity, exchange their signals, and coordinately resorb and form bone matrix (8). Such events are controlled by molecules present in the local microenvironment. These include cytokines, their modulators, and matrix proteins secreted by osteoblasts and osteoclasts (9–11). However, the bone environment is quite heterogeneous, and there are also cells other than these two types. Microvasculatures are serving as a root to supply osteoclast progenitors, which are derived from hematopoietic lineage cells. Vasculatures in bone are also considered to give rise to progenitors for osteoblastic cells from their perivascular regions (12). In addition to the anatomical relationship between the vascular cells and bone cells, these cells may be functionally involved in the coordinate regulation of bone mass.

Recent clinical studies indicated that beta blockers and anti-hypertension drugs would reduce the risk of bone fractures in the elderly populations (13, 14). This suggests a possible link between vascular and skeletal systems. Renin angiotensin system (RAS) is operating not only systemically but also locally in several tissues, and bone microenvironments have been studied in this regard (15, 16). Osteoblasts and osteoclasts express angiotensin II type 1 receptor in cell cultures (17–19), suggesting the existence of local RAS in bone. However, whether RAS components are expressed in bone *in vivo* is not known.

Angiotensin II (Ang II) acts via angiotensin II type 1 (AT1) and type 2 (AT2) receptors, which are members of the 7-transmembrane-spanning G-protein-coupled receptors. AT1 and AT2 receptors exhibit limited sequence homology (~34% amino acid sequence identity) (20). Many actions of Ang II appear to be through AT1 receptors. In bone tissue, Ang II was reported to promote bone resorption via the AT1 receptor in cell culture system and in ovariectomized mice and rats (19). Expression of AT1 receptor was observed in cultured osteoblasts (21), and Ang II inhibit differentiation and bone formation via the AT1 receptor in rat calvarial osteoblastic cells (22). In contrast to the AT1 receptor, no significant effect was

* This work was supported by the Grants-in-aid from the Japanese Ministry of Education (21st Century Center of Excellence Program, Frontier Research for Molecular Destruction and Reconstitution of Tooth and Bone) 17012008, 18109011, 18659438, and 18123456, grants from Japan Space Forum, NASDA, and Advanced Bone and Joint Science Strategic Research Networks Projects (Japan Society for Promotion of Science Core to Core Program, Research for the Future Program, Genome Science). The costs of publication of this article were defrayed in part by the payment of page charges. This article must therefore be hereby marked "advertisement" in accordance with 18 U.S.C. Section 1734 solely to indicate this fact.

[†] To whom correspondence may be addressed: 3-10 Kanda-Surugadai, 2-Chome Chiyoda-ku, Tokyo 101-0062, Japan. Tel.: 81-3-5280-8067; Fax: 81-3-5280-8067; E-mail: ezura.mph@mri.tmd.ac.jp.

[‡] To whom correspondence may be addressed: 3-10 Kanda-Surugadai, 2-Chome Chiyoda-ku, Tokyo 101-0062, Japan. Tel.: 81-3-5280-8066; Fax: 81-3-5280-8066; E-mail: noda.mph@mri.tmd.ac.jp.

[§] The abbreviations used are: PTH, parathyroid hormone; RAS, renin angiotensin system; Ang II, angiotensin II; ACE, angiotensin-converting enzyme; AT1, angiotensin II type 1 receptor; AT2, angiotensin II type 2 receptor; BV/TV, bone volume per tissue volume; TRAP, tartrate-resistant acid phosphatase; PBS, phosphate-buffered saline; RT, reverse transcription; Tb.N, trabecular number; Tb.Sp, trabecular spacing; BS, bone surface; BFR, bone formation rate; MS/BS, mineralized surface per bone surface; Oc,

osteoclast; Tb.N, trabecular number; μ CT, micro x-ray computed tomography; MAR, mineral apposition rate; ENaC, epithelial sodium channels.

AT2 Receptor Blockade Increases Bone Mass

observed in cells by the AT2 receptor blocker in rat calvarial cell (22) or in the co-cultures of human osteoblast and osteoclast precursor cells (19).

In this study, we examined the expression of renin, angiotensin-converting enzyme (ACE), and Ang II receptors in bone *in vivo*. The effects of AT2 receptor blocker on bone mass were also investigated. These experiments revealed that AT2 receptor as well as renin and ACE were expressed in bone *in vivo* and that AT2 receptor blocker treatment enhanced bone mass through both enhancement of osteoblastic activity and suppression of osteoclastic activity *in vivo*.

EXPERIMENTAL PROCEDURES

Animals—9-Week-old C57BL/6J male mice were purchased from Oriental Yeast Co. (Tokyo, Japan). Angiotensin II type 2 receptor-deficient mice were generated on a C57BL/6 background as described previously (23). The mice were kindly gifted from Dr. Tadashi Inagami, Vanderbilt University School of Medicine. We used 15-week-old male mice. All experiments were conducted according to the guidelines from the Animal Welfare Committee of Tokyo Medical and Dental University.

Histochemistry for Tartrate-resistant Acid Phosphatase (TRAP)—The animals were deeply anesthetized with ether and perfused through the cardiac left ventricle with 4% paraformaldehyde in 0.1 M phosphate buffer (pH 7.4). Tibiae were removed and immersed in the same fixation buffer at 4 °C overnight. Then tissues were decalcified in 15% EDTA in 0.01 M phosphate buffer, pH 7.4, at 4 °C for 1 week. After dehydration through a graded series of ethanol at 4 °C, they were embedded in paraffin and sectioned at 3 μ m. The histochemistry for TRAP was performed as described previously (24). Briefly, after the preincubation of the deparaffinized sections with a tartrate buffer solution (50 mM tartrate in 100 mM NaOAc, pH 5.0) for 5 min, the sections were incubated with the substrate solution for 20 min. The substrate solution was prepared by dissolving 10 mg of AS mix (Sigma) in 500 ml of dimethyl formamide together with 60 mg of fast red violet/LB in 100 ml of tartrate buffer. Finally, the sections were counterstained with hematoxylin.

Immunohistochemistry—After preparation of tibia sections by the same procedure described above, the sections were processed for immunohistochemistry for AT1, and AT2 receptors were performed using antibodies against these molecules according to the manufacturer's instructions (Santa Cruz Biotechnology). Briefly, deparaffinized sections were treated with 0.3% hydrogen peroxidase for 30 min to inhibit endogenous peroxidase and preincubated with 0.1% swine serum for 30 min at room temperature. Rabbit antisera against human AT1 and AT2 receptors (Santa Cruz Biotechnology) were applied to the sections, respectively, at 4 °C overnight. After treatment with the swine anti-rabbit immunoglobulin (DAKO A/S, Glostrup, Denmark), the sections were incubated in a streptavidin-biotin-peroxidase complex (sABC) (DAKO A/S). To visualize the antigen-antibody reaction, the sections were treated with 0.02% diaminobenzidine tetrahydrochloride and 0.005% H_2O_2 . Finally, the sections were counterstained with hematoxylin. Immunohistochemistry for ACE was performed according to Ref. 25. In brief, after deparaffinized sections were treated by inhibition of endogenous peroxidase, antigen retrieval was per-

formed with 0.01 M citrate buffer, pH 6.0, at 65 °C for 30 min. Following the similar process of AT1 and AT2 receptor antibodies, the sections were preincubated with 0.1% swine serum and incubated with rabbit antiserum against human ACE in sequence.

In Situ Hybridization—Bone and kidney were removed and processed as described above. For the paraffin sections, the samples were dehydrated through a graded series of ethanol solutions at 4 °C, embedded in paraffin, and sectioned at 3 μ m. For the detection of *renin* mRNA, a 508-bp fragment of *renin* cDNA was amplified by the PCR method using the primer pair (5'-GAA CCA GAT GGA CAG GAG GA-3', 5'-CAC AGT GAT TCC ACC CAC AG-3'), designed according to the reports of the mouse *renin* sequences. For experiments with riboprobes, digoxigenin-labeled antisense and sense RNA probes were prepared using a digoxigenin RNA labeling kit (Roche Applied Science) according to the manufacturer's instructions. *In situ* hybridization was performed at 45 °C on the deparaffinized sections. Hybridized riboprobes were detected with an alkaline phosphatase-conjugated anti-digoxigenin antibody (Roche Applied Science), and visualized with nitro blue tetrazolium and 5-bromo-4-chloro-3-indolyl phosphate (Roche Applied Science).

PCR Analysis—For RT-PCR analysis, kidney, bone marrow, and primary osteoblastic cells obtained from mouse neonatal calvarial cells were used. Total RNA was isolated with TRIzol reagent (Invitrogen) according to the manufacturer's protocol. Reverse transcription (RT) was performed using 1 μ g of total RNA, containing (dT)₁₂₋₁₈ primers for quantitative real time PCR and SuperScriptII transcriptase (Invitrogen). Complementary DNA was amplified in reaction mixture containing 2.5 mM deoxynucleotide triphosphate mix, 10 mM specific primers, and rTaq DNA polymerase (Takara, Ohtsu, Japan) under the following conditions: 95 °C for 30 s, 55 or 60 °C for 30 s, and 72 °C for 30 s for 40 cycles in a GeneAmp PCR system 9700 (Applied Biosystems, Foster City, CA). After PCR amplification, the PCR products were sequenced. The primer sequence was as follows: 5'-CAC CTA TGT AAG ATC GCT TC-3' and 5'-GCA CAA TCG CCA TAA TTA TCC-3' for AT1 receptor; 5'-GAA GGA CAA CTT CAG TTT TGC-3' and 5'-CAA GGG GAA CTA CAT AAG ATG C-3' for AT2 receptor; 5'-CAG AGG CCA ACT GGC ATT AT-3' and 5'-CTG GAA GTT GCT CAC GTC AA-3' for ACE; and 5'-ACC ACA GTC CAT GCC ATC AC-3' and 5'-TCC ACC ACC CTG TTG CTG TA-3' for glyceraldehyde-3-phosphate dehydrogenase gene (*gapdh*). *renin* primer was described above.

Treatment with an AT1 or AT2 Receptor Blockers—Animals were divided into two groups (eight in each group). One group was treated with an oral administration of an AT1-R blocker (losartan potassium; LKT Laboratories, Inc., St. Paul, MN) or water daily for 2 weeks. The other group was treated with intraperitoneal injection of AT2-R blocker (PD12319; Sigma) or phosphate-buffered saline (PBS) daily for 2 weeks. Mice were treated with losartan and PD12319 at 10 mg/kg body weight. A number of AT1 receptor antagonists exist. Among those losartan is the most widely used antagonist for AT1 in experimental studies as reported in the literature; therefore, we chose losartan. The dosages were chosen based on preliminary three-di-

AT2 Receptor Blockade Increases Bone Mass

mensional μ CT analysis as well as the hypertension experiments (data not shown) (26). These animals were anesthetized using the method described above. Femora and tibiae were removed and immersed the 4% paraformaldehyde in 0.1 M phosphate buffer (pH 7.4) at 4 °C overnight. Femora were stored in 70% ethanol followed by histomorphometric analysis. Tibiae were decalcified and embedded in paraffin for TRAP staining.

Three-dimensional Micro X-ray Computed Tomography (μ CT) Analysis—Three-dimensional μ CT analysis was conducted using Scan-Xmate-E090 (Comscan Techno Co., Ltd., Sagami-hara, Japan) and TRI/3D-Bon (Ratoc System Engineering Co., Ltd., Tokyo, Japan) as computer software. Bone volume/tissue volume (BV/TV), trabecular number (Tb.N), trabecular spacing (Tb.Spac), and other microarchitectural parameters were analyzed in the secondary trabecular regions from 0.2 to 1.2 mm away from the chondro-osseous junction.

Histomorphometric Analysis—Calcein labeling was conducted to estimate the levels of newly formed bone within a unit time period according to the methods described elsewhere (27). Briefly, calcein (10 mg/kg body weight) was injected intraperitoneally 2 and 7 days before sacrifice. Femora were fixed in 4% paraformaldehyde and rinsed in 0.1 M phosphate buffer. Then tissues were embedded in 4% carboxymethylcellulose and sectioned into 5 mm with a cryostat. Sagittal histological sections were prepared, and the calcein bands were observed by fluorescent microscopy. Single labeled bone surface, double labeled bone surface, and total bone surface (BS) were separately measured. Mineralizing surface (MS) per BS was calculated as (double labeled bone surface + single labeled bone surface/2)/BS. The distance between parallel calcein lines was measured to yield mineral apposition rate (MAR (μ m/day)). Bone formation rate (BFR) was calculated as MAR multiplied by MS/BS. Histomorphometric analysis was performed by focusing the area where the same region of femora were analyzed by μ CT analysis. Osteoclast number per bone surface (N.S/BS, N/mm) and osteoclasts surface per bone surface (Oc.S/BS, %) were analyzed by TRAP staining in sagittal sections of tibiae.

Mineralized Nodule Analysis—Bone marrow cells were seeded to 12-well plates (2.0 cm²/well) at a density of 2×10^6 cells/well. The bone marrow cells were cultured in a standard growth medium containing 50 μ g/ml ascorbic acid and 10 mM β -glycerophosphate. The medium was changed every 2 days. The cultures were stained with alizarin red solution on day 21. The area of mineralized nodules/total dish was measured with ImageJ analysis program.

Primary Osteoblast Culture—Primary mouse osteoblastic cells were obtained by sequential enzyme digestion of excised calvarial bones from 2-day-old neonatal mice using 0.5% trypsin and 1% collagenase in PBS for 15 min. The first three digests were discarded, and the cells were resuspended in α -minimum essential medium (Invitrogen) supplemented with 10% fetal bovine serum (Invitrogen) and antibiotics (Invitrogen). Osteoblasts were initially seeded at a density of 5×10^3 cells/96-well plate. When confluent, we changed to the growth medium containing 50 μ g/ml ascorbic acid and 10 mM β -glycerophosphate. The medium was changed every 2 days. The cells were collected on days 0, 3, 7, 10, 14, 21, and 28 after changing the growth

medium. The collected cells were used for the analysis of real time PCR and Western blotting.

Western Blotting Analysis—To confirm the expression of AT1 and AT2 in osteoblasts at the developmental stage, primary osteoblastic cells were lysed in RIPA buffer (150 mM NaCl, 1.0% Nonidet P-40, 0.5% sodium deoxycholate, 0.1% SDS, 50 mM Tris-HCl (pH 8.0)) supplemented with complete mini (Roche Applied Science), as a protein inhibitor and protein extracts were cleared by centrifugation. The proteins were eluted in SDS sample buffer with heating at 95 °C for 2 min. The proteins were electrophoresed in SDS-PAGE. AT1 and AT2 receptors were detected by rabbit polyclonal anti-human AT1 and AT2 receptors (Santa Cruz Biotechnology), respectively, using ECL Plus Western blotting Detection System (GE Healthcare). β -Actin detected by mouse monoclonal anti-actin antibody (Sigma) was used as internal control.

Organ Culture—Organ culture was examined as described previously (28). Briefly, newborn mice (1 day after birth, P1) were sacrificed with ether, and the radii and ulnae were dissected out under a binocular microscope. The removed bones were rinsed in PBS with antibiotics and then placed in a 96-well plate (Corning Glass, Corning, NY) containing 50 ml of α -modified minimum essential medium (Sigma) supplemented with 10% bovine serum (Invitrogen). The bones were subsequently cultured in fresh media for 5 days under an atmosphere of 5% CO₂ at 37 °C, changing the medium every day. In each experiment, bones from the right and left side of the P1 mice were collected. The bone from one side was used as an experimental group and treated with either PD123319 (10^{-8} M) plus angiotensin II (10^{-8} M), and the other was used as control with PD123319 plus PBS. The experiments were conducted with four samples from each group. The samples were then fixed in 4% paraformaldehyde and embedded in paraffin. The paraffin sections were stained for TRAP activity. TRAP-positive cells were counted in six sections per each sample.

Statistical Analysis—To test the histological and histomorphometric parameter effects of AT1 or AT2 receptor blockers, Student's *t* test was used to compare between control (water or PBS) group and the experimental group treated with these blockers. The difference was judged to be statistically significant when *p* values were less than 0.05. All the numeral data in the results were presented as means \pm S.D.

RESULTS

Expression of Angiotensin II Type 2 (AT2) Receptor, Renin, and ACE in Bone in Vivo—To find out whether bone cells *in vivo* are the targets of Ang II, we first examined the expression of Ang II receptor proteins in the bones of adult mice. Immunohistochemistry was conducted using antibodies against these molecules. Osteoblasts were recognized as cuboidal mononuclear cells lining the trabecular bone, and these cells were positive for AT2 receptor staining (Fig. 1A, arrowheads). Examination of serial sections revealed that multinucleated cells, which attached to the bone matrix surface and expressed AT2 receptors (Fig. 1A, arrows), were also positive for TRAP (Fig. 1B, arrows), suggesting that osteoclastic cells or chondroclastic cells expressed AT2 receptor. These osteoblasts and osteoclasts

AT2 Receptor Blockade Increases Bone Mass

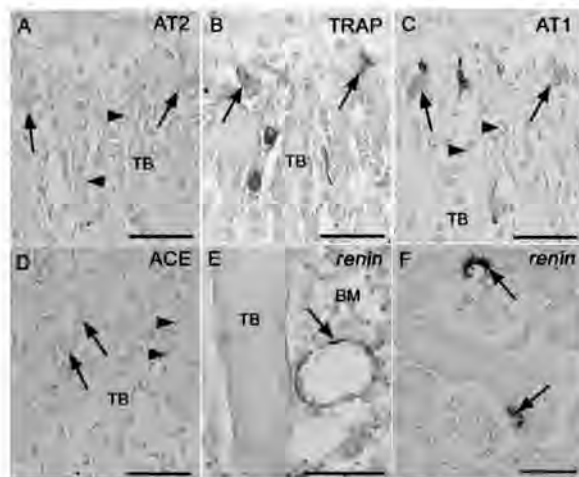


FIGURE 1. Expression of Ang II receptors, ACE, and renin in the proximal tibiae of 9-week-old male mice. Immunohistochemistry and *in situ* hybridization were carried out as described under "Experimental Procedures." A, AT2 receptor is expressed in osteoblasts (arrowheads) attached to trabecular bones and multinucleated osteoclasts (arrows). B, serial sections to A reveal that multinucleated osteoclasts are TRAP-positive. C, AT1 receptor is expressed in osteoblasts (arrowheads) and osteoclasts (arrows). D, ACE is expressed in osteoblasts (arrowheads) and osteoclasts (arrows). E and F, *in situ* hybridization for *renin* mRNA. Positive signal for *renin* mRNA (arrow) is detected in bone marrow cells located close to the trabecular bone (E). Juxtaglomerular cells in kidney show *renin* signals (arrows) as positive control (F). PB, primary bone trabecula; HC, hypertrophic chondrocyte; TB, trabecular bone; BM, bone marrow. Bar = 50 μm.

also expressed AT1 receptor (Fig. 1C, arrowheads and arrows, respectively).

Ang II, a ligand for these receptors, is generated by ACE cleavage of angiotensin I. Therefore, we examined whether ACE was expressed in bone cells. ACE signals were detected in osteoblasts and osteoclasts (Fig. 1D, arrowheads and arrows, respectively), the distribution of which was consistent with those expressing AT2 and AT1 receptors. As antibody against renin was not available, *in situ* hybridization was conducted. *renin* mRNA was expressed in the cells adjacent to trabecular bone (Fig. 1E, arrow). These cells exhibited vacuole-like morphology. The cells expressing *renin* were neither osteoblasts nor osteoclasts, although they were present in the bone microenvironment. These observations indicated that AT2 receptor as well as ACE and *renin* mRNA were expressed in the cells within a close proximity in the bone microenvironment. As positive control, *renin* signal was detected in juxtaglomerular cells in kidney (Fig. 1F). Furthermore, AT1, AT2, ACE, and *renin* mRNAs were expressed in primary cultures of osteoblastic cells derived from mouse neonatal calvarial cells and adult bone marrow based on RT-PCR analysis (Fig. 2). Thus, components of RAS are expressed locally in bone microenvironment. Real time PCR using RNA from bone marrow of tibiae indicated the expression of mRNAs encoding osteoclastic markers (Trap, Nfatc1, and Rank) as well as osteoblastic markers (alkaline phosphatase, osteocalcin, type I collagen, and Runx2) (data not shown).

Time course experiments were conducted to examine the expression levels of AT1 and AT2 in primary cultures of osteo-

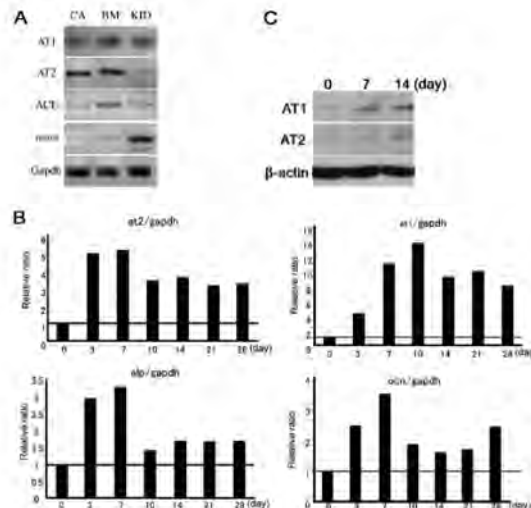


FIGURE 2. Expression of ACE and renin transcripts in primary culture of osteoblastic cells. A, ACE and *renin* mRNAs were detected as 614- or 194-bp bands, respectively, in bone marrow and osteoblastic cells as well as kidney. RT-PCR analyses were carried out as described under "Experimental Procedures." Glyceraldehyde-3-phosphate dehydrogenase (*gapdh*) levels serve as control. CA, calvaria; BM, bone marrow; KID, kidney; *alp*, alkaline phosphatase; *ocn*, osteocalcin. B, time course data on the expression of mRNAs. C, Western blot data on the levels of AT1 and AT2 proteins.

blasts derived from neonatal calvariae. In these cultures, we observed an increase in the levels of alkaline phosphatase and osteocalcin mRNAs. Real time PCR data indicated that mRNA expression levels of AT1 and AT2 were increased with time with a peak on day 7 for AT2 and day 10 for AT1, respectively (Fig. 2B). Western blotting of AT1 and AT2 revealed that the expression levels were increased with time (Fig. 2C). We also examined the effects of AT2 blocker on Trap mRNA in bone marrow and observed that AT2 blocker treatment suppressed Trap mRNA levels in the bone marrow (data not shown).

Angiotensin II Type 2 Receptor Blockade Increases Bone Mass—To examine the functional role of the angiotensin II receptors in bone, mice (9-week-old male) were treated with an AT2 receptor blocker (AT2-B, PD123319) or control (PBS) daily for 2 weeks. AT2 receptor blockade resulted in crowded patterning of the trabecular bone in these mice compared with control as shown in three-dimensional μ CT pictures (Fig. 3A). Analysis of morphological parameters based on three-dimensional μ CT revealed that AT2 receptor blocker treatment increased BV/TV by about 20% (Fig. 3B). In addition, AT2 receptor blocker treatment also increased the Tb.N by about 10% (Fig. 3C). On the other hand, Tb.Spac was reduced by about 10% (Fig. 3D). Other morphological parameters such as the thickness and separation of trabecular bone showed a similar trend, but the differences were not statistically significant (data not shown). As AT1 receptor was expressed in the bone cells, we also conducted oral treatment with a blocker for AT1 receptor (losartan) or control (water). In contrast to the blockade of AT2 receptor, AT1 blockade did not affect bone mass in terms of the patterning of the trabecular bone as well as the levels of BV/TV, Tb.N, and Tb.Spac in mice (Fig. 3, E–H). Thus, AT2 receptor blockade specifically enhances bone mass in adult mice.

AT2 Receptor Blockade Increases Bone Mass

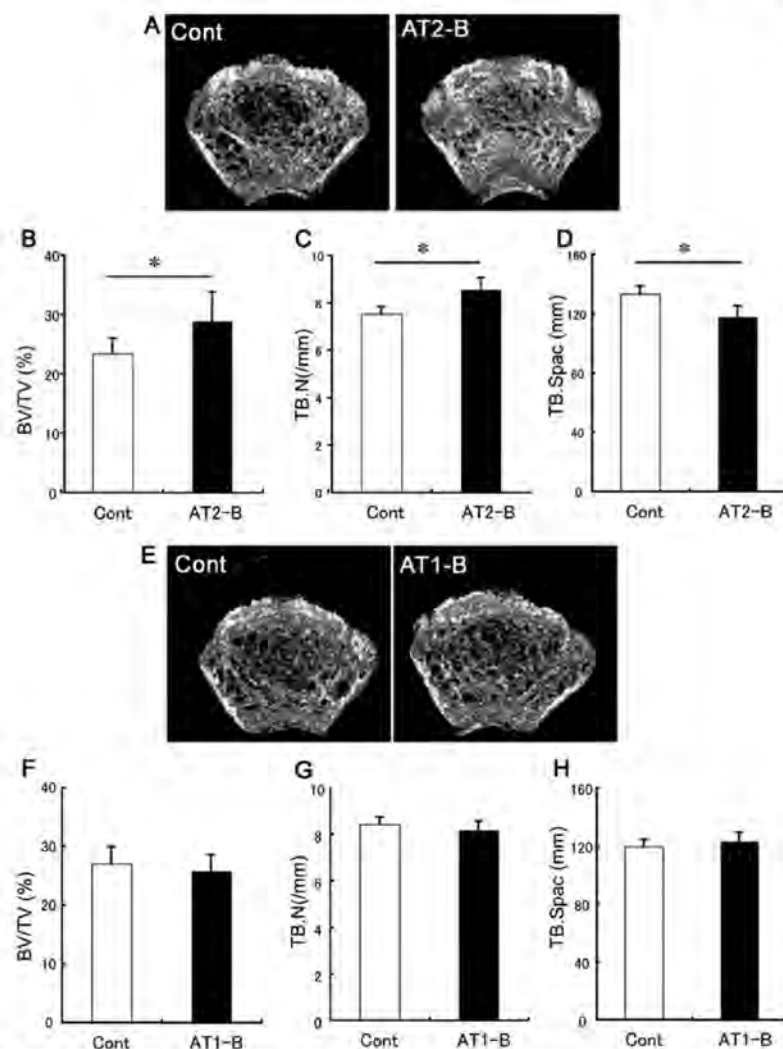


FIGURE 3. Treatment with AT2 blocker enhances bone mass. A, representative three-dimensional μ CT images of the distal metaphyseal regions of femora in mice treated with vehicle (PBS) or AT2 blocker (PD123319) (AT2-B). Treatment with AT2 blocker increased bone mass compared with control (Cont). B–D, quantification of the three-dimensional parameters of bone. AT2 blocker significantly increased BV/TV (B). AT2 blocker treatment increased the Tb.N (C). AT2 blocker treatment reduced the Tb.Spac (D). E, representative three-dimensional μ CT images of the distal metaphyseal regions of femora in mice treated with vehicle (water) or AT1 blocker (losartan) (AT1-B). Treatment with AT1 blocker did not affect bone mass compared with control (Cont). F–H, quantification of the three-dimensional parameter in femora. AT1 blocker treatment did not affect BV/TV (F), Tb.N (G), or Tb.Spac (H). Asterisk indicates that the difference is statistically significant ($p < 0.05$).

AT2 Receptor Blockade Enhances Bone Formation Activity—Because AT2 receptor blockade enhanced bone volume, we examined the effects of this blocker on the dynamic metabolic parameters in bone. Bone formation parameters were examined based on the analysis using calcein double labeling as described under “Experimental Procedures.” AT2 receptor blockade significantly increased BFR (Fig. 4A). AT2 receptor blockade did not significantly alter MAR levels, although there were trends for enhancement. MS/BS also tended to be increased by the treatment with AT2 receptor blocker, although the difference was not statistically significant (Fig. 4B

and C). Nodule formation assay *in vitro* revealed no major difference between the bone marrow cells obtained from mice after 2 weeks of treatment with AT2 blockade compared with control (data not shown). These observations indicated that AT2 receptor blockade enhanced bone volume at least in part through the enhancement of the bone formation activity *in vivo*.

AT2 Receptor Blockade Suppresses Bone Resorption—Increase in the bone volume would be either due to the activation of bone formation or the suppression of bone resorption or both. Therefore, we examined the osteoclastic parameters *in vivo* as well. AT2 receptor blockade reduced the presence of the TRAP-positive area in the histological sections (Fig. 5A). Quantification of osteoclast number/BS in the secondary trabecular region indicated that AT2 receptor blocker treatment decreased the level by about 20% (Fig. 5B). AT2 receptor blocker treatment also decreased the levels of osteoclast surface per bone surface (Oc/BS) (Fig. 5C). These observations indicated that AT2 receptor blockade suppressed bone resorption activities *in vivo*.

AT2 Receptor Blockade Suppresses Increasing Number of Osteoclasts by Angiotensin II in Organ Culture—We looked into whether RAS has any critical function in bone directly. To determine the effects of RAS in bone, we performed organ cultures using newborn mouse (1 day after birth, P1). Ulnae and radii were removed from the mice and were placed in 96-well plates (one bone per well) containing Ang II and/or AT2 blocker (AT2B, PD123319). We found that

angiotensin II treatment increased the number of TRAP-positive osteoclasts in the cultured bone. Such increase in osteoclasts in bone by Ang II was suppressed by AT2 blocker (Fig. 6). These findings indicate that direct action of angiotensin II to stimulate osteoclasts is present in bone and that AT2 blocker suppressed the osteoclastic cell differentiation in bone induced by angiotensin II. These data were consistent with our observations on the AT2 blocker suppression of osteoclast number in *in vivo* analysis.

AT2 Deficiency Increases Bone Mass—To further clarify whether AT2 receptor signaling can regulate bone mass, we

AT2 Receptor Blockade Increases Bone Mass

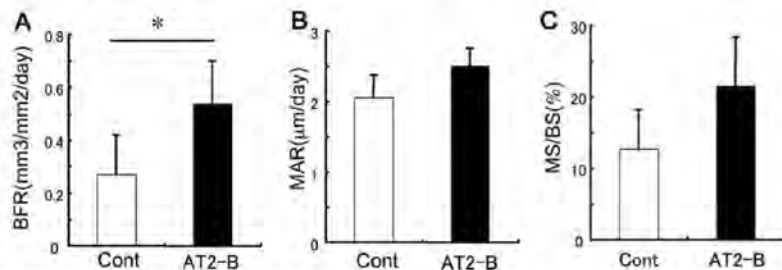


FIGURE 4. Treatment with AT2 blocker enhances bone formation *in vivo*. Dynamic histomorphometric parameters were evaluated based on calcein labeling. A, AT2-R blocker treatment increased BFR. B and C, AT2-R blocker treatment tended to increase MAR (B) and MS/BS (C). Asterisk indicates that the difference is statistically significant ($p < 0.05$). Cont, control.

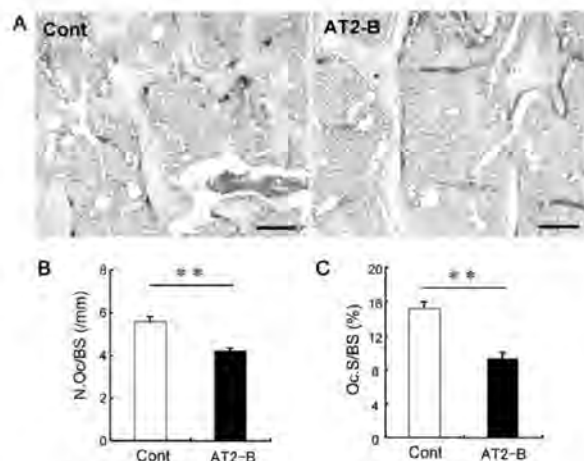


FIGURE 5. Treatment with AT2 blocker reduces the levels of bone resorption parameters *in vivo*. A, TRAP staining in the secondary trabecular region. B and C, quantification of TRAP-positive multinucleated osteoclasts. AT2-R blocker treatment reduced the number of osteoclasts (osteoclasts number per bone surface N.Oc/BS) and the osteoclasts surface per bone surface (Oc.S/BS). Asterisks indicate that the difference is statistically significant ($p < 0.01$). Cont, control.

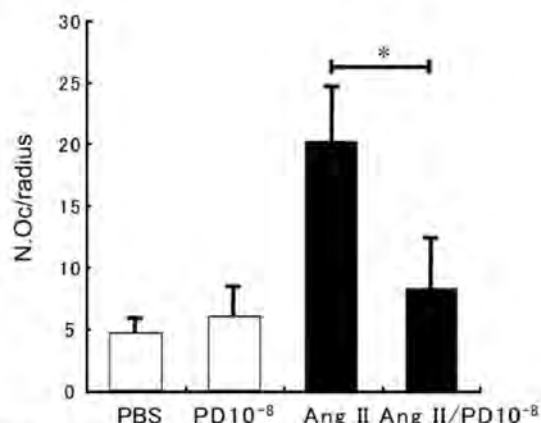


FIGURE 6. Treatment with AT2 blocker suppresses angiotensin II-induced increase in the number of osteoclasts in organ cultures of bone. Organ cultures were carried out as described under "Experimental Procedures." AT2 blocker suppressed angiotensin II-induced increase in osteoclast number in the bone. Asterisk indicates that the difference is statistically significant ($p < 0.05$).

analyzed AT2 receptor-deficient mice (15-week-old male mice). Three-dimensional μ CT revealed that AT2 deficiency showed a crowded pattern of trabecular bone compared with those in wild type mice. The analysis of three-dimensional μ CT parameters revealed that AT2 deficiency increased the levels of BV/TV by about 60% (Fig. 7). In addition, AT2 deficiency also increased the levels of Tb.N and thickness of trabecular bone by about 30%, respectively, although

AT2 deficiency decreased the levels of separation of trabecular bone and Tb.Spac by about 30 and 20% respectively. These observations further supported the role of AT2 in regulation of bone mass.

DISCUSSION

Here we reported that AT2 receptor blockade increased bone mass in adult mice. In addition, AT2 knock-out mice revealed an increase in bone mass. Furthermore, AT2 receptor was involved in basal suppression of osteoblastic activity *in vivo* as shown by the blockade-induced increase in BFR. At the same time, AT2 receptor blockade suppressed bone resorption *in vivo* based on the analysis of osteoclast number and osteoclast surface and in organ culture. Thus, AT2 receptor has a dual role in both the suppression of bone formation activity and the enhancement in bone resorption activity. Our observations on the presence of AT2 receptor, ACE, and renin in bone microenvironment suggest that bone is also regulated by local RAS and angiotensin II functions at least in part via AT2 receptor.

Our experiments on AT2 receptor blockade increased bone mass. In addition, three-dimensional μ CT data of AT2-deficient mice revealed that AT2 deficiency significantly increased bone mass compared with wild type mice. These findings indicate that the functional disruption of AT2 receptor increased bone mass *in vivo*.

In contrast, AT1 receptor blockade indicated no obvious bone change. Such observations on AT1 blocker (losartan) were consistent with other reports where AT1 receptor blocker (losartan) did not affect bone mass levels (29). However, one study using rats reported that exogenous Ang II administration suppressed bone mass levels through AT1 receptor in animals subjected to ovariectomy and five-sixths nephrectomy (19). Also, a recent study of mice with complete NO synthase deficiencies revealed that increased bone mass by genetic disruption was normalized by AT1 blockade (olmesartan). Our current data as well as *in vitro* reports by others revealed expression of AT1 receptors in bone cells (17–19, 22). The reasons for such diversity in terms of AT1 receptor function in bone may include the difference in the ligand (Ang II) concentration; however, these are still to be elucidated.

Several publications raise the possibility that AT1 receptor and AT2 receptor carry out negative cross-talk within fibroblasts and vascular endothelial cells with respect to each other's

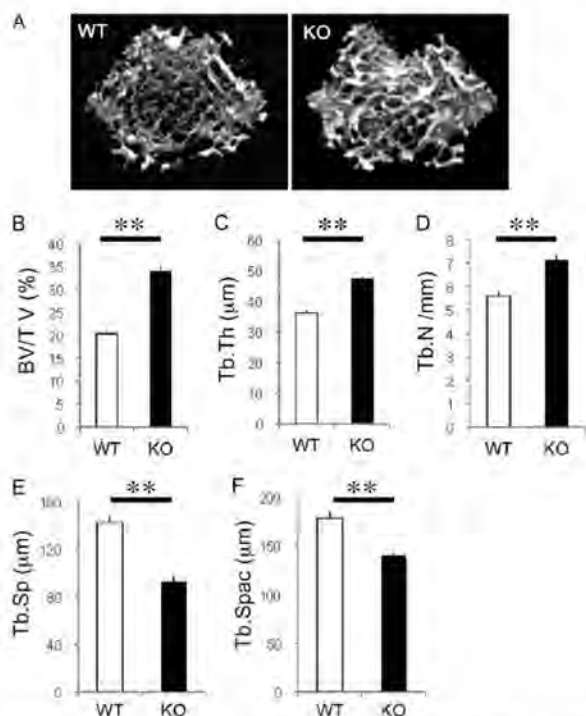


FIGURE 7. AT2 deficiency enhances bone mass. A, representative three-dimensional μ CT images of the distal metaphyseal regions of femora in wild type mice (WT) or AT2-deficient mice (KO). AT2-deficient mice increased bone mass compared with wild type. B–F, quantification of the three-dimensional parameters of bone. AT2 deficiency significantly increased BV/TV (B), thickness of trabecular bone (Tb.Th) (C), Tb.N (D), and separation of trabecular bone (Tb.Sp) (E). AT2 blocker treatment reduced the Tb.Spac (F). Asterisk indicates that the difference is statistically significant ($p < 0.01$).

signaling pathways and responses. Similar antagonism may also exist in bone. Although we did not observe such a relationship between AT2 blocker and AT1 blocker in the regulation of bone mass at the dosages we tested, other range of dosages may reveal antagonism. Negative cross-talk observed in previous angiotensin studies was in a hypertensive situation or in cell culture conditions where angiotensin II was used at nonphysiological concentrations. In addition, a previous study using spontaneous hypertensive rats revealed that AT1 blocker inhibited the reduction of bone loss, but no effect of AT2 was observed. These observations suggest that the role of angiotensin II via AT1 or AT2 may vary depending on the conditions such as background of animals or the levels of angiotensin II.

Previously published work provides several potential mechanistic connections for the control of bone resorption by the AT1 receptor. For example, first AT1 receptor signaling has been shown to inhibit development of osteoclast development (19) and to block macrophage infiltration in inflammatory situations (26). AT1 receptor antagonists also interfere with lipopolysaccharide activation of RAW264.7 osteoclast-like cells (26). Second, ultrasound (mechanical strain) has been shown to increase RANKL, MCP-1, and MIP in osteoblasts by signaling via the AT1 receptor (21). Third, high blood pressure has been associated with bone loss in various clinical studies in humans

AT2 Receptor Blockade Increases Bone Mass

(14, 30). Fourth, in the epithelia of the distal renal tubule, amiloride-sensitive epithelial sodium channels (ENaCs), which are controlled by the RAS-aldosterone system, represent the rate-limiting step for sodium reabsorption. ENaC not only controls blood volume and pressure but also are expressed in cartilage (31) and bone (32). These possibilities remain to be tested further in the future.

The dual role of AT2 receptor on both bone formation and bone resorption sides would be intriguing with respect to the treatment of osteoporosis in aged population. Currently, the drugs used for the suppression of the bone resorption, such as bisphosphonate, were shown to be efficacious to reduce fracture rate up to 50% (33). However, this means that the effects are still not complete. To reduce fracture rate further, enhancement of bone formation should be considered. This direction has been pursued in the case of PTH (teriparatide). However, simultaneous treatment with PTH and bisphosphonate was not successful in improving bone mass levels (34, 35). Furthermore, PTH treatment requires injection, and it has been limited to treat patients up to 2 years in western countries. Even for the treatment with PTH, the fracture rate has been shown to be improved up to 70%. Therefore, 30% of the fractures still remain to be solved. The idea of the possible utilization of the drugs to block the AT2 receptor in bone has two advantages. One is that AT2 receptor blockade decreases bone resorption, and the other is that it increases bone formation. The two beneficial directions of the effects of the AT2 blocker on bone are as unique for this blocker as it is different from bisphosphonates and PTH. Importantly, the safety profile of the drugs for the selective Ang II receptors for humans has been well confirmed. If one could contemplate developing more bone-effective drugs for the AT2 receptor, this would render possible options for the treatment of osteoporosis in the future.

In conclusion, we found that AT2 receptor blockade enhances bone mass in adult mice. This was based on the dual effect of the AT2 receptor blocker, including enhancement of bone formation and suppression of bone resorption. Importantly, such effects could be induced by the treatment of animals using drugs with chemical properties rather than peptide properties. Furthermore, these chemical drugs have exhibited a high safety profile even for a long term use. Therefore, the future development of drugs for the bone mass starting from the available chemical structures as the prototypes may benefit the treatment of patients with both osteoporosis and hypertension, diseases with a high prevalence in the modern aging societies.

REFERENCES

1. Kitahara, K., Ishijima, M., Rittling, S., Tsuji, K., Kurosawa, H., Nifuji, A., Denhardt, D., and Noda, M. (2003) *Endocrinology* **144**, 2132–2140
2. Girotra, M., Rubin, M., and Bilezikian, J. (2006) *Rev. Endocr. Metab. Disord.* **7**, 113–121
3. Ono, N., Nakashima, K., Schipani, E., Hayata, T., Ezura, Y., Soma, K., Kronenberg, H., and Noda, M. (2007) *J. Biol. Chem.* **282**, 25509–25516
4. Takeda, S., Eleftheriou, F., Levasseur, R., Liu, X., Zhao, L., Parker, K. L., Armstrong, D., Ducy, P., and Karsenty, G. (2002) *Cell* **111**, 305–317
5. Eleftheriou, F., Ahn, J. D., Takeda, S., Starbuck, M., Yang, X., Liu, X., Kondo, H., Richards, W. G., Bannon, T. W., Noda, M., Clement, K., Vaisse, C., and Karsenty, G. (2005) *Nature* **434**, 514–520
6. Kondo, H., Nifuji, A., Takeda, S., Ezura, Y., Rittling, S., Denhardt, D.,

AT2 Receptor Blockade Increases Bone Mass

- Nakashima, K., Karsenty, G., and Noda, M. (2005) *J. Biol. Chem.* **280**, 30192–30200
7. Katayama, Y., Battista, M., Kao, W. M., Hidalgo, A., Peired, A. J., Thomas, S. A., and Frenette, P. S. (2006) *Cell* **124**, 407–421
8. Zhao, C., Irie, N., Takada, Y., Shimoda, K., Miyamoto, T., Nishiwaki, T., Suda, T., and Matsuo, K. (2006) *Cell Metab.* **4**, 111–121
9. Miyazono, K., Maeda, S., and Imamura, T. (2004) *Oncogene* **23**, 4232–4237
10. Usui, M., Yoshida, Y., Tsuji, K., Oikawa, K., Miyazono, K., Ishikawa, I., Yamamoto, T., Nifuji, A., and Noda, M. (2004) *Proc. Natl. Acad. Sci. U. S. A.* **101**, 6653–6658
11. Morinobu, M., Nakamoto, T., Hino, K., Tsuji, K., Shen, Z., Nakashima, K., Nifuji, A., Yamamoto, H., Hirai, H., and Noda, M. (2005) *J. Exp. Med.* **201**, 961–970
12. Sacchetti, B., Funari, A., Michienzi, S., Cesare, S. D., Piersanti, S., Saggio, I., Tagliacico, E., Ferrari, S., Robey, P. G., Rinnucci, M., and Bianco, P. (2007) *Cell* **131**, 324–336
13. Sanada, M., Taguchi, A., Higashi, Y., Tsuda, M., Kodama, L., Yoshizumi, M., and Ohama, K. (2004) *Atherosclerosis* **176**, 387–392
14. Lynn, H., Kwok, T., Wong, S. Y. S., Woo, J., and Leung, P. C. (2006) *Bone (New York)* **38**, 584–588
15. Lavoie, J., and Sigmund, C. (2003) *Endocrinology* **144**, 2179–2183
16. Sakai, K., Agassandian, K., Morimoto, S., Sinnayah, P., Cassell, M. D., Davissón, R. L., and Sigmund, C. D. (2007) *J. Clin. Invest.* **117**, 1088–1095
17. Hatton, R., Stimpel, M., and Chambers, T. (1997) *J. Endocrinol.* **152**, 5–10
18. Hiruma, Y., Inoue, A., Hirose, S., and Hagiwara, H. (1997) *Biochem. Biophys. Res. Commun.* **230**, 176–178
19. Shimizu, H., Nakagami, H., Osako, M., Hanayama, R., Kunugiza, Y., Kizawa, T., Tomita, T., Yoshikawa, H., Ogihara, T., and Morishita, R. (2008) *FASEB J.* **22**, 2465–2475
20. Senbonmatsu, T., Saito, T., Landon, E., Watanabe, O., Price, E. J., Roberts, R., Imboden, H., Fitzgerald, T., Gaffney, F., and Inagami, T. (2003) *EMBO J.* **22**, 6471–6482
21. Bandow, K., Nishikawa, Y., Ohnishi, T., Kakimoto, K., Soejima, K., Iwabuchi, S., Kuroe, K., and Matsuguchi, T. (2007) *J. Cell. Physiol.* **211**, 392–398
22. Hagiwara, H., Hiruma, Y., Inoue, A., Yamaguchi, A., and Hirose, S. (1998) *J. Endocrinol.* **156**, 543–550
23. Ichiki, T., Labosky, P. A., Shiota, C., Okuyama, S., Imagawa, Y., Fogó, A., Nilmura, F., Ichikawa, I., Hogman, B. L. M., and Inagami, T. (1995) *Nature* **377**, 748–750
24. Ishijima, M., Tsuji, K., Rittling, S. R., Yamashita, T., Kurosawa, H., Denhardt, D. T., Nifuji, A., Ezura, Y., and Noda, M. (2007) *J. Endocrinol.* **193**, 235–243
25. Loghman-Adham, M., Soto, C. E., Inagami, T., and Sotelo-Avila, C. (2005) *J. Histochem. Cytochem.* **53**, 979–988
26. Nagai, N., Oike, Y., Izumi-Nagai, K., Urano, T., Kubota, Y., Noda, K., Ozawa, Y., Inoue, M., Tsubota, K., Suda, T., and Ishida, S. (2006) *Arterioscler. Thromb. Vasc. Biol.* **26**, 2252–2259
27. Mizoguchi, F., Mizuno, A., Hayata, T., Nakashima, K., Heller, S., Ushida, T., Sokabe, M., Miyasaka, N., Suzuki, M., Ezura, Y., and Noda, M. (2008) *J. Cell. Physiol.* **216**, 47–53
28. Ihara, H., Denhardt, D. T., Furuya, K., Yamashita, T., Muguruma, Y., Tsuji, K., Hruska, K. A., Higashio, K., Enomoto, S., Nifuji, A., Rittling, S. R., and Noda, M. (2001) *J. Biol. Chem.* **276**, 13065–13071
29. Broulik, P. D., Tesa, V., Zima, T., and Jirsa, M. (2001) *Physiol. Res.* **50**, 353–358
30. Reinmark, L., Vestergaard, P., and Mosekilde, L. (2006) *J. Hypertens.* **24**, 581–589
31. Trujillo, E., Alvarez, R. D., Molasharu, A., González, T., Canessa, C. M., and Martín-Vasallo, P. (1999) *Histol. Histopathol.* **14**, 1023–1031
32. Kizer, N., Guo, X. L., and Hruska, K. (1997) *Proc. Natl. Acad. Sci. U. S. A.* **94**, 1013–1018
33. Kanis, J. A., Adams, J., Borgström, F., Cooper, C., Jönsson, B., Preedy, D., Selby, P., and Compston, J. (2008) *Bone (New York)* **42**, 4–15
34. Aspenberg, P., Wernelin, K., Tengwall, P., and Fahlgren, A. (2008) *Acta Orthop.* **79**, 111–115
35. Migliaccio, S., Brama, M., and Spera, G. (2007) *Clin. Interv. Aging* **2**, 55–64

ADDITIONS AND CORRECTIONS

This paper is available online at www.jbc.org

THE JOURNAL OF BIOLOGICAL CHEMISTRY VOL. 284, NO. 31, pp. 21100–21101, July 31, 2009
© 2009 by The American Society for Biochemistry and Molecular Biology, Inc. Printed in the U.S.A.

VOLUME 278 (2003) PAGES 51722–51734

DOI 10.1074/jbc.A308740200

Dsl1p, an essential component of the Golgi-endoplasmic reticulum retrieval system in yeast, uses the same sequence motif to interact with different subunits of the COPI vesicle coat.

Uwe Andag and Hans Dieter Schmitt

On page 51726, we misleadingly stated that the central acidic domain in Dsl1p is essential for viability. Evidence for this was presented in Fig. 3C. This figure shows that a mutant carrying two Trp-to-Ala replacements in this region did not support growth of a *dsl1* deletion mutant. However, we recently created a GAL-regulated TAP-tagged version of *DSL1* carrying five Trp-to-Ala substitutions in this region to use as a negative control in pulldown experiments. Surprisingly, this mutant complemented the *dsl1* knock-out. Even a single-copy untaged version of this allele could replace the wild-type gene. However, these cells grow poorly at all temperatures tested and show phenotypes similar to those of Dsl1p-depleted cells.

Sequencing showed that the plasmid used for the growth assay in our previous work contained a C-terminal truncation in addition to the Trp-to-Ala substitutions at positions 413 and 455. A mutant clone with an intact C terminus supported growth of a *dsl1* deletion mutant.

Our recent data are still consistent with the notion that the outer tryptophan motifs in the acidic domain of Dsl1p (Trp⁴¹³/Trp⁴¹⁵ and Trp⁴⁵³/Trp⁴⁵⁹) mediate binding to δ -COP, whereas the central tryptophan residue at position 425 is involved in the interaction with α -COP. Obviously, all motifs must be destroyed to affect the growth of cells.

We sincerely apologize for any confusion that this may have caused.

VOLUME 284 (2009) PAGES 4857–4864

DOI 10.1074/jbc.A807610200

Angiotensin II type 2 receptor blockade increases bone mass.

Yayoi Izu, Fumitaka Mizoguchi, Aya Kawamata, Tadayoshi Hayata, Testuya Nakamoto, Kazuhisa Nakashima, Tadashi Inagami, Yoichi Ezura, and Masaki Noda

This work was supported by Grants-in-aid 17012008, 18109011, 18659438, and 18123456 from the Japanese Ministry of Education (21st Century Center of Excellence Program, Frontier Research for Molecular Destruction and Reconstitution of Tooth and Bone); by grants from the Japan Space Forum, NASDA, and the Advanced Bone and Joint Science Strategic Research Networks Projects (Japan Society for Promotion of Science Core to Core Program, Research for the Future Program, Genome Science); and by National Institutes of Health Grant HL58205.

VOLUME 280 (2005) PAGES 24839–24848

DOI 10.1074/jbc.A500253200

The ATPase activity of BfpD is greatly enhanced by zinc and allosteric interactions with other Bfp proteins.

Lynette J. Crowther, Atsushi Yamagata, Lisa Craig, John A. Tainer, and Michael S. Donnenberg

This article has been withdrawn at the request of the authors.

VOLUME 284 (2009) PAGES 13602–13609

DOI 10.1074/jbc.A900894200

Determination of *in vivo* dissociation constant, K_D , of Cdc42-effector complexes in live mammalian cells using single wavelength fluorescence cross-correlation spectroscopy.

Thankiah Sudhaharan, Ping Liu, Yong Hwee Foo, Wenyu Bu, Kim Buay Lim, Thorsten Wohland, and Sohail Ahmed

On page 13603, the following sentence should be added to the legend of Fig. 1: The SH3 in the N-WASP schematic indicates a polyproline sequence that binds SH3 domains.

VOLUME 284 (2009) PAGES 7385–7394

DOI 10.1074/jbc.A807820200

Autotaxin/lysopholipase D and lysophosphatidic acid regulate murine hemostasis and thrombosis.

Zehra Pamuklar, Lorenzo Federico, Shuying Liu, Makiko Umezu-Goto, Anping Dong, Manikandan Panchatcharam, Zachary Fulkerson, Evgeny Berdyshev, Viswanathan Natarajan, Xianjun Fang, Laurens A. van Meeteren, Wouter H. Moolenaar, Gordon B. Mills, Andrew J. Morris, and Susan S. Smyth
Dr. Fulkerson's name was misspelled. The correct spelling is shown above.

We suggest that subscribers photocopy these corrections and insert the photocopies in the original publication at the location of the original article. Authors are urged to introduce these corrections into any reprints they distribute. Secondary (abstract) services are urged to carry notice of these corrections as prominently as they carried the original abstracts.

う蝕制御学分野

田上 順次

医歯学総合研究科・口腔機能再構築学系専攻
齲蝕制御学・教授

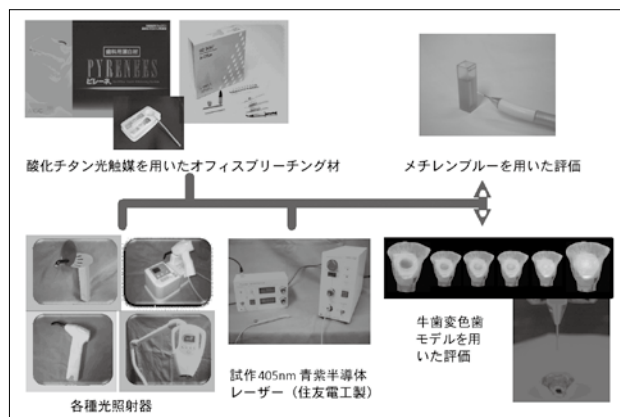


1) 研究の課題名

光触媒と405nm青紫レーザーを用いた歯の漂白

Teeth bleaching using visible-light activating titanium oxide photocatalyst and 405 nm violet diode laser

オフィスブリーチングは、高濃度の過酸化水素を歯面に塗布し、これを光・熱・触媒等で活性化して行ってきた。近年、可視光応答型酸化チタン光触媒を用いたオフィスブリーチング材が開発・市販された。本触媒を用いることにより、より低濃度の過酸化水素でも歯の漂白が可能となったが、照射光源の種類・光量が漂白効果に及ぼす影響は明らかではない。一方で、405nm青紫半導体レーザーが開発され、歯科への応用が試みられている。本研究では、可視光応答型酸化チタン光触媒を含有するオフィスブリーチング材の漂白効果に、照射光源の種類・光量が及ぼす影響と、405nmレーザー光源を用いた際の漂白効果についてin vitroで検討した。その結果、メチレンブルー水溶液を用いて、光量の異なるハロゲン照射器、青色LED照射器を用いて、漂白効果を評価したところ、照射光源・光量ともに漂白効果に影響を及ぼすことが明らかになった。また、405nm青紫レーザーは、漂白に有効であり、照射エネルギーの大きい方が、漂白効果が高いことが明らかになった。また、牛歯変色歯モデルを用いて評価を行ったところ同様の結果が得られた。

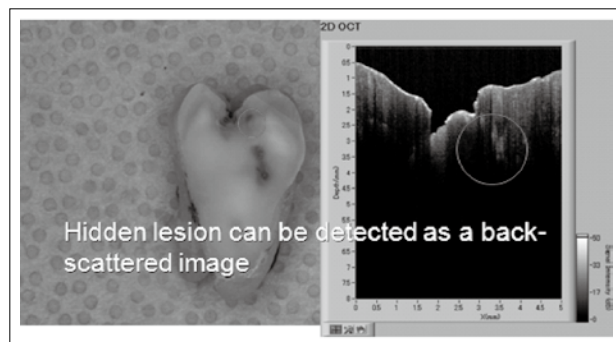


臨床診断に用いる歯科用OCTの開発

Development of dental OCT for clinical diagnosis

生体に無害な1310nm付近の近赤外線光は、歯質への透過性の高いことが知られており、う蝕診断への導入が試みられていた。一方、医療用として用いられているOCTは、多くの改良が加えられ、近年、フーリエ変換の導入により、画像解像度の向上が図られている。しかしながら、光源に可視光線を用いており、歯質への透過性が低く、精度の高い断層画像を得ることができなかった。

口腔内用OCTとして開発がすすめられている走査型OCTは、光源として近赤外線光を採用しており、歯質への透過性を飛躍的に向上させている。X線を用いない、画期的な精密断層画像診断技術であり、非侵襲的で高解像度の画像を得ることができる。したがって、従来の診断技術では検知できない初期う蝕病変をも診断が可能であり、しかもX線診断が困難であった小児や妊産婦への使用も可能と思われる。このような利点から、OCTの臨床導入は歯科医療の発展に資するところが大いと考えられる。



エナメル質酸蝕症モデルの作成と予防処置に関する研究

Establishment of enamel erosion model and assessment of preventive treatment

酸蝕症に関する病態の解析、及びその治療法について

検討する目的で、牛歯を用いてエナメル質酸蝕症モデルを作製した。さらに、その表面の分析をQLF (quantitative light-induced fluorescence) 及びSEM/EDSを用いて定性的、定量的解析を行った。その結果、QLF値と脱灰深度、ミネラル喪失量との間には相関が認められた。さらに脱灰抑制効果が期待されるCPP-ACPペーストを用いてその効果を検討するためにマイクロCTを用いて検討した。その結果、CPP-ACPペーストによるエナメル質表面の脱灰抑制はフッ化物の添加によって向上することが明らかとなった。

INTコーティングによるジルコニアオールセラミック修復に対する接着強さの向上

Enhancement of bond strength using the INT coating in zirconia all ceramic restorations

患者からの審美的要求の向上とともにオールセラミック修復が注目され、とくに高い破壊靱性を有するジルコニアは、CAD/CAMによる加工技術の向上とともに金属に代わるコーピング材料として注目される。ジルコニア表面に対するレジンセメントの接着では、シリカを含むセラミックスと異なり、シラン処理が効かないが、MDPなどの機能性モノマーの有効性が明らかとなった。さらに我々は、新たなシリカコーティング法であるINTコーティング法を開発した。INTコーティング法は、製作したジルコニアのコーピング面にシリカを含む陶材を薄く焼成する方法であり、CAD/CAMでコーピングを製作した後、ラボサイドで行う作業を想定している。INTコーティングを行った場合、表面のシラン処理が可能になり、レジンセメントの接着強さが著しく向上することがわかった。

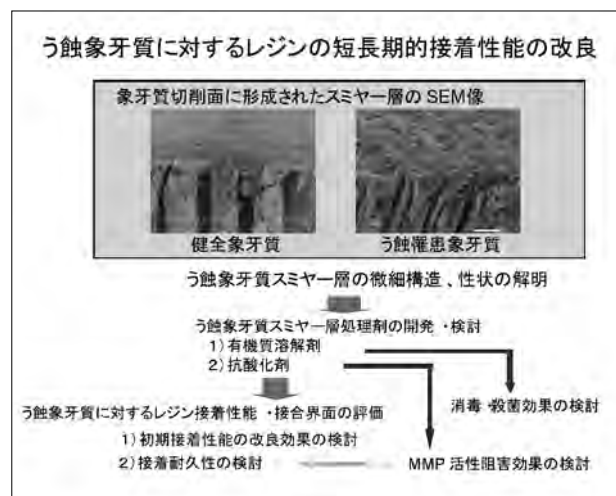
う蝕象牙質に対するレジンの短長期的接着性能の改良

Improvement of bonding to caries-affected dentin

近年確立されたミニマルインターベンションの概念による修復では、被着象牙質のほとんどが感染象牙質削除後に保存されたう蝕罹患象牙質となる。う蝕象牙質と健全象牙質では、その機械的性質のみならず化学的性質（有機成分、無機成分、水分量）も大きく異なるため、う蝕罹患象牙質に対するレジンの接着性能は、健全象牙質に比べ低いことが報告されている。さらにう蝕象牙質を切削した場合に形成されるスマー層の性状は、被切削体の成分と同じであると報告されていることから、健全象牙質のものとは大きく異なる。そのため、特にセルフエッチ接着システムでは、う蝕罹患象牙質に対する接着性

能が健全象牙質に比べ低下する大きな一因になっている可能性がある。

本研究では、う蝕象牙質切削表面に形成されるスマー層に着目し、その形態学的、化学的性状を分析し、窩洞の清掃・消毒効果を持ち、レジンの初期接着性および接着耐久性の向上を目指した臨床技法の開発を図ることにより、接着性コンポジットレジンを用いた修復法の信頼性を高め、生活歯のみならず失活歯の歯質欠損修復治療におけるミニマルインターベンションの構築を目指している。



う蝕象牙質におけるマトリックスメタロプロテアーゼ (MMP) 局在性の評価

Localization of matrix metalloproteinases in carious dentin

象牙質う蝕の進行は、う蝕病原性細菌の産生する酸やプロテアーゼの影響のみならず、象牙質固有のマトリックスメタロプロテアーゼ (MMP) などが細菌の刺激によって活性化しており、これらの病巣拡大への関与が明らかとなっている。う蝕象牙質のコラーゲン変性の主体は、これら象牙質固有のプロテアーゼであり、むしろ細菌による影響は少ないことも指摘されている。再石灰化を期待し、う蝕象牙質を修復するには、活性化したコラーゲナーゼ (MMP1,2,8,13 など) やゼラチナーゼ (MMP2,9) など有機質を分解・変性する酵素の活性を抑制し、変性した有機質成分を再生する必要があると思われる。そこで、まずヒト抜去歯を収集し、ウェスタンブロット法による各種MMPの検出を行ったが、う蝕象牙質という限局された部位における情報の収集は困難を極めた。そこで未脱灰の薄切切片を作成し、金抗体法による免疫電子顕微鏡観察を行ったところ、健全象牙質とう蝕象牙質における形態的観察と、各種MMPの局在性についての半定量的な分析が可能となった。

結果、う蝕象牙質にはコラゲナーゼ (MMP2,8) やゼラチナーゼ (MMP9) など、病変部の拡大に関与する酵素が含まれており、特に感染部のう蝕象牙質ではMMP8,9など、唾液に含まれる酵素が侵入していることが明らかとなった。

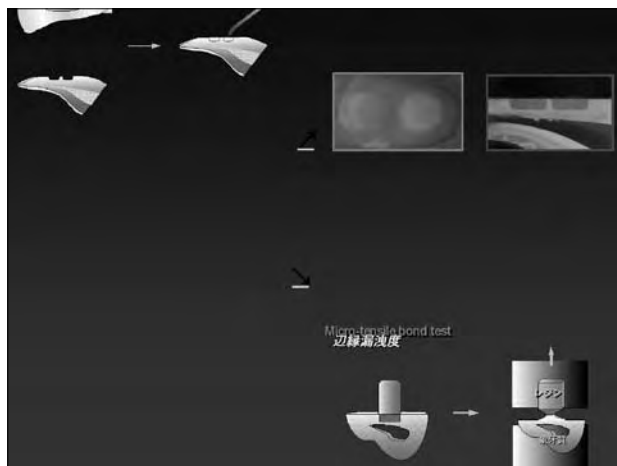
I 級窩洞における象牙質接着強さと窩壁適合性の関係について

Correlation between Bond Strength and Cavity Wall Adaptation

弾性のある接着材を用いると、レジン修復物の辺縁封鎖性と窩壁適合性を向上させるが、窩底部象牙質におけるレジンの接着強さが低下することを既に報告している。一方、フロアブルレジン、レジン修復物の窩壁適合性を向上させることを確認している。しかしながら、レジン修復物の窩壁適合性と窩洞内各部の微少接着強さに与える影響を同時に評価した研究は僅かである。本研究では、レジン修復物の辺縁封鎖性ならびに窩壁適合性に及ぼす影響を色素浸透法を用いて数値的に評価すると同時に、レジンと窩底部象牙質との微小接着強さに与える影響についても評価検討した。牛下顎永久切歯の唇側象牙質面に、直径3 mm、深さ1 mmの円柱状の窩洞 (C-factor = 2.3) を形成した。窩洞面を業者指示に従い Clearfil Mega Bond (クラレ メディカル) を用いて処理した後、Photo Clearfil Bright (PB: クラレ メディカル) のshade USのハイブリッドまたは、Filtek Flow (FF: 3M ESPE) のshade A3のフロアブルレジンで充填した。光照射器を用い出力600 mW/cm²で40秒間光照射を行い重合硬化させた。37℃ 暗所水中に24時間保管後、試料から約1mmの厚みの薄板を切り出した。残存象牙質厚みを計測した後、レジン-象牙質界面が約1mm²となるようトリミングし、micro-tensile bond testに供した。試片を試験装置に接着し、クロスヘッドスピード1mm/minで引張り接着強さを測定した。これらの結果について、Fisher's PLSD testを用いて統計処理を行った。次に、レジン修復物の辺縁封鎖性ならびに窩壁適合性を評価するため、同様に作製した試料の窩洞辺縁と半切面上で1.0%アシッドレッドプロピレングリコール溶液による色素浸透試験を行った。色素浸入度は、色素浸入部位の長さの窩縁または窩壁全周に対する百分率を算出した。これらの結果について、Kruskal-Wallis testとMann-Whitney U testで統計処理を行った。

フロアブルレジンのFiltek Flowの窩壁適合性は、ハイブリッドレジンであるPhoto Clearfil Brightより有意に

高かった。しかしながら、その窩底部象牙質に対する接着強さは、Photo Clearfil Brightより有意に低かった。



コンポジットレジン修復物の象牙質接着強さ及ぼす治療用放射線照射の影響

The effect of radiotherapy on resin-dentin bond strength

口腔領域の悪性腫瘍に対して放射線治療を行うと "radiation caries" が生じる。唾液腺を含む口腔顔面組織や味蕾、歯は頸部や頭部の放射線治療により影響を受けると考えられる。しかしながら、象牙質に対する放射線照射の影響については明らかではない。そこで、放射線照射がレジンと象牙質の接着強さ、ならびに象牙質の硬さと弾性に与える影響について評価検討した。ウシ下顎永久切歯の一方の群にコバルト60治療用装置を用いて60Gyのγ線を照射した。一方の群はコントロールとしてγ線の照射を行わなかった。唇側象牙質平坦面を作製し、その面をClearfil Mega Bondを用いて処理した後、Clearfil AP-Xを築盛し、出力600 mW/cm²で40秒間光照射を行い重合硬化させた。24時間水中保管後試片を切り出し、micro-tensile bond testに供し、引張り接着強さを測定した。次に、両群における象牙質の硬さと弾性をnano-indentation testerにより測定した。

γ線の照射は短期的なコンポジットレジンと象牙質の接着強さに直接的には影響を及ぼさなかったが、硬さと弾性率を低下させることが分かった。これらのことより、60Gyのγ線の照射は、コラーゲン組織等に何らかの変性を引き起こし、より長期的には接着強さを低下させる可能性が示唆された。

コンポジットレジン修復物の窩壁適合性に及ぼす治療用放射線照射の影響

The effect of radiotherapy on resin composite adaptation to

the cavity wall

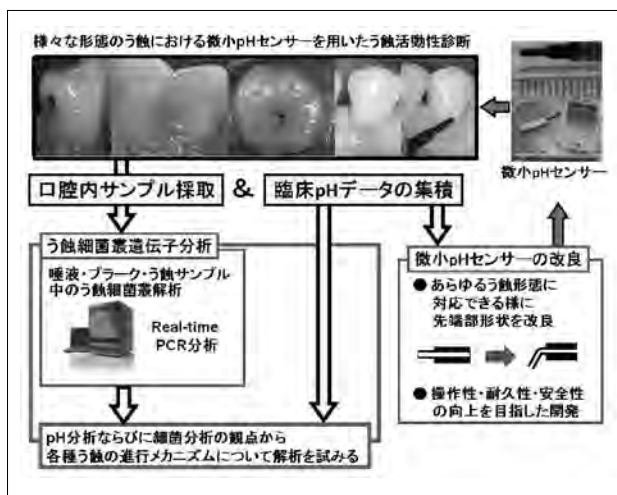
口腔領域の悪性腫瘍に対して放射線治療を行うと"radiation caries"が生じる。唾液腺を含む口腔顔面組織や味蕾、歯は頸部や頭部の放射線治療により影響を受けると考えられる。しかしながら、象牙質に対する放射線照射の影響については明らかではない。そこで、放射線照射がレジンと象牙質の窩壁適合性に与える影響について評価検討した。ウシ下顎永久切歯の一方の群にコバルト60治療用装置を用いて60Gyの γ 線を照射した。一方の群はコントロールとして γ 線の照射を行わなかった。直径3 mm、深さ1.5 mm (C-factor=3) の円柱状の窩洞を象牙質平坦面に形成した後、Clearfil SE BondとワンステップボンディングシステムであるTokuyama Bond ForceかClearfil tri-S Bondの接着システムを使用して、Clearfil AP-Xを填塞し、重合硬化させた。コントロール群はサーマルストレスをかけず、一方の群は5000回のサーマルサイクルに供し、窩縁と半切面の窩壁に色素浸透試験を行った。色素浸透度は、色素浸入部位の長さの窩壁全周に対する百分率を算出して評価した。

γ 線の照射は短期的なコンポジットレジン修復物の窩壁適合性に直接的には影響を及ぼさなかったが、 γ 線を照射した象牙質は、窩壁適合性において、接着システム間で健全象牙質と異なった挙動を示した。これらのことから、60Gyの γ 線の照射は、コラーゲン組織等に何らかの変性を引き起こし、より長期的には窩壁適合性に影響を及ぼす可能性が示唆された。

pH値を指標としたう蝕活動性評価とう蝕原因細菌遺伝子分析

Intraoral pH measurement of carious lesions with qPCR of role playing cariogens to differentiate caries activity

株)堀場製作所と臨床用微小pHセンサーを共同開発



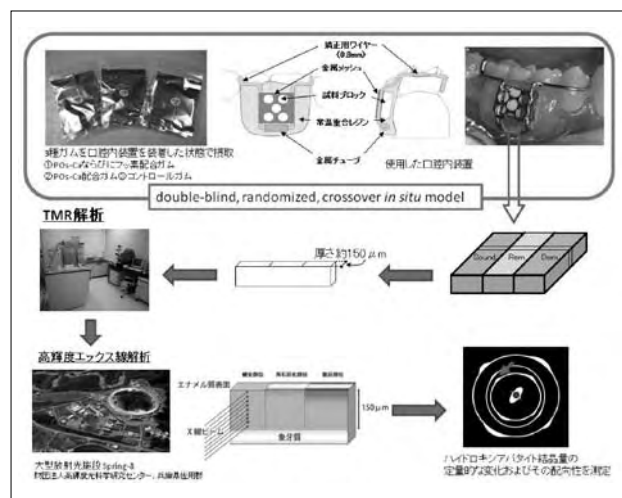
し、学内倫理審査承認のもと、ヒト口腔内にて象牙質う蝕表層pH値を測定した。その結果、急性う蝕の方が慢性う蝕よりも有意に低い値を示した。また、両う蝕サンプル中のう蝕原因細菌分布に関してReal-time PCR分析を行ったところ、*S. mutans*は急性・慢性両う蝕において高い検出率を認めたほか、急性う蝕では*Lactobacillus*が、慢性う蝕では*S.sobrinus*が有意に高い検出率を示した。従って、pH値を指標とした定量的う蝕象牙質活動性診断が可能であり、また細菌分布の違いから、各種細菌がう蝕活動性に及ぼす特異性について推察することによるう蝕進行における細菌学的検討が可能であることが示唆された。

リン酸化オリゴ糖カルシウム (POs-Ca) ならびに茶抽出フッ素配合ガム咀嚼後のエナメル質初期う蝕の再石灰化効果および結晶構造の変化

Effect of chewing gum containing Phosphoryl Oligosaccharides of Calcium (POs-Ca) and fluoride on remineralization and nanoindentation of enamel subsurface lesions in situ

馬鈴薯澱粉より酵素処理した分解物から抽出されたリン酸化オリゴ糖カルシウム (Phosphoryl Oligosaccharides of Calcium 以下POs-Ca) は、水溶性が極めて高く、デンタルガムポスカ (ポスカ[®]、江崎グリコ) の再石灰化促進成分として配合利用されている。しかし、実際の口腔内環境下におけるPOs-Caの再石灰化効果についての報告は少なく、また加えてフッ素を配合した場合の再石灰化効果および再石灰化部の微細構造変化に関する報告はない。そこで本実験では、POs-Caならびにフッ素配合ガムならびに口腔内装置を用いた群間並行臨床試験を実施し、Transversal Microradiography (以下TMR) 法を用いて観察し、その再石灰化効果について定量的に評価するとともに、高輝度エックス線を用いてハイドロキシアパタイト結晶量の定量的な変化およびその配向性を測定し、再石灰化前後におけるエナメル質初期う蝕のミネラル量変化と微細結晶構造変化について大型放射光施設SPRING-8にて検討を加えた。その結果、POs-Caならびにフッ素配合ガム摂取群では、POs-Ca配合ガムならびにPOs-Ca非配合ガム摂取群に比べ有意に高いミネラル密度の回復が認められ、また、POs-Caならびにフッ素配合ガム摂取群では、POs-Ca配合ガムならびにPOs-Ca非配合ガム摂取群に比べ有意に高い結晶量の回復が認められた。さらに、ハイドロキシアパタイト結晶量の回復した部位において、健全部と同じ配向性を有した部位

が認められた。以上より、ヒト口腔内環境下において、POs-Caならびにフッ素配合ガムを摂取することで、エナメル質初期う蝕の再石灰化が促進されることが示唆された。また、その再石灰化は安定したハイドロキシアパタイト結晶の形成によるものと推察された。これにより、POs-Caならびにフッ素配合ガムの摂取を行うことは、エナメル質初期う蝕における再石灰化レベルを、配向性の整ったハイドロキシアパタイトの再結晶化まで引き上げ、より健全歯質に近接した状態まで回復することが期待された。

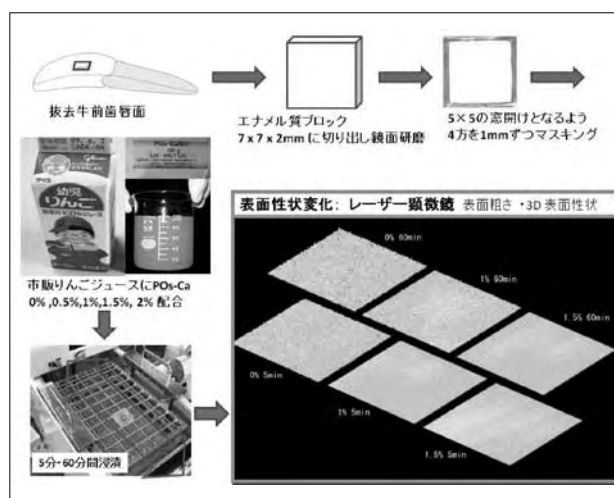


POs-Ca配合りんごジュースの酸蝕抑制効果

Development and evaluation of a low erosive apple juice drink with Phosphoryl Oligosaccharides of Calcium (POs-Ca)

リン酸化オリゴ糖カルシウム (Phosphoryl Oligosaccharides of Calcium: POs-Ca) は、水溶性が極めて高く、デンタルガム（江崎グリコ株式会社）の再石灰化促進成分として配合されている。一方、近年、飲み物のエナメル質酸蝕に関する研究が数多く報告されているが、その抑制効果を目指す開発ならびに研究報告は少ない。そこで本研究では、POs-Caを配合した幼児向けりんごジュースのエナメル質酸蝕抑制効果について検討した。すなわち、各種濃度POs-Ca配合りんごジュースに牛歯エナメル質ブロックを浸漬した場合の表面粗さ等について比較検討を加えた。その結果、各種濃度POs-Ca配合時のpH値は、いずれも臨界pH 5.5以下を示した（0% pH 3.6、0.5% pH 3.7、1% pH 3.8、2% pH 3.9、5% pH 4.1）。また、食味評価の結果、5%配合では、飲み物として適さない食味を示した為、その後の測定対象から除外した。一方、レーザー顕微鏡を用いた表面粗さ測定の結果、5分浸漬後でPOs-Ca未配合の表面粗さに対し、0.5%配合、1%配合、2%配合で顕著な酸蝕抑制効果を各々

示した（いずれも $p < 0.05$ ）。また、0.5%、1%の配合で経時的な表面粗さ変化を認めたのに対し、2%配合では60分浸漬後も5分浸漬後と同等の表面性状を示した。なお、無添加の0%の条件下では5分浸漬状態と60分浸漬状態でも共に高い粗さを示し、その表面粗さ程度に有意差はみられなかった。このことから、60分浸漬後に脱灰抑制効果を得るためにはPOs-Caを2%程度配合することが必要と考えられる。これらの要因として、POs-Caを配合することで、ジュース内のCa濃度が高まり、エナメル質のハイドロキシアパタイトの溶出を抑制したものと推察された。



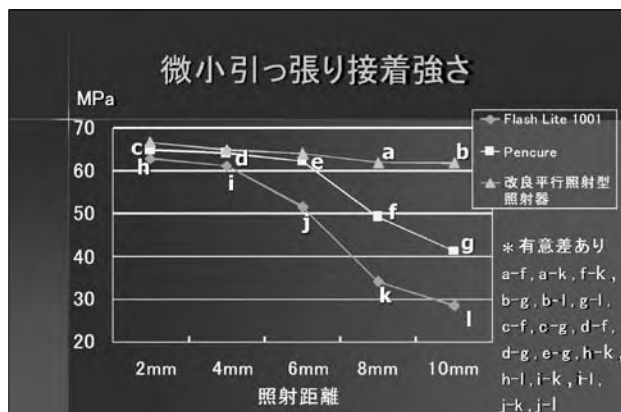
LEDの収束光照射によるレジンの象牙質接着強さ

Effect of convergent light-irradiation of LED on bond strength of resin composite to dentin

近年、歯質接着材料、光照射器の開発に伴い、大小様々な窩洞形態に対する直接修復の適応が広がっている。また、ファイバーポスト等のコア材の発達により歯内療法後の直接修復の適応が増えてきている。そのような場合、窩洞の深さの増大や、口腔内の限られた条件において接着面に対する光照射器の照射口の位置で、照射距離に伴う光強度の減弱が起きることによって、接着強さに影響を及ぼすことが考えられる。そこで本実験では、照射光の収束が異なる3種類のLED照射器を用い、照射距離が異なった場合におけるレジンの象牙質接着強さに照射光が及ぼす影響を調べた。

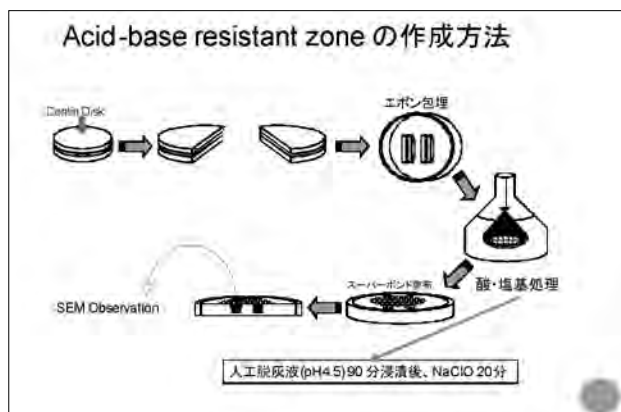
照射光の収束が異なる3種類のLED照射器を用い、照射距離が異なった場合におけるレジンの象牙質接着強さに及ぼす影響を調べた。照射器は、Flash Lite 1001, Pencureと今回、照射光を収束させるようにモリタと共同開発したDENTAPORT (Experimental LED Light Cure Handpiece for DENTAPORT ZX) を使用し、接

着剤に Clearfil Liner Bond II Σ を、レジンに Clearfil Photo Coreを用いて照射距離別の光量測定と微小引っ張り試験を行った。結果、照射光の拡散を抑えることにより照射距離の増大に伴う光量の低下が抑えられ、また、象牙質接着強さの低下が抑えられることが分かった。



接着界面における酸一塩基耐久性をもった象牙質の生成 Acid-base resistant zone formation of adhesive interface in dentin

象牙質接着界面におけるSEMを用いた詳細な検討を基に、コンポジットレジンをを用いた接着性修復において、これまで樹脂含浸層と呼ばれていた層の直下にpH4.5の人工脱灰液を用いて接着界面を脱灰した場合に、酸・塩基抵抗層の存在が確認されている。これまでの研究でその層を Acid-base resistant zone と呼び、特にセルフエッチングシステムに特有の層であることが確認されてきた。また数々のボンディングシステムにおいてその形態は異なり、特にフッ素含有のボンディング材を用いた場合に特有の形態を持つことが確認されてきた。その層内にはTEM観察においてアパタイトクリスタル存在も確認されており、ボンディング材に含有されている機能性モノマーとのカルシウムの結合が何らかの影響を及ぼしていることが考えられている。現在ではその形態学的観



察だけでなく、構成要素の精査や、長期耐久性の確認など多岐にわたる研究が進められており、これからの保存修復学が進むべき道の1つでもある、歯の改質による強化の方向性に大きく関与する可能性を持っている。

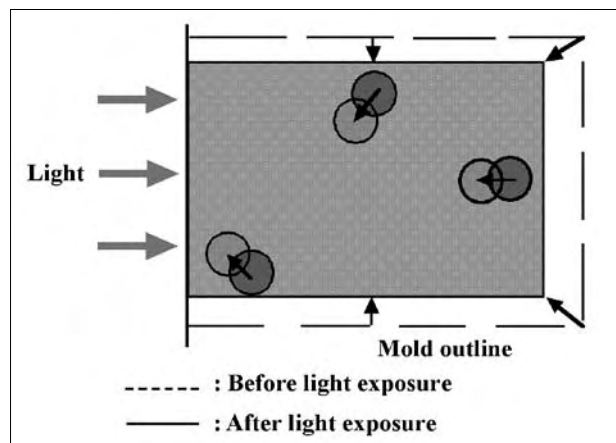
コンポジットレジンフィラーのトレースによる重合収縮の評価

Evaluation of polymerization shrinkage mechanism, tracing filler movement in light cured resin composite.

本研究の目的は、光重合型コンポジットレジンを窩洞内で重合させ、その収縮挙動をマイクロフォーカスX線CTを使用して非破壊的に重合挙動を評価し、その重合収縮理論を確立することにある。近年、ボンディング・コンポジット材料のみならず、重合器としての照射器にも改良がみられ、これら器材の応用を含めて光重合型コンポジットレジンの重合収縮挙動を評価する。また、接着材の有無や窩洞形態の違いによる収縮挙動の相違を検討し、臨床に応用すべく最良の修復技法の確立を目指している。

本研究の主たる目的である、光重合型コンポジットレジンの重合収縮解析に、マイクロフォーカスX線CTを使用する。これまでは、充填物を一塊のバルクとして、体収縮・線収縮などが評価されていたことに対し、窩洞に充填したコンポジットレジ内各所における収縮挙動を、個別に、さらに視覚的に評価することができる。マイクロフォーカスX線CTは近年その解析能力が著しく改良され、本研究の評価にも応用できるところまで分解能が小さくなっている。すなわち、光重合型コンポジットレジ内での測定に関しては、マーカーとして配合された特殊なフィラーの移動量を、マイクロ単位で測定することが可能となっている。

X線造影性のない歯質に弾性率が近似したコンポジットレジ製のマールド内にて、上記の特殊コンポジット



レジンを使い、重合前と重合後のフィラーの移動量をマイクロフォーカスX線CTにて測定している。得られたデータは、特別にプログラムされた重合収縮解析ソフトにてフィラー挙動の解析を行っている。本研究により詳細な光重合型コンポジットレジンの重合収縮挙動の解析を行うことができ、充填方法の評価を理論的できるようになった。

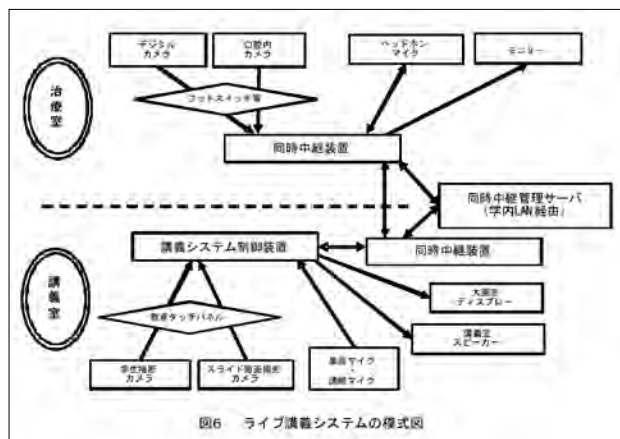
歯科診療室と講義室のインターネットライブ講義システムの開発と評価

Development and assessment of internet live seminar system between dental clinic and lecture room

歯学部教育において、外来見学や診療補助によって臨床現場を体験させることは必須である。しかし、臨床現場での体験実習には多くの教員と協力患者が必要であり、狭い術野のため学生が口腔内を十分に観察することは困難である。そこで、講義室の学生が口腔内の詳細まで含めた実際の歯科診療をリアルタイムに視聴でき、かつ体験を共有できるライブ講義システムを開発し、活用すると共に、その有効性等を評価した。

開発したシステムでは、術者が、可動アームに取り付けられたデジタルカメラや口腔内カメラからの映像を適宜切り替え、診療室のモニターとヘッドセットで、講義室の学生の反応を見聞きしながら授業できる。さらに、このような授業で蓄積された診療映像や講義映像をサーバに登録し、履修学生がいつでも学内外から視聴できるようなシステムとした。今回、歯学科4年生に対し、外来にて、保存修復治療の同時中継講義を行い、学生と教員による評価を行った。

学生は、臨場感を感じた(95%)、ビデオより良かった(100%)、外来見学より良かった(95%)と評価した。本システムにより、従来学生全員に対しては見せることのできなかった臨床現場を、直接全学生に臨場感をもつ

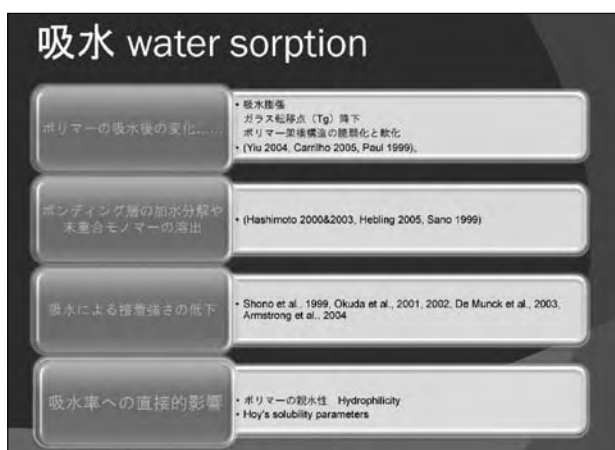


て効果的に体験させることができたと思われる。学生および教員からの高い評価や、ビデオ視聴や外来見学に無い長所が認められたことから、同時中継講義は、歯学部教育における新しい教育手法として有効と思われる。

象牙質接着性材料の基礎的研究とその臨床応用

Fundamental analysis and clinical application of dentin adhesives

ワンステップボンディング材は親水性であることが知られており、その親水性から吸水することが知られている。象牙質接着の耐久性には吸水によるボンディング材の劣化が影響を与えると考えられ、ボンディング材硬化体を作製し、3点曲げ試験を行うことにより得られたその弾性率と、吸水性及び溶解性試験を行って得られた吸水率と溶解率の結果を比較検討しその相関について検討を行った。また、ツーステップのエッチアンドリンシステムについてはより疎水性のボンディング層をつくることが重要であると考えられており、リン酸エッチングを行った象牙質に対して、従来の水を用いたウエットボンディング法を改良し、エタノールを用いるエタノールウエットボンディング法の初期接着強さが改良されていることに注目し、その長期耐久性について微小接着強さの観点からその長期耐久性を検討した。結果、ワンステップボンディング材には乾燥後も溶媒が残存し、重合率を低下させたり、その機械的強度を低下させる可能性が示唆された。またエタノールウエットボンディング法を用いることで1年後の接着強さは向上することが判明した。

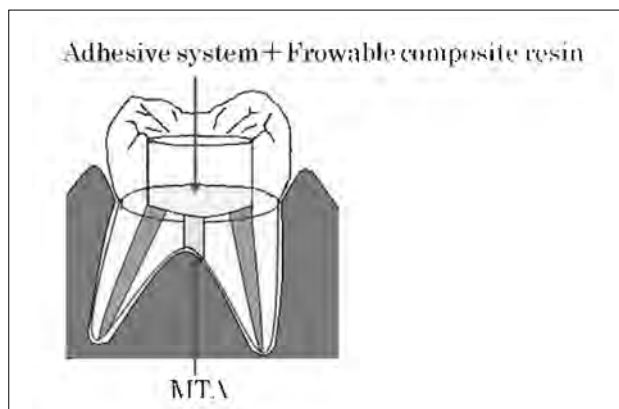


根管壁穿孔症例に対する新規穿孔部封鎖法の考案

Discovering the new way to treat perforations successfully using the combination of MTA and the adhesive technique

本研究の目的は、これまで予後不良であるとされてきた根管壁および髄床底部象牙質の穿孔症例において、

穿孔部を緊密に封鎖し、再感染を回避することで、歯の寿命の延長を実現させることである。1990年にLoma Linda大学を中心に開発された歯内療法用材料である mineral trioxide aggregate (MTA) は、湿潤下でも硬化し、高い封鎖性および生体親和性を有することから、近年、穿孔封鎖材として注目され始めている。MTAはケイ酸三カルシウム、ケイ酸二カルシウム、アルミン酸三カルシウム、鉄アルミン酸四カルシウム、石膏、酸化ビスマス等を成分とするポルトランドセメントに近似する材料であり、良好な封鎖性、生体親和性、硬組織誘導能などを有することから、穿孔封鎖材としてのみならず、逆根管充填、直接覆髄、apexification時の根尖封鎖など、根管と歯周組織の交通路の封鎖を目的とする様々な用途に使用されてきた。しかし、MTAは穿孔封鎖材として最も重要であると考えられる歯質接着性能を持たないことから、単独での使用では、長期的な視点から封鎖を実現できたとは明言しにくい。そこで、MTAで穿孔部を封鎖し、さらにその上から、コンポジットレジンを用いて、穿孔部周囲の象牙質表面に接着層を作る手法を用いることで、より確実な穿孔部の封鎖を実現することが期待される。本研究においては、MTAとコンポジットレジンとの接着性を明らかにするとともに、相互が及ぼす影響についても解析する。また、両者を用いて穿孔部を封鎖した際の、封鎖性、および生体組織側の反応についても追究する。

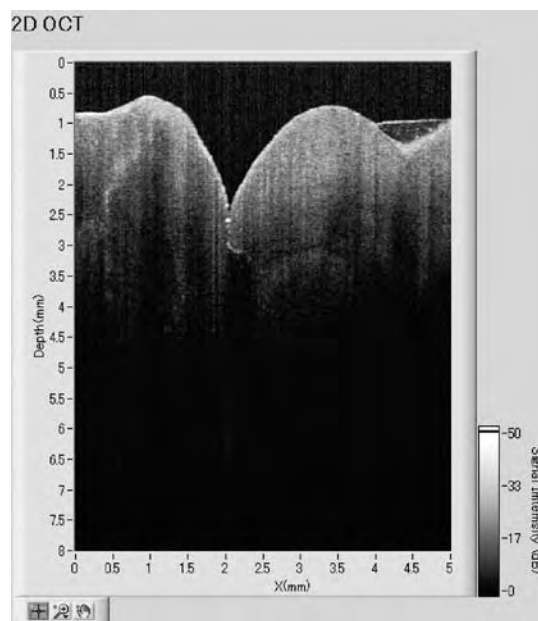


OCTを用いた隣接面う蝕モデルの非侵襲断層画像診査

Non-invasive cross-sectional imaging of the interproximal cavity at contact region using OCT

OCT (Optical Coherence Tomography) は生体に無害な近赤外線光を用いた光干渉断層画像法である。1991年の報告以来、電離放射線による被曝を伴わないため、非侵襲的な診断技術として医学領域の臨床現場に普及しつつあるが、歯科・口腔領域での臨床応用は極めて少なく、

この分野においても、OCTの可能性の検証が求められている。近年、う蝕の中でも、特に隣接面に生じたう蝕は視診や触診のみでの発見は困難であり、画像診断に頼るところが大きい。OCTは、隣接面う蝕の観察においても有用であることが期待できるが、観察範囲に限界があることから隣接する歯のコンタクト直下まで画像を構築する事が可能かという点については疑問が残る。そこで、本研究では、隣接面う蝕を想定したモデルを作製し、OCTによる断層画像診査を試みた。人抜去歯の隣接面コンタクト直下にダイヤモンドラウンドバーを用いて窩洞を形成し、OCT (Santec OCT-2000®, Santec) で咬合面方向から観察を行った。窩洞の大きさ、および位置を変えることで、画像がどのように変化するかについて検討した上で、実際に隣接面う蝕が存在する歯についても、観察を行った。結果として、本実験からOCTを用いることでコンタクト直下に存在する隣接面窩洞を検出できることが分かり、それに伴い臨床における隣接面う蝕もOCTにより検出できる可能性が示唆された。



ジルコニア切削用ダイヤモンドポイントにおける切削効率の検討

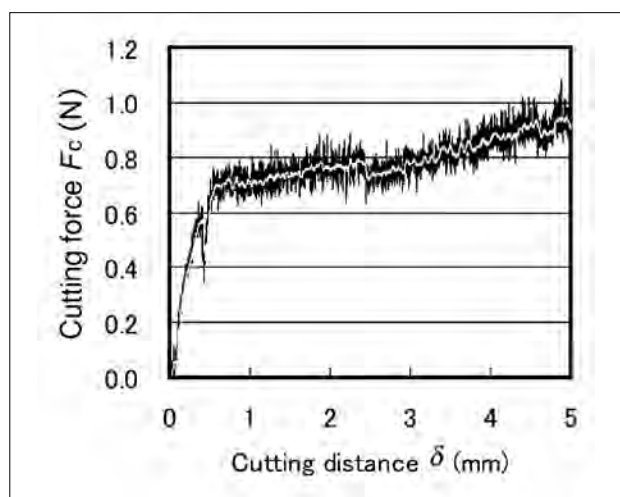
Cutting performance of diamond burs for zirconia

オールセラミック修復は、患者からの審美的な要求の高まりとともに広く臨床に普及している。とくに高い破壊靱性を有するジルコニアは、“白いメタル”と呼ばれ、CAD/CAMによる加工技術の向上とともに金属に代わるコーピング材料として注目され、臼歯部におけるクラウンブリッジやインプラント上部構造などへの臨床応用

が拡大している。しかし、ジルコニアオールセラミック修復は、その高い物性ゆえに切削が困難であり、技工操作における微調整や臨床におけるジルコニアフレームの除去は困難を極め、ジルコニアオールセラミック修復における解決すべき最重要課題の一つである。最近、ジルコニアをより効率的に切削するためのバーが開発されているが、これらの切削効率についての客観的な評価はないのが現状である。

本研究では、歯科用ダイヤモンドポイント及び回転切削器具の違いがジルコニアの切削効率に及ぼす影響について評価した。

結果として、バーの種類により切削性能に差が認められたが、エアタービンと5倍速マイクロモーターとの間に明らかな違いは認められなことが分かった。今後、SEM観察を行い、ダイヤモンドポイントの砥粒の違いが切削性能に及ぼす影響についてさらに検討が必要である。



2) 研究内容の英文要約

Effects of light sources and visible light-activated titanium dioxide photocatalyst on bleaching

The objective of this study was to evaluate, using methylene blue (MB), the effects of various light sources on the bleaching action of hydrogen peroxide (H_2O_2) with two titanium dioxide (TiO_2) photocatalysts - an ultraviolet light-activated TiO_2 photocatalyst (UVTiO₂) versus a visible light-activated TiO_2 photocatalyst (VLTiO₂). Five experimental solutions (VLTiO₂ + H_2O_2 , UVTiO₂ + H_2O_2 , H_2O_2 , VLTiO₂, UVTiO₂) were prepared by mixing varying concentrations of H_2O_2 and/or TiO_2 photocatalyst with MB solution. For H_2O_2 -containing solutions (VLTiO₂ + H_2O_2 , UVTiO₂ + H_2O_2 , and H_2O_2), the concentration of H_2O_2 was adjusted to 3.5%. For the four different light sources, low- and high-intensity halogen lamps and blue

LED LCUs were used. All the experimental solutions were irradiated by each of the light sources for 7 minutes, and the absorbance at 660 nm was measured every 30 seconds to determine the concentration of MB as an indicator of the bleaching effect. On the interaction between the effects of light source and bleaching treatment, the high-intensity halogen with VLTiO₂ + H_2O_2 caused the most significant reduction in MB concentration. On the effect of light sources, the halogen lamps resulted in a greater bleaching effect than the blue LED LCUs.

Effect of filler content of flowable composites on resin-cavity interface

The purpose of this in vitro study was to evaluate marginal integrity and wall adaptation in 1- and 2-mm-deep cavities restored with a high filler-loaded flowable composite in comparison to a flowable composite with lower filler content and a conventional hybrid composite. 1-mm-deep dentin and 2-mm-deep enamel-dentin Class I cavities were prepared and restored with a self-etch adhesive and with one of the composites. Samples were crosscut and evaluated for marginal integrity and gap formation using a digital microscope. Selected samples were also observed using a scanning electron microscope. For 1-mm-deep cavities, no differences in marginal integrity and wall adaptation were observed among the three composites. For 2-mm-deep cavities, those restored with the bulk technique and with the higher filler-loaded flowable composite demonstrated a similar outcome as that of the conventional hybrid composite. On the effect of restorative techniques, cohesive enamel defects were observed in bulk-filled 2-mm-deep cavities. However, when the incremental technique was used in conjunction with the higher filler-loaded flowable composite and the conventional hybrid composite for 2-mm-deep cavities, superior results were obtained.

Effect of Er:YAG Laser on Dentin Bonding Durability Under Simulated Pulpal Pressure

Purpose: To evaluate the effects of Er:YAG laser ablation on the microtensile bond strength and the nanoleakage of Er:YAG-lased dentin bonded to a self-etching adhesive system with and without pulpal pressure. Materials and Methods: Twenty flat dentin surfaces were obtained from extracted molars. Ten specimens were irradiated by Er:YAG laser, other specimens (control group) were ground using #600 SiC paper. Direct communication to the pulp chamber was created by cutting at a level approximately 1 mm below the cemento-enamel junction and parallel to the occlusal surface. The experimental groups were exposed to a simulated pulpal pressure of 15 cm H_2O . Each specimen was restored using an adhesive and a photocured composite. The specimens were then sectioned vertically to obtain dentin/adhesive slabs. Ninety-six slabs

were prepared for microtensile bond testing. Sixty-four slabs were immersed in ammoniacal silver nitrate tracer solution for 18 h, then rinsed thoroughly, and immersed in photodeveloping solution for 6 h prior to their examination by FE-SEM. Results: The method of dentin preparation and the pulpal pressure storage condition significantly affected the μ TBS, while the storage duration did not ($p < 0.05$). The nanoleakage patterns observed in the dentin/bond interface differed depending on whether the dentin was conventionally prepared or ablated by Er:YAG laser. Conclusion: Er:YAG laser ablation to dentin adversely affected the μ TBS and the sealing ability of SE Bond bonded to dentin under simulated pulpal condition.

Non-invasive cross-sectional imaging of the interproximal cavity at contact region using OCT

Detection of pit and fissure caries by current methods is not highly sensitive. The approximal surface is considered a very important site of caries expression. Diagnosis and treatment of contacting approximal cavitated caries lesions not detected by conventional clinical examination have been a subject of investigation in the literature. The OCT (Optical Coherence Tomography) is an optical signal acquisition and processing method allowing extremely high-quality, μ m-resolution, three-dimensional images from within optical scattering media (e.g., biological tissue) to be obtained. In this ex vivo study, we examined a swept-source OCT (SS-OCT) as a diagnostic tool for contacting approximal cavitated caries lesions. SS-OCT could clearly detect the interproximal cavity at contact region.

Preservation in the liquid media produces alterations in enamel surface properties

OBJECTIVE: The aim of the study was to elucidate any alterations in nanomechanical properties and structural integrity of enamel surfaces after preservation in different liquid media. **METHODS:** The nanohardness and modulus of elasticity of bovine enamel blocks were measured before (control) and after storage in all of the following liquid media: human pooled saliva, physiological saline (NaCl), Deionized water (Milli-Q water) and phosphate buffered saline (PBS) for 1, 7, 14 and 30 days. Control and the 30 days preserved samples were examined by scanning electron microscopy (SEM). Data were analysed by one-way ANOVA and Dunnett T (3) test. **RESULTS:** Hardness and modulus of elasticity of enamel in saliva up to 14 days showed no significant decrease compared to controls. In the case of PBS, both hardness and modulus did not change up to 30 days. The hardness values of Milli-Q water (12.06%) and NaCl (14.19%) samples were reduced significantly after just for 1 day and after 30 days were reduced to 55.59% and 61.18%, respectively. The Young's modulus of NaCl samples showed significant reduction (8.35%) after 1

day, but not for Milli-Q water samples. From 7 to 30 days, significant reductions for both samples were detected. SEM photomicrographs of samples in saliva showed widening of the inter-prismal space, while in PBS samples the structural damage was less. In the Milli-Q water group, prominent structural damage was observed and in case of NaCl, the enamel prisms were eroded. **CONCLUSIONS:** Human saliva and PBS are better for short term preservation of enamel samples compared to NaCl and Deionized water.

Acid resistance of dentin after erbium:yttrium -aluminum-garnet laser irradiation

The purpose of this study was to evaluate the acid resistance of erbium:yttrium-aluminum-garnet (Er:YAG) lased sub-surface dentin using a scanning electron microscope (SEM). Dentin disks were exposed to a single pulse of Er:YAG laser irradiation at 80 mJ/pulse under water spray, with the contact sapphire tip vertical to the dentin surfaces ($n = 15$). Five specimens from the laser-ablated dentin surfaces were observed. Ten specimens were crosscut, exposing the center of the lased point. For five of the specimens, the sub-surface of the lased dentin, with or without 10% phosphoric acid treatment, was evaluated. We used the remaining five specimens to analyze the degree of acid treatment on crosscut surface by observing the re-crosscut surfaces at the lased point. The irradiated dentin surfaces were irregular, scaly or flaky. Three sub-layers were observed in the sub-surface: a superficial, less decalcified layer; an intermediate most decalcified layer; and a deep, normal shade layer. Er:YAG laser irradiation affected the acid resistance of sub-surface dentin.

Assessment of nanostructure of "Super Dentin" formation by application of all-in-one adhesive systems

There are no reports on detailed examination of the recurrent caries inhibition potential of dentin adhesive systems. This study characterizes the ultramorphology and secondary caries inhibition potential of different dentin adhesive systems in order to find a satisfactory method to resist recurrent caries. Human premolar dentin was treated with self-etching adhesive systems Clearfil SE Bond, Clearfil Protect Bond or acid-etching adhesive system Single Bond. Bonded interface was exposed to an acid challenge. Transmission electron microscopic observation was performed at the resin dentin interface. An acid resistant zone was found adjacent to the hybrid layer in the outer lesion front with only Clearfil SE Bond and Clearfil Protect Bond. However Single Bond was devoid of this protective zone. Crystallites in the zone were confirmed as apatite. This special acid resistant dentin created by self-etching adhesive systems was introduced as a new concept "The super dentin".

Relationship between fluorescence loss of QLF and depth of demineralization in an enamel erosion model

The purpose of this study was to assess the relationship between quantitative light-induced fluorescence (QLF) values and demineralization depths in an enamel erosion model in vitro. Flat labial enamel surfaces of bovine incisors were ground with 800-grit SiC and coated with nail varnish, but also leaving rectangular windows of enamel uncoated. Subsequently, they were immersed in a lactic acid gel (pH 5.0) for 0 to 7 weeks to make an enamel erosion model. Carious lesions thus induced were analyzed by QLF and the demineralization depths measured using SEM/EDS method at the end of each period. A wide range of erosive lesions were produced with a steady increase in both demineralizing depth and fluorescence loss (ΔF) over time. With this model, a good correlation was exhibited between each ΔF value and the demineralization depth. Results of this study indicated that QLF could detect and quantify mineral loss under the eroded surface of the enamel erosion model.

Effect of an internal coating technique on tensile bond strengths of resin cements to zirconia ceramics

Specimens (Cercon Base) and twenty-eight silica-based ceramic specimens (GN-1, GN-1 Ceramic Block) were air-abraded using alumina. Thereafter, the zirconia ceramic specimens were divided into two subgroups of 28 each according to the surface pretreatment; no pretreatment (Zr) ; and the internal coating technique (INT) . For INT, the surface of zirconia was coated by fusing silica-based ceramics (Cercon Ceram Kiss) . Ceramic surfaces were conditioned with/without a silane coupling agent followed by bonding with one of two resin cements; Panavia F 2.0 (PF) and Superbond C&B (SB) . After 24 hours storage in water, the tensile bond strengths were tested ($n=7$) . For both PF and SB, silanization significantly improved the bond strength to GN-1 and INT ($p<0.05$) . The INT coating followed by silanization demonstrated enhancement of bonding to zirconia ceramics.

Localization of matrix metalloproteinases (MMPs-2, 8, 9 and 20) in normal and carious dentin

Dentine matrix metalloproteinases (MMPs) may participate in destruction of dentine following demineralization by bacterial acids. This study investigated the localization of MMPs in carious dentine. Frozen sections of dentine caries were prepared without demineralization and immersed in monoclonal antibody against MMP-2, -8, -9 and -20. The sections were labeled by IgG conjugated with gold colloidal particles, and observed under FE-SEM. Labeling indexes (number of gold particles / μm^2) of outer and inner carious dentine, respectively, with and without bacterial infection, were compared to that of normal dentine. MMP-

2 was distributed in both carious and normal dentine; the level of MMP-2 showed no significant difference among the outer caries, inner caries, and normal dentine. The labeling indexes of MMP-8 and MMP-9 both significantly decreased at the inner carious dentine compared to the level of normal dentine, but intensified again at the outer caries region. The labeling index of MMP 20 was the highest at normal dentine. The localization of MMPs was visibly detected using immunogold labeling. The localization of MMP-2 showed no significant difference among the three regions, while MMP-8 and MMP-9 showed significant reduction at the inner caries layer, and MMP-20 reduced toward the outer caries.

Effect of Double-application of Three All-in-one Adhesives on Dentin Bonding and Mechanical Properties of Resin-dentin Area

The aim of this study was to investigate whether double-application influences the bond strength of all-in-one adhesives and the mechanical properties of resin-dentin area.

Materials and Methods: Three all-in-one adhesives (EXL-683, experimental, 3M ESPE; Clearfil Tri-S Bond, Kuraray Medical; G-BOND, GC) were applied on the dentin surfaces by using single-application or double-application method. The manufacturers' instructions stated single-application method. Resin composite (Clearfil AP-X, shade A3, Kuraray Medical) was then placed and light cured for 40 s. Micro-shear bond test was carried out and bond strength data were analyzed using one-way ANOVA and Dunnett T3 tests. The hardness (H) of bonding layer, resin-dentin interface and dentin beneath the interface at 10 μm and 100 μm depth were measured with a nanoindentation tester. The H data were analyzed using two-way ANOVA, one-way ANOVA and independent t-test at a significance level of $p = 0.05$.

Results: The mean bond strength with single-application of EXL-683, Clearfil Tri-S Bond and G-BOND were 39.1, 36.9 and 30.0MPa, while as with double-application were 46.9, 40.2 and 32.2MPa, respectively. Double-application for EXL-683 to dentin showed significantly higher bond strength than single-application ($p < 0.05$) . However, there was no significant difference between single- and double-application methods for other two adhesives ($p > 0.05$) . The H of bonding layer was significantly influenced by both the adhesive material and application method ($p < 0.05$) ; The H of bonding layer with double-application was significantly improved compared to single-application. The H of resin-dentin interface was significantly affected by the application method ($p < 0.05$) , but not by the adhesive material ($p > 0.05$) . Neither the H value of dentin at 10 μm nor 100 μm depth were affected by adhesive material or application method ($p > 0.05$) .

Conclusions: Double-application of EXL-683 did improve the bond strength to dentin. The hardness of bonding layer and resin-dentin interface were significantly affected by double-application for each material used.

Effect of dentin pretreatment with mild acidic HOCl solution on microtensile bond strength and surface pH

To evaluate the pretreatment effect of mild acidic HOCl solution on the microtensile bond strength (μ TBS) of a two-step self-etch adhesive to dentin and the alteration of dentin surface pH. Thirty-nine flat ground coronal dentin specimens were treated with 6% NaOCl or 50, 100 and 200 ppm HOCl (Comfosy[®]) solutions for 5, 15 and 30 s. All the dentin surfaces were applied with Clearfil SE Bond. After 24h water storage, the bonded specimens were subjected to the μ TBS test. Dentin surface pH with or without pretreatment was examined using a pH-imaging microscope (SCHEM-100). The 50 ppm Comfosy[®] pretreatments for 5, 15 and 30 s did not affect the μ TBS of the two-step self-etch adhesive to dentin and dentin surface pH.

Influence of bonded enamel margins on dentin bonding stability of one-step self-etching adhesives

To evaluate the dentin bonding durability of two one-step self-etch adhesive systems with and without the presence of surrounding enamel. Tri-S Bond and G-Bond were applied to both the dentin and the surrounding enamel surfaces. Half the bonded teeth were sectioned to the shape for microtensile bond strength testing, followed by storage in water for 6 months (direct water exposure group). The other half were left untrimmed and stored in water for 6 months (Indirect water exposure group). After the designated periods of water storage, the specimens were subjected to bond strength testing. Indirect water exposure of the resin-dentin interface did not affect the μ TBS of both adhesives after 6-months water storage. However, direct exposure to water significantly reduced the μ TBS of both adhesives to dentin. The durability of resin-dentin bonds was found to be dependent on the method in which the bonded specimens were aged in water.

Improving the effect of NaOCl pretreatment on bonding to caries-affected dentin using self-etch adhesives

To evaluate the effect of sodium hypochlorite pretreatment on adhesion to normal and caries-affected dentin using self-etch adhesives. Twenty extracted human molars with coronal carious lesions were used in this experiment. The occlusal dentin surfaces including the caries-affected dentin in each group were treated as follows: group 1, rinsed with water; group 2, treated with 6 % NaOCl for 15 s; group 3, treated with 6 % NaOCl for 30 s; group 4, application with Accel, a reducing agent, for 30 s after NaOCl-30s pretreatment. The treated dentin surfaces were applied

with one- or two-step self-etch systems (Bond Force and Clearfil Protect Bond). After 24h water storage, the bonded specimens were subjected to the μ TBS test. NaOCl pretreatment for 15 s significantly improved the μ TBS of both self-etch adhesives to caries-affected dentin, while the 30 s pretreatment did not affect them. For normal dentin, NaOCl pretreatment for 30 s significantly reduced the μ TBS of both self-etch adhesives although the 15 s pretreatment did not alter them. Furthermore, the application of Accel with a reducing effect increased the μ TBS to normal and caries-affected dentin treated, which was treated with NaOCl for 30 s.

Correlation between Bond Strength and Cavity Wall Adaptation

The purpose of this study was to evaluate the correlation between bond strength and cavity wall adaptation. Cylindrical cavities, 1 mm deep and 3 mm in diameter (C-factor = 2.3) were prepared on flat bovine dentin surfaces. The teeth were restored with Clearfil SE Bond adhesive system followed by Photo Clearfil Bright hybrid composite or Filtek Flow flowable composite. The resins were light cured with 600 mW/cm² for 40 s. After 24 h storage, the teeth were sectioned about 1.0 mm thick. The remaining dentin thickness was measured. The slabs were trimmed (ca. 1 mm²) at the adhesive-dentin interface for micro-tensile bond strength test (μ -TBS). The trimmed specimens were stressed to failure in tension at 1 mm/min. Bond strength and RDT data were analyzed using the Fisher's PLSD test. Dye penetration test was carried out on cut surface. Dye penetration scores were analyzed using the Kruskal-Wallis test Mann-Whitney U test. The flowable composite significantly improved resin composite adaptation to the cavity wall. However, the tensile bond strength to the dentin cavity floor of flowable composite was significantly decreased.

There was no correlation between resin composite bond strength and cavity wall adaptation for the dentin cavity.

Effect of Radiotherapy on Resin-Dentin Bond Strength

The purpose of this study was to evaluate the effect of γ -rays irradiation on resin/dentin bond strength, dentin microhardness and elastic modulus. One group of bovine incisors was irradiated with 60Gy γ -rays. Flat dentin surfaces were prepared on labial side. The teeth were treated with Clearfil SE Bond adhesive system. Clearfil AP-X hybrid composite was built up of 3 x 4 x 2 mm. The resins were light cured with 600 mW/cm² for 40 s. After 24-h storage, the teeth were sectioned about 1.0 mm thick. Remaining dentin thickness was measured. The slabs were trimmed (ca. 1 mm²) at the adhesive-dentin interface for micro-tensile bond strength test (μ -TBS). The trimmed specimens stressed to failure in tension at 1 mm / min.

Nano indentation hardness and elastic modulus on both dentin surfaces were measured using Nano-indentation tester. μ -TBS, microhardness and elastic modulus data were analyzed using the Fisher's PLSD test. There was no significantly different μ -TBS between intact group and irradiated group. Nano hardness and elastic modulus of irradiated group was significantly lower compared with that of intact group.

Irradiation with 60Gy γ -rays had no effect on resin-dentin bond strength. However, 60Gy γ -rays irradiation significantly decreased microhardness and elastic modulus of dentin.

The effect of Radiotherapy on resin composite adaptation to the cavity wall

Radiotherapy for oral cancer causes radiation caries. However, the effect of radiotherapy on dentin is not to be solved. The purpose of this study was to evaluate the effect of γ -rays irradiation on the marginal sealing and cavity wall adaptation of composite restorations using one-step adhesive system. One group of bovine incisors was irradiated with 60Gy γ -rays using a cobalt 60 therapeutic machine. Cylindrical cavities, 1.5mm deep and 3mm in diameter (C-factor=3) were prepared on flat bovine dentin surfaces. The teeth were restored with Clearfil SE Bond, One-step bonding system; Tokuyama Bond Force or Clearfil Tri-S Bond adhesive system followed by Clearfil AP-X hybrid composite; shade A3. The resins were light-cured with 600 mW / cm² for 40 s. After 24-h, one group specimens were thermocycled for 5000 cycles between 5°C and 55°C. Dye penetration tests around the cavity margin and cavity wall on cut surface were carried out for before and after thermocycled specimens.

Irradiation with 60Gy γ -rays had no effect on resin composite adaptation to the cavity wall regardless of bonding system. However, one-step bonding system showed significantly decreased cavity wall adaptation compared with two-step bonding system Clearfil SE Bond for non-irradiated dentin.

Intraoral pH measurement of carious lesions with qPCR of role playing cariogens to differentiate caries activity

The purpose of this study was to evaluate the feasibility of a micro-pH sensor to assess caries risks clinically in relation to population of cariogenic bacteria. A total of 32 carious samples were classified active and arrested carious lesion selected on clinical and radiological examinations. The pH values of carious lesion were directly measured using a micro-pH sensor. All carious samples were collected with a spoon excavator and round bur. On isolation of genomic DNA a real-time polymerase chain reaction (qPCR) was performed for quantitatively detection of target cariogenic bacteria. All samples were diagnosed as active 15 and

arrested 17. The pH values of active lesion were lower than that of arrested lesion. Detection percentages of *S. sobrinus* and *Lactobacilli* have displayed co-relationships in opposite directions with low pH of active lesion, while *S. mutans* was highest detection percentage of regardless of the caries activity. It suggested that cariogenic bacteria population was difference between active and arrested lesion. It was understood that the micro-pH sensor has the potentiality of assessing caries activities clinically and suggested that the pH of caries lesion might be related to the population of cariogenic bacteria which eventually generate the acids to produce the lesions.

Effect of chewing gum containing Phosphoryl Oligosaccharides of Calcium (POs-Ca) and fluoride on remineralization and hydroxyapatite crystallites of enamel subsurface lesions in situ

Phosphoryl Oligosaccharides of Calcium (POs-Ca) have been demonstrated to have an effect on remineralization of enamel subsurface lesions. The aim of this clinical study was to evaluate the effect of chewing gum containing POs-Ca and fluoride on remineralization and hydroxyapatite crystallites in enamel subsurface lesions in a human in situ model. The study utilized a double-blind, randomized design with three treatments: (i) gum containing 2.5% of POs-Ca and fluoride, (ii) gum containing 2.5% of POs-Ca and (iii) gum not containing POs-Ca and fluoride as control. Twenty subjects wore removable oral appliances with insets of bovine enamel blocks containing demineralized subsurface lesions and chewed the gum for 20 min 3 times per day for 14 days. After each treatment the enamel blocks were removed, embedded, sectioned, and subjected to microradiography for measurement of the level of remineralization and X-ray microbeam diffraction for measurement of the level of hydroxyapatite crystallites. Synchrotron radiation from SPring-8 was used to obtain a microbeam. Wide-angle X-ray diffraction demonstrated the amount of hydroxyapatite crystals. The results of this study showed that gum containing POs-Ca and fluoride is superior to an equivalent gum containing POs-Ca or non containing both POs-Ca and fluoride in remineralization of enamel subsurface lesions in situ with remodeling the hydroxyapatite crystallites.

Development and evaluation of a low erosive apple juice drink with Phosphoryl Oligosaccharides of Calcium

The aim of this study was to evaluate the erosive potential of an experimental apple juice containing Pos-Ca (0%, 0.5%, 1%, 1.5% and 2%) to polished bovine enamel using the laser scanning microscope throughout exposure periods of 5 or 60 min. For 5 minute specimen, there were statistical differences on the average of surface roughness values (Ra) between 0% and the others ($p < 0.05$). For 60 minute

specimen, there were statistical differences on the average of surface roughness values (Ra) between 0% and 1.5%, 2% ($p < 0.05$). Adding 1.5% to 2.0% POs-Ca to apple juice could eliminate the erosive steps produced by immersion in apple juice alone.

Effect of convergent light-irradiation on microtensile bond strength of resin composite to dentin

This study investigated the effects of curing light convergence and irradiation distance on the microtensile bond strength of resin composite to dentin using three light emitted diode (LED) light-curing units. Three light curing units were investigated in this study; Flash Lite (FL), Pencure (PN), and an experimental light-curing hand-piece developed for Dentaport ZX (DP), which was designed to emit convergent light. The light intensity of each unit was measured at irradiation distances up to 10 mm. For bond strength test, bonding area was demarcated on prepared dentin using black plastic rings, in which a self-etching adhesive and a resin composite (Clearfil Liner Bond II Σ and Clearfil Photo Core) were light-cured at different distances (2, 4, 6, 8, and 10 mm). After 24 hours storage in 37°C water, the specimens were sectioned into beams. Microtensile bond strength was then measured and failure modes were observed. The light intensity of all units significantly decreased with increasing irradiation distance. DP showed a smaller range of decrease, significantly higher intensity values at irradiation distances over 2 mm and significantly higher bond strengths at 8 and 10 mm compared to FL and PN ($p < 0.05$). Percentage of cohesive failures in dentin decreased at 8 and 10 mm for FL and PN. Irradiation distance did not significantly affect light curing performance of DP. Convergent light-irradiation was effective in maintaining adequate light intensity and bond strength as the irradiation distance increased.

Ultrastructural observations of the acid-base resistant zone of all-in-one adhesives using three different acid-base challenges.

The aim of this study was to analyze the effects of three different acid-base challenges on morphology of the resin-dentin interface. An all-in-one system was applied onto the human dentin disks. A resin composite was then put between them and light cured to make a dentin disk sandwich. After storing in water for 24h, each specimen was treated with one of the three acid-base challenges; pH 4.5 demineralizing solution, 15% phosphoric acid and 0.05N hydrochloric acid. The hybrid layer was not detected clearly under 3500x magnification in all groups. The acid-base resistant zone of the adhesive with fluoride was thicker than that without fluoride, whereas the ABRZ was thinner in phosphoric acid and hydrochloric acid and an increase was not observed in both solutions.

Effect of F:Ca:P ratio on F deposition by FCP Complex

An FCP with F:Ca:P molar ratio of 6:10:1 produced higher F deposition than NaF in an in vitro model. To determine F deposition by FCP of varying F:Ca:P ratios with the goal of maximizing the F deposition at a fixed F concentration ([F]) of 12 mmol/L. The FCP solutions, prepared using NaF, CaCl_2 , H_3PO_4 and de-ionized water, had a [Ca] of (7, 20, or 50) mmol/L, a [P] of (0.5, 2, or 10) mmol/L, and pH in the range of 2.73 to 3.43. A 12mmol NaF solution was used as a control. A previously reported in vitro model [Takagi et al, 2001] was used for accessing F deposition. F deposition, ranging from (3.08 to 4.57) $\mu\text{g}/\text{cm}^2$, were at least 3.5 times greater than that produced by the NaF control. Higher [Ca] and [P] did not necessarily increase F deposition. Conclusion: FCP has the potential for use in F rinses and dentifrices that will produce greater F deposition without increasing the F dose. All FCP solutions have acidic pHs, and further studies are needed to formulating FCP solutions with higher pHs while maintaining their efficacies.

Assessments on F deposition by FCP Complexes

To determine F-deposition by FCP of varying F:Ca:P ratios with the goal of maximizing the F-deposition at a fixed F-concentration ([F]) of 12 mmol/L. The FCP solutions, prepared using NaF, CaCl_2 , and H_3PO_4 , had a [Ca] of (7, 20, or 50) mmol/L, a [P] of (0.5, 2, or 10) mmol/L. A 12mmol NaF solution was used as a control. A previously reported in vitro model [Takagi et al, 2001] was used for accessing F-deposition. For prophylaxis examination, HA discs were used. The FCP solution ([F]:[Ca]:[P] = 1.2:3.4:2.75 (mol/L)) was added into no-fluoride commercial product and pumice powder. Each disk was blotted dry and the prophylaxis was applied for 30s using a standard rubber cup/hand piece arrangement. The disk was washed in CaF_2 saturated solution to remove residual paste. The disc was then etched in 0.5M perchloric acid. All FCP solutions were stable as expected. Both the [Ca] and [P] effects and their interactions were significant ($p < 0.01$). As shown in Table, F-deposition, ranging from (3.08 to 4.7) $\mu\text{g}/\text{cm}^2$, were at least 3.5 times greater than that produced by the NaF control. Higher [Ca] and [P] did not necessarily increase F-deposition. Also F-depositions (8.2 and 4.63 $\mu\text{g}/\text{cm}^2$) of the prophylaxis which FCP solution added into were more than 4 times greater than that from commercial product with fluoride (1.15 $\mu\text{g}/\text{cm}^2$).

Development and evaluation of live broadcast lecture system on dental education.

In dental education, it is essential for dental students to experience clinics by observation and treatment assistance. However, for clinical on-site experience training, many instructors and cooperative patients need to be involved,

and also it is difficult for students to get a wide view of an oral cavity due to a small site of operation. Therefore, we developed a live broadcast lecture system, with which students in a lecture room could experience the real-time treatment being made in clinics. We utilized this system and evaluated its effectiveness. In a live broadcast lecture system, an operator takes movies using a digital camera which is attached to a movable arm, or an intraoral camera. The operator can give a lecture to students in a lecture room by showing the real-time movies and see their reaction using a monitor and headphones.

Effect of water sorption on the mechanical property of one-step adhesives

Recently, clinical use of one-step self-etch adhesives has increased. They contain water and hydrophilic monomers as ingredients in order to promote effective acid-etching and resin-dentin bonding. Consequently, they are intrinsically hydrophilic. These hydrophilic adhesives tend to rapidly absorb water. It is possible that these changes would make resin-dentin interface created by hydrophilic one-step self-etch adhesives much unstable over time. Since the water sorption of adhesives within hybrid layer could affect the long-term durability of resin-dentin bond, the influence of water sorption on the mechanical properties of resins must be understood in terms of bond strengths.

It has also been reported that water sorption by hydrophilic resins contributes to the commonly observed decrease in their mechanical properties. Although more and more one-step self-etch adhesives have been marketed, the relationship between water sorption and the mechanical properties of one-step self-etch adhesives has not been well understood. The purposes was to evaluate the mechanical properties of five currently used one step self-etch adhesive after polymerization, while dry or after water sorption and the amount of water sorption that occurs after immersion in water for 24 h. Finally, the quantitative relationship between water sorption and mechanical properties of five one-step adhesives was examined.

3) 本事業に関連して世界的な研究拠点形成に向けて、以下の点で改善・整備等されたこと

A (研究拠点体制)

パナソニック株式会社ならびに国立長寿医療センターと提携し、口腔内用 OCT の共同開発ならびに研究協力を推進する体制を確立した。

B (研究教育環境)

研究施設として医歯学総合研究棟 10 階に位置する GCOE 研究室を活用し、最新の研究機器を設置し、バイオフィルムならびに石灰化に関する研究を推進した。

C (人材確保)

イラン国テヘラン大学より、Arileza Sadr を特任講師として採用した。

ライオン株式会社研究所より、中嶋省志を特任講師として採用した。

香港大学より、平石典子を特任助教として採用した。

池田一郎を特任助教として採用した。

D (人材育成)

リサーチアシスタントとして、大学院生の高橋礼奈、高橋真広、篠田祐子、半場秀典を採用し、積極的な研究参加を促し、学会発表・論文作成を行うよう指導した。

E (国際化)

- ・田上 順次. 学部間交流協定締結式に出席し、Masaryk University, Faculty of Medicine, Internacional de Catalunya, School of Dentistry と学部間協定を締結、2009 年 4 月 26 日から 2009 年 5 月 3 日

- ・田上 順次. 学生の the second professional examination の学外試験官・教育研究の視察として、International Islamic University Malaysia, Faculty of Dentistry に出張、2009 年 6 月 4 日から 8 日まで

- ・田上順次. 学部間学術交流協定の締結、セミナー参加・発表、ならびに研究打ち合わせとして、ナレスアン大学歯学部・チュラロンコン大学歯学部に出張、2009 年 6 月 14 日から 18 日

- ・田上順次. 学部間交流協定締結を、内蒙古医学院と締結、2009 年 8 月 16 日から 18 日

- ・2009 年 11 月 19, 26 日、12 月 3, 10 日の 4 日間にわたり、スペイン国バルセロナ市のカタローニャ大学とネットワークによる臨床研究セミナーを開催し、以後ネットワークによる交流を継続することに合意

4) GCOE 事業を推進するに当たって力を入れた点

う蝕に罹患しにくい歯質として、高度に石灰化し耐酸性に優れたスーパーエナメル及びスーパーデンチンの生成を目指しており、特にその手法の開発に力を注いでいる。その遂行のため、国内を問わず、海外からも優れた研究者を招聘し、また研究機関と共同研究を行う締結を結び、数多くの研究手段から模索を続けている。

また、口腔内用 OCT として走査型 OCT の開発と改良を行っているが、光源として近赤外線光を採用しており、

歯質への透過性を飛躍的に向上させている。X線を用いない、画期的な精密断層画像診断技術であり、非侵襲的で高解像度の画像を得ることができる。しかも、X線診断が困難であった小児や妊産婦への使用も可能と思われる。このような利点から、OCTの臨床導入は歯科医療の発展に資するところが大きいと考えており、産学官協同の研究体制を整え、鋭意努力している。

5) 英文原著論文

1. Suyama Y, Otsuki M, Ogisu S, Kishikawa R, Tagami J, Ikeda M, Kurata H, Cho T. Effects of light sources and visible light-activated titanium dioxide photocatalyst on bleaching. *Dent Mater J* 28 (6) 693-699, 2009.
2. Ikeda I, Otsuki M, Sadr A, Nomura T, Kishikawa R, Tagami J. Effect of filler content of flowable composites on resin-cavity interface. *Dent Mater J* 28 (6) 679-685, 2009.
3. Bakry AS, Nakajima M, Otsuki M, Tagami J. Effect of Er-YAG Laser on Dentin Bonding Durability Under Simulated Pulpal Pressure. *J Adhes Dent* 11 (5) 361-368, 2009.
4. Anjum A, Otsuki M, Matin K, Tagami J. Preservation in the liquid media produces alterations in enamel surface properties. *J Dent* 37 (11) 884-890, 2009.
5. He Z, Otsuki M, Sadr A, Tagami J. Acid resistance of dentin after erbium:yttrium -aluminum-garnet laser irradiation. *Lasers Med Sci* 24 (4) 507-513, 2009.
6. ©Waidyasekera K, Nikaido T, Weerasinghe DS, Ichinose S, Tagami J. Reinforcement of dentin in self-etch adhesive technology: A new concept. *J Dent* 37(8):604-609, 2009.
7. ©Toru Nikaido, Dinesh D. S. Weerasinghe, Kanchana Waidyasekera, Go Inoue, Richard M. Foxton, Junji Tagami. Assessment of the nanostructure of acid-base resistant zone by the application of all-in-one adhesive systems: Super dentin formation. *Bio-Med Mater Eng* 19(2):163-171, 2009.
8. ©Kitayama S, Pilecki P, Nasser NA, Bravis T, Wilson RF, Nikaido T, Tagami J, Watson TF, Foxton RM. Effect of resin coating on adhesion and microleakage of computer-aided design/computer-aided manufacturing fabricated all-ceramic crowns after occlusal loading: a laboratory study. *Eur J Oral Sci*. 2009 Aug;117(4):454-62.
9. Shinohara MS, De Goes MF, Schneider LF, Ferracane JL, Pereira PN, Di Hipolito V, Nikaido T. Fluoride-containing adhesive: Durability on dentin bonding. *Dent Mater*. 2009 Jul 29.
10. Zhu L, Nikaido T, Kitayama S, Ikeda M, Foxton RM, Tagami J. Effect of surface abrasion and silica coating on tensile bond strength of a resin cement to zirconia ceramics. *Int Chin J Dent* 9:23-30, 2009.
11. ©Kitayama S, Nikaido T, Maruoka R, Zhu L, Ikeda M, Watanabe A, M Foxton R, Miura H, Tagami J. Effect of an internal coating technique on tensile bond strengths of resin cements to zirconia ceramics. *Dent Mater J*. 2009 Jul;28(4):446-53.
12. ©Tajima K, Nikaido T, Inoue G, Ikeda M, Tagami J. Effects of coating root dentin surfaces with adhesive materials. *Dent Mater J*. 2009;28 (5):578-586.
13. Nakata K, Nikaido T, Ikeda M, Foxton RM, Tagami J. Relationship between fluorescence loss of QLF and depth of demineralization in an enamel erosion model. *Dent Mater J* 28(5): 523-529, 2009.
14. ©Kunawarote S, Nakajima M, Shida K, Kitasako Y, Foxton RM, Tagami J. Effect of dentin pretreatment with mild acidic HOCl solution on microtensile bond strength and surface pH. *J Dent*, .
15. Torkabadi S, Nakajima M, Ikeda M, Foxton RM, Tagami J. Influence of bonded enamel margins on dentin bonding stability of one-step self-etching adhesives. *Journal of Adhesive Dentistry* 11(5): 347-353, 2009.
16. ©Taniguchi G, Nakajima M, Hosaka K, Iwamoto N, Ikeda M, Foxton RM, Tagami J. Improving the effect of NaOCl pretreatment on bonding to caries-affected dentin using self-etch adhesives. *J Dent* 37(10): 769-775, 2009.
17. ©Shida K, Kitasako Y, Burrow MF, Tagami J. Micro-shear bond strengths and etching efficacy of a two-step self-etching adhesive system to fluorosed and non-fluorosed enamel. *Eur J Oral Sci* 117(2):182-186, 2009.
18. ©Kitasako Y, Burrow MF, Huq LN, Stacey MA, Reynolds EC, Tagami J. A simplified quantitative test-adapted Checkbuf test-for resting saliva buffering capacity compared with a standard test. *Oral Surg Oral Med Oral Pathol Oral Radiol Endod* 108(4):551-556, 2009.
19. ©Shinichiro Ogisu, Ryuzo Kishikawa, Alireza Sadr, Kazunari Matoba, Norimichi Inai, Masayuki Otsuki, and Junji Tagami, Effect of convergent light-irradiation on microtensile bond strength of resin composite to dentin *Int Chin Dent* 2010
20. Iida Y, Nikaido T, Kitayama S, Takagaki T, Inoue G, Ikeda I, Foxton RM, Tagami J. Evaluation of dentin bonding performance and acid-base resistance of the interface of two-step self-etching adhesive systems. *Dent Mater J* 28(4): 493-500, 2009.
21. Tajima K, Nikaido T, Inoue G, Ikeda M, Tagami J. Effects of coating root dentin surfaces with adhesive materials. *Dent Mater J* 28(5): 578-586, 2009.
22. Inoue G, Nikaido T, M Foxton R, Tagami J. The acid-base resistant zone in three dentin bonding systems. *Dent Mater J* 28(6): 717-721, 2009.
23. ©Hosaka K, Nakajima M, Takahashi M, Itoh S, Ikeda M, Tagami J, Pashley DH. Relationship between water sorption and mechanical properties of one-step self-etch adhesives. *Dent Mater*

24. Hosaka K, Nishitani Y, Tagami J, Yoshiyama M, Brackett WW, Agee KA, Tay FR, Pashley DH. Durability of resin-dentin bonds to water- vs. ethanol-saturated dentin. J Dent Res. 2009 Feb;88(2):146-51、2009
25. Carrilho MR, Tay FR, Donnelly AM, Agee KA, Carvalho RM, Hosaka K, Reis A, Loguercio AD, Pashley DH. Membrane permeability properties of dental adhesive films. J Biomed Mater Res B Appl Biomater. 88(2):312-320、2009
26. Shimada Y, Ichinose S, Sadr A, Burrow MF, Tagami J. Localization of matrix metalloproteinases (MMPs-2,8,9 and 20) in normal and carious dentine. Australian Dental Journal 54(4): 347-354, 2009.
27. Wei S, Shimada Y, Sadr A, Tagami J. Effect of double-application of three single-step self-etch adhesives on dentin bonding and mechanical properties of resin-dentin area. Operative Dentistry 34(6): 716-724, 2009.
28. © Okada H, Sadr A, Shimada Y, Tagami J. Micro-shear bond strength of current one-step adhesives to cementum and dentin. American Journal of Dentistry .

6) 著書

田上順次、小柳岳大、マティン カイルール 次亜塩素酸電解水「パーフェクトペリオ」の臨床応用 日本歯科評論 別刷 Vol.69 (8) 通刊第802号,2009.8

田上順次. 直接修復による審美修復, 歯科審美第21巻 第2号別刷 P132-136, 2009.3

田上順次. 保存修復クリニカルガイド 第二版 医歯薬出版株式会社 2009.11.10

田上順次. 名医のセカンドオピニオン 自分の歯を残すむし歯治療を 週刊朝日. P.106 2009.07.17

田上順次. マキア必修ゼミ 歯科の時間 歯のリカバリー 第一回 MAQIA. P212 2009.09

田上順次. マキア必修ゼミ 歯科の時間 歯のリカバリー 第二回 MAQIA. P251 2009.10

田上順次、池田正臣. 歯科技工技術を活用した直接法審美修復 日本歯科技工学会雑誌 第30巻代1号 別刷 (平成21年7月20日 発行)

田上順次 フロアブルコンポジットレジン誕生から現

状 THE JOURNAL OF DENTAL ENGINEERING. No.169 Spring 2009.04.25

田上順次. `Super Tooth`の創出に向けて Voice to the Editorial Board ザ・クインテッセンス vol.28 no.7 July 別刷 2009.07

田上順次. 審美歯科も cure から care へ 歯科審美 第22巻 第1号 別刷 (平成21年9月 発行) Reprinted Journal of Esthetic Dentistry Vol.22, No.1, 2009

田上順次. フロアブルコンポジットレジンの基礎と臨床 日本歯科医師会雑誌 第62巻 第8号 別刷 (平成21年11月)

大槻昌幸: 安心安全なホワイトニングのためにおさえたいこのステップ STEP1 ホワイトニングの基本を知ろう!

デンタルハイジーン 29 (10) 1054-1057、2009

Maruoka R, Nikaido T, Kitayama S, Kunzelmann KH, Tagami J. Resin coating technique. Aesthetische Zahnmedizin. 12: 1: 24-29, 2009.

二階堂徹、田上順次. う蝕治療 (1) 象牙質の保護 (レジンコーティング法) について、別冊 the Quintessence Year Book 2009、現代の治療指針 欠損・審美補綴と全治療分野編、クインテッセンス出版、東京、160-161、2009年1月10日.

二階堂徹、池田正臣、來山修三、朱蕾、三浦宏之、田上順次. オールセラミック材料に対する接着、オールセラミック修復の有効性と新素材、歯冠修復の新たな潮流、歯科医療、23:3:23-31、2009.

二階堂徹、來山修三、高橋礼奈、有吉芽生、高垣智博、井上剛、田上順次. より確かな象牙質の保護が可能にした着実な臨床、2. 間接法修復におけるレジンコーティングについて—“Super Dentin”の形成、「歯をまもる—接着の進歩と歯質・歯髓の保護に関する最新情報」、日本歯科評論,69 (9) :85-90,2009.

北迫勇一、田上順次、歯が溶ける!? 酸蝕歯って知ってい

ますか?、クインテッセンス出版、12ページ、2009年。

7) 平成21年度までの自己評価

Super Tooth 創出のための、歯質強化法、接着界面強化法および歯の硬組織の診断技術に関する研究をバランスよく推進することができた。特にOCTによる歯の診断法の確立については、本年度臨床応用、実用化に向けて基礎的な情報を得た。接着界面の耐久性向上には、Super Dentinの役割が重要であることを指摘し、国際誌にもその用語とともに概念を発表した。

8) 和文原著論文

吉川 孝子, WATTANAWONGPITAK Nipaporn, 田上 順次. I級窩洞における象牙質接着強さと窩壁適合性の関係について. 日本歯科保存学雑誌 52 (6) : 441-445, 2009.

田中美由紀、北迫勇一、二階堂徹、半場秀典、池田正臣、田中智子、滝井寛、釜阪寛、田上順次. リン酸化オリゴ糖カルシウム (POs-Ca) 配合ガム咀嚼後のエナメル質初期う蝕の再石灰化効果および結晶構造の変化. 日本歯科保存学会雑誌 (印刷中) .

岸川隆蔵、田代浩史、趙 永哲、稲井紀通、田上順次. 光照射の有無がデュアルキュア型レジメンメントの象牙質接着強さに与える影響
接着歯学2010

趙 永哲, 木下淳博, 須永昌代, 岸川隆蔵, 南 一郎, 田上順次, 歯科診療室一講義室間のインターネット同時中継によるライブ講義システムの開発と評価 歯科医学教育学会誌 第25巻第3号 (印刷中)

島田康史、田上順次. 象牙質う蝕病巣におけるマトリックスメタロプロテアーゼ (MMP2,8,9,20) の局在性について. 接着歯学27 (2) : 57-62, 2009.

9) 学会発表 (英文)

©Bakry AS, Matin K, Tanaka Y, Otsuki M, Takahashi H, Yamashita K, Tagami J. Evaluating the Durability of Phosphoric Acid Promoted Bioglass-dentin Interaction Layer, 87th IADR, poster, Miami, oral, April 1-4, 2009.

Nakata K, Nikaido T, Tagami J. Remineralization Speed Analysis in a Subsurface Lesion Model using Micro-CT. 87th

IADR, Miami, poster, April 1-4, 2009.

Carvalho A, Oliveira MT, Ambrosano GMB, Nikaido T, Tagami J, Giannini M. Effect of adhesive system application modes on dentin permeability, 87th IADR2009, Miami, oral, April 1-4, 2009.2009.

Itoh S, Nakajima M, Hosaka K, Okuma M, Shinoda Y, Takahashi M, Seki N, Kishikawa R, Ikeda M, Tagami J. Dentin bonding durability of recent self-etching adhesives. 87th IADR, Miami, oral, April 1-4, 2009.

Okuma M, Nakajima M, Hosaka K, Itoh S, Kishikawa R, Ikeda M, Tagami J. Effect of indirect-post placement on bonding to root canal dentin. 87th IADR, Miami, oral, April 1-4, 2009.

Kunawarote S, Taniguchi G, Nakajima M, Tagami J. Pre-treatment effect of oxidizing solutions on bond-strength to caries-affected dentin. 87th IADR, Miami, oral, April 1-4, 2009

©Yoshikawa T, Miura M, Tagami J. Effect of Radiotherapy on Resin/Dentin Adaptation using Various Bonding Systems. 87th IADR, Miami, oral, April 1-4, 2009.

©Kitasako Y, Shida K, Matin K, Ikeda M, Tagami J. Effects of CPP-ACP on enamel pH and salivary cariogenic bacteria, 87th International Academy of Dental Research, 87th IADR, Miami, poster, April 1-4, 2009.

©Shida K, Kitasako Y, Matin K, Ikeda M, Tagami J. Intraoral pH measurement of caries and quantification of cariogenic bacteria. 87th IADR, Miami, poster, April 1-4, 2009.

Tsujimoto M, Inoue G, Nikaido T, Tagami J. Characterization of the Acid-Base Resistant Zone in three Different Acids. IADR2009, Miami, poster, 2009 April 4th.

Nikaido T, Tsujimoto M, Inoue G, Tagami J. Morphological Change of Adhesive-dentin Interface Using Two Different Acid-base Challenges. IADR2009, Miami, oral, 2009 April 4th.

Inoue G, Tagami J, Takagi S, Chong AM, Chow LC. Fluoride, Calcium, and Phosphate Deposition from Experimental Dental Prophylaxis. IADR2009, Miami, poster, 2009 April 4th

Chow LC, Inoue G, Tagami J, Takagi S. Unique Handling and Setting Properties of Dual-paste Premixed CPC. IADR2009, Miami, oral, 2009 April 4th

Takagi S, Inoue G, Tagami J, Chow LC. Relationship of Strength and Hydroxyapatite Formation in Dual-paste Premixed CPC. IADR2009, Miami, oral, 2009 April 4th

Inoue G, Takagi S, Tagami J, Chow LC. Effects of F:Ca:P ratio on F deposition by FCP Complexes. IADR2009, Miami, poster, 2009 April 4th

Chow LC, Inoue G, Tagami J, Sun L, Takagi S. Determination of Fluoride Release Rate from Varnishes by Constant-composition Titration. IADR2009, Miami, oral, 2009 April 4th

Inoue G, Takagi S, Tagami J, Chow LC. Assessments on F deposition by FCP Complexes. JADR2009, Wuhan, China, poster, 2009 Sep 22-25

©Sadr A, Tagami J, Shimada Y, Sumi Y. Optical coherence tomography for in-vivo assessment of class III composite restoration. IADR2009, Miami, oral, 2009 April 4th.

Sadr A, Mayoral Molina JR, Shimada Y, Bakhsh TA, Tagami J. Real-time Tomographic Monitoring Restoration Placement Using SS-OCT. AADR/CADR

10) 学会発表 (和文)

野村知正、池田一郎、大槻昌幸、田上順次、高出力LED照射器がレジンの象牙質接着に及ぼす影響、日本歯科保存学会秋季学術大会 (第131回)、仙台市、2009年10月29日

高岡丈博、田野絵里、岸綾香、岸川隆蔵、加藤純二、大槻昌幸、田上順次、405nm 青紫半導体レーザーが漂白効果に及ぼす影響、日本歯科保存学会春季学術大会 (第130回)、札幌市、2009年6月12日

岸綾香、大槻昌幸、田上順次、各種光源が光触媒含有の漂白材 (TiON in Office) の漂白効果に及ぼす影響、日本歯科保存学会春季学術大会 (第130回)、札幌市、2009年6月12日

岸川隆蔵、大槻昌幸、趙永哲、池田正臣、三浦宏之、田上順次、ホームホワイトニング材 (ティオン ホーム) の臨床評価についての報告、日本歯科保存学会春季学術大会 (第130回)、札幌市、2009年6月12日

篠木毅、加藤純二、大槻昌幸、田上順次、濱田和典、岩根聖二、西村己貴則、岡上吉秀、Er:YAGレーザー照射

がレジンの窩壁適合に及ぼす影響、第21回日本レーザー歯学会総会・学術大会、福岡市、2009年11月22日

藤田由美子、大槻昌幸、田上順次、可視光応答型酸化チタン光触媒を含有する漂白材の評価、第20回日本歯科審美学会学術大会、東京都、2009年9月19日

大山篤、須永昌代、駒田亘、南一郎、内田達郎、吉岡隆知、大槻昌幸、北迫勇一、秀島雅之、水口俊介、荒木孝二、俣木志朗、木下淳博、歯学科4年における臨床体験実習の実施と評価、第74回口腔病学会学術大会、東京都、2009年12月5日

半場秀典、二階堂徹、中田景子、田上順次、CPP-ACPペーストによるエナメル質の脱灰抑制効果、日本歯科保存学会2009年度春季学術大会 (130回)、札幌、2009年6月11日、12日。

ハミド ヌロマン、高垣智博、カンチャナ ワイディアセケラ、二階堂徹、田上順次、MMA系レジンセメントにおける象牙質微小引張り接着強さと Acid-base resistant zoneのSEM観察、第54回日本歯科技工学会学術講演会、鹿児島、2009年10月1日、2日。

李娜、高垣智博、カンチャナ ワイディアセケラ、池田正臣、二階堂徹、田上順次、デュアルキュア型レジンコアシステムの重合方式が象牙質に対する微小引張り接着強さと Acid-base resistant zoneの形成に及ぼす影響、第54回日本歯科技工学会学術講演会、鹿児島、2009年10月1日、2日。

高橋真広、保坂啓一、伊藤志麻、中島正俊、田上順次、長期水中浸漬がワンステップボンディング材硬化体の吸水性・溶解性およびその機械的性能に及ぼす影響について、第131回日本歯科保存学会学術大会、仙台、2009年10月29,30日。

坪根真子、中島正俊、池田正臣、田上順次、光重合型コンポジットレジンのカメレオン効果について、第130回日本歯科保存学会学術大会、札幌、2009年6月11、12日。

吉川孝子、Nipaporn Wattanawongpitak、田上順次、各種接着システムを用いたコンポジットレジン修復物の象牙質窩底部における接着強さについて、第73回口腔病学

会、東京、2009年12月4、5日

吉川 孝子、Nipaporn Wattanawongpitak、田上 順次、I
級窩洞窩底部における接着強さについて、第28回接着歯
学会、松江、2010年1月23、24日

美田瞳、北迫勇一、高垣智博、藤井美恵、池田正臣、田
中智子、滝井寛、田上 順次、POs-Ca配合飲み物のエナ
メル質酸蝕抑制効果、日本歯科保存学会、仙台、2009
年10月29-30日。

田中美由紀、北迫勇一、二階堂徹、半場秀典、池田正臣、
田中智子、滝井寛、釜阪寛、田上順次、リン酸化オリゴ
糖カルシウム（POs-Ca）配合ガム咀嚼後のエナメル質
初期う蝕の再石灰化効果および結晶構造の変化、日本歯
科保存学会、仙台、2009年10月29-30日。

小柳岳大、マティン カイルール、岡田彩子、田上順次
次亜塩素酸電解水及び洗口剤の短時間作用によるう蝕病
原菌に及ぼす効果、日本歯科保存学会春季学術大会（第
130回）、札幌市、2009年6月11日

マティン カイルール、暁万里子、岡田彩子、志田加奈子、
永山正仁、才原康弘、田上順次 第8回日本機能水学会
学術大会、富山市、2009年11月17日

内田僚一郎、マティン カイルール、暁万里子、永山正
仁、才原康弘、田上順次 第8回日本機能水学会学術大会、
富山市、2009年11月17日

鵜鷹佐知子、マティン カイルール、小柳岳大、岡田彩
子、暁万里子、田上順次 第8回日本機能水学会学術大会、
富山市、2009年11月16日

市川千秋、井上剛、二階堂徹、田上順次 長期水中保管
後のAcid-base Resistant ZoneのSEM観察、第53回日本
歯科理工学会学術講演会、東京、2009年4月11、12日。

趙 永哲、南 一郎、須永昌代、吉岡隆知、岸川隆蔵、川島
伸之、和達礼子、木下淳博、須田英明、田上順次、歯科診療
室—講義空間のインターネット同時中継によるライブ講
義システムの開発と評価 口腔病学会学術大会 東京
2009年12月5日

保坂啓一、中島正俊、高橋真広、駒田亘、大竹志保、三浦宏
之、池田正臣、坂野若詠、岸川隆蔵、田上順次 セルフエッ
チングシステムにおける吸水と機械的強度との関係 平
成21年度秋期第54回日本歯科理工学会学術講演会 鹿
児島 2009年10月1、2日

夏目悠子、島田康史、Sadr Alireza、田上順次.OCTを
用いた根面う蝕の非侵襲診断、第131回日本歯科保存学
会2009年度春季学術大会 札幌 2009年6月11、12日

島田康史、Sadr Alireza、田上順次.OCTによる咬合面
う蝕の非破壊断層画像診断、第131回日本歯科保存学会
2009年度春季学術大会 札幌 2009年6月11、12日

有吉芽生、島田康史、Sadr Alireza、田上順次.OCTを
用いた隣接面う蝕モデルの非侵襲断層画像診断、第131
回日本歯科保存学会2009年度秋季学術大会 仙台
2009年10月29、30日

今井加奈子、島田康史、Sadr Alireza、田上順次、エナ
メル質亀裂の非侵襲断層画像診断、第131回日本歯科保存学
会2009年度秋季学術大会 仙台 2009年10月29、30日

Hariri Ilnaz, Shimada Yasushi, Sadr Alireza, Tagami
Junji. The effect of increasing thermal cycling regimens
on shear bond strength and nanoleakage. 第131回日本
歯科保存学会2009年度秋季学術大会 仙台 2009年10
月29、30日

Nazari Amir, Tagami Junji, Shimada Yasushi, Sadr
Alirezai. Surface characterization and bond strength of
two adhesive systems to intact vs. ground enamel. 第
131回日本歯科保存学会2009年度秋季学術大会 仙台
2009年10月29、30日

サダルアリレザ、田上順次、島田康史.OCTを用いたエ
ナメル質および象牙質の厚さと屈折率の測定について、第
131回日本歯科保存学会2009年度秋季学術大会 仙台
2009年10月29、30日

吉岡俊彦、吉岡隆知、海老原新、須田英明、島田康史、
田上順次、垂直性歯根破折の診断におけるOCTの有
用性、第131回日本歯科保存学会2009年度秋季学術大会
仙台 2009年10月29、30日

11) 外部資金の獲得状況

長寿医療研究委託費

研究題目:近赤外光・レーザー等を用いた新たな歯科疾患診断・治療用機器の開発に関する研究

代表者:角保徳

期間:平成21-23年

研究総額:5000万円

科学研究費補助金、基盤C

研究題目:非侵襲的トモグラフィーを用いた修復物の欠陥と二次う蝕の精密画像診断

代表者:島田康史

期間:平成21-23年

研究費総額:407万円

科学研究費補助金、基盤C

研究題目:各種う蝕形態における罹患象牙質除去前後のpH変化とう蝕細菌叢遺伝子解析

代表者:北迫 勇一

期間:平成21-23年

研究費総額:340万円

科学研究費補助金、若手研究B

研究題目:光干渉断層画像診断法の歯科臨床への応用

代表者:岸川隆蔵

期間:平成21-23年

研究費総額:380万円

科学研究費補助金、若手(B)

研究題目:マイクロフォーカスX線CTを使ったレジンの重合収縮におけるフィラー挙動の追跡

代表者:趙 永哲

期間:平成20-22年

研究費総額:312万円

科学研究費補助金、若手研究B

研究題目:象牙質コラーゲンナノスペースを利用した新しい接着性レジンの開発

代表者:保坂啓一

期間:平成20-23年

研究費総額:320万円

科学研究費補助金、若手研究(スタートアップ)

研究題目:根管壁穿孔症例に対する新規穿孔部封鎖法

の考案

代表者:有吉 芽生

期間:平成20-22年

研究費総額:312万円

12) 特別講演、招待講演

1. 田上順次.Tooth Wear Sensitivityへの取り組み、学生のための講演会(4年生対象)、愛知学院大学歯学部、2009年4月18日
2. 田上順次.TOOTH WEARと象牙質知覚過敏、社団法人日本歯科衛生士会 生涯研修制度 専門研修Ⅰ 都道府県歯科衛生士会 研修会、松本勤労会館、2009年5月17日
3. 田上順次.日本歯科大学 特別講義、日本歯科大学生命歯学部、2009年5月28日
4. 田上順次.セラミックに代わる最新CRテクニック、東京医科歯科大学歯科同窓会主催 実習コース、東京医科歯科大学歯学部、2009年5月31日
5. 田上順次.MIの概念に基づく新時代の審美修復、北二会学術講演会、コール田無、2009年7月11日
6. 田上順次.歯を守るための接着と審美、社団法人京都府歯科医師会 平成21年度第一回学術講演会、社団法人京都府歯科医師会、2009年8月1日
7. 田上順次.患者満足度の高いMIの概念に基づく新時代の審美修復、2009年度トクヤマデンタル審美セミナー【保存編】 2009年8月2日 福岡、2010年1月31日 大阪
8. 田上順次.いつまでも白くてきれいな歯でいるために、平成21年度経済産業省における教育講演、経済産業省会議室、2009年9月7日
9. 田上順次.TOOTH WEARと象牙質知覚過敏、社団法人日本歯科衛生士会 生涯研修制度 専門研修Ⅰ 都道府県歯科衛生士会 研修会、長崎県歯科医師会館、2009年10月11日
10. 田上順次.審美修復セミナー、ジーシー東京支店セミナールーム、2009年10月25日
11. 田上順次.歯がしみる!放っておいたらどうなる?、東京都歯科医師会 第9回都民向け講演会、東京ビックサイト、2009年11月7日
12. 田上順次.教育研究視察、講演、「Introduction of TMDU, Direct aesthetic restoration with innovative materials」中山大学光化口腔医学院、2009年9月3日から5日
13. 田上順次.アジアQLF会議、「QLF in experimental

cariology (in vitro model)」ルブラ王山、2009年10月12日

14. 田上 順次 .The Annual Scientific Meeting of the Association for Dental Sciences of the Republic of China「Creating the super tooth」、Garden Villa Kaohsiung、2009年11月26-29日
15. 田上 順次 .The 2nd Minimal Intervention Dentistry-International Network Meeting「Historical perspective and future development」、チュラロンコン大学歯学部、2009年12月13-16日
16. 田上 順次 .学会出席、講演、IADR General sessionに参加、「Keynote Address: Evaluation of Bond Durability and Characteristics of interface」Miami Beach Convention Center、2009年3月31日-4月5日
17. 田上 順次 .学会出席、講演、東北三省第10回口腔医学学会学術会議吉林大学白求恩医学院成立七十周年学術報告会「可以無限巧拡張の即時美容修復技術」中国武漢、2009年9月26,27日
18. 田上 順次 .学会出席、Dental Breakthrough in the 21st Century Where Science meets Technology、「single visit esthetic dentistry with innovative technologies」インドネシア大学歯学部、ジャカルタ、2009年10月14-17日
19. 田上 順次 .二階堂徹、中島正俊、島田康史 .Academy of Dental Materials Meeting、「Relationship Between Bond Strength Tests and Other In Vitro Phenomena」Portland, Oregon、2009年10月29-31日

13) 新聞、雑誌、TV報道

1. 田上 順次 .日本テレビ「おもいっきりドン」出演、2009年10月26日
2. 田上 順次 .日本テレビ「おもいっきりドン」出演、2009年12月21日
3. マティンカイイール .TBSテレビ「夢の扉」放送日 2009年9月13日

14) 教室、分野や講座の准教授、講師、助教、特別研究員、ポスドク、指導を受けた大学院生の名前(AISSには○印)のリスト

准教授:大槻昌幸

講師:二階堂徹、中島正俊

助教:吉川孝子、島田康史、北迫勇一、岸川隆蔵、井上剛、趙永哲、保坂啓一

医員:有吉芽生、高垣智博、高岡文博、内藤万里子

大学院GP特任講師:Matin Khairul

大学院GP特任助教:園田秀一

GCOE特任講師:Alireza Sadr

特任講師:中嶋省志

特任助教:平石典子

特任助教:池田一郎

技術補佐員:

Peththahandi Gayani Kanchana
Waidyasekera, Atia Anjum

大学院4年:

伊藤志麻、志田嘉奈子、田中義子、
大熊麻紗子、篠木毅、有本綾子、
辻本美穂、Fahimeh Hayati、
Sitthikorn Kunawarote

3年:

市川千秋、内田遼太郎、荒牧音、
篠田祐子、堀江加奈子、関奈央子、
高橋礼奈、高橋真広、岸綾香、青木香那子、
藤井美恵、高井智行、森文彦、丹野恵造、
○Patricia Makishi

2年:

田中美由紀、矢作智花、小柳岳大、
夏目悠子、坪根真子、田野絵里、半場秀典、
神原啓介、Hamid Nurrohaman、
Amir Nazari、○Ilnaz Hariri、
Prasansuttiporn Taweesak

1年:

今井加奈子、今村友美、鶴鷹佐知子、
丸藤伊織、桐原大、栗林恵美、
坂野若詠、美田瞳、
Suppason Thitthaweerat、
Turki Abdulsam Bakhsh

15) GCOE 活動についての感想、コメント、改善を望む点など

業績についてはデータベースを構築して、逐次、アップデートできるようにすれば、何度も同じような業績調査を繰り返さずにすみ、また、お互いに負担も減ると思います。

Effects of coating root dentin surfaces with adhesive materials

Kenichi TAJIMA¹, Toru NIKAI², Go INOUE¹, Masaomi IKEDA³ and Junji TAGAMI^{1,2}

¹Cariology and Operative Dentistry, Department of Restorative Sciences, Graduate School, Tokyo Medical and Dental University, 1-5-45 Yushima, Bunkyo-ku, Tokyo 113-8549, Japan

²Global Center of Excellence Program, International Research Center for Molecular Science in Tooth and Bone Diseases, Tokyo Medical and Dental University, 1-5-45 Yushima, Bunkyo-ku, Tokyo 113-8549, Japan

³Faculty of Dentistry, School for Dental Technology, Tokyo Medical and Dental University, 1-5-45 Yushima, Bunkyo-ku, Tokyo 113-8549, Japan
Corresponding author: Kenichi TAJIMA; E-mail: infiniteaspiration2000@yahoo.co.jp

The aim of this study was to evaluate the effects of coating root dentin surfaces with adhesives vis-à-vis the prevention of root dentin demineralization. Root dentin surface was ground with #600 SiC, and then either a single coat of Clearfil SE Bond (SE), Clearfil Tri-S Bond (TS), G-Bond (GB), Hybrid Bond (HB-1), or two coats of HB (HB-2) were applied. Specimens were immersed in an artificial demineralizing solution, then sectioned through the center of the root and polished. Thickness of the coating layer and depth of the demineralized dentin layer were observed under a confocal laser scanning microscope (CLSM). Nanohardness values of the coating layer and underlying dentin were measured using a nanoindentation tester. All obtained data were statistically analyzed. Dentin demineralization was not observed in the surface coating groups with the exception of HB-1, and nanohardness of the underlying dentin was comparable to that of normal dentin. Based on the results obtained, it seemed that coating root dentin surfaces with an adhesive material is a promising good practice to prevent demineralization.

Keywords: Self-etching adhesive, Root dentin, Surface-coating

Received Jan 9, 2009; Accepted Apr 18, 2009

INTRODUCTION

Recent years have seen a rapid increase in the dentate elderly population, especially in developed countries, due to increase in life expectancy, awareness of dental health measures, and availability of dental care delivery systems⁽¹⁾. A concomitant development is the high incidence of root caries in the middle-aged and elderly, due to gingival recession and exposure of susceptible root surfaces of the retained dentition. Poor oral hygiene and low salivary flow resulting in dry mouths are also potentially important risk factors for root caries⁽²⁾.

Several methods have been proposed to prevent root caries initiation and to promote remineralization prior to contemplating invasive treatments. These include the daily use of fluoride-containing mouth-rinses⁽³⁾ or professional application of fluoridated gels⁽⁴⁾ and antimicrobial varnishes⁽⁵⁾. However, a simple method to protect the exposed root surfaces from long-term caries attack is not yet currently available. To inhibit the initiation and progression of root caries, especially for elderly patients who require home care, there is indeed an urgent need for simple treatment options to be developed and made easily available.

In this pursuit of a simple preventive treatment option against root caries, the coating of root dentin surfaces with adhesive systems has been investigated. During the last decade, self-etching adhesive systems have become widely used because of a myriad of advantages: simplified bonding procedure that requires only one application step; reduced chairside time; reliable bonding to dentin; and low technique sensitivity and consistent performance that auger well

for strong bonding of composite materials to both enamel and dentin^(6,7).

During cavity preparation for indirect restorations, sealing the exposed dentin with a resin coating has been proposed as a means to protect the tooth preparation. The resin coating is applied to the prepared cavity immediately after tooth preparation and before making an impression by assembling a dentin bonding system and a flowable composite^(8,9). It has been reported that resin coatings minimized pulp irritation as well as improved the bond strength between resin cement and dentin^(10,11).

Recently, thin-film coating materials based on all-in-one adhesive technology were introduced for resin coating of indirect restorations⁽¹²⁾. The thin coating materials created a barrier-like film layer on the prepared dentin and played an important role in protecting the dentin from physical, chemical, and biological irritation⁽¹³⁾. In addition, these thin-film coating materials reportedly improved the bond strength of resin cements to dentin⁽¹⁴⁾, thereby preventing marginal leakage beneath inlays or crown restorations⁽¹⁵⁾. In light of the many benefits provided by such a protective layer, these all-in-one adhesive materials may therefore also have the potential to cover exposed root dentin surfaces and prevent caries formation⁽¹⁶⁾.

Using several all-in-one adhesive systems, the aim of this study was to examine the effects of coating root dentin surfaces with these materials in relation to preventing root dentin demineralization.

MATERIALS AND METHODS

The research protocol of this study was designed according to the guidelines of the Ethics Committee of the Graduate School and Hospital, Tokyo Medical and Dental University.

Tooth specimens

A total of 35 intact roots of human premolars, freshly extracted for orthodontic reasons, were used in this study. Prior to extraction, the patients from whom the teeth were extracted gave informed consent to the use of their teeth for this *in vitro* study. The specimen preparation procedure is illustrated in Fig. 1, where the teeth were stored in distilled water at -20°C until use, and then assigned into seven groups of five teeth each.

The cementum was removed using a carborundum point (HP20, Shofu Inc.) to expose the root dentin surface. The latter was then ground flat with #600 SiC under running water. Roots were obtained by separating them from the crown at the cemento-enamel junction with a low-speed diamond saw (Isomet 1000, Buehler Ltd., Lake Bluff, IL, USA) under water spray coolant. To prevent root dentin dehydration during the restoration procedure, pulp tissue was left *in situ* and the cut surface and root apex were sealed with wax (Utility Wax, GC Corp., Tokyo, Japan).

Three grooves (approximately 0.3 mm wide, 3 mm deep) were prepared on the buccal or lingual dentin surface of each root using a low-speed diamond saw

(Isomet 1000), whereby the distance between each groove was approximately 5 mm. An MMA-based resin (Super-Bond C&B, Sun Medical, Siga, Japan) was used to fill the grooves without any dentin pretreatment. Surfaces of the filled resin and surrounding root dentin were re-polished flat with #600 SiC, such that this flattened surface level was defined as the original undemineralized level. Following which, the specimen surfaces were coated with two layers of nail varnish with the exception of the ground surface.

Root dentin surface coating with adhesives

Four dentin adhesive systems were used in this study: Clearfil SE Bond (SE; Kuraray Medical, Tokyo, Japan), Clearfil Tri-S Bond (TS; Kuraray Medical), G-Bond (GB; GC Corp., Tokyo, Japan), and Hybrid Bond (HB; Sun Medical, Siga, Japan). Clearfil SE Bond was a two-step self-etching adhesive system, while Clearfil Tri-S Bond and G-Bond were all-in-one adhesive systems. Hybrid Bond was also an all-in-one adhesive system, which was developed to be used as a thin coating material for indirect restorations.

Each adhesive system was applied as a coating material on the root dentin surface according to the manufacturers' instructions (Table 1). A single coat of SE, TS, and GB was applied on the root dentin surface, while HB was applied in a single coat (HB-1) or a double coat (HB-2). A halogen light curing unit (Optilux 501, Demetron-Kerr, Danbury, CT, USA) was used to polymerize the adhesive resins in this study. Root dentin surface without resin coating was used as

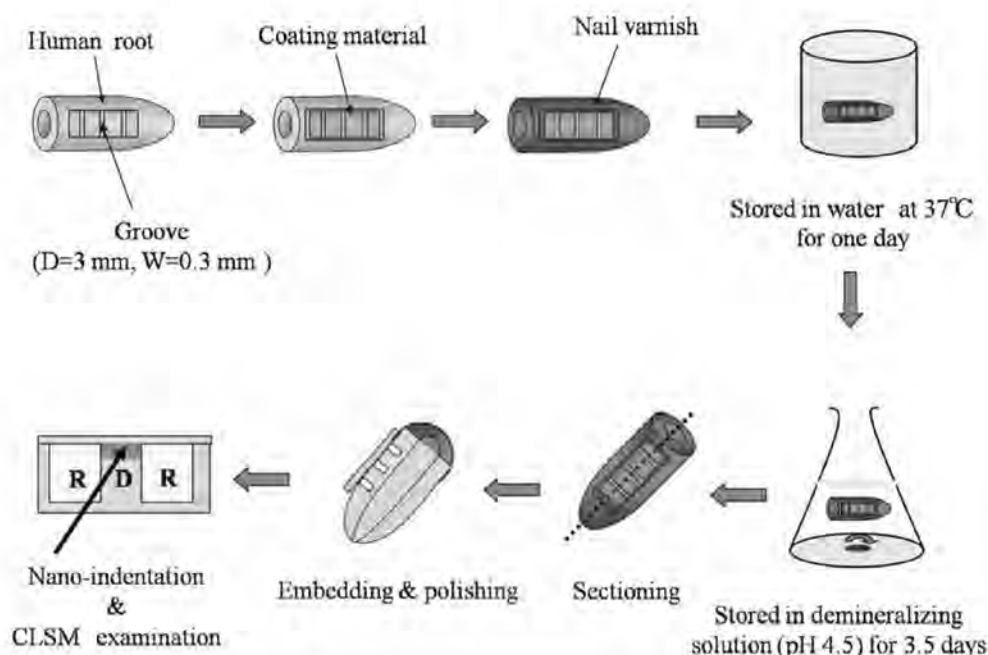


Fig. 1 Specimen preparation procedure.

Table 1 Materials used in this study

Code	Material	Manufacturers	Batch no.	Composition	Application instructions
SE	Clearfil SE Bond	Kuraray Medical, Tokyo Japan	11391	Primer: MDP, HEMA, PI, accelerators, CA, water Adhesive: MDP, HEMA, Bis-GMA, MFM, PI, accelerators, CA, microfiller	Apply the primer on the surface for 20 s. Air-blow and apply the adhesive. Then, air-blow and light-cure for 10 s.
TS	Clearfil Tri-S Bond	Kuraray Medical, Tokyo, Japan.	011142	MDP, HEMA, Bis-GMA, PI, water, ethanol, microfiller	Apply the adhesive on the surface for 20 s. Air-blow for 5 s and light-cure for 10 s.
GB	GC G-BOND	GC, Tokyo, Japan	0503071	4-MET, MDP, PI, water, acetone, microfiller	Apply the adhesive on the surface for 10 s. Air-blow for 10 s and light-cure for 10 s.
HB	Hybrid Bond	Sun Medical, Siga, Japan	LG1 LE1	Cata-brush: p-amine p-sulfonic acid Liquid: 4-META, methacrylate ester, multi-functional acrylate, methacrylate, water, acetone	Apply the adhesive on the surface for 20 s. Air-blow for 10 s and light-cure for 5 s.

Abbreviations: MMA = methyl methacrylate; MDP = 10-methacryloxydecyl dihydrogen phosphate; Bis-GMA = bisphenyl glycidyl methacrylate; 4-MET = 4-methacryloxyethyl trimellitic acid; 4-META = 4-methacryloxyethyl trimellitic anhydride; HEMA = 2-hydroxyethyl methacrylate; MFM = multifunctional methacrylate; PI = photoinitiator; CA = catalyst;

a control.

After storage in distilled water at 37°C for 1 day, the specimens were divided into their individual groups and subjected to the following demineralization challenge: 100 ml of an acid buffer solution (2.2 mmol/L CaCl_2 , 2.2 mmol/L NaH_2PO_4 , and 50 mmol/L acetic acid adjusted to pH 4.5 with NaOH)¹⁷⁻²⁰ for 3.5 days at 37°C, with the exception of five undemineralized control specimens.

Confocal laser scanning microscopic (CLSM) observation

The specimens were removed from the demineralizing solution and thoroughly rinsed under running water for 15 seconds. A cut parallel to the long axis of the root was made using a water-cooled, low-speed diamond saw, resulting in two halves (Fig. 1). Each sectioned specimen was then embedded in an epoxy resin (Epon 815, Nissin EM Co. Ltd., Tokyo, Japan) for 24 hours. The surfaces of the sectioned specimens were polished consecutively with #600, #800, #1,000, and #1,200 SiC, followed by diamond pastes (6, 3, 1, and 0.25 μm ; DP-Paste, Struers A/S, Copenhagen, Denmark). The polished surfaces were cleaned in an ultrasonic bath, and then observed under a CLSM (1LM21, Lasertec, Kanagawa, Japan) at $\times 200$ magnification ($\times 20$ objective lens). The undemineralized control specimens were also treated in



Fig. 2 CLSM observations of depth of demineralized dentin and thickness of coating layer.

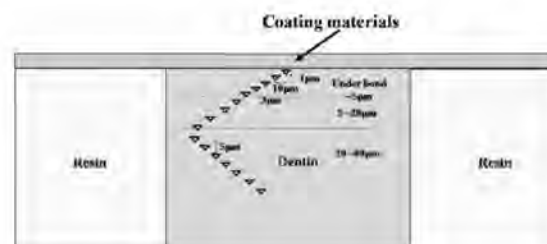


Fig. 3 Indentation locations in the dentin layer to measure the nanohardness of root dentin.

the same manner as described above.

The features evaluated were depth of the demineralized dentin layer beneath the surface coating and the thickness of the resin coating layer (Fig. 2). The depth of demineralized dentin layer was measured from the original undemineralized level — defined by the top surfaces of the two adjacent MMA-based resin blocks at both sides — to the demineralization front. Measurement was performed at three points for each specimen — namely the midpoint of the specimen which was between the two resin blocks, and two locations which were each 5 μm from the midpoint. The depth of demineralization for each specimen was determined by averaging the values obtained at these three measurement points. The thickness of the coating layer for each specimen was determined by averaging the values at the thickest and the thinnest portions of the coating layer in each specimen.

Nanoindentation test

After CLSM observation, an indentation test of the specimens was carried out to confirm the changes in hardness of the coating layers and the root dentin beneath the surface coating after demineralization. The specimens were placed on the stage of a nanoindentation tester (ENT-1100, Elionix, Tokyo, Japan), in which was programmed the locations for indentation. The instrument used for this experiment was a depth-sensing, computer-controlled instrument which had a three-sided pyramidal diamond probe with an included angle of 115° . Load on the indenter was 400 mgf.

Figure 3 illustrates the programmed indentation locations in the dentin layer for both demineralized and undemineralized control specimens. Indentation started at the interface between the surface coating and dentin. Six indentations at 1- μm intervals were made immediately under the coating materials. Five indentations at 3- μm intervals were made in the dentin layer starting from a depth of 5 μm , and 13 indentations at 5- μm intervals from the depth of 20 μm . These measurements were repeated twice for each specimen to yield a total of 48 indentations. This was so because the dentin layer to be assessed comprised two regions amongst three MMA-based resin blocks. However, in the deeper layer from 80 μm to 250 μm ,

indentations were made at 5- μm intervals. After executing the indentations, nanohardness was calculated using the attached computer. After the nanoindentation test, the geometry of the indentation marks produced in the dentin layer was further confirmed using CLSM.

To measure the nanohardness of the surface coating, nanoindentation was performed at the midpoint of the surface coating for SE, TS, GB, and HB-1. For HB-2, indentation was made at 3 μm above the resin-dentin interface in the lower coating layer, which was presumed to be the same indentation location as HB-1.

Statistical analysis

Pertaining to the thickness and nanohardness of the coating materials, the data were compared by one-way analysis of variance (ANOVA) and t-test with Bonferroni correction at 95% level of confidence.

To analyze the nanohardness values in the control groups without surface coating, the data were compared using t-test at 95% level of confidence. Regression analysis was also performed for the nanohardness values of the dentin with/without demineralization from the surface to the depth of 250 μm .

To analyze the nanohardness values of dentin with/without surface coating, dentin from the surface to the depth of 80 μm was divided into three regions — namely depth ranges of 0–5 μm , 5–20 μm , and 20–80 μm . For each region, the data were compared by two-way analysis of variance (ANOVA) and t-test with Bonferroni correction at 95% level of confidence. Two factors evaluated were “surface coating” and “depth of demineralized dentin”. To avoid an accumulation of errors due to multiple comparisons, the significance level was modified by Bonferroni correction at 95% level of confidence. Statistical tests were performed using a computerized statistical program (SPSS for Windows Ver. 11, SPSS Inc., USA).

RESULTS

CLSM observation

The depths of the demineralized dentin layer and the thicknesses of the surface coating materials are summarized in Table 2. Typical CLSM images of

Table 2 Depths of demineralized dentin (μm)

Surface coating	Depth of demineralized dentin (μm)	Thickness of coating material (μm)
Control (none)	215.5 (2.5)	—
SE	0	24.1 (0.8)
TS	0	8.2 (0.7)
GB	0	6.6 (1.1) ^a
HB-1	42.7 (1.1)	5.9 (0.4) ^a
HB-2	0	12.7 (1.4)

n=5; mean (SD)

Same superscript letter means no significant difference ($p>0.05$).

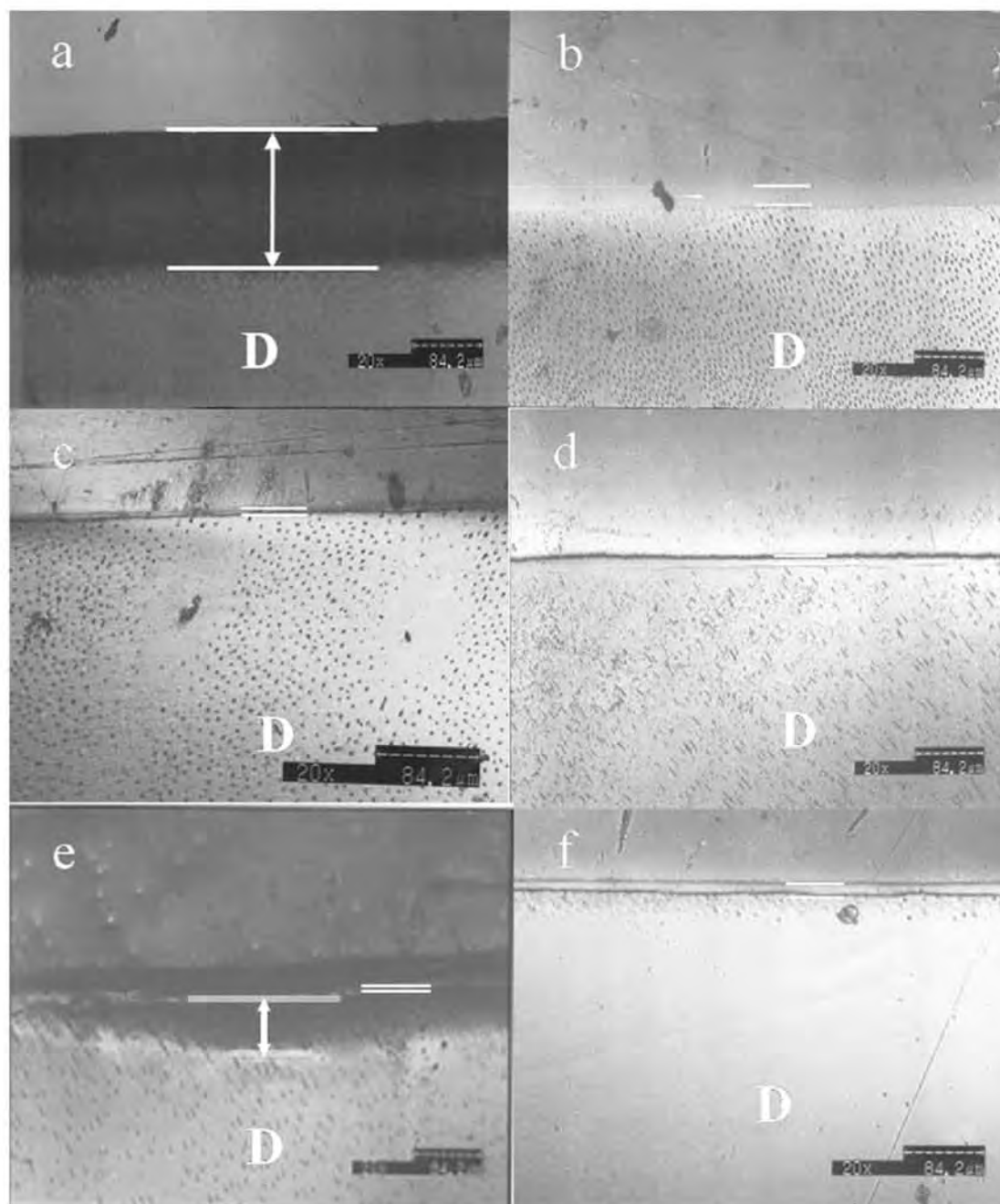


Fig. 4 CLSM images showing the coating layer and the dentin layer underneath ($\times 200$). In all the images, the arrows (\leftrightarrow) indicate the "thickness" of adhesive materials and demineralized dentin.

- a: control (demineralized); thickness of demineralized dentin layer was approximately $215 \mu\text{m}$.
- b: SE; no demineralized dentin layer was observed.
- c: GB; no demineralized dentin layer was observed.
- d: TS; no demineralized dentin layer was observed.
- e: HG-1; thickness of demineralized dentin layer was approximately $42 \mu\text{m}$.
- f: HG-2; no demineralized dentin layer was observed.

dentin with/without surface coating are shown in Fig. 4. Be it with or without surface coating, all the CLSM images showed that no gaps were formed between the surface coating and dentin. Without surface coating, the mean depth of demineralized dentin was $215.5 \mu\text{m}$. With the surface coating of SE, TS, GB, or HB-2, no demineralization of the dentin surface was observed, while there was slight demineralization with HB-1.

Regarding the surface coating, the descending order of thickness was $\text{SE} > \text{HB-2} > \text{TS} > \text{GB} > \text{HB-1}$. However, there was no significant difference in thickness between GB and HB-1 ($p > 0.05$).

Nanohardness

Nanohardness values of both the intact and demineralized dentin are shown in Fig. 5. For intact dentin, nanohardness gradually increased from the top to the deeper layers of dentin and reached a plateau at depths exceeding $50 \mu\text{m}$. With demineralized dentin, nanohardness was significantly lower than that of

intact dentin ($p < 0.05$) and gradually increased from the top surface toward the deeper dentin layers at depths exceeding $200 \mu\text{m}$ ($R^2 = 0.9772$, $p < 0.05$). These nanohardness results were in agreement with the results obtained from CLSM observation.

Figure 6 shows the nanohardness values of root dentin with/without surface coating after demineralization exposure. Two-way ANOVA revealed that the nanohardness of demineralized dentin was influenced by the factors of "surface coating" and "depth of demineralized dentin" ($p < 0.05$). Further, there was significant interaction between surface coating and depth of demineralized dentin ($p < 0.05$). At all measurement depths, demineralized dentin without any surface coating exhibited the lowest nanohardness among all the groups — except at $5 \mu\text{m}$ depth by HB-1 ($p < 0.05$). Up to a depth of $60 \mu\text{m}$, there were no significant differences in nanohardness between the intact dentin and the dentin coated with SE, TS, GB, or HB-2 ($p > 0.05$). At depths exceeding $60 \mu\text{m}$, there

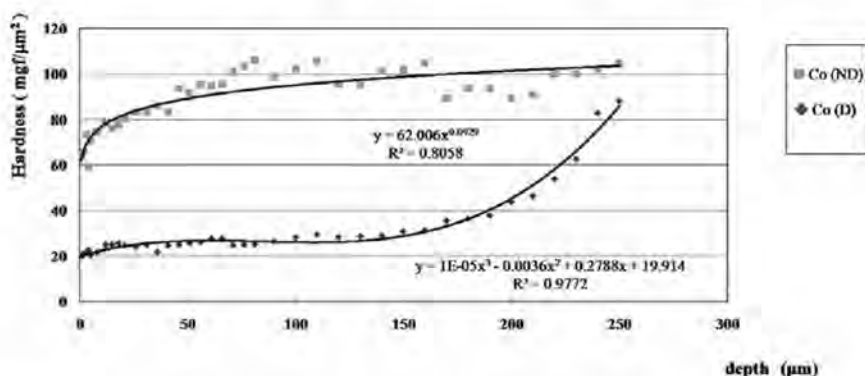


Fig. 5 Nanohardness of root dentin across the longitudinal tooth section. Co (D): control with demineralized dentin; Co (ND): control with no demineralized dentin.

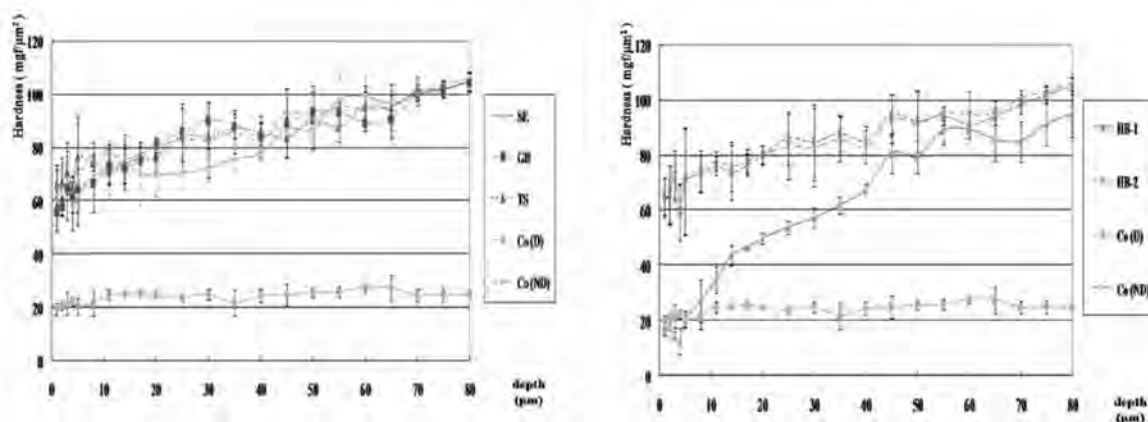


Fig. 6 Nanohardness of root dentin across the longitudinal tooth section with and without surface coating after demineralization exposure.

Table 3 Mean nanohardness values of surface coating materials

Surface coating	Nanohardness
SE	45.6 (2.5)
TS	38.8 (2.1)
GB	41.2 (1.2)
HB-1	31.2 (1.9)
HB-2	44.4 (1.3)

n=5; mean (SD)

Same superscript letter means no significant difference ($p>0.05$)

were no significant differences in nanohardness among all the coated specimens ($p>0.05$). Further, among all the surface-coated specimens, the nanohardness of the specimens coated with HB-1 was consistently the lowest ($p<0.05$).

Table 3 shows the nanohardness values of the surface coating materials. SE was significantly harder than the other adhesive resin materials ($p<0.05$), whereas the lowest hardness value was obtained with HB-1. The hardness of HB-2 was significantly higher than that of HB-1 ($p<0.05$).

DISCUSSION

Cementum is the first layer to be encountered when the root surface is exposed to the oral environment. However, the cementum formation exists as a superficial layer on the root and is easily peeled off by intensive root planing during the treatment of periodontal diseases or by toothbrushing. Therefore, the peel-off vulnerability of the cementum layer causes the underlying dentin to be prone to exposure, hence increasing the risk of root caries formation. For this reason, the chief focus of this study was on surface coating of root dentin with a view to preventing root dentin caries formation.

It has been reported that dentin bonding systems, by providing a strong physical barrier with the formation of a hybrid layer, are well poised to be an effective preventive option against root caries²¹. Indeed, studies have demonstrated that dentin bonding systems could prevent secondary caries formation around and under composite restorations²². In particular, self-etching primer adhesive systems have been shown in scanning electron microscope (SEM) studies that they were capable of creating an acid-base resistant zone adjacent to the hybrid layer after acid-base challenge²³⁻²⁴. The exact mechanism by which the acid-base resistant zone is formed still remained unclear, but these findings strongly suggested that the dentin adjacent to the adhesive-dentin interface is different from intact dentin and that it has a limited

potential to resist an acid attack from secondary caries. Therefore, reinforced dentin which has an ability to prevent primary caries was termed "super dentin"²⁵.

In the present study, four self-etching adhesive systems were employed for root surface coating. Clearfil SE Bond was a two-step self-etching adhesive system and a water- and solvent-free microfilled adhesive. On the contrary, Clearfil Tri-S Bond, G Bond, and Hybrid Bond were one-bottle/all-in-one adhesive systems, which were in essence water- and solvent-based adhesives. As such, manufacturers of the latter adhesives recommended strong air-blowing before curing to remove both water and solvent in the adhesives, resulting in the formation of a thin adhesive layer. Despite the strong air-blowing, residual water and solvent still remained in the adhesive resins. For this reason, cured all-in-one adhesive systems tend to be more permeable than two-step adhesive systems^{26,27}. On permeability, it is noteworthy that self-etching primer adhesive systems contain one or two different monomers in the composition, which demineralize dentin and promote monomer penetration into the underlying dentin. Clearfil SE Bond and Clearfil Tri-S Bond contained MDP²⁸. Hybrid Bond contained 4-META¹², while G-Bond contained MDP and 4-MET²⁹ (hydrated 4-META). However, the effect of these acidic monomers on the permeability of coating materials after curing remained unclear³⁰.

To investigate tooth demineralization *in vivo* and *in vitro*, several methods have been employed, such as hardness test³¹, microradiography³², contact microradiography³³, energy dispersive spectroscopy³⁴, and electron probe microanalysis³⁵. In the present study, the effect of root surface coating on prevention of dentin demineralization was evaluated using CLSM observation and nanoindentation test. CLSM evaluation can be performed under near-normal environmental conditions, resulting in fewer artifacts in the specimens³⁶. Subsequently, the nanoindentation test was conducted to confirm dentin demineralization as changes in dentin hardness reflect the mineral loss in dentin after demineralization. By means of ultra-light loads, the nanoindentation test is a useful method — which has been used in previous studies — to determine the hardness of small areas such as the dentin-enamel junction, inter- and intra-tubular dentin, and the resin-dentin hybrid layer³⁷.

The current *in vitro* study demonstrated that prevention of dentin demineralization using surface coatings was material-dependent. In particular, two factors were identified to strongly influence the prevention of dentin demineralization: composition of the adhesive material and its thickness. With SE, TS, and GB, root dentin demineralization was completely prevented with only one coat of the adhesive materials. With HB, one coat of the adhesive material (HB-1) resulted in slight demineralization, but demineralization was completely prevented when two coats (HB-2) were applied.

HB was developed as a resin coating material to

protect dentin prepared for indirect restorations⁹⁾. It was reported that coating the prepared dentin surface with HB resin reaped favorable benefits: improved dentin bond strength¹²⁾ and minimized microleakage in crown restorations¹⁰⁾. In terms of material composition, the catalytic system of HB was composed of an aromatic amine and p-sulfonic acid salt in the accessory sponge. In terms of results, the current result showed that one coat of HB yielded the lowest hardness among all the adhesives tested; however, hardness increased with two coats of HB. This suggested that the unpolymerized layer of the first adhesive layer might be hardened upon curing the second layer.

In clinical applications, two mandatory prerequisites for coating materials are durability and wear resistance. In a study by Kaneshiro *et al.* on the prevention of root surface demineralization, an experimental coating system was investigated by being applied as an appropriately thick layer³⁶⁾. In the current study, only a thin layer of the adhesive materials was applied on the root dentin surface for surface coating. Therefore, future studies should be undertaken to investigate if differences in surface coating thickness would result in in-tandem differences in the durability and wear resistance of the coating layer.

Another practical consideration for clinical applications is biofilm adherence on the coating material. In a study by Daneshmehr *et al.*, it was reported that a root surface coating using a fluoride-releasing all-in-one adhesive was more effective than a fluoride-free adhesive system in preventing biofilm adherence on the root dentin surface¹⁶⁾. Similarly, Gyo *et al.* also evaluated the surface response of resin composites incorporated with a fluorine polymer in relation to inhibiting cariogenic biofilm adherence⁴⁹⁾. In continuance of this effort against biofilm adherence and formation, a newly developed coating material was investigated using an oral simulator and found to possess self-cleaning properties that inhibited biofilm adherence⁴⁰⁾. In light of these encouraging results and findings, it may be probable that a root surface coating material which embodies these properties would be developed and available in the near future: possesses good durability and wear resistance, and in particular prevents dentin demineralization and root caries formation.

CONCLUSIONS

Within the limitation of this *in vitro* study, it was concluded that root dentin surface coating using all-in-one adhesive systems might be effective in preventing root dentin demineralization. However, the ability to inhibit root dentin demineralization was material-dependent.

ACKNOWLEDGMENTS

This work was supported by the Global Center of

Excellence Program; International Research Center for Molecular Science in Tooth and Bone Diseases, Tokyo Medical and Dental University, Tokyo, Japan, and by a Grant-in-aid from the Japan Society for the Promotion of Science (JSPS) (No. 16390544).

REFERENCES

- 1) Griffin SO, Griffin PM, Swann JL, Zlobin N. Estimating rates of new root caries in older adults. *J Dent Res* 2004; 83: 634-638.
- 2) Imazato S, Ikebe K, Nokubi T, Ebisu S, Walls AW. Prevalence of root caries in a selected population of older adults in Japan. *J Oral Rehabil* 2006; 33: 137-143.
- 3) Wallace MC, Retief DH, Bradley EL. The 48-month increment of root caries in an urban population of older adults participating in a preventive dental program. *J Public Health Dent* 1993; 53: 133-137.
- 4) Billings RJ, Brown LR, Kaster AG. Contemporary treatment strategies for root surface dental caries. *Gerodontology* 1985; 1: 20-27.
- 5) Schaeken MJ, Keltjens HM, Van Der Hoeven JS. Effects of fluoride and chlorhexidine on the microflora of dental root surfaces and progression of root-surface caries. *J Dent Res* 1991; 70: 150-153.
- 6) Sidhu SK, Omata Y, Tanaka T, Koshiro K, Spreafico D, Semeraro S, Mezzanzanica D, Sano H. Bonding characteristics of newly developed all-in-one adhesives. *J Biomed Mater Res Part B Appl Biomater* 2007; 80: 297-303.
- 7) Kitasato T, Nakajima M, Pereira PN, Okuda M, Sonoda H, Otsuki M, Tagami J. Monkey pulpal response and microtensile bond strength beneath a one-application resin bonding system *in vivo*. *J Dent* 2000; 28: 193-198.
- 8) Jayasooriya PR, Pereira PN, Nikaido T, Tagami J. Efficacy of a resin coating on bond strengths of resin cement to dentin. *J Esthet Restor Dent* 2003; 15: 105-113.
- 9) Islam MR, Takada T, Weerasinghe DS, Uzzaman MA, Foxton RM, Nikaido T, Tagami J. Effect of resin coating on adhesion of composite crown restoration. *Dent Mater J* 2006; 25: 272-279.
- 10) dos Santos-Daroz CB, Oliveira MT, Fernando de Góes M, Nikaido T, Tagami J, Giannini M. Bond strength of a resin cement to dentin using the resin coating technique. *Braz Oral Res* 2008; 22: 198-204.
- 11) Ariyoshi M, Nikaido T, Foxton RM, Tagami J. Microtensile bond strengths of composite cores to pulpal floor dentin with resin coating. *Dent Mater J* 2008; 27: 400-407.
- 12) Nikaido T, Nakaoki Y, Ogata M, Foxton RM, Tagami J. The resin-coating technique. Effect of a single-step bonding system on dentin bond strengths. *J Adhes Dent* 2003; 5: 293-300.
- 13) Tagami J, Kitasako Y, Sonoda H. Pulp protection and restoration with adhesive resin. *Jpn Adhes Dent* 1999; 17: 56-60.
- 14) Okuda M, Nikaido T, Maruoka R, Foxton RM, Tagami J. Microtensile bond strengths to cavity floor dentin in indirect composite restorations using resin coating. *J Esthet Restor Dent* 2007; 19: 38-46.
- 15) Kosaka S, Kajihara H, Kurashige H, Tanaka T. Effect of resin coating as a means of preventing marginal leakage beneath full cast crowns. *Dent Mater J* 2005; 24: 117-122.
- 16) Daneshmehr L, Matin K, Nikaido T, Tagami J. Effect of root dentin surface coating with all-in one adhesive materials on biofilm adherence. *J Dent* 2008; 36: 33-41.
- 17) Valk JW, Duijsters PP, ten Cate JM, Davidson CL. Long-term retention and effectiveness of APF and neutral KF fluoridation agents on sound and etched bovine enamel. *Caries Res* 1985; 19: 46-52.

- 18) ten Cate JM, Duijsters PP. Alternating demineralization and remineralization of artificial enamel lesions. *Caries Res* 1982; 16: 201-210.
- 19) ten Cate JM, Duijsters PP. Influence of fluoride in solution on tooth demineralization. I. Chemical data. *Caries Res* 1983; 17: 193-199.
- 20) ten Cate JM, Duijsters PP. Influence of fluoride in solution on tooth demineralization. II. Microradiographic data. *Caries Res* 1983; 17: 513-519.
- 21) Nakabayashi N. Bonding of restorative materials to dentine: the present status in Japan. *Int Dent J* 1985; 35: 145-154.
- 22) Tsuchiya S, Nikaido T, Sonoda H, Foxton RM, Tagami J. Ultrastructure of the dentin-adhesive interface after acid-base challenge. *J Adhes Dent* 2004; 6: 183-190.
- 23) Inoue G, Tsuchiya S, Nikaido T, Foxton RM, Tagami J. Morphological and mechanical characterization of the acid-base resistant zone at the adhesive-dentin interface of intact and caries-affected dentin. *Oper Dent* 2006; 31: 466-472.
- 24) Shinohara MS, Yamauti M, Inoue G, Nikaido T, Tagami J, Giannini M, de Goes MF. Evaluation of antibacterial and fluoride-releasing adhesive system on dentin — microtensile bond strength and acid-base challenge. *Dent Mater J* 2006; 25: 545-552.
- 25) Nikaido T, Weerasinghe DD, Waidyasekera K, Inoue G, Foxton RM, Tagami J. Assessment of the nanostructure of acid-base resistant zone by application of all-in-one adhesive systems: Super dentin formation. *Biomed Mater Eng* 2009; 19: 163-171.
- 26) Ito S, Tay FR, Hashimoto M, Yoshiyama M, Saito T, Brackett WW, Waller JL, Pashley DH. Effects of multiple coatings of two all-in-one adhesives on dentin bonding. *J Adhes Dent* 2005; 7: 133-141.
- 27) Nakaoki Y, Sasakawa W, Horiuchi S, Nagano F, Ikeda T, Tanaka T, Inoue S, Uno S, Sano H, Sidhu SK. Effect of double-application of all-in-one adhesives on dentin bonding. *J Dent* 2005; 33: 765-772.
- 28) Nakabayashi N, Kojima K, Masuhara E. The promotion of adhesion by the infiltration of monomers into tooth substrates. *J Biomed Mater Res* 1982; 16: 265-273.
- 29) Yoshida Y, Nagakane K, Fukuda R, Nakayama Y, Okazaki M, Shintani H, Inoue S, Tagawa Y, Suzuki K, De Munck J, Van Meerbeek B. Comparative study on adhesive performance of functional monomers. *J Dent Res* 2004; 83: 454-458.
- 30) Sauro S, Watson TF, Tay FR, Chersoni S, Breschi L, Bernardi F, Prati C. Water uptake of bonding systems applied on root dentin surfaces: a SEM and confocal microscopic study. *Dent Mater J* 2006; 22: 671-680.
- 31) Pereira PNR, Inokoshi S, Yamada T, Tagami J. Microhardness of *in vitro* caries inhibition zone adjacent to conventional and resin-modified glass ionomer cements. *Dent Mater* 1988; 14: 179-185.
- 32) ten Cate JM. Remineralization of caries lesions extending into dentin. *J Dent Res* 2001; 80: 1407-1411.
- 33) Creanor SL, Awawdeh LA, Saunders WP, Foye RH, Gilmour WH. The effect of a resin-modified glass ionomer restorative material on artificially demineralized dentine caries *in vitro*. *J Dent* 1988; 26: 527-531.
- 34) Akimoto N, Yokoyama G, Ohmori K, Suzuki S, Kohno A, Cox CF. Remineralization across the resin-dentin interface: *in vivo* evaluation with nanoindentation measurements, EDS and SEM. *Quintessence Int* 2001; 32: 561-570.
- 35) Kitasako Y, Nakajima M, Foxton RM, Aoki K, Pereira PNR, Tagami J. Physiological remineralization of artificially demineralized dentin beneath glass ionomer cements with or without bacterial contamination *in vivo*. *Oper Dent* 2003; 28: 274-280.
- 36) Okuda M, Pereira PN, Nikaido T, Tagami J. Evaluation of *in vitro* secondary caries using confocal laser scanning microscope and X-ray analytical microscope. *Am J Dent* 2003; 16: 191-196.
- 37) Urabe I, Nakajima S, Sano H, Tagami J. Physical properties of the dentin-enamel junction region. *Am J Dent* 2000; 13: 129-135.
- 38) Kaneshiro AV, Imazato S, Ebisu S, Tanaka S, Tanaka Y, Sano H. Effects of a self-etching resin coating system to prevent demineralization of root surfaces. *Dent Mater* 2008; 24: 1420-1427.
- 39) Gyo M, Nikaido T, Okada K, Yamauchi J, Tagami J, Matin K. Surface response of fluorine polymer-incorporated resin composites to cariogenic biofilm adherence. *Appl Environ Microbiol* 2008; 74: 1428-1435.
- 40) Okada A, Nikaido T, Ikeda M, Okada K, Yamauchi J, Foxton RM, Sawada H, Tagami J, Matin K. Inhibition of biofilm formation using newly developed coating materials with self-cleaning properties. *Dent Mater J* 2008; 27: 565-572.

M E M O

[illegible]

分子情報伝達学分野

高柳 広

東京医科歯科大学大学院医歯学総合研究科
分子情報伝達学・教授



1) 研究の課題名

研究の題目

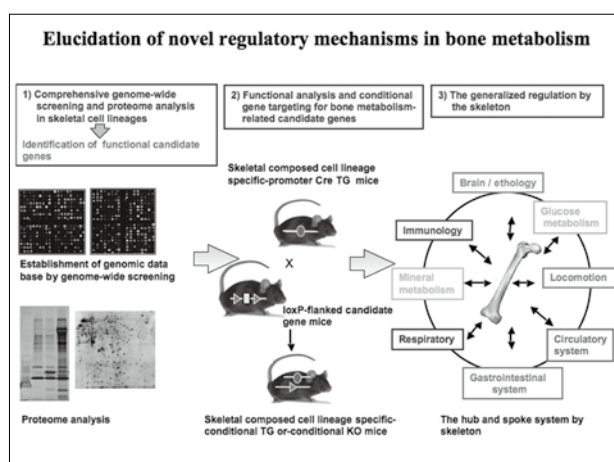
骨代謝制御ネットワークの解明:

Elucidation of novel regulatory mechanisms in bone metabolism

研究内容

骨代謝は、骨自身だけではなく他臓器や組織の恒常性維持にも重要である事が明らかにされている。しかしながら、骨による全身へのマクロな制御機構だけでなく、破骨細胞や骨芽細胞といった骨構成細胞間や細胞内シグナルのようなミクロな制御機構も依然として不明な点が多い。本研究は骨代謝制御ネットワークを、骨を構成する個々の細胞間から最終的に全身の組織、臓器レベルで解明する。この実現の為に、研究内容は3つの項目から構成され、段階的に遂行することになっている。A) 骨構成細胞に発現する遺伝子・タンパク質の網羅解析; B) コンディショナル遺伝子改変マウスを用いた骨代謝制御遺伝子の機能解析; C) 骨による全身性制御機構の解明である。本年度は、昨年度に実施した各細胞の網羅的なトランスクリプトーム解析とプロテオーム解析を基に、標的候補遺伝子群に対するshRNAを用いた遺伝子ノックダウンによる各細胞の分化や機能に与える影響を解析した。その結果、複数の候補分子を同定した。現在、これら候補分子群の機能や役割を生体レベルで解析する為に、次のステップである各候補遺伝子のコンディショナル遺伝子改変マウスを作製しており、いくつかのマウスは既に骨構成細胞特異的にCreを発現するマウスと交配している。マウスが樹立され次第、各候補分子の骨代謝における役割を、生体レベルで解析する。

2)



3) 研究内容の英文要約

- (1) Identification of the negative regulator of osteoclastogenesis: We identified that interferon regulatory factor-8 (IRF-8) negatively regulates the development of osteoclast. Mice deficient in *Irf8* showed severe osteoporosis, owing to increased number of osteoclasts. IRF-8 inhibits the function and expression of NFATc1 (ref. 7) .
- (2) Identification of a unique domain of RANK required for long-term activation of both RANK and ITAM signals during osteoclastogenesis: We identified that highly conserved domain in RANK (HCR) is essential for sustained activation of NF- κ B and PLC- γ 2 leading to NFATc1 activation. HCR recruits an adaptor protein, Gab2, which further associates with PLC- γ 2 in the late phase of RANK and ITAM signaling (ref. 4) .
- (3) Elucidation of new roles of NFATc1 in dendritic cells: We found that *Myd88*^{-/-}*Trif*^{-/-} mice lacking TLR signaling showed normal *Trypanosoma cruzi*-induced Th1 responses. We revealed that NFATc1 plays crucial roles in dendritic cells and mediates TLR-independent innate immune responses in *T. cruzi* infection (ref. 10) .

- (4) Elucidation of roles of IL-6 and PTHrP in osteoclast formation associated with oral cancers: We found that some of oral cancer cell lines produce both PTHrP and IL-6 and induce the expression of Rankl in stromal cells. We revealed that oral squamous cell carcinoma provides a suitable microenvironment for osteoclast formation (ref. 2) .
- (5) Identification of the patients bearing rheumatoid arthritis associated with osteopetrosis: We found the patient who was diagnosed with ADO type II osteopetrosis in his youth and further developed RA in adulthood. In spite of the severe inflammation and rapid progression of cartilage destruction, the progression of bone erosion was slow in this patient. This indicates that osteoclasts are critically involved in bone destruction but that joint inflammation and cartilage destruction in RA are independent of osteoclast function (ref. 11) .

4) 本事業に関連して世界的な研究拠点形成に向けて、以下の点で改善・整備等されたこと

A (研究拠点体制)

骨研究に従事する拠点内研究者のみならず、他分野(特に免疫学)の学外研究者との共同研究を通じて、世界的な成果を発表できた。

B (研究教育環境)

本年度は GCOE AISS 学生の博士号取得に向けた確実な研究指導を行った結果、GCOE AISS 学生は博士号を取得見込みとなった。

C (人材確保)、D (人材育成)

国内外から他分野に精通したポスドク、大学院生、技術補佐員を増員し、学際的環境下での骨代謝研究を推進できる環境を整備した。

E (国際化)

多数の海外での講演、国際学会のorganizeを行った。また、海外からのポスドクが常時研究に参画しており、ラボ内セミナーでの公用語は英語としている。

5) GCOE 事業を推進するに当たって力を入れた点

GCOE シンポジウムや国際学会を活用して、世界の優れた研究者と意見交換を行い、第一線の研究レベルを意識した研究推進を行った。さらに本年度は、GCOE 拠点内にとどまらず東京医科歯科大学や他大学の研究者と広く密接な連携を行うことで、各分野の先端的な発想を自分の研究領域と融合させ、研究成果として結実させることを心がけた。

6) 英文原著論文

1. Takayanagi, H.: New immune connections in osteoclast formation. *Annals of the New York Academy of Sciences*.
2. Kayamori, K., Sakamoto, K., Nakashima, T., Takayanagi, H., Morita, K., Nguyen, S.T., Omura, K., Miki, Y., Akashi, T., Ogata, E. and Yamaguchi, A.: Roles of IL-6 and PTHrP in osteoclast formation associated with oral cancers: The significance of IL-6 synthesized by stromal cells in response to cancer cells. *Am J Pathol*.
3. Takayanagi, H.: The unexpected link between osteoclasts and the immune system. *Adv Exp Med Biol*. 657:61、2010
4. Taguchi Y., Gohda J., Koga T., Takayanagi, H. and Inoue J.: A unique domain in RANK is required for Gab2 and PLC-2 binding to establish osteoclastogenic signals. *Genes Cells*. 14(11):1331、2009
5. Takayanagi, H.: Osteoimmunology and the effects of the immune system on bone. *Nat Rev Rheumatol*. 5(12):667、2009
6. Gober, H. J. and Takayanagi, H.: The interactions and shared mechanisms of T cells and osteoclasts. *Inflammation and Regeneration*. 29 (4):239-248、2009
7. Negishi-Koga, T. and Takayanagi, H.: Ca²⁺-NFATc1 signaling is an essential axis of osteoclast differentiation. *Immunological Reviews*. 231(1):241、2009
8. Zhao, B., Takami, M., Yamada, A., Wang, X., Koga, T., Hu, X., Tamura, T., Ozato, K., Choi, Y., Ivashkiv, L. B., Takayanagi, H. and Kamijo, R.: Interferon Regulatory Factor-8 Regulates Bone Metabolism by Suppressing Osteoclastogenesis. *Nat Med*. 15(9):1066、2009
9. Negishi-Koga, T. and Takayanagi, H.: Mysteries in Ca²⁺ signaling during osteoclast differentiation. *IBMS BoneKEy*. 301-306、2009
10. Kayama, H., Koga, R., Atarashi, K., Okuyama, M., Kimura, T., Mak, T. W., Uematsu, S., Akira, S., Takayanagi, H., Honda, K., Yamamoto, M., and Takeda, K.: NFATc1 mediates Toll-Like receptor-independent innate immune responses during

Trypanosoma cruzi Infection. PLoS Pathogens. 5 (7):e1000514、2009.

11. Kadono, Y., Tanaka, S., Nishino, J., Nishimura, K., Nakamura, I., Miyazaki, T., Takayanagi, H. and Nakamura, K.: Rheumatoid arthritis associated with osteopetrosis. Mod Rheumatol. 19(6):687、2009
12. Nakashima, T. and Takayanagi, H.: Osteoimmunology: crosstalk between the immune and bone systems. J Clin Immunol. 29(5):555、2009
13. Nakashima, T. and Takayanagi, H.: Osteoclasts and the immune systems. J Bone Miner Metab. 27(5):519、2009

7) 著書

©Takayanagi, H.: Cytokine and growth factor regulation of osteoclastogenesis. The Skeletal System. 263-270、2009

高柳 広 :5. 骨・関節 - b. 破骨細胞
炎症・再生医学事典、247 - 250、2009

8) 特許取得、特許申請

発明名称:カテプシン阻害剤を有効成分として含有する Toll 様受容体のシグナル伝達の調整剤 (特願:2007-276937) (PCT/JP2008/069235)

- ①発明者:高柳広、朝霧成拳、平井利武
- ②出願日:2007年10月24日 PCT:2008年10月23日
- ③出願人:国立大学法人 東京医科歯科大学、日本ケミファ株式会社

9) 平成21年度までの自己評価

本年度は、免疫細胞特異的に機能すると考えられていた IRF-8 が、破骨細胞のマスター転写因子である NFATc1 の発現と機能を抑制することによって、破骨細胞の分化を負に制御していることを発見した。また、破骨細胞分化における RANK と ITAM シグナルの長期間の活性化を担う RANK 受容体の重要な領域を同定した。さらに、NFATc1 が、トリパノソーマ原虫感染時に、樹状細胞における Toll 様受容体非依存的な自然免疫応答に重要な役割を果たしている事を明らかにした。以上、本年度は骨と免疫系が密接に関与している事を多数発見でき、5本の論文として発表した。また本年度は、各骨構成細胞の網羅的なトランスクリプトーム解析やプロテ

オーム解析を行った結果、骨代謝系と免疫系に関わる有望な候補遺伝子を複数同定し、それらのコンディショナル遺伝子改変マウスを作製した。今後、これらの遺伝子改変マウスの解析を進め、骨と免疫の相互作用の解明に取り組む予定である。

10) 和文原著論文

高柳広:A Special Edition 骨・軟骨疾患の分子医学 ③ Osteoimmunology の現状と展望 Bio Clinica Vol. 25 No.1 JAN.2010

高柳広:<企画>特集「骨免疫学II」
THE BONE 23 (4) (10月号)、2009

高柳広:Overview - Osteoimmunology-
THE BONE 23 (4) (10月号) : 25-29、2009

岡本一男、高柳広:自己免疫性関節炎とカテプシン K の関連を探索
分子リウマチ治療 2 (4) (11月号) : 13-18、2009

中島友紀、高柳広:骨破壊制御の新たなアプローチ
医薬ジャーナル 45 (10) (10月号) : 87-92、2009

高柳広:破骨細胞分化決定の分子メカニズムと骨免疫学
臨床血液 50 (6) : 447-452、2009

高柳広 :5. 骨・関節 - b. 破骨細胞
炎症・再生医学事典、247-250、2009

高柳広:骨免疫学のアップデート - 臨床への展開 -
日本臨床 67 (5) : 1031-1037、2009

高柳広:<企画>骨免疫制御のメカニズム
実験医学 27 (6) (4月号)、2009

高柳広:概論 骨と免疫の不可分な関係に立脚した新たな生体理解
実験医学 27 (6) (4月号) :846-851、2009

篠原正浩、高柳広:破骨細胞分化を司る免疫制御分子ネットワーク
実験医学 27 (6) (4月号) :852-859、2009

11) 学会発表 (英文)

Authors: Hans-Jürgen Guber, Takako Koga, Hiroshi Takayanagi

Title: Fc γ Receptors Control Bone Homeostasis by Regulating Costimulation Signals in Osteoclast Lineage Cells.

27th Annual Meeting of the Japanese Society for Bone and Mineral Research

Oral Presentation

Osaka Japan, 2009 July 23-25.

Authors: Tomoki Nakashima, Mikihiro Hayashi, Hiroshi Takayanagi

Title: Identification of novel genes regulated by NFATc1 in osteoclastogenesis.

The 26th Naito Conference on "Osteobiology"

Poster Presentation

Awaji Japan, 2009 November 5.

Authors: Masatsugu Oh-hora, Hiroshi Takayanagi, Anjana Rao.

Title: Different Ca²⁺ sensitivity of the development of T-lineage cells

Keystone Symposia

Poster Presentation

Colorado USA, 2010 February 27 - March 4

12) 学会発表 (和文)

発表者: 中島友紀

演題名: 骨の恒常性を司る骨リモデリングシステムの解明

学会名: 第3回 Skeletal Research Meeting

京都、平成21年6月27日

発表者: 岡本一男

演題名: 骨の恒常性を司る骨リモデリングシステムの解明

学会名: 第27回長崎骨粗鬆症研究会

大阪、平成21年10月6日

発表者: 岡本一男

演題名: 転写因子 I κ B ζ による Th17 細胞分化制御

学会名: 第5回骨免疫ワークショップ

東京、平成21年11月27日

発表者: 本郷 敏雄

演題名: 血清とヒト唾液中における歯科用モノマーの分解

学会名: 第54回日本歯科理工学会学術講演会

鹿児島、平成21年10月2日

13) 受賞

財団法人 井上科学振興財団 井上学術賞 2009.2.4

日本骨代謝学会 学術賞 2009.7.24

14) 外部資金の獲得状況

(独) 科学技術振興機構 (JST)

戦略的創造研究推進事業 (ERATO 型研究)

平成21年度発足

研究題目: ERATO 高柳オステオネットワークプロジェクト

代表: 高柳 広

期間: 平成21年度～平成26年度

研究費総額: 150,000 万円 (概算)

文部科学省科学研究費補助金 学術創成研究費

研究題目: 骨免疫学の創成

代表: 高柳 広

期間: 平成17年度～平成21年度

研究費総額: 70,343 万円

文部科学省科学研究費補助金 若手研究 (A)

研究題目: 骨リモデリングの開始と制御機構の解明

代表: 中島 友紀

期間: 平成19年度～平成21年度

研究費総額: 2,407 万円

文部科学省科学研究費補助金 若手研究 (A)

研究題目: 骨破壊性疾患における非ヒストンタンパク質のメチル化修飾の意義

代表: 古賀 貴子

期間: 平成20年度～平成22年度

研究費総額: 2,452 万円

文部科学省科学研究費補助金 挑戦的萌芽研究

研究題目: 炎症性破骨細胞の同定とその特異的プロテアーゼに着目した骨破壊防御法の開発

代表: 高柳 広

期間: 平成19年度～平成21年度

研究費総額: 320 万円

文部科学省科学研究費補助金 挑戦的萌芽研究

研究題目: 骨代謝を制御するカップリング因子の同定と機能解析

代表: 中島 友紀

期間:平成21年度～平成23年度

研究費総額:320万円

文部科学省科学研究費補助金 挑戦的萌芽研究

研究題目:軸策ガイダンス、セマフォリン分子による
硬組織代謝細胞間制御

代表:古賀 貴子

期間:平成21年度～平成22年度

研究費総額:310万円

文部科学省科学研究費補助金 挑戦的萌芽研究

研究題目:破骨細胞分化に関与するリン酸化シグナル
伝達機構のプロテオーム解析

代表:春宮 覚

期間:平成21年度～平成22年度

研究費総額:310万円

文部科学省科学研究費補助金 若手研究(スタートアップ)

研究題目:加齢に伴う骨芽細胞・脂肪細胞分化スイッチ
における転写因子Mafの役割代表:西川 恵三

期間:平成20年度～平成21年度

研究費総額:330万円

文部科学省科学研究費補助金 若手研究(スタートアップ)

研究題目:カルシウム流入制御機構を介した自己免疫
疾患発症機序の理解と解析

代表:大洞 将嗣

期間:平成21年度～平成22年度

研究費総額:236万円

文部科学省科学研究費補助金 若手研究(スタートアップ)

研究題目:制御性T細胞を用いた関節リウマチ治療法
の開発

代表:小松 紀子

期間:平成21年度～平成22年度

研究費総額:236万円

文部科学省科学研究費補助金 特別研究員奨励費

研究題目:性ホルモンを介した骨代謝制御における制
御性T細胞の意義

代表:高柳 広

期間:平成20年度～平成22年度

研究費総額:180万円

文部科学省科学研究費補助金 特別研究員奨励費

研究題目:p62結合蛋白KFB14の破骨細胞分化におけ
る役割の研究

代表:高柳 広

期間:平成21年度～平成22年度

研究費総額:200万円

文部科学省科学研究費補助金 基盤研究(B)

研究題目:生理的骨改造および炎症性骨破壊における
転写因子IRF-8の機能解析

代表:高見 正道(分担:高柳 広)

期間:平成20年度～平成22年度

研究費総額:40万円

横山臨床薬理研究助成基金

研究題目:硬組織再構築制御による骨破壊性疾患治療
薬の開発

代表:高柳 広

期間:平成19年度～平成21年度

研究費総額:1,500万円

金原一郎記念医学医療振興財団

第24回基礎医学医療研究助成金

研究題目:破骨細胞分化におけるPI3K下流シグナル
の解明

代表:篠原 正浩

期間:平成21年度

研究費総額:50万円

(財)内藤記念科学振興財団研究助成金

第41回(2009年度)内藤記念科学奨励費

研究題目:破骨細胞におけるイノシトールリン脂質シ
グナルの解明

代表:篠原 正浩

期間:平成21年度

研究費総額:300万円

(財)武田科学振興財団

研究題目:T細胞におけるカルシウム流入機構を介し
た自己免疫疾患発症機序の理解と解析

代表:大洞 将嗣

期間:平成21年度～平成22年度

研究費総額:300万円

(財) 上原記念生命科学財団 研究奨励金

研究題目:骨構成細胞が産生する細胞外分泌因子の同定と生理機能の解明

代表:篠原 正浩

期間:平成21年度

研究費総額:200万円

15) 特別講演、招待講演

14th International Congress of Endocrinology ICE2010
JES-Sponsored Symposia、

Mechanism of osteoclast differentiation 2010.3.29、京都

第9回 日本再生医療学会総会 ランチョンセミナー
骨免疫学とオステオネットワーク、2010.3.18、広島

技術情報協会 セミナー (確定)

骨代謝制御の分子メカニズムと新規創薬標的、
2010.1.22、東京

第32回日本分子生物学会 リウマチサイトカイン研究会、
リウマチにおける新たなサイトカインについて、
2009.12.11、横浜

Rheumatology Association, R.O.C. (Taiwan)
Bone destruction in arthritis and osteoimmunology,
2009.12.6, Yilan, Taiwan.

第37回日本臨床免疫学会総会
Osteoimmunologyの最先端、2009.11.14、東京

第29回コスモ・バイオ バイオプロダクトセミナー
骨免疫学研究の現状・課題・展望、2009.10.24、東京、
2009.11.7、大阪

第26回内藤コンファレンス
RANK Ligand and Osteoimmunology、2009.11.7、淡路

ACR/ARHP Scientific Meeting
Molecular Mechanisms of Monocyte Lineage
Commitment and Function、2009.10.18,
Philadelphia, U.S.A.

第34回東京都リウマチ膠原病懇話会
関節リウマチにおける骨破壊とRANKL、2009.10.3、東京

Beckman Research Institute of the City of Hope,
Division of Hematopoietic Stem Cell and
Leukemia Research
Osteoimmunology – interaction between bone and the
immune system, 2009.9.9, Los Angeles, U.S.A.

第27回日本骨代謝学会
破骨細胞と骨免疫学、2009.7.24、大阪

The Bones & Teeth Gordon Research Conference
New immune regulator of bone, 2009.7.15, Maine, U.S.A.

The 9th World Congress on Inflammation
Anti-Osteoclast Therapy for Bone Destruction in
Inflammation, 2009.7.10, Tokyo

The 9th World Congress on Inflammation
TNF- α and Bone Destruction in Arthritis - from the
Viewpoint of Basic Research - 2009.7.8, Tokyo

The 3rd Global COE International Symposium, Tokyo
Medical and Dental University,
Immune Regulation of Osteoclastogenesis, 2009.6.10,
Tokyo

第82回日本整形外科学会学術集会
関節リウマチの骨破壊とIL-6、2009.5.17、福岡

The 66th KSBMB Annual Meeting
RANKL Signaling and Osteoimmunology, 2009.5.13,
World Trade Center, Seoul, Korea

The 3rd New York Skeletal Biology and Medicine
Conference
New Immune Connections During Osteoclastogenesis,
2009.4.30 Mount Sinai School of Medicine,
New York, U.S.A.

第53回日本リウマチ学会総会・学術集会、第18回国際
リウマチシンポジウム
関節リウマチ骨破壊への新たなアプローチ、2009.4.23、
東京

16) 教室、分野や講座の准教授、講師、助教、特別研究員、ポスドク、指導を受けた大学院生の名前 (AISSには○印) のリスト

准教授	本郷敏雄
特任准教授	大洞将嗣
助 教	篠原正浩
	中島友紀
	春宮覚
特任助教	古賀貴子
特別研究員	Ling Wang
	Feng Haotian
ポスドク	西川恵三
	Hans-Juergen Gober
	小松紀子
	福永鷹信
	姚皇治
指導を受けた大学院生	○林幹人、○Erik Idrus、○武智香織、 ○Abdul Alim Al-Bari

17) GCOE 活動についての感想、コメント、改善を望む点など

シャペロン教官以外にも、ポスドク研究者の配置を増員できることが望ましい。病理組織作成と解析、ノックアウトマウス作成、トランスクリプトーム・プロテオーム解析、セルソーティング等にあたって、専門の技術補佐員の増員、あるいは共同研究施設と専属の技術員による管理・支援があると有益である。

Nat Rev Rheumatology 5, 667-676 December 2009 ---

Review

(Correction)

Please note that there is a mistake in the PDF file.

In Table 1, Th1 associated cytokines (IL12, IL18, GMCSF) are indicated with

Stimulation, but this is a mistake in the production process.

Th1 associated cytokines (IL12, IL18, GMCSF) should be indicated with Inhibition.

Interferon regulatory factor-8 regulates bone metabolism by suppressing osteoclastogenesis

Baohong Zhao^{1,2}, Masamichi Takami¹, Atsushi Yamada¹, Xiaogu Wang¹, Takako Koga^{3,4}, Xiaoyu Hu^{2,5}, Tomohiko Tamura⁶, Keiko Ozato⁶, Yongwon Choi⁷, Lionel B Ivashkiv^{2,5,8}, Hiroshi Takayanagi^{3,4} & Ryutaro Kamijo¹

Bone metabolism results from a balance between osteoclast-driven bone resorption and osteoblast-mediated bone formation. Diseases such as periodontitis and rheumatoid arthritis are characterized by increased bone destruction due to enhanced osteoclastogenesis^{1,2}. Here we report that interferon regulatory factor-8 (IRF-8), a transcription factor expressed in immune cells, is a key regulatory molecule for osteoclastogenesis. IRF-8 expression in osteoclast precursors was downregulated during the initial phase of osteoclast differentiation induced by receptor activator of nuclear factor- κ B ligand (RANKL), which is encoded by the *Tnfrsf11* gene. Mice deficient in *Irf8* showed severe osteoporosis, owing to increased numbers of osteoclasts, and also showed enhanced bone destruction after lipopolysaccharide (LPS) administration. *Irf8*^{-/-} osteoclast precursors underwent increased osteoclastogenesis in response to RANKL and tumor necrosis factor- α (TNF- α). IRF-8 suppressed osteoclastogenesis by inhibiting the function and expression of nuclear factor of activated T cells c1 (NFATc1). Our results show that IRF-8 inhibits osteoclast formation under physiological and pathological conditions and suggest a model where downregulation of inhibitory factors such as IRF-8 contributes to RANKL-mediated osteoclastogenesis.

Osteoclasts are multinucleated giant cells derived from the monocyte and macrophage lineage. Their differentiation is triggered by RANKL in the presence of macrophage colony-stimulating factor (M-CSF, encoded by the *Csf1* gene), which is produced by osteoblasts^{1,2}. RANKL induces intracellular signals via its receptor RANK, and it upregulates the expression of various genes, such as *Nfatc1*, *Fos*, *Oscar*, *Ctsk* and *Calcr*, which encode NFATc1, c-Fos, osteoclast-associated receptor (OSCAR), cathepsin K and calcitonin receptor, respectively³⁻⁵. Numerous studies have focused on these upregulated genes and their roles in osteoclastogenesis. However, the expression of various genes is also simultaneously downregulated during osteoclastogenesis⁶. The biological role of the downregulated

expression of these genes after RANK activation, has not been fully elucidated.

To identify genes that show reduced expression in response to RANK signaling, we performed a genome-wide screen of messenger RNAs from osteoclast precursors and osteoclasts using a DNA microarray technique (data deposited in the Gene Expression Omnibus). Among the identified genes, we found that expression of the transcription factor *Irf8* was reduced to one-quarter during the initial phase of osteoclastogenesis triggered by RANKL. IRF-8 is known to be specifically expressed in immune cells, including monocytes and macrophages, B lymphocytes and activated T lymphocytes⁷⁻⁹. It is a member of the IRF family and has been shown to regulate myeloid cell development by interacting with Ets family transcription factors^{10,11}. Hence, *Irf8*^{-/-} mice show a large number of myeloid progenitors, defects in macrophage function including impaired interleukin-12 production, developmental defects in CD8 α ⁺ and plasmacytoid dendritic cells, and systemic expansion of the granulocyte population, which frequently leads to a fatal blast crisis¹²⁻¹⁴.

Using RT-PCR and immunoblot analysis, we detected *Irf8* expression in bone marrow-derived macrophages (BMMs) and spleen-derived macrophages prepared from wild-type mice, which are capable of differentiating into osteoclasts (Fig. 1a,b). As previously shown³, *Nfatc1* was modestly expressed at a basal level in unstimulated BMMs, and *Nfatc1* expression was strongly induced after RANKL stimulation (Fig. 1b); robust induction of NFATc1 by RANKL is a necessary and pivotal step for osteoclast differentiation characterized by enhanced expression of osteoclast marker genes such as *Oscar*, *Itgb3* (encoding integrin β_3 protein) and *Ctsk* (ref. 3). In contrast, *Irf8* expression was lower after RANKL stimulation (Fig. 1a,b), resulting in substantially lower nuclear Irf-8 protein 24 h after RANKL addition (Fig. 1b). We hypothesized that IRF-8 downregulation may be required for osteoclast differentiation and that IRF-8 may inhibit early stages of osteoclastogenesis.

To examine the role of IRF-8 in osteoclastogenesis, we constructed a retroviral vector, pMX-Irf8-IRES-EGFP, which was engineered to express both *Irf8* and EGFP downstream of an internal ribosomal

¹Department of Biochemistry, School of Dentistry, Showa University, Shinagawa, Tokyo, Japan. ²Arthritis and Tissue Degeneration Program, Hospital for Special Surgery, New York, New York, USA. ³Department of Cell Signaling, Graduate School, Tokyo Medical and Dental University, Bunkyo-ku, Tokyo, Japan. ⁴Global Center of Excellence Program, International Research Center for Molecular Science in Tooth and Bone Diseases, Tokyo, Japan. ⁵Department of Medicine, Weill Cornell Medical College, New York, New York, USA. ⁶Laboratory of Molecular Growth Regulation, National Institute of Child Health and Human Development, National Institutes of Health, Bethesda, Maryland, USA. ⁷Department of Pathology and Laboratory Medicine, University of Pennsylvania School of Medicine, Philadelphia, Pennsylvania, USA. ⁸Graduate Program in Immunology and Microbial Pathogenesis, Weill Graduate School of Medical Sciences of Cornell University, New York, New York, USA. Correspondence should be addressed to M.T. (takami@dent.showa-u.ac.jp).

Received 25 February 2008; accepted 16 June 2009; published online 30 August 2009; doi:10.1038/nm.2007

LETTERS

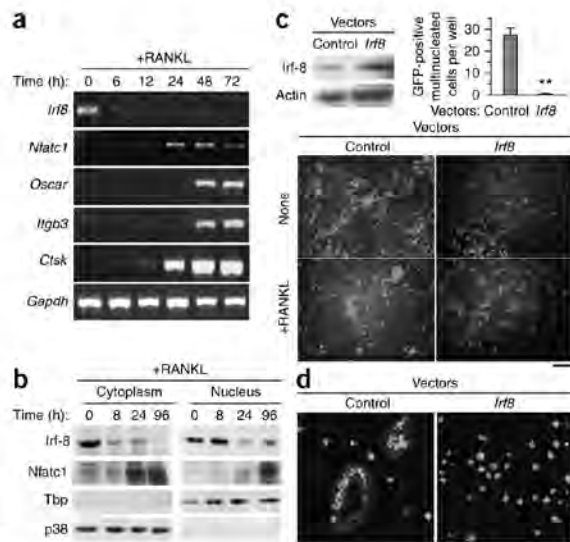


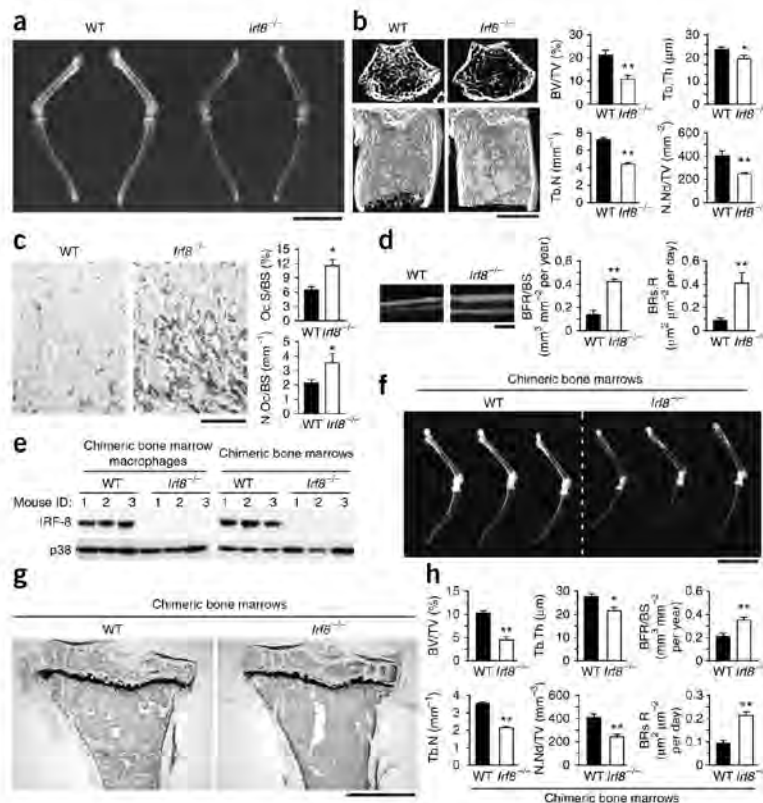
Figure 1 IRF-8 inhibits osteoclastogenesis in BMMs stimulated with M-CSF and RANKL. (a) mRNA expression of *Irfb*, *Nfatc1*, *Oscar*, *Itgb3*, *Ctsk* and glyceraldehyde-3-phosphate dehydrogenase (*Gapdh*) in BMMs 0, 6, 12, 24, 48 and 72 h after M-CSF (50 ng ml⁻¹) and RANKL (150 ng ml⁻¹) stimulation. (b) Immunoblot analysis of Irfb and Nfatc1 expression in cytoplasmic and nuclear fractions of BMMs obtained 0, 8, 24 and 96 h after stimulation with M-CSF and RANKL. Expression levels of TATA-binding protein (Tbp) and p38 were measured as loading controls for nuclear and cytoplasmic fractions, respectively. (c) Inhibition of GFP-positive multinucleated cell (osteoclast) formation due to retrovirus-mediated overexpression of *Irfb* in BMMs. Top left, immunoblot showing overexpression of Irfb protein in BMMs. Top right, quantification of GFP-positive multinucleated cell counts. Bottom, fluorescent images of GFP-positive multinucleated cells (osteoclasts) appeared as green giant cells. Control, pMX-IRES-EGFP; *Irfb*, pMX-Irf8-IRES-EGFP. *n* = 4, ***P* < 0.01. Scale bar, 50 μm. Data are means ± s.d. (d) Fluorescent images of FITC-conjugated zymosan bioparticles (green) to show phagocytic activity, rhodamine-conjugated phalloidin (red) staining of F-actin and DAPI (blue) staining of nuclei. BMMs were transduced with pMX-puro (control) or pMX-Irf8-puro (*Irfb*) and stimulated with M-CSF and RANKL for 3 d. Yellow fluorescent signals denotes colocalization of zymosan and actin. Scale bar, 100 μm.

entry site (IRES). We transduced wild-type osteoclast precursors with retroviral particles encoding *Irfb* or control viral particles that lacked the *Irfb* sequence (pMX-IRES-EGFP). *Irfb*-overexpressing precursors failed to differentiate into osteoclasts in response to RANKL stimulation (Fig. 1c). Furthermore, these cells were able to phagocytose

zymosan particles, whereas multinucleated osteoclasts failed to do so (Fig. 1d). These results suggest that IRF-8 inhibits osteoclastogenesis from precursor cells, which instead retain the characteristics of phagocytic macrophages.

Next, we analyzed the *Irfb*^{-/-} mice for abnormal bone phenotypes. Radiographic and microcomputed tomographic analyses showed that these mice had severe osteoporosis accompanied by markedly lower trabecular bone volume, number, and thickness, as well as a smaller

Figure 2 *Irfb*^{-/-} mice show severe osteoporosis due to enhanced osteoclast formation. (a) Radiographic analysis of the femur and tibia in wild-type and *Irfb*^{-/-} mice. Scale bar, 1 cm. (b) Microcomputed tomography of the femurs of 8-week-old wild-type and *Irfb*^{-/-} mice (left), and bone morphometric analysis of femurs isolated from 8-week-old mice (right). BV/TV, bone volume per tissue volume; Tb.Th, trabecular bone thickness; Tb.N, trabecular number; N.Nd/TV, number of nodules per tissue volume, *n* = 6, ***P* < 0.01 and **P* < 0.05. Scale bar, 500 μm. (c) Histology of femurs from 8-week-old mice in which osteoclasts were stained by TRAP (left), and histomorphometric analysis of tibias from 8-week-old mice (right). Oc.S/BS, osteoclast surface per bone surface; N.Oc/BS, number of osteoclasts per bone surface, *n* = 5, **P* < 0.05. Scale bar, 100 μm. (d) Histological photographs of bone formation that show tetracycline-calcein double labeling, which were administered with an interval of 72 h (left), and histomorphometric analysis of the bone formation rate and bone resorption rate in 8-week-old mice (right). BFR/BS, bone formation rate per bone surface; BRs.R, bone resorption rate. *n* = 4, ***P* < 0.01. Scale bar, 20 μm. (e) Analysis of Irfb protein levels in M-CSF-induced bone marrow macrophages (left) or bone marrow (right) from recipient chimeric mice. (f) Soft X-ray photographs of long bones (tibias and femurs) isolated from chimeric mice. Scale bar, 1 cm. (g) Photographs of proximal end of tibias isolated from chimeric mice (Villanueva bone staining). Scale bar, 500 μm. (h) Bone morphometric analysis of femurs isolated from chimeric mice. Representative data from one of two independent experiments is shown (*n* = 3 (WT) and 3 (*Irfb*^{-/-})) in each experiment. *n* = 3, ***P* < 0.01; **P* < 0.05. Error bars represent means ± s.d.



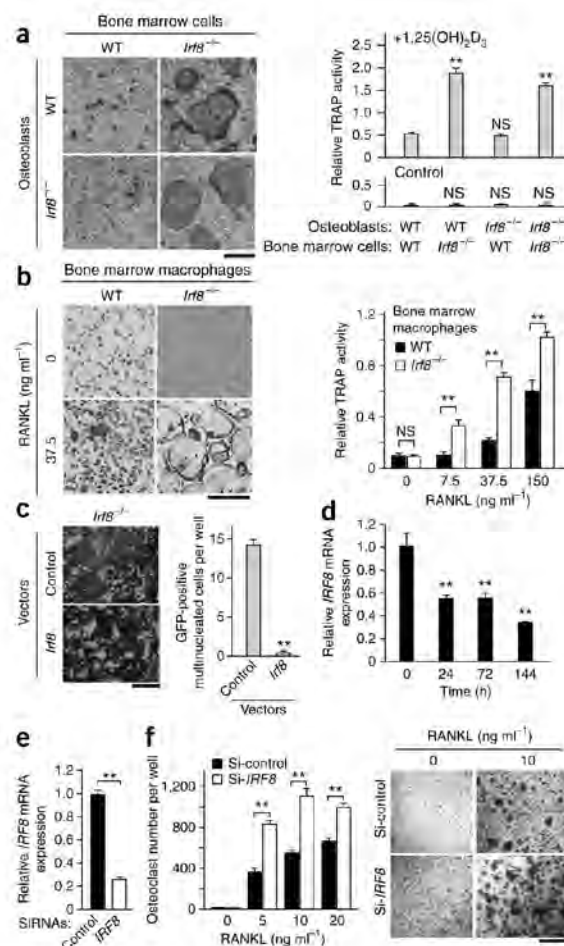
LETTERS

Figure 3 IRF-8 deficiency or RNA interference-mediated silencing in osteoclast precursors leads to enhanced osteoclast formation. (a) TRAP staining (left) and TRAP activity (right) of cultures of primary calvarial osteoblasts and bone marrow cells obtained from wild-type and *Irf8*^{-/-} mice cocultured in the presence of 10^{-8} M $1,25(\text{OH})_2\text{D}_3$ and 10^{-6} M prostaglandin E_2 (inducers of RANKL expression in osteoblasts) for 6 d. $n = 4$; $**P < 0.01$; NS, no statistical difference. Scale bar, 100 μm . (b) TRAP staining (left) and TRAP activity (right) of osteoclast formation induced by 50 ng ml^{-1} M-CSF and the indicated doses of RANKL in BMM cultures. Scale bar, 100 μm . (c) Fluorescent images of *Irf8*^{-/-} macrophages transduced with the vectors pMX-IRES-EGFP (Control) or pMX-Irf8-IRES-EGFP (*Irf8*) followed by the stimulation with 150 ng ml^{-1} RANKL for 3 d (left). GFP-positive multinucleated cells were counted as osteoclasts (right). $n = 4$; $**P < 0.01$, NS, no statistical difference. Scale bar, 100 μm . (d) Kinetics of *IRF8* mRNA expression during human osteoclastogenesis induced by 40 ng ml^{-1} RANKL at the indicated time points. $n = 4$; $**P < 0.01$. (e) Quantitative real-time PCR analysis of *IRF8* mRNA in human CD14-positive monocytic cells transfected with human *IRF8*-specific short interfering RNAs (*IRF8*) or nontargeting control siRNAs (Control), cultured for 2 d in the presence of 20 ng ml^{-1} M-CSF. $n = 4$; $**P < 0.01$. (f) Osteoclastogenesis of human monocytic cells transfected with si-*IRF8* or nontargeting control siRNAs (Control) in the presence of RANKL for 6 d. Number of TRAP-positive multinucleated cells was counted as osteoclasts (left). TRAP-positive cells appear red in the photograph (right). Representative data from one of three donors is shown; similar results were obtained using a distinct *IRF8*-specific siRNA in an additional three experiments. $n = 4$; $**P < 0.01$; NS, no statistical difference. Scale bar, 200 μm . Error bars represent means \pm s.d.

number of bone nodules compared to wild-type mice (Fig. 2a,b). Histomorphometric analysis also revealed reduced bone mass in the *Irf8*^{-/-} mice (data not shown). Notably, we observed higher osteoclast numbers and larger osteoclast surface areas in these mice (Fig. 2c). There were no significant differences between wild-type and *Irf8*^{-/-} mice in the serum concentration of osteoprotegerin, a decoy RANKL receptor that inhibits osteoclastogenesis, or in RANKL levels in primary cultured osteoblasts (Supplementary Fig. 1). Moreover, we observed a higher rate of bone formation accompanying the accelerated bone resorption rate in the *Irf8*^{-/-} mice, suggesting that their osteoporosis was caused by enhanced bone turnover and remodeling (Fig. 2d). Together, these observations indicate that IRF-8 has a suppressive role in osteoclastogenesis during *in vivo* bone remodeling.

To address whether the bone phenotype could be explained by *Irf8* deficiency in osteoclast precursors or whether *Irf8* deficiency in osteoblasts or bone marrow stromal cells could play a part, we established chimeric mouse models in which we transplanted either wild-type or *Irf8*^{-/-} littermate bone marrow into lethally irradiated wild-type recipients. Consistent with the results in *Irf8*-knockout mice, *Irf8*^{-/-} bone marrow chimeric mice showed severe, high-turnover osteoporosis (Fig. 2e-h). Further, IRF-8 is mainly expressed in hematopoietic cells⁷⁻⁹ and, indeed, we did not detect *Irf8* expression in primary calvarial osteoblasts (data not shown). Lastly, primary *Irf8*^{-/-} osteoblast differentiation and matrix calcification were not affected compared to wild-type cells (Supplementary Fig. 2). Thus, the osteoporosis resulted from enhanced osteoclastogenesis, which is a cell autonomous consequence of *Irf8* deficiency in osteoclast precursors but not osteoblasts.

On the basis of these results, we examined the differentiation potential of osteoclast precursors obtained from *Irf8*^{-/-} mice. When we cultured wild-type or *Irf8*^{-/-} osteoclast precursors with wild-type or *Irf8*^{-/-} primary osteoblasts in the presence of active vitamin D_3 (an inducer of RANKL expression in osteoblasts), a larger number of osteoclasts formed from the *Irf8*^{-/-} precursors than from the wild-type cells, independent of whether the osteoblasts were from *Irf8*^{-/-} or wild-type mice (Fig. 3a). These data further support the notion that there is no difference between wild-type and *Irf8*^{-/-} osteoblasts in

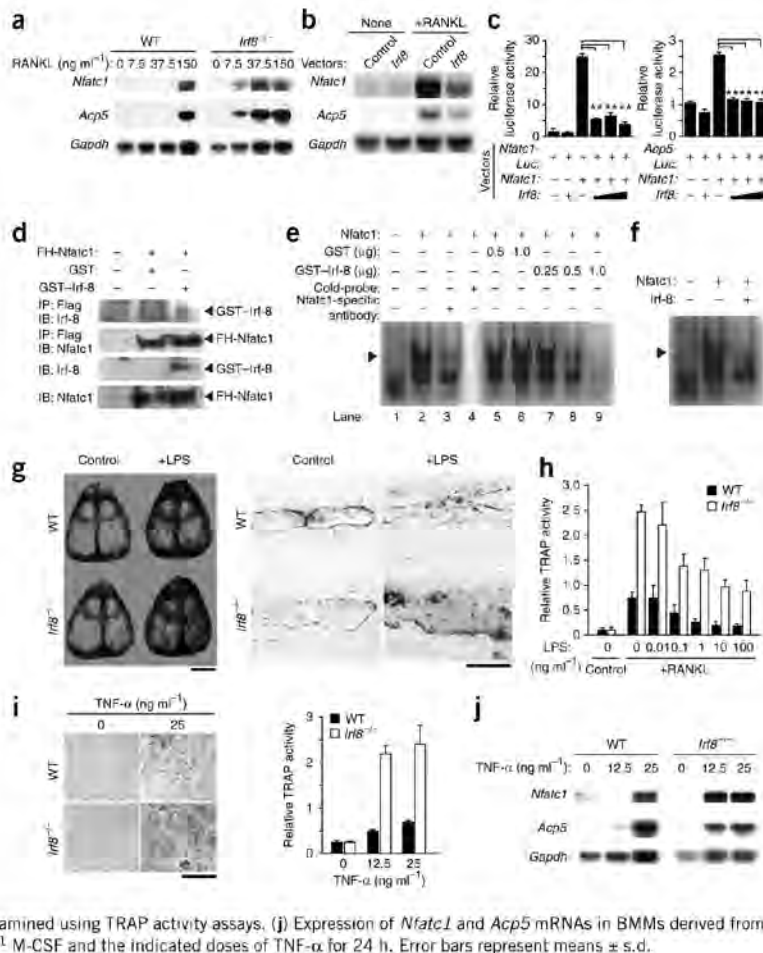


their ability to induce osteoclastogenic activity and that *Irf8* deficiency in osteoclast precursors has a decisive role in promoting osteoclast differentiation. Indeed, macrophage cultures prepared from *Irf8*^{-/-} mice also showed augmented osteoclastogenesis in the presence of RANKL and M-CSF (Fig. 3b), which led to an increase in resorption on dentin slices *in vitro* (data not shown). In contrast, retrovirus-mediated reconstitution of *Irf8* expression in *Irf8*^{-/-} macrophages inhibited RANKL-induced osteoclastogenesis (Fig. 3c). These results indicate that IRF-8 in osteoclast precursors is involved in the inhibition of osteoclastogenesis *in vitro* and *in vivo*. Furthermore, we found that IRF-8 expression was also lower during RANKL-induced human osteoclastogenesis, although with slower kinetics (Fig. 3d). Silencing of *IRF8* mRNA in human osteoclast precursors with small interfering RNAs (siRNAs) resulted in enhanced osteoclast differentiation (Fig. 3e-f), indicating that the function of IRF-8 in osteoclastogenesis is well conserved in humans and mice.

Consistent with the results regarding osteoclastogenesis, the mRNA expression profiles of various osteoclast markers were more strongly upregulated by RANKL stimulation in macrophages prepared from *Irf8*^{-/-} mice than in those obtained from wild-type mice (Supplementary Fig. 3). However, *Tnfrsf11a* and *Csf1r* (encoding Rank and M-CSf receptor protein, respectively) mRNA expression and cell surface Rank protein expression were comparable in wild-type

LETTERS

Figure 4 IRF-8 inhibits NFATc1 transcriptional activity and expression, and reduced IRF-8 expression may contribute to pathological bone destruction. **(a)** Expression of *Nfatc1* and *Acp5* mRNAs induced by 24 h stimulation of BMMs derived from wild-type and *Irf8*^{-/-} mice with 50 ng ml⁻¹ M-CSF and the indicated doses of RANKL. **(b)** Expression of *Nfatc1* and *Acp5* mRNAs in retrovirus-infected BMMs (Control, pMX-puro; *Irf8*, pMX-Irf8-puro) in the absence or presence of 150 ng ml⁻¹ RANKL with 50 ng ml⁻¹ M-CSF for 24 h. *Gapdh* was used as an internal control. **(c)** A luciferase activity assay to examine the effect of Irf-8 on the transcriptional activity of *Nfatc1*. *n* = 4, ***P* < 0.01. **(d)** The interaction between *Nfatc1* and *Irf8*. IP, immunoprecipitation; IB, immunoblotting. **(e, f)** Analysis of the inhibition of NFATc1 binding to its target DNA sequences by EMSAs (Supplementary Methods). The arrowheads indicate a specific binding complex, which included the *Nfatc1*-DNA complex; this was confirmed in a supershift assay (lane 1–3) and a cold competition experiment (lane 4). The intensity of *Nfatc1*-DNA bands decreased with increasing amounts of GST-Irf-8 (lanes 7–9), or when nuclear extracts from HEK293 cells cotransfected with pcDNA3-*Nfatc1* and pcDNA3-*Irf8* were used (f), but not with GST alone (lanes 5 and 6). **(g)** TRAP staining of mouse whole calvaria (left) and histological sections (right) obtained from wild-type and *Irf8*^{-/-} mice with or without administration of LPS. Scale bars, 1 cm (left) and 100 μm (right). **(h)** Osteoclast formation in BMMs stimulated with various doses of LPS in the presence of M-CSF (50 ng ml⁻¹) and RANKL (150 ng ml⁻¹) for 5 d. *n* = 4. **(i)** Left, BMM cultures in the presence of 50 ng ml⁻¹ M-CSF and 0 or 25 ng ml⁻¹ TNF-α on day 5, shown by TRAP staining. *n* = 4. Scale bar, 100 μm. Right, TNF-α dose-dependent induction of osteoclast formation examined using TRAP activity assays. **(j)** Expression of *Nfatc1* and *Acp5* mRNAs in BMMs derived from wild-type and *Irf8*^{-/-} mice stimulated with 50 ng ml⁻¹ M-CSF and the indicated doses of TNF-α for 24 h. Error bars represent means ± s.d.



and *Irf8*^{-/-} osteoclast precursors (Supplementary Fig. 4a and data not shown). During osteoclast precursor generation from bone marrow cells, M-CSF treatment did not lead to a greater increase in *Tnfrsf11a* mRNA expression in *Irf8*^{-/-} cells than in control cells (Supplementary Fig. 4b). These results suggest that enhanced osteoclastogenesis in *Irf8*^{-/-} macrophages is not due to changes in these receptor levels.

Expression of the *Nfatc1* gene and the osteoclast marker *Acp5*, which encodes tartrate-resistant acid phosphatase (TRAP), in *Irf8*^{-/-} precursors was induced by concentrations of RANKL that were 5–25% of those required for the expression of the genes in wild-type precursors (Fig. 4a). Furthermore, overexpression of *Irf8* in the precursor cells repressed the RANKL-induced expression of *Nfatc1* and *Acp5* mRNAs (Fig. 4b).

These observations led us to examine the effect of IRF-8 on the transcriptional activity of NFATc1, which was previously reported to interact with IRF-8 (ref. 15). For these experiments, we used luciferase reporter plasmids driven by three copies of the NFATc1 binding site from the human *IL2* (encoding interleukin-2) distal promoter (p3x *Nfatc1*-Luc) or by the mouse *Acp5* promoter (pAcp5-Luc). Overexpression of *Nfatc1* gene activated these promoters, whereas simultaneous expression of *Irf8* gene reduced the activities of the promoters to control levels (Fig. 4c), indicating that IRF-8 inhibits the transcriptional activity of NFATc1.

When GST-tagged Irf-8 proteins were incubated with nuclear lysates containing Flag-hemagglutinin-tagged *Nfatc1* (FH-*Nfatc1*), addition of Flag-specific antibodies to the mixture resulted in the immunoprecipitation of GST-Irf-8 with FH-*Nfatc1*, suggesting that IRF-8 physically interacts with NFATc1 (Fig. 4d). Furthermore, we identified an association between endogenous IRF-8 and NFATc1 by coimmunoprecipitation from nuclear extracts of human monocytic cells (Supplementary Fig. 5). We further examined the effects of Irf-8 on the binding of *Nfatc1* to its target DNA elements in an electrophoretic mobility shift assay (EMSA). We detected *Nfatc1*-DNA complexes, which we confirmed by adding competitive probes or NFATc1-specific antibodies (Fig. 4e). When we increased the levels of GST-Irf-8 (Fig. 4e) or added nuclear lysates containing excess Irf-8 (Fig. 4f) in the reaction mixture, *Nfatc1* binding to the labeled probes was substantially diminished, demonstrating the inhibitory effect of IRF-8 on NFATc1 binding to its target DNA elements.

We then attempted to examine the roles of IRF-8 in the processes underlying pathological bone destruction. Because several members of the IRF family of transcription factors, including IRF-8, have been shown to be crucial in Toll-like receptor (TLR) signaling in response to such microbial components as LPS and unmethylated CpG DNA^{16,17}, we examined the role of IRF-8 in the bone destruction

LETTERS

observed during TLR-mediated inflammation. Administration of LPS to the calvarial periosteum resulted in enhanced osteoclast formation in wild-type mice, whereas more extensive bone destruction was observed in *Irf8*^{-/-} mice (Fig. 4g). These results suggest that IRF-8 is a major negative regulator of osteoclastogenesis and a mediator of the maintenance of bone integrity during inflammatory bone destruction. We also examined the effects of TLR ligands on osteoclastogenesis in wild-type and *Irf8*^{-/-} osteoclast precursors. As previously reported¹⁸, LPS at high doses completely inhibited RANKL-induced osteoclastogenesis in wild-type cell cultures. In contrast, corresponding high doses of LPS, and also of the TLR3 ligand poly(I:C) and the TLR9 ligand CpG DNA, only partially inhibited osteoclast differentiation in *Irf8*^{-/-} cell cultures (Fig. 4h and Supplementary Fig. 6). *Irf8*-deficient cells were almost completely refractory to the inhibitory effects of the TLR2 ligand peptidoglycan (Supplementary Fig. 6a). These results suggest a potential inhibitory role of IRF-8 in the regulation of osteoclastogenesis by TLRs, although TLRs can also activate IRF-8-independent inhibitory mechanisms. We further found that expression of *Ifna* and *Ifnb* mRNAs (encoding Ifn- α and Ifn- β , respectively) was not diminished in *Irf8*-deficient cells and that IFN- γ completely inhibited osteoclastogenesis in *Irf8*^{-/-} macrophages, similar to wild-type cells (data not shown), thus suggesting that IRF-8 can inhibit osteoclastogenesis independently of IFN- γ .

Finally, we examined the effect of TNF- α on osteoclastogenesis using *Irf8*^{-/-} precursors, because TNF- α is a major mediator of inflammation induced by TLRs^{19–21} and has been suggested to be able to induce osteoclastogenesis^{22–24}. Consistent with previous reports, TNF- α induced the development of a small number of osteoclasts in cultures of wild-type precursor cells (Fig. 4i). Notably, osteoclastogenesis was enhanced in cultures of *Irf8*^{-/-} precursor cells treated with TNF- α (Fig. 4i). The mRNA expression levels of *Nfatc1* and *Acp5* in the *Irf8*^{-/-} osteoclast precursors were also augmented by TNF- α (Fig. 4j), indicating that IRF-8 also has a suppressive role in TNF- α -induced osteoclastogenesis.

Our data provide a mechanism by which IRF-8 suppresses osteoclastogenesis (depicted in Supplementary Fig. 7). In osteoclast precursors, abundant IRF-8 interacts with basally expressed NFATc1 to suppress its transcriptional activity and thus prevent its activation of target genes, including autoamplification of its own promoter. Stimulation of osteoclast precursors with RANKL results in the activation of nuclear factor- κ B (NF- κ B) and activator protein-1 (AP-1) that bind the *Nfatc1* promoter to induce its activity. At the same time, RANKL induces the downregulation of IRF-8, thereby releasing NFATc1 from IRF-8-mediated suppression and augmenting NFATc1-mediated autoamplification of its own expression. Together, these mechanisms result in robust NFATc1 expression and induction of downstream genes required for osteoclast differentiation.

Bone erosion that occurs in the setting of infection and chronic inflammation, termed inflammatory osteolysis, contributes to the pathogenesis of infectious and inflammatory diseases such as rheumatoid arthritis²⁵. Inflammatory bone erosion is driven by microbial products such as LPS and inflammatory cytokines, including TNF- α , that activate osteoclastogenesis directly or indirectly via activation of stromal cells and osteoblasts²⁵. Our findings show that IRF-8 is crucial in attenuating LPS-induced inflammatory bone resorption and LPS- and TNF- α -induced osteoclastogenesis. This homeostatic role of IRF-8 may be required during acute infections and also in chronic inflammatory conditions such as rheumatoid arthritis. Identification of additional factors and mechanisms that augment IRF-8 expression

or function may represent a fruitful clinical approach to therapeutic suppression of inflammatory bone erosion.

Overall, our findings support a model of RANKL-induced NFATc1 expression and osteoclast differentiation that involves cooperation between RANKL-mediated induction of positive regulators of osteoclastogenesis and suppression of negative regulators of osteoclast differentiation, such as IRF-8.

METHODS

Methods and any associated references are available in the online version of the paper at <http://www.nature.com/naturemedicine/>.

Accession codes. Microarray data have been deposited in Gene Expression Omnibus with accession code GSE17563.

Note: Supplementary information is available on the Nature Medicine website.

ACKNOWLEDGMENTS

We are grateful to M. Asagiri for technical assistance. We thank T. Kitamura (University of Tokyo) for providing the retrovirus expression system. We also thank A. Mochizuki and all members of the Department of Biochemistry, School of Dentistry, Showa University for valuable discussions. This work is supported in part by the High-Tech Research Center Project for Private Universities from the Ministry of Education, Culture, Sports, Science and Technology, Japan, 2005–2009, by Grants-in-Aid for Scientific Research from the Japan Society for the Promotion of Science (20390474 to M.T.) and by grants from the US National Institutes of Health (AR053843 and DE19381 to Y.C. and DE019420 and AR46713 to L.B.L.).

AUTHOR CONTRIBUTIONS

B.Z. performed most of the experiments with substantial assistance from M.T. X.W. conducted the histological analysis. A.Y., T.K., X.H. and T.T. assisted with the experiments. K.O. provided the *Irf8*^{-/-} mice. B.Z. and M.T. designed the project and wrote the manuscript. Y.C. provided recombinant RANKL and contributed to manuscript preparation. L.B.L. oversaw the bone marrow chimera and human cell experiments and contributed to manuscript revision. H.T. oversaw the inflammatory bone destruction experiments and provided crucial advice for the experiments. M.T. and R.K. supervised the project.

Published online at <http://www.nature.com/naturemedicine/>.

Reprints and permissions information is available online at <http://npg.nature.com/reprintsandpermissions/>.

- Wada, T., Nakashima, T., Hiroshi, N. & Penninger, J.M. RANKL-RANK signaling in osteoclastogenesis and bone disease. *Trends Mol. Med.* **12**, 17–25 (2006).
- Lee, S.K. & Lorenzo, J. Cytokines regulating osteoclast formation and function. *Curr. Opin. Rheumatol.* **18**, 411–418 (2006).
- Takayanagi, H. *et al.* Induction and activation of the transcription factor NFATc1 (NFAT2) integrate RANKL signaling in terminal differentiation of osteoclasts. *Dev. Cell* **3**, 889–901 (2002).
- Grigoriadis, A.E. *et al.* c-Fos: a key regulator of osteoclast-macrophage lineage determination and bone remodelling. *Science* **266**, 443–448 (1994).
- Kim, N., Takami, M., Rho, J., Josien, R. & Choi, Y. A novel member of the leukocyte receptor complex regulates osteoclast differentiation. *J. Exp. Med.* **195**, 201–209 (2002).
- Ishida, N. *et al.* Large scale gene expression analysis of osteoclastogenesis *in vitro* and elucidation of NFAT2 as a key regulator. *J. Biol. Chem.* **277**, 41147–41156 (2002).
- Kantakamalakul, W. *et al.* Regulation of IFN consensus sequence binding protein expression in murine macrophages. *J. Immunol.* **162**, 7417–7425 (1999).
- Nelson, N. *et al.* Expression of IFN regulatory factor family proteins in lymphocytes. Induction of Stat-1 and IFN consensus sequence binding protein expression by T cell activation. *J. Immunol.* **156**, 3711–3720 (1996).
- Driggers, P.H. *et al.* An interferon γ -regulated protein that binds the interferon-inducible enhancer element of major histocompatibility complex class I genes. *Proc. Natl. Acad. Sci. USA* **87**, 3743–3747 (1990).
- Tamura, T. & Ozato, K. ICSBP/IRF-8: its regulatory roles in the development of myeloid cells. *J. Interferon Cytokine Res.* **22**, 145–152 (2002).
- Marecki, S. & Fenton, M.J. PU.1/interferon regulatory factor interactions: mechanisms of transcriptional regulation. *Cell Biochem. Biophys.* **33**, 127–148 (2000).
- Holtzman, T. *et al.* Immunodeficiency and chronic myelogenous leukemia-like syndrome in mice with a targeted mutation of the ICSBP gene. *Cell* **87**, 307–317 (1996).

LETTERS

13. Tamura, T., Nagamura-Inoue, T., Shmeltzer, Z., Kuwata, T. & Ozato, K. ICSBP directs bipotential myeloid progenitor cells to differentiate into mature macrophages. *Immunity* **13**, 155–165 (2000).
14. Schievoni, G. *et al.* ICSBP is essential for the development of mouse type I interferon-producing cells and for the generation and activation of CD8 α^+ dendritic cells. *J. Exp. Med.* **196**, 1415–1425 (2002).
15. Zhu, C. *et al.* Activation of the murine interleukin-12 p40 promoter by functional interactions between NFAT and ICSBP. *J. Biol. Chem.* **278**, 39372–39382 (2003).
16. Tsujimura, H. *et al.* Toll-like receptor 9 signaling activates NF- κ B through IFN regulatory factor-8/IFN consensus sequence binding protein in dendritic cells. *J. Immunol.* **172**, 5820–5827 (2004).
17. Zhao, J. *et al.* IRF-8/interferon (IFN) consensus sequence-binding protein is involved in Toll-like receptor (TLR) signaling and contributes to the cross-talk between TLR and IFN- γ signaling pathways. *J. Biol. Chem.* **281**, 10073–10080 (2006).
18. Takami, M., Kim, N., Rho, J. & Choi, Y. Stimulation by Toll-like receptors inhibits osteoclast differentiation. *J. Immunol.* **169**, 1516–1523 (2002).
19. O'Neill, L.A. How Toll-like receptors signal: what we know and what we don't know. *Curr. Opin. Immunol.* **18**, 3–9 (2006).
20. Akira, S., Uematsu, S. & Takeuchi, O. Pathogen recognition and innate immunity. *Cell* **124**, 783–801 (2006).
21. Takaoka, A. *et al.* Integral role of IRF-5 in the gene induction programme activated by Toll-like receptors. *Nature* **434**, 243–249 (2005).
22. Azuma, Y., Kaji, K., Katogi, R., Takeshita, S. & Kudo, A. Tumor necrosis factor- α induces differentiation of and bone resorption by osteoclasts. *J. Biol. Chem.* **275**, 4858–4864 (2000).
23. Kobayashi, K. *et al.* Tumor necrosis factor α stimulates osteoclast differentiation by a mechanism independent of the ODF/RANKL-RANK interaction. *J. Exp. Med.* **191**, 275–286 (2000).
24. Kim, N. *et al.* Osteoclast differentiation independent of the TRANCE-RANK-TRAF6 axis. *J. Exp. Med.* **202**, 589–595 (2005).
25. Lorenzo, J., Horowitz, M. & Choi, Y. Osteoimmunology: interactions of the bone and immune system. *Endocr. Rev.* **29**, 403–440 (2008).



ONLINE METHODS

Mice and analysis of bone phenotypes. The *Irf8*^{-/-} mice (C57BL/6) used in this study have been described previously¹². We injected tetracycline hydrochloride (20 mg per kg body weight; Sigma) and, 72 h later, calcein (10 mg per kg body weight; Wako) subcutaneously into 8-week-old wild-type and *Irf8*^{-/-} mice. We then killed the mice 32 h after the second injection. The LPS-induced model of bone loss has been described previously²⁶, except that we used 12.5 mg per kg body weight LPS (Sigma). We subjected the mice to histomorphometric and microradiographic examinations as described previously²⁷. All mice were born and were maintained under specific pathogen-free conditions. All mouse experiments were approved by and conducted according to the guidelines of the Showa University Animal Care and Use Committee (approval number 17079).

Generation of bone marrow chimeric mice. We collected donor bone marrow cells from wild-type or *Irf8*^{-/-} littermate mice (on the C57/BL6 background) and injected one-fourth of total bone marrow cells from each donor intravenously via tail vein into each of the irradiated wild-type recipients. We obtained recipient mice (3-week-old C57/BL6 mice) from The Jackson Laboratory, and we lethally irradiated them with a single dose of 875 rad 1 d before transplantation. We killed chimeric mice 8 weeks after bone marrow transplantation. The experiments using chimeric mice were approved by the Hospital for Special Surgery Institutional Animal Care and Use Committee.

In vitro assays of osteoclast differentiation and macrophage function. The method used to analyze osteoclast differentiation *in vitro* has been described previously²⁸. Briefly, we cultured mouse bone marrow or spleen cells with 50 ng ml⁻¹ human M-CSF (Koyowa Hakko Kogyo) for 3 d. We further stimulated the obtained BMMs or spleen-derived macrophages with 150 ng ml⁻¹ RANKL in the presence of 50 ng ml⁻¹ M-CSF for 3–4 d. We also cocultured bone marrow cells, BMMs or spleen-derived macrophages with primary osteoblasts derived from mouse calvaria in the presence of 10⁻⁸ M 1,25(OH)₂D₃ (Sigma-Aldrich) and 10⁻⁶ M prostaglandin E₂ (Sigma-Aldrich) for 6 d. We changed the medium every 2 d. We evaluated the generation of osteoclasts by TRAP staining and TRAP activity assays²⁹. Methods used for the phagocytosis assay and labeling of actin have been described previously²⁸.

Human osteoclast culture system and RNA interference. We obtained fresh human peripheral blood mononuclear cells from whole blood from disease-free volunteers with their informed consent. The experiments using human cells were approved by the Hospital for Special Surgery Institutional Review Board. We then purified human CD14⁺ monocytes from peripheral blood mononuclear cells with CD14-specific magnetic beads (Miltenyi Biotec) and cultured them in α -MEM medium with 10% FBS (HyClone) and 20 ng ml⁻¹ M-CSF (Peprotech) for 2 d to induce osteoclast

precursors that we further stimulated with RANKL in the presence of 20 ng ml⁻¹ of M-CSF for 3–6 d to generate human osteoclasts. We transfected siRNAs specifically targeting human *IRF8* or control siRNAs (Dharmacon, Invitrogen) into primary human CD14⁺ monocytes with the Amara Nucleofector device set to program Y-001 using the Human Monocyte Nucleofector kit (Amara). We used two different targeting siRNAs and control siRNAs with comparable results in a total of six independent experiments with multiple blood donors.

Plasmid constructs. We prepared and amplified *Irf8* cDNA in RT-PCRs using RNA from BMMs. We PCR-amplified the coding region of *Irf8* with the following primers: 5'-GCAGGATGTGTGACCGGAAC-3' (sense) and 5'-ACTGAGGCTTAGACGGTGAT-3' (antisense). We subcloned the amplified PCR fragment into a pCR-Blunt vector to produce pCR-Blunt-*Irf8* using a Zero Blunt PCR Cloning kit (Invitrogen). We constructed the pMX-*Irf8*-IRES-EGFP retroviral vector by inserting a 1.3-kilobase EcoRI-flanked DNA fragment encoding *Irf8* from pCR-Blunt-*Irf8* into the same site in the pMX-IRES-EGFP vector. We then inserted the 1.3-kilobase BamHI- and XhoI-flanked DNA fragment encoding *Irf8* from pMX-*Irf8*-IRES-EGFP into the same site in the pMX-*parv* vector to construct the pMX-*Irf8*-*parv* retroviral vector. We constructed the pcDNA3-*Irf8* expression vector by inserting a 1.3-kb BamHI- and NotI-flanked DNA fragment encoding *IRF8* from pMX-*Irf8*-IRES-EGFP into the same site in the pcDNA3 vector. We constructed pcDNA3-*Nfatc1* by inserting an EcoRI-flanked DNA fragment encoding *NEATc1* from pMX-*Nfatc1*-IRES-EGFP³ into the same site in the pcDNA3 vector. The pFH-*Nfatc1*, p3 \times *Nfatc1*-Luc, and pAcp5-Luc vectors were previously described^{3,29}.

Statistical analyses. We used the Student's *t* test for statistical analyses (*P* < 0.05 was taken as statistically significant), and all data are presented as the mean \pm s.d. Results are representative of more than four individual experiments.

Additional methods. Details of the methods including retroviral gene transduction, GeneChip, RT-PCR, northern blot assay, real-time PCR, luciferase reporter assay, preparation of GST fusion proteins, immunoprecipitation and immunoblot analyses, and EMSA are described in the **Supplementary Methods**.

26. Takayanagi, H. *et al.* T-cell-mediated regulation of osteoclastogenesis by signalling cross-talk between RANKL and IFN- γ . *Nature* **408**, 600–605 (2000).
27. Takayanagi, H. *et al.* RANKL maintains bone homeostasis through c-Fos-dependent induction of interferon- β . *Nature* **416**, 744–749 (2002).
28. Mochizuki, A. *et al.* Identification and characterization of the precursors committed to osteoclasts induced by TNF-related activation-induced cytokine/receptor activator of NF- κ B ligand. *J. Immunol.* **177**, 4360–4368 (2006).
29. Koga, T. *et al.* NFAT and Osterix cooperatively regulate bone formation. *Nat. Med.* **11**, 880–885 (2005).

分子細胞機能学

森田 育男

医歯学総合研究科・顎顔面頸部機能再建学系専攻
分子細胞機能学・教授



1) 研究の課題名

1. PGI2と骨代謝

骨代謝においてプロスタグランジン E2 (PGE2) は骨吸収、骨形成を調節する重要な因子であることが明らかになっている。しかし、骨で産生されることが知られているプロスタサイクリン (PGI2) に関する研究は、ほとんど行われていなかった。そこで、本研究においては、PGI産生酵素 (PGIS) のノックアウトマウス (PGIS^{-/-}マウス) を用いて、PGI2の骨への作用を検討した。その結果、PGIS^{-/-}マウスにおいては、週齢を重ねるごとに、海面骨の骨塩含量の増加が認められた。そこで、37週齢の大腿骨における組織の解析を行うとともに、血清中の骨代謝マーカーを調べたところ、PGIS^{-/-}マウスにおいては、骨形成、骨吸収がともに促進しているが、骨形成によりシフトした結果、骨量の増加が促進したことが明らかとなった。以上の結果より、PGIS^{-/-}マウスにおける海面骨の骨量増加は、高回転型の骨代謝異常であるが、エストロゲン欠損とは逆の骨形成へのシフトであることが明らかとなった。その機序の解明のため行ったPGIS^{-/-}マウスから単離した細胞を用いた骨芽細胞の分化能、石灰化能、破骨細胞への分化能、骨吸収活性などは、controlとの差が認められなかった。このことは、PGIS^{-/-}マウスにおける骨代謝異常は骨代謝関連細胞に直接影響があると考えられるより、PGI2の生理作用などを考慮すると、骨細胞と血管内皮細胞との相互作用で考える必要があるかもしれない。

Prostaglandins (PGs) are key regulatory factors that affect bone metabolism. Prostaglandin E2 (PGE2) regulates bone resorption and bone formation. Prostacyclin (PGI2) is one of the major products derived from arachidonic acid by the action of cyclooxygenase and PGI2 synthase (PGIS). Unlike PGE2, there are few reports about the role of PGI2 in bone regulation. Therefore, we investigated the potential effect of PGI2 on bone metabolism. We used PGIS

knockout (PGIS^{-/-}), PGIS heterozygous (PGIS^{+/-}) and wild-type mice to investigate the role of PGI2. Notably, PGIS^{-/-} mice gradually displayed an increase in trabecular bone mass in adolescence. Adult PGIS^{-/-} mice showed an increase in trabecular BV/TV. Histomorphometric analysis showed that PGIS^{-/-} mice displayed increases in both bone formation and bone resorption parameters. Levels of serum osteocalcin and C-telopeptides (CTX) were increased in adult PGIS^{-/-} mice. Furthermore, the increased bone mass patterns were rescued in PGIS^{-/-}tg mice. In conclusion, adult PGIS^{-/-} mice displayed an overall increase in the levels of both bone formation and bone resorption parameters, which suggests that PGI2 deficiency accelerates high bone turnover activity with a greater increase in bone mass in ageing. These results indicated that PGI2 may contribute to the maintenance of normal bone mass and micro-architecture in mice in age-dependent manner. Our findings demonstrate for the first time that PGI2 is involved in bone metabolism in vivo.

2. ギャップ結合の調節機構の解明とその応用

ギャップ結合を構成しているコネキシン 43 (Cx43) は骨の成長およびその恒常性維持に重要な働きをしていると考えられている。そのため、骨組織においてコネキシン 43の発現を高いレベルで維持する必要がある。そこで著者らはコネキシン 43の発現維持機構を解明するために、各種タンパクリン酸化酵素に対する阻害剤を用い定常状態でのコネキシン 43発現に対する影響を調べ、PI3K/Aktのシグナル伝達経路が定常状態のコネキシン 43の発現に重要であることを示した。その機序としては、このシグナルがCx43のmRNAの安定化させていることを明らかにした。

さらに、ギャップ結合の安定化に関し、annular gap形成機序を検討している、

一方、ギャップ結合をDDSに応用するための秋吉研との共同研究で研究を行ってきたが、リボソームへのタ

ンパクの組み入れ方法に新たな展開がなされた。

The gap junction protein connexin43 (Cx43) plays an important role in bone development and its homeostasis. Therefore, it is important that the Cx43 expression is kept at a high-level in bone tissues under normal conditions. To investigate the mechanism to keep Cx43 expression level, the effects of protein kinase inhibitors on the basal expression of Cx43 were examined. It was found that the specific PI3K inhibitor LY294002 significantly decreased the steady-state expression levels of Cx43 mRNA and protein in osteoblastic cell line, MC3T3-E1 cells. Furthermore, dominant-negative Akt expression reduced both Cx43 expression and gap junction activity. These results suggest an important role of PI3K/Akt in the regulation of basal Cx43 expression. A promoter assay for Cx43 and an actinomycin D chase experiment revealed that PI3K/Akt modulated Cx43 expression post-transcriptionally via mRNA stability. The present findings could provide new insights into the molecular understanding of Cx43 expression. Liposomes are widely utilized in molecular biology and medicine as drug carriers. Here we report a new liposome-cell interaction through connexins. Connexin 43 (Cx43) -containing liposomes were prepared by using cell-free transcription/translation systems with plasmids encoding Cx43 in the presence of liposome. The expressed membrane protein, Cx43, was directly constituted to the liposome membrane upon in vitro synthesis, leading to pure membrane protein-containing liposomes. The hydrophilic dye calcein was efficiently transferred from Cx43-expressing liposomes to cultured cells (Cx43 expressing). The transfer is significantly blocked in the presence of gap junction inhibitor (18beta-glycyrrhetic acid) and in the case of the other type of connexin (Cx32) -expressing cell. The results show that calcein entered the cell through connexin-mediated pathway. Cx43 liposomes containing a soluble NEMO-binding domain peptide suppressed the intracellular signaling cascade IL-1beta-induced NF-kappaB activation and cyclooxygenase-2 expression in Cx43-expressing cells, confirming effective peptide transfer into the cell. This is a new method for direct cytosolic delivery of hydrophilic molecules.

3. 低酸素によるサイトカイン産生調節機序の解明

低酸素下でのサイトカイン産生の調節機序に関し、HIFによる制御が注目されているが、多くのサイトカインのプロモーター領域にはHIFに対するレスポンスエレメントがないことより、その制御機構の解明を行っている、本年度は、低酸素下で上昇するIL-8と低下するMCP-1に注目して実験を行い、NF- κ Bが両サイトカイン産生の制御に重要であるが、MCP-1賛成の低下に関しては、HDACが低酸素で活性化し、負の制御を行っているこ

とが明らかとなった。

Hypoxia is a microenvironmental factor frequently associated with tumors and inflammation. This study addresses the question of how hypoxia modulates the basal and IL-1 beta-induced production of cytokines and aims to identify the underlying mechanism of hypoxic transcriptional repression. We found that despite the similarities of the promoter structures of IL-8 and MCP-1, these chemokines were differently regulated by hypoxia (an increase in IL-8, but a decrease in MCP-1 mRNA and protein expression). Such differences were not observed in a reporter gene assay, in which both of the promoters were activated by hypoxia. The difference in the response to hypoxia between MCP-1 expression and the promoter assay was not due to mRNA instability. Using proteasome inhibitor MG132 and I kappaB overexpression we demonstrated that an NF-kappaB-dependent mechanism was involved in both the activation of IL-8 and the repression of MCP-1 mRNA expression in response to hypoxia. The histone deacetylase inhibitor Trihostatin A abolished the inhibitory actions of hypoxia on IL-1 beta-induced MCP-1 gene expression. Furthermore, hypoxia induced histone deacetylase activity in the nuclear extracts. Although stimulation with IL-1 beta and/or hypoxia increased the acetylation of histones H3 and H4 in the presence of Trihostatin A, histone acetylation remained unchanged when the cells were treated without histone deacetylase inhibitor. Collectively, our findings suggest that transiently transfected promoters are not subject to the same NF-kappaB regulatory mechanisms as their chromatinized counterparts. NF-kappaB, activated by hypoxia, can act as a transcriptional repressor via a mechanism that involves deacetylation of histones.

4. 印刷技術を用いた血管再建術

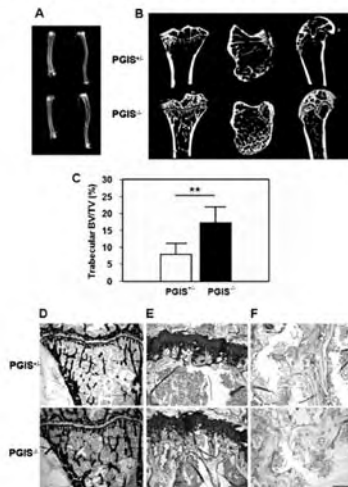
再生医療において、血管再生は大きな意義を持っている。そこで、in vitroでパターンニングした血管内皮細胞をマトリクスに転写することにより毛細血管を構築する系を考案した。すなわち、1) 光触媒を用いた独自の親疎水パターン形成技術を応用し培養基板を作成する。2) 血管内皮細胞をデザインされた基板上に培養後、高気圧で脱細胞化した羊膜に接触させることで毛細血管構造物を形成し、基盤の剥離により基質側に転写する。3) 羊膜上に作成した管腔をマウスに移植し、血流回復、機能回復を調べる。次に用いるべき細胞の選択に移り、大網由来血管内皮細胞を用いるための方法論、臍帯血、自己血より血管内皮細胞を単離・培養する系を確立した。その結果、自己の末梢血を用いた血管再生が可能となり、今後の再生医療への応用が期待される。

We previously reported a novel optical lithographic

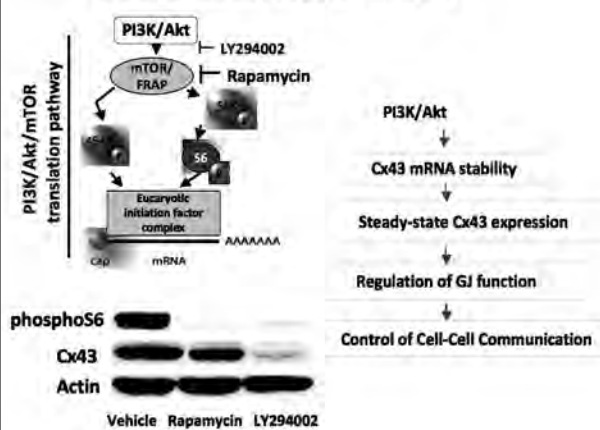
technique for the construction of a capillary network consisting of endothelial cells. To investigate the feasibility of clinical application in the treatment of ischemic diseases, capillary structures were formed on scaffolds made from amniotic membrane (AM) and implanted into mice. The capillary network remained in place for at least 5 days and blood perfusion through the implanted capillaries was histologically detected in an ear flap model. Moreover, blood was observed flowing through the capillary network implanted in abdominal subcutaneous tissue of mice at 5 days after insertion. Implantation of the AM capillary structure into the ischemic hind limbs of mice significantly increased reperfusion compared with controls (AM only). Blood flow was restored in the ischemic limbs to the level of corresponding nonischemic limbs as early as 9 days after surgical implantation. The treatment reversed ischemic symptoms, and ambulatory impairment was significantly improved. Thus, the implantation of a capillary network engineered ex vivo could have therapeutic potential for ischemic diseases.

2)

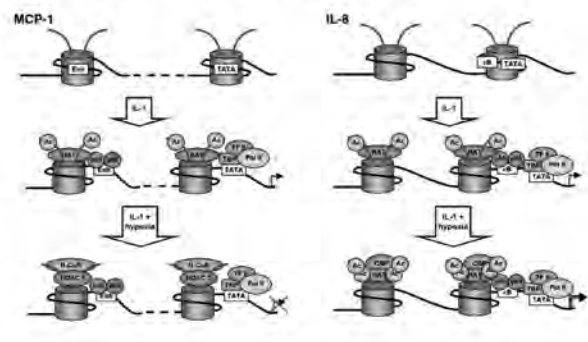
1. PGI2ノックアウトマウスにおける骨代謝の変動



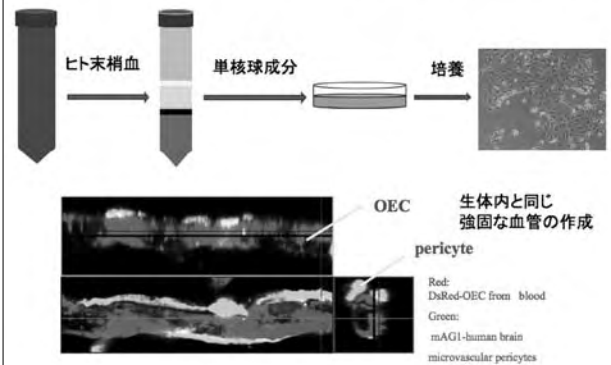
2. 骨芽細胞におけるコネキシン43の発現維持機構



3. 低酸素下におけるサイトカイン産生調節機構



4. ヒト末梢血から単離・増幅させたOECとペリサイトから形成された毛細血管



3) 研究内容の英文要約

Implantation of Capillary Structure Engineered by Optical Lithography Improves Hind Limb Ischemia in Mice

We previously reported a novel optical lithographic technique for the construction of a capillary network consisting of endothelial cells. To investigate the feasibility of clinical application in the treatment of ischemic diseases, capillary structures were formed on scaffolds made from amniotic membrane (AM) and implanted into mice. The capillary network remained in place for at least 5 days and blood perfusion through the implanted capillaries was histologically detected in an ear flap model. Moreover, blood was observed flowing through the capillary network implanted in abdominal subcutaneous tissue of mice at 5 days after insertion. Implantation of the AM capillary structure into the ischemic hind limbs of mice significantly increased reperfusion compared with controls (AM only). Blood flow was restored in the ischemic limbs to the level of corresponding nonischemic limbs as early as 9 days after surgical implantation. The treatment reversed ischemic symptoms, and ambulatory impairment was significantly improved. Thus, the implantation of a capillary network engineered ex vivo could have therapeutic potential for ischemic diseases.

Increased Bone Mass in Adult Prostacyclin Deficient Mice

Prostaglandins (PGs) are key regulatory factors that affect bone metabolism. Prostaglandin E2 (PGE2) regulates bone resorption and bone formation. Prostacyclin (PGI2) is one of the major products derived from arachidonic acid by the action of cyclooxygenase and PGI2 synthase (PGIS). Unlike PGE2, there are few reports about the role of PGI2 in bone regulation. Therefore, we investigated the potential effect of PGI2 on bone metabolism. We used PGIS knockout (PGIS^{-/-}), PGIS heterozygous (PGIS^{+/-}) and wild-type mice to investigate the role of PGI2. Notably, PGIS^{-/-} mice gradually displayed an increase in trabecular bone mass in adolescence. Adult PGIS^{-/-} mice showed an increase in trabecular BV/TV. Histomorphometric analysis showed that PGIS^{-/-} mice displayed increases in both bone formation and bone resorption parameters. Levels of serum osteocalcin and C-telopeptides (CTX) were increased in adult PGIS^{-/-} mice. Furthermore, the increased bone mass patterns were rescued in PGIS^{-/-}tg mice. In conclusion, adult PGIS^{-/-} mice displayed an overall increase in the levels of both bone formation and bone resorption parameters, which suggests that PGI2 deficiency accelerates high bone turnover activity with a greater increase in bone mass in ageing. These results indicated that PGI2 may contribute to the maintenance of normal bone mass and micro-architecture in mice in age-dependent manner. Our findings demonstrate for the first time that PGI2 is involved in bone metabolism *in vivo*.

Potential enhancement of osteoclastogenesis by severe acute respiratory syndrome coronavirus 3a/X1 protein

Severe acute respiratory syndrome coronavirus (SARS-CoV) causes a lung disease with high mortality. In addition, osteonecrosis and bone abnormalities with reduced bone density have been observed in patients following recovery from SARS, which were partly but not entirely explained by the short-term use of steroids. Here, we demonstrate that human monocytes, potential precursors of osteoclasts, partly express angiotensin converting enzyme 2 (ACE2), a cellular receptor of SARS-CoV, and that expression of an accessory protein of SARS-CoV, 3a/X1, in murine macrophage cell line RAW264.7 cells, enhanced NF-kappaB activity and differentiation into osteoclast-like cells in the presence of receptor activator of NF-kappaB ligand (RANKL). Furthermore, human epithelial A549 cells expressed ACE2, and expression of 3a/X1 in these cells up-regulated TNF-alpha, which is known to accelerate osteoclastogenesis. 3a/X1 also enhanced RANKL expression in mouse stromal ST2 cells. These findings indicate that SARS-CoV 3a/X1 might promote osteoclastogenesis by direct and indirect mechanisms.

Regulation of chemokine gene expression by hypoxia via cooperative activation of NF-kappaB and histone deacetylase

Hypoxia is a microenvironmental factor frequently associated with tumors and inflammation. This study addresses the question of how hypoxia modulates the basal and IL-1 beta-induced production of cytokines and aims to identify the underlying mechanism of hypoxic transcriptional repression. We found that despite the similarities of the promoter structures of IL-8 and MCP-1, these chemokines were differently regulated by hypoxia (an increase in IL-8, but a decrease in MCP-1 mRNA and protein expression). Such differences were not observed in a reporter gene assay, in which both of the promoters were activated by hypoxia. The difference in the response to hypoxia between MCP-1 expression and the promoter assay was not due to mRNA instability. Using proteasome inhibitor MG132 and I kappaB overexpression we demonstrated that an NF-kappaB-dependent mechanism was involved in both the activation of IL-8 and the repression of MCP-1 mRNA expression in response to hypoxia. The histone deacetylase inhibitor Trihostatin A abolished the inhibitory actions of hypoxia on IL-1 beta-induced MCP-1 gene expression. Furthermore, hypoxia induced histone deacetylase activity in the nuclear extracts. Although stimulation with IL-1 beta and/or hypoxia increased the acetylation of histones H3 and H4 in the presence of Trihostatin A, histone acetylation remained unchanged when the cells were treated without histone deacetylase inhibitor. Collectively, our findings suggest that transiently transfected promoters are not subject to the same NF-kappaB regulatory mechanisms as their chromatinized counterparts. NF-kappaB, activated by hypoxia, can act as a transcriptional repressor via a mechanism that involves deacetylation of histones.

Direct formation of proteo-liposomes by in vitro synthesis and cellular cytosolic delivery with connexin-expressing liposomes.

Liposomes are widely utilized in molecular biology and medicine as drug carriers. Here we report a new liposome-cell interaction through connexins. Connexin 43 (Cx43)-containing liposomes were prepared by using cell-free transcription/translation systems with plasmids encoding Cx43 in the presence of liposome. The expressed membrane protein, Cx43, was directly constituted to the liposome membrane upon *in vitro* synthesis, leading to pure membrane protein-containing liposomes. The hydrophilic dye calcein was efficiently transferred from Cx43-expressing liposomes to cultured cells (Cx43 expressing). The transfer is significantly blocked in the presence of gap junction inhibitor (18beta-glycyrrhetinic acid) and in the case of the other type of connexin (Cx32)-expressing cell. The results show that calcein entered the cell through

connexin-mediated pathway. Cx43 liposomes containing a soluble NEMO-binding domain peptide suppressed the intracellular signaling cascade IL-1 β -induced NF- κ B activation and cyclooxygenase-2 expression in Cx43-expressing cells, confirming effective peptide transfer into the cell. This is a new method for direct cytosolic delivery of hydrophilic molecules.

The steady-state expression of connexin43 is maintained by the PI3K/Akt in osteoblasts

The gap junction protein connexin43 (Cx43) plays an important role in bone development and its homeostasis. Therefore, it is important that the Cx43 expression is kept at a high-level in bone tissues under normal conditions. To investigate the mechanism to keep Cx43 expression level, the effects of protein kinase inhibitors on the basal expression of Cx43 were examined. It was found that the specific PI3K inhibitor LY294002 significantly decreased the steady-state expression levels of Cx43 mRNA and protein in osteoblastic cell line, MC3T3-E1 cells. Furthermore, dominant-negative Akt expression reduced both Cx43 expression and gap junction activity. These results suggest an important role of PI3K/Akt in the regulation of basal Cx43 expression. A promoter assay for Cx43 and an actinomycin D chase experiment revealed that PI3K/Akt modulated Cx43 expression post-transcriptionally via mRNA stability. The present findings could provide new insights into the molecular understanding of Cx43 expression.

Amyloid-beta up-regulates complement factor B in retinal pigment epithelial cells through cytokines released from recruited macrophages/microglia: Another mechanism of complement activation in age-related macular degeneration.

One of the earliest signs of age-related macular degeneration (AMD) is the formation of drusen which are extracellular deposits beneath the retinal pigmented epithelium (RPE). To investigate the relationship between drusen and AMD, we focused on amyloid beta (Abeta), a major component of drusen and also of senile plaques in the brain of Alzheimer's patients. We previously reported that Abeta was accumulated in drusen-like structure in senescent neprilysin gene-disrupted mice. The purpose of this study was to investigate the influence of Abeta on factor B, the main activator of the complement alternative pathway. The results showed that Abeta did not directly modulate factor B expression in RPE cells, but increased the production of monocyte chemoattractant protein-1 (MCP-1). Abeta also increased the production of IL-1 β and TNF- α in macrophages/microglia, and exposure of RPE cells to IL-1 β and TNF- α significantly up-regulated factor B. Co-cultures of RPE cells and macrophages/microglia in the presence of Abeta significantly increased the

expression of factor B in RPE. These findings indicate that cytokines produced by macrophages/microglia that were recruited by MCP-1 produced in RPE cells stimulated by Abeta up-regulate factor B in RPE cells. Thus, a combined mechanism exists for Abeta-induced for the activation of the complement alternative pathway in the subretinal space; cytokine-induced up-regulation of activator factor B and dysfunction of the inhibitor factor I by direct binding to Abeta as suggested in our earlier study.

The reduction in pigment epithelium-derived factor is a sign of malignancy in ovarian cancer expressing low-level of vascular endothelial growth factor.

Angiogenesis is a critical factor in the progression of solid tumors and metastasis. The aim of this study was to characterise the roles of angiogenic and anti-angiogenic factors on ovarian cancer. METHODS: The expression levels of vascular endothelial growth factor (VEGF, angiogenic factor) and pigment epithelial growth factor (PEDF, anti-angiogenic factor) were measured by real-time polymerase chain reaction and Western blotting in ovarian tumors. Microvessel density (MVD) was evaluated by the total microvessel length in high-power field of tumor tissue preparations. RESULTS: MVD correlated with tumor malignancy. The tissues with the highest expression levels of VEGF (VEGF-H) were malignant tumors. The VEGF expression levels in some malignant tumors (VEGF-L) were as low as that in benign tumors. Therefore, the expression of PEDF was examined. The PEDF expression levels in VEGF-L malignant tumors were significantly lower than those in benign tumors. On the other hand, the PEDF expression levels in VEGF-H malignant tumor tissues were not significantly different from those in benign tumors. CONCLUSION: The reduction in PEDF expression levels may be, in part, responsible for tumor malignancy in VEGF-L ovarian tumors. Furthermore, PEDF may be a useful marker of malignancy in VEGF-L ovarian tumors.

4) 本事業に関連して世界的な研究拠点形成に向けて、以下の点で改善・整備等されたこと

A (研究拠点体制)

シャベロン教員として齊藤先生を2009年10月まで雇用したことにより、教室内セミナーなどでの討議が活発化した。

B (研究教育環境)

毎週の講義を大学院博士課程の単位化をしたことにより、本G-COEに選ばれなかった学生たちも受講できるようになり、ボトムアップが図られた。また、講義アンケートの実施により学生たちの授業への取り組みがより真剣になるとともに、説教性が増した。また講義をする教員側の意識改革もはかられた。

E (国際化)

自分の分野に所属するSS学生を積極的に海外におけるインターンシップやリサーチデイでの発表を行わせた。

5) GCOE事業を推進するに当たって力を入れた点

若手育成委員会委員長として、SS学生の質の担保、モチベーションの向上に力を入れた。その例としては、SS学生に関し、半年ごとのヒアリングおよび1年ごとの評価に伴う再任システムを採用した。さらに、その評価には、ホンG-COEプログラムへの積極的参加（授業態度、海外派遣など）を加味し、きめ細かい評価を行った。さらに、毎週の講義後のアンケートにより、教員評価などをさせることにより、より積極的な受講態度を身につけさせた。

年3回にわたる海外リサーチデイでの発表、海外インターンシップなど海外的派遣事業を行うことにより、国際化を図った。

6) 英文原著論文

1. ©Nakalekha C, Yokoyama C, Miura Y, Alles N, Aoki K, Ohya K, Morita I. Increased Bone Mass in Adult Prostacyclin Deficient Mice. *J. Endocrinology*,
2. ©Akahori T, Kobayashi A, Komaki M, Hattori H, Kahahama K, Ichinose S, Abe M, Takeda S, Morita I. Implantation of capillary structure engineered by optical lithography improves hindlimb ischemia in mice, *Tissue Engendering*,
3. Obitsu S, Hironori NA, Hasegawa A, Nakahama K, Morita I, Nishigaki N, Hayashi, Masuda T, Kannagi M., Potential enhancement of osteoclastogenesis by severe acute 3 respiratory syndrome coronavirus 3a/X1 protein *Arch Virol* 154(9):1457-1464. 2009
4. Safronova O, Pluemsampant S, Nakahama K, Morita I Regulation of chemokine gene expression by hypoxia via cooperative activation of NFkB and histone deacetylase. *Int J Biochem Cell Biology* 41(11) 2270-2280., 2009
5. Kaneda M, Nomura, MS, Ichinose S, Kondo S, Nakahama k, Akiyoshi K, Morita I. Direct formation of proteo-liposomes by in vitro synthesis and cellular cytosolic delivery with connexin-expressing liposomes., *Materials* 30(23-24): 3971-3977, 2009
6. Wang J, Ohno-Matsui K, Yoshida T, Shimada N, Ichinose S, Sato T, Mochizuki M, Morita I. Amyloid-up-regulates complement factor B in retinal pigment epithelial cells through cytokines released from recruited macrophages/microglia; Another mechanism of complement activation in age-related macular

degeneration *J Cell Physiol* 220(1): 119-128, 2009

7. Bhattacharjee R, Kaneda M, Nakahama K, Morita I. The steady-state expression of connexin43 is maintained by the PI3K/Akt in osteoblasts. *Biochem Biophys Res Commun.* 382(2): 440-444, 2009.
8. Tsuchiya T, Nakahama K, Asakawa Y, Maemura T, Tanaka M, Takeda S, Morita M, Morita I, The reduction in pigment epithelium-derived factor is a sign of malignancy in ovarian cancer expressing low-level of vascular endothelial growth factor. *Gynecol Endocrinol* 25(2) 104-109, 2009

7) 著書

森田育男 :2.血管新生 /C.血管の再生 /II.再生医学、炎症・再生医学辞典（編集 松島綱治、西脇 徹）.P484-488. 朝倉書店.東京.2009年

8) 特許取得、特許申請

発明の名称 :人工細胞組織の作成方法、
及びそのための基材

発明者 :森田育男、中村真人、三宅秀之、服部秀志、
小林弘典、栗原正彰

特許権者 :森田育男、大日本印刷株式会社

国内特許 :第4247231号

特許承認日 :平成21年1月16日

出願番号 :特願2005-514873

出願年月日 :平成16年10月15日

発明の名称 :人工細胞体およびその製造方法

発明者 :森田育男、三宅秀之、服部秀志、小林弘典、
栗原正彰

特許権者 :森田育男、大日本印刷株式会社

国内特許 :第4303643号

特許承認日 :平成21年5月1日

出願番号 :特願2004-163512

出願年月日 :平成16年6月1日

9) 平成21年度までの自己評価

平成21年4月より、研究担当理事に就任したため、G-COEに関する業務に割かれる時間が少なくなってしまった。各推進委員の先生方にも迷惑をおかけして申し訳なく思っています。また、私の分野に所属しているSS学生にも迷惑をかけているが、その分自立心が芽生え、G-COEプログラムに積極的に取り組んでいることはたのもしく思う。研究に関しては、G-COE所属の論文が多くなり、実績は上がりつつあると考えている。

10) 和文原著論文

森田育男. アラキドン酸代謝物. 血管作動性物質-生合成、分泌、生理作用-V. 循環生理活性物質の最新知見. 日本臨床. Nippon Rinsho Vol. 67 (6) :232-238, 2009

森田育男. 序. 特集I/血管新生. 先端医学社. 炎症と免疫 17 (6) :627-628, 2009

11) 学会発表 (英文)

○Yoko Aoi. The involvement of methylation and acetylation in the repression of IL-1 β -induced MCP-1 production by hypoxia. Ph.D. Student Session. US-Japanese Symposium: Network for International Education and Research in Advanced Dental Science. Niigata, February 12-13, 2009. 口腔からQOL向上を目指す連携研究/先端歯学国際教育研究ネットワーク 日・米シンポジウム. 新潟. 2009年2月12~13日

○Aoi Y, Safronova O, Nakahama K, Morita I. The involvement of methylation and acetylation in the repression of IL-1 β -induced MCP-1 production by hypoxia. Harvard School of Dental Medicine, 2008 Student Research Day, HSDM RED LOBBY, Boston, USA, April 14, 2009

○Bhattacharjee R, Kaneda M, Nakahama K and Morita I. The steady-state expression of connexin 43 is maintained by the PI3K/Akt in osteoblasts. Harvard School of Dental Medicine, 2008 Student Research Day, HSDM RED LOBBY, Boston, USA, April 14, 2009

○Bhattacharjee R, Kaneda M, Nakahama K and Morita I. The steady-state expression level of connexin43 is maintained by the PI3K/Act pathway. Oral 6, Endothelial cells, 10th International Symposium on Mechanism of Vasodilatation, Matsushima, Miyagi, Japan, June 1-3, 2009

Safronova O, Nakahama K, Morita I. Regulation of chemokine gene expression by hypoxia via cooperative activation of NF- κ B and HDAC. GA (General Abstracts) 02: Basic Studies on Inflammation and Immunity, Japan-Taiwan Joint Symposium on Inflammation Research. The 9th World Congress on Inflammation (第30回日本炎症・再生医学会、第9回国際炎症学会 合同開催). Tokyo, Japan, June6-10, 2009

Wang J, Ohono-Matsui K, Yoshida T, Shimada N, Ichinose S, Sato T, Mochizuki M, Morita I. The crucial role of amyloid β on complement alternative pathway activation: Implication for pathogenesis of age-related macular degeneration. GA (General Abstracts) 05: Inflammatory Mediators, Such as Lipid Mediators, Coagulation, Complements, Cytokines, Chemokines, Free Radicals, and Proteases. The 9th World

Congress on Inflammation (第30回日本炎症・再生医学会、第9回国際炎症学会 合同開催). Tokyo, Japan, June6-10, 2009

Yoshida T, Komaki M, Morita I, Abe M. Therapeutic angiogenesis using EX vivo formed-capillary networks by human omental microvascular endothelial cells. GA (General Abstracts) 15 (O/P). Regenerative Medicine: Cell Therapy, Mesenchymal Stem Cells, ES, Neural and Other Organ Specific Stem/Progenitor Cells, Materials, Etc. The 9th World Congress on Inflammation (第30回日本炎症・再生医学会、第9回国際炎症学会 合同開催). Tokyo, Japan, June6-10, 2009

Safronova O, Aoi Y, Morita I. Promoter specific repression of RNA polymerase II in hypoxic inflammation is mediated by inhibition of P-TEFb elongation complex. The 32nd Annual Meeting of the Molecular Biology Society of Japan, Yokohama, November 9-12, 2009

Yuan J, Akiyama M, Nakahama K, Sato T, Uematsu H, Morita I. Effect of polyunsaturated fatty acids on osteoclastogenesis. The 32nd Annual Meeting of the Molecular Biology Society of Japan, Yokohama, November 9-12, 2009

12) 学会発表 (和文)

須藤乃里子、星野優子、中浜健一、小牧基浩、安部まゆみ、久保田俊郎、森田育男. 臍帯血を利用した血管内皮前駆細胞採取法の確立および転写技術を応用した毛細血管の作成. 第41回血管研究会. 東京. 2009年5月21日

長岡亮介、奥原 滋、森田育男、天笠光雄、井関祥子. 胎児期低酸素症が顔面形成に与える影響についての検討. ポスター発表. 第49回日本先天異常学会学術集会. 鹿児島. 2009年6月25~27日

滝 敦子、安部まゆみ、森田育男、水谷修紀. 合併症妊娠の胎盤および臍帯動静脈組織における血管新生関連因子の発現異常. 第42回血管研究会. 東京. 2009年11月5日

Jizhong Yuan, 穂山雅子、中浜健一、佐藤孝浩、植松 宏、森田育男. 破骨細胞分化に及ぼす多価不飽和脂肪酸の影響. 第32回日本分子生物学会年会. 横浜. 2009年12月9~12日

13) 受賞

IAIS Poster Award : Yoshida T, Komaki M, Morita I, Abe M. Therapeutic angiogenesis using ex vivo formed-capillary

networks by human omental microvascular endothelial cells.
The 9th World Congress on Inflammation, Tokyo, July 6-10,
2009

14) 外部資金の獲得状況

科学研究費補助金、基盤研究 (B)

研究題目:コネキシン43を介した組織の高次機能恒常性機構の解明
代表:森田育男
期間:平成20年-22年
研究費総額:14,600千円

科学研究費補助金、基盤研究 (B)

研究題目:骨リモデリングにおける破骨細胞分化の時空的制御機構の解明
代表:中浜健一
期間:平成20年-22年
研究費総額:14,700千円

科学研究費補助金、萌芽研究

研究題目:転写技術を応用した歯槽骨再生医療法の開発
代表:森田育男
期間:平成20年-21年
研究費総額:3,200千円

科学研究費補助金、挑戦的萌芽研究

研究題目:破骨細胞分化を司る接着分子の同定、その制御機構と破綻による病態の解明
代表:森田育男
期間:平成21年-22年
研究費総額:3,000千円

科学研究費補助金、特別研究員 (DC1)

研究題目:低酸素下におけるサイトカイン産生変動機序-メチル化の関与
代表:青井陽子
期間:平成20年-22年
研究費総額:1,800千円

共同研究費:森田育男・大日本印刷 (株)

研究題目:ナノテクノロジーを応用した再生医療および薬物導入技術の開発とその応用
期間:平成17年-22年
研究費総額:15,000千円

15) 特別講演、招待講演

1. 森田育男 (東京医科歯科大学大学院博士課程教育委員会).招待講演.ワークショップ.歯科医学における基礎融合型ボーダーレス教育研究拠点の形成 (Interdisciplinary Borderless Education System between Basic and Clinical Research in Dental Science / The first Workshop for Bio-dental education and research).平成20年度広島大学大学院医歯薬学総合研究科バイオデンティスト育成プログラム国際ワークショップ.広島.2009年2月7-8日
2. 森田育男 特別講演.血管新生の調節と再生医療への新展開、第27回東京母性衛生学会、東京、2009年5月17日
3. 森田育男.講演.大学院における高度歯学教育の問題点ならびに改革方針に関する提言のまとめ.第2回岡山医療教育国際シンポジウム.岡山.2009年5月17-19日
4. 森田育男 大学院FD招待講演 歯学系大学院における問題点とその対応、松本、2009年7月17日
5. 森田育男.教育講演.一研究者の生きざま.平成21年度先端歯学国際教育研究ネットワーク.先端歯学スクール2009.淡路.2009年8月27-28日
6. Ikuo Morita Special Lecture A possible mechanism for choroidal neovascularization - Involvement of amyloid β . Tainan, Taiwan, 2009. 9 21
7. 森田育男.特別講演.再生医療の将来.第129回日本輸血・細胞治療学会関東甲信越支部例会(例会長:藤田 浩、都立墨東病院 輸血科).東京.2009年9月26日
8. 森田育男.講演.東京医科歯科大学の研究展望.東京医科歯科大学歯学部歯学科4年生、平成21年度研究体験実習、第4回学生発表会.東京.2009年9月29日
9. 森田育男.特別講演.COXとNSAID_sの新展開.基調講演3/テーマNSAID_sの多面的作用.第13回壁細胞研究会.京都.2009年10月14日
10. 森田育男.ギャップ結合の調節機序とDDSへの応用.創剤フォーラム第15回シンポジウム「タイトジャンクションをめぐる最近の件給成果と創薬への応用」.東京.2009年10月23日
11. 森田育男.特別講演.血管新生の調節と再生医療への新展開.千葉大学薬友会東京支部総会.東京.2009年11月27日

16) 教室、分野や講座の准教授、講師、助教、特別研究員、ポスドク、指導を受けた大学院生の名前 (AISSには○印) のリスト

教 授	森田育男
准教授	中浜健一
シャペロン (准教授)	齊藤正夫 2009.9.30 退職
G-COE 特任講師	Olga Safronova
助 教	加藤幸太郎
特任助教	穂山雅子
大学院生	Rajib Bhattacharjee
	2009.9.30 修了
	Jiying Wang
	Chalida Nakalekha
	元 吉鐘
	青井 陽子
	滝 敦子
	須藤典子
	津川順一
	奥石太郎
	李香蘭

17) GCOE 活動についての感想、コメント、改善を望む点など

すみやかな推進教員の増員をお願いします。

ステアリング委員会の開催もよろしくお願いします。



Contents lists available at ScienceDirect

The International Journal of Biochemistry
& Cell Biologyjournal homepage: www.elsevier.com/locate/biocyRegulation of chemokine gene expression by hypoxia via cooperative activation of NF- κ B and histone deacetylaseOlga Safronova^{a,b}, Sireerat Pluemsampan^{a,b}, Ken-ichi Nakahama^a, Ikuo Morita^{a,b,*}^a Department of Cellular Physiological Chemistry, Tokyo Medical and Dental University, 1-5-45, Yushima, Bunkyo-ku, Tokyo 113-8549, Japan^b 21st Century Center of Excellence Program for Frontier Research on Molecular Destruction and Reconstitution of Tooth and Bone, Tokyo 113-8549, Japan

ARTICLE INFO

Article history:

Received 5 February 2009

Received in revised form 1 May 2009

Accepted 6 May 2009

Available online xxx

Keywords:

Hypoxia

Transcriptional repression

MCP-1

Histone deacetylase

NF- κ B

ABSTRACT

Hypoxia is a microenvironmental factor frequently associated with tumors and inflammation. This study addresses the question of how hypoxia modulates the basal and IL-1 β -induced production of cytokines and aims to identify the underlying mechanism of hypoxic transcriptional repression. We found that despite the similarities of the promoter structures of IL-8 and MCP-1, these chemokines were differently regulated by hypoxia (an increase in IL-8, but a decrease in MCP-1 mRNA and protein expression). Such differences were not observed in a reporter gene assay, in which both of the promoters were activated by hypoxia. The difference in the response to hypoxia between MCP-1 expression and the promoter assay was not due to mRNA instability. Using proteasome inhibitor MG132 and I κ B overexpression we demonstrated that an NF- κ B-dependent mechanism was involved in both the activation of IL-8 and the repression of MCP-1 mRNA expression in response to hypoxia. The histone deacetylase inhibitor Triostatin A abolished the inhibitory actions of hypoxia on IL-1 β -induced MCP-1 gene expression. Furthermore, hypoxia induced histone deacetylase activity in the nuclear extracts. Although stimulation with IL-1 β and/or hypoxia increased the acetylation of histones H3 and H4 in the presence of Triostatin A, histone acetylation remained unchanged when the cells were treated without histone deacetylase inhibitor. Collectively, our findings suggest that transiently transfected promoters are not subject to the same NF- κ B regulatory mechanisms as their chromatinized counterparts. NF- κ B, activated by hypoxia, can act as a transcriptional repressor via a mechanism that involves deacetylation of histones.

© 2009 Published by Elsevier Ltd.

1. Introduction

Hypoxia is a common pathological factor of inflamed tissue with a profound impact on the cellular transcriptome. Hypoxic areas can be detected from one of the earliest responses to injury, and progressive inflammation further exacerbates oxygen deficiency. Metabolic activity of immune cells (respiratory burst), reduced blood flow, production of adhesion factors, proliferative response, and tissue fibrosis all contribute to the reduction of oxygen supply (Bjornheden et al., 1999; Crowther et al., 2001; Lund-Olesen, 1970; Vaupel et al., 2001). Together with early response proinflammatory cytokines, hypoxia affects the profile of the cytokine/chemokine network and therefore directs the natural evolution of proinflammatory response.

The transcriptional response to hypoxia involves the activation of a number of transcriptional regulators associated with

inflammation, tumor invasion, angiogenesis, cell-cycle arrest, and apoptosis. Hypoxia-responsive transcription factors include hypoxia-inducible factors (HIF-1 and HIF-2), NF- κ B, AP-1, SP-1, CREB, etc. and have been reviewed in detail elsewhere (Cummins and Taylor, 2005; Kenneth and Rocha, 2008). In general, activation of HIF-1 leads to the expression of genes involved in hypoxia-adaptive response, such as GLUTs, iNOS, VEGF and erythropoietin (Manalo et al., 2005). Alternatively, activated NF- κ B mediates inflammatory responses and corresponds to the overlap of expression profiles under inflammation and hypoxia and is therefore an important regulator of transcription in hypoxia-associated inflammation (Barnes and Karin, 1997).

MCP-1 and IL-8 are prototypical members of the CC and CXC families of chemokines. MCP-1 expression results in the tissue infiltration of monocytes/macrophages (Leonard and Yoshimura, 1990), NK cells (Allavena et al., 1994), and subpopulations of T lymphocytes (Carr et al., 1994). IL-8 induces the chemotaxis of neutrophils (Matsushima and Oppenheim, 1989) and also displays angiogenic properties (Koch et al., 1992). Because of their biological functions, MCP-1 and IL-8 are associated with the pathogenesis of acute and chronic inflammatory diseases, such as atherosclerosis, rheumatoid arthritis, and various tumors (Balkwill, 2004; Strieter et al., 1994).

* Corresponding author at: Department of Cellular Physiological Chemistry, Tokyo Medical and Dental University, 1-5-45, Yushima, Bunkyo-ku, Tokyo 113-8549, Japan. Tel.: +81 5803 5575; fax: +81 5803 0212.

E-mail address: morita.ceu@tmd.ac.jp (I. Morita).

Comparative analysis of the 5'-genomic regions of MCP-1 and IL-8 revealed similarities in the transcription factor binding sites. Both genes are TATA-dependent and contain κ B and AP-1 binding sites. However, in the IL-8 gene, these binding sites are located within the minimal 133 bp promoter (Kikuchi et al., 2002; Xu et al., 1999), while in the MCP-1 gene they are grouped in the distal enhancer approximately 2.5 kbp upstream from the basic promoter (Finzer et al., 2000; Ueda et al., 1994). The distal enhancer region of MCP-1 has two functioning κ B sites (κ B1 and κ B2), both of which are required for gene regulation (Ueda et al., 1994). The κ B3 site of the proximal regulatory region shows homology to the κ B binding sequence, but does not bind NF- κ B family members (Ping et al., 1996).

The κ B-sites are required for the induction of the MCP-1 and IL-8 genes by inflammatory mediators, such as IL-1, TNF α , and LPS. The classical NF- κ B complex is a heterodimer of p65 and p50 subunits. In resting cells, most NF- κ B dimers are retained in the cytoplasm in a complex with inhibitory protein- κ B (I κ B). Release of the NF- κ B dimer from the complex with I κ B allows its translocation to the nucleus, where it is recruited to target promoters and promotes gene transcription (Chen and Greene, 2004).

Cytoplasmic events provide stimulus-specific activation of NF- κ B. In addition, gene transcription is governed by chromatin assembly and covalent modifications of core histones. Transcriptionally repressed chromatin is compact and correlates with the hypoacetylation of histone tails. In contrast, the acetylation of histone tails occurs at transcriptionally active loci and provides docking sites for the bromodomains of chromatin remodeling enzymes (Clayton et al., 2006). The remodeling cascade is usually initiated by the acetylation of histones H3 and H4 within regulatory regions and depends on p65-dependent recruitment of co-activators (Gerritsen et al., 1997). Conversely, p65 interaction with various transcriptional co-repressors, such as histone deacetylases HDAC1, HDAC2, HDAC3, or SIRT1, and subsequent co-recruitment leads to negative regulation of gene expression (Ashburner et al., 2001; Campbell et al., 2004; Shetty et al., 2005; Yeung et al., 2004).

This study addressed the question of how hypoxia affects the cytokine network. We demonstrated that hypoxia acts as a selective inhibitor of MCP-1 gene expression, but induces the transcription of IL-8. Our data provide new evidence that hypoxic MCP-1 repression is mediated by NF- κ B through a mechanism that involves the deacetylase activity of HDAC.

2. Materials and methods

2.1. Antibodies and inhibitors

Anti-acetyl-histone H3 (06-599), anti-acetyl-histone H4 (06-866), anti-histone H3 (06-755), and anti-histone H4 (07-108) antibodies were purchased from Upstate, Lake Placid, NY, USA. Anti-NF κ B p65 rabbit polyclonal antibody (sc-109) and anti-NF κ B p65 mouse monoclonal antibody (sc-8008) were from Santa Cruz Biotechnology. Anti-histone deacetylase 1 (SA-401) and anti-histone deacetylase 2 (SA-402) rabbit polyclonal antibodies were from BIOMOL. MG132, trichostatin A, actinomycin D, and cycloheximide were purchased from Sigma-Aldrich.

2.2. Cell culture and hypoxia treatment

HeLa and COS7 cells were cultured in Dulbecco's modified Eagle's medium (DMEM) supplemented with 10% fetal bovine serum. A hypoxic gas mixture containing 5% CO₂, 5% or 0.5% O₂, balanced with N₂ was used for hypoxia treatment. Long-term hypoxia (4, 6, or 24 h) was achieved with the use of a modular incubator chamber (Billups-Rothenberg, Inc.). O₂ concentrations were

routinely checked using an Oxygen Monitor JKO-25S. Short-term hypoxia (15 or 30 min) was achieved by bubbling a hypoxic gas mixture through the medium for 15 min. Hypoxic conditioned medium was then applied to the cells for the designated time periods. For hypoxia treatments of 1 h, hypoxic conditioned medium was used in combination with the modular incubator chamber. Treatment of HeLa cells was performed either with or without 50 ng/ml IL-1 β or 10 ng/ml TNF- α (PeproTech EC) for the indicated time periods.

2.3. Quantification of cytokines in conditioned medium

Cytokine protein secretion was analyzed in cell culture supernatants. The cytokine expression profile of HeLa cells was studied using a RayBio Human Cytokine Antibody Array III kit (RayBiotech, Inc.) according to the manufacturer's protocol. Chemiluminescence was analyzed using an Image Reader LAS-1000 Lite (Fujifilm). Densitometric analysis was performed using ImageJ software. MCP-1 and IL-8 protein expression was further confirmed in the same culture supernatants with the use of Human IL-8/NAP-1 and Human MCP-1 Immunoassay Kits (BioSource International, Inc.).

2.4. mRNA expression

Total RNA was extracted, reverse transcribed, and analyzed by quantitative real-time PCR (RT-qPCR) as described previously (Safronova et al., 2003) with the exception of using 1 μ l of 0.4 μ g/ μ l random primer (Amersham Pharmacia Biotech, Inc.) for cDNA synthesis and normalization by 18S rRNA. Data are expressed as a percentage of the expression level in the control and represented as means \pm SEM ($n = 3$).

2.5. Transient transfection and luciferase assay

For the reporter gene assay, HeLa cells were plated at a concentration of 1.4×10^5 cells/well and 24 h later transfected with the 0.5 μ g of the test plasmid DNA using Lipofectamine 2000 transfection reagent (Invitrogen). Each construct was co-transfected with 0.1 μ g of pRL-TK as an internal control for transfection efficiency. After 24 h, cells were treated with or without 50 ng/ml IL-1 β and incubated under normoxia or hypoxia (0.5% O₂) for 6 h.

The luciferase assay was performed on each sample using a Dual-Luciferase Reporter assay system (Promega). The luciferase activity was normalized by the Renilla luciferase activity and expressed as relative luciferase activity (RLA). Data represent the means \pm SEM ($n = 4$).

2.6. Plasmid constructs

Individual deletion fragments of the MCP-1 (D26087) or IL-8 (M28130) 5'-genomic flanking regions were placed upstream of the luciferase gene in the pGL3-basic vector (Promega). The NF- κ B reporter vector was purchased from Clontech. Three hypoxia response element (HRE) sequences from the erythropoietin gene (Krones et al., 2001) were subcloned into a pGL3-basic vector to obtain the HRE-reporter.

A fusion protein of the p65 subunit (NM_021975) with GFP linked to its C terminus was created with the use of a pEGFP-C1 vector (Clontech Laboratories Inc, Palo Alto, CA, USA). The pCMV-I κ B α vector was from BD Biosciences.

2.7. HDAC activity measurement

HDAC activity was measured in HeLa nuclear extracts using a HDAC Colorimetric Activity Assay/Drug Discovery kit (BIOMOL) in accordance with the manufacturer's protocol.

Please cite this article in press as: Safronova O, et al. Regulation of chemokine gene expression by hypoxia via cooperative activation of NF- κ B and histone deacetylase. Int J Biochem Cell Biol (2009), doi:10.1016/j.biocel.2009.05.003

2.8. Western blotting

Cells were lysed in a buffer containing 50 mM Tris-HCl (pH 7.5), 150 mM NaCl, 1% Triton X-100, 2 mM EDTA, 1 mM EGTA, supplemented with protease inhibitor cocktail (Sigma), and sheared by sonication.

Samples were separated by SDS-PAGE and transferred to a PVDF membrane. After incubation with primary antibody and secondary HRP-conjugated antibody, detection was performed using a Lumi-Light Western Blotting Substrate (Roche Applied Science).

2.9. Immunocytochemistry

HeLa cells were cultured on glass bottomed dishes. After treatment, the cells were fixed with 10% formaldehyde solution for 15 min at room temperature, permeabilized for 20 min using 0.2% Triton X-100, and incubated with blocking solution (1% FBS in PBS). Incubation with primary anti-p65 antibody was carried out overnight at 4 °C, followed by incubation for 2 h with appropriate Alexa Fluor 488-conjugated secondary antibodies (Molecular Probes). Cellular fluorescence was monitored using a ZEISS 510 META laser scanning confocal microscopy.

2.10. Chromatin immunoprecipitation (ChIP)

The ChIP assay was performed using a Chromatin Immunoprecipitation Assay Kit (Upstate Biotechnology) in accordance with the manufacturer's protocol with the following exceptions: cross-linking was carried out at room temperature by adding formaldehyde for 10 min with subsequent termination with glycine at a final concentration 0.125 M; and chromatin was sheared using a sonicator Bioruptor UCD-200T (Cosmo Bio Co., Ltd.). Chromatin from 3×10^6 HeLa cells was used per antibody. Samples were analyzed by Q-PCR in a 7500 Real-Time PCR System (Applied Biosystems) using a DyNAmo Probe qPCR kit (Finnzymes Oy, Espoo, Finland). TaqMan probes were labeled with 5'-FAM (reporter) and 3'-BHQ1 non-fluorescent quencher. For Q-PCR, 2 μ l from a 40 μ l DNA extraction were used. Each cycle threshold (Ct) value was determined from three parallel PCRs. Immunoprecipitated DNA was normalized by 10% input DNA. Data are expressed as a percentage of histone acetylation under normoxia. The MCP-1 and IL-8 promoter regions were subcloned into pGL3 and used to obtain the calibration curve.

2.11. Immunoprecipitation

Immunoprecipitations were carried out as recommended by Millipore Technical Library (<http://www.millipore.com/techpublications/tech1/mcproto424>) with the exception of using EBC lysis buffer (50 mM Tris [pH 8.0], 120 mM NaCl, 0.5% NP-40, 10% glycerol supplemented with 1 mM PMSF, complete mini protease inhibitor cocktail (Roche), 1 mM NaF and 1 mM sodium orthovanadate) for cell lysate preparation and washing. Cell lysates were diluted to 4.5 μ g/ μ l total cell protein and immunoprecipitated overnight with monoclonal anti-p65 antibody. Immunocomplexes were captured by Protein G Sepharose (Amersham Biosciences) and 25 μ l of immunoprecipitates were used for the analysis.

To measure HDAC activity associated with p65, Protein G Sepharose beads from immunoprecipitation step were resuspended in Color de Lys substrate from HDAC activity assay kit and incubated at 37 °C for 1 h. Supernatants were transferred to the microplates, mixed with Color de Lys developer and analyzed in microplate reader.

2.12. Statistical analysis

All quantitative data in this study are represented as means \pm standard error of the mean (SEM) of three experiments, if not stated otherwise, and were calculated using the Data Analysis package of Microsoft Excel software. Comparisons between groups were made using the unpaired two-tailed Student's *t*-test assuming equal variances. Differences were considered to be statistically significant at a level of $p < 0.05$.

3. Results

3.1. Identification of IL-8 and MCP-1 as hypoxia-responsive cytokines

First, the effect of hypoxia and IL-1 β on the cytokine secretion profile of HeLa cell line was studied. Cells were incubated under hypoxic or normoxic conditions in the presence or absence of IL-1 β for 24 h. Cell culture supernatants were then collected and analyzed using a RayBio Human Cytokine Protein Array. Cytokine expression was quantified by densitometric analysis. Under normoxic condition, HeLa cells did not produce large amounts of cytokines with the exception of abundant constitutive expression of Monocyte Chemoattractant Protein-1 (MCP-1) (Fig. 1). Treatment with IL-1 β caused a 30% increase in MCP-1 expression and led to a high level of production of IL-8 and IL-6. Exposure to hypoxia led to further changes in the cytokine expression pattern. An induction in the expression level of IL-8 was observed in response to IL-1 β with a 60% increase in the absence of IL-1 β and a 30% increase under simultaneous treatment with hypoxia and IL-1 β . In contrast, in response to hypoxia, secretion of MCP-1 protein declined (Fig. 1).

To confirm this observation, MCP-1 and IL-8 protein secretion levels were further quantified by ELISA. As shown in Fig. 2A, HeLa cells constitutively expressed MCP-1 protein. This constitutive expression was strongly inhibited by exposure to hypoxia with a 4-fold reduction. Treatment with IL-1 β -induced MCP-1 secretion by ~2-fold, and hypoxia abolished this response (Fig. 2A). Consistent with the Cytokine Protein Array data, quantification using ELISA confirmed that IL-1 β -induced IL-8 secretion was significantly enhanced by hypoxia (Fig. 2B).

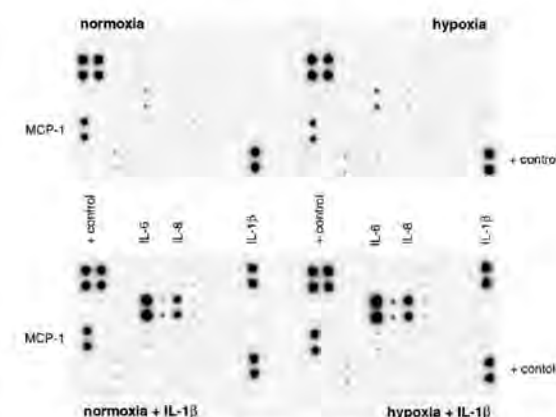


Fig. 1. Effect of hypoxia and IL-1 β on the profile of cytokine protein secretion by HeLa cells. HeLa cell cultures were treated with IL-1 β (50 ng/ml), or hypoxia (0.5% O₂) or both for 24 h. Cell culture supernatants were then collected and analyzed using a RayBio Human Cytokine Protein Array.

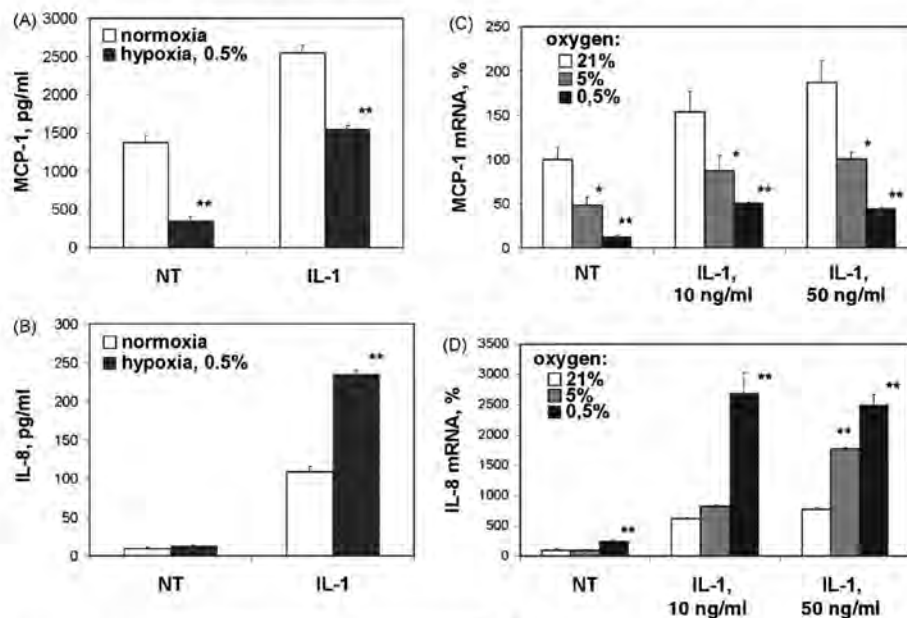


Fig. 2. Effect of hypoxia on protein secretion and mRNA expression of MCP-1 and IL-8. The amounts of MCP-1 (A) and IL-8 (B) proteins secreted into the culture supernatants were measured using ELISA. Cultures were subjected to normoxia or hypoxia in the absence (NT) or presence of 50 ng/ml IL-1 β for 24 h. Data are expressed as mean \pm SEM of four independent experiments. ** p < 0.01, significantly different as compared with normoxia in each data series. (C) Concentration-dependent response of MCP-1 mRNA expression to hypoxia. HeLa cells were treated with gas mixtures containing the indicated concentrations of O₂ without (NT) or with increasing concentrations of IL-1 β for 24 h. Total RNA was isolated and analyzed by RT-qPCR. Quantities of MCP-1 mRNA were normalized by the expression of 18S rRNA. The value of normoxic samples without IL-1 β treatment was set as 100%. The average of three experiments is shown with SEM. (D) Concentration-dependent response of IL-8 mRNA expression level to hypoxia. Analysis was performed as described in (C). * p < 0.05; ** p < 0.01, as compared with 21% O₂ in each data series.

3.2. Hypoxia activates IL-8, but represses MCP-1 mRNA expression

Next, we checked whether the mRNA expression level followed the pattern of protein secretion. HeLa cells were treated with increasing concentrations of IL-1 β and simultaneously incubated under various conditions of oxygenation. RT-qPCR analysis was performed to evaluate mRNA expression. Consistent with the observation on protein secretion, both MCP-1 and IL-8 mRNA expressions were significantly induced by IL-1 β (Fig. 2C, D). Strong suppression of MCP-1 mRNA expression was observed as the extent of oxygen deprivation increased (21%, 5%, and 0.5% of O₂) (Fig. 2C). Hypoxia

synergized with IL-1 β in inducing IL-8 mRNA expression (Fig. 2D). Therefore, MCP-1 and IL-8 mRNA expressions followed the same pattern of protein secretion.

To determine whether hypoxia possesses a similar effect on chemokines up-regulated by other proinflammatory mediators, in addition to that elicited by IL-1 β , the response to TNF α was studied. A considerable increase in MCP-1 and IL-8 mRNA expression levels over the basal levels was observed after 24 h of treatment with TNF α (Fig. 3A, B). The strong repressive effect of hypoxia on TNF α -induced MCP-1 mRNA expression was consistent with that shown in cells treated with IL-1 β (Fig. 3A). The effect of hypoxia on IL-8 mRNA expression induced by TNF α was much

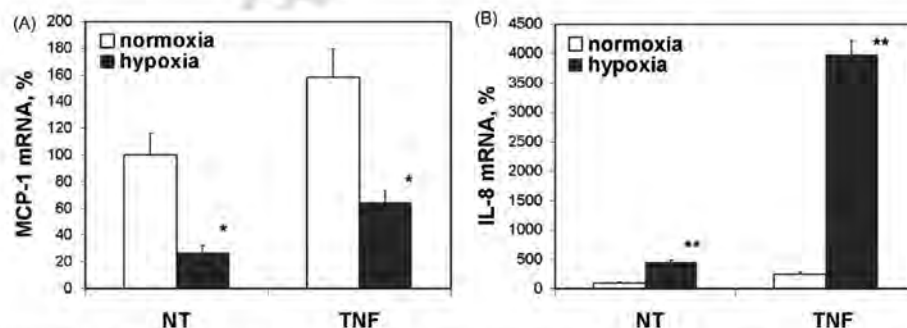


Fig. 3. Hypoxia inhibited TNF α -stimulated MCP-1 mRNA expression, but induced IL-8 mRNA expression. (A) Effect of hypoxia on TNF α -elicited MCP-1 mRNA expression. HeLa cells were treated without (NT) or with 10 ng/ml TNF α and exposed to normoxic or hypoxic gas mixtures for 24 h. MCP-1 mRNA levels were quantitated by RT-qPCR and normalized by 18S rRNA levels. Data are expressed as a percentage of expression under normoxia of triplicate assays. (B) Effect of hypoxia on TNF α -elicited IL-8 mRNA expression level. Analysis was performed as described in (A). * p < 0.05; ** p < 0.01, as compared with normoxia in each data series.

Please cite this article in press as: Safronova O, et al. Regulation of chemokine gene expression by hypoxia via cooperative activation of NF- κ B and histone deacetylase. Int J Biochem Cell Biol (2009), doi:10.1016/j.biocel.2009.05.003

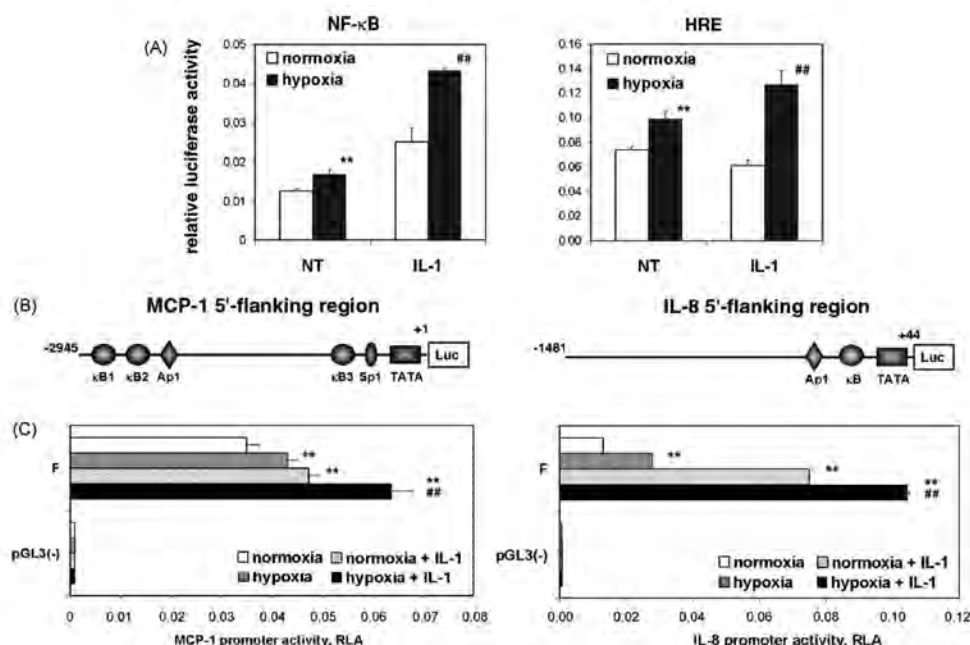


Fig. 4. Hypoxia induces the activity of transiently transfected promoters of both *MCP-1* and *IL-8* genes. (A) Relative luciferase activities (RLA) of NF-κB and hypoxia response element (HRE) reporter vectors in response to hypoxia, IL-1β, or their combination. Cells were transfected with the indicated reporter plasmid and co-transfected with pRL-TK vector as an internal control of transfection efficiency. After 24 h, cultures were treated without (NT) or with 50 ng/ml IL-1β with simultaneous exposure to normoxia or hypoxia for 6 h. Luciferase activities were measured in cell lysates, normalized by the activities of the control vector and expressed as mean ± SEM of four independent experiments. (B) Schematic representation of luciferase reporter plasmids containing *MCP-1* and *IL-8* 5'-regulatory regions. (C) Relative activities of luciferase reporters containing 5'-flanking regulatory regions of *MCP-1* and *IL-8* genes in response to hypoxia and/or IL-1β. Cells were treated and analyzed as described in (A). ***p* < 0.01, significantly different versus normoxia; ##*p* < 0.01, significantly different versus normoxic IL-1β-treated samples.

more potent in comparison with the synergistic effect with IL-1β (Fig. 3B).

3.3. Activities of transiently transfected promoters of *MCP-1* and *IL-8* genes are induced by hypoxia

The regulatory regions of *MCP-1* and *IL-8* genes contain κB binding sites (Fig. 4B). Thus, a reporter assay was performed to identify the activity of NF-κB transcription factor in HeLa cells in response to hypoxia and IL-1β. As shown in Fig. 4A, NF-κB was activated in response to hypoxia and IL-1β. Simultaneous treatment with hypoxia and IL-1β had a synergistic effect on NF-κB activity. The activity of the hypoxia response element is shown as a positive reference of hypoxic response (Fig. 4A).

To characterize the hypoxia-responsive DNA sequences of the *MCP-1* and *IL-8* genes, the 5'-flanking regions of the *MCP-1* and *IL-8* genes were cloned into the pGL3 vector, which contains the luciferase reporter gene. HeLa cells were transiently transfected with vectors and after 24 h of incubation were treated with hypoxia, IL-1β, or the combination for 42 h. As shown in Fig. 4C, exposure to hypoxia caused a 2-fold increase in IL-8 reporter activity. IL-1β was also a potent inducer of IL-8 transcription, with synergistic action in co-treatment with hypoxia. Unexpectedly, we could not observe hypoxic repression of the *MCP-1* reporter transfected into HeLa cells (Fig. 4C). IL-1β or hypoxia-induced luciferase activity in the cells transfected with the reporter containing the full-length (F) *MCP-1* reporter. Unlike *MCP-1* mRNA expression, hypoxia co-enhanced IL-1β-induced *MCP-1* reporter activity. Therefore, luciferase reporters containing full-length regulatory regions (F) of both *MCP-1* and *IL-8* were activated by hypoxia in HeLa cells (Fig. 4C). Furthermore,

different hypoxic responses of *MCP-1* and *IL-8* reporters also could not be observed in COS7 cells (data not shown).

3.4. Hypoxia does not affect *MCP-1* and *IL-8* mRNA stability

The different responsiveness of *MCP-1* mRNA expression and promoter activity in the reporter gene assay to hypoxia could be due to increased degradation of *MCP-1* mRNA in hypoxic cells. To clarify this assumption, the stability of *MCP-1* and *IL-8* mRNAs was examined in hypoxic and normoxic conditions using an inhibitor of transcription, actinomycin D. There was no difference in the rate of degradation of the *MCP-1* mRNA over the time period studied (Fig. 5A), suggesting that the decreased *MCP-1* expression in HeLa cells by hypoxia mainly occurs at the transcriptional level.

3.5. The effect of hypoxia on *MCP-1* and *IL-8* expressions does not require de novo protein synthesis

To examine the possible involvement of newly synthesized proteins in the hypoxic response of chemokine genes expression, HeLa cells were treated with cycloheximide, a protein synthesis inhibitor. Cycloheximide caused superinduction of *MCP-1* and *IL-8* mRNAs under hypoxia and normoxia (Fig. 5B). Hypoxia down-regulated the *MCP-1* mRNA expression, and enhanced *IL-8* mRNA expression in the presence of cycloheximide and the rate of these changes was similar to that without inhibitor (Fig. 5B). These data suggest that newly synthesized proteins were not required for the effect on the expression of *MCP-1* and *IL-8* mRNAs in response to hypoxia.

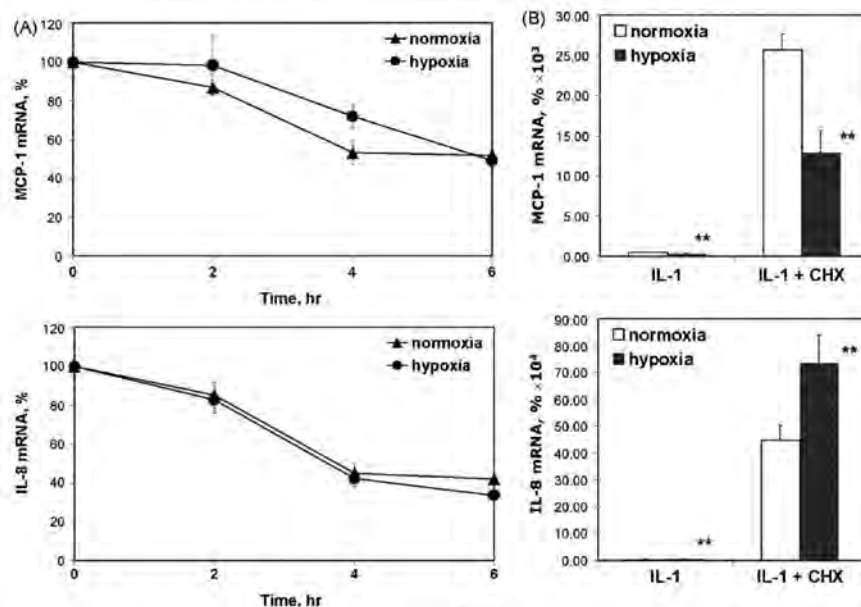


Fig. 5. Effect of actinomycin D and cycloheximide on MCP-1 and IL-8 gene expression under hypoxia. (A) Effect of hypoxia on MCP-1 and IL-8 mRNA stability. Cells were exposed to IL-1 β for 12 h, then treated with 5 μ g/ml actinomycin D to block mRNA synthesis and further incubated under normoxia or hypoxia for 0, 2, 4, or 6 h. mRNA was quantified by RT-qPCR, normalized by 18S rRNA and expressed as a percentage of expression at a 0 h time point. The average of three experiments is shown with SEM. (B) Effect of cycloheximide (CHX), a protein synthesis inhibitor, on hypoxic response of MCP-1 and IL-8 mRNA expression level. Cells were pretreated with 10 μ g/ml cycloheximide for 1 h then IL-1 β was added and cells were further incubated for 6 h under normoxia or hypoxia. Data shown as a percentage of expression under IL-1 β stimulation in normoxia and represent means \pm SEM ($n = 3$).

3.6. The role of NF- κ B in hypoxic response of MCP-1 and IL-8 genes

Recent evidence suggests that NF- κ B may act not only as an activator of transcription, but also as a transcriptional repressor (Campbell et al., 2004). Therefore, next we analyzed the possible involvement of NF- κ B in the hypoxic responses of MCP-1 and IL-8.

First, it was evaluated whether NF- κ B is inducible by hypoxia in the HeLa cell line. Treatment with either IL-1 β or hypoxia alone led to p65 nuclear translocation, though with different kinetics (Fig. 6A). Simultaneous treatment with IL-1 β and hypoxia caused stronger NF- κ B activation that was also longer in duration.

Next, we studied the role of NF- κ B in the hypoxia-mediated activities of MCP-1 and IL-8 genes. HeLa cells were treated with MG132, a proteasome inhibitor that abolishes NF- κ B activation by inhibition of I κ B proteolysis. As shown in Fig. 6B, under treatment with MG132, hypoxia induced MCP-1 mRNA expression, in contrast to repression in untreated cells.

To assess more definitively whether NF- κ B activation was required for the hypoxic response of chemokine expression, we used an expression vector encoding the NF- κ B inhibitory protein I κ B α linked to the CMV immediate early promoter. I κ B α binds NF- κ B and inhibits its activation by preventing NF- κ B from translocating to the nucleus. First we checked whether transfection with the pCMV-I κ B vector was sufficient to inhibit NF- κ B in HeLa cells. Cells were transfected with pEGFP-p65 expression vector in combination with a pCMV vector, which was empty or contained an I κ B α coding region. Overexpression of p65 led to its accumulation in the nucleus due to imbalance with inhibitory I κ B α (Fig. 6C). Co-transfection with pCMV-I κ B effectively prevented p65-GFP nuclear accumulation (Fig. 6C). I κ B α repressor abolished the response to hypoxia of both MCP-1 and IL-8 genes (Fig. 6D, E). These findings suggest that NF- κ B, activated by hypoxia, can act both as an acti-

vator of the IL-8 gene expression and as a repressor of MCP-1 gene expression.

3.7. HDAC is responsible for hypoxic down-regulation of MCP-1 expression

Recent studies have shown that the association of p65 with distinct histone modifying enzymes (acetyltransferases CBP/p300 or deacetylases HDAC1, HDAC2, and HDAC3) determines whether an activating or inhibitory transcription program will go into effect (Vanden Berghe et al., 2006). To test the possibility that HDAC may be involved in NF- κ B-mediated MCP-1 repression by hypoxia, we used trichostatin A (TSA), an HDAC inhibitor. IL-1 β -stimulated HeLa cells, which were the positive control, and cells stimulated with IL-1 β in the presence of increasing concentrations of TSA were subjected to hypoxia for 6 h. Treatment with TSA dose-dependently increased IL-1 β -induced expression of both MCP-1 and IL-8 genes (Fig. 7A). TSA at a low concentration (50 ng/ml) abolished the hypoxic response of MCP-1 expression. Furthermore, in the presence of a high concentration of TSA (100 ng/ml), hypoxia lost its inhibitory activity towards MCP-1 gene expression and strongly activated its transcription (Fig. 7A). Inhibition of HDAC activity caused increased expression of the IL-8 gene, but responsiveness to hypoxia was not changed (Fig. 7A).

HDACs inhibit gene transcription by deacetylating the tails of histone core proteins. Therefore, next we checked whether hypoxia affected histone acetylation. The intracellular levels of acetylated histones H3 and H4 were not changed in the cells treated with hypoxia or IL-1 β alone, or with co-treatment (Fig. 7C). The level of histone acetylation *in vivo* is mainly determined by the balance between HAT and HDAC. The acetylation of histones was analyzed in cells treated with TSA. The level of histone H4 acetylation was increased dramatically by treatment with TSA due to unopposed

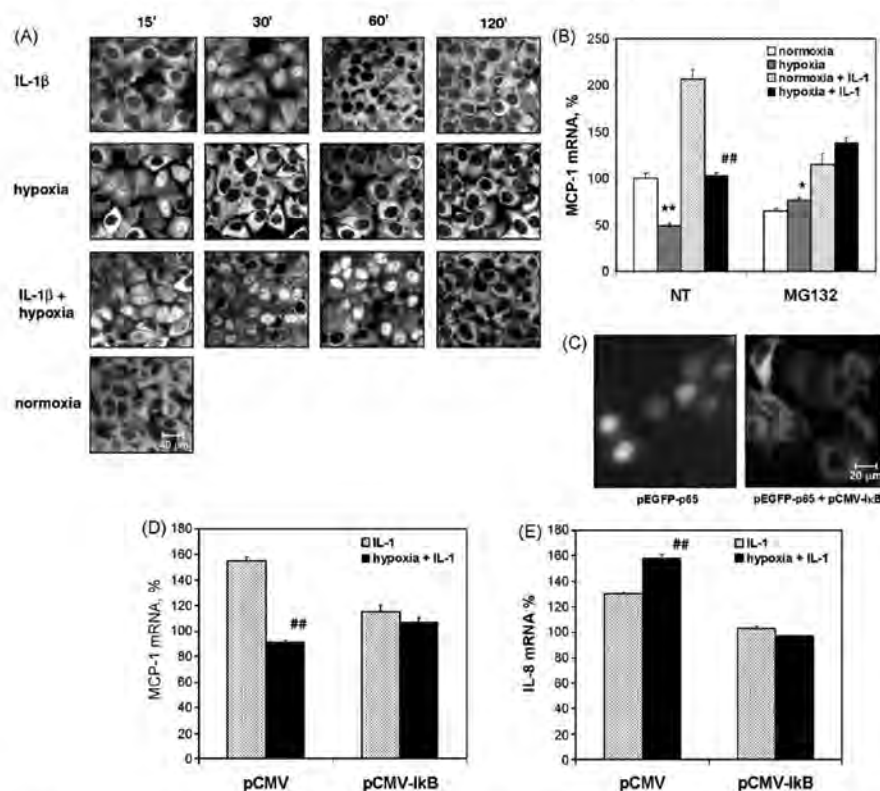


Fig. 6. NF-κB mediates the transcriptional hypoxic response of MCP-1 and IL-8 genes. (A) Confocal laser microscopic images showing subcellular localization of p65 in HeLa cells treated with IL-1β, hypoxia, or their combination. Cells were treated for the indicated periods of time, fixed, and incubated with p65 antibody for overnight, followed by incubation for 2 h with secondary antibodies. (B) Cells were pretreated or not (NT) with 10 mM MG132 for 1 h followed by 6 h exposure to hypoxia with or without IL-1β. Total RNA was isolated and analyzed by RT-qPCR. The quantities of MCP-1 mRNA were normalized by the expression of 18S rRNA. The average of three experiments is shown with SEM. Data are expressed as a percentage of expression under normoxia without IL-1β or MG132 treatment. (C) Transfection with the pCMV-IκB expression vector inhibits NF-κB activation, induced by overexpression of p65-GFP protein. Images represent p65-GFP intracellular localization 24 h after transfection. (D, E) Overexpression of IκB abolished the hypoxic response of the MCP-1 and IL-8 genes. MCP-1 (D) and IL-8 (E) mRNAs were quantified by RT-qPCR from mRNA isolated from HeLa cells that were transiently transfected with 2.5 μg of pCMV expression vector with or without an IκB coding region. Cells were treated with IL-1β and exposed to normoxia or hypoxia for 6 h. Expression in the cells transfected with empty pCMV vector followed by IL-1β treatment was set equal to 100%. Data represent the average of triplicate measurements with the SEM. **p* < 0.05; ***p* < 0.01, significantly different versus normoxia of each data series; ##*p* < 0.01, significantly different versus normoxic IL-1β-treated samples of each data series.

HAT activity (Fig. 7B) and was further elevated in cells treated with either hypoxia or IL-1β, reaching a maximum level with co-treatment (Fig. 7B, C). Therefore, hypoxia causes simultaneous activation of both HAT and HDAC and maintains the overall cellular level of histone acetylation at an unchanged level. Consistent with these observations, the induction of HDAC enzymatic activity in HeLa cells nuclear extracts was observed at 1 h after hypoxic treatment (Fig. 7D). These activities may allow hypoxia signaling to perform gene specific activation or repression by the selective recruitment of transcriptional co-regulators.

To correlate the effects of hypoxia on MCP-1 and IL-8 gene expression with histone acetylation, ChIP assays were performed with antibodies specific to acetylated forms of histones H3 and H4. Treatment with IL-1β caused a significant increase in histone H3 and H4 acetylation at the κB sites of the MCP-1 gene, consistent with the activation of transcription (Fig. 7E). Simultaneous treatment with IL-1β and hypoxia abolished the acetylation of histones on the MCP-1 promoter. Hypoxia alone led to the reduced acetylation of histone H4, thus correlating histone deacetylation with repression of transcription of the MCP-1 gene. Acetylation of his-

tone H4, but not H3, was seen on the IL-8 promoter upon IL-1β treatment (Fig. 4E). Hypoxia alone did not affect histone acetylation of the κB site of the IL-8 promoter, but co-stimulation with hypoxia and IL-1β led to the acetylation of histone H4, which was stronger than with IL-1β treatment alone.

3.8. Hypoxia leads to the increase of p65-associated HDAC activity

In order to determine if inhibitory function of NF-κB in hypoxia is connected with HDAC, series of co-immunoprecipitation experiments were performed. Cells were incubated under IL-1β, hypoxia or their simultaneous treatment for indicated periods of time. The p65 immunoprecipitates were isolated and examined for the association with class I HDACs. Precipitation of p65/HDAC2 immunocomplex suggested a physical interaction between these two proteins (Fig. 8A). In contrast, no interaction between p65 and HDAC1 was detected (data not shown). We observed that p65 associated with HDAC2 under the treatment with IL-1β or hypoxia across a similar time frame, reaching maximum at 1 h time point. However, in the cells simultaneously treated with IL-1β and

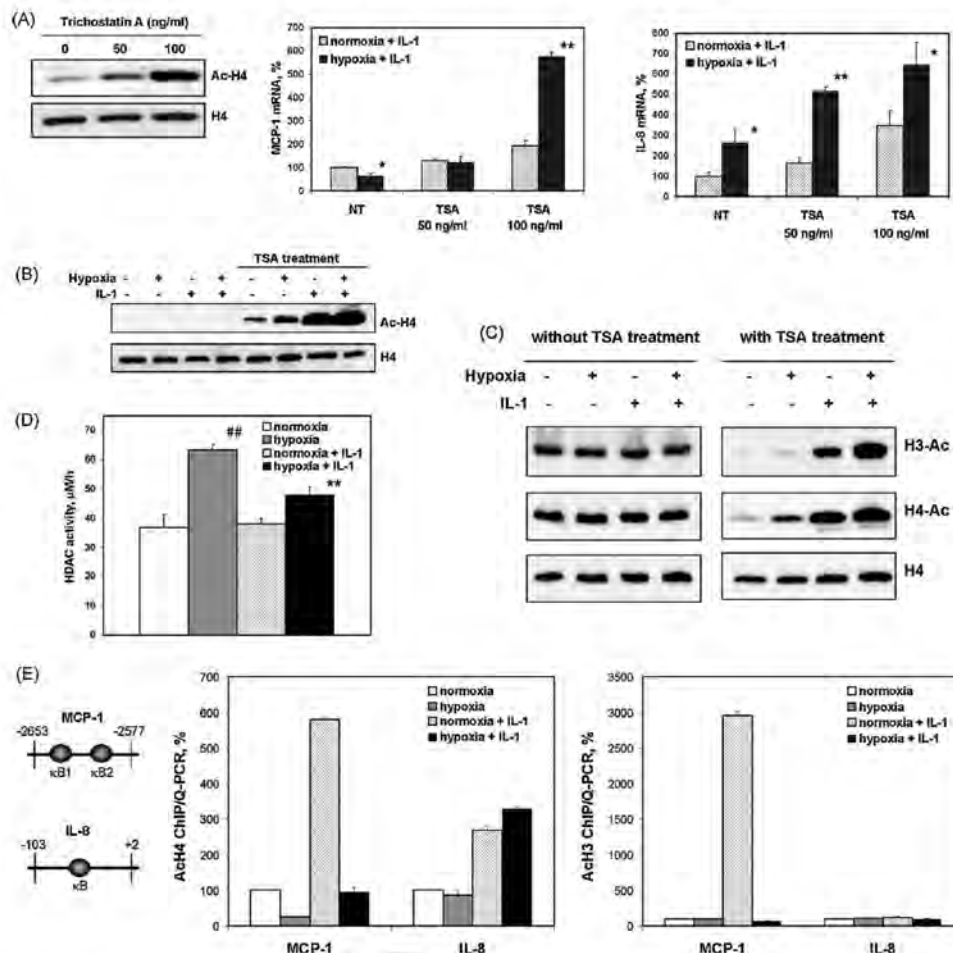


Fig. 7. HDAC activity and histone deacetylation are involved in hypoxia-induced repression of MCP-1. (A) Cells were pretreated without (NT) or with the indicated concentrations of TSA for 1 h prior to incubation under normoxia or hypoxia in the presence of 50 ng/ml IL-1 β for 6 h. MCP-1 and IL-8 mRNA levels were quantified by RT-qPCR. The expression level in normoxic cells treated with IL-1 β was set as 100%. Data are shown as mean \pm SEM of triplicate measurements. Left panel represents Western blot analysis showing dose-dependent induction of histone H4 acetylation (Ac-H4) after treatment with the TSA. (B) Western blotting for histone acetylation was performed on equal amounts of whole cell lysates generated from cells that were pretreated with or without 100 ng/ml of TSA for 1 h and then treated with IL-1 β and/or hypoxia for 4 h. Immunoblots were probed with anti-acetyl-histone 4 (Ac-H4) and anti-histone 4 (H4) antibodies. (C) Effect of hypoxia and IL-1 β on the acetylation of histones H3 and H4 in HeLa Cells. Cells were treated as in (B). Western blotting was performed using 15 μ g of total cell lysate with anti-acetyl-histone 4 (Ac-H4) and anti-acetyl-histone 3 (Ac-H3) antibodies. The amount of histone 4 (H4) was used as an internal control. Histone acetylation from cells treated with TSA and from untreated cells was analyzed on separate membranes. (D) HDAC activity was measured in nuclear extracts of HeLa cells after exposure to hypoxia and/or IL-1 β for 1 h. (E) Using antibodies against the acetylated forms of histones H4 (Ac-H4) and H3 (Ac-H3) ChIP assays were performed on HeLa cells treated with IL-1 β or hypoxia alone, or in co-treatment for 1 h. Immunoprecipitated DNA was quantified by Q-PCR using primers specific to the promoter regions of MCP-1 and IL-8 genes containing kB sites and normalized by 10% input. Data are expressed as a percentage of histone acetylation under normoxia. The relative positions of primers are indicated in left-hand panel. ## p < 0.01, significantly different versus normoxia; * p < 0.05; ** p < 0.01, significantly different versus normoxic IL-1 β treated samples.

hypoxia association of HDAC2 with p65 occurred at earlier time point and was persistent in time (Fig. 8A).

Because strong immunocomplexes of p65 and HDAC were detected after 1 h of treatment under all experimental conditions, next we investigated whether HDACs associated with p65 at this time point possessed similar histone deacetylase activity or not. In normoxic cells, p65-associated histone deacetylase activity was very weak (Fig. 8B). In the p65 immunoprecipitates from IL-1 β -treated cells histone deacetylase activity was higher than that from control cells. Hypoxia in combination with or without IL-1 β treatment strongly induced HDAC activity associated with p65 in comparison to that under the treatment by IL-1 β itself (Fig. 8B).

4. Discussion

Hypoxia can be referred as an oxygenation status that is below the norm for particular tissue. It has been traditionally viewed as pathological condition. Hypoxic regions are likely occurred in the tissues with increased proliferation, like arthritic joints and tumors. It is important to understand two types of hypoxia known to be present in such tissues. Chronically hypoxic cells appeared as a result of increased metabolic activities. Regions of acute hypoxia develop at the distances greater than 100–150 μ m from blood vessels, where oxygen tension becomes near zero (Brown, 1990). Besides pathophysiology, hypoxia has diverse roles in the function

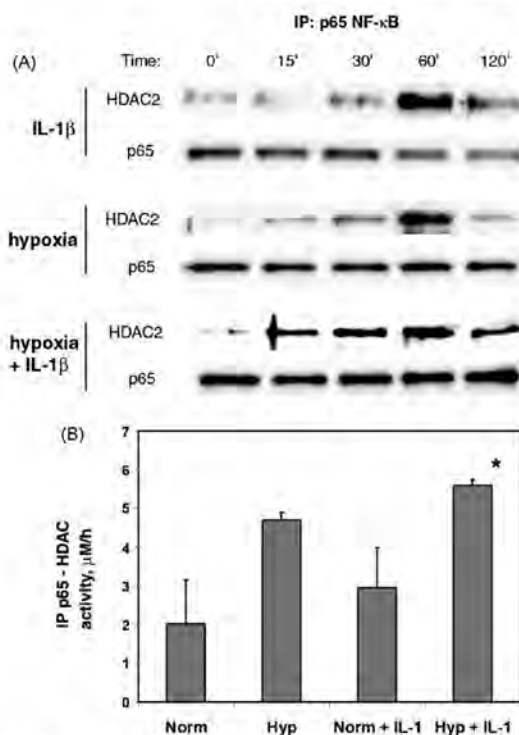


Fig. 8. Effect of hypoxia on p65-associated HDAC activity. (A) HDAC2 interacts with p65 in cells treated with hypoxia and IL-1 β . Whole cell lysates from HeLa cells treated with IL-1 β , hypoxia or combination for indicated periods of time were immunoprecipitated (IP) with monoclonal anti-p65 antibody followed by Western blotting with polyclonal HDAC2 or p65. (B) Hypoxia induces HDAC activity associated with p65. Cells were treated with hypoxia and/or IL-1 β for 1 h. HDAC activity was measured by incubation of p65 immunoprecipitates with Color de Lys substrate for 1 h. Data represent the average of triplicate measurements with the SEM, and are representative of two independent experiments. * $p < 0.05$, significantly different versus normoxic IL-1 β -treated samples.

of normal tissues. In the bone marrow, the most primitive stem cells are maintained in the hypoxic niche (Parmar et al., 2007). Mammalian development also normally transpires in a hypoxic environment (Maltepe and Simon, 1998).

The cellular transcriptome responds to hypoxia not only by the activation of specific genes, but also by selective repression. Such selectivity suggests an active process rather than a passive decline of macromolecular synthesis due to reduced energy supply. These assume that hypoxia-regulated transcriptional repression occurred through widely conserved regulatory elements. In response to hypoxia, genes containing HREs (like iNOS or VEGF) are generally activated by HIF-1 binding (Schofield and Ratcliffe, 2004). Unlike hypoxia-adaptive responses, the majority of genes involved in inflammatory responses lacks HRE but contains κ B sites. Therefore hypoxia directs the development of inflammation via two central transcription factors HIF-1 and NF- κ B (Taylor, 2008). Transcription factors interact with both HATs and HDACs, which are components of large multiprotein complexes, and therefore can lead to dual transcriptional responses. Interestingly, the content of physiological hypoxia during placental development HDAC activity is shown to be regulated in HIF-dependent manner (Maltepe et al., 2005).

In this study, it was demonstrated that hypoxia acts as a selective inhibitor of MCP-1, while inducing IL-8 chemokine expression in

HeLa cells. Earlier works from our laboratory and others observed a hypoxic repression of MCP-1 in the most of primary cultures and cell lines, including synovial cells, macrophages, cardiac cells, and ovarian carcinomas (Bosco et al., 2004; Hohensinner et al., 2006; Negus et al., 1998; Safronova et al., 2003). However, cell-specific induction of MCP-1 has also been reported in human dermal fibroblasts and hypoxic brains (Deng et al., 2008; Galindo et al., 2001). Here, we identified that the activation of NF- κ B was required for both the induction of IL-8 and repression of MCP-1 mRNA expression in response to hypoxia.

Although the role of NF- κ B as a transcriptional activator is well established and proven, growing evidence highlights its role as a transcriptional repressor (Ashburner et al., 2001; Shaw et al., 2006). These findings further support the possibility that NF- κ B is a main transcription factor involved in alteration of the cytokine network under various physiological and pathological conditions. The function of NF- κ B at specific promoters and enhancers depends on its association with different co-activators and co-repressors. Basal repression of NF- κ B in resting cells is controlled by p50 homodimers in a complex with HDAC1 or SMRT/HDAC3 co-repressors (Hoberg et al., 2004; Zhong et al., 2002). De-repression of NF- κ B-regulated genes governs the exchange of repressor complexes for acetyltransferases CBP/p300 or Tip60 (Baek et al., 2002; Hoberg et al., 2006). p65-associated HDAC activity was found to be important also for the active repression of anti-apoptotic genes after treatment with cytotoxic stimuli (Campbell et al., 2004). Consistent with this notion, the present study provides new evidence that hypoxic transcriptional repression by NF- κ B also involves the catalytic activity of HDAC.

Gene expression correlates with posttranslational modifications of the N-terminal tails of histones, which include methylation, phosphorylation, and acetylation (Kouzarides, 2007). In the case of acetylation, the hypoacetylation of lysine residues corresponds to gene repression and silencing. The balance between HAT and HDAC activities is important in maintaining the steady-state levels of histone acetylation *in vivo*. The fact that TSA completely abrogated the inhibitory actions of hypoxia on MCP-1 gene transcription strongly suggested the involvement of HDAC proteins in the repression. This finding supplements previous observation that induction of HDAC under hypoxia also involved in the repression of p53 and von Hippel-Lindau tumor suppressor genes (Kim et al., 2001).

Interestingly, we noted that a high concentration of TSA converted the inhibitory actions of hypoxia into stimulatory ones. This indirectly suggests that hypoxia simultaneously activates HAT and HDAC activities. By inhibiting histone deacetylases, TSA should allow acetyltransferases to replace the repressor complexes, which might lead to the induction of genes that are normally suppressed by hypoxia. This possibility was further supported by the observation that under the treatment with hypoxia the cellular levels of acetylated histones were not changed. TSA interrupted the balance between HAT and HDAC; therefore, an increase in histone acetylation can be observed. Moreover, it was found that hypoxia abolished IL-1 β -induced histones H3 and H4 acetylation on κ B sites of MCP-1 gene, while it enhanced histone H4 acetylation on the IL-8 promoter. These findings explained the possibility of simultaneous actions of hypoxia as an inducer of IL-8 and inhibitor of MCP-1. Interestingly, suppression of MCP-1, but not IL-8, was also demonstrated with the effect of alprazolam (Oda et al., 2002).

Finally, an interesting observation from the present study is that there is a critical difference in function of the MCP-1 gene *in vivo* versus the transiently transfected reporter under hypoxia. Inconsistent with the repression of mRNA expression, in the reporter gene assay the MCP-1 promoter was activated by hypoxia. These findings suggest that the chromatin structure of the endogenous MCP-1 gene is crucial in determining the specific gene expression program. Therefore, it is important to identify the chromatin-based mech-

anisms involved in hypoxia-mediated gene regulation. Although nucleosome-like particles are formed on transfected plasmid DNA, the overall structure is atypical and incompletely organized (Jeong and Stein, 1994). Previous reports suggested that in the uninduced state, nucleosome positioning in the proximal regulatory region of the *MCP-1* gene *in vivo* is not strictly ordered. However, chromatin configurations do not permit the binding of Sp1 until NF- κ B is recruited to the distal regulatory region. In contrast, in the distal region, a strong hypersensitive banding pattern suggested a degree of order in the nucleosomes (Boekhoudt et al., 2003; Ping et al., 2000, 1996). The induction of MCP-1 by TNF α switches nucleosome positioning from a random to a more orderly configuration, leads to histone modification and occupancy of both regulatory regions, and allows a direct interaction between the distal and proximal regulatory regions (Boekhoudt et al., 2003; Ping et al., 1996; Teferedegne et al., 2006).

The majority of genes manifests similar responses between transiently transfected promoters and their chromatinized counterparts. However, a growing number of genes have shown significant differences between the behavior of transfected and chromosomal versions, such as the MMTV LTR promoter, integrated HIV genome, α_1 -antitrypsin gene, etc. (reviewed in Smith and Hager, 1997). Chromatin structure also defines genes' behavior in distinct cell types. As shown for the human *IL-8* gene, the cell-specific chromatin architecture on the enhancer determines the cell-lineage-specific expression program (Agelopoulos and Thanos, 2006). Differences in nucleosome and nuclease-hypersensitive site distribution of the *MCP-1* gene accounted for its differential transcriptional responses in malignant and non-malignant HPV18-positive cells (Finzer et al., 2000).

Therefore, our data provide the first evidence that transcriptional repression of MCP-1 in response to oxygen deprivation requires the cooperative actions of NF- κ B and HDAC. Furthermore, our observations support the notion that the native chromatin structure within the 5'-regulatory region of MCP-1 is crucial in determining the transcriptional response to hypoxia. However, the detailed molecular mechanism of hypoxic repression is yet to be determined.

Acknowledgments

This work was supported by grants from the Japan Society for the Promotion of Science (15.52341 and 17.05243) and from the 21st Century Center of Excellence Program for Frontier Research on Molecular Destruction and Reconstitution of Tooth and Bone.

References

- Agelopoulos M, Thanos D. Epigenetic determination of a cell-specific gene expression program by ATF-2 and the histone variant macroH2A. *Embo J* 2006;25:4843–51.
- Allavena P, Bianchi G, Zhou D, van Damme J, Jilek P, Sozzani S, et al. Induction of natural killer cell migration by monocyte chemoattractant protein-1, -2, and -3. *Eur J Immunol* 1994;24:3233–6.
- Ashburner BP, Westerheide SD, Baldwin Jr AS. The p65 (RelA) subunit of NF- κ B interacts with the histone deacetylase (HDAC) corepressors HDAC1 and HDAC2 to negatively regulate gene expression. *Mol Cell Biol* 2001;21:7065–77.
- Baek SH, Ohgi KA, Rose DW, Koo EH, Glass CK, Rosenfeld MG. Exchange of N-CoR corepressor and Tip60 coactivator complexes links gene expression by NF- κ B and beta-amyloid precursor protein. *Cell* 2002;110:55–67.
- Balkwill F. Cancer and the chemokine network. *Nat Rev Cancer* 2004;4:540–50.
- Barnes PJ, Karin M. Nuclear factor- κ B: a pivotal transcription factor in chronic inflammatory diseases. *N Engl J Med* 1997;336:1066–71.
- Bjornheden T, Levin M, Ewaldsson M, Wiklund O. Evidence of hypoxic areas within the arterial wall *in vivo*. *Arterioscler Thromb Vasc Biol* 1999;19:870–6.
- Boekhoudt GH, Guo Z, Beesford GW, Boss JM. Communication between NF- κ B and Sp1 controls histone acetylation within the proximal promoter of the monocyte chemoattractant protein 1 gene. *J Immunol* 2003;170:4139–47.
- Bosco MC, Puppo M, Pastorino S, Mi Z, Melillo G, Massazza S, et al. Hypoxia selectively inhibits monocyte chemoattractant protein-1 production by macrophages. *J Immunol* 2004;172:1681–90.

- Brown JM. Tumor hypoxia, drug resistance, and metastases. *J Natl Cancer Inst* 1990;82:338–9.
- Campbell KJ, Rocha S, Perkins ND. Active repression of antiapoptotic gene expression by RelA(p65) NF- κ B. *Mol Cell* 2004;13:853–65.
- Carr MW, Roth SJ, Luther E, Rose SS, Springer TA. Monocyte chemoattractant protein 1 acts as a T-lymphocyte chemoattractant. *Proc Natl Acad Sci USA* 1994;91:3652–6.
- Chen LF, Greene WC. Shaping the nuclear action of NF- κ B. *Nat Rev Mol Cell Biol* 2004;5:392–401.
- Clayton AL, Hazzalin CA, Mahadevan LC. Enhanced histone acetylation and transcription: a dynamic perspective. *Mol Cell* 2006;23:289–96.
- Crowther M, Brown NJ, Bishop ET, Lewis CE. Microenvironmental influence on macrophage regulation of angiogenesis in wounds and malignant tumors. *J Leukoc Biol* 2001;70:478–90.
- Cummins EP, Taylor CT. Hypoxia-responsive transcription factors. *Pharmacol Ther* 2005;450:363–71.
- Deng YY, Lu J, Ling EA, Kaur C. Monocyte chemoattractant protein-1 (MCP-1) produced via NF- κ B signaling pathway mediates migration of amoeboid microglia in the periventricular white matter in hypoxic neonatal rats. *Glia* 2008;64:123–36.
- Finzer P, Soto U, Delius H, Patzelt A, Coy JE, Poustka A, et al. Differential transcriptional regulation of the monocyte chemoattractant protein-1 (MCP-1) gene in tumorigenic and non-tumorigenic HPV 18 positive cells: the role of the chromatin structure and AP-1 composition. *Oncogene* 2000;19:3235–44.
- Galindo M, Santiago B, Alcami J, Rivero M, Martin-Serrano J, Pablos JL. Hypoxia induces expression of the chemokines monocyte chemoattractant protein-1 (MCP-1) and IL-8 in human dermal fibroblasts. *Clin Exp Immunol* 2005;123:36–41.
- Gerlitsen ME, Williams AJ, Neish AS, Moore S, Shi Y, Collins T. CREB-binding protein/p300 are transcriptional coactivators of p65. *Proc Natl Acad Sci USA* 1997;94:2971–72.
- Hoberg JE, Popko AE, Ramsey CS, Mayo MW. IkappaB kinase alpha-mediated derepression of SMRT potentiates acetylation of RelA/p65 by p300. *Mol Cell Biol* 2006;26:457–71.
- Hoberg JE, Yeung T, Mayo MW. SMRT derepression by the IkappaB kinase alpha: a prerequisite to NF- κ B transcription and survival. *Mol Cell* 2004;16:245–55.
- Hollensinner PJ, Kaun C, Rychlik K, Ben-Tal Cohen E, Kastl SP, Denysanets S, et al. Monocyte chemoattractant protein (MCP-1) is expressed in human cardiac cells and is differentially regulated by inflammatory mediators and hypoxia. *FEBS Lett* 2006;580:3532–8.
- Jeong S, Stein A. Micrococcal nuclease digestion of nuclei reveals extended nucleosome ladders having anomalous DNA lengths for chromatin assembled on non-replicating plasmids in transfected cells. *Nucleic Acids Res* 1994;22:370–5.
- Kenneth NS, Rocha S. Regulation of gene expression by hypoxia. *Biochem J* 2008;414:19–29.
- Kikuchi T, Hagiwara K, Honda Y, Gomi K, Kobayashi T, Takahashi H, et al. Clarithromycin suppresses lipopolysaccharide-induced interleukin-8 production by human monocytes through AP-1 and NF- κ B transcription factors. *J Antimicrob Chemother* 2002;49:745–55.
- Kim MS, Kwon HJ, Lee YM, Baek JH, Jang JE, Lee SW, et al. Histone deacetylases induce angiogenesis by negative regulation of tumor suppressor genes. *Nat Med* 2001;7:437–43.
- Koch AE, Polverini PJ, Kunkel SL, Harlow LA, DiPietro LA, Elner VM, et al. Interleukin-8 as a macrophage-derived mediator of angiogenesis. *Science* 1992;258:1798–801.
- Kouzarides T. Chromatin modifications and their function. *Cell* 2007;128:693–705.
- Krones A, Jungermann K, Kietzmann T. Cross-talk between the signals hypoxia and glucose at the glucose response element of the L-type pyruvate kinase gene. *Endocrinology* 2001;142:7707–18.
- Leonard EJ, Yoshimura T. Human monocyte chemoattractant protein-1 (MCP-1). *Immunol Today* 1990;11:97–101.
- Lund-Olesen K. Oxygen tension in synovial fluids. *Arthritis Rheum* 1970;13:769–76.
- Maltepe E, Krampitz GW, Okazaki KM, Red-Horse K, Mak W, Simon MC, et al. Hypoxia-inducible factor-dependent histone deacetylase activity determines stem cell fate in the placenta. *Development* 2005;132:3393–403.
- Maltepe E, Simon MC. Oxygen, genes, and development: an analysis of the role of hypoxic gene regulation during murine vascular development. *J Mol Med* 1998;76:391–401.
- Manalo DJ, Rowan A, Lavoie T, Natarajan L, Kelly BD, Ye SQ, et al. Transcriptional regulation of vascular endothelial cell responses to hypoxia by HIF-1. *Blood* 2005;105:659–69.
- Matsushima K, Oppenheim JJ. Interleukin 8 and MCAF: novel inflammatory cytokines inducible by IL-1 and TNF. *Cytokine* 1989;1:2–13.
- Negus RP, Turner I, Burke F, Balkwill FR. Hypoxia down-regulates MCP-1 expression: implications for macrophage distribution in tumors. *J Leukoc Biol* 1998;63:758–65.
- Oda T, Ueda A, Shimizu N, Handa H, Kasahara T. Suppression of monocyte chemoattractant protein 1, but not IL-8, by alprazolam; effect of alprazolam on c-Rel/p65 and c-Rel/p50 binding to the monocyte chemoattractant protein 1 promoter region. *J Immunol* 2002;169:3329–35.
- Pamarik M, Mauch P, Vergilio JA, Sackstein R, Down JD. Distribution of hematopoietic stem cells in the bone marrow according to regional hypoxia. *Proc Natl Acad Sci USA* 2007;104:5431–6.
- Ping D, Boekhoudt G, Zhang F, Morris A, Philipsen S, Warren ST, et al. Sp1 binding is critical for promoter assembly and activation of the MCP-1 gene by tumor necrosis factor. *J Biol Chem* 2000;275:1708–14.
- Ping D, Jones PL, Ross JM. TNF regulates the *in vivo* occupancy of both distal and proximal regulatory regions of the MCP-1/JE gene. *Immunity* 1996;4:455–69.

Please cite this article in press as: Safronova O, et al. Regulation of chemokine gene expression by hypoxia via cooperative activation of NF- κ B and histone deacetylase. *Int J Biochem Cell Biol* (2009), doi:10.1016/j.ijbio.2009.05.003

G Model
BC3013.1-11

ARTICLE IN PRESS

O. Safronova et al. / The International Journal of Biochemistry & Cell Biology xxx (2009) xxx–xxx

11

- 710 Safronova O, Nakahama K, Onodera M, Muneta I, Morita I. Effect of hypoxia
711 on monocyte chemoattractant protein-1 (MCP-1) gene expression induced by
712 interleukin-1 β in human synovial fibroblasts. *Inflamm Res* 2003;52:480–6.
713 Schofield CJ, Ratcliffe PJ. Oxygen sensing by HIF hydroxylases. *Nat Rev Mol Cell Biol*
714 2004;5:343–54.
715 Shaw J, Zhang T, Rzesutek M, Yurkova N, Baetz D, Davie JR, et al. Transcriptional
716 silencing of the death gene BNIP3 by cooperative action of NF-kappaB and his-
717 tone deacetylase 1 in ventricular myocytes. *Circ Res* 2006;99:1347–54.
718 Shetty S, Graham BA, Brown JG, Hu X, Vegh-Yarema N, Harding G, et al. Transcription
719 factor NF-kappaB differentially regulates death receptor 5 expression involving
720 histone deacetylase 1. *Mol Cell Biol* 2005;25:5404–16.
721 Smith CL, Hager GL. Transcriptional regulation of mammalian genes in vivo. A tale
722 of two templates. *J Biol Chem* 1997;272:27493–6.
723 Strieter RM, Koch AE, Antony VB, Fick Jr RB, Standiford TJ, Kunkel SL. The
724 immunopathology of chemotactic cytokines: the role of interleukin-8 and
725 monocyte chemoattractant protein-1. *J Lab Clin Med* 1994;123:183–97.
726 Taylor CT. Interdependent roles for hypoxia inducible factor and nuclear factor-
727 kappaB in hypoxic inflammation. *J Physiol* 2008;585:4055–9.
- Teferedegne B, Green MR, Guo Z, Boss JM. Mechanism of action of a distal NF-kappaB-
dependent enhancer. *Mol Cell Biol* 2006;26:5759–70.
Ueda A, Okuda K, Ohno S, Shirai A, Igarashi T, Matsunaga K, et al. NF-kappa B and
Sp1 regulate transcription of the human monocyte chemoattractant protein 1
gene. *J Immunol* 1994;153:2052–63.
Vanden Berghe W, Ndlovu MN, Hoya-Arias R, Dijsselbloem N, Gerlo S, Haeghe-
man G. Keeping up NF-kappaB appearances: epigenetic control of immunity
or inflammation triggered epigenetics. *Biochem Pharmacol* 2006;72:1114–31.
Vaupel P, Kelleher DK, Hockel M. Oxygen status of malignant tumors: pathogenesis
of hypoxia and significance for tumor therapy. *Semin Oncol* 2001;28:29–35.
Xu L, Xie K, Mukaida N, Matsushima K, Fidler IJ. Hypoxia-induced elevation
in interleukin-8 expression by human ovarian carcinoma cells. *Cancer Res*
1999;59:5822–9.
Yeung F, Hoberg JE, Ramsey CS, Keller MD, Jones DR, Frye RA, et al. Modulation of
NF-kappaB dependent transcription and cell survival by the SIRT1 deacetylase.
Embo J 2004;23:2369–80.
Zhong H, May MJ, Jimi E, Ghosh S. The phosphorylation status of nuclear NF-kappa B
determines its association with CBP/p300 or HDAC-1. *Mol Cell* 2002;9:625–36.

Please cite this article in press as: Safronova O, et al. Regulation of chemokine gene expression by hypoxia via cooperative activation of NF- κ B and histone deacetylase. *Int J Biochem Cell Biol* (2009). doi:10.1016/j.biocel.2009.05.003

顎口腔外科分野

小村 健

医歯学総合研究科・口腔機能再構築学系専攻
口腔機能再建学／医学博士・教授



1) 研究の課題名

研究課題が複数の場合、各題目毎に平成21年12月までの研究内容（in pressは可、平成22年3月までの予定も可）についておまとめ下さい（和文400-800字）。研究開始時期は問いません。

「口腔扁平上皮癌におけるFADDのDNA増幅および発現」 DNA amplification and expression of FADD in oral squamous cell carcinoma

FADDは細胞死シグナル伝達を中継するアダプター分子であるが、細胞増殖に関与するとの報告も散見される。本研究の目的は、口腔扁平上皮癌におけるFADD発現の役割を明らかにすることである。対象症例は、当科で切除手術を施行した舌扁平上皮癌60例とした。また、6種の培養細胞を用いた。DNAの増幅およびRNAの発現解析には、リアルタイムPCRを用いた。タンパク発現については、免疫組織染色またはウエスタンブロット法を用いた。

30症例におけるFADDのDNA増幅を調べたところ、13症例で増幅が認められ、癌の組織学的分化度分類と関連が認められた。次に、60症例における免疫組織染色の結果、非癌組織部（6.2%）と比較して癌組織部（34.4%）でFADDの発現は有意に増加していた。癌組織部におけるFADDの発現増加とT1症例に限った分化度分類との間に関連が見られ、また、リンパ節転移および5年生存率との間にも関連が認められた。培養細胞においても、いくつかの細胞でFADDの増幅および高発現が認められ、切除標本の解析を裏付ける結果となった。FADDの高発現は様々な癌組織で認められるとされているが、今回、舌扁平上皮癌においても同様な結果が示された。本研究結果は、FADDを含む領域のDNA増幅によるFADDの発現上昇はその癌の分化度に影響を与え、さらにリンパ節転移や5年生存率にも影響を与えること

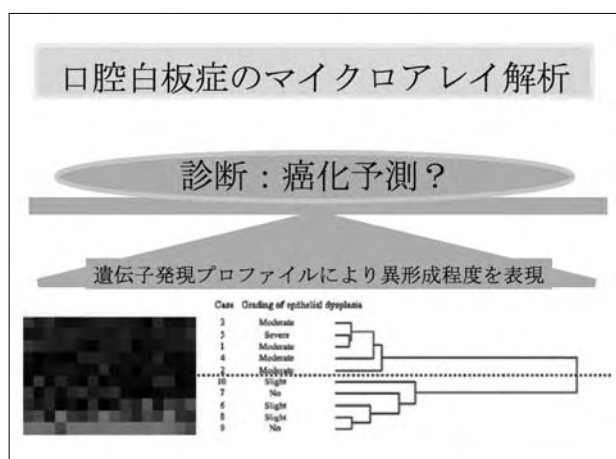
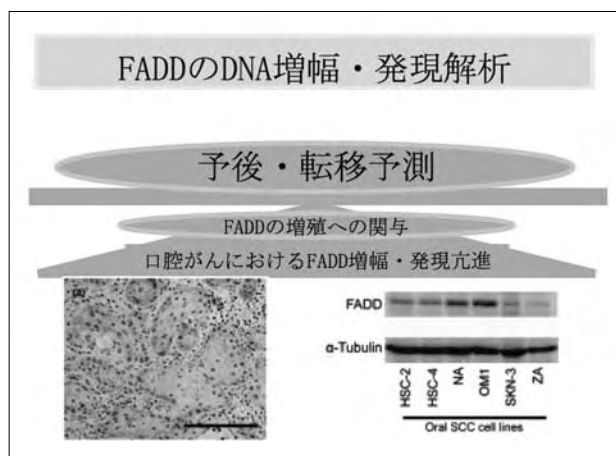
を示唆している。対象とした症例数が少ないことなどから、さらなる解析が必要であるが、FADDが有用な予後予測因子となる可能性が示された。

「口腔白板症のoligonucleotide microarrayによる遺伝子発現解析」

Gene expression analysis by oligonucleotide microarray in oral leukoplakia

口腔白板症は前癌病変として知られ、臨床的に非均一型や可動粘膜に認めるもの、あるいは病理組織学的に中等度以上の異形成を伴ったものに悪性化の可能性が高いと言われているが、明確な指標は明らかとなっていない。今回われわれは、新規癌化マーカー開発に先立ち、病理組織学的上皮異形成を鑑別する新規遺伝子マーカーの検索を行った。対象は、臨床病理組織学的に口腔白板症と診断された10例とした。対象症例の年齢は、37～77歳、平均65.8歳であった。性別は、男性6例、女性4例であった。部位は、舌6例、歯肉4例であった。病理組織学的上皮異形成の程度を便宜的にmild dysplasia group（異形成なし、およびslight dysplasia）とsevere dysplasia group（moderateおよびsevere dysplasia）の2群（各5例）に分類した。それぞれの症例の生検切除標本および一定の遺伝子発現パターンを示す対照としての培養細胞からtotal RNAを抽出し、oligonucleotideチップを用いてヒト遺伝子の発現解析を行った。上皮性異形成の程度を鑑別しうる遺伝子群を示す抽出するために、severe dysplasia groupで高発現を示し、mild dysplasia groupで低発現を示す遺伝子群を同定し、t検定により発現に有意差を認める96遺伝子を抽出した。このうちの3遺伝子に対してRT-PCR法を用いて発現を確認したところ、マイクロアレイによる発現パターンとほぼ同様の傾向を示していた。このことより、上皮性異形成の程度が96遺伝子の発現プロファイルで表現可能であることが示唆された。

2)



3) 研究内容の英文要約

[DNA amplification and expression of FADD in oral squamous cell carcinoma]

The Fas-associated death domain-containing protein, FADD, is an adaptor for relaying apoptotic signals. However, recent studies have shown that FADD also plays an important role in the growth and regulation of the cell cycle. The purpose of this study was to elucidate the role of FADD in oral squamous cell carcinoma (SCC). The DNA amplification of FADD from 30 samples of tongue SCC was analyzed using real-time PCR and the protein expression of FADD from 60 samples of tongue SCC was analyzed using immunohistochemistry. The DNA amplifications of FADD were observed in 13 cases (44.3%) and were significantly correlated with the histopathological differentiation grade of SCCs. FADD expression levels compared with the matched adjacent epithelium increased significantly. Additionally, the positive expressions of FADD were significantly correlated with lymph node metastasis of SCCs and the 5-year disease-specific survival rates. A positive association between FADD expression level and the histopathological differentiation grade was found to be limited to T1 SCCs.

DNA amplification was moderately correlated (correlation coefficient = 0.406, with expression of FADD in 30 samples of tongue SCC. In tongue SCCs, the expression of FADD was higher when compared with that of adjacent areas, which might be determined via genomic amplification in 11q13.3. Thus, SCC cells with the expression of FADD are possibly more likely to become metastatic and to worsen survival rates.

[Gene expression analysis by oligonucleotide microarray in oral leukoplakia]

Oral leukoplakias (LP) are the most frequent types of oral precancerous lesions, but there is no accurate assessment of this malignant transformation or even genetic diagnosis of the oral epithelial dysplasia. We need to identify the new genetic diagnosis system of the epithelial dysplasia. Oligonucleotide microarray was used to analyze expression patterns of 29952 genes in 10 LP patients. We compared the different gene expressions between mild dysplasia cases and severe dysplasia cases. Ninety-six genes expressed differentially were selected as candidates for up-regulated in severe dysplasia. Subsequently, we further selected 16 genes with highest differentially expression. By hierarchical clustering analysis, the 10 cases were divided mild dysplasia from severe dysplasia. The 16 genes are suggested as biomarker gene sets of efficacy and quickly recognized in the development of oral epithelial dysplasia.

[Metastasis of oral cancer to the parotid node]

The parotid node is an uncommon site of metastasis in head and neck cancer. This study was intended to clarify the incidence and indicators of oral cancer metastases to the parotid node. We reviewed the records of 253 patients with oral carcinomas who had undergone a total of 289 neck dissections between April 2001 and December 2006. The histologic diagnoses of the primary tumors were squamous cell carcinoma in 239 patients, mucoepidermoid carcinoma in 5, adenoid cystic carcinoma in 4, and miscellaneous others in 5. In all neck dissections, the tail of the parotid gland below the marginal mandibular branch of the facial nerve was resected. The cervical and parotid lymph nodes were isolated from the surgical specimens. One section through the maximum cross-sectional area of each node was examined histologically. From 183 of the 289 neck specimens, we collected 539 parotid nodes: 222 extraglandular and 317 intraglandular. Of the 253 patients, 10 (4.0%) had 19 parotid node metastases, of which 4 were extraglandular and 15 intraglandular. Parotid node involvement occurred in 2.5% of oral squamous cell carcinoma cases. For the other cancers, there were too few cases to determine a meaningful frequency. In terms of indicators, the likelihood of metastasis to the parotid nodes increased with the number of cancer-positive cervical

nodes. Metastasis to the parotid nodes should be considered in patients with oral cancer. Resection of the tail of the parotid gland is warranted during the neck dissection.

[Quantitative proteomics using formalin-fixed paraffin-embedded tissues of oral squamous cell carcinoma]

Clinical proteomics using a large archive of formalin-fixed paraffinembedded (FFPE) tissue blocks has long been a challenge. Recently, a method for extracting proteins from FFPE tissue in the form of tryptic peptides was developed. Here we report the application of a highly sensitive mass spectrometry (MS)-based quantitative proteome method to a small amount of samples obtained by laser microdissection from FFPE tissues. Cancerous and adjacent normal epithelia were microdissected from FFPE tissue blocks of 10 squamous cell carcinomas of the tongue. Proteins were extracted in the form of tryptic peptides and analyzed by 2-dimensional image-converted analysis of liquid chromatography and mass spectrometry (2DICAL), a label-free quantitative proteomics method developed in our laboratory. From a total of 25 018 peaks we selected 72 mass peaks whose expression differed significantly between cancer and normal tissues ($P < 0.001$, paired ttest). The expression of transglutaminase 3 (TGM3) was significantly down-regulated in cancer and correlated with loss of histological differentiation. Hypermethylation of TGM3 gene CpG islands was observed in 12 oral squamous cell carcinoma (OSCC) cell lines with reduced TGM3 expression. These results suggest that epigenetic silencing of TGM3 plays certain roles in the process of oral carcinogenesis. The method for quantitative proteomic analysis of FFPE tissue described here offers new opportunities to identify disease-specific biomarkers and therapeutic targets using widely available archival samples with corresponding detailed pathological and clinical records.

4) 本事業に関連して世界的な研究拠点形成に向けて、以下の点で改善・整備等されたこと

A (研究拠点体制)

硬組織領域における教育、研究、臨床について優れた実績を上げるため、平成15年度より開始の21世紀COEプログラム「歯と骨の分子破壊と再構築のフロンティア」において形成した研究基盤をさらに発展させ、一方、特別教育研究経費による「硬組織疾患ゲノムセンター」との密なる連携を図りつつ、口腔扁平上皮癌などの口腔外科学領域における悪性腫瘍を中心とした硬組織疾患のテーラーメイド医療の実現とともに、トランスレーショナル・リサーチへの発展を視野にいたした研究を展開している。

B (研究教育環境)

教育・研究基盤をさらに発展させ、基礎医・歯学分野から臨床分野までの融合型国際教育研究拠点の強化・拡大を図ることによって、博士課程学生に優れた教育環境・プログラムを提供し、国内外の研究機関とも連携して“国際的創造型科学者”の育成を目指す。

C (人材確保)

基礎医・歯学分野から臨床分野までの様々な情報・技術交流を目指し、学外研究所等との大学院生・教員の相互的な派遣・受け入れの体制を整備し、基礎研究、臨床研究の両分野について先端的かつ十分な知識と技術を持つ人材の確保に取り組んでいる。

D (人材育成)

顎顔面疾患におけるテーラーメイド医療の実現とQOLの向上をも目指したトランスレーショナル・リサーチを推進することによって、基礎医・歯学分野から臨床・応用医学分野までを両立させた“国際的創造型科学者”を養成する。

E (国際化)

国際的な情報交換と技術交流を目指し、アジア各国からの留学生を大学院生として受け入れて研究を遂行し、また基礎研究、臨床研究の両分野についてシンポジウムを開催するなどして、相互の発展に寄与している。

5) GCOE事業を推進するに当たって力を入れた点

臨床情報を具備した口腔扁平上皮癌症例の外科切除試料の系統的な収集と本学に既に設置済みのバイオリソースセンターにおける保存を進めつつ、これらの臨床検体を用いた網羅的発現解析によって口腔扁平上皮癌の頸部リンパ節転移診断モデルを構築するとともに、口腔扁平上皮癌細胞株での網羅的ゲノム・エピゲノム解析などにより新規口腔癌抑制遺伝子や口腔癌抑制microRNAを単離・同定し、口腔扁平上皮癌における遺伝子変異の同定などについても明らかにすべく研究を推進してきた。また、硬組織疾患ゲノムセンターとの密接な学内連携のもと、これらのバイオリソースを用いた分子・細胞・組織・個体すべてのレベルにおける分子メカニズムの解明、顎顔面疾患の新たな診断から外科的治療法の開発を目指した系統的研究基盤の整備をすすめている。

6) 英文原著論文

1. ©Harada H, K Omura: Metastasis of oral cancer to the

- parotid node. *Eur J Surg Oncol.* 35(8):890-894, 2009.
2. Hirai H, Omura K, Harada H, Tohara H: Sequential evaluation of swallowing function in patients with unilateral neck dissection. *Head & Neck.*
 3. Kaneoya A, Hasegawa S, Tanaka Y, Omura K: Quantitative analysis of invasive front in tongue cancer using ultrasonography. *J Oral Maxillofac Surg.* 67(1):40-46, 2009.
 4. ©Kayamori K, Sakamoto K, Nakashima T, Takayanagi H, Morita K, Omura K, Nguyen ST, Miki Y, Akashi T, Yamada-Okabe H, Ogata E, Yamaguchi A: Roles of IL-6 and PTHrP in osteoclast formation associated with oral cancers: The significance of IL-6 synthesized by stromal cells in response to cancer cells. *Am J Pathol.*
 5. Kawano T, Kabasawa Y, Ashikawa S, Sato Y, Jinno S, Omura K: Accuracy and reliability of thermal threshold measurement in the chin using heat flux technique. *Oral Surg Oral Med Oral Pathol Oral Radiol Endod.* 108:500-504, 2009.
 6. Komatsu S, Takenobu H, Ozaki T, Ando K, Koida N, Suenaga Y, Ichikawa T, Hishiki T, Chiba T, Iwama A, Yoshida H, Ohnuma N, Nakagawara A, Kamijo T: Plk1 regulates liver tumor cell death by phosphorylation of TAp63. *Oncogene.* 28(41):3631-3641, 2009.
 7. ©Kuribayashi Y, Morita K, Tomioka H, Uekusa M, Ito D, Omura K: Gene expression analysis by oligonucleotide microarray in oral leukoplakia. *J Oral Pathol Med.* 38(4):356-361, 2009.
 8. Matsubara J, Ono M, Negishi A, Ueno H, Okusaka T, Furuse J, Furuta K, Sugiyama E, Saito Y, Kaniwa N, Sawada J, Honda K, Sakuma T, Chiba T, Saijo N, Hirohashi S, Yamada T: Identification of a predictive biomarker for hematologic toxicities of gemcitabine. *J Clin Oncol.* 27(13): 2261-2268, 2009.
 9. Miyazaki H, Kato J, Kakizaki H, Nagata T, Uetake H, Okudera H, Watanabe H, Hashimoto K, Omura K: Submucosal glycerol injection-assisted laser surgical treatment of oral lesions. *Lasers Med Sci.* 24: 13-19, 2009.
 10. Miyazaki H, Kato J, Watanabe H, Harada H, Kakizaki H, Tetsumura A, Sato A, Omura K. Intralesional laser treatment of voluminous vascular lesions in the oral cavity. *Oral Surg Oral Med Oral Pathol Oral Radiol Endod.* 107(2):164-172, 2009.
 11. Miyazaki H, Omura K, Kakizaki H: Orbital approach via swinging eyelid procedure. *Asian J Oral Maxillofac Surg.*
 12. Mochizuki Y, Omura K, Kayamori K, Kaneoya A, Yamaguchi, Y: Osteonecrosis of the mandible associated with bisphosphonate therapy: Report of a case with surgical intervention. *Oral Surg.*
 13. Mochizuki Y, Matsushima E, Omura K: Perioperative assessment of psychological states and quality of life of head and neck cancer patients undergoing surgery. *Int J Oral Maxillofac Surg.* 38(2):151-159, 2009.
 14. Momin MA, Kiyoshi Okochi K, Watanabe H, Imaizumi A, Omura K, Amagasa T, Okada N, Ohbayashi N, Kurabayashi T: Diagnostic accuracy of cone-beam CT in the assessment of mandibular invasion of lower gingival carcinoma: Comparison with conventional panoramic radiography. *Eur J Radiol.* 72(1):75-81, 2009.
 15. Negishi A, Ono M, Handa Y, Kato H, Yamashita K, Honda K, Shitashige M, Satow R, Sakuma T, Kuwabara H, Omura K, Hirohashi S, Yamada T: Large-scale quantitative clinical proteomics by label-free liquid chromatography and mass spectrometry. *Cancer Sci.* 100(3): 514-519, 2009.
 16. ©Negishi A, Masuda M, Ono M, Honda K, Shitashige M, Satow R, Sakuma T, Kuwabara H, Nakanishi Y, Kanai Y, Omura K, Hirohashi S, Yamada T: Quantitative proteomics using formalin-fixed paraffin-embedded tissues of oral squamous cell carcinoma. *Cancer Sci.* 100(9): 1605-1611, 2009.
 17. Ono M, Matsubara J, Honda K, Sakuma T, Hashiguchi T, Nose H, Nakamori S, Okusaka T, Kosuge T, Sata N, Nagai H, Ioka T, Tanaka S, Tsuchida A, Aoki T, Shimahara M, Yasunami Y, Itoi T, Moriyasu F, Negishi A, Kuwabara H, Shoji A, Hirohashi S, Yamada T: Prolyl 4-hydroxylation of alpha-fibrinogen: a novel protein modification revealed by plasma proteomics. *J Biol Chem.* 284(42): 29041-29049, 2009.
 18. Piao Y, Bold B, Tayier A, Ishida R, Omura K, Okada N, Shibuya H: Evaluation of 18F-FDG PET/CT for diagnosing cervical nodal metastases in patients with oral cavity or oropharynx carcinoma. *Oral Surg Oral Med Oral Pathol Oral Radiol Endod.* 108(6):933-938, 2009.
 19. ©Prapinjumrune C, Morita K, Kuribayashi Y, Hanabata Y, Shi Q, Nakajima Y, Inazawa J, Omura K: DNA amplification and expression of FADD in oral squamous cell carcinoma. *J Oral Pathol Med.*
 20. Sang M, Ando K, Okoshi R, Koida N, Li Y, Zhu Y, Shimozato O, Geng C, Shan B, Nakagawara A, Ozaki T: Plk3 inhibits pro-apoptotic activity of p73 through physical interaction and phosphorylation. *Genes Cells.* 14(7):775-788, 2009.
 21. Yoda T, Sato T, Abe T, Sakamoto I, Tomaru Y, Omura K, Hatano N, Takato T, Ishii Y: Long-term results of surgical therapy for masticatory muscle tendon-aponeurosis hyperplasia accompanied by limited mouth opening. *Int J Oral Maxillofac Surg.* 38(11):1143-1147, 2009.
 22. Yoshida S, Ito D, Nagumo T, Shirota T, Hatori M, and Shintani S: Hypoxia induces resistance to 5-fluorouracil in oral cancer cells via G1 phase cell cycle arrest. *Oral Oncology.* 45:109-115, 2009.

7) 著書

1. 小村 健:科学的根拠に基づく口腔癌診療ガイドライン 2009年度版. 金原出版 共著 2009年.
2. 小村 健:口腔外科疾患 再建外科. 看護のための最新医学講座 第2版 第23巻 歯科口腔系疾患 中山書店 153-168, 2009年.
3. 尾野雅哉, 松原淳一, 根岸綾子, 山田哲司: 2DICALを用いた疾患バイオマーカーの探索. 細胞工学別冊 明日を拓く新次元プロテオミクス 122-130, 2009年.

8) 平成21年度までの自己評価

平成15年度より開始の21世紀COEプログラム「歯と骨の分子破壊と再構築のフロンティア」において形成した研究基盤をさらに発展させ、硬組織領域における教育、研究、臨床については世界的にトップレベルの優れた実績を上げ、一方、特別教育研究経費による「硬組織疾患ゲノムセンター」との密なる連携を図りつつ、口腔扁平上皮癌などの口腔外科学領域における悪性腫瘍を中心とした硬組織疾患のテーラーメイド医療の実現とともに、トランスレーショナル・リサーチへの発展を視野にいたれた研究が展開できた。

9) 和文原著論文

1. 伊東大典, 佐藤 昌, 栗林悠里, プラピンチャムルーン・チャンウィット, 小村 健: 口腔扁平苔癬135例の臨床的検討. 日本口腔粘膜学会雑誌 15 (1) :22-28, 2009
2. 田中香衣, 原田浩之, 生田 稔, 小村 健, 柏森 高: 顎骨に発生したランゲルハンス細胞組織球症の3例. 頭頸部癌 35 (3) :310-315, 2009.
3. 富岡寛文, 原田浩之, 岡田憲彦, 小村 健: 口腔に発生した顆粒細胞腫12例の臨床病理学的検討. 日本口腔科学会雑誌 58 (3) :97-102, 2009.
4. 畑山 均, 村上 孝, 柏田智徳, 井上 享, 宮崎英隆, 加藤純二: 青紫半導体レーザーの歯科治療への応用. 電子情報通信学会技術研究報告 IEICE technical report 109 (59) :1-6, 2009.
5. 望月裕美, 小村 健, 松島英介: 口腔がん手術患者の心理特性とQOLの経時的変化. 口腔病学会雑誌 76 (1) :16-24, 2009.

10) 学会発表 (英文)

1. Harada H, Omura K: Metastasis of oral cancer to the parotid node. The 50th anniversary congress of the

Korean Association of Oral and Maxillofacial Surgeons. April 9-11 2009. Seoul, Korea 口演

2. Shimamoto H, Harada H and Omura K: Recent advances in mandibular reconstruction. The 50th anniversary congress of the Korean association of oral and maxillofacial surgeons. April 9-11 2009. Seoul, Korea 口演
3. Ida M, Kuribayashi A, Kurabayashi T, Amagasa T, Okaga N, Omura K: Clinico-radiological study of the primary intraosseous carcinoma of the jaw. 17th International Congress of DentoMaxillofacial Radiology. 28 June-02 July, 2009. Amsterdam 示説

11) 学会発表 (和文)

1. 植草 優, 中島雄介, 原田浩之, 生田 稔, 島本裕彰, 富岡寛文, 田中香衣, 栗林悠里, 平井秀明, 小村 健: 含嗽液を用いた口腔癌スクリーニングの検討. 第27回日本口腔腫瘍学会総会 2009年1月29-30日 宇都宮市
2. 田中香衣, 原田浩之, 中島雄介, 生田 稔, 島本裕彰, 富岡寛文, 植草 優, 平井秀明, 小村 健: 小唾液腺癌30例の臨床病理学的検討. 第26回日本口腔腫瘍学会総会 2009年1月29-30日 宇都宮市
3. 富岡寛文, 原田浩之, 中島雄介, 生田 稔, 島本裕彰, 田中香衣, 植草 優, 平井秀明, 小村 健: 顎下腺腫瘍の臨床学的検討. 第26回日本口腔腫瘍学会総会 2009年1月29-30日 宇都宮市
4. 原田浩之, 中島雄介, 生田 稔, 島本裕彰, 富岡寛文, 田中香衣, 植草 優, 平井秀明, 小村 健: 口腔扁平上皮癌Stage III, IV症例の予後因子の検討. 第27回日本口腔腫瘍学会総会 2009年1月29-30日 宇都宮市
5. プラピンチャムルーン・チャンウィット, 森田圭一, 栗林悠里, 小村 健: 口腔扁平上皮癌におけるFas associated death domain (FADD) の発現解析. 第27回日本口腔腫瘍学会総会 2009年1月29-30日 宇都宮市
6. 樺沢勇司, 佐藤 昌, 菊池 剛, 樋口佑輔, 小村 健: ロッキングプレートシステムを用いた下顎枝矢状分割術の術後臨床経過の検討-チタンスクリューとの比較-. 第63回日本口腔科学会学術集会 2009年4月16-17日 浜松市
7. 工藤雅範, 中島雄介, 原田浩之, 小村 健: 上顎に発生した巨大な石灰化嚢胞性歯源性腫瘍の1例. 第63回日本口腔科学会学術集会 2009年4月16-17日 浜松市
8. 原田浩之, 小村 健: 口腔扁平上皮癌におけるTS-1・放射線同時併用療法による手術回避・縮小

- 手術の能性. 第63回日本口腔科学会総会 2009年4月16-17日 浜松市
9. 丸川恵理子、猪俣謙次、生田 稔、平井秀明、高橋由貴子、高橋幸伸、原田浩之、小村 健: 肩甲骨皮弁による下顎骨再建後の機能評価. 第63回日本口腔科学会 2009年4月16-17日 浜松市
 10. 森田圭一、辻美千子、今泉史子、森田綾子、森山啓司、小村 健: 新規創内固定型上顎仮骨延長装置の使用経験. 第33回日本口蓋裂学会総会・学術集会 2009年5月28-29日 東京
 11. 片岡恵一、鈴木聖一、馬場祥行、森山啓司、森田圭一、小村 健: Le Fort I型骨切り術によるセグメントの前方移動を行い顎裂閉鎖した口唇口蓋裂症例. 第33回日本口蓋裂学会総会・学術集会 2009年5月28-29日 東京
 12. 菊池 剛、樺沢勇司、佐藤 昌、佐藤百合子、樋口佑輔、丸岡 豊、小村 健: 外科的矯正治療における咬合力・咬合接触面積の推移についての検討. 第18回日本顎変形症学会総会 2009年6月4-5日 仙台市
 13. 佐藤 昌、樺沢勇司、菊池 剛、佐藤百合子、樋口佑輔、丸岡 豊、小村 健: 上顎前方歯槽部骨切り術後の形態的・機能的検討. 第18回日本顎変形症学会総会 2009年6月4-5日 仙台市
 14. 伊東大典、櫻井仁亨、小村 健: 口腔扁平苔癬におけるIL-22/IL-23およびそれらの受容体発現の免疫組織化学的解析. 第19回日本口腔粘膜学会総会・学術集会 2009年6月5-6日 葉山町
 15. 島本裕彰、原田浩之、中島雄介、富岡寛文、田中香衣、平井秀明、小村 健: 下顎骨再建における工夫. 第33回日本頭頸部癌学会 2009年6月11-12日 札幌市
 16. 富岡寛文、原田浩之、栗林悠里、平井秀明、田中香衣、島本裕彰、中島雄介、小村 健: 口腔に発生したbasaloid squamous cell carcinomaの3例. 第33回日本頭頸部癌学会 2009年6月11-12日 札幌市
 17. 原田浩之、中島雄介、島本裕彰、富岡寛文、田中香衣、小村 健: 舌リンパ節転移例の臨床病理学的検討. 第33回日本頭頸部癌学会 2009年6月11-12日 札幌市
 18. 釘本琢磨、島本裕彰、原田浩之、小村 健: 副耳下腺多形腺腫再発例の治療経験. 第187回日本口腔外科学会関東地方会 2009年6月27日 千葉市
 19. 佐藤麻緒、川元龍夫、井口隆人、八木優子、小村 健、天願俊泉、砂川 元、森山啓司: 外科的矯正治療を行った統合失調症を伴う顎変形症の2症例について. 第68回 東京矯正歯科学会大会 2009年7月16日 東京
 20. 山本信祐、生田 稔、樺沢 勇司、小村 健: 治療不全を契機に血友病Aが判明した舌裂傷の1例. 第11回日本口腔顎顔面外傷学会総会 2009年7月18日 札幌市
 21. 高 楠旻、今井英樹、櫻井仁亨、角倉可奈子、塚原宏泰、依田 泰、宮村壽一、森田 伸、小村 健: 全身性エリテマトーデスと慢性関節リウマチの重複症例において開咬を認めた1例. 第22回日本顎関節学会総会・学術大会 2009年7月25-26日 東京
 22. 角倉可奈子、高 楠旻、今井英樹、須田里香、依田 泰、宮村壽一、塚原宏泰、森田 伸、小村 健: 一次診断における顎関節症Ⅱ型とⅢb型の鑑別. 第22回日本顎関節学会総会・学術大会 2009年7月25-26日 東京
 23. 小松秀吾、竹信尚典、尾崎俊文、安藤清宏、小井田奈美、末永雄介、菱木知郎、千葉哲博、岩間厚志、吉田英生、中川原章、上條岳彦: Plk1はTAp63のリン酸化を介して肝腫瘍細胞死を制御する. 第68回日本癌学会学術総会 2009年10月1-3日 横浜市
 24. 松川 祥、原田浩之、丸川恵理子、小村 健、坂本 啓、岡田憲彦: 硬口蓋に発生した筋上皮腫の1例. 第43回日本口腔科学会関東地方部会 2009年10月3日 東京
 25. 樺沢勇司、佐藤 昌、菊池 剛、佐藤百合子、樋口祐輔、小村 健: ロッキングプレートシステムを用いた非対称症例への下顎枝矢状分割術の術後臨床経過の検討-顔面非対称症例におけるチタンスクリュー固定との比較-. 第54回日本口腔外科学会総会・学術大会 2009年10月9-11日 札幌市
 26. 櫻井仁亨、角倉可奈子、高 楠旻、小村 健: 著明な下顎頭骨吸収を示したシェーグレン症候群の1例. 第54回日本口腔外科学会総会・学術大会 2009年10月9-11日 札幌市
 27. 中島雄介、小村 健: 当科におけるビスフォスフォネート系薬剤投与患者の取り扱い. 第54回日本口腔外科学会総会・学術大会 2009年10月9-11日 札幌市
 28. 松本佳奈子、島本裕彰、栢森 高、小村 健: VELscopeを用いた口腔粘膜病変の観察. 第54回日本口腔外科学会総会・学術大会 2009年10月9-11日 札幌市
 29. 丸川恵理子、猪俣謙次、高橋幸伸、依田泰、塚原宏泰、小村 健: 自家骨・ β -TCP混合移植による上顎洞底挙上術後のX線学的・組織学的評価. 第54回日本口腔外科学会総会・学術大会 2009年10月9-11日 札幌市

30. 森田圭一、菊池 剛、今泉史子、根岸綾子、小村 健: 新規創内固定型上顎骨延長装置の使用経験. 第54回日本口腔外科学会総会・学術大会 2009年10月9-11日 札幌市
31. 宮崎英隆、小村 健、菊池 剛、加藤純二: 波長405nm半導体レーザーによる軟組織蒸散効果の実験的系統. 第54回日本口腔外科学会総会・学術大会 2009年10月9-11日 札幌市
32. 原田浩之、小村 健、中島雄介、生田 稔、島本裕彰、富岡寛文、田中香衣、金親あや乃: 口腔扁平上皮癌における遠隔転移発現に関与する因子の検討. 第47回日本癌治療学会総会 2009年10月22-24日 横浜市
33. 望月裕美: 手術治療を受けた頭頸部がん患者における社会復帰後の生活の質向上支援プログラムの検討ー手術を受ける口腔がん患者の心理特性および生活の質の経時的変化の傾向ー. 財団法人 慢性疾患・リハビリテーション研究振興財団 平成19年度助成研究成果報告発表会 2009年12月5日 京都市
34. 猪俣謙次、丸川恵理子、高橋幸伸、大林尚人、小村 健: 頬側裂開を伴う顎骨欠損における β -リン酸三カルシウム(β -TCP)を応用した歯槽堤保存法についての検討. 第13回日本顎顔面インプラント学会 2009年12月12-13日 佐賀市
35. 田口貴英、森田圭一、菊池 剛、角倉可奈子、島田泰如、小村 健: 過去9年間に当科で経験した角化嚢胞性歯源性腫瘍93例の臨床的検討. 第28回日本口腔腫瘍学会総会・学術大会 2010年1月27-29日 東京
36. 花畑泰子、中島雄介、森田圭一、栢森 高、小村 健: EGFRのkinase independent pathwayにおけるSGLT1の発現解析. 第28回日本口腔腫瘍学会総会・学術大会 2010年1月27-29日 東京
37. 平井秀明、三澤常美、河西八郎: 下唇に発生した血管平滑筋腫の1例. 第28回日本口腔腫瘍学会総会・学術大会 2010年1月27-29日 東京
38. 望月裕美、小村 健、坂本 啓、中西正一、丸川恵理子、佐藤 潔、山口 朗: 上顎歯肉に発生した複合型神経内分泌がんの1例. 第28回日本口腔腫瘍学会総会・学術大会 2010年1月27-29日 東京
39. 島田泰如、森田圭一、菊池 剛、中川 聡、栗林悠里、田口 貴英、小村 健: 基底細胞母斑症候群14例の臨床的検討. 第28回日本口腔腫瘍学会総会・学術大会 2010年1月27-29日 東京
40. 磯部 薫、森田 圭一、菊池 剛、小村 健: 治療方針に苦慮したエナメル上皮線維腫の1例. 第28回

日本口腔腫瘍学会総会・学術大会 2010年1月27-29日 東京

41. 富岡 寛文、釘本 琢磨、金親 あや乃、田中 香衣、島本 裕彰、生田 稔、中島 雄介、原田 浩之、小村 健: 治療前の外科処置が下顎歯肉扁平上皮癌に与える影響. 第28回日本口腔腫瘍学会総会・学術大会 2010年1月27-29日 東京
42. 吉本 光洋、森田 圭一、小村 健: 経過観察中に癌化した口腔白板症19例の検討. 第28回日本口腔腫瘍学会総会・学術大会 2010年1月27-29日 東京

12) 受賞

1. 小井田奈美: 平成20年度小林育英会奨学金 2009年3月17日 「Inhibitory role of Plk1 in the regulation of p73-dependent apoptosis through physical interaction and phosphorylation.」
2. 原田浩之、小村 健、中島雄介、生田 稔、島本裕彰、富岡寛文、田中香衣、金親あや乃: 第47回日本癌治療学会総会 優秀演題賞 2009年10月22-24日 横浜「口腔扁平上皮癌における遠隔転移発現に関与する因子の検討.」

13) 外部資金の獲得状況

1. 日本学術振興会科学研究費補助金・萌芽研究
研究題目: 「含嗽液による口腔癌検診システムの開発」
代表: 小村 健
期間: 平成19-21年度
研究費総額: 320万円
2. 日本学術振興会科学研究費補助金・若手研究B
研究題目: 「口腔癌幹細胞同定法の確立」
代表: 島本裕彰
期間: 平成19-21年度
研究費総額: 330万円
3. 日本学術振興会科学研究費補助金・若手研究B
研究題目: 「ビスフォスフォネート長期投与による骨髄炎モデルの確立とその骨代謝機構に対する解明」
代表: 今泉史子
期間: 平成20-23年度
研究費総額: 330万円
4. 日本学術振興会科学研究費補助金・若手研究B
研究題目: 「口腔がん顎骨浸潤における骨破壊分子メカニズムの解明」
代表: 森田圭一
期間: 平成20-21年度
研究費総額: 320万円

5. 日本学術振興会科学研究費補助金・基盤研究C

研究題目:「TGF 阻害と新規癌抗原を組み合わせた強化型口腔癌樹状細胞療法開発のための研究」

代表:伊東大典

期間:平成20-22年度

研究費総額:350万円

6. 日本学術振興会科学研究費補助金・基盤研究C

研究題目:「405nm半導体レーザーを用いた低侵襲的診断・治療法の口腔外科領域への導入」

代表:宮崎英隆

期間:平成21-23年度

研究費総額:350万円

7. 日本学術振興会科学研究費補助金・若手研究B

「新規免疫療法の確立を目指した口腔癌患者に誘導されている多能性免疫担当細胞の解析」

代表:田中香衣

期間:平成21-24年度

研究費総額:290万円

8. 研究助成費 やずや 食と健康研究所

「手術を施行された口腔癌患者における摂食嚥下機能の状態,食事内容,これらとQOLとの関連性の検証」

代表:望月裕美

期間:平成21年12月1日から平成22年11月30日

研究費総額:50万円

9. 厚生労働科学研究費補助金

「進行性下顎頭吸収の診断基準策定とその治療に関する研究」

研究分担者:小村 健

期間:平成21年度

研究費総額:200万円

10. 受託研究費 オリンパス テルモ バイオマテリアル株式会社

「新規材料 β -リン酸三カルシウム/コラーゲン複合体の抜歯窩への応用」

代表:小村 健

期間:平成21年10月1日～平成22年3月31日

研究費総額:4,753,260円 (直接経費 3,656,354円)

11. 共同研究 オリンパス株式会社

「有機酸誘導体と生体高分子から構成される2成分系接着剤の口腔粘膜間接着に関する研究」

代表:小村 健

期間:平成19年10月1日～平成21年9月30日

研究費総額:研究費:10,000,000円(直接経費 9,090,909円)

14) 特別講演、招待講演

1. Omura K: Mandibulectomy in cancer surgery. AO Craniomaxillofacial Course 2009 2009年7月10日 東京

2. Omura K: Mandibular reconstruction -subscapular artery system-. AO Craniomaxillofacial Course 2009 2009年7月10日 東京

3. 小村 健: Oral Cancer Treatment in Japan. 東京医科大学大学院歯学部・内蒙古医学院大学院医歯学総合研究科 学術交流協定締結特別記念講演 2009年8月18日 中国 内蒙古

4. 島本裕彰、小村 健: 下顎骨中心性癌と下顎再建の工夫. 東京医科大学大学院歯学部・内蒙古医学院大学院医歯学総合研究科 学術交流協定締結特別記念講演 2009年8月18日 中国 内蒙古

5. 丸川恵理子、小村 健: 下顎骨再建における基礎から臨床応用まで. 東京医科大学大学院歯学部・内蒙古医学院大学院医歯学総合研究科 学術交流協定締結特別記念講演 2009年8月18日 中国 内蒙古

6. 小村 健: 見逃さない口腔がん -診断・治療の変遷と今後の課題-. 船橋歯科医師会学術講演会 2009年2月5日 船橋市

7. 中島雄介: 当科におけるビスフォスフォネート投与患者の取り扱い. 第7回文京区医師会学術集会 2009年2月21日 東京

8. 小村 健: 見逃さない口腔がん -検診にむけて-. 海老名市歯科医師会 口腔癌検診スキルアップ研修会 2009年3月15日 海老名市

9. 小村 健: 口腔顎顔面外傷の診断と治療. 日本外傷歯学会 東日本セミナー 2009年4月5日 東京

10. 小村 健: 口腔癌の診断・治療の変遷と現況. 医科・歯科連携協議会講演会 2009年4月11日 小松市

11. 小村 健: ビスフォスフォネート投与患者の歯科治療における注意事項 -顎骨壊死の予防と治療-. 臨床歯科研究会 2009年10月22日 横浜市

12. 小村 健: すぐに役立つ口腔がんの知識 -あなたは口腔癌を見逃してはいませんか-. 港区芝歯科医師会 口腔癌検診研修会 2009年11月19日 東京

15) 主催学会

1. 第28回日本口腔腫瘍学会総会・学術大会 2010年1月27-29日 参加者500名 東京

2. C.E.D. 日常診療に活かす口腔外科の知識と基本 2009年7月19日, 21日 参加者12名 東京

3. 第4回 紹介医のための口腔外科セミナー「インプラントにおける骨造成法」2009年1月25日 参加者 200名 東京
4. 第5回 紹介医のための口腔外科セミナー「最近の口唇口蓋裂治療」、「口腔外科疾患のX線画像診断」参加者 150名 2009年11月15日 東京

16) 新聞、雑誌、TV報道

1. 小村 健:「病院の実力 口腔がん」2009年4月25日 夕刊フジ

17) 先生の講座の准教授、講師、助教、特別研究員、ポスドク、指導を受けた大学院生 の名称 (AISSには○印) のリスト

講 師 原田浩之, 中島雄介,
助 教 生田 稔, 森田圭一, 樺沢勇司,
島本裕彰, 丸川恵理子, 宮崎英隆,
佐藤 昌

硬組織疾患ゲノムセンター特任講師 伊東大典
大学院生 根岸綾子 (～3月), 小井田奈美 (～3月),
平井秀明 (～3月), 樋口佑輔 (～3月),
栗林悠里 (～3月),
プラピンチャムルーン・チャーンウィット (～9月), 花畑泰子, 上杉篤史,
猪俣謙次, 松本佳奈子, 釘本琢磨,
佐藤 潔, 高橋幸伸, 吉本光洋,
山本信祐 (4月～), 田口貴英 (4月～),
島田泰如 (4月～), 松川 祥 (4月～),
大迫利光 (4月～), 畠山一郎 (4月～)

doi: 10.1111/j.1600-0714.2008.00731.x

J Oral Pathol Med
 © 2009 John Wiley & Sons A/S. All rights reserved.
 interscience.wiley.com/journal/jop

Gene expression analysis by oligonucleotide microarray in oral leukoplakia

Yuri Kuribayashi¹, Kei-ichi Morita¹, Hirofumi Tomioka¹, Masaru Uekusa¹, Daisuke Ito^{1,2}, Ken Omura^{1,2,3}

¹Oral and Maxillofacial Surgery, Department of Oral Reconstitution, Division of Oral Health Sciences, Graduate School; ²Department of Advanced Molecular Diagnosis and Maxillofacial Surgery, Hard Tissue Genome Research Center; ³Global Center of Excellence Program, International Research Center for Molecular Science in Tooth and Bone Diseases, Tokyo Medical and Dental University, Yushima, Bunkyo-ku, Tokyo, Japan

BACKGROUND: Oral leukoplakias (LP) are the most frequent types of oral pre-cancerous lesions, but there is no accurate assessment of this malignant transformation or even genetic diagnosis of the oral epithelial dysplasia. We need to identify the new genetic diagnosis system of the epithelial dysplasia.

METHODS: Oligonucleotide microarray was used to analyze expression patterns of 29 952 genes in 10 LP patients. We compared the different gene expressions between mild dysplasia cases and severe dysplasia cases.

RESULTS: Ninety-six genes expressed differentially were selected as candidates for up-regulated in severe dysplasia. Subsequently, we further selected 16 genes with highest differentially expression. By hierarchical clustering analysis, the 10 cases were divided mild dysplasia from severe dysplasia.

CONCLUSIONS: The 16 genes are suggested as biomarker gene sets of efficacy and quickly recognized in the development of oral epithelial dysplasia.

J Oral Pathol Med (2009)

Keywords: epithelial dysplasia; gene expression; leukoplakia; microarray; oral cancer

Introduction

Oral leukoplakias (LP) are the most frequent type of oral pre-cancerous lesions; they show a variable rate of malignant transformation to oral squamous cell carcinoma (OSCC). Previous studies have shown that the overall prevalence of malignant change is 3–33% over 10 years (1). At present, there are no means of predict-

ing with certainty the risk of cancerous transformation. Malignancy risk of LP includes clinical type, site, presence and grade of epithelial dysplasia, and smoking (2–4).

Oral epithelial dysplasia is classified as either none, mild, moderate or severe, based on histopathological findings. In addition, the grade of epithelial dysplasia seems to be an indicator for malignant development. Nevertheless, it is recognized that occasionally non-dysplastic lesions may turn into cancer, while not all dysplastic lesions become malignant (5, 6). There are several reports on the application of molecular biological markers for the assessment of cancer risk, such as heterozygosity or microsatellite instability (7–9). However, no general agreement has been reached for the use of either of them in routine diagnosis. The diagnosis of LP was still, for the most part, dependent on traditional clinico- and histo-pathological observations (10). Therefore, we need to identify the reliable biomarkers that are potential for malignant transformation (11).

The final deciphering of the complete sequencing of the human genome, together with the improvement of high throughput technologies, is causing a fundamental transformation in cancer research. Microarray analysis allows the evaluation of a large number of potential candidate genes and pathways that may be related to carcinogenesis and cervical lymph node metastasis in head and neck squamous cell carcinoma. Several studies have already demonstrated the usefulness of this technique for identifying novel cancer-related genes and predictive genes of cervical lymph node metastasis (12, 13).

To identify the new biomarkers that predict their potential for malignant transformation of LP, we initially investigated the gene expression profiles of LP that differentiate between mild dysplasia cases and severe dysplasia cases. Our study suggests that gene expression profiling by oligonucleotide microarrays could prove to be the new genetic diagnosis of the oral epithelial dysplasia and could also provide important

Correspondence: Yuri Kuribayashi, DDS, Oral and Maxillofacial Surgery, Department of Oral Reconstitution, Division of Oral Health Sciences, Graduate School, Tokyo Medical and Dental University, 1-5-45, Yushima, Bunkyo-ku, Tokyo 113-8549, Japan. Tel: +81 3 5803 5506; Fax: +81 3 5803 0199; E-mail: kurisur@tmd.ac.jp
 Accepted for publication October 22, 2008

2

information concerning the molecular mechanisms for the oral carcinogenesis.

Materials and methods

Patients and cell lines

The study subjects included 20 patients with histopathologically defined LP.

These samples had been surgically resected in the Tokyo Medical and Dental University Hospital. The male:female ratio was 13:7 and the mean age was 65.2 years. The patient clinical and pathological data was summarized in Table 1.

The histopathological assessment scoring based on the architectural and cytological changes of grading epithelial dysplasia that was described in the WHO classification was made by evaluating (14): (i) the loss of the polarity of the basal cells; (ii) the presence of more than one layer having a basaloid appearance; (iii) the increased nuclear-cytoplasmic ratio; (iv) the drop-shaped rete-ridges; (v) the irregular epithelial stratification; (vi) the increased number of mitotic figures; (vii) the mitotic figures that are abnormal in form; (viii) the presence of mitotic figures in the superficial half of the epithelium; (ix) the cellular and nuclear pleomorphism; (x) the nuclear hyperchromatism; (xi) the enlarged nucleoli; (xii) the loss of intercellular adherence; and (xiii) the keratinization of single cells or cell groups in the prickle cell layer. For each case, each pathologist recorded the grade and details of the criteria on which the decision was based. Lesions were classified as no dysplasia, mild dysplasia, moderate dysplasia, and severe dysplasia. Based on these parameters, these samples were classified into two groups: no or mild dysplasia (mild dysplasia cases, $n = 5$) and moderate or severe dysplasia (severe dysplasia cases, $n = 5$). All tissue samples were immediately snap-frozen in liquid nitrogen and stored at -80°C until use.

Table 1 Clinical and pathological data

Case	Sex	Age	Site	Grading of epithelial dysplasia
1	M	66	Tongue	Moderate
2	F	64	Upper gingiva	Moderate
3	F	54	Tongue	Moderate
4	M	76	Tongue	Moderate
5	F	76	Tongue	Severe
6	F	77	Lower gingiva	Slight
7	M	68	Lower gingiva	No
8	M	69	Tongue	Slight
9	M	37	Lower gingiva	No
10	M	71	Tongue	Slight
11	M	64	Tongue	Moderate
12	M	81	Buccal mucosa	Moderate
13	M	67	Upper gingiva	Moderate
14	F	54	Tongue	Moderate
15	M	52	Buccal mucosa	No
16	M	64	Buccal mucosa	No
17	M	66	Lower gingiva	No
18	F	54	Tongue	No
19	M	67	Tongue	Slight
20	F	76	Upper gingiva	No

Based on showing a constant expression in the internal control of the microarray analysis, we chose a Ca9-22 cell that was identified as a human squamous cell carcinoma gingival-derived cell line (15, 16).

Isolation of total RNA and microarray analysis

Total RNA was extracted from each sample by using the RNeasy mini Kit (Qiagen, Tokyo, Japan) according to the manufacture's protocol treating with DNase (Qiagen). The quality of the isolated RNA samples was routinely confirmed by examining the integrity of 28S and 18S ribosomal RNA bands using the RNA Picochip 6000 kit in a Bioanalyser (Agilent Technologies, Santa Clara, CA, USA).

Total RNA was extracted from each sample by using the RNeasy mini Kit (Qiagen) according to the manufacturer's protocol treating with DNase (Qiagen). The quality of the isolated RNA samples was routinely confirmed by examining the integrity of 28S and 18S ribosomal RNA bands using the RNA Picochip 6000 kit in a Bioanalyser (Agilent Technologies).

Total RNA from ten surgical specimens (case number 1–10) and the internal control cell line (Ca9-22) was used for oligonucleotide microarray analysis. For Two-Cycle cDNA synthesis and amplified aminoallyl antisense RNA (aRNA) synthesis, the RiboAmpTM RNA amplification kit (Arcturus, Sunnyvale, CA, USA) and the amino-allyl RNA amplification kit (Sigma, Tokyo, Japan) were used. The standard protocols and reagents recommended by Sigma were used for coupling with either Cy3-UTP (the control) or Cy5-UTP (LP tissue) (Amersham Biosciences Corp, Piscataway, NJ, USA), and the labeled aRNA combining hybridization to AceGene[®] Human 30 K 1Chip (HitachiSoft, Hitachi, Japan). These microarray chips were scanned using GMS418 Array Scanner (BioDiscovery, El Segundo, CA, USA). The scanned Cy3 and Cy5 fluorescent signals were imported into the DNASIS Array[®] (HitachiSoft) and were normalized by the internal control spots including *GAPDH* and β -actin. The intensities of corresponding spots were subsequently converted into the ratios of the intensity for oral LP (Cy5) to the control (Cy3).

Semi-quantitative reverse transcriptase-polymerase chain reaction

Aliquots of total RNA from each of the seventeen samples (except in case two, in which sample a small quantity of total RNA was extracted) and the control were used in reverse transcriptase-polymerase chain reaction (RT-PCR) as the template. RT-PCR was carried out using TaKaRa Ex Taq(Takara, Shiga, Japan) and the gene-specific primers as follows: *GAPDH* sense 5'-TGCCTCCTGCACCACCACTTGC-3'; *GAPDH* antisense 5'-AATGCCAGCCCCAGCGTCAAAG-3'; *SLC25A11* sense 5'-TCCAAGCAGTTCTTACTGGAC-3' and *SLC25A11* antisense the 5'-CGTAGCGGACAACCTTTGAACA-3'; *TXNIP* sense 5'-TAATTGGCAGCAGATCAGGTC-3' and *TXNIP* antisense 5'-CATTGTTGTTGAGGATGCAGG-3'; *FZRI* sense 5'-GTGCAATCTGGCCTGGTCCAA-3' and

FZR1 antisense 5'-GGTGAAGAGGTTGAGCACA-GA-3'.

The amplification cycle for each gene fragment was in the linear range. The PCR products were then fractionated by 2% agarose gel electrophoresis followed by photography. In 18 cases, the image data processing software, imageJ, was used to digitize the intensity of each PCR product, and these values were subsequently converted into ratios of the intensity for LP tissue to the intensity for the control.

Real time reverse transcriptase – polymerase chain reaction

Aliquots of total RNA from each of the six samples and the control were used in real time reverse transcriptase-polymerase chain reaction (real time – PCR) as the template. All real time – PCR reactions were performed using the Lightcycler TaqMan Master and the Universal ProbeLibrary Probes (Roche Molecular Biochemicals, Mannheim, Germany) and the gene-specific primers as follows: *GAPDH* sense 5'-AGCCACATCGCTCAGACAC-3'; *GAPDH* antisense 5'-GCCCAATACGACCAATCC-3'; *TXNIP* sense 5'-TCCCTGATACCCCAAGAGC-3' and *TXNIP* antisense 5'-CTTGAGAGCATCCATGTCA-3'; *FZR1* sense 5'-CTACCGCGTGCTGTACCTG-3' and *FZR1* antisense 5'-GGGTTTTGCTAAAGACGTTCC-3'.

The comparative threshold cycle values were normalized to that of *GAPDH*, and these values were subsequently converted into ratios of the mRNA expression for LP tissue to the mRNA expression for the control.

Hierarchical clustering analysis

Following the log-transformation of the ratio (LP tissue vs. the control for each gene), we then used the clustering analysis software Expression Profiler (<http://ep.ebi.ac.uk/EP/EPCLUST/>), a web-based platform for

microarray gene expression and other functional genomics-related data analysis, to perform hierarchical clustering analysis. The resulting expression map was visualized with Treeview using the average-linkage clustering algorithms in the same software package. Those genes that were increased in LP tissue were indicated by a red color, while those that were decreased in LP tissue were indicated by a green color. A black color indicated that those genes were not changed between LP tissue and the control.

Results

Differential gene expression profiles in leukoplakias

We identified the differential expression of the 29952 genes in 10 samples of LP analyzed using AceGene[®] Human 30 K 1Chip.

To identify the markers that differentiate between mild dysplasia cases and severe dysplasia cases, the candidate genes were selected on the basis of the following criteria.

If the ratios of the intensity for LP (Cy5) to the control (Cy3) were more than 2.0-fold in three or more of the five severe dysplasia cases and were <0.5-fold in three or more of the five mild dysplasia cases, the gene was selected as a candidate. The 246 genes were selected as candidates for up-regulated in severe dysplasia. None of the down-regulated genes in severe dysplasia were selected. Then, two-group *t*-tests were used with a threshold of $P < 0.05$ and the 96 most differentially expressed genes allowing distinction of the two groups were selected. The 16 highest differentially expressed genes are extracted (Table 2). Hierarchical clustering of 96 genes resulted in a dendrogram separating mild dysplasia group from severe dysplasia group (Fig. 1a). The 16 highest differentially expressed genes are extracted (Fig. 2), and the hierarchical clustering of

Table 2 Significantly different genes between the mild dysplasia group and the severe dysplasia group

Accession number	Name	Description	P-value
BC003695	<i>KIAA1632</i>	Unknown (protein for image:3456134)	0.000474
NM_003562	<i>SLC25A11</i>	Solute carrier family 25 (mitochondrial carrier; oxoglutarate carrier), member 11; slc25a11	0.000539
NM_016332	<i>SEPX1</i>	Selenoprotein x, 1; sepx1	0.001503
NM_004306	<i>ANXA13</i>	Annexin a13; anxa13	0.003445
NM_000529	<i>MC2R</i>	Melanocortin 2 receptor; mc2r	0.003646
NM_004957	<i>FPGS</i>	Folypolyglutamate synthase; fpgs	0.004753
NM_004173	<i>SLC7A4</i>	Solute carrier family 7 (cationic amino acid transporter, y+ system), member 4; slc7a4	0.005313
NM_021948	<i>BCAN</i>	Chondroitin sulfate proteoglycan behab/brevican; bean	0.008361
AL021578	<i>DBNDD2</i>	dj453e12.4.4 (novel protein (similar to drosophila cg11753), isoform 4); dj453e12.4	0.008917
AF110465	<i>TCL1B</i>	T-cell leukemia/lymphoma 1b; tel1b	0.009348
NM_006423	<i>RABAC1</i>	Ensembl gencan prediction AceGene oligo matches these RefSeq numbers	0.00982
D45399	<i>PDE6H</i>	cgmp phosphodiesterase gamma subunit	0.00992
BC008196	<i>PGAM5</i>	Unknown (protein for mge:5352)	0.012351
NM_006472	<i>TXNIP</i>	Thioredoxin interacting protein; txnip	0.024796
AY007134	<i>CSNK1G2</i>	Clone cdabp0048 mrna sequence; similar to casein kinase i gamma 2 primary transcript with genbank accession number af001177.1	0.029344
NM_016263	<i>FZR1</i>	fzr1 protein; fzr1	0.035707

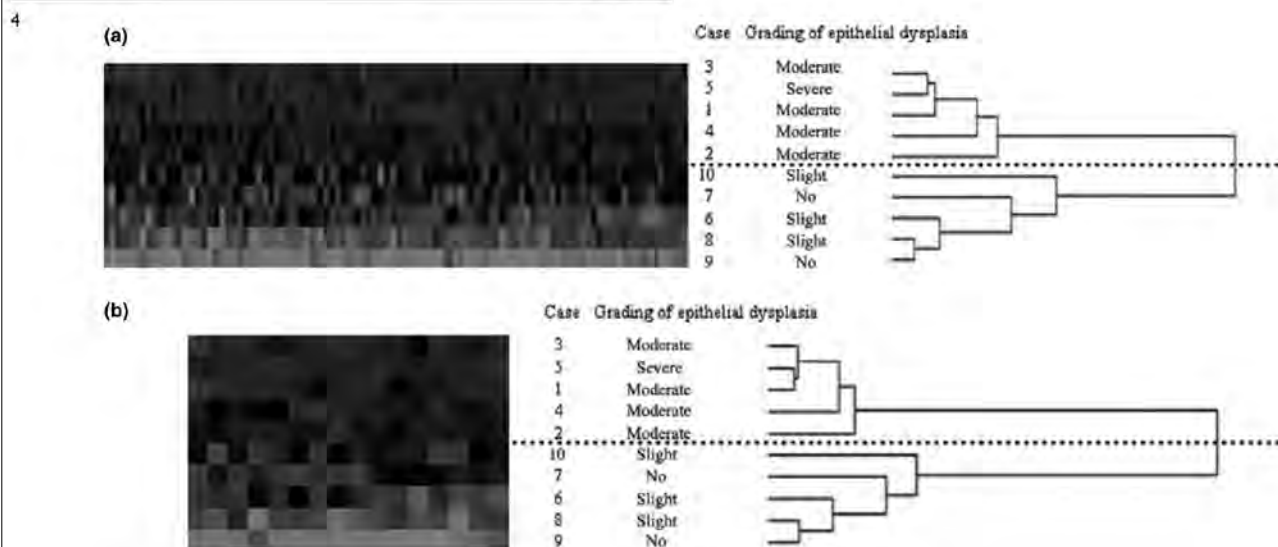


Figure 1 Hierarchical clustering based on differentially expressed genes that distinguished the mild dysplasia group from the severe dysplasia group. (a) Hierarchical clustering based on the 96 genes that distinguished the mild dysplasia group from the severe dysplasia group. (b) Hierarchical clustering based on the 16 most significantly different genes between the mild dysplasia group and the severe dysplasia group.

Case no.	Severe dysplasia group				Mild dysplasia group					C	
	1	3	4	5	6	7	8	9	10		
											<i>SLC25A11</i>
	2.0	1.8	3.0	2.7	1.5	1.0	1.0	1.0	0.9	1.0	Fold
	(3.0)	(4.8)	(3.5)	(2.9)	(1.1)	(0.5)	(0.1)	(0.1)	(1.0)	(1.0)	
											<i>TXNIP</i>
	6.5	9.1	3.3	3.3	2.0	2.3	1.8	2.1	1.0	1.0	Fold
	(3.8)	(3.8)	(2.2)	(6.8)	(0.2)	(0.7)	(0.4)	(0.3)	(1.6)	(1.0)	
											<i>FZR1</i>
	4.8	3.3	6.1	6.0	2.4	1.6	1.7	1.7	1.3	1.0	Fold
	(5.7)	(3.2)	(1.0)	(2.4)	(0.6)	(0.8)	(0.3)	(0.1)	(0.4)	(1.0)	
											<i>GAPDH</i>

Figure 2 Validation of the expression pattern of *SLC25A11*, *TXNIP*, and *FZR1* from nine cases by semi-quantitative RT-PCR. *GAPDH* was used as a loading control. Consistent with the cDNA microarray data, the expression of *SLC25A11*, *TXNIP*, and *FZR1* genes were up-regulated in the severe dysplasia group and down-regulated in the mild dysplasia group. Arabic numerals represent fold changes of each PCR product by imageJ, and numerals in parentheses represent fold changes of microarray data by ImaGene. C, control sample with cell line (Ca9-22).

16 genes resulted in a nearly identical dendrogram (Fig. 1b).

Validation of microarray data by semi-quantitative RT-PCR and real time-PCR

To confirm these gene expression data identified by oligonucleotide microarray analysis, the three candidate genes (*SLC25A11*, *TXNIP*, and *FZR1*) were selected for RT-PCR and Real time-PCR assay. The cDNA derived from total RNA was subsequently used as a template for *GAPDH* (housekeeping gene) and the three candidate genes (*SLC25A11*, *TXNIP*, and *FZR1*). Additionally, to confirm the expression pattern of *SLC25A11*, *TXNIP*, and *FZR1*, total RNA isolated from different subset of clinical specimens (case number 11–20) was harvested for

RT-PCR and real time-PCR. Consistent with case 1–10, the up and down-regulation of *SLC25A11*, *TXNIP*, and *FZR1* was also observed in different LP samples (Figs 2–4). The results of RT-PCR and real time-PCR were in accord with those of our microarray analysis, suggesting that the data obtained by our microarray gene expression analysis were valid and that these genes could potentially serve as a genetic diagnosis system.

Discussion

The ability to change our current paradigms of diagnosis and treatment of pre-malignant lesions depends in large part on the development of refined and clinically significant molecular risk markers that can assist the

Gene expression analysis in oral leukoplakia
Kuribayashi et al.





Case no.	Severe dysplasia group				Mild dysplasia group				C	
	11	12	13	14	15	16	17	18		
										<i>SLC25A11</i>
	2.0	1.3	1.5	2.1	1.0	0.7	1.2	0.7	1.0	Fold
										<i>TXNIP</i>
	3.6	3.8	3.1	3.7	2.1	1.3	3.1	0.7	1.0	Fold
										<i>FZR1</i>
	1.4	1.5	1.7	1.6	1.0	0.9	0.9	0.9	1.0	Fold
										<i>GAPDH</i>

Figure 3 Validation of the expression pattern of *SLC25A11*, *TXNIP*, and *FZR1* by semi-quantitative RT-PCR. Total RNA isolated from case 11–18 was used. The expression of *SLC25A11*, *TXNIP*, and *FZR1* was consistent with case 1–10.

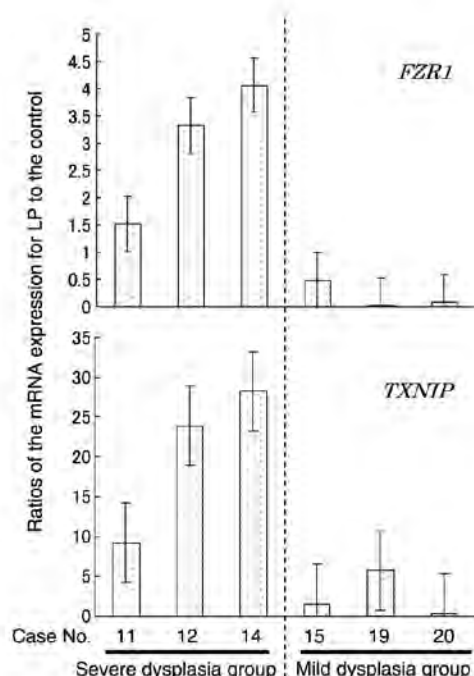


Figure 4 Validation of the expression pattern of *TXNIP*, and *FZR1* by Real time-PCR. Total RNA isolated from case 11, 12, 14, 15, 19, 20 was used. Results are the means of triplicate determinations \pm SD. The comparative threshold cycle values were normalized to that of *GAPDH*, and these values were subsequently converted into ratios of the mRNA expression for leukoplakias (LP) tissue to the mRNA expression for the control.

microscopic grading of oral epithelial dysplasia (17). There are a few reports that focus on oral pre-cancerous lesions by means of microarray technology.

By comparison of normal tissues with both mild and severe dysplasia, this study reveals alterations in gene expression patterns related to progression toward malignancy and include genes involved in DNA repair oxidative stress, cell adhesion/motility, cell cycle regulation and others (1). In this study, matched 'normal' epithelium may confound interpretations of gene expression changes occurring in OSCC tumorigenesis, given

that histologically normal tissue samples may already harbor pre-neoplastic genetic changes that have yet to manifest phenotypically. These gene subsets might be associated with the pathogenesis and malignant transformation of oral epithelial dysplasia, but might not exactly be prediction biomarkers of cancer development.

Using cDNA microarray and RT-PCR technologies, a comprehensive gene expression profile was compared among OSCC and LP tissues (18). The *decorin* gene expression was identified using oligonucleotide microarray analysis in representative cell lines of an OSCC progression model as well as oral matched and unmatched patients (19). Through an OSCC progression model composed of cell lines, organotypic cultures, and tissue specimens, the data show that up-regulation of EMMPRIN expression occurs during the early stage of oral pre-malignancy lesions and appears to be a critical phenotypic alteration that precedes the development of OSCC (20). When the results from these studies are evaluated together, the expression of marker gene candidates may provide the role of the tumor micro-environment in oral pre-malignancy to search genetic changes.

Another study identified microarray-based transcriptional profiling as a primarily affected metabolic pathway that may be responsible for irreversible transition to progressive stages of oral cancer (21). The study also showed the protective role of these enzyme-derived metabolites in inhibiting cell proliferation using an *in vitro* oral cancer model. A molecular basis and innovative approaches for clinical intervention may prevent oral cancer progression in the future.

The ultimate goal of our study is to discover biomarkers of oral cancer progression that will provide a more accurate diagnosis. Expression profiling using oligonucleotide microarray is a useful tool in identifying tumors, in distinguishing different tumor entities, and in differentiating between progressing and non-progressing pre-malignant lesions (22). In the present study, we selected 96 differentially expressed genes of the development of oral epithelial dysplasia using the oligonucleotide microarray analysis. The expression patterns of the 96 genes could differentiate between mild dysplasia and severe dysplasia. To identify biomarker gene sets of efficacy and to quickly discriminate between the mild

6

dysplasia group and the severe dysplasia group, the 16 highest differentially expressed genes are extracted and we verified the expression of three genes by using RT-PCR.

In the future, on the occasion that the number of cases accumulated for the expression data using our gene sets increases and each case is observed over a long term, the data of the 10-year malignant transformation rate will be added. Additionally, to investigate into genes differentially expressed carcinogenesis using microarray, we need to designate normal tissue or OSCC tissue as samples compared with the internal control (Ca9-22).

In conclusion, our study demonstrates that the gene expression profiling that we have identified through oligonucleotide microarrays could prove to be the new genetic-diagnostic oral epithelial transformation markers and could also provide valuable information for our further understanding of the oral carcinogenesis.

References

1. Francesco C, Lorenzo LM, Adriano P, et al. Genetic portrait of mild and severe lingual dysplasia. *Oral Oncol* 2005; **41**: 365–74.
2. Holmstrup P, Vedtofte P, Reibel J, et al. Long-term treatment outcome of oral premalignant lesions. *Oral Oncol* 2006; **42**: 461–74.
3. Epstein JB, Gorsky M, Fischer D, et al. A survey of the current approaches to diagnosis and management of oral premalignant lesions. *J Am Dent Assoc* 2007; **138**: 1555–62.
4. van der Waal I, Axell T. Oral leukoplakia: a proposal for uniform reporting. *Oral Oncol* 2002; **38**: 521–6.
5. Schepman K, der Meij E, Smele L, et al. Concomitant leukoplakia in patients with oral squamous cell carcinoma. *Oral Dis* 1999; **5**: 206–9.
6. Warnakulasuriya S. Lack of molecular markers to predict malignant potential of oral precancer. *J Pathol* 2000; **190**: 407–9.
7. Brennan M, Migliorati CA, Lockhart PB, et al. Management of oral epithelial dysplasia: a review. *Oral Surg Oral Med Oral Pathol Oral Radiol Endod* 2007; **103**(Suppl. 1): S19 e1–e12.
8. Patmore HS, Cawthell L, Stafford ND, et al. Unraveling the chromosomal aberrations of head and neck squamous cell carcinoma: a review. *Ann Surg Oncol* 2005; **12**: 831–42.
9. Zhang L, Cheung KJ Jr, Lam WL, et al. Increased genetic damage in oral leukoplakia from high risk sites: potential impact on staging and clinical management. *Cancer* 2001; **91**: 2148–55.
10. Holmstrup P, Vedtofte P, Reibel J, et al. Oral premalignant lesions: is a biopsy reliable? *J Oral Pathol Med* 2007; **36**: 262–6.
11. Ohkura S, Kondoh N, Hada A, et al. Differential expression of the keratin-4, -13, -14, -17 and transglutaminase 3 genes during the development of oral squamous cell carcinoma from leukoplakia. *Oral Oncol* 2005; **41**: 601–13.
12. Tomioka H, Morita K, Hasegawa S, et al. Gene expression analysis by cDNA microarray in oral squamous cell carcinoma. *J Oral Pathol Med* 2006; **35**: 206–11.
13. Nguyen ST, Hasegawa S, Tsuda H, et al. Identification of a predictive gene expression signature of cervical lymph node metastasis in oral cell carcinoma. *Cancer Sci* 2007; **98**: 740–6.
14. Pindborg JJ, Reichart PA, Smith CJ, et al. Histological typing of cancer and precancer of the oral mucosa. In: Pindborg JJ, Wahl PN, eds. *World Health Organization international histological classification of tumors*, 2nd edn. Berlin Heidelberg, New York: Springer-Verlag, 1997; 551–7.
15. Yamamoto K, Konishi N, Inui T, et al. Genomic alterations in oral squamous cell carcinoma cell lines detected by two-dimensional gel analysis. *Oral Oncol* 1998; **34**: 508–12.
16. Ikuta M, Podyma KA, Maruyama K, et al. Expression of heparanase in oral cancer cell lines and oral cancer tissues. *Oral Oncol* 2001; **37**: 177–84.
17. Scott M, Lippman JS, Waun KH. Oral cancer prevention and evolution of molecular-targeted drug development. *J Clin Oncol* 2005; **23**: 346–56.
18. Kondoh N, Ohkura S, Arai M, et al. Gene expression signatures that can discriminate oral leukoplakia subtypes and squamous cell carcinoma. *Oral Oncol* 2007; **43**: 455–62.
19. Abhijit GB, Indraneel B, William ML, et al. Aberrant expression and localization of decorin in human oral dysplasia and squamous cell carcinoma. *Cancer Res* 2003; **63**: 7769–76.
20. Vigneswaran N, Beckers S, Waigel S, et al. Increased EMMPRIN expression during oral carcinogenesis. *Exp Mol Pathol* 2006; **80**: 147–59.
21. Abhijit GB, Indraneel B, Vishwanatha JK, et al. Identification of genes and molecular pathways involved in the progression of premalignant oral epithelia. *Mol Cancer Ther* 2005; **4**: 865–75.
22. Odani T, Ito D, Li MH, et al. Gene expression profiles of oral leukoplakia and carcinoma: genome-wide comparison analysis using oligonucleotide microarray technology. *Int J Oncol* 2006; **28**: 619–24.

M E M O

This image shows a single sheet of white paper with horizontal ruling lines. The lines are evenly spaced and run across the width of the page. There are no margins, text, or other markings on the paper.

インプラント 口腔再生医学分野

春日井 昇平

医歯学総合研究科・口腔機能再構築学系専攻
摂食機能制御学・教授



1) 研究の課題名

歯科インプラント治療に必要な骨および軟組織再生

(Bone and Soft Tissue Renertion for Dental Implant Treatment)

歯が欠損した場合の治療法として歯科インプラント（以下インプラント）治療は確実な治療法となっており、従来の治療法に比較して利点も多い。しかしインプラント埋入予定部位に骨および軟組織が存在しない場合には治療が困難となる。骨造成法のゴールドスタンダードは自家骨移植であるが、骨採取部位の炎症と採取骨量に限度があることが問題である。また、現在臨床で使用されているハイドロキシアパタイトやbeta-TCPは骨形成の足場となるが、自家骨の代用としては力不足である。骨芽細胞のBMP2転写活性増加作用を示すシンバスタチンとalpha-TCPを組み合わせた骨補填材を開発し、この骨補填材の臨床試験をおこない良好な結果を得た。膜を用いて骨再生のスペースを確保するGuided Bone Regeneration (GBR) がおこなわれている。架橋ゼラチンとbeta-TCPを組み合わせた膜およびCHPナノゲルを用いた膜を開発し、これらの膜が現在使用されている膜に比べて骨再生を著しく促進し、またCHPナノゲルは軟組織の治癒を促進することも明らかになった。これらの2種類の膜はFGFやBMP等のシグナル分子のキャリアーとして優れており、細胞の増殖や分化を促進するシグナル分子を組み合わせることでSuper GBR膜を開発することが可能である。

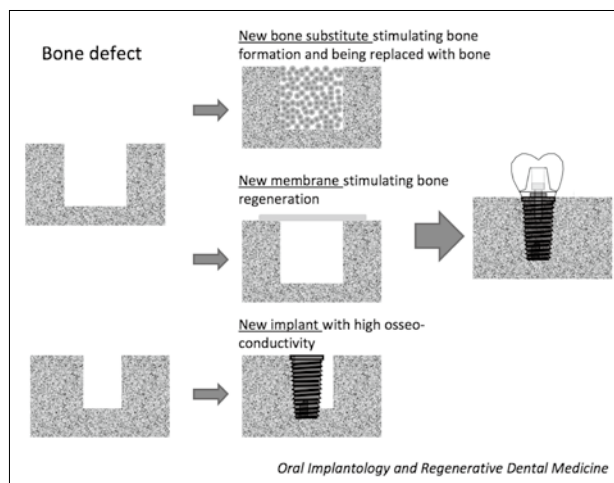
歯科インプラントの開発

(Develotment of Dental Implant)

我々が共同で開発したチタン表面にハイドロキシアパタイトを薄膜コーティングしたインプラントの臨床試験を継続しておこなっており、4年間の良好な臨床結果を報告した。このインプラントはミニブタへ埋入試

験において他のインプラントを遥かに凌ぐ100%のbone implant contactを示した。

2)



3) 研究内容の英文要約

Prosthetic treatment with dental implants is advantageous and predictable; however, deficiency of bone and soft tissue makes dental implant treatment difficult. Although autogenous bone graft is a gold standard for bone augmentation, mobility of the donor site and limitation of harvestable bone volume are problems. To solve these problems, bone substitutes, such as hydroxyapatite (HA) and beta-TCP, are clinically applied; however, these materials do not stimulate bone formation. We developed a bone substitute consisting of alpha-TCP and simvastatin, which stimulates BMP2 expression in osteoblasts. In animal and clinical experiences we demonstrated that alpha-TCP containing simvastatin stimulated bone formation and that this material was finally replaced with new bone. We also developed HA fiber material and demonstrated that this material worked efficiently as a scaffold for BMP2 gene delivery resulting in ectopic new bone formation. Guided bone regeneration (GBR) is a regenerative technique

with a membrane, which maintains a space for new bone formation. We developed gelatin cross-linked membrane and CHP nanogel membrane. Both of these membranes worked efficiently as GBR membranes compared to the GBR membrane available in the market. We also found CHP nanogel alone promoted wound healing while CHP nanogel combining with prostaglandin E1 stimulated wound healing more efficiently. These newly-developed materials would be useful to regenerate bone and soft tissue required in dental implant treatment.

4) 本事業に関連して世界的な研究拠点形成に向けて、以下の点で改善・整備等されたこと

A (研究拠点体制)

世界に向けて歯科インプラント治療に関連した研究に関して情報を発信している。

D (人材育成)

博士過程大学院生に対して、通常の研究指導に加えて、英語での発表とディスカッションの指導をおこない、海外での学会発表を積極的に推奨した。

E (国際化)

海外からの大学院博士課程および臨床研修希望者が増加している。現在、韓国、中華人民共和国、中華民国、タイ、ミャンマー、インド、ヨルダン、エジプト、リビア、ドミニカ、アルゼンチンの計11の国の博士過程大学院学生および臨床研修生を教育している。

5) GCOE 事業を推進するに当たって力を入れた点

常に世界のトップを目標に研究と教育をおこなうこと。

6) 英文原著論文

1. Nyan M, Miyahara T, Noritake K, Hao J, Rodriguez R, Kuroda S, Kasugai S. Molecular and tissue responses in the healing of rat calvarial defects after local application of simvastatin combined with alpha tricalcium phosphate. *Journal of Biomedical Materials Research Part B: Applied Biomaterials*
2. Kon K, Shiota M, Ozeki M, Yamashita Y, Kasugai S. Bone augmentation ability of autogenous bone graft particles with different sizes: a histological and micro-computed tomography study. *Clinical Oral Implants Research* 20(11):1240-6, 2009
3. Ikeda E, Morita R, Nakao K, Ishida K, Nakamura T, Takano-Yamamoto T, Ogawa M, Mizuno M, Kasugai S, Tsuji T. Fully functional bioengineered tooth replacement as an organ replacement therapy. *Proc Natl Acad Sci U S A*. 106(32):13475-80, 2009

4. Kobayashi H, Katakura O, Morimoto N, Akiyoshi K, Kasugai S. Effects of cholesterol-bearing pullulan (CHP)-nanogels in combination with prostaglandin E1 on wound healing. *Journal of Biomedical Material Research, Part B: Applied Biomaterials* 91(1):55-60, 2009
5. Oda M, Kuroda S, Kondo H, Kasugai S. Hydroxyapatite fiber material with BMP-2 gene induces ectopic bone formation. *Journal of Biomedical Material Research, Part B: Applied Biomaterials* 90(1):101-9, 2009
6. Nyan M, Sato D, Kihara H, Machida T, Ohya K, Kasugai S. Effects of the combination with alpha-tricalcium phosphate and simvastatin on bone regeneration. *Clinical Oral Implant Research* 20(3):280-7, 2009

7) 著書

春日井昇平. 成功するインプラント治療のための留意点. 日本歯科医学会雑誌 63 印刷中

春日井昇平. 歯科領域での骨の再生の基礎と臨床: 歯科インプラント治療と骨造成 東京都歯科医師会雑誌 57 (9) :447-454, 2009

春日井昇平. インプラント治療の現状と最近の進歩: 再生医療との関わり. Minimally Intervention 時代の歯科知識 (吉山昌宏、伊藤博夫、十河基文編)、永末書店、pp10-26, 144 ページ、2009

春日井昇平. 細胞増殖のためのバイオマテリアルの利用 再生部位確保膜 歯周組織 (GTR). 患者まで届いている再生誘導治療 (田畑泰彦 編)、株式会社メディカルドウ、pp81-84, 308 ページ、2009

春日井昇平. インプラント手術をマスターするための関連機材マニュアル 診断機材からピエゾサージェリーまで (春日井昇平、古賀剛人、嶋田淳 編)、クインテッセンス出版、127 ページ、2009

8) 平成21年度までの自己評価

平成12年(2000年)に教授となってから、歯学部附属病院インプラント外来の科長として、当外来の治療を世界のトップレベルにすることを目標に努力してきたが、その目標は到達できた。歯科インプラント治療に必要な骨および軟組織の再生に関連した研究、歯科インプラントの開発において、世界に向けて情報を発信している点は評価できる。今後は、長期の臨床の前向き研究をおこない、世界に向けて情報を発信していきたい。

9) 学会発表 (英文)

Miyahara T, Nyan M, Nagayama T, Hao J, Rodoriguez R, Yamamoto Y, Shimoda A, Kuroda S, Tachikawa N, Shiota M, Akiyoshi K, Kasugai S. Novel GBR membrane consisting of cholesterol-bearing pullulan nanogel. The 25th Annual Meeting of Academy of Osseointegration 2010.3.4-7 Walt Disney World Dolphin Resort Hotel, Orland, USA 口頭

Kasugai S, Takebayashi A, Furusawa K. Novel surgical guiding system with a laser beam. 25th Annual Meeting of Academy of Osseointegration 2010.3.4-7 Walt Disney World Dolphin Resort Hotel, Orland, USA 口頭

Nakata H, Tachikawa N, Takefuji K, Shiota M, Kasugai S. Anterior tooth replacement with implants in alveolar cleft site: A clinical evaluation of aesthetics. 18th Annual Scientific Meeting of European Association for Osseointegration 2009.9.30-10.3 Grimaldi Forum, Monaco 示説

Kasugai S, Shiota M, Tachikawa N, Kondo H, Kuroda S, Fujimori T, Munakata M, Nakata H, Kobayashi H. Four year clinical observation of thin hydroxyapatite-coated implant. 18th Annual Scientific Meeting of European Association for Osseointegration 2009.9.30-10.3 Grimaldi Forum, Monaco 示説

Yamaguchi Y, Tachikawa N, Kondo H, Munakata M, Ichinose S, Shiota M, Kasugai S. Analysis of fractures of splinted posterior implants. 18th Annual Scientific Meeting of European Association for Osseointegration 2009.9.30-10.3 Grimaldi Forum, Monaco 示説

Kasugai S. Patient-oriented implant treatment: Immediate protocol. Annual Congress of Academy of Oral Implantology, Republic of China (AOIRC) 2009.10.8-10 Howard International House, Taipei, Taiwan 口頭

Kasugai S. Prosthesis or regeneration?: Dental implant vs. tissue-engineered tooth. The 2nd Thailand International Conference on Oral Biology, Biology of Mineralized Tissue 2009.5.7-8 Chulalongkorn University, Bangkok, Thailand 口頭

Ueno N, Sato D, Nyan M, Kondo H, Kasugai S. Bone substitute of alpha-TCP containing simvastatin: Clinical study. 24th Annual Meeting of Academy of Osseointegration 2009.2.26-28 San Diego Convention Center, San Diego, USA 口頭

Kasugai S. IT-based safe, simple and predictable implant treatment. International Symposium 第21回日本歯科医学会総会 2008.11.14-16 パシフィコ横浜 横浜 口頭

Kasugai S. Immediate protocol in dental implant treatment: Keys to avoid failures in this attractive protocol. Invited Lecture Annual Meeting of Thai Dental Implant Society 2008.10.23-25 Landmark Bangkok Hotel, Bangkok, Thailand 口頭

Kasugai S. Dental implant treatment in the near future: Prosthesis or regeneration? 特別講演 第4回日中歯科医学学会 2008.9.27-29 西安 中華人民共和国 口頭

Kon K, Shiota M, Ozeki M, Kimura J, Kasugai S. Particle size effect on augmented bone volume in autologous graft. The 17th Annual Scientific Meeting of European Association of Osseointegration 2008.09.18-20 PKIN Convention Center, Warsaw, Poland 示説

Nyan M, Kihara H, Machida T, Ueno H, Kasugai S. Combination with alpha-tricalcium phosphate and simvastatin stimulates bone regeneration. The 17th Annual Scientific Meeting of European Association of Osseointegration 2008.09.18-20 PKIN Convention Center, Warsaw, Poland 示説

Yamaguchi Y, Tachikawa N, Kondo H, Ichinose S, Kasugai S. Analysis of fractured commercially pure titanium implants. The 17th Annual Scientific Meeting of European Association of Osseointegration 2008.09.18-20 PKIN Convention Center, Warsaw, Poland 示説

Kasugai S. Immediate function vs. conventional protocol. Esthetic Forum Bali 2008.5.2-4 Grand Hyatt Bali, Bali, Indonesia 口頭

Sato M, Fujii S, Amagasa T, Kasugai S. Hydroxyapatite fiber material as bone substitute: Clinical study for sinus elevation. The 23rd Annual Meeting of Academy of Osseointegration 2008.2.28-3.1 The Hynes Convention Center, Boston, USA 示説

Kasugai S, Ochi M, Shiota M, Hirose Y, Tachikawa N, Kuniyasu H, Kondo H, Matubara H, Kuroda S, Taira H, Fujimori T, Murata M, Kitajo H, Kusano K. Clinical trial of thin hydroxyapatite-coated one-piece implant. The 23rd Annual Meeting of Academy of Osseointegration 2008.2.28-3.1 The Hynes Convention Center, Boston, USA 示説

10) 学会発表 (和文)

春日井昇平. インプラント治療と骨補填材. 第2回 Academy of Minimally Invasive Implant Treatment 学術大会 2010.1.24 学術センター、東京

春日井昇平. 上顎洞底が近接する上顎臼歯欠損部に対する

るインプラント治療のガイドライン.シンポジウム 口腔インプラントの臨床エビデンスはどのくらい整ったのか 診療ガイドラインの策定に向けて 第39回日本口腔インプラント学会学術大会 2009.9.25-27 大阪国際会議場、大阪

春日井昇平.骨折治療機LIPUSはインプラントの救世主となるか? ランチョンセミナー (伊藤超短波株式会社) 第39回日本口腔インプラント学会学術大会 2009.9.25-27 大阪国際会議場、大阪

上野憲秀、近藤尚知、鬼原英道、佐藤大輔、春日井昇平.シンバスタチンを含有するalpha-TCPの骨補填材としての有効性:臨床研究.第39回日本口腔インプラント学会学術大会 2009.9.25-27 大阪国際会議場、大阪

朴浚喜、春日井昇平.超音波厚み測定器を用いた粘膜厚さ測定に関する研究.第39回日本口腔インプラント学会学術大会 2009.9.25-27 大阪国際会議場、大阪

近藤尚知、黒田真司、立川敬子、中村貴弘、春日井昇平.インプラント手術支援ナビゲーションシステムの有用性:症例報告.第39回日本口腔インプラント学会学術大会 2009.9.25-27 大阪国際会議場、大阪

武山秀子、黒田真司、長田紀子、則武加奈子、春日井昇平.Split crestと骨移植によって上顎前歯部にインプラント治療をおこなった一症例.第39回日本口腔インプラント学会学術大会 2009.9.25-27 大阪国際会議場、大阪

藤井政樹、塩田真、木村純一、今一裕、春日井昇平.インプラント補綴形態が機能回復に及ぼす影響.第39回日本口腔インプラント学会学術大会 2009.9.25-27 大阪国際会議場、大阪

春日井昇平.インプラント治療に必要な骨補填材.第7回日本再生歯科医学会総会・学術大会 2009.9.12九州歯科大学 小倉

黒田真司、中田秀美、則武加奈子、Hao Ja、春日井昇平.脂肪細胞分化におけるOsterixの骨芽細胞分化誘導の可能性.第7回日本再生歯科医学会総会・学術大会 2009.9.12九州歯科大学 小倉

春日井昇平.安全安心なインプラント治療.第2回日本先進インプラント医療学会総会・学術大会2009.9.6 学術総合センター 東京

春日井昇平.骨形成促進作用を示す吸収性の骨補填材.第27回日本骨代謝学会総会・学術大会 シンポジウム 歯周組織と骨の再生 2009.7.23-25 大阪国際会議場 大阪

春日井昇平.高齢者へのインプラント治療において考慮すべきこと.第20回日本老年歯科医学会総会・学術大会 2009.06.18-20 パシフィコ横浜 横浜

春日井昇平.骨形成を促進する化合物を含む吸収性骨補填材.日本バイオマテリアル学会シンポジウム2008 2008.11.17-18 東京大学 東京

Kasugai S. IT-based safe, simple and predictable implant treatment. International Symposium 第21回日本歯科医学会総会 2008.11.14-16 パシフィコ横浜 横浜

春日井昇平.Academy of minimally-invasive Implantology (AMII) の研究会発足の主旨.AMII第1回Conference 2008.11.15 ランドマークホール 横浜

春日井昇平.EBMとガイドライン.インプラント治療のガイドラインのためのエビデンス どのような考え方が提唱されてきたか シンポジウム 第38回日本口腔インプラント学会学術大会 2008.09.12-14 東京フォーラム 東京

川勝敦子、宗像源博、大庭容子、塩田真、立川敬子、春日井昇平.上顎臼歯欠損部の骨形態に関する検討.シンポジウム 第38回日本口腔インプラント学会学術大会 2008.09.12-14 東京フォーラム 東京

町田哲、丸尾勝一郎、佐藤仁、春日井昇平.繊維性ハイドロキシアパタイト材料がラット抜歯窩治癒に及ぼす影響:放射線学的評価.シンポジウム 第38回日本口腔インプラント学会学術大会 2008.09.12-14 東京フォーラム 東京

大藪祐子、塩田真、森川俊彦、黒田真司、近藤尚知、立川敬子、春日井昇平.糖尿病患者へのインプラント治療.シンポジウム 第38回日本口腔インプラント学会学術大会 2008.09.12-14 東京フォーラム 東京

小林裕史、近藤尚知、黒田真司、立川敬子、塩田真、春日井昇平. 当科におけるインプラント脱落に関する調査. シンポジウム 第38回日本口腔インプラント学会学術大会 2008.09.12-14 東京フォーラム 東京

藤森達也、塩田真、春日井昇平、作山葵. 超薄膜ハイドロキシアパタイトコーティングインプラント周囲における新生骨形成: ピーグル犬における早期負荷の組織観察. シンポジウム 第38回日本口腔インプラント学会学術大会 2008.09.12-14 東京フォーラム 東京

春日井昇平. 骨形成促進作用を示す骨補填材. シンポジウム Periodontal Tissue Engineeringの現状と将来展望. 第29回日本炎症・再生医学会 2008.7.8-10 都市センターホテル 東京

春日井昇平. 歯科インプラント治療と再生医療の融合. 第7回日本再生医療学会総会 2008.3.13-14 名古屋国際会議場

塩田真、木村純一、大藪祐子、今一裕、春日井昇平. インプラント上部構造に応用した陶材の破折について 第27回日本口腔インプラント学会関東・甲信越支部学術大会 2008.2.3-4 都市センター 東京

藤森達也、作山葵、塩田真、春日井昇平. 血液供給不足部位へのVEGFの応用による血管ならびに骨新生に関する組織学的研究. 第27回日本口腔インプラント学会関東・甲信越支部学術大会 2008.2.3-4 都市センター 東京

北爪孝昌、塩田真、大庭容子、立川敬子、近藤尚知、黒田真司、春日井昇平. 当科新来患者の中でインプラント治療に到った患者の内訳. 第27回日本口腔インプラント学会関東・甲信越支部学術大会 2008.2.3-4 都市センター 東京

長田紀子、塩田真、大庭容子、北爪孝昌、寺前智人、近藤尚智、立川敬子、春日井昇平. 東京医科歯科大学歯学部附属病院インプラント外来における無歯顎患者の治療動向. 第27回日本口腔インプラント学会関東・甲信越支部学術大会 2008.2.3-4 都市センター 東京

森川俊彦、近藤尚知、立川敬子、大庭容子、北爪孝昌、塩田真、春日井昇平. インプラント患者の有病率について.

第27回日本口腔インプラント学会関東・甲信越支部学術大会 2008.2.3-4 都市センター 東京

11) 受賞

Best Clinical Innovation Presentation, Academy of Osseointegration 2009年3月27日

12) 外部資金の獲得状況

科学研究補助金 基盤研究B

研究題目: 歯科領域における骨補填材の適正化

代表: 春日井昇平

期間: 平成19年—平成21年

研究費総額: 16,500千円

科学技術新興機構委託開発事業

研究題目: スタチンを用いた骨増加材

代表: 春日井昇平

期間: 平成16年—平成21年

研究費総額: 125,000千円

科学研究費補助金 基盤研究C

研究題目: 生分解性ポリマーステントを利用した口腔軟組織再建

代表: 立川敬子

期間: 平成20年—平成22年

研究費総額: 千円

科学研究費補助金 萌芽研究

研究題目: エンヴェロープベクターとsiRNAを応用した歯周組織再生療法

代表: 近藤尚知

科学研究費補助金 萌芽研究

研究題目: 粘膜・骨再生法による、新しい口蓋瘻孔閉鎖の試み

代表: 黒田 真司

科学研究費補助金 若手研究B

研究題目: 新規骨補填剤による骨新生に関する基礎的研究

代表: 鬼原英道

科学研究費補助金 若手研究B

研究題目: Msx1 遺伝子の調節エレメントの解析

代表:中田秀美

科学研究費補助金 若手研究 (スタートアップ)
ソノポレーション法による骨膜への遺伝子導入
代表:金井 亨

13) 特別講演、招待講演

Kasugai S. Surface modification and design of dental implant. 東京医科歯科大学 GCOE プログラムシンポジウム 2010.2.11 東京医科歯科大学、東京

春日井昇平.ここまでのインプラント治療.第39回日本口腔インプラント学会学術大会市民フォーラム、第3回徳島市歯科医師会市民公開講座 あわぎんホール、徳島

春日井昇平.インプラント治療と骨補填材.第2回 Academy of Minimally Invasive Implant Treatment 学術大会 2010.1.24 学術センター、東京

春日井昇平.インプラント治療のトラブルと対策:失敗しないインプラント治療のための留意点.補綴学会教育セミナー 2010.1.10 パシフィコ横浜、横浜

春日井昇平.インプラント治療は両刃の剣:問題症例からの考察 Detistry Quo Vadis? 2009.12.5-6 野口英世記念館 東京

春日井昇平.インプラント治療の現状と将来:患者中心のインプラント治療と再生医療の台頭.日本インプラント臨床研究会講演会 2009.12.5 松風東京支社 東京

春日井昇平.インプラント治療の現状と将来:治療期間の短縮と再生医療との関わり 2009.11.29 五群市(朝霞、入間、川越、所沢、比企) 歯科医師会学術講演会 2009.11.29 東武ホテル川越 川越

春日井昇平.上顎洞内の骨造成:再生医学的見地からの考察 UCLA デンタルアソシエートシンポジウム サイナスリフト 2009.11.15 昭和大学歯学部 東京

春日井昇平.はじめて臨床にインプラントを取り入れるには.歯科医学会平成21年度学術講演会 ニーズに応える21世紀最新歯科医療 口腔インプラントと日常臨床 2009.10.18 ベルクラシック甲府、甲府、山梨

Kasugai S. Patient-oriented implant treatment: Immediate protocol. Annual Congress of Academy of Oral Implantology, Republic of China (AOIRC) 2009.10.8-10 Howard International House, Taipei, Taiwan

春日井昇平.上顎洞底が近接する上顎臼歯欠損部に対するインプラント治療のガイドライン.シンポジウム 口腔インプラントの臨床エビデンスはどのくらい整ったのか 診療ガイドラインの策定に向けて 第39回日本口腔インプラント学会学術大会 2009.9.25-27 大阪国際会議場、大阪

春日井昇平.骨折治療機LIPUSはインプラントの救世主となるか? ランチョンセミナー (伊藤超短波株式会社) 第39回日本口腔インプラント学会学術大会 2009.9.25-27 大阪国際会議場、大阪

春日井昇平.インプラント治療に必要な骨補填材について .Clinical Dentistry Research Institute, Monthly Meeting 2009.9.25 ヨシダ本社、東京

春日井昇平.インプラント治療に必要な骨補填材.第7回日本再生歯科医学会総会・学術大会 2009.9.12 九州歯科大学 小倉

春日井昇平.安全安心なインプラント治療.第2回日本先進インプラント医療学会総会・学術大会 2009.9.6 学術総合センター 東京

春日井昇平.はじめて臨床にインプラントを取り入れるには.歯科医学会平成21年度学術講演会 ニーズに応える21世紀最新歯科医療 口腔インプラントと日常臨床 2009.8.30 和歌山県歯科医師会館 和歌山

春日井昇平.歯科医療の現状と将来:歯科インプラント治療と再生医療との関わり.岩手大学歯学部オープンリサーチプロジェクト 難治性歯科疾患克服に向けたCell Therapyの基礎構築とDentistryの育成 シンポジウム 再生医療の現状と将来 2009.7.25 岩手医科大学循環器医療センター 盛岡

春日井昇平.骨形成促進作用を示す吸収性の骨補填材.第27回日本骨代謝学会総会・学術大会 シンポジウム 歯周組織と骨の再生 2009.7.23-25 大阪国際会議場 大阪

春日井昇平.最近のインプラント治療のトピック:骨造成、即時荷重 埼玉インプラント研究会講演会 2009.7.19 浦和保健センター 浦和

春日井昇平.最近のインプラント治療のトピック:再生医療、即時荷重、即時埋入 歯植義歯研究所講演会 2009.7.12 仙台衛生士学院 仙台

春日井昇平.高齢者へのインプラント治療において考慮すべきこと.第20回日本老年歯科医学会総会・学術大会 2009.06.18-20 パシフィコ横浜 横浜

春日井昇平.歯科インプラント治療の現状と再生医療と関わり.再生医療にまつわる材料 有機エレクトロニクス研究会 2009.4.15 自動車会館 東京

Kasugai S. Prosthesis or regeneration?: Dental implant vs. tissue-engineered tooth. The 2nd Thailand International Conference on Oral Biology, Biology of Mineralized Tissue 2009.5.7-8 Chulalongkorn University, Bangkok, Thailand

春日井昇平.歯科インプラント治療における治療期間の短縮.チタン研究会 2009.02.14 日本大学工学部 東京
春日井昇平.歯科医療の近未来:補綴か再生医療か? 奥羽歯科大学歯学部FDセミナー 2009.01.23

春日井昇平.インプラント治療に必要な骨補填材.長崎大学口腔再建外科学分野セミナー 2009.01.14 長崎大学 長崎

春日井昇平.歯が無くなった場合の治療法として、インプラント治療はベストか? 食育市民フォーラム「食べる知恵と大切な歯」 2009.01.10 西日本新聞ホール 鹿児島

春日井昇平.歯科インプラント治療における治療期間の短縮.鹿児島大学歯学部セミナー 2009.01.9 鹿児島大学 鹿児島

春日井昇平.即時荷重、即時埋入の落とし穴.プラトニンミーティング大阪 2008.11.30 ホテルコスモスクエア 国際交流センター 大阪

春日井昇平.インプラント治療に必要な骨造成と骨補填材.日本歯科大学再生医療セミナー 2008.11.27 日本歯科大学 東京

春日井昇平.骨形成を促進する化合物を含む吸収性骨補填材.日本バイオマテリアル学会シンポジウム 2008.11.17-18 東京大学 東京

Kasugai S. IT-based safe, simple and predictable implant treatment. International Symposium 第21回日本歯科医学会総会 2008.11.14-16 パシフィコ横浜 横浜

春日井昇平.Academy of minimally-invasive Implantology (AMII) の研究会発足の主旨.AMII第1回 Conference 2008.11.15 ランドマークホール 横浜

春日井昇平.インプラント治療の最近の進歩と再生医療との関わり.歯植義歯研究所セミナー 2008.11.08 歯植義歯研究所研修室 仙台

Kasugai S. Immediate protocol in dental implant treatment: Keys to avoid failures in this attractive protocol. Invited Lecture Annual Meeting of Thai Dental Implant Society 2008.10.23-25 Landmark Bangkok Hotel, Bangkok, Thailand

春日井昇平.インプラント治療の進歩と低出力超音波刺激装置(LIPUS)への期待. LIPUSセミナー 2008.10.5 新宿NSビル 東京

Kasugai S. Dental implant treatment in the near future: Prosthesis or regeneration? 特別講演 第4回日中歯科医学会 2008.9.27-29 西安 中華人民共和国

春日井昇平.EBMとガイドライン.インプラント治療のガイドラインのためのエビデンス どのような考え方が提唱されてきたか シンポジウム 第38回日本口腔インプラント学会学術大会 2008.09.12-14 東京フォーラム 東京

春日井昇平. 歯科インプラント治療の進歩と再生医療との関わり. 総合インプラント研究センターセミナー 2008.8.24 新宿ニューシティホテル 東京

春日井昇平. インプラント治療を導入される(されている)先生方へ. ストロマンインプラントセミナー 2008.7.31 ストロマン・ジャパン株式会社 東京

春日井昇平. 即時過重、即時埋入の落とし穴. プラトニンセミナー2008 2008.7.27 パシフィコ横浜 横浜

春日井昇平.骨形成促進作用を示す骨補填材.シンポジウム
Periodontal Tissue Engineeringの現状と将来展望.第
29回日本炎症・再生医学会 2008.7.8-10 都市センターホテ
ル 東京

春日井昇平.歯科インプラント治療の最近の進歩と再生
医療との関わり.九州御茶ノ水会セミナー 2008.7.6 タ
カクラホテル 福岡

春日井昇平.歯科インプラント治療の最近の進歩と再
生医療との関わり.新潟大学歯学部大学院セミナー
2008.6.25 新潟大学歯学部 新潟

春日井昇平.歯が無くなった場合の治療法として、イン
プラント治療はベストか? 食育市民フォーラム「食べ
る知恵と大切な歯」 2008.6.15 時事通信ホール 銀座
東京

春日井昇平.インプラント治療に必要な骨組織の再生.日
本歯科先端技術研究所講演会 2008.6.7 東京

春日井昇平.歯科インプラント治療は今後再生医療とど
のように関わっていくか.東京形成歯科研究会講演会
2008.5.18 東京形成歯科研究会研修会場 王子 東京

春日井昇平.再生医療の現状と将来展開.社団法人日本総
合歯科研究会講演会 2008.5.15 霞ヶ関ビル 東京

Kasugai S. Immediate function vs. conventional protocol.
Esthetic Forum Bali 2008.5.24 Grand Hyatt Bali, Bali,
Indonesia

春日井昇平.歯科インプラント治療と再生医療の融合.第
7回日本再生医療学会総会 2008.3.13-14 名古屋国際会
議場

Kasugai S. Bone substitute in dental implant treatment.
2008.1.7 Khonkaen University, Thailand

14) 主催学会

第2回 AMII (Academy of minimally invasive Implantology)
2010.1.24 学術総合センター、東京 (大会長)

The 2nd Pacific Osseointegration Conference Tokyo
2009.5.30-31 都市センター、東京 (大会長)

15) 新聞、雑誌、TV報道

週刊朝日増刊号 新「名医」の最新治療2010 インブ
ラント人工歯根 2009年11月30日

週刊朝日 「知らないと怖いインプラント治療」 2009
年10月20日

毎日新聞 「マウスの歯再生」 2009年8月4日

日本経済新聞 「歯の再生医療に成功」 2009年8月4日

日刊工業新聞 「マウスの歯を完全再生 上皮細胞など
から作製」 2009年8月4日

朝日新聞 「インプラント治療 注意点は?」 2009年5
月13日朝刊

長陽 「QOLを高めるインプラント」2009年5月号

ニュースJAPAN 「インプラント治療の光と影」 2009
年2月13日

16) 教室、分野や講座の准教授、講師、助教、 特別研究員、ポスドク、指導を受けた大学 院生の名前 (AISSには○印) のリスト

准教授:塩田 真

講師:立川敬子

助教:近藤尚知 (平成21年6月まで)、黒田真司、
宗像源博 (平成21年12月より)

大学院生:朴浚喜、上野憲秀、○Myat Nyan、

○Hudieb, Malik Ismail、木村純一、

伊達佑生、○則武加奈子、宮原宇将、

Rojbani, Hisham Khalifa、○郝佳、

○Reena Rodriguez、

Bharagava Srilatha、秋野徳雄、

永山友子、藤井政樹、古市祥子、

Osama Zakaria、高尚、下岸将博、

陳康、羽田康叙、湯川健、

Madi Marwa Ibrahim

CLINICAL ORAL IMPLANTS RESEARCH

Kazuhiro Kon
Makoto Shiota
Maho Ozeki
Yasuo Yamashita
Shohei Kasugai

Bone augmentation ability of autogenous bone graft particles with different sizes: a histological and micro-computed tomography study

Authors' affiliations:

Kazuhiro Kon, Makoto Shiota, Maho Ozeki, Shohei Kasugai, Department of Oral Implantology and Regenerative Dental Medicine, Tokyo Medical and Dental University, Bunkyo-ku, Tokyo, Japan
Yasuo Yamashita, Department of Maxillofacial Anatomy, Tokyo Medical and Dental University, Bunkyo-ku, Tokyo, Japan

Correspondence to:

Kazuhiro Kon
Department of Oral Implantology and Regenerative Dental Medicine
Tokyo Medical and Dental University
1-5-45 Yushima
Bunkyo-ku
Tokyo 113-8549
Japan
Tel./Fax: +81 3 5803 5774
e-mail: k.kon.irm@tmd.ac.jp

Key words: bone graft, dental implant, histology, micro-CT analysis

Abstract

Objectives: The purpose of this study was to investigate the augmentation process and ability of autogenous bone graft particles of two different sizes in a vertical augmentation chamber.

Material and methods: The cranial bones of 24 rabbits were used. Two polytetrafluoroethylene chambers were filled with harvested bone from tibia with small bone (SB; 150–400 µm) and large bone (LB; 1.0–2.0 mm) of the same weight. Animals were sacrificed after 1, 2, 4 and 8 weeks. The samples were analyzed by micro-computed tomography (micro-CT) for quantitative analysis, and embedded in polyester resin as non-decalcified specimens for histological analysis. Total bone volume (TBV), bone height (BH) and distribution of bone structure were calculated by micro-CT.

Results: Micro-CT evaluation and histology revealed a significant difference between the investigated specimens. TBV and BH of SB decreased to about 50% of the initial situation, and there was a statistically significant difference between 1 and 8 weeks. In contrast, TBV and BH of LB were almost retained at all experimental time points. Significant differences in TBV and BH were also observed between LB and SB at 8 weeks. Bone volume of SB decreased predominantly in the upper half of the chamber at 4 and 8 weeks. In the histological observations, SB showed favorable new bone formation and rapid bone resorption in a time-dependent manner during the entire experimental period. However, LB exhibited favorable morphological stability and continued new bone formation.

Conclusion: SB follows a smooth osteogenic process, whereas it is not effective in volume augmentation. LB is superior to SB in augmentation ability.

Oral implant therapy is now widely accepted as it provides a satisfactory esthetic and functional outcome (Ferrigno et al. 2002; Boronat-Lopez et al. 2009). To achieve these results, edentulous jaws should have adequate bone volume, which enables the placement of implants in an ideal position. In many cases, implant placement was restricted by bone resorption after teeth extraction, or the position of the mandibular canal and maxillary sinus. Therefore, bone augmentation is

frequently planned in association with implant therapy (Lustmann & Lewinstein 1995; Chiapasco et al. 2004; Fugazzotto & Vlassis 2007; Hämmerle et al. 2008).

Currently, autogenous bone, allogeneic bone, xenogeneic bone and synthetic bone are being used as bone grafting materials (Moy et al. 1993; Yildirim et al. 2000; Rodriguez et al. 2003; Scabbia & Trombelli 2004; Turunen et al. 2004; Kihara et al. 2006). Among them, autogenous bone is widely regarded as the gold standard (Boyne

Date:

Accepted 26 May 2009

To cite this article:

Kon K, Shiota M, Ozeki M, Yamashita Y, Kasugai S. Bone augmentation ability of autogenous bone graft particles with different sizes: a histological and micro-computed tomography study. *Clin. Oral Impl. Res.* 20, 2009; 1240–1246. doi: 10.1111/j.1600-0501.2009.01798.x

& James 1980; Moy et al. 1993]. However, autogenous bone grafts have several disadvantages, including morbidity of the donor site, limited amount of harvestable bone and ongoing volume reduction during the healing period. Especially, many researchers have demonstrated resorption of the grafted autogenous bone after surgery. Clinically, reduction of the buccal tissue volume was observed after autogenous block bone grafting in long-term follow-up studies [Widmark et al. 1997; Jemt & Lekholm 2003]. The authors described this phenomenon as the result of grafted bone resorption. Moreover, autogenous bone grafted for maxillary sinus augmentation was reduced 6 months after surgery [Johansson et al. 2001].

The particle size of autogenous bone, which is considered to be one of the important factors that determine the augmentation ability, was studied in some articles [Zaner & Yukna 1984; Fucini et al. 1993; Springer et al. 2004; Murai et al. 2006; Coradazzi et al. 2007; Kuroki et al. 2008; Walsh et al. 2008]. However, the conclusions of these investigations varied.

The purpose of this study was to investigate the augmentation process of autogenous bone graft particles of two different sizes in a vertical augmentation chamber and evaluate their augmentation ability.

Material and methods

Experimental protocols were approved by the Institutional Committee of Animal Care and Use at Tokyo Medical and Dental University. Japanese male white rabbits of weight (3.2–3.8 kg) and size were used ($n = 24$).

Surgical procedures

Animals were anesthetized preoperatively with an intramuscular injection of ketamine (50 mg/kg, Ketalar, Sankyo, Tokyo, Japan) and thiopental sodium (25 mg/kg Rabonal, Tanabe, Tokyo, Japan). The surgical area was shaved and disinfected. In addition, 1.8 ml of a local anesthetic (2% xylocaine/epinephrine 1:80,000, Dentsply Sankin, Tokyo, Japan) was injected into the surgical sites before the start of surgery. Autogenous bone particles of two sizes were harvested from the tibia. The large particle bone (LB), which was cuboidal in

shape (about 1 mm thickness and width with 2 mm length, standardized by sieves), was harvested with bone forceps. The small particle bone (SB), which was bone debris (150–400 μ m diameter, average 250 μ m), was harvested by a 3.2-mm-diameter trephine-bone-mill system (K-System, DentaK, Paris, France). Parietal bone was chosen as the augmentation model site. Skin incision and subperiosteal dissection were carried out sagittally between the parietal and the frontal bone, and the periosteum was raised. Polytetrafluoroethylene chambers (hollow cylinders with 5.0 mm inner diameter and 3.0 mm height having an outer brim) were fixed with stainless-steel screws (FKG Dentaire, Chaux-de-Fonds, Switzerland) to the parietal bone on the right and left sides. Bone of the same weight (60 mg) was grafted into each chamber with peripheral blood. The skin flaps were sutured with 3-0 silk. During the observation period, all rabbits were given water and a standard rabbit feed *ad libitum*. Rabbits were sacrificed at 1 week ($n = 6$), 2 weeks ($n = 6$), 4 weeks ($n = 6$) and 8 weeks ($n = 6$) with a lethal dose of thiopental sodium. The entire cranial bone was removed and fixed for 10 days in neutral 10% formalin.

Micro-computed tomography (micro-CT) analysis

Following the fixation period, grafted regions of specimens were quantified via micro-CT analysis (SMX-90CT, Shimadzu, Kyoto, Japan). Total bone volume (TBV) and bone height (BH) were calculated. TBV was acquired by the radiopaque voxels (cube 60 μ m on one side) observed in the chamber. BH was evaluated from the distance between the basal host bone and the highest point of the bone fragment in the chamber and was measured in the center 3.0 mm diameter part of the chamber in each animal. The bone volume distribution in the upper and lower halves was also described as a percentile.

Histological processing

To obtain non-decalcified sections, cranial bone ($n = 24$) was dehydrated in ascending grades of ethanol, following fixation, and then embedded in polyester resin (Rigolac-70F, Rigolac-2004, Nissin EM Co., Tokyo, Japan). These sections were cut (Exakt, Mesmer, Ost Einbeck, Germany)

in the sagittal direction and ground to a thickness of about 300 μ m. The sections were finally stained with 0.1% toluidine blue. Histological observation was performed under a light microscope.

Statistical analysis

To evaluate the influence of particle size on TBV and BH, intergroup data at each time point were statistically compared using the Kruskal–Wallis test and non-parametric multiple comparisons by Dunnett T3. Particle comparison within the same time point was analyzed using the Mann–Whitney test. P -values ≤ 0.05 were considered statistically significant. All statistical analyses were performed using a commercial computer program (SPSS 11.5, SPSS Inc., Chicago, IL, USA).

Results

Histology

SB-grafted sites

1 week. SB densely occupied almost the entire augmentation chamber and blood cells filled the inter-SB space. SB, which stained strongly with toluidine blue, retained its original chip-like shape. No osteoclast- or osteoblast-like cells were observed at this stage (Fig. 1a and b).

2 weeks. SB occupied nearly entire the chamber as in the first week, and the height of SB did not change (Fig. 2a). At the lower part of the chamber, numerous multinuclear giant cells were observed on the surface of SB, newly formed bone was partially observed on the surface of grafted bone and large amounts of fibrous connective tissue were observed in the interspace of the graft. Especially, in the region close to host bone, new blood vessels had formed. However, at the upper part of the chamber, there was no new bone formation; instead, part of the SB had undergone resorption by multi nuclear giant cells (Fig. 2c).

4 weeks. Bone area that exhibited constricted bone trabeculae occupied about half or more of the height of the chamber. Grafted SB had resorbed mostly in the upper part (Fig. 3a). Loose fibrous connective tissue was observed in the upper half of the chamber, and some fibrous connective tissue ran in a direction parallel to the bone

Kon et al. Augmentation ability of different-sized autogenous bone

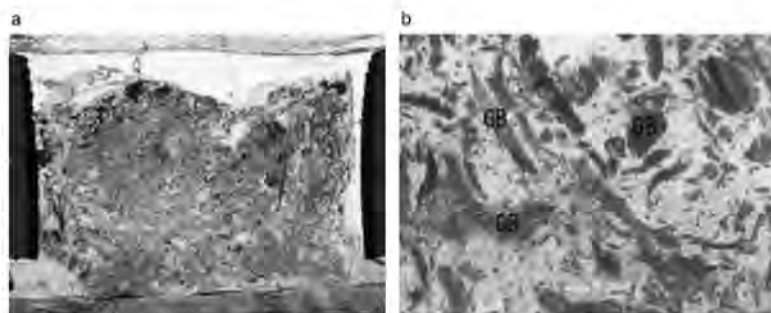


Fig. 1. Small bone grafted site at 1 week. (a) Grafted bone (GB) was observed over the entire augmentation chamber. GB retained its original chip-like shape. However, no newly formed bone was observed. Magnification $\times 2.5$. (b) High-magnification image of (a). GB was strongly stained with toluidine blue. The interparticular space was occupied by blood cells. Magnification $\times 50$.

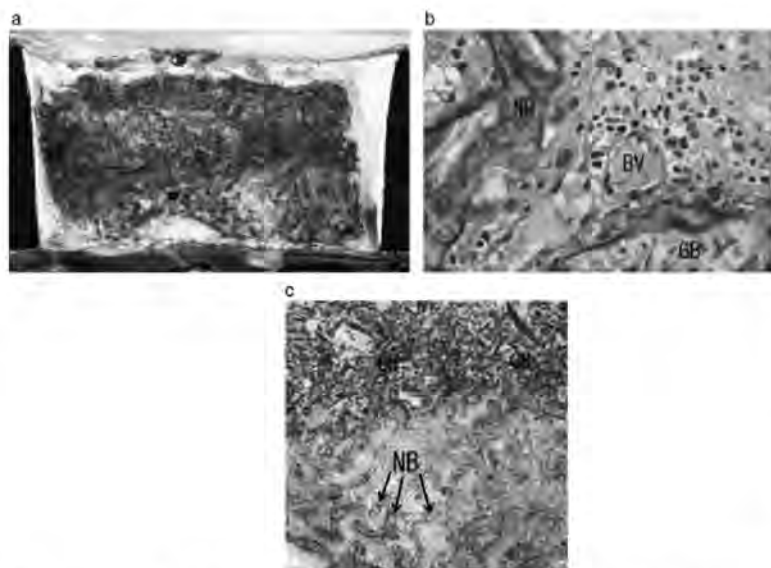


Fig. 2. Small bone grafted site at 2 weeks. (a) Grafted bone (GB) occupied the the entire chamber same as the 1-week model. The GB height was almost preserved. Magnification $\times 2.5$. (b) High-magnification image of (a). New bone formation was observed from the region close to the host bone surface toward the GB. Blood vessels (BV) were also observed. Magnification $\times 100$. (c) In the lower part of the chamber, near the host bone, newly formed bone (NB) was observed on the GB surface. In the upper part of the chamber, there was no new bone formation; instead, a part of GB underwent resorption by a multinuclear giant cell. Magnification $\times 10$.

area. At higher magnification, grafted SB was mostly resorbed and replaced by newly formed bone. Mature blood vessels were observed in the interspace of the bone structure, and many fat cells were observed around the host bone (Fig. 3b).

8 weeks. The height of bone area was about a quarter of the chamber and the number of trabeculae had reduced when compared with the 4-week specimens. Loose fibrous connective tissue was observed in the upper region of the chamber.

A large number of fat cells were observed over the entire chamber (Fig. 4a). Grafted bone was almost completely replaced by new bone that was surrounded by blood vessels and fat cells. Osteoclast-like cells were observed in the resorption lacunae within newly formed bone (Fig. 4b).

LB-graft sites

1 week. LB occupied a large part of the chamber. LB stained less with toluidine blue and resorption lacuna were not de-

tected on the surface of grafted bone at this time point (Fig. 5a). In the interspace of grafted bone, very loose fibrous connective tissue and a few blood vessels were observed (Fig. 5b).

2 weeks. LB preserved its original block-like shape and low stainability. The height and space of the bone structure was maintained. The interspace of the grafted bone was filled with fibrous connective tissue (Fig. 6a). A few osteoclast-like cells were observed on the grafted bone. In the vicinity of the host bone, moderately mature blood vessels were found, and new bone had formed from the host bone surface toward the grafted bone (Fig. 6b).

4 weeks. LB was positioned at a higher level in the chamber and it retained its original form and low stainability (Fig. 7a). However, new bone formation was observed from the host bone surface to the grafted bone surface and Howship's lacunae with many osteoclast-like cells were found on the surface of the grafted bone in the upper part of the chamber (Fig. 7b). Fibrous connective tissue and blood vessels were observed around the grafted bone, and fat cells were detected around the host bone surface.

8 weeks. LB was only modestly integrated with newly formed bone that had high stainability, and the graft stained slightly stronger than at 4 weeks. Many osteocyte-like cells were observed on the grafted bone and a few osteoclast-like cells were also detected in the resorption lacunae (Fig. 8a). Around this bone architecture, numerous blood vessels were observed (Fig. 8b). There were many fat cells over the entire chamber, especially, near the host bone surface.

Micro-CT analysis

Radiological quantitative analysis was performed by micro-CT (Fig. 9)

Intergroup comparisons. TBV showed significant differences for 1 week/8 weeks in the SB group ($P=0.026$), and 2/4 weeks in the LB group ($P=0.025$). BH showed significant differences for 1 week/4 weeks ($P<0.001$), 1 week/8 weeks ($P<0.001$), 2/4 weeks ($P<0.001$) and 2/8 weeks ($P<0.001$) in the SB group. No other significant differences were found (Fig. 10a and b).

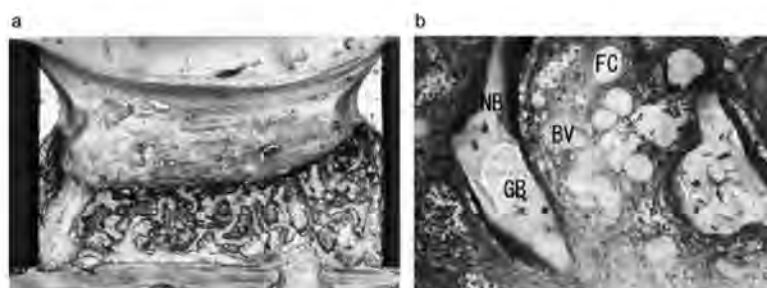


Fig. 3. Small bone grafted site at 4 weeks. (a) Newly formed bone (NB) occupied about half or more the height of the chamber. NB constricted bone trabeculae. Magnification $\times 2.5$. (b) High-magnification image of (a). NB was observed around the grafted bone (GB). Mature blood vessels (BV) and fat cells (FC) were also observed in the interspace of the bone structure. Magnification $\times 50$.

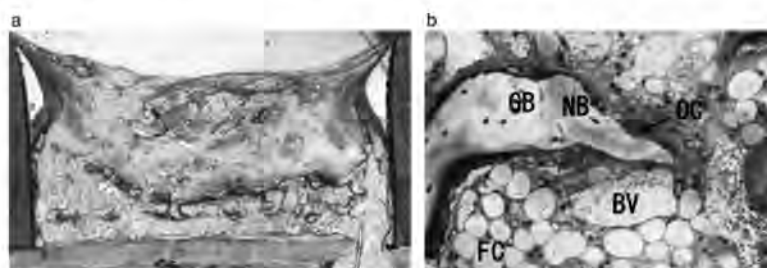


Fig. 4. Small bone grafted site at 8 weeks. (a) Accelerated bone resorption was observed in the 8-week model. A large number of fat cells were observed over the entire chamber. Magnification $\times 2.5$. (b) High-magnification image of (a). Mature blood vessels (BV) were observed around the newly formed bone (NB). Grafted bone (GB) was almost completely replaced by new bone. An osteoclast-like cell (OC) was observed in the NB. Magnification $\times 100$. FC, fat cell.



Fig. 5. Large bone grafted site at 1 week. (a) Grafted bone (GB) was observed over the entire chamber. Bone resorption was not observed around the surface of GB at this time point. Magnification $\times 2.5$. (b) High-magnification image of (a). In the interspace of the GB, there was very loose fibrous connective tissue (CT), and a few blood vessels (BV) were also observed. Magnification $\times 25$.

SB vs. LB

TBV and BH showed notable significant differences at 4 weeks (TBV: $P=0.004$, BH: $P=0.002$) and 8 weeks (TBV: $P=0.006$, BH: $P=0.004$). At 1 week and 2 weeks, there was no significant difference (Fig. 10a and b).

Distribution of bone structure

LB groups exhibited no remarkable changes. In contrast, bone volume reduc-

tion of the upper half was prominent in the 4- and 8-weeks of SB groups (Fig. 10c).

Discussion

Autogenous bone has long been considered the most excellent material for bone augmentation (Boyne & James 1980; Moy et al. 1993). However, it was recently reported that autogenous bone grafts

showed continuous volume reduction during the healing and follow-up periods. During maxillary sinus augmentation, the volume of autogenous grafts was reduced to 49.5% of the initial volume after 6 months (Johansson et al. 2001). In addition, it was demonstrated that the surgically augmented height with an autogenous block graft decreased to 60% after 10 months (Widmark et al. 1997).

The particle size of graft material has been regarded as one of the major factors that determine the ability of augmentation, and it has been studied by many researchers. However, these studies have reported variable conclusions so far. The aim of this study was to investigate the augmentation process and the ability of autogenous bone graft particles of two different sizes.

In the present study, TBV of the SB group decreased in a time-dependent manner; it decreased to 51.3% of the initial volume. Histological analysis showed that the grafted bone in the lower half had resorbed by multinuclear giant cells at 2 weeks, and was partially replaced by newly formed bone at 4 weeks. A great deal of newly formed bone had resorbed at 8 weeks. Thus, SB groups were considered to follow the remodeling process. In the upper part of the chamber, strongly stained SB observed at 2 weeks had resorbed by 4 weeks. This resorption caused volume reduction between 2 and 4 weeks. On the other hand, TBV of the LB group exhibited a volume increase at 4 weeks, and it was almost maintained at 8 weeks. Histologically, LB almost preserved its shape at 2 weeks and new bone formation was observed from the host bone to the LB surface at 4 weeks. The formation and resorption of bone was observed at 8 weeks. In addition, in the 4-week LB group, the original grafted bone of the upper half had the same low stainability, although numerous osteoclast-like cells were observed on the surface of the grafted bone. A greater part of the original grafted bone was maintained in the LB-grafted site at 8 weeks; meanwhile, the original grafted bone almost disappeared in the SB groups. This behavior of bone remodeling was thought to cause the difference in TBV between LB and SB.

The larger particle size of the grafting material was more beneficial than the small size bone grafts in augmentation. Demineralized freeze-dried bone allografts

Kon et al. Augmentation ability of different-sized autogenous bone

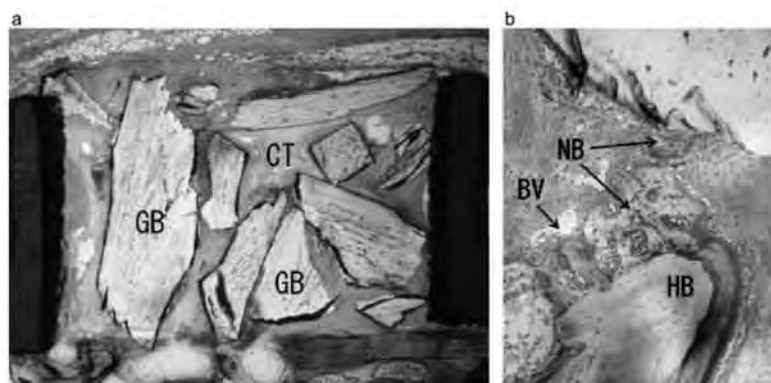


Fig. 6. Large bone grafted site at 2 weeks. (a) Grafted bone (GB) almost preserved its original shape. In the interspace of the GB, fibrous connective tissue (CT) was observed. Magnification $\times 2.5$. (b) High-magnification image of (a). In the region close to the host bone (HB), blood vessels (BV) were found, and new bone (NB) formation occurred from the host bone surface to the GB surface. Magnification $\times 25$.

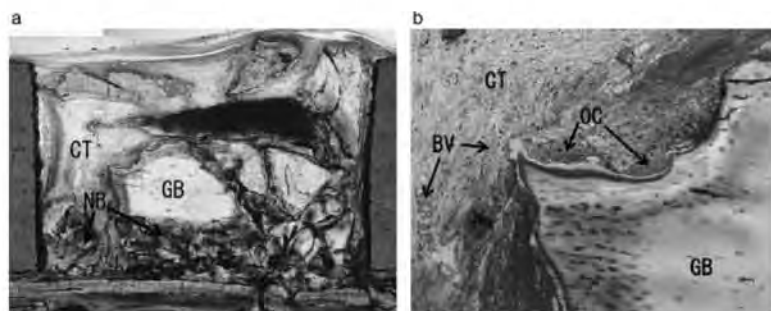


Fig. 7. Large bone grafted site at 4 weeks. (a) The center of grafted bone (GB) retained its original form. Fibrous connective tissue (CT) was observed around GB. A large amount of new bone (NB) was formed from the host bone surface to the GB surface. Magnification $\times 2.5$. (b) High-magnification image of (a). Howship's lacunae with osteoclast-like cells (OC) were found at the surface of GB. Fibrous connective tissue and blood vessels (BV) were observed around the GB. Magnification $\times 40$.

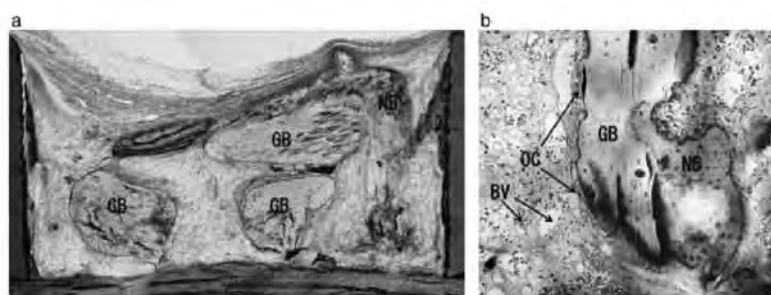


Fig. 8. Large bone grafted site at 8 weeks. (a) Newly formed bone (NB) was observed around the grafted bone (GB). GB was covered by NB, and many osteocytes were observed. Magnification $\times 2.5$. (b) High-magnification image of (a). Osteoclast-like cells (OC) were observed on the surface of the GB. Around this bone architecture, many blood vessels (BV) were observed. Magnification $\times 40$.

with 850–1000 μm particles yielded favorable results than the 250–500 μm particles in human periodontal defects (Fucini et al. 1993). Unmilled bone particle had more osteoblast than milled and drilled bone

(Springer et al. 2004). In another study, application of 250–500 μm particle β -tricalcium phosphate particles exhibited more advantages in terms of bone formation than the 100–250 μm -sized particles (Murai

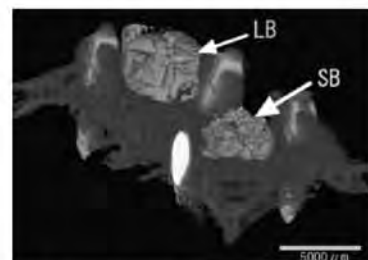


Fig. 9. Extracted image of bone-grafted site with micro-computed tomography (micro-CT). Both small bone (SB)- and large bone (LB)-grafted sites were extracted with micro-CT (grafted site image at 4 weeks).

et al. 2006). These results agree with the present study. However, the observations about particle size varied. In a rabbit autogenous graft defect model, there was no difference between the non-graft control, collected debris and particles collected by a manual bone crusher (Coradazzi et al. 2007). In addition, no significant difference was detected between the control defect and two sizes of β -tricalcium phosphate particles, 500–1000 and 1000–2000 μm , applied to a cynomolgus monkey mandible defect model (Kuroki et al. 2008). In these two studies, augmentation material was applied to the defect model, which was different from the chamber model in other studies, and is considered not suitable for confirming the augmentation potency. Hence, it would appear that application of large graft materials is preferable for bone augmentation. However, Pallesen et al. (2002) reported that 0.5–2.0 mm^3 particle autogenous bone exhibited more newly formed bone than 10 mm^3 in a rabbit cranial defect model. Thus, excessively large particles applied to a bone defect might have lower augmentation ability.

The SB groups showed a considerable reduction of bone volume in the upper half of the chamber. The bone volumes of the upper half were 50.2%, 45.1%, 25.8% and 18.1% at 1, 2, 4 and 8 weeks, respectively. For this reason, BH of SB decreased at all experimental time points. Advanced biodegradability of small-sized grafted bone is considered to be responsible for these results. In contrast, LB could maintain the original shape of grafted bone in the upper half of the chamber; thus, BH was preserved during the entire period. Although the biodegradability of a bone substitute is

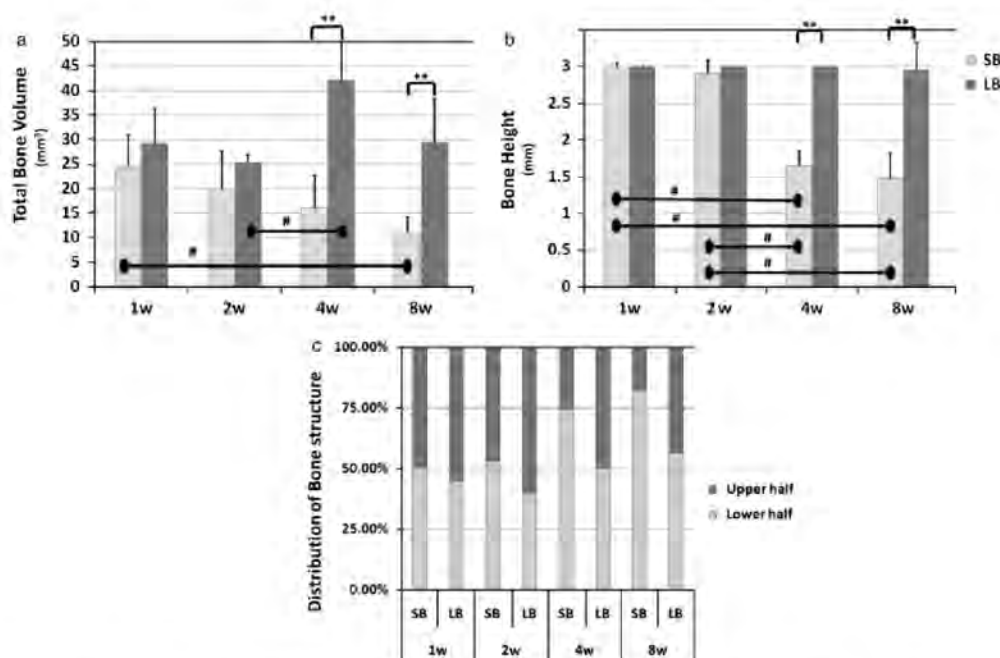


Fig. 10. Micro-computed tomography analysis. (a) Total bone volume change. Comparison between two groups – Mann-Whitney test, $^{**}P < 0.01$; comparison within each group – non-parametric multiple comparison test, $^{\#}P < 0.05$. Error bar indicates 95% confidence interval. (b) Bone height change. Comparison between two groups – Mann-Whitney test, $^{**}P < 0.01$; comparison within each group – non-parametric multiple comparison test, $^{\#}P < 0.05$. Error bar indicates 95% confidence interval. (c) Distribution of bone structure. Notably, bone volume reduction of the upper half was observed in small bone (SB) models. In contrast, large bone (LB) models exhibited no dramatic change.

thought to be very important, taking into account the volumetric augmentation ability, morphological stability is essentially required.

Clinically, autogenous bone is believed to be the gold standard for bone augmentation. However, the augmentation ability could differ with particle size. The present study indicates that small autogenous bone debris would be easily resorbed, having a poor outcome for augmentation. Therefore, to achieve sufficient bone augmentation,

small autogenous bone debris should be applied in combination with a slow or a non-resorbable bone substitute. On the other hand, LB exhibited favorable augmentation with morphological stability. However, the osteogenesis in the interspace of grafted LB was limited, and newly trabecula formation progressed slowly throughout the entire experimental period. Therefore, to enhance osteogenesis in the interspace, application of SB might be effective.

Within the limitations of the present study, it is concluded that SB decreased to 51.3% and 51.0% of the initial volume and height, respectively, and LB could maintain the volume and height at 8 weeks in this augmentation model. SB follows smooth osteogenic process, whereas it is not effective in volume augmentation. However, LB is superior to SB in augmentation ability, although further studies are needed to evaluate the longitudinal bone augmentation condition.

References

- Boronat Lopez, A., Carrillo, C., Peñarrocha, M. & Peñarrocha-Diago, M. (2009) Immediately restored dental implants for partial-arch applications: a study of 12 cases. *Journal of Oral and Maxillofacial Surgery* 67: 195–199.
- Boyne, P. & James, R. (1980) Grafting of the maxillary sinus floor with autogenous marrow and bone. *Journal of Oral Surgery* 38: 613–616.
- Chiapasco, M., Consolo, U., Bianchi, A. & Ronchi, P. (2004) Alveolar distraction osteogenesis for the correction of vertically deficient edentulous ridges: a multicenter prospective study on humans. *International Journal of Oral & Maxillofacial Implants* 19: 399–407.
- Coradazzi, L., Garcia, I.J. & Manfrin, T. (2007) Evaluation of autogenous bone grafts, particulate or collected during osteotomy with implant bars: histologic and histomorphometric analysis in rabbits. *International Journal of Oral & Maxillofacial Implants* 22: 201–207.
- Ferrigno, N., Laureti, M., Fanali, S. & Grippaudou, G. (2002) A long-term follow-up study of non-submerged ITI implants in the treatment of totally edentulous jaws. Part I: ten-year life table analysis of a prospective multicenter study with 1286 implants. *Clinical Oral Implants Research* 13: 260–273.
- Fucini, S., Quintero, G., Glier, M., Black, B. & Richardson, A. (1993) Small versus large particles of demineralized freeze-dried bone allografts in human intrabony periodontal defects. *Journal of Periodontology* 64: 844–847.
- Fugazzotto, P. & Vlassis, J. (2007) Report of 1633 implants in 814 augmented sinus areas in function for up to 180 months. *Implant Dentistry* 16: 369–378.
- Hämmerle, C., Jung, R., Yaman, D. & Lang, N. (2008) Ridge augmentation by applying bioresorbable

Kon et al. Augmentation ability of different-sized autogenous bone

- membranes and deproteinized bovine bone mineral: a report of twelve consecutive cases. *Clinical Oral Implants Research* 19: 19–25.
- Jemt, T. & Lekholm, U. (2003) Measurements of buccal tissue volumes at single-implant restorations after local bone grafting in maxillas: a 3-year clinical prospective study case series. *Clinical Implant Dentistry & Related Research* 5: 63–70.
- Johansson, B., Grepe, A., Wännfors, K. & Hirsch, J. (2001) A clinical study of changes in the volume of bone grafts in the atrophic maxilla. *Dentomaxillofacial Radiology* 30: 157–161.
- Kihara, H., Shiota, M., Yamashita, Y. & Kasugai, S. (2006) Biodegradation process of alpha-TCP particles and new bone formation in a rabbit cranial defect model. *Journal of Biomedical Material Research B Applied Biomaterial* 79: 284–291.
- Kuroki, H., Toda, I. & Suwa, F. (2008) Experimental study of bone defect repair process with different sizes of β -TCP granules. *Journals of Japanese Society of Oral Implantology* 21: 21–31.
- Lustmann, J. & Lewinstein, I. (1995) Interpositional bone grafting technique to widen narrow maxillary ridge. *International Journal of Oral & Maxillofacial Implants* 10: 568–577.
- Moy, P., Lundgren, S. & Holmes, R. (1993) Maxillary sinus augmentation: histomorphometric analysis of graft materials for maxillary sinus floor augmentation. *Journal of Oral and Maxillofacial Surgery* 51: 857–862.
- Murai, M., Sato, S., Fukase, Y., Yamada, Y., Komiya, K. & Ito, K. (2006) Effects of different sizes of beta-tricalcium phosphate particles on bone augmentation within a titanium cap in rabbit calvarium. *Dentistry Material Journal* 25: 87–96.
- Pallese, L., Schou, S., Aaboe, M., Hjorting-Hansen, E., Nattestad, A. & Melsen, F. (2002) Influence of particle size of autogenous bone grafts on the early stages of bone regeneration: a histologic and stereologic study in rabbit calvarium. *International Journal of Oral & Maxillofacial Implants* 17: 498–506.
- Rodríguez, A., Anastasov, G., Lee, H., Buchbinder, D. & Wettan, H. (2003) Maxillary sinus augmentation with deproteinized bovine bone and platelet rich plasma with simultaneous insertion of endosseous implants. *Journal of Oral and Maxillofacial Surgery* 61: 157–163.
- Scabbia, A. & Trombelli, L. (2004) A comparative study on the use of a HA/collagen/chondroitin sulphate biomaterial (Biostite) and a bovine-derived HA xenograft (Bio-oss) in the treatment of deep intra-osseous defects. *Journal of Clinical Periodontology* 31: 348–355.
- Springer, INC., Terheyden, H., Geiß, S., Härle, F., Hedderich, J. & Açil, Y. (2004) Particulated bone grafts – effectiveness of bone cell supply. *Clinical Oral Implants Research* 15: 205–212.
- Turunen, T., Peltola, J., Yli-Urpo, A. & Happonen, R. (2004) Bioactive glass granules as a bone adjunctive material in maxillary sinus floor augmentation. *Clinical Oral Implants Research* 15: 135–141.
- Walsh, W., Vizesi, F., Michael, D., Auld, I., Langdown, A., Oliver, R., Yu, Y., Irie, H. & Bruce, W. (2008) Beta-TCP bone graft substitutes in a bilateral rabbit tibial defect model. *Biomaterials* 29: 266–271.
- Widmark, G., Andersson, B. & Ivanoff, C. (1997) Mandibular bone graft in the anterior maxilla for single-tooth implants. Presentation of surgical method. *International Journal of Oral and Maxillofacial Surgery* 26: 106–109.
- Yildirim, M., Spiekermann, H., Biesterfeld, S. & Edelhoff, D. (2000) Maxillary sinus augmentation using xenogenic bone substitute material Bio-oss in combination with venous blood. A histologic and histomorphometric study in humans. *Clinical Oral Implants Research* 11: 217–229.
- Zaner, D. & Yukna, R. (1984) Particle size of periodontal bone grafting materials. *Journal of Periodontology* 55: 406–409.

M E M O

This image shows a single page of white paper with horizontal ruling lines. The lines are evenly spaced and run across the width of the page. There are no margins, text, or other markings on the paper.

歯髄生物学分野

須田 英明

医歯学総合研究科・口腔機能再構築学系専攻
歯髄生物学・教授



1) 研究の課題名

Pulp Biology Field

1. 未分化間葉細胞から骨芽細胞・象牙芽細胞への分化プロセスにかかわるシグナルネットワークの解析

Signal network of osteoblast- and odontoblast-differentiation from undifferentiated mesenchymal cells

<Notch-Hey1>

骨芽細胞の分化において、Runx2およびOsxがマスター遺伝子として基本的な分化の方向付けをするといわれているが、分化メカニズムの詳細においてはいまだ不明な点が多い。これまでにNotchのConstitutive Active Formにより、骨髄未分化間葉由来で骨芽細胞への分化傾向の高い細胞:Kusa-A1細胞の骨芽細胞への分化が抑制されることを報告した。その制御に深くかかわっている因子として、Notchシグナルの下流に置いて働く転写調節因子Hey1を同定し、Hey1がNotchシグナルの下流において、骨芽細胞マーカーであるオステオカルシンなどの発現を制御していることが明らかになった。骨芽細胞のみならず、歯髄細胞においても同様の系が動いていることが明らかになった。

<Mef2c>

筋芽細胞分化に重要な因子であるMef2cは、骨髄未分化間葉由来で骨芽細胞への分化傾向の高い細胞:Kusa-A1と同じ骨髄未分化間葉由来で骨芽細胞への分化傾向の低い細胞:Kusa-Oとの間で遺伝子発現の相違を調べた結果、芽細胞への分化傾向の高い細胞において強く発現している因子として同定された。このMef2cを弱く発現しているKusa-OにMef2cを強制発現させると、骨芽細胞マーカーの発現が増加し、石灰化結節形成が促進された。Mef2cが骨芽細胞分化を正の方向に制御していることが明らかになった。骨芽細胞のみならず、歯髄細胞においても同様の

系が動いていることが明らかになった。

<Sp7>

Sp7 (Osx:Osterix) は骨芽細胞分化のマスター遺伝子の一つで、そのノックアウトマウスにおいては骨形成が高度に障害される。ところで、歯胚間葉組織にもSp7の弱い発現は観察されるが、歯胚の形成は阻害されないで、歯の形成における関与は低いと考えられている。このSp7が成体の歯髄、特に象牙芽細胞に強く発現していることを明らかにした。Sp7の発現は未分化な象牙芽細胞においては弱く、成熟に伴って強く発現し、さらに成熟が進むと弱くなる。Sp7は象牙芽細胞の成熟において重要な因子であると推測される。さらに、Sp7の発現によりDsppプロモーター発現が亢進した。Sp7は直接あるいは間接にDspp発現を調節し、象牙芽細胞分化を制御していると推察された。

2. 歯髄幹細胞の分離と、幹細胞を用いた歯髄組織再構築の可能性

Isolation of stem cells from pulp tissues, and reconstruction of pulp tissues from stem cells

<幹細胞の分離>

幹細胞を分離するに当たり、ヘキスト色素を用いてSP分画を分離する方法が用いられているが、ヘキスト色素はDNA結合性があり臨床応用は難しい。間葉系幹細胞を分離するにあたり、細胞を疎の状態でき、その中からコロニーを形成した細胞を取ってくることで、幹細胞として用いることが可能である。了解を得た患者より、抜歯した歯を提供してもらい、歯髄組織を摘出し、そこに含まれる幹細胞の分離を試みた。その結果、歯髄組織より間葉系幹細胞の分離が可能であった。

<移植後の感染コントロール>

細胞を局所に移植する場合、その部分における感染および炎症のコントロールは必須である。今回、歯髄組織

の再生を図るにあたり、歯髄の炎症をコントロールする手段について検討を行った。まず、歯髄炎において最も多く存在するマクロファージに着目し、マクロファージからの炎症性メディエーター産生を制御することを試みた。ラット腹腔より安静状態なマクロファージを摘出し、そこにLPSを加えて刺激したところNO（一酸化窒素）産生が亢進した。そこにMMP3（マトリックスメタロプロテアーゼ3）を加えたところ、NO産生は有意に減少した。また、同様の系を用いてメディエーター遺伝子の発現を解析したところ、IL6およびCox2の発現をMMP3が抑制することが明らかになった。

3. ラット実験的根尖性歯周炎の進展におけるカテプシンK阻害剤の抑制効果

Inhibitory effects of the cathepsin K inhibitor on the progress of rat periapical lesions

カテプシンKは破骨細胞に発現し、骨吸収において重要な役割を果たしている。カテプシンK阻害剤であるNC-2300（日本ケミファ）は、新たに開発された関節リウマチの治療薬であり、関節リウマチモデルにおいて、関節の骨破壊ばかりでなく炎症反応も抑制することが報告されている。本研究の目的は、ラットに実験的に誘発した根尖性歯周炎のモデルを用い、根尖性歯周炎の進展におけるNC-2300の抑制効果を検討することである。ラット下顎第一臼歯を露髄後、抜髄し、口腔内に開放することにより根尖性歯周炎を誘発した。露髄開放時よりNC-2300を1日2回経口投与した。21日後に屠殺して下顎臼歯を周囲の顎骨ごと摘出し、左側はマイクロCT撮影により根尖病変の大きさを測定した後、組織学的に検討した。右側は、根尖周囲の病変部を根尖とともに一塊として摘出し、RNA抽出後、リアルタイムPCRにて起炎症性サイトカインの発現量を測定した。マイクロCTによる評価の結果、NC-2300投与群における根尖病変の大きさは、コントロール（非投与）群と比較して有意に小さかった。また、組織学的検討により、コントロール群においては多数の破骨細胞が根尖周囲の歯槽骨上に観察され、活発な骨吸収が行われている像が認められたのに対し、NC-2300群では破骨細胞は認められるものの、その数は少ない傾向にあった。病変中の炎症性サイトカイン発現を比較したところ、NC-2300投与群においてはIL-1 α およびIL-6の発現が有意に抑制されていた。以上の結果より、NC-2300の投与によって、破骨細胞におけるカテプシンK阻害作用による骨吸収抑制に加えて、炎症性サイトカインの発現が減少することにより破骨細胞

形成が抑制され、その結果として根尖周囲の骨吸収が抑制された可能性が示唆された。

4. 幹細胞と血管内皮細胞を用いた歯髄組織の再生と臨床応用

Improved pulp tissue regeneration from stem cells induced by accelerated revascularization

歯髄の失活した歯の寿命は、生活歯髄を有する歯よりも極端に短くなる。故に歯髄組織の再生療法が成功すると、当該歯の寿命が延長し、患者のQuality of Lifeの維持も期待される。本研究は歯髄組織の再生療法の確立を目指し、以下の3項目に大別して行われる。

1. 歯髄腔内に再生する細胞に適切な機能を持たせ、最適な密度で維持させる方法および因子の解明

本プロジェクトは細胞培養を用いた実験分子生物学的実験を主体に行い、幹細胞から象牙芽細胞を含む歯髄細胞への分化の機序の解明を行う。象牙芽細胞を含む歯髄固有の細胞を効率的に再生できる幹細胞と血管内皮細胞の選択、および象牙質と歯髄組織の再生に適した足場の選択実験も並行する。

2. 歯髄腔内に速やかに血管新生を生じさせる方法および因子の解明

象牙質という硬組織で取り囲まれている歯髄腔は血管の侵入が根管口に限られ、移植した細胞が壊死に陥りやすいと考えられる。そのため移植細胞への速やかな血管新生を促す必要がある。本プロジェクトは免疫不全マウスを用いた分子生物学的実験を主体とし、実験的に抜去歯内に再生された歯髄組織内に速やかに血管新生を促すための方法および因子を解明する。

3. 臨床治療へ向けた歯髄組織再生療法の開発

実際にヒトの口腔内で効果的かつ安全な歯髄再生治療を具現することを目指す。細胞を移植するための足場をヒト歯髄腔内に設置するためのインジェクションタイプの移植法の開発なども並行して行い、ラットを用いた動物実験による再生療法の効果および術式を検討する。これまでの実験成果をふまえ、臨床治療に向けた準備を行う。

5. ヒト象牙細管の機能的幅径計測の試み

An attempt to measure functional space of dentinal tubules in human dentin

象牙質には高密度の象牙細管が存在し、外界と歯髄を結ぶルートとして、外來刺激とのバランスをとりながら歯髄生活性は維持されている。すなわち、細菌およびそ

の分解産物、化学的刺激物質の歯髄内への侵入に対しては、歯髄組織圧に由来する象牙細管内容液の外向きの流れが、生体防御機構として働いている。また、象牙質刺激によって生じる鋭痛が動水力学説に基づくことも広く知られている。

しかし、象牙細管はエナメル質側に向かって先細りし、内部には象牙芽細胞突起や感覚神経終末などが存在しているので、水力学的圧の及ぶスペースは複雑な形状であることが推測される。電子顕微鏡写真から細胞成分と象牙細管壁との距離を推測できるが、収縮変形を考慮しなければならない。そこで本研究は、生体に近い状態で、ヒト象牙細管がどれほど大きい機能的幅径を有しているかを計測することを目的とした。

本研究は東京医科歯科大学歯学系倫理審査委員会の承認を得て行われた。研究内容に関する説明を行い、歯の提供に同意の得られた患者から、矯正治療目的で拔牙された新鮮ヒト小白歯6本を用いた（年齢14、14、15、23、27、29歳）。4歯では拔牙後速やかに、歯冠象牙質を露出させる直径2mmの窩洞を歯冠中央の近遠心、頬舌側の4カ所に形成した。半数の窩洞で象牙質のエッチング処理を行った。事前に演者Aが混和した、外径と励起波長の異なるfluorescent microsphereを混和した液を、内容物を知らない演者Bが窩洞内に30分間作用させた。残りの2歯（14、15歳例）では脱臼し、拔牙直前に4窩洞を形成し、microsphere混和液を2分間作用後直ちに拔牙した。固定、脱灰後、凍結標本作製し、蛍光顕微鏡下でmicrosphereの象牙質、歯髄進入深度を画像解析ソフト上で計測した。

Microsphere液を脱臼状態で作用させた歯では、象牙質外側1/3～中央1/3に0.1～0.5 μm までのmicrosphereが集積し、内側1/3では数個のみ確認できた。象牙芽細胞層および歯髄では、microsphereは確認されなかった。

microsphere液を拔牙後作用させた歯では、窩洞直下から象牙質外側1/3にかけて0.1～0.5 μm のmicrosphereが確認できた。しかし、1.0～4.0 μm のmicrosphereの集積は、象牙質外側1/3のみに限られていた。1歯（14歳例）のみ、数個の0.1～0.5 μm のmicrosphereが内側1/3に確認された。

エッチングの有無、窩洞の位置は到達深度に影響しなかった。

ヒト歯冠部象牙質の内側1/3には、0.5～1.0 μm の隙間が存在し、象牙細管内容液はそのスペースを移動することが推測された。それより大きいmicrosphereは、通

過が困難であることが示唆された。外向きの組織圧がmicrosphereの侵入を妨げるとともに、象牙芽細胞突起を外側に伸展させているのかもしれない。

6. 細胞内外の環境がヒト象牙芽細胞機能複合体の協調に及ぼす影響

Influence of cytosolic and extracellular environments on functional syncytium in human odontoblastic

象牙芽細胞は、その単極性突起をエナメル側に向けて象牙細管内容液中に置きながら、細胞体を象牙質直下の歯髄最外層に整列させているが、受容器電位あるいは起動電位を発生させる純正の感覚受容器に匹敵する機能を有するという科学的証拠は現在のところ揃っていない。本研究では、細胞内外の環境を変えることで、機能的複合体として協調する象牙芽細胞間 Ca^{2+} 伝播への影響をさらに明らかにすることを目的とした。

研究内容に関する説明を行い、歯の提供に同意の得られた患者から、矯正治療目的で拔牙された6本の新鮮ヒト小白歯を使用した。HEPE-baseのplating液を満したディッシュ内に単離した、長さ120 μm を超す細胞突起を有する細胞を、倒置型顕微鏡で観察しながら還流下で使用した。クラスター内の単一細胞の細胞膜に動水圧を機械的刺激として使用した。またイノシトール3リン酸を細胞内注入し、ギャップジャンクションブロッカーの影響も観察した。これらの刺激による細胞内 Ca^{2+} の伝播を経時的にモニターした。

ガラス電極を用いた細胞膜の機械的変形により、細胞内 Ca^{2+} は刺激部位から同一細胞内で広がった。

還流による機械的刺激が生じる隣接象牙芽細胞へのカルシウムイオンの伝播様式には、2種のタイプがあることがわかった。一方は、変形方向に一致する成分で、より早い伝播がみられた。他方は、変形方向とは逆行する成分で、スピードが遅く伝播距離も小さかった。

イノシトール3リン酸依存性の Ca^{2+} 伝播は、ギャップジャンクションブロッカーで抑制を受けた。

象牙細管壁と細胞成分とのスペースを移動する象牙細管内容液の動水力学的水圧が象牙芽細胞膜を併せて変形させることは注目されなかった。本研究で示されたように、この動水圧は象牙芽細胞膜を歪ませ、細胞内伝達物質としての Ca^{2+} が細胞間カップリングネットワークを介し、象牙芽細胞間を広く伝播することが推察された。

7. ヒトエナメル質内の物質透過性を交流イオン導入が促進する

Facilitated chemical transfer through human enamel with AC iontophoresis

目的: ヒトエナメル質の物質透過性を、交流イオン導入法で促進できるかについて定量的に分析した。

方法: プラチナ製電極を用いて塩酸リドカイン濃度と電気コンダクタンスの関係をプロットした。2つのチャンバーの間に6本の新鮮抜去歯冠をOリングで挟んだ。エナメル質チャンバーに塩酸リドカイン、歯髄側チャンバーに超純水を満たした。後者には模擬的歯髄組織圧を加えた。両チャンバー端にプラチナ製板電極を置き、電極間に交流イオン導入を加えた。電気インピーダンスの経時変化を歯髄側チャンバー中央に置いた電極で計測した。

結果: 電気コンダクタンス (G, mho) は塩酸リドカイン濃度 (x, mmol/L) と高い相関 ($G=2.16x^2+0.0289x+0.000376$, $r^2=0.999$) を示し、交流イオン導入はコンダクタンスの上昇を加速させた。

結論: エナメル質を通過した塩酸リドカインの電気伝導度は交流イオン導入で増加した。

8. マスタードオイルにより誘発された視床における遺伝子発現に対する p38MAPK インヒビター SB203580 の脳内マイクロインジェクションの効果

The effect of p38MAPK inhibitor SB203580 intra-endocranial microinjection on the MO-induced gene expressions in the thalamus.

これまでの研究で、ラット上顎第一臼歯歯髄への Mustard oil (MO) 適用は、その直後から対側視床内の NMDAR, p38MAPK, 及び GFAP mRNA のアップレグレーションをもたらすことが示されてきた。これら視床 mRNA の発現に対する p38MAPK 抑制薬 SB203580 の脳硬膜内への微小投与の影響を検索した。Pentobarbital sodium で麻酔したラット (体重: 300g) を用い、開頭後、硬膜下に SB203580 とその対照薬 SB202474 を微小投与した。ついで、左側上顎第一臼歯を露髄させ、MO を適用し化学的に歯髄神経を刺激した。MO 適用後 60 分後に視床組織を摘出し、RT-PCR 法により NMDAR-2A, NMDAR-2D, p38MAPK 及び GFAP の mRNA 発現様式の解析を行った。対側視床内の p38MAPK 及び GFAP mRNA のアップレグレーションは、SB203580 の脳硬膜内微小投与によりそのレベルが低下したが、NMDAR mRNA の発現には影響がなかった。また、対照薬 SB202474 は、こ

れらの mRNA の発現に影響を及ぼさなかった。この結果は、視床における p38MAPK mRNA 発現は同部位の GFAP mRNA 発現を制御している可能性を示唆している。

Endodontic Field

9. レーザーの外科的歯内療法への応用について

Application of laser to apicoectomy

レーザーの外科的歯内療法への応用により、患部の殺菌、根尖切除面からのスメア層の除去、切除面のコラーゲンの露出といった効果が期待され、それにより切除面に細胞接着を促進し、早期の治癒を誘導することが期待される。レーザー照射により切除面の微細構造を変化させることにより、周囲細胞の生物学的な活性化を促すこと期待される。そこで、Er:YAG レーザーをヒト象牙質面に照射し、その後、骨芽細胞を播種、培養した後に、SEM による観察を行い、切除面の表面性状の形態観察および細胞接着能について基礎的に検討した。その結果、Er:YAG レーザーの象牙質照射によりスメア層は除去され、表面は凹凸状の不整形となっていた。これに対し、非照射群では象牙質面は平滑ではあるもののスメア層で覆われていた。細胞接着に関してはレーザー照射群で非照射群より有意な接着した細胞数の増加を認めた。従って、象牙質面への低出力 Er:YAG レーザー照射により骨芽細胞接着能が向上し、骨形成に寄与する可能性が示唆された。

10. ニッケルチタンファイルに対する熱処理の効果

Effect of heat treatment for Ni-Ti rotary endodontic instruments

ニッケルチタン合金の機械的性質は相変態挙動に密接な関連性があり、その相変態挙動は熱処理によって影響を受けることが知られている。そこで、市販の K3 ファイルにそれぞれ 400、450、500°C で 30 分間の熱処理を施した後、冷却したファイルを実験群として、片持ち梁による曲げ試験と根管模型を用いた根管形成を行い、根管の移動について評価する 2 つの実験を行った。熱処理を施さなかったファイルを対照群とした。その結果、曲げ試験ではファイルの先端が 0.5mm 変形した弾性領域では対照群と 500°C 群で 400、450°C 群と比較して有意に曲げ応力が大きかった。ファイルの先端が 2.0mm 変形した超弾性領域では対照群の曲げ応力が熱処理を施した全ての実験群より有意に大きかった。根管形成については対照群で実験群と比較して有意に根尖部で外側への根管の移動が認められた。K3 ファイルを熱処理により、フ

レキシビリティが向上し、湾曲根管の根管形成に有用であることが示唆された。

11. 超音波吸引洗浄法に関する研究

New root canal irrigation method using ultrasonic aspiration technique

歯内治療の成功のためには、根管形成と洗浄により細菌を根管内から取り除くことが重要であるが、完全な根管形成と洗浄は極めて困難である。

我々は、新しい根管洗浄方法、超音波吸引洗浄法(UAT:Ultrasonic aspiration technique)を開発した。この方法は福元らのINP(根管吸引洗浄法)を改良したものである。INPの最大の欠点はその細い洗浄針がデブリで簡単に詰まってしまうことであった。UATでは吸引針の詰まりを避けるために、INPの吸引針が超音波ユニットで振動させられる。

UATの有効性は透過光を用いた我々の評価方法で調べられた。この方法では半透明の根管模型(マイクロピペット)を透過する光の強度を検出する。この根管模型では、デブリの替りに水酸化カルシウムペーストが詰められた。UATの安全性は根管洗浄中に根尖孔外で生じる圧力を測定することによって評価された。シリンジによる洗浄(プラント針、サイドホール針)、受動的超音波洗浄(PUI)、INP、そしてUATが評価された。データはTukey-Kramer法で統計的に分析された。我々の実験では、UATが一番安全かつ時間を要しなかった。

12. 水硬性仮封材の硬度に及ぼす消毒液の影響に関する研究

Effects of disinfectant solution on hydraulic temporary sealing material

根管治療時の仮封材として水硬性セメントを使用する際、乾燥綿球に代わり消毒薬を含有した綿球を髄室内に置くことは、歯髄腔内の無菌化に有用であると予想される。本研究の目的は、消毒薬が水硬性仮封材の硬化に及ぼす影響を検討することである。

髄室を模したポリエチレンテレフタレート製チューブ100本のうち、50本に水硬性仮封材(Cavition[®],GC)を填塞し、残りの50本には各10本ずつ以下の被験薬剤を含ませた綿球を封入した。A群:6.0%次亜塩素酸ナトリウム水溶液(次亜塩6%「ヨシダ」,吉田製薬)、B群:83%エタノールおよび3.7%イソプロパノール(メディアルコットME-S,白十字)、C群:水酸化カルシウム材(カルシベックスII[®],日本歯科薬品工業)、D群:蒸留水、E群:なし(乾燥綿球のみ、コントロール群)。これらのチューブは接

合し、Cavition[®]の上面以外をユーティリティワックスにて固定、封鎖した。37℃の水中で3日間保管後、Cavition[®]の表面を耐水研磨紙にて#2000まで研磨し、硬度試験機(EZ-TEST,島津製作所)にてCavition[®]の被験材料側の硬度を測定した。統計学的解析は、一元配置分散分析およびTukey-Kramer testを用い、有意水準5%で行った。

その結果、D群と比較しC群およびE群では被験材料に接するCavition[®]の硬度は有意に低かった。一方、A群およびB群では、D群との統計学的な有意差は認められなかった。

以上の結果から、Cavition[®]を根管治療時の仮封材として用いる場合、髄室に次亜塩素酸ナトリウム水溶液、エタノール、あるいは蒸留水を含む綿球を置くことにより、乾燥綿球と比較し深層のCavition[®]の硬化が促進されることが示された。

13. 象牙質形成不全症の永久歯列に対する実体顕微鏡およびコーンビームCTを用いた歯内治療学的アプローチ

Endodontic treatment of dentinogenesis imperfecta using microscope and cone beam computed tomography

象牙質形成不全症は、約6000人~8000人に1人の割合で発生する常染色体遺伝の疾患である。乳歯および永久歯の双方に発症するが、通常青灰色や黄褐色に変色した乳歯により発見される。歯髄腔は初期から著しく狭窄する。ひとたびエナメルを喪失すると象牙質は急速に磨耗する。小児歯科医の下で適切な管理が行われれば、その後理想的に見える永久歯列を得る事も可能である。

しかし、乳歯列同様永久歯のエナメル質は破折あるいは剥離しやすく、歯髄疾患や根尖性歯周炎に陥りやすい。多くは歯髄腔の狭窄ゆえ根管へアクセスすることが出来ず、抜歯に至る。それゆえ、象牙質形成不全症の永久歯を保存するために新たな根管へのアプローチ法が求められる。

本症例では、象牙質形成不全症患者の2本の失活歯に対し、実体顕微鏡およびコーンビームCTを用いて歯内治療を行い歯の保存を試みた。解剖学的あるいは組織学的異常を伴う永久歯列を保存するための歯内治療の可能性に関し情報を提供するものである。

2) 研究内容の英文要約

1. Signal network of osteoblast- and odontoblast-differentiation form undifferentiated mesenchymal cells <Notch-Hey1>

In the course of osteoblast differentiation, Runx2 and Osx

work as master genes, which determine the direction of osteoblast differentiation. However, precise mechanisms of molecular signal network in this process are not clearly elucidated. We revealed that the constitutive active form of Notch prohibited the osteoblastic differentiation of Kusa-A1 cells, which are bone marrow stromal cell-derived undifferentiated mesenchymal cells and are highly committed to differentiate into mature osteoblasts. Hey1, which is a member of the Notch signaling network, was an essential factor of the major phenomena induced by the Notch activation in Kusa-A1 cells. Furthermore, Notch signaling is revealed to be important even in the differentiation of pulp cells.

<Mef2c>

We revealed that high expression of Mef2c, which is one of the master genes of myoblast differentiation, in Kusa-A1 cells, which are bone marrow stromal cell-derived undifferentiated mesenchymal cells and are highly committed to differentiate into mature osteoblasts. Its expression was low in Kusa-O cells, which are also bone marrow stromal cell-derived undifferentiated mesenchymal cells but are not highly committed to differentiate into mature osteoblasts. Enforced expression of Mef2c in Kusa-O cells promoted osteoblastic marker expression and mineralized nodule formation. Mef2c may be one of the positive regulators of osteoblast differentiation. Mef2c was also a positive regulator of odontoblasts.

<Sp7>

Sp7 (Osterix) is a major transcriptional factor, along with Runx2, in the osteoblast differentiation, and severe disturbance of bone formation is observed in Sp7 null mouse, which suggests that Sp7 may be one of the essential regulators for undifferentiated mesenchymal cells into hard tissue forming cells. Various cells in rat pulp tissues showed the expression of Sp7, and its high expression was detected especially in mature odontoblasts. Its expression in immature odontoblasts was rare. These results indicated that Sp7 may be an essential factor for odontoblast differentiation.

2. Isolation of stem cells from pulp tissues, and reconstruction of pulp tissues from stem cells

<Isolation of mesenchymal stem cells from pulp tissues>

SP cells, which are side population cells determined by Hoechst dye, are popularly used as a stem cell population. However, they can not be used clinically, because the Hoechst dye binds to DNA, which may induce mutagenesis. We tried to separate the stem cells from pulp tissues using the low density culture method, which is popularly applied to isolate mesenchymal stem cell populations. Stem cells were successfully isolated from pulp tissues using this method.

<Infection and inflammation control in the pulp chamber>

The control of infection and inflammation in the remained pulp tissue is essential in case of transplantation of stem cells into the pulp chamber. In order to control the inflammation, we focused on the MMP3 (matrix metalloproteinase 3), which is reported to accelerate the healing of pulp tissue wound. MMP3 down-regulated the inflammatory mediator synthesis in LPS-stimulated peritoneal macrophages. MMP3 may be a potent candidate to control the pulpal inflammation.

3. Inhibitory effects of the cathepsin K inhibitor on the progress of rat periapical lesions

In this study, we investigated the inhibitory effects of a cathepsin K inhibitor (NC-2300) on the progress of rat periapical lesions. The periapical lesions were induced experimentally in the rat first lower molars, and NC-2300 was administrated orally in the experimental group. The micro CT and the histological analyses revealed that the size of the periapical lesion and the number of osteoclasts in the experimental group were significantly reduced compared to those in the control group. The expression of pro-inflammatory cytokines (IL-1 α and IL-6) in the experimental group was also significantly suppressed compared to that of the control group. These results suggest that NC-2300 may inhibit not only the cathepsin K activity in the osteoclasts but also the osteoclastogenesis induced by the inflammatory cytokines, which contribute the down-regulation of active bone destruction.

4. Improved pulp tissue regeneration from stem cells induced by accelerated revascularization

Caries is a common dental problem leading to damage of tooth structure and in many cases, pulp tissue. The regeneration of the pulp-dentin complex is the ultimate goal of operative dentistry and endodontics. This treatment will regenerate the pulp tissue in non-vital teeth and further stimulate the growth of reparative dentin. Thus, the regenerated vital tooth structure reinforces the tooth, as compared to a non-vital tooth with restoratives. Therefore, the dentin/pulp complex regeneration is our prospect of interest, which potentially improves quality of endodontic treatments.

The purposes of the study are classified as follows;

- Seeking a signaling molecule capable of cell differentiation into odontoblasts and dental pulp cells.
- Searching factors that promote angiogenesis quickly into a pulp cavity, as vascularization is one of the key elements for tissue regeneration.
- Searching a methodology to maintain an appropriate function of the cells in order to regenerate pulp tissue complex.

- Seeking an appropriate strategy to regenerate dentin/pulp complex in human pulp cavity aiming at clinical application.

5. Attempt to Measure Functional Space of Dentinal Tubules in Human Dentin

The aim of this study was to measure the functional space that would simulate in situ in dentinal tubules.

For 5 teeth (aged 14-29 years), dentin cavities (2mm in diameter) were prepared on the surfaces of the tooth crown. Fluorescent microspheres which had individual external diameters and excitation wave-lengths were mixed and applied to the cavities for 30min. Samples were fixed and decalcified. Cryostat sections were cut and the localization of applied microspheres were confirmed with a fluorescent microscope and analyzed using an image-analysis software.

First, microspheres (0.1-0.5 μ m) applied to dislocated teeth were accumulated in the outer third-middle third of dentin. Only a few of microspheres were observed in the inner third. No microspheres were found in the odontoblastic layer and the core pulp. Second, microspheres (0.1-0.5 μ m) applied to extracted teeth were found just beneath the bottom of cavities and in the outer third of dentin. A small number of bigger ones (1.0~4.0 μ m) were accumulated only in outer third. In case (aged 14 years) a small number of 0.1~0.5 μ m microspheres were found in the inner third of dentin.

These results suggest that dentinal tubules in the inner third of human tooth crown may have a space of about 0.5~1.0 μ m through which dentinal fluid can move, and that microspheres larger than 1.0 μ m may not be able to pass this space.

6. Influence of Cytosolic and Extracellular Environments on Functional Syncytium in Human Odontoblastic

Objectives: Odontoblasts (OBs) are well-known to be associated with dentinogenesis. They have a monopolar process in dentinal tubule and align in the outermost dentin. Thus, they seem suitable to be a possible sensor even though clear evidence for a role of OBs as sensory receptor cells has not been clarified. But, technical difficulties have hampered approach to them. We have demonstrated cell-to-cell communication between odontoblasts. Many important cell functions are controlled by Ca^{2+} release from intracellular stores via the inositol 1,4,5-trisphosphate receptor (IP3R). We designed the present study to determine intra-/intercellular Ca^{2+} propagation in mechanically stimulated and IP3-injected human OBs and surrounding OBs.

Methods: Six freshly extracted premolars for an orthodontic reason from informed patients were used. Cells with a monopolar process (>100 μ m) were placed in HEPE-

based buffer with fura-2 acetoxymethyl ester (3 μ M). Intracellular Ca^{2+} concentrations were monitored when mechanically stimulated with a fire-polished glass micropipette using a micromanipulator or when IP3 was intracellularly applied either with or without a gapjunction blocker (25mM 2-bromo-2-chloro-1,1,1-trifluoroethane) together with extracellular Ca^{2+} .

Results: (1) Mechanical stimulation of a single OB resulted in a significant ($p<0.05$) increase of cytosolic Ca^{2+} in the stimulated OB that propagated from the point of stimulation throughout the cell cytoplasm. (2) Mechanical stimulation to OB cell membrane significantly increased intracellular Ca^{2+} of the surrounding OBs. (3) Intracellularly injected IP3 also increased intracellular Ca^{2+} significantly. The IP3 dependent-intracellular Ca^{2+} propagation to adjacent OBs was inhibited by the gap-junction blocker.

Conclusions: (1) Intracellular Ca^{2+} signaling system exists in the human OB layer and may play an important role in mechano-transduction mechanism triggered by deformation of cell membrane. (2) Influx of extracellular Ca^{2+} into the mechanically stimulated OB may contribute to intracellular increase of Ca^{2+} propagation. (3) Cell-to-cell Ca^{2+} propagation may be mainly mediated by IP3 dependent Ca^{2+} release from intracellular pool.

7. Facilitated Chemical Transfer through Human Enamel with AC iontophoresis

Objectives: We have shown monomeric substances can pass through the intact human enamel and dentin that are defensive barriers against external irritation. The objectives of the present study were to quantitatively evaluate chemical permeability through human enamel/dentin with conductometry and to clarify the effect of AC iontophoresis on its permeability.

Methods: Electrical impedance of different concentrations of lidocaine hydrochloride (LH) was measured using a bipolar platinum electrode. The relation between concentration and conductance of the solution was examined. Two chambers were used; one was filled with ultrapure water and the other with different concentrations of LH. Six premolars extracted for orthodontic treatment were sectioned at the cemento-enamel junction. Tooth crowns were held between two chambers with a double O-ring. The enamel side chamber was filled with LH, the pulp side one with ultrapure water. A simulated interstitial pulp pressure was applied to the pulp side chamber. Change in the concentrations of LH was measured every 2 minutes with a platinum recording electrode positioned at the center of the pulp side chamber. Two platinum plates were set at the both ends of the chambers to pass alternating current. Passive diffusion without the iontophoresis was used as control. After the measurements, the enamel surfaces of sample teeth were examined by scanning electron

microscopy.

Results: One sample that had enamel cracks was excluded from the study. Electrical conductance (G , mho) correlated closely to the concentration (x , mmol/L) of LH ($G=2.16x^2+0.0289x+0.000376$, $r^2=0.999$). LH that passed through enamel/dentin against dentinal fluid flow increased with time.

Conclusions: Conductometry showed LH diffusion through enamel/dentin was increased in quantity by AC iontophoresis. Anion delivery through human enamel/dentin could be increased by AC iontophoresis.

8. Effect of p38MAPK inhibitor SB203580 intra-endocranial microinjection on the MO-induced gene expressions in the thalamus.

The expression levels of NMDA receptor, p38MAPK, GFAP mRNAs were upregulated in the thalamus, responding immediately to pulpal afferents excitation by mustard oil (MO) application in rats. To elucidate the functional properties of these genes, the effect of the intra-endocranial microinjection of p38MAPK inhibitor, SB203580, was examined on the above mentioned mRNA expressions in the thalamus. Using pentobarbital sodium anesthetized male SD rats (weighing 300g), the left maxillary first molar pulp was exposed to stimulate pulpal afferents by the MO application. Animals were sacrificed at 60 mins after the MO application, and the effect of SB203580 or SB202474 (negative control) administration on the gene expressions was examined ($n=3$ each), and gene expression analyses of GFAP, p38MAPK, NMDAR2A and NMDAR2D mRNA were performed by using RT-PCR. The upregulations of p38MAPK and GFAP mRNAs in the contralateral thalamus were notably suppressed by SB203580 administration, but not NMDAR mRNA expression. The administration of SB202474, used as a control, had no effect on these genes. In this analysis, the p38MAPK inhibitor, SB203580, suppressed remarkably not only p38MAPK mRNA but also GFAP mRNA expressions. These results suggest that p38MAPK might have some roles to regulate GFAP mRNA expression in the thalamus.

Endodontic Field

9. Application of laser to apicoectomy

The use of laser in apical endodontic surgery has become well-known for the sterilization of contaminated root apex, removal of the smear layer, and exposure of collagen fibers on the root surface. Those benefits of laser apicoectomy may be a main factor for rapid bone healing by enhancing cell attachment. During the laser irradiation, various morphological changes occur in the ultrastructure of resected root surface, which may cause biological activation

for surrounding cells. The entire surfaces in the control group were covered with debris. The surfaces of laser-treated samples showed an irregular or scaly morphology, and the smear layer was completely removed. Er:YAG laser irradiation group exhibited the largest number of attached cells/specimen compared with non laser irradiated groups. Morphology of the dentin surface irradiated with low level Er:YAG laser might enhance osteoblastic cell attachment. Rough surfaces produced by Er:YAG laser might allow increased mineralization of osteoblastic cells.

10. Effect of Heat Treatment for Ni-Ti Rotary Endodontic Instruments

The bending properties of Ni-Ti endodontic files are closely related to the transformation behavior, and it is noted that the behavior is transformed by heat treatment. The purpose of this investigation was to evaluate the bending property and shaping ability of Ni-Ti rotary endodontic instruments that were processed by heat treatment. K3 files were heated for 30 minutes at 400 (Group 400), 450 (Group 450), and 500 (Group 500) °C. Files as received were served as control. A cantilever bending test apparatus was used to evaluate the changes in the specimen flexibility caused by heat treatment. Moreover, standardized curved root canal models were prepared using those files. At 0.5 mm deflection, load values of the control group and Group 500 were higher than those of Groups 400 and 450 ($p<0.05$). At 2.0 mm deflection, the bending load values of the control group showed the highest value among all groups ($p<0.05$). In the control group, root canals at the apex were transported to the outer side of the curvature compared to all heat treated groups ($p<0.05$). Heat treatment for the K3 might be effective for the preparation of curved canal because of flexibility.

11. New root canal irrigation method using ultrasonic aspiration technique

For an endodontic success, it is very important to remove microorganisms from the root canal by instrumentation and irrigation. Complete instrumentation and irrigation of the canal seem to be very difficult. We developed a new root canal irrigation method, the ultrasonic aspiration technique (UAT). This technique modified the INP (Irrigation with Negative Pressure) by Fukumoto et al. The biggest problem of INP was its thin aspiration needle was very easily choked with debris. In UAT, the aspiration needle of the INP is vibrated with an ultrasonic unit to avoid choking of the needle. The efficacy of UAT was evaluated using our evaluating system using permeating light. This system detects the magnitude of the permeating light through the semi-transparent root canal model (micro-pipette). In the model canal, calcium hydroxide paste was filled in place of debris. The safety of UAT was evaluated

by a measurement of the pressure generated outside the apical foramen during root canal irrigation. We evaluated syringe irrigations (blunt and side-hole needles), passive ultrasonic irrigation (PUI), INP, and UAT. The data were statistically analyzed using Tukey-Kramer test. In our experiments, UAT was safest and most effective and least time consuming.

12. Effects of Disinfectant Solution on Hydraulic Temporary Sealing Material

The cotton pellet soaked with disinfectant under the hydraulic sealing cement is expected to maintain aseptic conditions in the pulp chamber during root canal treatment. The aim of this study was to examine the effect of disinfectant on the hardness of hydraulic sealing cement.

One hundred pulp chamber models were made with polyethylene terephthalate tubing. Fifty of them were filled with hydraulic sealing cement (Cavition®, GC). The remainder were divided to five groups and filled with a cotton pellet soaked with one of the following agents. Group A: 6% sodium hypochlorite (Jiaen6% "Yoshida", Yoshida Pharmaceutical), Group B: 83vol% ethanol and 3.7vol% isopropanol (Medialcotto ME-S, Hakujuji), Group C: Calcium hydroxide (Calcipec® , Nippon Shika Yakuhin Kogyo), Group D: Distilled water. In Group E, no agent was soaked and used as control. Each of them was joined to the tube filled with Cavition® and covered with utility wax except the surface of Cavition®. They were kept in 37° C water for 3 days. The surfaces of Cavition® were polished with water-resident paper #2000. The hardness of the surface contacting to disinfectants was measured by a hardness tester (EZ-TEST, Shimadzu). Statistical analyses were performed by one-way ANOVA and Turkey-Kramer test with a 0.05 confidence.

The hardness of Group C and E was significantly lower than that of group D. There were no significant differences among Groups A, B and D. It was suggested that a cotton pellet soaked with 6% sodium hypochlorite, 70% ethanol or distilled water in the pulp chamber may increase the hardness of Cavition® in the deep layer compared with dry one.

13. Endodontic Treatment of Dentinogenesis Imperfecta Using Microscope and Cone Beam Computed Tomography

Dentinogenesis imperfecta is an autosomal dominant inheritable disorder affecting approximately one person out of 6,000 to 8,000 people. It was usually found as an opalescent blue-gray or yellow-brown color dentin in deciduous teeth. The enamel is prone to exfoliation or fracture and the dentin promptly wears, resulting in pulpitis or apical periodontitis. As pulp obliteration is typically too severe for the conventional root canal treatment, extraction

is often indicated. This case report describes the endodontic treatment to preserve a non-vital permanent tooth of dentinogenesis imperfecta using microscope and cone beam computed tomography.

3) 本事業に関連して世界的な研究拠点形成に向けて、以下の点で改善・整備等されたこと

A (研究拠点体制)

グローバルな視点に立って、歯学の中でも歯髄生物学および歯内療法学の発展に寄与できる研究を行うことができるよう研究の環境整備を進めている。そのため、幅広く研究領域をカバーするとともに、それぞれの領域で先端的な研究を行うことができるよう、専任の指導教官を配備している。指導教員にはその領域において世界の第一線で活躍できる知識および経験を備えていることが求められる。

B (研究教育環境)

大学院生には、常に臨床と研究の接点を見失うことのないよう、週に最低3コマの診療コマが与えられている。また、専任の指導教官は個別に研究指導を行い、研究遂行上問題が生じた場合にはすぐに対応できる環境が整えられている。

C (人材確保)

大学院を終了した後に教室に残り、研究を続けることができるよう、大学院終了時に医員として大学に残ることが出来るように配慮している。医員は病院職員として臨床業務に携わるが、時間を有効に活用し研究業務に当たることが可能である。

D (人材育成)

研究課題を自ら考えて、それを解明するための実験系を遂行できる人材の育成に力をいれている。そのために、研究の内容について指導者と突っ込んだ話し合いを行い、自らの考えをきちんとまとめることができるよう指導している。

E (国際化)

海外からの留学生も多くいることから、各研究グループのセミナーおよび医局のセミナー用のスライドは原則英語にしている。また、当教室で行う大学院講義はスライド、講義ともに英語で行っている。

4) GCOE事業を推進するに当たって力を入れた点

本事業を推進するにあたり、世界的な研究拠点づくりとのことから海外の研究機関との情報交換および人

材交流に力を入れている。アメリカ、カナダ、イギリス、韓国、中国、タイなどの研究機関と現在交流を持っている。

5) 英文原著論文

1. Kawashima N, Wadachi R, Yeng T., Parashos P., Suda H.. Contemporary Meaning of Intracanal Medicaments IDJ 59, 5-11, 2009.
2. Carlos G Adorno, Takatomo Yoshioka, Hideaki Suda. The Effect of Root Preparation Technique and Instrumentation Length on the Development of Apical Root Cracks Journal of Endodontics 35(3)389-392, 2009.
3. Saegusa H, Watanabe S, Anjo T, Ebihara A, Suda H. Safety of Laser use under the Dental Microscope Australian Endodontic Journal , 2009.
4. Ikeda H, Matthews B, Holley M. Monoclonal antibodies raised against cat odontoblasts with in vitro immunisation Cell and Tissue Research , 2009.
5. Hanada T, Quevedo C, Okitsu M, Yoshioka T, Iwasaki N, Takahashi H, Suda H. Effects of new adhesive resin root canal filling materials on vertical root fractures. Australian Endodontic Journal , 2009.
6. Rittling S, Zetterberg C, Yagiz K, Skinner S, Suzuki N, Fujimura A, Sasaki H. Protective Role of Osteopontin in Endodontic Infection Immunology Published online, 2009.
7. Kaneko T, Okiji T, Kaneko R, Suda H. Gene expression analysis of immunostained endothelial cells isolated from formaldehyde-fixated paraffin embedded tumors using laser capture microdissection-A technical report Microsc Res Tech 72(12)908-912, 2009.
8. Watanabe S, Saegusa H , Anjo T, Ebihara A, Kobayashi T, Suda H. Dentin strain induced by laser irradiation Australian Endodontic Journal , 2009.
9. Yahata Y, Yoneyama T, Hayashi Y, Ebihara A, Doi H, Hanawa T, Suda H. Effect of heat treatment on transformation temperatures and bending properties of nickel-titanium endodontic instruments International Endodontic Journal 42(7)621-626, 2009.
10. Sun H, Kawashima N, Xu J., Takahashi S., Suda H.. Expression of Notch-signaling-related Genes Australian Endodontic Journal , 2009.
11. Carlos G Adorno, Takatomo Yoshioka, Hideaki Suda. Incidence of accessory canals in Japanese anterior maxillary teeth following root canal filling ex vivo International Endodontic Journal 43 2009.
12. Carlos G Adorno, Takatomo Yoshioka, Hideaki Suda. The effect of working length and root canal preparation technique on crack development in the apical root canal wall. International Endodontic Journal 43 2009.

6) 著書

Ikeda H, Suda H. Chapter 6 Circulation of the Pulp Seltzer and Bender's The Dental Pulp Quintessence International Publishing (2nd) , in press 2009.

Ikeda H, Suda H. Chapter7 Intraoral Pain Disorder Guideline of Orofacial Pain Quintessence International Publishing (2nd) , in press 2009.

吉岡隆知, . 歯科用CTと歯内療法 歯界展望特別号 めざせ! 健・口・美 - 未来に向けた歯科医療 - 第21回日本歯科医学会総会 医歯薬出版株式会社, 154.

吉岡隆知, 須田英明. ビジュアライズドエンドドンテックス - セカンドジェネレーション - 歯界展望特別号 めざせ! 健・口・美 - 未来に向けた歯科医療 - 第21回日本歯科医学会総会 医歯薬出版株式会社, 237.

吉岡隆知, 石村瞳. コーンビームCTを用いた画像診断 歯界展望別冊 エンド難症例 医歯薬出版株式会社別冊, 96-104.

須田英明, . 歯槽膿漏 暮らしと健康 保健同人社第64巻, 73.

須田英明, . 和、輪、話 第58回 御茶ノ水祭プログラム, 3.

Suda H, . Welcome message The 15th Asian Pacific Endodontic Confederation. 第30回日本歯内療法学会学術大会, 2.

須田英明、田中義弘、牟田悟朗、山口育子, . 座談会「これからの歯科医療に望まれる形は何か Part.3」 - 良質な歯科医療をあまねく実践するために - 日本歯科医学会誌 日本歯科医学会, 8.

須田英明, . 特定非営利活動法人 日本歯科保存学会 日本歯科医学会誌 日本歯科医学会, 97.

須田英明, . 歯髄はどこまで残せる、どうして処置する 別冊 the Quintessence クインテッセンス出版株式会社 (第1版) 別冊, 166-167.

池田英治, 須田英明. 口腔内疼痛症 口腔顎顔面痛の最新ガイドライン クインテッセンス出版株式会社 (改定第4版) , 115-141.

須田英明, . 編集後記 歯科薬物療法 日本歯科薬物療法学会28巻2号.

Suda H, . APEC News Australian Endodontic Journal Australian Society of Endodontology35, 112.

池田英治, . 第17章 偶発事故の予防と処置 改訂版エントドンティックス21 須田英明, 戸田忠夫 (編集主幹) 永末書店, 京都 (第3版)

池田英治, . 歯内治療に関連する歯の形態異常 歯界展望 特別号 めざせ! 健・口・美 - 未来に向けた歯科医療 - 第21回日本歯科医学会総会 医歯薬出版株式会社, 306.

7) 特許取得、特許申請

<国内>

川島伸之、鈴木規元、日本ケミファ株式会社, 歯周病又は根尖性歯周炎の予防又は治療剤. 特許出願中 40080 特願2009-218590.

三井宗洋、栗橋行雄、吉岡隆知, 歯牙模型およびその製造方法. 特許出願中 40099 特願2009-235930.

8) 平成21年度までの自己評価

世界の中心としての研究拠点を構築していくにあたり、各指導教員および大学院生あるいはポスドクが一体となって研究活動に邁進する環境を整備する必要があるが、その整備が十分に行われていない。指導教員は自らの研究を行うと共に指導している大学院生の研究を補助し、さらに臨床、教育、雑務に従事せざるをえず、あまりの多忙に研究に対する熱意が薄れがちである。その一つの解決策として、他分野との共同研究を行うことが考えられる。共同研究を行うことにより、多方面からのアプローチが行えると共に、研究の効率化を進めることも可能となると期待される。

9) 和文原著論文

吉岡隆知, 石村瞳, 菊地和泉, 小林千尋, 須田英明. 根尖に適合するファイルサイズの決定 日本歯内療法学会雑誌 30 (1) 1-4, 2009.

砂川光宏, 松本宏之. 本学歯学部歯学科における包括的臨床実習 Phase I 履修学生に対する院内感染予防対策教育とその問題点 口腔病学会誌 76 (1) 25-30, 2009.

大山篤, 清水チエ, 佐藤光生, 濱野英也, 礪波健一、大原里子、吉岡隆知、樺沢勇司、新田浩、塩沢育巳、荒木孝二、木下淳博、俣木志朗. 本学歯学部附属病院歯科総合診療部における医歯学シミュレーション教育システムの実施と評価 日本口腔診断学雑誌 22 (1) 1-10, 2009.

石村瞳, 吉岡隆知, 須田英明. 接着性根管充填材のコロナルリーケージに関する評価 日本歯科保存学雑誌 52 (2) 131-137, 2009.

吉岡隆知, 花田隆周, 石村瞳, 菊地和泉, 小林千尋, 須田英明. 穿孔封鎖を行った根管治療歯にみられた垂直性歯根破折 日本歯内療法学会雑誌 30 (2) 65-70, 2009.

小林千尋, 吉岡隆知, 須田英明. 根管洗浄の新しい評価法 日本歯内療法学会雑誌 30 (2) 79-83, 2009.

八幡祥生, 吉岡隆知, 須田英明. ラバーダムのために distal wedge operation を行った1例 日本歯内療法学会雑誌 30 (2) 84-88, 2009.

金子友厚, 興地隆史, 砂川光宏, 金子実弘, CHOKECHANACHAISAKUL Uraiwan, 河村隼, 須田英明. ラット臼歯に誘発した根分岐部病変の初期発症過程における免疫機能分子および Toll-like レセプター mRNA 発現の亢進 日本歯科保存学会雑誌 52 (2) 154-160, 2009.

渡辺聡, 三枝英敏、安生智朗、海老原新、須田英明. 根管照射用チップを用いた Er:YAG レーザー照射による象牙質切削の基礎的検討 日本レーザー歯学会誌, 2009.

池田英治, 須田英明. 歯内治療に関連する慢性痛 日本歯内療法学会雑誌 29 (2) 107-112, 2009.

小林千尋, 福元康恵、吉岡隆知、須田英明. 超音波吸引洗浄法の開発 日本歯内療法学会雑誌 31 (2) in press, 2009.

10) 学会発表 (英文)

Carlos Gabriel Adorno Quevedo, Takatomo Yoshioka, Hideaki Suda, Apical crack development caused by root canal instrumentation The 15th asian pacific endodontic

confederation poster,Tokyo, 2009/4/25.

Xu J,Kawashima N, Suzuki N, Okuhara S, Wei S, Takahashi S, Zhou M, Koizumi Y, Suda H,VIP receptor expression in tooth development The 15th Asian Pacific Endodontic Confederation poster,Tokyo, 2009/4/25.

Wei S,Kawashima N, Suzuki N, Xu J, Takahashi S, Zhou M, Koizumi Y, Suda H,Expression of Th17 related cytokines in experimentally-induced rat periapical lesions The 15th Asian Pacific Endodontic Confederation poster,Tokyo, 2009/4/25.

Sasaki N,Alshwaimi E, Suzuki N, Stashenko P,18-glycyrrhetic acid inhibits periodontal bone loss in rats IADR 87th General Session poster,Miami, 2009/4/4.

U. Chokechanachaisakul, J. Kawamura, T. Kaneko, M. Sunakawa, M. Kaneko, T. Okiji, and H. Suda ,Tooth-pulp stimulation upregulates antigen presentation-associated genes in the thalamus FDI FDI 2009 poster,Singapore,2009/9/2,3.

J. Kawamura,U.Chokechanachaisakul, T. Kaneko, M. Sunakawa, M. Kaneko, T. Okiji, and H. Suda,Up-regulation of TLR mRNA in furcal inflammation of endodontic origin FDI FDI 2009 poster,Singapore,2009/9/2,3.

U. Chokechanachaisakul,T. Kaneko, J. Kawamura, M. Kaneko, T. Okiji, and H. Suda ,A technical report of immune-LCM from paraffin embedded tumors The Japanese Society of Microscopy 2009 poster,Sendai,2009/5/27~29.

M. Sunakawa,, T. Kaneko, J. Kawamura,U. Chokechanachaisakul, , M. Kaneko and H. Suda,The effect of p38MAPK inhibitor SB203580 intra-endocranial microinjection on the MO-induced gene expressions in the thalamus The 11th Joint Meeting between KACD & JSCD poster, Jeju, 2009/11/13.

Kawashima N,Xu J, Iwata T, Zhou M, Takimoto K, Koizumi Y, Ohi C, Takahashi S, Suzuki N, Suda H,Expression of Sp7 in the rat dental pulp The 11th Joint Meeting between KACD & JSCD Poster,Jeju, 2009/11/13.

Ikeda H,Suda H,Long-term follow-up after endodontic treatment of young patients having severe endodontic problems -a marvel healing ability- The 11th Joint Meeting between KACD & JSCD Poster,Jeju, 2009/11/13.

Wadachi R,Miwa Z, Suda H,Endodontic treatment for dentinogenesis imperfecta using microscope and cone beam computed tomography The 15th Asian Pacific Endodontic

Confederation poster,Tokyo, 2009/4/25.

Ebihara A,Yahata Y, Nakano K, Hayashi Y, Suda H,Effect of heat treatment for NiTi rotary endodontic instruments: change of bending properties American Association of Endodontists, 2009 annual session poster,Orlando, 2009/5/2.

Hayashi Y,Yahata Y, Ebihara A, Doi H, Suda H,Phase transformation behavior and bending properties of GT series X rotary endodontic file American Association of Endodontists, 2009 annual session poster,Orlando, 2009/5/2.

Nakano K,Ebihara A, Yahata Y, Hayashi Y, Suda H,Effect of heat treatment for NiTi rotary endodontic instruments: evaluation of root canal preparation American Association of Endodontists, 2009 annual session poster,Orlando, 2009/5/2.

Watanabe S,Kokuzawa C, Gomb B, Saegusa H, Anjo T, Ebihara A, Kobayashi C, Suda H,Dentin strain caused by removal of root canal obturation with Er:YAG laser irradiation American Association of Endodontists, 2009 annual session poster, Orlando, 2009/5/2.

Yahata Y,Hayashi Y, Ebihara A, Kobayashi C, Suda H,Influence of radius of curvature and load on fatigue fracture of nickel-titanium rotary instruments American Association of Endodontists, 2009 annual session poster,Orlando, 2009/5/2.

Ikeda H,Suda H,Facilitated Chemical Transfer through Human Enamel with AC iontophoresis. International Association for Dental Research poster,Miami, 2009/4/2.

Ikeda H,Suda H, Influence of mechanical distortion of human odontoblast membrane on transjunctional Ca²⁺ conductance. International Association for Dental Research, IADR PAPF/1st Meeting of IADR poster,Wuhan, 2009/9/23.

11) 学会発表 (和文)

吉岡隆知,, 歯の根管を洗浄するための新しい吸引用ニードルの開発 国際バイオフィォラム oral,東京, 2009/7/2.

吉岡隆知,花田隆周、石村瞳、小林千尋、須田英明,根管形成における困難性 -根管の探索と穿通について - 第30回日本歯内療法学会 テーブルクリニック,東京, 2009/4/26.

小林千尋,吉岡隆知、福元康恵、須田英明,根管洗浄 - より良い歯内療法のために - 第30回日本歯内療法学会 テ

ーブルクリニック,東京,2009/4/26.

池田英治,須田英明,象牙芽細胞膜の撓みが細胞間カルシウム移動に及ぼす影響 第130回日本歯科保存学会春期大会 口演,札幌,2009/6/12.

河村隼,金子友厚,チョクチャナチャイサクン ウライワン、金子実弘、須田英明、砂川光宏、興地隆史,実験的歯髄炎に伴うラット脳幹内抗原提示細胞関連分子 mRNA 発現の亢進 第130回日本歯科保存学会春期大会 ポスター,札幌,2009/6/11.

チョクチャナチャイサクン ウライワン,金子友厚、金子実弘、須田英明、河村隼、興地隆史、砂川光宏,露髄によって実験的に惹起させたラット臼歯根分岐部歯根膜の炎症部における Toll 様受容体 mRNA 発現の亢進 第130回日本歯科保存学会春期大会 ポスター,札幌,2009/6/12.

坂上斉,吉岡俊彦、須藤享、花田隆周、石村瞳、吉岡隆知、須田英明,接着性材料を用いた根管充填における空隙について 第130回日本歯科保存学会春期大会 ポスター,札幌,2009/6/12.

須藤享,吉岡隆知、小林千尋、須田英明,根管拡大・形成による電氣的根管長測定値の変化 第130回日本歯科保存学会春期大会 ポスター,札幌,2009/6/11.

Adorno Carlos G,吉岡隆知、須田英明,The Effect of Working Length and Root Canal Instrumentation Techniques on Crack Development in the Apical Root Canal Wall 第130回日本歯科保存学会春期大会 ポスター,札幌,2009/6/12.

吉岡俊彦,萩谷洋子、吉岡隆知、須田英明,歯科用CT画像を用いた垂直性歯根破折の診断 第130回日本歯科保存学会春期大会 ポスター,札幌,2009/6/12.

大山篤,須永昌代、吉岡隆知、樺沢勇司、荒木孝二、俣木志朗、木下淳博,医歯学シミュレーション教育システムの活用 総合歯科医療に関する学術研究セミナー2009 テーブルクリニック,松戸,2009/7/20.

小川卓也,須藤享、吉岡隆知,根管の乾燥が電氣的根管長測定法に与える影響 2009年学生発表会 ポスター,東京,

2009/9/29.

時田大輔,須藤享、吉岡隆知,電氣的根管長測定法における、太い根管での測定値の変化 2009年学生発表会 ポスター,東京,2009/9/29.

安川知里,須藤享、吉岡隆知,電氣的根管長測定における根管内容液および歯種の影響 2009年学生発表会 ポスター,東京,2009/9/29.

小林千尋,吉岡隆知、須田英明,超音波吸引洗浄法の開発 第131回日本歯科保存学会秋季大会 口演,仙台,2009/10/29.

石村瞳,坂上斉、吉岡隆知、須田英明,レジン系根管充填用シーラーを用いた際の根管封鎖性に関する研究 第131回日本歯科保存学会秋季大会 ポスター,仙台,2009/10/29.

吉岡隆知,八幡祥生、中野生和子、花田隆周、石村瞳、菊地和泉、鈴木規元、川島伸之、砂川光宏、須田英明,先進医療「X線CT画像診断に基づく手術用顕微鏡を用いた歯根端切除手術」の治療成績 第131回日本歯科保存学会秋季大会 ポスター,仙台,2009/10/30.

坂上斉,吉岡俊彦、須藤享、花田隆周、石村瞳、吉岡隆知、須田英明,接着性材料を用いた根管充填における coronal リークエッジの評価 第131回日本歯科保存学会秋季大会 ポスター,仙台,2009/10/29.

須藤享,吉岡隆知、小林千尋、須田英明,根管内容液とその作用時間が電氣的根管長測定値に与える影響 第131回日本歯科保存学会秋季大会 ポスター,仙台,2009/10/30.

花田隆周,坂上斉、石村瞳、吉岡隆知、岩崎直彦、高橋英和、須田英明,垂直性歯根破折における破折線の進展 第131回日本歯科保存学会秋季大会 ポスター,仙台,2009/10/30.

吉岡俊彦,吉岡隆知、海老原新、須田英明、島田康史、田上順次,垂直性歯根破折の診断における OCT の有用性 第131回日本歯科保存学会秋季大会 ポスター,仙台,2009/10/29.

山内隆守, 辺見浩一, 石村瞳, 福元康恵, 吉岡隆知, 小林千尋, 須田英明, 根管内吸引洗浄法の洗浄効果に関する検討 第131回日本歯科保存学会秋季大会 ポスター, 仙台, 2009/10/29.

鈴木規元, 川島伸之, 許 婧, 須田英明, ラット実験的根尖性歯周炎の進展におけるカテプシンK阻害剤の抑制効果 第131回日本歯科保存学会秋季大会 ポスター, 仙台, 2009/10/30.

瀧本晃陽, 川島伸之, 小泉悠, 中島美砂子, 須田英明, マクロファージのNO産生能に対するMMP-3の影響 第131回日本歯科保存学会秋季大会 ポスター, 仙台, 2009/10/29.

石澤千鶴子, ゴムボ ボロルトヤ, 渡辺聡, 三枝英敏, 安生智郎, 海老原新, 須田英明, 根管用チップを用いたEr:YAGレーザー照射による根管形成の基礎的研究 第131回日本歯科保存学会秋季大会 ポスター, 仙台, 2009/10/29.

ゴムボ ボロルトヤ, 海老原新, 川島伸之, 渡辺聡, 安生智郎, 石澤千鶴子, 須田英明, Evaluation of osteoblastic mesenchymal cell attachment on dentin surface treated with low level Er:YAG laser irradiation 第21回日本レーザー歯学会総会・学術大会 口演, 福岡, 2009/11/21.

渡辺聡, 石澤千鶴子, Gombo Bolortuya, 安生智郎, 海老原新, 須田英明, Er:YAGレーザーによる逆根管充填窩洞形成が垂直性歯根破折に与える影響 第21回日本レーザー歯学会総会・学術大会 口演, 福岡, 2009/11/21.

池田英治, 李穎, 須田英明, 細胞内外の環境がヒト象牙芽細胞機能複合体の協調に及ぼす影響 第131回日本歯科保存学会秋季大会 ポスター, 仙台, 2009/10/29.

竹田淳志, 瀧本晃陽, 辺見浩一, 花田隆周, 石村瞳, 安生智郎, 須田英明, 大林尚人, モーションアーチファクトが歯科用CT画像に及ぼす影響 第131回日本歯科保存学会秋季大会 ポスター, 仙台, 2009/10/30.

八幡祥生, 林洋介, 海老原新, 小林千尋, 須田英明, 低サイクル疲労領域におけるニッケルチタンファイルの疲労

挙動 第131回日本歯科保存学会秋季大会 ポスター, 仙台, 2009/10/30.

李穎, 池田英治, 須田英明, ヒト象細管の機能的幅径計測の試み 第131回日本歯科保存学会秋季大会 ポスター, 仙台, 2009/10/30.

宮本智行, 三輪全三, 鶴沢成一, 岡田大蔵, 和達礼子, 和達重郎, 俣木志朗, 倉林亨, 嶋田昌彦, 東京医科歯科大学歯学部附属病院における医療安全ポケットマニュアル 第28回日本歯科医学教育学会 口演, 広島, 2009/11/6.

森尾郁子, 小野芳明, 和達礼子, 鶴田潤, 海外歯科学士の短期研修受入の現状と課題 第74回口腔病学会 口演, 東京, 2009/12/5.

宮本智行, 三輪全三, 倉林亨, 嶋田昌彦, 和達礼子, 鶴沢成一, 和達重郎, 岡田大蔵, 深山智子, 三浦佳子, 石井牧子, 小畑佳代子, 多田浩, 東京医科歯科大学歯学部附属病院へ異性21年度安全対策研修会(前期)におけるアンケート調査について 第74回口腔病学会 口演, 東京, 2009/12/5.

大山篤, 須永昌代, 駒田亘, 南一郎, 内田達郎, 吉岡隆知, 大槻昌幸, 北迫勇一, 秀島雅之, 水口俊介, 荒木孝二, 俣木志朗, 木下淳博, 歯学科4年次における臨床体験実習の実施と評価 第74回口腔病学会学術大会 口演, 東京, 2009/12/5.

趙永哲, 南一郎, 須永昌代, 吉岡隆知, 岸川隆蔵, 川島伸之, 和達礼子, 木下淳博, 須田英明, 田上順次, 歯科診療室-講義室間の学内LAN同時中継によるライブ講義システムの開発と評価 第74回口腔病学会学術大会 口演, 東京, 2009/12/5.

12) 受賞

花田隆周, ファイバーポイントが垂直性歯根破折に与える影響. 日本歯科保存学会デンツプライ賞 受賞 39975 第130回日本歯科保存学会春期大会,

石 村 瞳, Sealing Ability of New Adhesive Root Canal Filling Materials Measured by a New Dye Penetration Method. 日本歯科保存学会奨励賞 受賞 39975 第130回日本歯科保存学会春期大会,

川 島 伸 之, Expression of Sp7 in the rat dental pulp.
Endo 大 賞 40130 The 11th Joint Meeting between
KACD & JSCD,

池田英治, 歯内治療に関連する慢性痛. 日本歯内療法学会
最優秀論文賞 39927 第30回日本歯内療法学会学術大会,

13) 外部資金の獲得状況

科学研究費補助金、基盤研究 (A)

研究題目:垂直性歯根破折のメカニズム解析と臨床的
対応
代表:須田英明
期間:平成19年—平成22年
研究費総額:3460万円

科学研究費補助金、基盤研究 (B)

研究題目:Notchシグナルの歯髄細胞分化におけるメ
カニズムの解明とその臨床的展開
代表:川島伸之
期間:平成19年—平成22年
研究費総額:1460万円

科学研究費補助金、若手研究 (B)

研究題目:歯髄細胞におけるFgf18シグナルの機能解
析とその臨床的展開
代表:大井智恵
期間:平成19年—平成21年
研究費総額:330万円

科学研究費補助金、若手研究 (スタートアップ)

研究題目:接着性根管充填用シーラーに適した根管治
療システムの開発
代表:石村瞳
期間:平成20年—平成21年
研究費総額:217万円

科学研究費補助金、基盤研究 (B)

研究題目:Gap-junctionを介した象牙芽細胞複合体の
電気的・化学的細胞間連絡の解析
代表:池田英治
期間:平成20年—平成24年
研究費総額:1200万円

科学研究費補助金、基盤研究 (C)

研究題目:根尖性歯周炎の発症・拡大におけるIL-10
の機能的役割
代表:鈴木規元
期間:平成20年—平成22年
研究費総額:350万円

科学研究費補助金、基盤研究 (C)

研究題目:根尖性歯周炎の発症・拡大におけるIL-10
の機能的役割
代表:鈴木規元
期間:平成20年—平成22年
研究費総額:350万円

長寿医療研究委託費

研究題目:近赤外光・レーザー等を用いた新たな歯科
疾患診断・治療用機器の開発に関する研究
代表:角保徳
期間:平成21年—平成23年
研究費総額:500万円

長寿医療研究委託費

研究題目:歯髄幹細胞を用いた象牙質・歯髄再生医療
によるう蝕・歯髄疾患等のための治療技術の開発
代表:川島伸之
期間:平成21年—平成24年
研究費総額:150万円

先端医療開発特区補助金

研究題目:歯髄・象牙質再生用解析機器
代表:川島伸之
期間:平成21年—平成21年
研究費総額:2982万円

GCOEイノベーション研究費

研究題目:歯髄・歯肉・歯根膜由来の幹細胞の特性
代表:川島伸之
期間:平成21年—平成21年
研究費総額:150万円

科学研究費補助金、若手研究 B

研究題目:エナメル芽細胞におけるShhおよびBmpシ
グナルのクロストークと歯の再生への展望
代表:高橋里美

期間:平成21年—平成23年

研究費総額:374万円

科学研究費補助金、若手研究（スタートアップ）

研究題目:接着性根管充填用シーラーによる垂直性歯根破折の予防

代表:花田隆周

期間:平成21年—平成22年

研究費総額:200万円

学術振興会、タイ若手研究者支援事業費

研究題目:Permeability of human dentin and odontoblasts

代表:池田英治

期間:平成21年—平成21年

研究費総額:54万円

GCOE イノベーション研究費、GCOE 海外研究者招聘費

研究題目:Mechanisms of Dentine in Man, Electrophysiological Evidence on the properties of Intradental Surgery Receptors

代表:池田英治

期間:平成21年—平成21年

研究費総額:40万円

14) 特別講演、招待講演

Suda H

Tooth pulp nerves and odontogenic pain
The 11th Joint Meeting between KACD & JSCD
Ramada plaza Jeju Korea
2009/11/13

Ikeda H

Functional Syncytium of Human Odontoblasts (c)
Enamel permeability
Chiangmai University Chiangmai Thailand
2009/1/4

Ikeda H

Human pulp sensation
Mahidol University Bangkok Thailand 2
009/1/4

Ikeda H

(a-1) Gap-junctional communication in the human odontoblastic layer (a-2) Circulation of the pulp, (c) Dentin permeability"

Naresuan University Pitsanulok Thailand

2009/1/4

Ikeda H

Electrical coupling between odontoblasts
"University of Lyon,Facult? d'Odontologie, Molecular cell biology" Lyon France
2009/3/6

Ikeda H

" (1) Odontoblasts -Functional syncytium underneath dentinal tubules, (2) Microcirculation of the dental pulp -from the 6th chapter, the 2nd edition of Seltzer and Bender's The Dental Pulp"
Capital Medical University Beijing China
2009/9/19

Ebihara A

Lasers' Endodontics
National University of Singapore Singapore
Singapore
2009/9/2

吉岡隆知

生涯教育講座: 歯内療法の前線 顕微鏡下の治療「先端医療 X線CT 画像診断に基づく手術用顕微鏡を用いた歯根端切除手術」
第63回特定非営利活動法人 日本口腔科学会学術集会
アクトシティ浜松 2009年4月16日

吉岡隆知

最新の根管充填法
JEA 関東甲信越静支部第13回ベーシックセミナー
実行委員長 ヨシダ（上野） 2009年8月27日

海老原新

歯内治療におけるレーザー応用の効果
第21回日本レーザー歯学会総会・学術大会
福岡県歯 2009年11月22日

須田英明

市民・患者を中心とした医療円形（連携医療）の方向性と学会のかかわり
日本歯学系学会協議会シンポジウム
昭和大学歯科病院 2009年3月21日

海老原新

マイクロエンドドンティクスにおけるEr:YAGレーザー使用の安全性の検討

第12回Er:YAGレーザー臨床研究会

大阪国際会議場 2009年7月26日

15) 教室、分野や講座の准教授、講師、助教、特別研究員、ポスドク、指導を受けた大学院生の名前(AISSには○印) のリスト

准教授 :小林千尋,
砂川光宏(感染対策歯科治療部 兼任)

講師 :竹田淳志, 池田英治

助教 :海老原新, 川島伸之,
松本宏之(感染対策歯科治療部 兼任),
吉岡隆知, 和達礼子, 鈴木規元

ポスドク(医員):金子友厚, 石村瞳, 花田隆周,
八幡祥生, 渡辺聡, 中野生和子

大学院生 :Adrno Quevedo Carlos Gabriel,
○許婧, 河村隼, 小泉悠, 石澤千鶴子,
坂上斉, ○Bolortuya Gombo,
吉岡俊彦,
○Uraiwan Chokechanachaisakul,
本晃陽, ○周夢宇, ○李穎

Basic Research—Technology

The Effect of Root Preparation Technique and Instrumentation Length on the Development of Apical Root Cracks

Carlos G. Adorno, DDS, Takatomo Yosbioka, PhD, and Hideaki Suda, PhD

Abstract

The purpose of this study was to compare the effects of root canal preparation techniques and instrumentation length on the development of apical root cracks. Forty extracted mandibular premolars with straight roots were randomly selected and mounted on resin blocks with simulated periodontal ligaments, and the apex was exposed. The teeth were divided into four groups of 10 teeth each for different canal preparation techniques and instrumentation lengths: group A: step-back preparation (SB) with stainless steel files (SF) using root canal length (RCL) to guide instrumentation length; group B: SB using RCL – 1 mm; group C: crown-down preparation (CD) with Profile using RCL; and group D: CD with PF using RCL – 1 mm. Digital images of the instrumentation sequence were compared for each tooth. Statistical analysis revealed a significant effect of instrumentation length ($p < 0.05$) but no significant effect of preparation technique ($p > 0.05$) on the development of apical cracks. (*J Endod* 2009;35:389–392)

Key Words

Apical root cracks, preparation, vertical root fracture, working length

From the Tokyo Medical and Dental University, Pulp Biology and Endodontics, Tokyo, Japan.

Address requests for reprints to Dr Carlos G. Adorno, Tokyo Medical and Dental University, Pulp Biology and Endodontics, Yushima 1-5-45, Bunkyo-ku, Tokyo 113-8549, Japan. E-mail address: c.adorno.endo@tmd.ac.jp.

0099-2399/09 - see front matter

Copyright © 2009 American Association of Endodontists. doi:10.1016/j.joen.2008.12.008

Root canal preparation is one of the most important steps in any root canal treatment. Ideally, instrumentation should terminate at a suitable location, which is not necessarily the same for both vital and infected cases (1). Kuttler (2) reported that the root canal usually narrows toward the apex and expands to form the apical foramen. The narrowest part of the canal forms the apical constriction. Another study, however, found that the apical constriction was present in less than half of the teeth, and the apical portion of the root was frequently tapered or parallel (3). The frequency of deviation of the apical foramen from the anatomic apex and the mean distance between the major foramen and the anatomical root apex were found to be 76% and 0.99 mm, respectively (4). In addition, a single apical foramen may be found in mandibular first premolar teeth in four of five cases, but two or more foramina may occur over 20% of the time (5).

Instrumentation of root canals alone significantly weakens the roots (6). Root stresses generated from inside the root canal are higher in the apical region and along the canal wall than on the external surface (7). Moreover, the forces developed during canal preparation with a Profile (PF) taper 0.04 (Dentsply Maillefer, Ballaigues, Switzerland) were located at or near the tip of the file (8). The pattern of stress distribution in the apical area could lead to the development of cracks and fracture propagation. In addition, a debilitated root, as a result of flaring and instrumentation, could suffer vertical root fractures during obturation procedures (9). Increasing the apical enlargement with Lightspeed (LightSpeed Technology Inc., San Antonio, TX) nickel-titanium files and increasing the taper with GT files, however, did not weaken the root any more than the conventional step-back K-file preparations and might even increase fracture resistance (10).

To date, no study has reported the relationship between instrumentation length and the development of apical cracks. The purpose of this study was to compare the effects of two canal preparation techniques and instrumentation length on the development of root fractures.

Materials and Methods

Mandibular premolar teeth with straight roots, stored in distilled water immediately after extraction, were randomly selected for this study. The radicular surfaces of each tooth were examined for evidence of fracture lines, open apices, or anatomic irregularities and were discarded if any of these characteristics were found. Forty teeth were finally selected and stored in distilled water throughout the study.

Tooth Preparation

The root was wrapped with a single layer of aluminum foil and embedded in autopolymerizing resin (Ostron; GC Corporation, Tokyo, Japan) set in an acrylic tube (12 mm high and 20 mm in diameter). The root was then removed from the tube, and the aluminum foil peeled off. The acrylic tube was cut on the apical end so that 2 to 3 mm of the root apex was exposed. The root surface and the "socket" were coated with a hydrophilic vinyl polysiloxane impression material (Examixfine, GC Corporation), and the root was immediately repositioned. Thus, the polysiloxane replaced the space created by the foil. Then, the crown was removed at 2 mm above the proximal cemento-enamel junction to ensure a straight access line and to provide a reference plane.

Three initial (0° Ortho, 30° Disto, and 30° Mesioradial) photomicrographs of the apex were taken by a Digital Microscope ($\times 100$) (VH-8000; Keyence, Osaka, Japan).

Basic Research—Technology

TABLE 1. The Mean Number of Teeth with Apical Cracks or Dentinal Detachment and the Smallest and Largest Files that Caused the First Crack in Relation to Instrumentation Length and Techniques

Group (n = 10)	Instrumentation length (technique)	Mean number of teeth with apical cracks	Mean number of teeth with dentinal detachment	Smallest file size to cause the first crack	Largest file size to cause the first crack
Group A	RCL (SF)	1	0.6	#15	#40
Group B	RCL – 1 mm (SF)	0.5	0	#20	#40
Group C	RCL (PF)	0.6	0.4	#15	#60
Group D	RCL – 1 mm (PF)	0.1	0	#25	#25

The teeth were randomly distributed into four experimental groups of 10 teeth per group. A size 10 K-file was inserted into the canal until the tip of the file became visible at the major apical foramen. The distance between the reference plane and the tip of the file was defined as the root canal length (RCL).

Root Canal Preparation

The teeth in groups A and B were instrumented with stainless steel files (SF) (Zipperer, Munich, Germany) with a noncutting tip using a step-back technique with a balanced force concept (11). To enlarge the canal, the balanced force technique is performed with the use of successive files screwed into the canal with a clockwise movement of 60° to 90° and slight inward pressure. Then, a counterclockwise movement of 120° to 180°, under apical-directed pressure, cuts the dentin. The instrumentation sequence followed an incremental size increase (15, 20, 25, 30, 35, 40, 45, and 60), and all canals were irrigated with 1% sodium hypochlorite solution followed by recapitulation with a size 15 file after each file change. The instrumentation length of groups A and B were RCL and 1 mm short of RCL (RCL – 1 mm), respectively.

The teeth in groups C and D were instrumented with a crown-down technique using PF .04 taper followed by the same incremental instrumentation sequence used for groups A and B. A low-torque motor (Dentaport ZX; J Morita MFG Corp, Kyoto, Japan) was used at a constant speed of 300 rpm according to the manufacturer's recommendations. Each instrument was used with a pecking motion and low-force apically directed pressure was applied. The instrumentation lengths in groups C and D were RCL and RCL – 1 mm, respectively. A sequence of incremental decreasing size was used (60, 45, 40, 35, 30, 25, 20, and 15), and each file was changed after 8 to 10 seconds of use. In all samples in groups C and D, the instrumentation length was reached with a size 15 file. After the file reached the instrumentation length, the samples were, once again, examined for cracks caused by the decrement sequence. Using PF, the increment sequence was the same as for groups A and B. The canals were thoroughly irrigated with 1% sodium hypochlorite solution between each file change.

Evaluation

Once the instrumentation length was reached, after each file change, India Ink (Salis International Ink, Hollywood, FL) was used to stain the root apex in order to reveal any cracks, and the teeth were then rinsed with water. The teeth in acrylic tubes were placed under the digital microscope to record standardized images. Then, three photomicrographs (ortho, 30° disto, and 30° mesioradial) ($\times 100$) of the root apex were digitally recorded and stored as JPEGs. A slideshow presentation using Office PowerPoint 2003 (Microsoft Corporation, Redmond, WA) was created for each sample, and every presentation consisted of 8 slides corresponding to the sequential order of instrumentation. On each slide were the three photomicrographs taken at each file change in incremental order (#15, #20, #25, #30, #35, #40,

#45, and #60). A crack was defined as any visible discontinuity on the root surface not detectable by the dental explorer. The photomicrographs for each sample were examined by comparing the PowerPoint slide corresponding to each file used to the PowerPoint slide of the previous file used. The presence or absence of cracks, number of cracks originating at the apical foramen, file size that produced the first crack, and file size that caused dentinal detachment (missing portion of the apex that was present in the preceding image) were recorded.

Statistical Analysis

Using Statview 5.0 (SAS Institute Inc, Cary, NC), logistic regression analysis was performed to compare file size and dentinal detachment in association with preparation technique and instrumentation length. One-way analysis of variance was used to compare the number of cracks between root preparation techniques and instrumentation lengths. All statistical analyses were performed at a 5% significance level.

Results

Table 1 summarizes the mean number of teeth with apical cracks and dentinal detachment as well as the smallest and largest files used that produce a crack. The first crack produced in relation to the file size is shown in Table 2 along with the total number of teeth affected by cracks (17 teeth) and the cumulative total. Figure 1 depicts a representative image showing an apical crack formed after using file #15. Logistic regression analysis revealed a significant effect of working length on file size that produced first crack ($p = 0.036$) and dentinal detachment ($p = 0.002$). In contrast, the root preparation technique had no significant effect on either file size that produced first crack ($p = 0.054$) or dentinal detachment ($p = 0.245$). One-way analysis of variance showed no significant effect of root canal preparation technique ($p = 0.08$) on the number of cracks present. However, working length had a significant effect on the number of cracks present ($p = 0.031$).

Discussion

External reinforcement was avoided using a thin layer of silicone as a simulated periodontal ligament (12–14). Because an “exposed” apex is not uncommon in teeth with chronic apical periodontitis or periapical cysts, the apical 2- to 3-mm portion of the root was exposed to allow for intraoperative image recordings. The instrumentation sequence was chosen based on the files available for PF.

Although three teeth did develop cracks after using the size 60 file, these teeth belonged to group C (Table 2). The transition of the file size #45 to #60 represents the same proportional increase as #15 to #20 because the ratio of 45/60 is equal to 15/20.

All of the cracks that appeared in the SF groups appeared before using the size 45 file (Table 2). The apical pressure used in the balanced force technique (15) might concentrate the force on the external root surface surrounding the apical foramen and cause a crack if the tooth

Basic Research—Technology

TABLE 2. File Size to Produce the First Crack in Affected Teeth ($n = 17$) and Cumulative Total

Group	#15	#20	#25	#30	#35	#40	#45	#60	Total
A	3	2	1	0	0	1	0	0	7
B	0	2	0	1	0	1	0	0	4
C	1	1	0	0	0	0	0	3	5
D	0	0	1	0	0	0	0	0	1
Total	4	5	2	1	0	2	0	3	17
Cumulative total	4	9	11	12	12	14	14	17	

structure is not tough enough. Nevertheless, the canal preparation technique proved to be nonsignificant with regards to the first file that produced a crack.

By contrast, the instrumentation length had significant effects on the first file that produced a crack (Table 2) and also on the file that produced dentinal detachment. Dentinal detachment was observed in half of the samples prepared to the RCL (Table 1). Eighty percent of the detachments were produced after using the size 45 file. There were no cases of dentinal detachment in groups B and D (Table 1) in which the file tip was positioned 1 mm short of the RCL.

Three teeth in group A and one in group C showed cracks after only using a #15 file (Fig. 1). The possibility of causing cracks after

the use of what is usually considered a "safe" file size has not been previously reported in the literature. The external root stresses caused by the SF used with the balanced force technique was concentrated near the tip of the file (16). This might explain why group A showed the highest mean number of cracks (Table 1).

Fourteen samples exhibited cracks before the use of file size 45 (Table 2). In a recent study (17), only an apical debridement larger than normally recommended could achieve bacteria-free root canal samples. Weiger et al (18) suggested that the apical preparation size should generally be at least 6 to 8 files sizes larger than the first apical binding file. Consequently, if the first apical binding file is #10, the apical preparation size should be size 45 to 55, and the sensitivity to generate apical cracks would increase.

The results of this study indicate that a crack is more likely to appear when the working length was RCL rather than RCL - 1 mm. Conservation of the dentin adjacent to the apical root canal is crucial to maintain strength and fracture resistance of the tooth structure (19). It has been suggested that the clinician could reduce fracture susceptibility by maintaining the canal size as small as practical and striving for a smooth round canal without irregularities (20). The excessive removal of dentin would predispose the tooth structure to catastrophic fractures (21). Furthermore, because of the proximity to the apical foramen, the file tips reaching RCL might have been able to cause cracks that were observable on the surface of the apex. This could explain why 11 samples exhibited cracks before using file #30. On the other hand, the file tips reaching RCL - 1 mm might have had a sufficient amount of dentin around the file tip to resist the formation of cracks, although cracks were found in five teeth (Table 2). More debridement means better apical disinfection but also an increased chance of crack development.

This study focused on the development of cracks on the surface of the apex during mechanical preparation that might lead to future fractures of the tooth structure. Root canal obturation and final restoration, frequently with a post, have been shown to stress and strain the tooth structure and could by themselves cause cracks or help propagate cracks previously provoked by mechanical preparation.

References

1. Wu MK, Wesselink PR, Walton RE. Apical terminus location of root canal treatment procedures. *Oral Surg Oral Med Oral Pathol Oral Radiol Endod* 2000;89:99-103.
2. Kuttler Y. Microscopic investigation of root apices. *J Am Dent Assoc* 1955;50:544-52.
3. Dummer PMH, McGinn JH, Rees DG. The position and topography of the apical canal constriction and apical foramen. *Int Endod J* 1984;17:192-8.
4. Blašković-Šubat V, Matić B, Šutalo J. Asymmetry of the root canal foramen. *Int Endod J* 1992;25:158-64.
5. Cleghorn BM, Christie WH, Dong CCS. The root and root canal morphology of the human mandibular first premolar: A literature review. *J Endod* 2007;33:509-16.
6. Zandbiglari T, Davids H, Schäfer E. Influence of instrument taper on the resistance to fracture of endodontically treated roots. *Oral Surg Oral Med Oral Pathol Oral Radiol Endod* 2006;101:126-31.
7. Versluis A, Messer HH, Pintado MR. Changes in compaction stress distributions in roots resulting from canal preparation. *Int Endod J* 2006;39:931-9.

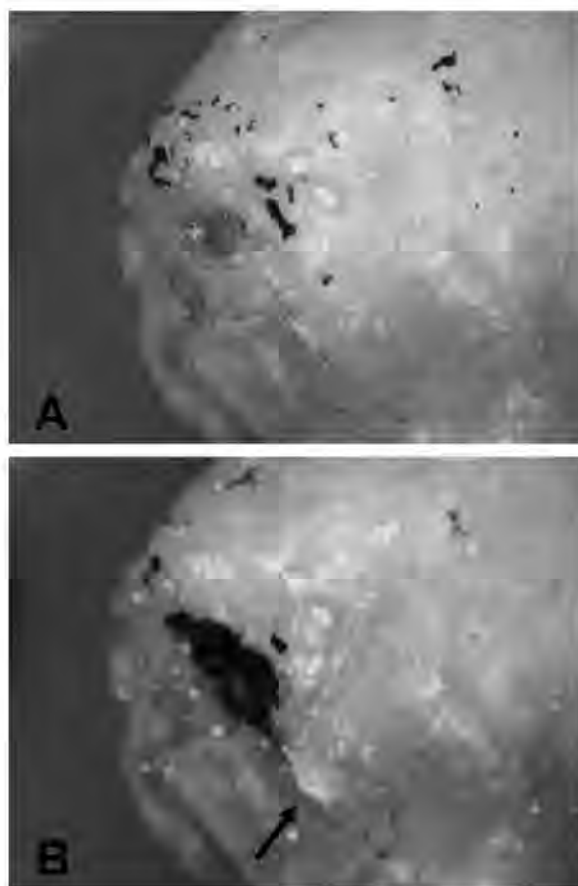


Figure 1. Representative image of an apical crack in group A. (A) Preoperative image. (B) Image obtained after using a #15 SF file. The arrow indicates the crack.

Basic Research—Technology

8. Blum JY, Machtou P, Micallef JP. Location of contact areas on rotary Profile instruments in relationship to the forces developed during mechanical preparation on extracted teeth. *Int Endod J* 1999;32:108–14.
9. Isom TL, Marshall JG, Baumgartner JC. Evaluation of root thickness in curved canals after flaring. *J Endod* 1995;21:368–71.
10. Lam PPS, Palamara JEA, Messer HH. Fracture strength of tooth roots following canal preparation by hand and rotary instrumentation. *J Endod* 2005;31:529–32.
11. Roane JB, Sabala CL, Meredith N, et al. The “balanced force” concept for the instrumentation of curved canals. *J Endod* 1985;11:205–11.
12. Okitsu M, Takahashi H, Yoshioka T, et al. Effective factors including periodontal ligament on vertical root fractures. *Dent Mater J* 2005;24:66–9.
13. Akkayan B, Gülmez T. Resistance to fracture of endodontically treated teeth restored with different post systems. *J Prosthet Dent* 2002;87:431–7.
14. Sirimai S, Riis DN, Morgano SM. An in vitro study of the fracture resistance and the incidence of vertical root fracture of pulpless teeth restored with six post-and-core systems. *J Prosthet Dent* 1999;81:262–9.
15. Blum JY, Machtou P, Esber S, et al. Analysis of forces developed during root canal preparation with the balanced force technique. *Int Endod J* 1997;30:386–96.
16. Maybaw JT, Eleazer PD, Hnat WP. Stress analysis of human tooth root using various root canal instruments. *J Endod* 2000;26:523–4.
17. Card SJ, Sigurdsson A, Ørstavik D, et al. The effectiveness of increased apical enlargement in reducing intracanal bacteria. *J Endod* 2002;55:752–8.
18. Weiger R, Barthel T, Kalwitski M, et al. A clinical method to determine the optimal apical preparation size. Part I. *Oral Surg Oral Med Oral Pathol Endod* 2006;102:686–91.
19. Kishen A. Mechanisms and risk factors for fracture predilection in endodontically treated teeth. *Endod Top* 2006;13:57–83.
20. Sathorn C, Palamara JEA, Messer HH. A comparison of the effects of two canal preparation techniques on root fracture susceptibility and fracture pattern. *J Endod* 2005;31:283–7.
21. Kishen A, Kumar GV, Chen NN. Stress-strain response in human dentine: rethinking fracture predilection in postcore restored teeth. *Dent Traumatol* 2004;20:90–100.

M E M O

[illegible]

歯周病学分野

和泉 雄一

医歯学総合研究科・生体支持組織学系専攻・教授
歯周病学／歯学博士



1) 研究の課題名

全身疾患（糖尿病およびバジュー病）とリスクファクターとしての歯周病：その連関と関連メカニズム

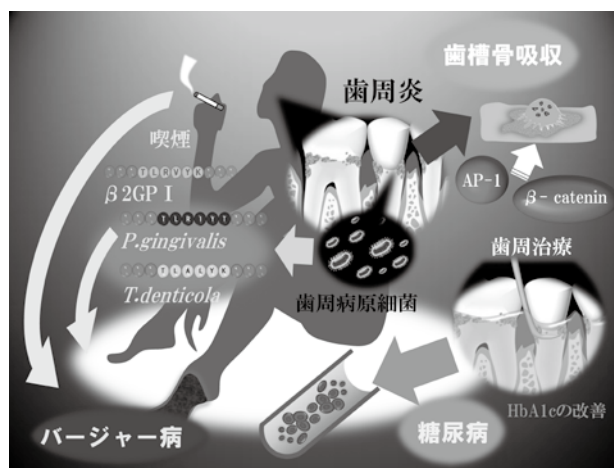
Study on association between periodontitis and systemic diseases (diabetes and Buerger's disease) : The link and relevant mechanisms

歯周病と全身疾患との関連性について研究を進めている。今回、2型糖尿病について、局所抗菌療法を含む歯周治療の多施設介入試験を行い、歯周治療がグリコヘモグロビン（HbA1c）レベルと高感度C-反応性蛋白（hs-CRP）に及ぼす影響およびCRPと血糖コントロールとの関係について検討した。5施設で総計49名（年齢:39-75歳、HbA1c:6.5-10%）の2型糖尿病患者が参加した。2ヵ月間の歯周治療を行い、術後1、3、6ヵ月に検査を実施した。その結果、歯周病を伴う2型糖尿病患者には抗菌剤の局所投与が有効であり、HbA1cレベルの低下すなわち血糖コントロールの改善とhs-CRPの低下に寄与することを認めた。

バジュー病は四肢抹消血管に閉塞をきたす閉塞性血栓血管炎である。今回、バジュー病に誘導される抗cardiolipin抗体と歯周病との関連について検討した。

Osteoprotegerin（OPG）はRANKLのおとりレセプターであり、歯周病患者の歯槽骨吸収はOPGとRANKLとのバランスの上に成り立っている。今回、 β -cateninとAP-1が歯根膜細胞（PDL）および歯肉線維芽細胞（hGFs）のOPG産生を違った形で調節していること、c-fosの発現がhGFsよりPDLでより高度であることを明らかにした。

2)



3) 研究内容の英文要約

Multi-center intervention study revealed periodontal treatment improved HbA1c through reduction of CRP, which may relate to amelioration of insulin resistance, in type 2 diabetic patients with periodontal disease. Buerger's disease is a non-atherosclerotic, segmental, inflammatory occlusive vascular disease. Periodontopathic bacteria such as *P. gingivalis* and *T. denticola* were detected in both saliva and arterial specimens of the Buerger's disease patients by a PCR analysis, while none of the control arterial samples without Buerger's disease was positive for these bacteria. Higher IgG titers against periodontopathic bacteria and also elevated anti-cardiolipin antibody levels were associated with periodontal destruction in Buerger's disease patient, thus indicating that these bacteria might trigger immune responses and play a significant role in the pathogenesis of Buerger's disease. Osteoprotegerin (OPG) plays a suppressive role in cytokine-induced osteoclastogenesis. We carried out to examine the regulatory roles of β -catenin and AP-1 on OPG production in interleukin-1 α -stimulated periodontal ligament cells. The present study suggests that

β -catenin enhances IL-1 α -induced OPG production in both PDL cells and hGFs, whereas AP-1 suppresses IL-1 α -induced OPG production in PDL cells. Higher expression of c-fos in PDL cells than in hGFs may implicate a role of PDL cells in alveolar bone resorption in periodontitis.

4) 本事業に関連しての改善・整備等

A (研究拠点体制)

米国UCSFのMark Raider教授およびタイ国Khon Kaen大学のNawarat W Charoen准教授との研究協力体制を樹立した。

B (研究教育環境)

大学院講義を英語で実施し英語に親しむ環境の構築に努めた。4月の医局の引越しに際して、実験室の整備および改修を実施した。

C (人材確保)

7人のAISSを獲得した。大学院院生を新規に9名受け入れた。

D (人材育成)

新人教育に力を入れ、研究面ではNawarat先生に何人かの大学院生の指導をお願いした。

E (国際化)

- 1) 第16回GCOE海外研究者招聘講演会(Dr. Nawarat W Charoen: IL-1 β gene expression control and IL-1 signaling. 2009.9.18)を主催した。
- 2) タイ国Srinakharinwirot大学との大学間交流の準備に携わった。

5) GCOE事業を推進するに当たって力を入れた点

若い研究者に出来る限り国際化の意識を植え付けるように努めた。

6) 英文論文(原著、総説)

1. ©Chen YW, Nagasawa T, Nawarat WA, Ushida Y, Wang DQ, Takeuchi Y, Kobayashi H, Umeda M, Inoue Y, Iwai T, Ishikawa I, Izumi Y. Association between periodontitis and anti-cardiolipin antibodies in Buerger disease. J Clin Periodontol 36(10): 830-835, 2009.
2. ©Eguro T, Aoki A, Maeda T, Takasaki AA, Hasegawa M, Ogawa M, Suzuki T, Yonemoto K, Ishikawa I, Izumi Y, Katsuumi I. Energy Output Reduction and Surface Alteration of Quartz and Sapphire Tips Following Er:YAG Laser Contact Irradiation for Tooth Enamel Ablation. Laser Surg Med 41:595-604, 2009.
3. ©Kayamori K, Sakamoto K, Nakashima T,

Takayanagi H, Morita K, Omura K, Nguyen ST, Miki Y, Iimura T, Himeno A, Akashi T, Yamada-Okabe H, Ogata E, Yamaguchi A. Roles of IL-6 and PTHrP in osteoclast formation associated with oral cancers: The significance of IL-6 synthesized by stromal cells in response to cancer cells. The American Journal of Pathology

4. Katagiri S, Nitta H, Nagasawa T, Uchimura I, Izumiyama H, Inagaki K, Kikuchi T, Noguchi T, Kanazawa M, Matsuo A, Chiba H, Nakamura N, Kanamura N, Inoue S, Ishikawa I, Izumi Y. Multi-center intervention study on glycohemoglobin (HbA1c) and serum, high-sensitivity CRP (hs-CRP) after local anti-infectious periodontal treatment in type 2 diabetic patients with periodontal disease. Diabetes Research and Clinical Practice 83: 308-315, 2009.
5. Kobayashi T, Nagata T, Murakami S, Takashiba S, Kurihara H, Izumi Y, Numabe Y, Watanabe H, Kataoka M, Nagai A, Hayashi J, Ohshima H, Okamoto Y, Inagaki Y, Tai H, Yoshie H, Genetic risk factor for periodontitis in a Japanese population. J Dent Res 88(12):1137-1141, 2009.
6. Miyazaki H, Kato J, Kakizaki H, Nagata T, Uetake H, Okudera H, Watanabe H, Hashimoto K, Omura K. Submucosal glycerol injection assisted laser surgical treatment of oral lesions. Lasers Med Sci 24:13-19, 2009.
7. Miyazaki H, Kato J, Watanabe H, Harada H, Kakizaki H, Tetsumura A, Sato A, Omura K. Intralesional laser treatment of voluminous vascular lesions in the oral cavity. Oral Surgery, Oral Med Oral Pathol Oral Radiol Endodont 107(2):164-172, 2009.
8. ©Sato I, Akizuki T, Oda S, Tsuchioka H, Hayashi C, Takasaki AA, Mizutani K, Kawakatsu N, Kinoshita A, Ishikawa I, Izumi Y. Histological evaluation of alveolar ridge augmentation using injectable calcium phosphate bone cement in dogs. J Oral Rehabil 36 762-769, 2009.
9. ©Suda T, Nagasawa T, Wara-aswapati N, Kobayashi H, Iwasaki I, Yashiro R, Hormdee D, Nitta H, Ishikawa I and Izumi I. Regulatory roles of β -catenin and AP-1 on OPG production in IL-1 α -stimulated periodontal ligament cells. Oral Microbiol Immunol 24(5):384-389, 2009.
10. Yamashita D, Machigashira M, Miyamoto M, Takeuchi H, Noguchi K, Izumi Y, Ban S. Effect of surface roughness on initial responses of osteoblast-like cells on two types of zirconia Dent Mater J 28(4): 461-470, 2009
11. Yoshino T, Aoki A, Oda S, Takasaki AA, Mizutani K, Sasaki KM, Kinoshita A, Watanabe H, Ishikawa I, Izumi Y. Long-term Histologic Analysis of Bone Tissue Alteration and Healing Following Er:YAG Laser

- Irradiation Compared to Electrosurgery. J Periodontol 80(1): 82-92, 2009.
12. Ishikawa I, Aoki A, Takasaki AA, Mizutani K, Sasaki KM, Izumi Y. Application of lasers in periodontics - true innovation or myth? Periodontology 2000, 50(1): 90-126, 2009.
 13. © Izumi Y, Nagasawa T, Umeda M, Kobayashi H, Takeuchi Y, Yashiro R, Hormdee D, Suda T, Ushida Y, Nawarat WA. Periodontitis and cardiovascular diseases: The link and relevant mechanisms. Japanese Dental Science Review 45: 98-108, 2009.
 14. Schwarz F, Aoki A, Sculean A, Becker J. Impact of laser application to support periodontal and peri-implant wound healing. Periodontology 2000 51:79-108, 2009.
 15. Takasaki AA, Aoki A, Mizutani K, Schwarz F, Sculean A, Wang C-Y, Koshy G, Romanos G, Ishikawa I, Izumi Y. Application of Antimicrobial Photodynamic Therapy in Periodontal and Peri-implant Diseases. Periodontology 2000 51:109-140, 2009.
 16. Aoki A, Mizutani K, Takasaki AA, Sasaki KM, Nagai S, Schwarz F, Yoshida I, Eguro T, Zeredo JL, Izumi Y. Part-I. Dentists of Taipei County, No.173: 22-26, Jan-Feb 2009.
 17. Aoki A, Mizutani K, Takasaki AA, Sasaki KM, Nagai S, Schwarz F, Yoshida I, Eguro T, Zeredo JL, Izumi Y. Part-II. Dentists of Taipei County, No.174: 8-23, Mar-Apr 2009.
- ## 7) 著書
1. 長澤敏行, 和泉雄一. 歯周疾患 (歯周病) について. 編集/和泉雄一, 沼部幸博, 山本松男, 木下淳博. ザ・ペリオドントロジー 全294項. 永末書店 京都. 2009 p.22-23
 2. 梅田誠, 和泉雄一. 小児の歯周疾患. 編集/和泉雄一, 沼部幸博, 山本松男, 木下淳博. ザ・ペリオドントロジー 全294項. 永末書店 京都. 2009 p.86-87
 3. 矢代麗子, 和泉雄一. 歯周疾患の検査 2. その他の検査 5) ~6). 編集/和泉雄一, 沼部幸博, 山本松男, 木下淳博. ザ・ペリオドントロジー 全294項. 永末書店 京都. 2009 p.108-109
 4. 水谷幸嗣, 和泉雄一. スケーリング・ルートプレーニング〈アドバンス編〉象牙質知覚過敏症. 編集/和泉雄一, 沼部幸博, 山本松男, 木下淳博. ザ・ペリオドントロジー 全294項. 永末書店 京都. 2009 p.139
 5. 矢代麗子, 小田 茂. 暫間固定, 和泉雄一, 沼部幸博, 山本松男, 木下淳博編集, ザ・ペリオドントロジー, 永末書店, 京都, 2009年10月, 140-141.
 6. 青木 章, 渡辺 久. 歯周形成手術〈アドバンス編〉レーザー. 編集/和泉雄一, 沼部幸博, 山本松男, 木下淳博. ザ・ペリオドントロジー 全294項. 永末書店 京都. 2009 p.165-168.
 7. 荒川真一, 和泉雄一. エナメルマトリックス. 編集/和泉雄一, 沼部幸博, 山本松男, 木下淳博. ザ・ペリオドントロジー 全294項. 永末書店 京都. 2009 p.177-178
 8. 秋月達也, 小田 茂. 再生治療アドバンス編3, 和泉雄一, 沼部幸博, 山本松男, 木下淳博編集, ザ・ペリオドントロジー, 永末書店, 京都, 2009年10月, 182-183.
 9. 秋月達也, 小田 茂. 咬合治療, 和泉雄一, 沼部幸博, 山本松男, 木下淳博編集, ザ・ペリオドントロジー, 永末書店, 京都, 2009年10月, 190-192.
 10. 宮田 敦, 小田 茂. 咬合治療アドバンス, 和泉雄一, 沼部幸博, 山本松男, 木下淳博編集, ザ・ペリオドントロジー, 永末書店, 京都, 2009年10月, 193-195.
 11. 竹内康雄, 小田 茂. 歯周治療での修復・補綴治療, 和泉雄一, 沼部幸博, 山本松男, 木下淳博編集, ザ・ペリオドントロジー, 永末書店, 京都, 2009年10月, 200-2003.
 12. 荒川真一, 和泉雄一. 高齢者の歯周治療 高齢者の歯周疾患. 編集/和泉雄一, 沼部幸博, 山本松男, 木下淳博. ザ・ペリオドントロジー 全294項. 永末書店 京都. 2009 p.221-224
 13. 荒川真一, 和泉雄一. Down症と歯周炎. 編集/和泉雄一, 沼部幸博, 山本松男, 木下淳博. ザ・ペリオドントロジー 全294項. 永末書店 京都. 2009 p.244-246
 14. 渡辺 久. 低ホスファターゼ症. 編集/和泉雄一, 沼部幸博, 山本松男, 木下淳博. ザ・ペリオドントロジー 全294項. 永末書店 京都. 2009 p.247-248
 15. 荒川真一, 和泉雄一. 歯周病のリスクファクター. 編集/和泉雄一, 沼部幸博, 山本松男, 木下淳博. ザ・ペリオドントロジー 全294項. 永末書店 京都. 2009 p.256-259
 16. 片桐さやか, 和泉雄一. 歯周病と糖尿病. 編集/和泉雄一, 沼部幸博, 山本松男, 木下淳博. ザ・ペリオドントロジー 全294項. 永末書店 京都. 2009 p.261-262
 17. 小林宏明, 和泉雄一. 歯周病と肥満. 編集/和泉雄一, 沼部幸博, 山本松男, 木下淳博. ザ・ペリオドントロジー. 全294項. 永末書店 京都. 2009 p.263-264
 18. 梅田誠, 和泉雄一. 歯周病と動脈疾患 (動脈硬化疾患). 編集/和泉雄一, 沼部幸博, 山本松男, 木下淳博. ザ・ペリオドントロジー 全294項. 永末書店 京都. 2009 p.265-266
 19. 岩崎剣吾, 和泉雄一. 歯周病と骨粗鬆症. 編集/和泉雄一, 沼部幸博, 山本松男, 木下淳博. ザ・ペリオドントロジー 全294項. 永末書店 京都. 2009 p.268

20. 青木章, 和泉雄一. 歯周病と早産・低体重児出産. 編集/和泉雄一, 沼部幸博, 山本松男, 木下淳博. ザ・ペリオドントロジー 全294項. 永末書店 京都. 2009 p.270-271
21. 萩原さつき, 和泉雄一. 歯周病と肺炎. 編集/和泉雄一, 沼部幸博, 山本松男, 木下淳博. ザ・ペリオドントロジー 全294項. 永末書店 京都. 2009 p.272
22. 和泉雄一, 古市保志, 野口和行, 長谷川梢. 早産・低体重児出産. 編著: 中原泉, 鴨井久一. 口腔と全身疾患歯科医療は医学を補完する. クインテッセンス出版株式会社 東京. 2009年6月 p.156-162
23. 和泉雄一, 迫田賢二. インプラント治療に必要な解剖学的知識. 古谷野潔, 松浦正朗編著. エッセンシャル 口腔インプラント学. 医歯薬出版株式会社. 2009 p.24-29
24. 和泉雄一, 中村利明. インプラントの骨および軟組織の界面の反応. 古谷野潔, 松浦正朗編著. エッセンシャル 口腔インプラント学. 医歯薬出版株式会社. 2009 p.30-33
25. 和泉雄一, 町頭三保. インプラント治療の特徴 リスクファクター. 古谷野潔, 松浦正朗編著. エッセンシャル 口腔インプラント学. 医歯薬出版株式会社. 2009 p.64-67
26. 和泉雄一, 小田茂, 秋月達也, 高崎アリストオ敦志, 須田智也. GTR法の術式. 山田了編. ステップアップ GTR 歯周組織再生誘導法. 医歯薬出版株式会社. 2009 p.36-47
27. 竹内康雄, 和泉雄一. Column9 おさえておきたい歯周病に関連する細菌の知識. デンタルハイジーン別冊 歯科衛生士のためのペリオドンタルメディシン 全身の健康と歯周病とのかかわり. 医歯薬出版, 東京. p.88-89, 2009.
28. 和泉雄一, 荒川真一. クインテッセンス イヤーブック 2009 現代の治療指針 歯周治療と全治療分野編 (190-191) モチベーションとプラークコントロールの実践 クインテッセンス出版株式会社 2009年1月10日.
29. 和泉雄一. 序文. 編集: 和泉雄一. 季刊 歯科医療 vol.23 No.2 特集 進歩する歯周組織再生治療の分類と臨床. 第一歯科出版 2009春号 p.4-5
30. 秋月達也, 和泉雄一. 歯周組織再生療法の分類 基礎と臨床 2) GTR. 編集: 和泉雄一 季刊 歯科医療 vol.23 No.2 特集 進歩する歯周組織再生治療の分類と臨床. 第一歯科出版 2009春号 p.14-18
31. 和泉雄一, 荒川真一. 季刊・歯科医療 2009年春号 Vol.23, No.2. p.19-23. 進歩する歯周組織再生治療の分類と臨床: 1. 歯周組織再生治療の分類と基礎と臨床 3) 根面処理 化学的根面処理 (クエン酸等)、生物学的根面処理 (エムドゲイン処理) 第一歯科出版株式会社.
32. 荒川真一, 和泉雄一, 眞野喜洋, 月刊 Materials Integration Vol 22, No.5 (2009) 2009年5月号 特集 特集 マイクロ・ナノバブル (1) いろいろつかえる マイクロ・ナノバブル 6. ナノバブル水の歯周治療への応用 p. 36-43.
33. 和泉雄一, 荒川真一. 遺伝子医学 p. 126-130. MOOK 13, 患者まで届いている再生誘導治療 第2章 生体シグナル因子の利用 1. 細胞増殖因子 9) 歯周組織: 歯周組織再生療法への応用 発行: 株式会社メディカルドゥ、2009年5月31日 第一版 田端康彦編集.
34. 吉江弘正, 川浪雅光, 池田雅彦, 坂上竜資, 高柴正悟, 角田正健, 三辺正人, 渡辺 久, 菅谷 勉, 内藤 徹, 児玉利朗, 三上 格, 宮田 敦 編著: 歯周病の検査・診断・治療計画の指針 2008. 日本歯周病学会 東京 2009 総頁: 49頁
35. 青木 章, 水谷幸嗣, 和泉雄一. Er:YAG レーザーの歯周治療への臨床応用. めざせ! 健・口・美—未来に向けた歯科医療—, 第21回日本歯科医学会総会, 歯科医展望特別号, pp.238, 2009.
36. 渡辺 久, 青木 章, 和泉雄一. レーザーの Biostimulation 効果のメカニズムに関する研究. めざせ! 健・口・美—未来に向けた歯科医療—, 第21回日本歯科医学会総会, 歯科医展望特別号, pp.280, 2009.
37. Schwarz F, Takasaki A, Aoki A, Sager M, Becker J. Antimicrobial photodynamic therapy. In: Schwarz F and Becker J. Peri-implant Infection: Etiology, Diagnosis and Treatment. Pp. 191-195. Quintessence, 2009.
38. 小田 茂, 坂井雅子, 岩崎剣吾, 秋月達也. 3章治療計画と歯科衛生士との関わり, 日本歯周病学会編, 歯科衛生士のための歯周治療ガイドブック キャリアアップ・認定資格取得をめざして, 医歯薬出版, 東京, 2009年9月, 43-66.
39. 和泉雄一, 小田 茂, 秋月達也, 水谷幸嗣, 鈴木充文. GC 友の会 SRP トレーニング DVD マスターしよう! SRP -SRP Basic-, 2009年8月, 株式会社GC, 東京.
40. 和泉雄一, 荒川真一. モチベーションとプラークコ

- ントロールの実際,別冊 The Quintessence YEAR BOOK2009・現代の治療指針 欠損・審美補綴と全治療分野編.クインテッセンス出版株式会社.2009年1月 p.190-191
41. 和泉雄一.サテライトシンポジウム② あすの歯科臨床につながる基礎研究とその成果.歯界展望 特別号 めざせ!健・口・美 未来に向けた歯科医療 第21回日本歯科医学会総会.医歯薬出版株式会社.2009年6月 p.217
42. 中村利明,野口和行,和泉雄一.循環器疾患の患者さんへの歯周治療 高血圧患者への歯周治療.沼部幸博,和泉雄一 編著.月刊デンタルハイジーン別冊 歯科衛生士のためのペリオドンタルメディシン 全身の健康と歯周病とのかかわり.医歯薬出版株式会社.2009年5月 p.30-33
43. 長谷川梢,野口和行,和泉雄一.妊産婦への歯周治療.沼部幸博,和泉雄一 編著.月刊デンタルハイジーン別冊 歯科衛生士のためのペリオドンタルメディシン 全身の健康と歯周病とのかかわり.医歯薬出版株式会社.2009年5月 p.42-47
44. 梅田誠,和泉雄一.循環器疾患(心疾患・脳血管疾患等)と歯周病.沼部幸博,和泉雄一 編著.月刊デンタルハイジーン別冊 歯科衛生士のためのペリオドンタルメディシン 全身の健康と歯周病とのかかわり.医歯薬出版株式会社.2009年5月 p.82-89
45. 古市保志,長谷川梢,和泉雄一.早産・低体重児出産と歯周病.沼部幸博,和泉雄一 編著.月刊デンタルハイジーン別冊 歯科衛生士のためのペリオドンタルメディシン 全身の健康と歯周病とのかかわり.医歯薬出版株式会社.2009年5月 p.96-101
46. 水谷幸嗣,和泉雄一.服用薬剤による口腔内への影響と歯周治療.沼部幸博,和泉雄一 編著.月刊デンタルハイジーン別冊 歯科衛生士のためのペリオドンタルメディシン 全身の健康と歯周病とのかかわり 医歯薬出版株式会社 2009年5月 p.23
47. 梅田誠,和泉雄一.バーチャ病と歯周病.沼部幸博,和泉雄一 編著.月刊デンタルハイジーン別冊 歯科衛生士のためのペリオドンタルメディシン 全身の健康と歯周病とのかかわり.医歯薬出版株式会社.2009年5月 p.34-35
48. 竹内康雄,和泉雄一.おさえたい歯周病に関連する細菌の知識.沼部幸博,和泉雄一 編著.月刊デンタルハイジーン別冊 歯科衛生士のためのペリオドンタルメディシン 全身の健康と歯周病とのかかわ

り.医歯薬出版株式会社.2009年5月 p.88・89

49. 和泉雄一,片桐さやか.糖尿病と相互に関連し合う全身疾患 歯周病.PRACTICE別冊プラクティス 糖尿病と全身疾患.(社)日本糖尿病協会 医歯薬出版株式会社.P.134-140
50. 塩山秀裕,水谷幸嗣,和泉雄一.ヒトの歯肉退縮欠損に対する、歯肉弁歯冠側移動術と組換え型精製ヒト血小板由来成長因子-BB含有 β リン酸三カルシウムもしくは結合組織移植併用治療.組織評価およびマイクロコンピュータ断層撮影(マイクロCT)による評価(翻訳). Int J Periodont Rest Dent 日本語版. 2009; 17 (2) : 11-21.

8) 特許取得、特許申請

青木章,小田茂.歯科用歯石除去ヘッド.意匠登録第1176973号,2009.

9) 自己評価

今年度の研究課題についてはほぼ予定通りの進行を示している。また、研究拠点体制作りでは、タイのKhon Kaen大学のNawarat W Charoen准教授とのコラボレーションが順調に進んでいる。

10) 和文論文(原著、総説)

- 津久井 明、渡辺 久:Er:YAGレーザーによる根面被覆(半月弁切開移動術)への応用 日レ歯誌 20:2-8,2009.
- 荒川真一,和泉雄一,眞野喜洋.オゾン,酸素ナノバブル水の臨床応用に向けて 総説 p/253-259 東京都病院薬剤師会雑誌 Vol. 58, No. 4, 2009.8.31.
- 和泉雄一,水谷幸嗣,青木章.国際歯科ニュース:光による新しい歯周治療-antimicrobial Photodynamic Therapy.日本歯科医師会雑誌 62 (8) : 94-96 (888-890), 2009.
- 石橋寛二、吉江弘正、川浪雅光、池田雅彦、山森徹雄、坂上竜資、池田和博、角田正健、安田 登、高柴正悟、渡邊文彦、三邊正人、伊藤創造、渡辺 久、山田 了、平井敏博:「歯周病患者に対する補綴歯科治療のありかた」に関する提案書 日歯周誌 51 (2) :191-212, 2009.
- 小田 茂,竹内康雄.5.非外科治療,季刊歯科医療,23巻,No.2,64-71,2009.
- 小田 茂,岩崎剣吾.根拠ある!歯周治療の診査・検査～すべての対応には理由がある～ 第2回.時間軸で変わる診査・検査の意義,歯科衛生士,33巻,No.4,44-

48,2009.

7. 小田 茂, 岩崎剣吾. 根拠ある! 歯周治療の診査・検査 ~すべての対応には理由がある~ 第1回. 診査・検査の意義を理解しよう, 歯科衛生士, 33巻, No.3, 38-42, 2009.

11) 学会発表 (英文)

1. Tanaka K, Iwasaki K, Feghali K, Yashiro R, Izumi Y. : Characteristics of periodontal ligament cells isolated using different methods. 87th General session of international association of dental research. (2009.4.1-4. maiami)
2. Aoki A, Namiki N, Takasaki AA, Sasaki KM, Mizutani K, Takagi C, Yoshino J, Umeda M, Watanabe H, Ishikawa I, Izumi Y. The bactericidal effect of blue lights on a periodontal pathogen. Academy of Laser Dentistry 16th Annual Conference, Las Vegas, Nevada, USA, Apr 22-25, 2009.
3. Watanabe H, Takeuchi Y. Persimmon polyphenol oligomer shows bacteriostatic activity against *Porphyromonas gingivalis*. *Europrio* 6, J Clin Periodontol 36 (suppl 9) : 1 (2009. 6. 4-6, Stockholm, Sweden)
4. ©Aleksic V, Aoki A, Iwasaki K, Takasaki AA, Izumi Y. Low-level Er:YAG laser irradiation can enhance proliferation of osteoblasts. 6th Congress of the European Federation of Periodontology (*Europrio* 6) , Stockholm, Sweden, June 4 - 6, 2009.
5. ©Ebe N, Yokoyama M, Iwasaki K, Yanagishita M, Izumi Y. High-mobility group box 1 release from human gingival epithelial cells during apoptosis. J Clin Periodontol 36 (Suppl. 9) pp. 6, 2006. *Europrio* 6 (2009. 6.4-6.6, stockholm, sweden)
6. Onishi H, Arakawa S, Nakajima T, Izumi Y. Protective role of anti-FDF antibody in gingival crevicular fluid of periodontitis patients. J Clin Periodontol 36 (Suppl. 9) pp. 6, 2006. *Europrio* 6 (2009. 6.4-6.6, stockholm, sweden)
7. Aoyama N, Suzuki J, Wang D, Ogawa M, Takeuchi Y, Isobe M, Izumi Y. Infection of periodontal bacteria accelerates progression of abdominal aortic aneurysms with altered expression of MMPs and TIMPs. The American Academy of Periodontology (AAP) 95th annual meeting. (2009.9.12-15. Boston)
8. Yashiro R, Wara-aswapati N, Nagasawa T, Nanbara H, Bando Y, Kobayashi H, Izumi Y. Modulation of Wnt5a Expression by Periodontopathic Bacteria. The American Academy of Periodontology (2009.9.12-15 Boston. USA)
9. Aoyama N, Suzuki J, Ogawa M, Kobayashi N, Hanatani T, Takeuchi Y, Izumi Y, Isobe M. Matrix Metalloproteinases play a key role in the progression of abdominal aortic aneurysms with infection of periodontal bacteria. Asian Chapter Meeting of the International Union of Angiology 2009. (2009.10.29-30. Tokyo)
10. ©Himeno A, Sugiyama M, Sakaue-Sawan A, Miyawaki A, Izumi Y, Yamaguchi A, Iimura T. Spatio-temporal mapping of cell cycle progression during skeletogenesis and odontogenesis. The 26th Naito Conference on OSTEOBIOLOGY. (2009. 11. 4-7. Awaji Yumebutai International Conference Center)
11. Aoyama N, Suzuki J, Ogawa M, Izumi Y, Hirata Y, Nagai R, Isobe M. Clarithromycin Attenuates Periodontal Bacteria-Induced Abdominal Aortic Aneurysms with Altered Expression of Matrix Metalloproteinases. American Heart Association Scientific Sessions 2009. (2009.11.14-18. Orlando)
12. Taniguchi Y, Aoki A, Mizutani K, Takeuchi Y, Takasaki AA, Y. Izumi Y. Determination of optimal irradiation parameters for debridement of micro-structured surface of titanium implant with a high-pulse-rate Er:YAG laser. The 12th congress of the World Federation for lasers Dentistry (WFLD) , Dubai, 2010. 3. 9-11.
13. ©Aleksic V, Aoki A, Iwasaki K, Takasaki AA, Wang C-Y, Abiko Y, Ishikawa I, Izumi Y. Low-level Er:YAG laser irradiation enhances osteoblast proliferation through activation of MAPK/ERK. The 12th congress of the World Federation for lasers Dentistry (WFLD) , Dubai, 2010. 3. 9-11.
14. Watanabe H, Taniguchi Y, Izumi Y. The precise incision by Er:YAG laser for making flap in periodontal surgery. The 12th congress of the World Federation for lasers Dentistry (WFLD) , Dubai, 2010. 3. 9-11.

12) 学会発表 (和文)

1. 青山典生, 鈴木淳一, 王冬青, 小川真仁, 田村典子, 竹内康雄, 和泉雄一, 磯部光章: *Porphyromonas gingivalis* Infection Promotes Development of Abdominal Aortic Aneurysm in Mice. 第73回日本循環器学会学術集会 (2009.3.20-22. 大阪)
2. 青木 章, 木下淳博, 和泉雄一. 侵襲性歯周炎患者の長期治療経過. 第52回春季日本歯周病学会学術大会, 岡山, 2009.5.15-16.
3. アレクシチ ヴェリツァ, 青木 章, 岩崎剣吾, 王 振穎, 和泉雄一. Low-level Er:YAG laser irradiation can enhance proliferation of osteoblasts. 第52回春季日本歯周病学会学術大会, 岡山, 2009.5.15-16.
4. 江部 典子, 横山 三紀, 岩崎 剣吾, 柳下 正樹, 和泉 雄一. アポトーシスによるヒト歯肉上皮細胞からの HMGB1 放出 日歯周誌51 (春季特別号) pp.107, 2009. 第51回春季日本歯周病学会 (2009.5.15, 岡山)
5. 青山典生, 鈴木淳一, 竹内康雄, 磯部光章, 和泉雄一: *Porphyromonas gingivalis* 感染による腹部大動脈

- 瘤の形成促進.第52回春季日本歯周病学会学術大会 (2009.5.15-16. 岡山)
6. 竹内康雄,坂東由記子,長澤敏行,南原弘美,小林宏明,和泉雄一.次亜塩素酸電解水の抗菌作用と細胞毒性の検討.日本歯科保存学会プログラムおよび講演抄録集 p49,2009.第130回日本歯科保存学会春期学術大会 (2009.6.11. 札幌)
 7. 高松 秀行,片桐 さやか,新田 浩,長澤 敏行,牛田 由佳,小林 宏明,小柳 達郎,鈴木 允文,高橋 充,谷口 陽一,寺地 真由,南原 弘美,早雲 彩絵,姫野 彰子,和田 真由子,和泉 雄一.2型糖尿病患者の歯周基本治療におけるHbA1c及び歯周病原細菌に対する血清IgG抗体価への影響 日歯周誌51 (秋季特別号) p100, 2009. 第52回秋季日本歯周病学会学術大会 (2009.10.11. 宮崎)
 8. 青山典生,鈴木淳一,小林奈穂,花谷智哉,竹内康雄,磯部光章,和泉雄一:動脈壁でのmatrix metalloproteinase発現量と血管病変に対する歯周病原細菌感染の影響.第52回秋季日本歯周病学会学術大会 (2009.10.11. 宮崎)
 9. 田中敬子,岩崎剣吾,矢代麗子,石川烈,和泉雄一:細胞移植に有用なヒト歯根膜細胞の採取法.第51回秋季日本歯周病学会学術大会 (2009.10.18-19. 宮崎)
 10. 和田真由子,片桐さやか,小林宏明,竹内康雄,谷口陽一,南原弘美,高松秀行,新田浩,長澤敏行,Bharti Pariksha,和泉雄一.2型糖尿病患者における歯周治療の影響.日本歯科保存学会プログラムおよび講演抄録集 p226,2009.第131回日本歯科保存学会秋期学術大会 (2009.10.29. 仙台)
 11. 渡辺 久,竹内康雄,和泉雄一.柿ポリフェノールオリゴマーによる抗菌および抗酸化作用.日本歯科保存学会プログラムおよび講演抄録集 p226,50.第131回日本歯科保存学会秋期学術大会 (2009.10.29. 仙台)
 12. 水谷 幸嗣,青木 章,谷口 陽一,和泉 雄一. Er:YAGレーザーによるフラップレス骨整形.第21回日本レーザー歯学会総会・学術大会,福岡,2009.11.22-23.
 13. 渡辺 久,谷口陽一,和泉雄一.Er:YAGレーザーによる軟組織切開能の検討.第21回日本レーザー歯学会総会・学術大会,福岡,2009.11.22-23.
 14. 萩原さつき,山口博之,和泉雄一:歯周治療のメンテナンスに影響する臨床的な要因について.第74回口腔病学会学術大会 (2009.12.5. 東京)
 15. 大塚鉦未,須永昌代,吉田有里,木下淳博,小林宏明,片桐さやか,和泉雄一,趙 永哲,田上 順次:歯周

外科治療におけるライブ講義の実施と評価 第74回口腔病学会学術大会 (2008.12.5)

16. 江部典子,横山三紀,岩崎剣吾,柳下正樹,和泉雄一.アポトーシスによるヒト歯肉上皮細胞からのHMGB1放出.第74回口腔病学会学術大会 (2009.12.5. 東京)
17. 穂山文彦,青木 章,和泉 雄一.Er:YAGレーザーの歯周病罹患根面に対する除菌効果.第74回口腔病学会学術大会 (2009.12.5. 東京)

13) 受賞

1. Izumi Y: R Earl Robinson Periodontal Regeneration Award, American Academy of Periodontology. (2009.9.15. Boston)
2. 青木 章.日本歯周病学会優秀臨床ポスター賞受賞.侵襲性歯周炎患者の長期治療経過 (青木 章,木下淳博,和泉雄一.侵襲性歯周炎患者の長期治療経過.第52回春季日本歯周病学会学術大会,岡山, 2009.5.16) .第52回秋期歯周病学会, 2009.10.11.
3. Himeno A, Sugiyama M, Sakaue-Sawano A, Miyawaki A, Izumi Y, Yamaguchi A, Iimura T. 第38回内藤記念特定研究助成金受賞. Spatio-temporal mapping of cell cycle progression during skeletogenesis and odontogenesis. (The 26th Naito Conference on OSTEOBIOLOGY, Awaji, 2009. 11. 5, Poster Presentation) (2009.11.7, Awaji)

14) 外部資金獲得状況

1. 和泉雄一 (代表): 器官形成シグナルのコントロールを基盤にした歯周病に対する新規治療戦略. 科学研究費補助金,基盤研究 (B) (新規) 平成21~23年度.研究費総額:935万円
2. 梅田 誠 (代表): 血管系疾患に関与する歯周病原細菌の特定と検証. 科学研究費補助金, 基盤研究 (C) (新規) 平成21~23年度.研究費総額:182万円
3. 荒川真一 (代表): 歯周病原細菌由来FDFの細胞への影響及び歯周炎病態への関与の解析. 科学研究費補助金, 基盤研究 (C) (新規) 平成21~23年度.研究費総額:361万円
4. 長澤敏行 (代表), 竹内康雄 (分担). 歯槽骨破壊の防止と動脈硬化抑制のためのWntシグナル制御による新規治療の開発. 科学研究費補助金,基盤研究C,平成20年度~22年度.
5. 青木 章 (代表), 渡辺 久,小田 茂,小林 宏明,岩崎 剣吾,竹内 康雄,秋月 達也,水谷 幸嗣. 科学

- 研究費補助金,基盤研究 (C) エルビウム・レーザーの歯周治療への応用とその生物学的効果の解明 (継続) 平成19~21年度.研究費総額:130万円
6. 小林宏明 (代表):Th17免疫細胞を主軸とした歯周炎進行機序に関する研究.若手研究 (B) (継続) 平成20~21年度.研究費総額:169万円
7. 竹内康雄.歯周炎・インプラント周囲炎細菌叢の総合的解析と弱アルカリ水による治療効果. 科学研究費補助金,若手研究B,平成21年度~23年度.研究費総額:182万円
8. 矢代麗子:ヒト歯根膜幹細胞シートを用いた歯周組織の再生. 科学研究費補助金,若手研究 (B) 平成21年度~22年度.研究費総額:210万円
9. 片桐さやか:早期低体重児出産における歯周病由来anti-cardiolipine抗体の役割. 科学研究費補助金,若手研究 (B) 平成21年度~22年度.研究費総額:273万円

奨学寄附金

オムロン株式会社	47万5千円
株式会社 松風	123万5千円
ファイザー株式会社	47万5千円

受託研究

和泉雄一: 新規ビスフォスフォネート歯周病治療薬の局所投与試験 昭和薬品化工株式会社 (H21年~H24年)	261万9千円
和泉雄一: 歯肉溝滲出液 (GCF) 成分を用いた歯周病罹患部位の診断と治療効果のモニタリングの有用性 日本歯科医師会 (H21年)	50万円
渡辺 久: べにふうき緑茶粉末含有ガム剤の口腔症状への効果に関する研究 やまと興業株式会社 (H21年)	82万5千円

15) 特別講演、招待講演

- 和泉雄一:歯周組織の健康と全身の健康とのかかわり—生活習慣病と歯周病との関係
平成20年度歯の健康づくり研修会、(2009.1.19. 横浜、2009.1.29. 小田原)
- 和泉雄一:歯周組織の健康と全身の健康とのかかわり、平成20年度東京都特別区職員歯科衛生士会研修会、(2009.2.13. 東京)
- 和泉雄一:インプラント治療と全身的风险ファク

- ター、ITI Congress Japan 2009 Tokyo (2009. 2. 14-15 東京)
- 和泉雄一:インプラント治療とインプラント周囲炎、インプラント実践パーフェクトセミナー、(2009. 3. 8. 東京)
 - 和泉雄一:歯周病と糖尿病—その密接な関係、平成20年度多摩府中保健所課題別地域保健医療推進プラン事業、(2009.3.17 東京)
 - 和泉雄一:歯周治療の進め方と歯周外科治療、2009年度日本インプラント臨床研究会 (2009.5.31 東京)
 - 和泉雄一:歯周病と糖尿病—その密接な関係、第25回兵庫県歯科医学大会 (2009.6.14 神戸)
 - 和泉雄一:ここまで来た歯周病と歯周治療—歯科医科連携の必要性—、一歯周組織再生治療—、徳島県歯科医師会学術講演会 (2009.6.21 徳島)
 - 和泉雄一:生活習慣病の黒幕—それは歯周病!、東京顕微鏡院、(2009.7.29 東京)
 - 和泉雄一:歯周外科治療とインプラント治療、平成21年度愛歯学術講演会 (2009.8.2 名古屋)
 - 和泉雄一:歯周病の最新治療、インプラント周囲炎の診断と治療、徳島インプラント研究会 (2009.8.11 徳島)
 - 和泉雄一:歯周治療を考える—全身との関わりから歯周組織再生まで—、北埼玉郡市歯科医師会学術講演会、(2009.8.30 埼玉)
 - 和泉雄一:歯周組織再生治療を俯瞰する、第24回北海道医療大学歯周病研究会、(2009.9.5 札幌)
 - Izumi Y.: Periodontal Treatment from Conventional to Regenerative Therapy. Seminar on Recent Advances in Dentistry –Oral Health and Systemic Diseases- (2009.10.19 Dhaka)
 - Izumi Y.: Periodontal Treatment from Conventional to Regenerative Therapy. Current Concepts on Periodontal, Vascular diseases and Oral Infectious Control. (2009.10.19 Dhaka)
 - 和泉雄一:日常臨床のための歯周組織再生療法、エムドゲイン®ゲル特別講演会、(2009. 11. 3. 東京)
 - 和泉雄一:若年者の歯周病、平成21年度幼児・児童・生徒についての歯科保健講演会、(2009.11.5. 東京)
 - 和泉雄一:最新*糖尿病と歯周病との深い関係、平成21年度多摩小平保健所口腔機能工場研修 (2009.11.5. 東京)
 - 和泉雄一:歯周炎と糖尿病—その密接な関係、西東京臨床糖尿病研究会第46回例会、(2009.11.21. 東京)
 - 和泉雄一:歯周病と全身の健康とのかかわり—歯周病の最新情報—、平成21年度保健衛生研修会、(2009.11.30. 鎌倉)

21. 和泉雄一:糖尿病と歯周病との関係、平成21年度歯の健康づくり研修会、(2009.12.7. 横浜)
22. 和泉雄一:ここまで来た歯周病と歯周治療、東京医科歯科大学小児歯科学教室同門会平成21年度総会講演会、(2009.12.20. 東京)
23. 和泉雄一:メタボリックシンドロームの黒幕—それは歯周病、8020運動推進特別事業地域保健セミナー、(2010.1.10. 横浜)
24. 和泉雄一:歯周病と早産・低体重児出産との関わり、平成21年度横浜市保健所保健衛生研修会、(2010.1.30. 横浜)
25. 渡辺 久:歯周治療へのEr:YAGレーザーの活用—その基礎と臨床—、シンポジウム「歯周治療へのレーザーの応用」、第9回日本歯科用レーザー学会、(2009.9.26. 新潟)
26. 渡辺 久:レーザーによる歯石除去、市民公開講座、第9回日本歯科用レーザー学会、(2009.9.26. 新潟)
27. 渡辺 久:歯周病の本質とその治療法、GCデンタルカレッジセミナー、(2009.10.27. 東京)
28. Aoki A. Current Status of Er:YAG laser in Periodontics and Implant Dentistry-I. Annual Wulai Advanced Laser Training, Taiwan Branch of World Clinical Laser Institute, Wulai, Taiwan, Oct 17 (17-18), 2009.
29. Aoki A. Hands-on seminar for Er:YAG laser clinical application. Annual Wulai Advanced Laser Training, Taiwan Branch of World Clinical Laser Institute, Wulai, Taiwan, Oct 17-18, 2009.
30. Aoki A. Current Status of Er:YAG laser in Periodontics and Implant Dentistry-II. Annual Wulai Advanced Laser Training, Taiwan Branch of World Clinical Laser Institute, Wulai, Taiwan, Oct 17-18, 2009.
31. Aoki A. Er:YAG Laser in periodontal and peri-implant therapies. National Taiwan University, Taipei, Taiwan, Oct 17-18, 2009.
32. 青木 章:歯周治療におけるEr:YAGレーザーの臨床応用(ランチョンセミナー).第52回秋期歯周病学会, 宮崎, 2009.10.11.
33. 青木 章:光エネルギーを用いた歯周病の新しい治療—レーザー療法.国立大学法人東京医科歯科大学公開講座「健康を創る(V)—新しい治療法を知ろう—」, 東京,お茶の水,2009.11.4.
34. 青木 章:歯周治療におけるレーザー応用の効

果.第21回日本レーザー歯学会総会・学術大会,福岡,2009.11.22-23.

35. 青木 章:Er:YAGレーザーの骨組織への照射の影響と歯周外科治療への臨床応用.臨床医学シンポジウム3: 骨・関節外科領域へのレーザーの応用.第30回日本レーザー医学会総会,市ヶ谷,東京,2009.12.2-3.
36. Aoki. Er:YAG laser-assited periodontal therapy. The 12th congress of the World Federation for lasers Dentistry (WFLD), Dubai, 2010.3.9-11.
37. 竹内康雄,和泉雄一.歯周治療を考慮したパーフェクトペリオ®の抗菌作用と細胞毒性の検討.パーフェクトペリオワールドクラス第一回学術大会(2009.10.3. 千葉)

16) 新聞、雑誌、TV報道

1. 内藤正裕,和泉雄一,小宮山彌太郎.座談会 インプラント治療の正道とは 歯科医師の良心を問う.DENTAL TRIBUNE.2009年8月 Vol.5 No.8 p.16-19
2. 和泉雄一.50歳が近付いてきたら本気で歯周病ケアを!ブルミエクリニックススペシャル vol.6. Nikkei Health Premie 2009-12.p.124-129
3. 荒川真一,和泉雄一.歯周組織再生療法の分類 基礎と臨床 3) 根面処理.和泉雄一編著 季刊 歯科医療 vol.23 No.2 特集 進歩する歯周組織再生治療の分類と臨床.第一歯科出版2009春号 p.19-23
4. 和泉雄一,荒川真一.歯周組織:歯周組織再生療法への応用.編集:田端泰彦.遺伝子医学MOOK13 患者まで届いている再生誘導治療 バイオマテリアル、生体シグナル因子、細胞を利用した患者のための再生医療の実際.株式会社メディカルドゥ.2009年5月 p.126
5. 和泉雄一,長澤敏行,古市保志.Q65 SRPはなぜ6ブロックに分けて行う必要があるのですか?また、全顎を一度に行う方法(FMD)との違いはあるのですか?.DHstyle増刊号 歯周1st ペリオ治療の疑問をスピード解決!.株式会社デンタルダイヤモンド社.2009年9月 p.110-111
6. 和泉雄一.歯周組織再生手術におけるエナメルマトリックス・デリバティブ:手技と臨床的・組織的症例報告 論文解説.THE INTERNATIONAL JOURNAL OF PERIODONTAL & RESTORATIVE DENTISTRY Vol.17 Number4 2009 〈日本語版〉.クインテッセンス出版株式会社.2009年8月

- p.106-107
7. 和泉雄一. 歯周病が全身をおびやかす!? 日本人の70%以上が歯周病患者。あなたの歯ぐきは大丈夫? Newton. 株式会社ニュートンプレス 2009年6月 p.86-91
 8. 和泉雄一. 新 名医の最新治療 名医のセカンドオピニオン. 週刊朝日. 朝日新聞出版. 2009年5月
 9. 和泉雄一, 鷺野崇, 小野寺良修, 関根秀志, 木津康博. インプラント周囲組織評価シート-メンテナンス時に見るべきポイント 評価シートの今後の展開. DENTAL DIAMOND 2009 NOV. Vol.34 No.497. p.36-42
 10. 和泉雄一, 小川伸子, 加藤光敏, 小島麻里. 一般歯科医院への糖尿病患者の来院は無視できない! THE JOURNAL OF DENTAL HYGINE. 医歯薬出版株式会社. NOVEMBER 2009 vol.29 no.11 p.1165-1175
 11. 和泉雄一. ヘルスケアあどばいす (歯周病). さわやか (株) 社会保険研究所 春号 2009 p.6-8
 12. 和泉雄一. 名医のセカンドオピニオン. 新「名医」の最新治療 2010. 朝日新聞出版. P.239
 13. 和泉雄一. メタボを悪化させる歯周病. ヘルスアンドライフ 2009 6月号. (株) 研友企画出版. P.8-11
 14. 和泉雄一. 歯周病. 健康情報番組明日も元気. アステラス製薬. 09/04/13-09/04/17. TBS ラジオ 15:45~, SBS ラジオ 16:10~, CBC ラジオ 14:30~
 15. 渡辺 久: Q&A. 「マスティック入り歯磨剤の抗菌作用」 DENTAL DIAMOND 2009 JUN. Vol.34 No.490. p.104-105
 16. 渡辺 久: 海外ジャーナル Watching. 「One-stage, full-mouth disinfection は虚構か現実か?」 DENTAL DIAMOND 2009 AUG. Vol.34 No.493. p.114
 17. 渡辺 久: ワールドミーティング・レポート. 「第6回ユーロペリオ学会に参加して」 DENTAL DIAMOND 2009 SEP. Vol.34 No.494. p.172-174
 18. 渡辺 久: 歯周病の放置が糖尿病、心筋梗塞を誘発する! 週刊アサヒ芸能 2009.9.10, 116-117.
 19. 渡辺 久: 歯周病が重症化しても歯は守れる. 日刊ゲンザイ 2009.6.12
 20. 渡辺 久. テレビ出演, 『歯周病恐怖』 ラボマイスター フジテレビ系列 2009.9.9. 24:45-1:08 放映
 21. 小田 茂. 歯周病の治療法, 暮らしと健康, 2009年2月号, p.74, 保健同人社, 2009.2.1.
 22. 荒川真一 テレビ出演, 『見えない泡で食の安心・安全を実現したい』, 夢の扉, TBS 系列 2009.2.1. 18:30-19:00 放映.

17) 教室、分野や講座の准教授、講師、助教、特別研究員、ポスドク、指導を受けた大学院生 の名前 (AISSには○印) のリスト

准教授 渡辺 久
 講師 小田 茂、萩原さつき
 助教 梅田 誠、青木 章、荒川真一、小林宏明、竹内康雄
 大学院 田中敬子、大西英知、○江部典子、
 ○Aleksic Verica
 青山典生、小林知映、春田千裕、小柳達郎、
 ○鈴木允文、谷口陽一、寺地真由、
 南原弘美、早雲彩絵、○姫野彰子、
 ○GAAslam AL Mehdi、
 ○GA Rajakaruna、○Bharti Pariksha、
 高橋茉莉香、妻沼有香、澤辺正規、
 山田 梓、小林奈穂、藤原 香、花谷智哉、
 伊藤康夫、江尻健一郎 (○:AISS)

18) GCOE 活動についての感想、コメント、 改善を望む点など

GCOE 活動について、若手研究者の育成には大いなる成果が認められ、また、国際交流の点でも徐々に成果を上げつつある。ただ、日頃の研究資金の増額を望みたい。

Association between periodontitis and anti-cardiolipin antibodies in Buerger disease

Chen Y-W, Nagasawa T, Wara-Aswapati N, Ushida Y, Wang D, Takeuchi Y, Kobayashi H, Umeda M, Inoue Y, Iwai T, Ishikawa I, Izumi Y. Association between periodontitis and anti-cardiolipin antibodies in Buerger disease. *J Clin Periodontol* 2009; 36: 830–835. doi: 10.1111/j.1600-051X.2009.01467.x.

Abstract

Aim: Anti-cardiolipin (CL) antibodies can be induced in Buerger disease (BD), an inflammatory occlusive disorder affecting peripheral blood vessels, in response to bacteria bearing homology to the TLRVYK peptide of a phospholipid-binding plasma protein β -2-glycoprotein I. TLRVYK homologies are present in *Porphyromonas gingivalis* (TLRIYT) and *Treponema denticola* (TLALYK). This study investigated the association between periodontal infection and anti-CL antibodies in BD patients. **Material and Methods:** Periodontal conditions were examined in 19 BD patients and 25 systemically healthy control subjects. All subjects were heavy smokers. Serum anti-CL, anti-TLRVYK, anti-TLRIYT, and anti-TLALYK antibodies were assessed using the enzyme-linked immunosorbent assay.

Results: BD patients had a significantly higher prevalence of periodontitis, more severe periodontal destruction and increased titres of serum anti-CL, anti-TLRVYK, anti-TLRIYT, and anti-TLALYK antibodies compared with healthy subjects. The levels of anti-CL antibodies positively correlated with those of the three anti-peptide antibodies. Anti-CL antibody titres were significantly associated with the percentage of sites with clinical attachment level ≥ 4 mm in BD patients.

Conclusion: Elevated anti-CL antibody levels were associated with periodontal destruction in BD patients. Periodontopathic bacteria may serve as exogenous antigens that stimulate the anti-CL antibody production through molecular mimicry between the bacterial peptides and a host plasma protein.

Yi-Wen Chen^{1,2}, Toshiyuki Nagasawa^{1,9}, Nawarat Wara-Aswapati³, Yuka Ushida¹, Dongqing Wang^{1,4}, Yasuo Takeuchi¹, Hiroaki Kobayashi¹, Makoto Umeda¹, Yoshinori Inoue⁵, Takehisa Iwai⁶, Isao Ishikawa^{1,7} and Yuichi Izumi^{1,8}

¹Section of Periodontology, Department of Hard Tissue Engineering, Graduate School, Tokyo Medical and Dental University, Tokyo, Japan; ²National Taiwan University Hospital, National Taiwan University, Taipei, Taiwan; ³Department of Periodontology, Faculty of Dentistry, Khon Kaen University, Khon Kaen, Thailand; ⁴Department of Periodontics & Oral Medicine, Beijing Stomatological Hospital, Capital Medical University, Beijing, China; ⁵Department of Vascular and Applied Surgery, Graduate School, Tokyo Medical and Dental University, Tokyo, Japan; ⁶Tsukuba Vascular Center and Buerger Disease Research Institute, Ibaragi, Japan; ⁷Institute of Advanced Biomedical Engineering and Science, Tokyo Women's Medical University, Tokyo, Japan; ⁸Global Center of Excellence Program, International Research Center for Molecular Science in Tooth and Bone Diseases, Tokyo Medical and Dental University, Tokyo, Japan; ⁹Department of Periodontology and Endodontology, Health Science University of Hokkaido, Hokkaido, Japan

Key words: anti-cardiolipin antibody; β -2-glycoprotein I; Buerger disease; molecular mimicry; periodontitis

Accepted for publication 29 June 2009

Buerger disease (BD) is an inflammatory occlusive disorder affecting small-

Conflict of interest and source of funding statement

The authors declare that they have no conflicts of interests.

This study was supported in part by Grants-in-Aid for Scientific Research from the Japan Society for the Promotion of Science (JSPS) (nos. 18390561, 18592258, and 20592425), JSPS Invitation Fellowship for Research in Japan (N. W.), and a grant from the Center for Excellence Program for Frontier Research on Molecular Destruction and Reconstruction of Tooth and Bone at the Tokyo Medical and Dental University.

and medium-sized arteries and veins, and occurs predominantly in males younger than 40–45 years (Buerger 1952, Mills & Porter 1993, Olin 2000, Olin & Shih 2006). Pathological findings showed well-organized intra-luminal vascular thrombosis in the surgically resected arterial specimens from patients with BD (Shionoya 1990, Tanaka 1998). Although the cause of BD remains unclear, there is a strong association between heavy tobacco use and BD (Allen & Brown 1928, Olin et al. 1990, Shionoya 1998). A high prevalence of anti-cardiolipin (CL) antibodies and increased anti-CL antibody titres were reported in patients with

BD (Olin et al. 1996, Maslowski et al. 2002).

Anti-CL antibodies and lupus anticoagulant are different classes of anti-phospholipid antibodies associated with the anti-phospholipid antibody syndrome (Ginsburg et al. 1992, Nahass 1997, Greaves 1999). Anti-phospholipid antibodies interact with a phospholipid-binding plasma protein, β -2-glycoprotein I (β 2GPI) (Galli et al. 1990, McNeil et al. 1990, Roubey et al. 1992), and may lead to a thrombotic predisposition. Some phospholipid-binding viral and bacterial proteins function like β 2GPI in inducing the production of anti-phospholipid antibodies and anti- β 2GPI anti-

bodies (Gharavi et al. 1999, 2002, Blank & Shoenfeld 2004), suggesting a mechanism of molecular mimicry. Blank et al. (2002) demonstrated that pathogenic anti- β 2GPI antibodies could be induced by immunizing mice with *Hemophilus influenzae* or *Neisseria gonorrhoeae*, which possesses peptide sequences that are homologous to the TLRVYK peptide of β 2GPI.

Schenkein et al. (2003, 2007) reported that the prevalence of patients with chronic periodontitis and a generalized aggressive periodontitis positive for anti-CL antibodies was greater than that in healthy controls. In addition, systemic markers of vascular inflammation in patients with aggressive periodontitis are associated with elevated levels of β 2GPI-dependent anti-CL antibodies. We reported previously that patients with BD exhibited severe periodontitis and higher serum IgG titres against periodontopathic bacteria, suggesting that periodontal infection may also be associated with BD (Iwai et al. 2005, Chen et al. 2007).

According to the Swiss Prot database, sequences homologous to the TLRVYK peptide of β 2GPI are present in the arg-gingipain protease of *Porphyromonas gingivalis* (TLRIYT) and the phosphoglycerate kinase of *Treponema denticola* (TLALYK). We hypothesized that homologous peptides in periodontopathic bacteria could induce the production of pathogenic anti-CL antibodies in patients with BD. The aim of the present study was to examine whether periodontal infection was associated with increased anti-CL antibody titres in patients with BD.

Material and Methods

Study population

Twenty-six BD and 38 healthy control subjects were recruited during September 2005–December 2006. Nineteen male patients with a diagnosis of BD, based on Shionoya's criteria and angiographic findings from the Clinic of Vascular and Applied Surgery in the Tokyo Medical and Dental University, were included in this study (participation rate = 73.1%). One female BD patient, four with hypertension, and two with diabetes mellitus were excluded. All patients had the typical characteristics of BD, including a history of smoking, disease onset before the age of 50 years, occlusive lesions in

the infrapopliteal artery, either upper limb involvement or phlebitis migrans, and an absence of risk factors for atherosclerosis (with the exception of smoking). Occluded arterial segments were removed during surgery, and histopathological examinations were performed to confirm a diagnosis of BD.

Twenty-five healthy control subjects, defined as those without BD or any other systemic disease, were matched against the patient population by age, gender, smoking status, and systemic status (participation rate = 65.8%). Seven females and six non-smokers were excluded. Information about their current health status, medical history, drug use, and smoking behaviour was obtained via a questionnaire. Subjects were excluded if they had received antibiotics in the last 3 months or treatment for periodontal disease in the last 6 months. The socio-economic status of the subjects was homogenous without a considerable difference between BD patients and control subjects. All subjects provided informed consent, and all protocols were approved by the Ethical Committee of Tokyo Medical and Dental University.

Clinical periodontal examinations

Periodontal status was evaluated using various clinical parameters by a well-trained calibrated periodontist (M. U.). Periodontal probing depth (PD) and clinical attachment level (CAL) were recorded at six points for each tooth. CAL was calculated from the sum of the PD and the gingival margin. Participants who presented with at least one site with PD \geq 4 mm and CAL \geq 4 mm in each quadrant were defined as patients with periodontitis. The number of residual teeth was also recorded. Periodontal examinations were performed before patients received surgical treatment.

Determination of serum anti-CL IgG antibodies

Whole-blood samples were taken from all study subjects at the time of the dental visit. Blood samples were centrifuged at 1500 g for 10 min at 4°C. The serum was filtered and immediately stored at -80°C until analysis. Serum anti-CL antibodies were measured using the AngioMax anti-CL IgG ELISA kit (Assaypro, St. Charles, MO, USA) according to the manufacturer's instructions, and the results are presented as

GPL units, which is the international standard for the measurement of anti-CL IgG antibodies (Harris 1990).

Determination of serum IgG antibody titres against TLRVYK, TLRIYT, and TLALYK peptides

Serum anti-TLRVYK, anti-TLRIYT, and anti-TLALYK antibodies were determined using an enzyme-linked immunosorbent assay method, as described previously (Wang et al. 2008). Briefly, 96-well micro-titre plates were coated with TLRVYK, TLRIYT, or TLALYK peptides (10 μ g/mL) and blocked with 3% bovine serum albumin. In order to prepare a positive control, rabbits were immunized with TLRVYK peptide, and the anti-TLRVYK rabbit IgG was purified by affinity chromatography with a sepharose column conjugated with TLRVYK peptide. After washing with phosphate-buffered saline (PBS), a twofold serial dilution (50 to 0.098 ng/mL) of rabbit anti-TLRVYK IgG was added to the top two rows of the plate as a standard. Diluted serum samples (1:128) from subjects were added in duplicate to the remaining rows of the plate, followed by overnight incubation. After washing with PBS, peroxidase-conjugated protein A was added to bind both rabbit and human IgG antibody, and the binding was detected using the tetramethylbenzidine liquid substrate system (Sigma, St. Louis, MO, USA). The reaction was stopped with 1 M H₂SO₄ (Sigma) after 30 min. The optical density at 450 nm for each well was determined using a Microplate Reader (SOFT MaxTM, Sunnyvale, CA, USA).

Statistical analysis

Descriptive statistics and statistical analyses were performed using a computerized statistical package (SPSS). The Kolmogorov–Smirnov normality test and the Levene variance homogeneity test were applied to study the distribution normality of the data. The statistical difference of the periodontitis prevalence between the two groups was examined using Fisher's exact test. The Mann–Whitney *U*-test was applied to detect differences in the percentages of sites with PD and CAL, number of residual teeth, and serum IgG antibody titres. Spearman's rank-correlation test was applied to test the correlations between anti-CL antibodies and the per-

832 Chen et al.

centage of sites with PD ≥ 4 mm or CAL ≥ 4 mm, and three anti-peptide IgG antibodies. Statistical significance was set at $p < 0.05$. Multivariate logistic regression analysis was performed to examine the association between BD and several risk factors.

Results

Characteristics and the periodontal status of participants

The demographics of BD patients and healthy control subjects are summarized in Table 1. There were no significant differences in age, gender, and smoking status on comparing the two groups. Because smoking was regarded as an important risk factor for both BD (Allen & Brown 1928, Shionoya 1998, Olin & Shih 2006) and periodontitis (Haber et al. 1993, Bergström et al. 2000, Tomar & Asma 2000, Hyman 2006), all subjects in our study were heavy smokers. The prevalence of periodontitis and the percentage of sites with PD ≥ 4 mm and CAL ≥ 4 mm were significantly higher in patients with BD than in the control subjects ($p < 0.001$, $p < 0.001$, and $p = 0.037$, respectively). Furthermore, patients with BD had fewer residual teeth when compared with healthy controls, but the difference between the two study groups was not statistically significant ($p = 0.216$).

Serum anti-CL, anti-TLRVYK, anti-TLRIYT, and anti-TLALYK antibodies

Patients with BD had significantly higher anti-CL antibody titres when compared with control subjects ($p < 0.001$, Fig. 1a). Further, anti-TLRVYK (Fig. 1b), anti-TLRIYT (Fig. 1c), and anti-TLALYK (Fig. 1d) antibody titres were significantly higher in patients with BD than in control subjects ($p < 0.001$, $p < 0.001$, and $p = 0.017$, respectively). Figure 2 illustrates the correlations between anti-CL IgG antibody titres and three anti-peptide antibody titres. Anti-CL antibody titres positively correlated with anti-TLRVYK, anti-TLRIYT, and anti-TLALYK antibody titres ($p < 0.001$, $p = 0.002$, and $p = 0.028$, respectively).

Association between anti-CL antibody titres and periodontal status

Overall, anti-CL antibody titres significantly correlated with the percentage of

Table 1. Characteristics of the study subjects

	Buerger disease patients	Control subjects
Number of subjects (<i>n</i>)	19	25
Age (years; mean \pm SD)	56.6 \pm 11	59.6 \pm 14
Gender (male/female)	19/0	25/0
Heavy smoker [†] (<i>n</i>)	19	25
Prevalence of periodontitis**	89.5% (17/19)	28% (7/25)
Percentage of sites with PD ≥ 4 mm**	14.3%	2.4%
Percentage of sites with CAL ≥ 4 mm*	22.6%	13.2%
Number of residual teeth	20.2	24.2

[†]Heavy smoker: subject who has or had a history of smoking, as defined by ≥ 20 cigarettes per day for > 20 years.

PD, probing depth; CAL, clinical attachment level.

Significantly different between the study groups at

** $p < 0.001$, * $p = 0.037$.

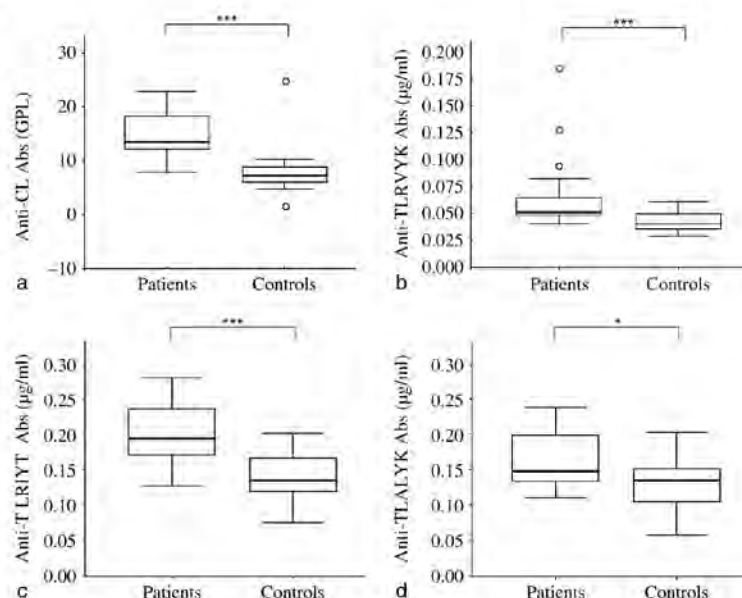


Fig. 1. Serum IgG levels of anti-cardiolipin (CL) (a), anti-TLRVYK (b), anti-TLRIYT (c), and anti-TLALYK (d) antibodies in 19 patients with Buerger disease and 25 healthy control subjects. Box plots show medians with 25th and 75th percentiles, and outliers are marked as open circles. *** $p < 0.001$, * $p < 0.05$ (Mann-Whitney *U*-test).

sites with CAL ≥ 4 mm and the percentage of sites with PD ≥ 4 mm (Fig. 3a, all subjects, $r = 0.428$, $p = 0.004$; and Fig. 3b, all subjects, $r = 0.426$, $p = 0.004$; respectively). In BD patients, anti-CL antibody titres positively correlated with the percentage of sites with CAL ≥ 4 mm (Fig. 3a, $r = 0.471$, $p = 0.042$). Although the trend for an association between anti-CL antibody titres and the percentage of sites with PD ≥ 4 mm was observed, it did not reach a level of statistical significance (Fig. 3b, $r = 0.175$, $p = 0.474$).

Association between BD and risk factors

Logistic regression analysis was performed to examine the association between BD and several risk factors. BD was associated with anti-CL antibodies [odds ratio (OR) = 1.43, $p = 0.008$] and periodontitis (OR = 7.71, $p = 0.046$) (Table 2).

Discussion

The association between anti-CL antibodies and BD has been reported pre-

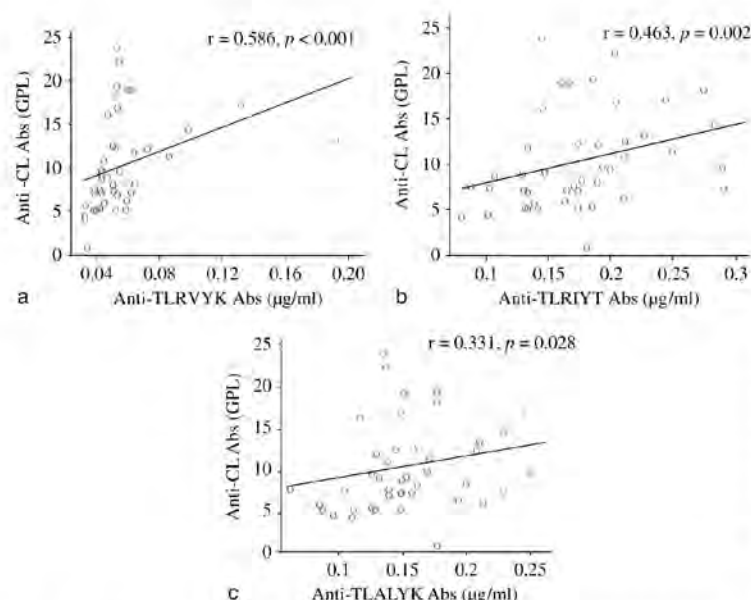


Fig. 2. The plot shows associations between serum anti-cardiolipin (CL) antibody levels and anti-TLRVYK (a), anti-TLRIYT (b), and anti-TLALYK (c) antibody levels in all subjects. Each subject is shown as an open circle, and the regression line represents the trend. r represents the correlation coefficient; $p < 0.05$ represents statistical significance (linear regression analysis; Spearman's rank-correlation test).

viously (Olin et al. 1996, Olin 2002, Maslowski et al. 2002). Our present study also found that patients with BD displayed significantly higher anti-CL antibody titres when compared with control subjects. Logistic regression analysis confirmed that increased levels of anti-CL antibodies were related to BD. In addition, our results showed that periodontitis was strongly associated with BD. All subjects in the present study were heavy smokers. Therefore, we could not evaluate the effect of periodontitis on BD in non-smokers. It is possible that the correlation between periodontitis and BD may be limited only to the smokers.

In this study, BD patients exhibited severe periodontitis, and the anti-CL antibody titres significantly correlated with the percentage of sites with CAL ≥ 4 mm, implying that the elevated anti-CL antibody levels may be related to periodontal destruction in patients with BD. These findings are consistent with observations from previous studies suggesting that periodontitis may increase serum $\beta 2$ GPI-dependent anti-CL antibody titres (Schenkein et al. 2003, 2007). However, the mechanistic link between periodontal infection and anti-CL antibodies was not investigated

in those studies. Because most BD patients in our study had periodontitis, further studies comparing BD patients with periodontitis with BD patients without periodontitis are warranted to confirm the contribution of periodontitis on BD pathogenesis through elevated levels of anti-CL antibodies.

We previously reported that *P. gingivalis* and *T. denticola* DNA were frequently detected in arterial specimens taken from patients with BD (Iwai et al. 2005), and that IgG antibody titres against *P. gingivalis* and *T. denticola* were significantly increased in patients with BD. These observations implicate a possible aetiological linkage between BD and periodontitis (Chen et al. 2007). Indeed, bacteria that possess peptide sequences homologous to the TLRVYK peptide of $\beta 2$ GPI were demonstrated to induce pathogenic anti- $\beta 2$ GPI antibodies in mice (Blank et al. 2002). TLRVYK homologues are present in *P. gingivalis* (TLRIYT) and *T. denticola* (TLALYK). In this study, patients with BD had increased antibody titres against TLRVYK, TLRIYT, and TLALYK peptides, suggesting that infection with *P. gingivalis* and *T. denticola* may induce anti-TLRIYT, anti-TLALYK, and anti-TLRVYK antibodies. TLRVYK

is a peptide on the $\beta 2$ GPI molecule, and anti-TLRVYK antibody is believed to be a part of the anti- $\beta 2$ GPI or anti-CL antibodies. Our results showed that the levels of serum anti-TLRVYK, anti-TLRIYT, and anti-TLALYK antibodies positively correlated with the levels of serum anti-CL antibodies. Recently, we have demonstrated that *Aggregatibacter actinomycetemcomitans* infection can elicit and modify the anti-TLRVYK antibody response via molecular mimicry between the SIRVYK peptide in *A. actinomycetemcomitans* leucotoxin c and the TLRVYK peptide of $\beta 2$ GPI (Wang et al. 2008). Therefore, the findings in the present study supported that periodontal infection by *P. gingivalis* and *T. denticola* may augment antibody responses against CL and/or $\beta 2$ GPI via molecular mimicry in patients with BD.

Molecular mimicry between periodontopathic bacteria and host-antigens has been reported in other disease (Tabeta et al. 2000, 2001, Yamazaki et al. 2004). Yamazaki et al. (2004) showed that antibody levels to human heat shock protein 60 (HSP60) and *P. gingivalis* HSP60 (GroEL) were the highest in patients with atherosclerosis, followed by periodontitis patients and healthy subjects. It was also demonstrated that patients with atherosclerosis had HSP60-reactive as well as GroEL-reactive T cells and that atherosclerotic lesions were infiltrated with HSP60 reactive T cells. These studies suggested the mechanism of molecular mimicry between self-antigens and periodontopathic bacteria as a possible link between periodontitis and vascular diseases. Although the scope of our present study was limited to BD, it is reasonable to assume that periodontitis may influence other systemic diseases via a similar mechanism of molecular mimicry. Further studies are warranted to investigate the association between periodontitis and other anti-CL antibody-related diseases.

In conclusion, our study demonstrated that periodontal destruction was associated with increased anti-CL antibody titres in patients with BD. The periodontopathic bacterial peptides homologous to the TLRVYK peptide of $\beta 2$ GPI, which are presented in *P. gingivalis* (TLRIYT) and *T. denticola* (TLALYK), may induce the production of anti-CL antibodies in BD patients. Since the improvement of anti-phospholipid antibody syndrome after *Helico-*

834 Chen et al.

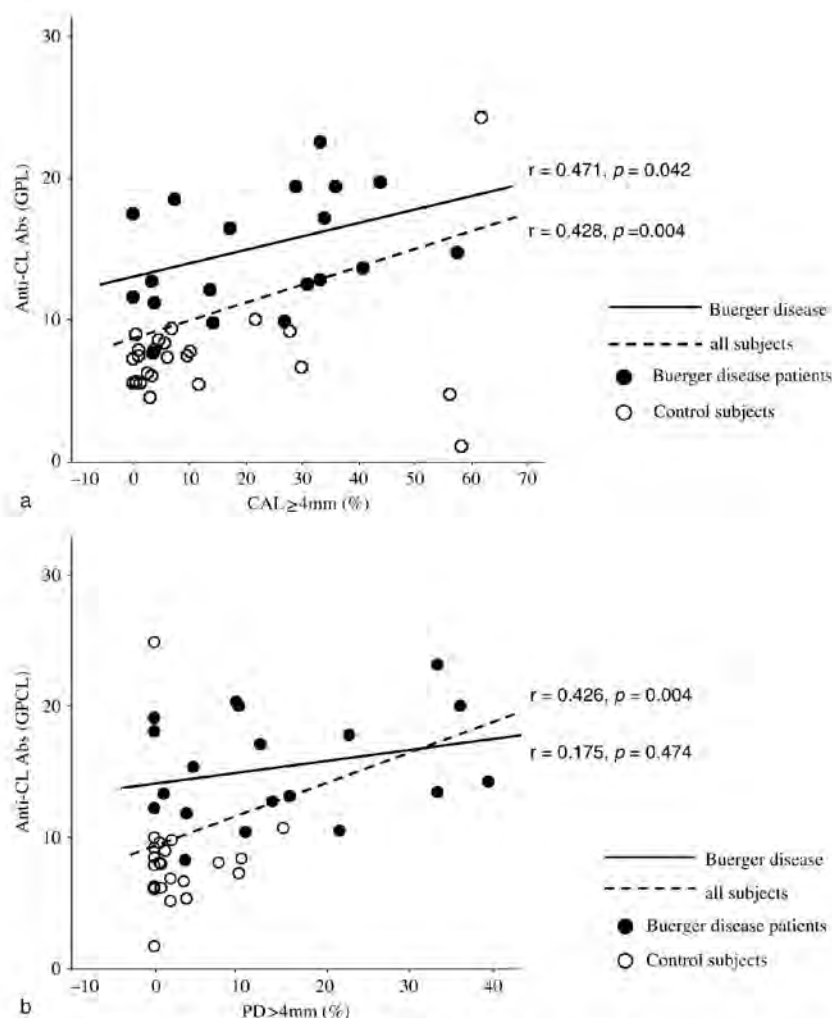


Fig. 3. The plot shows associations between serum anti-cardiolipin (CL) antibody levels and the percentage of sites with clinical attachment level (CAL) ≥ 4 mm (a) or probing depth (PD) ≥ 4 mm (b). Patients with Buerger disease are shown as black dots, and the straight line represents the trend. Control subjects are shown as open circles, and the dashed line represents the trend. "r" represents the correlation coefficient; $p < 0.05$ represents statistical significance (linear regression analysis; Spearman's rank-correlation test).

Table 2. Association of risk factors with Buerger disease in a logistic regression model. Independent variables include anti-CL antibodies and periodontitis

Independent variables	Dependent variable: Buerger disease odds ratio (95% CI)	p-value
Anti-CL antibodies	1.43 (1.10–1.85)	0.008**
Periodontitis	7.71 (1.04–57.24)	0.046*

95% CI: 95% confidence interval. * $p < 0.05$, ** $p < 0.01$.

bacter pylori eradication was reported (Cicconi et al. 2001), periodontal treatment to eliminate periodontopathic bacteria may reduce anti-CL antibody titres leading to an improvement of the BD condition.

References

- Allen, E. V. & Brown, G. E. (1928) Thromboangiitis obliterans. A clinical study of 200 cases. *Annals Internal Medicine* **1**, 535–549.
- Bergström, J., Eliasson, S. & Dock, J. (2000) Exposure to tobacco smoking and periodontal

health. *Journal of Clinical Periodontology* **27**, 61–68.

- Blank, M., Krause, I., Fridkin, M., Keller, N., Kopelovic, J., Goldberg, I., Tobar, A. & Shoenfeld, Y. (2002) Bacterial induction of autoantibodies to beta2-glycoprotein-I accounts for the infectious etiology of antiphospholipid syndrome. *The Journal of Clinical Investigation* **109**, 797–804.
- Blank, M. & Shoenfeld, Y. (2004) Beta-2-glycoprotein-I, infections, antiphospholipid syndrome and therapeutic considerations. *Clinical Immunology* **112**, 190–199.
- Buerger, I. (1952) Thrombo-angiitis obliterans; a study of the vascular lesions leading to presenile spontaneous gangrene. *The American Journal of Medicine* **13**, 526–532.

© 2009 John Wiley & Sons A/S

- Chen, Y. W., Iwai, T., Umeda, M., Nagasawa, T., Huang, Y., Takeuchi, Y. & Ishikawa, I. (2007) Elevated IgG titers to periodontal pathogens related to Buerger disease. *International Journal of Cardiology* **122**, 79–81.
- Cicconi, V., Carloni, E., Franceschi, F., Nocente, R., Silveri, N. G., Manna, R., Servidei, S., Bentivoglio, A. R., Gasbarrini, A. & Gasbarrini, G. (2001) Disappearance of antiphospholipid antibodies syndrome after *Helicobacter pylori* eradication. *The American Journal of Medicine* **111**, 163–164.
- Galli, M., Comfurius, P., Maassen, C., Hemker, H. C., de Baets, M. H., van Breda-Vriesman, P. J., Barbui, T., Zwaal, R. F. & Bevers, E. M. (1990) Anticardiolipin antibodies (ACA) directed not to cardiolipin but to a plasma protein cofactor. *Lancet* **335**, 1544–1547.
- Gharavi, A. E., Pierangeli, S. S., Espinola, R. G., Liu, X., Colden-Stanfield, M. & Harris, E. N. (2002) Antiphospholipid antibodies induced in mice by immunization with a cytomegalovirus-derived peptide cause thrombosis and activation of endothelial cells in vivo. *Arthritis and Rheumatism* **46**, 545–552.
- Gharavi, E. E., Chaimovich, H., Cucunull, E., Celli, C. M., Tang, H., Wilson, W. A. & Gharavi, A. E. (1999) Induction of antiphospholipid antibodies by immunization with synthetic viral and bacterial peptides. *Lupus* **8**, 449–455.
- Ginsburg, K. S., Liang, M. H., Newcomer, L., Goldhaber, S. Z., Schur, P. H., Hennekens, C. H. & Stampfer, M. J. (1992) Anticardiolipin antibodies and the risk for ischemic stroke and venous thrombosis. *Annals of Internal Medicine* **117**, 997–1002.
- Greaves, M. (1999) Antiphospholipid antibodies and thrombosis. *Lancet* **353**, 1348–1353.
- Haber, J., Wattles, J., Crowley, M., Mandell, R., Joshipura, K. & Kent, R. L. (1993) Evidence for cigarette smoking as a major risk factor for periodontitis. *Journal of Periodontology* **64**, 16–23.
- Harris, E. N. (1990) Special report. The Second International Anti-cardiolipin Standardization Workshop/the Kingston Anti-Phospholipid Antibody Study (KAPS) group. *American Journal of Clinical Pathology* **94**, 476–484.
- Hyman, J. (2006) Guest Editorial. The importance of assessing confounding and effect modification in research involving periodontal disease and systemic diseases. *Journal of Clinical Periodontology* **33**, 102–103.
- Iwai, T., Inoue, Y., Umeda, M., Huang, Y., Kurihara, N., Koike, M. & Ishikawa, I. (2005) Oral bacteria in the occluded arteries of patients with Buerger disease. *Journal of Vascular Surgery* **42**, 107–115.
- Maslowski, L., McBane, R., Alexewicz, P. & Wysokinski, W. E. (2002) Antiphospholipid antibodies in thromboangiitis obliterans. *Vascular Medicine* **7**, 259–264.
- McNeil, H. P., Simpson, R. J., Chesterman, C. N. & Krilis, S. A. (1990) Anti-phospholipid antibodies are directed against a complex antigen that includes a lipid-binding inhibitor of coagulation: beta 2-glycoprotein I (apolipoprotein H). *Proceedings of the National Academy of Sciences of the United States of America* **87**, 4120–4124.
- Mills, J. L. & Porter, J. M. (1993) Buerger's disease: a review and update. *Seminars in Vascular Surgery* **6**, 14–23.
- Nahass, G. T. (1997) Antiphospholipid antibodies and the antiphospholipid antibody syndrome. *Journal of American Academy of Dermatology* **36**, 149–172.
- Olin, J. W. (2000) Thromboangiitis obliterans (Buerger's disease). *The New England Journal of Medicine* **343**, 864–869.
- Olin, J. W. (2002) Are anticardiolipin antibodies really important in thromboangiitis obliterans (Buerger's disease)? *Vascular Medicine* **7**, 257–258.
- Olin, J. W., Childs, M. B., Bartholomew, J. R., Calabrese, L. H. & Young, J. R. (1996) Anticardiolipin antibodies and homocysteine levels in patients with thromboangiitis obliterans. *Arthritis and Rheumatism* **39**, S47.
- Olin, J. W. & Shih, A. (2006) Thromboangiitis obliterans (Buerger's disease). *Current Opinion in Rheumatology* **18**, 18–24.
- Olin, J. W., Young, J. R., Graor, R. A., Ruschhaupt, W. F. & Bartholomew, J. R. (1990) The changing clinical spectrum of thromboangiitis obliterans (Buerger's disease). *Circulation* **82**, IV3–IV8.
- Roubey, R. A., Pratt, C. W., Buyon, J. P. & Winfield, J. B. (1992) Lupus anticoagulant activity of autoimmune antiphospholipid antibodies is dependent upon beta 2-glycoprotein I. *The Journal of Clinical Investigation* **90**, 1100–1104.
- Schenkein, H. A., Berry, C. R., Burmeister, J. A., Brooks, C. N., Barbour, S. E., Best, A. M. & Tew, J. G. (2003) Anti-cardiolipin antibodies in sera from patients with periodontitis. *Journal of Dental Research* **82**, 919–922.
- Schenkein, H. A., Best, A. M., Brooks, C. N., Burmeister, J. A., Arrowood, J. A., Kontos, M. C. & Tew, J. G. (2007) Anti-cardiolipin and increased serum adhesion molecule levels in patients with aggressive periodontitis. *Journal of Periodontology* **78**, 459–466.
- Shionoya, S. (1990) Etiology, pathology, pathophysiology, clinical manifestation, diagnosis. In: Shionoya, S. (ed) *Buerger's Disease. Pathology, Diagnosis and Treatment*. Nagoya, Japan: University of Nagoya Press, pp. 38–198.
- Shionoya, S. (1998) Diagnostic criteria of Buerger's disease. *International Journal of Cardiology* **66**, S243–S245, discussion S247.
- Tabeta, K., Yamazaki, K., Hotokezaka, H., Yoshie, H. & Hara, K. (2000) Elevated humoral immune response to heat shock protein 60 (hsp60) family in periodontitis patients. *Clinical and Experimental Immunology* **120**, 285–293.
- Tabeta, K., Yoshie, H. & Yamazaki, K. (2001) Characterization of serum antibody to A actinomycescomitans GroEL-like protein in periodontitis patients and healthy subjects. *Oral Microbiology and Immunology* **16**, 290–295.
- Tanaka, K. (1998) Pathology and pathogenesis of Buerger's disease. *International Journal of Cardiology* **66**, S237–S242.
- Tomar, S. L. & Asma, S. (2000) Smoking-attributable periodontitis in the United States: findings from NHANES III. National Health and Nutrition Examination Survey. *Journal of Periodontology* **71**, 743–751.
- Wang, D., Nagasawa, T., Chen, Y. W., Ushida, Y., Kobayashi, H., Takeuchi, Y., Umeda, M. & Izumi, Y. (2008) Molecular mimicry of *Aggregatibacter actinomycetemcomitans* with beta2 glycoprotein I. *Oral Microbiology and Immunology* **23**, 401–405.
- Yamazaki, K., Ohsawa, Y., Itoh, H., Ueki, K., Tabeta, K., Oda, T., Nakajima, T., Yoshie, H., Saito, S., Oguma, F., Kodama, M., Aizawa, Y. & Seymour, G. J. (2004) T-cell clonality to *Porphyromonas gingivalis* and human heat shock protein 60s in patients with atherosclerosis and periodontitis. *Oral Microbiology and Immunology* **19**, 160–167.

Address:
Toshiyuki Nagasawa
Department of Periodontology
and Endodontology
Health Science University of Hokkaido
1757 Kanazawa Tobetsu-cho
Ishikari-gun
Hokkaido, 061-0293
Japan
E-mail: nagasawa@hoku-iryo-u.av.jp

Clinical Relevance

Scientific rationale for the study: Evidences suggest that periodontitis can influence systemic diseases, including BD. However, the mechanism of this interaction remains unclear.

Principal findings: Periodontal destruction is associated with an

increased production of anti-CL antibodies in patients with BD. Periodontopathic bacteria may act as exogenous antigens to stimulate the production of anti-CL antibodies through molecular mimicry between the bacterial peptides and a plasma protein β 2GPI.

Practical implications: This study implies an association between periodontitis and BD. Periodontal treatment to eradicate periodontopathic bacteria may reduce anti-CL antibody titres, leading to an improvement of the BD condition.

硬組織病態制御学

柳下 正樹

医歯学総合研究科・生体支持組織学系専攻
硬組織病態制御学・教授



1) 研究課題名

歯周組織炎症部位における酸化ストレスの組織学的・生化学的解析

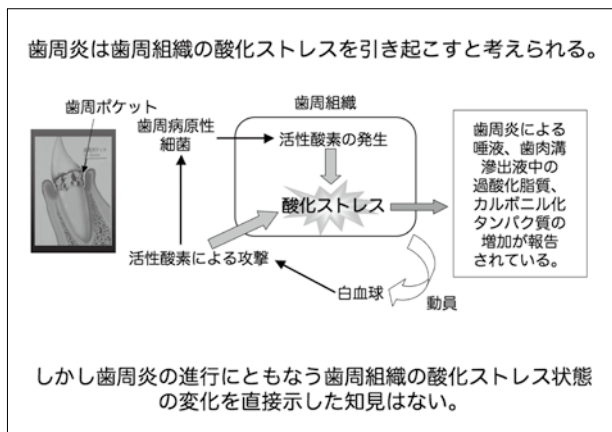
Histological and biochemical analyses of oxidation stress at the inflammation site of periodontal diseases

歯周病は歯周病原菌の感染による歯周組織の炎症を特徴とする慢性炎症性疾患である。日本人の歯周病罹患率は非常に高く45歳以上では40%を越えている（厚生労働省の平成17年歯科疾患実態調査）。歯周病の進行とともに歯周ポケットは深さを増し、ポケット内に嫌気性菌を中心として歯周病原菌が増加する。これに反応して歯周炎局部には様々な免疫応答が惹起され結果的に歯周組織の破壊が生じ、最後には歯の喪失に至る。また歯周疾患の炎症部位に由来する細菌由来成分や炎症性サイトカインが血流を介して全身に作用し糖尿病、心臓血管病、低体重児出産・早産、呼吸疾患、骨粗しょう症などの疾患の誘発に関与すると考えられている。歯周病および歯周病と関連する全身疾患の治療や予防のためには原因となる炎症部位の特殊性、すなわち「嫌気性細菌が繁殖する場となる低酸素領域（歯周ポケット）に隣接していること」の意味を明らかにすることが不可欠である。

歯周病原菌から放出される内毒素（LPS）、外毒素、短鎖脂肪酸などは *in vitro* の実験系において細胞内の活性酸素産生を引き起こす。LPS に対して組織から放出される炎症性サイトカインも組織自身に作用して活性酸素産生を促進する。また歯周ポケット内が低酸素状態であることにより隣接する歯周組織の活性酸素産生が亢進する可能性がある。そこで歯周疾患の炎症部位は歯周ポケットに存在する細菌の種類や繁殖状況および免疫系、循環系の状態などの複数の因子の寄与を反映した酸化ストレスの状況を呈すると考えられる。しかし現在までに歯周疾患の病態と炎症部位の酸化ストレス状態とを直接結びつける知見はほとんど報告されていない。本研究では

歯周病の炎症部位の臨床サンプルの酸化ストレスの状態を組織学的、生化学的に解析する。

2)



3) 研究内容の英文要約

During the years of 2009 and 2010, we initiated a new study developing a technique directly demonstrating oxydative status in periodontal tissue associated with bacterial periodontitis. This will clarify factors involved in initiation and continuation of immunological responses toward bacterial infection in periodontium.

We also continued our study identifying the presence of a molecular complex on the cell surface involving heparan sulfate proteoglycans, and the role of heparan sulfate chains on the integrity of membrane raft structure. Biochemical properties of heparan sulfate proteoglycans point to the presence of intimate molecular interactions in specialized domains of cell surface and their importance in the cellular signaling mechanisms. Research results, using isolation procedures of plasma membrane and identification of several membrane proteins together with heparan sulfate proteoglycans, indicated that cholesterol-rich, cell surface microdomains constitute one of specialized functional units of the plasma membrane and are associated with a species

of cell surface heparan sulfate proteoglycan, syndecan-4. Biological significance of heparan sulfate proteoglycans in specialized membrane domains will be further investigated.

4) 本事業に関連して世界的な研究拠点形成に向けて、以下の点で改善・整備等されたこと

A (研究拠点体制)

GCOEの国内評価会準備に参画。

異なる分野のInnovationの確立する研究「歯周組織炎症部位における酸化ストレスの組織学的・生化学的解析」を提案。

B (研究教育環境)

活発なシンポジウム、セミナーの開催

C (人材確保)

特任講師中村博幸博士との共同研究体制確立。

D (人材育成)

大学院生(AISS)への奨学金授与、大学院生セミナーの開催

E (国際化)

国際セミナーへの参加、発表。

5) GCOE事業を推進するに当たって力を入れた点

特任講師の招聘、大学院生への教育活動に参加することを心がけた。

6) 英文原著論文

1. Masaki Yanagishita, Katarzyna Anna Podyma-Inoue and Miki Yokoyama. Extraction and separation of proteoglycans. Glycoconj. J. (2009) 26:953-959

7) 平成21年度までの自己評価

中村博幸特任講師との共同研究体制確立に努力した。その他の活動内容のうち私の参加できる主な項目としては大学院生、GCOE教官に対する評価関連の活動および、大学院生に対するセミナーシリーズでの講義であった。これらの活動はGCOE事業全体からすると微力とは思いますが、可能な限り参加させていただきました。

8) 学会発表 (英文)

1. Ebe, N., Yokoyama, M., Iwasaki, K., Yanagishita, M. and Izumi, Y., High-mobility group box 1 release from human gingival epithelial cells during apoptosis, Europerio 6, July 4, 2009, Stockholm, Sweden
2. Katarzyna A. Podyma Inoue, Miki Yokoyama and

Masaki Yanagishita, Heparan sulfate proteoglycans on the plasma membrane; association with detergent-resistant membranes, 6th International Conference on proteoglycans, September 13-17, Aix-les-Bains, France

3. Katarzyna A. Podyma Inoue, Miki Yokoyama and Masaki Yanagishita, Remodeling of extracellular matrix and low gravity, Meeting of the Japanese Society for Biological Sciences in Space, JSBSS23, October 2-4, Tsukuba

9) 学会発表 (和文)

1. 江部典子、横山三紀、岩崎剣吾、柳下正樹、和泉雄一、「アポトーシスによるヒト歯肉上皮細胞からのHMGB1放出」、日本歯周病学会、2009年5月15,16日、岡山コンベンションセンター、岡山
2. 横山三紀、寺澤和恵、渡辺明彦、秋吉一成、五十嵐靖之、平林義雄、柳下正樹、「スフィンゴシンキナーゼ2阻害剤による細胞崩壊の促進」、第51回脂質生化学会、2009年7月30,31日、名古屋
3. 横山三紀、寺澤和恵、五十嵐靖之、平林義雄、柳下正樹、「スフィンゴシンキナーゼ2阻害剤によるFas依存性の活性酸素産生の促進」、第4回スフィンゴセラピー(STC)研究会、2009年7月17-18日、大山ロイヤルホテル、鳥取県
4. 横山三紀、新野睦子、寺澤和恵、井上カタジナアンナ、三嶋智恵美、梅津陽子、松本知子、脇山素明、白水美香子、横山茂之、柳下正樹、「N結合型糖鎖は膜貫通タンパク質CD38の膜ラフト局在化の制御を可能にする」、第29回日本糖質学会、2009年9月9日、高山、岐阜県
5. 横山三紀、寺澤和恵、渡辺明彦、秋吉一成、市野瀬志津子、五十嵐靖之、平林義雄、柳下正樹、「スフィンゴシンキナーゼ2阻害剤によるFas依存性細胞死過程での液胞形成」、第2回セラミド研究会、2009年11月6日、札幌
6. 竹原祥子、柳下正樹、Katarzyna A. Podyma Inoue、植野正之、品田佳代子、川口陽子、「口臭有無と唾液タンパク質の関連について」、第74回口腔病学会、2009年12月5日、東京医科歯科大学、東京
7. 江部典子、柳下正樹、横山三紀、岩崎剣吾、和泉雄一、「ヒト歯肉上皮細胞における細胞死によるHMGB1放出」、第74回口腔病学会、2009年12月5日、東京医科歯科大学、東京
8. 横山三紀、「膜貫通タンパク質の膜ラフト局在化における糖質の役割」、GlycoTokyo 2009、2009年11月14日、お茶の水大学、東京

10) 特別講演、招待講演

(受託研究)

糖質科学研究所、「グリコサミノグリカンオリゴ糖の生理活性解析と医薬応用」、期間:平成17年-平成21年、総額:840万円

11) 教室、分野や講座の准教授、講師、助教、特別研究員、ポスドク、指導を受けた大学院生の名前(AISSには○印)のリスト

(助教授) 横山三紀

(講師) 糸井康宏

(助教) 井上-Podyma Katarzyna Anna

(大学院生) 歯周病学分野より○江部典子

12) GCOE 活動についての感想、コメント、改善を望む点など

執行上の細かい決定に了承を求める必要はないと思います。

Glycoconj J (2009) 26:953–959
DOI 10.1007/s10719-008-9138-4

Extraction and separation of proteoglycans

Masaki Yanagishita · Katarzyna Anna Podyma-Inoue ·
Miki Yokoyama

Received: 3 April 2008 / Revised: 14 April 2008 / Accepted: 15 April 2008 / Published online: 21 May 2008
© Springer Science + Business Media, LLC 2008

Abstract Proteoglycans contain a unique carbohydrate component, glycosaminoglycan, which consists of repeating, typically sulfated disaccharides, and is capable of interacting with diverse molecules. Specific, clustered arrangements of sulfate on the glycosaminoglycan backbone form binding sites for many biologically important ligands such as extracellular matrix molecules and growth factors. Core proteins of proteoglycans also show molecular interactions necessary for organizing scaffolds in the extracellular matrix or for anchoring proteoglycans to the plasma membrane. Experimental protocols aiming at extracting maximal amounts of proteoglycans from tissues or cells require disruption of molecular interactions involving proteoglycans by denaturing solvents. Among many of the proteoglycan separation procedures, anion exchange chromatography, which takes advantage of the presence of highly negatively charged glycosaminoglycans in all proteoglycans, serves one of the most convenient general separation techniques.

Keywords Proteoglycan · Glycosaminoglycan · Extraction · Separation

Introduction

Proteoglycans are a class of glycosylated proteins characterized by the presence of glycosaminoglycans as a carbohydrate component, which endows proteoglycans with unique biochemical as well as biological properties.

The composition of proteoglycans vary widely, for example, the number of glycosaminoglycan chains per molecule could be as many as over 100 in aggrecan, the major proteoglycan in cartilage, or as few as just one in decorin. There are four general classes of glycosaminoglycans:¹ (1) chondroitin sulfate and dermatan sulfate, (2) heparan sulfate and heparin, (3) keratan sulfate, and (4) hyaluronan (which is not synthesized on a core protein and, therefore, is not classified as a component of a proteoglycan). Glycosaminoglycans consist of linear polymers of repeating (typically 50–100 repeats²) disaccharides of defined structure which consists of one hexosamine, which often contains one or more sulfate residues,³ and either a hexuronic acid or a

¹ Discussions on biochemical and biological characteristics of each glycosaminoglycan can be found in excellent reviews published elsewhere [1–4].

² Except hyaluronan, which is synthesized at the plasma membrane, contains many more repeating disaccharides up to ~25,000 per chain, and does not undergo sulfation.

³ In many studies on biological functions of proteoglycans, cell culture and tissue explant systems in combination with metabolic radiolabeling techniques are employed. In these experiments, monitoring incorporated radioactivity provides excellent measures to follow proteoglycans through extraction and purification steps and to evaluate recoveries at each experimental step. Due to characteristic sulfation in the glycosaminoglycan moiety, [³⁵S]sulfate is an excellent precursor for metabolic labeling of glycosaminoglycans, thus proteoglycans. In many cell culture systems, more than ~90% of radioactive incorporation of ³⁵S from [³⁵S]sulfate is accounted for by the incorporation into glycosaminoglycans. Concomitant use of other radioactive precursors such as those labeled with ³H, which can be differentiated from ³⁵S by spectral analysis, provides further detailed information about molecular structures and metabolic state of the cell. For example, the use of [³H]glucosamine, as shown in the present manuscript, allows labeling hexosamines ([³H]glucosamine is metabolically converted into both [³H]glucosamine and [³H]galactosamine) in all glycoconjugates synthesized by the cell. Further details on metabolic labeling techniques using cell cultures should be consulted elsewhere [5].

M. Yanagishita (✉) · K. A. Podyma-Inoue · M. Yokoyama
Biochemistry, Department of Hard Tissue Engineering,
Graduate School, Tokyo Medical and Dental University,
1–5–45 Yushima, Bunkyo-ku,
Tokyo 113–8549, Japan
e-mail: m.yanagishita.bch@tmd.ac.jp

hexose in keratan sulfate. Specific spatial arrangements of clustered sulfate residues on glycosaminoglycans provide binding sites for various biologically active molecules, which regulate cell functions (an aspect of proteoglycan functions extensively studied [1–4]). In many biological circumstances, highly negatively charged glycosaminoglycan structures also attract many positively charged molecules in less specific manners.

Proteoglycans widely distribute as major molecular components in most extracellular matrices (representative molecules include aggrecan, versican, decorin and perlecan among many), as integral plasma membrane proteins (including syndecan and glypican families), and as an intracellular molecule (serglycin) associated with storage granules in mast cells. Relatively limited number, over 50 separate gene products, of core proteins have been identified, and they show specific spatial as well as temporal expression patterns. The core proteins fundamentally define biochemical compositions of proteoglycans under genetic control and direct cell biological behavior of the molecules, *e.g.*, posttranslational modification, trafficking through intracellular compartments, and targeting to their destinations *etc.* In extracellular matrices, proteoglycans form highly ordered scaffolds through specific molecular interactions with other major matrix molecules (binding of core proteins of aggrecan and versican to hyaluronan, and binding of decorin to collagens are good examples). On the plasma membrane, core proteins of syndecan family proteoglycans are intercalated into the plasma membrane, while those of glypicans are linked to glycosylphosphatidylinositol (GPI)-anchors. Understanding molecular interactions involving proteoglycans, especially those with major extracellular molecules, is key in studying biological functions of proteoglycans and in designing experiments extracting proteoglycans from extracellular matrices.

General considerations on extraction and separation of proteoglycans Proteoglycans have been recognized as a crucial hub in organizing supramolecular scaffolds in the extracellular matrices by their binding to many extracellular matrix molecules through multiple binding domains in glycosaminoglycans and core protein. Thus, intact proteoglycans generally resist extraction in associative solvent conditions, which preserve molecular interactions, and require the use of dissociative solvent conditions for efficient extraction from the tissue [5, 6]. Dissociative conditions of high guanidine HCl concentrations (ordinarily at 4 M) have been most widely employed. For the extraction of cell-associated proteoglycans, the concomitant use of a detergent is necessary. Most non-ionic detergents (such as Triton X-100 and NP-40 with low critical micellar

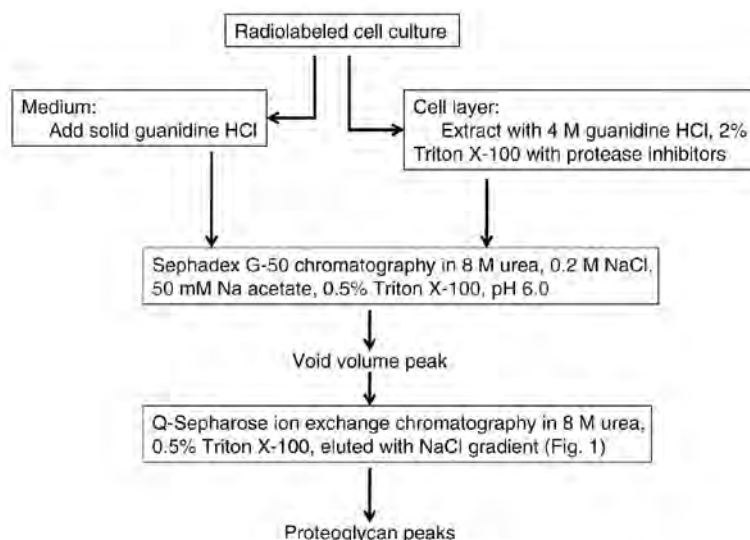
concentration, CMC) or zwitter-ionic detergents (such as 3-[(3-cholamidopropyl)-dimethylammonio]-1-propanesulfonate, CHAPS, with high CMC) are compatible with 4 M guanidine HCl. In addition, the use of detergent, not only at the time of proteoglycan solubilization from the cell membrane, but also throughout purification procedures, has been shown to dramatically improve recoveries of proteoglycans in most experimental procedures.

Because of their exceptional diversity in molecular constructions and in properties of molecular interactions, there is no single set of extraction or separation procedure which is usable for every proteoglycan. Therefore, the techniques described below illustrate general principles that can be successfully modified in different combination for characterizing a particular proteoglycan. This manuscript focuses on experimental procedures, which are particularly useful obtaining total proteoglycan and glycosaminoglycan species non-selectively and in high yield from various biological sources. Other reviews on similar subjects should be consulted for more detailed discussions on specific subjects [5–8].

Materials and methods

Proteoglycan material Rat ovarian granulosa cell cultures radiolabeled with [35 S]sulfate and [3 H]glucosamine are used as a starting material containing proteoglycans [9]. See footnote 3 for detailed discussion on metabolic labeling experiments using cell cultures.

Extraction At the conclusion of cell culture, medium is removed from the cell culture dish and analyzed separately (Scheme 1). Approximately 2 ml (per 35 mm diameter cell culture dish) of extraction buffer (4 M guanidine HCl, 0.05 M Na acetate, pH 6.0, containing 2% (w/v) Triton X-100 and a cocktail of protease inhibitors [*i.e.*, 1 mM 4-(2-aminoethyl)benzenesulfonylfluoride (AEBSF, from Calbiochem), 10 mM *N*-ethylmaleimide (NEM), 10 mM disodium ethylenediaminetetraacetic acid (EDTA)] [10] is then added to a culture plate. AEBSF and a stock solution of NEM (100 × concentrated in ethanol) are added to the buffer just prior to use (as they are relatively unstable in aqueous solutions). Proteoglycans are extracted within 2–3 h of constant shaking at 4°C. When the extraction is complete, vigorous vortexing of the sample for 1–2 min allows fragmentation of macromolecular DNA by shear forces, making samples amenable for easy handling in the subsequent chromatographic procedures. As used originally in the extraction of proteoglycans from the cartilage tissue [6], guanidine HCl at 4 M concentration generally provides

Scheme 1 A flow diagram of proteoglycan separation using radiolabeled cell culture

excellent solubilization of proteoglycans from most tissues. When solid tissues are to be extracted, approximately ten times volume of 4 M guanidine HCl buffer is used to solubilize proteoglycans after finely mincing the tissue and incubating for 12 h at 4°C. Ordinarily, only gentle agitation is required for efficient extraction. Extraction of proteoglycans from calcified tissues often requires additional decalcification solvents, which can be prepared by including a high concentration of EDTA (*e.g.*, at 0.5 M) [11]. Although secreted proteoglycans in cell culture media are generally already soluble, in order to minimize interactions between highly charged proteoglycans and other molecules, solid guanidine HCl (0.53 g solid guanidine HCl per ml of media makes 4 M guanidine HCl solution) and a protease inhibitor cocktail at concentrations described above are directly added to the medium. Usually, omission of detergents for the extraction of proteoglycans in the medium compartment is not critical at this stage, as, perhaps, samples contain only limited amounts of hydrophobic elements (as long as detergents are included in subsequent chromatographic steps, see below).

The cells or tissues usually contain several different species of proteoglycans, some of which are integrated in the extracellular matrix by noncovalent interactions, associated with the plasma membrane through hydrophobic interactions either by intercalation of core protein or by phosphatidylinositol anchors, and as a content of intracellular granules. The extraction of proteoglycans usually aims at solubilizing maximum amounts of proteoglycan without degradation, which requires the use of denaturing solvents. For this purpose, 4 M guanidine HCl containing detergent

is the solvent employed most often.⁴ Inclusion of an appropriate detergent is not only crucial when extracting cell-associated proteoglycans, but also is generally beneficial achieving good recovery in many experimental procedures. Since proteoglycans can be easily degraded, especially by proteases, inclusion of a protease inhibitor cocktail is desirable. Inhibitors, which introduce covalent modification of amino acids, have been shown to be most effective [10]. For solid tissues such as tissue explants, efficiency of extraction can be drastically improved by fine mincing [6].

Solvent exchange In order to prepare the extracted proteoglycans in 4 M guanidine HCl for anion exchange chromatography procedure in the next step, guanidine

⁴ Additional consideration should be made when one is attempting to extract cell-associated proteoglycans; *i.e.*, inclusion of sufficient amounts of detergent may be necessary (such as 2% Triton X-100, a non-ionic detergent, or 1% CHAPS, a zwitter-ionic detergent) for the solubilization of proteoglycans [5]. It should be noted that critical micellar concentration of detergents could change drastically in chaotropic solvents such as guanidine HCl or urea [12], and some of the detergents are not soluble in such solvents. Adding the detergent from the beginning of extraction is highly preferred in order to completely disrupt hydrophobic interactions, since irreversible, artificial molecular complexes may be formed between newly exposed hydrophobic sites in proteins during the process of denaturation by 4 M guanidine HCl.

HCl has to be replaced with a solvent compatible with the procedure. A preferred solvent is a urea buffer since it disrupts molecular interactions by interfering with the formation of hydrogen bonds. A convenient buffer exchange procedure can be done by gel filtration (such as Sephadex G-50 chromatography) using a small disposable pipette.⁵ This process is also convenient to remove unincorporated radioactive precursors, when radiolabeled cell cultures were extracted with 4 M guanidine HCl solvent.

Separation of proteoglycans Separation of proteoglycan species can be achieved by taking advantage of their biochemical characteristics, especially those of glycosaminoglycans, including high negative charge, large hydrodynamic size, high buoyant density, *etc.* Hydrophobicity or biological recognition by various ligands can also be utilized.

A. Charge—Anion exchange chromatography described here is an excellent single step procedure to separate

proteoglycans from other molecules⁶; all proteoglycan species can be collected since they all possess highly negatively charged glycosaminoglycan components by definition. In some experiments, this separation technique alone provides samples of sufficient purity in proteoglycan content. In addition, since different kinds of glycosaminoglycans tend to have distinct charge properties based on the extent of sulfation, separation of proteoglycan species based on their glycosaminoglycan composition may, at least partially, be achieved. For example, chondroitin sulfate is generally more negatively charged than most heparan sulfate (in Fig. 1, two distinct ³⁵S-labeled proteoglycan peaks are observed in the NaCl gradient; a peak eluting at lower NaCl concentrations (indicated by a horizontal

⁵ Solvent exchange by Sephadex G-50 chromatography in a disposable pipette—Preswell Sephadex G-50, fine (obtained from GE Healthcare Life Science) in hot water off the heater, which achieves sterilization, degassing and shortening of swelling time. An extreme caution should be exercised when adding Sephadex powder to boiling water to avoid flushing. A convenient concentration of gel (50% slurry) can be made by mixing 5 g of Sephadex G-50 with 100 ml water. Bacteriostatic agents (*e.g.*, 0.02% Na azide) should be added for a long-term storage. Pour preswollen Sephadex G-50 into a 10 ml plastic disposable pipette (Falcon), which was cut at the top with a file and plugged with glass wool (no. 3950, Corning) at the bottom, to make 8 ml bed volume. Remove excess water and equilibrate the column with a buffer (8 M urea, 0.20 M NaCl, 0.05 M Na acetate, 0.5% Triton X-100, pH 6.0, a total of 9 ml is sufficient to equilibrate the column). Carefully prepare a flat gel surface with a glass Pasteur pipette and remove excess urea buffer. Apply 2 ml sample and discard the eluent. After the entire sample is in the column, carefully overlay 3 ml of buffer and collect eluent until the entire buffer is in the column (3 ml of V₀ fraction collected). This fraction contains proteoglycans and other macromolecules in 8 M urea buffer, while leaving small molecules in the original extract (guanidine HCl, isotope precursors *etc.*) behind in the column. At this point, column can be safely disposed as a radioactive waste. Dimension of the column may be changed proportionately when sample size varies.

⁶ Q-Sepharose chromatography—Q-Sepharose, fast flow (GE Healthcare Life Science) has to be pre-equilibrated with the low salt buffer (8 M urea, 0.20 M NaCl, 0.05 M Na acetate, 0.5% Triton X-100, pH 6.0) used in the NaCl gradient. Two ml of pre-equilibrated Q-Sepharose (1 ml of Q-Sepharose can bind up to 3–5 mg of proteoglycans) is packed into a small column (10 ml plastic pipette is cut by a file and plugged with glass wool at the bottom). Alternatively, 2 ml of pre-equilibrated Q-Sepharose is mixed with the sample in 8 M urea buffer (of any volume) and gently shaken for 1 h, then packed into the column; this latter method gives uniform binding of proteoglycans to Q-Sepharose gel resulting in a better flow property, especially when a large quantity of materials (proteoglycan, protein, nucleic acid, *etc.*) is used. After sample application, the column is washed with 10 ml of the low salt buffer. Then the column is connected to a gradient former (using, for an example, a high salt buffer: 8 M urea, 1.5 M NaCl, 0.05 M Na acetate, 0.5% Triton X-100, pH 6.0) and eluted with approximately a total 40 ml of buffer with a flow rate of 10–15 ml/h. Every 1–2 ml fraction is collected and monitored for NaCl concentration by conductivity measurement, Fig. 2. Eluent fractions are monitored for proteoglycans by radioactivity detection or colorimetric procedures, such as a convenient and safe colorimetric procedure using Safranin O [6, 13] or a classic procedure measuring uronic acid by m-phenylphenol reactants [14], which can be modified to use a microtiter plate for easier handling. Typically, heparan sulfate proteoglycans are eluted in a peak at approximately 0.5 M NaCl and chondroitin sulfate proteoglycans at 0.65 M NaCl. The use of step elution for the purpose of differentially eluting proteoglycan species is not recommended unless salt concentrations in which individual proteoglycans elute are widely separate. Determination of the exact salt concentration which enables clear separation of proteoglycan species may be rather delicate. One of the major technical problems associated with anion exchange chromatography of proteoglycans, especially when purifying molecules are present in small quantities (*e.g.*, isolation of proteoglycans from cell cultures), is poor recovery. This can be, in most cases, overcome by the use of detergents (either non-ionic or zwitter-ionic) in elution buffer. Routinely, the use of 0.5% (w/v) Triton X-100 dramatically improves recovery of proteoglycans (even glycosaminoglycans) from ion exchange columns. Most non-ionic detergents (such as Triton X-100 and NP-40) possess strong absorbance in the UV range, thus making the UV tracing for protein detection difficult. If this causes problems in the analysis, non-UV absorbing, non-ionic detergents such as Genapol X-100® (Calbiochem) can be used with virtually the same chromatographic result. Also, when the removal of detergents in later experimental steps is required, the use of ones with high CMC (such as CHAPS, Calbiochem) in place of Triton X-100 is beneficial.

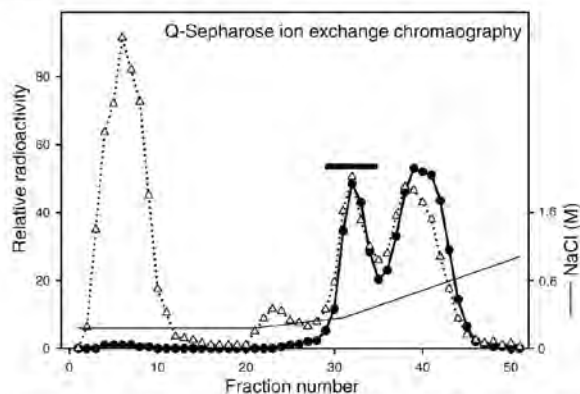


Fig. 1 Q-Sepharose anion exchange chromatography. Extract of a cell culture metabolically labeled with [^{35}S]sulfate and [^3H]glucosamine [9] is analyzed. A large peak at the breakthrough containing ^3H -labeled (unfilled triangle and dot line) macromolecules, which mostly represented glycoproteins, is efficiently separated from ^{35}S -labeled (filled circle with solid line) proteoglycan peaks eluting later in high salt fractions. The earlier ^{35}S -labeled peak (indicated by a horizontal bar and used for gel filtration analysis shown in Fig. 2) contains mostly heparan sulfate proteoglycans and the latter mostly chondroitin/dermatan sulfate proteoglycans

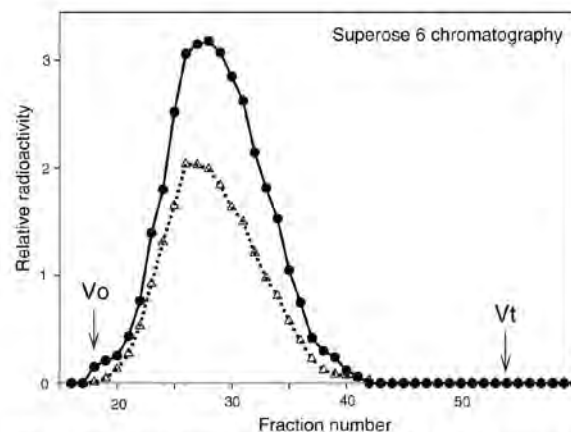


Fig. 2 Superose 6 chromatography of the first ^{35}S -labeled proteoglycan peak (as indicated by a bar in Fig. 1, representing heparan sulfate proteoglycan) is analyzed in 4 M guanidine HCl, 0.5% Triton X-100. A cell culture is metabolically labeled using [^3H]glucosamine (unfilled triangle and dot line) and [^{35}S]sulfate (filled circle with solid line). Void volume (V_0) and the column total volume (V_t) are indicated by arrows

bar) contains mostly heparan sulfate proteoglycans, while that eluting in higher NaCl concentrations contains mostly chondroitin/dermatan sulfate proteoglycans). Heparin is more highly sulfated than chondroitin sulfate and is eluted at even higher concentrations of NaCl. Ion exchange chromatography is generally a step allowing both purification and concentration at the same time, a useful tip to remember, when performing multiple sequential procedures.

- B. Molecular size—Hydrodynamic sizes of proteoglycans are generally large because of the contribution by glycosaminoglycans, but vary greatly by species. In addition, proteoglycans typically show considerable molecular size microheterogeneity because of variation in glycosaminoglycan number or composition in a single proteoglycan molecule. Because of these molecular characteristics, many frequently used procedures such as gel electrophoresis do not provide desirable, clear separation of proteoglycans (see later section on analytical methods). Gel filtration chromatography has been used more successfully in many experiments. It also has additional advantages of providing quantitative information about the recovery of materials in the procedure, and if appropriate combinations of elution buffer and gel material are used, excellent recovery may be expected. For the analysis of proteoglycan species with large hydrodynamic sizes such as aggrecan and perlecan, Sephacryl S-500 or S-1000, Sepharose CL-2B (gel filtration media all from GE Healthcare Life Science) are appropriate, while proteoglycans with smaller hydrodynamic sizes such as decorin, biglycan,

cell surface heparan sulfate proteoglycans or partially degraded proteoglycans can be analyzed by Superose 6, HR 10/30 (GE Healthcare Life Science). In all cases, the use of 4 M guanidine HCl, 0.05 M Na acetate, 0.5% (w/v) Triton X-100, pH 6.0 allows analysis of molecules in dissociated, monomeric forms. The use of associative solvents, such as guanidine HCl buffer below 0.5 M concentrations, on the other hand, permits some specific molecular interactions involving proteoglycans to occur, for example, association of aggrecan or versican with hyaluronan. As an illustration, gel filtration analysis of cell surface heparan sulfate proteoglycan purified by Q-Sepharose chromatography⁷ is shown in Fig. 2.

- C. Buoyant density—Glycosaminoglycans have high buoyant densities in CsCl equilibrium density gradient because of their intrinsically high buoyant density and the presence of a large number of anionic groups, which bind to dense cesium ion. Thus, this procedure allows efficient separation of proteoglycans with high glycosaminoglycan-to-protein ratios (their densities often reach almost as high as those of nucleic acids) from bulk proteins. This procedure is particularly

⁷ Superose 6 chromatography—A Superose 6 column (HR 10/30, 1 × 30 cm) is preequilibrated with 4 M guanidine HCl, 50 mM Na acetate, pH 6.0 containing 0.5% Triton X-100 and eluted with the same buffer at a flow rate of 0.4 ml/min and fractions of 0.4 ml are collected for measurement of proteoglycan content (by radioactivity or colorimetric analysis [6, 13, 14]). Inclusion of detergent in the elution buffer is critical to obtain quantitative recovery. Most efficient detergents in this respect have been non-ionic detergent such as Triton X-100.

suited for the purification of proteoglycans with many glycosaminoglycan chains (*i.e.*, the procedure has been extensively used to separate and characterize proteoglycans in cartilage tissues [6]). On the other hand, the procedure is not suitable for isolating proteoglycans with only few glycosaminoglycans or with high protein contents (*e.g.*, 'small, leucine-rich proteoglycans' and cell surface heparan sulfate proteoglycans). One advantage of the procedure is that experiments can be performed in associative solvent conditions retaining specific molecular interactions involving proteoglycans, thus enabling to isolate molecules which show specific interactions with proteoglycans [6].

Separation of selective proteoglycans Above described separation techniques, namely, anion exchange chromatography, gel filtration and buoyant density ultracentrifugation, separate proteoglycans non-selectively as long as their physical characteristics are similar. However, in some cases when individual proteoglycan species are analyzed, particular cells/tissues are used or experimental design demands special requirements, *etc.*, additional separation techniques are required. Many such example cases have been compiled elsewhere [8], and can be consulted. Here, two additional relatively general procedures are discussed. They add further dimensions to the principles of proteoglycan separation and could provide means to separate hard-to-separate proteoglycans or hard-to-remove contaminants (such as nucleic acid, highly negatively charged glycoproteins, *etc.*). Again, the procedures have been optimized mainly for separation and quantitative recovery.

Hydrophobic chromatography Hydrophobic [5] nature of core proteins could be used to separate proteoglycan species otherwise difficult to separate. Excellent separation of two similar proteoglycan species was achieved by the use of Octyl-Sepharose chromatography in the presence of 4 M guanidine HCl eluted with a detergent gradient [15].

Lectin affinity chromatography There have been reports of lectins, such as annexins and galectins, which specifically bind to glycosaminoglycans. As an example, an annexin, which specifically binds to heparan sulfate, has been used to purify heparan sulfate proteoglycans by affinity chromatography^{*} [16], Fig. 3. One of the major contaminants

^{*} Annexin affinity chromatography—SH-derivatized Magnetic beads[®] (obtained from Promega) is conjugated with annexin. Binding of radiolabeled heparan sulfate proteoglycan to the beads is performed in 200 μ l of buffer consisting of 10 mM Hepes, 50 mM NaCl, pH 7.0, containing 0.5% Triton X-100 and 1% BSA. Supernatant is removed after incubation at 4°C for 1 h. Washed beads are then eluted with 10 mM Hepes, 500 mM NaCl, 5 mM EDTA, pH 7.0, containing 0.5% Triton X-100, and the eluant is counted for radioactivity.

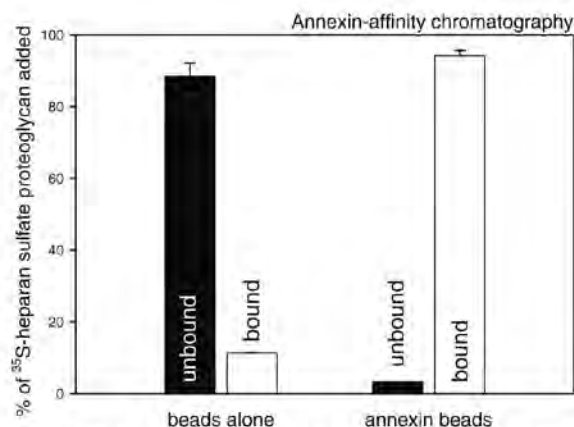


Fig. 3 Affinity chromatography using a lectin, annexin, which specifically binds to heparan sulfate [14]. Binding of radiolabeled heparan sulfate proteoglycan to unconjugated beads (*left columns*) and annexin-conjugated beads (*right columns*) is compared

encountered in proteoglycan specimens obtained by anion exchange chromatography, gel filtration and equilibrium density gradient centrifugation includes nucleic acid, and it could be efficiently removed by this procedure. Applicability of this method in other situations, however, needs to be further examined. Specific hyaluronan-binding properties of some proteoglycans (*i.e.*, hyaluronan-binding proteoglycans, such as aggrecan and versican) have been used extensively [6] for the purification and characterization of proteoglycans. In this case, lectin-like properties of proteoglycan are used.

Other analytical methods For non-radiolabeled samples, chemical or immunological detection of proteoglycans is required during separation procedures. It is not the objective of this manuscript to detail a comprehensive list of analytical procedures for proteoglycans, which can be consulted elsewhere [8]. Here, some of the selected analytical methods, which are recently developed and/or convenient to use, are discussed briefly. The use of polyacrylamide gel electrophoresis for the molecular size analysis of intact proteoglycans has been hampered because of extremely large hydrodynamic sizes of some proteoglycans (especially aggrecan, versican and perlecan, *etc.*) However, the use of polyacrylamide/agarose composite gel allows electrophoretic analysis of these large proteoglycans [17]. However, the poor transfer of proteoglycans from gel to membrane often precludes some useful procedures such as immunological detection with Western blot analysis. Identification of core proteins, on the other hand, is most often done with polyacrylamide gel electrophoresis, using core protein preparations generated by the treatment of proteoglycans with glycosaminoglycan degrading enzymes (*i.e.*, bacterial eliminases such as chondroitin-

nase and heparitinase). Core proteins prepared by such a method form tight bands suitable for accurate molecular weight estimation as ordinary proteins, and they are also efficiently transferred to membranes used for immunological identification by specific antibodies raised against individual core proteins [18]. Some of the excellent analytical methods for glycosaminoglycans and their constituent disaccharides developed recently are also worth mentioning. They include capillary electrophoresis of fluorescently labeled glycosaminoglycans [19], and fluorophore-assisted carbohydrate electrophoresis [20, 21] for the analysis of constituent disaccharides of glycosaminoglycans. The former provides high speed and sensitivity analysis suitable for studying molecular interactions, such as those between glycosaminoglycans and growth factors.

Conclusion and future directions

Explosive expansion of genetic information and molecular biological techniques, together with rapidly accumulating knowledge on molecules using structural biological techniques greatly demands renewed efforts and refinements in biochemical analyses of proteins. Proteoglycans are no exception with this argument. The general techniques for proteoglycan separation described in this article only fulfill minimum necessities of proteoglycan research in the new generation, but hopefully they would aid us to catch up with the developments in other field of life sciences. Some of the already available high resolution analytical techniques, such as mass spectroscopy, for example, would provide extremely powerful biochemical analytical tool, when it becomes more accessible and is combined with other newer separation techniques. We hope that the days are not too far when the studies of life sciences are further accelerated by the concerted developments in all fields of life sciences to answer many more fundamental questions on life.

References

- Kimata, K., Habuchi, O., Habuchi, H., Watanabe, H.: Knockout mice and proteoglycans, in comprehensive glycoscience. In: Kamerling J. P., et al. (eds.) Elsevier, Amsterdam (2007)
- Shipp, E.L., Hsieh-Wilson, L.C.: Profiling the sulfation specificities of glycosaminoglycan interactions with growth factors and chemotactic proteins using microarrays. *Chem. Biol.* **14**, 195–208 (2007)
- Habuchi, H., Habuchi, O., Kimata, K.: Sulfation pattern in glycosaminoglycan: Does it have a code? *Glycoconj. J.* **21**, 47–52 (2004)
- In: Conrad, H.E. (ed.) *Heparin-Binding Proteins*. Academic, San Diego (1998)
- Hascall, V.C., Calabro, A., Midura, R.J., Yanagishita, M.: Isolation and characterization of proteoglycans. *Methods Enzymol.* **230**, 390–417 (1994)
- Hascall, V.C., Kimura, J.H.: Proteoglycans: Isolation and characterization. *Methods Enzymol.* **82**, 769–800 (1982)
- Yanagishita, M., Midura, R.J., Hascall, V.C.: Proteoglycans: Isolation and purification from tissue cultures. *Methods Enzymol.* **138**, 279–289 (1987)
- In: Iozzo, R.V. (ed.) *Proteoglycan Protocols*. Humana, New Jersey (2001)
- Yanagishita, M., Hascall, V.C.: Proteoglycans synthesized by rat ovarian granulosa cells in culture; isolation, fractionation, and characterization of proteoglycans associated with the cell layer. *J. Biol. Chem.* **259**, 10260–10269 (1984)
- Oike, Y., Kimata, K., Shinomura, T., Nakazawa, K., Suzuki, S.: Structural analysis of chick-embryo cartilage proteoglycan by selective degradation with chondroitin lyases (chondroitinases) and endo-beta-D-galactosidase (keratanase). *Biochem. J.* **191**, 193–207 (1980)
- Fisher, L.W., Termine, J.D., DeJler Jr., S.W., Whitson, S.W., Yanagishita, M., Kimura, J.H., Hascall, V.C., Kleinman, H.K., Hassell, J.R., Nilsson, B.: Proteoglycans of developing bone. *J. Biol. Chem.* **258**, 6588–6594 (1983)
- Midura, R.J., Yanagishita, M.: Chaotropic solvents increase the critical micellar concentrations of detergents. *Anal. Biochem.* **228**, 318–322 (1995)
- Lammi, M., Tammi, M.: Densitometric assay of nanogram quantities of proteoglycans precipitated on nitrocellulose membrane with Safranin O. *Anal. Biochem.* **168**, 352–357 (1988)
- Blumenkrantz, N., Asboe-Hansen, G.: New method for quantitative determination of uronic acids. *Anal. Biochem.* **54**, 484–489 (1973)
- Midura, R.J., Hascall, V.C.: Analysis of proteoglycans synthesized by corneal explants from embryonic chicken II. Structural characterization of keratan sulfate and dermatan sulfate proteoglycans from corneal stroma. *J. Biol. Chem.* **264**, 1423–1430 (1989)
- Ishitsuka, R., Kojima, K., Utsumi, H., Ogawa, H., Matsumoto, I.: Glycosaminoglycan binding properties of Annexin IV, V, and VI. *J. Biol. Chem.* **273**, 9935–9941 (1998)
- Heinegård, D., Wieslander, J., Sheehan, J., Paulsson, M., Sommarin, Y.: Separation and characterization of two populations of aggregating proteoglycans from cartilage. *Biochem. J.* **225**, 95–106 (1985)
- Couchman, J.R., Tapanadechopone, P.: Detection of proteoglycan core proteins with glycosaminoglycan lyases and antibodies. In: Iozzo, R.V. (ed.) *Proteoglycan Protocols*, pp. 329–333. Humana, New Jersey (2001)
- Militopoulou, M., Lamari, F., Karamanos, N.K.: Capillary electrophoresis: A tool for studying interactions of glycans/proteoglycans with growth factors. *J. Pharm. Biomed. Anal.* **32**, 823–828 (2003)
- Karousou, E.G., Viola, M., Genasetti, A., Vigetti, D., De Luca, G., Karamanos, N.K., Passi, A.: Application of polyacrylamide gel electrophoresis of fluorophore-labeled saccharides for analysis of hyaluronan and chondroitin sulfate in human and animal tissues and cell cultures. *Biomed. Chromatogr.* **19**, 761–765 (2005)
- Calabro, A., Benavides, M., Tammi, M., Hascall, V.C., Midura, R.J.: Microanalysis of enzyme digests of hyaluronan and chondroitin/dermatan sulfate by fluorophore-assisted carbohydrate electrophoresis (FACE). *Glycobiology* **10**, 273–281 (2000)

口腔病理学分野

山口 朗

医歯学総合研究科・口腔機能再構築学系専攻
口腔病理学・教授



1) 研究課題名

(1) 口腔癌による顎骨破壊の分子メカニズム (図A)

Molecular mechanism of bone destruction by oral cancer

我々は歯肉癌の顎骨浸潤部では、癌巣と骨の間に必ず線維性結合組織が介在し、癌による顎骨吸収部にはRANKL陽性の線維芽細胞様細胞が出現していることを明らかにした (BONE 43:621-627,2008)。これらの結果は、癌細胞が何らかの因子を介して線維芽細胞様細胞のRANKL発現を誘導し、癌による骨破壊を亢進していることを示唆している。我々はこの点を詳細に検討するために、口腔扁平上皮癌による骨破壊過程におけるIL-6, PTHrPの役割を解析した。その結果、口腔扁平上皮癌細胞は自らIL-6を産生しているが、間質の線維芽細胞におけるIL6産生を強力に促進していることを明らかにした。また、癌細胞の産生するPTHrPが間質線維芽細胞のIL6産生にも関与していることを示した。さらに、口腔扁平上皮癌細胞株をヌードマウスの頭蓋部皮下に移植することにより、ヒト口腔癌の顎骨浸潤に酷似したモデルを作製することにも成功した。(Amer J Pathol, in press)

(2) 骨芽細胞分化におけるNotch, BMP, CCN3の役割 (図B)

Role of Notch, BMP and CCN3 in osteoblast differentiation

我々はCCN3がBMPおよびNotchに細胞外で結合することにより、BMPのシグナルを抑制し、Notchシグナルを活性化することを明らかにしてきた。本研究ではCCN3が骨髄造血系細胞にも関与することを示すと同時に、CCN3の骨格系への作用をさらに検討するために、骨芽細胞特異的にCCN3を過剰発現するtransgenic miceとCCN3 knockout miceの骨格を解析している。また、これらのマウスにおける骨再生過程の解析も行っている。(J Cell Commun Signal. 3:135-145,2009, Dev

Growth Differ 51:55-67,2009)

(3) 歯および骨組織のin vivo 蛍光イメージングとその生物医学的応用基盤の確立 (図C)

最新のin vivo 蛍光イメージング法を駆使して歯および骨組織の新たな解析法を確立し、それによって新規の生物医学的知見を得ることを目的として以下の研究を行った。

① 発生・骨再生における細胞群の細胞周期in vivo イメージング解析

細胞周期インディケータを組み込んだトランスジェニックマウス (Fucciマウス、増殖停止期 (G1期) を赤、増殖期 (S,G2,M期) を緑で識別できる) の歯および骨組織の発生・発達過程を観察した。その結果、それらの組織の発生・発達過程では、細胞周期パターンが巧妙に、領域および時間特異的に調節を受けていることを観察し、形態形成や機能分化との相関が示唆された。また、骨再生過程に出現する細胞群の細胞周期調節を観察することで、再生に関与する前駆細胞 (幹細胞) 集団の時空間的動態を観察することに成功している。さらに、ゼブラフィッシュの発生過程における細胞周期のin vivo imagingに成功した (Proc Natl Acad Sci USA in press)。

② 蛍光3次元イメージングによる骨系細胞モルフォメリー (形態計測) の確立

新規の蛍光3次元イメージング技術を駆使して骨格の発生・形成過程における骨芽細胞、骨細胞、破骨細胞のモルフォメリー (形態計測) を行い、その細胞内小器官や細胞の大きさや形態・周辺細胞との細胞突起による接着の数などを、計測・数値化した。さらにこれらの骨系細胞の各細胞内小器官や細胞形態さらには細胞間ネットワークの定量解析から、骨組織の成長および代謝機能との相関を見いだす基礎を確立した。

(4) 滑膜性軟骨腫症における BMP の役割 (図 D)

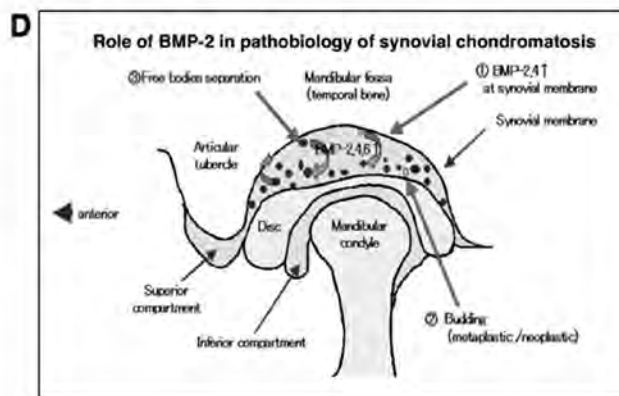
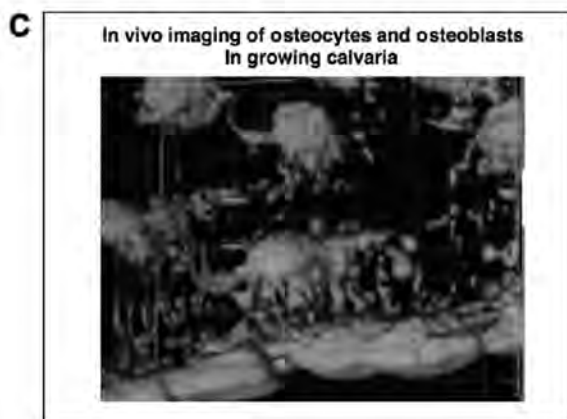
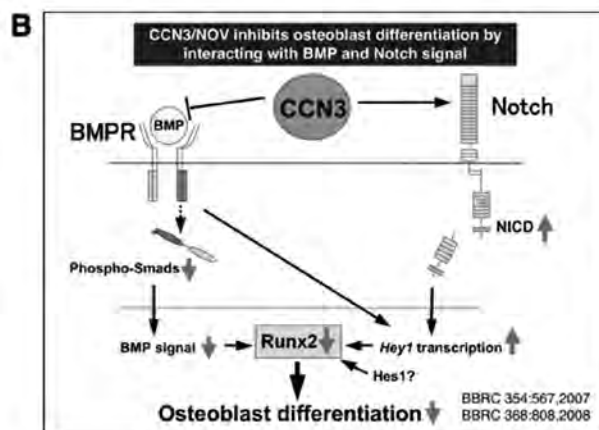
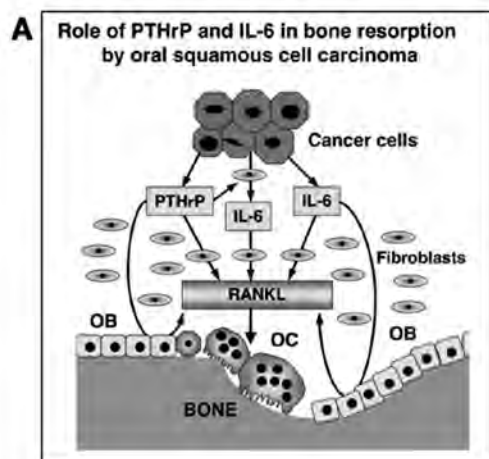
滑膜性軟骨腫症は関節滑膜下に骨・軟骨性結節で構成される遊離体を生じる疾患で、滑膜の化生による疾患と考えられているが、本症における軟骨・骨化生の病態制御機構は十分に明らかにされていない。そのため、本研究では滑膜性軟骨腫症における BMP の役割を検討した。その結果、滑膜性軟骨腫症における遊離体細胞、滑膜細胞は共に BMP-2, BMP-4 を発現しており、遊離体より採取した培養細胞の軟骨細胞への分化は BMP antagonist である Noggin により抑制された。さらに、BMP-2 は培養滑膜細胞における軟骨細胞の分化マーカーの発現を促進した。これらの結果は、滑膜性軟骨腫症では滑膜細胞、遊離体の細胞が自ら BMPs を産生し、それらがオートクライン・パラクライン的に作用して滑膜性軟骨腫症の主たる病態である軟骨・骨化生の誘導に関与していることを示しており、Noggin などの BMP アンタゴニストにより滑膜性軟骨腫症における軟骨・骨化生を抑制できる可能性も示唆した。(Biochem Biophys Res Commun 379:914-919,2009)

2)

3) 研究内容の英文要約

① Nakanishi S, Sakamoto K, Yoshitake H, Kino K, Amagasa T, Yamaguchi A: Bone morphogenetic proteins are involved in the pathobiology of synovial chondromatosis. Biochem Biophys Res Commun 379:914-919,2009

Synovial chondromatosis is characterized by the formation of osteocartilaginous nodules (free bodies) under the surface of the synovial membrane in joints. Free bodies and synovium isolated from synovial chondromatosis patients expressed high levels of BMP-2 and BMP-4 mRNAs. BMP-2 stimulated the expression of Sox9, Col2a1, and Aggrecan mRNAs in free-body and synovial cells and that of Runx2, Col1a1, and Osteocalcin mRNAs in the free-body cells only. BMP-2 increased the number of alcian blue-positive colonies in the free-body cell culture but not in the synovial cell culture. Noggin suppressed the expression of Sox9, Col2a1, Aggrecan, and Runx2 mRNAs in both the free-body and synovial cells. Further, it inhibited Osteocalcin expression in the free-body cells. These results suggest that BMPs are involved in the pathobiology of cartilaginous and osteogenic metaplasia observed in synovial chondromatosis.



- ② Kadouchi I, Sakamoto K, Liu T, Murakami T, Kobayashi E, Hoshino Y, Yamaguchi A: Latexin is involved in bone morphogenetic protein-2-induced chondrocyte differentiation. *Biochem Biophys Res Commun* 378:6000-6004,2009

Latexin is the only known carboxypeptidase A inhibitor in mammals. We previously demonstrated that BMP-2 significantly induced latexin expression in Runx2-deficient mesenchymal cells (RD-C6 cells), during chondrocyte and osteoblast differentiation. In this study, we investigated latexin expression in the skeleton and its role in chondrocyte differentiation. Immunohistochemical studies revealed that proliferating and prehypertrophic chondrocytes expressed latexin during skeletogenesis and bone fracture repair. In the early phase of bone fracture, latexin mRNA expression was dramatically upregulated. BMP-2 upregulated the expression of the mRNAs of latexin, Col2a1, and the gene encoding aggrecan (Agc1) in a micromass culture of C3H10T1/2 cells. Overexpression of latexin additively stimulated the BMP-2-induced expression of the mRNAs of Col2a, Agc1, and Col10a1. BMP-2 treatment upregulated Sox9 expression, and Sox9 stimulated the promoter activity of latexin. These results indicate that latexin is involved in BMP-2-induced chondrocyte differentiation and plays an important role in skeletogenesis and skeletal regeneration.

- ③ Katsube K, Ichikawa S, Katsuki Y, Kihara T, Terai M, Lau LF, Tamamura Y, Takeda S, Umezawa A, Sakamoto K, Yamaguchi A. CCN3 and bone marrow cells. *J Cell Commun Signal*. 3:135-145,2009

CCN3 expression was observed in a broad variety of tissues from the early stage of development. However, a kind of loss of function in mice (CCN3 del VWC domain -/-) demonstrated mild abnormality, which indicates that CCN3 may not be critical for the normal embryogenesis as a single gene. The importance of CCN3 in bone marrow environment becomes to be recognized by the studies of hematopoietic stem cells and Chronic Myeloid Leukemia cells. CCN3 expression in bone marrow has been denied by several investigations, but we found CCN3 positive stromal and hematopoietic cells at bone extremities with a new antibody although they are a very few populations. We investigated the expression pattern of CCN3 in the cultured bone marrow derived mesenchymal stem cells and found its preference for osteogenic differentiation. From the analyses of in vitro experiment using an osteogenic mesenchymal stem cell line, Kusa-A1, we found that CCN3 downregulates osteogenesis by two different pathways; suppression

of BMP and stimulation of Notch. Secreted CCN3 from Kusa cells inhibited the differentiation of osteoblasts in separate culture, which indicates the paracrine manner of CCN3 activity. CCN3 may also affect the extracellular environment of the niche for hematopoietic stem cells.

- ④ Katsube K, Sakamoto K, Tamamura Y, Yamaguchi A. Role of CCN, a vertebrate specific gene family, in development. *Dev Growth Differ* 51:55-67,2009

The CCN family of genes constitutes six members of small secreted cysteine rich proteins, which exists only in vertebrates. The major members of CCN are CCN1 (Cyr61), CCN2 (CTGF), and CCN3 (Nov). CCN4, CCN5, and CCN6 were formerly reported to be in the Wisp family, but they are now integrated into CCN due to the resemblance of their four principal modules: insulin like growth factor binding protein, von Willebrand factor type C, thrombospondin type 1, and carboxy-terminal domain. CCNs show a wide and highly variable expression pattern in adult and in embryonic tissues, but most studies have focused on their principal role in osteo/chondrogenesis and vasculo/angiogenesis from the aspect of migration, growth, and differentiation of mesenchymal cells. CCN proteins simultaneously integrate and modulate the signals of integrins, bone morphogenetic protein, vascular endothelial growth factor, Wnt, and Notch by direct binding. However, the priority in the use of the signals is different depending on the cell status. Even the equivalent counterparts show a difference in signal usage among species. It may be that the evolution of the CCN family continues to keep pace with vertebrate evolution itself.

- ⑤ Kayamori K, Sakamoto K, Nakashima T, Takayanagi T, Morita K, Omura K, Nguyen ST, Miki Y, Iimura T, Himeno A, Akashi T, Yamada-Okabe H, Ogata E, Yamaguchi A: Roles of IL-6 and PTHrP in osteoclast formation associated with oral cancers: The significance of IL-6 synthesized by stromal cells in response to cancer cells. *Amer J Pathol* (in press)

We investigated the roles of interleukin-6 (IL-6) and parathyroid hormone-related peptide (PTHrP) in oral squamous cell carcinoma (OSCC)-induced osteoclast formation. Microarray analyses performed on 43 human OSCC specimens revealed that many of the specimens overexpressed PTHrP mRNA, but a few overexpressed IL-6 mRNA. Immunohistochemical analysis revealed that IL-6 was expressed not only in cancer cells but also in fibroblasts and osteoclasts at the tumor-bone interface. Many of the IL-6-positive cells coexpressed vimentin. Conditioned medium (CM) derived from the

culture of oral cancer cell lines (BHY, Ca9-22, HSC3, and HO1-u-1) stimulated Rankl expression in stromal cells and osteoclast formation. Antibodies against both human PTHrP and mouse IL-6 receptor suppressed Rankl in ST2 cells and osteoclast formation induced by CM from BHY and Ca9-22, although the inhibitory effects of IL6 antibody were greater than those of PTHrP antibody. CM derived from all of the OSCC cell lines effectively induced IL-6 expression in stromal cells, and the induction was partially blocked by anti-PTHrP antibody. Xenografts of HSC3 cells onto the periosteal region of the parietal bone in athymic mice presented histology and expression profiles of RANKL and IL-6 similar to those observed in bone-invasive human OSCC specimens. These results indicate that OSCC provides a suitable microenvironment for osteoclast formation not only by producing IL-6 and PTHrP but also by stimulating stromal cells to synthesize IL-6.

- ⑥ Sugiyama M, Sakaue-Sawano A, Iimura T, Fukami K, Kitaguchi T, Kawakami K, Okamoto H, Higashijima SI, Miyawaki A. Illuminating cell-cycle progression in the developing zebrafish embryo. *Proc Natl Acad Sci U S A*. 2009 Nov 18. [Epub ahead of print]

By exploiting the cell-cycle-dependent proteolysis of two ubiquitination oscillators, human Cdt1 and geminin, which are the direct substrates of SCF (Skp2) and APC (Cdh1) complexes, respectively, Fucci technique labels mammalian cell nuclei in G (1) and S/G (2) / M phases with different colors. Transgenic mice expressing these G (1) and S/G (2) /M markers offer a powerful means to investigate the coordination of the cell cycle with morphogenetic processes. We attempted to introduce these markers into zebrafish embryos to take advantage of their favorable optical properties. However, although the fundamental mechanisms for cell-cycle control appear to be well conserved among species, the G (1) marker based on the SCF (Skp2) -mediated degradation of human Cdt1 did not work in fish cells, probably because the marker was not ubiquitinated properly by a fish E3 ligase complex. We describe here the generation of a Fucci derivative using zebrafish homologs of Cdt1 and geminin, which provides sweeping views of cell proliferation in whole fish embryos. Remarkably, we discovered two anterior-to-posterior waves of cell-cycle transitions, G (1) /S and M/G (1) , in the differentiating notochord. Our study demonstrates the effectiveness of using the Cul4 (Ddb1) -mediated Cdt1 degradation pathway common to all metazoans for the development of a G (1) marker that works in the nonmammalian animal model.

4) 本事業に関連して世界的な研究拠点形成に向けて、改善・整備等したこと

A (研究拠点体制)

研究テーマが散漫にならないように以下の3つのテーマに重点をおいて研究を推進した。

- ① 口腔癌による顎骨破壊の分子メカニズム
- ② 骨代謝、骨再生における Notch シグナルの役割
- ③ 歯・骨組織の in vivo 蛍光イメージングとその生物医学的応用基盤の確立

B (研究教育環境)

綿密な実験計画の立案と実験結果に対する discussion

C (人材確保)

臨床系分野から大学院生を確保している

D (人材育成)

SSと指導教官の綿密な実験計画の立案と研究の推進

E (国際化)

- ・ 研究室の progress meeting を3ヶ月間英語で発表、討論した。
- ・ 外国からの招聘研究者と大学院生の discussion

5) GCOE 事業を推進するに当たって力を入れた点

諸外国や国内の他大学で報告された研究の追試ではなく、originality の高い研究テーマの選定と推進。

6) 英文原著論文

1. ©Nakanishi S, Sakamoto K, Yoshitake H, Kino K, Amagasa T, Yamaguchi A: Bone morphogenetic proteins are involved in the pathobiology of synovial chondromatosis. *Biochem Biophys Res Commun* 379:914-919,2009
2. ©Kadouchi I, Sakamoto K, Liu T, Murakami T, Kobayashi E, Hoshino Y, Yamaguchi A: Latexin is involved in bone morphogenetic protein-2-induced chondrocyte differentiation. *Biochem Biophys Res Commun* 378:6000-6004,2009
3. Katsube K, Ichikawa S, Katsuki Y, Kihara T, Terai M, Lau LF, Tamamura Y, Takeda S, Umezawa A, Sakamoto K, Yamaguchi A. CCN3 and bone marrow cells. *J Cell Commun Signal*. 3:135-145,2009
4. Katsube K, Sakamoto K, Tamamura Y, Yamaguchi A. Role of CCN, a vertebrate specific gene family, in development. *Dev Growth Differ* 51:55-67,2009
5. ©Kayamori K, Sakamoto K, Nakashima T, Takayanagi T, Morita K, Omura K, Nguyen ST, Miki Y, Iimura T, Himeno A, Akashi T, Yamada-Okabe H, Ogata E, Yamaguchi A: Roles of IL-6 and PTHrP in osteoclast

formation associated with oral cancers: The significance of IL-6 synthesized by stromal cells in response to cancer cells. Amer J Pathol

6. ©Sugiyama M, Sakaue-Sawano A, Iimura T, Fukami K, Kitaguchi T, Kawakami K, Okamoto H, Higashijima SI, Miyawaki A. Illuminating cell-cycle progression in the developing zebrafish embryo. Proc Natl Acad Sci U S A. 2009 Nov 18.

7) 著書

1. 山口 朗:骨形成と骨再生. 59-68, 口腔外科ハンドマニュアル09 (日本口腔外科学会編)、クインテッセンス出版株式会社、2009

8) 平成21年度までの自己評価

口腔癌による顎骨浸潤メカニズムの解析と歯・骨の in vivo imaging法の確立に関しては研究が順調に進行し、当初の目的を達成することができた。しかし、骨形成における Notch シグナルの解析に関しては、我々の作成した遺伝子改変マウスに当初予想した phenotype がみられず、予定より研究の進行が遅れており、論文発表には至らなかった。これらのマウスの解析は次年度に向けてさらに解析を続けている。

9) 和文原著論文

1. 芝原孝彦、森田章介、杉原一正、箕輪和行、山口朗、玉田隆文、野村武史:本邦におけるエナメル上皮腫の病態と治療法に関する疫学的研究. 日本口腔腫瘍学会雑誌 21:171-181,2009

10) 学会発表 (和文)

1. 栢森高、坂本啓、明石巧、山口朗:口腔扁平上皮癌の顎骨浸潤における IL-6 と PTHrP の役割、第98回に本病理学会総会、国立京都国際会館、2009年5月3日
2. 坂本啓、山口朗:口腔白板症・扁平上皮癌のバイオマーカーとなるケラチン4、ケラチン13の発現調節機構の解明の試み、第98回に本病理学会総会、国立京都国際会館、2009年5月3日
3. 栢森高、山口朗:口腔扁平上皮癌による骨破壊メカニズム、害12回癌と骨病変研究会、千里阪急ホテル (大阪)、2009年11月20日

11) 外部資金の獲得状況

・科学研究費補助金 基盤研究 (A)

研究題目:骨再生過程における細胞・分子間クロストークの解析

代表:山口 朗

期間:平成19 - 21年

研究費総額:3820万円

・科学研究費補助金 挑戦的萌芽研究

研究題目:骨再生過程における Osteocrine factor の同定

代表:山口 朗

期間:平成21 - 22年

研究費総額:150万円 (平成21年度)

・厚生労働省科学研究費補助金 (再生医療実用化研究事業)

研究題目:実験的再生歯の臨床応用に関する研究

代表:山口 朗

期間:平成21 - 23年

研究費総額:833万円 (平成21年度)

・科学研究費補助金 挑戦的萌芽研究

研究題目:頭蓋骨および顎顔面頸部の発生・発達における4次元蛍光イメージング法の確立

代表:飯村忠浩

期間:平成21年

研究費総額:310万円

・科学研究費補助金 基盤研究 (C)

研究題目:上皮間葉移行の口腔腫瘍での役割

代表:勝部憲一

期間:平成20 - 22年

研究費総額:250万円 (平成20 - 21年度)

・科学研究費補助金 基盤研究 (C)

研究題目:口腔癌におけるケラチン発現異常の病院病理的研究

代表:坂本啓

期間:平成21 - 23年

研究費総額:120万円 (平成21年度)

・科学研究費補助金 若手研究 (B)

研究題目:Fgf23 遺伝子の発現を制御する新規遺伝子の検索と機能解析

代表:玉村禎宏

期間:平成21 - 23年

研究費総額:170万円 (平成21年度)

12) 特別講演、招待講演

- ・山口 朗:ビスフォスフォネート関連顎骨壊死の病理学的所見(招待講演)、ビスフォスフォネート関連顎骨壊死—現状と対策—、神奈川県臨床整形医会、2009年10月24日(横浜ベイシェラトンホテル)
- ・山口 朗:水棲動物と陸棲動物における骨の形態と機能の相違. シンポジウム:系統組織学から見た骨改造の顕微解剖学、第114回日本解剖学会、岡山理科大学、2009年3月28日
- ・山口 朗:骨再生の分子メカニズムの解析とその応用. 第22回日本創外固定・骨延長学会(教育講演). 2009年3月6日
- ・Akira Yamaguchi: Role of BMP and Notch signaling in osteoblast differentiation. The 26th Naito Conference. Awaji Yumebutai International Conference Center, Nov. 5, 2009

13) 講義サマリー

口腔扁平上皮癌は進行すると速やかに顎骨へと浸潤し、患者のその後のQOLを著しく低下させる。口腔癌による顎骨破壊は患者の予後を規定する重要な因子であるが、その詳細なメカニズムは明らかではない。本講義ではその機序を病理組織学的、分子生物学的手法により解析し、癌による骨破壊に対する治療法の開発に寄与する事を概説した。特に以下の点を詳細に講義した。1) 口腔癌の顎骨浸潤部では、癌巣と骨の間には必ず線維性結合組織より成る間質が介在している、2) 口腔癌細胞はPTHrPやIL-6を産生して、間質結合組織におけるRANKL発現を上昇させる、3) 口腔癌細胞が産生する液性因子により間質結合組織のIL-6産生が亢進する、4) 口腔癌細胞及び間質の産生するIL-6が口腔癌による顎骨破壊過程で重要な役割を担っている。

14) 教室、分野や講座の准教授、講師、助教、特別研究員、ポスドク、指導を受けた大学院生の名前(AISSには○印)のリスト

- 飯村忠浩 (GCOE 特任准教授)
- 勝部憲一 (講師)
- 坂本啓 (助教)
- 玉村禎宏 (特任助教)
- 新垣理宣 (顎顔面外科学分野大学院生 AISS から QISS へ)
- 木原翼 (顎顔面外科学分野大学院生)
- 姫野彰子 (歯周病学分野大学院生)

- Samir Kumar Pal (口腔病理学分野大学院生)
- 松本力 (顎顔面矯正学分野大学院生)
- 曹 雷 (口腔病理学分野大学院生)
- 梅原康祐 (部分床義歯学分野大学院生)
- 寺地真由 (歯周病学分野大学院生)
- 大上えりか (顎顔面外科学分野大学院生)
- 渡辺高 (顎顔面外科学分野大学院生)
- 門内一郎 (自治医科大学整形外科大学院生)

15) GCOE 活動についての感想、コメント、改善を望む点

シャペロン教官やSSも決まり、順調に進行していると思います。



Contents lists available at ScienceDirect

Biochemical and Biophysical Research Communications

journal homepage: www.elsevier.com/locate/ybbrc

Bone morphogenetic proteins are involved in the pathobiology of synovial chondromatosis

Shoichi Nakanishi^{a,d}, Kei Sskamoto^a, Hiroyuki Yoshitake^b, Koji Kino^c,
Teruo Amagasa^b, Akira Yamaguchi^{a,d,*}

^aSection of Oral Pathology, Graduate School of Tokyo Medical and Dental University, 1-5-45 Yushima, Bunkyo-ku, Tokyo 113-8549, Japan

^bSection of Maxillofacial Surgery, Tokyo Medical and Dental University, Tokyo, Japan

^cSection of Temporomandibular Joint and Occlusion, Graduate School of Tokyo Medical and Dental University, Tokyo, Japan

^dGlobal Center of Excellence (GCOE) Program, International Research Center for Molecular Science in Tooth and Bone Diseases, Tokyo Medical and Dental University, Tokyo, Japan

ARTICLE INFO

Article history:

Received 20 December 2008

Available online 10 January 2009

Keywords:

Synovial chondromatosis

BMP

Cartilage

Chondrocyte

Bone

Osteoblast

ABSTRACT

Synovial chondromatosis is characterized by the formation of osteocartilaginous nodules (free bodies) under the surface of the synovial membrane in joints. Free bodies and synovium isolated from synovial chondromatosis patients expressed high levels of *BMP-2* and *BMP-4* mRNAs. *BMP-2* stimulated the expression of *Sox9*, *Col2a1*, and *Aggrecan* mRNAs in free-body and synovial cells and that of *Runx2*, *Col1a1*, and *Osteocalcin* mRNAs in the free-body cells only. *BMP-2* increased the number of alcian blue-positive colonies in the free-body cell culture but not in the synovial cell culture. Noggin suppressed the expression of *Sox9*, *Col2a1*, *Aggrecan*, and *Runx2* mRNAs in both the free-body and synovial cells. Further, it inhibited *Osteocalcin* expression in the synovial cells. These results suggest that BMPs are involved in the pathobiology of cartilaginous and osteogenic metaplasia observed in synovial chondromatosis.

© 2009 Elsevier Inc. All rights reserved.

Synovial chondromatosis is characterized by the formation of osteocartilaginous nodules (free bodies) under the surface of the synovial membrane in joints [1]. This disease occurs most commonly in the knee joints [1] and occasionally in the temporomandibular joint [2,3]. Although clonal karyotypic abnormalities [4,5] and rare malignant changes [6,7] have been reported in synovial chondromatosis, this disease is generally considered to be a metaplastic, and not a neoplastic, disease of synovial cells. However, the precise pathobiology involved in cartilaginous metaplasia in this disease has not been elucidated.

Mesenchymal stem cells differentiate into various types of mesenchymal cells such as osteoblasts, chondrocytes, adipocytes, and muscle [8]. During the differentiation of these cells, various local factors are involved in determining cell lineage by the regulation of lineage-specific transcription factors [9]. In the case of chondrocyte differentiation, bone morphogenetic proteins (BMPs) activate *Sox9* [10], which is an essential transcription factor for chondrocyte differentiation [11,12]. BMPs also stimulate osteoblast differentiation by regulating *Runx2* [8,13], which is an essential transcription factor for osteoblast differentiation [13,14]. Further,

BMP-2 converts the differentiation pathway of myogenic cells to osteoblast lineage cells by inhibiting the MyoD family transcription factors [15] and activating *Runx2*. Thus, BMPs play critical roles in the differentiation of various types of mesenchymal cells from mesenchymal stem cells. It has been demonstrated that synovial tissues express *BMP-2*, *BMP-6*, and *BMP-7* in chronic arthritis [16–18]. Several lines of evidence indicate that synovial fibroblasts are capable of differentiating into chondrocytes by stimulation of BMPs [19–21]. These results suggest that synovial cells express BMPs under pathological conditions, and these BMPs induce the differentiation of synovial cells into chondrocytes. This prompted us to explore the role of BMPs in the pathobiology of synovial chondromatosis.

In the present study, we investigated the role of BMPs in regulating chondrocyte differentiation by using cells isolated from synovial chondromatosis patients. Here, we propose that BMPs are involved in the pathobiology of synovial chondromatosis. Our results also provide evidence that BMPs play important roles in mesenchymal cell differentiation not only in the normal developmental process but also under pathological conditions.

Materials and methods

Samples. Synovium and enucleated free bodies were obtained from two synovial chondromatosis patients, who visited the Dental

* Corresponding author. Address: Section of Oral Pathology, Graduate School of Tokyo Medical and Dental University, 1-5-45 Yushima, Bunkyo-ku, Tokyo 113-8549, Japan. Fax: +81 3 5803 0188.

E-mail address: akira.mpa@tmd.ac.jp (A. Yamaguchi).

Hospital at Tokyo Medical and Dental University. These patients had synovial chondromatosis in the temporomandibular joint. Written informed consent was obtained from both the patients, and the experiments were approved by the hospital's Ethical Review Board.

BMP production by the synovium and free bodies in synovial chondromatosis. BMPs were detected by reverse transcription-polymerase chain reaction (RT-PCR) and immunohistochemistry. For the RT-PCR analysis, total RNA was extracted from unfixed frozen samples of the synovium and free bodies maintained at -80°C and from cultured synovial cells by using NucleoSpin (Macherey-Nagel, Duren, Germany). RNA aliquots were reverse transcribed to complementary DNAs by using Oligo(dT) primer (Roche, Mannheim, Germany), deoxynucleotide triphosphate (dNTP; Promega), and Moloney murine leukemia virus (M-MuLV) reverse transcriptase (Fermentas, Hanover, MD). The complementary DNA products were subjected to PCR amplification, using gene-specific primers for BMP-2, BMP-4, BMP-6, and BMP-7 (Table 1). The amplified products were electrophoresed on 2% agarose gel containing ethidium bromide, using OneSTEP ladder 100 (Nippon Gene, Japan).

For immunohistochemistry, synovium and a few enucleated free bodies were fixed in 10% phosphate-buffered formalin and embedded in paraffin. The free bodies were decalcified by treatment with 10% ethylenediaminetetraacetic acid (EDTA) at 4°C for 1 week before embedding in paraffin. The embedded specimens were cut into $4\text{ }\mu\text{m}$ sections. Endogenous peroxidase activity was blocked with 10% hydrogen peroxidase/methanol, and nonspecific binding was blocked with 10% horse serum. Antigen retrieval was performed by incubating the specimens in an antigen retrieval buffer (10 mM Tris, 1 mM EDTA; pH 9.0) in a microwave at 80°C for 60 min. The sections were incubated with goat anti-BMP-2/BMP-4 antibody (dilution, 1:500; Santa Cruz Biotechnology, Santa Cruz, CA), which specifically recognizes both BMP-2 and BMP-4. Anti-goat immunoglobulin G (IgG) (Vector laboratories, Burlingame, CA) was used as the secondary antibody. The antigen-bound peroxidase activity was visualized using 3,3'-diaminobenzidine chromogen.

Cell culture. To isolate cells from the free bodies and synovium obtained from our two patients, each tissue was cut into small pieces (approximately less than $1 \times 1\text{ mm}$), and the pieces were treated with 0.25% trypsin–EDTA solution at 37°C for 20 min. After washing with phosphate-buffered saline (PBS) and Dulbecco's modified minimum essential medium (DMEM; Nacalai Tesque, Kyoto, Japan), the cells were re-incubated with DMEM containing 0.15% collagenase (Collagenase type II; Worthington Biochemical Corporation, Lakewood, NJ) and 0.25% trypsin (Becton, Dickinson and Company, Franklin Lakes, NJ) at 37°C for 4 h. The harvested cells were inoculated into 24-well plates at a density of 2.0×10^4 cells per well and cultured in DMEM containing 10% fetal bovine serum (Invitrogen/Gibco, Carlsbad, CA), penicillin G (50 U/ml),

and streptomycin (50 mg/ml). The culture medium was changed every 3 days and maintained for 6 days with or without 500 ng/ml of recombinant human BMP-2 (rhBMP-2), which was provided by Astellas Pharma, Inc., Tokyo, Japan. To investigate the role of BMPs in chondrocyte and osteoblast differentiation, the cells isolated from the free bodies and synovium were cultured in the presence or absence of 500 ng/ml of noggin (R&D Systems, Minneapolis, MN).

RT-PCR analysis. Total RNA was extracted from the cultured cells and RNA aliquots were reverse transcribed to complementary DNAs as described above. The complementary DNA products were subjected to PCR amplification, using gene-specific primers for Sox9, Col1a1, Col2a1, Col10a1, Aggrecan (Agc1), Runx2, and Osteocalcin (Table 1). Real-time RT-PCR amplification was performed using a LightCycler System (Roche) with a Platinum SYBR Green qPCR SuperMix UDG kit (Invitrogen, Carlsbad, CA). The relative amount of each mRNA was normalized to β -actin mRNA.

Histochemical staining. Cultured cells were fixed in 10% phosphate-buffered formalin for 5 min, washed twice with 10 mM Tris–HCl (pH 7.5), and then double stained with alkaline phosphatase (ALP) and alcian blue. ALP staining was performed at 37°C for 20 min by using 2-(4-iodophenyl)-3-(4-nitrophenyl)-5-phenyl-2H-tetrazolium chloride (INT) as a formazan dye with 5-bromo-4-chloro-3-indolyl phosphate (BCIP) as an enhancer (Roche). After the ALP staining, alcian blue (pH 2.5) staining was performed. Alcian blue-positive nodules were defined as those having a diameter of more than $50\text{ }\mu\text{m}$.

Measurement of ALP activity. Cultured cells were sonicated in radioimmunoprecipitation assay (RIPA) buffer to obtain the cell lysate. ALP activity was determined using *p*-nitrophenylphosphate solution (Wako Pure Chemicals, Osaka, Japan) as the substrate. The amount of *p*-nitrophenylphosphate released was estimated by measuring the absorbance at 405 nm after 30 min of incubation at 37°C . The protein concentration was determined using a bicinchoninic acid (BCA) protein assay kit (Thermo, Waltham, MA).

Statistical analyses. We used *t*-test for the statistical analysis of the influence of rhBMP-2 and noggin. *P* values less than 0.05 were considered significant. Each analysis was performed at least 3 times. The data are presented as mean \pm standard error of mean (SEM) of independent replicates ($n \geq 3$).

Results and discussion

The synovium and free bodies expressed BMPs in synovial chondromatosis

In synovial chondromatosis, free bodies were produced in the joints (Fig. 1A), which are composed of cartilaginous tissues (Fig. 1B). We hypothesized that the synovium and free bodies synthesized BMPs, which might be involved in the excess formation of

Table 1
Primers sequences used for RT-PCR.

Gene	Forward primer	Reverse primer
BMP-2	5'-GCAGTGCTACTGTTGAG	3'-AGATCAGCAATGCTGGT
BMP-4	5'-AAGCGTAGCCTAAGCATCA	3'-TGGTTGAGTTGAGGTGGTCA
BMP-6	5'-GCGACACCAAGAGAGTTCA	3'-CCCATACTACACGGGTGTC
BMP-7	5'-GGCTATGAGCTTCGTCAACC	3'-GCAGCAAGAGATCCGATTCC
Sox9	5'-AGCAAGGAGATGAAATCTGTCG	3'-AGAGTCTCTGGTCTCAATTGGA
Aggrecan	5'-AAGTATCATCAGTCCAGAAATCTAGCA	3'-TTGGTGGAGACCTAAGCTGC
Col1a1	5'-CACCAATCACCTGCGTACAGAA	3'-CAACACGCTACTGCACTAGACA
Col2a1	5'-CGAGTACCGATCACAGA	3'-ACTGCGGTTAGAAAGTATTTC
Col10a1	5'-GCCCGATCTTGTTGTC	3'-CTTACCTGGTGTCTGG
Runx2	5'-AGAAGGCACAGACAGAAAGCTTGA	3'-TCACTAAATCCCGCTAAGGA
Ocn	5'-GGCAGCGAGGTAGTGAAGAG	3'-CTGGAGAGGAGAGAACTGG
β -Actin	5'-AACTGGAAACGGTGAAGGTG	3'-TCAAGTTGGGGGACAAAAAG

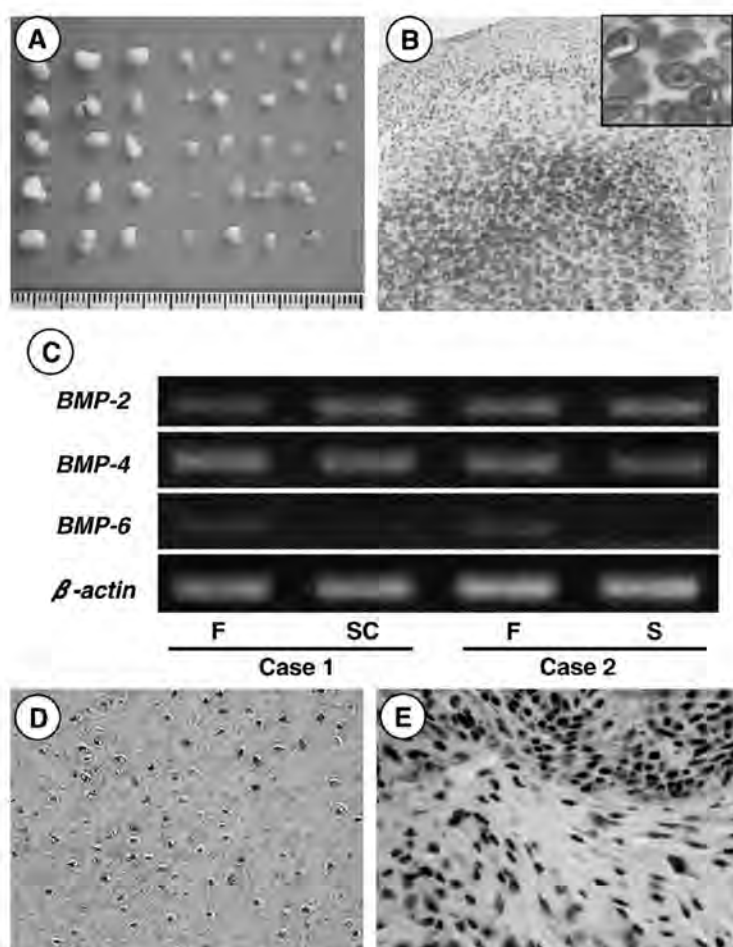


Fig. 1. Free bodies and BMP expression in synovial chondromatosis. (A) Gross findings of free bodies used for isolation of culture cells. Thirty-eight enucleated nodules were isolated from the temporomandibular joint in one patient. (B) Typical histology of a free body, which is composed of hyaline cartilage. Right upper insert shows a high magnification view of cartilage. (C) Expression of BMP-2, BMP-4, and BMP-6 mRNAs in the free bodies (F) and synovium (S) or cultured synovial cells (Sc). RT-PCR analysis was performed as described in Materials and methods. (D,E) Immunohistochemical detection of BMP-2/BMP-4 in the free bodies (D) and synovium (E). Immunoreactivity (brown) is seen in chondrocytes (D) and some fibroblastic cells (E). Immunohistochemistry was performed as described in Materials and methods.

cartilage or bone in synovial chondromatosis. To corroborate our hypothesis, we first investigated BMP expression in the synovium or cultured synovial cells and the free bodies isolated from two synovial chondromatosis patients. RT-PCR analysis revealed that the synovium or cultured synovial cells and the free bodies expressed high levels of *BMP-2* and *BMP-4* mRNAs (Fig. 1C). *BMP-6* expression was weak in the free bodies and undetectable in the synovium or cultured synovial cells (Fig. 1C). No apparent *BMP-7* expression was detected in either the synovium or the free bodies. Immunohistochemical study demonstrated that chondrocytes in the free bodies (Fig. 1D) and some fibroblastic cells in the synovium (Fig. 1E) expressed BMP-2/BMP-4. These results indicate the production of BMP-2 and BMP-4 by the free bodies and synovium in synovial chondromatosis and suggest the possible involvement of BMPs in the pathobiology of synovial chondromatosis. These results prompted us to further investigate the effects of rhBMP-2 on chondrogenic and osteogenic differentiation in the free-body and synovial cells isolated from synovial chondromatosis patients.

rhBMP-2 stimulated the production of cartilaginous nodules and ALP-positive cells in the culture of cells isolated from synovial chondromatosis patients

We first assessed the effects of rhBMP-2 on chondrogenic and osteogenic differentiation of cells by dual staining with ALP and alcian blue in the cells isolated from the free bodies and synovium. In the culture of free-body cells isolated from Case 1, we found numerous nodules composed of spherical cells associated with alcian blue-positive extracellular matrices, indicating chondrogenic differentiation (Fig. 2A). BMP-2 treatment (500 ng/ml) for 6 days increased the number of these nodules by 1.5 times than that in the BMP-2-untreated culture (Fig. 2B). Free-body cells isolated from Case 2 formed a few such nodules (Fig. 2B). Cultured synovial cells exhibited no apparent alcian blue-positive nodules in the presence or absence of BMP-2 (data not shown). These results indicate that free-body cells are capable of differentiating into chondrocytes more effectively than synovial cells.

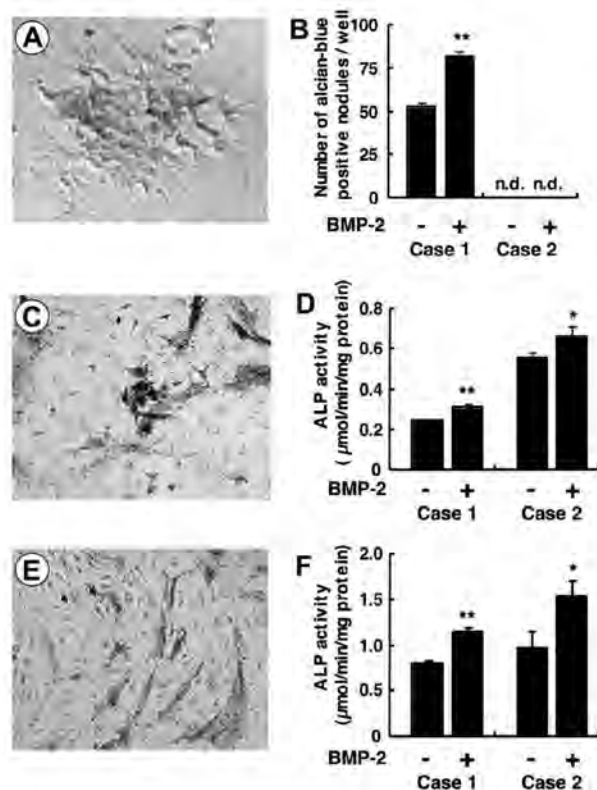


Fig. 2. Effects of rhBMP-2 on cartilaginous nodule formation (A,B) and ALP activity (C–F). (A) Double staining of the cultured cells isolated from the free bodies with ALP and alcian blue in the presence of rhBMP-2. Note that round-shaped alcian blue-positive cells (blue) form a cartilaginous colony. No ALP-positive cells are observed. (B) The number of alcian blue-positive colonies observed in culture of free-body cells and synovial cells in the presence or absence of rhBMP-2 (500 ng/ml). No positive colonies were observed in the synovial cell culture. (C,E) ALP histochemistry in free-body cells (C) and synovial cells (E). Numerous ALP-positive cells (brown) were observed in the cultures of free-body and synovial cells in the presence of rhBMP-2. (D,F) ALP activity in the free-body cells (D) and synovial cells (F) cultured with or without rhBMP-2.

ALP-positive cells were scattered in the cultures of both free-body (Fig. 2C) and synovial cells (Fig. 2E). Almost all the cells were polyhedral or spindle-shaped without any close association with the alcian blue-positive nodules (Fig. 2C and E). BMP-2 treatment increased the number of ALP-positive cells in the cultures of both the free-body and synovial cells (data not shown). Further, BMP-2 treatment significantly increased ALP activity in both the free-body cells (Fig. 2D) and the synovial cells (Fig. 2F). ALP activity is exhibited from early differentiated osteoblasts through mature osteoblasts [8], but it appears in only mature hypertrophic cells during chondrocyte differentiation. We found few nodules double-positive for ALP and alcian blue even in the cultures treated with rhBMP-2. These suggest that ALP-positive polyhedral or spindle-shaped cells are osteoblast lineage cells.

BMP-2 stimulated the expression of mRNAs related to chondrocyte and osteoblast differentiation in the culture of cells isolated from synovial chondromatosis patients

We investigated the effects of rhBMP-2 on the expression of mRNAs related to chondrocyte differentiation. The basal expres-

sion levels of *Sox9*, *Col2a1*, *Aggrecan*, and *Col10a1* mRNAs were significantly higher in the free-body cells than in the synovial cells (data not shown). BMP-2 treatment increased *Sox9* mRNA expression over 20-fold in the free-body cells (Fig. 3A). BMP-2 also significantly increased the expression of *Col12a1* and *Aggrecan* mRNAs, which are involved in the early differentiation of chondrocytes [22] (Fig. 3A). The expression of *Col10a1* mRNA, which is mainly expressed by hypertrophic chondrocytes [22], was also stimulated by the BMP-2 treatment, but its induction in the treated culture was less than 2-fold as compared with that in the control cultures (Fig. 3A). In the synovial cells, rhBMP-2 treatment significantly increased the expression of *Sox9*, *Col2a1*, and *Aggrecan* mRNAs (Fig. 3B). BMP-2 increased *Col10a1* expression more effectively in the synovial cells than in the free-body cells. These results indicate that rhBMP-2 stimulates the free-body and synovial cells to differentiate into chondrogenic cells.

We next investigated the effects of rhBMP-2 on the expression of mRNAs related to osteoblast differentiation. BMP-2 treatment significantly increased *Runx2* expression but failed to stimulate *Col1a1* expression in the free-body cells. rhBMP-2 slightly, but significantly, increased *Osteocalcin* expression in only Case 2. In the synovial cells, BMP-2 treatment significantly increased the expression of *Runx2*, *Col1a1*, and *Osteocalcin* mRNAs. These results suggest that rhBMP-2 induces osteoblast differentiation more effectively in synovial cells than in free-body cells.

Taken together, these results indicate that BMP-2 treatment stimulates chondrocyte and osteoblast differentiation in free-body and synovial cells. Our histopathological examination of eight patients with synovial chondromatosis in the temporomandibular joint revealed that free bodies in all the cases exhibited extensive cartilage formation, and only one case was associated with bone formation (unpublished results). These findings support that the

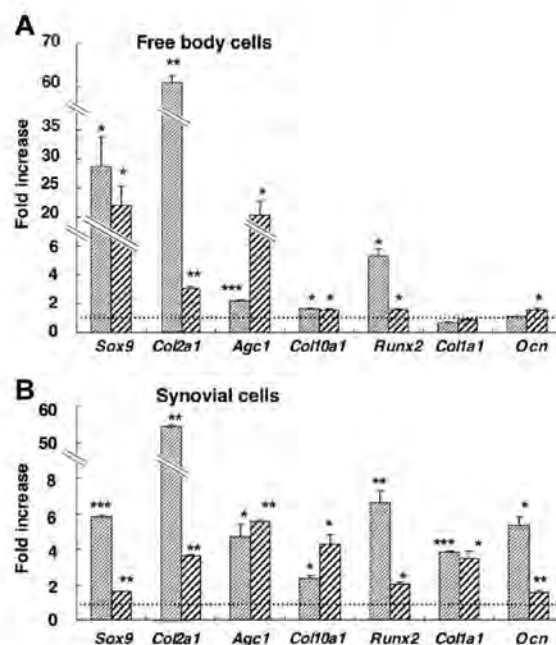


Fig. 3. Effects of BMP-2 on the expression of mRNAs related to chondrocyte and osteoblast differentiation in the free-body cells (A) and synovial cells (B). The cells were cultured for 6 days in the presence or absence of BMP-2 (500 ng/ml), and the expression of mRNAs was determined by real-time RT-PCR analysis as described in Materials and methods. *Agc1*, Aggrecan. Thin slash bars indicate the data of Case 1, and thick slash bars show that of Case 2. * $P < 0.05$, ** $P < 0.01$, *** $P < 0.001$ ($n = 3$).

free-body cells used in the present study had differentiated into chondrogenic cells, and the synovial cells retained bipotency to differentiate into both chondrocytes and osteoblasts.

Noggin inhibited the expression of marker genes related to chondrocyte and osteoblast differentiation in the cultured cells

The free-body and synovial cells expressed substantial levels of mRNAs related to chondrocyte and osteoblast differentiation in the absence of exogenous BMP-2. We also demonstrated that the free-body and synovial cells expressed BMPs. These results suggested that endogenous BMPs synthesized by the free-body and synovial cells stimulated chondrocyte and osteoblast differentiation in an autocrine or a paracrine fashion. To address this issue, we investigated the effects of noggin, which is a specific antagonist for BMPs [23,24], on chondrogenic and osteoblastic differentiation in the free-body and synovial cells.

Noggin significantly inhibited *Sox9* and *Col2a1* expression in both the free-body and synovial cells (Fig. 4A and B). Noggin also inhibited aggrecan expression in the free-body cells but not in the synovial cells (Fig. 4A and B), which might be due to the low level of basal aggrecan mRNA expression in the latter. The inhibitory effect of noggin on *Col10a1* expression was observed in only one case each in the free-body and synovial cells (Fig. 4A and B). These results indicate that BMPs synthesized by free-body and synovial cells are involved in chondrogenic differentiation in synovial chondromatosis.

Noggin significantly inhibited *Runx2* expression in the free-body and synovial cells, but its inhibitory effect on *Col1a1* expression was observed in only synovial cells isolated from Case 1 (Fig. 4A and B). Noggin inhibited *Osteocalcin* expression in the synovial cells but not in the free-body cells (Fig. 4A and B). The ALP activity in the free-body (Fig. 4C) and synovial cells (Fig. 4D) was also inhibited by noggin. These results suggest that BMPs synthesized by free-body and synovial cells also participate in the regulation of osteoblast differentiation in synovial chondromatosis.

In conclusion, the present study demonstrated that the free bodies and synovium isolated from synovial chondromatosis patients produced BMPs and that the free-body and synovial cells are capable of differentiating into chondrocyte and osteoblast lineage cells in response to BMPs. Thus, we propose that BMPs synthesized by synovial and free-body cells promote cartilaginous and osteogenic metaplasia in synovial chondromatosis in an autocrine or a paracrine fashion. The present study also indicates that BMPs play important roles in not only skeleton formation but also in the cartilaginous and osteogenic metaplasia observed under pathological conditions. Thus, BMP antagonists such as noggin might be useful therapeutic tools for preventing chondrogenic metaplasia occurred in synovial chondromatosis.

Acknowledgments

This work was supported by a Grant-in-Aid for Scientific Research from the Japan Society for the Promotion of Science (to A.Y.), and the grant from the Japanese Ministry of Education, Global Center of Excellence (GCOE) Program, "International Research Center for Molecular Science in Tooth and Bone Diseases".

References

- [1] F.P. Murphy, D.C. Dahlin, C.R. Sullivan, Articular synovial chondromatosis, *J. Bone Joint Surg. Am.* 44 (1962) 77–86.
- [2] V. Karlis, R.S. Grickman, M. Zaslow, Synovial chondromatosis of the temporomandibular joint with intracranial extension, *Oral Surg. Oral Med. Oral Pathol. Oral Radiol. Endod.* 86 (1998) 664–666.
- [3] J.J. von Lindern, I. Theuerkauf, B. Niederhagen, S. Bergé, T. Appel, R.H. Reich, Synovial chondromatosis of the temporomandibular joint: clinical, diagnostic, and histomorphologic findings, *Oral Surg. Oral Med. Oral Pathol. Oral Radiol. Endod.* 94 (2002) 31–38.
- [4] F. Mertens, K. Jonsson, H. Willén, A. Rydholm, A. Kreicbergs, L. Eriksson, G. Olsson-Sandén, F. Mitelman, N. Mandahl, Chromosome rearrangements in synovial chondromatous lesions, *Br. J. Cancer* 74 (1996) 251–254.
- [5] R. Sciort, P. Dal Cin, J. Bellemans, I. Samson, H. Van den Bergh, V.B. Damme, Synovial chondromatosis: clonal chromosome changes provide further evidence for a neoplastic disorder, *Virchows Arch.* 433 (1998) 189–191.
- [6] B.L. Sperling, S. Angel, G. Stoneham, V. Chow, A. McFadden, R. Chibbar, Synovial chondromatosis and chondrosarcoma: a diagnostic dilemma, *Sarcoma* 7 (2003) 69–73.
- [7] R.L. Davis, H. Foster, K. Arthur, S. Trewin, P.W. Hamilton, D.J. Biggart, Cell proliferation studies in primary synovial chondromatosis, *J. Pathol.* 184 (1998) 18–23.
- [8] A. Yamaguchi, T. Komori, T. Suda, Regulation of osteoblast differentiation mediated by bone morphogenetic proteins, hedgehogs, and *Cbfa1*, *Endocr. Rev.* 21 (2000) 393–411.
- [9] G.A. Rodan, S. Harada, The missing bone, *Cell* 30 (1997) 677–680.
- [10] E.J. Jin, S.Y. Lee, Y.A. Choi, J.C. Jung, O.S. Bang, S.S. Kang, BMP-2-enhanced chondrogenesis involves p38 MAPK-mediated down-regulation of Wnt-7a pathway, *Mol. Cells* 22 (2006) 353–359.
- [11] W. Bi, J. Min Deng, Z. Zhang, R. Behringer, B. de Crombrughe, *Sox9* is required for cartilage formation, *Nat. Genet.* 22 (1999) 85–89.
- [12] Y. Mori-Akiyama, H. Akiyama, D.H. Rowitch, B. de Crombrughe, *Sox9* is required for determination of the chondrogenic cell lineage in the cranial neural crest, *Proc. Natl. Acad. Sci. USA* 100 (2003) 9360–9365.
- [13] P. Ducy, R. Zhang, V. Geoffroy, A.L. Ridall, G. Karsenty, *Osf2/Cbfa1*: a transcriptional activator of osteoblast differentiation, *Cell* 89 (1997) 747–754.
- [14] T. Komori, H. Yagi, S. Nomura, A. Yamaguchi, K. Sasaki, K. Deguchi, Y. Shimizu, R.T. Bronson, Y.-H. Gao, M. Inada, M. Sato, R. Okamoto, Y. Kitamura, S. Yoshiki, T. Kishimoto, Targeted disruption of *Cbfa1* results in a complete lack of bone formation owing to maturational arrest of osteoblasts, *Cell* 89 (1997) 755–764.
- [15] K. Katagiri, A. Yamaguchi, K. Komaki, E. Abe, N. Takahashi, T. Ikeda, V. Rosen, J.M. Wozney, A. Fujisawa-Sehara, T. Suda, Bone morphogenetic protein-2 converts the differentiation pathway of C2C12 myoblasts into the osteoblast lineage, *J. Cell. Biol.* 127 (1994) 1755–1766.

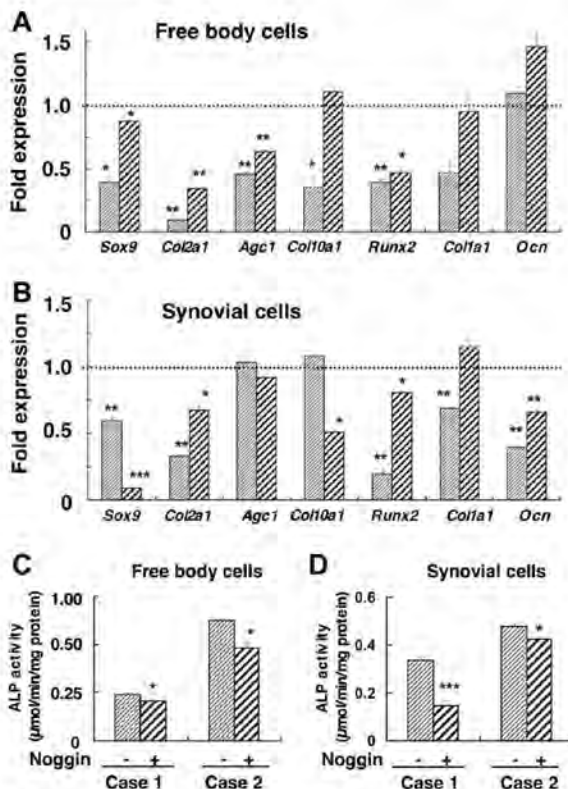


Fig. 4. Effects of noggin on the expression of mRNAs related to chondrocyte and osteoblast differentiation in the free-body cells (A) and synovial cells (B). The cells were cultured for 6 days in the presence or absence of noggin (500 ng/ml), and the expression of mRNAs was determined by real-time RT-PCR analysis as described in Materials and methods. *Agc1*, Aggrecan. Thin slash bars indicate the data of Case 1, and thick slash bars show that of Case 2. * $P < 0.05$, ** $P < 0.01$, *** $P < 0.001$ ($n = 3$).

- [16] R.J. Lories, I. Derese, J.L. Ceuppens, F.P. Luyten, Bone morphogenetic proteins 2 and 6, expressed in arthritic synovium, are regulated by proinflammatory cytokines and differentially modulate fibroblast-like synoviocyte apoptosis, *Arthritis Rheum.* 48 (2003) 2807–2818.
- [17] R.J.U. Lories, F.P. Luyten, Bone morphogenetic protein signaling in joint homeostasis and disease, *Cytokine Growth Factor Rev.* 16 (2005) 287–298.
- [18] K. Bobacz, I.G. Suuk, S. Hayer, L. Amoy, M. Tohidast-Akrad, G. Kollias, J.S. Smolen, G. Schett, Differentially regulated expression of growth differentiation factor 5 and bone morphogenetic protein 7 in articular cartilage and synovium in murine chronic arthritis: potential importance for cartilage breakdown and synovial hypertrophy, *Arthritis Rheum.* 58 (2008) 109–118.
- [19] H. Iwata, S. Ono, K. Sato, T. Sato, M. Kawamura, Bone morphogenetic protein-induced muscle- and synovium-derived cartilage differentiation in vitro, *Clin. Orthop. Relat. Res.* 296 (1993) 295–300.
- [20] N. Shintani, E.B. Hunziker, Chondrogenic differentiation of bovine synovium: bone morphogenetic proteins 2 and 7 and transforming growth factor beta1 induce the formation of different types of cartilaginous tissue, *Arthritis Rheum.* 56 (2007) 1869–1879.
- [21] S. Yamane, A.H. Reddi, Induction of chondrogenesis and superficial zone protein accumulation in synovial side population cells by BMP-7 and TGF-beta1, *J. Orthop. Res.* 26 (2008) 485–492.
- [22] M.B. Goldring, K. Tsuchimochi, K. Ijiri, The control of chondrogenesis, *J. Cell. Biochem.* 97 (2006) 33–44.
- [23] V. Rosen, BMP and BMP inhibitors in bone, *Ann. N. Y. Acad. Sci.* 1068 (2006) 19–25.
- [24] L.J. Brunet, J.A. McMahon, A.P. McMahon, R.M. Harland, Noggin, cartilage morphogenesis, and joint formation in the mammalian skeleton, *Science* 280 (1998) 1455–1457.

顎顔面矯正学分野

森山 啓司

医歯学総合研究科・顎顔面頸部機能再構築学系専攻
顎顔面矯正学・教授



1) 研究の課題名

頭蓋早期癒合症のモデルマウスの解析と可溶型 FGFR2 の効果

Analysis of a model mouse of craniosynostosis and the effect of soluble FGFR2

Apert syndrome の原因は Fibroblast Growth Factor 2 (FGFR2) の細胞外ドメインである Ig II と Ig III の結合領域における S252W および P253R の変異である。しかしながら、その発症の分子細胞メカニズムには不明な点が多く残されている。そこで FGFR2 IIIc S252W を受精卵に遺伝子導入した transgenic mouse (S252W) と、FGFR2 IIIc S252W から細胞内ドメインを欠如する可溶型のコンストラクトを遺伝子導入した transgenic mouse (SOL) を作製し、解析した。S252W 由来の細胞は、アリザリンレッド染色で強染され、アルカリフォスファターゼ活性が亢進した。さらに免疫不全マウスの背側皮下に S252W 由来の細胞を移植したところ、異所性骨形成が誘導された。一方、SOL の細胞を移植したところ、骨組織誘導は全くみられなかった。さらに S252W と SOL の両マウスを交配して得られたマウス由来の細胞は、SW06 の頭蓋冠由来のマウスの細胞と比較して、アリザリンレッド染色で淡染され、アルカリフォスファターゼ活性も低値を示した。興味深いことに、この細胞を免疫不全マウスの背側皮下に移植した結果、SOL 由来の細胞移植によって誘導される骨形成を有意に抑制した。上記の結果は、FGFR2 IIIc S252W の遺伝子機能に対して、その細胞内ドメインを欠如する可溶型のコンストラクトが治療ターゲットとして有用なことを示唆する。

習慣性咀嚼側に依存した舌感覚の弁別能および脳賦活パターン

Preferred chewing side-dependent two-point discrimination and cortical activation pattern of tactile tongue sensation

本研究の目的は、1) 舌の感覚閾値に左右差があるか、2) 舌感覚刺激の皮質投射パターンに左右差があるか、習慣性咀嚼側 (PCS) との関連を調べることである。12名の健康者において、最初に顎運動記録装置を用いて PCS を同定した。次に、舌の前歯・犬歯・臼歯相当部に触覚刺激を与え、左右の2点弁別 (TPD) 閾値を比較した。最後に、機能的磁気共鳴画像法 (fMRI) を用いて舌縁刺激時の左右一次体性感覚野 (S1) における賦活ボクセル数を比較した。その結果、TPD 閾値は前歯、犬歯、臼歯部と後方に進むにつれ増加した。また、犬歯・臼歯相当部において PCS 側の方が非 PCS 側に比べて有意に小さかった。一方、PCS の対側 S1 における賦活ボクセル数の方が非 PCS の対側 S1 に比べて有意に多かった。以上の結果から、舌感覚と皮質投射パターンに PCS 依存性が存在することが示唆された。このような特性は、咀嚼効率を増大させることに寄与していると考えられた。

fMRI および MRI 動画法を用いた口蓋裂言語の脳および末梢機能解析

Brain and peripheral functional analysis of cleft speech using fMRI and MRI movie

口唇口蓋裂 (CLP) 患者における構音障害は口蓋裂言語と呼ばれている。口蓋裂言語の有無と CLP の有無との関連を知る目的で機能的磁気共鳴画像法 (fMRI) および MRI 動画法 (MRI movie) を用いて、軟口蓋破裂音 (/k/) 発音 (内言語および外言語) 時における脳賦活パターンと末梢構音器官運動を解析した。被験者は、健康成人10名と術後成人口唇口蓋裂患者3名 (片側性1名および両側性2名、うち両側性の1名のみ軟口蓋音に構音障害あり) であった。その結果、fMRI 実験からは、内言語発音時には、CLP の有無にかかわらず運動前野が賦活した。外言語発音時には、健康者ならびに構音障害を有しない CLP 患者においては運動前野、一次運動

野および小脳が賦活したが、構音障害を有するCLP患者においては後帯状回が賦活した。一方、MRI movie実験からは、外言語発音時の舌形状は、健常者および構音障害を有しないCLP患者では類似していたが、構音障害を有するCLP患者ではほとんど変化しなかった。これらの結果から、発音時において脳賦活パターンおよび末梢構音器官運動は、構音障害の有無に依存し相互に関連していることが示唆された。

マルファン症候群の重篤な歯周炎に関する分子機構

Molecular mechanism of severe periodontitis in Marfan syndrome

弾性線維の主要構成タンパク fibrillin-1 をコードするFBN1 遺伝子は、心血管（大動脈乖離や拡張）、骨格（高身長）、目（水晶体脱臼）などを主症状とする1型Marfan 症候群の責任遺伝子である。この疾患ではさらに重篤な歯周疾患に罹患することが知られているが、その発症機構は不明である。そこでFbn1 の遺伝子を改変したhypomorphic mice (Mg Δ) に実験的に歯周疾患を誘発し解析を行った。

昨年度に引き続き本年度も、Mg Δヘテロ接合子に歯周病原菌P.gingivalisを上顎側歯肉に2日毎計3回播種させて惹起した歯周炎モデルを用いた。本年度は、最近Marfan 症候群の心血管治療薬として使用されることが多いAngiotensin II receptor blocker (ARB) の一つであるテルミサルタンの歯周疾患に対する作用を中心に検討した。テルミサルタンの飲料水中への添加は、P.gingivalisをMg Δヘテロ接合子に惹起させた歯槽骨吸収を有意に抑制した。さらにこの抑制は、血中の活性化TGF-βレベルとTNF-αレベルを有意に抑制した。

これらの結果より、Angiotensin II receptor blocker (ARB) は心血管のみならず、歯周疾患の予防や進行抑制に効果的な薬剤であることが示唆された。

歯の再生に向けたヒト遺伝子解析

Gene analysis for human tooth regeneration

歯の喪失や欠損が多数歯は、咀嚼、発音、摂食といった口腔機能に重大な障害を引き起こし、患者のQOLに深刻な影響を与える。歯の再生に対するreverse geneticなアプローチとして本課題では、6本以上の多数歯欠損が家族性にみられ、非症候群性に発症するケース(Familial oligodontia)の遺伝子解析を行ってきた。本年度は、3世代にわたってFamilial oligodontia を呈する家系の遺伝子解析を行った。

1. 遺伝子解析の結果、この家系においてFamilial oligodontiaを示す3名に、動物実験より歯の発生における機能が既に報告されている転写因子PAX9に、フレームシフト型の遺伝子変異(321_322insG)を同定した。この変異は様々な種間で保存され、DNA 結合能を持つpaired domainに存在した。
2. この家系内でFamilial oligodontiaを伴わない方からもDNA 試料を提供いただき、遺伝子解析を行った結果、321_322insGは見られなかった。
3. 321_322insGの変異遺伝子機能をin vitroで解析した。この変異遺伝子をCOS-7に遺伝子導入した結果、野生型タンパクと異なり、321_322insGは分解されやすく、タンパクの安定性に劣ることが示唆された。

先天性多数歯欠損を呈する症例における口腔内および顎態の特徴の抽出

Dentofacial characteristics in patients with oligodontia

先天性多数歯欠損症(oligodontia:OD)とは、智歯以外に先天的に6歯以上の永久歯胚の欠損を認める状態をいい、外胚葉異形成症(ectodermal dysplasia: ED)をはじめとする先天性疾患の一表現系として発症する症候群性のものと、歯以外の組織に異常を認めない非症候群性のものに分類される。平成20年度より本邦において、ED患者の歯科矯正治療に保険が適用されている。その一方、ODを呈する患者の顎口腔領域についての詳細な報告は少ない。そこで本研究の目的は、ODの顎顔面領域の特徴を抽出し、歯科矯正治療における治療方針立案の一助とするものとした。なお、症候群性ODにはEDおよびEEC(ectrodactyly-ectodermal dysplasia-clefting)症候群の症例を含む。結果: 1) 永久歯胚の平均欠損数は、症候性ODで10.4本、非症候性ODで9.0本であった。2) ED、非症候群性ODは下顎枝が反時計回りに回転し、skeletal Class III傾向の顎態を示し、上顎大臼歯部の垂直成分が小さかった。3) EEC症候群では、下顎骨体長に問題はないが、下顎前歯部の永久歯先天欠如が原因と考えられるB点の後方位を認めた。4) 永久歯先天欠如は症候群性、非症候群性共に上下顎小臼歯部に最も高頻度に認められた。5) 症候群性ODでは永久歯の形態異常を高頻度で認める一方、非症候群性ODでは稀であった。これらの症例の成人期に欠損補綴治療を行うにあたっては、スペースの管理や咬合高径の適正化を図る必要があり、咬合機能の獲得および審美性の改善には矯正および補綴治療を含めた包括的歯科治療が必要である。したがって、成長期の歯科矯正治療においては、

上顎臼歯部の挺出により下顎の時計まわりの回転を促す治療計画と欠損部のスペース管理の必要性が示唆された。

先天性多数歯欠損を引き起こすPAX9の変異と表現系の関係

Pathogenic mechanisms of tooth agenesis linked to paired domain mutations in human PAX9.

近年、転写因子であるPAX9の変異によって常染色体性優性に家族性に先天性多数歯欠損が引き起こされることが報告された。しかし、変異部位や変異の種類により欠損する部位や欠損歯数に一貫性を見ず、たとえPAX9の変異が同定されたとしても、欠損する歯を特定するのは困難なことが現状である。そこで、先天性に永久歯胚の欠損を引き起こすPAX9の変異と表現系の関係(genotype-phenotype correlation)を明らかにすることを目的とした計画を立案した。方法として、PAX9のDNA結合領域であるpaired domain内に認められる今まで報告されている8つのmissense変異を有する変異タンパクの機能解析、ならびに構造インフォマティクスの手法を用いることとした。DNA結合能やPax9が直接結合すると考えられているBmp4やMsx1のプロモーター活性に大きな減少を認めるmissense変異を有する家系では多くの欠損歯数を認めた。以上より、DNA結合能が欠損部位や欠損歯数に影響を与えている可能性を示唆し、この結果は遺伝子診断さらに、遺伝カウンセリングにも大きく役に立つと考えられる。

COBRA-DHPLC法によるラッセルシルバー症候群の遺伝子診断システムの開発

Development of a diagnostic system of Russell-Silver Syndrome based on the combined bisulfite restriction analysis-denaturing high-performance liquid chromatography (COBRA-DHPLC) assay

ラッセルシルバー症候群(RSS)(MIM %180860)は、成長遅延、逆三角形の顔貌、彎指症を主徴とし、小下顎症と顔面非対称も好発する。矯正治療の対象となるケースが多く(平成16年より健康保険適用疾患)、疾患の診断は治療やその計画立案に大きな意義を持つ。RSSの半数は、11p15.5上に座位を持つH19遺伝子のdifferentially methylated region(DMR)が非メチル化され、遺伝子解析が疾患の診断上重要である。これまで遺伝子解析にはbisulfite-clone-sequencing法が用いられてきたが、長時間を要し煩雑なため、簡便なシステムの開発が待たれてきた。そこで、combined bisulfite

restriction analysis-denaturing high-performance liquid chromatography(COBRA-DHPLC)法を用いたRSSの診断システムの簡略化を試みた。末梢血からゲノムDNAを抽出しバイサルファイト処理後、H19のDMR領域をPCRで増幅した。PCR産物を制限酵素(Hinf I)処理し、DHPLCにより切断・非切断の両者に分け、メチル化率を算出した。今回解析検体として、日本人RSS患者7名と健常者22名を用いた。今回のCOBRA-DHPLC法と従来のbisulfite-clone-sequencing法を比較した結果、H19遺伝子のメチル化率に関し、両者に高い相関が有意にみられ、本法の有用性が実証された。COBRA-DHPLC法による健常者22名のメチル化の平均値は83%であったのに対し、RSS患者7名中3名が10%前後と低いメチル化率を示した。本法によりRSSの遺伝子診断が、迅速かつ簡便に実施可能となった。

口唇裂・口蓋裂患者に対する骨延長法の適用

Application of distraction osteogenesis in patients with cleft lip and palate

近年、著しい上顎の劣成長を呈する口唇裂・口蓋裂患者に対して骨延長法が適用されている。当分野では、口唇裂・口蓋裂患者における上顎骨の劣成長に対してLe Fort I型骨延長術を、また顎裂の閉鎖や叢生の改善を目的として歯槽骨延長術を適用し、良好な結果を得ている。本研究では骨延長法の適用に関して、臨床および基礎的な多角的見地より検討を行い以下の結果を得た。1) 延長に適用する牽引力の測定:創外型延長器の牽引ワイヤーに小型張力計を組み込むことにより、上顎の牽引力を測定し力学的検討を行った結果、延長効率が低い症例において、延長器のアクチベートに伴う牽引力の上昇率が高いことが示唆された。2) 硬・軟組織の3次元データの統合:骨延長術前後のCT、歯列模型、および顔面の色彩データ等の3次元情報を解析ソフトウェア(STL-Rugle®, Medic Engineering、京都)を用いて同一座標系に統合することにより、硬・軟組織の変化を評価する手法を構築した。3) 顔貌軟組織変化のシミュレーション:Le Fort I型骨延長術による顔面軟組織変化と3次元シミュレーションソフト(SimPlant® OMS ver 12、マテリアライズ デンタル ジャパン、千葉)を用いた変化予測と比較した結果、特に鼻形態において両者の不一致を認めた。

歯槽骨延長部への歯の移動に高気圧酸素が与える影響

The effects of hyperbaric oxygen to tooth movement into the regenerated area after distraction osteogenesis

近年骨延長によって生じた新生骨への歯の移動に関する報告は散見されるものの、口唇口蓋裂患者を想定した上顎骨に対して評価した基礎的報告はまだない。一方、骨延長術に高気圧酸素を適用させると延長部位における血流量の増加・骨化促進・末梢循環の増加による血管新生が確認されており、延長部位での新生骨の有意な形成が報告されている。しかし歯の移動に対しての高気圧酸素療法に関する報告はほとんど認められないのが現状である。そこで、骨延長によって新生した骨内に歯の移動を行った際の高気圧酸素の影響を移動歯の歯根周囲の骨改造様相において組織学的・放射線学的に解析を加えることを本研究の目的とした。10匹のビーグル犬を用い、上顎左側切歯3本相当部に顎裂を想定した10mmの人為的骨欠損を作成し、その骨欠損部位に向かい1mm/日の割合で10日間骨延長を行い、骨延長終了後第二前臼歯を骨延長部位に向かって牽引した。20日間2.5ATAで高気圧酸素に曝露した5匹を高気圧酸素群とし、屠殺後、移動歯の近心根・遠心根それぞれの近心側（牽引側）・遠心側（圧迫側）において骨密度解析、骨組織形態計測法による構造計測を行った。また、有意差検定はMann-Whitney U-testを行った。骨密度解析から新生骨内に移動された遠心根の近心側において高気圧酸素群の骨密度が有意に高かった。また、同部位では骨形態計測からも高気圧酸素群では新生骨の骨梁間隙・骨梁数・血管数において有意に高い値を示した。今回得られた骨密度・骨梁幅・血管数の有意な差は、高気圧酸素適用下で骨延長部位への歯の移動を行うことにより、新生骨内の牽引側において血管新生が促進された結果と考えられた。骨延長により新生した骨内に歯の移動を行う際に高気圧酸素を用いることで、移動歯の牽引側では骨形成が促進される可能性が示唆された。

先天異常診断エキスパートシステムのための三次元バーチャルフェイスの合成

Evaluation of the three-dimensional-virtual-face for diagnosis of congenital anomalies

当分野は国内の矯正歯科で最も多くの先天異常患者を有し、長年蓄積してきたデータを広く社会に発信し、先天異常患者の診断・治療に役立てたいと考え、以前から診断・矯正治療を支援する先天異常診断エキスパートシステムを構築し、仮想外来システムの実現を進めてきた。

先天異常疾患の約70%に頭蓋顔面領域の異常を認め、本システムのさらなる発展のためには、顔貌の視覚情報を組み込むことが必須であると考え、個人情報保護の観点から公開は極めて困難である。本システムに個人情報保護対策を取り入れた視覚的な頭蓋顔面情報を取り入れるため、先天異常患者の頭蓋顔面領域の三次元情報から、先天異常疾患の特徴を有し、個人として特定できない三次元バーチャルフェイスを作成し、本システムに組み込むことを本研究課題の目的とした。3Dデジタイザを用いて、先天異常疾患の複数患者の三次元顔データの計測を行い、所定のデータ形式に変換後、顔画像へのワイヤフレームのフィッティングを行い、三次元先天異常バーチャルフェイスを作成した。今後はバーチャルフェイスの先天異常疾患としての妥当性の評価を行い、アンケート結果集計・解析し、バーチャルフェイスの個人としての異同評価を行い、総合判定とする。先天異常バーチャルフェイスの種類の加増の後、診断エキスパートシステムへのバーチャルフェイスの導入、E-learningへ登用し、情報の発信・普及につとめ、患者のQOLの向上につとめる。

石灰化組織における象牙質細胞外基質タンパクの生物学的役割

The roles of dentin extracellular matrix proteins in mineralized tissues.

これまでBMPなどを用いた歯髄腔側二次象牙質形成の促進や、乳歯より得られた歯髄幹細胞をもちいた歯の象牙質再生が活発に研究されてきたが、現在までウ蝕で脱灰された象牙質部分の正常な再生には成功していない。これには象牙質に侵入したバクテリア成分を取り除いた上で、最終的にコラーゲンとその他の基質を中心とした石灰化メカニズムを正確に再現することが求められるからである。象牙質の基質タンパクとして、非コラーゲン性タンパク質で最も多く分泌されているのはDSPP（象牙質シアロリン酸化タンパク）である。今回DSPPが象牙質石灰化を如何にコントロールしているか、つまり象牙質石灰化のメカニズムについて新たな知見を得ることができた。DSPPノックアウト（KO）マウスの象牙質組織では未石灰化部分である象牙前質が拡大しているが、今回DSPPKOマウスとデコリンKOマウスを交配したダブルKOマウスの歯を解析したところ、DSPPKOマウスにみられた象牙前質の拡大が回復し、野生型に近い象牙質の厚みになった。よって、象牙前質の石灰化前線で起こる基質の石灰化にはデコリンの発現量が重要である

ことがわかった。ところで、DSPPは1本のmRNAから合成されその直後に主にDSPとDPPの2つのタンパクに分解されて機能すると考えられているが、それぞれのタンパクについての役割は不明であった。そこで、今回DSPのみを象牙質に過剰発現するトランスジェニックマウスをDSPPKOマウスと交配させ解析したところ、石灰化前線において石灰化を促進した所見を得た。しかしDPPが存在しなかったため、最終的な石灰度は正常な象牙質ほどは上昇しなかった。以上のことから、発生時に起こる正常な象牙質形成と同等の構造・物理的強度をもつ象牙質再生や、in vitroにおける象牙質類似石灰化物質など、コラーゲンベースのバイオマテリアルの開発につながる基礎的データを得られたと考えられる。

エナメル質細胞外基質タンパクの機能解析

Functional analysis of enamel extracellular matrix proteins

エナメル質形成不全症(AI)は全體的にエナメル質形成が損なわれ、審美的な障害はもちろん、重篤な知覚過敏や咬合の崩壊など患者に重篤な不利益をもたらす。エナメル質形成期にエナメル芽細胞から分泌されるタンパク質のうち最も多くを占めるのはアメロジェニンであり、2番目に多いのはアメロプラスチンであるが、これらのヒトにおける遺伝子欠損や変異動物ではAIを引き起こすことが知られている。今回我々は、この2つの基質タンパクを同時に欠損させたマウスの表現型について解析した。アメロジェニン/アメロプラスチンダブルノックアウト(Amel X^{-/-}/Ambn^{-/-})マウスは、アメロジェニンノックアウト(Amel X^{-/-})およびアメロプラスチンノックアウト(Ambn^{-/-})と比較して有意に薄いエナメル質を有していたが、エナメル質が消失することにはなかった。Amel X^{-/-}/Ambn^{-/-}およびAmbn^{-/-}マウスでは、エナメル芽細胞がエナメル表面から剥がれ、本来円柱状のエナメル芽細胞の高さが減少していることが確認された。エナメル芽細胞のタンパク質発現プロファイルを2次元電気泳動で比較したところ、Ambn^{-/-}欠失時にRhoGDI(Arhgdi: Rhoファミリー特異的Gアニンヌクレオチド解離阻害因子)の発現上昇が見られた。RhoファミリーGタンパクは、活性型Rhoにのみ結合できる標的タンパク質群を介して、微小管の安定化、アクチン重合、アクチンミオシンの収縮などを誘導し、ひいては細胞骨格の制御を担っていることから、Ambnは細胞骨格制御に影響を与え結果的にエナメル芽細胞の形態変化を引き起こしていることが示唆された。エナメル質減形成が起こる歯のフッ素症では、エナメル芽細胞の細胞骨格制

御異常が起こることが示唆されており、今後フッ素症患者においてアメロプラスチンの発現変化などを検討する必要があると考えられた。

毛髪・歯・骨症候群

(Trichodontoosseous (TDO) syndrome) の

歯と骨の表現型発現メカニズムの解析

In vivo impact of a 4 bp deletion mutation in the DLX3 gene: understanding the mechanisms of TDO syndrome phenotypes.

毛髪・歯・骨症候群(Trichodontoosseous (TDO) syndrome)は、常染色体優性遺伝の外胚葉異形成症(Ectodermal dysplasia; ED)の1つであるとされている。典型的な毛髪・歯・骨症候群では、巻き毛やエナメル質形成不全のほか、頭蓋冠や長管骨の骨硬化症をおこす。まれに頭蓋骨縫合早期癒合症が見られるが、その場合は長頭症となり、上下顎の咬合状態に影響を及ぼすだけでなくエナメル質形成不全から口腔機能に重大な障害を引き起こす可能性がある。現在までに、毛髪・歯・骨症候群の原因遺伝子であるDLX3遺伝子上の変異のタイプによって表現型に様々なバリエーションがあることが判明しているが、その表現型発現のメカニズムに関しては不明な点が多い。我々は今回、骨症状を引き起こすことで知られるc.571_574delGGGG変異についてトランスジェニック(TG)マウスを作成し、個体レベルの表現型(病態)の理解を目標とした。マウス2.3kb-Collalプロモーター下に変異DLX3を発現させたところ、長管骨における骨密度及び海綿骨の占める体積が上昇した。TGマウス由来の骨髄間葉系細胞を培養したところ骨芽細胞への分化促進及び骨形成マーカーの上昇が見られたが、マウス生体内では骨形成速度の上昇は見られなかった。破骨細胞形成能は、TGマウス由来培養細胞で低下し、これは骨幹端で見られた生体内での破骨細胞数の減少、および骨吸収マーカーの減少と一致した。一方で血清中のIFN- γ 濃度上昇が見られたことから、生体内では破骨細胞数が減少することによって骨硬化が引き起こされていると推測された。今回解析したマウスは、骨と象牙質について変異DLX3を発現させたマウスモデルであり、現在歯におけるマウスの表現型(タウロドンティズム)について研究成果を投稿中である。

2)

25th GDOE general presentation
"Special Lecture of Advanced Medical and Dental Study"

Functional analysis of extra cellular matrix proteins as signaling molecules predominantly expressed in tooth enamel and dentin.

エナメル質および象牙質細胞外基質タンパクのシグナル分子としての生物学的機能の解析

Tokyo Medical & Dental University
Department of Maxillofacial Orthognathics

Naoto Haruyama
(春山直人)

Overview

■ Enamel matrix proteins and Amelogenesis imperfecta (AI)

(エナメル基質タンパクとエナメル質形成不全症)

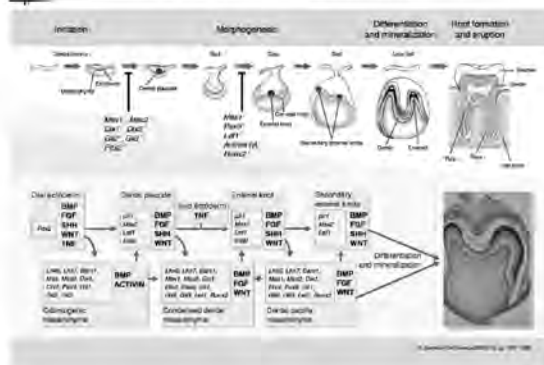
■ Dentin matrix proteins and Dentinogenesis imperfecta (DI)

(象牙質基質タンパクと象牙質形成不全症)

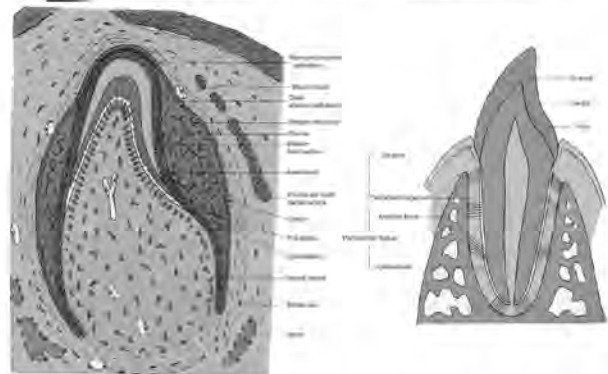
■ Research introduction and Future research plans

(最近の研究紹介と研究計画)

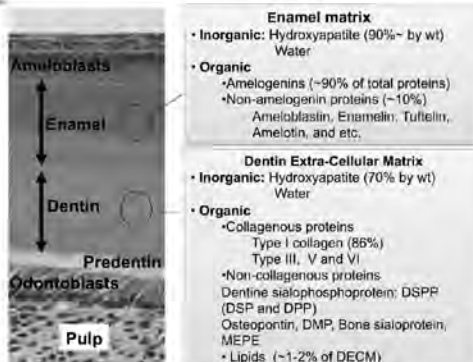
Tooth development



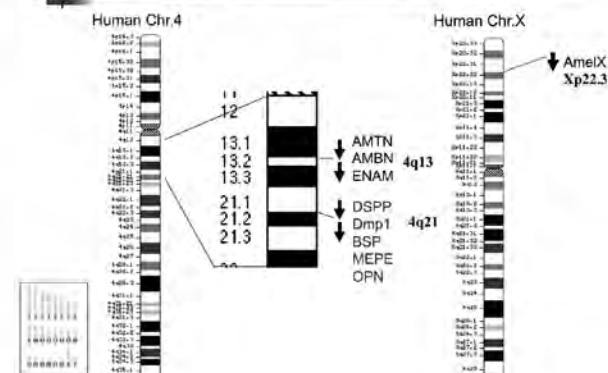
Tooth development



Extra-Cellular matrix in tooth



Locus (position on chromosomes) of tooth related genes



Overview

■ Enamel matrix proteins and Amelogenesis imperfecta (AI)

(エナメル基質タンパクとエナメル質形成不全症)

■ Dentin matrix proteins and Dentinogenesis imperfecta (DI)

(象牙質基質タンパクと象牙質形成不全症)

■ Research introduction and Future research plans

(最近の研究紹介と研究計画)

Hereditary enamel defects- Amelogenesis Imperfecta

Frequency: 1/20,000

Type	Inheritance
Hypoplastic (type 1)	Autosomal dominant, recessive, or X-linked
Hypomaturation (type 2)	Autosomal dominant, recessive, or X-linked
Hypocalcified (type 3)	Autosomal dominant, recessive
Hypomaturation/ hypoplasia/ taurodontism (type 4)	Autosomal dominant

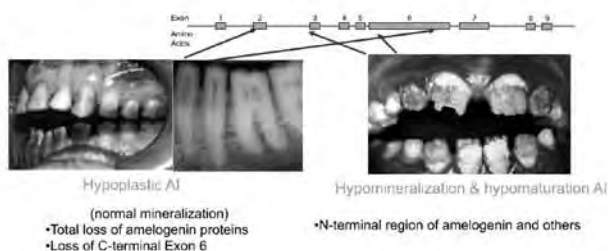
Amelogenin (AMELX)
Enamelin (ENAM) Matrix proteins

Kallikrein 4 (KLK4)
Matrix metalloproteinase 20 (MMP20) Proteases

Amelogenin and Amelogenesis Imperfecta (AI)

Amelogenin

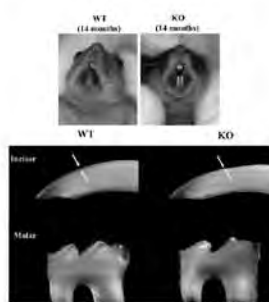
Genome locus (human) Xp22.31-p22.1 Yp11.2 (almost inactive)



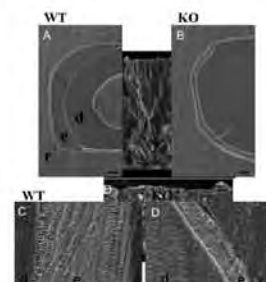
M. Nisener, Oral surg Oral med Oral pathol, 9/23/2004

Amelogenin KO mice phenotype

Amelogenin KO mice display amelogenesis imperfecta phenotype



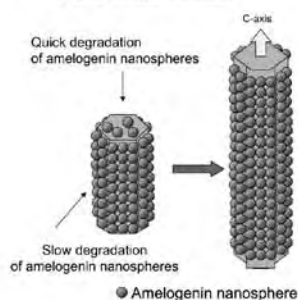
Amelogenin KO mice display well mineralized hypoplastic enamel (thin enamel).



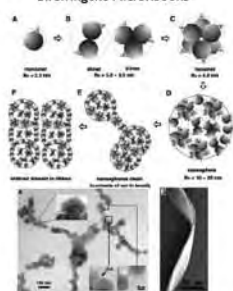
J Dent Res, 2007, 2009

The role of amelogenin (full length) on enamel crystal formation

Hypothetical mechanisms of HA crystal growth in enamel



Supramolecular Assembly of Amelogenin Nanospheres into Birefringent Microribbons



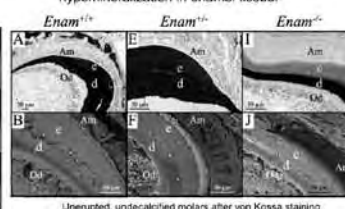
Du et al. Science, 2005

Enamelin KO mice phenotype

Enamelin KO mice display phenotypes similar to AI patients in hetero and homozygote



Enamelin KO mice show hypomineralization in enamel tissue.



Unruptured, undecalcified molars after von Kossa staining

Ho et al. J Biol Chem, 2008

The role of major enamel matrix proteins in enamel mineralization

Amelogenin: 90%

• Amelogenins are the most abundant proteins in enamel.

- Regulation of HA crystal orientation and growth.

(アメロジェニン、エナメル質形成時のハイドロキシアパタイト結晶の方向制御および伸張に重要な役割を果たす)

Non-amelogenins: 10% (ameloblastin, MMP20 and etc.)

• Ameloblastin is a critical component of the enamel mineralization.

- Promotes or catalyzes the extension of enamel crystals.

(エナメルリンは、エナメル質形成時のハイドロキシアパタイト結晶の形成促進に重要な役割を果たす)

Overview

■ Enamel matrix proteins and Amelogenesis imperfecta (AI)

(エナメル基質タンパクとエナメル質形成不全症)

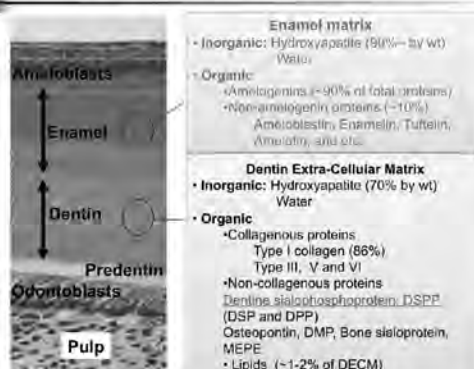
■ Dentin matrix proteins and Dentinogenesis imperfecta (DI)

(象牙質基質タンパクと象牙質形成不全症)

■ Research introduction and Future research plans

(最近の研究紹介と研究計画)

Extra-Cellular matrix in tooth



Hereditary dentin defects- Dentinogenesis Imperfecta

Frequency: 1 in 6000 to 8000

Type I	diminished or obliterated pulp chamber	Associated with osteogenesis imperfecta and type I collagen defects
Type II	obliterated pulp chamber, disorganized dentinal tubules	Not associated with osteogenesis imperfecta, Autosomal dominant or recessive
Type III	Enlarged pulp chamber, widened predentin, pulp exposure, irregular mineralization front	Often associated with a genetically isolated population, Autosomal dominant

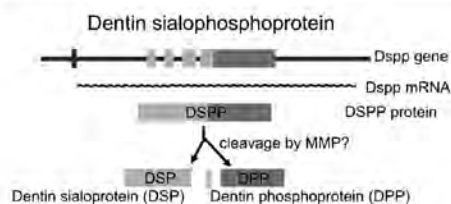
Type II, III
-- variable, opalescent blue-gray to yellow-brown discoloration
-- due to mutations in *DSPP*



from Witkop JT, Probst CJ, Heath AM (2001)

Dentin sialophosphoprotein (DSPP)

- Most abundant non-collagenous matrix protein in dentin.
- Belonging to SIBLING (Small integrin-binding ligand N-linked glycoprotein) family such as OPN, BSP, DMP1 and MEPE.
- Highly phosphorylated with high acidity.



Phenotypes of *dspp* null mice

Broken incisors found in *dspp* null teeth



Widened predentin in *dspp* null teeth

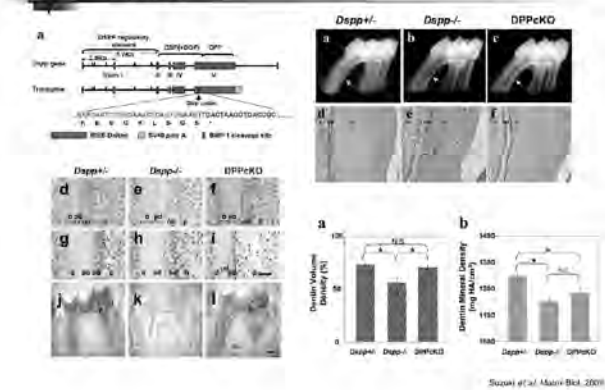


Dental caries found in *dspp* null teeth



Shenoy et al. J Biol Chem 2003

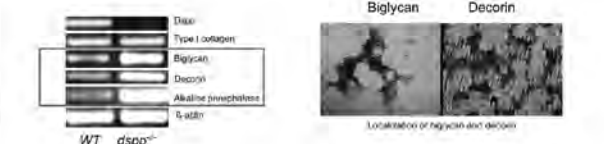
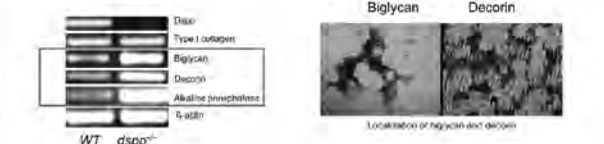
Partial rescue of the DSPP null phenotypes with DSP



Altered gene expressions in DSPP null teeth

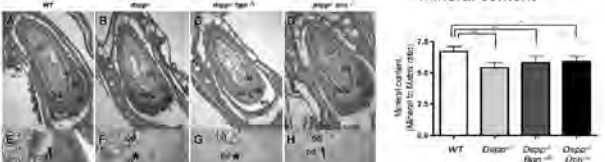
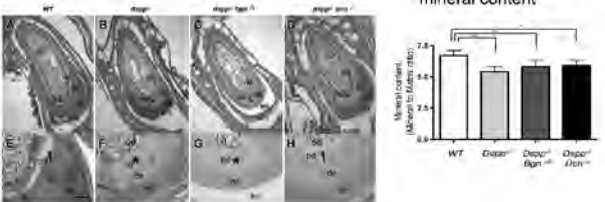
Altered gene expression in *dspp*^{-/-} teeth Biglycan and Decorin localization of Human DI patient

Altered gene expression in *dspp*^{-/-} teeth Biglycan and Decorin localization of Human DI patient



DSP(P) may affects the dentin mineralization front though the regulation of decorin / biglycan expression

The widened predentin observed in *dspp*^{-/-} was restored in *dspp*^{-/-} *dcn*^{-/-} mice



The role of DSPP in dentin mineralization

The major non-collagenous protein in dentin

*The disruption of mouse *Dspp* gene, encoding dentin sialoprotein (DSP) and dentin phosphoprotein (DPP), causes the phenotypes resembling human dentinogenesis imperfecta Type III.
(DSP遺伝子欠損マウスはヒト象牙質形成不全症(Ⅲ型)に似た表現系を示す)

・DSP(P) null affects the dentin mineralization front possibly though the regulation of decorin / biglycan expression.
(DSP(P)欠損は、デコリンやバイグリアンの遺伝子発現を変化させることで象牙前質の石灰化前線形成に影響を与える可能性がある)

・DPP might be important for the quality of dentin maturation, but not for the mineral initiation.
(DPPは象牙前質から象牙質への変換(石灰化開始)ではなく、象牙質の石灰化度に影響をおよぼす可能性が示唆された)

Overview

- Enamel matrix proteins and Amelogenesis imperfecta (AI)
(エナメル基質タンパクとエナメル質形成不全症)
- Dentin matrix proteins and Dentinogenesis imperfecta (DI)
(象牙質基質タンパクと象牙質形成不全症)
- Research introduction and Future research plans
(最近の研究紹介と研究計画)

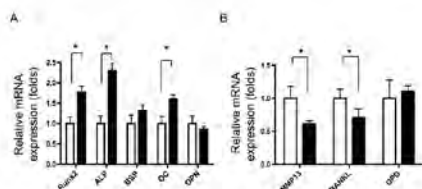
Functional analysis of extra cellular matrix proteins as signaling molecules predominantly expressed in tooth enamel and dentin.

エナメル質および象牙質細胞外基質タンパクの
シグナル分子としての生物学的機能の解析

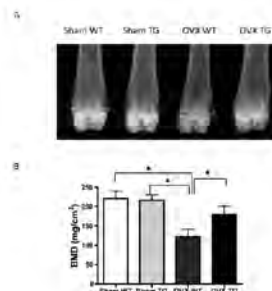
Tokyo Medical & Dental University
Department of Maxillofacial Orthognathics

Naoto Haruyama
(春山直人)

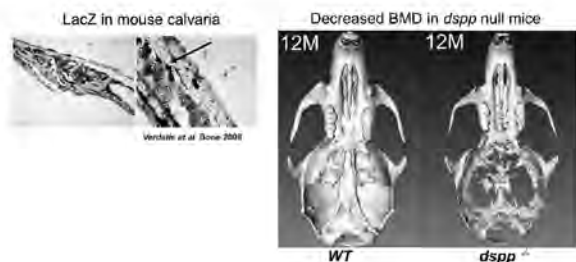
Altered gene expression level in LRAP transgenic calvarial cells.



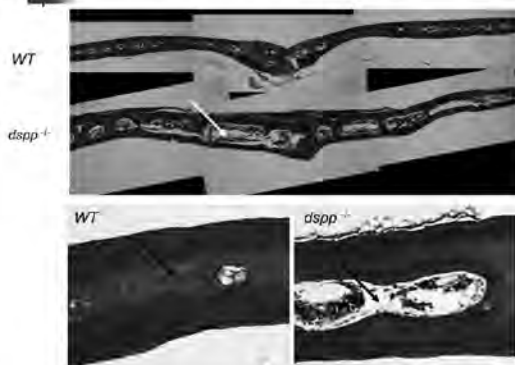
Changes in femoral bone parameters in WT and TG mice



dspp gene expression in mouse calvaria

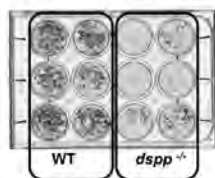


Histological changes in *dspp*^{-/-} calvaria



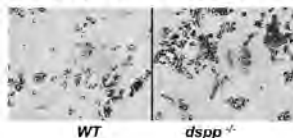
Calvarial cell culture

in vitro mineralization assay



Mineralization was reduced ~3 folds in *dspp*^{-/-} calvaria cell cultures

Adipocyte differentiation assay



dspp^{-/-} calvarial cells showed increased differentiation of adipocyte lineage

Summary

- Enamel matrix proteins and dentin matrix proteins are essential for proper enamel matrix organization and mineralization in teeth.
(エナメル基質タンパクと象牙質基質タンパクは、歯における基質組織の形成と石灰化に重要な役割を果たす。)
- Amelogenin and DSPP may have additional functions in bone tissues.
(アメロジェニンとDSPPは、骨組織において、基質タンパクとしての役割ではなく他の機能を担っている可能性が示唆される。)



3) 研究内容英文要約

Preferred chewing side-dependent two-point discrimination and cortical activation pattern of tactile tongue sensation

The purpose of this study was to investigate (1) whether the sensory threshold of the tongue differed according to the side and (2) whether the pattern of hemispheric cortical activation by tactile tongue stimulation differed, with special attention to the preferred chewing side (PCS). The PCS was determined with a mandibular kinesiograph in 12 healthy adults. The mean thresholds for two-point discrimination (TPD) in the anterior, canine and posterior regions on both sides of the tongue, and those between PCS and non-PCS in each region were statistically compared. In the functional magnetic resonance imaging study, tactile stimulation was delivered to either side of the tongue with acrylic balls via a mandibular splint. Activated voxel numbers in the bilateral primary somatosensory cortex (S1) were statistically compared. The threshold of TPD increased in the order of the anterior, canine and posterior regions. Moreover, this threshold was significantly smaller on the PCS than on the non-PCS in both the canine and posterior regions. Moreover, the number of activated voxels in S1 contralateral to the PCS was significantly greater than that in S1 contralateral to the non-PCS.

Diagnosis of Russell-Silver Syndrome by the Combined Bisulfite Restriction Analysis - Denaturing High-performance Liquid Chromatography Assay

Russell-Silver syndrome (RSS) is characterized by prenatal and postnatal growth retardation, triangular facies, and fifth-finger clinodactyly. Half of all patients with RSS have hypomethylation of the differentially methylated region (DMR) of the H19 gene on chromosome 11p15.5. Hence, a quantitative methylation analysis of this region can

be useful for the molecular diagnosis of RSS. However, conventional assays based on bisulfite-clone-sequencing are rather time and labor consuming and are not suitable for clinical use. In the present study, we investigated a possible method of quantitatively determining H19 hypomethylation in RSS patients using a combined COBRA (combined bisulfite restriction analysis) -DHPLC (denaturing high-performance liquid chromatography) assay. An analysis of 7 RSS patients using the COBRA-DHPLC assay demonstrated that 3 of the 7 RSS patients had a low methylation index of around 10%. A comparison of the methylation indices obtained using COBRA-DHPLC and conventional bisulfite-clone-sequencing revealed an excellent intermethod agreement. In summary, we have developed a robust, rapid, and cost-effective COBRA-DHPLC based screening system for Russell-Silver syndrome.

Systemic and maxillofacial characteristics of individuals affected by Beckwith-Wiedemann syndrome who have not received a glossectomy

Beckwith-Wiedemann syndrome (BWS) is a genetic disorder characterized by exomphalos, macroglossia and gigantism. Previous studies reported a wide variation in the skeletal and occlusal characteristics in individuals affected by BWS. However, these studies were performed by analyzing individuals both who had and had not received a glossectomy, which has a high impact on the jaw growth and occlusion. To highlight the intrinsic characteristics of BWS, seven Japanese affected individuals without glossectomy were analyzed in this study. Seven individuals who had been diagnosed as BWS by medical specialists and had not undergone glossectomy, were analyzed. Cephalograms and dental casts were taken and systemic complications were recorded at the first visit. Individuals uniformly showed a higher birth height and weight, macroglossia, large anterior cranial base and mandibular body. They exhibited a wide dental arch and an anterior open bite due to the undererupted and proclined anterior teeth. A wide variation was seen in the gonial angle but a facial height was overall large. As intrinsic characteristics of BWS, individuals exhibited macroglossia resulting in an anterior open bite and a wide dental arch. A long facial height and an enlarged anterior cranial base and mandibular body were also noted.

A Mongolian hypohidrotic ectodermal dysplasia patient with a novel P121S variant

Hypohidrotic ectodermal dysplasia is a genetic disorder characterized by diminished or a lack of sweating, congenital missing teeth, and sparse or an absence of hair. Three genes, EDA, EDAR, and EDARADD, all related to tumor necrosis factor (TNF) signaling, have been reported as responsible genes for this disorder. DNA

analysis of EDA, EDAR, and EDARADD was performed on a Mongolian patient by polymerase chain reaction-direct sequencing. The 5-year-old Mongolian individual had no erupted deciduous or permanent teeth. A panoramic radiograph showed only one tooth in the right mandible. His hair and eyebrows were sparse, but he did not show short stature. He showed diminished sweating, but the nails of his fingers and toes were normal. Based on these conditions, he was diagnosed with hypohidrotic ectodermal dysplasia. There was no gene mutation of EDA or EDAR. A novel heterozygous variant (P121S; c.361C>T) was identified in the death domain of EDARADD (NM_080738). No other member of his family was affected, and this variant was not identified in his parents or maternal grandparents. This study reports an individual affected with hypohidrotic ectodermal dysplasia with a novel heterozygous P121S variant in the death domain of EDARADD.

Marfan Syndrome and Its Disorder in Periodontal Tissues

Fibrillin-1 is a major microfibrillar protein and characterized by calcium binding EGF-like (cbEGF) domain. Association between fibrillin-1 and TGF- β is a recent topic of this field and this interaction is known to inactivate and target TGF- β action. FBN1 encoding fibrillin-1 is a responsible gene for Marfan syndrome type 1 (MIM 154700), characterized by increased height and long limbs, ectopia lentis, and cardiovascular disorders, such as mitral valve prolapse and aortic dilation and regurgitation. Animal models suggest that the abnormal TGF- β signaling is underlying as the pathogenesis of these conditions. Besides skeletal, ocular and cardiovascular conditions, severe periodontitis is frequently seen in affected patients. To clarify the unknown function of elastic system fibers in the periodontal ligament (PDL), PDL-cells were isolated from a Marfan syndrome type 1 patient who was with the severe periodontitis and had a mutation in one of the cbEGF domain of fibrillin-1. These results suggested that wild-type fibrillin-1 was required for the normal cell alignment and tissue architecture of PDLs. Evidences are now accumulated to suggest that fibrillin-1 is one of the molecule involved in the interaction between cell and extracellular matrix.

Human diseases accompanied with abnormal tooth roots

Tooth development is a complicated process characterized by reciprocal interactions between the dental epithelia and mesenchyme. During this process, inner and outer enamel epithelia form a double-layer sheath, Hertwig's epithelial root sheath, after crown formation. A close association is suggested between this root sheath and root dentin. Many genetic human diseases are associated with abnormal roots. Down syndrome, caused by trisomy 21, is frequently associated with short roots. In Turner syndrome, which is caused by monosomy or partial absence of the

X chromosome, characteristic extra multiroots are seen in the mandibular premolars. Oculo-facio-cardio-dental (OFCD) syndrome is associated with extremely long roots. Clinical observations postulate the following two points: 1) Abnormal tooth roots are accompanied by abnormal crowns. This indicates that crown and root formation is a sequential process and the latter is closely related to the former. 2) Multiple root abnormality is seen syndromically but not solely as a dental condition. This implies that regulators of tooth development are likely to be involved in the development of other tissues, such as the limbs, eyes and heart.

Application of distraction osteogenesis in patients with cleft lip and palate

Recently, distraction osteogenesis (DOG) has been applied to patients showing severe maxillary deficiency with cleft lip and palate. We have reported excellent outcomes relating to Le Fort I distraction for maxillary retardation and dentoalveolar distraction aiming at cleft closure and alveolar bone augmentation. In this field, clinical studies were carried out and following results were obtained. 1) Measurement of distraction force: The results of force measurement using micro tension gauges indicated that cases with low distraction efficiency would demonstrate high tension/activation ratio. 2) Integration of three-dimensional (3D) hard/soft tissue data: The framework for evaluating the change of hard and soft tissue in DOG was established by using image analysis software (STL-Rugle[®], Medic Engineering, Kyoto). Hard and soft tissue data of CT, hard tissue data of dental cast model incorporated by 3D scanner, and facial surface data incorporated by 3D digitizer were integrated into a common reference frame. 3) Simulation of soft tissue change in DOG: Soft tissue change in Le Fort I DOG was simulated by 3D software (SimPlant[®] OMS ver.12, Materialized Dental Japan, Chiba). As the result, discordance between the real soft tissue change and the simulation was detected especially in the nasal region.

Pathogenic mechanisms of tooth agenesis linked to paired domain mutations in human PAX9.

Mutations in the paired-domain transcription factor PAX9 are associated with non-syndromic tooth agenesis that preferentially affects posterior dentition. Of the 18 mutations identified to date, eight are phenotypically well-characterized missense mutations within the DNA-binding paired domain. We determined the structural and functional consequences of these paired domain missense mutations and correlated our findings with the associated dental phenotype variations. In vitro testing included subcellular localization, protein-protein interactions between MSX1 and mutant PAX9 proteins, binding of PAX9 mutants to a DNA consensus site and transcriptional activation from the

Pax9 effector promoters Bmp4 and Msx1 with and without MSX1 as co-activator. Our structure-based studies, which modeled DNA binding and subdomain stability, were able to predict functional consequences quite reliably.

Dentofacial characteristics in patients with oligodontia

Oligodontia (OD) is congenital agenesis of six permanent teeth or more, excluding third molars. Syndromic oligodontia (S-OD) is one of phenotype associated with congenital anomalies, such as ectodermal dysplasia (ED). On the other hand, oligodontia involving anomalies with only teeth is termed nonsyndromic oligodontia (NS-OD). This study aimed to investigate dentofacial characteristics in OD cases and to help planning the treatment. S-OD cases in this study included ED and EEC (ectrodactyly-ectodermal dysplasia-clefting) syndrome. The results were as follows: 1) Mean numbers of congenital missing permanent teeth were 10.4 and 9.0 in S-OD and NS-OD cases, respectively. 2) ED and NS-OD showed counterclockwise rotation of mandible and skeletal Class III. 3) EEC syndrome revealed retarded point B possibly induced by missing lower incisors. 4) Congenital missing of permanent premolars was most frequent in both S-OD and NS-OD cases. 5) Abnormal crown shape and amelogenesis imperfecta of permanent teeth were found more commonly in S-OD than those in NS-OD. For attainment of occlusal function and aesthetical profile in comprehensive orthodontic/prosthetic treatment of OD cases, elongation of maxillary molars aiming at mandibular clockwise rotation and space maintenance for prosthetics would be required in their growing stage.

The effects of hyperbaric oxygen to tooth movement into the regenerated area after distraction osteogenesis

To analyze the effect of hyperbaric oxygen (HBO) on regenerated bone in distracted areas by histological and radiological analysis. It was hypothesized the application of HBO to a tooth movement into the distracted area would accelerate ossification and vascularization of newly formed bone in the distracted space. 10 dogs were used. After creating a 10-mm length bone defect, a bony segment was translocated into the defect area. Following the distraction period, tooth movement was started and the dogs were divided into two groups. 150 days after osteotomy, the distracted area around the moving tooth was evaluated radiologically and histologically. Differences between groups were confirmed by Mann-Whitney rank test. Trabecular bone density and cortical and subcortical bone area measured by peripheral quantitative computed tomography in the HBO group were significantly higher than those in the control group. Histological observations revealed regenerated bone and blood vessels formation in the tension site of the moving tooth in the HBO group. The regenerated bone structure measured by bone histomorphometry was

larger, more active in bone formation in the HBO group. Applying HBO to tooth movement into a distracted area appears to accelerate ossification and vascularization of regenerated bone in the distracted area.

Dental information that can be offered in the genetic counseling of Turner syndrome

The aim of this study is to provide with useful information for the genetic counseling of Turner syndrome. We examined 7 patients in orthodontic clinic of Turner syndrome about their characteristics of oral manifestations. The following is the result. 1. Chief complaint: malocclusion 2. Initial visit: 7 years 3 months to 11 years 11 months. 3. Type of malocclusion: maxillary protrusion 5 cases, spaced arch 2 cases. 4. High palate: 6 cases. The most of them have maxillary protrusion caused by their small mandible. They need to guide their mandible forward during growth spurt with maxillary expansion correcting of narrow palate. For the success of their orthodontic treatment, we have to know their effect of growth hormone therapy and estimate the skeletal maturation.

Clinical experience with the use of the new internal device for maxillary distraction osteogenesis

We clinically applied a new internal device for maxillary distraction osteogenesis; The Maxillary Distractor System. This internal distractor was used in a 17-year-old man with a bilateral cleft lip and palate. Before distraction, he presented with a retrognathic maxilla with a minus 11 mm overjet. Following a bilateral alveolar bone graft with iliac bone 5 months before maxillary distraction, a Le Fort I osteotomy was performed and an internal distractor was placed under general anesthesia. After a 4-day latency period, internal maxillary distraction was performed at a rate of 1 mm/day achieved by two activations per day. Cephalometric analysis showed a 15 mm maxillary advancement. After a 4-day consolidation period, a removal of the device and plate fixation surgery was performed under general anesthesia. The intraoral finding 8 months after plate fixation was showed good occlusion. The bone formation at the front of the maxillary sinus was evaluated using computed tomography (CT), showing partial bone formation 3 months after plate fixation surgery. This device is more useful for larger maxillary distraction than other internal devices used previously by incorporating parts of various lengths.

Non-Prosthetic treatment with segmental osteotomy and bone grafting in patients with cleft lip and palate

The aim of this study is to present surgical combined comprehensive orthodontic treatment of two adult cases with unilateral CLP. Case 1: A male with left-CLP. The midline of upper central incisors was shifted 7 mm to the

right, the lateral incisor on the right (#12) showed palatal transposition, and the size of residual alveolar cleft was 7 mm. Le Fort I segmental osteotomy of major segment with incision between #11 and #13 to make space for alignment of #12, and simultaneous bone grafting into the extended alveolar bone were performed at age 18 years 4 months. Case 2: A male with left-CLP. The midline of upper central incisors was shifted 8 mm to the right, the size of residual alveolar cleft was 14 mm. For the purpose of midline correction and cleft closure, segmental osteotomy of major and minor segments and simultaneous bone grafting were performed at age 22 years 4 months. The present cases did not require prosthetic treatment. Segmental osteotomy in combination with bone grafting would be the treatment alternatives in the comprehensive orthodontic treatment for adult patients with CLP.

Assessment of bone maturity applying modal analysis after orthognathic surgery

The purpose of this study is to assess bone maturity after orthognathic surgery applying modal analysis that is one of the noninvasive methods of revealing the dynamic characteristics of a structure by investigating how each component vibrates at its own natural frequency. Two female patients diagnosed to apply maxillary orthognathic surgery were included. One of the subjects had left unilateral complete cleft lip and palate. Modal testing was carried out at the pre-operation, 3 months post-operation and over 12 months post-operation. The measurement system was composed of an impact hammer, Laser-Doppler Vibrometer, Fast Fourier Transform (FFT) -analyzer and personal computer installed with modal analysis software. The upper right central incisor was struck with the impact hammer, and the response at each measurement point on the upper anterior teeth was detected using Laser-Doppler Vibrometer. Then the transfer function was obtained from each measurement point using FFT-analyzer. Finally, a computer analysis was performed and modal parameters such as modal shape, natural frequency and damping ratio were calculated. The modal parameters had varied as the progress after the operation. The parameters of over 12 months post-operation got to be close to those of pre-operation.

Osteogenesis by gradually expanding the interface between bone surface and periosteum enhanced by bone marrow stem cell administration in Rabbits.

Periosteal distraction for osteogenesis is expected to generate new bone without limitations resulting from the width of the osteotomized segment in distraction osteogenesis. However, the bone tissue newly formed by periosteal distraction is generally not suitable for occlusal forces because it is rich in interstitial fatty tissue. Therefore,

the development of alternative strategies for periosteal distraction is necessary to induce effective bone formation that will lead to a reduction of the treatment period and to obtain functional bone capable of withstanding occlusal force. This study was performed to investigate whether the administration of mesencymal stem cells (MSCs) promotes bone formation at the gap created by periosteal distraction. Following elevation of the mesh plate placed subperiosteally in rabbit parietal bones, rabbit MSCs were administered into the gap. Controls received phosphate-buffered saline. The MSC administrated group showed significantly increased volume, height, bone mineral density, and bone mineral content in newly formed bone tissues at the gaps compared with the control group ($P < .05$), which was examined by microcomputed tomography. Histological analysis revealed that the newly formed bone tissues showed both type I collagen and osteocalcin expression in the MSC-administration group. MSC administration may be useful to induce osteogenesis at sites of periosteal distraction.

Dentin sialoprotein and dentin phosphoprotein have distinct roles in dentin mineralization.

Dentin sialophosphoprotein (DSPP), a major non-collagenous matrix protein of odontoblasts, is proteolytically cleaved into dentin sialoprotein (DSP) and dentin phosphoprotein (DPP). Previous studies revealed that DSPP null mice display a phenotype similar to human autosomal dominant dentinogenesis imperfecta, in which teeth have widened predentin and irregular dentin mineralization resulting in sporadic unmineralized areas in dentin and frequent pulp exposure. Earlier in vitro studies suggested that DPP, but not DSP, plays a significant role in initiation and maturation of dentin mineralization. However, the precise in vivo roles of DSP and DPP are far from clear. Here we report the generation of DPPcKO mice, in which only DSP is expressed in a DSPP null background, resulting in a conditional DPP knockout. DPPcKO teeth show a partial rescue of the DSPP null phenotype with the restored predentin width, an absence of irregular unmineralized areas in dentin, and less frequent pulp exposure. Micro-computed tomography analysis of DPPcKO molars further confirmed this partial rescue with a significant recovery in the dentin volume, but not in the dentin mineral density. These results indicate distinct roles of DSP and DPP in dentin mineralization, with DSP regulating initiation of dentin mineralization, and DPP being involved in the maturation of mineralized dentin.

Synthesis and intracellular transportation of type I procollagen during functional differentiation of odontoblasts.

The expression of type I collagen, the most component of

dentin extracellular matrix proteins (ECMs) in odontoblast is correlated with the activity of dentin formation. Since odontoblast possesses a distinct cellular process for protein transport into the dentinal tubule, it may possess important roles on intracellular protein localization. Type I collagen is synthesized as procollagen, which is immediately converted to collagen upon secretion. After characterization of antiserum to rat type I procollagen, we investigated the intracellular localization of type I procollagen in odontoblasts during and after dentinogenesis, using immunohistochemistry and in situ hybridization. The level of mRNA expression decreased during dentinogenesis, whereas the intracellular localization of type I procollagen in odontoblast processes become more distinct. The percentage of dentinal tubules with type I procollagen increased significantly with aging. Odontoblasts in pulp horn, in particular, showed moderate expression of type I procollagen after dentinogenesis. Since loss of occlusion also caused a significant decrease in type I procollagen, we concluded that occlusal stimulation activated type I procollagen synthesis in odontoblasts. We also suggest that analysis of intracellular transport of type I procollagen via odontoblast processes may be a new approach to evaluation of odontoblast function.

Genetic evidence for key roles of decorin and biglycan in dentin mineralization.

Targeted disruption of the dentin sialophosphoprotein (DSPP) gene in the mice (Dsp^{-/-}) results in dentin mineralization defects with enlarged predentin phenotype similar to human dentinogenesis imperfecta type III. Using DSPP/biglycan (Dsp^{-/-}Bgn^{-/-}) and DSPP/decorin (Dsp^{-/-}Dcn^{-/-}) double knockout mice, here we determined that the enlarged predentin layer in Dsp^{-/-} teeth is rescued in the absence of decorin, but not in the absence of biglycan. However, Fourier transform infrared (FTIR) spectroscopy analysis reveals similar hypomineralization of dentin in both Dsp^{-/-}Bgn^{-/-} and Dsp^{-/-}Dcn^{-/-} teeth. Atomic force microscopy (AFM) analysis of collagen fibrils in dentin shows subtle differences in the collagen fibril morphology in these genotypes. The reduction of enlarged predentin in Dsp^{-/-}Dcn^{-/-} mice suggests that the elevated level of decorin in Dsp^{-/-} predentin interferes with the mineralization process at the dentin mineralization front. On the other hand, the lack of DSPP and biglycan leads to the increased number of calcospherites in Dsp^{-/-}Bgn^{-/-} predentin, suggesting that a failure in coalescence of calcospherites was augmented in Dsp^{-/-}Bgn^{-/-} teeth as compared to Dsp^{-/-} teeth. These findings indicate that normal expression of small leucine rich proteoglycans, such as biglycan and decorin, plays an important role in the highly orchestrated process of dentin mineralization.

Synergistic Roles of Amelogenin and Ameloblastin.

Amelogenin and ameloblastin, the major enamel matrix proteins, are important for enamel mineralization. To identify their synergistic roles in enamel development, we generated Amel X^{-/-}Ambn^{-/-} mice. These mice showed additional enamel defects in comparison with Amel X^{-/-} or Ambn^{-/-} mice. In 7-day-old Amel X^{-/-}Ambn^{-/-} mice, not only was the ameloblast layer irregular and detached from the enamel surface, as in Ambn^{-/-}, but also, the enamel width was significantly reduced in the double-null mice as compared with Amel X^{-/-} or Ambn^{-/-} mice. Proteomic analysis of the double-null teeth revealed increased levels of RhoGDI (Arhgdia), a Rho-family-specific guanine nucleotide dissociation inhibitor, which is involved in important cellular processes, such as cell attachment. Both Amel X^{-/-}Ambn^{-/-} mice and Ambn^{-/-} mice displayed positive staining with RhoGDI antibody in the irregularly shaped ameloblasts detached from the matrix. Ameloblastin-regulated expression of RhoGDI suggests that Rho-mediated signaling pathway might play a role in enamel formation.

In vivo impact of a 4 bp deletion mutation in the DLX3 gene on bone development.

Distal-less 3 (DLX3) gene mutations are etiologic for Tricho-Dento-Osseous syndrome. To investigate the in vivo impact of mutant DLX3 on bone development, we established transgenic (TG) mice expressing the c.571_574delGGGG DLX-3 gene mutation (MT-DLX3) driven by a mouse 2.3kb-Coll1a1 promoter. Micro-computed tomographic analyses demonstrated markedly increased trabecular bone volume and bone mineral density in femora from TG mice. In ex vivo experiments, TG mice showed enhanced differentiation of bone marrow stromal cells to osteoblasts and increased expression levels of bone formation markers. However, TG mice did not show enhanced dynamic bone formation rates in in vivo fluorochrome double labeling experiments. Osteoclastic differentiation capacities of bone marrow monocytes were reduced in TG mice in the presence of osteoclastogenic factors and the numbers of TRAP (+) osteoclasts on distal metaphyseal trabecular bone surfaces were significantly decreased. TRACP 5b and CTX serum levels were significantly decreased in TG mice, while IFN- γ levels were significantly increased. These data demonstrate that increased levels of IFN- γ decrease osteoclast bone resorption activities, contributing to the enhanced trabecular bone volume and mineral density in these TG mice. These data suggest a novel role for this DLX3 mutation in osteoclast differentiation and bone resorption.

4) 本事業に関連して世界的な研究拠点形成に向けて、以下の点で改善・整備等されたこと

A (研究拠点体制)

昨年度に整備したGCOEの事業に携わる他の事業推進者との連携をさらに強化するとともに、国立保健医療科学院とも連携することで公衆衛生の分野にも裾野を広げ、疾患に関わる情報を幅広く得られる基盤を確立した。

B (研究教育環境)

当分野では疾患に即した研究グループ分けが行われており、各グループにおいて、その疾患の原因の解明、検査診断や治療法の改良を目的とした研究が行われている。各大学院生は各研究グループに所属しており、そこで定期的にミーティングを行うなど、グループを基盤とした教育体制の充実化を図っている。また大学院生を含めた新人教育の一環として、先天性疾患をテーマにあげ、疾患の成因から臨床的な側面を含めた幅広い内容を求めた発表を課している。

C (人材確保)

本年度、大学院生が5人新たに加わり、各々GCOEのテーマである歯と骨の疾患の分子病態成立のメカニズムの解明を目指した研究だけでなく、当分野の特色である疾患を有する患者の咬合機能の回復のための治療法の開発にも携わっている。

D (人材育成)

GCOEプログラムでは、シャペロン制度やスーパースチューデント制度を創設して、若手研究者の人材の育成に取り組んでいるが、当分野において、現在のところ3名の大学院生がこの制度を利用している研究に携わっている。当分野の特色である臨床研究と基礎研究の橋渡しが出来た幅広い視野を持った研究者の育成が期待される。

E (国際化)

積極的に海外の学会発表や学術誌に投稿し、成果を発表した。さらに、モンゴル、タイ、ホンジュラスならびに中国とさまざまな国からの留学生を受け入れている。

5) GCOE事業を推進するに当たって力を入れた点

GCOEのテーマである歯と骨の疾患の分子病態成立のメカニズムを明らかにするには、ヒトから得られる情報を多角的に集積することが非常に大切であると思われる。そこで本年度は、国立保健医療科学院生涯保健部の藤原

武男先生と連携することで、疾患に関わる情報を幅広く得られる基盤を確立した。公衆衛生の分野にも裾野を広げることは、当分野で得られた情報ならびに成果を幅広く社会に発信する可能性を有すると期待できる。

6) 英文原著論文

1. ©Ono T, Okuma M, Hamada T, Motohashi N, Moriyama K. A case of ring chromosome 18 syndrome treated with a combined orthodontic-prosthetic approach. *Cleft Palate Craniofac J*.
2. Inokuchi T, Kawamoto T, Aoki K, Aoki A, Nagahama K, Baba Y, Suzuki S, Shibayama M, Mano Y, Ohya K, Moriyama K. The effects of hyperbaric oxygen on tooth movement into the regenerated area after distraction osteogenesis. *Cleft Palate Craniofac J*.
3. ©Aoki A, Moriyama K, Kawamoto T, Aoki K, Inokuchi T, Kudoh A, Nagahama K, Baba Y, Suzuki S, Ohya K. Amount of bone lengthening affects blood flow recovery and bone mineralization after distraction osteogenesis in a canine cleft palate model. *Cleft Palate Craniofac J*.
4. ©Sato K, Haruyama N, Shimizu Y, Hara J, Kawamura H. Osteogenesis by gradually expanding the interface between bone surface and periosteum enhanced by bone marrow stem cell administration in Rabbits. *Oral Surg Oral Med Oral Pathol Oral Radiol Endod*.
5. Kawafuji A, Suda N, Suzuki T, Ichikawa N, Kakara S, Baba Y, Ogawa T, Tsuji M, Moriyama K. Systemic and maxillofacial characteristics of individuals affected by Beckwith-Wiedemann syndrome who have not received a glossectomy. *Am J Orthod Dentofacial Orthop*.
6. Suda, N, Moriyama K. Human diseases accompanied with abnormal tooth roots. *Journal of Oral Biosciences. J Oral Biosci* 51(4):199-204, 2009
7. Hiasa M, Abe M, Nakano A, Oda A, Amou H, Kido S, Takeuchi K, Kagawa K, Yata K, Hashimoto T, Ozaki S, Asaoka K, Tanaka E, Moriyama K, Matsumoto T. GM-CSF and IL-4 induce dendritic cell differentiation and disrupt osteoclastogenesis through M-CSF receptor shedding by up-regulation of TNF- α converting enzyme (TACE). *Blood* 114(20):4517-26, 2009
8. ©Kusumah SW, Suzuki S, Itoh K, Higashino R, Ohbayashi N, Kurabayashi T, Moriyama K. Morphological observation of the medial pterygoid muscle by the superimposition of images obtained by lateral cephalogram and MRI. *J Orthod*. 36(4):243-52, 2009
9. Kondo Y, Takahashi T, Oba Y, Tanaka E, Moriyama K. Blood flow distribution of repaired lip in cleft lip patients. *Angle Orthodont*. 79(6):1182-7, 2009
10. ©Hattori M, Torii C, Yagihashi T, Izumi K, Suda N, Ohya K, Takahashi T, Moriyama K, Kosaki K. Diagnosis of Russell-Silver syndrome by the

- combined bisulfite restriction analysis-denaturing high-performance liquid chromatography assay. *Genet Test Mol Biomarkers*. 13(5):623-30, 2009
11. Jinno K, Takahashi T, Tsuchida K, Tanaka E, Moriyama K. Acceleration of palatal wound healing in Smad3-deficient mice. *J. Dent. Res.* 88(8):757-61, 2009
 12. Wang Y, Groppe JC, Wu J, Ogawa T, Mues G, D'Souza RN, Kapadia H. Pathogenic mechanisms of tooth agenesis linked to paired domain mutations in human PAX9. *Hum Mol Genet.* 18(15):2863-74, 2009
 13. Kitase Y, Yokozeki M, Fujihara S, Izawa T, Kuroda S, Tanimoto K, Moriyama K, Tanaka E. Analysis of gene expression profiles in human periodontal ligament cells under hypoxia: the protective effect of CC chemokine ligand 2 to oxygen shortage. *Arch Oral Biol.* 54(7):618-24, 2009
 14. ◎Minato A, Ono T, Miyamoto JJ, Honda E, Kurabayashi T, Moriyama K. Preferred chewing side-dependent two-point discrimination and cortical activation pattern of tactile tongue sensation. *Behav Brain Res.* 203(1):118-26, 2009
 15. ◎Inoue-Arai MS, Ono T, Honda E, Kurabayashi T, Moriyama K. Motor coordination of articulators depends on the place of articulation. *Behav Brain Res.* 16:199(2):307-16, 2009
 16. Miraoui H, Oudina K, Petite H, Tanimoto Y, Moriyama K, Marie PJ. Fibroblast growth factor receptor 2 promotes osteogenic differentiation in mesenchymal cells via ERK1/2 and protein kinase C signaling. *J Biol Chem.* 284(8):4897-904, 2009
 17. ◎Yagi Y, Suda N, Yamakoshi Y, Baba O, Moriyama K. In vivo application of amelogenin suppresses root resorption. *J Dent Res.* 88(2):176-81, 2009
 18. Suda N, Shiga M, Ganburged G, Moriyama K. Marfan syndrome and its disorder in periodontal tissues. *J Exp Zool B Mol Dev Evol.* 312B(5):503-9, 2009
 19. Suzuki S, Sreenath T, Haruyama N, Honeycutt C, Terse A, Cho A, Kohler T, Müller R, Goldberg M, Kulkarni AB. Dentin sialoprotein and dentin phosphoprotein have distinct roles in dentin mineralization. *Matrix Biol.* 28(4):221-9, 2009
 20. Sato S, Tsuchiya M, Komaki K, Kusunoki S, Tsuchiya S, Haruyama N, Takahashi I, Sasano Y, Watanabe M. Synthesis and intracellular transportation of type I procollagen during functional differentiation of odontoblasts. *Histochem Cell Biol.* 131(5):583-91, 2009
 21. Haruyama N, Sreenath TL, Suzuki S, Yao X, Wang Z, Wang Y, Honeycutt C, Iozzo RV, Young MF, Kulkarni AB. Genetic evidence for key roles of decorin and biglycan in dentin mineralization. *Matrix Biol.* 28(3):129-136, 2009
 22. Hatakeyama J, Fukumoto S, Nakamura T, Haruyama N, Suzuki S, Hatakeyama Y, Shum L, Gibson CW, Yamada Y, Kulkarni AB. Synergistic Roles of Amelogenin and Ameloblastin. *J Dent Res.* 88(4):318-322, 2009
 23. Choi SJ, Roodman GD, Feng JQ, Song IS, Amin K, Hart PS, Wright JT, Haruyama N, Hart TC. In vivo impact of a 4 bp deletion mutation in the DLX3 gene on bone development. *Dev Biol.* 325(1): 129-37, 2009
- ## 7) 著書
1. Haruyama N, Hatakeyama J, Hatakeyama Y, Gibson CW, Kulkarni AB. Chapter 3, Lessons from the amelogenin knockout mice. In: *Amelogenins: multifaceted proteins for dental and bone formation and repair*. 7 pages, (in press)
 2. Haruyama N, Cho A, Kulkarni AB. Overview: engineering transgenic constructs and mice. In: *Current Protocols in Cell Biology*. Chapter 19: Unit 19.10, 9 pages, 2009
 3. Cho A, Haruyama N, and Kulkarni AB. Generation of transgenic mice. In: *Current Protocols in Cell Biology*. Mar; Chapter 19: Unit 19.11, 22 pages, 2009
 4. 小野卓史. 頭部X線規格写真(セファロ)分析. 睡眠学、朝倉書店、622-624, 2009
- ## 8) 平成21年度までの自己評価
- 研究面においては、基礎研究の成果と臨床的要素を融合した研究を遂行することが可能であったとともに、公衆衛生の分野にも裾野を広げることで、疾患に関連した情報を幅広く得られる基盤を確立することができた。さらに、各々の大学院生が積極的に海外を含めた学会等で発表するとともに、発表した学術大会で受賞している大学院生も多数見られ、教育面でも充実化が図られた。
- ## 9) 和文原著論文
1. 森田圭一、菊池剛、今泉史子、根岸綾子、辻美千子、小村健. 新規創内固定型上顎骨延長装置の使用経験. 日本口腔外科学会誌(印刷中)
 2. 青木朝里. イヌ顎裂モデルを用いた上顎歯槽骨延長術後の歯髄血流量および硬組織変化の観察. 口腔病学会雑誌. 76 (1) :37-44, 2009
- ## 10) 学会発表 (英文)
1. ◎Mitani K, Haruyama N, Igarashi K. Amelogenin splice isoforms stimulate chondrogenic differentiation of ATDC5 cells. The 39th Annual Meeting & Exhibition of

- the AADR/CADR, Washington, DC, March 3-6, 2010 示説
2. ©Hashimoto K, Ono T, Sato M, Honda E, Kurabayashi T, Mataka S, Hasegawa M, Moriyama K. Effects of oral appliance treatment on brain activation during inspiratory loading in obstructive sleep apnea patients: a preliminary functional magnetic resonance imaging study. 7th International Orthodontic Congress, Sydney, February 6-9, 2010 示説
 3. Inoue-Arai MS, Ono T, Honda E, Moriyama K. Avaliação da Articulação da Fala Utilizando RM funcional e RM movie em Pacientes Fissurado e Não Fissurado. 7th ABOR (Associação Brasileira de Ortodontia e Ortopedia Facial), Brasília-DF · Brasil, October 8-11, 2009 示説
 4. Tsuji M, Baba Y, Suzuki S, Moriyama K. Non-prosthetic treatment with segmental osteotomies and bone grafting in patients with cleft lip and palate. 11th International Congress on Cleft Lip and Palate and Related Craniofacial Anomalies, Fortaleza, September 10-13, 2009 示説
 5. Kataoka K, Baba Y, Honda A, Suzuki S, Ohbayashi N, Kurabayashi T, Moriyama K. Integration of three-dimensional hard/soft tissue data in patients treated with orthognathic surgery. 11th International Congress on Cleft Lip and Palate and Related Craniofacial Anomalies, Fortaleza, September 10-13, 2009 示説
 6. Honda A, Baba Y, Kataoka K, Suzuki S, Moriyama K. Long-term study of skeletal changes after maxillary distraction in growing children with cleft lip and palate. 11th International Congress on Cleft Lip and Palate and Related Craniofacial Anomalies, Fortaleza, September 10-13, 2009 口頭
 7. Iida T, Hoshiai H, Hatsuno K, Taniguchi H, Tsuji M, Baba Y, Suzuki S, Moriyama K. Assessment of bone maturity by modal analysis after orthognathic surgery. 11th International Congress on Cleft Lip and Palate and Related Craniofacial Anomalies, Fortaleza, September 10-13, 2009 示説
 8. Inoue-Arai MS, Ono T, Honda E, Kurabayashi T, Moriyama K. Geometrical changes in the tongue shape during articulation in subjects with and without CLP revealed by MRI movie. 11th International Congress on Cleft Lip and Palate and Related Craniofacial Anomalies, Fortaleza, September 10-13, 2009 口頭
 9. Inoue-Arai MS, Sato-Wakabayashi M, Ono T, Honda E, Kurabayashi T, Moriyama K. Mapping of brain activation areas in covert and overt articulation in subjects with and without cleft lip and palate. 11th International Congress on Cleft Lip and Palate and Related Craniofacial Anomalies, Fortaleza, September 10-13, 2009 示説
 10. Suda N, Kawafuji A, Ogawa T, Tsuji M, Moriyama. Characteristics of Japanese Beckwith-Wiedemann syndrome patients without glossectomy. 85th Congress of the European Orthodontic Society, Helsinki, June 10-14, 2009 口頭
 11. Ogawa T, Wirahadi Kusumah S, Moriyama K. Dentofacial changes of a congenital myopathy patient after orthodontic treatment. 85th Congress of the European Orthodontic Society, Helsinki, June 10-14, 2009 示説
 12. Yokota T, Ono T, Miyamoto JJ, Takada J, Moriyama K. Mandibular hinge axis in skeletal Class III subjects with posterior unilateral crossbite. 85th Congress of the European Orthodontic Society, Helsinki, June 10-14, 2009 示説
 13. Takada J, Ono T, Miyamoto JJ, Yokota T, Moriyama K. Relationship between buccolingual position and angle of molars and intraoral pressure in subjects with facial asymmetry. 85th Congress of the European Orthodontic Society, Helsinki, June 10-14, 2009 示説
 14. Kataoka K, Baba Y, Honda A, Kawafuji A, Ishizaki T, Suzuki S, Moriyama K. Measurement of traction force using micro tension gauges in maxillary distraction osteogenesis. 66th American Cleft Palate Association Annual Meeting, Scottsdale, Arizona, April 20-25, 2009 示説
 15. Takahashi Y, Suda N, Yamakoshi Y, Baba O, Moriyama K. Amelogenin is a potent inhibitor of odontoclastic root resorption. 88th General Session & Exhibition of the International Association for Dental Research, Miami, April 1-4, 2009 口頭
 16. Ganjargal G, Suda N, Takahashi, Y, Hamada N, Moriyama K. Accelerated alveolar bone resorption in mouse model of Marfan syndrome. 88th General Session & Exhibition of the International Association for Dental Research, Miami, April 1-4, 2009 示説

11) 学会発表 (和文)

1. 須田直人、志賀百年、Ganjargal Ganburged、齊藤正寛、山崎洋介、磯川桂太郎、森山啓司. 歯根膜に局在する弾性線維の機能解析に関するアプローチ. 第7回エラスチン研究会学術集会、北九州市、平成21年12月4-5日
2. 齊藤正寛、須田直人、Ganjargal Ganburged、辻孝. 新規細胞外マトリックスである ADAMTSL-5 は歯根膜のマイクロフィブリル形成を促進する. 第7回エラスチン研究会学術集会. 北九州市、12月4-5日
3. 疋田理奈、川元龍夫、佐藤麻緒、茂木和久、井口隆人、八木優子、豊福明、森山啓司. 精神的問題が疑われ矯正歯科治療において対応に苦慮した3症例. 第68回日本矯正歯科学会、福岡、平成21年11月16-18日

4. 湊亜紀子、小野卓史、宮本順、菅田栄一、倉林亨、森山啓司. 舌感覚の皮質投影パターンにおける習慣性咀嚼の関与. 第68回日本矯正歯科学会、福岡、平成21年11月16-18日
5. 破裂音発生時における舌の形状および重心の構音点依存性の経時的変化. 井上マリステラ小百合、小野卓史、本田栄一、倉林亨、森山啓司. 第68回日本矯正歯科学会、福岡、平成21年11月16-18日
6. 金谷和宏、鈴木聖一、五島健一、三浦不二夫、三浦宏之、森山啓司. 球形樹脂微粒子含有ガムを用いた咀嚼効率の研究(第1報). 第68回日本矯正歯科学会、福岡、平成21年11月16-18日
7. 鎌田秀樹、鈴木聖一、塙隆夫、森山啓司. コラーゲン電着固定化Tiの創製と耐久性評価. 第68回日本矯正歯科学会、福岡、平成21年11月16-18日
8. 佐藤麻緒、馬場祥行、井口隆人、本田綾、片岡恵一、辻美千子、鈴木聖一、森山啓司. 口唇裂・口蓋裂症例の永久歯の先天性欠如に関する臨床統計学的検討. 第68回日本矯正歯科学会、福岡、平成21年11月16-18日
9. 服部架、鳥居千春、須田直人、小崎健次郎、森山啓司. COBRA-DHPLC法によるラッセルシルバー症候群の遺伝子診断システムの開発. 第68回日本矯正歯科学会、福岡、平成21年11月16-18日
10. 鈴木一史、辻美千子、大隈瑞恵、岡本奈那、武智香織、疋田理奈、福岡裕樹、馬場祥行、森山啓司. 外胚葉異形成症患者の顎顔面領域における形態的特徴. 第68回日本矯正歯科学会、福岡、平成21年11月16-18日.
11. 中澤佑紀、馬場祥行、福岡裕樹、松本力、須田直人、森山啓司. 先天性多数歯欠損症患者における永久歯の形成異常に関する報告. 第68回日本矯正歯科学会、福岡、平成21年11月16-18日
12. 茂木和久、福岡裕樹、小川卓也、阿彦希、岡村絵里花、中山友美子、馬場祥行、森山啓司. 先天性多数歯欠損症患者の顎顔面形態に関する頭部X線規格写真を用いた検討. 第68回日本矯正歯科学会、福岡、平成21年11月16-18日
13. 辻美千子、馬場祥行、鈴木聖一、森山啓司. 新規創内型上顎骨延長器を用いて咬合および顔貌の改善をはかった両側性口唇口蓋裂の1症例. 第68回日本矯正歯科学会、福岡、平成21年11月16-18日
14. 三戸天元、春山直人、五十嵐薫. 筋ジストロフィーマウスにおける筋機能活性化が下顎骨の成長に与える影響. 第68回日本矯正歯科学会、福岡、平成21年11月16-18日
15. 本田綾、馬場祥行、山田大輔、鈴木聖一、大林尚人、倉林亨、森山啓司. Le Fort I型上顎骨延長法を適用した口唇口蓋裂症例の軟組織変化に対するCT画像を用いた三次元的検討. 第19回日本シミュレーション外科学会、東京、平成21年10月31日
16. 佐藤光一郎、春山直人、清水良央、原純一、川村仁. 骨-骨膜延長による骨誘導に対する骨髄由来間葉系幹細胞の有効性の検討. 第54回社団法人日本口腔外科学会総会・学術大会、札幌、平成21年10月9-11日
17. 岡本那奈、林深、黒澤健司、水野誠司、蒔田芳男、羽田明、井本逸勢、森山啓司、稲澤譲治. 新規症候群の可能性のある10q24微細欠失を伴う2症例の報告. 第54回日本人類遺伝学会、品川、平成21年9月23-26日
18. 鈴木尋之、須田直人、志賀百年、井関祥子、森山啓司. Apert 症候群型変異FGFR2とその可溶性変異体を過剰発現するトランスジェニックマウス頭蓋冠由来骨芽細胞の解析. 第51回歯科基礎医学会学術大会、新潟、平成21年9月9-11日
19. 辻美千子、森山啓司. Turner 症候群の遺伝カウンセリング時に提供できる歯科領域からの情報. 第33回日本遺伝カウンセリング学会学術集会、兵庫、平成21年7月24-26日
20. 鈴木尋之、須田直人、志賀百年、中村正孝、井関祥子、森山啓司. Apert 症候群型変異FGFR2とその可溶性変異体を過剰発現するトランスジェニックマウス由来骨芽細胞の分化形質. 第27回日本骨代謝学会、大阪、平成21年7月23-25日
21. 佐藤麻緒、川元龍夫、井口隆人、八木優子、小村健、天願俊泉、砂川元、森山啓司. 外科的矯正治療を行った統合失調症を伴う顎変形症の2症例について. 第68回東京矯正歯科学会、東京、平成21年7月16日
22. 岡村絵里花、阿彦希、福岡裕樹、辻美千子、馬場祥行、森山啓司. EEC 症候群の顎顔面領域に関する歯科の検討. 第49回日本先天異常学会、鹿児島、平成21年6月25-27日.
23. 中山 友美子、鈴木一史、中澤佑紀、茂木和久、福岡裕樹、辻美千子、馬場祥行、森山啓司. 外胚葉異形成症の顎顔面領域に関する歯科の検討. 第49回日本先天異常学会、鹿児島、平成21年6月25-27日
24. 佐藤繁久、土谷昌広、小牧健一郎、楠慎一郎、土谷忍、春山直人、高橋一郎、笹野泰之、渡辺誠. 象牙芽細

胞分化過程におけるI型コラーゲンの合成および細胞内輸送に関する検討. 第118回社団法人日本補綴歯科学会学術大会、京都、平成21年6月5-8日

25. 福岡裕樹、辻美千子、出井彩乃、本田彩、岡本奈那、森山啓司. RED systemで前下方へ上顎骨延長を行ったoverclosureを呈する成人口唇口蓋裂3症例. 第19回日本顎変形症学会総会、仙台、平成21年6月4-5日
26. 鈴木剛史、福岡裕樹、青木朝里、北村良平、富永直子、川元龍夫、森山啓司. 下顎枝矢状分割法を用いた外科的矯正治療を行った下顎後退症例の術後安定性について. 第19回日本顎変形症学会総会、仙台、平成21年6月4-5日
27. 北村良平、鈴木剛史、富永直子、青木朝里、福岡裕樹、川元龍夫、森山啓司. 馬蹄形骨切り術を施行した下顎前突症例の顎態変化に関する検討. 第19回日本顎変形症学会総会、仙台、平成21年6月4-5日
28. 本田綾、馬場祥行、片岡恵一、鈴木聖一、大林尚人、倉林亨、森山啓司. Le Fort I型上顎骨延長法を適用した口唇口蓋裂症例の軟組織変化に対するCT画像を用いた三次元的検討. 第33回日本口蓋裂学会総会、東京、平成21年5月28-29日
29. 井口隆人、川元龍夫、青木朝里、長濱浩平、馬場祥行、鈴木聖一、森山啓司. 歯槽骨延長部への歯の移動に高気圧酸素が与える影響. 第33回日本口蓋裂学会総会、東京、平成21年5月28-29日
30. 片岡恵一、馬場祥行、森田圭一、小村健、鈴木聖一、森山啓司. Le Fort I型骨切り術によるセグメントの前方移動を行い顎裂閉鎖した口唇口蓋裂症例. 第33回日本口蓋裂学会総会、東京、平成21年5月28-29日
31. 飯田敏朗、星合泰治、初野有人、辻美千子、馬場祥行、鈴木聖一、森山啓司、谷口尚. モード解析による骨成熟過程の評価の試み. Assessment of bone maturity using modal analysis after orthognathic surgery. 第33回日本口蓋裂学会総会、東京、平成21年5月28-29日
32. 森田圭一、辻美千子、今泉史子、森田綾子、森山啓司、小村健. 新規創内固定型上顎仮骨延長装置の使用経験. 第33回日本口蓋裂学会総会・学術集会、東京、平成21年5月28-29日

12) 受賞

1. 湊亜紀子、小野卓史、宮本順、菅田栄一、倉林亨、森山啓司. 舌感覚の皮質投影パターンにおける習慣性咀嚼の関与. 第68回日本矯正歯科学会・優秀発表賞、

福岡、平成21年11月16-18日

2. 服部架、鳥居千春、須田直人、小崎健次郎、森山啓司. COBRA-DHPLC法によるラッセルシルバー症候群の遺伝子診断システムの開発. 第68回日本矯正歯科学会・優秀発表賞、福岡、平成21年11月16-18日
3. 疋田理奈、川元龍夫、佐藤麻緒、茂木和久、井口隆人、八木優子、豊福明、森山啓司. 精神的問題が疑われ矯正歯科治療において対応に苦慮した3症例. 第68回日本矯正歯科学会・優秀発表賞、福岡、平成21年11月16-18日
4. 鎌田秀樹、鈴木聖一、塙隆夫、森山啓司. コラーゲン電着固定化Tiの創製と耐久性評価. 第68回日本矯正歯科学会・優秀発表賞、福岡、平成21年11月16-18日
5. 鈴木尋之、須田直人、志賀百年、中村正孝、井関祥子、森山啓司. Apert 症候群型変異FGFR2とその可溶性変異体を過剰発現するトランスジェニックマウス由来骨芽細胞の分化形質. 第27回日本骨代謝学会・優秀ポスター演題賞、大阪、平成21年7月23-25日
6. 片岡恵一. 超音波画像を用いた片側性口唇裂・口蓋裂症例に対する上顎骨延長術後の骨形成の評価. 日本顎変形症学会総会・平成20年度学会賞、仙台、平成21年6月5日
7. 井口隆人、川元龍夫、青木朝里、長濱浩平、馬場祥行、鈴木聖一、森山啓司. 歯槽骨延長部への歯の移動に高気圧酸素が与える影響. 第33回日本口蓋裂学会総会・優秀ポスター賞、東京、2009年5月28-29日
8. Takahashi Y, Suda N, Yamakoshi Y, Baba O, Moriyama K. Amelogenin is a potent inhibitor of odontoclastic root resorption. International Association for Dental Research/ Unilever Travel Award. International Association for Dental Research, 88th General Session & Exhibition of the International Association for Dental Research, Miami, April 1-4, 2009

13) 外部資金の獲得状況

1. 科学研究費補助金 萌芽 研究題目:コラーゲン電着固定化によるチタンの組織適合性向上 代表:森山啓司 期間:平成21年-平成22年 研究費総額:3,000千円
2. 独立行政法人日本学術振興会 科学研究費補助金 (特別研究員奨励費):口唇口蓋裂患者の発話時における脳活動と構音器官運動相関 研究代表者 森山啓司 研究分担者 Inoue MS 期間:平成19年-平成21年

- 研究費総額:2,300千円
3. 科学研究費補助金 基盤C 研究題目:骨延長統合モニタリングシステムの開発 代表:鈴木聖一 期間:平成21年-平成23年 研究費総額:3,700千円
 4. 科学研究費補助金 基盤B 研究題目:口唇口蓋裂をモデルとした音声言語の生成、障害および可塑性のメカニズムの解明 代表:小野卓史 期間:平成20年-平成23年 研究費総額:14,700千円
 5. 科学研究費補助金 萌芽 研究題目:ニューロイメージング法を用いた咬合と全身機能の脳神経生理学的解析 代表:小野卓史 期間:20年-平成22年 研究費総額:3,200千円
 6. 科学研究費補助金 基盤B(海外学術) 研究題目:アジアにおける先天性多数歯欠損に関する遺伝学的調査 代表:須田直人 期間:平成19年-平成22年 研究費総額:12,900千円
 7. 科学研究費補助金 基盤B 研究題目:ヒトiPS細胞を用いた歯根再生への画期的アプローチ 代表:須田直人 期間:平成21年-平成23年 研究費総額:14,100千円
 8. 科学研究費補助金 基盤C 研究題目:張力センサを用いた骨延長術時の牽引力の解析 代表:馬場祥行 期間:平成20年-平成22年 研究費総額:3,600千円
 9. 科学研究費補助金 基盤C 研究題目:上顎歯槽部骨延長への歯の移動と移植に高気圧酸素療法が与える影響 代表:川元龍夫 期間:平成21年-平成23年 研究費総額:3,500千円
 10. 科学研究費補助金 若手B 研究題目:先天性多数歯欠損の家系における変異と表現系に関する研究 代表:小川卓也 期間:平成20年-平成21年 研究費総額:3,200千円
 11. 科学研究費補助金 若手B 研究題目:頭蓋顎顔面の形成における転写因子TWIST1の役割に関する研究 代表:大隈瑞恵 期間:平成20年-平成21年 研究費総額:3,200千円
 12. 独立行政法人日本学術振興会 科学研究費補助金(特別研究員奨励費) 研究題目:非侵襲的脳機能画像法を用いた咀嚼運動時のヒト脳機能の解明 代表:宮本順 期間:平成20年-平成22年 研究費総額:2,400千円
 13. 科学研究費補助金 若手研究スタートアップ 研究題目:超小型圧力センサを用いた顔面非対称症例の治療前後における口腔圧の変化の解析 代表:高田潤一 期間:平成20年-平成21年 研究費総額:2,420千円
 14. 文部科学省科学研究費補助金 若手研究スタートアップ 研究題目:片側性臼歯部反対咬合を有する骨格性下顎前突症患者の下顎蝶番運動回転軸に関する研究 代表:横田俊明 期間:平成20年-平成21年 研究費総額:2,000千円
 15. 文部科学省科学研究費補助金 若手研究スタートアップ 研究題目:ヒト吸収歯根にセメント芽細胞を移入し歯根再生を試みる基礎研究 代表:高橋優子 期間:平成20年-平成21年 研究費総額:2,540千円

14) 特別講演、招待講演

1. Takashi Ono: Neuro-orthodontics: an intersection of orthodontics with applied neurophysiology. Symposium "Basic Science – Physiology", 7th International Orthodontic Congress, Feb 6-9, 2010, Sydney
2. Takashi Ono: Control mechanisms of tongue posture. 36th Annual International Conference on Craniofacial Research ("Presymposium"), Feb 26, 2010, University of Michigan
3. Keiji Moriyama: Differential Diagnosis and Treatment for Class III malocclusion 7^o Congresso da Associação Brasileira Ortodontia e Ortopedia Facial (ABOR), October 11, 2009, Brasilia, Brazil
4. Keiji Moriyama: Special Lecture -Some Considerations in the Treatment of Cleft Lip/Palate Patients. Hospital De Reabilitação De Anomalias Craniofaciais Da Universidade de São Paulo, October 9, 2009, Bauru, Brazil
5. Keiji Moriyama: Symposium Orthognathic surgery, Surgical Orthodontic Treatment for Cleft Lip/Palate Patients. 11th International Congress on Cleft Lip and Palate and Related Craniofacial Anomalies, September 11, 2009, Fortaleza, Brazil
6. Takashi Ono: An application of MRI technology to analyze speech-related central/peripheral function in cleft lip/palate. Symposium "Imaging and new technology in CLP", 11th International Congress on Cleft Lip and Palate and Related Craniofacial Anomalies, Sept 10-13, 2009, Fortaleza/Brazil
7. Yoshiyuki Baba: Distraction Osteogenesis in the Treatment of Cleft Lip and Palate. 3th Annual Meeting of Korean CLPA, June 14, 2009, Seoul
8. Keiji Moriyama: Symposium; Molecular Mechanisms of Craniofacial Development and Craniosynostosis.

- Characterization of the Osteoblast Phenotype in Apert Syndrome. IADR/AADR/CADR 87th General Session and Exhibition, April 1, 2009, Miami Florida, U.S.A.
- 9. Keiji Morioyama: Function and regulation of osteopontin during orthodontic tooth movement. 2009 The Angle Society East Component Meeting, March 29, 2009, Newport, Rhode Island, U.S.A.
- 10. 森山啓司:口蓋裂患者に対する上顎骨延長法を用いた外科的矯正治療. 神戸大学大学院医科学研究科大学院特別講義 平成21年12月18日 神戸
- 11. 須田直人: 歯根膜弾性線維の新規機能に関する考察 - 遺伝性疾患の歯科的問題点から - 北海道大学大学院歯学研究セミナー 2009年12月2日 札幌
- 12. 川元龍夫:垂直的咬合異常に対する外科的矯正治療の予後について. 第68回日本矯正歯科学会 平成21年11月17日 福岡
- 13. 須田直人: 歯数異常に関する遺伝子型とその表現型の多様性. 第2回 顎顔面の器官発生・形態形成研究会 平成21年10月17-18日 軽井沢
- 14. 春山直人: DSPPの象牙質石灰化における役割〜マウスモデルの表現型解析から〜 第2回 顎顔面の器官発生・形態形成研究会 平成21年10月17-18日 軽井沢
- 15. 森山啓司:シンポジウム 歯科医療の安全・安心をどのように考えるか:とくにインプラント治療に関して - 矯正用インプラントアンカーの安全・安心使用に向けた日本矯正歯科学会の取り組み. 第39回(社)日本口腔インプラント学会学術大会 平成21年9月25-27日 大阪
- 16. 辻美千子:日本家族計画協会 遺伝カウンセリングセミナー(第37回実践コース) 多因子遺伝. 平成21年8月27日 東京
- 17. 辻美千子:BWS親の会.ベックウィズ症候群のかみ合わせについて. 平成21年8月2日 東京
- 18. 森山啓司、小長谷光、笛木賢治、和達礼子:PHMI (Partner Harvard Medical Institute) リーダーシップコースに参加して - ハーバード大学における医学・歯学教育の視察と教育改革研修について. 口腔病学会6月例会 平成21年7月2日 東京
- 19. 辻美千子:東京医科歯科大学分子細胞遺伝分野教室セミナー. 歯に異常がある先天異常疾患について. 平成21年6月17日 東京
- 20. 森山啓司、白土 雄司:シンポジウム 特定非営利法

人日本顎変形症学会のこれからを考える - 日本顎変形症学会認定医制度の検討について、第19回日本顎変形症学会総会 平成21年6月5日 仙台

- 21. 鈴木聖一:シンポジウム 当分野における骨格性不正咬合患者に対する治療のアプローチ. 第19回日本顎変形症学会総会 平成21年6月4日 仙台
- 22. 片岡恵一:超音波画像を用いた片側性口唇裂・口蓋裂症例に対する上顎骨延長術後の骨形成の評価. 第19回日本顎変形症学会総会・平成20年度学会賞受賞講演 平成21年6月5日 仙台
- 23. 春山直人: エナメル質および象牙質細胞外基質タンパクのシグナル分子としての生物学的機能の解析 第25回 グローバルCOE総合プレゼンテーション 平成21年5月25日 東京
- 24. 辻美千子:日本家族計画協会 第33回遺伝カウンセリングリフレッシュセミナー. 口唇裂・口蓋裂の遺伝カウンセリング 平成21年1月10-11日 大阪

15) 第25回GCOE総合プレゼンテーション サマリー

エナメル質および象牙質細胞外基質タンパクのシグナル分子としての生物学的機能の解析

Functional analysis of extra cellular matrix proteins as signaling molecules predominantly expressed in tooth enamel and dentin.

春山直人

歯の発生段階において、上皮系細胞由来のエナメル芽細胞と間葉系細胞由来の象牙芽細胞からは、それぞれユニークな基質タンパクが分泌されている。近年のノックアウトマウスの表現型解析から、エナメル芽細胞から分泌される代表的な基質タンパクであるアメロジェニン、ハイドロキシアパタイトの結晶の長さを制御し、エナメル質の厚みに影響を及ぼすことがわかった。また、非コラーゲン性象牙質基質タンパクのDSPPは、象牙質の石灰化度と象牙前質の厚みを制御していることがわかった。これら、アメロジェニンとDSPPは、実は他組織においても少量の発現がみられ、最近特に骨組織においては基質タンパクとしての役割ではなくシグナル伝達の機能を担っている可能性が示唆されている。これらのタンパク質の新たな生物学的機能について、最近の我々のグループの結果を交え、歯と骨という2つの組織におけるこれらのタンパクの持つユニークな側面を紹介する。

16) 教室、分野や講座の准教授、講師、助教、特別研究員、ポスドク、指導を受けた大学院生の名前(AISSには○印)のリスト

准 教 授 :鈴木聖一

講 師 :小野卓史、須田直人

助 教 :馬場祥行、川元龍夫、辻美千子、
小川卓也

特別研究員 :宮本順、
井上マリステラ小百合 (学術振興会)

大 学 院 :井口隆人 (3月まで)、
服部架 (3月まで)、
湊亜紀子 (3月まで)、
シント・ウィラハディ・クスマ (3月まで)、
○ガンブルゲド・ガンジャルガル、
鎌田英樹、
○鈴木尋之、ウン・イン・ウー、
岡本奈那、○武智香織、正田理奈、
松本力、伊藤洋介 (4月から)、
菅野直美 (4月から)、
森田淳平 (4月から)、
保田裕子 (4月から)、
渡辺千穂 (4月から)

17) GCOE 活動についての感想、コメント、改善を望む点など

本年度は、昨年度に整備したGCOE事業推進者との研究体制をさらに強化することができた。各研究分野でトップを走る他の事業推進者と連携して研究を進めていくことができる環境は、いち早く最先端の情報を得られることで、今後の研究の展開に大変有意義であると思われた。

Marfan Syndrome and Its Disorder in Periodontal Tissues

NAOTO SUDA*, MOMOTOSHI SHIGA, GANJARGAL GANBURGED, AND KEIJI MORIYAMA

Maxillofacial Orthognathics, Department of Maxillofacial Reconstruction and Function, Division of Maxillofacial/Neck Reconstruction, Graduate School, Tokyo Medical and Dental University, Tokyo, Japan

ABSTRACT Elastic system fibers are composed of two distinct elements, elastin, which is an amorphous component crosslinked in the core, and microfibril, localized in the periphery of elastin. As microfibrillar proteins, fibrillins, microfibril-associated glycoproteins (MAGPs), latent TGF- β -binding proteins (LTBPs), microfibril-associated proteins (MFAPs), and fibulins are known. Fibrillin-1 is a major microfibrillar protein and characterized by calcium binding EGF-like (cbEGF) domain. Association between fibrillin-1 and TGF- β is a recent topic of this field and this interaction is known to inactivate and target TGF- β action. *FBN1* encoding fibrillin-1 is a responsible gene for Marfan syndrome type 1 (MIM #154700), characterized by increased height and long limbs, ectopia lentis, and cardiovascular disorders, such as mitral valve prolapse and aortic dilation and regurgitation. Animal models suggest that the abnormal TGF- β signaling is underlying as the pathogenesis of these conditions. Besides skeletal, ocular and cardiovascular conditions, severe periodontitis is frequently seen in affected patients. To clarify the unknown function of elastic system fibers in the periodontal ligament (PDL), PDL-cells were isolated from a Marfan syndrome type 1 patient who was with the severe periodontitis and had a mutation in one of the cbEGF domain of fibrillin-1. These results suggested that wild-type fibrillin-1 was required for the normal cell alignment and tissue architecture of PDLs. Evidences are now accumulated to suggest that fibrillin-1 is one of the molecule involved in the interaction between cell and extracellular matrix. *J. Exp. Zool. (Mol. Dev. Evol.)* 312B:503–509, 2009. © 2009 Wiley-Liss, Inc.

How to cite this article: Suda N, Shiga M, Ganburged G, Moriyama K. 2009. Marfan syndrome and its disorder in periodontal tissues. *J. Exp. Zool. (Mol. Dev. Evol.)* 312B:503–509.

BIOLOGY OF ELASTIC SYSTEM FIBERS

There is a complexity of the word usage of “elastic fibers.” “Elastic fiber” is used for entire elastic fibers in a broad sense and this is also used for one type of elastic fibers that contains a high proportion of elastin. Thus, in this review, the former is represented as “elastic system fibers” and the latter “elastic fiber.” The elastic system fibers are the major insoluble extracellular matrices (ECM) in various structures, e.g., artery, ligament, lung, and dermis that require elasticity and stiffness (Rosenbloom et al., '93; Kielty et al., 2002).

Elastic system fibers are composed of two distinct elements, elastin, which is an amorphous component crosslinked in the core, and microfibril, which is localized in the periphery of elastin

and serve as a scaffold (Mecham and Davies, '94) (Fig. 1A). In the process of elastic fiber assembly, elastin precursor, tropoelastin, is deposited on microfibrils and crosslinked by lysyl oxidase (LOX enzymes) to form mature elastin (Rosenbloom et al., '93). Depending on the relative proportions and morphological arrangement of elastin and microfibril, three types of elastic system fibers, elastic, elaunin, and oxytalan fibers, are classified.

Grant sponsor: Ministry of Education, Culture, Sports, Science, and Technology of Japan; Grant numbers: 16390604; 16659570; 18390552.

*Correspondence to: Naoto Suda, Maxillofacial Orthognathics, Department of Maxillofacial Reconstruction and Function, Division of Maxillofacial/Neck Reconstruction, Graduate School, Tokyo Medical and Dental University, 1-5-45 Yushima, Bunkyo-ku, Tokyo 113-8510, Japan. E-mail: n-suda.mort@tmd.ac.jp

Received 30 November 2008; Accepted 8 December 2008
Published online 6 February 2009 in Wiley InterScience (www.interscience.wiley.com). DOI: 10.1002/jez.b.21278

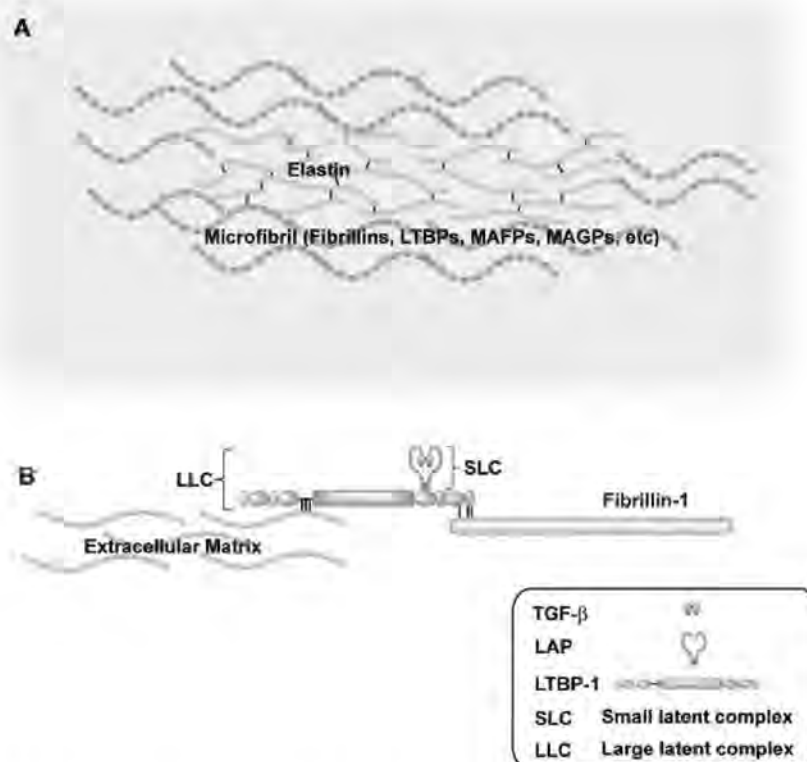


Fig. 1. Structure of elastic system fibers and complex formation of microfibrillar proteins. Structure of elastic system fibers (A). Each elastin crosslinks on the microfibrils serving as the scaffold for elastins. TGF- β and microfibrillar proteins form a complex in the elastic system fiber (B). LAP, latency-associated propeptide; LTBP, latent TGF- β -binding protein; MAGP, microfibril-associated glycoprotein.

Elastic fibers contain a large amount of elastin and oxytalan fibers are bundles of elastin-free microfibrils. Elaunin fibers only contain relatively small elastin.

Recently, numerous microfibrillar molecules are reported, e.g., fibrillins (Pereira et al., '93; Zhang et al., '94), microfibril-associated glycoproteins (MAGPs) (Brown-Augsburger et al., '96), latent TGF- β -binding proteins (LTBPs) (Gibson et al., '95), microfibril-associated proteins (MFAPs) (Liu et al., '97), fibulins (Nakamura et al., 2002; Yanagisawa et al., 2002), decorin, emilins, versican (Isogai et al., 2002), vitronectin (Dahlbäck et al., '90) and type VI, VIII and XVI collagens (Finnis and Gibson, '97). Among them, fibrillin-1 and -2 are 350 kDa proteins and major structural components (Carta et al., 2006). The structure of these two molecules is characterized by calcium binding EGF-like (cbEGF) domain (Downing et al., '96). Fibulin-5 (also called DANCE) is localized in the

interface of elastin and microfibril, and promote alignment and crosslink of elastins on microfibrils (Hirai et al., 2007). MAGP-1 is thought as an integral microfibril molecule important for structural integrity.

INTERACTION OF MICROFIBRILLAR PROTEIN

Interactions between microfibrillar molecules are the recent topic of this field. Especially, accumulating evidences highlight the regulation of TGF- β signaling by these molecules (Chaudhry et al., 2007). TGF- β s are the multifunctional growth factors that can induce series of cellular events including matrix synthesis and deposition, cell differentiation and proliferation, cell cycle arrest, and apoptosis (Miyazono et al., '91). TGF- β s are secreted from cells as a dimeric small complex comprising latency-associated propeptide

(LAP) (Annes et al., 2003), and the dimers of TGF- β and LAP form a tight complex, small latent complex (SLC) (Fig. 1B). Linkages are formed between cysteine residues of LAP and LTBP-1, to form a large complex termed large latent complex (LLC). LTBP-1 is structurally related to fibrillins and belong to the LTBP/fibrillin protein family with fibrillin-1, -2, -3 and LTBP-1, -2, -3, -4 (Todorovic et al., 2005). LTBP-1 but not LTBP-3 can bind to fibrillin-1 (Isogai et al., 2003). It is known that the formation of complex has dual roles, (i) inactivating and controlling TGF- β activity in the matrix, (ii) targeting and concentrating TGF- β in a specific site to facilitate temporal and spatial control (Karttunen and Warburton, 2003).

PATHOGENESIS OF MARFAN SYNDROME

FBN1 encoding fibrillin-1 is the responsible gene for Marfan syndrome type 1 (MIM #154700) (Dietz et al., '91; Maslen et al., '91). This genetic disorder is characterized by increased height, disproportionately long limbs and digits, and anterior chest deformity. Myopia and ectopia lentis are ocular findings. Mitral valve prolapse, mitral regurgitation, dilatation of the aortic root, and aortic regurgitation are cardiovascular features. The pathogenesis of Marfan syndrome type 1 has been explained by the mutated fibrillin-1 molecule which is unable to supply enough tissue elasticity. Since fibrillin-1 forms a large complex

with TGF- β and inactivates its activity in the matrix as shown in Figure 1B, it is recently proposed that mutated fibrillin-1 is susceptible to proteolysis and results in the excess activation of TGF- β signaling in this disorder (Chaudhry et al., 2007; Ramirez et al., 2007) (Fig. 2A). Using mice with a missense mutation of *FBN1* (C1039G) that eliminates one of the cysteine residues of cbEGF domain, antagonism of TGF- β signal has been shown to prevent histological sign of aneurysm progression (Habashi et al., 2006). Moreover, families with heterozygous gain-of-function mutation in both type I and II TGF- β receptors, in which phosphorylation of Smad2 and expression of collagen and connective tissue growth factors are increased, show aortic root aneurysm (Loeys et al., 2005) (Fig. 2B). These studies support that abnormal TGF- β signaling underlies as the pathogenesis of Marfan syndrome (Judge et al., 2004; Mizuguchi et al., 2004; Habashi et al., 2006).

However, it is still under the debate that either activation or inactivation of TGF- β signaling accounts for the pathogenesis. A second type of Marfan syndrome (Marfan syndrome type 2, MIM #154705) has overlapping phenotype as type 1 but does not have any mutation in *FBN1*. *TGFBR2* encoding type II TGF- β receptor has been identified as the responsible gene for this disorder (Mizuguchi et al., 2004). Unexpectedly, the identified gene mutations of *TGFBR2* (L308P, S449F, R537C), all showed the loss-of-function type of mutations. To clear up this

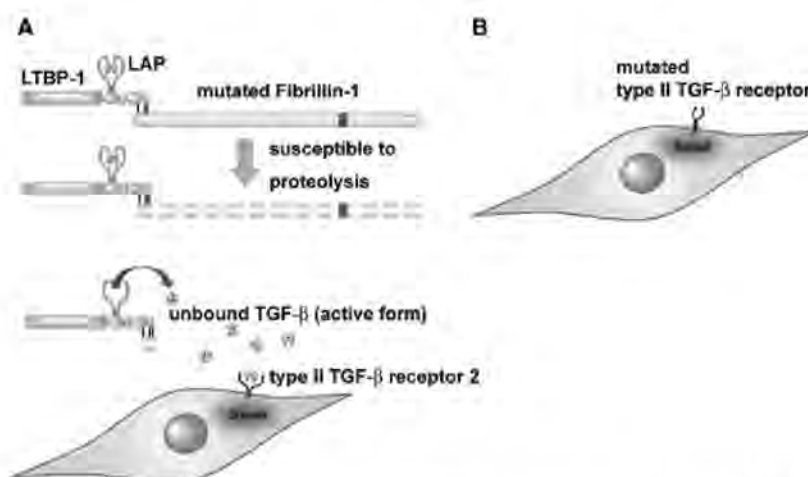


Fig. 2. Pathogenesis for Marfan syndrome type 1 and 2. In Marfan syndrome type 1, mutated fibrillin-1 is susceptible to proteolysis and prone to activate TGF- β signaling (A). Mutation in the gene encoding type II TGF- β receptor (*TGFBR2*) is responsible for Marfan syndrome type 2 (B).

controversy the complex processes of TGF- β secretion, localization, activation, and signaling, together with the consideration of compensatory events under the altered TGF- β expression, have to be examined further.

MARFAN SYNDROME AND ITS DISORDER IN PERIODONTAL TISSUES

Periodontal tissues consists of cementum, periodontal ligament (PDL), alveolar bone and gingiva (Nanci, 2007). The PDL is a characteristic and specialized connective tissue that locates between the socket of alveolar bone and cementum covering the root of teeth. PDLs are composed of fibers and various kinds of cells, e.g., fibroblasts, epithelial cell remnants of Malassez, macrophages, undifferentiated mesenchymal cells, cementoblasts, osteoblasts, and osteoclasts (Nanci, 2007). Besides collagen fibers, elastic system fibers are also seen in PDLs. It is known that the majority of elastic system fibers in PDLs are elastin-free oxytalan fibers and those in gingiva are elaunin fibers. This was also shown by in vitro studies that cultured gingival fibroblasts expressed both microfibrils and elastin (Tsuruga et al., 2002a), and PDL-cells only expressed microfibrils, fibrillin-1 and fibrillin-2 (Tsuruga et al., 2002b). The immunolocalization of elastin and fibrillins in the rat PDL is reported (Sawada et al., 2006). It is shown that a small amount of elastin is localized in the apical region of the PDL. Fibrillins are the major elastic system fibers and widely distributed throughout the ligament. Fibulin-5/DANCE, which is known to promote crosslink of elastins (Hirai et al., 2007), is lacked in PDLs but is expressed in cultured gingival cells (Tsuruga et al., 2004).

In general, elastin-free oxytalan fibers are known to function for tissue stiffness and stabilization of blood vessels, but not for elasticity (Beertsen et al., '74; Kielty et al., 2002; Tashiro et al., 2002). In PDLs, elastin-free microfibrils are also seen close to blood vessels (Sawada et al., 2006). However, the exact function is still obscure and has been long awaited in this field.

In Marfan syndrome, in addition to skeletal, ocular, and cardiovascular systems, patients also exhibit characteristic oral features including maxillary protrusion, high palate, narrowed arch, crowding of teeth, and fragility of the temporomandibular joint (Westling et al., '98; Bauss et al., 2004). Periodontitis is a chronic inflammation of gingiva, PDL, and alveolar bone, and

known as a major cause for tooth loss. It is reported that the severe periodontitis is frequently associated with Marfan syndrome (De Coster et al., 2002; Straub et al., 2002; Shiga et al., 2008). In contrast to the periodontitis, the prevalence of dental caries is not higher in affected patients (De Coster et al., 2002). These studies suggest that the genetic disorder causes structural and cellular defects of the periodontal tissues susceptible to the severe periodontitis in Marfan syndrome.

In order to clarify the unknown function of elastic system fibers in PDLs, PDL-cells were isolated from a type 1 patient with severe periodontitis (Shiga et al., 2008). A heterozygous mutation of *FBN1* seen in this patient, resulted in the replacement of Asn by Ser at the amino acid position 2144 (N2144S) in the 32nd cbEGF domain. N2144S in fibrillin-1 is predicted to alter one of the key calcium-binding residue ligands within the 32nd cbEGF domain (Kettle et al., '99). This mutation is reported to increase the flexibility in the peptide backbone (Yuan et al., 2002).

Immortalized PDL-cells from a patient with N2144S (M-HPL1) and from a healthy volunteer (HPDL2) showed the same growth rate, in vitro. Both the cells expressed various PDL-related molecules, e.g., asporin, periostin, type I and XII, osteocalcin, bone sialoprotein. All these are characteristics of cultured PDL-cells (Cho et al., '92; Giannopoulou and Cimasoni, '96; Nohutcu et al., '97; Chien et al., '99).

Ectopic tissue formation by M-HPL1 and HPDL2 in the subcutaneous tissues of SCID mice was examined by implanting these cells for 4 weeks (Fig. 3). In bone and tooth, more than half of the inorganic components are known to be incorporated in hydroxyapatite (Freeman, '98). To examine how M-HPL1 and HPDL2 behave around inorganic components of tooth and bone, M-HPL1 and HPDL2 were implanted with hydroxyapatite particles in SCID mice. When transplanted tissues were immunostained with the anti-human fibrillin-1 antibody, the elaborate network of immunoreactive fibrillin-1 is formed by HPDL2 (Fig. 3A). In contrast, impaired microfibril-assembly was seen by M-PDL1 (Fig. 3B). When stained by the human-vimentin antibody, HPDL2 aligned in an organized manner between the particles (Fig. 3D), but most M-PDL1 attached to the particles and aligned irregularly (Fig. 3E). It was noted that there was also lack or impairment of the microfibril-assembly in areas adjacent to the hydroxyapatite particles, where many M-HPL1 localized

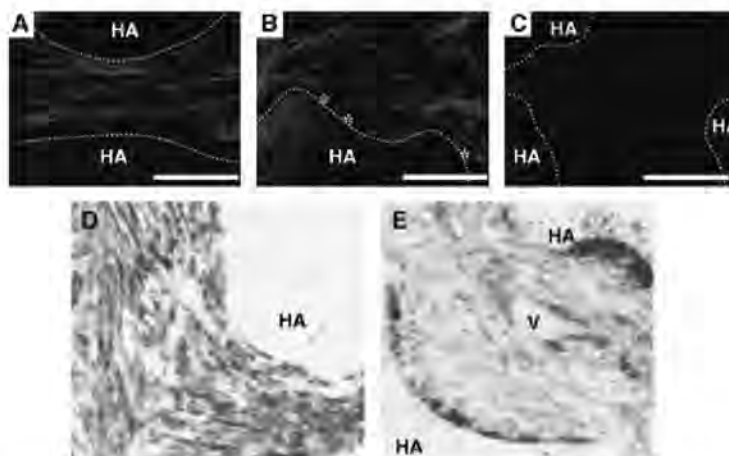


Fig. 3. Fiber formation and cell alignment of PDL-cells isolated from a Marfan syndrome patient (M-HPL1) and a healthy volunteer (HPDL2) in SCID mice. Tissues were immunostained with anti-human fibrillin-1 antibody (A–C). Sections of HPDL2 (A), M-HPL1 (B), and without implanting human cells (C). M-HPL1 induced the disorganized microfibril-assembly, which was not seen in sections of HPDL2. The mouse tissue without implanting human cells was not immunoreactive to the used antibody (C). Dotted line, interface of hydroxyapatite particles. Scale bar, 50 μ m. Sections were immunostained with anti-vimentin antibody, which recognizes only human but not mouse cells (D, E). Sections of HPDL2 (D) and M-HPL1 (E). Compared with HPDL2, M-HPL1 were mainly located around hydroxyapatite particles and aligned irregularly. Note that the microfibril-assembly was also lacked or impaired in areas adjacent to the hydroxyapatite particles (indicated by asterisks in B) where many M-HPL1 localized. HA, hydroxyapatite particles. V, blood vessel.

(Fig. 3B and 3E). The exact cell numbers of HPDL2 and M-HPL1 at the end of implantation were not known. However, the same numbers of cells were implanted and the growth of two cells did not differ, in vitro. Thus, the interaction between cells and ECM have determined the cell behaviour and fate of the implanted tissues. Interestingly, vimentin-positive M-HPL1 cells migrated around the blood vessel (Fig. 3E). Factor(s) from blood vessels might induce the migration of M-HPL1. The disorganized cell alignment was also seen in PDLs of fibrillin-1 hypomorphic mice (MgR/MgR) (Pereira et al., '99, Ganburged et al., manuscript in preparation). These observations suggest that the wild-type fibrillin-1 is essential for the normal cell alignment and tissue architecture of PDLs. This notion is supported by the studies, that mutant mice with C1039G showed architectural alternations in the mitral valves (Ng et al., 2004), and that *Fbn1* null mutant mice showed abnormal vessel development and the disorganized medial layer (Carta et al., 2006).

ECM and cells have important interactions that can determine the phenotype and behavior of cells during various tissue development. Evidences are now accumulated to suggest that fibrillin-1 is one of ECM fulfilling this interaction.

LITERATURE CITED

- Annes JP, Munger JS, Rifkin DB. 2003. Making sense of latent TGF beta activation. *J Cell Sci* 116:217–224.
- Baass O, Sadat-Khonsari R, Fenske C, Engelke W, Schweska-Polly R. 2004. Temporomandibular joint dysfunction in Marfan syndrome. *Oral Surg Oral Med Oral Pathol Oral Radiol Endod* 97:592–598.
- Beertsen W, Everts V, van den Hooff A. 1974. Fine structure of fibroblasts in the periodontal ligament of the rat incisor and their possible role in tooth eruption. *Arch Oral Biol* 19:1087–1098.
- Brown-Augsburger P, Broekelmann T, Rosenbloom J, Mecham RP. 1996. Functional domains on elastin and microfibril-associated glycoprotein involved in elastic fibre assembly. *Biochem J* 318:149–155.
- Carta L, Pereira L, Arteaga-Solis E, Lee-Arteaga SY, Lenart B, Starcher B, Merkel CA, Sukoyan M, Kerkis A, Hazeki N, Keene DR, Sakai LY, Ramirez F. 2006. Fibrillins 1 and 2 perform partially overlapping functions during aortic development. *J Biol Chem* 281:8016–8023.
- Chaudhry SS, Cain SA, Morgan A, Dallas SL, Shuttleworth CA, Kielty CM. 2007. Fibrillin-1 regulates the bioavailability of TGFbeta1. *J Cell Biol* 176:355–367.
- Chien HH, Lin WL, Cho MI. 1999. Interleukin-1beta-induced release of matrix proteins into culture media causes inhibition of mineralization of nodules formed by periodontal ligament cells in vitro. *Calcif Tissue Int* 64:402–413.
- Cho MI, Matsuda N, Lin WL, Moshier A, Ramakrishnan PR. 1992. In vitro formation of mineralized nodules by periodontal ligament cells from the rat. *Calcif Tissue Int* 50:459–467.

- Dahlbäck K, Ljungquist A, Löfberg H, Dahlbäck B, Engvall E, Sakai LY. 1990. Fibrillin immunoreactive fibers constitute a unique network in the human dermis: immunohistochemical comparison of the distributions of fibrillin, vitronectin, amyloid P component, and orcein stainable structures in normal skin and elastosis. *J Invest Dermatol* 94:284-291.
- De Coster PJ, Martens LC, De Paepe A. 2002. Oral manifestations of patients with Marfan syndrome: a case-control study. *Oral Surg Oral Med Oral Pathol Oral Radiol Endod* 93:564-572.
- Dietz HC, Cutting GR, Pyeritz RE, Maslen CL, Sakai LY, Corson GM, Puffenberger EG, Hamosh A, Nanthakumar EJ, Currstin SM, Stetten G, Meyers DA, Francomano CA. 1991. Marfan syndrome caused by a recurrent de novo missense mutation in the fibrillin gene. *Nature* 352:337-339.
- Downing AK, Knott V, Werner JM, Cardy CM, Campbell ID, Handford PA. 1996. Solution structure of a pair of calcium-binding epidermal growth factor-like domains: implications for the Marfan syndrome and other genetic disorders. *Cell* 85:597-605.
- Finnis ML, Gibson MA. 1997. Microfibril-associated glycoprotein-1 (MAGP-1) binds to the pepsin-resistant domain of the alpha3(VI) chain of type VI collagen. *J Biol Chem* 272:22817-22823.
- Freeman E. 1998. Periodontium. In: TenCate AR, editor. *Ten cate's oral histology: development, structure, and function*, 6th edition. St. Louis: Mosby Elsevier. p 253-288.
- Giannopoulos C, Cimasoni G. 1996. Functional characteristics of gingival and periodontal ligament fibroblasts. *J Dent Res* 75:895-902.
- Gibson MA, Hatzinikolas G, Davis EC, Baker E, Sutherland GR, Mecham RP. 1995. Bovine latent transforming growth factor beta 1-binding protein 2: molecular cloning, identification of tissue isoforms, and immunolocalization to elastin-associated microfibrils. *Mol Cell Biol* 15:6932-6942.
- Habashi JP, Judge DP, Holm TM, Cohn RD, Loeys BL, Cooper TK, Myers L, Klein EC, Liu G, Calvi C, Podowski M, Neptune ER, Halushka MK, Bedja D, Gabrielson K, Rifkin DB, Carta L, Ramirez F, Huso DL, Dietz HC. 2006. Losartan, an AT1 antagonist, prevents aortic aneurysm in a mouse model of Marfan syndrome. *Science* 312:117-121.
- Hirai M, Horiguchi M, Ohbayashi T, Kita T, Chien KR, Nakamura T. 2007. Latent TGF-beta-binding protein 2 binds to DANCE/fibulin-5 and regulates elastic fiber assembly. *EMBO J* 26:3283-3295.
- Isogai Z, Aspberg A, Keene DR, Ono RN, Reinhardt DP, Sakai LY. 2002. Versican interacts with fibrillin-1 and links extracellular microfibrils to other connective tissue networks. *J Biol Chem* 277:4565-4572.
- Isogai Z, Ono RN, Ushiro S, Keene DR, Chen Y, Mazzieri R, Charbonneau NL, Reinhardt DP, Rifkin DB, Sakai LY. 2003. Latent transforming growth factor beta-binding protein 1 interacts with fibrillin and is a microfibril-associated protein. *J Biol Chem* 278:2750-2757.
- Judge DP, Biery NJ, Keene DR, Geubtner J, Myers L, Huso DL, Sakai LY, Dietz HC. 2004. Evidence for a critical contribution of haploinsufficiency in the complex pathogenesis of Marfan syndrome. *J Clin Invest* 114:172-181.
- Kaartinen V, Warburton D. 2003. Fibrillin controls TGF-beta activation. *Nat Genet* 33:331-332.
- Kettle S, Yuan X, Grundy G, Knott V, Downing AK, Handford PA. 1999. Defective calcium binding to fibrillin-1: consequence of an N2144S change for fibrillin-1 structure and function. *J Mol Biol* 285:1277-1287.
- Kielty CM, Sherratt MJ, Shuttleworth CA. 2002. Elastic fibres. *J Cell Sci* 115:2817-2828.
- Liu W, Faraco J, Qian C, Francke U. 1997. The gene for microfibril-associated protein-1 (MFAP1) is located several megabases centromeric to FBN1 and is not mutated in Marfan syndrome. *Hum Genet* 99:578-584.
- Loeys BL, Chen J, Neptune ER, Judge DP, Podowski M, Holm T, Meyers J, Leitch CC, Katsanis N, Sharifi N, Xu FL, Myers LA, Spevak PJ, Cameron DE, De Backer J, Hellemans J, Chen Y, Davis EC, Webb CL, Kress W, Coucke P, Rifkin DB, De Paepe AM, Dietz HC. 2005. A syndrome of altered cardiovascular, craniofacial, neurocognitive and skeletal development caused by mutations in TGFBR1 or TGFBR2. *Nat Genet* 37:275-281.
- Maslen CL, Corson GM, Maddox BK, Glanville RW, Sakai LY. 1991. Partial sequence of a candidate gene for the Marfan syndrome. *Nature* 352:334-337.
- Mecham RP, Davies E. 1994. Elastic fiber structure and assembly. In: Yuchenco PD, Birk DE, Mecham RP, editors. *Extracellular matrix assembly and structure*. New York: Academic Press. p 281-314.
- Miyazono K, Olofsson A, Colosetti P, Heldin CH. 1991. A role of the latent TGF-beta 1-binding protein in the assembly and secretion of TGF-beta 1. *EMBO J* 10:1091-1101.
- Mizuguchi T, Collod-Beroud G, Akiyama T, Abifadel M, Harada N, Morisaki T, Allard D, Varret M, Claustres M, Morisaki H, Ihara M, Kinoshita A, Yoshiura K, Junien C, Kajii T, Jondeau G, Ohta T, Kishino T, Furukawa Y, Nakamura Y, Niihara N, Boileau C, Matsumoto N. 2004. Heterozygous TGFBR2 mutations in Marfan syndrome. *Nat Genet* 36:855-860.
- Nakamura T, Lozano PR, Ikeda Y, Iwanaga Y, Hinek A, Minamisawa S, Cheng CF, Kobuke K, Dalton N, Takada Y, Tashiro K, Ross Jr J, Honjo T, Chien KR. 2002. Fibulin-5/DANCE is essential for elastogenesis in vivo. *Nature* 415:171-175.
- Nanci A. 2007. Periodontium. In: Nanci, A, editor. *Ten cate's oral histology: development, structure and function*, 7th edition. St. Louis: Mosby Elsevier. p 239-267.
- Ng CM, Cheng A, Myers LA, Martinez-Murillo F, Jie C, Bedja D, Gabrielson KL, Mecham RP, Judge DP, Dietz HC. 2004. TGF-beta-dependent pathogenesis of mitral valve prolapse in a mouse model of Marfan syndrome. 1. *J Clin Invest* 114:1586-1592.
- Nohutcu RM, McCauley LK, Koh AJ, Somerman MJ. 1997. Expression of extracellular matrix proteins in human periodontal ligament cells during mineralization in vitro. *J Periodontol* 68:320-327.
- Pereira L, D'Alessio M, Ramirez F, Lynch JR, Sykes B, Pangilinan T, Bonadio J. 1993. Genomic organization of the sequence coding for fibrillin, the defective gene product in Marfan syndrome. *Hum Mol Genet* 2:961-968.
- Pereira L, Lee SY, Gayraud B, Andrikopoulos K, Shapiro SD, Bunton T, Biery NJ, Dietz HC, Sakai LY, Ramirez F. 1999. Pathogenetic sequence for aneurysm revealed in mice underexpressing fibrillin-1. *Proc Natl Acad Sci USA* 96:3819-3823.
- Ramirez F, Sakai LY, Rifkin DB, Dietz HC. 2007. Extracellular microfibrils in development and disease. *Cell Mol Life Sci* 64:2437-2446.
- Rosenbloom J, Abrams WR, Mecham R. 1993. Extracellular matrix 4: the elastic fiber. *FASEB J* 7:1208-1218.

PERIODONTAL TISSUES IN MARFAN SYNDROME

509

- Sawada T, Sugawara Y, Asai T, Aida N, Yanagisawa T, Ohta K, Inoue S. 2006. Immunohistochemical characterization of elastic system fibers in rat molar periodontal ligament. *J Histochem Cytochem* 54:1095–1103.
- Shiga M, Saito M, Hattori M, Torii C, Kosaki K, Kiyono T, Suda N. 2008. Characteristic phenotype of immortalized periodontal cells isolated from a Marfan syndrome type 1 patient. *Cell Tissue Res* 331:461–472.
- Straub AM, Grahame R, Scully C, Tonetti MS. 2002. Severe periodontitis in Marfan's syndrome: a case report. *J Periodontol* 73:823–826.
- Tashiro K, Sawada T, Inoue S, Yanagisawa T. 2002. Development of oxytalan fibers in the rat molar periodontal ligament. *J Periodontal Res* 37:345–352.
- Todorovic V, Jurukovski V, Chen Y, Fontana L, Dabovic B, Rifkin DB. 2005. Latent TGF-beta binding proteins. *Int J Biochem Cell Biol* 37:38–41.
- Tsuruga E, Irie K, Sakakura Y, Yajima T. 2002a. Expression of fibrillins and tropoelastin by human gingival and periodontal ligament fibroblasts in vitro. *J Periodontal Res* 37:23–28.
- Tsuruga E, Irie K, Yajima T. 2002b. Gene expression and accumulation of fibrillin-1, fibrillin-2, and tropoelastin in cultured periodontal fibroblasts. *J Dent Res* 81:771–775.
- Tsuruga E, Yajima T, Irie K. 2004. Induction of fibulin-5 gene is regulated by tropoelastin gene, and correlated with tropoelastin accumulation in vitro. *Int J Biochem Cell Biol* 36:395–400.
- Westling L, Mohlin B, Bresin A. 1998. Craniofacial manifestations in the Marfan syndrome: palatal dimensions and a comparative cephalometric analysis. *J Craniofac Genet Dev Biol* 18:211–218.
- Yanagisawa H, Davis EC, Starcher BC, Ouchi T, Yanagisawa M, Richardson JA, Olson EN. 2002. Fibulin-5 is an elastin-binding protein essential for elastic fibre development in vivo. *Nature* 415:168–171.
- Yuan X, Werner JM, Lack J, Knott V, Handford PA, Campbell ID, Downing AK. 2002. Effects of the N2144S mutation on backbone dynamics of a TB-cbEGF domain pair from human fibrillin-1. *J Mol Biol* 316:113–125.
- Zhang H, Apfelroth SD, Hu W, Davis EC, Sanguineti C, Bonadio J, Mecham RP, Ramirez F. 1994. Structure and expression of fibrillin-2, a novel microfibrillar component preferentially located in elastic matrices. *J Cell Biol* 124:855–863.

M E M O

This image shows a full page of a handwriting practice worksheet. It consists of numerous horizontal dashed lines spaced evenly across the page, providing a guide for letter height and placement. The lines are light gray and extend from the left margin to the right edge of the page. There are no margins, text, or other markings present.

整形外科学分野

四宮 謙一

医歯学総合研究科・先端医療開発学系専攻
脊椎・脊髄神経外科学・教授



1) 研究の課題名

1.ビスフォスフォネートが多孔質ハイドロキシアパタイト・コラーゲン複合体 (HAp/Col) の吸収と骨形成に与える影響

Development and evaluation of a novel artificial bone – porous hydroxyapatite / collagen composite.

HAp/Colは生体吸収性であり、またその高い骨伝導性の理由として、破骨細胞と骨芽細胞のカップリングが考えられていることから、骨粗鬆症治療薬であるビスフォスフォネートにより、移植後の骨形成、インプラントの吸収性に影響を受ける可能性が高いと考えられた。そこでウサギ大腿骨に多孔質HAp/Colを移植し、術前、術後のビスフォスフォネート投与の有無で4群に分け検討を行った。その結果、ビスフォスフォネート投与によりインプラントの吸収が遅延しただけでなく、形成される骨のmineralizationも遅延することが確認された。また、術前に投与を行い、術後投与を中止した群でも術後投与群と同じ傾向を示したことから、術前のみのビスフォスフォネートも移植後の骨形成などに影響を与えることが確認された。実際にHAp/Colを患者に使用する際には、術後の投与だけでなく、術前の投与の有無も考慮する必要が示唆された。

2.γ線滅菌による多孔質ハイドロキシアパタイト・コラーゲン複合体 (HAp/Col) の機械的強度、吸収性、及び骨形成能への影響

Effects of gamma ray irradiation on mechanical property, osteoconductivity, and absorption of porous hydroxyapatite/collagen (HAp/Col)

HAp/Colはガンマ線により滅菌されるが、ガンマ線はHAp/Colに含まれるコラーゲン線維も破壊してしまう。そこでガンマ線滅菌による骨補填剤としての性能に与える影響について検討を行った。検討を行ったガンマ

線量は0, 16, 25, 35, 50kGyであるが35kGy以上の線量では、HAp/Colの急激な力学強度の低下、コラーゲンゼによる分解促進を認め、また移植した際の吸収速度も著しく促進されることが確認された。骨髄内でのHAp/Colによる骨伝導は影響を受けなかったものの、実際に移植する場合は、HAp/Colの一部が骨髄外に露出されることも考えられ、この場合、インプラントの吸収が早すぎると、骨形成を阻止する軟部組織の侵入を招くことになる。これらのことからHAp/Colを滅菌する際には16kGy (滅菌バリデーションで滅菌性を保証済み) 以上25kGy以下が望ましいと考えられた。

3.多孔質HAp/ColとFGF-2を用いた骨軟骨欠損再生に関する検討

Repair of Large Osteochondral Defects in Rabbits Using Porous Hydroxyapatite/Collagen (HAp/Col) and Fibroblast Growth Factor-2 (FGF-2)

HAp/Colと細胞増殖因子であるFGF-2を用いた骨軟骨欠損の修復について検討した。日本白色家兎36羽の両大腿骨膝蓋関節面に直径5mm、深さ5mmの骨軟骨欠損を作成し、FGF-2 (10 μg/ml) 50 μlをHAp/Colに滴下し、24時間、4℃で静置し移植 (FGF10群)、同様に100 μgのFGF-2溶液を含浸させたFGF100群、PBS 50 μlを滴下したHAp/Col移植 (H群)、欠損のみ (D群) の4群に分けた。なお、HAp/Colは直径5mm、高さ3mmの円柱形とし、関節表面から2mm髓腔側の軟骨下骨層に移植した。術後3,6,12,24週で屠殺後、肉眼的・組織学的評価、マイクロCTによる軟骨下骨の骨形成評価を行った。

FGF10群では、群での軟骨面は術後3週から欠損部周囲、骨髄腔側より修復されて行き、軟骨下骨形成も良好であった。また24週という長期観察においても修復軟骨の変性はわずかだった。FGF100群、H群も軟骨下骨

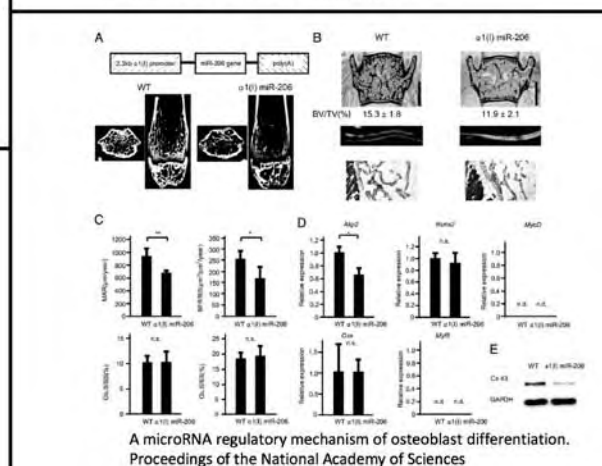
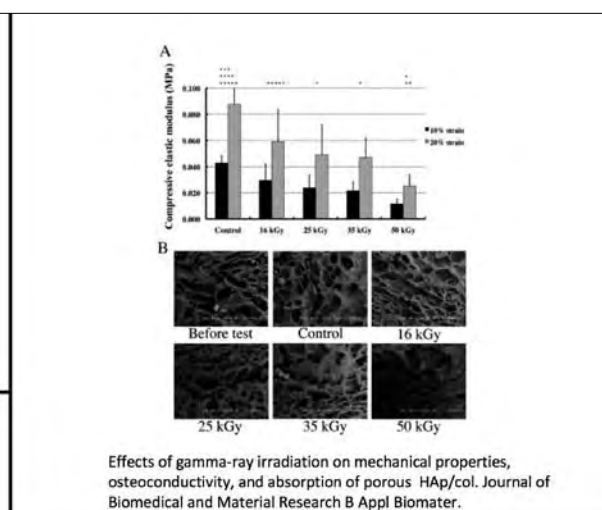
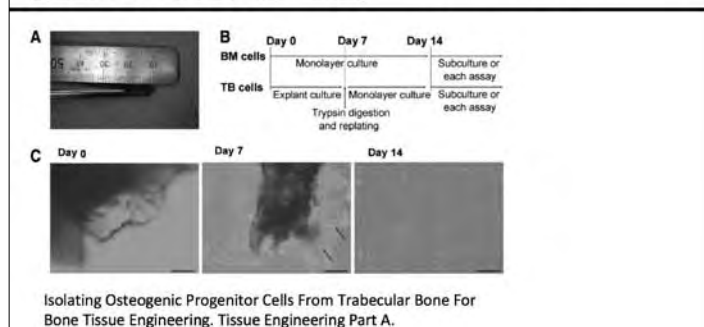
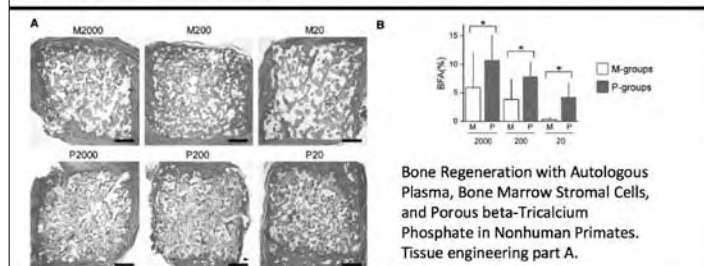
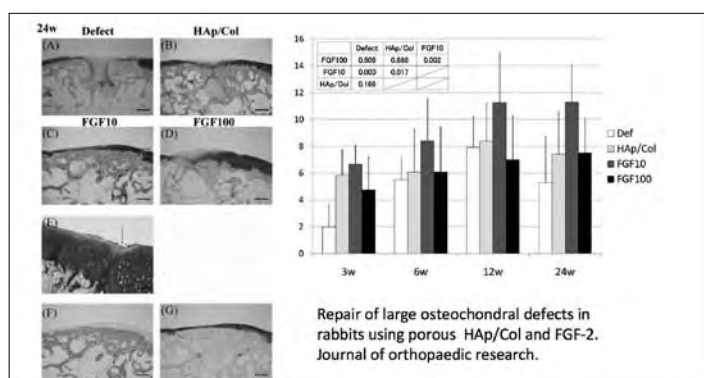
の形成は良好であるが、軟骨下骨、軟骨面の修復ともに FGF10 群に劣っていた。D 群においては線維性組織による修復が主であった。本法は Critical size の骨軟骨欠損修復に対する新たな試みとして期待できるものと考えられた。また、BMP などとも軟骨修復を期待できる薬剤であることから、BMP などとも複合させることでさらに軟骨修復が促進されることが考えられた。

4. 骨芽細胞分化におけるマイクロ RNA の生理的意義の解明

骨芽細胞分化過程におけるマイクロ RNA の発現の変化を網羅的に検討した。骨芽細胞分化に伴い発現の減少がもっとも著しい miR-206 についてその生理的意義を解明した。miR-206 は in vivo で幼弱な骨芽細胞に発現し、分化とともに発現は消失した。骨芽細胞に miR-206 を過剰に発現すると骨芽細胞の分化は抑制された。逆

に miR-206 の骨芽細胞における発現をノックダウンすると骨芽細胞の分化は促進された。続いて、miR-206 の標的をデータベースを用いて探索し、候補の一つとしてコネキシン 43 を同定した。miR-206 の過剰発現により、コネキシン 43 のタンパクの発現はたしかに減弱し、また、miR-206 による骨芽細胞分化の抑制はコネキシン 43 の発現を回復してやることで救済された。これらの結果より、miR-206 の骨芽細胞分化の抑制作用はコネキシン 43 の発現調節を介するものであることが明らかになった。さらに骨芽細胞特異的に miR-206 を発現するトランスジェニックマウスを作製したところ、その骨量の顕著な減少が認められた。以上のことより、miR-206 は骨芽細胞分化を in vivo において生理的に制御する因子であることを世界で初めて明らかにした。

2)



3) 研究内容の英文要約

Bone regeneration with autologous plasma, bone marrow stromal cells, and porous beta-tricalcium phosphate in nonhuman primates.

To potentiate the bone formation capability of bone marrow stromal cell (BMSC) /beta-tricalcium phosphate (beta-TCP) constructs, we devised an autologous plasma-based construct. We tested its effectiveness and investigated the effects of its components on a monkey ectopic bone formation model. The autologous plasma (platelet-rich plasma, PRP, or platelet-poor plasma, PPP) /BMSC/beta-TCP construct (R group or P group) showed significantly more bone formation at 3 and 6 weeks after implantation than a conventional BMSC/beta-TCP construct using a culture medium (M group). There was no significant difference between the P and R groups. Moreover, the P group constructs with a 10-fold lower cell concentration yielded equivalent bone formation to the M group at 5 weeks after implantation. To elucidate the effect of fibrin and serum contained in the plasma, five constructs were prepared using the following cell vehicles: autologous serum + fibrinogen (0, 1, 4, or 16 mg/mL) or phosphate-buffered saline + fibrinogen (4 mg/mL). The serum + fibrinogen (4 mg/mL, physiological concentration of monkeys) construct showed the most abundant bone formation at 3 weeks after implantation, though at 5 weeks no statistical difference existed among the groups. Autologous plasma efficiently promoted osteogenesis of BMSCs/porous beta-TCP constructs, and both fibrin and serum proved to play significant roles in the mechanism.

Effects of gamma-ray irradiation on mechanical properties, osteoconductivity, and absorption of porous hydroxyapatite/collagen.

In this study, the effects of gamma-ray irradiation on the mechanical properties, absorbability, and osteoconductivity of porous hydroxyapatite/collagen (HAp/Col) were investigated. Porous HAp/Col was exposed to 16, 25, 35, or 50 kGy of gamma-ray irradiation. The compressive elastic modulus showed irradiation dose-dependence, with a particularly pronounced decrease in the 50-kGy treatment group. An in vitro enzymatic digestion test showed that gamma-ray irradiation of porous HAp/Col resulted in accelerated degradation by collagenase. For in vivo studies, porous HAp/Col was transplanted into the back muscles or bone defects in the femoral condyle of rats. Specimens were obtained at 2, 4, and 8 weeks postoperatively. Absorption of the implants in the muscle was time- and irradiation dose-dependent, with notable absorption for the 35- and 50-kGy groups at 2 weeks. At the skeletal sites, porous HAp/Col demonstrated high osteoconductivity in all irradiation treatment groups. Interestingly, not only implant absorption but also bone formation was irradiation dose-dependent at

early time points.

Isolating Osteogenic Progenitor Cells From Trabecular Bone For Bone Tissue Engineering.

Trabecular bone fragments can be percutaneously harvested from the ilium using methods that are similar in invasiveness to aspiration of bone marrow. In this study, we investigated the use of the trabecular bone as a cell source for bone tissue engineering. Trabecular bone derived progenitor cells (TB cells) were isolated with a simple method in which trabecular fragments were first cultured as explants, and then the cells were released by trypsin digestion and advanced to a monolayer culture. The properties of TB cells prepared in this procedure were compared with bone marrow derived progenitor cells (BM cells). A large number of TB cells could be obtained with less variation among donors, compared to BM cells. In multiple harvests of donor tissue through the same aspiration hole at the cortex, TB cells could be more consistently obtained in primary culture. The proliferative potential of BM and TB cells was similar in serial subculture. TB cells showed a higher ALP expression in the surface marker analysis and greater in vitro osteogenic abilities than BM cells after the initial 14 days of culture. In in vivo bone formation studies, TB cells also showed a higher osteogenic potential than BM cells. The results of this study suggest that TB cells can be considered an attractive source for clinical bone regeneration.

Repair of large osteochondral defects in rabbits using porous hydroxyapatite/collagen (HAp/Col) and fibroblast growth factor-2 (FGF-2).

Articular cartilage has a limited capacity for self-renewal. This article reports the development of a porous hydroxyapatite/collagen (HAp/Col) scaffold as a bone void filler and a vehicle for drug administration. The scaffold consists of HAp nanocrystals and type I atelocollagen. The purpose of this study was to investigate the efficacy of porous HAp/Col impregnated with FGF-2 to repair large osteochondral defects in a rabbit model. Ninety-six cylindrical osteochondral defects 5 mm in diameter and 5 mm in depth were created in the femoral trochlear groove of the right knee. Animals were assigned to one of four treatment groups: porous HAp/Col impregnated with 50 microl of FGF-2 at a concentration of 10 or 100 microg/ml (FGF10 or FGF100 group); porous HAp/Col with 50 microl of PBS (HAp/Col group); and no implantation (defect group). The defect areas were examined grossly and histologically. Subchondral bone regeneration was quantified 3, 6, 12, and 24 weeks after surgery. Abundant bone formation was observed in the HAp/Col implanted groups as compared to the defect group. The FGF10 group displayed not only the most abundant bone regeneration

but also the most satisfactory cartilage regeneration, with cartilage presenting a hyaline-like appearance. These findings suggest that porous HAp/Col with FGF-2 augments the cartilage repair process. Elucidation of a microRNA regulatory mechanism of osteoblast differentiation

Growing evidence shows that microRNAs (miRNAs) regulate various developmental and homeostatic events in vertebrates and invertebrates. Osteoblast differentiation is a key step in proper skeletal development and acquisition of bone mass; however, the physiological role of non-coding small RNAs, especially miRNAs, in osteoblast differentiation remains elusive. Here, through comprehensive analysis of miRNAs expression during osteoblast differentiation, we show that miR-206, previously viewed as a muscle-specific miRNA, is a key regulator of this process. miR-206 was expressed in osteoblasts, and its expression decreased over the course of osteoblast differentiation. Overexpression of miR-206 in osteoblasts inhibited their differentiation, and conversely, knockdown of miR-206 expression promoted osteoblast differentiation. In silico analysis and molecular experiments revealed Connexin 43 (Cx43), a major gap junction protein in osteoblasts, as a target of miR-206, and restoration of Cx43 expression in miR-206-expressing osteoblasts rescued them from the inhibitory effect of miR-206 on osteoblast differentiation. Finally, transgenic mice expressing miR-206 in osteoblasts developed a low bone mass phenotype due to impaired osteoblast differentiation. Our data show that miRNA is a novel regulator of osteoblast differentiation.

4) 本事業に関連して世界的な研究拠点形成に向けて、以下の点で改善・整備等されたこと

A (研究拠点体制)

- ・大学外との連携を図り、また研究環境（設備など）を整備することによって、研究拠点の基礎を立ち上げた（物質材料研究機構・産業技術総合研究所）。
- ・また、大学内連携を図り、他分野と共同で研究を行っている。（生体材料工学研究所・有機材料分野、難治研究所・分子薬理学）
- ・企業との連携（オリンパス、HOYA、ストライカー）により、研究設備の充実を図るとともに、基礎と臨床との橋渡し研究領域を充実させた。
- ・研究専門部門として寄附講座を運営

B (研究教育環境)

- ・週に3回、論文の抄読会や研究報告会を実施することにより、分子生物学、骨・軟骨組織学、骨再生学の研究、教育体制を確立した。
- ・科学研究費補助金や企業との共同研究により外部

資金を得ることによって、研究環境を整備（研究室の整備）し得た。

C (人材確保)

寄附講座を開設・運営し、研究に専念できる人材を確保した。

D (人材育成)

- ・11名（内留学生2名、他大大学院生1名）の大学院生および1名の専攻生（留学生）に対して、骨・軟骨に関する研究教育、指導を行った。
- ・医学部4学年を対象としたプロジェクトセメスターの制度のもと、2名の大学生に5ヶ月間研究の指導を行った。
- ・Imperial collegeからの短期留学生を受け入れ、3ヶ月間研究指導を行った。

E (国際化)

- ・4名の留学生（大学院生2名、専攻生1名、短期留学生1名）に研究教育、指導を行った。

5) GCOE 事業を推進するに当たって力を入れた点

- ・企業を含む大学内外との連携を強化するなどして、骨・軟骨に関する基礎領域だけでなく、臨床応用を目指した研究にも重点を置いた。
- ・分野内で研究経過・成果に関する discussion を重ねるとともに、外部への研究成果の発表の機会を増やすよう努力した。

6) 英文原著論文

1. © Inose H, Ochi H, Kimura A, Fujita K, Xu R, Sato S, Iwasaki M, Sunamura S, Takeuchi Y, Fukumoto S, Saito K, Nakamura T, Siomi H, Ito H, Arai Y, Shinomiya K-i, Takeda S: A microRNA regulatory mechanism of osteoblast differentiation. *Proceedings of the National Academy of Sciences* 106(49): 20794-20799, 2009.
2. © Maehara H, Sotome S, Yoshii T, Torigoe I, Kawasaki Y, Sugata Y, Yuasa M, Hirano M, Mochizuki N, Kikuchi M, Shinomiya K, Okawa A. Repair of large osteochondral defects in rabbits using porous hydroxyapatite/collagen (HAp/Col) and fibroblast growth factor-2 (FGF-2). *Journal of orthopaedic research*. 2009 Nov 13.
3. © Yoshii T, Sotome S, Torigoe I, Maehara H, Sugata Y, Yamada T, Shinomiya K, Okawa A. Isolating Osteogenic Progenitor Cells From Trabecular Bone For Bone Tissue Engineering. *Tissue Engineering Part A*. 2009 Oct 14.
4. © Kawasaki Y, Sotome S, Yoshii T, Torigoe I, Maehara H, Sugata Y, Hirano M, Mochizuki N, Shinomiya K, Okawa A. Effects of gamma-ray irradiation on

mechanical properties, osteoconductivity, and absorption of porous hydroxyapatite/collagen. Journal of Biomedical and Material Research B Appl Biomater. 2010 Jan;92(1):161-7.

5. ©Torigoe I, Sotome S, Tsuchiya A, Yoshii T, Maehara H, Sugata Y, Ichinose S, Shinomiya K, Okawa A. Bone Regeneration with Autologous Plasma, Bone Marrow Stromal Cells, and Porous beta-Tricalcium Phosphate in Nonhuman Primates. Tissue engineering part A. 2009 Jul;15(7):1489-99.
6. Yoshii T, Sotome S, Torigoe I, Tsuchiya A, Maehara H, Ichinose S, Shinomiya K. Fresh Bone marrow introduction into porous scaffolds using a simple low-pressure loading method for effective osteogenesis in a rabbit model. Journal of orthopaedic research. 27:1, 2009

7) 特許取得、特許申請

「生体内薬物徐放材料の製造方法」

発明者:早乙女進一、四宮謙一他、特許番号4204772、特許取得日2008年10月24日

「多孔質複合材料の製造方法」

発明者:早乙女進一、四宮謙一他、国内:特許番号3727059、特許取得日2005年10月7日、アメリカ合衆国:特許番号7163965、特許取得日2007年1月16日

「複合生体材料」

発明者:早乙女進一、四宮謙一他、特許番号3770555、特許取得日2006年2月17日 その他米国、カナダ取得

8) 平成21年度までの自己評価

研究も概ね計画通り進めることができ、学会発表、論文発表も、質、内容的ともに十分な成果を得ることができたと考えている。

9) 学会発表 (英文)

©Sugata Y, Sotome S, Maehara H, Kawasaki Y, Yuasa M, Mochizuki N, Hirano M, Shinomiya K. The Influence of Bisphosphonate Treatment on a Hydroxyapatite-Collagen Composite. 55th Annual meeting of the orthopaedic research society. July 22-25, 2009, poster presentation, Las Vegas

A. Kimura, H. Inose, K. Fujita, F. Yano, H. Kawaguchi, U. Chung, K. Shinomiya, S. Takeda. Requirement of Runx1 for chondrocyte lineage commitment 31 th Annual Meeting of the American Society for Bone and Mineral Research, 示説 MO0065, Colorado, Denver, USA, 9月, 2009.

Koji Fujita, Hiroyuki Inose, Ayako Kimura, Yoshiyasu Arai, Kenichi Shinomiya, Shu Takeda Regulation of osteoblast differentiation by microRNA 第26回内藤コンファレンスオステオバイオロジー 示説 淡路夢舞台国際会議場 2009年11月5日

A. Kimura, H. Inose, K. Fujita, F. Yano, H. Kawaguchi, U. Chung, H. Itoh, K. Shinomiya, S. Takeda. Requirement of Runx1 for chondrocyte lineage commitment 第26回内藤コンファレンスオステオバイオロジー 示説 淡路夢舞台国際会議場 2009年11月5日

10) 学会発表 (和文)

◎早乙女進一、土谷明男、前原秀二、菅田祐美、阿江啓介、若林良明、四宮謙一、上坂優子、高山知士、望月直美、塩谷慎吾、平野昌弘、石突雅文、森岡秀雄、松本誠一、中村孝志、阿部哲、別府保男:多孔質ハイドロキシアパタイト・コラーゲン複合体 (HAp/Col) の開発と臨床応用.第27回日本骨代謝学会 大阪 7/23-25

菅田祐美、早乙女進一、前原秀二、川崎雄一、湯浅将人、望月直美、平野昌弘、四宮謙一、大川淳:ビスフォスフォネートが生体吸収性骨補填剤に吸収と骨形成に与える影響 (第2報).第24回日本整形外科学会基礎学術集会 横浜 11/5-6

小柳広高、阿江啓介、早乙女進一、前原秀二、菅田祐美、湯浅将人、正岡智和、山田剛史、船内雄生、四宮謙一、大川淳:温熱処理骨と骨髓由来間質細胞導入 β -TCPを用いた大型犬の骨欠損モデルにおける骨再生.第24回日本整形外科学会基礎学術集会 横浜 11/5-6

前原秀二、早乙女進一、菅田祐美、湯浅将人、正岡智和、山田剛史、平野昌弘、望月直美、四宮謙一、大川淳:多孔質ハイドロキシアパタイト/コラーゲン複合体 (HAp/Col) のosteogenic protein-1 (OP-1) 担体としての有用性に関する検討.第24回日本整形外科学会基礎学術集会 横浜 11/5-6

早乙女進一、川崎雄一、吉井俊貴、鳥越一郎、前原秀二、菅田祐美、望月直美、平野昌弘、四宮謙一、大川淳: γ 線滅菌による多孔質ハイドロキシアパタイト・コラーゲン複合体 (HAp/Col) の機械的強度、吸収性、および骨形成能への影響.第24回日本整形外科学会基礎学術集会 横浜 11/5-6

猪瀬弘之 竹田秀 藤田浩二 岩崎牧子 四宮謙一 マイクロRNAによる骨芽細胞分化の調節第24回日本整形外科学会基礎学術集会2009年11月5日 横浜

11) 外部資金の獲得状況

厚生労働科学研究費補助金（長寿科学総合研究事業）

研究題目:骨粗鬆症椎体骨折に対する低侵襲治療法の開発

代表:四宮 謙一

期間:平成21年-平成24年

研究費総額:平成21年度 ¥14,000,000.-

厚生労働科学研究費補助金（難治性疾患克服研究事業）

研究題目:脊柱靱帯骨化症に関する調査研究

分担:四宮 謙一

期間:平成20年-平成22年

研究費総額:平成20年度¥1,000,000.- 平成21年度 ¥1,000,000.-

厚生労働科学研究費補助金

（地域医療基盤開発推進研究事業）

研究題目:診療ガイドラインの新たな可能性と課題:患者・一般国民との情報共有と医療者の生涯学習

分担:大川 淳

期間:平成19年-平成21年

研究費総額:平成19年度¥500,000.- 平成20年度 ¥500,000.- 平成21年度¥200,000.-

科学研究費補助金（基盤研究B）

研究題目:骨髄間葉系幹細胞を利用した巨大骨組織再生のための基礎技術の確立

代表:四宮 謙一

期間:平成21年-平成24年

研究費総額:平成21年度¥5,720,000.-

科学研究費補助金（基盤研究C）

研究題目:SQUID磁束計を用いた脊髄機能診断法の臨床応用

代表:川端 茂徳

期間:平成19年-平成21年

研究費総額:平成19年度¥1,560,000.- 平成20年度 ¥1,430,000.- 平成21年度¥1,430,000.-

科学研究費補助金（基盤研究C）

研究題目:危険因子分析法（HAZOP）に基づいた医療安全演習ソフトウェアの開発

代表:大川 淳

期間:平成21年-平成22年

研究費総額:平成21年度¥1,170,000.-

科学研究費補助金（基盤研究C）

研究題目:Runx1による軟骨初期分化調節の分子機構の解明と軟骨再生医療への応用

代表:神野 哲也

期間:平成21年度-平成22年度

研究費総額:平成21年度¥1,170,000.-

科学研究費補助金（基盤研究C）

研究題目:靱帯骨化症の分子基盤-Run × 3遺伝子欠損マウスを用いた検討-

代表:阿江 啓介

期間:平成20年度-平成22年度

研究費総額:平成20年度¥1,560,000.- 平成21年度 ¥1,430,000.-

科学研究費補助金（基盤研究C）

研究題目:マイクロRNAによる骨芽細胞・骨細胞分化調節機構の解明

代表:早乙女 進一

期間:平成21年-平成23年

研究費総額:平成21年度¥1,950,000.-

科学研究費補助金（基盤研究C）

研究題目:末梢神経損傷に対する低分子Gタンパク質発現制御を標的とした遺伝子治療法の確立

代表:若林 良明

期間:平成20年-平成22年

研究費総額:平成20年度¥1,430,000.- 平成21年度 ¥1,170,000.-

科学研究費補助金（基盤研究C）

研究題目:メタボリックシンドロームに伴う関節軟骨変性の分子機構解析

代表:加藤 剛

期間:平成19年-平成21年

研究費総額:平成19年度¥1,560,000.- 平成20年度 ¥1,430,000.- 平成21年度¥1,430,000.-

科学研究費補助金（基盤研究C）

研究題目: 脊髄損傷慢性期での細胞移植を併用した再髄鞘化と運動機能再建

代表: 榎本 光裕

期間: 平成21年-平成23年

研究費総額: 平成21年度¥1,430,000,-

科学研究費補助金（基盤研究C）

研究題目: 関節軟骨代謝における老化制御因子SIRT1の機能解析

代表: 麻生 義則

期間: 平成21年度-平成23年度

研究費総額: 平成21年度¥1,560,000,-

科学研究費補助金（基盤研究C）

研究題目: 関節軟骨細胞に発現する破骨細胞分化制御因子の機能に関する研究

代表: 古賀 大介

期間: 平成21年度-平成23年度

研究費総額: 平成21年度¥1,560,000,-

科学研究費補助金（萌芽研究）

研究題目: 3次元磁界測定により神経細胞内・細胞外電流を評価し、神経障害の病態を解明する

代表: 平成19年度 富澤 将司 平成20年度-平成21年度 友利 正樹

期間: 平成19年-平成21

研究費総額: 平成19年度¥1,100,000,- 平成20年度¥1,000,000,- 平成21年度¥1,000,000,-

交通事故医療特定課題の研究助成（日本損害保険協会）

研究題目: 骨誘導性注入型骨補填剤の開発および難治性骨折への応用

代表: 早乙女 進一

期間: 平成21年-平成23年（2年間）

研究費総額: 4,000,000,-

共同研究費（帝人ファーマ株式会社）

研究題目: 椎間板ヘルニア治療薬の創薬研究. 民間との共同研究

代表: 加藤 剛

期間: 平成21年度-平成22年度（単年度）

研究費総額: ¥1,420,000,-

共同研究費（オリンパス株式会社）

研究題目: 骨髄間葉系細胞/ β TCP複合体による骨形成能の検討. 民間との共同研究

代表: 四宮 謙一

期間: 平成21年度-平成22年度（単年度）

研究費総額: ¥2,200,000,-

共同研究費（横河電機株式会社）

研究題目: 川端茂徳: 多部位対応普及型脊髄誘発磁場計測装置の開発.

代表: 四宮 謙一

期間: 平成21年度-平成22年度

研究費総額: ¥4,700,000,-

共同研究費（HOYA株式会社）

研究題目: 多孔質ハイドロキシアパタイト/コラーゲン複合体 (HAp/Col) のOsteogenicprotein-1 (Op-1) 担体としての有用性に関する検討

代表: 早乙女 進一

期間: 平成21年-平成22年度（単年度）

研究費総額: 平成21年度¥1,430,000,-

共同研究費（キッコーマン株式会社）

研究題目: 関節軟骨代謝に対するプロアントシアニジンとオリゴヒアルロン酸の作用に関する研究

代表: 早乙女 進一

期間: 平成21年度

研究費総額: ¥1,000,000,-

12) 特別講演、招待講演

2009/4/9

第112回中部日本整形外科災害外科学会・学術集会
国立京都国際会館（京都府）
教育研修講演4

2009/5/4

東京医科歯科大学医師会産業医研修会
東京医科歯科大学5号館講堂（東京都）
「職場の腰痛対策」

2009/7/10

第27回二豊整形外科フォーラム
マリエールオークパイン中津（大分県）
特別講演「人工骨を用いた骨再生の現状と未来」

2009/7/11

名古屋脊椎脊髄セミナー2009

名古屋大学病院 第1研究棟地下1階 (愛知県)

教育講演「術中脊髄モニタリングの現状と未来」

2009/10/17

第24回福岡運動器カンファレンス

タカクラホテル福岡 (福岡県)

特別講演「頸椎後縦靱帯骨化症に対する治療戦略」

13) 主催学会

第17回日本腰痛学会

2009年11月21日～22日

東京コンファレンスセンター・品川

14) 教室、分野や講座の准教授、講師、助教、特別研究員、ポスドク、指導を受けた大学院生の名前(AISSには○印)のリスト

(整形外科学分野)

准 教 授 : 大川 淳

講 師 : 神野 哲也、

助 教 : 若林良明、川端茂徳、阿江啓介、
加藤剛、古賀大介、富沢将司

大 学 院 生 : 岩崎牧子、五木田茶舞、小柳広高、
石井宣一、山内裕樹、猪瀬弘之、
草野和生、○木村文子、
○菅田祐美、○藤田浩二、
正岡智和、榊経平、平井高志、
○湯浅将人、○山田剛史、
請川大

(整形外科先端治療開発学講座)

寄付講座准教授 : 早乙女進一

寄 付 講 座 講 師 : 榎本光裕、麻生義則

A microRNA regulatory mechanism of osteoblast differentiation

Hiroyuki Inose^a, Hiroki Ochi^b, Ayako Kimura^{a,c}, Koji Fujita^{a,c}, Ren Xu^a, Shingo Sato^a, Makiko Iwasaki^a, Satoko Sunamura^d, Yasuhiro Takeuchi^e, Seiji Fukumoto^f, Kuniaki Saito^g, Takashi Nakamura^h, Haruhiko Siomiⁱ, Hiroshi Ito^d, Yoshiyasu Arai^a, Ken-ichi Shinomiya^{a,c}, and Shu Takeda^{a,d,1}

^aDepartment of Orthopedics, Graduate School, ^cGlobal Center of Excellence Program, and ^bDepartment of Developmental and Regenerative Biology, Tokyo Medical and Dental University, 1-5-45 Yushima, Bunkyo-ku, Tokyo 113-8519, Japan; ^dDepartment of Veterinary Science, Faculty of Veterinary Medicine, Nippon Veterinary and Life Science University, 1-7-1 Kyonan-cho, Musashino-shi, Tokyo 180-8602, Japan; ^eToranomon Hospital Endocrine Center, 2-2-2 Toranomon, Minato-ku, Tokyo 105-8470, Japan; ^fDivision of Nephrology and Endocrinology, Department of Internal Medicine, University of Tokyo Hospital, 7-3-1 Hongo, Bunkyo-ku, Tokyo 113-8655, Japan; and ^gSection of Nephrology, Endocrinology and Metabolism, Department of Internal Medicine and ^hDepartment of Molecular Biology, Keio University School of Medicine, 35 Shinanomachi, Shinjuku-ku, Tokyo 160-8582, Japan

Edited by Clifford J. Tabin, Harvard Medical School, Boston, MA, and approved October 13, 2009 (received for review August 17, 2009)

Growing evidence shows that microRNAs (miRNAs) regulate various developmental and homeostatic events in vertebrates and invertebrates. Osteoblast differentiation is a key step in proper skeletal development and acquisition of bone mass; however, the physiological role of non-coding small RNAs, especially miRNAs, in osteoblast differentiation remains elusive. Here, through comprehensive analysis of miRNAs expression during osteoblast differentiation, we show that miR-206, previously viewed as a muscle-specific miRNA, is a key regulator of this process. miR-206 was expressed in osteoblasts, and its expression decreased over the course of osteoblast differentiation. Overexpression of miR-206 in osteoblasts inhibited their differentiation, and conversely, knock-down of miR-206 expression promoted osteoblast differentiation. In silico analysis and molecular experiments revealed connexin 43 (Cx43), a major gap junction protein in osteoblasts, as a target of miR-206, and restoration of Cx43 expression in miR-206-expressing osteoblasts rescued them from the inhibitory effect of miR-206 on osteoblast differentiation. Finally, transgenic mice expressing miR-206 in osteoblasts developed a low bone mass phenotype due to impaired osteoblast differentiation. Our data show that miRNA is a regulator of osteoblast differentiation.

Connexin43 | miR-206

The osteoblast, a cell type of a mesenchymal origin, plays a major role in skeletal development and bone formation (1, 2). Understanding the regulatory mechanism of osteoblast differentiation is a prerequisite for developing strategies to treat bone loss diseases such as osteoporosis (3–5). In the last two decades, progress in molecular and genetic research has uncovered various regulatory processes of osteoblast differentiation (1, 2, 4). Central to this regulation are transcription factors: Runx2, Osterix, and β -catenin are, to date, the transcription factors known to be essential for osteoblast differentiation (2). In addition, while some transcription factors, including C/EBP β , Smad1, and Smad5, bind to Runx2 and enhance its transcriptional activity, others, such as Twist, inhibit Runx2 transcriptional activity (6). However, given the fact that the number of coding genes in vertebrates and invertebrates (which lack a skeleton) is comparable (7), there must be additional mechanisms for controlling skeletal development other than transcriptional regulation of gene expression.

Recently, miRNAs have emerged as important regulators in various developmental, physiological, and pathological conditions such as tumorigenesis, viral infection, and cell differentiation and function (8–10). miRNAs are single-stranded small RNA molecules that are approximately 21 or 22 nucleotides long (9). They do not encode protein; instead, they regulate the level of other proteins by decreasing messenger RNA (mRNA) levels or inhibiting translation by binding the 3'UTR of the target mRNA (8). Surprisingly, non-coding RNA accounts for 98% of

all genomic output in humans (11), and it has been proposed that the proportion of non-coding RNA to protein-coding RNA is correlated with developmental complexity (12).

Previous reports implicated miRNAs in the differentiation of osteoclasts and osteoblasts (13–21). However, their importance in the regulation of osteoblast differentiation in vivo, if any, remains to be established. Here we show that one particular miRNA, miR-206, is expressed in the osteoblastic cell lineage and that its expression gradually decreases in parallel with osteoblast differentiation. Interestingly, modulating miR-206 expression in osteoblasts markedly affects their differentiation potential in part by altering the accumulation of connexin 43 (Cx43). Finally, osteoblast-specific expression of miR-206 in vivo leads to severe bone loss due to impairment of osteoblast differentiation. Thus, this study reveals a physiological regulatory mechanism of osteoblast differentiation mediated by miRNA.

Results

Identification of miRNAs Whose Expression Varies During Osteoblast Differentiation. To study the potential involvement of miRNAs in osteoblast differentiation, we first attempted to identify miRNAs that are expressed in the osteoblastic cell lineage, particularly miRNAs whose expression is altered during osteoblast differentiation. To that end, we treated multipotent C2C12 mesenchymal progenitor cells with recombinant BMP-2 for 2 days, an established model for studying osteoblast differentiation (22). We then comprehensively analyzed the expression of miRNAs before and after BMP-2 treatment using a microarray that detects all known miRNAs (23). miR-133a was downregulated by BMP-2 treatment (Fig. 1A and Figs. S1 and S2A) as previously reported (13), suggesting that the experiment was properly conducted. Osteoblasts express many miRNAs, and most of the miRNAs (36%) were downregulated by BMP-2 treatment, while only 4% of them were upregulated (Fig. 1A and Fig. S1). Of these, we were interested in miR-206 because its expression was most significantly downregulated during osteoblast differentiation (Fig. 1A). As miR-206 was originally shown to be expressed exclusively in skeletal muscle and heart (24–28), we first verified its expression in the osteoblastic lineage using primary mouse osteoblasts and bones by four different experiments. First, as

Author contributions: Y.T., S.F., T.N., H.S., H. Ito, Y.A., K. Shinomiya, and S.T. designed research; H. Inose, H.O., A.K., K.F., R.X., S. Sato, M.I., S. Sunamura, and K. Saito performed research; H. Inose and S.T. analyzed data; and S.T. wrote the paper.

The authors declare no conflict of interest.

This article is a PNAS Direct Submission.

¹To whom correspondence should be addressed. E-mail: shu-tky@umin.ac.jp.

This article contains supporting information online at www.pnas.org/cgi/content/full/0909311106/DCSupplemental.

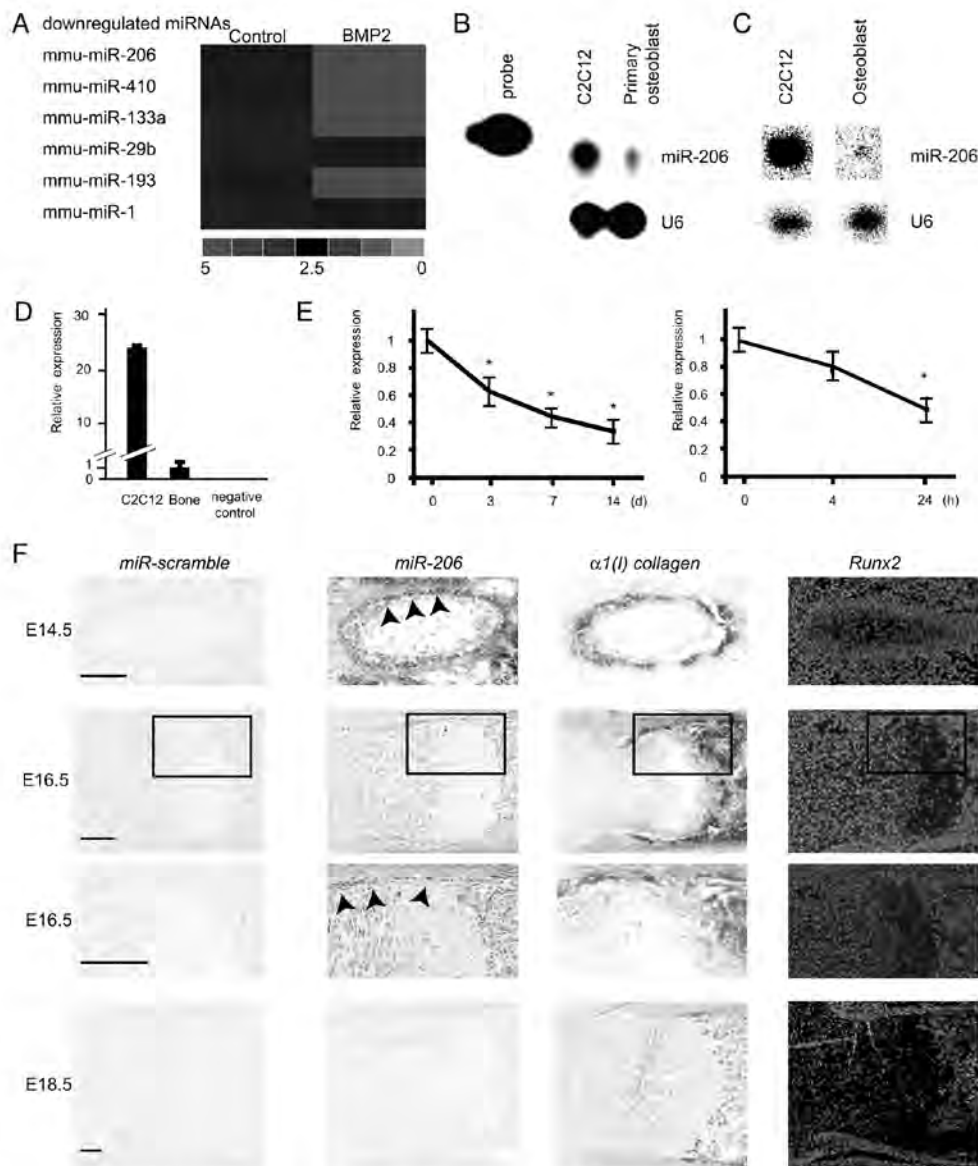


Fig. 1. Expression of miR-206 during osteoblast differentiation. (A) miRNA array expression data from C2C12 cells cultured in growth medium (Control) or in differentiation medium containing BMP-2. Red denotes high expression and green denotes low expression relative to the median; only the representative miRNA nodes that were significantly downregulated in the differentiation medium are shown. (B–D) Expression of miR-206 in osteoblasts: RNase protection assay (B), Northern blot analysis (C), and quantitative RT-PCR analysis (D) to detect miR-206 expression in osteoblasts. Total RNA was isolated from primary mouse osteoblasts, mouse femur or C2C12 cells. U6 RNA was used as a loading control. Note the distinct expression of miR-206 in primary osteoblasts and bone (B–D). (E) Change in miR-206 expression during osteoblast differentiation: quantitative RT-PCR analysis. Mouse primary osteoblasts were treated in differentiation medium (Left) or with the addition of BMP-2 (Right) for each indicated length of time. Note the significant decrease in parallel with the progression of osteoblast differentiation. *, $P < 0.05$ vs. 0 time point, $n = 6$. (F) In situ hybridization analysis of miR-206 expression in mouse embryos: Rib (E14.5, Top) and femur (E16.5, middle and E18.5, Bottom) cryosections. Bottom panel of E16.5 embryo shows the higher magnification of the black rectangular region in the top panel. Adjacent sections were hybridized with scramble-miRNA (left), miR-206 (Middle Left), $\alpha 1(I)$ collagen (Middle Right), and Runx2 (Right) probes. Note the miR-206 expression in perichondrium osteoblastic cells at E14.5 (arrowheads) and in cells of bone collar at E16.5 (arrowheads). (Scale bar, 100 μ m.)

shown by an RNase protection assay, miR-206 was clearly expressed in primary osteoblasts (Fig. 1B). Second, by Northern blot analysis, which is almost 10 times less sensitive than an

RNase protection assay (29, 30), miR-206 was also shown to be expressed in primary osteoblasts (Fig. 1C). Third, by real-time PCR analysis specific to miR-206, we observed miR-206 expres-

sion both in femur and primary osteoblasts (Fig. 1D and E), and interestingly, miR-206 expression gradually decreased during the course of osteoblast differentiation (Fig. 1E). Fourth and most importantly, to investigate the dynamic pattern of miR-206 expression in bone, we performed in situ hybridization analysis using DIG-labeled probes. At E14.5, miR-206 was expressed in muscle and perichondrium osteoblastic cells, whose identity was verified by the coexpression of $\alpha 1(I)$ collagen and *Runx2*, markers for osteoblasts (Fig. 1F). At E16.5, miR-206 was still expressed in the cells of the bone collar, although the expression was decreased compared to the expression at E14.5 (Fig. 1F). At E18.5, miR-206 expression in bone was close to background level (Fig. 1F). The gradual decrease of miR-206 expression during skeletogenesis in vivo is consistent with its gradual decrease of expression during the course of in vitro osteoblast differentiation. To further confirm in vivo expression of miR-206 in osteoblasts, we also performed double staining for in situ hybridization to detect miR-206 and immunohistochemistry to detect *Runx2*. High resolution confocal microscopic analysis revealed that miR-206 colocalize with *Runx2* in osteoblast (Fig. S3). Taken together, these four independent experiments confirmed that miR-206 is expressed in the osteoblastic cell lineage.

miR-206 Regulates Osteoblast Differentiation. The decrease in the expression of miR-206 during osteoblast differentiation prompted us to test if miR-206 inhibits osteoblast differentiation. To this end, we infected a vector expressing both miR-206 and a blasticidin-resistance gene into C2C12 cells and isolated five stable blasticidin-resistant clones that also express miR-206 to determine if continuous expression of miR-206 affected their ability to differentiate into osteoblasts. As controls, we also infected either an empty vector or a miR-133-expressing vector. C2C12 cells expressing empty vector differentiated normally into the osteoblastic lineage upon BMP-2 treatment. In contrast, osteoblastic differentiation of C2C12 cells expressing miR-133 was significantly impaired (Fig. S2B), as previously reported. Importantly, none of the five clones expressing miR-206 differentiated into the osteoblastic lineage, as shown by the lack of induction of alkaline phosphatase activity (Fig. 2A). To rule out the possibility that stable expression of miR-206 altered the properties of C2C12 cells, we also transiently transfected a miR-206-expressing vector into C2C12 cells. In this transient DNA transfection assay, miR-206 also repressed osteoblastic differentiation (Fig. 2B). To test if miR-206 regulates osteoblast differentiation in a physiological manner, we next used primary mouse osteoblasts because C2C12 is a myogenic cell line. The results showed that continuous expression of miR-206 significantly inhibited osteoblast differentiation as demonstrated by the decrease in alkaline phosphatase activity and *bglap* expression (Fig. 2C and Fig. S4). Interestingly, miR-206 expression did not affect *Runx2* mRNA expression, indicating that miR-206 regulates osteoblast differentiation independently of *Runx2* (Fig. 2C).

Because it has been shown that expression of miR-206 induces myogenic differentiation (24, 27, 28), we asked whether miR-206 expression induces myogenic transdifferentiation of osteoblasts; however, no expression of myogenic genes such as *MyoD* or *Myf5* (31) was detected, indicating that miR-206 does not induce myogenic differentiation (Fig. 2C).

Since overexpression of miR-206 inhibits osteoblast differentiation, we next asked whether decreasing miR-206 expression would accelerate their differentiation. Indeed, knockdown of miR-206 significantly induced osteoblast differentiation (Fig. 2D). Taken together, these results demonstrate that miR-206, which is expressed in the osteoblastic cell lineage, physiologically regulates osteoblast differentiation.

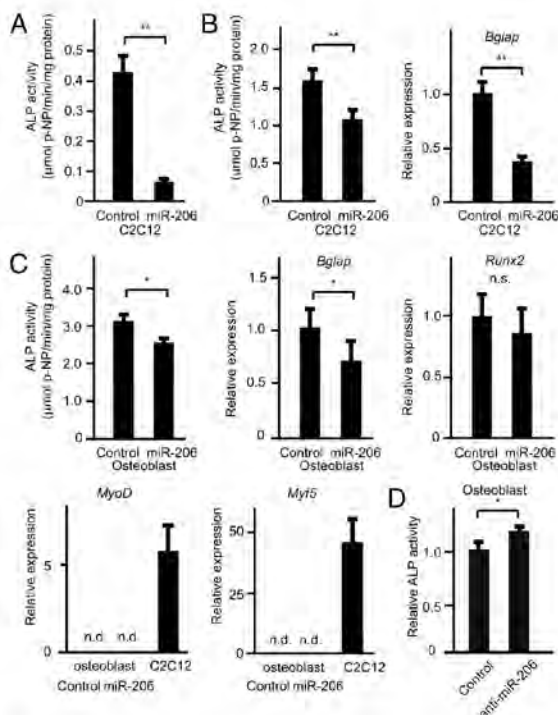


Fig. 2. Regulation of osteoblast differentiation by miR-206. (A and B) Effect of miR-206 expression on BMP-2-dependent C2C12 cell differentiation: C2C12 cells constitutively expressing miR-206 (A) or transiently transfected with miR-206 (B). Alkaline phosphatase activity (A and B, Left) and *bglap* gene expression (B, Right) were analyzed. Note the decreased osteoblastic differentiation in miR-206 expressing cells. **, $P < 0.01$, $n = 6-8$. (C) Effect of miR-206 continuous expression on primary mouse osteoblast differentiation: primary mouse osteoblasts infected with pAd-miR-206 or control adenovirus were cultured. Subsequently, alkaline phosphatase activity assay (Top Left) and quantitative RT-PCR analysis for the indicated genes were analyzed. GAPDH was used as an internal control. n.s., not significant. n.d., not detected. +, $P < 0.05$, $n = 6-8$. (D) Effect of miR-206 knockdown on osteoblast differentiation: osteoblasts were transfected with a miR-206 inhibitor or control. Subsequently, alkaline phosphatase activity was analyzed. Note the significant increase by the miR-206 inhibitor. *, $P < 0.05$, $n = 6$.

Connexin 43 Is One Molecular Target of miR-206 in Osteoblasts. We next studied the molecular mechanism by which miR-206 inhibits osteoblast differentiation. To identify target genes of miR-206, we relied on a computational approach using two different established databases (32, 33). Among the many genes that were predicted to be potential targets by both databases, we focused on Cx43, a gap junction protein expressed in osteoblasts that plays a major role in osteoblast differentiation and function; indeed, Cx43-deficient mice display low bone mass due to osteoblast dysfunction (34, 35). Two putative target sequences for miR-206 were found in the 3'UTR region of Cx43 (Fig. 3A). At first, we tested if miR-206 regulated Cx43 expression using a reporter plasmid in which the two putative binding sites of the Cx43 3'UTR were cloned into the 3'UTR of the luciferase gene (Fig. 3B). As expected from in silico analysis, ectopic expression of miR-206 significantly decreased luciferase activity (Fig. 3B); furthermore, ectopic expression of miR-206 downregulated endogenous Cx43 protein expression without affecting Cx43 mRNA expression (Fig. 3C). Taken together, these results identify Cx43 as a bona fide target of miR-206 in vivo.

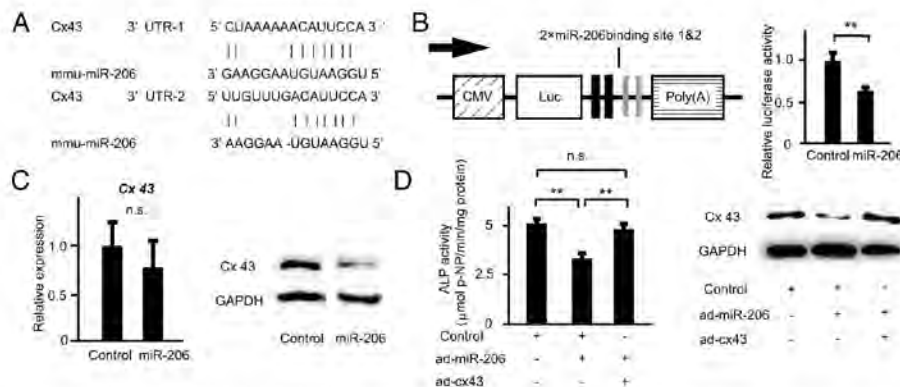


Fig. 3. Identification of miR-206 target genes in osteoblast differentiation. (A) Alignment of miR-206 showing complementary pairing to the Cx43 3' UTR. (B) Schematic presentation of the reporter plasmid used to analyze the effect of the Cx43 3' UTR on luciferase activity (Left). Effect of miR-206 expression on a luciferase reporter plasmid carrying the Cx43 3' UTR was analyzed (Right). Cells were transfected with either the miR-206 expression plasmid or a control. The ratio of reporter (firefly) to control (renilla) was plotted. CMV, cytomegalovirus promoter; Luc, luciferase. **, $P < 0.01$, $n = 6$. (C) miR-206 targets Cx43 and regulates its expression. Cells were transfected with the miR-206 expression plasmid or a control. Quantitative RT-PCR analysis (Left) and Western blot analysis for Cx43 (Right) were subsequently performed. GAPDH was used as an internal control. n.s., not significant; $n = 6-8$. (D) Cx43 rescues the inhibitory effect of miR-206 on osteoblast differentiation. Primary osteoblasts expressing miR-206 were infected with either the Cx43-expressing virus (pAd-Cx43) or control adenovirus. Subsequently, alkaline phosphatase activity was analyzed. Note that the inhibitory effect of miR-206 on osteoblast differentiation was reversed by co-expression of Cx43. (Left, alkaline phosphatase activity; Right, Western blot) **, $P < 0.01$, $n = 6$.

To address if Cx43 is a physiologically important target of miR-206 during osteoblast differentiation, we asked whether restoring Cx43 expression rescued the impairment of osteoblast differentiation caused by continuous miR-206 expression. Continuous expression of miR-206 in osteoblasts decreased osteoblast differentiation and Cx43 protein expression (Fig. 3C). However, when we co-expressed Cx43 together with miR-206, the inhibitory effect of miR-206 on osteoblast differentiation was markedly rescued (Fig. 3D). Importantly, the expression level of Cx43 protein was similar between control cells and cells co-expressing both miR-206 and Cx43, which indicates that restoration of Cx43 protein expression is sufficient to obtain normal osteoblast differentiation in miR-206-expressing osteoblasts (Fig. 3D).

miR-206 Is a Regulator of Bone Formation in Vivo. Lastly, to address the in vivo role of miR-206 in bone formation, we generated transgenic (tg) mice specifically expressing miR-206 in osteoblasts using the $\alpha 1(I)$ collagen promoter (Fig. 4A and Fig. S5). $\alpha 1(I)$ miR-206 tg mice displayed a low bone mass phenotype both in trabecular and cortical bones by μ CT analysis and histology (Fig. 4A and B). Furthermore, bone histomorphometric analysis revealed that the bone formation rate, an indicator of osteoblast function, was significantly decreased in $\alpha 1(I)$ miR-206 mice (Fig. 4B and C). In contrast, osteoclast surface, a marker of bone resorption, was similar in wild-type mice and $\alpha 1(I)$ miR-206 tg mice, indicating that osteoclastic bone resorption was not affected (Fig. 4C). The expression of osteoblastic marker genes such as *Akp2* was significantly downregulated in $\alpha 1(I)$ miR-206 tg mice (Fig. 4D). Importantly, Cx43 protein expression was significantly reduced in $\alpha 1(I)$ miR-206 tg mice, while the expression of Runx2 and Osterix was not affected in these mice (Fig. 4D and E), further indicating that miR-206 regulates osteoblast differentiation through Cx43 independently of Runx2 and Osterix. Of note, the lack of expression of myogenic marker genes in real-time PCR and the absence of Troponin I protein in immunohistochemistry (36) clearly demonstrated that there was no ectopic muscle differentiation in $\alpha 1(I)$ miR-206 tg mice (Fig. 4B and D). Collectively, overex-

pression of miR-206 in osteoblasts inhibited osteoblast differentiation, which led to low bone mass in vivo.

Discussion

We demonstrate here an inhibitory role of miR-206 during osteoblast differentiation. First, we showed that miR-206 is expressed in the osteoblastic lineage and that this expression gradually decreases during osteoblast differentiation. Then we demonstrated that modulating the expression of miR-206 in osteoblasts affects osteoblast differentiation and that one of the targets of miR-206 is Cx43. Finally, we showed that miR-206 regulates osteoblast differentiation in vivo. Recent reports suggested the involvement of miRNAs in osteoblast differentiation (13–20). However, these reports were based only on in vitro observations using a cell line. To our knowledge, this study demonstrates an in vivo regulatory role of miRNA in osteoblast differentiation.

It was previously shown that miR-206 induces myogenic differentiation (24, 27, 28). Therefore, we were concerned that the observed inhibitory effect of miR-206 in osteoblast differentiation was attributable only to an increase of differentiation into the myoblastic lineage, or alternatively, that miR-206 transdifferentiates osteoblasts into the myoblastic lineage. However, the experimental evidence argues against these hypotheses. Indeed, primary osteoblasts continuously expressing miR-206 do not express myogenic markers such as *MyoD* or *Myf5*. Furthermore, $\alpha 1(I)$ miR-206 tg mice do not demonstrate any evidence of ectopic muscle differentiation in bone. Notably, the fact that to overexpress miR-206 we used the $\alpha 1(I)$ collagen promoter, which is active only in cells committed to the osteoblastic lineage (37), and that these tg mice developed bone abnormalities strongly suggests that miR-206 directly affects osteoblast differentiation independently from any function it has during myogenic differentiation.

There was also another concern that miR-206 was expressed only in myogenic cells and inhibited osteoblastic genes in them. However, we observed that miR-206 was expressed in osteoblastic cells by four different experimental procedures. Moreover, the fact that the knockdown of miR-206 in osteoblasts

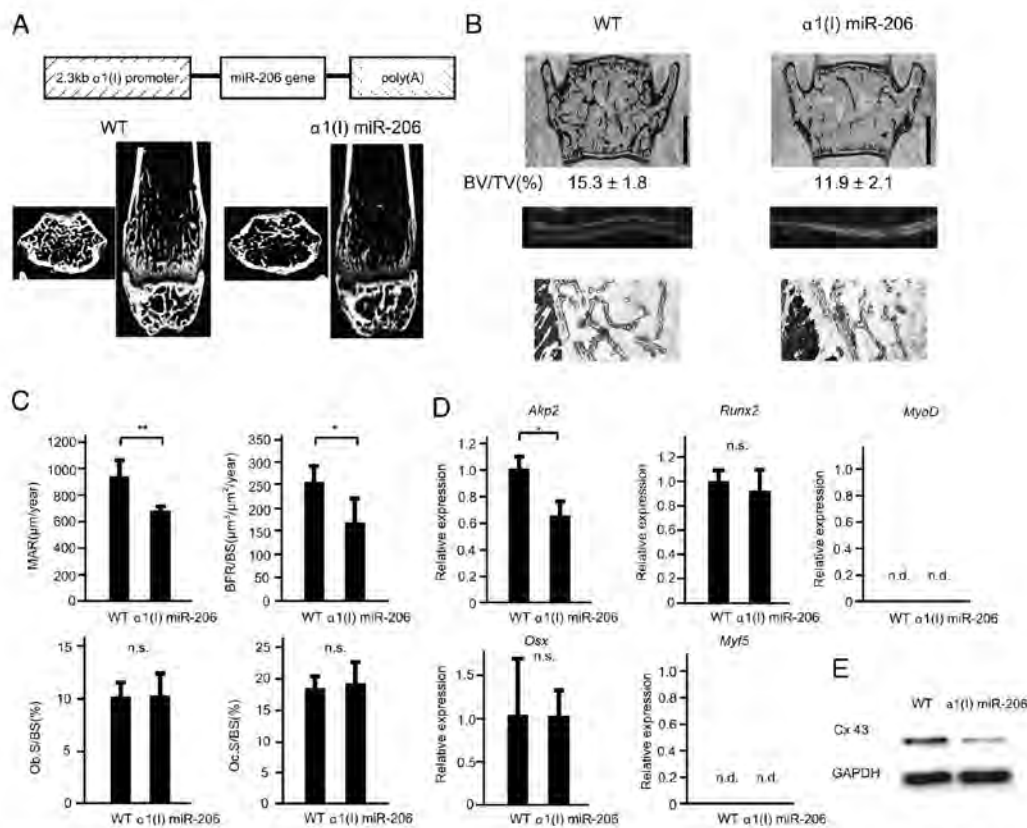


Fig. 4. Low bone mass in $\alpha 1(I)$ miR-206 tg mice due to reduced bone formation. (A) Structure of the construct for osteoblast-specific $\alpha 1(I)$ miR-206 tg mice (Top). μ CT analysis of the femurs of 6-week-old female wild-type (WT) or $\alpha 1(I)$ miR-206 tg mice (Bottom). Axial section (Left) and coronal section (Right). (B) Histological analysis of the vertebrae of 6-week-old female WT or $\alpha 1(I)$ miR-206 tg mice. Von Kossa staining (Top). Bone volume per tissue volume (BV/TV). (Scale bars, 1 mm.) The distance between the two calcein labels represents the bone formation rate (middle). Note the significant decrease in bone formation in $\alpha 1(I)$ miR-206 tg mice. Immunohistochemical staining for Troponin I (Bottom). Note the absence of Troponin I immunoreactivity (brown) in the vertebrae of $\alpha 1(I)$ miR-206 tg mice in contrast to the intense staining in skeletal muscle. (C) Histomorphometric analysis of the vertebrae of 6-week-old female mice. Mineral apposition rate (MAR), bone formation rate over bone surface area (BFR/BS), osteoblast surface area over bone surface area (Ob.S/BS), osteoclast surface area over bone surface area (Oc.S/BS). n.s., not significant. *, $P < 0.05$, **, $P < 0.01$, $n = 6-7$. (D) Gene expression in $\alpha 1(I)$ miR-206 tg mice. Quantitative RT-PCR analysis of osteoblastic genes (*Akp2*, *Runx2*, and *Osx*) and myogenic genes (*Myf5*, *MyoD*). Primary calvarial osteoblasts were isolated from WT or $\alpha 1(I)$ miR-206 tg mice and used for subsequent analyses. n.s.: not significant. *, $P < 0.05$, $n = 6$. (E) Western blot analysis of calvarial bones of 2-week-old female mice. Note the decrease in Cx43 protein expression in $\alpha 1(I)$ miR-206 tg mice.

accelerated their differentiation demonstrates that miR-206 is expressed in osteoblasts and plays a role in their differentiation.

Muscle-specific miRNAs comprise a well-defined family consisting of miR-1, miR-133, and miR-206. Interestingly, while miR-1 and -133 are expressed in *Drosophila* and vertebrates, miR-206 is not expressed in *Drosophila*. Instead, it is only expressed in vertebrates. This suggests that miR-206 evolved at a different period from miR-1 and miR-133 and thus may play a role other than the regulation of myogenic differentiation exhibited by miR-1 and miR-133.

Our observation that the inhibitory effect of miR-206 on osteoblast differentiation was rescued by the restoration of Cx43 suggests that Cx43 is a bona fide target of miR-206 in osteoblast differentiation. Indeed, while miR-206-expressing osteoblasts have a defect in osteoblast differentiation, they do not show any proliferative abnormality. This result is consistent with the normal proliferation of Cx43-deficient osteoblasts (34, 35). However, given that a miRNA can regulate multiple target genes

(8), the effect of miR-206 may not depend solely on Cx43. Indeed, although osteoblast-specific Cx43-deficient mice have a normal mineral apposition rate (34), $\alpha 1(I)$ miR-206 tg mice have a 30% decrease in the same parameter, suggesting the involvement of other molecules in miR-206-mediated bone formation defects.

Interestingly, parathyroid hormone (PTH), a well-known regulator of osteoblast differentiation, has been shown to regulate Cx43 expression through a posttranscriptional modification of Cx43 mRNA (38), and the anabolic response of PTH is attenuated in Cx43-deficient mice (34). Because miR-206 regulates both osteoblast differentiation and Cx43 mRNA stability, we tested whether PTH regulates Cx43 through a modification of miR-206 expression. However, PTH did not affect miR-206 expression.

It is interesting that miR-206 is strongly expressed in perichondrium, whereas its expression in trabecular bone is less (Fig. 1F). Considering that osteoblasts are derived from immature

osteoprogenitor cells located in the perichondrium (39), strong expression of miR-206 in the perichondrium suggests that miR-206 may work to keep osteoblast immature and decrease of miR-206 expression is important for proper osteoblastic differentiation, which is in agreement with our *in vitro* observations. Currently, the molecular mechanism accounting for the down-regulation of miR-206 expression during osteoblast differentiation is unknown. Because miR-206 is expressed in myogenic (24–28), adipocytic (40), and osteoblastic cells, all of mesenchymal origin, and miR-206 regulates both myogenic and osteoblastic differentiation, it is tempting to hypothesize that transcription factors involved in the differentiation of mesenchymal stem cells into specific cell lineages also regulate miR-206 expression. In this context, myogenic factors were shown to bind the upstream sequences of miR-206 (26). Therefore, it is possible that essential transcription factors for osteoblast differentiation, such as Runx2 and Osterix, also regulate miR-206 expression. Indeed, there are many putative binding sites for these factors in the sequence upstream of miR-206.

In conclusion, we demonstrated a regulatory role of miRNA in osteoblast differentiation *in vivo*. From a clinical point of view, inhibiting miRNA expression (41) may lead to therapies for bone degenerative diseases such as osteoporosis.

Materials and Methods

Cell Culture, Microarrays, Alkaline Phosphatase Assay, and Dual-Luciferase Reporter Assay. Primary osteoblast and C2C12 cells were cultured and alkaline phosphatase activity (Wako, LabAssay ALP) was measured as previously described (42). Microarray analysis was performed as previously described (23).

The activities of luciferase were determined by the dual-luciferase reporter assay (Promega). Further details are provided in the *SI Text*.

Cloning and Gene Expression. Genomic fragments of miR-206 precursors were amplified by PCR. miRNA expression was detected by an RNase protection assay using a mirVANA miRNA kit (Ambion) or quantitative RT-PCR with Mx3000P (Stratagene). Northern blot analysis was performed as previously reported (43). 3'-UTR of Cx43 was subcloned into downstream of the luciferase gene for Cx43-3'-UTR reporter construction.

Western Blot Analysis, Immunohistochemistry, and *In Situ* Hybridization. Western blot analysis and immunohistochemistry were performed according to a standard protocol (42). *In situ* hybridization was performed using DIG labeled probe [miR-206, miR-scramble and $\alpha 1(I)$ collagen] and 35 S-labeled riboprobe (Runx2) as reported in ref. 44 with modifications. Further details are provided in the *SI Text*.

Transgenic Mice, Histology, and Histomorphometry. The genomic fragment of the miR-206 precursor was cloned into a plasmid containing a 2.3-kb $\alpha 1(I)$ collagen promoter and microinjected as described in ref. 37. We performed histomorphometric analysis using the Osteomeasure System (Osteometrics) as described in ref. 42. Further details are provided in the *SI Text*.

Statistics. All data are presented as means \pm SE. ($n \geq 6$). We performed statistical analysis by Student's *t* test, and $P < 0.05$ was considered statistically significant.

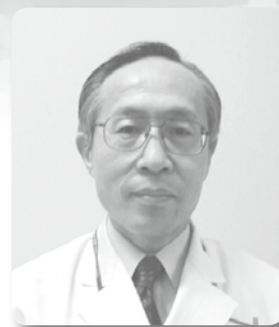
ACKNOWLEDGMENTS. We thank Dr. Gerard Karsenty for discussion and Takako Usami for technical assistance. This work was supported by the Japan Society for the Promotion of Science grants (to Y.A., K.S., and S.T.) and Uehara Memorial Foundation grant (to S.T.).

- Karsenty G, Kronenberg HM, Settembre C (2009) Genetic control of bone formation. *Annu Rev Cell Dev Biol*, in press.
- Komori T (2006) Regulation of osteoblast differentiation by transcription factors. *J Cell Biochem* 99:1233–1239.
- Khosla S, Westendorf JJ, Oursler MJ (2008) Building bone to reverse osteoporosis and repair fractures. *J Clin Invest* 118:421–428.
- Rosen CJ (2005) Clinical practice. Postmenopausal osteoporosis. *N Engl J Med* 353:595–603.
- Sambrook P, Cooper C (2006) Osteoporosis. *Lancet* 367:2010–2018.
- Fianchini RT, Ge C, Xiao G, Roca H, Jiang D (2007) Transcriptional regulation of osteoblasts. *Ann N Y Acad Sci* 1116:196–207.
- Venter JC, et al. (2001) The sequence of the human genome. *Science* 291:1304–1351.
- Robert O (2008) Gene regulation by transcription factors and microRNAs. *Science* 319:1785–1786.
- Klosterman WP, Plasterk RH (2006) The diverse functions of microRNAs in animal development and disease. *Dev Cell* 11:441–450.
- Stefani G, Slack FJ (2008) Small non-coding RNAs in animal development. *Nat Rev Mol Cell Biol* 9:219–230.
- Mattick JS (2001) Non-coding RNAs: The architects of eukaryotic complexity. *EMBO Rep* 2:986–991.
- Mattick JS, Makunin IV (2006) Non-coding RNA. *Hum Mol Genet* 15:R17–29.
- Li Z, et al. (2008) A microRNA signature for a BMP2-induced osteoblast lineage commitment program. *Proc Natl Acad Sci USA* 105:13906–13911.
- Luzi E, et al. (2008) Osteogenic differentiation of human adipose tissue-derived stem cells is modulated by the miR-26a targeting of the SMAD1 transcription factor. *J Bone Miner Res* 23:287–295.
- Mizuno Y, et al. (2008) miR-125b inhibits osteoblastic differentiation by down-regulation of cell proliferation. *Biochem Biophys Res Commun* 368:267–272.
- Kobayashi T, et al. (2008) Dicer-dependent pathways regulate chondrocyte proliferation and differentiation. *Proc Natl Acad Sci USA* 105:1949–1954.
- Davis BN, Hilyard AC, Lagna G, Hata A (2008) SMAD proteins control DROSHA-mediated microRNA maturation. *Nature* 454:56–61.
- Tuddenham L, et al. (2006) The cartilage specific microRNA-140 targets histone deacetylase 4 in mouse cells. *FEBS Lett* 580:4214–4217.
- Harfe BD, McManus MT, Mansfield JH, Hornstein E, Tabin CJ (2005) The RNaseIII enzyme Dicer is required for morphogenesis but not patterning of the vertebrate limb. *Proc Natl Acad Sci USA* 102:10898–10903.
- Watanabe T, et al. (2008) Dnm3os, a non-coding RNA, is required for normal growth and skeletal development in mice. *Dev Dyn* 237:3738–3748.
- Sugatani T, Hruska KA (2007) MicroRNA-223 is a key factor in osteoclast differentiation. *J Cell Biochem* 101:996–999.
- Katagiri T, et al. (1994) Bone morphogenetic protein-2 converts the differentiation pathway of C2C12 myoblasts into the osteoblast lineage. *J Cell Biol* 127:1755–1766.
- Hohjoh H, Fukushima T (2007) Marked change in microRNA expression during neuronal differentiation of human teratocarcinoma NTera2D1 and mouse embryonal carcinoma F19 cells. *Biochem Biophys Res Commun* 362:360–367.
- Kim HK, Lee YS, Sivaprasad U, Malhotra A, Dutta A (2006) Muscle-specific microRNA miR-206 promotes muscle differentiation. *J Cell Biol* 174:677–687.
- Pollitz JC, Zhang F, Pederson T (2006) MicroRNA-206 colocalizes with ribosome-rich regions in both the nucleolus and cytoplasm of rat myogenic cells. *Proc Natl Acad Sci USA* 103:18957–18962.
- Rao PK, Kumar RM, Farkhondeh M, Baskerville S, Lodish HF (2006) Myogenic factors that regulate expression of muscle-specific microRNAs. *Proc Natl Acad Sci USA* 103:8721–8726.
- Rosenberg MI, Georges SA, Asawachalcharn A, Analau E, Tapscott SJ (2006) MyoD inhibits *Irf1* and *Utrn* expression by inducing transcription of miR-206. *J Cell Biol* 175:77–85.
- Sweetman D, et al. (2008) Specific requirements of MRFs for the expression of muscle specific microRNAs, miR-1, miR-206, and miR-133. *Dev Biol* 321:491–499.
- Sambrook J, Fritsch EF, Maniatis T (1989) In *Molecular Cloning: A Laboratory Manual* (Cold Spring Harbor Laboratory, Cold Spring Harbor, NY), pp 7.2–7.87.
- Reue K (1998) mRNA quantitation techniques: Considerations for experimental design and application. *J Nutr* 128:2038–2044.
- McKinsey TA, Zhang CL, Olson EN (2002) Signaling chromatin to make muscle. *Curr Opin Cell Biol* 14:763–772.
- Krek A, et al. (2005) Combinatorial microRNA target predictions. *Nat Genet* 37:495–500.
- Lewis BP, Burge CB, Bartel DP (2005) Conserved seed pairing, often flanked by adenosines, indicates that thousands of human genes are microRNA targets. *Cell* 120:15–20.
- Chung DJ, et al. (2006) Low peak bone mass and attenuated anabolic response to parathyroid hormone in mice with an osteoblast-specific deletion of connexin43. *J Cell Sci* 119:4187–4198.
- Lecanda F, et al. (2000) Connexin43 deficiency causes delayed ossification, craniofacial abnormalities, and osteoblast dysfunction. *J Cell Biol* 151:931–944.
- Tiso N, et al. (1997) Fine mapping of five human skeletal muscle genes: alpha-tropomyosin, beta-tropomyosin, troponin-I slow-twitch, troponin-I fast-twitch, and troponin-C fast. *Biochem Biophys Res Commun* 230:347–350.
- Dacquin R, Starbuck M, Schinke T, Karsenty G (2002) Mouse alpha1(I)-collagen promoter is the best known promoter to drive efficient Cre recombinase expression in osteoblast. *Dev Dyn* 224:245–251.
- Mitchell JA, Ou C, Chen Z, Nishimura T, Lye SJ (2001) Parathyroid hormone-induced up-regulation of connexin-43 messenger ribonucleic acid (mRNA) is mediated by sequences within both the promoter and the 3' untranslated region of the mRNA. *Endocrinology* 142:907–915.
- Caplan AL, Pechak DG (1987) In *Bone and Mineral Research*, ed Peck WA (Elsevier, New York), pp 117–183.
- Walden TB, Timmons JA, Keller P, Nedergaard J, Cannon B (2009) Distinct expression of muscle-specific microRNAs (myomirs) in brown adipocytes. *J Cell Physiol* 218:444–449.
- Care A, et al. (2007) MicroRNA-133 controls cardiac hypertrophy. *Nat Med* 13:613–618.
- Sato S, et al. (2007) Central control of bone remodeling by neuromedin U. *Nat Med* 13:1234–1240.
- Saito K, et al. (2006) Specific association of Piwi with rasiRNAs derived from retrotransposon and heterochromatic regions in the Drosophila genome. *Genes Dev* 20:2214–2222.
- Obernosterer G, Martinez J, Alenius M (2007) Locked nucleic acid-based *in situ* detection of microRNAs in mouse tissue sections. *Nat Protoc* 2:1508–1514.

膠原病・リウマチ内科学

宮坂 信之

医歯学総合研究科・生体環境応答学系専攻
臨床免疫学・教授



1) 研究の課題名

1. 関節リウマチにおける chemerin/ChemR23 の発現: これらをターゲットとした新規治療法の開発

Chemerin は近年同定されたケモカイン様分子である。ChemR23 は chemerin のレセプターであり、マクロファージや樹状細胞に発現し、炎症局所への抗原提示細胞の遊走に関わることが報告されている。我々は、関節リウマチ (RA) 滑膜組織における chemerin および ChemR23 の発現を解析した。免疫組織染色にて、chemerin は RA 滑膜表層細胞および血管内皮細胞に、ChemR23 は RA 滑膜表層および表層下領域に広く発現していた。また、RA 滑膜組織より樹立した線維芽細胞様滑膜細胞株の培養上清に chemerin 産生がみられ、TNF- α および IFN- γ 刺激により産生亢進を認めた。マウスコラーゲン誘導関節炎 (CIA) 滑膜細胞においても ChemR23 の発現が認められた。さらに、chemerin 由来 C15 ペプチドを、CIA マウスに対して第一回免疫時から5週間連日腹腔内投与することで、関節炎の程度と骨破壊は有意に抑制された。また C15 の前処置により、chemerin によるマウス腹腔内マクロファージの ERK1/2 リン酸化が抑制された。C15 は chemerin 刺激を阻害していると考えられる。chemerin/ChemR23 は RA および CIA 滑膜に発現し、病態形成において重要な役割を担っている可能性がある。この pathway が、RA 新規治療法の新たなターゲットとなることが期待される。

Chemerin and ChemR23 expression in rheumatoid arthritis: the therapeutic implication of the pathway

Chemerin is a novel chemoattractant protein that was identified as a ligand for ChemR23. It is reported that chemerin has a chemoattractant ability for macrophages and dendritic cells to the inflammatory site. In this study, we analyzed the expression of chemerin and ChemR23 in the synovium of rheumatoid arthritis (RA), and examined the effect of chemerin-derived peptide (C15) on murine

collagen-induced arthritis (CIA). Chemerin and ChemR23 were expressed in the RA synovial tissue. Chemerin was expressed by unstimulated RA fibroblast-like synoviocytes, and the production was upregulated by stimulation with TNF- α and IFN- γ . ChemR23 was also expressed by the synoviocyte from CIA. Treatment with synthesized C15 peptide significantly reduced the arthritis score and bone erosion of CIA compared to control peptide. Pretreatment of C15 peptide suppressed chemerin-induced ERK1/2 phosphorylation of mouse peritoneal macrophage. These results indicate that chemerin/ChemR23 pathway plays an important role for the pathogenesis of RA, and the pathway could be a therapeutic target for new RA treatment.

2. 関節リウマチの病態形成における CXCR7 の役割について

CXCL12 (SDF-1) は関節リウマチ (RA) の滑膜組織で産生が亢進し、CXCR4 を介して炎症細胞の滑膜への浸潤・集簇、炎症細胞の活性化、血管新生などに重要な役割を担っていると考えられている。近年 CXCL12 の新規レセプターとして CXCR7 が同定された。そこで、我々は滑膜組織における CXCR7 の発現、その機能について解析した。免疫染色にて、CXCR7 は RA 滑膜組織の血管内皮細胞に発現していた。変形性関節症の滑膜にはほとんど発現がみられなかった。正常ヒト臍帯静脈内皮細胞 (HUVECs) においても CXCR4, CXCR7 mRNA は発現し、CXCR7 mRNA 発現は IL-1 β 刺激により著明に亢進した。血管新生能を tube formation assay で解析すると、CXCL12 は HUVECs の管腔形成を亢進したが、CXCR4 阻害剤、CXCR7 阻害剤いずれによってもその亢進は抑制された。マウスコラーゲン関節炎に対し CXCR7 阻害剤を投与すると、関節炎の程度、骨破壊が抑制された。また滑膜組織中の血管数も減少した。CXCR7 は RA の病態形成において重要な役割を担っている可能性があり、特に血管新生抑制を標的とした RA の新たな治療ターゲットとなることが期待される。

Pathogenic Role of CXCR7 in Rheumatoid Arthritis
Interaction between CXCL12 (SDF-1) and the receptor, CXCR4, plays an important role in the pathogenesis of rheumatoid arthritis (RA). Recently, CXCR7 was identified as an alternative receptor for CXCL12. We analyzed CXCR7 expression in the synovium, and examined the pathogenic role in RA. CXCR7 was expressed on endothelial cells in the RA synovium. CXCR7 mRNA was detected in HUVECs, and the expression was upregulated by stimulation with IL-1 β . CXCL12 promoted tube formation by HUVECs. However, the tube formation was inhibited either by CXCR7 antagonist or CXCR4 antagonist. Treatment with CXCR7 antagonist reduced arthritis score and bone destruction of ankle joint in murine collagen-induced arthritis (CIA). The number of vessels in the synovial tissue was also reduced by the treatment. These results indicate that CXCR7 plays an important role for angiogenesis in RA synovium. CXCR7 could be a target molecule in novel therapies for RA by blocking angiogenesis.

3. レチノイドによる関節炎抑制効果

ビタミンAの活性体であるレチノイドには、Th1, Th17細胞への分化抑制、Th2, Treg細胞への分化亢進能があることが報告され、Th1, Th17に関連する疾患に対する抑制効果が期待されている。我々は、レチノイドの一種であるAm80が筋炎モデルマウスを抑制することを見出した。そこで、Am80による関節炎への影響を解析した。マウスコラーゲン誘導関節炎は、day 1およびday 22にコラーゲン免疫をすることにより発症するが、Am80を免疫初日 (day 1) から経口投与すると関節炎スコアは抑制された。また足関節の骨破壊も抑制された。マウス脾細胞をコラーゲン刺激しサイトカイン産生能を解析すると、IL-17産生は著明に低下したが、IFN- γ 産生は増加した。また脾臓CD4 T細胞のFoxp3陽性細胞の割合は有意に減少していた。血清中の抗コラーゲン抗体産生も抑制された。一方、初回免疫2週間からのAm80投与では関節炎抑制効果はみられなかった。コラーゲン刺激した脾細胞からのIL-17, IFN- γ 産生も有意な変化を認めなかった。脾臓CD4 T細胞のFoxp3陽性細胞の割合はday 1からのAm80投与と同様に有意に減少していた。血清中の抗コラーゲン抗体産生も抑制されていた。Am80はTh細胞分化の制御、抗体産生などに関与し、関節炎抑制効果があると考えられる。

Retinoid ameliorates collagen-induced arthritis with modulating Th cell development and antibody production
Retinoids are compounds that have biological activities of vitamin A. Recent studies indicate that retinoids promote differentiation into Th2 cells and Treg cells,

and suppress Th1 and Th17 cell differentiation. In this study, we examined the effects of a synthetic retinoid, Am80, on collagen-induced arthritis (CIA), and also on Th phenotype development and antibody production. We induced murine CIA by immunization with bovine type II collagen at days 1 and 22. When Am80 was orally administrated from day 1, clinical arthritis score and radiographic findings were significantly reduced. Moreover, Am80 decreased IL-17 production by collagen-stimulated splenic T cells. However, IFN- γ production was upregulated by the treatment. Frequency of Foxp3-positive in CD4+ spleen T cell was decreased by the Am80 treatment. Production of serum anti-collagen Abs was also decreased. When we treat the mice from day 15, arthritis score was not changed. IL-17 and IFN- γ production was not changed by the treatment. Proportion of Foxp3-expressing CD4+ splenic T cells was decreased, as similar to the mice treated from day 1. Production of serum anti-collagen Abs was also decreased. Am80 might reduce arthritis by regulation of Th development and antibody production.

4. 関節リウマチ新規治療法の開発

Development of new therapeutic approaches to rheumatoid arthritis

関節リウマチに対する抗サイトカイン療法が実用化され治療の革命がもたらされたものの、易感染性などの副作用があり、かつ疾患完全制圧に至らない。今年度は、triggering receptor expressed on myeloid cell (TREM)-1を阻害することで感染防御能を落とさない程度に炎症性サイトカインを抑制することができ、この治療法で関節リウマチ動物モデルを治療しうることを見いだした。Triggering receptor expressed on myeloid cells (TREM)-1 is a transmembrane receptor inducible on monocytes/macrophages and neutrophils. It has been known that it is involved in human and animal diseases related to bacterial infections. We have found its involvement in pathology of rheumatoid arthritis (RA). TREM-1 blockade exerted therapeutic effects on collagen-induced arthritis, a murine model of RA. Since TREM-1 blockade does not impair host defense against bacterial infections significantly, it should be a new anti-rheumatic approach that is safer than presently available immunosuppressive treatment.

5. 炎症性筋難病の克服

成人筋疾患の代表は多発性筋炎・皮膚筋炎であるが、その病態解明や治療法開発は遅れていた。かかる中、我々は、多発性筋炎の病態に極めて類似するマウスモデルの開発に成功し (Cタンパク誘導性筋炎:CIM)、今年度は、近年、自己免疫に重要とされるIL-6/17経路の関与につ

いて探索した。IL-6や17は、筋組織内炎症細胞に発現していた。IL-6変異マウスはCIMに抵抗性であったが、IL-17変異マウスは感受性であった。一方、抗IL-6受容体抗体による治療は奏功した。IL-6阻害は、IL-17産生T細胞分化を阻害して自己免疫疾患に奏功すると考えられてきたが、必ずしもこれがすべての自己免疫に当てはまるわけではないことを示した（発表論文は、Nature Review Rheumatologyで速報された）。

A new murine model of PM, C protein-induced myositis (CIM) was examined for involvement of an interleukin-6 (IL-6) /IL-17A pathway. IL-6 and 17 were expressed by mononuclear cells infiltrating in the muscles. IL-6-null mice developed myositis with significantly lower incidence and milder severity than wild type mice. In contrast, IL-17A-null mice were as susceptible to CIM as wild-type mice. Intraperitoneal administration of anti-IL-6R monoclonal antibodies ameliorated CIM both preventively and therapeutically. These findings indicate that IL-6 is critically involved in the development of CIM. Although many other autoimmune models require IL-6 for differentiation of pathogenic T cells producing IL-17A, IL-17A was dispensable in CIM. IL-6 blockade is potentially a new approach to the treatment of autoimmune myositis, via processes distinct from interference in the IL-6/IL-17A pathway.

3) 研究内容の英文要約

Main target of our research is rheumatoid arthritis (RA) which causes destruction of the cartilage and bones resulting in joint dysfunction. Another target of our study is polymyositis/dermatomyositis (PM/DM) which greatly affects motor functions of patients. Both diseases are refractory to conventional treatments and significantly disturb activity of daily living (ADL) and quality of life (QOL) of patients. We tried to elucidate their pathophysiology at molecular levels and to develop new modes of treatment. We found that interaction between chemokines and corresponding receptors; i.e. chemerin (Chem) /ChemR23 and CXCL12 (SDF-1) /CXCR7, played important roles in the pathophysiology of arthritis and inhibition of their interaction ameliorated murine models of RA. Blockade of TREM-1 (triggering receptor expressed on myeloid cells-1) and administration of Am80, a synthetic retinoid, also exerted therapeutic effects in collagen-induced arthritis, a murine model of RA. We also demonstrated that IL-6 blockade is potentially a new approach to the treatment of autoimmune myositis.

4) 本事業に関連して世界的な拠点形成に向けて改善・整備されたこと

A (研究拠点体制)

GCOE内の研究ネットワークを活用して相互の情報交換に可能となった。

B (研究教育環境)

本年11月に旧来の研究室から新たな研究教育棟に移転し、研究スペースが拡充されたことによって研究教育環境が著しく改善された。

C (人材確保)

米国スタンフォード大学医学部に留学中だった岩井秀之を国際PIシャベロンとしてリクルートし、人材確保を行った。

D (人材育成)

現在、大学院生を1名AISSとして養成中である。

5) GCOE事業を推進するにあたって力を入れた点

global standardに合致し、これを凌駕する質の高い研究を推進するよう努力した。

6) 英文原著論文

1. Nishimoto N, Miyasaka N, Yamamoto K, Kawai S, Takeuchi T, Azuma J, Kishimoto T. Study of Active controlled Tocilizumab monotherapy for Rheumatoid Arthritis Patients with an Inadequate Response to Methotrexate (SATORI) : significantly reduction in disease activity and serum vascular endothelial growth factor by IL-6 receptor inhibition therapy. *Mod. Rheumatol.* 19:12-19, 2009
2. Hashimoto J, Garner P, Heijde D. van der, Miyasaka N, Yamamoto K, Kawai S, Takeuchi T, Yoshikawa H, Nishimoto N. A combination of biochemical markers of cartilage and bone turnover, radiographic damage and body mass index to predict progression of joint destruction in patients with rheumatoid arthritis treated with disease modifying anti-rheumatic drugs. *Mod. Rheumatol.* 19:273-282, 2009
3. Komano Y, Harigai M, Koike R, Sugiyama H, Ogawa J, Saito K, Sekiguchi N, Inoo M, Onishi I, Ohashi H, Amamoto F, Miyata M, Ohtsubo H, Hiramatsu K, Iwamoto M, Minota S, Matsuoka N, Kageyama G, Imaizumi K, Tokuda H, Okochi Y, Kudo K, Tanaka Y, Takeuchi T, Miyasaka N. Pneumocystis jiroveci pneumonia in patients with rheumatoid arthritis treated with infliximab : a retrospective review and case-control study of 21 patients. *Arthritis & Rheumatism* 61(3):305-312, 2009

4. Watanabe K, Nanki T, Sugihara T, Miyasaka N. A case of polyarteritis nodosa with periurethral aseptic abscesses and testicular lesions. *Clin. Exp. Rheumatol.* 26:1113-1115, 2009
5. Nii T, Kubota T, Nanki T, Komano Y, Harigai M, Kohsaka H, Hirose W, Nagasaka K, Sakurai T, Miyasaka N. Reevaluation of antibody titers 1 year after influenza vaccination in patients with rheumatoid arthritis receiving TNF blockers. *Mod. Rheumatol. LETTER* 19:216-218, 2009
6. Nonomura Y, Mizoguchi F, Suzuki A, Nanki T, Kato H, Miyasaka N, Kohsaka H. Hypoxia-induced abrogation of contact-dependent inhibition of rheumatoid arthritis synovial fibroblast proliferation. *J. Rheumatol.* 36(4):698-705, 2009
7. Kishi J, Nanki T, Watanabe K, Takamura A, Miyasaka N. A case of rituximab-induced interstitial pneumonitis observed in systemic lupus erythematosus. *Letters to Editor Rheumatology* 48:447-448, 2009
8. Koike R, Harigai M, Atsumi T, Amano K, Kawai S, Saito K, Saito T, Yamamura M, Matsubara T, Miyasaka N. Japan college of rheumatology 2009 guidelines for the use of Tocilizumab, a humanized anti-interleukin-6 receptor monoclonal antibody, in rheumatoid arthritis. *Mod. Rheumatol.* 19:351-357, 2009
9. Kubota T, Fukuya Y, Hashimoto R, Kanda T, Suzuki H, Okamura Y, Nanki T, Miyasaka N, Umezawa K. Possible involvement of chemokine-induced platelet activation in thrombophilic diathesis of antiphospholipid syndrome. *Ann. N.Y. Acad. Sci.* 1173:137-145, 2009
10. ©Ohyanagi N, Ishido M, Suzuki F, Kaneko K, Kubota T, Miyasaka N, Nanki T. Retinoid ameliorates experimental autoimmune myositis, with modulation of th cell differentiation and antibody production in vivo. *Arthritis & Rheum.* 60(10):3118-3127, 2009
11. Nishimoto N, Miyasaka N, Yamamoto K, Kawai S, Takeuchi T, Azuma J. Long-term safety and efficacy of tocilizumab, an anti-IL-6 receptor monoclonal antibody, in monotherapy, in patients with rheumatoid arthritis (the STREAM study) : evidence of safety and efficacy in a 5-year extension study. *Ann. Rheum. Dis.* 68:1580-1584, 2009
12. Ochi S, Nanki T, Kaneko H, Honne K, Miyazaki Y, Komano Y, Miyasaka N. Successful treatment of ankylosing spondylitis coexisting with pulmonary sarcoidosis by infliximab. *Clin. Experimental Rheumatol.* 27:698-699, 2009
13. ©Murakami Y, Akahoshi T, Aoki N, Toyomoto M, Miyasaka N, Kohsaka H. Triggering receptor expressed on myeloid cells-1 as a new therapeutic target of rheumatoid arthritis. *Arthritis Rheum* 60 (6), 1615-1623, 2009
14. ©Okiyama N, Sugihara T, Iwakura Y, Yokozeki H, Miyasaka N, Kohsaka H. Therapeutic effects of IL-6 blockade on a murine model of polymyositis that does not require IL-17A. *Arthritis Rheum* 60 (8), 2505-2512, 2009
15. ©Nanki T, Takada K, Komano Y, Morio T, Kanegane H, Nakajima A, Lipsky Peter E, Miyasaka N. Chemokine receptor expression and functional effects of chemokines on B cells: Implication in the pathogenesis of rheumatoid arthritis. *Arthritis Res. Ther.* 11(5): R149, 2009.
16. Souto-Carneiro M M, Mahadevan V, Takada K, Fritsch-Stork R, Nanki T, Brown M, Fleisher T A, Wilson M, Goldbach-Mansky R, Lipsky Peter E. Alterations in peripheral blood memory B cells in patients with active rheumatoid arthritis are dependent on the action of tumour necrosis factor. *Arthritis Res. Ther.* 11(3): R84, 2009.
17. Takahashi N, Matsumoto K, Saito H, Nanki T, Miyasaka N, Kobata T, Azuma M, Lee Sang-Kyou, Mizutani S, Morio T. Impaired CD4 and CD8 effector function and decreased memory T cell populations in ICOS-deficient patients. *J. Immunol.* 182(9): 5515-5527, 2009.
18. Hirose W, Nishikawa K, Hirose M, Nanki T, Sugimoto H. Response of early active rheumatoid arthritis to tumor necrosis factor inhibitors: evaluation by magnetic resonance imaging. *Mod. Rheumatol.* 19(1): 20-26, 2009.
19. ©Kohsaka H. Current insights in polymyositis and dermatomyositis. *Clin Exp Neuroimmunol*
20. Nonomura Y, Miyabe Y, Tanaka M, Tsubata R, Nanki T, Harigai M, Miyasaka N. Prominent splenic microcalcifications in a patient with systemic lupus erythematosus complicated with antiphospholipid syndrome. *J. Clin. Rheumatol.*
21. Takeuchi T, Miyasaka N, Inoue K, Abe T, Koike T. Impact of trough serum level on radiographic and clinical response to infliximab plus methotrexate in patients with theumatoid arthritis: results from the RISING study. *Mod. Rheumatol.*
22. Miyasaka N, Kawai S, Hashimoto H. Efficacy and safety of tacrolimus for lupus nephritis: a placebo-controlled double-blind multicenter study. *Mod. Rheumatol.*

7) 著書

1. 骨・関節－a.関節リウマチ・骨粗鬆症.宮坂信之 「炎症・再生医学事典」 松島綱治、西脇徹編集 朝倉書店 pp243-246, 2009
2. 総論 生物学的製剤とは?—定義とその種類 宮坂信之 「正しい生物学的製剤の使い方—関節リウマチ—」 宮坂信之の編 医薬ジャーナル社
3. Felty症候群.「今日の治療指針 第6版」金澤一郎、永井良三編 医学書院
4. 全身性エリテマトーデス (SLE) 病態・臨床所見・

診断.宮坂信之「リウマチ病学テキスト」日本リウマチ財団・日本リウマチ学会編集

5. 関節リウマチ (RA) における NSAIDs の使い方.野々村美紀、宮坂信之.「NSAIDs の選び方、使い方ハンドブック」佐野統編 羊土社
6. H. Kohsaka Recent Research Developments in Rheumatic Diseases - Polymyositis / dermatomyositis Recent Research Developments in Rheumatology Editor: Antonio La Cava Transworld Research Network 166-184 (total pages 184) 2009
7. 上阪 等 ステロイド薬の適応と副作用 「よくわかる関節リウマチのすべて」 宮坂信之編集 179-185 頁 永井書店 2009年

8) 平成21年度までの自己評価

研究目標を筋骨格系を侵す関節リウマチと多発性筋炎・皮膚筋炎に絞り、その病態形成に関する分子機構の解析を行った結果、あらたなケモカインおよびケモカインレセプター、細胞表面分子、サイトカインなどの関与を明らかにすることができ、いずれも現在、peer-review journals に投稿中あるいは受理をされている。したがって、当初の目標は十分に達成できたものとする。

9) 学会発表 (英文)

1. Naoko Okiyama, Takehiko Sugihara, Hiroo Yokozeki, Nobuyuki Miyasaka, Hitoshi Kohsaka. Effector CD8 T cells and local innate immunity need to act in concert for development of autoimmune myositis. Keystone Symposia, Banff, Alberta, March 28-April 3, 2009
2. N. Okiyama, T. Kitajima, Y. Ito, N. Miyasaka, H. Yokozeki, H. Kohsaka. Promotion of Cutaneous Wound Healing with a Fusion Protein of Hepatocyte Growth Factor and Collagen-Binding Domain of Fibronectin., Society for Investigative Dermatology Annual Meeting, Montreal, Canada, May 8, 2009
3. Naoko Okiyama, Takehiko Sugihara, Hiroo Yokozeki, Nobuyuki Miyasaka, Hitoshi Kohsaka Effector CD8 T cells and local innate immunity need to act in concert for development of autoimmune myositis 9th World Congress on Inflammation, Tokyo, July 6-10, 2009
4. Masayasu Toyomoto, Satoshi Ishido, Nobuyuki Miyasaka, Hitoshi Kohsaka. Treatment of arthritis by anti-inflammatory effect of E3 ubiquitin ligase, c-MIR. American College of Rheumatology 73rd National Meetings, Philadelphia, Pennsylvania, October 16-21, 2009
5. Ryuji Koike, Michi Tanaka, Yukiko Komano, Fumikazu Sakai, Haruhito Sugiyama, Toshihiro Nanki, Nobuyuki

Miyasaka, Masayoshi Harigai Study Group for Tacrolimus-induced Pulmonary Injury. Tacrolimus-Induced Pulmonary Injury in Patients with Rheumatoid Arthritis. American College of Rheumatology 73rd National Meetings, Philadelphia, Pennsylvania, October 19, 2009

6. Yukiko Komano, Nobuhiro Yagi, Ikumi Onoue, Kayoko Kaneko, Nobuyuki Miyasaka Toshihiro Nanki. Arthritic Joint-Targeting siRNA/Wrapsome® as a Treatment Strategy for Rheumatoid Arthritis. American College of Rheumatology 73rd National Meetings, Philadelphia, Pennsylvania, October 18, 2009
7. Toshihiro Nanki, Aya Sato, Kaori Watanabe, Kayoko Kaneko, Yousuke Murakami, Miwako Ishido Nobuyuki Miyasaka. The Effect of Synthetic Retinoid, Am80, On T Helper Cell Development and Antibody Production in Murine Collagen-Induced Arthritis. American College of Rheumatology 73rd National Meetings, Philadelphia, Pennsylvania, October 18, 2009
8. Kaori Watanabe, Toshihiro Nanki, Kayoko Kaneko, Thomas J. Schall, Nobuyuki Miyasaka. Pathogenic Role of CXCR7 in Rheumatoid Arthritis. 9th World Congress on Inflammation, Tokyo, July 7, 2009
9. Michi Tanaka, Ryoko Sakai, Toshihiro Nanki, Nobuyuki Miyasaka, Masayoshi Harigai. Pneumocystis jiroveci Pneumonia (PCP) Associated with Etanercept in Patients with Rheumatoid Arthritis. 9th World Congress on Inflammation, Tokyo, July 7, 2009
10. Yukiko Komano, Toshihiro Nanki, Michi Tanaka, Ryoko Sakai, Ryuji Koike, Nobuyuki Miyasaka, Masayoshi Harigai, for the REAL Study Group. Analysis of serious adverse events in patients with rheumatoid arthritis under the treatment with biologics; a report from the Registry of Japanese Rheumatoid Arthritis Patients for Long-term Safety. Annual European Congress of Rheumatology, Copenhagen, Denmark 2009
11. Michi Tanaka, Ryoko Sakai, Ryuji Koike, Yukiko Komano, Toshihiro Nanki, Nobuyuki Miyasaka, Masayoshi Harigai. Pneumocystis jiroveci pneumonia associated with etanercept in patients with rheumatoid arthritis. Annual European Congress of Rheumatology, Copenhagen, Denmark 2009
12. Toshihiro Nanki, Aya Sato, Kaori Watanabe, Kayoko Kaneko, Miwako Ishido, Nobuyuki Miyasaka. Retinoid ameliorates collagen-induced arthritis with modulating Th cell development and antibody production. Keystone symposia, TH17 Cells in Health and Disease. バンクーバー、カナダ。2009/2。

10) 学会発表 (和文)

1. 沖山奈緒子, 杉原毅彦, 宮坂信之, 上阪 等 自己免疫性筋炎発症には自己反応性T細胞と局所自然免疫の

- 協調が必要である 第53回 日本リウマチ学会総会・学術集会 東京 2009年4月23-26日
2. 沖山奈緒子, 杉原毅彦, 宮坂信之, 上阪 等 新たな多発性筋炎モデルにみる獲得免疫と自然免疫の協調関係 第1回筋炎ワークショップ 東京 2009年4月11日
 3. 細矢 匡, 高田 和生, 溝口 史高, 鈴木 文仁, 南木敏宏, 上阪 等, 宮坂 信之 臨床的にTRAPS (TNF receptor-associated periodic syndrome) が疑われトシリズマブが有効であった1例 第53回 日本リウマチ学会総会・学術集会 東京 2009年4月23-26日
 4. 沖山奈緒子, 杉原毅彦, 横関博雄, 宮坂信之, 上阪 等 新たな多発性筋炎モデルにみる獲得免疫と自然免疫の協調関係 第37回日本臨床免疫学会総会 東京 2009年11月13日-15日
 5. 豊本雅康, 石戸 聡, 宮坂信之, 上阪 等 E3ユビクチンリガーゼc-MIRの抗炎症効果による関節炎治療 第5回骨免疫ワークショップ 東京 2009年11月27日
 6. 豊本雅康, 石戸 聡, 宮坂信之, 上阪 等 E3ユビクチンリガーゼc-MIRの抗炎症効果による関節炎治療 第39回日本臨床免疫学会総会・学術集会 大阪 2009年12月2日-3日
 7. 南木敏宏. シンポジウム1「膠原病の新展開」PM/DM。第20回日本リウマチ学会関東支部学術集会 横浜 2009年12月6日
 8. Aya Sato, Kaori Watanabe, Kayoko Kaneko, Yousuke Murakami, Nobuyuki Miyasaka, Toshihiro Nanki. The effect of synthetic retinoid, Am80, on T helper cell development and antibody production in murine collagen-induced arthritis. 第39回日本免疫学会総会。大阪。2009/12/3。
 9. Kayoko Kaneko, Kaori Watanabe, Nobuyuki Miyasaka, Toshihiro Nanki. Chemerin and ChemR23 expression in rheumatoid arthritis: the therapeutic implication of the pathway. 第39回日本免疫学会総会 大阪 2009年12月4日
 10. 駒野有希子, 八木信宏, 尾上育美, 金子佳代子, 宮坂信之, 南木敏宏 siRNA/WrapsomeRを用いた関節リウマチに対する新規治療法の開発 第37回日本臨床免疫学会 東京 2009年11月13日
 11. 尾上育美, 南木敏宏, 長坂憲治, 白井俊純, 針谷正祥, 赤星透, 宮坂信之, 窪田哲朗 重症細菌感染症に際してCRPが上昇せず抗IL-6自己抗体が検出された症例 日本臨床検査医学会学術集会 札幌 2009年8月
 12. 細矢匡, 南木敏宏, 尾上育美, 長坂憲治, 窪田哲朗, 針谷正祥, 赤星透, 宮坂信之 黄色ブドウ球菌による全身性多発膿瘍を認めたが, CRP陰性で抗IL-6抗体が同定された悪性関節リウマチの一例 関東リウマチ 東京 2009年6月20日
 13. 酒井良子, 駒野有希子, 田中みち, 南木敏宏, 小池竜司, 宮坂信之, 針谷正祥 関節リウマチ患者におけるメトトレキサートの安全性:8mg/週以下と8mg/週超の比較 第53回日本リウマチ学会総会 東京 2009年4月
 14. 田中みち, 酒井良子, 駒野有希子, 南木敏宏, 小池竜司, 針谷正祥, 宮坂信之 膠原病の肺合併症診断および治療法に関する後ろ向き研究 第53回日本リウマチ学会総会 東京 2009年4月
 15. 田中みち, 酒井良子, 駒野有希子, 南木敏宏, 小池竜司, 宮坂信之, 針谷正祥 エタネルセプト投与下での関節リウマチ患者におけるニューモシスチス肺炎 第53回日本リウマチ学会総会 東京 2009年4月
 16. 細矢匡, 高田和生, 溝口史高, 鈴木文仁, 南木敏宏, 上阪 等, 宮坂 信之 臨床的にTRAPS (TNF receptor-associated periodic syndrome) が疑われトシリズマブが有効であった1例 第53回日本リウマチ学会総会 東京 2009年4月
 17. 駒野有希子, 南木敏宏, 八木信宏, 尾上育美, 金子佳代子, 宮坂信之 siRNA/wrapped liposome複合体を用いた関節リウマチに対する新規治療法の開発 第53回日本リウマチ学会総会 東京 2009年4月
 18. 鈴木文仁, 南木敏宏, 今井俊夫, 廣畑俊成, 宮坂信之 多発性筋炎/皮膚筋炎におけるCX3CL1 (fractalkine) 発現の解析 第53回日本リウマチ学会総会 東京 2009年4月
 19. 渡部香織, 南木敏宏, 金子佳代子, 宮坂信之 関節リウマチの病態形成におけるCXCR7の役割について 第53回日本リウマチ学会総会 東京 2009年4月

11) 外部資金の獲得状況

1. 宮坂信之:厚生労働科学研究費補助金(治験推進研究事業)「多発性筋炎・皮膚筋炎に合併する間質性肺炎に対するタクロリムスの臨床試験」の調整・管理に関する研究」研究代表者 平成18年度-平成21年度(継続) 研究費総額261,403千円
2. 宮坂信之:厚生労働科学研究費補助金(治験推進研究

- 事業)「治験の実施に関する研究【タクロリムス水和物】」 研究代表者 平成18年度-平成21年度(継続) 研究費総額3850千円
3. 宮坂信之:厚生労働科学研究費補助金(免疫・アレルギー疾患等予防・治療研究事業)「膠原病の生命予後規程因子である肺合併症の診断及び治療法の再評価と新規開発に関する研究」 研究代表者 平成19年度-平成21年度 研究費総額111,000千円
4. 宮坂信之:厚生労働科学研究費補助金(免疫アレルギー疾患等予防・治療研究事業)「関節リウマチの関節破壊ゼロを目指す治療指針の確立、及び根治・修復療法の開発に関する研究」 研究分担者 平成20年度-21年度(継続) 研究費総額5,000千円
5. 宮坂信之:厚生労働科学研究費補助金(難治性疾患克服研究事業)「難治性疾患克服研究の評価ならびに研究の方向性に関する研究」 研究分担者 平成21年度(継続) 研究費総額2,000千円
6. 宮坂信之:厚生労働科学研究費補助金(難治性疾患克服研究事業)「難治性疾患腸管病変の病態に関する研究」 研究分担者 平成21年度(継続) 研究費総額1,000千円
7. 宮坂信之:厚生労働科学研究費補助金(難治性疾患克服研究事業)「抗好中球細胞質抗体関連血管炎患者のgenomic DNA収集に関する研究」 研究分担者 平成21年度 研究費総額500千円
8. 上阪 等:文部科学研究費補助金 基盤研究(B)「関節リウマチ新治療戦略としてのサイクリン依存性キナーゼ4/6阻害療法」 6,100千円
9. 上阪 等:厚生労働科学研究費補助金(難治性疾患克服研究事業)「新たな診断・治療法開発のための免疫学的手法の開発に関する研究」 研究分担者 3,000千円
10. 上阪 等:厚生労働科学研究費補助金(免疫アレルギー疾患等予防・治療研究事業)「免疫疾患の病因・病態解析とその制御戦略へのアプローチ」 研究分担者 3,000千円
11. 上阪 等:共同研究(ベネシス)「多発性筋炎・皮膚筋炎などの難病に対する人免疫グロブリン療法的作用機序の解明」 1,000千円
12. 上阪 等:共同研究(ファルマエイト)「関節リウマチおよび糖尿病を対象とした評価・アッセイ技術および化合物の合成展開技術の融合による治療薬の開発」 420千円
13. 上阪 等:共同研究(田辺三菱製薬)「TREM-1の創

薬可能性評価」 2,000千円

14. 南木敏宏:厚生労働科学研究費補助金(免疫・アレルギー疾患等予防・治療研究事業)「関節リウマチの寛解導入療法体系化に関する研究」。分担研究者。平成19年-平成21年 研究費総額7,000千円
15. 南木敏宏:科学研究費補助金(基盤研究C)「フラクタリカイン阻害による血管炎症候群に対する新規治療法の開発」 期間平成20年-平成22年 研究費総額4,470千円。
16. 南木敏宏:科学研究費補助金(基盤研究B)「関節リウマチにおける生物学的製剤の長期安全性と副作用リスク因子に関する疫学研究」 分担研究者 平成20年-平成22年 研究費総額900千円
17. 南木敏宏:共同研究(エーザイ(株))「ケモカイン・接着分子等の関節リウマチなどの自己免疫疾患における役割の研究」 平成21年 1,000千円
18. 高田和生:厚生労働科学研究費補助金(難治性疾患克服研究事業)「自己免疫疾患に関する調査研究」 研究分担者 2,440千円
19. 沖山奈緒子:文部科学研究費補助金 特別研究員奨励費「新しい多発性筋炎モデルマウスを用いた至適抗サイトカイン療法の開発」 1,200千円
20. 村上洋介:文部科学研究費補助金 若手研究(B)「自然免疫および破骨細胞分化に及ぼすCDK4/6の新規機能の解析」 研究費総額2,210千円
21. 村上洋介:財団法人日本応用控訴協会 研究助成金「自然免疫および破骨細胞分化に及ぼすCDK4/6の新規機能の解析」 500千円

12) 特別講演、招待講演

1. 『BIO時代における関節リウマチ治療—現状と展望—』第53回日本リウマチ学会総会・学術集会サテライトシンポジウム4 リウマチフロンティア第7回学術講演会 平成21年4月24日
2. 『3e-Jの目的と方法』 3e-J研究会 Kick off Meeting 平成21年5月10日
3. 『新しい関節リウマチ治療を考える』 リウマチフロンティア市民公開講座 平成21年6月6日
4. 『アダリムマブの有効性と安全性』 Humira World Conference 平成21年7月4日
5. 『炎症と再生:総論』 第9回国際炎症学会/第30回日本炎症・再生医学会 市民公開講座 平成21年7月10日
6. 『関節リウマチとは?』 第9回国際炎症学会/第30回日本炎症・再生医学会 市民公開講座 平成21年7月

- 10日
7. 『関節リウマチという悪女に魅せられて—研究の足跡』
第5回リウマチヤングアカデミー 平成21年7月17日
 8. 『関節リウマチ治療におけるパラダイムシフトと今後の展望』 第5回血液免疫ネットワーク in 金沢 平成21年9月26日
 9. 『生物学的製剤は関節リウマチ治療に何をもたらしたのか?』 第59回日本アレルギー学会秋季学術大会
平成21年10月31日
 10. 『リウマチ治療の現在と未来について』 信州リウマチネットワーク 第2回市民公開講座 平成21年11月1日
 11. 『関節リウマチの新規治療の展望と問題点』 産業医科大学大学院特別講義 平成21年11月24日
 12. 『関節リウマチに対するトシリズマブの有効性と安全性』 トシリズマブ学術講演会 平成21年11月28日
 13. 『正しく知ろう、リウマチ治療の現在』 琉球新報市民公開講座 平成21年11月29日
 14. 『SLE:何がわかってきたか』 第39回日本免疫学会総会・学術集会クリニカルセミナー2 平成21年12月2日
 15. 『リウマチはここまでよくなる!』 平成21年度リウマチ・アレルギーシンポジウム in 仙台 平成21年12月5日
 16. 『RAにおける生物学的製剤の役割』 2010年 Kick-off meeting 社内講演会 平成22年1月12日
 17. 『免疫難病に対するIL-6阻害治療』 トシリズマブ学術講演会 平成22年1月15日
 18. 関節リウマチ治療薬がもたらしたパラダイムシフトとは?』 平成22年2月1日
 19. 『リウマチはここまでよくなる!』 平成21年度リウマチ・アレルギーシンポジウム in 東京 平成22年2月20日

高村聡人、酒井良子、鈴木晶子、
川口直子

リサーチレジデント:村上洋介

日本学術振興会特別研究員PD:沖山奈緒子

13) 教室員リスト

教 授 :宮坂信之
 併 任 教 授 :針谷正祥 (薬害監視学講座)
 准 教 授 :上阪 等
 併 任 准 教 授 :窪田哲朗 (保健衛生学科)、
 小池竜司 (臨床試験管理センター)、
 南木敏宏 (薬害監視学講座)
 講 師 :高田和生
 助 教 :溝口史高 (元 AISS)、平田真哉
 併 任 助 教 :田中みち、
 駒野有希子 (薬害監視学講座)
 大 学 院 生 :豊本雅靖、渡部香織、金子佳代子、

Arthritis & Rheumatism (Arthritis Care & Research)
Vol. 61, No. 3, March 15, 2009, pp 305–312
DOI 10.1002/art.24283
© 2009, American College of Rheumatology

ORIGINAL ARTICLE

Pneumocystis jiroveci Pneumonia in Patients With Rheumatoid Arthritis Treated With Infliximab: A Retrospective Review and Case–Control Study of 21 Patients

YUKIKO KOMANO,¹ MASAYOSHI HARIGAI,¹ RYUJI KOIKE,¹ HARUHIITO SUGIYAMA,² JUN OGAWA,¹ KAZUYOSHI SAITO,³ NAOYA SEKIGUCHI,⁴ MASAYUKI INOO,⁵ IKUKO ONISHI,⁵ HIROYUKI OHASHI,⁶ FUJIO AMAMOTO,⁷ MASAYUKI MIYATA,⁸ HIDEO OHTSUBO,⁹ KAZUKO HIRAMATSU,¹⁰ MASAHIRO IWAMOTO,¹¹ SEIJI MINOTA,¹¹ NAOKI MATSUOKA,¹² GOICHI KAGEYAMA,¹³ KAZUYOSHI IMAIZUMI,¹⁴ HITOSHI TOKUDA,¹⁵ YASUMI OKOCHI,¹⁵ KOICHIRO KUDO,² YOSHIYA TANAKA,³ TSUTOMU TAKEUCHI,⁴ AND NOBUYUKI MIYASAKA¹

Objective. To establish proper management of *Pneumocystis jiroveci* pneumonia (PCP) in rheumatoid arthritis (RA) patients treated with infliximab. PCP has been observed in 0.4% of patients with RA treated with infliximab in Japan.

Methods. Data from patients with RA (n = 21) who were diagnosed with PCP during infliximab treatment and from 102 patients with RA who did not develop PCP during infliximab therapy were collected from 14 rheumatology referral centers in Japan. A retrospective review of these patients and a case–control study to compare patients with and without PCP were performed.

Results. The median length of time from the first infliximab infusion to the development of PCP was 8.5 weeks. At the onset of PCP, the median dosages of prednisolone and methotrexate were 7.5 mg/day and 8 mg/week, respectively. *Pneumocystis jiroveci* was microscopically identified in only 2 patients, although the polymerase chain reaction test for the organism was positive in 20 patients. The patients with PCP had significantly lower serum albumin levels ($P < 0.001$) and lower serum IgG levels ($P < 0.001$) than the patients without PCP. Computed tomography of the chest in all patients with PCP revealed ground-glass opacity either with sharp demarcation by interlobular septa or without interlobular septal boundaries. Sixteen of the 21 patients with PCP developed acute respiratory failure, but all survived.

Conclusion. PCP is a serious complication that may occur early in the course of infliximab therapy in patients with RA. For the proper clinical management of this infectious disease, physicians need to be aware of the possibility of PCP developing during infliximab therapy.

INTRODUCTION

Rheumatoid arthritis (RA) is a systemic inflammatory disease that is characterized by chronic synovitis and the

destruction of articular structures of multiple joints. The discovery that high levels of tumor necrosis factor α (TNF α) contribute to chronic inflammation and joint de-

Dr. Harigai's work was supported by a grant-in-aid from the Japan Ministry of Health, Labor, and Welfare, and by a grant from Mitsubishi Tanabe Pharma. Dr. Koike's work was supported by the grant-in-aid for scientific research from the Japan Society for the promotion of science.

¹Yukiko Komano, MD, PhD; Masayoshi Harigai, MD, PhD; Ryuji Koike, MD, PhD; Jun Ogawa, MD, PhD; Nobuyuki Miyasaka, MD, PhD; Tokyo Medical and Dental University, Tokyo, Japan; ²Haruhito Sugiyama, MD, PhD; Koichiro Kudo, MD; International Medical Center of Japan, Tokyo, Japan; ³Kazuyoshi Saito, MD, PhD; Yoshiya Tanaka, MD, PhD; University of Occupational and Environmental Health, Kitakyushu, Japan; ⁴Naoya Sekiguchi, MD; Tsutomu Takeuchi, MD, PhD; Saitama Medical Center, Saitama Medical

University, Kawagoe, Japan; ⁵Masayuki Inoo, MD, PhD, Ikuko Onishi, MD, PhD; Utazu Hama Clinic, Kagawa, Japan; ⁶Hiroyuki Ohashi, MD, PhD; Hamamatsu University School of Medicine, Hamamatsu, Japan; ⁷Fujio Amamoto, MD; Kanto Rosai Hospital, Kawasaki, Japan; ⁸Masayuki Miyata, MD, PhD; Fukushima Red Cross Hospital, Fukushima, Japan; ⁹Hideo Ohtsubo, MD, PhD; Japanese Red Cross Society Kagoshima Hospital, Kagoshima, Japan; ¹⁰Kazuko Hiramatsu, MD, PhD; Tokyo Metropolitan Fuchu General Hospital, Tokyo, Japan; ¹¹Masahiro Iwamoto, MD, PhD; Seiji Minota, MD, PhD; Jichi Medical University, Shimotsuke, Japan; ¹²Naoki Matsuoka, MD; Nagasaki Medical Hospital of Rheumatology, Ohmura, Japan; ¹³Goichi Kageyama, MD,

struction in patients with RA heralded a new era of targeted and highly effective therapy for this disease.

Several clinical trials have demonstrated excellent efficacy for the treatment of RA with infliximab, an anti-TNF α chimeric monoclonal antibody (1,2). Because TNF α is one of the key molecules protecting against microorganisms *in vivo*, treatment with infliximab has been associated with increased risk of opportunistic and serious infections in cohort studies using RA patient registries, as well as in the meta-analysis of clinical trials (3–6). In Japan, a strict postmarketing surveillance program was implemented that mandated the registration of all patients with RA receiving infliximab, with a tracking period of 6 months for each patient. Of the 5,000 patients tracked, this postmarketing surveillance program identified 108 patients (2.2%) with bacterial pneumonia and 14 patients (0.3%) with tuberculosis (7). Notably, 22 patients (0.4%) with *Pneumocystis jiroveci* pneumonia (PCP) were identified in the same postmarketing surveillance program (7), a much higher number than was found in corresponding studies in the US (3). In addition, another anti-TNF α agent, etanercept, has been subject to a similarly strict postmarketing surveillance program in Japan, which identified 16 patients (0.23%) with PCP out of 7,091 patients with RA receiving etanercept (8). These 2 postmarketing surveillance programs show PCP to be more common than expected in patients receiving anti-TNF therapy in Japan (9).

PCP is an infectious disease caused by *P. jiroveci*, and has received increased attention since the emergence of the human immunodeficiency virus (HIV) infection more than 20 years prior (10). More recently, PCP has increasingly been reported in immunocompromised patients with connective tissue diseases, patients with malignancies, or in patients after organ transplantation (11,12). The postmarketing surveillance data in Japan and some anecdotal reports of PCP in patients receiving infliximab (13–16) suggest that patients receiving infliximab comprise a novel high-risk group for development of PCP. A thorough knowledge of the clinical and laboratory characteristics of PCP in patients treated with infliximab is indispensable

for prophylaxis, early diagnosis, and proper treatment of this infectious disease.

In a previous report (17), we compared 21 patients with RA receiving infliximab who developed PCP and 102 patients with RA receiving infliximab who did not develop PCP, and identified risk factors for PCP in patients with RA treated with infliximab. We demonstrated that patients with 2 or 3 risk factors showed significantly higher probability of developing PCP than those with 1 or those without risk factors. In this study, we report detailed clinical, laboratory, and radiographic features along with a case-control study of PCP in these 21 patients with RA treated with infliximab.

PATIENTS AND METHODS

The PCP Under Anti-TNF Therapy (PAT) study group was organized for the investigation of PCP in patients with RA treated with infliximab in Japan. Included in the present study were those patients who fulfilled the 1987 American College of Rheumatology (formerly the American Rheumatism Association) criteria for RA (18) and received infliximab (3 mg/kg every 8 weeks) with concomitant methotrexate (MTX). Between August 2003 and June 2006, 21 patients with PCP were selected from 14 hospitals through either the postmarketing surveillance program ($n = 15$) or through voluntary case reports by attending physicians either at scientific meetings or to a pharmaceutical company ($n = 6$). Patients without PCP ($n = 102$) were selected at random from a consecutive series of 523 patients with RA who did not develop PCP during infliximab therapy. These patients were selected from 3 hospitals: the University Hospital of Occupational and Environmental Health, the Saitama Medical Center, and the Tokyo Medical and Dental University Hospital. To increase the statistical power of the case-control study, the number of patients in the control group was designed to provide ~5 times the number of patients with PCP (19). Two pulmonologists (HS and KK) participated in the PAT study group.

Diagnostic criteria for PCP. Previously established diagnostic criteria for PCP (20,21) were used for the present study, with some modifications (17). A diagnosis of PCP was deemed definitive if *P. jiroveci* was found on microscopic analysis of respiratory samples with concurrent clinical manifestations (fever, dry cough, or dyspnea), hypoxemia, and radiologic findings indicative of PCP. The diagnosis of PCP was considered presumptive if a patient fulfilled these conditions in the absence of evidence of bacterial pneumonia and presence of either a positive polymerase chain reaction (PCR) test for *P. jiroveci* DNA or increased serum 1,3- β -D-glucan levels (Fungitec G test MK; Seikagaku, Tokyo, Japan or Wako β -D-glucan test; Wako Pure Chemical Industries, Tokyo, Japan) with response to standard treatments for PCP (22,23). The HIV status of the patient was not examined.

Collection and analysis of the clinical data. RA patients with definitive or presumptive PCP ($n = 21$) and those without PCP ($n = 102$) were referred to as the PCP group

PhD; Kurashiki Central Hospital, Kurashiki, Japan; ¹³Kazuyoshi Imaizumi, MD, PhD; Nagoya University Graduate School of Medicine, Nagoya, Japan; ¹⁴Hitoshi Tokuda, MD, PhD, Yasumi Okochi, MD; Social Insurance Central General Hospital, Tokyo, Japan.

Dr. Harigai has received honoraria (less than \$10,000) from Mitsubishi Tanabe Pharma. Dr. Ohtsubo has received speaking fees (less than \$10,000) from Mitsubishi Tanabe Pharma. Dr. Iwamoto has received honoraria (less than \$10,000) from Mitsubishi Tanabe Pharma. Dr. Minota has received honoraria (less than \$10,000) from Mitsubishi Tanabe Seiyaku. Dr. Takeuchi has received speaking fees (more than \$10,000) from Mitsubishi Tanabe Seiyaku. Dr. Miyasaka has received speaking fees and honoraria (less than \$10,000) from Mitsubishi Tanabe Seiyaku.

Address correspondence to Masayoshi Harigai, MD, PhD, Department of Pharmacovigilance, Graduate School, Tokyo Medical and Dental University, 1-5-45 Yushima, Bunkyo-ku, Tokyo, 113-8519, Japan. E-mail: mharigai.mpha@tmd.ac.jp.

Submitted for publication April 12, 2008; accepted in revised form October 24, 2008.

Table 1. Characteristics of rheumatoid arthritis patients with PCP who were treated with infliximab*

Patient	Age, years	Sex	No. of infusions†	Treatment duration, weeks‡	MTX, mg/week	PSL, mg/day	Lung disease	Diabetes mellitus	Clinical symptoms
1	52	F	3	12	7.5	7.5	IP	-	fever/cough/DOE
2	76	F	1	2	6	20	IP	-	fever/cough/DOE
3	61	M	3	8	15.5	6	-	-	fever/cough/DOE
4	69	F	4	16	6	20	IP	+	cough/DOE
5	54	F	2	7	20	8	-	-	fever
6	60	F	2	4	6	5	-	-	fever/cough
7	80	F	1	6	8	7.5	-	+	fever/cough/DOE
8	66	F	3	6	6	7	bronchiectasis	-	fever/DOE
9	52	M	2	5	10	10	follicular bronchiolitis	-	fever/cough
10	65	F	3	9	10.5	7.5	old tuberculosis	-	fever/cough/DOE
11	64	F	13	90	10	10	-	-	fever/cough
12	64	M	5	26	10	15	COPD	-	fever/DOE
13	71	F	4	17	8	5	-	-	fever/cough/DOE
14	56	F	3	12	6	8	IP	+	fever/DOE
15	71	M	3	9	8	8	chronic bronchitis	-	fever/cough/DOE
16	56	F	2	3	5	5	-	-	fever/cough/DOE
17	68	F	2	6	1	1	-	-	fever/cough/DOE
18	69	F	3	9	10	10	-	+	fever/cough/DOE
19	67	F	3	9	8	5	-	-	fever/cough/DOE
20	71	F	7	54	2.5	2.5	old tuberculosis	-	cough/DOE
21	56	F	3	8	7.5	7.5	-	+	DOE

* PCP = *Pneumocystis jirovecii* pneumonia; MTX = methotrexate; PSL = prednisolone; IP = interstitial pneumonia; cough = dry cough; DOE = dyspnea on effort; COPD = chronic obstructive pulmonary disease.

† Infliximab infusions prior to the diagnosis of PCP.

‡ With infliximab before the onset of PCP.

and the non-PCP group, respectively. Patient records were evaluated to determine demographic information, comorbidities, concomitant drugs, laboratory data, radiographic data, treatment, and outcome. Chest radiographs and computed tomography (CT) scans of the thorax were evaluated by the 2 pulmonologists. Inclusion in the study required that the patient be followed until January 31, 2006 (the date established as the common close-out date for the non-PCP group) or that the patient stopped receiving infliximab before that date.

Ethics. The guidelines of Helsinki declaration and the ethical guidelines for epidemiologic research in Japan were followed. The study protocol was approved by the Institutional Ethical Committee of the Tokyo Medical and Dental University Hospital.

Statistical analyses. Fisher's exact test was used for categorical variables and the Mann-Whitney U test was used for continuous variables with Bonferroni correction for multiple pair comparisons. All analyses were performed using SPSS software, version 15.0 (SPSS Japan, Tokyo, Japan).

RESULTS

Diagnosis and clinical characteristics of RA patients with PCP. We evaluated the cases of 21 patients with RA who were receiving infliximab treatment using the above diagnostic criteria. Two of the 21 cases were considered to

have a definitive PCP diagnosis and 19 had a presumptive PCP diagnosis. The clinical characteristics of each patient are summarized in Table 1. The mean age of the patients was 64 years (range 52–80 years) and 17 (81%) were women.

All patients were receiving both corticosteroids and MTX. At the onset of PCP, the median dosages of prednisolone and MTX were 7.5 mg/day (range 1–20 mg/day) and 8 mg/week (range 6–20 mg/week), respectively. None of the patients were receiving other immunosuppressive drugs. Ten patients had pulmonary comorbidities, including interstitial pneumonia (n = 4), chronic obstructive pulmonary disease (n = 1), bronchiectasis (n = 1), chronic bronchitis (n = 1), follicular bronchiolitis (n = 1), and prior pulmonary tuberculosis (n = 2). Five patients had diabetes mellitus. None of the patients were receiving chemoprophylaxis for PCP at the time of PCP diagnosis. The median interval between the first infusion of infliximab and the onset of PCP was 9 weeks (range 2–90 weeks). Sixteen patients (76%) developed PCP within 14 weeks after the first infusion (before the scheduled fourth infusion) and 19 patients (90%) developed PCP within 26 weeks. Fever was the most common clinical symptom, observed in 18 patients (86%), followed by effort-induced dyspnea (81%) and dry cough (76%).

Laboratory and radiographic features of the patients with PCP. Laboratory results data for the PCP group are summarized in Table 2. Sixteen patients either had severe hypoxia (with $\text{PaO}_2 < 60$ mm Hg on room air) or required immediate oxygen therapy at the onset of PCP. Peripheral

Table 2. Laboratory data of patients with rheumatoid arthritis treated with infliximab at the onset of PCP*

Patient	WBC, cells/ μ l	Lymphocytes, cells/ μ l	PaO ₂ mm Hg (O ₂ liter/minute)†	Serum β -D-glucan, pg/ml‡	<i>Pneumocystis jiroveci</i> PCR
1	7,950	539	46	39.0	+
2	6,900	1,249	44	30.5	+
3	8,400	1,008	81 (5)	67.1	+
4	6,500	2,210	56 (10)	27.2	+
5	5,700	570	71 (2)	325.3	NA
6	14,800	740	47 (3)	204.0	+
7	9,700	854	50	7.9	+
8	7,880	1,560	55	<5	+
9	13,100	524	76	1,720.0	+
10	7,400	592	74 (10)	928.0	+
11	8,280	1,520	44 (15)	241.0	+
12	7,200	288	63	36.1	+
13	11,500	1,840	62	256.0	+
14	4,900	147	43	35.7	+
15	10,660	320	NA§	863.0	+
16	6,300	1,348	53	267.5	+
17	9,700	NA	41	180.0	+
18	8,400	1,100	66	41.3	+¶
19	11,950	836	28	77.8	NA¶
20	6,900	1,573	34	334.0	+
21	11,600	1,856	102 (4)	103.5	+

* PCP = *Pneumocystis jiroveci* pneumonia; WBC = white blood cell; PCR = polymerase chain reaction; NA = not assessed.

† Oxygen therapy during the measurement of PaO₂.

‡ Normal ranges: <20 pg/ml by Fungitec G test (Seikagaku) for patients 1, 2, 8, 12, and 14–17, \leq 11 pg/ml by Wako β -D-glucan test (Pure Chemical Industries) for patients 3–7, 9–11, 13, and 18–21.

§ Oxygen saturation measured by a pulse oximeter was 93%.

¶ *Pneumocystis jiroveci* were microscopically detected in bronchoalveolar lavage fluid (patient 18) or sputum (patient 19).

blood lymphocyte (PBL) counts at the onset of PCP were <500 cells/ μ l in 3 patients, 500–1,000 cells/ μ l in 7 patients, and >1,000 cells/ μ l in 10 patients. The PCR test to detect *P jiroveci* was conducted in 19 patients, using either induced sputum (14 patients) or bronchoalveolar lavage fluid (5 patients). All test results were positive, although *P jiroveci* was microscopically identified in samples from only 2 patients (patients 18 and 19). Serum levels of 1,3- β -D-glucan, one of the major components of the cell walls of fungi and reportedly a reliable serum marker for PCP (22,23), were elevated in 19 patients. Results of sputum culture performed on 20 patients revealed no causative bacteria or fungus. The median serum levels of IgG, lactate dehydrogenase, and KL-6 antigen were 1,191.5 mg/dl (range 626–2,112 mg/dl, n = 12), 439.0 IU/liter (range 214–1,011 IU/liter, n = 16), and 521.5 units/ml (range 156–1,480 units/ml, n = 20), respectively. KL-6 antigen is a mucinous high molecular weight glycoprotein that is produced by type II pneumonocytes and is reported to increase in patients with active interstitial pneumonitis as well as in those with PCP (24).

Chest radiographs and CT scans were analyzed in all 21 patients. The most common CT finding was ground-glass opacity (in 21 patients), either with sharp demarcation by interlobular septa (in 7 patients) or without interlobular septal boundaries (in 15 patients) (Figure 1). One patient demonstrated both patterns.

Treatment and clinical course of PCP in patients with RA treated with infliximab. All of the patients were hospitalized on the same day that PCP was suspected. Eighteen patients (all except patients 9, 15, and 18) received oxygen therapy on admission. MTX and infliximab were discontinued in all patients. Twenty patients received therapeutic doses of trimethoprim/sulfamethoxazole (TMP/SMX) and 1 was given a therapeutic dose of pentamidine isethionate immediately after the laboratory and radiologic examinations. Because of adverse drug reactions that included skin eruptions, renal toxicity, and thrombocytopenia, therapy with TMP/SMX was changed to pentamidine isethionate in 7 patients. Nineteen patients were treated with high-dose corticosteroids within a few days after admission. Sixteen patients were empirically treated with antibiotics and 7 with antifungal agents. A 68-year-old woman (patient 17) was intubated on the day of admission because of progressive respiratory failure, but was successfully weaned from the respirator 4 days later. All of the patients responded well to treatment and all survived.

Case-control study. In order to characterize the PCP group of patients with RA more precisely, we compared demographic information, comorbidities, treatments, and laboratory data between the PCP and non-PCP groups

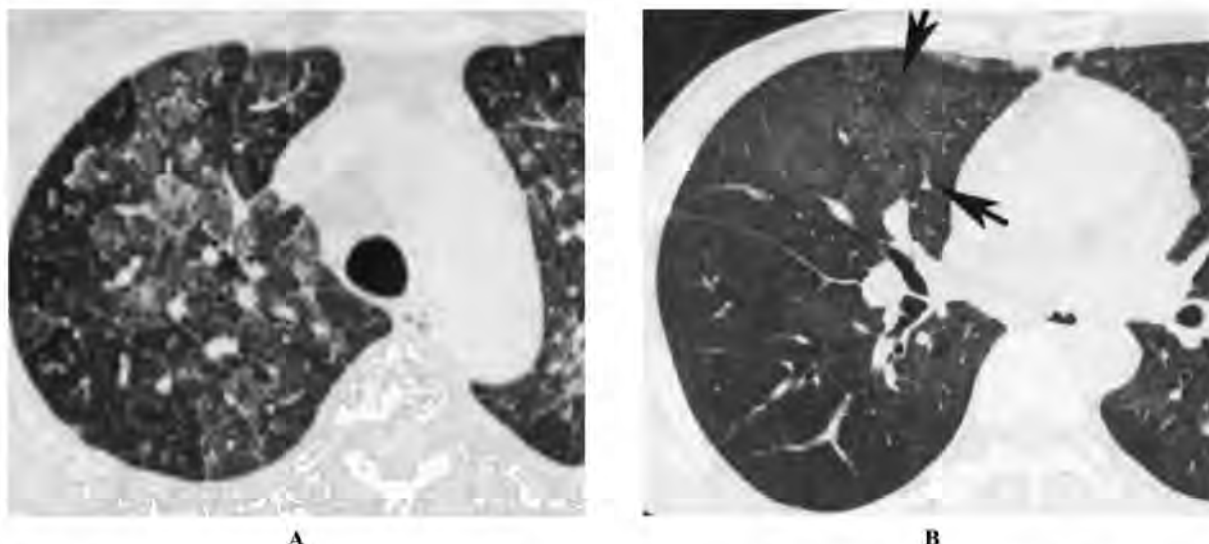


Figure 1. Representative computed tomography scans of patients with *Pneumocystis jiroveci* pneumonia taken at the time of diagnosis. **A**, Ground-glass opacity with sharp demarcation by interlobular septa (patient 21), and **B**, ground-glass opacity without interlobular septal boundaries (patient 9).

(Table 3). We have previously reported that the PCP group was significantly older ($P < 0.001$), had a higher percentage of pulmonary diseases ($P < 0.001$), and was treated with a higher prednisolone dose ($P = 0.001$) than the non-PCP group at baseline (i.e., at the initiation of treatment with infliximab) (17). The percentage of patients with diabetes mellitus was higher ($P = 0.046$) and serum IgG levels were lower ($P = 0.008$) in the PCP group; however, these differences were not considered to be statistically significant after Bonferroni correction.

We compared the treatment and laboratory data of the PCP group at the onset of PCP with those of the non-PCP

group at the most recent visit during infliximab therapy (as of January 31, 2006). The PCP group received higher prednisolone dosages than the non-PCP group (median 7.5 mg/day [range 1–15] and median 4 mg/day [range 0–15], respectively; $P < 0.001$). The PCP group also exhibited lower PBL counts compared with the non-PCP group (median 931 cells/ μ l [range 147–2,210] and median 1,330 cells/ μ l [range 119–4,788], respectively; $P = 0.015$), lower serum albumin levels than the non-PCP group (median 3.3 gm/dl [range 2.3–4.0] and 4.0 gm/dl [range 2.9–4.8], respectively; $P < 0.001$), and lower serum IgG levels

Table 3. Baseline characteristics of patients with rheumatoid arthritis treated with infliximab*

Characteristic	PCP group (n = 21)	Non-PCP group (n = 102)	P†
Age, mean \pm SD years	64 \pm 8	54 \pm 12	< 0.001
Women, n (%)	17 (81.0)	93 (91.2)	NS
Diabetes, n (%)	5 (23.8)	8 (7.8)	0.046
Pulmonary disease, n (%)	10 (47.6)‡	11 (10.8)§	< 0.001
Disease duration, years	8.9 (2.6–29)	7 (0.3–35)	NS
Methotrexate, mg/week	8 (6–20)	8 (2–15)	NS
Prednisolone, mg/day	7.5 (1–20)	5 (0–20)	0.001
Peripheral lymphocyte counts, cells/ μ l¶	1,148 (420–2,439)	1,192 (170–3,200)	NS
Serum albumin, gm/dl#	3.7 (2.9–4.4)	3.8 (2.9–4.6)	NS
Serum IgG, mg/dl**	1,192 (626–2,112)	1,540 (932–3,460)	0.008

* Values are the median (range) unless otherwise indicated. PCP = *Pneumocystis jiroveci* pneumonia; NS = not significant.

† Bonferroni correction was applied; difference considered significant if $P \leq 0.005$.

‡ Interstitial pneumonia (n = 4), chronic obstructive pulmonary disease (n = 1), bronchiectasis (n = 1), chronic bronchitis (n = 1), follicular bronchiolitis (n = 1), old pulmonary tuberculosis (n = 2).

§ Interstitial pneumonia (n = 1), chronic obstructive pulmonary diseases (n = 2), bronchiectasis (n = 2), chronic bronchitis (n = 3), old pulmonary tuberculosis (n = 3).

¶ PCP group n = 19, non-PCP group n = 95.

PCP group n = 17, non-PCP group n = 94.

** PCP group n = 12, non-PCP group n = 89.

than the non-PCP group (944 mg/dl [range 518–1,474] and 1,394 mg/dl [range 799–3,269], respectively; $P < 0.001$).

We prepared 21 case-control matches. In each match we collected data from 2 patients from the non-PCP group at the same point in time at which a patient from the PCP group was first diagnosed with PCP. Analyzing these data, we found that at time of onset of PCP, the PCP group had significantly lower serum albumin levels than the non-PCP group (median 3.3 gm/dl, $n = 20$ and median 3.9 gm/dl, $n = 32$, respectively; $P < 0.001$) and lower serum IgG levels than the non-PCP group (median 944 mg/dl, $n = 13$ and 1,347 mg/dl, $n = 32$, respectively; $P < 0.001$).

DISCUSSION

We accumulated the largest possible number of patients with RA who developed PCP during treatment with infliximab, and described clinical and radiologic characteristics of the 21 patients that we found. Sixteen patients presented with severe hypoxia and/or required immediate oxygen therapy, and all 21 patients were hospitalized. PCP in these patients with RA presented an acute and progressive course, which should alert clinicians to recognize PCP as an important opportunistic infection during infliximab therapy.

The incidences of PCP during the postmarketing surveillance programs of infliximab and etanercept in Japan were 0.4% and 0.23%, respectively (7,8). The corresponding incidence reported in the US is ~0.01% (25). Although the US incidence was derived from voluntary reports to the Food and Drug Administration, a 20–40-fold higher incidence of PCP with the use of anti-TNF therapy in Japan suggests that this phenomenon might be unique to Japanese patients. Possible explanations for the difference include: 1) anti-TNF therapy may more severely affect host defenses in Japanese patients with RA in vivo due to genetic or environmental differences, 2) Japanese patients with RA may have a higher prevalence of prolonged colonization of *P jiroveci*, or 3) the incidence of PCP in patients with RA receiving anti-TNF therapy in Western countries may be underestimated due to the voluntary reporting system for adverse events.

Several lines of evidence have suggested that TNF α plays a critical role in host defenses against a *Pneumocystis* infection. First, *Pneumocystis murina* was found to directly stimulate the secretion of TNF α from murine alveolar macrophages by activation of the Toll-like receptor (26). Second, *Pneumocystis*-induced TNF α in turn enhanced the production of the reactive nitrogen intermediates that are important mediators for killing the microorganism (27). Finally, adenoviral gene transfer of mouse IgG/p55 TNF receptor in immunocompetent mice delayed clearance of *P jiroveci* after intratracheal inoculation (28). These data clearly indicate that TNF α serves as a key cytokine in the host defenses during a *Pneumocystis* infection, and they explain the association between PCP and treatment with infliximab. In the 21 patients with PCP, 76% developed the disease within 14 weeks after the first infusion of infliximab and 90% developed PCP within 26 weeks (or 6 months). Although patients with RA who are

prescribed MTX alone sometimes develop PCP during their clinical course, the relatively short interval between the first infusions of infliximab and the onset of PCP indicate a strong causal relationship between the two.

Previous studies have revealed that there are significant differences in clinical presentations of PCP between patients with HIV infection and those without. PCP in patients with HIV infection develops insidiously, taking a subacute to chronic course that usually does not progress to respiratory failure (29). In contrast, patients without HIV infection develop PCP abruptly and progress to acute fulminating pneumonia with a high incidence of acute respiratory failure (30,31). Mortality due to PCP in patients with HIV infection ranges from 9.6–20%, whereas it exceeds 50% in patients without HIV infection (32,33). These differences probably resulted not only from the older age, more frequent comorbidities, and less standardized management of PCP in patients without HIV infection (31,32,34), but also from differing immunologic responses to *P jiroveci* (35). In our cohort, the clinical features of PCP are similar to those of previously reported cases without HIV infection (32) in terms of the high rate of progressive respiratory failure (observed in 16 [76%] of 21 patients) as well as the low rate of the microscopic detection of *P jiroveci* (found in 2 [9.5%] of 21 patients). All of our patients survived, which is distinctly different from the much higher mortality reported in PCP patients without HIV infection. Prompt diagnosis and treatment by attending physicians who have prior experience and are alert for the possible development of PCP probably contributed to the excellent prognosis for the patients in this study (36).

Double-blind, placebo-controlled trials have shown that adjunctive treatment with corticosteroids reduces the need for mechanical ventilation and mortality due to moderate-to-severe PCP in patients with HIV infection. An officially recommended regimen of adjunctive corticosteroid therapy for PCP in patients with HIV infection has been proposed (37). However, the clinical benefit of adjunctive corticosteroid therapy for PCP patients without HIV infection has not been established (35,38). In our study, 19 of 21 patients received adjunctive corticosteroid therapy, including intravenous pulse methylprednisolone. Secondary infections were not observed in these patients, only 1 required mechanical ventilation, and all recovered rapidly. Based on the limited existing reports and our sample of patients, adjunctive corticosteroid therapy for PCP in patients with RA treated with infliximab who show respiratory failure may have some clinical benefit, including an improved prognosis. Further studies will be required to establish an optimal regimen for adjunctive corticosteroid therapy in these patients.

Microscopic evidence of *P jiroveci* is required to make a definitive diagnosis of PCP. Studies have shown that the organism is detectable on microscopic examination of induced sputum in 55–92% of PCP patients with HIV infection (39,40). In patients with PCP but without HIV infection, detectability is <10%; thus, bronchoalveolar lavage fluid examination is often required (38). We included the PCR test for *P jiroveci* (41) or serum 1,3- β -D-glucan (22,42) in the diagnostic criteria for presumptive PCP diagnosis in the current study. Several studies have

demonstrated that the PCR test has greater sensitivity and specificity for the diagnosis of PCP compared with direct staining of *P jiroveci* (43). β -D-glucan, the major component of fungi cell walls (including the *Pneumocystis* cyst wall), has been also recognized as a useful serum marker for PCP (23). Because the PCR test results are sometimes positive in patients with colonization of *P jiroveci*, and because patients can have elevated serum β -D-glucan levels with various fungal infections, combining the results of these tests with clinical findings, laboratory data, and radiologic findings is mandatory for the presumptive diagnosis of PCP.

Monitoring and prophylaxis for PCP in patients with RA receiving infliximab is an important and challenging issue. There are no clinically useful biologic markers that guide the initiation of chemoprophylaxis for PCP in these patients. In individuals with HIV infection, the risk of developing PCP increases with a CD4+ T cell count $<200/\mu\text{L}$; this number serves as a clinically useful marker to identify patients at high risk for PCP (44). In patients with rheumatic diseases who are starting corticosteroid therapy, a PBL count of $<500/\mu\text{L}$ proved to be a major predictor for PCP infection (12). In the current study, however, only 3 of the 21 patients had lymphocyte counts $<500/\mu\text{L}$ at the time of disease onset, indicating that PCP can develop in patients with RA receiving infliximab both in a T cell-independent (i.e., TNF-dependent) and a T cell-dependent status. Recently, we reported that development of PCP in patients with RA treated with infliximab was best predicted by age (≥ 65 years), dosage of prednisolone (≥ 6 mg/day), and pulmonary comorbidities. Patients with 2 or 3 of the above risk factors developed PCP more frequently than those with only 1 or none.

In the present study we demonstrated that levels of serum albumin and serum IgG decreased upon onset of PCP. Therefore, prophylaxis should begin with a standard regimen in patients with 2 or 3 risk factors for PCP when results of serum albumin level or serum IgG level are seen to decrease. PBL counts could prove useful as a general predictor for PCP. Considering the seriousness and the relatively high incidence of PCP in RA patients in Japan, we also recommend that prophylaxis be initiated before treating patients with infliximab, at least in Japanese patients with RA, with 3 of these risk factors. Appropriate timing and length of PCP prophylaxis, as well as its efficacy in patients with RA receiving infliximab, need to be investigated.

In summary, the results of this study show that PCP is a serious complication in patients with RA who receive infliximab therapy. PCP developed early in the course of infliximab treatment and progressed to respiratory failure. The severity of PCP in the present series emphasizes the importance of the clinician's awareness of this opportunistic infection in patients treated for RA with infliximab. Early diagnosis and prompt intervention with specific antimicrobial drugs is vital. The evaluation of risk factors before treatment, as well as careful monitoring of clinical manifestations and laboratory tests, is beneficial for early diagnosis.

ACKNOWLEDGMENTS

We would like to thank Drs. Tatsuya Atsumi (Hokkaido University), Hiroaki Ida (Nagasaki University), and Mitsuhiko Iwahashi (Higashi Hiroshima Memorial Hospital) for their critical comments on this manuscript, and Drs. Yoshikazu Yamamoto (Tokyo Metropolitan Fuchu General Hospital), Takemasa Matsuda (Kagoshima Red Cross Hospital), Yoshinori Hasegawa (Nagoya University), and Seizo Yamana (Higashi Hiroshima Memorial Hospital) for supplementation of the clinical data for the patients. We also would like to thank Dr. Takahiro Nakamura (National Defense Medical College) for his help with the statistical analyses.

AUTHOR CONTRIBUTIONS

Dr. Harigai had full access to all of the data in the study and takes responsibility for the integrity of the data and the accuracy of the data analysis.

Study design. Komano, Harigai, Koike, Miyasaka.

Acquisition of data. Komano, Harigai, Sugiyama, Ogawa, Saito, Sekiguchi, Inoo, Oonishi, Ohashi, Amamoto, Miyata, Ohtsubo, Hiramatsu, Iwamoto, Minota, Matsuoka, Kageyama, Imaizumi, Tokuda, Okochi, Kudo, Tanaka, Takeuchi.

Analysis and interpretation of data. Komano, Harigai, Koike, Sugiyama, Ogawa, Saito, Sekiguchi, Inoo, Oonishi, Ohashi, Amamoto, Miyata, Ohtsubo, Hiramatsu, Iwamoto, Minota, Matsuoka, Kageyama, Imaizumi, Tokuda, Okochi, Kudo, Tanaka, Takeuchi, Miyasaka.

Manuscript preparation. Komano, Harigai, Koike, Sugiyama, Ogawa, Saito, Sekiguchi, Inoo, Oonishi, Ohashi, Amamoto, Miyata, Ohtsubo, Hiramatsu, Iwamoto, Minota, Matsuoka, Kageyama, Imaizumi, Tokuda, Okochi, Kudo, Tanaka, Takeuchi, Miyasaka.

Statistical analysis. Komano, Harigai, Koike, Ogawa, Miyasaka.

REFERENCES

1. Maini R, St Clair EW, Breedveld F, Furst D, Kalden J, Weisman M, et al, and the ATTRACT Study Group. Infliximab (chimeric anti-tumour necrosis factor α monoclonal antibody) versus placebo in rheumatoid arthritis patients receiving concomitant methotrexate: a randomised phase III trial. *Lancet* 1999;354:1932-9.
2. Goekoop-Ruiterman YP, de Vries-Bouwstra JK, Allaart CF, van Zeben D, Kerstens PJ, Hazes JM, et al. Clinical and radiographic outcomes of four different treatment strategies in patients with early rheumatoid arthritis (the BeSt study): a randomized, controlled trial. *Arthritis Rheum* 2005;52:3381-90.
3. Khanna D, McMahon M, Furst DE. Safety of tumour necrosis factor- α antagonists. *Drug Saf* 2004;27:307-24.
4. Mikuls TR, Moreland LW. Benefit-risk assessment of infliximab in the treatment of rheumatoid arthritis. *Drug Saf* 2003;26:23-32.
5. Bongartz T, Sutton AJ, Sweeting MJ, Buchan I, Matteson EL, Montori V. Anti-TNF antibody therapy in rheumatoid arthritis and the risk of serious infections and malignancies: systematic review and meta-analysis of rare harmful effects in randomized controlled trials. *JAMA* 2006;295:2275-85.
6. Dixon WG, Watson K, Lunt M, Hyrich KL, British Society for Rheumatology Biologics Register Control Centre Consortium, Silman AJ, et al, on behalf of the British Society for Rheumatology Biologics Register. Rates of serious infection, including site-specific and bacterial intracellular infection, in rheumatoid arthritis patients receiving anti-tumour necrosis factor therapy: results from the British Society for Rheumatology Biologics Register. *Arthritis Rheum* 2006;54:2368-76.
7. Takeuchi T, Tatsuki Y, Nogami Y, Ishiguro N, Tanaka Y, Yamanaka H, et al. Postmarketing surveillance of the safety

- profile of infliximab in 5000 Japanese patients with rheumatoid arthritis. *Ann Rheum Dis* 2008;67:189-94.
8. Koike T, Harigai M, Inokuma S, Inoue K, Ishiguro N, Ryu J, et al. Safety outcomes from a large Japanese post-marketing surveillance for etanercept [abstract]. *Arthritis Rheum* 2007;56 Suppl:S182.
 9. Koike R, Takeuchi T, Eguchi K, Miyasaka N. Update on the Japanese guidelines for the use of infliximab and etanercept in rheumatoid arthritis. *Mod Rheumatol* 2007;17:451-8.
 10. Phair J, Munoz A, Detels R, Kaslow R, Rinaldo C, Saah A, and the Multicenter AIDS Cohort Study Group. The risk of *Pneumocystis carinii* pneumonia among men infected with human immunodeficiency virus type 1. *N Engl J Med* 1990;322:161-5.
 11. Sepkowitz KA. Opportunistic infections in patients with and patients without acquired immunodeficiency syndrome. *Clin Infect Dis* 2002;34:1098-107.
 12. Ogawa J, Harigai M, Nagasaka K, Nakamura T, Miyasaka N. Prediction of and prophylaxis against *Pneumocystis pneumonia* in patients with connective tissue diseases undergoing medium- or high-dose corticosteroid therapy. *Mod Rheumatol* 2005;15:91-6.
 13. Mori S, Imamura F, Kiyofuji C, Ito K, Koga Y, Honda I, et al. *Pneumocystis jirovecii* pneumonia in a patient with rheumatoid arthritis as a complication of treatment with infliximab, anti-tumor necrosis factor α neutralizing antibody. *Mod Rheumatol* 2006;16:58-62.
 14. Seddik M, Melliez H, Seguy D, Viget N, Cortot A, Colombel JF. *Pneumocystis jirovecii* (carinii) pneumonia after initiation of infliximab and azathioprine therapy in a patient with Crohn's disease. *Inflamm Bowel Dis* 2005;11:618-20.
 15. Tai TL, O'Rourke KP, McWeeney M, Burke CM, Sheehan K, Barry M. *Pneumocystis carinii* pneumonia following a second infusion of infliximab [letter]. *Rheumatology (Oxford)* 2002;41:951-2.
 16. Velayos FS, Sandborn WJ. *Pneumocystis carinii* pneumonia during maintenance anti-tumor necrosis factor- α therapy with infliximab for Crohn's disease. *Inflamm Bowel Dis* 2004;10:657-60.
 17. Harigai M, Koike R, Miyasaka N. *Pneumocystis pneumonia* associated with infliximab in Japan. *N Engl J Med* 2007;357:1874-6.
 18. Arnett FC, Edworthy SM, Bloch DA, McShane DJ, Fries JF, Cooper NS, et al. The American Rheumatism Association 1987 revised criteria for the classification of rheumatoid arthritis. *Arthritis Rheum* 1988;31:315-24.
 19. Strom B. Sample size considerations for pharmacoepidemiology studies. In: Strom B, editor. *Pharmacoepidemiology*. West Sussex (UK): John Wiley & Sons; 2000. p. 31-9.
 20. Furrer H, Egger M, Opravil M, Bernasconi E, Hirschel B, Battegay M, et al, and the Swiss HIV Cohort Study. Discontinuation of primary prophylaxis against *Pneumocystis carinii* pneumonia in HIV-1-infected adults treated with combination antiretroviral therapy. *N Engl J Med* 1999;340:1301-6.
 21. Ledergerber B, Mocroft A, Reiss P, Furrer H, Kirk O, Bickel M, et al, and the Eight European Study Groups. Discontinuation of secondary prophylaxis against *Pneumocystis carinii* pneumonia in patients with HIV infection who have a response to antiretroviral therapy. *N Engl J Med* 2001;344:168-74.
 22. Yasuoka A, Tachikawa N, Shimada K, Kimura S, Oka S. (1,3) β -D-glucan as a quantitative serological marker for *Pneumocystis carinii* pneumonia. *Clin Diagn Lab Immunol* 1996;3:197-9.
 23. Marty FM, Koo S, Bryar J, Baden LR. (1,3) β -D-glucan assay positivity in patients with *Pneumocystis (carinii) jirovecii* pneumonia. *Ann Intern Med* 2007;147:70-2.
 24. Tasaka S, Hasegawa N, Kobayashi S, Yamada W, Nishimura T, Takeuchi T, et al. Serum indicators for the diagnosis of *Pneumocystis pneumonia*. *Chest* 2007;131:1173-80.
 25. Kaur N, Mahl TC. *Pneumocystis jirovecii* (carinii) pneumonia after infliximab therapy: a review of 84 cases. *Dig Dis Sci* 2007;52:1481-4.
 26. Zhang C, Wang SH, Lasbury ME, Tschang D, Liao CP, Durant PJ, et al. Toll-like receptor 2 mediates alveolar macrophage response to *Pneumocystis murina*. *Infect Immun* 2006;74:1857-64.
 27. Downing JF, Kachel DL, Pasula R, Martin WJ II. Gamma interferon stimulates rat alveolar macrophages to kill *Pneumocystis carinii* by L-arginine- and tumor necrosis factor-dependent mechanisms. *Infect Immun* 1999;67:1347-52.
 28. Kolls JK, Lei D, Vazquez C, Odom G, Summer WR, Nelson S, et al. Exacerbation of murine *Pneumocystis carinii* infection by adenoviral-mediated gene transfer of a TNF inhibitor. *Am J Respir Cell Mol Biol* 1997;16:112-8.
 29. Thomas CF Jr, Limper AH. *Pneumocystis pneumonia*: clinical presentation and diagnosis in patients with and without acquired immune deficiency syndrome. *Semin Respir Infect* 1998;13:289-95.
 30. Sepkowitz KA, Brown AE, Telzak EE, Gottlieb S, Armstrong D. *Pneumocystis carinii* pneumonia among patients without AIDS at a cancer hospital. *JAMA* 1992;267:832-7.
 31. Yale SH, Limper AH. *Pneumocystis carinii* pneumonia in patients without acquired immunodeficiency syndrome: associated illness and prior corticosteroid therapy. *Mayo Clin Proc* 1996;71:5-13.
 32. Geoffrey S, Gilmartin HK. *Pneumocystis carinii* pneumonia in adult non-HIV disorders. *J Intensive Care Med* 2002;17:283-301.
 33. Thomas CF Jr, Limper AH. *Pneumocystis pneumonia*. *N Engl J Med* 2004;350:2487-98.
 34. Festic E, Gajic O, Limper AH, Aksamit TR. Acute respiratory failure due to *Pneumocystis pneumonia* in patients without human immunodeficiency virus infection: outcome and associated features. *Chest* 2005;128:573-9.
 35. Limper AH, Offord KP, Smith TF, Martin WJ II. *Pneumocystis carinii* pneumonia: differences in lung parasite number and inflammation in patients with and without AIDS. *Am Rev Respir Dis* 1989;140:1204-9.
 36. Ward MM, Donald F. *Pneumocystis carinii* pneumonia in patients with connective tissue diseases: the role of hospital experience in diagnosis and mortality. *Arthritis Rheum* 1999;42:780-9.
 37. National Institutes of Health University of California expert panel for corticosteroids as adjunctive therapy for *Pneumocystis pneumonia*. Consensus statement on the use of corticosteroids as adjunctive therapy for *Pneumocystis pneumonia* in the acquired immunodeficiency syndrome. *N Engl J Med* 1990;323:1500-4.
 38. Pareja JG, Garland R, Koziel H. Use of adjunctive corticosteroids in severe adult non-HIV *Pneumocystis carinii* pneumonia. *Chest* 1998;113:1215-24.
 39. Zaman MK, Wooten OJ, Suprahmanya B, Ankobiah W, Finch PJ, Kamholz SL. Rapid noninvasive diagnosis of *Pneumocystis carinii* from induced liquefied sputum. *Ann Intern Med* 1988;109:7-10.
 40. Cruciani M, Marcati P, Malena M, Bosco O, Serpelloni G, Mengoli C. Meta-analysis of diagnostic procedures for *Pneumocystis carinii* pneumonia in HIV-1-infected patients. *Eur Respir J* 2002;20:982-9.
 41. Saito K, Nakayama S, Nakano K, Tokunaga M, Tsujimura S, Nakatsuka K, et al. Detection of *Pneumocystis carinii* by DNA amplification in patients with connective tissue diseases: reevaluation of clinical features of *P. carinii* pneumonia in rheumatic diseases. *Rheumatology (Oxford)* 2004;43:479-85.
 42. Shimizu A, Oka H, Matsuda T, Ozaki S. (1,3)- β -D glucan is a diagnostic and negative prognostic marker for *Pneumocystis carinii* pneumonia in patients with connective tissue disease. *Clin Exp Rheumatol* 2005;23:678-80.
 43. Wakefield AE, Guiver I, Miller RF, Hopkin JM. DNA amplification on induced sputum samples for diagnosis of *Pneumocystis carinii* pneumonia. *Lancet* 1991;337:1378-9.
 44. Kovacs JA, Masur H. Prophylaxis against opportunistic infections in patients with human immunodeficiency virus infection. *N Engl J Med* 2000;342:1416-29.

運動器外科学分野 軟骨再生学分野

宗田 大

医歯学総合研究科・生体支持組織学系専攻
運動機能再建学・教授



1) 研究の課題名

(1) 前十字靱帯 (ACL) 損傷膝の問題の解決

Solution of ACL injured knee related problems

スポーツ傷害の代表である前十字靱帯 (ACL) 損傷とその治療法の発展を長年のテーマとして取り組んでいる。人工靱帯の開発や移植腱の治癒の促進法を含む手術法の工夫 (1,2,3,4), 再再建術式 (5), 正常解剖と術式の検討 (6) などが手術治療に直結する研究である。ACL 損傷を放置すると外傷性関節症を発症する (7)。その発症素因について患者の検体を用いたマイクロアレイ解析により、重要な遺伝子を明らかにし関節症治療に結びつける取り組みを行っている。また ACL 損傷後の関節液の分析から、治癒傾向や関節症素因の割り出しを目指して検討している。ACL 損傷患者は遺伝子的な背景を持つ。マイクロアレイ解析、患者の形態評価、動作解析 (8) を行うことにより損傷の予防に効果的な目指している。

1. Hara K, Muneta, et al T. Am J Sports Med. 2008;36:333-9.
2. Kawai T, Muneta T, Takakuda K, et al Artif Organs. 2009 Oct 11
3. Kawai T, Muneta T, Takakuda K, et al J Biomed Mater Res B Appl Biomater. 2009;88:264-70.
4. Ju YJ, Muneta T, et al Cell Tissue Res. 2008;332:469-78
5. Muneta T, et al Arthroscopy 2009;25 (in press)
6. Hara K, Muneta T, et al Am J Sports Med. 2009;37:2386-91.
7. Morito T, Muneta T, Sekiya I, et al Rheumatology (Oxford) . 2008;47:1137-43
8. Yamazaki J, Muneta T, et al Knee Surg Sports Traumatol Arthrosc. 2009 Aug 20.

(2) 骨形成、ホメオスタシスにおける骨形成因子 BMP4, 7 の生理機能の解析

Roles of BMPs 4 and 7 during skeletal development and in postnatal bone homeostasis

骨形成因子 (BMP) は、胎生期の骨格形成に必須の分子であるだけでなく、生後の骨のホメオスタシス (骨量の維持、損傷の修復) にも深く関与することが示唆されている。私たちは、BMP2 欠損マウスの解析から、BMP2 は生後の骨のホメオスタシスにおいて必須の分子であり、その欠損により、骨折後の骨修復の過程が完全に阻害されることを、明らかとしてきた (Tsuji et al, Nature Genetics, 2006)。骨修復過程において、BMP2 は、BMP4 及び BMP7 の発現に先立って、早期に一過的に発現量が増大することが知られている。そこで、私たちは、骨折治癒過程におけるそれぞれの BMP の役割として、① BMP2 は、骨折治癒過程における BMP シグナルの開始に必須であり、② BMP4、BMP7 は BMP2 の下流で、内軟骨性骨化のプロセスを開始するために必要な分子である、との仮説を立て、その検証を試みている。四肢特異的、BMP4、BMP7 のコンディショナルノックアウトマウスの解析結果から、BMP4、BMP7 はそれぞれ骨のホメオスタシス、骨折治癒のプロセスに必須の分子ではなく、それらの単独欠損の骨の表現型は野生型マウスにはほぼ同等のものであることを示した (Tsuji et al JBJS Am 2008 for Bmp4 and Tsuji et al JOR in press for Bmp7)。ところが、BMP4、BMP7 を同時に欠損したマウスにおいては、胎生期の骨形成は生じるが、生後の骨形成に重篤な障害が生じることが明らかとなった。現在、BMP4、BMP7 の両方を同時に欠損したマウスの骨修復のプロセスの異常の解析を行っている。

(3) 関節症発症及び病態の進行の分子メカニズムの解析

Identification and characterization of the genes in the pathogenesis of osteoarthritis

本研究は、変形性関節症の発症及び進行に関与する遺伝子の同定及び生理機能の解析を通じて病態の分子メカニズムを明らかとすることを目的としている。ヒト変形

性関節症において、人工膝関節置換術を行った患者の了承のもと、滑膜サンプルにおける遺伝子発現パターンの網羅的解析を行った。その結果、骨棘形成の多寡と相關する遺伝子として、オステオポンチン及びその翻訳後修飾に関与する酵素であるプロトロンビナーゼを同定した。その後の解析より、オステオポンチンの滑膜における発現量、関節液中のタンパク量は、関節軟骨の損傷に伴い増加すること、トロンビン切断型オステオポンチンの関節液中における存在量は、リウマチ性関節炎において増大することを明らかとした。現在、関節症の病態におけるオステオポンチン並びにトロンビン切断型オステオポンチンの生理機能の解析をオステオポンチンノックアウトマウスの系を用いて行っている。

(4) 間葉幹細胞による再生医療の開発

Repair of intraarticular tissue injury by synovial mesenchymal stem cells

私たちのこれまでの解析によると、正常膝関節液中の間葉幹細胞はわずかにしか存在しないが、前十字靭帯損傷や軟骨損傷を有する膝の関節液中には100倍以上の間葉幹細胞が存在する。また、前十字靭帯、半月板、滑膜等の関節内組織由来の間葉幹細胞は、骨髄液、皮下脂肪、骨格筋等の関節外組織由来の間葉幹細胞と比較し、互いに遺伝子プロファイルが類似する。さらに滑膜由来の間葉幹細胞を関節内に投与すると、損傷組織部位に接着し、修復に寄与する。すでに1937年にKingらが報告しているように、関節内の組織損傷部が滑膜組織に被覆され、自然修復に寄与する現象がしばしば観察される。滑膜は間葉幹細胞を貯蔵し、修復に寄与するという仮説を私たちはたてている。すなわち、関節軟骨、半月板、靭帯等の関節内組織損傷により、間葉幹細胞が滑膜から関節液中に動員され、損傷部位に接着し、組織修復に貢献する機序の存在が予測される。しかし、実際には動員または損傷部位に接着する幹細胞の数が限られるため、自然治癒には限界があるものと推察される。私たちは、これまでの基礎研究の成果を踏まえ、滑膜の間葉幹細胞を体外で自己血清を使用して増殖させ、人工素材を使用せずに、関節鏡視下で、軟骨欠損部に移植する、関節軟骨の再生医療を開始している。滑膜間葉幹細胞は、高齢の方からも確実に多くの細胞を確保できることから、変形性関節症への応用も期待できる。

2)



3) 研究内容の英文要約

(1) Anatomy of normal human anterior cruciate ligament attachments evaluated by divided small bundles.

Am J Sports Med 37 (12) :2386-91, 2009

Hara K, Mochizuki T, Sekiya I, Yamaguchi K, Akita K, Muneta T.

BACKGROUND: Double-bundle anterior cruciate ligament (ACL) reconstruction has several potential advantages over single-bundle reconstruction with hamstring tendons. However, there are still controversies regarding tunnel placement in tibial and femoral attachments. HYPOTHESIS: The macroscopically normal ACL consists of small bundles about 1 mm in diameter. Detailed observation of the divided smaller bundles will achieve better understanding of the tunnel placement in anatomic ACL reconstruction. STUDY DESIGN: Descriptive laboratory study. METHODS: This study used 20 cadaveric knees. The ACL was divided into anteromedial and posterolateral bundles, then separated into 10 small bundles of 2-mm diameters, with preservation of their attachment sites marked with color markers. The positional relationship between the femoral and tibial attachments of each small bundle was investigated. RESULTS: A layered positional correlation of small bundles was found between the tibial and femoral attachments. Small bundles aligned in the anterior-posterior direction in the tibia corresponded to the bundles aligned in a high-low direction in the femur in flexion. The femoral attachment pattern was relatively similar in each specimen; however, the tibial attachment showed 2 patterns: an oblique type (12 of 20) and a transverse type (8 of 20). The posterior portion of the posterolateral bundle was separately attached to the medial and lateral portions of the tibial attachment. There was no fibrous insertion in the center of the posterior portion of the ACL tibial attachment in any specimen. In this bare area, there was fat tissue and vascular bundles. CONCLUSION: Small bundles constituting the ACL showed

a relatively layered arrangement between 2 attachments. The tibial attachment showed 2 patterns of oblique and transverse types, and the vascular bundles were located in the center of the posterolateral bundle. **CLINICAL RELEVANCE:** The results of this study of the normal ACL will provide insights for surgeons when placing grafts during anatomic ACL reconstruction.

(2) Anterior Cruciate Ligament Reconstruction Using Chitin-coated Fabrics in a Rabbit Model.

Kawai T, Yamada T, Yasukawa A, Koyama Y, Muneta T, Takakuda K.

Artif Organs. 2009 Oct 11.

Abstract Experimental anterior cruciate ligament (ACL) reconstruction was carried out in a rabbit model, in which a chitin-coated polyester graft was used as the scaffold, and a noncoated graft was used as a control graft. After 8 weeks implantation, a mechanical test of the knee and histometric measurement of the graft and surrounding tissues were carried out. A tensile test of the femur-graft-tibia specimen showed that the knee treated with the coated graft had a peak resistance force of 42.2 ± 12.7 N, which was significantly greater than the 19.2 ± 15.3 N of the knee treated with the control graft. The histometric measurement revealed that the area of bone tissue within the section of the coated graft in the femoral bone tunnel was 3.43 ± 1.73 mm², which was significantly greater than the area of 0.29

(3) Is a minimally invasive approach superior to a conventional approach for total knee arthroplasty? Early outcome and 2- to 4-year follow-up.

Watanabe T, Muneta T, Ishizuki M.

J Orthop Sci 14 (5) :589-95, 2009

BACKGROUND: Total knee arthroplasty (TKA) has been widely applied as an effective treatment for knee arthritis for several decades. More recently, minimally invasive surgery (MIS) has been developed for TKA. The purpose of this study was to clarify the difference in clinical results between MIS and conventional TKA. We hypothesized that knee function would recover earlier with MIS than with conventional TKA without major problems, and hence the middle-term outcome would be better with MIS TKA. **METHODS:** We retrospectively reviewed 48 primary TKAs performed using the same model of a posterior stabilized prosthesis by a single surgeon at our institution: 25 knees treated by a mini midvastus approach (MIS group) and 23 knees treated by a conventional midvastus approach (conventional group). Outcomes at the early stage and at the 2- to 4-year follow-up were evaluated and compared between the two groups. **RESULTS:** The average length of the skin incision was 10.9 cm in the MIS group and 17.1 cm in the conventional group. The duration

of the surgery did not differ significantly between the two groups. Most of the components were correctly implanted in both groups, and no complications were observed. Active straight-leg raising could be achieved significantly earlier in the MIS group. Knee function at the 2- to 4-year follow-up did not significantly differ between the two groups. **CONCLUSIONS:** The early results and the wide indication encourage us to apply the MIS approach instead of the conventional technique. The limitation of this study was the small number of cases in the retrospective point of view. If the number were larger, perhaps other significant differences could be detected. Further investigations on a larger scale are required to solve this problem.

(4) Tohyama H, Yasuda K, Minami A, Majima T, Iwasaki N, Muneta T, Sekiya I, Yagishita K, Takahashi S, Kurokouchi K, Uchio Y, Iwasa J, Deie M, Adachi N, Sugawara K, Ochi M.

Atelocollagen-associated autologous chondrocyte implantation for the repair of chondral defects of the knee: a prospective multicenter clinical trial in Japan.

J Orthop Sci. ;14 (5) :579-88, 2009

BACKGROUND: New tissue-engineering technology was developed to create a cartilage-like tissue in a three-dimensional culture using atelocollagen gel. The minimum 2-year followup outcome of transplanting autologous chondrocytes cultured in atelocollagen gel for the treatment of full-thickness defects of cartilage in knees was reported from the single institution. The present multicenter study was conducted to determine clinical and arthroscopic outcomes in patients who underwent atelocollagen-associated autologous chondrocyte implantation for the repair of chondral defects of the knees. **METHODS:** At six medical institutes in Japan, we prospectively evaluated the clinical and arthroscopic outcomes of transplanting autologous chondrocytes cultured in atelocollagen gel for the treatment of full-thickness defects of cartilage in 27 patients (27 knees) with cartilage lesions on a femoral condyle or on a patellar facet over 24 months. **RESULTS:** The Lysholm score significantly increased from 60.0 ± 13.7 points to 89.8 ± 9.5 points ($P = 0.001$). Concerning the ICRS grade for arthroscopic appearance, 6 knees (24%) were assessed as grade I (normal) and 17 knees (68%) as grade II (nearly normal). There were few adverse features, except for detachment of the graft in two cases. **CONCLUSIONS:** We concluded that transplanting chondrocytes in a newly formed matrix of atelocollagen gel can promote restoration of the articular cartilage of the knee.

(5) Yamazaki J, Muneta T, Ju YJ, Sekiya I.

Differences in kinematics of single leg squatting between anterior cruciate ligament-injured patients and healthy controls.

Knee Surg Sports Traumatol Arthrosc. 2009 Aug 20. Seventy to eighty percent of all anterior cruciate ligament (ACL) injuries are due to non-contact injury mechanisms. It has been reported that the majority of injuries due to single leg landing come from valgus positioning of the lower leg. Preventing valgus positioning during single leg landing is expected to help reduce the number of ACL injuries. We found that many ACL-deficient patients cannot perform stable single leg squatting. Therefore, we performed 3D motion analysis of the single-legged half squat for ACL-injured patients to evaluate its significance as a risk factor for ACL injuries. We evaluated the relative angles between the body, thigh, and lower leg using an electromagnetic device during single leg half squatting performed by 63 ACL-injured patients (32 males, 31 females) the day before ACL reconstruction and by 26 healthy control subjects with no knee problems. The uninjured leg of ACL-injured male subjects demonstrated significantly less external knee rotation than that of the dominant leg of the male control. The uninjured leg of ACL-injured female subjects demonstrated significantly more external hip rotation and knee flexion and less hip flexion than that of the dominant leg of the female control. Comparing injured and uninjured legs, the injured leg of male subjects demonstrated significantly less external knee and hip rotation, less knee flexion, and more knee varus than that of the uninjured leg of male subjects. The injured leg of female subjects demonstrated more knee varus than that of the uninjured leg of female subjects. Regarding gender differences, female subjects demonstrated significantly more external hip rotation and knee valgus than male subjects did in both the injured and uninjured legs ($P < 0.05$). The current kinematic study exhibited biomechanical characteristics of female ACL-injured subjects compared with that of control groups.

(6) Horie M, Sekiya I, Nakamura T, Tanaka H, Maekawa K, Nakanishi M, Muneta T, Kobayashi E.

In vivo pharmacokinetics of ketoprofen after patch application in the Mexican hairless pig. Biopharm Drug Dispos 30 (4) :204-8, 2009 To evaluate the pharmacokinetics of topical drugs, *in vitro* permeation studies are performed using sacrificed pig skin or human tissues resected at surgery; however, these methods have their limitations in *in vivo* pharmacokinetics. This study examined the usefulness of Mexican hairless pigs for *in vivo* pharmacokinetic study, especially the drug concentration in the tissues. A ketoprofen patch was applied on the back of Mexican hairless pigs for 24 h, followed by sequential collection of blood specimens from 0 to 36 h ($n=3$). Also, the skin, subcutaneous fat, fascia and muscle from the center of the site of application were excised at 12 h after the application ($n=4$). Ketoprofen

was first detected in the plasma at 8 h, the concentration increasing up to 24 h; the plasma concentration began to decrease after the removal of the ketoprofen patch. Ketoprofen concentrations in the tissues decreased with increasing depth of the tissues, but the values in the deep muscles, being the lowest among the tissues examined, were still higher than those in the plasma. While the data of drug concentration in human tissue are difficult to test, the Mexican hairless pig model appears to be attractive for *in vivo* pharmacokinetic studies of topically applied ketoprofen. Copyright (c) 2009 John Wiley & Sons, Ltd.

(7) Ezura Y, Sekiya I, Koga H, Muneta T, Noda M.

Methylation status of CpG islands in the promoter regions of signature genes during chondrogenesis of human synovium-derived mesenchymal stem cells.

Arthritis Rheum 60 (5) :1416-26, 2009

OBJECTIVE: Human synovium-derived mesenchymal stem cells (MSCs) can efficiently differentiate into mature chondrocytes. It has been suggested that DNA methylation is one mechanism that regulates human chondrogenesis; however, the methylation status of genes related to chondrogenic differentiation is not known. The purpose of this study was to investigate the CpG methylation status in human synovium-derived MSCs during experimental chondrogenesis, with a view toward potential therapeutic use in osteoarthritis. **METHODS:** Human synovium-derived MSCs were subjected to chondrogenic pellet culture for 3 weeks. The methylation status of 12 regions in the promoters of 10 candidate genes (SOX9, RUNX2, CHM1, FGFR3, CHAD, MATN4, SOX4, GREM1, GPR39, and SDF1) was analyzed by bisulfite sequencing before and after differentiation. The expression levels of these genes were analyzed by real-time reverse transcription-polymerase chain reaction. Methylation status was also examined in human articular cartilage. **RESULTS:** Bisulfite sequencing analysis indicated that 10 of the 11 CpG-rich regions analyzed were hypomethylated in human progenitor cells before and after 3 weeks of pellet culture, regardless of the expression levels of the genes. The methylation status was consistently low in SOX9, RUNX2, CHM1, CHAD, and FGFR3 following an increase in expression upon differentiation and was low in GREM1 and GPR39 following a decrease in expression upon chondrogenesis. One exceptional instance of a differentially methylated CpG-rich region was in a 1-kb upstream sequence of SDF1, the expression of which decreased upon differentiation. Paradoxically, the hypermethylation status of this region was reduced after 3 weeks of pellet culture. **CONCLUSION:** The DNA methylation levels of CpG-rich promoters of genes related to chondrocyte phenotypes are largely kept low during chondrogenesis in human synovium-derived MSCs.

(8) Horie M, Sekiya I, Muneta T, Ichinose S, Matsumoto K, Saito H, Murakami T, Kobayashi E.

Intra-articular Injected synovial stem cells differentiate into meniscal cells directly and promote meniscal regeneration without mobilization to distant organs in rat massive meniscal defect.

Stem Cells 27 (4) :878-87, 2009

Osteoarthritis in the knees, which can be caused by meniscal defect, constitutes an increasingly common medical problem. Repair for massive meniscal defect remains a challenge owing to a lack of cell kinetics for the menisci precursors in knee joint. The synovium plays pivotal roles during the natural course of meniscal healing and contains mesenchymal stem cells (MSCs) with high chondrogenic potential. Here, we investigated whether intra-articular injected synovium-MSCs enhanced meniscal regeneration in rat massive meniscal defect. To track the injected cells, we developed transgenic rats expressing dual luciferase (Luc) and LacZ. The cells derived from synovium of the rats demonstrated colony-forming ability and multipotentiality, both characteristics of MSCs. Hierarchical clustering analysis revealed that gene expression of meniscal cells was closer to that of synovium-MSCs than to that of bone marrow-MSCs. Two to 8 weeks after five million Luc/LacZ+ synovium-MSCs were injected into massive meniscectomized knee of wild-type rat, macroscopically, the menisci regenerated much better than it did in the control group. After 12 weeks, the regenerated menisci were LacZ positive, produced type 2 collagen, and showed meniscal features by transmission electron microscopy. In in-vivo luminescence analysis, photons increased in the meniscus-resected knee over a 3-day period, then decreased without detection in all other organs. LacZ gene derived from MSCs could not be detected in other organs except in synovium by real-time PCR. Synovium-MSCs injected into the massive meniscectomized knee adhered to the lesion, differentiated into meniscal cells directly, and promoted meniscal regeneration without mobilization to distant organs.

(9) Koga H, Engebretsen L, Brinchmann JE, Muneta T, Sekiya I.

Mesenchymal stem cell-based therapy for cartilage repair: a review.

Knee Surg Sports Traumatol

Arthrosc 17 (11) :1289-97, 2009

Articular cartilage injury remains one of the major concerns in orthopaedic surgery. Mesenchymal stem cell (MSC) transplantation has been introduced to avoid some of the side effects and complications of current techniques. The purpose of this paper is to review the literature on MSC-based cell therapy for articular cartilage repair to determine if it can be an alternative treatment for cartilage injury. MSCs retain both high proliferative

potential and multipotentiality, including chondrogenic differentiation potential, and a number of successful results in transplantation of MSCs into cartilage defects have been reported in animal studies. However, the use of MSCs for cartilage repair is still at the stage of preclinical and phase I studies, and no comparative clinical studies have been reported. Therefore, it is difficult to make conclusions in human studies. This requires randomized clinical trials to evaluate the effectiveness of MSC-based cell therapy for cartilage repair.

(10) Mochizuki T, Sugaya H, Uomizu M, Maeda K, Matsuki K, Sekiya I, Muneta T, Akita K.

Humeral insertion of the supraspinatus and infraspinatus. New anatomical findings regarding the footprint of the rotator cuff. Surgical technique.

J Bone Joint Surg Am 91 Suppl 2 Pt 1:1-7, 2009

BACKGROUND: It is generally believed that the supraspinatus is the most commonly involved tendon in rotator cuff tears. Clinically, however, atrophy of the infraspinatus muscle is frequently observed in patients with even small to medium-size rotator cuff tears. This fact cannot be fully explained by our current understanding of the anatomical insertions of the supraspinatus and infraspinatus. The purpose of this study was to reinvestigate the humeral insertions of these tendons. **METHODS:** The study included 113 shoulders from sixty-four cadavers. The humeral insertion areas of the supraspinatus and infraspinatus were investigated in ninety-seven specimens. In sixteen specimens, all muscular portions of the supraspinatus and infraspinatus were removed, leaving the tendinous portions intact, in order to define the specific characteristics of the tendinous portion of the muscles. Another twenty-six shoulders were used to obtain precise measurements of the footprints of the supraspinatus and infraspinatus. **RESULTS:** The supraspinatus had a long tendinous portion in the anterior half of the muscle, which always inserted into the anteriormost area of the highest impression on the greater tuberosity and which inserted into the superiormost area of the lesser tuberosity in 21% of the specimens. The footprint of the supraspinatus was triangular in shape, with an average maximum medial-to-lateral length of 6.9 mm and an average maximum anteroposterior width of 12.6 mm. The infraspinatus had a long tendinous portion in the superior half of the muscle, which curved anteriorly and extended to the anterolateral area of the highest impression of the greater tuberosity. The footprint of the infraspinatus was trapezoidal in shape, with an average maximum medial-to-lateral length of 10.2 mm and an average maximum anteroposterior width of 32.7 mm. **CONCLUSIONS:** The footprint of the supraspinatus on the greater tuberosity is much smaller than previously believed, and this area of the greater tuberosity is actually

occupied by a substantial amount of the infraspinatus.

(11) Sekiya I, Tang T, Hayashi M, Morito T, Ju YJ, Mochizuki T, Muneta T.

Periodic knee injections of BMP-7 delay cartilage degeneration induced by excessive running in rats. *J Orthop Res* 27 (8) :1088-92, 2009

Strenuous running of rats enhances mechanical stress on the knee, thereby inducing degeneration of articular cartilage. Bone morphogenetic protein-7 (BMP-7) has an inhibitory effect on cartilage degeneration, suggesting its usefulness for human osteoarthritis patients. However, its mode of administration should be investigated. We examined whether weekly knee injections of BMP-7 delayed the progression of cartilage degeneration. Wistar rats were forced to run 30 km in 6 weeks on a rodent treadmill, and BMP-7 was injected weekly into the knee. Macroscopically and histologically, this strenuous running regimen induced cartilage degeneration. Weekly injections of 250 ng BMP-7 delayed the progression of cartilage degeneration. Immunohistochemically, in the control knee, type II collagen expression decreased, while BMP-7 expression in chondrocytes slightly increased. Interestingly, weekly injection of BMP-7 increased BMP-7 expression even 9 days after the final injection. Disulfate disaccharide keratan sulfate in serum transiently increased in the control group, while it remained at a low level in the BMP-7 group. Weekly BMP-7 injection increased BMP-7 expression in chondrocytes and its effect seemed to last more than 7 days. The effect of BMP-7 could be monitored by serum keratan sulfate concentration. Periodical injections of BMP-7 delayed progression of cartilage degeneration induced by excessive running in rats. Copyright 2009 Orthopaedic Research Society. Published by Wiley Periodicals, Inc

(12) Segawa Y, Muneta T, Makino H, Nimura A, Mochizuki T, Ju YJ, Ezura Y, Umezawa A, Sekiya I.

Mesenchymal stem cells derived from synovium, meniscus, anterior cruciate ligament, and articular chondrocytes share similar gene expression profiles. *J Orthop Res* 27 (4) :435-41, 2009

Section of Orthopedic Surgery, Tokyo Medical and Dental University, Tokyo, Japan.

Mesenchymal stem cells (MSCs) can be obtained from various tissues, and contain common features. However, an increasing number of reports have described variant properties dependent of cell sources. We examined (1) whether MSCs existed in several intraarticular tissues, (2) whether gene expression profiles in intraarticular tissue MSCs closely resembled each other, and (3) whether identified genes were specific to intraarticular tissue MSCs. Human synovium, meniscus, intraarticular ligament, muscle, adipose tissue, and bone marrow were harvested, and

colony-forming cells were analyzed. All these cells showed multipotentiality and surface markers typical of MSCs. Gene profiles of intraarticular tissue MSCs and chondrocytes were closer to each other than those of extraarticular tissues MSCs. Among three characteristic genes specific for intraarticular tissue MSCs, we focused on proline arginine-rich end leucine-rich repeat protein (PRELP). Higher expression of PRELP was confirmed in chondrocytes and intraarticular tissue MSCs among three elderly and three young donors. Synovium MSCs stably expressed PRELP, contrarily, bone marrow MSCs increased PRELP expression during in vitro chondrogenesis. In conclusion, MSCs could be isolated from various intraarticular tissues including meniscus and ligament, gene expression profiles of intraarticular tissue MSCs closely resembled each other, and the higher expression of PRELP was characteristic of intraarticular tissue MSCs.

(13) Asano H, Muneta T, Sekiya I

Soft tissue tension in extension in total knee arthroplasty affects postoperative knee extension and stability.

Knee Surg Sports Traumatol Arthrosc. 2009 Apr;17 (4) :431.

The purpose of this study was to assess correlation of soft tissue tension in extension with postoperative extension deficit and valgus/varus instability. Sixty-four osteoarthritic knees that underwent primary total knee arthroplasty were investigated. Soft tissue tension in extension was measured during operation with a balancer/tensor device. Extension deficit was measured, and valgus/varus laxity was assessed by stress radiographs in extension and 30 degrees -flexion 1 year after operation. The extension deficit became larger with an increase of soft tissue tension a year after operation. ($P < 0.05$) The varus laxity in extension and 30 degrees -flexion and valgus laxity in 30 degrees -flexion became smaller with an increase of soft tissue tension ($P < 0.05$). Our results demonstrated that soft tissue tension during operation affects postoperative knee extension and stability.

(14) Kawai T, Yamada T, Yasukawa A, Koyama Y, Muneta T, Takakuda K.

Biological fixation of fibrous materials to bone using chitin/chitosan as a bone formation accelerator. *J Biomed Mater Res B Appl Biomater* 88 (1) :264-70, 2009

Biological fixation or anchorage of fibrous materials to bone by bone ingrowth into the spaces between fibers is a major concern in developing novel medical implants, including artificial ligaments. Toward this end, we evaluated the efficacy of chitin/chitosan as a bone formation accelerator. Specimens of polyester nonwoven fabric coated with chitin/chitosan were implanted into holes drilled into the

distal ends of rat femora. Uncoated fabric specimens were used as controls. At 1 or 2 weeks after implantation, the specimens were retrieved, and the fixation strength was measured by mechanical testing. Histological sections of 2-week implantation specimens were prepared, and the area of new bone tissue formed in the spaces between the fibers of the fabric was measured. The chitin/chitosan coating significantly increased the fixation strength and the area of bone tissue formed in the spaces between the fibers. The mean fixation strength of chitin/chitosan-coated fabric specimens was more than twice that of the controls at 2 weeks after implantation. These results demonstrated that the chitin/chitosan coating effectively induced bone formation in the spaces between the fibers and enhanced biological fixation of the fibrous materials to the bone. (c) 2008 Wiley Periodicals, Inc

(15) Tsuji K, Cox K, Gamer L, Graf D, Economides A, Rosen V.

Conditional deletion of BMP7 from the limb skeleton does not affect bone formation or fracture repair.

J Orthop Res. 2009 Sep 24.

While the osteoinductive activity of recombinant bone morphogenetic protein 7 (BMP7) is well established, evaluation of the role of endogenous BMP7 in bone formation and fracture healing has been hampered by perinatal lethality in BMP7 knockout mice. Here we employ conditional deletion of BMP7 from the embryonic limb prior to the onset of skeletogenesis to create limb bones lacking BMP7. We find that the absence of locally produced BMP7 has no effect on postnatal limb growth, articular cartilage formation, maintenance of bone mass, or fracture healing. Our data suggest that other BMPs present in adult bone are sufficient to compensate for the absence of BMP7.

(16) Ichinose S, Muneta T, Koga H, Segawa Y, Tagami M, Tsuji K, Sekiya I.

Morphological differences during in vitro chondrogenesis of bone marrow-, synovium-MSCs, and chondrocytes.

Lab Invest. [Epub ahead of print]

Instrumental Analysis Research Center, Tokyo Medical and Dental University, Tokyo, Japan.

Mesenchymal stem cells (MSCs) from a variety of mesenchymal tissue contain common features, but distinguishing properties dependent on their origin are emerging. We investigated morphological differences of human bone marrow-MSCs, synovium-MSCs, and chondrocytes during in vitro chondrogenesis. Two hundred thousands cells were pelleted after centrifugation and cultured in chondrogenic media that contained BMP-2, TGF-beta3, and dexamethasone. The pellets were analyzed histologically, immunohistologically, and electron microscopically. Before chondrogenic induction, trypsinized

MSCs and chondrocytes looked similar. At day 1, the structure of the three masses was divided into two layers, and the most obvious differences in the three populations were observed in the deep zone. In bone marrow-MSCs, round cells accumulated without intercellular space, and the cells were mainly connected through intermediate junctions. In synovium-MSCs, elongated cells accumulated with small desmosomes and intercellular spaces could occasionally be seen. In chondrocytes, separated oval and polygonal cells connected only in a narrow spotty area through a small desmosome. At day 7, the structure of the three masses was divided into three layers, and the most obvious differences in the three populations were observed in the middle zone. In bone marrow-MSCs, the middle zone consisted of dense smaller cells and apoptotic cells. In synovium-MSCs, the middle zone consisted of dense arrayed wider cells and apoptotic cells. In chondrocytes, the middle zone was acellular without apoptotic cells. At day 21, the morphology of cells and extracellular space became similar in that each cell was located separately with abundant extracellular matrix. The superficial zone was still obvious in bone marrow-MSCs, but hardly seen both in synovium-MSCs and chondrocytes. In this study, we revealed morphological differences of bone marrow-MSCs, synovium-MSCs, and chondrocytes during in vitro chondrogenesis. The most obvious differences in the three populations were observed at day 1 in the deep zone. Laboratory Investigation advance online publication, 14 December 2009; doi:10.1038/labinvest.2009.125.

(17) Muneta T, Hara K, Ju YJ, Mochizuki T, Morito T, Yagishita K, Sekiya I

Revision Anterior Cruciate Ligament Reconstruction By Double-Bundle Technique Using A Multi-Strand Semitendinosus Tendon

Arthroscopy 2009 (in press)

Purpose: The purpose of the study is to compare the outcome of revision anterior cruciate ligament (ACL) reconstruction by double-bundle (DB) technique with a multi-strand semitendinosus tendon with that of primary reconstruction using the same technique.

Methods: Twenty-one patients of revision ACL reconstructions (average 40 months follow-up) with the hamstring DB technique between 1995 and 2006, and 86 unilateral primary DB ACL reconstructions (average 33 months follow-up) between 2000 and 2004 were included in the study. The outcome of both groups was compared based on the difference between operated and unoperated limbs and modified IKDC grading. Both the overall and sports-related subjective scores were evaluated between the two groups. Results: The KT measurements averaged 1.7 mm (SD, 1.8 mm) in the revision group and 1.5 mm (SD, 1.6 mm) in the primary group. There was no significant

difference of KT measurements between the two groups. Eighty-three % of revision cases and 87 % of primary cases were negative in Lachman test, 83 % and 91 % were negative in anterior drawer test (ADT) , and 78% and 90 % were negative in pivot-shift test, respectively. There was a tendency of positive pivot-shift test in the revision group being higher. The Lysholm score and subjective recovery score were significantly lower in the revision group. There were no differences between the two groups regarding sports related parameters.

Conclusion: The semitendinosus tendon DB revision procedure provided range of motion and anterior stability comparable to that after primary DB surgery and a comparable return to athletic activities. However, the patients tended to have positive pivot-shift test results. The revision cases were also inferior in general evaluation recovery of knee strength. The outcome scores were lower overall in the revision group.

(18) Sekiya I, Morito T, Hara K, Yamazaki J, Ju YJ, Yagishita K, Mochizuki T, Tsuji K, Muneta T.

AAPS PharmSciTech (in press)

Ketoprofen Absorption by Muscle and Tendon after Topical or Oral Administration in Patients Undergoing Anterior Cruciate Ligament Reconstruction

Abstract. Topical ketoprofen patches are widely used in the treatment of musculoskeletal pain, but the pharmacokinetics of ketoprofen following topical application remain unclear.

This open-label, single-dose pharmacokinetic study was designed to determine the concentrations of ketoprofen in the semitendinosus muscle/tendon and plasma after topical application or oral administration to patients scheduled for anterior cruciate ligament reconstruction. Two ketoprofen patches (20mg each) were applied over the semitendinosus muscle/tendon for 1, 6, 14, or 20 h before surgery in 21 patients, while one sustained-release 150 mg ketoprofen capsule was administered to six patients 14 h before surgery. Ten untreated patients served as the control group. The main outcome measures were the semitendinosus muscle/tendon and plasma concentrations of ketoprofen at 1, 6, 14, and 20 h. Ketoprofen was detected in the semitendinosus muscle/ tendon from about 1 h after topical application. The peak concentration was reached at 6 h, and it decreased gradually until 20 h, although the concentration at 20 h was still higher than that at 1 h. Unlike the tissue concentration, the plasma concentration of ketoprofen increased gradually after topical application. At 14 h, there was no significant difference of the tissue concentration between the topical and oral groups, although the plasma concentration was about 17-fold higher in the oral group than in the topical group. In conclusion, following topical application in a patch, ketoprofen shows rapid and sustained delivery to the underlying tissues without a

significant increase of the plasma drug concentration.

4) 本事業に関連して世界的な研究拠点形成に向けて、以下の点で改善・整備等されたこと

A (研究拠点体制)

間葉幹細胞を用いた新規治療:これまで教室のメインテーマとして滑膜幹細胞の細胞移植による関節軟骨欠損の治療を臨床応用まで高めた。今後ともよりよい治療法の実現に向け基礎研究で裏付けながら取り組んでいく。滑膜幹細胞の臨床応用を米国の施設とも共同して臨床応用を進めていく計画が進んでいる。また関節軟骨欠損の治療ばかりでなく、他の関節構造の再建に滑膜幹細胞を応用する基礎的研究が進んでいる。さらに他の間葉幹細胞を用いた細胞治療についても積極的に取り組み臨床応用の実績を積み重ねる予定である。

各種BMPの機能解析と新規治療法の開発:各種BMPを発生過程さらに生後の必要な時期にノックアウト、ノックダウンする技術を駆使して研究をしてきた研究者をGCOEの国際シャペロン教官として教室に得た。M・Dタワーに教室が移転し、ノックアウトマウスの飼育スペースも確保された。Harvard大学との共同研究も引き続いて行われている。またBMP-7についてストライカーバイオテックとの共同研究も引き続き行われている。

膝前十字靱帯損傷治療の改善:高い臨床治療実績、長年のACL研究、解剖学的研究に基づいた再建手術の最適化に加えて、バイオメカ研究によってACL損傷患者の特徴を明らかにしつつある。またフィールドスタディも進みつつある。

B (研究教育環境)

M・Dタワーへの引っ越しにより教室の研究面積が3倍増した。新しい動物実験設備も完備し、遺伝子組み換え実験室も整った。GCOE事業担当分野間の共同研究も複数進行している。教育スタッフの増員によって大学院生各人に対する個別教育の時間が増し、その質が向上した。

C (人材確保)

国際シャペロンの分野への採用により研究の幅が広がり、教育の充実化が図られた。毎年3.4人の大学院生を受け入れ、国外からの留学生も慎重な選択のもとに受け入れている。

D (人材育成)

週3回の早朝カンファランスと勉強会により、研究

基盤として最新研究に遅れないように留意している。海外の著名な研究者や新進の研究者に積極的に依頼し、セミナーを適時開催している。セミナーの前後に大学院生に個別の指導を依頼し、実施している。国際シャペロンの分野への採用により教育の充実化が図られた。

E (国際化)

国際シャペロンとの関係から Harvard 大学歯学部との2つの共同研究プロジェクトを立ち上げた。滑膜幹細胞を用いた関節軟骨細胞治療の臨床研究が米国テキサス州の病院と進みつつある。

大学院生卒業生が米国に2名とノルウェーに留学し、業績を挙げている。来年度も1人留学する。大学院卒業生の留学率が増加している。

5) GCOE 事業を推進するに当たって力を入れた点

GCOEにより新たに教室に加わった国際シャペロン教官による各種改変マウスを駆使したBMP研究の推進。シャペロン教官による大学院生の個別教育の充実。滑膜幹細胞を用いた治療法の臨床応用の推進と間葉幹細胞研究の対象の広域化。国際的な共同研究の推進。事業者間の共同研究の立ち上げ。

6) 英文原著論文

- Hara K, Mochizuki T, Sekiya I, Yamaguchi K, Akita K, Muneta T. Anatomy of normal human anterior cruciate ligament attachments evaluated by divided small bundles. *Am J Sports Med* 37(12):2386-91, 2009
- Kawai T, Yamada T, Yasukawa A, Koyama Y, Muneta T, Takakuda K. Anterior Cruciate Ligament Reconstruction Using Chitin-coated Fabrics in a Rabbit Model. *Artif Organs*. 2009
- Watanabe T, Muneta T, Ishizuki M. Is a minimally invasive approach superior to a conventional approach for total knee arthroplasty? Early outcome and 2- to 4-year follow-up. *J Orthop Sci* 14(5):589-95, 2009
- Tohyama H, Yasuda K, Minami A, Majima T, Iwasaki N, Muneta T, Sekiya I, Yagishita K, Takahashi S, Kurokouchi K, Uchio Y, Iwasa J, Deie M, Adachi N, Sugawara K, Ochi M. Atelocollagen-associated autologous chondrocyte implantation for the repair of chondral defects of the knee: a prospective multicenter clinical trial in Japan. *J Orthop Sci* 14(5):579-88, 2009
- Yamazaki J, Muneta T, Ju YJ, Sekiya I. Differences in kinematics of single leg squatting between anterior cruciate ligament-injured patients and healthy controls. *Knee Surg Sports Traumatol Arthrosc*. 2009 Aug 20.
- Horie M, Sekiya I, Nakamura T, Tanaka H, Maekawa K, Nakanishi M, Muneta T, Kobayashi E. In vivo pharmacokinetics of ketoprofen after patch application in the Mexican hairless pig. *Biopharm Drug Dispos* 30(4):204-8, 2009
- Ezura Y, Sekiya I, Koga H, Muneta T, Noda M. Methylation status of CpG islands in the promoter regions of signature genes during chondrogenesis of human synovium-derived mesenchymal stem cells. *Arthritis Rheum* 60(5):1416-26, 2009
- Horie M, Sekiya I, Muneta T, Ichinose S, Matsumoto K, Saito H, Murakami T, Kobayashi E. Intra-articular Injected synovial stem cells differentiate into meniscal cells directly and promote meniscal regeneration without mobilization to distant organs in rat massive meniscal defect. *Stem Cells* 27(4):878-87, 2009
- Koga H, Engebretsen L, Brinchmann JE, Muneta T, Sekiya I. Mesenchymal stem cell-based therapy for cartilage repair: a review. *Knee Surg Sports Traumatol Arthrosc* 17(11):1289-97, 2009
- Mochizuki T, Sugaya H, Uomizu M, Maeda K, Matsuki K, Sekiya I, Muneta T, Akita K. Humeral insertion of the supraspinatus and infraspinatus. New anatomical findings regarding the footprint of the rotator cuff. Surgical technique. *J Bone Joint Surg Am*. ;91 Suppl 2 Pt 1:1-7, 2009
- Sekiya I, Tang T, Hayashi M, Morito T, Ju YJ, Mochizuki T, Muneta T. Periodic knee injections of BMP-7 delay cartilage degeneration induced by excessive running in rats. *J Orthop Res* 27(8):1088-92, 2009
- Segawa Y, Muneta T, Makino H, Nimura A, Mochizuki T, Ju YJ, Ezura Y, Umezawa A, Sekiya I. Mesenchymal stem cells derived from synovium, meniscus, anterior cruciate ligament, and articular chondrocytes share similar gene expression profiles. *J Orthop Res*. 27(4):435-41, 2009
- Asano H, Muneta T, Sekiya I. Soft tissue tension in extension in total knee arthroplasty affects postoperative knee extension and stability. *Knee Surg Sports Traumatol Arthrosc*. ;16(11):999-1003, 2008 Erratum in: *Knee Surg Sports Traumatol Arthrosc* 17(4):431, 2009 .
- Kawai T, Yamada T, Yasukawa A, Koyama Y, Muneta T, Takakuda K. Biological fixation of fibrous materials to bone using chitin/chitosan as a bone formation accelerator. *J Biomed Mater Res B Appl Biomater* 88(1):264-70, 2009
- Tsuji K, Cox K, Gamer L, Graf D, Economides A, Rosen V. Conditional deletion of BMP7 from the limb skeleton does not affect bone formation or fracture repair. *J Orthop Res*. 2009
- Ichinose S, Muneta T, Koga H, Segawa Y, Tagami M, Tsuji K, Sekiya I. Morphological differences during in

vitro chondrogenesis of bone marrow-, synovium-MSCs, and chondrocytes Laboratory Investigation

17. Muneta T, Hara K, Ju YJ, Mochizuki T, Morito T, Yagishita K, Sekiya I. Revision Anterior Cruciate Ligament Reconstruction by Double-Bundle Technique Using Multi-Strand Semitendinosus Tendon Arthroscopy: The Journal of Arthroscopic and Related Surgery,
18. Sekiya I, Morito T, Hara K, Yamazaki J, Ju YJ, Yagishita K, Mochizuki T, Muneta T. Ketoprofen absorption by muscle and tendon after topical or oral administration in patients undergoing anterior cruciate ligament reconstruction AAPS PharmSciTech

7) 著書

宗田 大、齋藤知行、井原秀俊:NHK ここが聞きたい! 名医にQ ひざの痛み。2009.3.20 日本放送出版協会 総ページ71

宗田 大、秋田恵一:第5章 膝関節への進入法 内側側方進入法。「手術進入法-下肢」最新整形外科学大系8 中山書店 p.212 - 217, 2009.5.8 総ページ330

宗田 大:膝部痛点ストレッチ。日常診療に役立つ整形外科領域の痛みの知識。企画 山下敏彦 整形・災害外科4月臨時増刊号 Vol.52.5:542, 2009. 総ページ200

宗田 大:前十字靭帯損傷の診断と治療。すぐに役立つ日常整形外科診療に対する私の工夫。Monthly Book Orthopaedics 2009 22 (5) : 231-242. 総ページ数282

宗田 大:皮膚切開。2.Medial parapatellar (MPP) 皮切 P.8-12 編集 松野誠夫他 人工膝関節置換術—手技と論点— 医学書院 2009.12.1 総ページ数336

関矢一郎、宗田大
関節液中の幹細胞
関節外科
p.108-110, vol 28, No. 2, 2009

関矢一郎
いま基礎研究がおもしろい -整形外科医のラボ日記-
臨床雑誌 整形外科
p.372-373, vol 60, No. 4, 2009

関矢一郎、堀江雅史
ダブルトランスジェニックラットを用いた再生医療研究—滑膜幹細胞による半月板再生—

医学のあゆみ
p.135-140, vol 230, No. 2, 2009

8) 平成21年度までの自己評価

平成20年度より開催されたGCOEにより、国際シャペロンが一名運動器外科学での研究に参加することになった。これにより教育の幅が広がり、新たな研究領域が開かれた。靭帯の研究は進んでいるもののそのスピードは速いとは言えない。これまで教室のメインテーマとして発展してきた滑膜幹細胞の研究は新たな進歩を遂げているがなお改善の余地を残している。シャペロンを中心としたBMP研究はようやくその基盤となる遺伝子改変マウスがそろい始めている。

教育面では大学院生に対するきめ細かで時間をかけたアプローチが実現した。研究でも新たな領域が広がりつつあるがなお成果をみない。臨床面での滑膜幹細胞を用いた軟骨治療に対する一層の改善が求められる。

9) 和文原著論文

宗田 大
整形外科手術・私のポイント。膝前十字靭帯の二重束再建術
整形・災害外科52:1098-1099, 2009

宗田 大
膝の痛みをとる-痛点ストレッチについて
Sportsmedicine 113:6-12, 2009

関矢一郎、宗田大
関節液中の幹細胞
関節外科
p.108-110, vol 28, No. 2, 2009

関矢一郎
いま基礎研究がおもしろい -整形外科医のラボ日記-
臨床雑誌 整形外科
p.372-373, vol 60, No. 4, 2009

関矢一郎、堀江雅史
ダブルトランスジェニックラットを用いた再生医療研究—滑膜幹細胞による半月板再生—
医学のあゆみ
p.135-140, vol 230, No. 2, 2009

清水 禎則、麻生 義則

破骨細胞形成抑制因子オステオプロテジェリンの関節内投与はマウス外傷性変形性関節症モデルにおける軟骨破壊を阻害する

整形外科 60 (2) : 185-190, 2009

清水 禎則、立石 智彦、長瀬 寅、朝比奈 信太郎、中川 照彦、土屋 正光

MPFL再建術後の膝蓋骨高位に関するX線学的検討

膝 33 (1) : 64-66, 2008

清水 禎則、立石 智彦、長瀬 寅、中川 照彦、土屋 正光

大相撲力士の頸椎外傷・障害の検討

日本整形外科スポーツ医学会誌 Vol.29 (3) :164-167, 2009.

10) 学会発表 (英文)

Takeshi Muneta

Symposium, Symposium: Double bundle ACL reconstruction: Any evidence based clinical advantages? Clinical evidence from the literature

ISAKOS 2009 in Osaka, 2009.4.5

Takeshi Muneta

ICL #12. Technical Considerations in Double Bundle ACL Reconstruction

ISAKOS in OSAKA 2009.4.7 Transtibial approach in figure-four position using moving-a-wire technique

Koga H, Nakamae A, Shima Y, Iwasa J, Krosshaug T. Updated results of analysis of non-contact ACL injury situation

Oslo Sports Trauma Research Center spring seminar. Oslo, Norway. 2009.5.13-15

Koga H, Nakamae A, Shima Y, Iwasa J, Myklebust G, Bahr R, Krosshaug T.

Reconstruction of the injury mechanisms for anterior cruciate ligament injuries among female basketball and team handball players

Idrettsmedisinsk Høstkongress (Norwegian Congress of Sports Medicine) . Trondheim, Norway. 2009.11.5-8

Toshiyuki Morito, Takeshi Muneta, Sheng Zhang, Tomoyuki Mochizuki, Ichiro Sekiya Autologous synovial fluid enhances expansion of mesenchymal stem cells through TGF-beta effect in tissue culture of synovium from osteoarthritis patients

ISAKOS 大阪 2009.4.5

11) 学会発表 (和文)

宗田 大、原 憲司、朱 寧進、山崎順也、森戸俊行、関矢一郎

FasT-Fixによる半月板修復術の経験。第49回関東整形災害外科学会パネル 2009.3.21 会長 里見 和彦

宗田 大

診療ガイドラインの活用と問題点:膝前十字靱帯損傷診療ガイドラインについて。

第49回関東整形災害外科学会シンポジウム 2009.3.21 会長 里見 和彦

宗田 大、山賀 美芽、朱 寧進、森戸俊行 山崎順也、関矢一郎、四宮 謙一

JOA シンポジウム5 変形性膝関節症の保存療法—エビデンスの構築をめざして— 積極的可動域訓練の効果。2009.5.14

宗田 大、関矢一郎、朱 寧進、森戸俊行、柳下和慶

多重折り半腱様筋腱を用いた2重束再ACL再建術

2009. 6. 26 JOSKAS2009 シンポジウム4 ACL再建術の成績向上を目指して

宗田 大

Anterior Knee Painの病態と治療についての私見。パネル5

第37回日本関節病学会。2009.11.20 会長 渥美 敬

星野明穂

「MISからLISへ」

第39回日本人工関節学会 東京2009.2.13-14

星野明穂

「MIS ; Misfortune In front of Surgeons」

第15回日本最小侵襲整形外科学会 2009/10/23

関矢一郎

両側同時TKAの実際

2009年2月13日人工関節学会 品川

関矢一郎

切除面を基準にして求めた人工膝関節大腿骨コンポーネントの設計

2009年2月14日人工関節学会 品川

関矢一郎

Local adherent technique for transplanting mesenchymal stem cells as a treatment of cartilage defect

2009年4月7日 ISAKOS 大阪

関矢一郎

軟骨損傷に対する鏡視下滑膜幹細胞移植術
移植細胞取り扱いの観点から

2009年5月14 - 17日 日整会総会 博多

関矢一郎

ケトプロフェンの半腱様筋・腱内濃度 貼付剤と経口剤
の比較

2009年6月4日 お茶の水膝スポーツ研究会

関矢一郎

ACL 損傷膝の病態と処置 軟骨損傷・変性の病態とそ
の対処

2009年6月25日 JOSKAS 札幌

関矢一郎

関節内投与した滑膜幹細胞は関節内にとどまり半月板再
生に寄与する

2009年6月27日 JOSKAS 札幌

関矢一郎

関節液中の間葉幹細胞による変形性膝関節症の早期診断
と予後予測

2009年9月26日

厚生労働科学研究費補助金（長寿科学総合研究事業）

膝痛の診断・治療に関する調査研究

-関節マーカーを用いた早期診断と予後予測の確立に関
する研究-

平成21年度 班会議長寿研究 名古屋

関矢一郎

膝関節軟骨病変と再生医療

整形外科初期研修セミナー2009年10月4日 千葉県

関矢一郎

滑膜幹細胞による軟骨再生医療

2009年10月4日 運動器科学研究会

関矢一郎

滑膜幹細胞による半月板再生ダブルトランスジェニック
ラットを用いた解析

2009年11月6日 日整会基礎 横浜

張 禎浩、星野明穂、池田浩夫、吉村英哉、岩澤大輔、
中川祐介

軟部組織緊張度が術後膝屈曲角度に与える影響

第39回人工関節学会 東京 2008.2.13-14

張 禎浩、星野明穂、池田浩夫、吉村英哉、岩澤大輔、
中川祐介

軟部組織バランス獲得困難例への対処法

第39回人工関節学会 東京 2008.2.13-14

張 禎浩、星野明穂、池田浩夫、吉村英哉、岩澤大輔、
中川祐介

人工膝関節術後深屈曲可能例における軟部組織緊張度の
検討

第82回日本整形外科学会学術総会 福岡 2009.5.14-17

朱寧進 関矢一郎 柳下和慶 原憲司 森戸俊行 四宮
謙一 宗田大

3D テンプレートを用いた術前計画

第39回日本人工関節学会 東京 2009.2.13-14

朱寧進 関矢一郎 柳下和慶 原憲司 森戸俊行
四宮謙一 宗田大

皮切の大小による人工膝関節置換術の術後早期回復と術
後成績の違い

第39回日本人工関節学会 東京 2009.2.13-14

朱寧進 関矢一郎 柳下和慶 森戸俊行 山崎順
也 片桐洋樹 四宮謙一 宗田大

鏡視下膝前十字靱帯再建術の長期成績

第82回日本整形外科学会学術集会 福岡 2009.5.14-17.

朱寧進 関矢一郎 柳下和慶 森戸俊行 山崎順
也 片桐洋樹 四宮謙一 宗田大

膝前十字靱帯損傷患者における血清グリコサミノグリカ
ン濃度の測定

お茶の水 膝スポーツ懇話会 東京 2009.6.4

朱寧進 関矢一郎 柳下和慶 森戸俊行 山崎順
也 片桐洋樹 四宮謙一 宗田大

膝前十字靱帯損傷患者の術中超音波測定器による膝関節軟骨のIntegrity、厚さの測定と他の因子との関連
第1回日本関節鏡・膝・スポーツ整形外科学会（JOSKAS 2009） 札幌 2009.6.25-27

朱寧進 関矢一郎 柳下和慶 森戸俊行 山崎順也 片桐洋樹 四宮謙一 宗田大
膝前十字靱帯損傷患者における血清グリコサミノグリカン濃度の測定
第1回日本関節鏡・膝・スポーツ整形外科学会（JOSKAS 2009） 札幌 2009.6.25-27

朱寧進 関矢一郎 柳下和慶 森戸俊行 山崎順也 片桐洋樹 四宮謙一 宗田大
滑膜由来の間葉系幹細胞による移植腱骨孔治癒促進の試み
第24回日本整形外科学会基礎学術集会 横浜 2009.11.5-6

朱寧進 関矢一郎 柳下和慶 森戸俊行 山崎順也 片桐洋樹 四宮謙一 宗田大
What would you do?
第10回TKAフォーラム 東京 2009.12.4.

森戸俊行、宗田大、柳下和慶、朱寧進、望月智之、原憲司、四宮 謙一、関矢 一郎
人工膝関節置換術後の静脈血栓塞栓症に対する低分子ヘパリン（エノキサパリン）の予防効果とその有用性
第39回日本人工関節学会 東京 2009.2.13.

森戸俊行、宗田大、神野哲也、関矢一郎、柳下和慶、山内裕樹、四宮謙一
関節外科手術における静脈血栓塞栓症の予防方法とその有用性
～人工股関節置換術と人工膝関節置換術において～
関東整形災害外科学会 2009.3.20

森戸俊行、宗田大、柳下和慶、朱寧進、望月智之、原憲司、四宮謙一、関矢一郎
低分子ヘパリン（エノキサパリン）による静脈血栓塞栓症の予防効果とその有用性
～人工膝関節置換術（TKA）後において～
日本整形外科学会 2009.5.14

森戸俊行、宗田大、柳下和慶、朱寧進、望月智之、

原憲司、四宮謙一、関矢一郎
2重束2ルート膝前十字靱帯再建術における 脛骨骨孔部位の選択
JOSKAS 札幌 2009.6.25

森戸俊行、宗田大、柳下和慶、朱寧進、望月智之、原憲司、四宮謙一、関矢一郎
低分子ヘパリン（エノキサパリン）を用いた人工膝関節置換術後の静脈血栓塞栓症（VTE）に対する予防効果
JOSKAS 札幌 2009.6.25

森戸俊行、宗田大、唐涛、関矢一郎
ヒアルロン酸は長距離ランナーの滑膜線維化を抑制する
ヒアルロン酸研究会 小樽 2009.9.11

森戸俊行、宗田大、柳下和慶、朱寧進、山崎順也、片桐洋樹、四宮謙一、関矢一郎
静脈血栓塞栓症に対する低分子ヘパリン（エノキサパリン）の効果
<人工膝関節置換術後において>
東日本整形災害外科学会 2009

森戸俊行、宗田大
膝蓋腱炎に対するヒアルロン酸注入療法
日本整形外科スポーツ医学会 群馬 2009.9.25

森戸俊行、宗田大、柳下和慶、朱寧進、山崎順也、片桐洋樹、四宮謙一、関矢一郎
骨端線閉鎖前膝前十字靱帯再建術の治療成績
日本小児整形外科学会 松山 2009.12.4
清水 禎則、立石 智彦、長瀬 寅、朝比奈 信太郎、中川 照彦、土屋 正光
大相撲力士の膝前十字靱帯損傷に関する検討
第1回日本関節鏡・膝・スポーツ整形外科学会（JOSKAS 2009） 札幌 2009.6.25-27

清水 禎則、立石 智彦、長瀬 寅、朝比奈 信太郎、中川 照彦、土屋 正光
膝蓋骨骨折に対するFiberWireを用いた整復固定術後に転位を生じた症例の検討
第58回東日本整形災害外科学会 小樽 2009.9.11-12

清水 禎則、立石 智彦、長瀬 寅、朝比奈 信太郎、中川 照彦、土屋 正光

大相撲力士の膝前十字靱帯損傷の検討 -靱帯再建例と保存治療例との比較

第35回日本整形外科学会スポーツ医学会 前橋 2009.9.25-26

清水 禎則、立石 智彦、長瀬 寅、朝比奈 信太郎、中川 照彦、土屋 正光

大相撲力士の大腿部肉離れ

第20回日本臨床スポーツ医学会 神戸 2009.11.14-15

島谷雅之、宗田大、朱寧進、森戸俊行、辻邦和、四宮謙一、関矢一郎

マグネシウムはインテグリンを介した滑膜間葉幹細胞の軟骨欠損部への接着と軟骨基質産生を促進する

第24回日本整形外科基礎学術集会 横浜 2009. 11.5-6

八木茂典、望月智之、吉村英哉、林将也、関矢一郎、宗田大

トッパスリートの難治性膝蓋腱炎に対する治療経験

お茶の水 膝スポーツ懇話会 東京 2009.6.4

八木茂典、望月智之、吉村英哉、林将也、関矢一郎、宗田大

トッパスリートの難治性膝蓋腱炎に対する治療経験

第35回日本整形外科学会スポーツ医学会学術集会 群馬 2009.9.26

八木茂典、望月智之、吉村英哉、林将也、森戸俊行、関矢一郎、宗田大

膝蓋腱炎に対し手術療法を施行した一例

第15回スポーツ傷害フォーラム 大阪 2010.1.30

高橋 徹、宗田 大、関矢 一郎

BMP-7はラットザイモサン関節炎において軟骨変性を抑制する

第1回Orthopedic Research Club 千葉 2009.10.31-11/1

12) 受賞

2009年度日本整形外科学会研究奨励賞

堀江雅史

Intra-articular Injected synovial stem cells differentiate into meniscal cells directly and promote meniscal regeneration without mobilization to distant organs in rat massive meniscal defect.

Stem Cells. 2009, 27 (4) :878-87.

古賀英之

Nycomed Pharma Award (Best paper Award)

Idrettsmedisinsk Høstkongress (Norwegian Congress of Sports Medicine) . Trondheim, Norway. 2009.11.5-8

Reconstruction of the injury mechanisms for anterior cruciate ligament injuries among female basketball and team handball players

Intra-articular Injected synovial stem cells differentiate into meniscal cells directly and promote meniscal regeneration without mobilization to distant organs in rat massive meniscal defect.

Stem Cells. 2009, 27 (4) :878-87.

13) 外部資金の獲得状況

科学研究費補助金 基盤研究 (C) .

滑膜由来の幹細胞を用いた軟骨損傷の治療促進術.

研究代表者 宗田 大.

期間:平成20-平成22

研究費総額:500万円

科学研究費補助金、基盤C

研究題目: 軟骨損傷に対する滑膜幹細胞浮遊液静置療法において細胞接着効率を向上させる為の検討

代表: 関矢一郎

期間: 平成21年—平成23年

研究費総額:500万円

厚生科研費

研究題目:厚生労働科学研究「膝痛の診断・治療に関する調査研究 -関節マーカーを用いた早期診断と予後予測の確立に関する研究-」

代表:藤田保健衛生大学整形外科

主任研究者 山田治基

分担研究者 宗田 大、関矢一郎

期間:平成20年-平成22年

分担金 平成20年 300万

21年 250万

14) 特別講演、招待講演

2008年

宗田 大:小児の膝疾患。第24回九州小児整形外科集談会。

2008.1.19 九州大学西新プラザ。会長 津村 弘

宗田 大:診療ガイドラインからみた前十字靱帯損傷と今後の課題。第110回中部整形災害外科学会(びわこセミナー) 会長 松末吉隆

宗田 大:膝痛の治療。厚木整形外科医会学術講演会。
2008.5.15

宗田 大:2重束 ACL 再建術の変遷と問題点。第5回横浜・
横須賀 Knee Frontier。代表世話人 齋藤知行 教授
2008.6.5

宗田 大:ACL 損傷と私。JOSKAS 2008 会長講演
2008.6.14

宗田 大:変形性膝関節症の治療—EBM とその裏側—
モーラスパップ 30mg 発売 20 周年記念講演会。ホテルグ
ランヴィア大阪 2008.7.19 座長 吉川秀樹 教授

2009 年

宗田 大:小児・思春期の膝スポーツ障害。熊谷市整形
外科医会学術講演会。2009.2.5

宗田 大:前十字靱帯再建術と術後リハビリテーション。
第7回徳島スポーツ整形外科研究会 阿波観光ホテル
座長 安井 夏生

宗田 大:前十字靱帯損傷と膝のリハビリテーション。
H21 年度第2回香川県臨床整形外科医会研修会。2009.9.4
ロイヤルパークホテル高松

宗田 大:膝の痛みに対するヒアルロン酸治療 ヒアル
ロン酸関節療法臨床と基礎研究会。東京女子医大東医
療センター千葉純二教授 2009.9.18

Takeshi Muneta: Technical aspects of ACL
augmentation. Session5 Anatomical Approach to ACL.
International ATOS LIVE Summit 2009, Heidelberg.
2009.9.25

Takeshi Muneta: Double Bundle ACL reconstruction.
Talk in Department of Orthopaedic Surgery of Uvella
University, Oslo, 29/9/2009

Takeshi Muneta: Knee Pain - Knowledge, Diagnosis and
Treatment - Evidence Level 5 Talk in Oslo 30/9/2009

宗田 大:外来における前十字靱帯損傷の診断と治療。
埼玉県南スポーツフォーラム 2009.10.29

宗田 大:私たちが行ってきた膝靱帯手術 第16回中越
整形外科手術手技講演会 2009.11.26 長岡

宗田 大:ACL 損傷膝を取り巻く諸問題と解決への模索。
第26回膝関節フォーラム モーニングレクチャー

Tsuji K.
Roles of BMPs in postnatal bone homeostasis
The 3rd Global COE International Symposium:
Frontiers in Bone Biology
2009.6.10-11, Tokyo

関矢一郎
両側同時 TKA の実際
2009 年 2 月 13 日人工関節学会 品川

関矢一郎
切除面を基準にして求めた人工膝関節大腿骨コンポーネ
ントの設計
2009 年 2 月 14 日人工関節学会 品川

関矢一郎
Local adherent technique for transplanting mesenchymal
stem cells as a treatment of cartilage defect
2009 年 4 月 7 日 ISAKOS 大阪

関矢一郎
軟骨損傷に対する鏡視下滑膜幹細胞移植術
移植細胞取り扱いの観点から
2009 年 5 月 14 - 17 日 日整会総会 博多

関矢一郎
ケトプロフェンの半腱様筋・腱内濃度 貼付剤と経口剤
の比較
2009 年 6 月 4 日お茶の水膝スポーツ研究会

関矢一郎
ACL 損傷膝の病態と処置 軟骨損傷・変性の病態とそ
の対処
2009 年 6 月 25 日 JOSKAS 札幌

関矢一郎
関節内投与した滑膜幹細胞は関節内にとどまり半月板再
生に寄与する

2009年6月27日 JOSKAS 札幌

関矢一郎

関節液中の間葉幹細胞による変形性膝関節症の早期診断
と予後予測

2009年9月26日

厚生労働科学研究費補助金（長寿科学総合研究事業）

膝痛の診断・治療に関する調査研究

-関節マーカーを用いた早期診断と予後予測の確立に関
する研究-

平成21年度 班会議長寿研究 名古屋

関矢一郎

膝関節軟骨病変と再生医療

整形外科初期研修セミナー2009年10月4日 千葉県

関矢一郎

滑膜幹細胞による軟骨再生医療

2009年10月4日運動器科学研究会

関矢一郎

滑膜幹細胞による半月板再生ダブルトランスジェニック
ラットを用いた解析

2009年11月6日日整会基礎 横浜

関矢一郎

滑膜幹細胞を鏡視下で移植する軟骨再生医療

2009年2月6日 青森県骨軟骨シンポジウム 青森

関矢一郎

関節軟骨欠損に対する低侵襲幹細胞移植術のミニブタを
用いた解析

2009年4月8日 自治医科大学先端医療技術開発センター
シンポジウム 自治医大

関矢一郎

Arthroscopic Transplantation of Synovial Stem Cells
into Cartilage Injury

2009年5月30日 International Symposium for
Orthopaedic Sports Medicine" Chang Gung Memorial
Hospital - Keelung Keelung, Taiwan

関矢一郎

Intraarticular injected synovial stem cells differentiate

into meniscal cells directly and promote meniscal
regeneration without mobilization to distant organs in
rat massive meniscal defect

2009年5月30日 International Symposium for
Orthopaedic Sports Medicine" Chang Gung Memorial
Hospital - Keelung Keelung, Taiwan

関矢一郎

Synovial fluid-derived mesenchymal stem cells increase
after anterior cruciate ligament injury in humans

2009年5月30日 International Symposium for
Orthopaedic Sports Medicine" Chang Gung Memorial
Hospital - Keelung Keelung, Taiwan

関矢一郎

Cartilage regeneration by transplantation of synovial
stem cells - Preliminary results in second look
arthroscopy and biopsy -

2009年6月1日 Taipei Veterans General Hospital 台湾

関矢一郎

Arthroscopic Transplantation of Synovial Stem Cells
into Cartilage Defect

2009年6月11日 Gordon Research Conference
"Cartilage Biology & Pathology"
Les Diablerets, Switzerland

関矢一郎

滑膜由来の幹細胞と再生医療への応用

2009年7月14日 慶応軟骨代謝研究会

関矢一郎

軟骨損傷に対する低侵襲な細胞治療の開発

2009年7月23日 第27回日本骨代謝学会 大阪

関矢一郎

ダブルトランスジェニックラットを用いた再生医療研究
滑膜幹細胞による半月板再生

2009年9月8日 東大腎臓内科

関矢一郎

滑膜幹細胞による軟骨再生医療

2009年9月19日運動器科学研究会 東京八重洲

関矢一郎

Arthroscopic Transplantation of Synovial Stem Cells
into Cartilage Defect

2009年11月14日

International Conference of Mesenchymal and
Nonhematopoietic Stem Cells (MSCs)

Austin, Texas

関矢一郎

幹細胞から考える膝関節疾患の病態と再生

2009年11月27日 杉並区医師会整形外科医会

15) 主催学会

第6回御茶ノ水関節症研修会

2009年1月30日(金) 18:30-20:30 東京医科歯科大学 I
期棟 2階 講義室 1

第7回東京スポーツ整形外科研修会

2009年4月25日(金) 東京ドームホテル 宗田主催

お茶の水膝スポーツ懇話会

2009年6月4日(木) 東京医科歯科大学 関矢世話人

第18回運動器外科学セミナー

2009年 7月13日(月) 18:00-19:00

第1回スポーツリハビリテーションワークショップ

2009年8月29日(土) 17:30-20:30 東京医科歯科大学
16F 大会議室

大学院特別講義(医歯学先端研究論)

2009年10月23日(金) 18:00-19:00 臨床講堂1(東京医科
歯科大学A棟地下1階)

第19回運動器外科学セミナー

2009年 12月8日(火) 18:0-19:00

16) 新聞、雑誌、TV報道

宗田 大:NHK きょうの健康「ひざの痛み」。

2008.3.31-4.2,4.4

宗田 大:NHK 名医にQ「膝の痛み」 2008.7.19、7.26

宗田 大:「ラジオあさいちばん」「健康ライフ」コーナー
出演 NHKラジオ 濱中博久さん、遠田恵子キャス
ター 5回シリーズ放送10.27-10.31 「膝を大切に〜

大事に長持ちさせる〜」

宗田 大:NHK 名医にQ「ロコモティブシンドローム」
2009.4.4;2009.4.9

宗田 大:BS-TBS「健康トリプルアンサー」変形性膝関
節症。平成21年12月18日放送

科学ニュース

幹細胞を利用して半月板の再生に成功、ラットでの実験

<http://www.kagakunavi.jp/topic/show/149>

17) GCOE 総合講義

Knee Joint Disorders and Joint Fluid Stem Cells- 関節
液幹細胞からみた膝関節障害 -

運動器外科学が臨床上ターゲットしている前十字靱帯
損傷はスポーツ膝傷害の代表である。一方変形性膝関節
症は高齢者において最も頻度の高い整形外科疾患の1つ
であり、50歳以上の1000万人の膝痛の原因と報告され
ている。ACL損傷膝では軟骨損傷の程度に相関して関
節液幹細胞が増加し、また術後6日目には有意な幹細胞
の増加を見た。関節液幹細胞の遺伝子プロファイルは滑
膜のそれに類似している。滑膜幹細胞を用いた関節軟骨
欠損の治療、腱移行術における骨髄移行部の治癒促進、
半月板再建における有意な治癒促進効果を動物実験にて
示した。さらに軟骨欠損に対する臨床応用も実績を重ね
ている。

<第31回GCOE国際総合プレゼンテーション>

大学院医歯学総合研究科「医歯学先端研究特論」

演題:『骨のホメオスタシスにおける骨形成因子(BMP)
の生理機能の解析』

演者:辻 邦和

日時:平成21年9月14日(月) 12:30~14:00

場所:歯学部4階 特別講堂

骨組織中に存在し、その高い組織修復能力を担う
分子の存在は40年以上前に予見され、BMP(Bone
Morphogenetic Protein)と名づけられた。その後BMP
ファミリーに属する遺伝子は数多く同定されたが、胎
生期、生後の骨形成、骨代謝、及び骨折後の組織修復
過程で各々のBMP分子がどのような生理機能を有し
ているかについては、未だ明らかとされていなかった。
本講演の前半では、骨形成、骨代謝における過去の
BMP研究のレビューと問題点についてイントロダクショ
ンを行った。講演の後半では、私が、米国留学期間に行っ
た、BMP2、BMP4、BNP7のコンディショナルノック

アウトマウスの骨の表現型の解析結果について紹介を行った。

18) 教室、分野や講座の准教授、講師、助教、特別研究員、ポスドク、指導を受けた大学院生の名前 (AISSには○印) のリスト

運動器外科学	教 授	宗田 大
軟骨再生学	准教授	関矢 一郎、
GCOE	講 師	辻 邦和、
運動器外科学	助 教	朱 寧進、
軟骨再生学	助 教	森戸 俊行、
医学部付属病院	医 員	山崎 順也
運動器外科学	大学院生	
		島谷 雅之、八木 茂典、
		中村 智祐、高橋 徹、
		宮本 崇、鈴木 志郎、
		山賀 美芽、宮武 和正、
		初鹿 大祐、小田辺 浩二、
		片桐 洋樹

19) GCOE 活動についての感想、コメント、改善を望む点

成果の割合に報告書作成、GCOE事業などに割かれる時間が多い。

国際シャペロンが教室を基盤として活動していただい、教室の研究・教育の内容が多様化し、深まった点は特筆に値する。

活動成果の評価は比較が必要であると思われる。

The American Journal of Sports Medicine

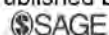
<http://ajs.sagepub.com/>

Anatomy of Normal Human Anterior Cruciate Ligament Attachments Evaluated by Divided Small Bundles

Kenji Hara, Tomoyuki Mochizuki, Ichiro Sekiya, Kumiko Yamaguchi, Keiichi Akita and Takeshi Muneta
Am J Sports Med 2009 37: 2386
DOI: 10.1177/0363546509340404

The online version of this article can be found at:
<http://ajs.sagepub.com/content/37/12/2386>

Published by:



<http://www.sagepublications.com>

On behalf of:



American Orthopaedic Society for Sports Medicine

Additional services and information for *The American Journal of Sports Medicine* can be found at:

Email Alerts: <http://ajs.sagepub.com/cgi/alerts>

Subscriptions: <http://ajs.sagepub.com/subscriptions>

Reprints: <http://www.sagepub.com/journalsReprints.nav>

Permissions: <http://www.sagepub.com/journalsPermissions.nav>

Anatomy of Normal Human Anterior Cruciate Ligament Attachments Evaluated by Divided Small Bundles

Kenji Hara,* MD, PhD, Tomoyuki Mochizuki,*[†] MD, PhD, Ichiro Sekiya,*[†] MD, PhD, Kumiko Yamaguchi,[‡] MD, PhD, Keiichi Akita,[‡] MD, PhD, and Takeshi Muneta,*^{§||} MD, PhD
 From the *Department of Orthopaedic Surgery, School of Medicine, Tokyo Medical and Dental University Hospital, Tokyo, Japan, [†]Section of Cartilage Regeneration, Graduate School, Tokyo Medical and Dental University, Tokyo, Japan, [‡]Section of Clinical Anatomy, Graduate School, Tokyo Medical and Dental University, Tokyo, Japan, and the [§]Section of Orthopedic Surgery, Graduate School, Tokyo Medical and Dental University, Tokyo, Japan

Background: Double-bundle anterior cruciate ligament (ACL) reconstruction has several potential advantages over single-bundle reconstruction with hamstring tendons. However, there are still controversies regarding tunnel placement in tibial and femoral attachments.

Hypothesis: The macroscopically normal ACL consists of small bundles about 1 mm in diameter. Detailed observation of the divided smaller bundles will achieve better understanding of the tunnel placement in anatomic ACL reconstruction.

Study Design: Descriptive laboratory study.

Methods: This study used 20 cadaveric knees. The ACL was divided into anteromedial and posterolateral bundles, then separated into 10 small bundles of 2-mm diameters, with preservation of their attachment sites marked with color markers. The positional relationship between the femoral and tibial attachments of each small bundle was investigated.

Results: A layered positional correlation of small bundles was found between the tibial and femoral attachments. Small bundles aligned in the anterior-posterior direction in the tibia corresponded to the bundles aligned in a high-low direction in the femur in flexion. The femoral attachment pattern was relatively similar in each specimen; however, the tibial attachment showed 2 patterns: an oblique type (12 of 20) and a transverse type (8 of 20). The posterior portion of the posterolateral bundle was separately attached to the medial and lateral portions of the tibial attachment. There was no fibrous insertion in the center of the posterior portion of the ACL tibial attachment in any specimen. In this bare area, there was fat tissue and vascular bundles.

Conclusion: Small bundles constituting the ACL showed a relatively layered arrangement between 2 attachments. The tibial attachment showed 2 patterns of oblique and transverse types, and the vascular bundles were located in the center of the posterolateral bundle.

Clinical Relevance: The results of this study of the normal ACL will provide insights for surgeons when placing grafts during anatomic ACL reconstruction.

Keywords: normal anatomy; anterior cruciate ligament; anterior cruciate ligament attachments; double-bundle anterior cruciate ligament reconstruction

Anterior cruciate ligament (ACL) reconstruction using multi-strand hamstring tendons has become not only a popular procedure but a new worldwide standard. The

number of reconstructions with hamstring tendons is now more than that with bone-patellar tendon-bone grafts. Some clinical researchers have suggested that reconstruction with hamstring tendons has advantages—namely, less harvest site morbidity, less postoperative pain, and earlier return to athletic activities.^{10,17} Yet, compared with bone-patellar tendon-bone reconstruction, these reconstructions have a tendency to be inferior in terms of stability.¹²

In terms of sports medicine, knee surgeons have recently paid attention to the double-bundle (DB) ACL procedure to improve stability after reconstruction with hamstring tendons.¹⁶ With regard to tunnel placement in

^{||}Address correspondence to Takeshi Muneta, MD, PhD, Section of Orthopedic Surgery, Graduate School, Tokyo Medical and Dental University 1-5-45 Yushima, Bunkyo-ku, Tokyo 113-8519 (e-mail: muneta.orj@tmd.ac.jp).

No potential conflict of interest declared.

DB reconstruction, Yasuda et al²³ proposed anatomic reconstruction with a DB procedure, for its superiority of stability over a single-bundle procedure; their study was followed by several others.^{14,19}

With respect to anatomic placement of the graft, several studies of the normal human ACL have been reported to achieve a better understanding of the anatomic tunnel placement in DB ACL reconstruction. Takahashi et al²² described each central point of the femoral and tibial insertions of the anteromedial (AM) and posterolateral (PL) bundles in millimeters of distance from the posterior femoral condyle margin and anterior tibial margin after dividing the human ACL into AM and PL parts. Mochizuki et al¹³ studied the central part of the AM and PL bundle after removing the ligament membrane; they described its position in millimeters from the posterior margin and as a time reference on a clock face on the intercondylar surface. Colombet et al⁶ used the line described by Amis and Jakob² on the tibia and the grid prepared by Bernard et al⁴ for the femur to define AM and PL bundle attachment positions using a radiograph. Zantop et al²⁴ measured the distances from the center of the AM and PL bundles to the articular cartilage; they also performed radiographic analyses using the techniques of Bernard et al⁴ on the femur, as well as the method by Stäubli and Rauschning²¹ on the tibia. Edwards et al⁷ measured and described the AM and PL bundles in terms of the o'clock positions parallel to the femoral long axis and parallel to the roof of the intercondylar notch. Siebold et al²⁰ described tibial insertions of the AM and PL bundles in the intercondylar anterior area of the tibia. They quantified the area of each AM and PL bundle and characterized arthroscopically identified landmarks for each bundle.

Every recent study divided the natural human ACL into 2 macroscopically separate bundles by a manual method; however, the human ACL cannot be clearly and completely divided into 2 separate parts, as determined in many studies.^{3,11,13,16} Amis and Dawkins¹ once described 3 functional bundles identified in cadaver knees—namely, the AM, intermediate, and PL; they then measured changes of length in flexion and extension and in tibial rotation of each bundle. In fact, the natural ACL consists of a number of smaller fibrous bundles with a 3-dimensional arrangement.

Surgeons need to understand the normal anatomy of the ACL femoral and tibial attachments to achieve satisfactory tunnel placement in anatomic ACL reconstruction. Thus, we performed a detailed anatomic study of the natural human ACL by dividing it into small bundles in each AM and PL bundle. Our hypothesis is that such detailed observation will achieve better understanding of the tunnel placement of AM and PL bundles on the tibial and femoral sides in anatomic ACL reconstruction, which would not be obtained by simply dividing the ACL into the 2 AM and PL bundles.

MATERIALS AND METHODS

This study used 20 knees from 10 cadavers. It excluded knees with ACL rupture, other ligament injury, or significant osteoarthritis. Specimens were prepared by the removal

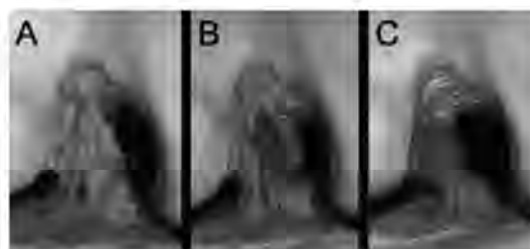


Figure 1. Preparation of cadaveric knees used in the study: A, specimens were prepared by removal of all soft tissues, with the exception of the ACL; B, the overlying synovium around the ACL was carefully removed to expose the surface fibrous structure of the ligament; C, each ACL looked as if it consisted of many small fibrous bundles of approximately 1 mm in diameter.

of all soft tissues, with the exception of the ACL; then, the overlying synovium around the ACL was carefully removed to expose the surface fibrous structure of the ligament (Figure 1). After careful removal of the ligament membrane, the superficial arrangement could be observed, and it consisted of small bundles 1 mm in diameter. In fact, every ACL appeared as if it consisted of many small fibrous bundles approximately 1 mm in diameter. The change in the surface of the small bundle arrangement more clearly indicated the border portion between the 2 main bundles in flexion. Knees were flexed to allow macroscopic identification of the AM and PL bundles. A cotton string was introduced into the border point between the AM and PL bundles at the central portion of the ACL in 90° of flexion. A small bundle of about 2 mm in diameter was picked up with a forceps from the ligament surface at the central portion of the ACL. The 2-mm-diameter bundle was strong enough that it did not break up when stripped with a forceps; this maneuver did not disturb the small bundle arrangement as well. Next, the string was moved up (toward the femoral attachment), then down (toward the tibial attachment). Each AM and PL bundle was separated into about 10 small bundles (2 mm in diameter) with preservation of their attachment sites. These preparations were performed using a string along each bundle course, as described above.

The femur was then cut in the sagittal plane with an oscillating saw, from the top of the roof of the intercondylar notch. After removal of the medial femoral condyle, the femoral attachment area of the ACL could be easily observed. After such preparation, each small bundle attachment of both the femur and the tibia was marked with 5 fine-tipped color markers (Figure 2). As shown in detail later, the small bundles do not run completely in parallel, with some twisting even in the extension position. Therefore, some of the small bundles, especially in the core portion, could not be isolated from end to end with a string. The shallower portion of the tibial attachment tended to extend anteriorly to the articular cartilage, and the deeper portion of the femoral attachment tended to extend posteriorly to the articular cartilage. The conjunction between the fibers

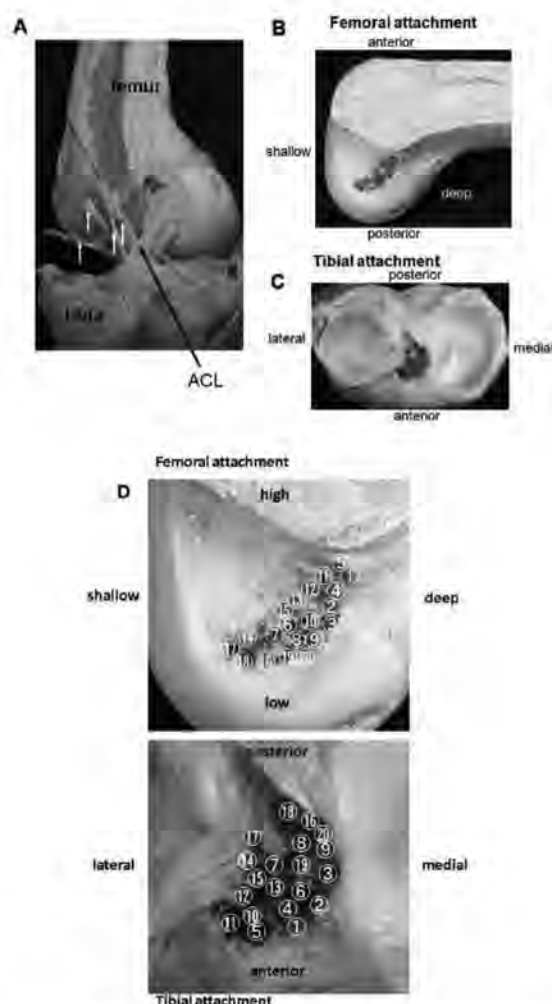


Figure 2. Preparation of the small bundles: A, after removal of the medial femoral condyle, the femoral attachment area of the ACL could be easily observed. Each AM and PL bundle was separated into about 10 small bundles (2 mm in diameter) with preservation of their attachment sites. These preparations were performed using a string along each bundle course. After such preparation, each small bundle attachment of the femur and the tibia was marked with 5 fine-tipped color markers. B, the small fibrous arrangement at the femoral attachment can be seen as dots in the lateral view. C, the small fibrous arrangement at the tibial attachment can be seen as colored dots in the view from above. D, the corresponding number for each small bundle at the femoral and tibial attachments was put on a magnified view.

and the articular cartilage was clearly separated during dissection. In both the shallower portion of the tibia and the deeper portion of the femur, the ACL attached to the joint surface in a fanlike extension. Therefore, the small

bundle of the shallower portion of the tibial attachment and that of the deeper portion of the femoral attachment showed a wider trumpetlike insertion. As such, the positional relationship between the femoral and tibial attachments of each small bundle were investigated.

RESULTS

Positional Relationship of the Small Bundles Between the Tibial and Femoral Attachments

In all specimens, the small bundles composing the ACL were aligned in parallel between the tibial and femoral attachments in extension; however, they were twisted in a 3-dimensional arrangement with knee flexion. A layered positional correlation of small bundles was found between the tibial and femoral attachments. The small bundles aligned in the anterior-posterior direction on the tibia corresponded to bundles aligned in the high-low direction on the femur in flexion (Figure 3).

The bundles that originated from the AM portion of tibial attachment were inserted into the high and deep portion of the femoral attachment in flexion, whereas those from the anterolateral portion of the tibial attachment were inserted into the high and shallow portion of the femoral footprint. The bundles that originated from the posteromedial portion of tibial attachment were inserted into the low and deep portion of the femoral attachment, whereas those from the PL portion of the tibial attachment were inserted into the low and shallow portion of the femoral footprint.

The femoral attachment pattern was relatively similar in each specimen (Figure 4A); however, the tibial attachment showed 2 patterns of the small bundle footprint location: an oblique type and a transverse type (Figure 4B). Oblique and transverse types were found in 12 and 8 of the 20 knees, respectively. The tibial attachment pattern was defined as an oblique type in both sides of 5 knees and as a transverse type in both sides of 3 knees. In the other 2 knees, the tibial attachment pattern was defined differently. In the oblique type, the AM fibers extended from anterolateral to posteromedial in the tibial attachment; however, in the transverse pattern, the AM fibers were attached in the anterior half, and the PL fibers were attached in the posterior half of the whole attachment site.

Change of Tibial and Femoral Attachment Sites Between in Extension and Flexion From Observation of Divided Small Bundles

Furthermore, each AM and PL bundle was divided into 2 half-portions, anterior and posterior, with respect to the femoral attachment area. Each small bundle of anterior and posterior portions runs parallel to the tibial attachment in extension (ie, in the AM bundles as well as in the PL bundles), whereas in flexion they could be seen twisting and crossing over each other, similar to when the ACL was divided into the AM and PL bundles (Figure 5).

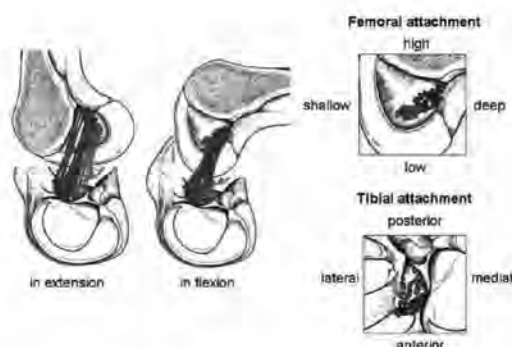


Figure 3. Small bundles composing the ACL were aligned in a rather parallel direction between the tibial and femoral attachments in extension; however, they were twisted in a 3-dimensional arrangement with knee flexion. A layered positional correlation of the small bundles was found in the tibial and femoral attachments. Small bundles aligned in a anterior-posterior direction on the tibia corresponded to bundles aligned in a deep-shallow direction on the femur in flexion.

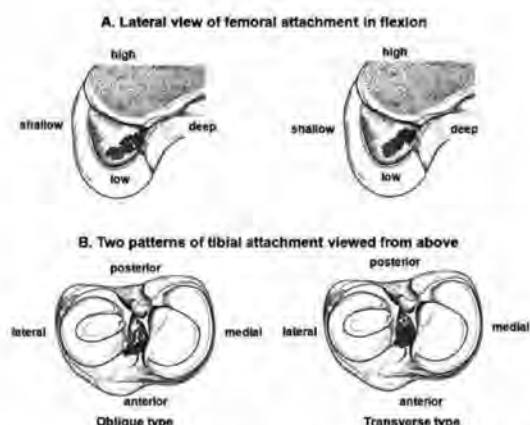


Figure 4. Femoral and tibial attachment patterns: A, the femoral attachment pattern was relatively similar among the specimens; B, on the contrary, the tibial attachment showed 2 patterns regarding the location of the footprints of the small bundles: an oblique type (left) and a transverse type (right).

Detailed Observation of the Tibial Attachment of the ACL With Histologic Analysis

We noticed that there was no fibrous insertion in the center of the posterior portion of the ACL tibial attachment in any of the specimens. The small bundles of the posterior-shallow portion of the PL bundle on the femur were found separately attached to the medial and lateral portions of the tibial attachment; therefore, we histologically evaluated the tibial attachment. In the bare area, there were fat tissue and vascular bundles (Figure 6).

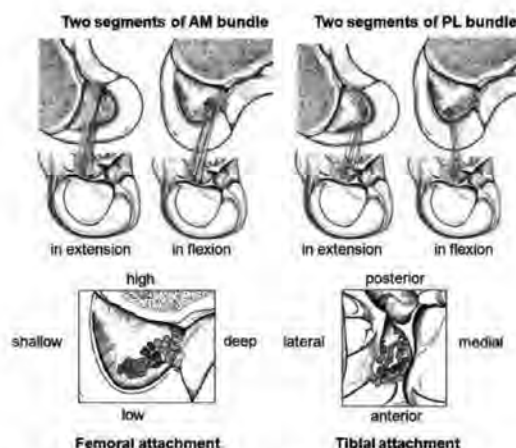


Figure 5. Each AM and PL bundle was divided into 2 half-portsions in relation to the femoral attachment area. Each small bundle of anterior and posterior portions runs parallel to the tibial attachment in extension (in the AM bundles as well as in the PL bundles), whereas in flexion they could be seen twisting and crossing over each other, as in the case when the ACL was divided into the AM and PL bundles.

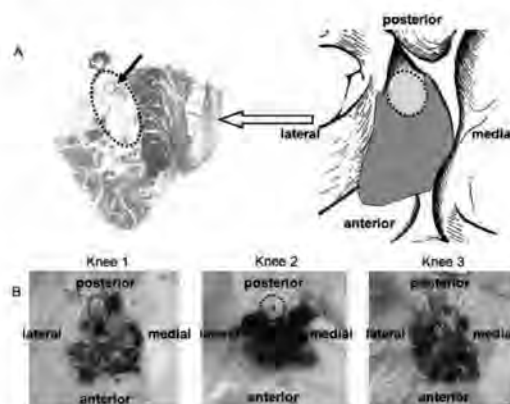


Figure 6. Histological evaluation of the tibial attachment: A, there was no fibrous insertion in the center of the posterior portion of the ACL tibial attachment (dotted circle in the right figure). The small bundles of the distal portion of the posterolateral bundle on the femur were found separately attached to the medial and lateral portions of the tibial attachment. The tibial attachment was evaluated histologically. In the bare area, there were fat tissue and vascular bundles (dotted circle in the left figure). B, each of 3 knee joints has a bare area with vascular bundles in the posterolateral bundle (dotted circle).

DISCUSSION

To accomplish anatomic ACL reconstruction correctly, surgeons must understand the normal ACL attachment on

the femur and tibia for accurate tunnel placement. In our study, the ACL could be morphologically divided into AM and PL portions in flexion only when the synovial ligament membrane was removed. Previous studies have provided various descriptions of attachment sites of AM and PL bundles. There are some controversies in the literature about the shape, length, and width of the femoral attachment and the center of the AM and PL bundle. Odensten and Gillquist¹⁶ and many others have stated that the femur has to be lifted around 25° to bring the femoral insertion area to horizontal. Siebold et al²⁰ reported that the center of the AM and PL bundles was horizontally aligned when the femoral shaft axis was lifted 12° from the horizontal plane. Ferretti et al⁵ described the identification of osseous landmarks on the femoral attachment of the ACL. They called the lateral intercondylar ridge the "resident's ridge," a structure first described by William Clancy Jr.¹⁵ They reported there was no ACL attachment anterior to this ridge. Our findings agree with their report.

The length of the ACL femoral attachment site was measured as 17.2 ± 1.2 mm and the width, 9.9 ± 0.8 mm.⁸ Colombet et al⁶ and Odensten and Gillquist¹⁶ reported size findings similar to those of Ferretti et al.⁵ On the contrary, Mochizuki et al¹³ reported that the natural ACL femoral attachment looked more oval and narrower after removal of the ligament membrane. They described the average lengths of the AM and PL bundle femoral attachments as 9.2 mm and 6.0 mm, respectively, and the width as 5 mm, which is smaller than that of other reports. The area of the AM and PL bundles of the femoral attachment was relatively similar in all specimens. The variations of the anatomic data from several studies are thought to be partly due to the interpretation of the ligament membrane and its attachment.

Findings regarding the shape, area, and center of the AM and PL bundles of the tibial ACL attachment are controversial. Siebold et al²⁰ reported that the average anterior-posterior length of all dissected ACL footprints was 14 mm, which is similar to the result of 15 mm recorded by Stäubli and Rauschning.²¹ Odensten and Gillquist¹⁶ reported the length to be 17 mm and Colombet et al⁶ reported the length to be 17.5 mm. Ferretti et al⁵ reported that the AM bundle was located anteriorly and medially to the PL bundle in relation to the tibial insertion. Colombet et al⁶ reported that the shape of the tibial attachments was more variable than that of the femoral attachments among specimens. In the current study, the tibial insertion was classified into 2 patterns, an oblique type and a transverse type (ie, when the ACL is divided into AM and PL bundles). This is the first description for the tibial attachment pattern, and it will provide insight into DB reconstruction based on real anatomy. The existence of the 2 types of insertion will explain the controversy of the present findings regarding tibial attachment. One described pattern involved the anterior and posterior portions of the tibia²⁴ and the other, the medial and lateral portions of the tibia.^{6,20} This finding is thought to be morphologically important as an anatomical finding, given that it reconciles the 2 previously described patterns. The variation of

tibial attachment pattern that we found will partly explain the different descriptions of tibial attachment.

There was no fibrous bundle in the center of the posterior portion of the PL bundle attachment. Histologic evaluation of the tibial attachment revealed that there were fat and vascular bundles in that area. To the best of our knowledge, this is the first observation showing no fibrous bundle in the center of the posterior portion of the PL bundle tibial attachment. This finding may result in some change of concept for the tibial attachment regarding the placement of the PL bundle.

Harner et al⁹ reported that the area of the insertion site of the ACL onto the tibia and femur is approximately 3 times larger than that of the midsubstance cross-sectional area. If those findings are correct, graft placement based on the whole natural attachment site in anatomic ACL reconstruction may inevitably lead to notch impingement without a large amount of notchplasty.

The current study reaffirmed that each small bundle of the natural ACL twists from extension to flexion in AM and PL bundles. These findings suggest the difficulty of real anatomic ACL reconstruction by current reconstruction techniques using a few straight bundles.

The DB reconstructions use 4 strands of tendons; as such, the tendons should be the 2 main bundles (AM and PL), which twist around in the same manner as a complete ACL. Perhaps surgeons should accordingly respect this finding during the operation by orienting each double strand for a single bundle. This new information regarding normal ACL attachment anatomy via divided small bundles will lead surgeons to a more precise understanding with respect to small bundle arrangement between the 2 attachment sites. More precise understanding might change the concept of anatomical ACL with regard to graft placement. Moreover, some new idea of anatomical ACL reconstruction procedures will be developed on the basis of these research findings. Yet, one promising method respecting the natural femoral and tibial insertion area is possible with bone-tendon-bone grafts, in which the knee is flexed to 115° and the bone block of the ligament graft is fixed safely in the bone tunnel with its cortex-ligament borderline lying horizontal in the insertion area of the femur. Because of oblique drilling, more than two thirds of the 15-mm insertion area are covered. The graft is fixed at the tibia in a way that all fiber bundles are parallel in extension. This technique has been used in Europe since 1990, under the term *press-fit fixation*.³

In conclusion, a detailed anatomic study of the normal ACL revealed the positional relationship between the tibial and femoral attachments of small bundles. For the first time, a study described 2 patterns of AM and PL bundle attachments in the tibial attachment, whereas a similar pattern was observed in the femoral attachment. There was no fibrous area in the posterior portion of the tibial attachment site of the PL bundle.

REFERENCES

1. Amis AA, Dawkins GP. Functional anatomy of the anterior cruciate ligament. *J Bone Joint Surg Br*. 1991;73:260-267.

2. Amis AA, Jakob RP. Anterior cruciate ligament graft positioning, tensioning and twisting. *Knee Surg Sports Traumatol Arthrosc.* 1998; 6(suppl 1):S2-12.
3. Arnoczky JP. Anatomy of the anterior cruciate ligament. *Clin Orthop Relat Res.* 1983;172:19-25.
4. Bernard M, Hertel P, Hornung H, Cierpinski T. Femoral insertion of the ACL: radiographic quadrant method. *Am J Knee Surg.* 1997;10:14-21.
5. Boszotta H. Arthroscopic anterior cruciate ligament reconstruction using a patellar tendon graft in press-fit technique: surgical technique and follow-up. *Arthroscopy.* 1997;13:332-339.
6. Colombet P, Robinson J, Christel P, et al. Morphology of anterior cruciate ligament attachments for anatomic reconstruction: a cadaveric dissection and radiographic study. *Arthroscopy.* 2006;22:984-992.
7. Edwards A, Bull AM, Amis AA. The attachments of the anteromedial and posterolateral fibre bundles of the anterior cruciate ligament, part 2: femoral attachment. *Knee Surg Sports Traumatol Arthrosc.* 2008; 16:29-36.
8. Ferretti M, Ekdahl M, Shen W, Fu FH. Osseous landmarks of the femoral attachment of the anterior cruciate ligament: an anatomic study. *Arthroscopy.* 2007;23:1218-1225.
9. Harner CD, Baek GH, Vogrin TM, Carlin GJ, Kashiwaguchi S, Woo SL. Quantitative analysis of human cruciate ligament insertions. *Arthroscopy.* 1999;15:741-749.
10. Kartus J, Movin T, Karlsson J. Donor-site morbidity and anterior knee problems after anterior cruciate ligament reconstruction using autografts. *Arthroscopy.* 2001;17:971-980.
11. Kennedy JC, Weinberg HW, Wilson AS. The anatomy and functions of the anterior cruciate ligament. *J Bone Joint Surg Am.* 1974;56:223-235.
12. Kim SJ, Kim TE, Lee DH, Oh KS. Anterior cruciate ligament reconstruction in patients who have excessive joint laxity. *J Bone Joint Surg Am.* 2008;90:735-741.
13. Mochizuki T, Muneta T, Nagase T, Shirasawa S, Akita KI, Sekiya I. Cadaveric knee observation study for describing anatomic femoral tunnel placement for two-bundle anterior cruciate ligament reconstruction. *Arthroscopy.* 2006;22:356-361.
14. Muneta T, Koga H, Mochizuki T, et al. A prospective randomized study of 4-strand semitendinosus tendon anterior cruciate ligament reconstruction comparing single-bundle and double-bundle techniques. *Arthroscopy.* 2007;23:618-628.
15. Muneta T, Sekiya I, Yagishita K, Ogiuchi T, Yamamoto H, Shinomiya K. Two-bundle reconstruction of the anterior cruciate ligament using semitendinosus tendon with endobuttons: operative technique and preliminary results. *Arthroscopy.* 1999;15:618-624.
16. Odensten M, Gillquist J. Functional anatomy of the anterior cruciate ligament and a rationale for reconstruction. *J Bone Joint Surg Am.* 1985;67:257-262.
17. Poolman RW, Farrokhyar F, Bhandari M. Hamstring tendon autograft better than bone patellar-tendon bone autograft in ACL reconstruction: a cumulative meta-analysis and clinically relevant sensitivity analysis applied to a previously published analysis. *Acta Orthop.* 2007; 78:350-354.
18. Purnell ML, Larson AJ, Clancy W. Anterior cruciate ligament insertions on the tibia and femur and their relationships to critical bony landmarks using high-resolution volume-rendering computed tomography. *Am J Sports Med.* 2008;36:2083-2090.
19. Siebold R, Dehler C, Ellert T. Prospective randomized comparison of double-bundle versus single-bundle anterior cruciate ligament reconstruction. *Arthroscopy.* 2008;24:137-145.
20. Siebold R, Ellert T, Metz S, Metz J. Tibial insertions of the anteromedial and posterolateral bundles of the anterior cruciate ligament: morphometry, arthroscopic landmarks, and orientation model for bone tunnel placement. *Arthroscopy.* 2008;24:154-161.
21. Stäubli HU, Rauschning W. Tibial attachment area of the anterior cruciate ligament in the extended knee position: anatomy and cryosections in vitro complemented by magnetic resonance arthrography in vivo. *Knee Surg Sports Traumatol Arthrosc.* 1994;2:138-146.
22. Takahashi M, Doi M, Abe M, Suzuki D, Nagano A. Anatomical study of the femoral and tibial insertions of the anteromedial and posterolateral bundles of human anterior cruciate ligament. *Am J Sports Med.* 2006;34:787-792.
23. Yasuda K, Kondo E, Ichiyama H, et al. Anatomic reconstruction of the anteromedial and posterolateral bundles of the anterior cruciate ligament using hamstring tendon grafts. *Arthroscopy.* 2004;20: 1015-1025.
24. Zantop T, Wellmann M, Fu FH, Petersen W. Tunnel positioning of anteromedial and posterolateral bundles in anatomic anterior cruciate ligament reconstruction: anatomic and radiographic findings. *Am J Sports Med.* 2008;36:65-72.

For reprints and permission queries, please visit SAGE's Web site at <http://www.sagepub.com/journalsPermissions.nav>.

M E M O

[illegible]

有機材料分野

秋吉 一成

生体材料工学研究所・素材研究部門
有機材料学・教授



1) 研究の課題名

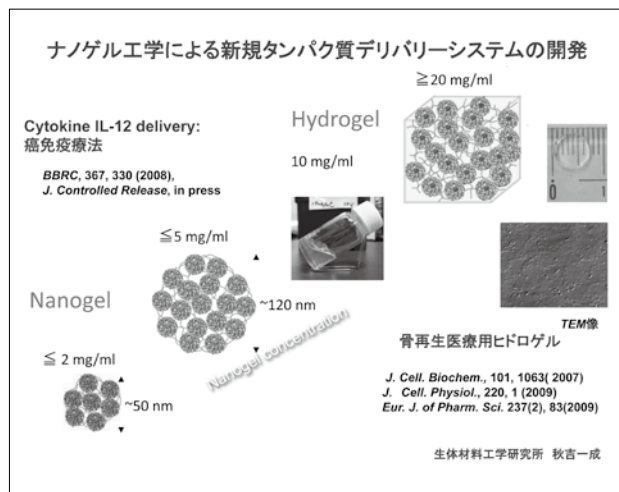
a) ナノゲル工学による新規ナノバイオマテリアル創製と医療応用

Development of novel nanobiomaterials by Nanogel engineering and medical applications

b) リポソーム工学による新規ナノバイオマテリアル創製と医療応用

Development of novel nanobiomaterials by Liposome engineering and medical applications

2)



3) 研究内容の英文要約

We develop tailor-made functional nanogels to create novel nanobiomaterials (nanogel engineering) by the self-assembly of functional associating polymers as building blocks. Macrogels with well-defined nanostructures can be obtained by self-assembly using these nanogels as building blocks. Raspberry-like assembly of nanogels (A-CHPNG) with a high potential as a carrier for protein delivery was prepared. A-CHPNG had a high potential to maintain a high IL-12 level in plasma after subcutaneous injection in mice.

Therefore, A-CHPNG is a promising carrier for long-term medications.

Connexin-containing liposomes were directly prepared by using cell-free transcription/translation systems with plasmids encoding connexin. The proteo-liposomes obtained were able to deliver a hydrophilic and bioactive oligo-peptide to cells through GJs mediated by Cx43 liposome-cell contacts to regulate cell functions. The functional connexin-bearing liposomes reported here should be useful as a tool for cell biology and for drug carrier research into cellular cytosolic delivery.

4) 本事業に関連して世界的な研究拠点形成に向けて、以下の点で改善・整備等されたこと

A (研究拠点体制)

昨年に引き続き、医歯工連携の共同研究を積極的に推進した。

B (研究教育環境)

講義内容を充実させ、質問も随時受け付ける窓口を開いた

C (人材確保)

当研究室の学生二人がスーパースチューデントとして採用された。

D (人材育成)

二人のスーパースチューデントは積極的に本プログラムに参加し、研究面でも大いにプラスとなった。

E (国際化)

外国人特別講師とSSとの討論する機会を年2回以上もった。

5) GCOE事業を推進するに当たって力を入れた点

SS学生も積極的に医歯工連携の共同研究に参画することで、研究の広がりや幅広い知識を身につけることに力を入れた。

6) 英文原著論文

1. N. Inomoto, N. Osaka, T. Suzuki, U. Hasegawa, Y. Ozawa, H. Endo, K. Akiyoshi, and M. Shibayama, Interaction of Nanogel with Cyclodextrin or Protein: Study by Dynamic Light Scattering and Small-angle Neutron Scattering, *Polymer*, 50, 541-546 (2009).
2. S. Yamane, A. Sugawara, A. Watanabe, and K. Akiyoshi, Hybrid Nanoapatite by Polysaccharide Nanogel-Templated Mineralization, *J. Bioactive and Compatible Polym.*, 24, 129-150 (2009).
3. S. Yamane, A. Sugawara, Y. Sasaki, and K. Akiyoshi, Nanogel-Calcium Phosphate Hybrid Nanoparticles with Negative or Positive Charges for Potential Biomedical Applications, *Bull. Chem. Soc. Jpn.*, 82, 416-418 (2009).
4. N. Morimoto, N. Ogino, T. Narita, and K. Akiyoshi, Enzyme-responsive artificial chaperone system with amphiphilic amylose primer, *J. Biotechnology*, 140, 246-249 (2009).
5. N. Alles, N. S. Soysa, A. H. Mian, N. Tomomatsu, H. Saito, R. Baron, N. Morimoto, K. Aoki, K. Akiyoshi, and K. Ohya, Polysaccharide nanogel delivery of a TNF- α and RANKL antagonist peptide allows systemic prevention of bone loss, *Eur. J. Pharm. Sci.*, 37(2), 83-88 (2009).
6. K. Miyai, M. Yoneda, U. Hasegawa, S. Toita, Y. Izu, H. Hemmi, T. Hayata, Y. Ezura, S. Mizutani, K. Miyazono, K. Akiyoshi, T. Yamamoto, and M. Noda, ANA deficiency enhances BMP-induced ectopic bone formation via transcriptional events, *J. Biol. Chem.*, 284(16), 10593-10600 (2009).
7. N. Morimoto, R. Obeid, S. Yamane, F. M. Winnik, and K. Akiyoshi, Composite Nanomaterials by Self-assembly and Controlled Crystallization of Poly(2-isopropyl-2-oxazoline)-Grafted Polysaccharide, *Soft Matter*, 5(8), 1597-1600 (2009).
8. N. Morimoto, J. Tamada, S. Sawada, N. Shimada, A. Kano, A. Maruyama, and K. Akiyoshi, Interaction of Self-assembled Cationic Nanogels with Oligo-DNA and Function as Artificial Nucleic Acid Chaperone, *Chem. Lett.*, 38, 496-497 (2009).
9. M. Kaneda, S. M. Nomura, S. Ichinose, S. Kondo, K. Nakahama, K. Akiyoshi, and I. Morita, Direct formation of proteo-liposomes by in vitro synthesis and cellular cytosolic delivery with connexin-expressing liposomes, *Biomaterials*, 30, 3971-3977 (2009).
10. Y. Ozawa, S. Sawada, N. Morimoto, and K. Akiyoshi, Self-assembled nanogel of hydrophobized dendritic dextrin for protein delivery, *Macromol. Biosci.*, 9, 694-701 (2009).
11. C. Hayashi, U. Hasegawa, Y. Saita, H. Hemmi, T. Hayata, K. Nakashima, Y. Ezura, T. Amagasa, K. Akiyoshi, and M. Noda, Osteoblastic bone formation is induced by using nanogel-crosslinking hydrogel as novel scaffold for bone growth factor, *J. Cell. Phys.*, 220(1), 1-7 (2009).
12. M. X. Chu, H. Kudo, T. Shirai, K. Miyajima, H. Saito, N. Morimoto, K. Yano, Y. Iwasaki, K. Akiyoshi, and K. Mitsubayashi, A soft and flexible biosensor using a phospholipid polymer for continuous glucose monitoring, *Biomedical Microdevices*, 11(4), 837-842 (2009).
13. S. Boridy, H. Takahashi, K. Akiyoshi, and D. Maysinger, The binding of pullulan modified cholesteryl nanogels to A β oligomers and their suppression of cytotoxicity, *Biomaterials*, 30(29), 5583-5591 (2009).
14. H. Kobayashi, O. Katakura, N. Morimoto, K. Akiyoshi, and S. Kasugai, Effects of cholesterol-bearing pullulan (CHP)-nanogels in combination with prostaglandin E1 on wound healing, *J. Biomed. Mater. Res. B.*, 91(1), 55-60 (2009).
15. S. Toita, Y. Soma, N. Morimoto, and K. Akiyoshi, Cycloamylose-based Biomaterial: Nanogels of Cholesterol-bearing Cationic Cycloamylose for siRNA Delivery, *Chem. Lett.*, 38, 1114-1115 (2009).
16. H. Tsutsumi, W. Nomura, S. Abe, T. Mino, A. Masuda, N. Ohashi, T. Tanaka, K. Ohba, N. Yamamoto, K. Akiyoshi, and H. Tamamura, Fluorogenically Active Leucine Zipper Peptides as New Tag-Probe Pairs for Protein Imaging in Living Cells, *Angew. Chem., Int. Ed.*, 48, 9164-9166 (2009).
17. U. Hasegawa, S. Sawada, T. Shimizu, T. Kishida, E. Otsuji, O. Mazda, and K. Akiyoshi, Raspberry-Like Assembly of Cross-Linked Nanogels for Protein Delivery, *J. Controlled Release*, 140, 312-317 (2009).
18. S. Sawada and K. Akiyoshi, Nano-encapsulation of lipase by self-assembled nanogels: induction of high enzyme activity and thermal stabilization, *Macromol. Biosci.*, .
19. T. Hirakura, K. Yasugi, T. Nemoto, M. Sato, T. Shimoboji, Y. Aso, N. Morimoto, K. Akiyoshi, Hybrid hyaluronan hydrogel encapsulating nanogel as a protein nanocarrier: new system for sustained delivery of protein with a chaperone-like function, *J. Controlled Release*, .
20. S. Toita, N. Morimoto, K. Akiyoshi, Functional cycloamylose-based biomaterial: application in a gene delivery system, *Biomacromolecules*,

7) 著書

1. 下田麻子, 秋吉一成, インジェクタブル高分子, ますます重要になる細胞周辺環境の科学技術, 遺伝子医学MOOK別冊, 田畑泰彦監修, メディカルドゥ, 77-80 (2009) .
2. 高橋治子, 秋吉一成, DDSナノデバイス, バイオ利用&健康デバイス, 三林浩二監修, シーエムシー出版, 158-167 (2009) .

3. 秋吉一成, 分子シャペロン機能工学, 超分子サイエンス & テクノロジー, 国武豊喜監修, NTS, 1018-1024 (2009) .
4. 秋吉一成, 生体の機能, 現代界面コロイド化学の基礎-原理・応用・測定ソリューション, 第3版日本化学会編, 丸善, 332-338 (2009) .
5. 秋吉一成, 進化するバイオ高分子・生体分子システムへの挑戦, 特集高分子学会研究会, 高分子, 58,756-760 (2009) .
6. 佐々木善浩, 秋吉一成, ナノゲル工学による新規ナノバイオ材料設計, 高分子科学最近の進歩, 高分子, 58,756-760 (2009) .

8) 平成21年度までの自己評価

我々の開発したDDSを利用した拠点内での協同研究を一層促進させるように努力した。

現在、野田教授、森田教授、春日井教授、大谷教授、小川教授との共同研究を進めている。それぞれの共同研究も順調に成果が得られており、本年度は、野田教授との論文、2報、森田教授、1報、大谷教授、1報、春日井教授、1報の計5報が欧文誌に受理された。

9) 学会発表 (英文)

(一般)

- 1) Shimoda A, Akiyoshi K. Design of Nanogel Cross-Linking Nanoparticles for Protein Delivery. 8th International Symposium on Frontiers in Biomedical Polymers. Mishima, Japan, May, 2009.
- 2) Kamiya K, Tsumoto K, Yoshimura T, Akiyoshi K. Preparation of connexin proteoliposomes using baculovirus expression systems for a novel drug carrier. 8th International Symposium on Frontiers in Biomedical Polymers. Mishima, Japan, May, 2009.
- 3) Toita S, Soma Y, Morimoto N, Akiyoshi K. Cationic Cycloamylose for pDNA/siRNA Delivery. 8th International Symposium on Frontiers in Biomedical Polymers, Mishima, Japan, May, 2009.
- 4) Takahashi H, Sawada S, Akiyoshi K. Functional polysaccharide nano-ball for protein delivery. 8th International Symposium on Frontiers in Biomedical Polymers, Mishima, Japan, May, 2009.
- 5) Sasaki Y, Yamane S, Akiyoshi K. Organic-Inorganic Dual Crosslinked Nanogels for Potential Biomedical Applications. 8th International Symposium on Frontiers

- in Biomedical Polymers, Mishima, Japan, May, 2009.
- 6) Shimoda A, Komaki M, Morita I, Akiyoshi K. Design of Nanogel-assembled Nanoparticles for protein delivery. 36th Annual Meeting and Exposition of the Controlled Release Society, Copenhagen, Denmark, July, 2009.
- 7) Kamiya K, Tsumoto K, Yoshimura T, Akiyoshi K. Preparation of connexin proteoliposomes using baculovirus expression systems for potential biomedical application. 36th Annual Meeting and Exposition of the Controlled Release Society, Copenhagen, Denmark, July, 2009.
- 8) Takahashi H, Sawada S, Akiyoshi K. Design of functional polysaccharide nano-ball and application to DDS. 36th Annual Meeting and Exposition of the Controlled Release Society, Copenhagen, Denmark, July, 2009.
- 9) Sasaki, Y, Yamane S, Akiyoshi K. Organic-Inorganic Hybrid Polysaccharide Nanogels Crosslinked with Siloxane. 36th Annual Meeting and Exposition of the Controlled Release Society, Copenhagen, Denmark, July, 2009.
- 10) Toita S, Soma Y, Morimoto N, Akiyoshi K. Functional Cycloamylose for siRNA Delivery. 22nd European Conference on Biomaterials, the annual conference of the European Society for Biomaterials, Lausanne, Switzerland, September, 2009.
- 11) Kamiya K, Tsumoto K, Yoshimura T, Akiyoshi K. New method of preparation of proteoliposomes: Baculovirus expression-liposome fusion systems. 2nd Switzerland-Japan Biomolecular Chemistry Symposium, Tokyo, Japan, September, 2009.
- 12) Toita S, Akiyoshi K. Functional Cycloamylose Nanogels for siRNA Delivery. GelSymposium2009, Osaka, Japan, December, 2009.
- 13) Takahashi H, Sawada S, Akiyoshi K. Function of polysaccharide nano-ball based nanogel. GelSymposium2009, Osaka, Japan, December, 2009.

10) 学会発表 (和文)

- 1) 高橋治子, 澤田晋一, 秋吉一成. 疎水化グリコーゲンのナノゲル形成と機能. 日本化学会第89春季年会, 千葉, 2009年3月.
- 2) 林純吾, 澤田晋一, 栗田公夫, 秋吉一成. ポリイオンコンプレックスナノゲルの設計. 日本化学会第89春季年会, 千葉, 2009年3月.
- 3) 土戸優志, 佐々木善浩, 秋吉一成. アミンをターゲットとする動的バイオコンジュゲーターの設計と合成. 日本化学会第89春季年会, 千葉, 2009年3月.
- 4) 酒井ゆうき, 土戸優志, 橋本剛, 早下隆士. デンドリマー表面へのボロン酸型アゾプロローブの自己組織化と糖認識機能. 日本化学会第89春季年会, 千葉, 2009年3月.

- 5) 森谷優貴, 野村慎一郎, 檜山聡, 須田達也, 秋吉一成. 分子通信の実現に向けたチャネル形成膜タンパク質組込リボソームの調製と機能評価. 日本化学会第89春季年会, 千葉, 2009年3月.
- 6) 下田麻子, 秋吉一成. ナノゲル架橋ナノ微粒子の設計とタンパク質デリバリーへの応用. 日本化学会第89春季年会, 千葉, 2009年3月.
- 7) 戸井田さやか, 相馬祐輝, 森本展行, 秋吉一成. 機能性サイクロアミロースによる核酸キャリアの開発. 日本化学会第89春季年会, 千葉, 2009年3月.
- 8) 神谷厚輝, 湊元幹太, 吉村哲郎, 秋吉一成. バキュロウイルス発現系を用いた新規コネキシンリボソームの構築と機能. 日本化学会第89春季年会, 千葉, 2009年3月.
- 9) 佐々木善浩, 山根説子, 秋吉一成. ナノ有機-無機ハイブリッドによるバイオ応用. 日本化学会第89春季年会, 千葉, 2009年3月.
- 10) 山根説子, 佐々木善浩, 秋吉一成. シロキサン結合を架橋点に有する多糖ナノゲルの設計と合成. 第58回高分子学会年次大会, 千葉, 2009年3月.
- 11) 中島新, 菊池純一, 佐々木善浩, 秋吉一成. 強度人工細胞膜「セラソーム」を用いる遺伝子発現. 日本化学会第89春季年会, 千葉, 2009年3月.
- 12) 高橋治子, 澤田晋一, 秋吉一成. 機能性ポリサッカライドナノボールの設計とDDS応用. 第58回高分子学会年次大会, 神戸, 2009年5月.
- 13) Tsuchido Y, Sasaki Y, Akiyoshi K. Synthesis and Function of Vitamin B6-bearing Polysaccharide. 第58回高分子学会年次大会, 神戸, 2009年5月.
- 14) Kamiya K, Tsumoto K, Yoshimura T, Akiyoshi K. Preparation of proteoliposome using baculovirus-liposome fusion method-Function of connexin liposomes. 第58回高分子学会年次大会, 神戸, 2009年5月.
- 15) 平野さやか, 森本展行, 栗田公夫, 秋吉一成. 刺激応答性ナノゲルの設計. 第58回高分子学会年次大会, 神戸, 2009年5月.
- 16) 林純吾, 澤田晋一, 栗田公夫, 秋吉一成. イオンコンプレックスナノゲルの設計. 第58回高分子学会年次大会, 神戸, 2009年5月.
- 17) 安岡潤一, 戸井田さやか, 澤田晋一, 秋吉一成. カチオン性ナノゲルによる核酸の細胞内デリバリー. 第58回高分子学会年次大会, 神戸, 2009年5月.
- 18) 下田麻子, 秋吉一成. ナノゲルボトムアップ法によるバイオ材料の設計- (1) ナノゲル集積ナノ微粒子. 第58回高分子学会年次大会, 神戸, 2009年5月.
- 19) Toita S, Soma Y, Morimoto N, Akiyoshi K. Functional Cycloamylose for Intracellular Delivery. 第58回高分子学会年次大会, 神戸, 2009年5月.
- 20) 早下隆士, 佐藤諒, 新福千枝, 酒井ゆうき, 土戸優志, 橋本剛. ボロン酸型アゾプローブの自己組織化と糖認識機能. 第5回ホスト・ゲスト化学シンポジウム, 宇都宮, 2009年5月.
- 21) 神谷厚輝, 杉浦裕展, 湊元 幹太, 吉村哲郎, 秋吉一成. 新規膜タンパク質再構成リボソーム作製法の開発. 第19回バイオ・高分子シンポジウム, 東京, 2009年7月.
- 22) 高橋治子, 澤田晋一, 秋吉一成. 酵素合成グリコーゲンの機能化とDDS応用. 第19回バイオ・高分子シンポジウム, 東京, 2009年7月.
- 23) 下田麻子, 小牧基浩, 森田育男, 岸田綱郎, 松田修, 秋吉一成. ナノゲルボトムアップ法によるバイオ材料の設計とタンパク質デリバリー. 第19回バイオ・高分子シンポジウム, 東京, 2009年7月.
- 24) 戸井田さやか, 相馬祐輝, 森本展行, 秋吉一成. 機能性サイクロアミロースによるsiRNAデリバリー. 遺伝子・デリバリー研究会第9回シンポジウム, 大阪, 2009年7月.
- 25) 高橋治子, 澤田晋一, 秋吉一成. 機能化ポリサッカライドナノボールの設計とタンパク質デリバリーへの応用. 第25回日本DDS学会, 東京, 2009年7月.
- 26) 下田麻子, 小牧基浩, 森田育男, 岸田綱郎, 松田修, 秋吉一成. インジェクタブルナノゲル架橋ナノ微粒子によるタンパク質デリバリー. 第25回日本DDS学会, 東京, 2009年7月.
- 27) 秋吉一成, 澤田晋一, 高橋治子, 原田直純, 村岡大輔, 珠玖洋. 癌免疫ワクチン療法におけるナノゲルキャリアの機能. 第25回日本DDS学会, 東京, 2009年7月.
- 28) 戸井田さやか, 相馬祐輝, 森本展行, 秋吉一成. 機能化サイクロアミロースによるsiRNAキャリアの開発. 第25回日本DDS学会, 東京, 2009年7月.
- 29) 澤田晋一, 多田陽子, 秋吉一成. ナノゲルを基盤としたタンパク質徐放シートの開発. 第25回日本DDS学会, 東京, 2009年7月.
- 30) 佐々木善浩, 阿部慶太, 菊池純一, 秋吉一成. バイオチップ作製へ向けた人工細胞アレイの構築. 第58回高分子討論会, 熊本, 2009年9月.
- 31) 高橋治子, 澤田晋一, 秋吉一成. 新規機能性グリコーゲン多糖ナノボールの設計とバイオ応用. 第58回高分子討論会, 熊本, 2009年9月.

- 32) 戸井田さやか, 相馬祐輝, 森本展行, 秋吉一成. siRNA キャリアとしてのサイクロアミロースの機能. 第58回高分子討論会, 熊本, 2009年9月.
- 33) 中島彩, 相馬祐輝, 戸井田さやか, 森本展行, 秋吉一成. 機能性サイクロアミロースによる細胞内タンパク質デリバリー. 第58回高分子討論会, 熊本, 2009年9月.
- 34) 下田麻子, 秋吉一成. ナノゲル架橋ハイドロゲルの設計とタンパク質デリバリーへの応用. 第58回高分子討論会, 熊本, 2009年9月.
- 35) 安岡潤一, 戸井田さやか, 澤田晋一, 秋吉一成. カチオン性ナノゲルによる CpG DNA デリバリーと免疫療法. 第58回高分子討論会, 熊本, 2009年9月.
- 36) 阿部慶太, 佐々木善浩, 秋吉一成. DNA セルフアセンブリによるリポソームアレイの構築. 第58回高分子討論会, 熊本, 2009年9月.
- 37) 土戸優志, 佐々木善浩, 秋吉一成. ビタミンB6-多糖コンジュゲートの設計と機能. 第58回高分子討論会, 熊本, 2009年9月.
- 38) 平野さやか, 森本展行, 清水繁, Thompson David H, 秋吉一成. pH応答性ナノゲルの設計. 第58回高分子討論会, 熊本, 2009年9月.
- 39) 林純吾, 澤田晋一, 清水繁, 秋吉一成. イオンコンプレックスナノゲルの設計と機能評価. 第58回高分子討論会, 熊本, 2009年9月.
- 40) 神谷厚輝, 湊元幹太, 吉村哲郎, 秋吉一成. バキュロウイルス-リポソーム融合法によるコネキシンプロテオリポソームの構築と機能. 第58回高分子討論会, 熊本, 2009年9月.
- 41) 神谷厚輝, 湊元幹太, 吉村哲郎, 秋吉一成. コネキシン巨大プロテオリポソームの構築と機能. 第47回日本生物物理学会年会, 徳島, 2009年10月.
- 42) 高橋治子, 澤田晋一, 秋吉一成. グリコーゲン多糖ナノボールの機能化とバイオ応用. 第31回日本バイオマテリアル学会大会, 京都, 2009年11月.
- 43) 戸井田さやか, 森本展行, 秋吉一成. 機能化サイクロアミロースによる siRNA デリバリーキャリアの開発. 第31回日本バイオマテリアル学会大会, 京都, 2009年11月.
- 44) 安岡潤一, 戸井田さやか, 澤田晋一, 秋吉一成. カチオン性ナノゲルによる CpG DNA デリバリーシステム. 第31回日本バイオマテリアル学会大会, 京都, 2009年11月.
- 45) 中島彩, 戸井田さやか, 森本展行, 秋吉一成. 機能化サイクロアミロースによるタンパク質デリバリー. 第31回日本

バイオマテリアル学会大会, 京都, 2009年11月.

11) 受賞

- 1) 神谷厚輝, 日本化学会第88春季年会, 学生講演賞, 2009年3月.
- 2) 高橋治子, 第25回日本DDS学会, ポスター賞, 2009年7月.

12) 外部資金の獲得状況

文部科学省科学研究費補助金 特定領域研究 統合がん

研究題目: 癌免疫治療のための新規ナノゲルキャリアの開発

代表: 秋吉 一成

期間: 平成20-21年度

研究費総額: 2200万円

文部科学省科学研究費補助金 基盤研究 (A)

研究題目: ナノゲルを基盤とした新規ドラッグデリバリーシステムの開発

代表: 秋吉 一成

期間: 平成20-24年度

研究費総額: 3910万円

文部科学省科学研究費補助金 学術創製研究費

研究題目: 物理科学を基盤とする人工細胞の構築と機能解析

分担: 秋吉 一成

期間: 平成18-22年度

研究費総額: 6300万円

戦略的創造研究推進事業 (CREST)

研究題目: 分子シャペロン工学に基づく遺伝子解析

分担: 秋吉 一成

期間: 平成17-21年度

研究費総額: 3000万円

医薬基盤研究所 保健医療分野における基礎研究推進事業

研究題目: 新規 siRNA テクノロジーを用いたC型肝炎の画期的治療法の開発

分担: 秋吉 一成

期間: 平成20-21年度

研究費総額: 1200万円

13) 特別講演、招待講演

- 1) 秋吉一成. シャペロン機能工学の創製とバイオ応用. 4 回理研「バイオ医工学シンポジウム」, 和光, 2009 年 3 月.
- 2) 秋吉一成. ナノゲル工学による新規タンパク質 DDS の開発. 慶応大学大学院薬学研究科 DDS・薬物動態クラスター・ドラッグデリバリー・薬物動態ミニシンポジウム, 東京, 2009 年 5 月.
- 3) 秋吉一成. ナノゲル工学による新規バイオマテリアルの設計と応用. 第 58 回高分子学会年次大会, 神戸, 2009 年 5 月.
- 4) 秋吉一成. ナノゲル工学による新規 DDS の設計. 第 27 回物性物理化学研究会「DDS と製剤基材の物性」, 京都, 2009 年 6 月.
- 5) 秋吉一成. Polysaccharide nanogel engineering. 遺伝子デリバリー研究会第 9 回シンポジウム. 第 15 回日本遺伝子治療学会, 大阪, 2009 年 7 月.
- 6) 秋吉一成. 多糖ナノゲル工学による新規バイオマテリアルの創製. 第 3 回多糖の未来フォーラム-多糖の資源活用と機能探求に向けて-, 仙台, 2009 年 11 月.
- 7) 秋吉一成. ナノゲル工学による新規バイオマテリアルの創製. 第 77 回千葉地区高分子研究交流講演会, 千葉, 2009 年 11 月.
- 8) 秋吉一成. 高機能バイオマテリアル: ナノゲルリポゾーム DDS の現況について. 医薬ライセンシング協会第 216 回月例会, 東京, 2009 年 11 月.
- 9) 秋吉一成. ナノゲル工学による新規タンパク質 DDS の開発. 第 3 回 NEDO 特別講座 DDS シンポジウム「次世代 DDS が切り拓く未来医療」, 東京, 2009 年 12 月.
- 10) Akiyoshi K. Nanogel protein delivery system with chaperone function. 14th International Symposium on Recent Advances in Drug Delivery Systems. Salt Lake City, Utah, USA, February, 2009.
- 11) Akiyoshi K. Nanogel Engineering for Protein Delivery. 8th International Symposium on Frontiers in Biomedical Polymers FBPS'09, Mishima, Japan, May, 2009.
- 12) Akiyoshi K. Polysaccharide nanogel engineering for protein delivery system. KIFEE workshop on environment, Energy and Materials, Trondheim, Norway, September, 2009.
- 13) Sasaki Y, Akiyoshi K. Drug Delivery System for Cancer Therapy. International Summer Program 2009, Recent Advances in Cancer Research, Tokyo, Japan, September, 2009.

14) Akiyoshi K. Design of New Hydrogel Biomaterials by Nanogel Engineering. The 4th International Symposium on Integrated Molecular/Materials Engineering (ISIMME2009), Chengdu, China, October, 2009.

15) Sasaki Y, Abe K, Kikuchi J, Akiyoshi K. Fabrication of Artificial Cell Array for Creation of Biochip. International Symposium on Nanobio-Interfaces Related to Molecular Mobility, Tokyo, Japan, November, 2009.

14) 新聞、雑誌、TV 報道

1. 2009 年 7 月 16 日 日経産業新聞
がん治療、効果持続 免疫タンパク質多糖類で包
2. 2009 年 8 月 1 日 日本経済新聞 技術ウオッチ (中外製薬との共同研究)
薬物送達で注射回数少なく 中外製薬、慢性疾患で成果
3. 2009 年 8 月 29 日 日本経済新聞 技術ウオッチ (三重大との共同研究)
癌免疫療法、事業化動く

15) GCOE 総合講義のサマリー

近年ゲノム科学やバイオテクノロジーの進歩により、抗体やホルモンに代表されるようなタンパク質バイオ医薬の実用化が急速に進んでいる。バイオ医薬は一般的に高い治療効果を示す一方で、安定性が低いことや複数回の投与が必要であり、患者への負担も大きい。また、製剤化におけるタンパク質のフォールディングや活性維持に関しても課題は多い。そこで活性を維持したままデリバリーし得る技術がますます重要となっている。本稿では、多糖ナノゲルをタンパク質 DDS キャリアとして用いる研究について、分子シャペロン機能を有するナノゲルキャリアの開発、ナノゲルによる効率的な細胞内導入から、免疫療法としての臨床応用にいたる研究成果を紹介した。また、ナノゲルをビルディングブロックとしたボトムアップゲル製造技術により、ナノゲル基盤ヒドロゲル材料の開発と再生医療用ヒドロゲルとしての応用について解説した。

16) 教室、分野や講座の准教授、講師、助教、特別研究員、ポスドク、指導を受けた大学院生の名前 (AISSには○印) のリスト

佐々木善浩	准教授
澤田晋一	助教
戸井田さやか	博士2年
神谷厚輝	博士2年
○下田麻子	博士1年
関根由莉奈	博士1年
○高橋治子	博士1年
土戸優志	修士2年
安岡潤一	修士2年
阿部慶太	修士1年
中島 彩	修士1年

17) GCOE 活動についての感想、コメント、改善を望む点など

本年度は、当研究室の二人が AISS に採用されて、充実した研究展開と共同研究が実施できた。

Provided for non-commercial research and education use.
Not for reproduction, distribution or commercial use.



This article appeared in a journal published by Elsevier. The attached copy is furnished to the author for internal non-commercial research and education use, including for instruction at the authors institution and sharing with colleagues.

Other uses, including reproduction and distribution, or selling or licensing copies, or posting to personal, institutional or third party websites are prohibited.

In most cases authors are permitted to post their version of the article (e.g. in Word or Tex form) to their personal website or institutional repository. Authors requiring further information regarding Elsevier's archiving and manuscript policies are encouraged to visit:

<http://www.elsevier.com/copyright>



Contents lists available at ScienceDirect

Biomaterials

journal homepage: www.elsevier.com/locate/biomaterials

Direct formation of proteo-liposomes by *in vitro* synthesis and cellular cytosolic delivery with connexin-expressing liposomes

Makoto Kaneda^{a,1}, Shin-ichiro M. Nomura^{b,1,2}, Shizuko Ichinose^c, Satoshi Kondo^b,
Ken-ichi Nakahama^a, Kazunari Akiyoshi^{b,d,*}, Ikuo Morita^{a,d,**}

^a Department of Cellular Physiological Chemistry, Tokyo Medical and Dental University, 1-5-45 Yushima, Bunkyo-ku, Tokyo 113-8549, Japan

^b Institute of Biomaterials and Bioengineering, Tokyo Medical and Dental University, 2-3-10 Kanda, Suruga-dai, Chiyoda-ku, Tokyo 101-0062, Japan

^c Instrumental Analysis Research Center, Tokyo Medical and Dental University, 1-5-45 Yushima, Bunkyo-ku, Tokyo 113-8510, Japan

^d Global Center of Excellence (GCOE) Program, International Research Center for Molecular Science in Tooth and Bone Diseases, Tokyo Medical and Dental University, Tokyo, Japan

ARTICLE INFO

Article history:

Received 3 January 2009

Accepted 2 April 2009

Available online 6 May 2009

Keywords:

Liposome

Membrane protein

Cell-free protein synthesis

Drug delivery

Peptide

Connexin

ABSTRACT

Liposomes are widely utilized in molecular biology and medicine as drug carriers. Here we report a new liposome–cell interaction through connexins. Connexin 43 (Cx43)-containing liposomes were prepared by using cell-free transcription/translation systems with plasmids encoding Cx43 in the presence of liposome. The expressed membrane protein, Cx43, was directly constituted to the liposome membrane upon *in vitro* synthesis, leading to pure membrane protein-containing liposomes. The hydrophilic dye calcein was efficiently transferred from Cx43-expressing liposomes to cultured cells (Cx43 expressing). The transfer is significantly blocked in the presence of gap junction inhibitor (18β-glycyrrhetic acid) and in the case of the other type of connexin (Cx32)-expressing cell. The results show that calcein entered the cell through connexin-mediated pathway. Cx43 liposomes containing a soluble NEMO-binding domain peptide suppressed the intracellular signaling cascade IL-1β-induced NF-κB activation and cyclooxygenase-2 expression in Cx43-expressing cells, confirming effective peptide transfer into the cell. This is a new method for direct cytosolic delivery of hydrophilic molecules.

© 2009 Elsevier Ltd. All rights reserved.

1. Introduction

Membrane proteins play crucial roles in diverse biological functions such as signal transduction, energy production, and cellular communication. Many membrane proteins have been widely studied by analytical molecular biology approaches. However, understanding their structures and functions has been complicated by difficulties in isolating and purifying functional membrane protein. Folding and function of integrated membrane proteins are assisted by addition of a lipid bilayer. In cellular membrane models, liposomes have been frequently used to analyze the function of reconstituted membrane proteins [1], including gap

junction forming connexins [2–4]. In these approaches, a target membrane protein is usually overexpressed in host cells, solubilised with detergents, purified by chromatography, and finally reconstituted into liposomes by detergent removal. However, this process is complicated and time-consuming, and the yield of functional reconstituted membrane protein is often low [5]. In constructive approach, liposome-encapsulated gene-expression systems have recently been investigated as possible artificial cell models [6–10], displaying a capacity for compartmentalized processes essential for gene transcription and protein product translation. Most of the research on *in vitro* gene-expression systems have been devoted to the synthesis of water-soluble proteins. Recently, *in vitro* membrane protein syntheses in the presence of artificial membranes have been reported [9–12]. However, the synthesis of membrane proteins is still limited due to the low solubility and folding problem. In this report, *in vitro* membrane protein synthesis for connexins was performed in the presence of liposomes, producing liposomes bearing a functional membrane protein. This method allows us direct formation of pure membrane protein-containing liposomes.

Connexins are a critical component of cellular gap junctions (GJs), forming structures that mediate intercellular communication [13,14]. Each GJ consists of two docked hemichannels (connexons)

* Corresponding author. Institute of Biomaterials and Bioengineering, Tokyo Medical and Dental University, 2-3-10 Kanda, Suruga-dai, Chiyoda-ku, Tokyo 101-0062, Japan.

** Corresponding author. Department of Cellular Physiological Chemistry, Tokyo Medical and Dental University, 1-5-45 Yushima, Bunkyo-ku, Tokyo 113-8549, Japan.

E-mail addresses: akiyoshi.ori@tmd.ac.jp (K. Akiyoshi), morita.cell@tmd.ac.jp (I. Morita).

¹ These authors contributed equally to this work.

² Present address: Institute for Integrated Cell Material Sciences (iCeMS), Kyoto University, and JST PRESTO, Yoshida ushinomiya-cyo, Sakyo-ku, Kyoto 606-8501, Japan.

Author's personal copy

3972

M. Kaneda et al. / Biomaterials 30 (2009) 3971–3977

between two neighboring cells. A connexon is comprised of six connexin proteins in self-assembly. Small molecules such as ions, second messengers, and metabolites in cytosol can be directly transferred from one cell to a neighboring cell through GJs. The driving force for the transfer is considered as a simple diffusion. The molecular mass cut-off for a GJ channel is generally given as below 1–1.8 kDa [13,14]. Mechanism of the transfer in detail does not understand well. The open state channel probabilities of the gap junction are regulated by pH, calcium ion, membrane potential, and other factors. Here we report usage of connexins in liposomes as a molecular carrier for direct cytosolic delivery.

2. Methods and materials

2.1. Connexin plasmid construction

The cloning of Cx43 cDNA has been described previously [15]. Plasmid pcDNA3.1-Cx43 was used as the template for polymerase chain reaction (PCR) amplification. The expression vector pCMVINT-Cx43 was generated using the following primers: 5'-AAAGAATTCGCCACCATGGGTGACTGGAGT-3' (forward) and 5'-AAATCTAGAGGTTTAAATCTCCAGGTCATC-3' (reverse). The PCR products were digested by EcoRI and XbaI and then inserted into pCMVINT (Promega, Madison, WI). For construction of pCMVINT-Cx43-EGFP, Cx43 cDNA was amplified using the primers 5'-AACCGAATTCATGGGTGACTGGAGTGCCTT-3' (forward) and 5'-TTGGATCCGTAATCTCCAGGTCATCAGG-3' (reverse). The PCR product was digested by EcoRI and BamHI and inserted into pEGFP-N3 (pEGFP-Cx43, clontech, Mountain View, CA). Then pCMVINT-Cx43-EGFP was generated using pEGFP-Cx43, forward for pCMVINT-Cx43 and 5'-AATCTAGAGCTTACTGTACAGCTCGTC-3' (reverse) as the template and primers, respectively. For construction of pcDNA3.1-Cx32 and pCMVINT-Cx32, rat liver cDNA was used as the template for polymerase chain reaction (PCR) amplification. The expression vectors pcDNA3.1-Cx32 and pCMVINT-Cx32 were generated using the following primers: 5'-AAAGAATTCAGGCGATGAAGTGGACAG-3' (forward) and 5'-AAATCTAGATGGTATGCGCATCAGCAGG-3' (reverse). The PCR products were digested by EcoRI and XbaI and then inserted into pcDNA3.1+ (Invitrogen Co., Carlsbad, CA) and pCMVINT. All of the purified plasmids had an average Abs. 260/280 ratio of approximately 1.8.

2.2. Liposome preparation and in vitro protein synthesis

Connexin 43-containing liposomes (Cx43-liposomes) were directly generated as follows; an *in vitro* transcription/translation solution of rabbit reticulocyte lysate with the Cx43 gene added into the procedure used to prepare liposomes by the natural swelling method. Protein synthesis was performed with liposomes over time *in vitro*. A solution of egg yolk phosphatidylcholine (Nakalai tesque, Kyoto, Japan) and a 10,000:1 molar ratio of Texas Red conjugated 1,2-dihexadecanoyl-sn-glycero-3-phosphatidylethanolamine (Texas Red DHPE, Invitrogen Co., Carlsbad, CA) in chloroform/methanol (2:1, v/v) were put in a glass test tube (8 × 33 mm). Texas Red DHPE stains the liposomal membrane. The solvent was gently evaporated in Argon gas flux, and then the residual lipid film was dried overnight under vacuum. For *in vitro* gene expression of Cx43, Cx43-EGFP and Cx32, rabbit reticulocyte lysate in TNT Quick Coupled Transcription/Translation Systems (Promega, Madison, WI) was used. The plasmid (1 µg) was dissolved in the transcription/translation mixture (25 µL) on ice for temporary inhibition of gene expression according to the manufacturer's protocol. In the experiment, reagents were used without further purification and treated with caution under RNase-free conditions. The lipid films were hydrated with this mixture solution; this is generally called the "natural swelling method" of gene-expressing liposome preparation [6]. The final concentration of the lipid was 5 mM. Samples containing hydrated lipid films were incubated for 90 min at 30 °C in the incubator PG-Mate (Invitroch, Kyoto, Japan). Liposome formation and protein synthesis were performed in parallel. After cooling to 4 °C, the liposome samples were immediately used for the various assays.

2.3. Immunoelectron microscopy

One hundred microliter sample solutions of Cx43 liposome were washed in cold PBS by centrifugation (10,000 × g, 10 min, 4 °C). The samples were immersed in 25% sucrose in 0.1 M PBS for 24 h at 4 °C, mounted in O.C.T. compound (Tissue tek) embedding medium with gentle mixing by pipetting and quickly frozen in liquid nitrogen. Frozen sections of thickness of 6 µm were cut on a CM1900 cryostat (Reichert, Vienna, Austria) at a knife and specimen temperature of -15 °C. The frozen sections were placed on silane-coated glass slides and washed in 0.1 M PBS. For immunoelectron microscopy of connexin 43, 8 µm cryostat sections were used. The sections were placed on silane-coated glass and then placed on droplets of 1% bovine serum albumin in 0.1 M PBS for 1 h at 4 °C to eliminate nonspecific antibody binding. Then the slides with the sections were placed on droplets of mouse monoclonal antibody against connexin 43 (1:20; BD Transduction Laboratories)

containing 1% bovine serum albumin for 24 h at 4 °C. Each slide was washed with 0.1 M PBS and incubated with goat anti-mouse IgG and IgM conjugated with 10-nm diameter gold colloidal particles (1:20; British Biocell International) containing 1% bovine serum albumin for 24 h at 4 °C. After incubation, the slides were washed with 0.1 M PBS for 2 h. The sections on the slide were subsequently fixed in 2.5% glutaraldehyde and then postfixed in 1% OsO₄ in 0.1 M PBS. The slides were dehydrated in a graded series of ethanol and embedded in Epon812. The ultrathin sections were stained with uranyl acetate and then examined with a transmission electron microscope H-7100 (Hitachi Ltd.) at 75 kV. The number of the immunogold particles on the cross-section of liposome was counted using ImageJ software (NIH). The relative amounts of each connexin in each Cx-liposome increase with the diameter of the liposome. Supplemental figure 6 showed the numbers of immunogold per one liposome as a function of diameter of liposome.

2.4. Dye-transfer assay

To investigate dye transfer from the liposomes to cells through gap junctions, Cx43-liposome encapsulating calcein dye (Dojindo, Kumamoto, Japan), which is membrane impermeable, was prepared. Dye-containing Cx43 liposomes were prepared by adding calcein dye (at a final concentration of 0.1 mM in liposome solution) to the transcription/translation reaction. FITC-Dextran with nominal molecular weights of 3000 and 10,000 Da (Molecular Probes, Invitrogen, USA) were adopted for investigation of the GJ gating. The dye conditions showed no significant effect on connexin synthesizing reaction. After the gene-expression reaction finished, 20 µL of the Cx43-liposome solution were applied to 1 mL subconfluent cultures of Cx43-expressing U2OS cells (in DMEM media containing 10% FBS). This step dilutes the un-encapsulated dye 50 times, and the dye encapsulated in the liposomes was clearly observed. 2 h after incubation in a 5% CO₂ atmosphere at 37 °C in a humidified incubator, the cells were observed by confocal laser-scanning microscopy (LSM 510 META, Carl Zeiss, Oberkochen, Germany) at 505–530 nm (for calcein) and at 560 nm for Texas Red DHPE (for liposome membranes). Under these conditions image analysis was performed using a Zeiss LSM image browser.

2.4.1. Time-lapse imaging

Twenty microliters of the calcein-containing Cx43-liposome solution were centrifuged (at 10,000 × g for 10 min at 4 °C) and removed the supernatant with free calcein. Giant liposomes (cell-size liposome) were mainly collected. Precipitate was rehydrated by 20 µL of ice-cold PBS. 5 min after application of the Cx43 liposomes to cultured cells, liposome was scanned at 10-s intervals, until a transfer of calcein was observed to enter the cells.

2.4.2. Dye-transfer ratio analysis

For evaluating the ratios of calcein dye transfer from the liposomes to cells, more than 490 cells were counted directly from the obtained microscopic images at specific time points ($n = 2-4$). The liposomes were washed out by PBS for critical counting. For investigation of the heterotypic gap junctions between Cx43 and Cx32, dye-containing Cx43 (or Cx32) liposomes were prepared by the method described above. After the expression reaction finished, 20 µL of the Cx43-liposome solution was applied to Cx43- or Cx32-expressing U2OS cells (cultured in 1 mL of DMEM media containing 10% FBS). 2 h after incubation in a 5% CO₂ atmosphere at 37 °C in a humidified incubator, the sample cells were washed 3 times with DMEM medium and then observed by LSM 510 at 505–530 nm (for calcein or FITC-Dextran). Dye positive cells were counted for the total cells on the observed cells.

2.5. NEMO-binding domain peptide (NBDp) preparation

The NBD peptide (TALDWSWLQTE), a partial sequence of IKKβ, and the mutant peptide (TALDASALQTE; sites of mutation underlined) were produced by Fmoc (fluorenylmethoxycarbonyl) synthesis (Qiagen, Hilden, Germany). Peptides were characterized by matrix-assisted laser desorption/ionization-time of flight mass spectrometry and reverse-phase high-performance liquid chromatography. The peptides were dissolved at 5 mM in deionized, distilled water. Cx43-liposomes entrapping NBDp (or the mutant) in several different concentrations were prepared as mentioned above. The entrapped NBDp concentrations were controlled by the initial condition of the liposome formation solution.

2.6. Peptide transfer assay: measurement of NF-κB activity

For the NF-κB reporter gene assay, cells grown on 24-well plates were transiently transfected with NF-κB promoter-conjugated luciferase vector (pGL3-Basic; Vector, Promega, Madison, WI) and the pRL-TK vector (for the dual-luciferase reporter gene assay). After transfection, these cells were cultured in DMEM without FBS to abrogate the NF-κB activation caused by FBS itself for 24 h. The cells were then treated with 18β-glycyrrhetinic acid (GA, 10 µM, Sigma, St. Louis, MO) for 12 h. Then the peptide (NBDp, and the mutant) within or without Cx43-liposomes was treated for 12 h (in DMEM media containing 10% FBS). The liposome outside NBDp was diluted to 1/50 (v/v) when added to the DMEM media. Next, IL-1β (10 nM, Peprotech, Rocky Hill, NJ) was applied to each well for 24 h. Luciferase activity in cells was measured using the Dual-Luciferase Reporter Assay System (Promega, Madison, WI).

Author's personal copy

M. Kameda et al. / Biomaterials 30 (2009) 3971–3977

3973

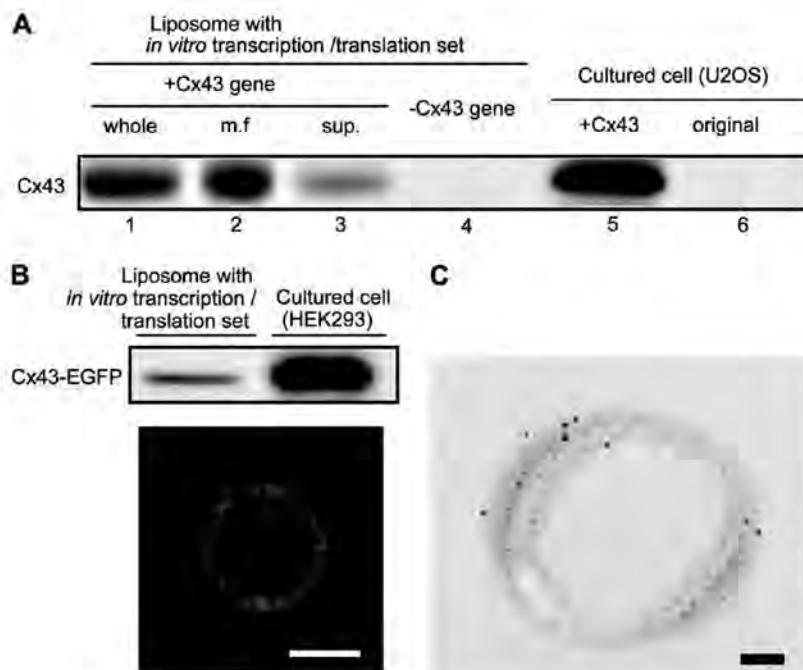


Fig. 1. Constructing Cx43-expressing liposomes. (A) Western blotting analysis of Cx43 protein expressed in liposomes. Reaction mixtures containing liposomes were separated by centrifugation at $100,000 \times g$ into membrane-rich fractions (m.f.) and supernatant (sup.). The lanes 1–3 represent the whole liposomal solutions, the membrane-rich fractions and supernatant, respectively. Lane 5: positive control obtained from the cells of Cx43 transfectant. (B) Cx43-conjugated-EGFP synthesized in the presence of the liposomes. The expression was confirmed by Western blotting analysis. Confocal microscopic image of giant liposomes prepared with Cx43-EGFP fusion protein expression. The giant liposome was selected for accurate imaging. Bar = 5 μm. (C) Immunoelectron microscopic images of the Cx43 liposomes. Cx43s were identified by immunogold labeling (black dots). Bar = 100 nm.

Comparisons were made with the Turkey test, and values of $p < 0.001$ were considered significant (Stat Mate III, ATMS, Tokyo, Japan).

2.7. Semi-quantitative RT-PCR analysis

Total RNA was prepared from the U2OS cells using TRIzol reagent (Invitrogen Co., Carlsbad, CA) according to the manufacturer's instructions. Total RNA (3–5 μg) was subjected to reverse-transcription using ReverTra Ace (Toyobo, Osaka, Japan) and an oligo(dT) primer. PCR primers for the cDNA amplification were designed as follows: for Cyclooxygenase-2 (COX-2), 5'-TTCAAATGAGATGTGGGAAATTGCT-3' (forward) and 5'-AGATCATCTCTGCTGAGTATCT-3' (reverse); and for glyceraldehyde-3-phosphate dehydrogenase (GAPDH), 5'-ACCACAGTCCATGCCATCAC-3' (forward) and 5'-TCCACCACCTGTGTGCTGA-3' (reverse). The PCR products were separated by electrophoresis on a 1% agarose gel containing ethidium bromide.

3. Results and discussion

3.1. Direct preparation of Cx43-containing liposomes by an in vitro transcription/translation system

To detect liposomal membrane localization of Cx43 proteins synthesized in vitro transcription/translation system, the membrane and water-soluble fractions of centrifuged Cx43 liposome were analyzed by western blotting (Supplemental fig. 1). Cx43 protein was detected predominantly (>80%) in the membrane fraction (Fig. 1A, lanes 1–3). We also expressed Cx43-enhanced green fluorescent protein (EGFP) fusion proteins in the presence of liposomes. Confocal fluorescent image analysis supports the expressed Cx43-EGFP fusion proteins being localized in the giant liposomal membranes (Fig. 1B). In addition, immunoelectron microscopy of Cx43 liposome supports the expressed Cx43 proteins being localized in the liposomal membranes (Fig. 1C). Several studies have prepared

connexin liposomes reconstituted by a detergent removal method from the cellular membrane. In pioneering work using in vitro expression of connexins [2,4], the translated connexins were incorporated into the microsomal membranes (canine pancreas rough microsomes). The method we have undertaken here provides

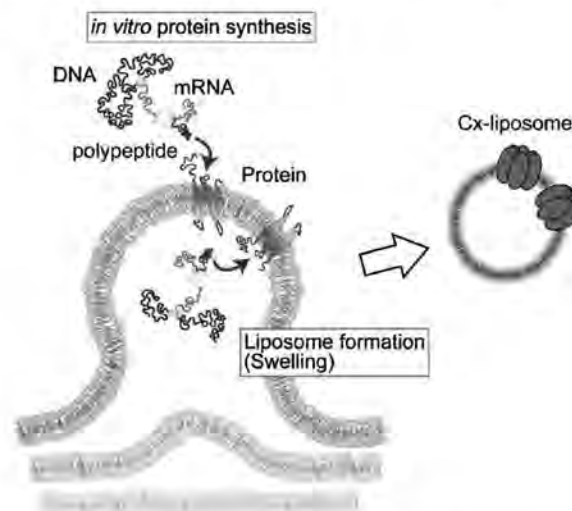


Fig. 2. Schematic illustration of constructing Cx43-expressing liposomes.

3974

M. Kaneda et al. / Biomaterials 30 (2009) 3971–3977

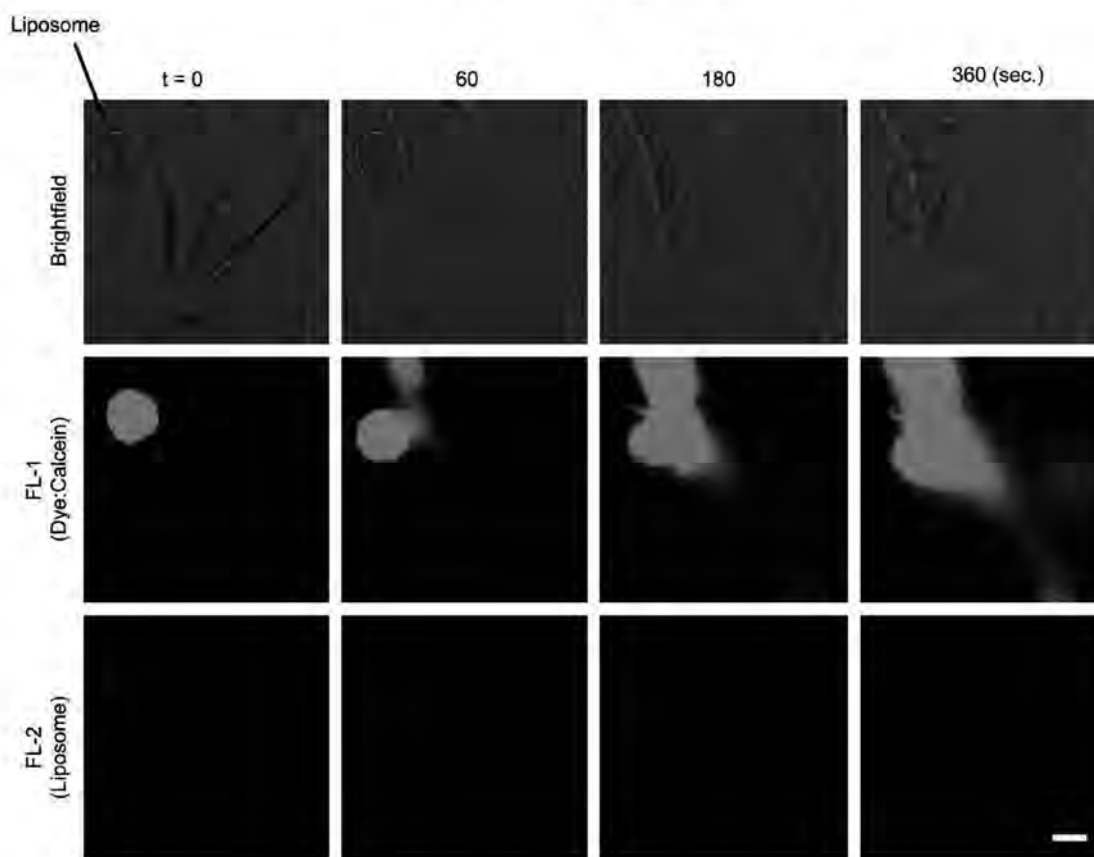


Fig. 3. Calcein dye transfer from Cx43-expressing liposomes to cells. Time-course images of Cx43 liposome attached to the Cx43-U2OS cells by confocal laser-scanning microscopy. The bottom images indicate liposomal membrane dye TexasRed-DHPE. Bar = 10 μ m.

a single-step direct constitution of Cx43 into artificial liposomes in place of microsomes. It is a presumable scenario that the continuous translation reaction ongoing nearby the membrane makes folded functional membrane protein [10–12].

During the liposome formation process by the 'swelling/hydration' method, gene-expression enzymes/substrates were stochastically trapped into the swelling lipid multilayer (Fig. 2). They located both inside and outside of the liposomes. We previously reported evidence of rsGFP protein synthesis inside a single cell-sized vesicle formed by the natural swelling of phospholipids, following encapsulation of the gene-expression system [6]. In this system, proteins are probably synthesized both inside and outside of the liposomes. Considering the volume of the liposomes, the proteins should locate predominantly on the liposome outer surface.

In cell systems, Cx43 is assembled into connexons (hexamers of Cx43) and form GJs between neighboring cells [13,14]. Images of connexin hexamers in the condensed states such as the two-dimensional crystal phase were observed by transmission electron microscopy (TEM) [16] or atomic force microscopy (AFM) [17,18]. In our system, however, it is difficult to directly observe the assembly of Cx43 in the liposomal membrane, even with immunoelectron microscopy. Connexon formation was investigated by a dye-leakage method with the connexin liposomes and/or by electrophysiological analysis with Cx43-reconstituted planar lipid membranes [2–4]. Here, we focused on the major role of connexins in forming the intercellular GJ channel.

3.2. Interaction between Cx43-containing liposomes and cells

The possibility of channel formation in Cx43 liposomes was investigated by dye-transfer assays with cultured cells (Cx43-expressing cells). The membrane-impermeable hydrophilic dye, calcein (molecular weight 623), was adopted. Calcein-loaded

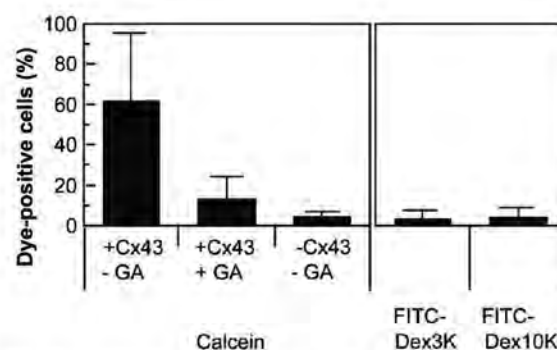


Fig. 4. Dye transferred into Cx43-U2OS cells. The number of the dye-transferred cell was counted from the confocal fluorescent images. 18 β -glycyrrhetic acid (GA) at 10 μ M was used as the GJ inhibitor. The molecular weights of Dex3 K and 10 K of FITC-Dextran are 3000 and 10,000 Da, respectively.

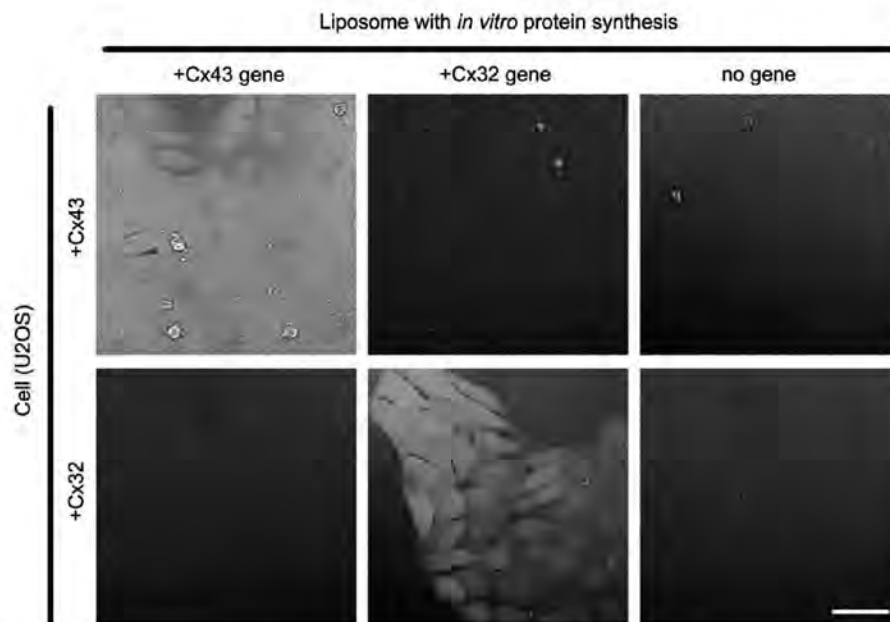


Fig. 5. Dye transfer through the homo/heterotypic connexins between liposomes and cells. A heterotypic pair between Cx43 and Cx32 was clearly non-functional compared with homotypic pairs (Cx43/Cx43 or Cx32/Cx32). The words “no gene” indicate that the added liposomes included a complete transcription/translation set without the plasmid coding connexin. The images were layered on their differential interference contrast images. In these observations, the liposomes were washed away. Bar = 50 μ m.

spherical giant liposomes were clearly identified on confocal microscopic analysis (Supplemental figure 2) even in the cell-culture medium (DMEM containing 10% FBS). The retention ratio of the dye in the Cx43-liposomes was not any lower than that in

liposomes without Cx43 (Supplemental figure 3). To directly visualize the dye-transfer, we investigated the interaction between a single giant Cx liposome and cells. Fig. 3 shows the time-lapsed images of the dye transfer from a calcein-loaded Cx43-liposome

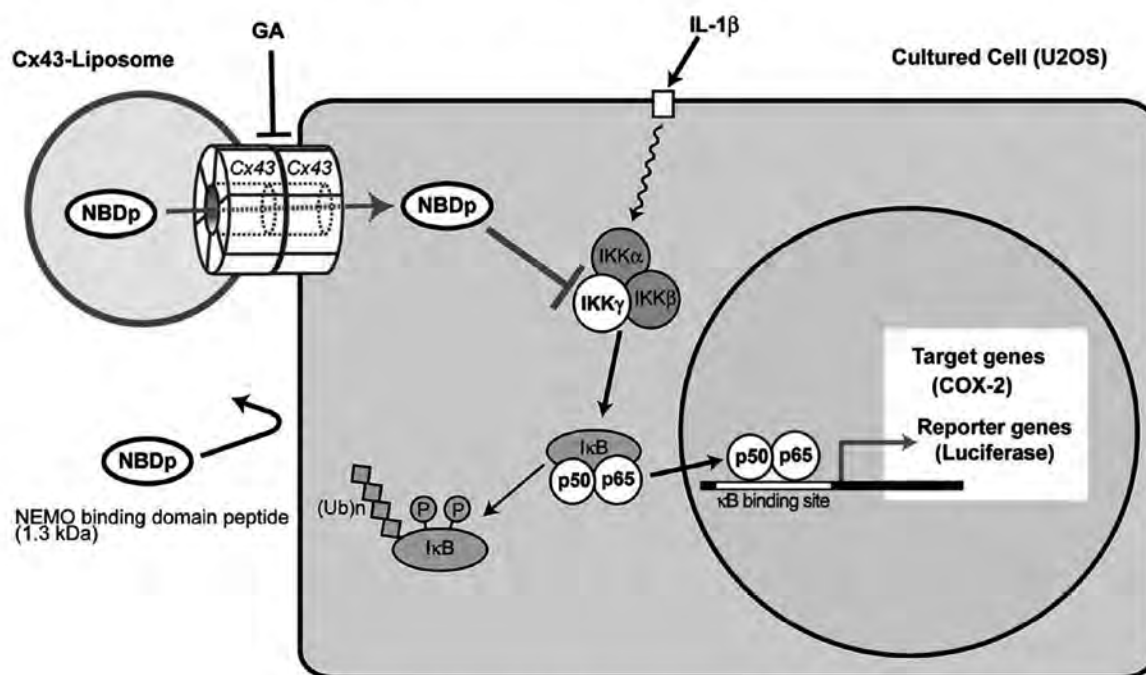


Fig. 6. Schematic illustration of bioactive peptide transfer experiment to cell by Cx43 liposomes.

Author's personal copy

3976

M. Kaneda et al. / Biomaterials 30 (2009) 3971–3977

(15 μ m) to Cx43-expressing U2OS cells. The giant liposome adsorbed on the liposome surface and then dyes were transferred into the cell for 6 min. During the transfer of dye, the giant Cx-containing liposome remained on the surface of cell.

The number of the dye-transferred cells was counted from the confocal fluorescent images. The calcein-positive cell number after Cx43 liposome treatment was 61.5 ± 33.6 (s.d.) % in 2 h (Fig. 4). In contrast, dye incorporated into control liposomes lacking Cx43 expression was not transferred into cultured Cx43-expressing cells (Fig. 4, $4.2 \pm 2.6\%$). The GJ inhibitor (18 β -glycyrrhetic acid (GA)) significantly inhibited the transfer of dye by reducing the positive cells to $13.0 \pm 10.7\%$. GA at the concentration of 10 μ M used here strongly inhibited GJ between Cx43-expressing U2OS (Supplemental figure 4). The confocal fluorescent image provides no observable indication of the fluorescence of Texas Red DHPE (as a marker of the liposomal membrane) inside the dye-transferred cells, regardless of the presence or absence of Cx43 plasmid expression. The transfer ratios of larger dyes, FITC-Dextran with a molecular mass of 3000 and 10,000 were $3.0 \pm 4.4\%$, $4.1 \pm 4.8\%$, respectively (Fig. 4). The results imply that calcein dye transfer occurred through channel between Cx43-liposomes and cells with a particular molecular mass cut-off. Thus, Cx43-expressed *in vitro* protein synthesis was directly constituted to liposomes in a functional form.

Cx43 is ubiquitously expressed in various organs in vertebrates. However, several connexins are expressed in specific organs, such as Cx32 in the liver (hepatocytes). It is believed that Cx43 and Cx32 do not pair to form functional GJs. Cx32-expressing liposomes were prepared by a similar method using cell-free transcription/translation systems with plasmids encoding Cx32 in the presence of liposomes (Supplemental figure 5). We investigated the dye transfer through the homotypic/heterotypic communication systems between liposomes and cells (Fig. 5). The transfer of calcein was only observed in the case of the Cx43 liposome and Cx43 presenting cell system or the Cx32-liposome and Cx32-presenting cell system. These results suggest that Cx liposomes can be used as a connexin-specific delivery system.

3.3. Transfer of bioactive peptide to cell by Cx43 liposomes

We examined next whether the Cx43 liposomes can be used to deliver a model drug into living cells (Fig. 6). We chose a synthetic oligo-peptide corresponding to the NBDp (NEMO-binding domain peptide) found on the C-terminus of both I κ B kinase (IKK)- α and - β . This peptide competitively inhibits the formation of the IKK complex and blocks interleukin (IL)-1 β -induced NF- κ B (p50/p65) activation. However, the NBD peptide (1.3 kDa) is so hydrophilic

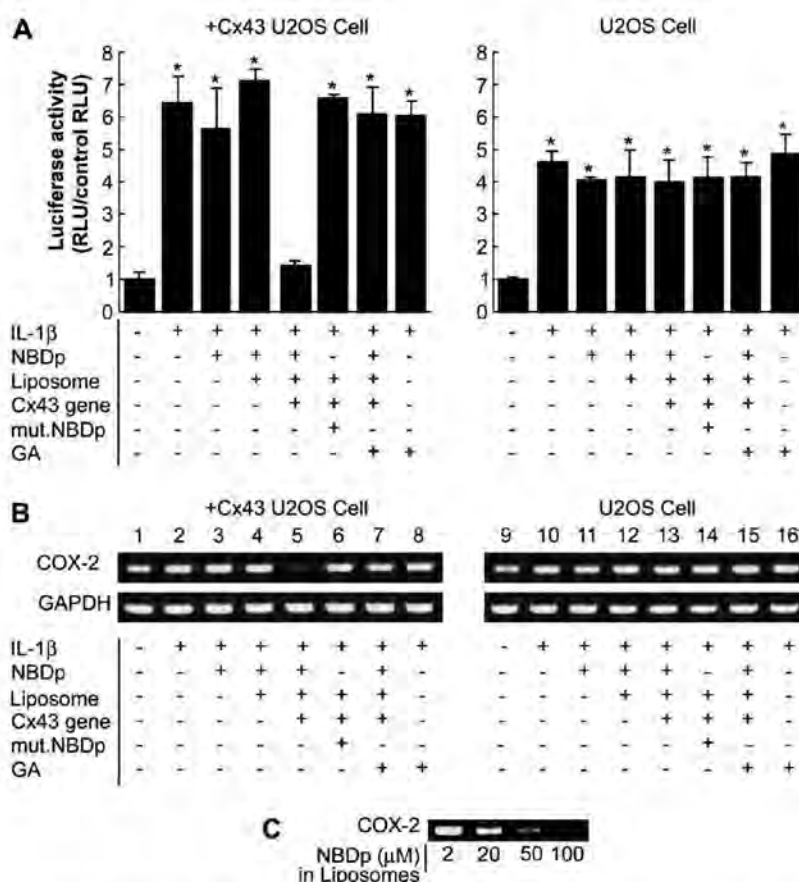


Fig. 7. Effects of Cx43 liposomes containing NBD peptide (NBDp) on cellular NF- κ B (p50/p65) activity. "Cx43 gene ±" means in the presence and absence of the plasmid (pCMV-TNT) coding Cx43. All samples added to the cell included the complete set of the transcription/translation reaction solution. (A) Measurement of NF- κ B activity by luciferase assay. Cx43-liposomes entrapping NBDp suppressed activation of NF- κ B by IL-1 β in Cx43-expressing cells, but not in parental cells. Values are shown as means \pm standard deviation. * $p < 0.001$. (B) COX-2 expression was measured by RT-PCR analysis. (C) Dose dependency of NBDp entrapped in Cx43 liposomes on COX-2 expression.

that it cannot enter cells without a membrane permeation sequence [19]. In this study, the peptide incorporated within Cx43 liposomes was applied to IL-1 β -stimulated Cx43-expressing U2OS cells and NF- κ B promoter activities were analyzed by luciferase assay (Fig. 7A). NBDp including Cx liposomes was prepared by similar method for calcein dye. In the presence of Cx43 liposomes, NBDp peptide decreased IL-1 β activation of NF- κ B in the Cx43-expressing U2OS cells. Neither a mutant of NBDp (1.1 kDa) in the Cx43-liposomes nor NBDp in liposomes lacking Cx43 affected NF- κ B activation. Furthermore, the GJ inhibitor, GA, blocked the reduction of NF- κ B activation by the NBDp-containing Cx43 liposomes. By contrast, parental U2OS cells not expressing Cx43 [15] were not affected by the administration of the NBDp-containing Cx43 liposomes. We further examined the effect of NBDp on the expression of cyclooxygenase (COX)-2, which is enhanced by IL-1 β [20]. NBDp-containing Cx43 liposomes significantly suppressed the upregulation of COX-2 by IL-1 β in Cx43-expressing cells (Fig. 7B, lanes 1, 2, and 5), and the addition of GA abolished this suppressive effect (Fig. 7B, lane 7). Application of NBDp without liposomes or by entrapment within liposomes lacking Cx43 did not suppress the enhancement of COX-2 expression by IL-1 β (Fig. 7B, lanes 3 and 4). Parental cells (lacking Cx43) also were unaffected by NBDp entrapped in Cx43 liposomes (Fig. 7B, lane 13). It was noted as well that the inhibition of COX-2 expression by NBDp was dose-dependent (Fig. 7C). Collectively, these results indicate that the NBD peptide acts on these cells by specifically entering through connexin-mediated pathway.

Problems for cytosolic delivery of hydrophilic drugs to cells and tissues still remain because the hydrophobic bilayer membrane barrier inhibits their reliable cell internalization, regardless of delivery mode. Using our Cx43-mediated procedure, it should be possible to noninvasively deliver even cell-impermeable drugs, such as the NBD peptide, that have no effect when applied alone. Moreover, by using specific interaction between connexin families, cell specific delivery system should be designed. However, the phenomenon was limited by the connexins' own properties such as upper transportation limit of ~ 2 kDa. Recently, direct antigen peptide transfer into the cytoplasm of adjacent cells through GJs, and resulting effective cytotoxic T cell responses were reported [21]. Interesting finding that RNAi goes through gap junction was reported [22]. These results have important implication for using our system as drug delivery system.

4. Conclusion

We demonstrate here a new example for obtaining proteo-liposomes by *in vitro* protein synthesis. Connexin-containing liposomes were directly prepared by using cell-free transcription/translation systems with plasmids encoding connexin. This method should create new opportunities for the formation and analysis of functional membrane proteins as useful biomaterials. The proteo-liposomes obtained were able to deliver a hydrophilic and bioactive oligo-peptide to cells through GJs mediated by Cx43-liposome–cell contacts to regulate cell functions. The functional connexin-bearing liposomes reported here should be useful as a tool for cell biology and for drug carrier research into cellular cytosolic delivery.

Acknowledgments

We thank Prof. D.W. Grainger and Prof. F.M. Winnik for critical reading of the manuscript. This research was supported by a grant from Center of Excellence for Frontier Research Program on Molecular Destruction and Reconstruction of Tooth and Bone at Tokyo Medical and Dental University. This work was also supported by Grant-in-Aid for Scientific Research and by JSPS (18GS0421,

19684015, 20034016, 20390463, 20390470, 20659306) from the Japanese Government. Pacific Edit reviewed the manuscript prior to submission.

Appendix

Figures with essential colour discrimination. Certain parts of Fig. 4 in this article may be difficult to interpret in black and white. The full colour images can be found in the on-line version, at doi: 10.1016/j.biomaterials.2009.04.006.

Appendix. Supplementary material

Supplementary material associated with this article can be found in the online version, at doi:10.1016/j.biomaterials.2009.04.006.

References

- [1] Rigaud JL, Pitard B, Levy D. Reconstitution of membrane proteins into liposomes: application to energy-transducing membrane proteins. *Biochim Biophys Acta* 1995;1231(3):223–46.
- [2] Ahmad S, Evans WH. Post-translational integration and oligomerization of connexin 26 in plasma membranes and evidence of formation of membrane pores: implications for the assembly of gap junctions. *Biochem J* 2002;365(Pt 3):693–9.
- [3] Kim DY, Kam Y, Koo SK, Joe CO. Gating connexin 43 channels reconstituted in lipid vesicles by mitogen-activated protein kinase phosphorylation. *J Biol Chem* 1999;274(9):5581–7.
- [4] Falk MM. Cell-free synthesis for analyzing the membrane integration, oligomerization, and assembly characteristics of gap junction connexins. *Methods* 2000;20(2):165–79.
- [5] Seddon AM, Curnow P, Booth PJ. Membrane proteins, lipids and detergents: not just a soap opera. *Biochim Biophys Acta* 2004;1666(1–2):105–17.
- [6] Nomura SM, Tsumoto K, Hamada T, Akiyoshi K, Nakatani Y, Yoshikawa K. Gene expression within cell-sized lipid vesicles. *ChemBiochem* 2003;4(11):1172–5.
- [7] Yu W, Sato K, Wakabayashi M, Nakaishi T, Ko-Mitamura EP, Shima Y, et al. Synthesis of functional protein in liposome. *J Biosci Bioeng* 2001;92(6):590–3.
- [8] Kita H, Matsuura T, Sunami T, Hosoda K, Ichihashi N, Tsukada K, et al. Replication of genetic information with self-encoded replicase in liposomes. *ChemBiochem* 2008;9(15):2403–10.
- [9] Noireaux V, Libchaber A. A vesicle bioreactor as a step toward an artificial cell assembly. *Proc Natl Acad Sci U S A* 2004;101(51):17669–74.
- [10] Nomura SM, Konishi S, Asayama W, Asada A, Nishikawa S, Akiyoshi K. Direct preparation of giant proteo-liposomes by *in vitro* membrane protein synthesis. *J Biotechnol* 2008;133(2):190–5.
- [11] Rohelek R, Lemker ES, Wiltisch B, Kirste V, Naumann R, Oesterheld D, et al. Incorporation of *in vitro* synthesized GPCR into a tethered artificial lipid membrane system. *Angew Chem Int Ed Engl* 2007;46(4):605–8.
- [12] Kalmbach R, Chizhov I, Schumacher MC, Friedrich T, Bamberg E, Engelhard M. Functional cell-free synthesis of a seven helix membrane protein: *in situ* insertion of Bacteriorhodopsin into liposomes. *J Mol Biol* 2007;371:639–48.
- [13] Bruzzone R, White TW, Paul DL. Connections with connexins: the molecular basis of direct intercellular signaling. *Eur J Biochem* 1996;238(1):1–27.
- [14] Kumar NM, Gilula NB. The gap junction communication channel. *Cell* 1996;84(3):381–8.
- [15] Zhang YW, Morita I, Ikeda M, Ma KW, Murota S. Connexin43 suppresses proliferation of osteosarcoma U2OS cells through post-transcriptional regulation of p27. *Oncogene* 2001;20(31):4138–49.
- [16] Stauffer KA, Kumar NM, Gilula NB, Unwin N. Isolation and purification of gap junctions. *J Cell Biol* 1991;115(1):141–50.
- [17] Müller DJ, Hand GM, Engel A, Sosinsky GE. Conformational changes in surface structures of isolated connexin 26 gap junctions. *EMBO J* 2002;21(14):3598–607.
- [18] Yu J, Bippes CA, Hand GM, Müller DJ, Sosinsky GE. Aminosulfonate modulated pH-induced conformational changes in connexin26 hemichannels. *J Biol Chem* 2007;282(12):8895–904.
- [19] May MJ, D'Acquisto F, Madge LA, Glöckner J, Pober JS, Ghosh S. Selective inhibition of NF- κ B activation by a peptide that blocks the interaction of NEMO with the I κ B kinase complex. *Science* 2000;289(5484):1550–4.
- [20] Jung YJ, Isaacs JS, Lee S, Trepel J, Neckers L. IL-1 β -mediated up-regulation of HIF-1 α via an NF- κ B/COX-2 pathway identifies HIF-1 as a critical link between inflammation and oncogenesis. *FASEB J* 2003;17(14):2115–7.
- [21] Neijssen J, Herberichs C, Drijfhout JW, Reits E, Janssen L, Neeffjes J. Cross-presentation by intercellular peptide transfer through gap junctions. *Nature* 2005;434(7029):83–8.
- [22] Valiunas V, Polosina YY, Müller H, Potapova IA, Valiuniene L, Doronin S, et al. Connexin-specific cell-to-cell transfer of short interfering RNA by gap junctions. *J Physiol* 2005;568(Pt 2):459–68.

Communications

Protein Imaging

DOI: 10.1002/anie.200903183

Fluorogenically Active Leucine Zipper Peptides as Tag–Probe Pairs for Protein Imaging in Living Cells**

Hiroshi Tsutsumi, Wataru Nomura, Seiichiro Abe, Tomoaki Mino, Akemi Masuda, Nami Ohashi, Tomohiro Tanaka, Kenji Ohba, Naoki Yamamoto, Kazunari Akiyoshi, and Hirokazu Tamamura*

Artificial functional peptides are valuable tools in various fields of chemical biology. Small peptides, such as an oligohistidine tag (His tag), can be genetically incorporated into target proteins and used for purification of recombinant proteins, immobilization of proteins on microplates, and bioimaging of proteins on the surface of living cells with their complementary partner molecules, such as Ni^{II} –nitrilotriacetic acid complex (Ni^{II} –NTA).^[1] Tsien and co-workers reported that pairs of tetracysteine motif peptides and biarsenical molecular probes, which specifically bind to tetracysteine peptides, are useful in the real-time fluorescence imaging of proteins in living cells.^[2] Several pairs of other tag peptides/proteins and their specific ligands have also been reported.^[3–4] In many cases, however, the bound/free (B/F) separation process of probes is necessary to avoid background emission from excess probe molecules. Fluorogenic tag–probe pairs can facilitate in distinguishing the labeled proteins from the free probes, without the B/F separation process. However, very few tag–probe pairs have been developed to date.^[5a]

Engineered leucine zipper peptides, which have complementary selectivity and strong binding affinity, have been applied to tags for the affinity purification of expressed proteins, to anchors for immobilization of proteins on microplates, and to allosteric modulators of engineered enzyme activity.^[5] Moreover, the hydrophobic cores of leucine zipper peptides can be engineered to form hydrophobic pockets in which small organic molecules can bind.^[6] It is thought that

selective binding of environmentally sensitive fluorescent dyes to these pockets inside the leucine zipper assembly might induce colorimetric changes and enhance their fluorescence intensity. The unique characteristics of leucine zipper peptides might enable production of fluorescent tag–probe pairs that are exchangeable. Herein, we describe the development of a fluorescent changeable tag–probe system based on artificial leucine zipper peptides, designated ZIP tag–probe pairs, and its application to the fluorescence imaging of ZIP tag–fused protein on the surface of living cells.

The design of ZIP tag–probe pairs is based on the crystal structure of an antiparallel coiled-coil trimer of a GCN4 mutant (Figure 1).^[7] The probe peptide is an α -helical peptide with 4-nitrobenzo-2-oxa-1,3-diazole (NBD), an environmentally sensitive fluorescent dye, attached to the side chain of L- α -2,3-diaminopropionic acid, that is, Dap(NBD). Tag peptides are designed as antiparallel 2 α -helical peptides linked through a Gly–Gly–Cys–Gly–Gly loop sequence. Two leucine residues, which are located at the positions complementary to the NBD in the probe peptide, are replaced by alanine or glycine so that hydrophobic pockets will be formed when the tag peptides bind to the probe peptide. Original tag peptides having two leucine residues at the complementary positions are designated as L2, and alanine- or glycine-substituted tag peptides are designated as A2 and G2, respectively.

In the UV/Vis analysis, the absorption spectra of the probe peptide changed on addition of A2 producing isosbestic points at 456, 403, and 333 nm, and thus the excitation wavelength was determined as 456 nm (Figure S1 in the Supporting Information). A fluorescence titration experiment revealed that the fluorescence spectra of the probe peptide changed remarkably with increasing A2 concentration. The emission maximum arising from the NBD dye showed a significant blue shift from 536 to 505 nm with a concurrent increase in the emission intensity (Figure 2a,b and Table 1). Such a spectral change clearly suggests that the NBD moiety of the probe peptide is located in the hydrophobic environment within the 3 α -helical peptide bundle structure, which is supported by the previous report of Uchiyama et al.^[8]

In the cases of L2 and G2, similar spectral changes were observed although the wavelength shifts and changes in fluorescence intensity were less than those in the case of A2 (Figure S2 in the Supporting Information and Table 1). As there is insufficient space to accommodate an NBD moiety in the complex of the L2–probe pair, the NBD moiety might bind only to the hydrophobic surface of two leucine residues of L2, thus causing the subtle fluorescence change. The

[*] S. Abe, T. Mino, A. Masuda, Prof. K. Akiyoshi, Prof. H. Tamamura
Institute of Biomaterials and Bioengineering
Tokyo Medical and Dental University
Chiyoda-ku, Tokyo 101-0062 (Japan)

and

School of Biomedical Science, Tokyo Medical and Dental University
Chiyoda-ku, Tokyo 101-0062 (Japan)
Fax: (+81) 3-5280-8036

E-mail: tamamura.mr@tmd.ac.jp

Dr. H. Tsutsumi, Dr. W. Nomura, N. Ohashi, T. Tanaka
Institute of Biomaterials and Bioengineering
Tokyo Medical and Dental University
Chiyoda-ku, Tokyo 101-0062 (Japan)

Dr. K. Ohba, Prof. N. Yamamoto
AIDS Research Center, National Institute of Infectious Diseases
Shinjuku-ku, Tokyo 162-8640 (Japan)

[**] This work was supported in part by a grant from the Naito Foundation.

Supporting information for this article is available on the WWW under <http://dx.doi.org/10.1002/anie.200903183>.

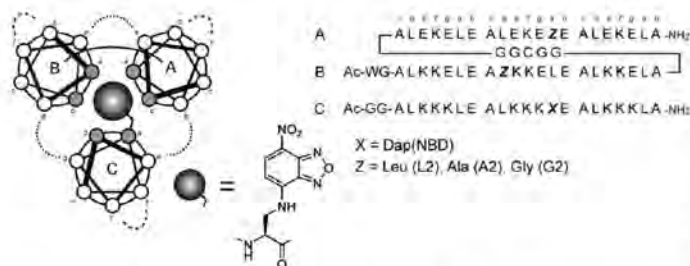


Figure 1. Structure and amino acid sequences of ZIP tag-probe pairs.

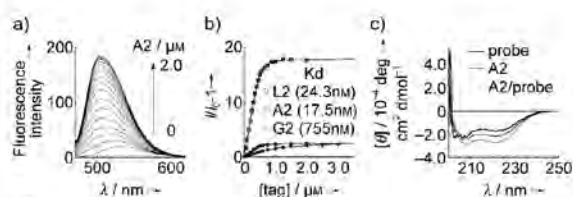


Figure 2. a) Fluorescence spectral change of the probe peptide upon addition of A2 at 25 °C in 50 mM 2-[4-(2-hydroxyethyl)piperazin-1-yl]ethanesulfonic acid (HEPES) buffer (pH 7.2, 100 mM NaCl): [probe] = 0.5 μM. b) Fluorescence titration curves of the probe peptide with L2, A2, and G2 at 516, 505, and 526 nm, respectively. I and I_0 represent the fluorescence intensity at various concentrations of tag peptides and the initial fluorescence intensity, respectively. c) Circular dichroism spectra of the A2 tag (solid line), the probe peptide (bold line), and their complex (dashed line) at 25 °C in 50 mM Tris-HCl buffer (pH 7.2, 100 mM NaCl).

Table 1: Emission maxima [nm] and $\Delta I_{\text{max}}/I_0$ values (in parentheses) of the probe peptide and tag-probe complexes, dissociation constants (K_d) [nM] between the tag and probe peptides, and the α -helix contents [%] of the probe, the tag peptides, and their complexes (in parentheses).

	Probe	L2	A2	G2
λ_{max} ($\Delta I_{\text{max}}/I_0$)	536 (–)	516 (2.7)	505 (17.9)	526 (2.5)
K_d [nM]	–	24.3	17.5	755
α -helix content [%]	53	81 (78)	58 (71)	18 (41)

[a] Measurement conditions: 50 mM HEPES buffer solution (pH 7.2, 100 mM NaCl) at 25 °C, [probe] = 0.5 μM. [b] Measurement conditions: 50 mM Tris-HCl buffer solution (pH 7.2, 100 mM NaCl) at 25 °C; [tag], [probe], [tag-probe] = 1.0 μM. The α -helix contents were determined according to a standard method.^[10]

wavelength shift and change in fluorescence intensity of the G2-probe pair were also small, which implies that the NBD moiety of the G2-probe peptide complex is located in a more hydrophilic area than those of the A2-probe peptide complex.

The dissociation constants of the probe peptide toward L2, A2, and G2 were estimated from the fluorescence titration curves by analysis with a nonlinear least-squares curve-fitting method^[9] (Table 1). L2 and A2 showed high affinity, comparable to that of a normal antigen-antibody interaction, for the probe peptide. In general, the hydrophobicity of leucine zipper peptides is essential for their self-assembly and L2, for example, is more hydrophobic than A2

because it has two leucine residues. However, the binding affinity of the A2-probe pair is slightly superior to that of the L2-probe peptide pair, indicative not only of the hydrophobic interaction but also of the steric complementarity between A2 and the probe peptide, which is critical for the strong binding affinity. The binding affinity of G2 for the probe peptide is much lower than that of L2 or A2. Since a glycine residue generally destabilizes an α -helical structure, the structure of the G2-probe pair might be less stable than those of the L2- and A2-probe peptide pairs.

Circular dichroism (CD) spectra revealed that L2 and A2 tags, the probe peptide, and their complexes form α -helical structures (Figure 2c and Figure S3 in the Supporting Information). The probe peptide showed a CD spectral pattern typical of α -helical structures with negative maxima at 208 and 222 nm. L2, A2, and their complexes with the probe peptide also showed CD spectral patterns typical of α -helical structures. The α -helical content of A2 is lower than that of L2, which indicates that A2 forms a less stable α -helical structure than L2. However, the α -helix content of the A2-probe complex is higher than those of A2 or the probe peptides alone, which suggests that the A2-probe pair forms a stable 3 α -helical bundle structure. Furthermore, the enhanced α -helical structure of the A2-probe complex is nearly equal to that in the L2-probe complex, which indicates that A2 can form a stable 3 α -helical leucine zipper structure with the probe peptide. The CD spectrum of G2, however, shows a random-coil pattern and the α -helix content of the G2-probe complex is only 41 %. These results imply that the mutation of the leucine or alanine residues to glycine causes the destabilization of the structure of G2 and of the G2-probe complex, and it is thought that this is the reason why the G2-probe pair has a lower binding affinity than the A2-probe pair.

The fluorescence titration experiment and the CD spectra suggest that formation of a stable α -helical structure with a hydrophobic pocket is necessary for high binding affinity and fluorogenic activity. A2 forms a stable α -helical structure with a pocket that can accommodate NBD and it is thought, therefore, that the combination of the A2 tag and the probe leads to expression of the remarkable fluorescence activity. In addition, the A2-probe pair showed the same fluorescence spectral change in the cell lysate solution (Figure S7 in the Supporting Information), thus indicating that A2 is the most appropriate partner of the probe peptide as a fluorogenic tag-probe pair for protein imaging in vivo.

Next, we investigated whether our ZIP tag-probe system is available for the fluorescence imaging of proteins in living cells. CXCR4 was chosen as a model protein. CXCR4 is one of the 7-transmembrane G-protein coupled receptors, a member of a chemokine receptor family.^[11] The A2 tag is genetically fused at the N terminus of CXCR4, which is an extracellular region, through the (Gly-Ser)₆ linker sequence. The A2-tag-fused CXCR4 is transiently expressed on the surface of Chinese hamster ovary K1 (CHO-K1) cells, and double labeling experiments of the A2-tag-fused CXCR4 using a fluorescent CXCR4 antagonist with tetramethylrhod-

Communications

amine (TAMRA)^[12] and the probe peptide with the NBD dye were performed. The A2-tag-fused CXCR4 was specifically stained with red fluorescence by TAMRA-appended CXCR4 antagonist (Figure S8a in the Supporting Information). Then, the sequential labeling of the A2-tag-fused CXCR4 was performed using the probe peptide. Before removal of the probe peptide, a bright green fluorescence was observed on the surface of cells in the presence of excess probe peptide, but the fluorescence resulting from this peptide was not observed in CHO-K1 cells without expression of the A2-tag-fused CXCR4 (Figure 3b). Fluorescence arising from the TAMRA-appended CXCR4 antagonist was also observed (Figure 3a), which suggests that the binding events between the A2 tag and the probe peptide, and between CXCR4 and the TAMRA-appended CXCR4 antagonist, are independent of each other. The fluorescence image derived from the probe peptide was merged well with the fluorescence image of the TAMRA-appended CXCR4 antagonist (Figure 3c,d). After removal of the probe peptide by the exchange of culture medium, similar fluorescence images were also observed (Figure S9 in the Supporting Information). These results suggest that CXCR4 can be successfully visualized using our ZIP tag–probe system without removal of excess probe molecules. This ZIP tag–probe system is consequently a useful fluorescence-imaging tool for proteins in living cells.

In conclusion, we have developed a new functional peptide pair with fluorogenic activity based on leucine zipper peptides. The alanine-substituted tag peptide A2 binds strongly to a probe peptide, and this binding is accompanied by a dramatic fluorescent colorimetric change from weak yellow to bright green. In addition, we have demonstrated that the fluorescence imaging of A2-tag-fused CXCR4, which is a membrane-bound protein, is successfully achieved by the probe peptide. Recently, Yano et al. reported that two α -helical leucine zipper tag–probe pairs are useful fluorescence imaging tools for membrane-bound proteins.^[13]

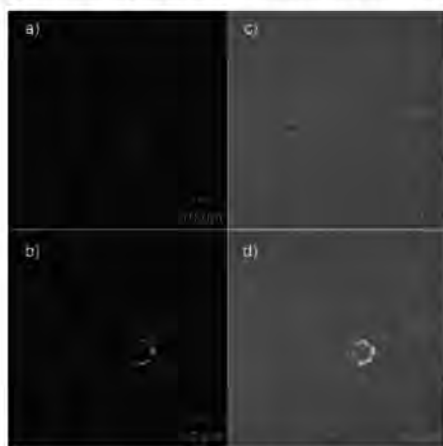


Figure 3. Sequential labeling of A2-tag-fused CXCR4 by the probe peptide after labeling by TAMRA-appended CXCR4 antagonist. a) Fluorescence image derived from TAMRA (excitation: 543 nm, emission filter: >560 nm). b) Fluorescence image derived from NBD (excitation: 458 nm, emission filter: 505–530 nm). c) Differential interference contrast. d) Merged image of (a)–(c).

Our ZIP tag–probe pairs have, in addition, fluorogenic activity which might facilitate the real-time imaging of proteins without the necessity to remove excess probe molecules. Thus, ZIP tag–probe pairs would become valuable imaging tools for target proteins in living cells.

Received: June 12, 2009

Revised: September 24, 2009

Published online: October 28, 2009

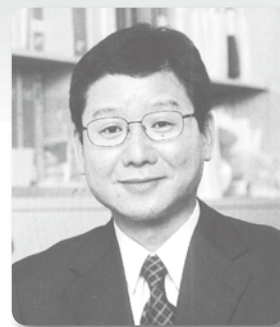
Keywords: fluorescent probes · imaging · living cells · peptides · proteins

- [1] a) K. Terpe, *Appl. Microbiol. Biotechnol.* **2003**, *60*, 523–533; b) M. Hedhammar, T. Gräslund, S. Hober, *Chem. Eng. Technol.* **2005**, *28*, 1315–1325; c) E. G. Guignet, R. Hovius, H. Vogel, *Nat. Biotechnol.* **2004**, *22*, 440–444; d) C. R. Goldsmith, J. Jaworski, M. Sheng, S. J. Lippard, *J. Am. Chem. Soc.* **2006**, *128*, 418–419; e) C. T. Hauser, R. Y. Tsien, *Proc. Natl. Acad. Sci. USA* **2007**, *104*, 3693–3697.
- [2] a) B. A. Griffin, S. R. Adams, R. Y. Tsien, *Science* **1998**, *281*, 269–272; b) G. Gaietta, T. J. Deerinck, S. R. Adams, J. Bouwer, O. Tour, D. W. Laird, G. E. Sosinsky, R. Y. Tsien, M. H. Ellisman, *Science* **2002**, *296*, 503–507.
- [3] a) K. M. Marks, M. Rosinov, G. P. Nolan, *Chem. Biol.* **2004**, *11*, 347–356; b) A. Ojida, K. Honda, D. Shinmi, S. Kiyonaka, Y. Mori, I. Hamachi, *J. Am. Chem. Soc.* **2006**, *128*, 10452–10459; c) I. Chen, Y.-A. Choi, A. Y. Ting, *J. Am. Chem. Soc.* **2007**, *129*, 6619–6625; d) H. M. O'Hare, K. Johnsson, A. Gautier, *Curr. Opin. Struct. Biol.* **2007**, *17*, 488–494.
- [4] a) A. Keppler, S. Gendreizig, T. Gronemeyer, H. Pick, K. Johnsson, *Nat. Biotechnol.* **2003**, *21*, 86–89; b) A. Gautier, A. Juillerat, C. Heinis, I. R. Corra, Jr., M. Kindermann, F. Beaufils, K. Johnsson, *Chem. Biol.* **2008**, *15*, 128–136; c) J. Yin, F. Liu, X. Li, C. T. Walsh, *J. Am. Chem. Soc.* **2004**, *126*, 7754–7755; d) G. V. Los, A. Darzins, N. Karassina, C. Zimprich, R. Learish, M. G. McDougall, L. P. Encell, R. Friedman-O'hana, M. Wood, G. Vidurgiris et al., *Promega Cell Notes* **2005**, *11*, 2–6.
- [5] a) B. Tripet, L. Yu, D. L. Bautista, W. Y. Wong, R. T. Irvin, R. S. Hodges, *Protein Eng.* **1996**, *9*, 1029–1042; b) K. Zhang, M. R. Diehl, D. A. Tirrell, *J. Am. Chem. Soc.* **2005**, *127*, 10136–10137; c) S. Yuzawa, T. Mizuno, T. Tanaka, *Chem. Eur. J.* **2006**, *12*, 7345–7352.
- [6] a) I. Obataya, S. Sakamoto, A. Ueno, H. Mihara, *Biopolymers* **2001**, *59*, 65–71; b) M. K. Yadav, J. E. Redman, L. J. Leman, J. M. Alvarez-Gutiérrez, Y. Zhang, C. D. Stout, M. R. Ghadiri, *Biochemistry* **2005**, *44*, 9723–9732.
- [7] B. Lovejoy, S. Choe, D. Cascio, D. K. McRorie, W. F. DeGrado, D. Eisenberg, *Science* **1993**, *259*, 1288–1293.
- [8] S. Uchiyama, T. Santa, K. Imai, *J. Chem. Soc. Perkin Trans. 2* **1999**, 2525–2532.
- [9] T. Kuwabara, A. Nakamura, A. Ueno, F. Toda, *J. Phys. Chem.* **1994**, *98*, 6297–6303.
- [10] a) Y.-H. Chen, J. T. Yang, K. H. Chau, *Biochemistry* **1974**, *13*, 3350–3359; b) P. J. Gans, P. C. Lyu, M. C. Manning, R. W. Woody, N. R. Kallenbach, *Biopolymers* **1991**, *31*, 1605–1614; c) D. Y. Jackson, D. S. King, J. Chmielewski, S. Singh, P. G. Schultz, *J. Am. Chem. Soc.* **1991**, *113*, 9391–9392.
- [11] a) S. G. Ward, J. Westwick, *Biochem. J.* **1998**, *333*, 457–470; b) H. Tamamura, H. Tsutsumi, W. Nomura, T. Tanaka, N. Fujii, *Expert Opin. Drug Discovery* **2008**, *3*, 1155–1166.
- [12] W. Nomura, Y. Tanabe, H. Tsutsumi, T. Tanaka, K. Ohba, N. Yamamoto, H. Tamamura, *Bioconjugate Chem.* **2008**, *19*, 1917–1920.
- [13] Y. Yano, A. Yano, S. Oishi, Y. Sugimoto, G. Tsujimoto, N. Fujii, K. Matsuzaki, *ACS Chem. Biol.* **2008**, *3*, 341–345.

分子細胞遺伝学分野

稲澤 譲治

難治疾患研究所・遺伝疾患研究部門
分子細胞遺伝学・教授



1) 研究の課題名

1. Identified novel genes responsible for cancer and unknown genetic diseases.
2. Development of high-density and high-resolution in-house CGH arrays and established their applications for detection of cryptic genomic and/or epigenetic aberrations in cancer and genomic disorders
3. Establishment of practically useful tools for diagnosis in personalized medicine of cancer and genome disorders.
1. がんと本態不明の遺伝疾患の病態に関連する遺伝子の同定と機能の解析
2. 高精度高密度ゲノムアレイならびにその応用技術の開発と、これらツールを駆使した癌と遺伝疾患のゲノム・エピゲノム解析の推進
3. がんとゲノム異常疾患の個別化医療に資する実用化レベルの診断法の開発

2)

先天異常疾患の診断用アレイを開発、2009年10月より
実用化供給と受託検査が開始される



東京医科歯科大学・難治研で開発した
先天異常疾患診断用SACアレイ
Genome Disorder (GD)-Array



アレイCGHを診断法として活用するた
めの解説書(平成20年3月)

3) 研究内容の英文要約

1. Gene-expression phenotypes for vascular invasiveness of hepatocellular carcinomas.

BACKGROUND: Gross vascular invasion is a well-established prognostic indicator in hepatocellular carcinoma (HCC), but the biological significance of microscopic invasion remains unclear. METHODS: Curatively resected primary HCCs were classified retrospectively into three groups: HCCs without vascular invasion (V0), HCCs with microvascular invasion (V1), and HCCs with macrovascular invasion (V2). Microarray profiling of patients with V0, V1, and V2 using Jonckheere-Terpstra (JT) tests and Wilcoxon rank sum tests was performed. RESULTS: Distinct patterns of gene expression were demonstrated between V0 and V2 groups; less (L) and highly (H) invasive phenotypes, respectively. It is noteworthy that 2 dendrograms by the hierarchical clustering provided exactly the same assignment results for V1 cases that were thus separated into L and H gene-expression phenotypes. Marked differences were found in overall ($P < .001$) and tumor-free survival ($P < .001$) between L and H gene-expression phenotypes. Multivariate analyses indicated that the phenotypes of the patterns of gene expression, rather than the clinicopathologic markers of vascular invasion, were independent predictors of tumor recurrence ($P = .031$). Using the gene-expression patterns identified by both JT and Wilcoxon rank sum test analyses, other V1 cases validated these differences in tumor-free survivals between gene-expression phenotypes within the group ($P = .039$). CONCLUSION: Gene profiling suggested that microvascular invasiveness consisted of a classable mixture of 2 distinct phenotypes. Thus, gene-array analyses may have clinical benefit, because they may in fact be more predictive than other clinical factors.

2. miR-124 and miR-203 are epigenetically silenced tumor-suppressive microRNAs in hepatocellular carcinoma.

MicroRNAs (miRNAs) are a class of small non-coding RNAs that, in general, negatively regulate gene expression.

They have been identified in various tumor types, showing that different sets of miRNAs are usually deregulated in different cancers. Some miRNA genes harboring CpG-islands undergo methylation-mediated silencing, a characteristic of many tumor-suppressor genes. To identify such miRNAs in hepatocellular carcinoma (HCC), we first examined the methylation status of 43 loci containing CpG-islands around 39 mature miRNA genes in a panel of HCC cell lines and non-cancerous liver tissues as controls. Among 11 miRNA genes frequently methylated in HCC cell lines but not in non-cancerous liver tissues, 3 miRNA genes, i.e. miR-124, miR-203, and miR-375, were selected as silenced miRNAs through CpG-island methylation by comparing methylation and expression status and evaluating restored expression after treatment with 5-aza-2'-deoxycytidine. In primary tumors of HCC with paired non-tumorous liver tissues, only miR-124 and miR-203 showed frequent tumor-specific methylation, and their expression status was inversely correlated with methylation status. Ectopic expression of miR-124 or miR-203 in HCC cells lacking their expression inhibited cell growth, with direct down-regulation of possible targets, cyclin-dependent kinase 6 (CDK6), vimentin (VIM), SET and MYND domain containing 3 (SMYD3), and IQ motif containing GTPase activating protein 1 (IQGAP1) or ATP-binding cassette, sub-family E, member 1 (ABCE1), respectively. Our results suggest that miR-124 and miR-203 are novel tumor-suppressive miRNAs for HCC epigenetically silenced and activating multiple targets during hepatocarcinogenesis.

3. Lysosomal-associated protein multispinning transmembrane 5 gene (LAPTM5) is associated with spontaneous regression of neuroblastomas.

BACKGROUND: Neuroblastoma (NB) is the most frequently occurring solid tumor in children, and shows heterogeneous clinical behavior. Favorable tumors, which are usually detected by mass screening based on increased levels of catecholamines in urine, regress spontaneously via programmed cell death (PCD) or mature through differentiation into benign ganglioneuroma (GN). In contrast, advanced-type NB tumors often grow aggressively, despite intensive chemotherapy. Understanding the molecular mechanisms of PCD during spontaneous regression in favorable NB tumors, as well as identifying genes with a pro-death role, is a matter of urgency for developing novel approaches to the treatment of advanced-type NB tumors. **PRINCIPAL FINDINGS:** We found that the expression of lysosomal associated protein multispinning transmembrane 5 (LAPTM5) was usually down-regulated due to DNA methylation in an NB cell-specific manner, but up-regulated in degenerating NB cells within locally regressing areas of favorable tumors detected by mass-screening. Experiments in vitro showed

that not only a restoration of its expression but also the accumulation of LAPTM5 protein, was required to induce non-apoptotic cell death with autophagic vacuoles and lysosomal destabilization with lysosomal-membrane permeabilization (LMP) in a caspase-independent manner. While autophagy is a membrane-trafficking pathway to degrade the proteins in lysosomes, the LAPTM5-mediated lysosomal destabilization with LMP leads to an interruption of autophagic flux, resulting in the accumulation of immature autophagic vacuoles, p62/SQSTM1, and ubiquitinated proteins as substrates of autophagic degradation. In addition, ubiquitin-positive inclusion bodies appeared in degenerating NB cells. **CONCLUSIONS:** We propose a novel molecular mechanism for PCD with the accumulation of autophagic vacuoles due to LAPTM5-mediated lysosomal destabilization. LAPTM5-induced cell death is lysosomal cell death with impaired autophagy, not cell death by autophagy, so-called autophagic cell death. Thus LAPTM5-mediated PCD is closely associated with the spontaneous regression of NBs and opens new avenues for exploring innovative clinical interventions for this tumor.

4. Genome-wide DNA methylation profiles in urothelial carcinomas and urothelia at the precancerous stage.

To clarify genome-wide DNA methylation profiles during multistage urothelial carcinogenesis, bacterial artificial chromosome (BAC) array-based methylated CpG island amplification (BAMCA) was performed in 18 normal urothelia obtained from patients without urothelial carcinomas (UCs) (C), 17 noncancerous urothelia obtained from patients with UCs (N), and 40 UCs. DNA hypo- and hypermethylation on multiple BAC clones was observed even in N compared to C. Principal component analysis revealed progressive DNA methylation alterations from C to N, and to UCs. DNA methylation profiles in N obtained from patients with invasive UCs were inherited by the invasive UCs themselves, that is DNA methylation alterations in N were correlated with the development of more malignant UCs. The combination of DNA methylation status on 83 BAC clones selected by Wilcoxon test was able to completely discriminate N from C, and diagnose N as having a high risk of carcinogenesis, with 100% sensitivity and specificity. The combination of DNA methylation status on 20 BAC clones selected by Wilcoxon test was able to completely discriminate patients who suffered from recurrence after surgery from patients who did not. The combination of DNA methylation status for 11 BAC clones selected by Wilcoxon test was able to completely discriminate patients with UCs of the renal pelvis or ureter who suffered from intravesical metachronous UC development from patients who did not. Genome-wide alterations of DNA methylation may participate in urothelial carcinogenesis from the precancerous stage to UC, and

DNA methylation profiling may provide optimal indicators for carcinogenetic risk estimation and prognostication. (Cancer Sci 2009) .

5. Resequencing and copy number analysis of the human tyrosine kinase gene family in poorly differentiated gastric cancer.

The tyrosine kinase (TK) family is an important regulator of signaling pathways that control a variety of physiological and pathological conditions, and a substantial proportion of TK genes are genetically altered in cancer. To clarify the somatic mutation profile of TK genes and discover potential targets for gastric cancer (GC) therapy, we undertook a systematic screening of mutations in the kinase domains of all human TK genes (636 exons of 90 genes) in 17 GC cell lines and 52 microdissected primary GCs with poorly differentiated histology. We identified 26 non-synonymous alterations (22 genes in total) that included 11 sequence alterations in cell lines and 15 somatic mutations in primary tumors. Recurrent mutations were found in four genes including a known oncogene (NTRK3), the Src kinase family (LTK and CSK) and a potential Wnt signal activator (ROR2). In addition, we analyzed copy number alterations of all the TK gene loci in the same cohort samples by array-based comparative genomic hybridization analysis and identified 24 high-level amplifications and two homozygous deletions. Both sequence alteration and frequent copy number aberration were detected in two TK genes (HCK and ERBB2), strongly suggesting that they encode potential oncogenes in GC. Our focused and integrated analyses of systemic resequencing and gene copy number have revealed the novel onco-kinome profile of GC and pave the way to a comprehensive understanding of the GC genome.

6. Identification of PAK4 as a putative target gene for amplification within 19q13.12-q13.2 in oral squamous-cell carcinoma.

Amplification of chromosomal DNA is thought to be one of the mechanisms activating cancer-related genes in tumors. To identify the most likely target for amplification in the region 19q13.12-q13.2, detected previously in SKN-3 cells by a genome-wide screening of DNA copy-number aberrations in a panel of oral squamous-cell carcinoma (OSCC) cell lines, we determined the extent of the amplicon, analyzed a panel of cell lines for the expression of candidate genes within the amplicon, and then evaluated growth-suppressive effects by knocking down genes of interest. Reported information about the function and/or expression of each gene, remarkable overexpression in SKN-3 cells and relatively frequent overexpression in additional OSCC lines compared with an immortalized normal oral epithelial cell line, and expression level-dependent

proliferation-promoting activity led us to conclude that the p21-activated kinase 4 (PAK4) gene was the most likely target. An immunohistochemical analysis of primary tumors from 105 cases of head and neck SCC including 50 cases of OSCC demonstrated the overexpression of PAK4 to be significantly associated with a poorer prognosis. These findings reveal that the PAK4 overexpression through amplification or other mechanisms promotes the proliferation and/or survival of OSCC cells, and that PAK4 might be a good diagnostic and/or therapeutic target.

7. Krüppel-like factor 12 plays a significant role in poorly differentiated gastric cancer progression.

Gastric cancer is the second common malignant neoplasia in Japan, and its poorly differentiated form is a deadly disease. To identify novel candidate oncogenes contributing to its genesis, we examined copy-number alterations in 50 primary poorly differentiated gastric cancers using an array-based comparative genomic hybridization (array-CGH). Many genetic changes were identified, including a novel amplification of the 13q22 locus. Several genes are located in this locus, and selective knockdown of one for the Krüppel-like factor 12 (KLF12) induced significant growth-arrest in the HGC27 gastric cancer cell line. Microarray analysis also demonstrated that genes associated with cell proliferation were mostly changed by KLF12 knockdown. To explore the oncogenic function of KLF12, we introduced a full length of human KLF12 cDNA into NIH3T3 and AZ-521 cell lines and found that overexpression significantly enhanced their invasive potential. In clinical samples, KLF12 mRNA in cancer tissue was increased in 11 of 28 cases (39%) when compared with normal gastric epithelium. Clinicopathological analysis further demonstrated a significant correlation between KLF12mRNA levels and tumor size ($p = 0.038$). These data suggest that the KLF12 gene plays an important role in poorly differentiated gastric cancer progression and is a potential target of therapeutic measures.

8. Genome-wide DNA methylation profiles in liver tissue at the precancerous stage and in hepatocellular carcinoma.

To clarify genome-wide DNA methylation profiles during hepatocarcinogenesis, bacterial artificial chromosome (BAC) array-based methylated CpG island amplification was performed on 126 tissue samples. The average numbers of BAC clones showing DNA hypo- or hypermethylation increased from noncancerous liver tissue obtained from patients with hepatocellular carcinomas (HCCs) (N) to HCCs. N appeared to be at the precancerous stage, showing DNA methylation alterations that were correlated with the future development of HCC. Using Wilcoxon test, 25 BAC clones, whose DNA methylation status was inherited

by HCCs from N and were able to discriminate 15 N samples from 10 samples of normal liver tissue obtained from patients without HCCs (C) with 100% sensitivity and specificity, were identified. The criteria using the 25 BAC clones were able to discriminate 24 additional N samples from 26 C samples in the validation set with 95.8% sensitivity and 96.2% specificity. Using Wilcoxon test, 41 BAC clones, whose DNA methylation status was able to discriminate patients who survived more than 4 years after hepatectomy from patients who suffered recurrence within 6 months and died within a year after hepatectomy, were identified. The DNA methylation status of the 41 BAC clones was correlated with the cancer-free and overall survival rates of patients with HCC. Multivariate analysis revealed that satisfying the criteria using the 41 BAC clones was an independent predictor of overall outcome. Genome-wide alterations of DNA methylation may participate in hepatocarcinogenesis from the precancerous stage, and DNA methylation profiling may provide optimal indicators for carcinogenetic risk estimation and prognostication.

9. Overexpression of SMYD2 relates to tumor cell proliferation and malignant outcome of esophageal squamous cell carcinoma.

Although we have identified two putative targets, ATF3 and CENPF, for a frequently gained/amplified region around 1q32-q41 in esophageal squamous cell carcinoma (ESCC), it is possible that other amplification targets remain to be identified. In this study, we tested whether SET and MYND domain-containing protein 2 (SMYD2), located between those two genes and encoding a lysine methyltransferase for histone H3K36 and p53K370 that regulates transcription and inhibits transactivation activity, respectively, acts as a cancer-promoting gene through activation/overexpression in ESCC. Frequent overexpression of SMYD2 messenger RNA and protein was observed in KYSE150 cells with remarkable amplification at 1q32-41.1 and other ESCC cell lines (11/43 lines, 25.6%). Overexpression of SMYD2 protein was frequently detected in primary tumor samples of ESCC (117/153 cases, 76.5%) as well and significantly correlated with gender, venous invasion, the pT category in the tumor-lymph node-metastases classification and status of recurrence. Patients with SMYD2-overexpressing tumors had a worse overall rate of survival than those with non-expressing tumors, and SMYD2 positivity was independently associated with a worse outcome in the multivariate analysis. Knockdown of SMYD2 expression inhibited and ectopic overexpression of SMYD2 promoted the proliferation of ESCC cells in a TP53 mutation-independent but SMYD2 expression-dependent manner. These findings suggest that SMYD2 plays an important role in tumor cell proliferation through its activation/overexpression and highlight its usefulness as

a prognosticator and potential therapeutic target in ESCC.

10. Molecular cloning of t (2;7) (p24.3;p14.2), a novel chromosomal translocation in myelodysplastic syndrome-derived acute myeloid leukemia.

In this study, we report the molecular structure of the breakpoint region in a new chromosomal translocation, t (2;7) (p24.3;p14.2), in a case of acute myeloid leukemia transformed from myelodysplastic syndrome (MDS). An extensive fluorescence in situ hybridization (FISH) analysis showed that NAG (2p24.3) and ELMO1 (7p14.2) were involved at the breakpoints of t (2;7) (p24.3;p14.2). Furthermore, we detected a novel chimeric transcript consisting of NAG and ELMO1. Interestingly, this transcript encoded a truncated molecular form of 3'ELMO1 as the result of a frameshift caused by the chromosomal translocation. Although this study does not provide direct evidence that a defect in NAG-ELMO1 plays a role in the pathogenesis or the leukemic change in MDS, it does suggest that defects in NAG-ELMO1 potentially contributed to the leukemic progression in this case.

11. Surgical contribution to recurrence-free survival in patients with macrovascular-invasion-negative hepatocellular carcinoma.

BACKGROUND: Macroscopic vascular invasion (MVI) is a well-known indicator of recurrence of hepatocellular carcinoma (HCC) even after curative hepatectomy, but the clinicopathologic and molecular features of the recurrence remain unclear in MVI-negative HCC. STUDY DESIGN: Two hundred seven consecutive patients with confirmed primary MVI-negative HCC were retrospectively assessed after curative resection, with special emphasis on the importance of anatomically systematized hepatectomy. HCC tissues were also analyzed for genome-wide gene expression profile of each tumor using a microarray technique. RESULTS: Univariate analysis of HCC recurrence revealed multiple tumors ($p < 0.001$), moderate to poor differentiation ($p = 0.044$), Child-Pugh B/C ($p = 0.047$), alpha-fetoprotein elevation ($p = 0.007$), and nonanatomic hepatectomy ($p = 0.010$) as risk factors. According to Cox hazard multivariate analysis, multiple tumors ($p = 0.002$), alpha-fetoprotein elevation ($p < 0.001$), and nonanatomic hepatectomy ($p = 0.002$) were identified as independent factors of the recurrence. In the recurrent cases after anatomic hepatectomy for HCC, local recurrence was significantly infrequent compared with those after nonanatomic hepatectomy ($p < 0.001$). Network expression analysis using cDNA microarray revealed distinct signaling pathways of epithelial-mesenchymal transitions are associated with recurrence after anatomically systematized hepatectomy. CONCLUSIONS: Anatomically systematized hepatectomy might contribute to recurrence-free survival

of HCC patients of HCC without MVI. Local recurrence could be mostly averted by anatomic hepatectomy, although specific epithelial-mesenchymal transitions signaling might regulate the biologic aggressiveness of HCC.

12. ASK1 and ASK2 differentially regulate the counteracting roles of apoptosis and inflammation in tumorigenesis.

Apoptosis and inflammation generally exert opposite effects on tumorigenesis: apoptosis serves as a barrier to tumour initiation, whereas inflammation promotes tumorigenesis. Although both events are induced by various common stressors, relatively little is known about the stress-induced signalling pathways regulating these events in tumorigenesis. Here, we show that stress-activated MAP3Ks, ASK1 and ASK2, which are involved in cellular responses to various stressors such as reactive oxygen species, differentially regulate the initiation and promotion of tumorigenesis. ASK2 in cooperation with ASK1 functioned as a tumour suppressor by exerting proapoptotic activity in epithelial cells, which was consistent with the reduction in ASK2 expression in human cancer cells and tissues. In contrast, ASK1-dependent cytokine production in inflammatory cells promoted tumorigenesis. Our findings suggest that ASK1 and ASK2 are critically involved in tumorigenesis by differentially regulating apoptosis and inflammation.

13. PH domain-only protein PHLDA3 is a p53-regulated repressor of Akt.

p53 And Akt are critical players regulating tumorigenesis with opposite effects: whereas p53 transactivates target genes to exert its function as a tumor suppressor, Akt phosphorylates its substrates and transduces downstream survival signals. In addition, p53 and Akt negatively regulate each other to balance survival and death signals within a cell. We now identify PHLDA3 as a p53 target gene that encodes a PH domain-only protein. We find that PHLDA3 competes with the PH domain of Akt for binding of membrane lipids, thereby inhibiting Akt translocation to the cellular membrane and activation. Ablation of endogenous PHLDA3 results in enhanced Akt activity and decrease of p53-dependent apoptosis. We also demonstrate the suppression of anchorage-independent cell growth by PHLDA3. Loss of the PHLDA3 genomic locus was frequently observed in primary lung cancers, suggesting a role of PHLDA3 in tumor suppression. Our results reveal a new mode of coordination between the p53 and Akt pathways.

14. Actinin-4 gene amplification in ovarian cancer: a candidate oncogene associated with poor patient prognosis and tumor chemoresistance.

Actinin-4, an isoform of non-muscular alpha-actinin, enhances cell motility by bundling the actin cytoskeleton. We previously reported a prognostic implication of high immunohistochemical expression of actinin-4 protein in ovarian cancers. Chromosomal gain or amplification of the 19q12-q13 region has been reported in ovarian cancer. We hypothesized that the actinin-4 (ACTN4) gene might be a target of the 19q12-q13 amplicon and play an essential role of ovarian cancer progression. In total, 136 advanced-stage ovarian cancers were investigated for the copy number of the ACTN4 gene on chromosome 19q13, using fluorescence in situ hybridization, and the correlation of the ACTN4 copy number with actinin-4 protein immunoreactivity and major clinicopathological factors was investigated. A higher copy number ($> \text{or } =4$ copies) of the ACTN4 gene was detected in 29 (21%) cases and was highly associated with the intensity of actinin-4 immunoreactivity ($P < 0.0001$), a high histological tumor grade ($P = 0.030$), a clear-cell adenocarcinoma histology ($P = 0.012$), resistance to first-line chemotherapies ($P = 0.028$), and poor patient outcome ($P = 0.0011$). Univariate analyses using the Cox regression model showed that a higher ACTN4 gene copy number was able to predict patient outcome more accurately than high actinin-4 immunoreactivity (relative risk: 2.48 vs 1.55). Multivariate analysis showed that a higher copy number of the ACTN4 gene and the degree of residual disease were independent prognostic factors for overall patient survival. The actinin-4 gene may be a target of the 19q amplicon, acting as a candidate oncogene, and serve as a predictor of poor outcome and tumor chemoresistance in patients with advanced-stage ovarian cancers.

15. SKI and MEL1 cooperate to inhibit transforming growth factor-beta signal in gastric cancer cells.

Chromosomal amplification occurs frequently in solid tumors and is associated with poor prognosis. Several reports demonstrated the cooperative effects of oncogenic factors in the same amplicon during cancer development. However, the functional correlation between the factors remains unclear. Transforming growth factor (TGF)-beta signaling plays important roles in cytodifferentiation and normal epithelium differentiation, and alterations in TGF-beta signaling have been identified in many malignancies. Here, we demonstrated that transcriptional co-repressors of TGF-beta signaling, SKI and MDS1/EVI1-like gene 1 (MEL1), were aberrantly expressed in MKN28 gastric cancer cells by chromosomal co-amplification of 1p36.32. SKI and MEL1 knockdown synergistically restored TGF-beta responsiveness in MKN28 cells and reduced tumor growth in vivo. MEL1 interacted with SKI and inhibited TGF-beta signaling by stabilizing the inactive Smad3-SKI complex on the promoter of TGF-beta target genes. These findings reveal a novel mechanism where distinct transcriptional co-

repressors are co-amplified and functionally interact, and provide molecular targets for gastric cancer treatment.

16. Genome-wide DNA methylation profiles in both precancerous conditions and clear cell renal cell carcinomas are correlated with malignant potential and patient outcome.

To clarify genome-wide DNA methylation profiles during multistage renal carcinogenesis, bacterial artificial chromosome array-based methylated CpG island amplification (BAMCA) was performed. Non-cancerous renal cortex tissue obtained from patients with clear cell renal cell carcinomas (RCCs) (N) was at the precancerous stage where DNA hypomethylation and DNA hypermethylation on multiple bacterial artificial chromosome (BAC) clones were observed. By unsupervised hierarchical clustering analysis based on BAMCA data for their N, 51 patients with clear cell RCCs were clustered into two subclasses, Clusters A (N) (n = 46) and B (N) (n = 5). Clinicopathologically aggressive clear cell RCCs were accumulated in Cluster B (N), and the overall survival rate of patients in Cluster B (N) was significantly lower than that of patients in Cluster A (N). By unsupervised hierarchical clustering analysis based on BAMCA data for their RCCs, 51 patients were clustered into two subclasses, Clusters A (T) (n = 43) and B (T) (n = 8). Clinicopathologically aggressive clear cell RCCs were accumulated in Cluster B (T), and the overall survival rate of patients in Cluster B (T) was significantly lower than that of patients in Cluster A (T). Multivariate analysis revealed that belonging to Cluster B (T) was an independent predictor of recurrence. Cluster B (N) was completely included in Cluster B (T), and the majority of the BAC clones that significantly discriminated Cluster B (N) from Cluster A (N) also discriminated Cluster B (T) from Cluster A (T). In individual patients, DNA methylation status in N was basically inherited by the corresponding clear cell RCC. DNA methylation alterations in the precancerous stage may generate more malignant clear cell RCCs and determine patient outcome.

17. ITCH is a putative target for a novel 20q11.22 amplification detected in anaplastic thyroid carcinoma cells by array-based comparative genomic hybridization.

Anaplastic thyroid carcinoma (ATC) is one of the most virulent of all human malignancies, with a mean survival time among patients of less than 1 year after diagnosis. To date, however, cytogenetic information on this disease has been very limited. During the course of a program to screen a panel of ATC cell lines for genomic copy-number aberrations using array-based comparative genomic hybridization, we identified a high-level amplification of the

ITCH gene, which is mapped to 20q11.22 and belongs to the homologous to the E6-associated protein carboxylterminus ubiquitin ligase family. The expression of ITCH was increased in 4 of 14 ATC cell lines (28.6%), including 8305C in which there was a copy-number amplification of this gene, and six of seven primary cases (85.7%). Among the primary thyroid tumors, a considerable number of ITCH high expressers was found in ATC (40/45, 88.9%), papillary thyroid carcinoma (25/25, 100%), and papillary microcarcinoma (25/25, 100%). Furthermore, knockdown of ITCH by specific small interfering RNA significantly inhibited the growth of ITCH-overexpressing cells, whereas ectopic overexpression of ITCH promoted growth of ATC cell lines with relatively weak expression. These observations indicate ITCH to be the most likely target for 20q11.22 amplification and to play a crucial role in the progression of thyroid carcinoma.

18. Heterozygous deletion at 14q22.1-q22.3 including the BMP4 gene in a patient with psychomotor retardation, congenital corneal opacity and feet polysyndactyly.

Here we report on a 1-year-old Japanese girl with psychomotor retardation, bilateral congenital corneal opacity and bilateral postaxial polysyndactyly of the feet. Although she had a normal female karyotype, our in-house bacterial artificial chromosome (BAC)-based array-CGH analysis successfully detected at least a 2.7-Mb heterozygous deletion at 14q22.1-q22.3 harboring 18 protein-coding genes. Among the genes, BMP4 was a candidate for the gene causing the abnormalities of both the eye and digits. It was previously reported that the BMP family was correlated with the morphogenesis of digits and ocular development, and Bmp4 heterozygous null mice revealed skeletal abnormalities including polydactyly and ocular anterior segment abnormalities. Patients with a deletion including BMP4 also had abnormalities of the eye and digits. These previous reports support that a haplo-insufficiency of the BMP4 gene likely caused the congenital ocular and digit abnormalities. Moreover, among the other genes contained in the deletion, GMFB is a candidate for the gene responsible for the psychomotor retardation. (c) 2008 Wiley-Liss, Inc.

19. Genetic clustering of clear cell renal cell carcinoma based on array-comparative genomic hybridization: its association with DNA methylation alteration and patient outcome.

PURPOSE: The aim of this study was to clarify genetic and epigenetic alterations occurring during renal carcinogenesis. EXPERIMENTAL DESIGN: Copy number alterations were examined by array-based comparative genomic hybridization analysis using an array harboring 4,361 bacterial artificial chromosome clones, and DNA

methylation alterations on CpG islands of the p16, human MutL homologue 1, von Hippel-Lindau, and thrombospondin 1 genes and the methylated in tumor (MINT-1, MINT-2, MINT-12, MINT-25, and MINT-31) clones were examined in 51 clear cell renal cell carcinomas (RCC). RESULTS: By unsupervised hierarchical clustering analysis based on copy number alterations, clear cell RCCs were clustered into the two subclasses, clusters A (n=34) and B (n=17). Copy number alterations were accumulated in cluster B. Loss of chromosome 3p and gain of 5q and 7 were frequent in both clusters A and B, whereas loss of 1p, 4, 9, 13q, and 14q was frequent only in cluster B. The average number of methylated CpG islands in cluster B was significantly higher than those in cluster A. Clear cell RCCs showing higher histologic grades, vascular involvement, renal vein tumor thrombi, and higher pathologic stages were accumulated in cluster B. The recurrence-free and overall survival rates of patients in cluster B were significantly lower than those of patients in cluster A. Multivariate analysis revealed that genetic clustering was a predictor of recurrence-free survival and was independent of histologic grade and pathologic stage. CONCLUSIONS: This genetic clustering of clear cell RCC is significantly associated with regional DNA hypermethylation and may become a prognostic indicator for patients with RCC.

20. Expression and gene amplification of actinin-4 in invasive ductal carcinoma of the pancreas.

PURPOSE: An invasive growth pattern is one of the hallmarks of pancreatic ductal carcinoma. Actinin-4 is an actin-binding protein associated with enhanced cell motility, invasive growth, and lymph node metastasis. Actinin-4 might play an important role in the development and progression of pancreatic cancer. EXPERIMENTAL DESIGN: The expression of actinin-4 was examined immunohistochemically in 173 cases of invasive pancreatic ductal carcinoma. The copy number of the actinin-4 (ACTN4) gene was calculated by fluorescence in situ hybridization. The expression of actinin-4 was stably knocked down by short hairpin RNA, and tumorigenicity was evaluated by orthotopic implantation into mice with severe combined immunodeficiency. RESULTS: The expression level of actinin-4 was increased in 109 (63.0%) of 173 cases of pancreatic cancer. Kaplan-Meier survival curves revealed that patients with increased expression of actinin-4 had a significantly poorer outcome ($P=0.00001$, log-rank test). Multivariate analysis by the Cox proportional hazard model showed that high expression of actinin-4 was the most significant independent negative predictor of survival (hazard ratio, 2.33; $P=0.000009$). Amplification (defined as more than four copies per interphase nucleus) of the ACTN4 gene was detected in 11 (37.9%) of 29 cases showing increased expression of actinin-4. Knockdown of

actinin-4 expression inhibited the destructive growth of cancer cells in the pancreatic parenchyma. CONCLUSION: Recurrent amplification of chromosome 19q13.1-2 has been reported in pancreatic cancer, but the exact target gene has not been identified. Actinin-4 contributes to the invasive growth of pancreatic ductal carcinoma, and ACTN4 is one of the candidate oncogenes in this chromosome locus.

21. Caffeine yields aneuploidy through asymmetrical cell division caused by misalignment of chromosomes.

Aneuploidy has been implicated as an important step leading to various neoplasias. Although genetic factors that block aneuploidy have been the subject of intense interest, the impact of pharmacological and environmental substances on the development of aneuploidy has not been studied. Here, we show that caffeine induces aneuploidy through asymmetrical cell division. Mitotic exits of HeLa, U2OS, and primary fibroblast cells were significantly delayed by 10 mmol/L caffeine. Most caffeine-treated mitotic cells showed misalignment of chromosomes at the metaphase plates, and were arrested at prometaphase. Mitotic arrest deficient 2 (MAD2) depletion rescued the caffeine-induced delay of mitotic exit, indicating that caffeine-induced prolongation of mitosis was caused by activation of a MAD2-dependent spindle checkpoint. Enumeration of centromeres by fluorescence in situ hybridization revealed that cell division in the presence of caffeine was not symmetrical and resulted in aneuploid cell production. Most of these cells survived and underwent DNA synthesis. Our findings reveal a novel pharmacological effect of a high concentration of caffeine on genomic stability in dividing cells.

22. The CASK gene harbored in a deletion detected by array-CGH as a potential candidate for a gene causative of X-linked dominant mental retardation.

Here we report on a 5-year-old Japanese girl with developmental delay and microcephaly. Although she had a normal karyotype, a bacterial artificial chromosome-based array-comparative genome hybridization analysis detected a de novo 4.0-Mb heterozygous deletion at Xp11.3-p11.4 harboring nine genes. By comparison with a healthy carrier mother of a boy with atypical Norrie disease having a smaller deletion in the same region, we excluded four genes as candidates whose haploinsufficiency would be causative for developmental delay. Among the other five genes, CASK seems to be the most likely candidate for a causative gene, because it is strongly expressed in fetal brain and plays important roles in neural development and synaptic function. We confirmed that the expression of CASK mRNA was decreased in the patient compared with healthy controls and the patient's X-chromosomal inactivation was not skewed. These results suggested that

the genetic deletion of CASK results in haploinsufficiency, which might be causative for the patient's developmental delay or mental retardation. (c) 2008 Wiley-Liss, Inc.

23. Activation of B-Myb by E2F1 in hepatocellular carcinoma.

Aim: Deregulation of E2F1 transcriptional activity is observed in a variety of cancers, including hepatocellular carcinoma (HCC). The aim of the present study is to identify transcriptional target genes of E2F1 in HCC. **Methods:** We determined expression levels for E2F1 and ten candidate genes thought to be targets of E2F1 in primary HCCs using a real-time quantitative reverse transcription-PCR assay. Following small interfering RNA (siRNA)-mediated knockdown of E2F1 in HCC cell lines, we quantified mRNA levels of the candidate E2F1 target genes. **Results:** E2F1 was significantly over-expressed in 41 primary HCCs as compared to non-tumorous liver tissues. Among the candidates, MYBL2, whose product is the transcriptional factor B-Myb, which is involved in controlling cell-cycle progression and apoptosis, was significantly over-expressed in primary HCCs. Additionally, expression levels of MYBL2 correlated with those of E2F1. Knockdown of E2F1 resulted in a decrease in expression of MYBL2. A copy-number gain for MYBL2 was observed in 36 of 66 primary HCCs, suggesting that MYBL2 expression is up-regulated by amplification in addition to being regulated by E2F1. Moreover, siRNA-mediated knockdown of MYBL2 led to reduced expression of CDC2 (which encodes CDC2), cyclin A2 (CCNA2), and topoisomerase II alpha (TOP2A), implicating these genes in the cell cycle and suggesting that they may be downstream targets of B-Myb. **Conclusion:** MYBL2 is a probable transcriptional target of E2F1 in HCC and may therefore be a useful biomarker for diagnosis and an attractive target for molecular therapies useful to treat HCC.

24. Expression of cIAP-1 correlates with nodal metastasis in squamous cell carcinoma of the tongue.

Cellular inhibitor-of-apoptosis protein 1 (cIAP-1) is a member of the inhibitor-of-apoptosis protein family, which predominantly regulates apoptosis. It has been suggested that expression of cIAP-1 correlates with certain clinicopathological features. The possible significance of cIAP-1 expression in cervical lymph node metastasis of tongue squamous cell carcinoma (SCC) is investigated. Seventy-five tongue SCCs were analyzed by immunohistochemistry. cIAP-1 immunoreactivity patterns were nuclear in 38 (51%), cytoplasmic in 47 (63%), and concurrent in 37 (49%) cases. Nuclear, cytoplasmic and concurrent cIAP-1 immunoreactions were significantly correlated with lymph node metastasis in tongue SCCs ($P=0.0011$, 0.0012 , and 0.0006 , respectively). The cleaved

caspase-3, which is a marker of tumor apoptosis, and Ki-67 index, which is a marker of tumor proliferation, were immunohistochemically examined in 21 tongue SCCs with concurrent nuclear and cytoplasmic cIAP-1 expression and with metastasis, and in 23 tongue SCCs without concurrent nuclear and cytoplasmic cIAP-1 expression and without metastasis. Concurrent cIAP-1 expression was inversely correlated with caspase-3 ($P=0.0066$), but was positively correlated with Ki-67 expression ($P=0.0028$). The mode of invasion was associated with lymph node metastasis ($P=0.014$) and differentiation ($P=0.013$), but was not correlated with cIAP-1 expression. There was no statistically significant correlation between nuclear or cytoplasmic cIAP-1 expression and the Clinicopathological factors of gender, age, clinical stage or differentiation. These results suggest that both patterns of cIAP-1 are useful markers for predicting cervical lymph node metastasis in tongue SCC.

25. Frequent inactivation of a putative tumor suppressor, angiopoietin-like protein 2, in ovarian cancer.

Angiopoietin-like protein 2 (ANGPTL2) is a secreted protein belonging to the angiopoietin family, the members of which are implicated in various biological processes, although its receptor remains unknown. We identified a homozygous loss of ANGPTL2 (9q33.3) in the course of screening a panel of ovarian cancer (OC) cell lines for genomic copy-number aberrations using in-house array-based comparative genomic hybridization. ANGPTL2 mRNA expression was observed in normal ovarian tissue and immortalized normal ovarian epithelial cells, but was reduced in some OC lines without its homozygous deletion (18 of 23 lines) and restored after treatment with 5-aza 2'-deoxycytidine. The methylation status of sequences around the ANGPTL2 CpG-island with clear promoter activity inversely correlated with expression. ANGPTL2 methylation was frequently observed in primary OC tissues as well. In an immunohistochemical analysis of primary OCs, ANGPTL2 expression was frequently reduced (51 of 100 cases), and inversely correlated with methylation status. Patients with OC showing reduced ANGPTL2 immunoreactivity had significantly worse survival in the earlier stages (stages I and II), but better survival in advanced stages (stages III and IV). The restoration of ANGPTL2 expression or treatment with conditioned medium containing ANGPTL2 inhibited the growth of OC cells originally lacking the expression of this gene, whereas the knockdown of endogenous ANGPTL2 accelerated the growth of OC cells with the expression of ANGPTL2. These results suggest that, at least partly, epigenetic silencing by hypermethylation of the ANGPTL2 promoter leads to a loss of ANGPTL2 function, which may be a factor in the carcinogenesis of OC in a stage-dependent manner.

26. Frequent silencing of a putative tumor suppressor gene melatonin receptor 1 A (MTNR1A) in oral squamous-cell carcinoma.

Array-based comparative genomic hybridization (array-CGH) has good potential for the high-throughput identification of genetic aberrations in cell genomes. In the course of a program to screen a panel of 21 oral squamous-cell carcinoma (OSCC) cell lines for genome-wide copy-number aberrations by array-CGH using our in-house bacterial artificial chromosome arrays, we identified a frequent homozygous deletion at 4q35 loci with approximately 1 Mb in extent. Among the seven genes located within this region, the expression of the melatonin receptor 1 A (MTNR1A) messenger RNA (mRNA) was not detected or decreased in 35 out of the 39 (89%) OSCC cell lines, but was detected in immortalized normal oral epithelial cell line, and was restored in gene-silenced OSCC cells without its homozygous loss after treatment with 5-aza-2'-deoxycytidine. The hypermethylation of the CpG (cytosine and guanine separated by phosphate) island in the promoter region of MTNR1A was inversely correlated with its expression in OSCC lines without a homozygous deletion. Methylation of this CpG island was also observed in primary OSCC tissues. In an immunohistochemical analysis of 50 primary OSCC tumors, the absence of immunoreactive MTNR1A was significantly associated with tumor size and a shorter overall survival in patients with OSCC tumors, and seems to be an independent prognosticator in a multivariate analysis. Exogenous restoration of MTNR1A expression inhibited the growth of OSCC cells lacking its expression. Together with the known tumor-suppressive function of melatonin and MTNR1A in various tumors, our results indicate MTNR1A to be the most likely target for epigenetic silencing at 4q35 and to play a pivotal role during oral carcinogenesis.

27. Exploration of tumor-suppressive microRNAs silenced by DNA hypermethylation in oral cancer.

In the last few years, microRNAs (miRNA) have started a revolution in molecular biology and emerged as key players in the carcinogenesis. They have been identified in various tumor types, showing that different sets of miRNAs are usually deregulated in different cancers. To identify the miRNA signature that was specific for oral squamous cell carcinoma (OSCC), we first examined expression profiles of 148 miRNAs in a panel of 18 OSCC cell lines and the immortalized oral keratinocyte line RT7 as a control. Compared with RT7, the expression of 54 miRNAs (36.5%) was frequently down-regulated in OSCC lines (<0.5-fold expression, >or=66.7% of 18 lines). Among these 54 miRNAs, we further analyzed four of these miRNAs (i.e., miR-34b, miR-137, miR-193a, and miR-203), located around CpG islands, to identify tumor-suppressive miRNAs silenced

through aberrant DNA methylation. The expression of those four genes was restored by treatment with 5-aza-2'-deoxycytidine in OSCC cells lacking their expression. In addition, expression levels of the four miRNAs were inversely correlated with their DNA methylation status in the OSCC lines. In primary tumors of OSCC with paired normal oral mucosa, down-regulation of miRNA expression through tumor-specific hypermethylation was more frequently observed for miR-137 and miR-193a than for miR-34b and miR-203. Moreover, the ectopic transfection of miR-137 or miR-193a into OSCC lines lacking their expressions significantly reduced cell growth, with down-regulation of the translation of cyclin-dependent kinase 6 or E2F transcription factor 6, respectively. Taken together, our results clearly show that miR-137 and miR-193a are tumor suppressor miRNAs epigenetically silenced during oral carcinogenesis.

28. Identification of SMURF1 as a possible target for 7q21.3-22.1 amplification detected in a pancreatic cancer cell line by in-house array-based comparative genomic hybridization.

Pancreatic cancer (PC) cell lines provide a useful starting point for the discovery and functional analysis of genes driving the genesis and progression of this lethal cancer. To increase our understanding of the gene copy number changes in pancreatic carcinomas and to identify key amplification and deletion targets, we applied genome-wide array-based comparative genomic hybridization using in-house array (MCG Cancer Array-800) to 24 PC cell lines. Overall, the analyses revealed high genomic complexity, with several copy number changes detected in each line. Homozygous deletions (log (2) ratio < -2) of eight genes (clones) were seen in 14 of the 24 cell lines, whereas high-level amplifications (log (2) ratio >2) of 10 genes (clones) were detected in seven lines. Among them, we focused on high-level amplification at 7q22.1, because target genes for this alteration remain unknown. Through precise mapping of the altered region by fluorescence in situ hybridization, determination of the expression status of genes located within those regions, and functional analysis using knockdown of the gene expression or the ectopic overexpression approach in PC cell lines, as well as immunohistochemical analyses of candidates in primary tumors of PC, we successfully identified SMURF1 as having the greatest potential as a 7q21.3-22.1 amplification target. SMURF1 may work as a growth-promoting gene in PC through overexpression and might be a good candidate as a therapeutic target. Our results suggest that array-based comparative genomic hybridization analysis combined with further genetic and functional examinations is a useful approach for identifying novel tumor-associated genes involved in the pathogenesis of this lethal disease.

29. Aurora kinase B is a predictive factor for the aggressive recurrence of hepatocellular carcinoma after curative hepatectomy.

BACKGROUND: Patterns of cancer recurrence hold the key to prognosis after curative resection. This retrospective study aimed to identify a predictor and therapeutic candidate for aggressive recurrence of hepatocellular carcinoma (HCC). **METHODS:** Primary HCC tissues from 107 patients who had curative resection were analysed. Genome-wide gene expression profiles were investigated using a microarray technique, and clustering analysis was carried out based on the first diagnosis of recurrence according to the Milan criteria. Immunohistochemical expression and array-based comparative genomic hybridization (array-CGH) were also assessed. **RESULTS:** Microarray analysis revealed overexpression of Aurora kinase B, a chromosome passenger protein kinase, as the most significant predictor of the aggressive recurrence of HCC. Aurora kinase B protein expression was significantly associated with aggressive recurrence ($P < 0.001$) and prognosis ($P < 0.001$). Multivariable analysis identified Aurora kinase B as the only independent predictor of aggressive recurrence of HCC ($P = 0.031$). Array-CGH analysis showed that genomic instability was closely related to Aurora kinase B expression ($P = 0.011$). **CONCLUSION:** Aurora kinase B is an effective predictor of aggressive HCC recurrence, in relation to the genomic instability. It might be worth considering as a molecular target for the adjuvant therapy of HCC.

30. Overexpressed NF-kappaB-inducing kinase contributes to the tumorigenesis of adult T-cell leukemia and Hodgkin Reed-Sternberg cells.

The nuclear factor-kappaB (NF-kappaB) transcription factors play important roles in cancer development by preventing apoptosis and facilitating the tumor cell growth. However, the precise mechanisms by which NF-kappaB is constitutively activated in specific cancer cells remain largely unknown. In our current study, we now report that NF-kappaB-inducing kinase (NIK) is overexpressed at the pretranslational level in adult T-cell leukemia (ATL) and Hodgkin Reed-Sternberg cells (H-RS) that do not express viral regulatory proteins. The overexpression of NIK causes cell transformation in rat fibroblasts, which is abolished by a super-repressor form of IkappaBalpha. Notably, depletion of NIK in ATL cells by RNA interference reduces the DNA-binding activity of NF-kappaB and NF-kappaB-dependent transcriptional activity, and efficiently suppresses tumor growth in NOD/SCID/gammac (null) mice. These results indicate that the deregulated expression of NIK plays a critical role in constitutive NF-kappaB activation in ATL and H-RS cells, and suggest also that NIK is an attractive molecular target for cancer therapy.

31. A loss-of-function mutation in the FTSJ1 gene causes nonsyndromic X-linked mental retardation in a Japanese family.

Mental retardation (MR) is a common trait, affecting approximately 2-3% of individuals in the general population. Although the etiology of MR remains largely unknown, genetics apparently play a major role. Recent molecular studies of X-linked form of MR in European and North American countries have revealed 24 nonsyndromic X-linked mental retardation (NS-XLMR) genes including FTSJ1, a human homolog of the Escherichia coli 2'-O-rRNA methyltransferase FtsJ/RrmJ gene. Here we identified a novel FTSJ1 mutation in an XLMR family through mutation screening of a cohort of 73 unrelated Japanese male probands with MR. Sequence analysis of the proband and his mother revealed a G > A substitution at the consensus for the donor splicing site in intron 8 (c.571 + 1G > A) of FTSJ1. This mutation prevented the removal of intron 8 from the pre-mRNA, thereby leading to a frameshift in the mutant FTSJ1 mRNA and resulting in a premature termination in exon 9. Quantitative RT-PCR showed a significant reduction of mutant FTSJ1 mRNA in the patient's lymphoblast cells, which was restored by treatment with cycloheximide, a potent inhibitor of nonsense-mediated mRNA decay (NMD). Therefore, mRNAs carrying this mutation are likely subject to degradation by NMD. Together, loss-of-function of FTSJ1 may be a mechanism for the cognitive dysfunction observed in this family. Our study also suggested that the FTSJ1 mutation probably accounts for XLMR in Japanese at a similar frequency (1-2%) as in Europeans.

4) 本事業に関連して世界的な研究拠点形成に向けて、以下の点で改善・整備等されたこと

A (研究拠点体制)

全国の臨床遺伝専門医と連携し遺伝疾患解析コンソーシアムを形成し、本態不明の先天異常症、精神発達遅滞等の潜在的ゲノム異常診断を実施するとともに、それらの全例で詳細な臨床病理学データベースを構築するとともにリンパ芽球細胞株化を実施しバイオリソースを構築した。

D (人材育成)

4名の大学院博士課程研究生(歯科医)において口腔がんの分子病態解析研究を指導し、うち1名は学位を取得した。他大学院博士課程研究生(歯科医)1名において顎顔面形成異常を伴う先天異常症のゲノム解析を指導中である。

その他、2名のSS、1名のQSSの研究を指導している。

E (国際化)

韓国ヨンセイ大学医学部小児科とアジア民族のCNVに関するゲノム疫学的共同研究を実施した。

5) GCOE事業を推進するに当たって力を入れた点

がんと遺伝疾患のゲノム・エピゲノム解析を実施し疾患関連遺伝子の同定と病態解明を推進することにより、実地医療にも十分に貢献する診断、治療、予防法の開発に繋がる価値の高い成果を得ることを目的に研究指導を行っている。また、積極的に国際学会等で発表し、国際的にも十分に評価される成果を得るよう注力している。

6) 英文原著論文

- Prapinjumrun C, Morita KI, Kuribayashi Y, Hanabata Y, Shi Q, Nakajima Y, Inazawa J, Omura K: DNA amplification and expression of FADD in oral squamous cell carcinoma. *J Oral Pathol Med*. 2009 Dec 22.
- Tanaka S, Mogushi K, Yasen M, Noguchi N, Kudo A, Nakamura N, Ito K, Miki Y, Inazawa J, Tanaka H, Arii S: Gene-expression phenotypes for vascular invasiveness of hepatocellular carcinomas. *Surgery*. 2009
- Furuta M, Kozaki K, Tanaka S, Arii S, Imoto I, Inazawa J: miR-124 and miR-203 are epigenetically silenced tumor-suppressive microRNAs in hepatocellular carcinoma. *Carcinogenesis*. 2009
- Inoue J, Misawa A, Tanaka Y, Ichinose S, Sugino Y, Hosoi H, Sugimoto T, Imoto I, Inazawa J: Lysosomal-associated protein multispinning transmembrane 5 gene (LAPTM5) is associated with spontaneous regression of neuroblastomas. *PLoS One*. 4:e7099. 2009
- Nishiyama N, Arai E, Chihara Y, Fujimoto H, Hosoda F, Shibata T, Kondo T, Tsukamoto T, Yokoi S, Imoto I, Inazawa J, Hirohashi S, Kanai Y: Genome-wide DNA methylation profiles in urothelial carcinomas and urothelia at the precancerous stage. *Cancer Sci*. 2009
- Kubo T, Kuroda Y, Shimizu H, Kokubo A, Okada N, Hosoda F, Arai Y, Nakamura Y, Taniguchi H, Yanagihara K, Imoto I, Inazawa J, Hirohashi S, Shibata T: Resequencing and Copy Number Analysis of the Human Tyrosine Kinase Gene Family in Poorly Differentiated Gastric Cancer. *Carcinogenesis*. 30:1857-64. 2009
- Begum A, Imoto I, Kozaki K, Tsuda H, Suzuki E, Amagasa T, Inazawa J: Identification of PAK4 as a putative target gene for amplification within 19q13.12-q13.2 in oral squamous-cell carcinoma. *Cancer Sci*. 100:1908-16. 2009
- Nakamura Y, Migita T, Hosoda F, Okada N, Gotoh M, Arai Y, Fukushima M, Ohki M, Miyata S, Takeuchi K, Imoto I, Katai H, Yamaguchi T, Inazawa J, Hirohashi S, Ishikawa Y, Shibata T: Krüppel-like factor 12 plays a significant role in poorly differentiated gastric cancer progression. *Int J Cancer*. 125:1859-67. 2009
- Arai E, Ushijima S, Gotoh M, Ojima H, Kosuge T, Hosoda F, Shibata T, Kondo T, Yokoi S, Imoto I, Inazawa J, Hirohashi S, Kanai Y: Genome-wide DNA methylation profiles in liver tissue at the precancerous stage and in hepatocellular carcinoma. *Int J Cancer*. 125:2854-62. 2009
- Komatsu S, Imoto I, Tsuda H, Kozaki K, Muramatsu T, Shimada Y, Aiko S, Yoshizumi Y, Ichikawa D, Otsuji E, Inazawa J: Overexpression of SMYD2 relates to tumor cell proliferation and malignant outcome of esophageal squamous-cell carcinoma. *Carcinogenesis*. 30:1139-46. 2009
- Fujita K, Sanada M, Harada H, Mori H, Niikura H, Omine M, Inazawa J, Imoto I: Molecular cloning of t(2;7)(p24.3;p14.2), a novel chromosomal translocation in myelodysplastic syndrome-derived acute myeloid leukemia. *J Hum Genet*. 54:355-9. 2009
- Tanaka S, Mogushi K, Yasen M, Noguchi N, Kudo A, Kurokawa T, Nakamura N, Inazawa J, Tanaka H, Arii S: Surgical contribution to recurrence-free survival in patients with macrovascular-invasion-negative hepatocellular carcinoma. *J Am Coll Surg*. 208:368-74. 2009
- Iriyama T, Takeda K, Nakamura H, Motimoto Y, Kuroiwa T, Mizukami J, Umeda T, Noguchi T, Naguro I, Nishitoh H, Saegusa K, Tobiume K, Homma T, Shimada Y, Tsuda H, Aiko S, Imoto I, Inazawa J, Chiba K, Kamei Y, Kozuma S, Taketani Y, Matsuzawa A, Ichijo H: ASK1 and ASK2 differentially regulate the counteracting roles of apoptosis and inflammation in tumorigenesis. *EMBO Journal*. 28:43-53, 2009
- Kawase T, Ohki R, Shibata T, Tsutsumi S, Kamimura N, Inazawa J, Ohta T, Ichikawa H, Aburatani H, Tashiro F, Taya Y: PH domain-only protein PHLDA3 is a p53-regulated repressor of akt. *Cell*. 36:535-550, 2009
- Yamamoto S, Tsuda H, Honda K, Onozato K, Takano M, Tamai S, Imoto I, Inazawa J, Yamada T, Matsubara O: Actinin-4 gene amplification in ovarian cancer: a candidate oncogene associated with poor patient prognosis and tumor chemoresistance. *Mod Pathol*. 22:499-507, 2009
- Takahata M, Inoue Y, Tsuda H, Imoto I, Koinuma D, Hayashi M, Ichikura T, Yamori T, Nagasaki K, Yoshida M, Matsuoka M, Morishita K, Yuki K, Hanyu A, Miyazawa K, Inazawa J, Miyazono K, Imamura T: SKI and MEL1 cooperate to inhibit transforming growth factor-beta signal in gastric cancer cells. *J Biol Chem*. 284:3334-44, 2009
- Arai E, Ushijima S, Fujimoto H, Hosoda F, Shibata T,

Kondo T, Yokoi S, Imoto I, Inazawa J, Hirohashi S, Kanai Y: Genome-wide DNA methylation profiles in both precancerous conditions and clear cell renal cell carcinomas are correlated with malignant potential and patient outcome. *Carcinogenesis*.30:214-21, 2009

7) 著書

1. (分担) 稲澤譲治:講義録 腫瘍学.株式会社メジカルビュー社 (東京) pp43-46, 2009,2,10 (4P)
2. (分担) 阿部達生、稲澤譲治、井本逸勢、井上純:造血器腫瘍アトラス-形態、免疫、染色体と遺伝子-改訂第4版.日本医事新報社 (東京) 2009,4,20 (574P)
3. (分担) 稲澤譲治:入門腫瘍内科学.篠原出版新社 (東京) 2009,10,1
4. (分担) 井本逸勢、稲澤譲治:がん化学療法・分子標的治療update.中外医学社 (東京) pp329-333,2009,10,30 (733P)
5. (分担) 稲澤譲治:新臨床腫瘍学 (改訂第2版) -がん薬物療法専門医のために-.株式会社南江堂 (東京) 2009,11,5

8) 特許取得、特許申請

特許取得

1. 2009.3.27 特許第4280878号、MASL1癌遺伝子 (1999/1/28特許出願平11-20696、特許公開2000-217578)

特許申請

〔国内〕

1. 2009.2.2、「医薬組織物、および腫瘍の治療用薬剤」、大木理恵子・川瀬竜也・柴田龍弘・田矢洋一・油谷浩幸・稲澤譲治・田代文夫、財団法人ヒューマンサイエンス振興財団・国立大学法人東京医科歯科大学・学校法人東京理科大学、特願2009-022048
2. 2009.3.3、「精神遅滞を伴う多発性奇形症候群の判別方法」、稲澤譲治・井本逸勢・林深・会津善紀、国立大学法人東京医科歯科大学・株式会社ビー・エム・エル・富士フィルム株式会社、特願2009-049864
3. 2009.3.11、「BACクローンを用いる尿路上皮癌の発生病リスク評価方法及び予後予測方法」、金井弥栄・新井恵史・西山直隆・稲澤譲治、(財)ヒューマンサイエンス財団・国立大学法人東京医科歯科大学、特願2009-058156
4. 2009.3.25、「食道癌の検出方法及び抑制剤」、井上純・井本逸勢・稲澤譲治、国立大学法人東京医科歯科大学・

富士フィルム株式会社、特願2009-073998

5. 2009.5.1、「薬剤耐性マーカーおよびその利用」、井上純・稲澤譲治、稲澤譲治・富士フィルム株式会社、特願2009-111725
6. 2009.5.26、「核酸アレイ及び核酸アレイの識別方法」、石井靖幸・吉田淳哉・氏原大・三好隼人・岩木義英・稲澤譲治・井本逸勢、富士フィルム株式会社・国立大学法人東京医科歯科大学、特願2009-126894
7. 2009.5.26、「核酸マイクロアレイを用いた解析方法」、氏原大・金原秀行・稲澤譲治・井本逸勢、富士フィルム株式会社・国立大学法人東京医科歯科大学、特願2009-126780
8. 2009.5.27、「核酸マイクロアレイの異常スポットを検出する方法」、金原秀行・吉田淳哉・稲澤譲治・井本逸勢、富士フィルム株式会社・国立大学法人東京医科歯科大学、特願2009-128162

〔米国〕

1. 「癌の検出方法及び癌抑制剤」、稲澤譲治・小崎健一・井本逸勢、国立大学法人東京医科歯科大学・富士写真フィルム株式会社、2009.1.22、12/357,894、特願2008-012256
2. 「甲状腺癌の検出方法」、稲澤譲治・井本逸勢・石原孝也・津田均、国立大学法人東京医科歯科大学・富士写真フィルム株式会社、2009.7.15、12/503,434、特願2008-184982
3. 「神経芽腫の検出方法」、稲澤譲治・井本逸勢・井上純、国立大学法人東京医科歯科大学・富士写真フィルム株式会社、2009.9.28、12/568,569、特願2008-275176

〔EP〕

1. 「癌の検出方法及び癌抑制剤」、稲澤譲治・小崎健一・井本逸勢、国立大学法人東京医科歯科大学・富士写真フィルム株式会社、2009.1.23、09151217.8、特願2008-012256

9) 学会発表 (英文)

1. Honda S, Hayashi S, Imoto I, Toyama J, Okamoto N, Kurosawa K, Nakagawa E, Goto Y, Inazawa J: Exploration of genes related to X-linked mental retardation (XLMR) by BAC-based X-tiling array. 59th Annual Meeting of the American Society of Human Genetics 2009 (Honolulu, Hawaii USA) 21/October/2009 示説
2. Hayashi S, Honda S, Mizuno S, Okamoto N, Makita Y, Hata A, Imoto I, Inazawa J: Analyses of 499 cases of multiple congenital anomalies with mental retardation

using array-CGH for investigation and diagnosis. 59th Annual Meeting of the American Society of Human Genetics 2009 (Honolulu, Hawaii USA) 21/October/2009 示説

10) 学会発表 (和文)

1. 本田尚三、林深、井本逸勢、當山潤、岡本伸彦、黒澤健司、中川栄二、後藤雄一、稲澤譲治:BAC-based X-tiling arrayを用いたX連鎖性精神発達遅滞(XLMR)の原因遺伝子探索.日本人類遺伝学会第54回大会.グランドプリンスホテル高輪.東京.2009年9月24日
2. 林深、岡本奈那、本田尚三、蒔田芳男、羽田明、井本逸勢、稲澤譲治:アレイ CGHを用いた多発奇形を伴う精神遅滞症例解析の4年間の実績.日本人類遺伝学会第54回大会.グランドプリンスホテル高輪.東京.2009年9月24日
3. 林深、岡本伸彦、水野誠司、小野正恵、小崎里華、奥山虎之、知念安紹、蒔田芳男、羽田明、井本逸勢、稲澤譲治:小頭症と小脳脳幹部低形成を伴う発達遅滞12例におけるCASK遺伝子の解析.日本人類遺伝学会第54回大会.グランドプリンスホテル高輪.東京.2009年9月24日
4. 会津善紀、井本逸勢、林深、小澤伸晃、左合治彦、山口敏和、永田欽也、宮本力、蒔田芳男、羽田明、稲澤譲治:GDA700による染色体微細異常解析受託システムの構築.日本人類遺伝学会第54回大会.グランドプリンスホテル高輪.東京.2009年9月24日
5. 小澤伸晃、佐々木愛子、須郷慶信、江川真希子、青木宏明、高橋宏典、三井真理、渡邊典芳、林聡、左合治彦、会津善紀、山口敏和、井本逸勢、稲澤譲治:アレイ CGH法による流産絨毛染色体分析.日本人類遺伝学会第54回大会.グランドプリンスホテル高輪.東京.2009年9月26日
6. 井本逸勢、松村聡、小崎健一、有井滋樹、稲澤譲治:ゲノムワイドな統合的DNAメチル化異常解析による肝癌抑制遺伝子候補探索.日本人類遺伝学会第54回大会.グランドプリンスホテル高輪.東京.2009年9月26日
7. 中川栄二、和田敬仁、久保田健夫、加藤光広、難波栄二、斉藤伸治、黒澤健司、戸田達史、岡澤均、松本直道、本田尚三、稲澤譲治、神田将和、岡崎康司、後藤雄一:自閉症スペクトラム障害を併存する精神遅滞の遺伝学的解析.日本人類遺伝学会第54回大会.グランドプリンスホテル高輪.東京.2009年9月26日
8. 田中真二、藍原有弘、茂樺薫、ヤーセン マームット、野口典男、入江工、工藤篤、中村典明、井本逸勢、三木義男、稲澤譲治、田中博、有井滋樹:肝癌再発ネットワーク解析に基づくAurora kinase B分子標的治療の開発.第68回日本癌学会学術総会.パシフィコ横浜.神奈川.2009年10月1日
9. 西山直隆、新井恵史、藤元博行、細田文恵、柴田龍弘、近藤格、塚本泰司、横井左奈、井本逸勢、稲澤譲治、廣橋説雄、金井弥栄:尿路上皮がんならびに前がん段階にある尿路上皮におけるDNAメチル化プロファイル-発がんリスク評価と予後予測.第68回日本癌学会学術総会.パシフィコ横浜.神奈川.2009年10月2日
10. 新井恵史、牛島抄織、後藤政広、尾島英知、小菅智男、細田文恵、柴田龍弘、近藤格、横井左奈、井本逸勢、稲澤譲治、廣橋説雄、金井弥栄:肝細胞がんとその前がん状態である慢性肝炎・肝硬変症におけるゲノム網羅的DNAメチル化プロファイル.第68回日本癌学会学術総会.パシフィコ横浜.神奈川.2009年10月2日
11. 古田繭子、小崎健一、田中真二、有井滋樹、井本逸勢、稲澤譲治:肝細胞癌において腫瘍特異的DNA過剰メチル化により発現抑制される癌抑制microRNA.第68回日本癌学会学術総会.パシフィコ横浜.神奈川.2009年10月2日
12. 小松周平、井本逸勢、津田均、小崎健一、嶋田裕、市川大輔、大辻英吾、稲澤譲治:食道扁平上皮癌における新規診断・治療標的遺伝子SMYD2の同定.第68回日本癌学会学術総会.パシフィコ横浜.神奈川.2009年10月2日
13. 横井左奈、津田均、稲澤譲治:乳癌における1p13増幅領域の標的遺伝子tripartite motif 33 (TRIM33)の解析.第68回日本癌学会学術総会.パシフィコ横浜.神奈川.2009年10月2日
14. 中村裕、右田敏郎、細田文恵、後藤政広、新井康仁、宮田敏、竹内賢吾、片井均、山口俊晴、稲澤譲治、廣橋説雄、石川雄一、柴田龍弘:低分化胃がん進展におけるKLF12転写因子の役割.第68回日本癌学会学術総会.パシフィコ横浜.神奈川.2009年10月2日
15. 鶴田智彦、小崎健一、平沢晃、阪空浩司、進伸幸、井本逸勢、青木大輔、稲澤譲治:子宮体癌細胞株の機能的スクリーニングを用いたエピゲノム異常により発現抑制される癌抑制遺伝子型microRNAの探索.第68回日本癌学会学術総会.パシフィコ横浜.神奈川.2009年10月2日
16. 松村聡、井本逸勢、小崎健一、有井滋樹、稲澤譲治:肝細胞癌においてエピゲノムで制御されるがん抑制遺伝子の統合的アレイ解析.第68回日本癌学会学術

総会.パシフィコ横浜.神奈川県.2009年10月2日

17. 村松智輝、井本逸勢、松井毅、小崎健一、津田均、嶋田裕、稲澤譲治:食道扁平上皮癌におけるYAP1とそのisoformの癌遺伝子としての機能.第68回日本癌学会学術総会.パシフィコ横浜.神奈川県.2009年10月3日
18. 大木理恵子、川瀬竜也、柴田龍弘、堤修一、太田力、市川仁、稲澤譲治、油谷浩幸、田代文夫、田矢洋一:p53標的遺伝子PHLDA3はAkt抑制因子として機能するPH domain-only protein をコードする.第68回日本癌学会学術総会.パシフィコ横浜.神奈川県.2009年10月3日
19. ベガム アスマ、井本逸勢、小崎健一、津田均、鈴木江美奈、天笠光雄、稲澤譲治:口腔扁平上皮癌における19q13.12-q13.2増幅の新規標的遺伝子PAK4.第68回日本癌学会学術総会.パシフィコ横浜.神奈川県.2009年10月3日
20. 岡本奈那、林深、黒澤健司、水野誠司、蒔田芳男、羽田明、井本逸勢、森山啓司、稲澤譲治:新規症候群の可能性のある10q24微細欠失を伴う2症例の報告.日本人類遺伝学会第54回大会.グランドプリンスホテル高輪.東京.2009年9月24日示説
21. 岡本伸彦、林深、井本逸勢、稲澤譲治、蒔田芳男、羽田明:アレイCGHで診断された1p34.3微細欠失例.日本人類遺伝学会第54回大会.グランドプリンスホテル高輪.東京.2009年9月24日示説
22. 横井左奈、津田均、井本逸勢、稲澤譲治:1p13増幅領域の標的遺伝子tripartite motif 33 (TRIM33)は乳癌の予後不良因子である.日本人類遺伝学会第54回大会.グランドプリンスホテル高輪.東京.2009年9月25日示説
23. 細田文恵、新井康仁、宮本正之、安田純、中西幸浩、井本逸勢、稲澤譲治、柳原五吉、廣橋説雄、大木操、柴田龍弘:胃がんにおける6p21ゲノム増幅と複数のがん関連遺伝子の協調的活性化.第68回日本癌学会学術総会.パシフィコ横浜.神奈川県.2009年10月1日示説
24. 春木茂男、井本逸勢、小松周平、村松智輝、松井毅、小崎健一、河内洋、嶋田裕、河野辰幸、稲澤譲治:食道扁平上皮癌において高頻度に発現抑制される癌関連抑制遺伝子DESC1の同定.第68回日本癌学会学術総会.パシフィコ横浜.神奈川県.2009年10月1日示説
25. 白樺、井上純、井本逸勢、稲澤譲治:ヒト癌におけるLC3A variant 1の発現低下の意義.第68回日本癌学会学術総会.パシフィコ横浜.神奈川県.2009年10月1日示説

11) 外部資金の獲得状況

科学研究費補助金、 特定領域

研究題目:がんの統合的ゲノム解析と個性診断法の開発

代表:稲澤 譲治

期間:平成21年

研究費総額:23,200,000円

科学研究費補助金、 特定領域

研究題目:ヒトゲノム構造解析ツールとして的高密度ゲノムDNAマイクロアレイの開発と応用

代表:井本 逸勢

期間:平成21年

研究費総額:11,500,000円

科学研究費補助金、 基盤研究C

研究題目:ゲノム情報と癌遺伝子・癌抑制遺伝子中毒を指標にした食道癌治療標的遺伝子の探索

代表:井本 逸勢

期間:平成21年

研究費総額:1,100,000円

科学研究費補助金、 基盤研究C

研究題目:癌特異的エピゲノム異常を指標とした口腔癌抑制microRNAの網羅的探索

代表:小崎 健一

期間:平成21年

研究費総額:1,100,000円

科学研究費補助金、 基盤研究A

研究題目:難治性消化器癌における転移・再発の分子診断と分子標的治療の開発

代表:有井 滋樹

期間:平成21年

研究費総額:1,000,000円(稲澤分担額)

独)新エネルギー・産業技術総合開発機構(NEDO)

委託研究費

研究題目:個別化医療の実現のための技術融合¹⁾付診断技術開発/染色体解析技術開発

代表:稲澤 譲治

期間:平成21年

研究費総額:97,598,000円

富士写真フイルム株式会社 共同研究費

研究題目:CGHマイクロレイシステム実用化研究

代表:稲澤 譲治

期間:平成21年

研究費総額:1,000,000円

富士写真フイルム株式会社 共同研究費

研究題目:CGHマイクロレイシステム実用化研究

代表:稲澤 譲治

期間:平成21年

研究費総額:1,000,000円

文部科学省 科学技術試験研究委託事業

研究題目:ゲノム網羅的解析情報を基盤とするオーダーメイドがん医療（胃がんの個別化医療を目指した新規胃がん関連遺伝子の探索と同定）

代表:稲澤 譲治

期間:平成21年

研究費総額:5,000,000円

文部科学省 科学技術試験研究委託事業

研究題目:ゲノム網羅的解析情報を基盤とするオーダーメイドがん医療（胃がんの個別化医療を目指した新規胃がん関連遺伝子の探索と同定）

代表:稲澤 譲治

期間:平成21年

研究費総額:5,000,000円（井本分担額）

厚生労働省 精神・神経疾患研究委託費

研究題目:精神・神経疾患バイオリソース・レポジトリの構築及び拡充と病因病態の解明に関する研究

代表:後藤 雄一

期間:平成21年

研究費総額:2,000,000円（稲澤分担額）

厚生労働省 精神・神経疾患研究委託費

研究題目:脳形成異常の成立機序の解明と治療法確立のための融合的研究

代表:中川 栄二

期間:平成21年

研究費総額:2,000,000円（井本分担額）

厚生労働科学研究費補助金 第3次対がん総合戦略

研究題目:網羅的なゲノム異常解析に基づく多段階発

がん過程並びに臨床病態の分子基盤の解明とその臨床応用に関する研究

代表:横田 淳

期間:平成21年

研究費総額:6,000,000円（稲澤分担額）

厚生労働科学研究費補助金

肝炎等克服緊急対策研究事業

研究題目:肝癌早期発見を目的とした分子マーカーおよび画像診断システムの開発

代表:有井 滋樹

期間:平成21年

研究費総額:3,500,000円（稲澤分担額）

厚生労働科学研究費補助金

肝炎等克服緊急対策研究事業

研究題目:肝癌早期発見を目的とした分子マーカーおよび画像診断システムの開発

代表:有井 滋樹

期間:平成21年

研究費総額:3,000,000円（井本分担額）

厚生労働科学研究費補助金 難治性疾患克服研究事業

研究題目:未分類疾患の情報集約に関する研究

代表:林 謙治

期間:平成21年

研究費総額:5,000,000円（稲澤分担額）

国立成育医療センター 成育医療研究委託費

研究題目:周産期医療における先進的診断技術の開発と応用に関する研究

代表:小澤 伸晃

期間:平成21年

研究費総額:2,000,000円（稲澤分担額）

12) 特別講演、招待講演

1. 稲澤譲治:「癌と遺伝疾患のゲノム・エピゲノム解析」.昭和大学歯学部口腔癌包括的研究センター 平成20年度公開シンポジウム.昭和大学歯科病院.東京.2009年3月14日
2. 稲澤譲治:「がんと遺伝子疾患の病態形成とゲノム多様性」.京都府立医科大学医学部がんプロフェッショナル養成プラン特別講義.臨床講義棟北臨床講義室.京都.2009年3月25日 稲澤譲治:「がんと遺伝疾患の統

合的ゲノム・エピゲノム解析」.琉球大学大学院セミナー.琉球大学医学部機器センターセミナー室.沖縄.2009年7月9日

3. 稲澤譲治:「ゲノム・エピゲノム解析によるがん関連遺伝子の探索」.広島がんセミナー学術講演会.広島大学.広島.2009年7月13日
4. 稲澤譲治:「アレイ CGH 法と新しい細胞遺伝学」.日本人類遺伝学会第54回大会.グランドプリンスホテル高輪.東京.2009年9月24日

13) 主催学会

1. 第16回癌ゲノムサイエンス研究会 2009年2月27日
東京ガーデンパレス
2. 第17回癌ゲノムサイエンス研究会 2009年7月16日
東京ガーデンパレス
3. 第18回癌ゲノムサイエンス研究会 2010年2月18日
予定 東京ガーデンパレス

14) 新聞、雑誌、TV 報道

1. CGH database: <http://www.cghtml.jp/index.html>
2. 分子細胞遺伝 HP: <http://www.tmd.ac.jp/mri/cgen/framepage.htm>

15) GCOE 総合講義のサマリー

課題: がんと遺伝疾患のゲノム・エピゲノム解析

要約: 日本人がどんな病気で亡くなるのかという病因別死亡率は、1981年から変わることなく“がん”がトップを占めています。世界に冠たる長寿国の我が国では、現在、二人に一人は生涯に一度はがんになり、さらに三人に一人はがんで死亡するという状況です。一人一人が健康で安心な生活をおくり、また、少しでも医療費の負担を軽減させて教育や文化活動、福祉の充実を図れるようにするという社会経済的な観点からも、“がんの克服”は、現在の日本にとって非常に大きな課題となっています。そこで、複雑ながんのゲノム異常を明らかにして、その情報にもとに画期的な診断、治療、予防法を開発することに大きな期待が寄せられています。また、網羅的ゲノムコピー数の解析が実施され、全く健康な人でも遺伝子の塩基配列や遺伝子を含むDNA断片のコピー数に変化が複数の箇所で行き起きていることも明らかになってきています。これら結果は、健康に日々を過ごす私たちにおいて、多くの遺伝子に変異が起きているものの、たまたま細胞や臓器、運動器や神経、さらにこころの発達などにおいて日常の生活に支障がない程度におさまっているこ

とを示しており、ゲノムの多様性の理解は人の多様性そのものを知るうえで重要といえます。

16) 教室、分野や講座の准教授、講師、助教、特別研究員、ポスドク、指導を受けた大学院生の名前 (AISS には○印) のリスト

准教授 : 井本逸勢
 特任准教授 : 小崎健一
 助教 : 井上純
 MTT 特任講師 : 松井毅
 特任助教 : 林深
 ポスドク研究員 : 石原孝也
 リサーチアシスタント : 高橋綾子、森留美、田山さやか

大学院生 医歯学総合研究科博士課程:
 坂本宙子、本田尚三、白樺、春木茂男、松村聡、
 倉沢泰浩、上杉篤史、小野宏晃、岡本奈那、小西博貴、
 遠藤寛則、村松智輝、宮脇豊

大学院生 生命情報科学教育部博士課程: 古田繭子

大学院生 医歯学総合研究科修士課程:
 大森逸美、川原正人、小林淳也

大学院生 生命情報科学教育部修士課程:
 大前明代、前田誠

大学院特別研究学生: 鶴田智彦

研究室アシスタント: 福川順子、篠崎優子

Lysosomal-Associated Protein Multispanning Transmembrane 5 Gene (*LAPTM5*) Is Associated with Spontaneous Regression of Neuroblastomas

Jun Inoue^{1,6}, Akiko Misawa^{1,6}, Yukichi Tanaka⁷, Shizuko Ichinose², Yuriko Sugino^{1,8}, Hajime Hosoi⁸, Tohru Sugimoto^{8,9}, Issei Imoto^{1,3,6}, Johji Inazawa^{1,3,4,5,6*}

1 Department of Molecular Cytogenetics, Medical Research Institute and School of Biomedical Science, Tokyo Medical and Dental University, Tokyo, Japan, **2** Instrumental Analysis Research Center, Tokyo Medical and Dental University, Tokyo, Japan, **3** Hard Tissue Genome research Center, Tokyo Medical and Dental University, Tokyo, Japan, **4** 21st Century Center of Excellence Program for Molecular Destruction and Reconstitution of Tooth and Bone, Tokyo Medical and Dental University, Tokyo, Japan, **5** Global Center of Excellence (GCOE) Program, International Research Center for Molecular Science in Tooth and Bone Disease, Saitama, Japan, **6** Core Research for Evolutionary Science and Technology of the Japan Science and Technology Corporation, Saitama, Japan, **7** Division of Pathology, Kanagawa Children's Medical Center, Kanagawa, Japan, **8** Department of Pediatrics, Graduate School of Medical Science, Kyoto Prefectural University of Medicine, Kyoto, Japan, **9** Saiseikai Shiga Hospital, Shiga, Japan

Abstract

Background: Neuroblastoma (NB) is the most frequently occurring solid tumor in children, and shows heterogeneous clinical behavior. Favorable tumors, which are usually detected by mass screening based on increased levels of catecholamines in urine, regress spontaneously via programmed cell death (PCD) or mature through differentiation into benign ganglioneuroma (GN). In contrast, advanced-type NB tumors often grow aggressively, despite intensive chemotherapy. Understanding the molecular mechanisms of PCD during spontaneous regression in favorable NB tumors, as well as identifying genes with a pro-death role, is a matter of urgency for developing novel approaches to the treatment of advanced-type NB tumors.

Principal Findings: We found that the expression of lysosomal associated protein multispanning transmembrane 5 (*LAPTM5*) was usually down-regulated due to DNA methylation in an NB cell-specific manner, but up-regulated in degenerating NB cells within locally regressing areas of favorable tumors detected by mass-screening. Experiments *in vitro* showed that not only a restoration of its expression but also the accumulation of *LAPTM5* protein, was required to induce non-apoptotic cell death with autophagic vacuoles and lysosomal destabilization with lysosomal-membrane permeabilization (LMP) in a caspase-independent manner. While autophagy is a membrane-trafficking pathway to degrade the proteins in lysosomes, the *LAPTM5*-mediated lysosomal destabilization with LMP leads to an interruption of autophagic flux, resulting in the accumulation of immature autophagic vacuoles, p62/SQSTM1, and ubiquitinated proteins as substrates of autophagic degradation. In addition, ubiquitin-positive inclusion bodies appeared in degenerating NB cells.

Conclusions: We propose a novel molecular mechanism for PCD with the accumulation of autophagic vacuoles due to *LAPTM5*-mediated lysosomal destabilization. *LAPTM5*-induced cell death is lysosomal cell death with impaired autophagy, not cell death by autophagy, so-called autophagic cell death. Thus *LAPTM5*-mediated PCD is closely associated with the spontaneous regression of NBs and opens new avenues for exploring innovative clinical interventions for this tumor.

Citation: Inoue J, Misawa A, Tanaka Y, Ichinose S, Sugino Y, et al. (2009) Lysosomal-Associated Protein Multispanning Transmembrane 5 Gene (*LAPTM5*) Is Associated with Spontaneous Regression of Neuroblastomas. PLoS ONE 4(9): e7099. doi:10.1371/journal.pone.0007099

Editor: Georg Häcker, Technical University Munich, Germany

Received: April 1, 2009; **Accepted:** August 5, 2009; **Published:** September 29, 2009

Copyright: © 2009 Inoue et al. This is an open-access article distributed under the terms of the Creative Commons Attribution License, which permits unrestricted use, distribution, and reproduction in any medium, provided the original author and source are credited.

Funding: Grant support: grants-in-aid for Scientific Research, Scientific Research on Priority Areas, and a 21st Century Center of Excellence Program for Molecular Destruction and Reconstitution of Tooth and Bone from the Ministry of Education, Culture, Sports, Science, and Technology, Japan; a grant-in-aid from the Ministry of Health, Labor and Welfare for the 3rd-Term Comprehensive 10-Year Strategy for Cancer Control and for Cancer Research; a grant from Core Research for Evolutional Science and Technology (CREST) of Japan Science and Technology Corporation (JST); and a grant from the New Energy and Industrial Technology Development Organization (NEDO). This work was supported by a grant from the Japanese Ministry of Education, Global Center of Excellence (GCOE) Program, "International Research Center for Molecular Science in Tooth and Bone Diseases". The funders had no role in study design, data collection and analysis, decision to publish, or preparation of the manuscript.

Competing Interests: The authors have declared that no competing interests exist.

* E-mail: johinaz.cgen@mri.tmd.ac.jp

Introduction

Neuroblastoma (NB) is a malignant tumor consisting of undifferentiated neuroectodermal cells from the neural crest and the most common solid tumor in children. Most primary tumors occur within the abdomen, with the adrenal medulla affected in

about 50% of NB patients [1–3]. The clinical behavior of NB is heterogeneous: favorable tumors, which are usually detected by mass screening based on increased levels of catecholamines in urine, regress spontaneously via programmed cell death (PCD) or mature through differentiation into benign ganglioneuromas (GN) in patients under 1 year of age, with minimal or no therapeutic

intervention; while advanced-type NBs, usually clinically detected, often grow rapidly to become fatal in older children, despite intensive chemotherapy [1–3].

The spontaneous regression and maturation of favorable NBs coincide with the neuronal differentiation and massive cellular suicide during the normal development of the nervous system, indicating that NB cells in favorable tumors may retain the genetic program of their normal counterparts [2]. Therefore, it has been considered that NB cells within regressing tumors may undergo apoptosis (a form of PCD), involving the neurotrophin signaling pathway through TrkA (receptor) and nerve growth factor (NGF) [3–9]. However some groups failed to find evidence of a correlation between apoptosis and factors associated with spontaneous regression [10–12]. On the other hand, a previous electron microscopic analysis revealed that degenerative changes including the accumulation of autophagic vacuoles are a conspicuous feature of NBs [13], and it has also been proposed that the spontaneous regression of NBs may occur via a H-Ras-associated non-apoptotic mechanism with the appearance of autophagic vacuoles in a caspase-independent manner [12]. Thus, evidence suggests that both apoptosis and non-apoptotic cell death play a role in the spontaneous regression of NBs [5].

The “wait and see” strategy has revealed that one third of mass-screened NB tumors undergo spontaneous regression, and a complete regression usually takes place over 4–20 months [4,14–17]. This slow process suggests that the degenerating NB cells in the late phase of PCD are a small proportion in favorable NB tumors found by mass-screening and then extirpated surgically, and therefore some genes having a pro-death role in PCD may yet to be expressed in mass-screened NB tumor samples. To develop a breakthrough in therapy against advanced-type NBs, which can not regress spontaneously, it is important to identify genes having a critical role in spontaneous regression/maturation and to understand those molecular mechanisms.

Here, we found *lysosomal associated protein multispansing transmembrane 5* (*LAPTM5*) to be closely associated with the spontaneous regression of mass-screened NB tumors. Whereas the expression of this gene was usually down-regulated through DNA methylation in favorable and unfavorable NB tumor samples, it was up-regulated in degenerating NB cells within locally regressing areas of mass-screened tumors. Moreover, overexpression of this gene induced caspase-independent lysosomal cell death due to lysosomal destabilization with lysosomal-membrane permeabilization (LMP), with the accumulation of immature autophagic vacuoles and ubiquitinated proteins, leading us to propose novel characteristics for PCD during the spontaneous regression of NBs.

Results

Down-regulation of *LAPTM5* expression through DNA methylation in NB cells

Previously, we developed a DNA methylation-screening system, bacterial artificial chromosome (BAC) array-based methylated CpG island amplification (MCA) [18] (BAMCA) [19], and identified tumor-related genes down-regulated through DNA methylation in human cancers, including neuroblastoma [20–22]. Using this system with an in-house “1p35–p36 contig BAC-array” [19], we identified one BAC at 1p35 as potentially methylated in NB cell lines, by comparing with two NB cell lines (GOTO and IMR32) and a reference (normal peripheral blood mononuclear cells, PBMCs) (Supplementary Figure S1, Supplementary Table S1, and Supplementary Methods S1). Screening for two candidate genes (*MLTN1* and *LAPTM5*) on this BAC revealed that the expression of *LAPTM5* was down-

regulated in NB cell lines and the CG sites around the transcriptional start site (TSS) of this gene were highly and widely methylated in both NB cell lines and primary NB tumors (Supplementary Figure S1, Supplementary Table S1, and Supplementary Methods S1), prompting us to focus on *LAPTM5* as a candidate for an NB-related gene down-regulated through DNA methylation.

First, we examined the mRNA level, frequency of methylation, and copy-number status of the *LAPTM5* gene in 10 NB cell lines. The expression of *LAPTM5* was down-regulated in all the cell lines and the down-regulation was inversely correlated with methylation at the CG sites around the TSS, compared with normal adrenal glands (Figure 1A and 1B), regardless of *MYCN* amplification or allelic loss of *LAPTM5* (Supplementary Figure S2, Supplementary Table S2, and Supplementary Methods S1). In addition, expression of *LAPTM5* was restored in correlation with a decrease of the methylation level after treatment with 5-aza-2'-deoxycytidine, a demethylating drug, in IMR32 and GOTO cells, although the expression level of *LAPTM5* after the restoration was lower than that in normal adrenal glands (Figure 1A, 1B). We next determined the mRNA level by quantitative RT-PCR and the frequency of methylation at two CG sites (CG-I and -II) upstream of TSS of *LAPTM5* by the methylation-sensitive single nucleotide primer extension (Ms-SNuPE) method in primary NB tumors, including favorable (stage-1, -2, -3 and 4S) tumors detected by mass screening and unfavorable (stage-4a) tumors (Supplementary Figure S3). Methylation was detected in all primary NB tumors examined and there was no significant difference in mRNA level and methylation status among tumors at each stage (Figure 1C). In addition, bisulfite sequencing revealed that the CG sites around the TSS of *LAPTM5* were highly and widely methylated in NB tumors and frequently demethylated in benign ganglioneuromas (GNs) that had developed from NB tumors (Figure 1D). Notably, the frequency of methylation at the two CG sites, especially CG-II, was significantly decreased in GNs compared with NB tumors (66.4% to 43.0% for CG-I; $p = 0.0002$, 50.3% to 20.9% for CG-II; $p < 0.0001$; Figure 1E). Furthermore, we examined the level of *LAPTM5* protein in NB tumor sections by conducting an immunohistochemical analysis using a specific antibody and confirmed that the protein is highly expressed in hematopoietic cells as reported [23] (Figure 1F). Although *LAPTM5* was also highly expressed in adjacent adrenal medulla cells within the tumor sections and weakly expressed in differentiated ganglion cells within GNs, its immunoreactivity in NB cells was much lower, regardless of the prognosis (Figure 1F). Taken together, these results suggested the expression of *LAPTM5* to be epigenetically down-regulated through DNA methylation in all NB cell lines and primary NB tumor samples and these conditions to be associated with the differentiation of tumors. Thus, the methylation and down-regulation of *LAPTM5* may be NB cell lineage-specific.

Up-regulation of *LAPTM5* expression in degenerating NB cells within regressing areas of mass-screened NB tumors

A focal regressing area is defined as a shrinking locus, accompanied by gaps or clefts within a tumor section, which occasionally appears in mass-screened NB tumors [12]. As shown in Figure 2A, we found two types of regressing areas on Hematoxylin-Eosin (HE) staining; type-I defined by a loss of cells within the area including a number of differentiating NB cells with an eosinophilic and large cytoplasm, and type-II defined by the loss of a large group of undifferentiating NB cells. Interestingly, our immunohistochemical analysis revealed the *LAPTM5* protein to be highly expressed in the NB cells within regressing areas (the

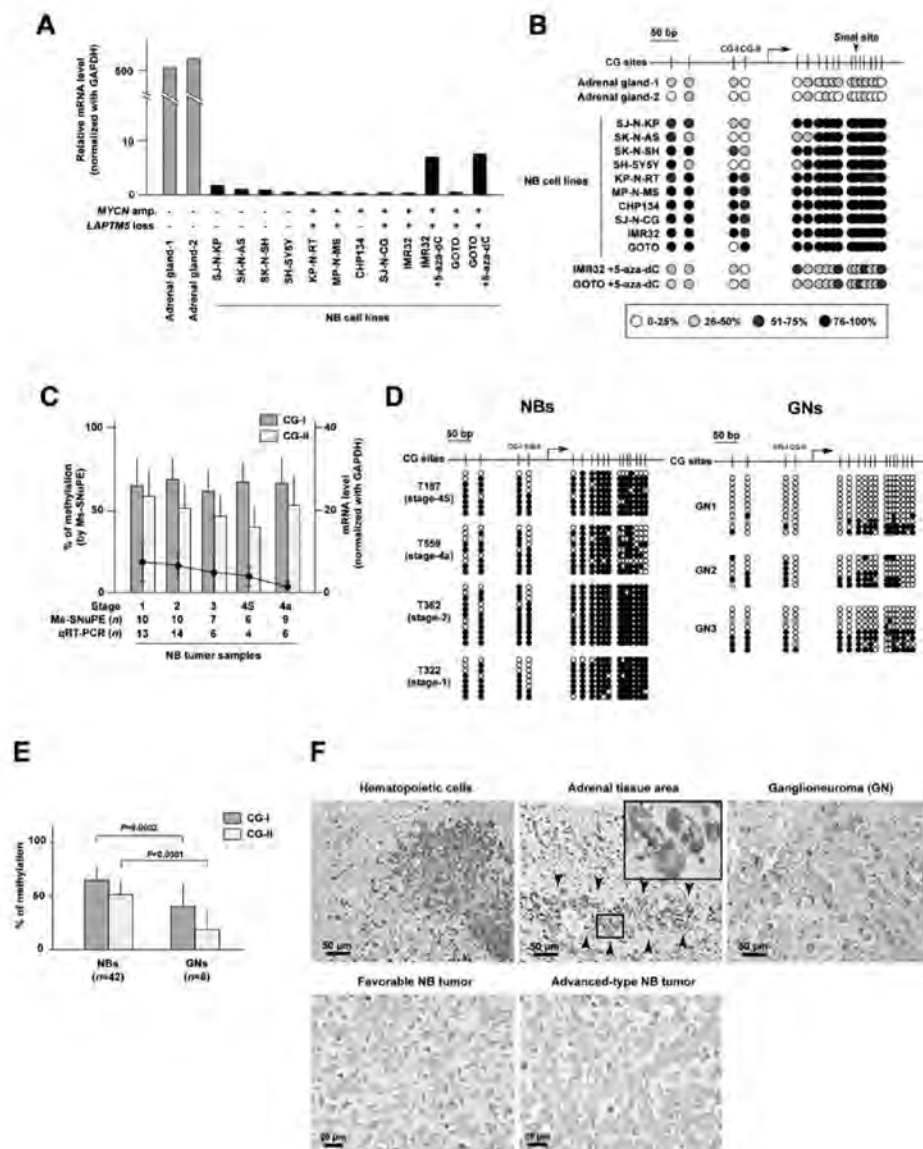


Figure 1. Identification of methylated DNA and down-regulation of *LAPTMS* expression in NB cell lines and primary NB tumors. (A) *LAPTMS* mRNA levels in NB cell lines with or without *MYCN* amplification (amp.) and/or allelic loss of the *LAPTMS* gene were determined by quantitative RT-PCR (qRT-PCR) and are indicated as bars. Levels of *LAPTMS* mRNA were normalized with levels of *GAPDH* mRNA. GOTO and IMR32 cells were treated with 5-aza-2'-deoxycytidine (5-aza-dC, 10 μ M for 5 days). (B) Frequencies of methylation at 17 CG sites within region-I around the transcriptional-start site (TSS) of the *LAPTMS* gene were determined by bisulfite sequencing, as indicated in **Supplementary Figure S1**. An arrow indicates the TSS. (C) Methylation frequency and mRNA level of *LAPTMS* in primary NB tumors at different stages. Levels of *LAPTMS* mRNA measured by qRT-PCR are indicated as dots; whereas methylation frequencies at two CG sites (CG-I or -II) measured by Ms-SNuPE are indicated as dark gray and light bars, respectively. Levels of *LAPTMS* mRNA were normalized with levels of *GAPDH* mRNA. *n* indicates the number of cases. Vertical lines, SD. (D) Representative results of bisulfite sequencing at CG sites around the TSS of *LAPTMS* in primary NB tumors and ganglioneuromas (GNs). Methylation status is indicated as white (unmethylated) or black (methylated) circles. An arrow indicates the TSS. (E) Methylation frequency of *LAPTMS* in primary NB tumors and GNs. The methylation frequencies at two CG site in 8 GNs were measured by Ms-SNuPE. The average frequency of methylation in primary NB tumors or GNs is indicated. *n* indicates the number of cases. Vertical lines, SD. (F) Representative images of immunostaining for *LAPTMS* in tissue sections. Upper; representative images of hematopoietic cells, adrenal tissue within tumor sections, and GN. The enlarged image shows the adrenal medulla cells within adrenal tissue indicated by arrowheads. Lower; representative images of NB cells within a favorable tumor (stage-1) detected by mass-screening and an advanced-type tumor (stage-4a) with *MYCN* amplification.

degenerating NB cells) (Figure 2A). We further confirmed a report [12] that H-Ras was also highly expressed in such areas (Supplementary Figure S4). Notably, while LAPTMS was weakly expressed in the differentiating NB cells within type-I

regressing areas, it appeared to be accumulated in the degenerating NB cells within type-I and -II regressing areas, compared with that in differentiating NB cells, adrenal medulla cells, or ganglion cells in GNs (Figure 1F and Figure 2A). These

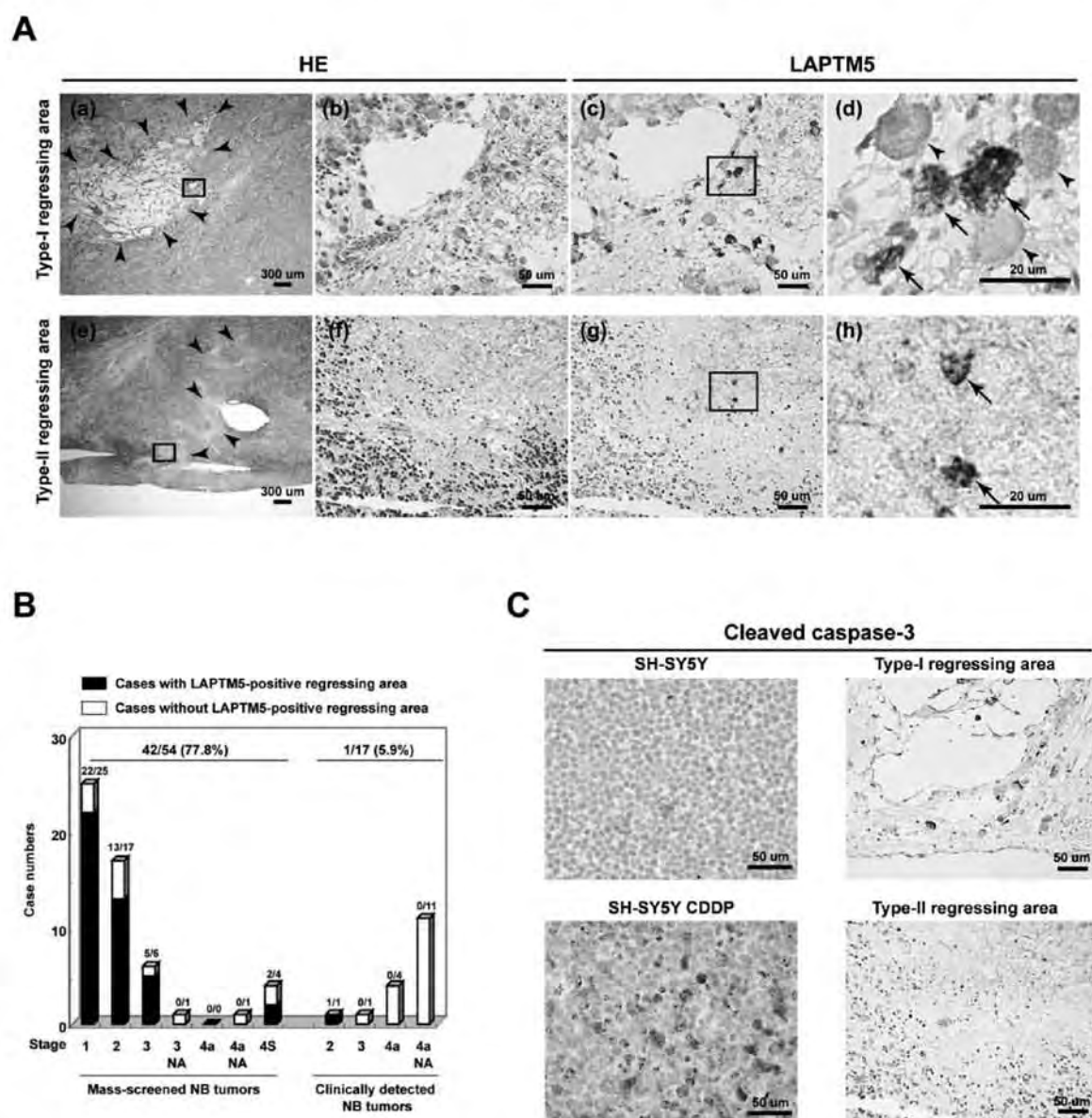


Figure 2. Immunostaining of LAPTMS protein in degenerating NB cells within regressing area in mass-screened NB tumors. (A) Serial tumor sections were stained with hematoxylin-eosin (HE) (a, b, e, and f) or with anti-LAPTMS (c, d, g, and h). a–d; representative image of a type-I regressing area, with a loss of cells including differentiating NB cells. e–h; representative image of a type-II regressing area, with a large loss of undifferentiated NB cells. The images of b, d, f, and h are the areas enlarged by the rectangle in a, c, e, and g, respectively. The area surrounded with arrowheads in a and e indicates a typical regressing area. In d and h images, arrowheads and arrows indicate differentiating NB cells and degenerating NB cells, respectively. **(B)** Relationship of between LAPTMS-associated regression with patients and tumor characteristics. A comparison was made of the proportion of positive cases between mass-screened NBs and clinically detected NBs. The stage of each tumor was determined using the INSS (International Neuroblastoma Staging System). NA; cases with MYCN amplification. **(C)** Representative image of immunostaining of cleaved caspase-3. SH-SY5Y cells with or without treatment with Cisplatin (CDDP; 1.5 µg/ml) for 2 days or serial tumor sections were stained with an antibody to cleaved caspase-3 antibody.

regressing areas with LAPTM5-positive degenerating NB cells were much more frequently observed in the mass-screened NB tumors (42 of 54 tumors, 77.8%), than in the clinically detected NB tumors (1 of 17 tumors, 5.9%) (**Figure 2B**). Furthermore, only one clinically detected tumor with LAPTM5-positive degenerating areas was classified as favorable (stage-2, well-differentiating). In addition, the immunostaining of cleaved caspase-3 revealed that LAPTM5-positive degenerating NB cells were essentially negative at least when the cleaved caspase-3 was present in SH-SY5Y cells induced into apoptosis by treatment with Cisplatin (CDDP) (**Figure 2C**), suggesting that caspase-independent cell death might occur in LAPTM5-positive degenerating NB cells. We further confirmed that the hematopoietic cells expressing the CD20 antigen (BCA-B20) specific for normal peripheral B lymphocytes could not be detected within the regressing areas of mass-screened NB tumors (**Supplementary Figure S4**). Those results suggest that the expression of LAPTM5 is closely associated with the spontaneous regression of mass-screened NB tumors and the accumulation of this protein rather than the restoration of its expression contributes to the PCD of NB cells in a caspase-independent manner.

LAPTM5 overexpression induces caspase-independent cell death and the accumulation of this protein is required to induce cell death in NB cell lines

To examine whether LAPTM5 contributes to the PCD of NB cells, the protein was overexpressed in NB cell lines using an adenovirus-mediated expression system. Strong expression of the LAPTM5 protein was detected at 4 days, rather than at 2 days, after infection in three cell lines, GOTO, IMR32, and SH-SY5Y (**Figure 3A**), and cell survival rates decreased in a dose-dependent manner on adenovirus-LAPTM5 (Ad-LAPTM5) infection (**Figure 3B**). Moreover, a remarkable increase in the number of dead cells with an increase in LAPTM5 protein level was observed at 4 days, after infection with Ad-LAPTM5, compared with adenovirus-LacZ (Ad-LacZ), in all cell lines. The cell death induced by Ad-LAPTM5 infection was not inhibited by treatment with 100 μ M of zVAD-fmk, a pan-caspase inhibitor, although the reduction of cell viability induced by CDDP was partially inhibited by treatment with the same concentration of zVAD-fmk in SH-SY5Y cells (**Figure 3C** and **Supplementary Figure S5**). In addition, on immunostaining and western blotting, we detected almost no cleaved caspase-3 in Ad-LAPTM5-infected NB cell lines (**Supplementary Figure S5**), and found none of the typical features of apoptosis, such as nuclear fragmentation and apoptotic bodies during LAPTM5-induced cell death (data not shown). These results suggest that overexpression of LAPTM5 mainly induces a non-apoptotic cell death in a caspase-independent manner in NB cells.

Based on the immunohistochemical observations that LAPTM5 seemed to be markedly accumulated in degenerating NB cells, together with the observation *in vitro* that no cell death was detected at 2 days after infection regardless of the expression of LAPTM5, we speculated that the protein accumulated due to a decrease in turnover efficiency for degradation and its accumulation is required to induce cell death. To test this idea, we first investigated whether LAPTM5 was accumulated on treatment with inhibitors for the intracellular protein degradation system (proteasomal or lysosomal degradation). When GOTO cells at 1 day after Ad-LAPTM5 infection were treated with a proteasomal inhibitor (ALLN or MG132) or a lysosomal inhibitor (Bafilomycin A1; BafA1 or NH₄Cl) for 1 day, a remarkable accumulation of LAPTM5 was detected by western blotting, compared with that in Ad-LAPTM5-infected GOTO cells without each of these

treatments (**Figure 3D**). In addition, we showed that the induction of cell death was significantly enhanced in correlation with the accumulation of LAPTM5 in Ad-LAPTM5-infected GOTO cells treated with BafA1, compared to Ad-LAPTM5-infected GOTO cells without BafA1-treatment or in Ad-LacZ-infected GOTO cells treated with BafA1 ($p = 0.027$ or $p = 0.042$) or with ALLN, compared to Ad-LAPTM5-infected GOTO cells without treatment or Ad-LacZ-infected GOTO cells treated with ALLN ($p = 0.022$ or $p = 0.028$) (**Figure 3E**). Moreover, we examined the effect of inhibiting the accumulation of LAPTM5 with specific siRNA to confirm that the accumulation is required for the induction of cell death. When LAPTM5 siRNA-transfected GOTO cells were infected with Ad-LAPTM5, and cultured with or without BafA1 or ALLN, a remarkable inhibition of LAPTM5's accumulation was confirmed by western blotting (**Figure 3F**). In this setting, the frequency of dead cells was significantly decreased in LAPTM5 siRNA-transfected GOTO cells, compared with that in control siRNA-transfected GOTO cells ($p = 0.035$ for BafA1; $p = 0.022$ for ALLN) (**Figure 3G**). Taken together, these results indicate that the introduced LAPTM5 is usually degraded by both proteasomal and lysosomal pathways and the accumulation of this protein is critical for the induction of cell death.

Appearance of autophagic vacuoles during LAPTM5-induced cell death

Non-apoptotic cell death in a caspase-independent manner is often accompanied by the appearance of numerous autophagic vacuoles in the cytoplasm [23], and has been proposed as one of the mechanisms for PCD during the spontaneous regression of NB tumors [12,13]. We therefore examined whether autophagic vacuoles appear in the cytoplasm during LAPTM5-induced cell death. Electron microscopic analysis revealed numerous autophagic vacuoles in the cytoplasm of most Ad-LAPTM5-infected GOTO cells, as compared with Ad-LacZ-infected cells (**Figure 4A**). In addition, when GOTO cells stably expressing GFP-LC3 and the parental GOTO cells were infected with Ad-LAPTM5, as well as when the cells were starved to activate autophagic flux, a remarkable increase in cells showing a punctuate distribution of GFP-LC3 or endogenous LC3B was observed by immunofluorescence microscopy, compared with untreated cells or Ad-LacZ-infected cells, respectively ($p = 0.0022$ in GOTO cells stably expressing GFP-LC3, $p = 0.0288$ in parental GOTO cells) (**Figure 4B**) [23,24]. Moreover, the cleaved form (LC3B-II) for endogenous LC3B, another indicator of the presence of autophagic vacuoles, was also clearly detected in GOTO cells during LAPTM5-induced cell death as well as starved cells by western blotting (**Figure 4C**) [23,24]. Similar results were observed in Ad-LAPTM5-infected GOTO cells stably expressing GFP-LC3 (**Supplementary Figure S6**). In addition, the cleaved form and a punctuate distribution for endogenous LC3B were observed during LAPTM5-induced cell death in SH-SY5Y cells (**Supplementary Figure S6**). These findings indicate that overexpression of LAPTM5 induces cell death with the appearance of autophagic vacuoles in NB cells.

Appearance of autophagic vacuoles during LAPTM5-induced cell death is attributed to an interruption of autophagic flux

The autophagic process functions as a flux, with portions of the cytosol and intracellular organelles sequestered into the autophagosome. The autophagosome fuses with intracellular vesicles and finally matures into the autolysosome through fusion with the

Mechanism of Tumor Regression

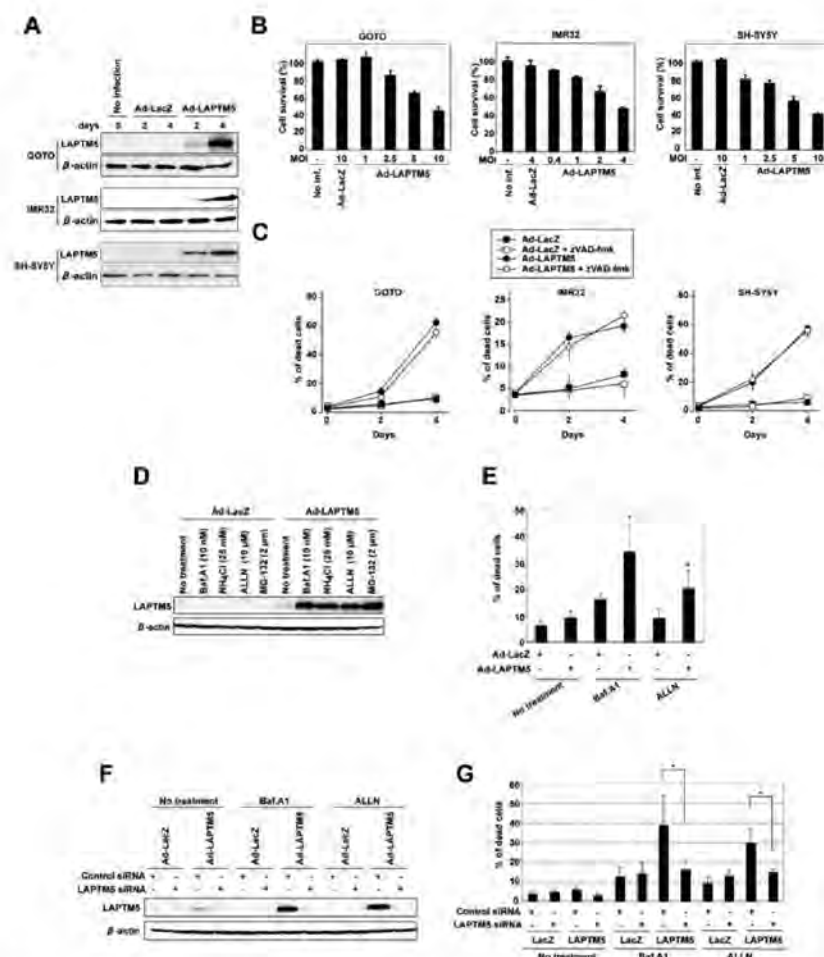


Figure 3. Induction of caspase-independent cell death by LAPTMS overexpression and effect of LAPTMS accumulation on the cell death. (A) Western blot analysis of adenovirus-infected GOTO, IMR32, and SH-SY5Y cells. The cells were infected with the *LacZ* (Ad-LacZ) or *LAPTMS* (Ad-LAPTMS) adenovirus at a MOI of 10 for GOTO and SH-SY5Y or 4 for IMR32. Two and four days after infection, whole-cell lysates were isolated, and analyzed by immunoblotting with an antibody to LAPTMS or β -actin (internal control). Results shown are representative of two independent experiments. (B) Viability of adenovirus-infected GOTO, IMR32, and SH-SY5Y cells. GOTO (5×10^4 cells/well), IMR32 (2×10^4 cells/well), or SH-SY5Y (5×10^4 cells/well) cells plated in 24-well plates were infected with Ad-LacZ or Ad-LAPTMS at the indicated MOIs. Four days after infection, the percentage of surviving cells was determined by a colorimetric water-soluble tetrazolium salt (WST) assay. Vertical lines, SD for three experiments. No inf., no infection. (C) Frequency of dead cells among adenovirus-infected GOTO, IMR32, and SH-SY5Y cells. The cells were infected with Ad-LacZ or Ad-LAPTMS under the same conditions as in (A) with or without treatment with the pan-caspase inhibitor zVAD-fmk at 100 μ M in each cell line. Dead cells were counted 2 and 4 days after infection using the trypan blue exclusion method, and indicated as percentages. Vertical lines, SD for three experiments. (D) Western blot analysis of LAPTMS in LAPTMS-infected GOTO cells treated with protein degradation inhibitors. Cells were infected with Ad-LacZ or Ad-LAPTMS at a MOI of 10. One day after infection, cells were treated with Bafilomycin A1 (BafA1, lysosomal inhibitor), NH₄Cl (lysosomal inhibitor), ALLN (proteasome inhibitor), or MG-132 (proteasome inhibitor) at indicated concentration for 1 day. Whole-cell lysate was analyzed by immunoblotting with indicated antibodies. The results shown represent two independent experiments. (E) Frequency of dead cells among LAPTMS-infected GOTO cells treated with protein degradation inhibitors. Cells were infected and treated with BafA1 or ALLN, as indicated in (D). Dead cells were counted using the trypan blue exclusion method, and indicated as percentages. Vertical lines, SD for three experiments. *t-test; $p < 0.05$. (F) Western blot analysis of LAPTMS inhibition by siRNA transfection in LAPTMS-infected GOTO cells treated with protein degradation inhibitors. Cells were transfected with control- or LAPTMS-siRNA, and infected with Ad-LacZ or -LAPTMS at a MOI of 10. The next day cells were treated with the inhibitor BafA1 or ALLN for 1 day. Whole-cell lysate was analyzed by immunoblotting with indicated antibodies. The results shown represent two independent experiments. (G) Effect of siRNA transfection on frequency of dead cells among LAPTMS-infected GOTO cells treated with protein degradation inhibitors. Cells were infected and treated with BafA1 or ALLN, as indicated in (F). Dead cells were counted using the trypan blue exclusion method, and indicated as percentages. Vertical lines, SD for three experiments. *t-test; $p < 0.05$. doi:10.1371/journal.pone.0007099.g003

lysosome, which supplies acid hydrolases, for bulk degradation. While the autophagic process is rapidly activated in the absence of nutrients for cell survival, the process also occurs constitutively at a

low level in cells (basal autophagic flux) [23,24]. Importantly, the appearance of numerous autophagic vacuoles during cell death does not necessarily reflect "so-called autophagic cell death"

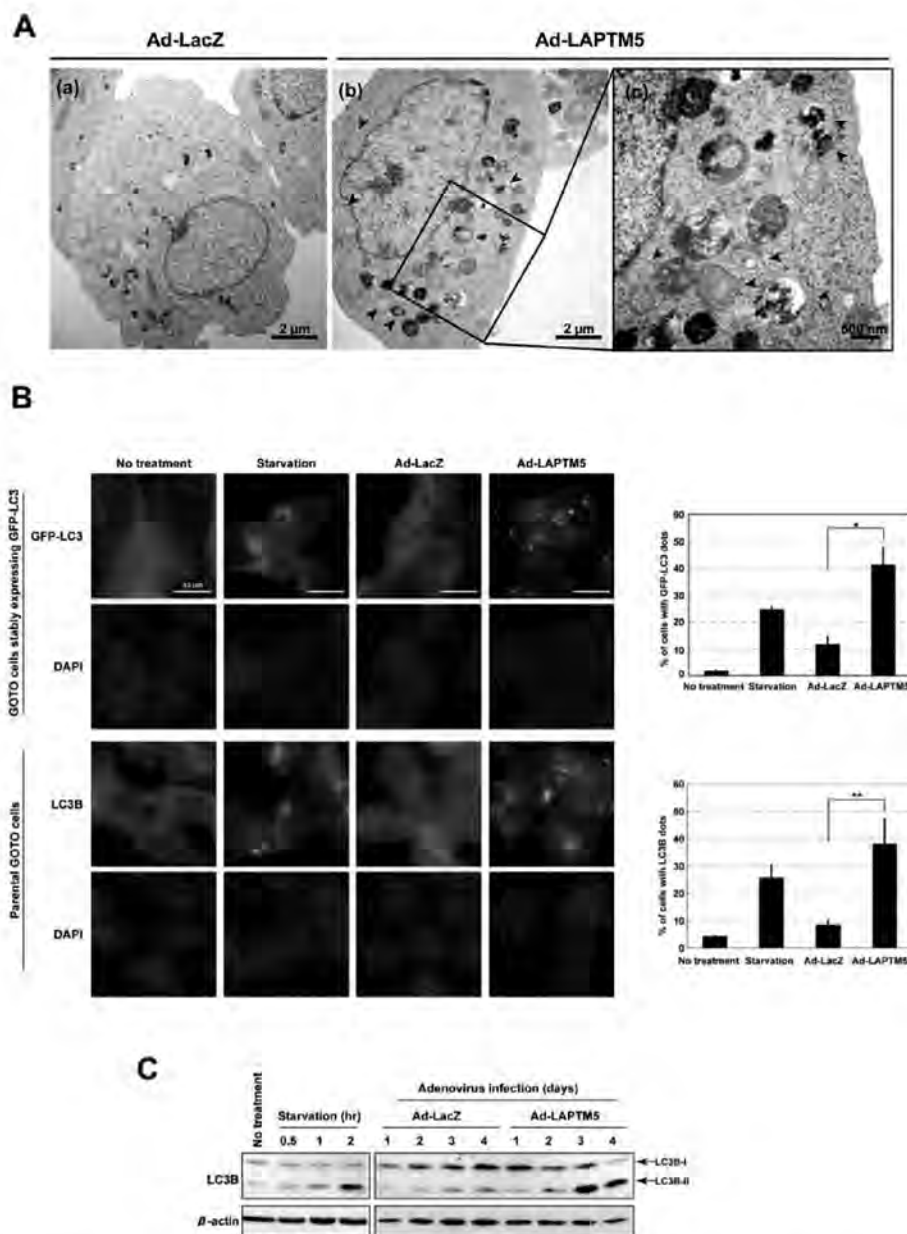


Figure 4. Appearance of autophagic vacuoles during LAPTM5-induced cell death. (A) Representative transmission-electron micrographs of Ad-LacZ (a) or Ad-LAPTM5 (b and c) -infected GOTO cells 4 days after infection. The (c) image was enlarged from the area enclosed by the rectangle in (b), showing the accumulation of autophagic vacuoles (arrowheads). (B) Localization of GFP-LC3 or endogenous LC3B detected by immunofluorescence microscopy. GOTO cells stably expressing GFP-LC3 (1×10^5 /well) (upper panel) or parental GOTO cells (1×10^5 /well) (lower panel) were plated on coverslips in 24-well plates, and the next day infected with Ad-LacZ or Ad-LAPTM5 at a MOI of 10. Four days later, the GOTO cells stably expressing GFP-LC3 were fixed in 4% formaldehyde, and observed under a fluorescence microscope. For parental GOTO cells, the cells were fixed in 10% TCA 4 days after infection, reacted with the LC3B antibody, and visualized with an FITC-conjugated secondary antibody. Control cells starved of nutrients were treated with EBSS for 2 hours at 5 days of plating. The frequency of cells with a punctate distribution (dot pattern) of GFP-LC3 or LC3B among all GFP-positive cells or total cells (at least 200 cells), respectively, was measured. * t -test, $p < 0.005$ and ** $p < 0.05$. Vertical lines, SD for three experiments. (C) Detection of LC3B-II by western blotting. As the time-courses indicated, whole-cell lysate from GOTO cells starved of nutrients or infected with Ad-LacZ and Ad-LAPTM5 at a MOI of 10 was analyzed by immunoblotting with an antibody to endogenous LC3B or β -actin (internal control). Arrows indicate form-I or -II of LC3B. Results shown are representative of two independent experiments. doi:10.1371/journal.pone.0007099.g004

attributed to activation of the autophagic process [23]. When the formation of autophagosomes was inhibited by treatment with wortmannin, an autophagic inhibitor, or by the knockdown of ATG5 expression during cultivation in a starved state or

LAPTM5-induced cell death in GOTO cells, the number of cells showing a punctate pattern of LC3B expression was significantly decreased (Figure 5A and Supplementary Figure S7). Even though the autophagic process was experimentally inhibited, the

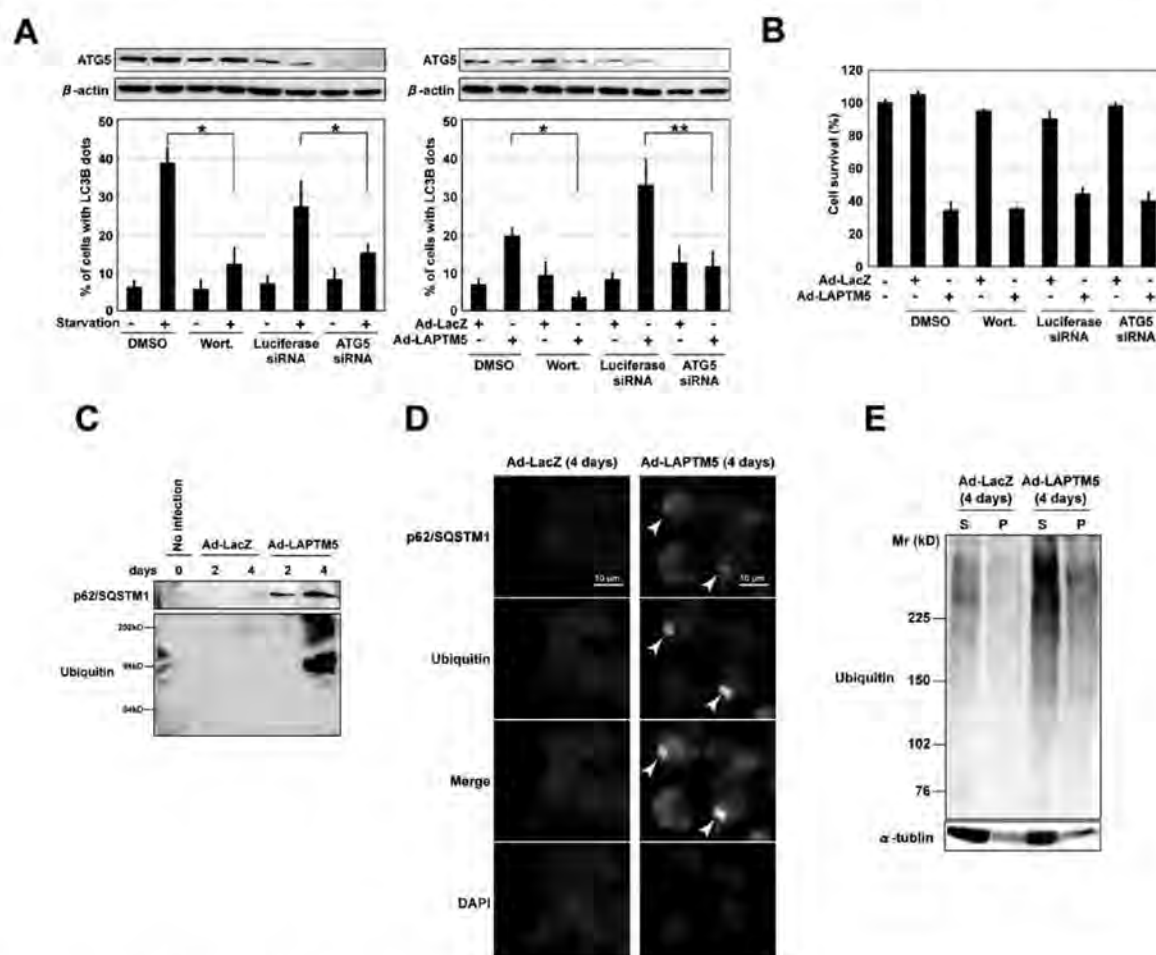


Figure 5. Interruption of autophagic flux during LAPTM5-induced cell death. (A) Effect of treatment with wortmannin or transfection with ATG5 siRNA in GOTO cells with a punctate distribution of LC3B. Cells (1×10^5 /well) were plated on coverslips in 24-well plates and the next day treated with wortmannin (Wort.; 200 nM) or DMSO (0.02%), or transfected with ATG5 siRNA (20 nM) or Luciferase siRNA (20 nM). Left; 4 days after the treatment or transfection, cells were treated with EBSS for 2 hours. Right; the plated cells were infected with Ad-LacZ or Ad-LAPTM5 at a MOI of 10 for 4 days with treatment with DMSO or wortmannin, or with transfection with Luciferase or ATG5 siRNA. Then, cells were fixed in 10% TCA, reacted with the LC3B antibody, and visualized with an FITC-conjugated secondary antibody. Upper; western blotting analysis of ATG5. Whole-cell lysate was analyzed by immunoblotting with an antibody to ATG5 or β -actin (internal control). Lower; frequency of cells showing a punctate distribution of LC3B among cells (at least 200 cells) was measured. *t-test, $p < 0.001$ and ** $p < 0.01$. Vertical lines, SD for three experiments. (B) Effect of treatment with wortmannin or the knockdown of ATG5 during LAPTM5-induced cell death. GOTO cells (1×10^4 /well) were plated in 96-well plates and infected with Ad-LacZ or LAPTM5 at a MOI of 10 with treatment with DMSO or wortmannin (Wort.), or with transfection with Luciferase or ATG5 siRNA. Four days after infection, numbers of viable cells were assessed by WST assay. Vertical lines, SD for three experiments. (C) Western blot analysis of p62/SQSTM1 and ubiquitin in LAPTM5-infected GOTO cells. The same whole-cell lysates indicated in Figure 3A were analyzed by immunoblotting with indicated antibodies. The results shown represent two independent experiments. (D) Immunofluorescence microscopy for p62/SQSTM1 and ubiquitin in LAPTM5-infected GOTO cells. Upper; GOTO cells (1×10^5 /well) were plated on coverslips in 24-well plates, and infected with Ad-LAPTM5 at a MOI of 10. Four days after infection, the cells were fixed in 4% formaldehyde, reacted with p62/SQSTM1 and ubiquitin antibodies, and visualized with an FITC- or Alexa Fluor 594-conjugated secondary antibody. Arrowheads indicate the cells with p62/SQSTM1-ubiquitin positive inclusion-like body. DAPI was used for counterstaining. (E) Western blotting of ubiquitinated proteins. Four days after infection, GOTO cells were lysed in a 0.1% Triton-X solution. The Triton-insoluble pellet (P) was lysed in a 2% SDS buffer. The Triton-X soluble (S) or -insoluble (P) lysate was loaded on a 6% SDS-PAGE gel and analyzed by immunoblotting with an antibody to ubiquitin or α -tubulin. For both soluble and insoluble samples, ubiquitinated proteins were found to be accumulated in Ad-LAPTM5-infected GOTO cells, compared with Ad-LacZ-infected GOTO cells. The results shown represent two independent experiments.

doi:10.1371/journal.pone.0007099.g005

frequency of LAPTM5-induced cell death was not affected (**Figure 5B**), indicating that LAPTM5-induced cell death is not "so-called autophagic cell death" [23] and the appearance of autophagic vacuoles during LAPTM5-induced cell death may result in the accumulation of immature autophagic vacuoles due to an interruption of basal autophagic flux.

Accumulating evidence suggests that p62/SQSTM1 and some ubiquitinated proteins are degraded during the autophagic process by which p62/SQSTM1 recruits ubiquitinated proteins into the autophagosome through interaction directly with LC3 protein to be degraded by autophagy [24–26]. In addition, the genetic disruption of autophagic flux in mouse neurons led to the accumulation of p62/SQSTM1 and ubiquitinated proteins and the formation of inclusion bodies with these proteins, resulting in a loss of neurons by cell death [27,28]. To further confirm that basal autophagic flux is interrupted during LAPTM5-induced cell death, we examined levels of p62/SQSTM1 protein and ubiquitinated proteins. As expected, a remarkable accumulation of both p62/SQSTM1 and ubiquitinated proteins was observed on western blotting (**Figure 5C**) and immunofluorescence analysis (**Supplementary Figure S8**). These proteins were frequently co-localized as inclusion-like bodies (**Figure 5D**) and ubiquitinated protein levels were increased in the Triton-X insoluble fraction, not only the soluble fraction, in Ad-LAPTM5-infected GOTO cells (**Figure 5E**). We also confirmed that p62/SQSTM1 and GFP-LC3 were occasionally co-localized to cytoplasmic spots (or ring-like structures) as autophagosomes in Ad-LAPTM5-infected GOTO cells (data not shown). These findings strongly suggest that overexpression of LAPTM5 leads to an interruption of basal autophagic flux, and results in the accumulation of p62/SQSTM1 and ubiquitinated proteins, as well as of immature autophagic vacuoles, that is, "cell death with impaired autophagy" [23].

Accumulation of LAPTM5-positive vesicles during LAPTM5-induced cell death

LAPTM5 is a multispanning transmembrane protein that resides in lysosomes [29]. Further, it has been demonstrated that LAPTM5 contributes to vesicle trafficking from the Golgi apparatus to the lysosome [30]. Therefore, we investigated the subcellular distribution of LAPTM5 in cells together with that of Golgi-58K (Golgi marker) or LAMP2 (Lysosome marker) by confocal microscopy. As shown in **Figure 6A**, the exogenously expressed LAPTM5 was localized to vesicles and exhibited a punctuate pattern, and the LAPTM5-positive vesicles did not colocalize with the Golgi apparatus, but partially colocalized with LAMP2-positive lysosomes 1 day after the infection with Ad-LAPTM5. Four days after the infection, LAPTM5-positive vesicles were remarkably accumulated as larger entities in dying cells and colocalized with neither the Golgi apparatus nor LAMP2-positive lysosomes. Rather, Golgi-58K-positive structures and LAMP2-positive punctuate pattern were shown to be reduced in dying cells with a strong accumulation of LAPTM5-positive vesicles.

Since treatment with lysosomal or proteasomal-degradation inhibitors significantly enhanced LAPTM5-induced cell death combined with the accumulation of exogenously expressed LAPTM5 (**Figure 3D and 3E**), we next examined the subcellular localization of accumulated LAPTM5 under such conditions. LAPTM5 protein was remarkably accumulated as large vesicles in Ad-LAPTM5-infected GOTO cells treated with 10 nM BafA1 or 10 μ M ALLN (**Figure 6B**) for one day, similar to the pattern observed 4 days after the infection with Ad-LAPTM5 (**Figure 6A**). In addition, a reduction in Golgi-58K-positive structure and LAMP2-positive punctuate pattern was also observed in dying

cells with a strong accumulation of LAPTM5-positive vesicles. Alternatively, when GOTO cells were infected with Ad-LAPTM5 for 2 days under mild treatment with 2 nM of BafA1 or 2 μ M of ALLN, LAPTM5-positive vesicles were frequently co-localized with LAMP2-positive lysosomes (**Supplementary Figure S9**). Based on these findings, it is considered that LAPTM5 intrinsically localizes to trafficking vesicles from Golgi to lysosomes in NB cells, and an increase of LAPTM5 protein leads to the production of LAPTM5-positive vesicles. Further the gradual accumulation of these vesicles by consecutive overexpression of LAPTM5 and/or a treatment with lysosomal or proteasomal inhibitor leads to losses of the Golgi apparatus and punctate pattern of lysosomes. Consequently, the accumulation of LAPTM5-positive vesicles might lead to lysosomal destabilization.

Induction of lysosomal destabilization with lysosomal-membrane permeabilization (LMP) during LAPTM5-induced cell death

Based on the results of the immunofluorescence analysis (**Figure 6**), we examined whether lysosomal destabilization occurs during LAPTM5-induced cell death. Along with the loss of a punctuate pattern of LysoTracker Rhodamine (LTR) staining (Pale cells) which reflects lysosomal destabilization via lysosomal-membrane permeabilization (LMP) [31–35], we observed the loss of the punctuate pattern in proportion to an increase in cell death among LAPTM5-infected GOTO cells (2.7-fold in GOTO, $p=0.0007$, compared with Ad-LacZ; **Figure 7A** and **Supplementary Figure S10**). In addition, we found a diminution in acridine orange (AO) uptake [31], another indicator for LMP, during LAPTM5-induced cell death, in a FACS analysis ($p=0.0001$ in Ad-LAPTM5-infected GOTO cells compared to those infected with Ad-LacZ; **Figure 7B**). Since lysosomal destabilization with LMP leads to the leakage of enzymes from the lysosome into the cytosol, we examined the subcellular distribution of cathepsin D (CTSD), a lysosomal enzyme [32]. The number of cells leaking CTSD into the cytosol was significantly increased among Ad-LAPTM5-infected GOTO cells compared with Ad-LacZ-infected GOTO cells ($p=0.0388$) (**Figure 7C**). In addition, we also observed that the fluorescein isothiocyanate-labelled dextran (FITC-dextran; 40kD), which was incorporated intact lysosomes, also was leaked into the cytosol (**Supplementary Figure S10** and **Supplementary Methods S1**) [31]. Moreover, treatment with ciprofloxacin (CPX), a known inducer of LMP [30], also resulted in the presence of the GFP-LC3-II form and the accumulation of p62/SQSTM1 proteins (**Supplementary Figure S11**). Taken together, these findings suggest the accumulation of LAPTM5 in NB cells to cause lysosomal cell death due to lysosomal destabilization with LMP. The lysosomal dysfunction caused by LAPTM5-mediated LMP might lead to an interruption to basal autophagy flux, probably resulting in the increased number of immature autophagic vacuoles.

To confirm whether levels of CTSD, p62/SQSTM1, and ubiquitinated proteins are increased in degenerating NB cells as observed *in vitro*, we performed an immunohistochemical analysis using each specific antibody in primary NB tumors. As shown in **Figure 7D**, levels for each of these proteins were remarkably increased in degenerating NB cells within regressing areas, compared with levels in non-degenerating NB cells, in the mass-screened NB tumors. Notably, ubiquitin-positive inclusion bodies were occasionally observed in degenerating NB cells. In addition, the CTSD protein appeared to fill the cytoplasm. These observations suggest that degenerating NB cells accumulating LAPTM5 protein undergo lysosomal cell death with LMP and

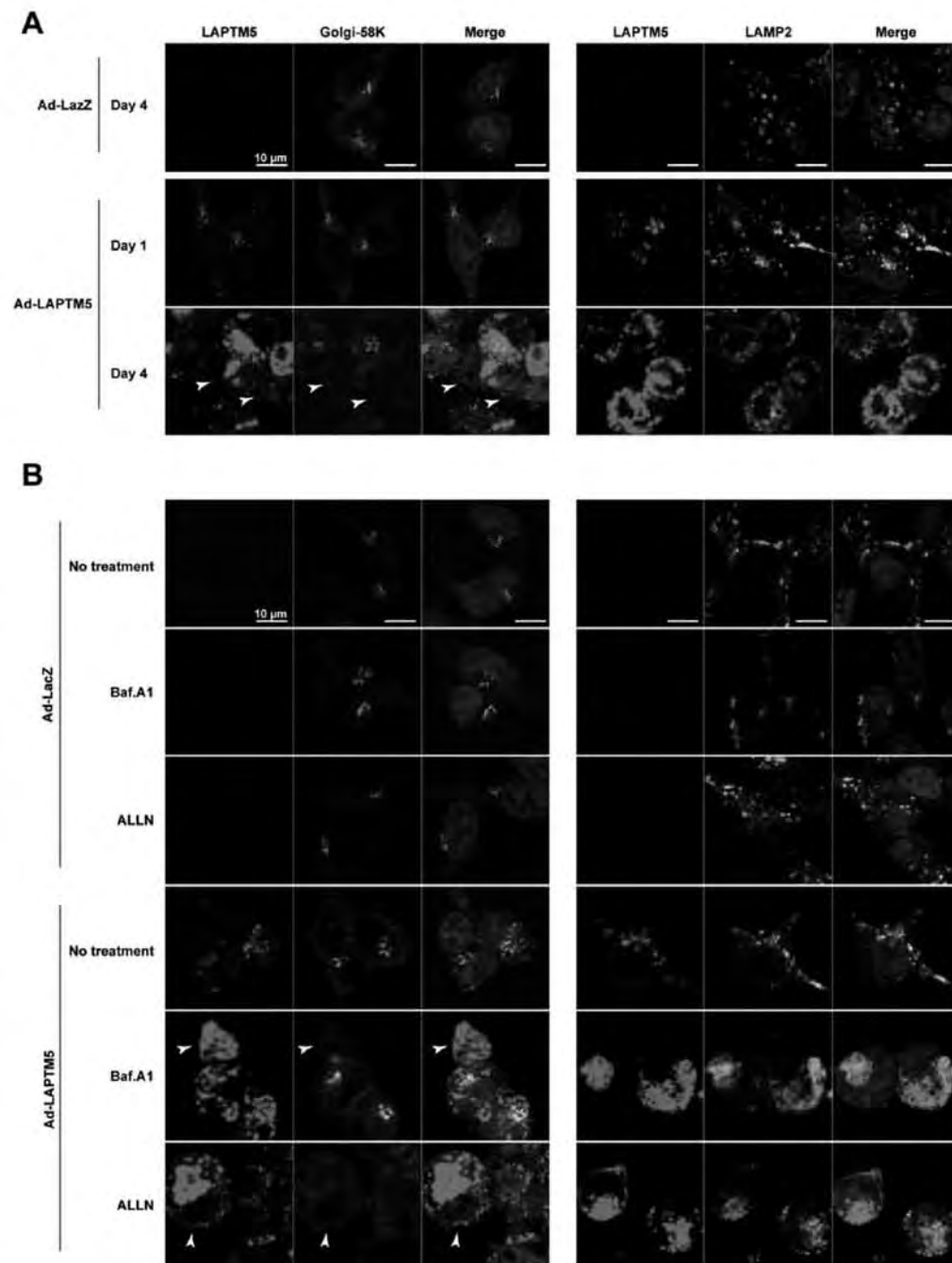


Figure 6. Localization of accumulated LPTM5 during LPTM5-induced cell death. (A) Representative image of the co-staining of Golgi-58K or LAMP2 (Green) and LPTM5 (Red). GOTO cells (1×10^5 /well) were plated on coverslips in 24-well plates and the next day infected with Ad-LacZ or Ad-LPTM5 at a MOI of 10. One or four days after infection, the cells were fixed in 10% TCA, reacted with Golgi-58K or LAMP2 and LPTM5 antibodies, and visualized with FITC- or Alexa Fluor 594-conjugated secondary antibodies. DAPI was used for counterstaining. Arrowheads indicate the cells with a loss of Golgi apparatus structures. (B) Representative image of the co-staining of Golgi-58K or LAMP2 (Green) and LPTM5 (Red). GOTO cells were infected with Ad-LacZ or Ad-LPTM5 a MOI of 10, and next day treated with Bafilomycin A1 (Baf.A1) or ALLN for 1 day. Arrowheads indicate the cells with a loss of Golgi apparatus structures. Then immunofluorescent images were obtained as in (A).
doi:10.1371/journal.pone.0007099.g006

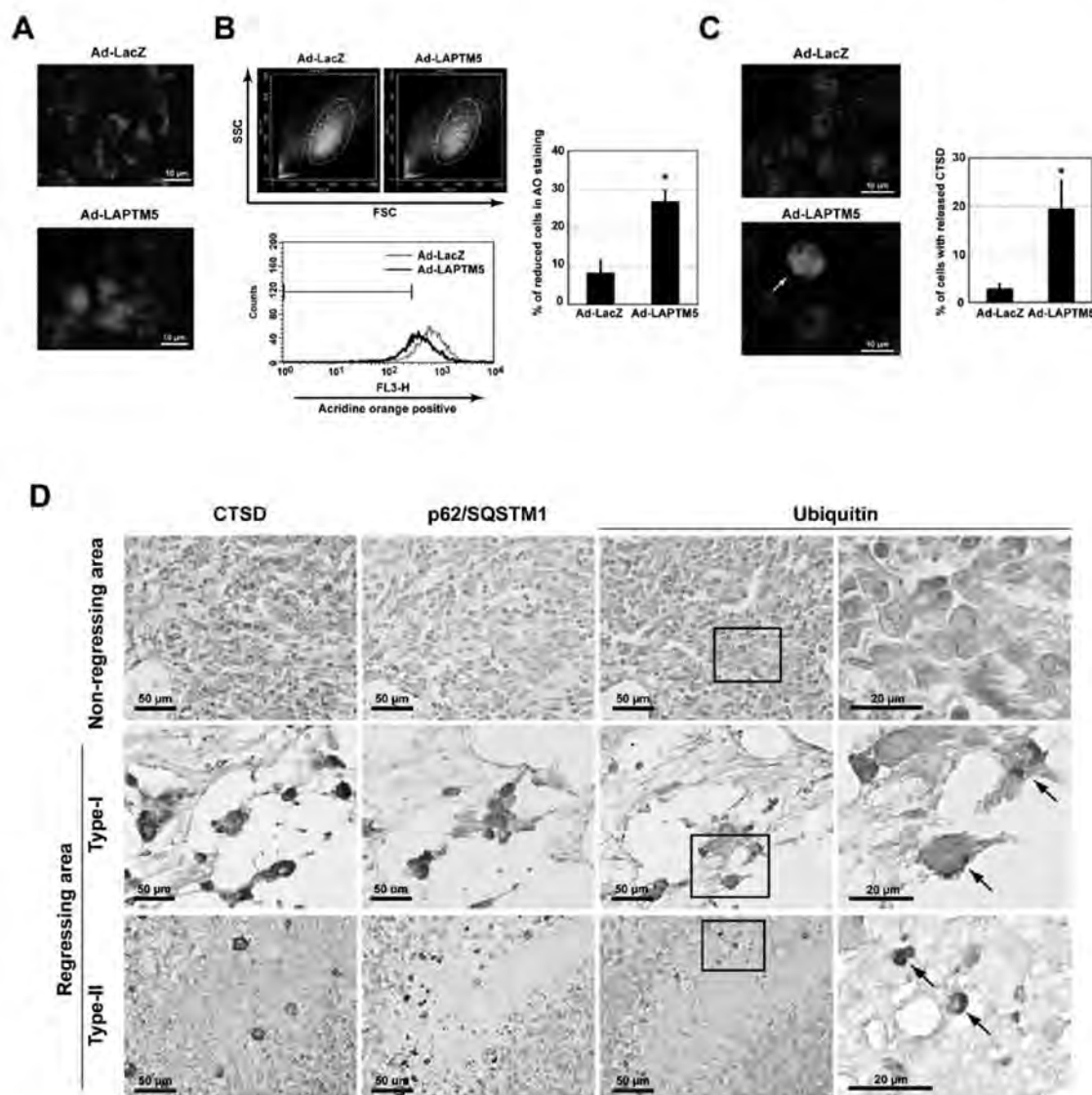


Figure 7. Induction of lysosomal-membrane permeabilization (LMP) during LAPTMS5-induced cell death. (A) Representative images of LysoTracker Rhodamine (LTR) staining in infected GOTO cells. GOTO cells (1×10^5 /well) were plated on coverslips in 24-well plates, and infected with Ad-LAPTMS5 at a MOI of 10. Four days after infection, cells were stained with LTR (100 nM) for 30 min at 37°C , washed twice and fixed in 4% formaldehyde, and observed by fluorescence microscopy. (B) Acridine orange (AO) uptake analysis in infected GOTO cells. GOTO cells (2×10^5 /well) were plated in 6 well plates, and infected with Ad-LAPTMS5 at a MOI of 10. Four days later, cells were stained with AO (5 $\mu\text{g}/\text{ml}$, 30 min). Detached cells were removed, and attached cells were collected by trypsinization and washed twice with PBS. Left-upper; scatter blots of FSC and SSC for Ad-LacZ or Ad-LAPTMS5-infected cells. The main population of cells was gated and analyzed by FACS. Left-lower; the intensity of staining was measured by FACS using a channel of FL3; the range containing $>99\%$ of the cells without AO fluorescence was gated. Black line indicates Ad-LAPTMS5-infected cells; red line, Ad-LacZ-infected cells. The frequency of cells with a reduction in AO staining was increased among Ad-LAPTMS5-infected GOTO cells. Right; percentage of cells with a reduction in AO fluorescence. Vertical lines, SD for four separate experiments. **t*-test, $p < 0.01$. (C) Representative images of staining for cathepsin D (CTSD) in infected GOTO cells. GOTO cells (1×10^5 /well) were plated on coverslips in 24-well plates, and the next day infected with Ad-LacZ or Ad-LAPTMS5 at a MOI of 10. Four days after infection, the cells were fixed in 10% TCA, reacted with a CTSD antibody, and visualized with an Alexa Fluor 594-conjugated secondary antibody. The percentage of cells that released CTSD (arrow) was measured. Vertical lines, SD for three separate experiments. **t*-test, $p < 0.05$. (D) Representative images of staining for CTSD, p62/SQSTM1, or ubiquitin in non-regressing or regressing areas within favorable NB tumors. Serial tumor sections were stained with each antibody. The area enclosed by the rectangle is enlarged at the right. Arrows indicate cells with ubiquitin-positive inclusion bodies.

impaired autophagy, and this process is closely associated with the PCD of NB cells during the spontaneous regression of favorable NB tumors.

Discussion

In the present study, the BAMCA method revealed that *LAPTM5* was highly methylated and its expression was transcriptionally down-regulated in NB cell lines. Unexpectedly, the methylation/down-regulation of this gene was detected in all the primary NB tumors and cell lines examined, and we further could detect no difference in methylation status and expression level between favorable and unfavorable NB tumors. Based on our findings that the mRNA level of *LAPTM5* restored after treatment with 5-aza-dC was still lower than in normal adrenal glands and the frequency with which *LAPTM5* was methylated was decreased in benign GNs, we conclude that the methylation of *LAPTM5* in NB cells is not aberrant methylation for an irreversible shut-off of the expression as occurs in CpG islands of classical tumor suppressor genes (indeed *LAPTM5* has no CpG islands) and may contribute to maintaining a constitutively down-regulated state and/or prevent leaking of the expression of this gene under conditions without transcriptional activation in an NB cell lineage-specific manner. Indeed, a recent report also found a decrease in the methylation of *LAPTM5* during normal lung development and in correlation with the differentiation state of lung tumors [36].

One key finding of the present study is that *LAPTM5*-mediated programmed cell death (PCD) was closely associated with the spontaneous regression of mass-screened NB tumors. As illustrated in **Figure 8**, although *LAPTM5* expression usually appears to be down-regulated through DNA methylation in both favorable and unfavorable NBs, it is up-regulated in degenerating NB cells within

locally limited regressing areas of favorable NBs. Our immunohistochemical analyses revealed that *LAPTM5*-positive degenerating NB cells were frequently detected in mass-screened NB tumors, but not in clinically detected unfavorable tumors, establishing a clear correlation between *LAPTM5*-mediated PCD and the propensity of NB tumors to undergo regression. The mass-screened NB tumors contained *LAPTM5*-positive degenerating NB cells, nonetheless we could not detect a significant difference in the mRNA expression of this gene between favorable and unfavorable tumor samples, suggesting the up-regulation of *LAPTM5* expression to be involved in the pro-death role in the late phase of PCD in regressing tumors and *LAPTM5*-positive degenerating NB cells are a small proportion in mass-screened NB tumors.

Our observations also revealed that the *LAPTM5* protein to be more significantly accumulated in degenerating NB cells than differentiating NB cells and the accumulation to be required to induce cell death in NB cells. Our *in vitro* study showed that the consecutive overexpression of *LAPTM5* led to the accumulation of *LAPTM5*-positive vesicles and the accumulation was enhanced by treatment with inhibitors for either the lysosomal or proteasomal pathway. Moreover, under cellular stress caused by treatment with a neurotoxin (such as 1-methyl-4-phenylpyridinium; MPP⁺) or H₂O₂, or on cell differentiation induced by treatment with retinoic acid (RA), we found a remarkable increase of *LAPTM5* expression at the transcriptional level. In addition, we showed an accumulation of *LAPTM5* protein level in RA-induced differentiated IMR32 cells treated with BafA1 or ALLN (**Supplementary Figure S12** and **Supplementary Methods S1**). Thus, the results suggest that lysosomal or proteasomal degradation of *LAPTM5*, whose impairment might enhance the accumulation of the protein and/or *LAPTM5*-positive vesicles, in addition to the

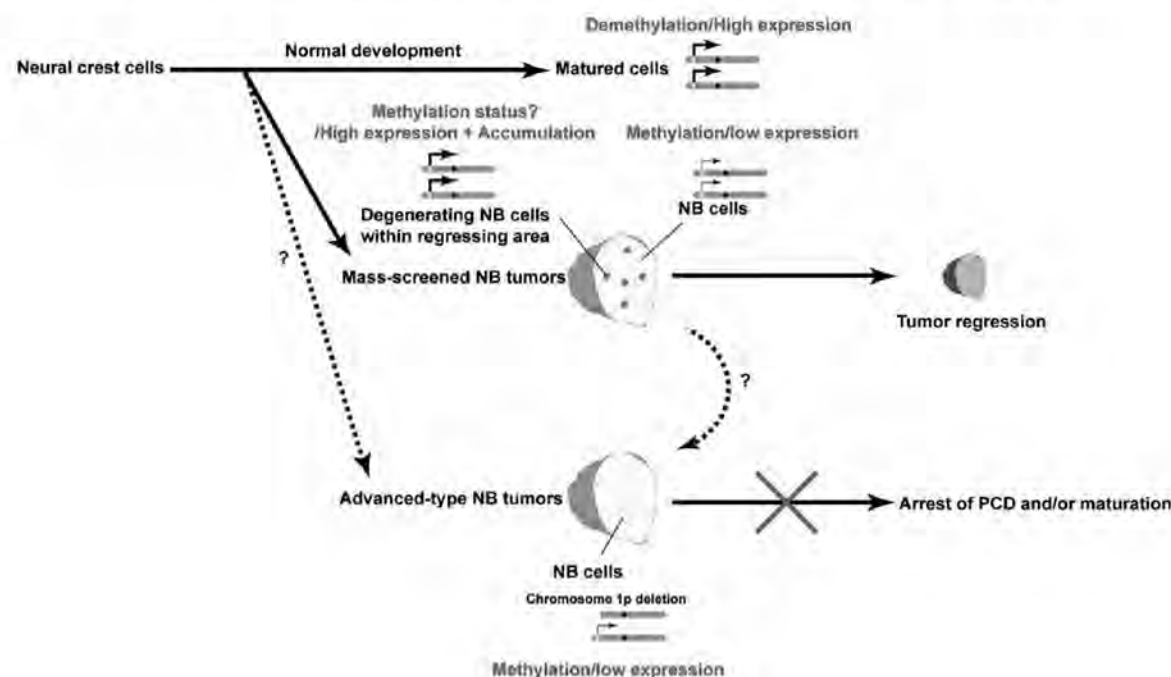


Figure 8. Model of the relationship between *LAPTM5*-mediated degeneration and propensity for spontaneous regression of NB tumors.

doi:10.1371/journal.pone.0007099.g008

consecutive transcriptional activation of *LAPTM5* by cellular stress, also plays a critical role in degeneration and cell death in NB cells. Indeed, the spontaneous regression of clinically favorable NB tumors is known to occur over a period of several months [4,14–17].

Advanced-type NB tumors are presumed to have a very low chance of regressing, and the final outcome for any NB tumor is likely to be attributable to cytogenetic aberrations as well as biological differences [1–3]. Deletion of the short arm of chromosome 1 (1p), observed in about 40% of NBs, is strongly associated with a poor prognosis, and highly associated with *MYCN* amplification, which is itself a strong indicator of a poor outcome for advanced-type NB tumors [1–3,37]. Accumulating evidence suggests that multiple candidates, including *p73*, *CDH5*, and *KIF1B*, for genes having a NB-suppressive role within the 1p36-critical region [1–3,38–40]. In addition, some of the 1p deletions in *MYCN*-amplified NB tumors are quite large, involving a proximal segment spanning 1p32–p36; tumors having this extensive loss of 1p make up a subset of advanced-type NBs with a poorer prognosis [41,42]. *LAPTM5* is mapped at 1p35, not at 1p36, and the copy-number of the *LAPTM5* gene locus is also frequently decreased in NB cell lines (Supplementary Figure S2). Therefore, the decrease of *LAPTM5* gene dosage may also act to prevent accumulation of LAPTM5-positive vesicles and LAPTM5-mediated PCD in advanced-type NB tumors with a large deletion of 1p.

A second key finding is that the cell death mediated by the accumulation of LAPTM5 protein in NB cells is a lysosomal cell death with the typical features of lysosomal destabilization through LMP and with the impaired autophagy in a caspase-independent manner, as a molecular mechanism for spontaneous regression of NB tumors. At this time, it is not clear how the accumulated LAPTM5 contributes to the lysosomal destabilization in degenerating NB cells and how the non-accumulated LAPTM5 functions in differentiating NB cells, adrenal medulla cells, or ganglion cells in GNS. A recent report demonstrated that LAPTM5 plays an important role in the lysosomal degradation of specific substrates in T cells [43]. Therefore, in “differentiating NB cells” or “matured neuroblastic cells” as well as in T cells, LAPTM5 may also function in the lysosomal degradation system for specific substrate(s). Our *in vitro* study showed that LAPTM5 intrinsically localizes to trafficking vesicles from the Golgi apparatus to the lysosomes in NB cells, and consecutive overexpression of LAPTM5 leads to the accumulation of LAPTM5-positive vesicles together with losses of the Golgi apparatus and punctate pattern of lysosomes. It has been reported that LAPTM5 contributes to vesicle trafficking from the Golgi apparatus to lysosome [30]. In addition, lysosomal membrane proteins such as LAMP1 and LAMP2 were transported from the Golgi apparatus to the lysosomes [44]. Therefore, the accumulation of LAPTM5-positive vesicles may lead to a disruption of intracellular vesicle trafficking in the Golgi-lysosome pathway, resulting in lysosomal destabilization, accompanied by interruption of provision of lysosomal contents into the lysosomes, in “degenerating NB cells”. Interestingly, a recent report showed that a down-regulation of lysosomal membrane proteins, LAMP1 and LAMP2, increased sensitivity to the lysosomal cell death and those accumulation induced by inhibition of lysosomal proteases contribute to the resistance to lysosomal cell death [45].

On the other hand, our study also revealed that the lysosomal disruption by treatment with lysosomal inhibitor led to the accumulation for these vesicles (by a decrease of removal in the lysosomes), although LAPTM5-positive vesicles were usually transported into the lysosomes, and to be degraded. A dysfunction

of proteasomal protein degradation also led to the accumulation of LAPTM5-positive vesicles. Thus, this protein may be also degraded by ubiquitin-proteasome system to regulate the production of LAPTM5-positive vesicles. Indeed, LAPTM5 protein can be ubiquitinated by NEDD4, an E3 ubiquitin ligase [30].

This cell death is also characterized by the accumulation of autophagic vacuoles and ubiquitinated proteins and the occasional formation of ubiquitin-positive inclusion bodies as occurs in neurodegenerative diseases (NDs) [46], suggesting that a common molecular mechanism underlies the degeneration of cells in the regression of NB tumors and in NDs. We consider the ND-like features of degenerating NB cells attributable to an interruption of autophagic flux caused by a loss of intact lysosomes through LAPTM5-mediated lysosomal destabilization, although we can not exclude the existence of some other mechanism, given results of studies where autophagic flux or lysosomal degradation were genetically disrupted in mice [27,28].

Finally, it has been reported that H-Ras is also highly expressed in degenerating NB cells and its overexpression can induce caspase-independent cell death with autophagic vacuoles in NB cells [12]. However, it has been not clarified whether this cell death is attributable to an interruption of autophagic flux. Clarification of the relationship between H-Ras and LAPTM5 in signal transduction will require further examination.

Methods

Cell lines and tumor samples

All 10 human NB cell lines used (GOTO, IMR32, SJ-N-CG, CHP134, MP-N-MS, KP-N-RT, SK-N-AS, SH-SY5Y, SK-N-SH, and SK-N-KP) had been established from surgically restricted tumors, and maintained as described elsewhere. Primary samples were obtained during surgery from NB patients undergoing tumor resection at University Hospital, Kyoto Prefectural University of Medicine from 1986 to 2003, with written consent by the parents of each patient in the formal style and after approval by the local ethics committee. Staging was evaluated according to the criteria of the International Staging System (INSS) [20]. Patients were treated according to previously described protocols [20]. Tumor samples were frozen immediately and stored at -80°C until required.

Cell culture and treatments

All cell lines were grown in RPMI1640 medium supplemented with 10% FCS, penicillin, and streptomycin. Earle's Balanced Salt Solution (EBSS) was from Invitrogen. For treatment with drugs in cell cultures, wortmannin (Sigma), zVAD-fmk (Peptide Institute), Bafilomycin A1 (Sigma), ALLN (Calbiochem), NH_4Cl (Wako), and MG-132 (Calbiochem) were used.

Generation of specific antibody for LAPTM5

An anti-LAPTM5 polyclonal antibody against a peptide, CEEALSLPSKTPEGG, from the carboxyl terminus was generated in rabbits (Qiagen), and affinity-purified.

DNA methylation analysis

For bisulfite sequencing, genomic DNA was treated with sodium bisulfite and amplified with primer sets for sequences of interest. PCR products were sub-cloned and sequenced.

To investigate methylation status in primary tumor samples, methylation-sensitive single nucleotide primer extension (MS-SNuPE) was performed [47]. Genomic regions containing two CG sites were amplified using sodium bisulfite-treated DNA; the PCR products were purified from agarose gels and used as

templates for analyzing methylation using Ms-SNuPE primers specific for each site. The MS-SNuPE products were run on 15% polyacrylamide gels, and the resulting signals were quantified with a Phosphorimager analysis system (Molecular Dynamics). Methylation values were calculated based on results from two CG sites, according to the following equation: $[\text{methylated C}/(\text{methylated C} + \text{unmethylated T})] \times 100$. Primer sequences used in the analysis are provided in **Supplementary Table S3**.

Reverse Transcription (RT)-PCR

Single-stranded cDNA generated from total RNA [20] was amplified with a primer set specific for the gene being examined. Real-time quantitative PCR experiments were done on an ABI-7900 with TaqMan probes (Applied Biosystems). The gene encoding glyceraldehyde-3-phosphate dehydrogenase (*GAPDH*) served as an endogenous control. Each sample was normalized on the basis of its *GAPDH* content. Primer sequences are provided in **Supplementary Table S3**.

Immunohistochemistry

Sections from paraffin-embedded tumor samples were deparaffinized by xylene, and rehydrated in ethanol. After the retrieval of antigens by boiling in 10 mM citrate buffer (pH 6.0), the sections were treated with 0.3% hydrogen peroxide in methanol to inactivate the endogenous peroxidase. Then, the sections were incubated with an antibody against LAPTM5 (1:200), cleaved caspase-3 (1:200, Cell signaling), CD20 (BCA-B20; 1:10, kindly provided by Dr H. Tsuda), p62/SQSTM1 (1:200, Santa Cruz Biotechnology), ubiquitin (1:200, Dako), or cathepsin D (1:200, Chemicon) for 1 hour at room temperature. The bound antibody was visualized using diaminobenzidine as a chromogen (VECTASTAIN-Elite ABC kit, Vector Laboratories), and the sections were lightly counterstained with hematoxylin. The specificity of LAPTM5 immunostaining was confirmed by omission of the primary antibody, using rabbit preimmune-serum as the primary antibody, or by the immunoblotting method.

Western blotting

Whole-cell extracts were prepared in RIPA buffer containing a proteinase inhibitor cocktail (Roche). Western blotting was performed as described previously [20]. Antibodies against LAPTM5 (1:1000), MYCN (1:500, Santa Cruz Biotechnology), p62/SQSTM1 (1:1000), ubiquitin (1:1000), ATG5 (1:500, Abgent), LC3B (1:4000, Sigma), β -actin (1:4000, Sigma), and GFP (1:1000, MBL) were used according to the manufacturer's instructions. As an internal control for western blotting, the blots were stripped and reprobed with a monoclonal antibody against β -actin (Sigma).

Isolation of cells stably expressing GFP-LC3

The GFP-LC3 expression vector was kindly provided by Dr T. Yoshimori. Cells were transfected with GFP-LC3 using Lipofectamine 2000 (Invitrogen) according to instructions. Then they were cultured in the presence of G418 (Sigma) for 3 weeks and the resistant colonies pooled in a mass were used as the cells stably expressing GFP-LC3.

Immunofluorescence microscopy

The cells were fixed in 4% formaldehyde or 10% trichloroacetic acid (TCA), permeabilized with 0.2% Triton X-100 and treated with blocking solution (1% BSA/0.01% Triton X-100 in PBS), and then incubated at 37°C with the primary antibody for 3 hours or overnight. The bound antibody was visualized using a FITC-

conjugated or Alexa Fluor 594-conjugated secondary antibody. After mounting with DAPI (4',6'-diamidino-2-phenylindole) to stain nuclei, the cells were observed under a fluorescence microscope (ECLIPSE 800; Nikon) or a confocal microscopy (Carl Zeiss). Antibodies against LAPTM5 (1:200), LC3B (1:1000), p62/SQSTM1 (1:200), ubiquitin (1:200), Golgi-58K (1:200, Sigma), and cathepsin D (1:200) were used according to the manufacturers' recommendations.

RNA interference

The siRNAs for LAPTM5 (siGENOME SMARTpool M-019880) and for Control (siControl, Non-targeting siRNA #2) were from Dharmacon. The siRNAs for Luciferase (CGUACGCGGAUACUUCGA) and for ATG5 (GCAACUCUGGAUGGGAUUC) were from Sigma. The siRNAs were transfected into cells using Lipofectamine RNAi MAX (Invitrogen) according to the manufacturer's directions and after 4–6 hours, the medium was renewed.

Recombinant Adenovirus

The replication-defective recombinant adenovirus was constructed with the Adenovirus Expression Vector Kit (Takara) following the manufacturer's recommendations. Cosmid vector-inserted full-length LAPTM5 cDNA (pAxCawit-LAPTM5) was generated and the adenovirus was propagated in HEK293 cells, and stored at -80°C prior to use. As a control, an Ad-LacZ adenovirus encoding the β -galactosidase gene was constructed from the cosmid pAxCaiLacZ (TaKaRa). Viral titers were measured in pfu/ml by a limiting-dilution method using the HEK293 cells. Cells were infected with each MOI (multiplicity of infection; PFU/cell). Primer sequences for the construction of vectors are provided in **Supplementary Table S3**.

Cell death and survival assays

For the cell death assay, numbers of dead cells were determined using the trypan blue exclusion method. A minimum of 100 cells were counted in each experiment. For cell survival assay, numbers of viable cells were assessed by a colorimetric water-soluble tetrazolium salt assay (WST assay, cell counting kit-8; Dojindo Laboratories).

Electron microscopy

The cells were fixed with 2.5% glutaraldehyde in 0.1 M phosphate-buffered saline (PBS) overnight. They were washed with 0.1 M PBS at 4°C and post-fixed with 1% OsO_4 buffered in 0.1 M PBS for 2 h. Then the cells were dehydrated in a graded series of ethanol solutions and embedded in Epon 812. Ultrathin (90 nm) sections were collected on copper grids, double-stained with uranyl acetate and lead citrate, and examined by transmission electron microscopy (H-7100, Hitachi).

LysoTracker Rhodamine (LTR) staining and Acridine orange (AO) uptake analysis

For LTR staining, the cells were stained with 100 nM of LTR (Molecular Probes) for 30 min at 37°C. After two washes with PBS, the cells were analyzed by fluorescence microscopy for LTR. For AO uptake analysis, the cells were stained with 5 $\mu\text{g}/\text{ml}$ of AO (Sigma) for 30 min at 37°C. Then, detached cells were removed, attached cells were collected by trypsinization and washed twice with PBS. The cells untaken AO were detected by flow cytometry using a FACScan (Becton-Dickinson).

Statistical analysis

The results of quantitative *in vitro* analyses are presented as the mean and SD. Differences were compared with a two-sided test (Student's *t*-test).

Supporting Information

Methods S1 Supplementary methods and Supplementary references

Found at: doi:10.1371/journal.pone.0007099.s001 (0.03 MB DOC)

Table S1 List of BACs containing possibly methylated regions in NB cell lines compared to PBMNCs by BAMCA analysis a; Distance from the top of short arm on chromosome 1. b; BAMCA ratios were indicated by resulting for duplicate spots (1 and 2). c; The presence ("yes") or absence ("no") of expression for each gene was determined by RT-PCR as indicated in Supplementary Figure S1. d; The presence ("yes") or absence ("no") of differential methylation in *Sma*I sites for each gene was determined by MS-PCR as indicated in supplementary Figure S1. e; The methylation status of LPTM5 in primary NB tumors was determined by COBRA as indicated in supplementary Figure S1. "-" indicates "not tested".

Found at: doi:10.1371/journal.pone.0007099.s002 (0.02 MB DOC)

Table S2 Summary of copy-number aberrations for MYCN, LPTM5, and 1p35 region in 13 NB cell lines a; Copy-number status for MYCN gene locus and 1p35 region was determined by array-CGH and conventional CGH analysis. "yes" indicates the presence of MYCN amplification or 1p35 loss, and "no" indicates the absence of them. b; Two probes were used for FISH analysis. 418B22 (BAC clone), spotted on 1p36-contig array, is mapped on 1p35 and contain LPTM5 gene locus. The pUC1.77 (plasmid) as a control is mapped on the pericentromeric region of chromosome 1.

Found at: doi:10.1371/journal.pone.0007099.s003 (0.02 MB DOC)

Table S3 Primer sequences

Found at: doi:10.1371/journal.pone.0007099.s004 (0.02 MB DOC)

Figure S1 Validation of candidate genes down-regulated through DNA methylation (A) Schematic diagram of BAMCA experiments. DNA fragments generated by the MCA method from NB cell lines (Green) and from the references (Red) were labeled with Cy3 or Cy5 respectively, and co-hybridized on the in-house 1p35-p36 contig array. (B) Screening of down-regulated genes by RT-PCR analysis. GAPDH served as an internal control. Adr, normal adrenal glands; S1 NBs, pooled samples from five stage-I NB tumors. (C) Determination of methylation status of *Sma*I sites within 418B22, a BAC clone that includes LPTM5, by MS-PCR in PBMNCs and the two NB cell lines GOTO and IMR32. Sixteen primer sets were used for PCR in genomic regions including at least two *Sma*I sites in a distance range of 200–2,000 bp, because the MCA procedure produced a genomic fragment having two adjacent methylated *Sma*I sites at each end. Black and white circles indicate the presence (methylated) or absence (unmethylated) of PCR products, respectively. The region (including no. 12–16) shown by a gray box indicates the NB-specific methylated region at the LPTM5 locus. (D) Determination of methylation status at CG sites around the transcriptional-start site of the LPTM5 gene by bisulfite sequencing. A total of 32 CG sites within 1 kb of the start site were analyzed using two primer sets (regions-I and -II). An arrow at the start-site shows the direction of transcription. Arrowheads indicate two *Sma*I sites that located within the PCR product

produced by no. 14 primers, as indicated in (C). GOTO and IMR32 cells were both widely methylated, whereas PBMNCs and an EBV-transformed lymphocyte cell line (LCL) were almost completely unmethylated. (E) Representative images of COBRA for LPTM5 in primary NB tumors. Methylation of this gene was detected in regions-I and -II in all NB tumors examined. Bisulfite-PCR products for each of the two regions indicated in (D) were digested with *Hinf*I (region-I) and *Taq*I (region-II). Arrows indicate where bands would show the presence of methylation.

Found at: doi:10.1371/journal.pone.0007099.s005 (0.85 MB TIF)

Figure S2 Analysis of DNA copy-number aberrations in the 1p region in NB cell lines Frequency of 1p loss in NB cell lines revealed by array-CGH. In house "MCG cancer array-800"-spotted arbitrary BACs, including 43 BACs on 1p, were used for analyzing 13 NB cell lines (GOTO, IMR32, SJ-N-CG, CHP134, MP-N-MS, KP-N-RT, SMS-KCN, SK-N-DZ, SMS-KAN, SK-N-AS, SH-SY5Y, SK-N-SH, and SK-N-KP). The sideways red (4 non-amplified NB cell lines) or blue (MYCN-amplified NB cell lines) bars indicate frequencies of loss on each BAC, respectively. A large range of loss on 1p, including the LPTM5 locus, was detected frequently in MYCN-amplified NB cell lines.

Found at: doi:10.1371/journal.pone.0007099.s006 (0.93 MB TIF)

Figure S3 Methylation analysis in primary NB tumors and ganglioneuromas (GNs) by the methylation-sensitive single-nucleotide primer extension (Ms-SNuPE) method (A) Positions of primers used in the Ms-SNuPE analysis. Bisulfite-PCR products for region-I (indicated in Supplementary Figure S1) were obtained. Arrows indicate the position of each primer used in primer-extension experiments. When a CG site is methylated or unmethylated, either "C" or "T" is appended, respectively. (B) Representative image of the Ms-SNuPE analysis at the CG-II site. Purified bisulfite-PCR products (25 ng), a primer, and radioisotope-labeled C or T were reacted for primer extension; products were purified and loaded on polyacrylamide gels for electrophoresis (PAGE). A methylation value for each CG site was computed using the following equation: methylated C/(methylated C + unmethylated T) × 100. GN sample numbers, T830, T1052, and T334, reflect GN1, GN2, and GN3 in Figure 1D.

Found at: doi:10.1371/journal.pone.0007099.s007 (0.46 MB TIF)

Figure S4 Representative images from immunohistochemical staining for LPTM5, H-Ras, or CD20 (BCA-B20) in degenerating NB cells within regressing areas in mass-screened NB tumors (A) Representative images of immunostaining for each protein in regressing areas within sections from Stage-4S NB tumors detected by mass-screening. Serial tumor sections were stained with hematoxylin-eosin (HE) (left), with LPTM5 (middle), or with H-Ras antibody (right). Arrowheads indicate a degenerated area. (B) Representative images of CD20 (BCA-B20) staining in regressing areas within sections from Stage-1 NB tumors detected by mass-screening. Arrowheads indicate CD20-positive hematopoietic cells.

Found at: doi:10.1371/journal.pone.0007099.s008 (5.55 MB TIF)

Figure S5 Detection of cleaved caspase-3 during CDDP- or LPTM5-induced cell death (A) Representative image of cleaved caspase-3 staining. The cells (2 × 10⁵/well for CDDP, 1 × 10⁵/well for infection) were plated on coverslips in 24-well plates, and the next day treated with Cisplatin (CDDP; 1.5 μg/ml in SH-SY5Y cells) for 2 days or infected with Ad-LacZ or Ad-LPTM5 at a MOI of 10 for 4 days. Cells were fixed, reacted with an antibody to cleaved caspase-3, and visualized with a Alexa Fluor 594-conjugated secondary antibody. (B) Quantitation of the percentage of cleaved caspase-3-positive cells during cell death in NB cell lines including SH-SY5Y in (A). The percentage of cleaved caspase-3-

positive cells among all cells (at least 500 nuclei) was counted. Vertical lines, SD for three experiments. (C) Western blotting for cleaved caspase-3. The cells were treated as indicated in (A) and whole-cell lysate was analyzed by immunoblotting with an antibody to cleaved caspase-3 or β -actin (internal control). (D) Effect of zVAD-fmk treatment during CDDP-induced cell death in SH-SY5Y cells. SH-SY5Y (1×10^4 /well) cells plated in 96-well plates were treated with CDDP (1.5 μ g/ml) in the absence or presence of zVAD-fmk (100 μ M). The percentage of surviving cells was determined two days after treatment by WST assay. Vertical lines, SD for three experiments. *t-test, $p < 0.05$. Found at: doi:10.1371/journal.pone.0007099.s009 (1.16 MB TIF)

Figure S6 Appearance of autophagic vacuoles during LAPTM5-induced cell death in SH-SY5Y and GOTO cells stably expressing GFP-LC3. (A) Localization of endogenous LC3B detected by immunofluorescence microscopy. SH-SY5Y cells (1×10^5 /well) were plated on coverslips in 24-well plates, and the next day infected with Ad-LacZ or Ad-LAPTM5 at a MOI of 10. Four days later, the cells were fixed in 10% TCA 4 days after infection, reacted with the LC3B antibody, and visualized with an Alexa Fluor 594-conjugated secondary antibody. (B) Detection of LC3 form-II by western blotting. As the time-courses indicated, whole-cell lysate from SH-SY5Y cells (left) or GOTO cells stably expressing GFP-LC3 (right) infected with Ad-LacZ and Ad-LAPTM5 at a MOI of 10 was analyzed by immunoblotting with an antibody to endogenous LC3B, GFP, or β -actin (internal control). Arrows indicate form-I or -II of LC3B or GFP-LC3. Found at: doi:10.1371/journal.pone.0007099.s010 (0.98 MB TIF)

Figure S7 Representative images of the subcellular localization of GFP-LC3 or endogenous LC3B by immunofluorescence microscopy. GOTO cells stably expressing GFP-LC3 (A) or parental GOTO cells (B) were prepared and treated as described in Figure 4B. The number of cells with a GFP-LC3 or LC3B punctate pattern was decreased by treatment with wortmannin (Wort; 200 nM) or knockdown of ATG5 during starvation or LAPTM5-induced cell death. Found at: doi:10.1371/journal.pone.0007099.s011 (2.30 MB TIF)

Figure S8 Accumulation of p62/SQSTM1 protein in Ad-LAPTM5-infected GOTO cells. The accumulation of p62/SQSTM1 protein in Ad-LAPTM5-infected GOTO cells was revealed by immunofluorescence microscopy. Four days after infection, cells were fixed, reacted with an antibody to p62/SQSTM1, and visualized with Alexa Fluor 594-conjugated secondary antibody. The images were obtained with different exposure times (0.2 and 0.02 seconds for Ad-LacZ and Ad-LAPTM5-infected cells, respectively). Found at: doi:10.1371/journal.pone.0007099.s012 (0.64 MB TIF)

Figure S9 Subcellular localization of accumulated LAPTM5 during LAPTM5-induced cell death. Representative image of the co-staining of LAMP2 (Green) and LAPTM5 (Red). GOTO cells were infected with Ad-LacZ or Ad-LAPTM5 at a MOI of 10 in medium containing Bafilomycin A1 (BafA1, 2 nM) or ALLN (2 μ M) for 2 days. Immunofluorescence microscopy was performed as in Figure 6A. DAPI was counterstained. In GOTO cells subjected to mild treatment with BafA1 or ALLN, LAPTM5 was frequently localized into LAMP2-positive lysosomes. Found at: doi:10.1371/journal.pone.0007099.s013 (4.81 MB TIF)

Figure S10 Lysosomal membrane permeabilization (LMP) during LAPTM5-induced cell death. (A) Frequency of cells with loss of a punctate pattern of LTR staining. One or four days after infection with Ad-LacZ or Ad-LAPTM5, cells that had lost the punctate pattern of LTR staining, so-called "Pale cells", were

counted, and the number recorded as a percentage of all cells. The graph indicates the percentages of cells in both cell lines. Vertical lines, SD for three separate experiments. *t-test, $p < 0.001$, ** $p < 0.05$. No inf., no infection. (B) Representative images of staining for FITC-dextran (40 kD) in infected GOTO cells. GOTO cells (1×10^5 /well) were plated on coverslips in 24-well plates, and the next day infected with Ad-LacZ or Ad-LAPTM5 at a MOI of 10, and then maintained in medium containing 100 μ g/ml of FITC-dextran (40kD). Right; Four days after infection, cells were washed twice, fixed in 4% formaldehyde, and observed by fluorescence microscope. Left; The percentage of cells that released FITC-dextran (40 kD) among cells at least 200 cells was measured. Vertical lines, SD for three separate experiments. *t-test, $p < 0.05$. Found at: doi:10.1371/journal.pone.0007099.s014 (1.10 MB TIF)

Figure S11 Detection of GFP-LC3 form-II and accumulation of p62/SQSTM1 on treatment with Ciprofloxacin (CPX). GOTO cells stably expressing GFP-LC3 (1×10^6 /well) were plated in 6-well plates, and treated with CPX (100 or 300 μ g/ml) for one day. As a solvent for CPX, 0.1N HCl was added with 1 or 3% of the medium. Whole-cell lysate from treated cells was analyzed by immunoblotting with antibodies to the indicated proteins. Found at: doi:10.1371/journal.pone.0007099.s015 (0.43 MB TIF)

Figure S12 Detection of endogenous LAPTM5 by western blotting. (A) Relative levels of LAPTM5 mRNA levels during induction of differentiation in IMR32 cells. Cells were induced to neuronal differentiation by maintaining in serum-free medium including retinoic acid (RA, 10 μ M) for 4 days. The levels of LAPTM5 mRNA at the indicated days were determined by quantitative RT-PCR and normalized with each level of GAPDH mRNA. Vertical lines, SD. (B) Morphological change during RA-induced differentiation and treatment with lysosomal or proteasomal inhibitor. IMR32 cells (2×10^6 /well) were plated in 10 cm dishes and maintained in serum-free medium including RA (10 μ M) (SFRA). At 3 days after induction, BafA1 (25 nM) or ALLN (10 μ M) were added in medium and then cultured for 1 day. Treatment with SFRA efficiently induced the appearance of cells with a number of axonal outgrowth in IMR32 cells (a; parental IMR32 cells and b; differentiated IMR32 cells). Additional treatment with BafA1 (c) or ALLN (d) frequently induced cell death with a loss of axon. (C) Detection of endogenous LAPTM5 protein by western blotting. Cells were treated as indicated in (b). As a positive control for detection, whole-cell lysate from LCL highly expressing with or without BafA1 (10 nM, 1 day) or ALLN (10 μ M 1 day) was used. Arrows indicate bands for endogenous LAPTM5 detected in expected size. TBS buffer including 0.05% Tween-20 and 1% Casein was used for blocking and reaction with antibody. Endogenous LAPTM5 was detected in expected size. Asterisks indicate non-specific bands. The results shown represent two independent experiments. Found at: doi:10.1371/journal.pone.0007099.s016 (2.52 MB TIF)

Acknowledgments

We thank Dr. Hitoshi Tsuda (National cancer center) and Dr. Toshio Terashima (Kobe University) for helpful discussions regarding the immunohistochemical study, Dr. Mio Tanaka (Kanagawa Children's Medical Center) for the preparation of archived NB tumors, and Ayako Takahashi and Rumi Mori for technical assistance.

Author Contributions

Conceived and designed the experiments: JI II JL. Performed the experiments: JI AM SI. Analyzed the data: JI AM SI YS II. Contributed reagents/materials/analysis tools: AM YT SI YS HH TS. Wrote the paper: JI II JL.

References

1. Brodeur GM (2003) Neuroblastoma: biological insights into a clinical enigma. *Nat Rev Cancer* 3: 203–216.
2. Schwab M, Westermann F, Hero B, Berthold F (2003) Neuroblastoma, biology and molecular and chromosomal pathology. *Lancet Oncol* 4: 472–480.
3. Maris JM, Hogarty MD, Bagatell R, Cohn SL (2007) Neuroblastoma. *Lancet* 369: 2106–2120.
4. Pritchard J, Hickman JA (1994) Why does stage 4s neuroblastoma regress spontaneously? *Lancet* 344: 869–870.
5. Reynolds CP (2002) Ras and Seppuku in neuroblastoma. *J Natl Cancer Inst* 94: 319–321.
6. Hoehner JG, Gestblom C, Olsen L, Pahlman S (1997) Spatial association of apoptosis-related gene expression and cellular death in clinical neuroblastoma. *Br J Cancer* 75: 1185–1194.
7. Ikeda H, Hirato J, Akami M, Matsuyama S, Suzuki N, et al. (1995) Bcl-2 oncoprotein expression and apoptosis in neuroblastoma. *J Pediatr Surg* 30: 805–808.
8. Koizumi H, Wakasaka M, Nakada K, Takakawa T, Fujioka T, et al. (1995) Demonstration of apoptosis in neuroblastoma and its relationship to tumour regression. *Vitrovi Arch* 42: 167–173.
9. Oue T, Fukuzawa M, Kusafuka T, Kohmoto Y, Imura K, et al. (1996) In situ detection of DNA fragmentation and expression of bcl-2 in human neuroblastoma. *J Pediatr Surg* 31: 251–257.
10. Tonini GP, Mazzeo K, di Vinci A, Grido E, de Bernardi B, et al. (1997) Evidence of apoptosis in neuroblastoma at onset and relapse: An analysis of a large series of tumors. *J Neurooncol* 31: 209–215.
11. Koizumi H, Hamano S, Doi M, Tsumanami S, Nakada K, et al. (2006) Increased occurrence of caspase-dependent apoptosis in unfavorable neuroblastomas. *Am J Surg Pathol* 30: 249–257.
12. Kitanaka C, Kato K, Ijiri R, Sakurada K, Tomiyama A, et al. (2002) Increased Ras expression and caspase-independent neuroblastoma cell death: possible mechanism of spontaneous neuroblastoma regression. *J Natl Cancer Inst* 94: 358–368.
13. Kodet R (1998) Ultrastructural observations on neuroblastic tumors in childhood: a study of tumor cell differentiation and regression on 89 cases. *Cesk Patol* 34: 123–130.
14. Yamamoto K, Hanada R, Kikuchi A, Ichikawa M, Aihara T, et al. (1998) Spontaneous regression of localized neuroblastoma detected by mass screening. *J Clin Oncol* 16: 1265–1269.
15. Frisch P, Kerbl R, Lackner H, Urban C (2004) "Wait and see" strategy in localized neuroblastoma in infants: an option not only for cases detected by mass screening. *Pediatr Blood Cancer* 43: 679–682.
16. Oue T, Inoue M, Yoneda A, Kubota A, Okuyama H, et al. (2005) Profile of neuroblastoma detected by mass screening, resected after observation without treatment: results of the Wait and See pilot study. *J Pediatr Surg* 40: 359–363.
17. Hero B, Simon T, Spitz R, Ernestus K, Guekov AK, et al. (2008) Localized infant neuroblastomas often show spontaneous regression: results of the prospective trials NB95-S and NB97. *J Clin Oncol* 26: 1504–1510.
18. Toyota M, Ho C, Ahuja N, Jia KW, Li Q, et al. (1999) Identification of differentially methylated sequences in colorectal cancer by methylated CpG island amplification. *Cancer Res* 59: 2307–2312.
19. Inazawa J, Inoue J, Imoto I (2004) Comparative genomic hybridization (CGH)-arrays pave the way for identification of novel cancer-related genes. *Cancer Sci* 95: 559–563.
20. Misawa A, Inoue J, Sugino Y, Hosoi H, Sugimoto T, et al. (2005) Methylation-associated silencing of the nuclear receptor I12 gene in advanced-type neuroblastomas, identified by bacterial artificial chromosome array-based methylated CpG island amplification. *Cancer Res* 65: 10233–10242.
21. Sugino Y, Misawa A, Inoue J, Kitagawa M, Hosoi H, et al. (2007) Epigenetic silencing of prostaglandin E receptor 2 (PTGER2) is associated with progression of neuroblastomas. *Oncogene* 26: 7101–7113.
22. Tanaka K, Imoto I, Inoue J, Kozaki K, Tsuda H, et al. (2007) Frequent methylation-associated silencing of a candidate tumor-suppressor, CRABP1, in esophageal squamous-cell carcinoma. *Oncogene* 26: 6456–6466.
23. Levine B, Kroemer G (2008) Autophagy in the pathogenesis of disease. *Cell* 132: 27–42.
24. Mizushima N (2007) Autophagy: process and function. *Genes Dev* 21: 2861–2873.
25. Bjorkoy G, Lamark T, Brech A, Outzen H, Perander M, et al. (2005) p62/SQSTM1 forms protein aggregates degraded by autophagy and has a protective effect on huntingtin-induced cell death. *J Cell Biol* 171: 603–614.
26. Pankiv S, Clausen TH, Lamark T, Brech A, Bruun JA, et al. (2007) p62/SQSTM1 binds directly to Atg8/LC3 to facilitate degradation of ubiquitinated protein aggregates by autophagy. *J Biol Chem* 282: 24131–24143.
27. Komatsu M, Waguri S, Chiba T, Murata S, Iwata J, et al. (2006) Loss of autophagy in the central nervous system causes neurodegeneration in mice. *Nature* 441: 880–884.
28. Hara T, Nakamura K, Matsui M, Yamamoto A, Nakahara Y, et al. (2006) Suppression of basal autophagy in neural cells causes neurodegenerative disease in mice. *Nature* 441: 885–889.
29. Adra CN, Zhu S, Ko JL, Guillemot JC, Cuervo AM, et al. (1996) LAMP5: a novel lysosomal-associated multispanning membrane protein preferentially expressed in hematopoietic cells. *Genomics* 35: 328–337.
30. Pak Y, Glowacka WK, Bruce MC, Pham N, Rotin D (2006) Transport of LAMP5 to lysosomes requires association with the ubiquitin ligase Nedd4, but not LAMP5 ubiquitination. *J Cell Biol* 175: 631–645.
31. Boya P, Andreu K, Poncet D, Zamzami N, Perfettini JL, et al. (2003) Lysosomal membrane permeabilization induces cell death in a mitochondrion-dependent fashion. *J Exp Med* 197: 1323–1334.
32. Boya P, Kroemer G (2008) Lysosomal membrane permeabilization in cell death. *Oncogene* 27: 6434–6451.
33. Kroemer G, Jaattela M (2005) Lysosomes and autophagy in cell death control. *Nat Rev Cancer* 5: 886–897.
34. Tardy C, Codogno P, Autefage H, Levade T, Andrieu-Abadie N (2006) Lysosomes and lysosomal proteins in cancer cell death (new players of an old struggle). *Biochim Biophys Acta* 1763: 101–125.
35. Yuan XM, Li W, Dalen H, Lotem J, Kama R, et al. (2002) Lysosomal destabilization in p53-induced apoptosis. *Proc Natl Acad Sci U S A* 99: 6286–6291.
36. Cortese R, Hartmann O, Berlin K, Eckhardt F (2008) Correlative gene expression and DNA methylation profiling in lung development nominate new biomarkers in lung cancer. *Int J Biochem Cell Biol* 40: 1494–1508.
37. Brodeur GM, Sekhon G, Goldstein MN (1977) Chromosomal aberrations in human neuroblastomas. *Cancer* 40: 2256–2263.
38. Ichimura S, Nimura Y, Kageyama H, Takada N, Sunahara M, et al. (2001) Genetic analysis of p73 localized at chromosome 1p36.3 in primary neuroblastomas. *Med Pediatr Oncol* 36: 42–44.
39. Fujita T, Igarashi J, Okawa ER, Gotoh T, Manne J, et al. (2008) CHD3, a tumor suppressor gene deleted from 1p36.31 in neuroblastomas. *J Natl Cancer Inst* 100: 910–919.
40. Munirajan AK, Ando K, Mukai A, Takahashi M, Suenaga Y, et al. (2008) KIF18A functions as a haploinsufficient tumor suppressor gene mapped to chromosome 1p36.2 by inducing apoptotic cell death. *J Biol Chem* 283: 24426–24434.
41. Caron H, van Sluis P, de Kraker J, Bokkerink J, Egder M, et al. (1996) Allelic loss of chromosome 1p as a predictor of unfavorable outcome in patients with neuroblastoma. *N Engl J Med* 334: 225–230.
42. Maris JM, White PS, Beltinger CP, Sulman EP, Castleberry RP, et al. (1995) Significance of chromosome 1p loss of heterozygosity in neuroblastoma. *Cancer Res* 55: 4664–4669.
43. Ouchida R, Yamasaki S, Hikida M, Masuda K, Kawamura K, et al. (2008) A lysosomal protein negatively regulates surface T cell antigen receptor expression by promoting CD3zeta-chain degradation. *Immunity* 29: 33–43.
44. Karlsson K, Carlsson SK (1998) Sorting of lysosomal membrane glycoproteins lamp-1 and lamp-2 into vesicles distinct from mannose 6-phosphate receptor/galactose-4-epitope vesicles at the trans-Golgi network. *J Biol Chem* 273: 18966–18973.
45. Fehrenbacher N, Bastholm L, Kirkegaard-Sorensen T, Rafn B, Bouzaaw T, et al. (2008) Sensitization to the lysosomal cell death pathway by oncogene-induced down-regulation of lysosome-associated membrane proteins 1 and 2. *Cancer Res* 68: 6623–6633.
46. Brundin P, Li JV, Holton JL, Lindvall O, Revez T (2008) Research in motion: the enigma of Parkinson's disease pathology spread. *Nat Rev Neurosci* 9: 711–715.
47. Gonzalez ML, Liang G (2007) Methylation-sensitive single-nucleotide primer extension (MS-SNuPE) for quantitative measurement of DNA methylation. *Nat Protoc* 2: 1931–1936.

PH Domain-Only Protein PHLDA3 Is a p53-Regulated Repressor of Akt

Tatsuya Kawase,^{1,8,9,11} Rieko Ohki,^{1,9,11,*} Tatsuhiro Shibata,^{2,3} Shuichi Tsutsumi,⁷ Naoko Kamimura,⁷ Johji Inazawa,⁶ Tsutomu Ohta,⁴ Hitoshi Ichikawa,⁵ Hiroyuki Aburatani,⁷ Fumio Tashiro,⁸ and Yoichi Taya^{1,9,10}

¹Radiobiology Division

²Cancer Genomics Project

³Pathology Division

⁴Center for Medical Genomics

⁵Cancer Transcriptome Project

National Cancer Center Research Institute, Tsukiji 5-1-1, Chuo-ku, Tokyo 104-0045, Japan

⁶Department of Molecular Cytogenetics, Medical Research Institute, Tokyo Medical and Dental University, 1-5-45 Yushima, Bunkyo-ku, Tokyo 113-8510, Japan

⁷Genome Science Division, Research Center for Advanced Science and Technology, University of Tokyo, 4-6-1 Komaba, Meguro-ku, Tokyo 153-8904, Japan

⁸Department of Biological Science and Technology, Faculty of Industrial Science and Technology, Tokyo University of Science, Yamazaki 2641, Noda-shi, Chiba 270-8510, Japan

⁹SORST/JST, Kawaguchi Center Building, 4-1-8 Honcho, Kawaguchi-shi, Saitama 332-0012, Japan

¹⁰Cancer Research Center of Excellence, Center for Life Sciences, #02-07, 28 Medical Drive, National University of Singapore, Singapore 117456

¹¹These authors contributed equally to the work.

*Correspondence: rohki@ncc.go.jp

DOI 10.1016/j.cell.2008.12.002

SUMMARY

p53 and Akt are critical players regulating tumorigenesis with opposite effects: whereas p53 transactivates target genes to exert its function as a tumor suppressor, Akt phosphorylates its substrates and transduces downstream survival signals. In addition, p53 and Akt negatively regulate each other to balance survival and death signals within a cell. We now identify *PHLDA3* as a p53 target gene that encodes a PH domain-only protein. We find that *PHLDA3* competes with the PH domain of Akt for binding of membrane lipids, thereby inhibiting Akt translocation to the cellular membrane and activation. Ablation of endogenous *PHLDA3* results in enhanced Akt activity and decrease of p53-dependent apoptosis. We also demonstrate the suppression of anchorage-independent cell growth by *PHLDA3*. Loss of the *PHLDA3* genomic locus was frequently observed in primary lung cancers, suggesting a role of *PHLDA3* in tumor suppression. Our results reveal a new mode of coordination between the p53 and Akt pathways.

INTRODUCTION

Proper regulation of cell death, survival, and proliferation is fundamental to ensuring homeostasis of a multicellular organism. Complex signal transduction pathways controlled by

oncoproteins and tumor suppressor proteins enable an elaborate balance of growth-promoting and growth-suppressing signals within a cell. One example of such a pathway is mutual regulatory crosstalk between tumor suppressor protein p53 and oncoprotein Akt, two key molecules regulating the life and death of a cell (Cully et al., 2006; Oren, 2003; Vousden and Prives, 2005).

The Akt signaling pathway plays a central role in cell survival and proliferation. Several components of this pathway are dysregulated in a wide spectrum of human cancers (i.e., Akt, PI3K, and PTEN), establishing its importance in oncogenesis (Luo et al., 2003). Mitogenic signals by receptor tyrosine kinases are first transmitted to phosphatidylinositol 3-kinase (PI3K), leading to production of a second messenger, phosphatidylinositol (3,4,5)-trisphosphate (PIP₃). PIP₃ generation on the inner side of the plasma membrane leads to translocation and activation of Akt. Akt activation is regulated by a dual mechanism that requires both translocation to the plasma membrane and phosphorylation at Thr308 and Ser473. Akt is recruited to the plasma membrane through direct interaction with its pleckstrin homology (PH) domain, functioning as lipid-binding modules. Downstream of Akt, Akt substrates contribute to the effects of Akt in cell survival and proliferation (Manning and Cantley, 2007).

In contrast, p53 plays a major role in the induction of growth arrest and cell death (Harris and Levine, 2005; Liu and Chen, 2006; Oda et al., 2000; Ohki et al., 2000). As the inactivation of p53 abrogates p53-mediated growth constraints, loss of functional p53 is a prerequisite for oncogenesis and is the most common anomaly in human cancers (Vogelstein et al., 2000; Vousden and Prives, 2005). Various stress signals stabilize and activate p53, which exerts its tumor-suppressive function mainly

Cell

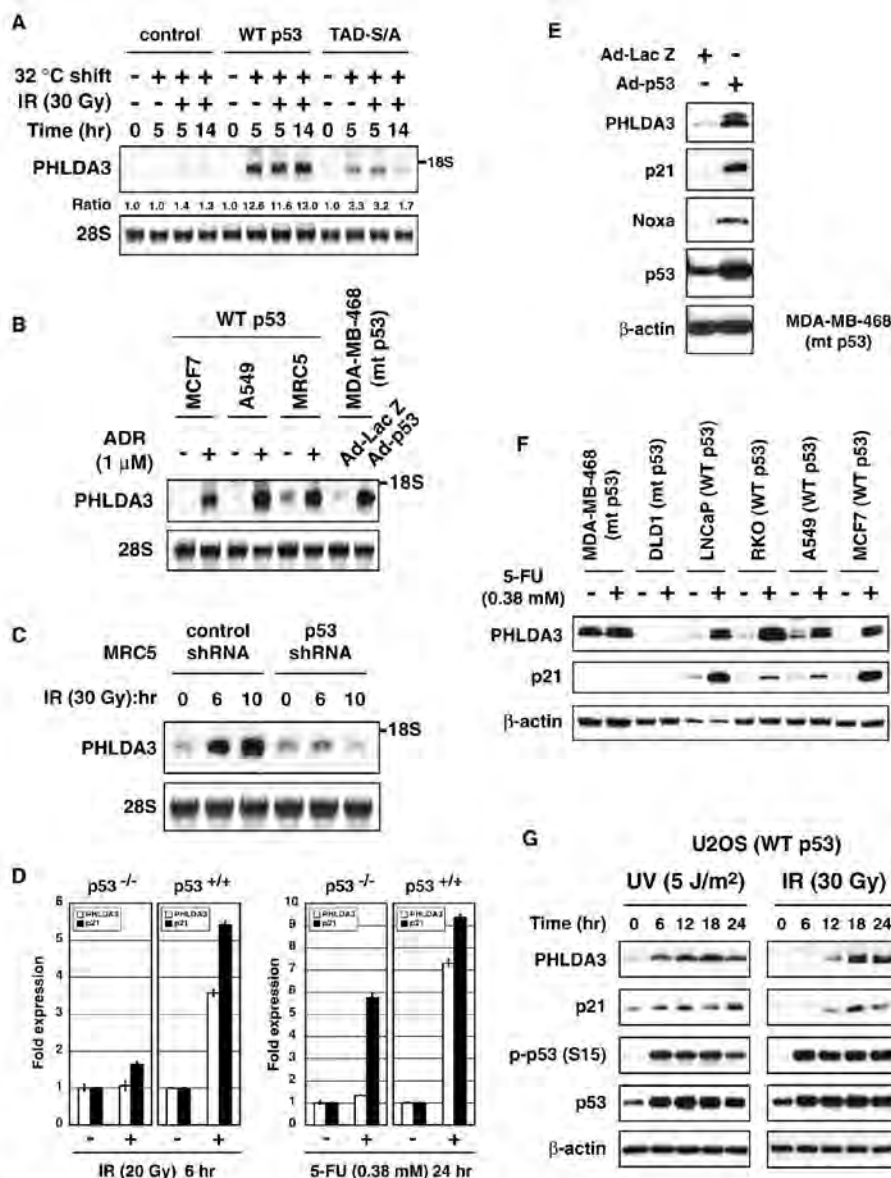


Figure 1. PHLDA3 is induced by p53

(A–C) PHLDA3 expression was analyzed by Northern blotting. Methylene blue staining of 28S ribosomal RNA was also shown to confirm equal loading of RNA in each lane.

(A) Temperature-sensitive (ts) WT p53- or ts-TAD-S/A-expressing Saos2 cell lines were tested for PHLDA3 induction ability upon temperature shift to the permissive temperature with or without γ -ray irradiation. Cells were subjected to γ -ray irradiation 2 hr after temperature shift to 32 °C. Cells were collected 5 or 14 hr post-temperature shift. Raw Northern blotting data are shown in the top panel, and the relative signal intensities for PHLDA3 expression (normalized by 28S intensities) were quantified by NIH Image J software and are shown below the panel.

(B) MCF7, A549, and MRC5 cells were treated with adriamycin for 18 hr. MDA-MB-468 cells were transduced with control LacZ-expressing (Ad-LacZ) or p53-expressing adenovirus (Ad-p53) at multiplicity of infection (moi) 15 and harvested 18 hr post-infection.

(C) MRC5 cells transduced with control lentivirus or lentivirus expressing p53 shRNA were subjected to γ -ray irradiation.

(D) HCT116 p53^{+/+} and HCT116 p53^{-/-} cells were subjected to γ -ray irradiation or 5-FU. Cells were harvested at the indicated times following treatment. RNA was purified from each sample and analyzed by quantitative real-time PCR. The mRNA levels of PHLDA3 and p21 were standardized by mRNA levels of GAPDH. All samples were run in triplicate, and data are represented as the mean fold expression \pm standard deviation (SD).

as a transcriptional activator. Many p53 target genes have been identified that regulate various processes involved in the prevention of tumorigenesis, such as the induction of cell-cycle arrest, cell death, DNA repair, and senescence. It has been postulated that target genes are selectively activated to implement different p53-mediated responses, depending on the stress signal that activates p53. Posttranslational modification of p53 is the candidate mechanism that makes p53 respond to different stress signals, and phosphorylation of p53 is a major posttranslational modification of p53 (Bode and Dong, 2004). Moreover, recent studies have shown the importance of p53 phosphorylation in the induction of several p53 target genes.

Akt-p53 mutual regulation involves Akt substrates and p53 target genes; for example, one target gene of p53, *PTEN*, negatively regulates Akt (Mayo and Donner, 2002). *PTEN* encodes a phosphatase that dephosphorylates lipid PIP₃, which is essential for Akt activation. On the other hand, p53 is also negatively regulated by Akt. Akt phosphorylates Mdm2, a negative regulator of p53 that targets p53 for degradation, and Mdm2 phosphorylation leads to accelerated degradation of p53. Moreover, the *mdm2* gene is transcriptionally regulated by p53, forming a p53-Mdm2 autoregulatory feedback loop (Brooks and Gu, 2006). Thus, Akt and p53 negatively regulate each other by a complex protein network to ensure coordinated growth control within a cell.

As is evident from the findings of *PTEN* and *Mdm2*, identification of p53 target genes led to the discovery of tumor-associated genes. *PTEN* is a tumor suppressor gene mutated in breast cancers and gliomas, while *mdm2* is an oncogene frequently amplified in tumors without p53 mutations (Mayo and Donner, 2002). In order to identify genes participating in the regulation of tumorigenesis, and to dissect the functional relevance of p53 phosphorylation in target gene induction, we performed exhaustive analysis to identify p53 target genes that are induced in a manner dependent on p53 phosphorylation status (Ohki et al., 2007; Kawase et al., 2008). We found that approximately 80% of genes depended on p53 phosphorylation, showing its importance in transcriptional activity of p53. Adding to the list of previously identified genes, we report here a p53 target gene, *PHLDA3*, that encodes a PH domain-only protein that suppresses Akt activity by directly interfering with Akt binding to membrane lipids. *PHLDA3* also inhibits anchorage-independent growth and is a candidate tumor suppressor of lung endocrine tumors.

RESULTS

PHLDA3 Is a Direct Target Gene of p53

Previously, we identified by microarray expression analysis genes induced by wild-type (WT) p53 and TAD-S/A, a phosphorylation-defective p53 mutant carrying point mutations at all Ser residues within the transactivation domain (TAD) (Ohki et al.,

2007). As shown in Figures 1A and S1A (available online), *PHLDA3* was one of the identified genes induced by WT p53 but not by TAD-S/A. *PHLDA3* transcript was also induced by exogenous expression of p53, adriamycin treatment in cells carrying WT p53, γ -ray irradiation, and 5-fluorouracil (5-FU) in a p53-dependent manner (Figures S1B, S1C, and 1B–1D). We also showed that the induction kinetics of *PHLDA3* mRNA was similar to that of representative target genes of p53 (Figure S1D). In addition, *PHLDA3* protein expression was induced by exogenous expression of p53 and various DNA-damaging agents, including 5-FU, ultraviolet (UV), and γ -ray irradiation, in cell lines carrying WT p53 (Figures 1E–1G and S2A–S2E). Furthermore, *PHLDA3* and p21 proteins were induced with similar kinetics by UV and γ -ray irradiation (Figures 1G and S2E).

It has been reported previously that the *PHLDA3* (also named *Tih1*) gene has sequence similarity to an imprinted gene, *Ipl* (Frank et al., 1999). As shown in Figure S3, *Ipl* transcript was not induced with a dependence on p53, and although *PHLDA3* and *Ipl* genes share sequence homology, they are regulated in different ways.

As it had been demonstrated that *PHLDA3* is a p53-responsive gene, we then explored whether *PHLDA3* is also a direct target gene of p53. The consensus binding motif of p53 is composed of two copies of 5'-RRRCWWGYYY-3' (R: purine, Y: pyrimidine, W: A or T) (Harris and Levine, 2005). As shown in Figure 2A, we found a putative p53-responsive element (p53RE) upstream of the *PHLDA3* gene, overlapping the transcription initiation site. Interestingly, this putative p53RE was highly conserved among the species. In order to clarify if this putative p53RE is activated by p53, the upstream region of the *PHLDA3* gene was cloned and assayed for p53 responsiveness. We first analyzed whether promoters with or without p53RE showed p53 responsiveness by luciferase reporter promoter assay. As shown in Figure 2B, p53 responsiveness strictly depended on intact p53RE. Furthermore, double-stranded synthetic oligonucleotide containing p53RE inserted upstream of the luciferase gene conferred strong p53 response on the promoter, which was abolished when p53RE was mutated (Figure 2C). On the other hand, the p53 mutant, V143A, which has no transactivation ability, did not activate the promoters, confirming that *PHLDA3* promoter activation depends on p53 transcriptional activity (Figures 2B and 2C).

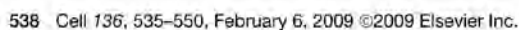
We next analyzed whether p53 protein binds to the *PHLDA3* promoter in vivo. As shown in Figure 2D, binding of WT p53 and TAD-S/A to the *PHLDA3* promoter was analyzed by chromatin immunoprecipitation (ChIP) assay, and it was strengthened when both p53s were active. Furthermore, we comprehensively analyzed p53 binding near the *PHLDA3* gene, utilizing ChIP-chip and ChIP sequence technology. As shown in Figures 2E and S4A, strong and specific binding of endogenous p53 at p53RE was detected upon DNA damage. The signal obtained by ChIP-chip analysis was proportional to the strength of p53 binding, and the signal obtained for the *PHLDA3* gene was as

(E–G) Western blotting was performed to detect *PHLDA3* protein expression. In all cases, *PHLDA3* protein migrated as a doublet (see also Figure S2A). Expression and activation (Ser15 phosphorylation) of p53 and expressions of representative p53 target genes (p21 and Noxa) were also analyzed.

(E) MM468 cells were transduced with Ad-LacZ or Ad-p53 at moi 15 and harvested 18 hr post-infection.

(F) Indicated cells were treated with 5-FU for 20 hr. Note that neither *PHLDA3* nor p21 protein is induced in cell lines carrying mutant p53.

(G) U2OS cells were treated with UV or γ -ray irradiation.



strong as other representative p53 target genes (Figure S4B). In addition, quantitative PCR was performed to analyze p53RE enrichment by ChIP. The relative enrichment of *PHLDA3* p53RE after ChIP was compared to a locus with no p53 binding and was concentrated more than 50-fold (Figure S4C). Moreover, ChIP sequence assay was performed for histone H3 trimethylated at Lys 4 (trimethyl K4/H3). It has been reported that trimethyl K4/H3 peaks in the 5' transcribed region and active genes can be discriminated from inactive genes by high levels of trimethyl K4/H3 (Schneider et al., 2004). Upon DNA damage, the *PHLDA3* gene was actively transcribed and increased trimethyl K4/H3 was detected in the 5' transcribed region simultaneously (Figures S1D and 2E). We finally analyzed, by p53 pull-down assay using biotinylated DNA probes containing one or two copies of p53RE, whether p53 binds directly to p53RE. As shown in Figure 2F, p53 was pulled down by WT but not by mutant p53RE. Collectively, these results identify *PHLDA3* as a bona fide target gene of p53 and p53RE as the p53-responsive element of the *PHLDA3* gene.

PHLDA3 Expression Is Regulated by p53 Phosphorylation Status

Multiple phosphorylation occurs within the TAD of p53 and regulates p53 transcriptional activity (Bode and Dong, 2004). As shown in Figures 1A and 2G, we found that *PHLDA3* expression and promoter activation was severely diminished in cells expressing TAD-S/A. We therefore analyzed which Ser residue within the TAD contributes to *PHLDA3* expression. We constructed p53 phosphorylation-deficient mutants carrying single amino acid conversions from Ser to Ala on all Ser residues within the TAD. As shown in Figure 2G, while p53 Ala mutants at Ser6,

9, 20, 33, and 37 showed activity similar to WT p53, the mutant at Ser15 showed decreased activity, similar to TAD-S/A. In addition, phosphorylation-mimic mutant S15D showed enhanced promoter response (Figure 2G, right panel). The requirements for Ser15 phosphorylation were also confirmed by analyzing endogenous *PHLDA3* transcriptional activation by WT p53, TAD-S/A, S15A, S15D, or S46A (Figure 2H) and by mutants carrying combined (S15, 20A and S6, 33, 46A) amino acid conversions (Figure S5A). On the other hand, although weak impairment of *PHLDA3* promoter activation was observed for S46A (Figure 2G left panel), it was not observed for endogenous *PHLDA3* induction (Figures 2H and S5A).

Phosphorylation of Ser15 upon genotoxic stress is dependent on ATM (Bode and Dong, 2004). Upon γ -ray irradiation, efficient Ser15 phosphorylation and *PHLDA3* expression were detected, whereas both were diminished in the same cells treated with caffeine, an ATM inhibitor (Figure 2I). Furthermore, when cells were treated with siRNA targeting ATM, Ser15 phosphorylation and *PHLDA3* expression reduced simultaneously upon γ -ray irradiation (Figure 2J). We also analyzed *PHLDA3* expression in ATM-proficient normal human fibroblast WI-38 and ATM-deficient AT2KY fibroblasts and showed that ATM is required for both Ser15 phosphorylation and *PHLDA3* expression (Figures S5B and S5C). These results collectively support the idea that p53 activation upon DNA damage is regulated by Ser15 phosphorylation, and *PHLDA3* expression is dependent on it. ChIP analysis results showed that TAD-S/A can bind to the *PHLDA3* promoter as efficiently as WT p53 (Figure 2D); however, TAD-S/A is unable to fully activate the *PHLDA3* promoter. The phosphorylation status of p53 may not affect p53 binding to the *PHLDA3* promoter

Figure 2. *PHLDA3* Is a Direct Target Gene of p53

- (A) Genomic organization of *PHLDA3* (chr1: 198,164,473–198,171,696) is shown together with the plots of pairwise genomic alignments between human and mouse, human and rat, and human and chicken. Genomic alignment plots were constructed using VISTA (<http://genome.lbl.gov/vista/index.shtml>). Based on genomic alignments, nucleotide conservation was calculated with a 100 bp window, and conservation percentage is shown as a plot. The position and nucleotide sequence of p53-responsive element are shown at the bottom.
- (B) *PHLDA3* promoter region with or without p53RE (shown as an oval) was cloned upstream of firefly luciferase reporter gene with a minimal promoter, and luciferase reporter assay was performed. Constructs contain indicated positions relative to the transcription initiation site. Nucleotides that matched p53 consensus binding sites, 4th and 7th nucleotides for promoter 2 mut.1 and 14th nucleotide for promoter 2 mut.2, were mutated. Constructs were tested for transactivation by WT p53 and p53-V143A. The assay was performed 24 hr post-transfection. The experiment was run in triplicate, and data are represented as the mean fold activation \pm SD.
- (C) One or two copies of double-stranded synthetic oligonucleotide containing p53RE were inserted into the luciferase reporter plasmid containing a minimal promoter. The assay was performed as in (B).
- (D) ChIP assay was performed for the *PHLDA3* promoter. The ts WT p53- and TAD-S/A-expressing Saos2 cell lines were used to analyze p53 binding to the *PHLDA3* promoter upon temperature shift to the permissive temperature. The positions of PCR primers within the *PHLDA3* promoter region are shown at the top.
- (E) HCT116 p53^{+/+} cells were treated with 5-FU, and p53 ChIP-chip or trimethyl K4/H3 ChIP sequence analysis was performed. Genomic locus of *PHLDA3* is shown together with the results obtained. Vertical axis shows the probability value ($-\log P$), which reflects the fold enrichment of ChIP-chip or ChIP sequence samples. Blue and red lines at the top indicate the p53-consensus region computed from TRANSFAC analysis. One p53-consensus region matched completely with p53RE obtained from our analysis (shown by a red line).
- (F) p53 pull-down using biotinylated DNA probes was performed. Two additional DNA probes served as controls: one containing the p21-derived sequence (p21-p53RE) as a positive control and another containing a nonrelevant sequence derived from a plasmid as a negative control. Bound p53 was analyzed by western blotting.
- (G–J) Full activation of the *PHLDA3* promoter requires p53 phosphorylation, especially at Ser15.
- (G) Luciferase assay was performed as in (B) using promoter 2. Saos2 cells were transfected with the indicated constructs and promoter 2 and analyzed 48 hr post-transfection.
- (H) Endogenous *PHLDA3* expression was analyzed by northern blotting. Saos2 cells were transfected with the indicated p53s and harvested 24 hr post-transfection. Relative signal intensities for *PHLDA3* expression were quantified as in Figure 1A and are shown below the panel. p53 protein levels were analyzed and are shown in the bottom panel. Asterisk denotes a nonspecific band detected by anti-p53 polyclonal antibody.
- (I) MCF7 cells were subjected to γ -ray irradiation with or without caffeine. Caffeine was added to the medium 1 hr prior to γ -ray irradiation. Cells were harvested 4 hr post-irradiation. Western blotting was performed to detect p53 expression and activation (Ser15 phosphorylation of p53).
- (J) MCF7 cells were transfected with siRNA targeting ATM and analyzed as in (I).

Cell

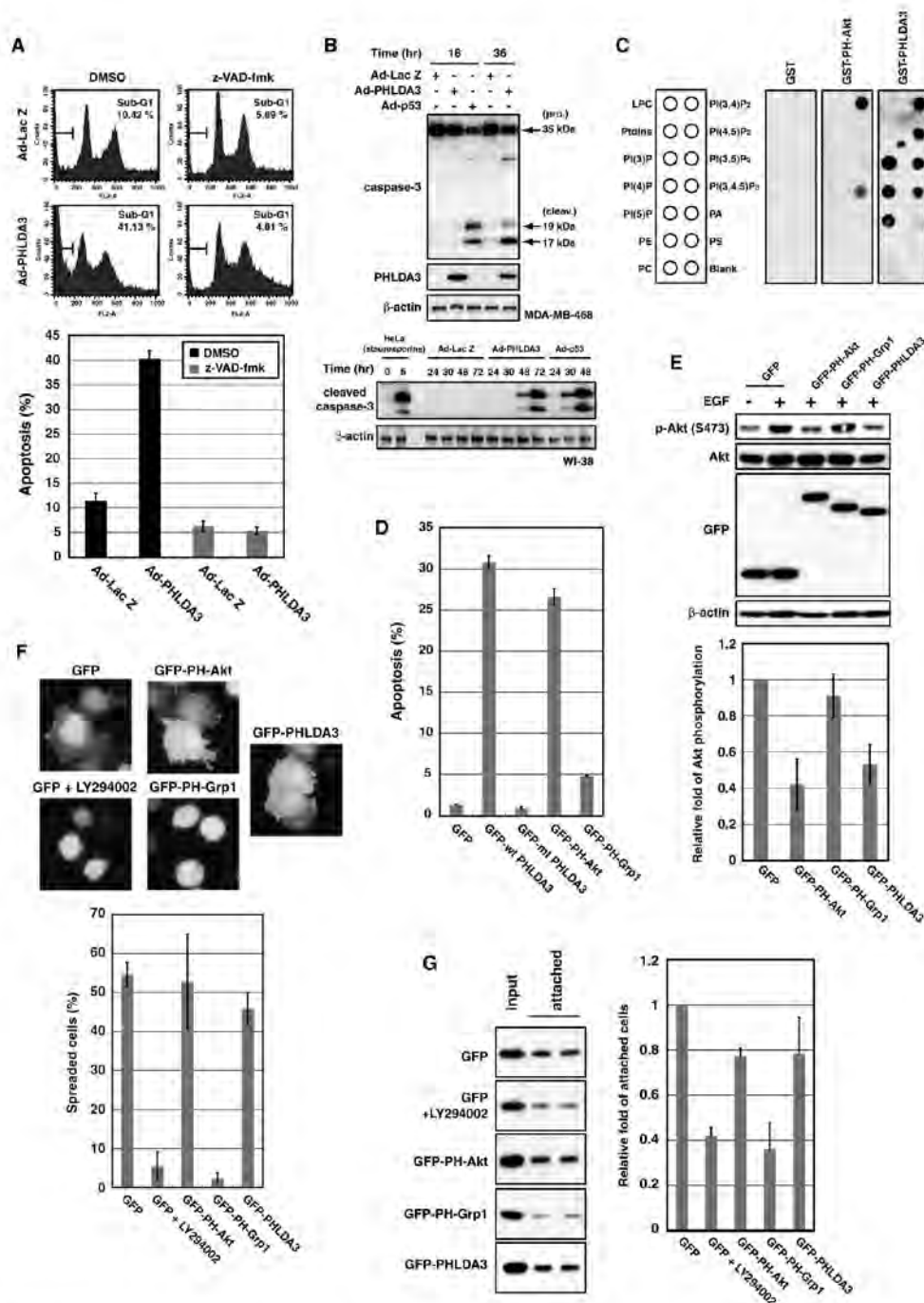


Figure 3. PHLDA3 Induces Apoptosis and Represses Akt
 (A) PHLDA3 induces caspase-dependent cell death. MM468 cells were transduced with Ad-LacZ or N-terminally HA-tagged PHLDA3-expressing adenovirus (Ad-PHLDA3) at moi 15. Cells were cultured with or without caspase-specific peptide inhibitor z-VAD-fmk. Cells were harvested 48 hr post-infection and analyzed by FACS. Percentages of cells with sub-G1 DNA content are shown (bottom panel).

but may affect other aspects of *PHLDA3* promoter activation, such as cofactor recruitment to the promoters, leading to its efficient activation.

PHLDA3 Is an Apoptosis Inducer

To explore the physiological functions of *PHLDA3*, we first transduced *PHLDA3* by adenovirus-mediated gene transfer and analyzed the effect of ectopic *PHLDA3* expression. As shown in Figures S6A and S9B, *PHLDA3* induced cell death in several cell lines irrespective of the p53 status, consistent with *PHLDA3* as a downstream mediator of p53. We found that cells with sub-G1 DNA content were increased by *PHLDA3* expression (Figure S6A), and this increase was inhibited by z-VAD-fmk addition, a specific caspase inhibitor, showing that *PHLDA3*-induced cell death is caspase dependent (Figure 3A). In addition, caspase 3 activation and increased annexin V-positive/PI-negative cells were observed upon *PHLDA3* expression (Figures 3B and S6B). We also compared the cell death-inducing ability of *PHLDA3* with that of p53 and Noxa, a representative p53 target gene that induces apoptosis (Figure S6C). Although cell-death induction was weaker than that with p53, *PHLDA3* induced cell death similarly to Noxa. Besides, we showed that endogenous *PHLDA3* is required for p53-dependent apoptosis (Figure 5, discussed in detail later). Collectively, it was shown that *PHLDA3* expression leads to apoptosis induction.

PHLDA3 Induces Apoptosis through Its PH Domain

PHLDA3 protein is highly conserved in vertebrates and is a small protein of 127 aa mostly comprised of the PH domain (Figure S7). Based on the results of the *in vitro* phosphatidylinositol phosphate (PIP) binding assay, the PH domain of *PHLDA3* is functional and binds to most PIP (Figure 3C and Saxena et al., 2002). *PHLDA3* binding to PIP occurs without stimulation and therefore *PHLDA3* is localized to the cellular membrane when expressed (Figure S8). Accordingly, we tested whether *PHLDA3*'s ability to induce apoptosis is dependent on the function of its PH domain. We fused WT *PHLDA3* (WT *PHLDA3*) and mt*PHLDA3*, a *PHLDA3* mutant with a small deletion within the PH domain (Figure S7), with GFP or DsRed, and subcellular localization was analyzed. As shown in Figures 4C and 4D, while DsRed-WT *PHLDA3* local-

ized to the plasma membrane as expected, DsRed-mt*PHLDA3* localized mainly in the cytoplasm, showing that the PH domain of mt*PHLDA3* is nonfunctional (equivalent GFP fusion proteins showed the same subcellular localizations; Figure 3F and data not shown). We next expressed GFP, GFP-WT *PHLDA3*, and GFP-mt*PHLDA3* in 293T cells and analyzed GFP-positive cells by flow cytometry. As shown in Figure 3D, compared to GFP-expressing cells, an increase of dead cells was observed in cells expressing GFP-WT *PHLDA3*, while no increase was observed for cells expressing GFP-mt*PHLDA3*. These results demonstrate that the functional PH domain is required for *PHLDA3*-induced apoptosis.

PHLDA3 Acts Similarly to the PH Domain of Akt

The PH domain is an approximately 100-residue protein module found in many signaling proteins and binds to PIP located on the inner plasma membrane. The PH domain mediates protein recruitment to cellular membranes, which is of paramount importance for signal transduction (Lemmon and Ferguson, 2000). Given that apoptosis induction of *PHLDA3* requires its PH domain, and *PHLDA3* has no distinct functional domain other than the PH domain, we speculated that the physiological role of *PHLDA3* is to function as a PH domain-only protein. We hypothesized that *PHLDA3* is induced by p53 under stressed conditions, functioning as a dominant-negative molecule for other PH domain-containing proteins to shut off the signal transduction pathway mediated by those proteins. In order to test our hypothesis, we tested whether PH domains derived from other PH domain-containing proteins function similarly to *PHLDA3* within the cell. We selected two well-known PH domain-containing proteins with distinct functions within the cell: serine/threonine kinase Akt, the main molecule that transduces survival signaling, and Grp1, a member of the GTP-binding protein exchange factor family that regulates cell adhesion and spreading (Lemmon and Ferguson, 2000). It has been reported that both PH domains of Akt and Grp1 bind to PIP₃, and when isolated PH domains are expressed in cells, they function as dominant-negative forms of the proteins (Songyang et al., 1997; Vamai et al., 2005). The PH domain of Akt or Grp1 was fused with GFP (GFP-PH-Akt, GFP-PH-Grp1) and expressed in 293T and COS7

(B) Cleavage and activation of caspase 3 upon *PHLDA3* expression. MM468 and WI-38 cells were transduced with Ad-LacZ, Ad-*PHLDA3*, or Ad-p53 at moi 35. Cells were harvested at the indicated times post-infection. HeLa cells treated with staurosporine for 6 hr were shown as a positive control for caspase 3 activation. *PHLDA3* expression was detected with anti-HA antibody. Caspase 3 activation induced by *PHLDA3* followed that by p53.

(C) Binding of GST-*PHLDA3*, GST-PH-Akt, or GST to immobilized PIP was assessed by protein-lipid overlay assay. Nitrocellulose membranes spotted with 100 pmol of different phospholipids were used for the assay. Bound proteins were detected with anti-GST antibody. Note that GST produced no signal under the conditions employed.

(D) 293T cells were transfected with GFP, GFP-WT *PHLDA3*, GFP-mt*PHLDA3*, GFP-PH-Akt, or GFP-PH-Grp1 and analyzed for GFP-positive cells 48 hr post-transfection. The apoptotic rate, measured by PI-positive cells (cells stained with PI without fixation), is shown. Mean apoptotic rates \pm SD from three experiments are shown.

(E) *PHLDA3* inhibits Akt activation. COS7 cells were transfected with the indicated fusion proteins for 24 hr and subsequently stimulated with EGF for 5 min. Induction of Akt phosphorylation was detected in control cells expressing GFP upon EGF treatment. Akt activity after EGF treatment was analyzed by western blotting, and Akt activity relative to the GFP-transfected control was calculated. The mean \pm SD from three experiments is shown. GFP fusion protein levels were also analyzed by western blotting.

(F) Cell spreading is not inhibited by *PHLDA3*. The cell-spreading assay was performed. LY294002 was added 10 min before re-plating. More than 150 cells were counted from three fields, and the percentages of fully spread cells are shown. Note that PI3K inhibitor LY294002 inhibited cell spreading under the conditions tested. Mean percentage \pm SD from three fields is shown. Representative images of cells are shown on the left.

(G) Cell attachment is only weakly inhibited by *PHLDA3*. Cell attachment assay was performed. Attached cells were harvested and analyzed by western blotting. The fraction of attached cells relative to input cells was calculated for each construct. LY294002 (added 10 min before plating) inhibited cell attachment under the conditions tested. Representative result is shown on the left, and the mean \pm SD from four experiments is shown.

Cell

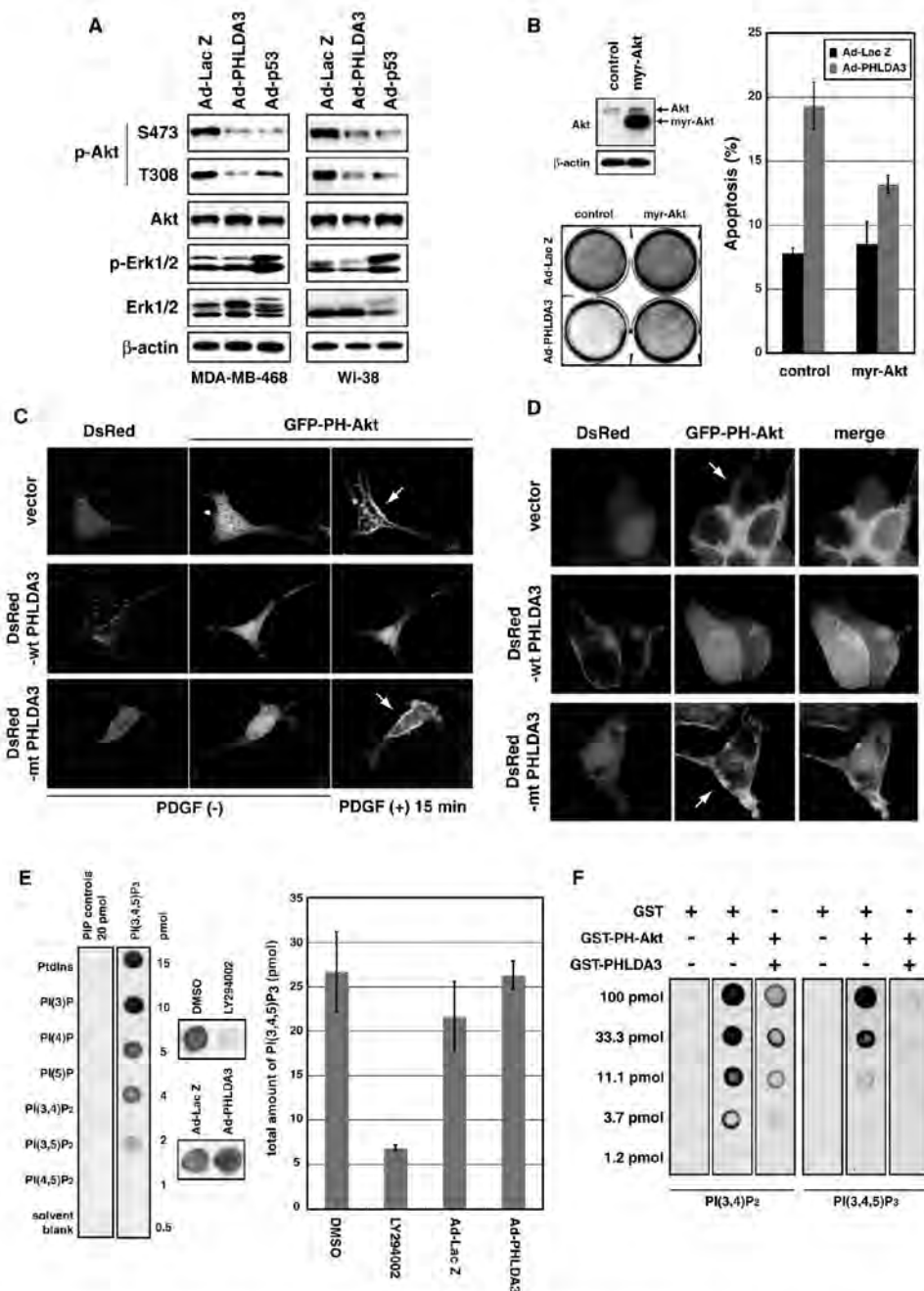


Figure 4. PHLDA3 Interferes with Akt Activation by Inhibiting Akt Binding to PI(3,4)P₂ and PI(3,4,5)P₃
 (A) Indicated cells were infected with Ad-LacZ, Ad-p53, or Ad-PHLDA3 at moi 35 and analyzed 18 hr post-infection, when apoptotic cells were not yet detected. Akt and Erk activities were assessed by analyzing phosphorylated Akt and Erk1/2 by western blotting.
 (B) Constitutively active Akt represses apoptosis induced by PHLDA3. MM468 cells stably expressing myr-Akt or control cells expressing only the Bsr drug resistance gene were infected with Ad-LacZ or Ad-PHLDA3 at moi 15. Myr-Akt was detected with anti-Akt antibody. Cells were fixed and stained with Giemsa 48 hr post-infection (left lower panel). Cells in sub-G1 were also analyzed by FACS (right panel). The data are represented as the mean \pm SD for triplicate samples.

cells. As expected, GFP-PH-Akt repressed Akt activity and induced apoptosis by inhibition of the Akt pathway (Figures 3D and 3E), whereas GFP-PH-Grp1 inhibited cell spreading on fibronectin and cell attachment to culture dishes by inhibiting endogenous Grp1 signaling (Figures 3F and 3G). GFP-PH-Akt had no effect on cell spreading and a very weak effect on cell attachment (Figures 3F and 3G), and GFP-PH-Grp1 had a very weak effect on cell survival and no effect on Akt activity (Figures 3D and 3E), showing the selective effect of these PH domains, as reported (Varnai et al., 2005). We found that GFP-WT PHLDA3 induced apoptosis and repressed Akt activity as GFP-PH-Akt, whereas it had a very weak effect on cell spreading and attachment, showing that PHLDA3 functions similarly to the PH domain of Akt (Figures 3D–3G).

PHLDA3 Induces Apoptosis by Inhibiting Akt Activity

PHLDA3 represses Akt activity and induces apoptosis, suggesting that it functions as a PH domain-only protein to inhibit Akt; therefore, we further examined whether PHLDA3 induces apoptosis by inhibiting Akt activation. As shown in Figure 4A, PHLDA3 expression resulted in diminished Akt phosphorylation at Ser473 and Thr308, both of which are essential for Akt activity, whereas the phosphorylation status of Erk was not changed by PHLDA3 expression, showing that inhibition of Akt activity is not a result of inhibition of the global cell survival signaling pathway. We also compared sensitivity to apoptosis induction by LY294002, a specific PI3K/Akt signaling pathway inhibitor, and apoptosis by PHLDA3 expression within several cell lines (Figures S9A and S9B). Cell lines sensitive to LY294002 treatment were also sensitive to PHLDA3 expression. Furthermore, when MM468 cells were treated with LY294002, PHLDA3 expression did not enhance apoptosis, indicating that PHLDA3 expression does not increase PI3K pathway inhibition in apoptosis induction (Figure S9C). These results collectively suggest that apoptosis induction by PHLDA3 is mediated by inhibition of the PI3K/Akt pathway.

We next tested whether the expression of constitutively active forms of Akt restrains apoptosis induced by PHLDA3. We selected two constitutively active forms of Akt, neither of which require PIP₃ binding for activation: a double mutant mimicking phosphorylated Akt (T308D/S473D-Akt) and myristoylated and PH domain-deleted constitutively active Akt (myr-Akt). We first transfected 293T cells with GFP-PHLDA3 and T308D/S473D-Akt. As shown in Figure S10A, by cotransfection of T308D/S473D-Akt, PHLDA3-induced apoptosis was rescued, and this rescue was dependent on T308D/S473D-Akt dosage. When the effect of T308D/S473D-Akt on apoptosis induced by PHLDA3 and PH-Akt was compared, T308D/S473D-Akt similarly

rescued both (Figure S10B). We next obtained cells stably expressing myr-Akt and analyzed apoptosis induction by ectopic PHLDA3 expression. As shown in Figure 4B, compared to control cells, apoptotic cells decreased and viable cells increased in myr-Akt-expressing cells, showing that myr-Akt efficiently repressed apoptosis induced by PHLDA3. Thus, these results reveal that PHLDA3 inhibits Akt activation, and Akt inhibition mainly contributes to apoptosis induction by PHLDA3.

PHLDA3 Interferes with Akt Translocation to the Plasma Membrane

Activation and phosphorylation of Akt require prior PIP binding at the plasma membrane (Stokoe et al., 1997). When PI(3,4,5)P₃ and PI(3,4)P₂ are generated by PI3K upon growth stimulation, Akt translocates from the cytoplasm to the plasma membrane by binding to PIP through its PH domain, which specifically binds to PI(3,4,5)P₃ or PI(3,4)P₂ (Figure 3C and Scheid and Woodgett, 2003). Since two constitutively active forms of Akt that do not require PIP binding for activation rescued PHLDA3-induced apoptosis, it was suggested that PHLDA3 inhibits Akt binding to PIP. We therefore analyzed whether PHLDA3 expression inhibits Akt translocation to the plasma membrane upon PIP₃ production. We coexpressed DsRed or DsRed-WT PHLDA3 together with GFP-PH-Akt in NIH 3T3 cells (Figures 4C and S11A). GFP-PH-Akt has been shown to mimic Akt translocation upon PI3K pathway activation (Harriague and Bismuth, 2002). As has been reported, PDGF treatment of control cells expressing DsRed resulted in GFP-PH-Akt translocation to the plasma membrane, whereas in cells expressing DsRed-WT PHLDA3, GFP-PH-Akt translocation was inhibited. Moreover, inhibition was not observed in cells expressing DsRed-mtPHLDA3, a PHLDA3 mutant with a defective PH domain, which cannot localize at the plasma membrane. To assess the effect of PHLDA3 expression on Akt localization in other cell lines, a similar experiment was performed using 293T cells with constitutively active PI3K activity. Again in 293T cells, DsRed-WT PHLDA3 interfered with GFP-PH-Akt localization to the plasma membrane, while DsRed or DsRed-mtPHLDA3 did not (Figures 4D and S11B). Taken together, the results show that PHLDA3 impedes Akt translocation to the cellular membrane and subsequent activation in a manner dependent on its PH domain function.

PHLDA3 Directly Interferes with Akt Binding to PIP₂ and PIP₃

Because PHLDA3 expression led to the inhibition of Akt translocation to the plasma membrane and subsequent phosphorylation and activation, we next analyzed the mechanism by which PHLDA3 inactivates Akt. We first tested whether PHLDA3

(C) Akt translocation to the plasma membrane upon PDGF treatment was analyzed by live-cell imaging. NIH 3T3 cells were transfected with GFP-PH-Akt together with DsRed, DsRed-WT PHLDA3, or DsRed-mtPHLDA3. GFP-PH-Akt subcellular localization was monitored before and after PDGF treatment (15 min). Note that Akt is localized at the plasma membrane in cells expressing DsRed or DsRed-mtPHLDA3 (shown by arrows).

(D) Akt subcellular localization in 293T cells with the constitutively active PI3K/Akt pathway. 293T cells were transfected with GFP-PH-Akt together with DsRed, DsRed-WT PHLDA3, or DsRed-mtPHLDA3, and GFP-PH-Akt subcellular localization was analyzed. Arrows indicate Akt localized at the plasma membrane.

(E) Quantification of PIP₃ in cells expressing PHLDA3. Amount of PIP₃ was quantified in lipids extracted from MM468 cells infected with Ad-LacZ and Ad-PHLDA3 and cells treated with LY294002. The data are represented as the mean ± SD from three experiments.

(F) PHLDA3 inhibits PH-Akt binding to PIP₂ and PIP₃. Binding of GST-PH-Akt to immobilized PIP was assessed by protein-lipid overlay assay. Nitrocellulose membranes spotted with serially diluted PIP₂ and PIP₃ were incubated with the indicated proteins. While GST did not interfere with Akt binding to PIP, PHLDA3 significantly interfered. Bound Akt was detected with anti-Akt PH domain antibody.

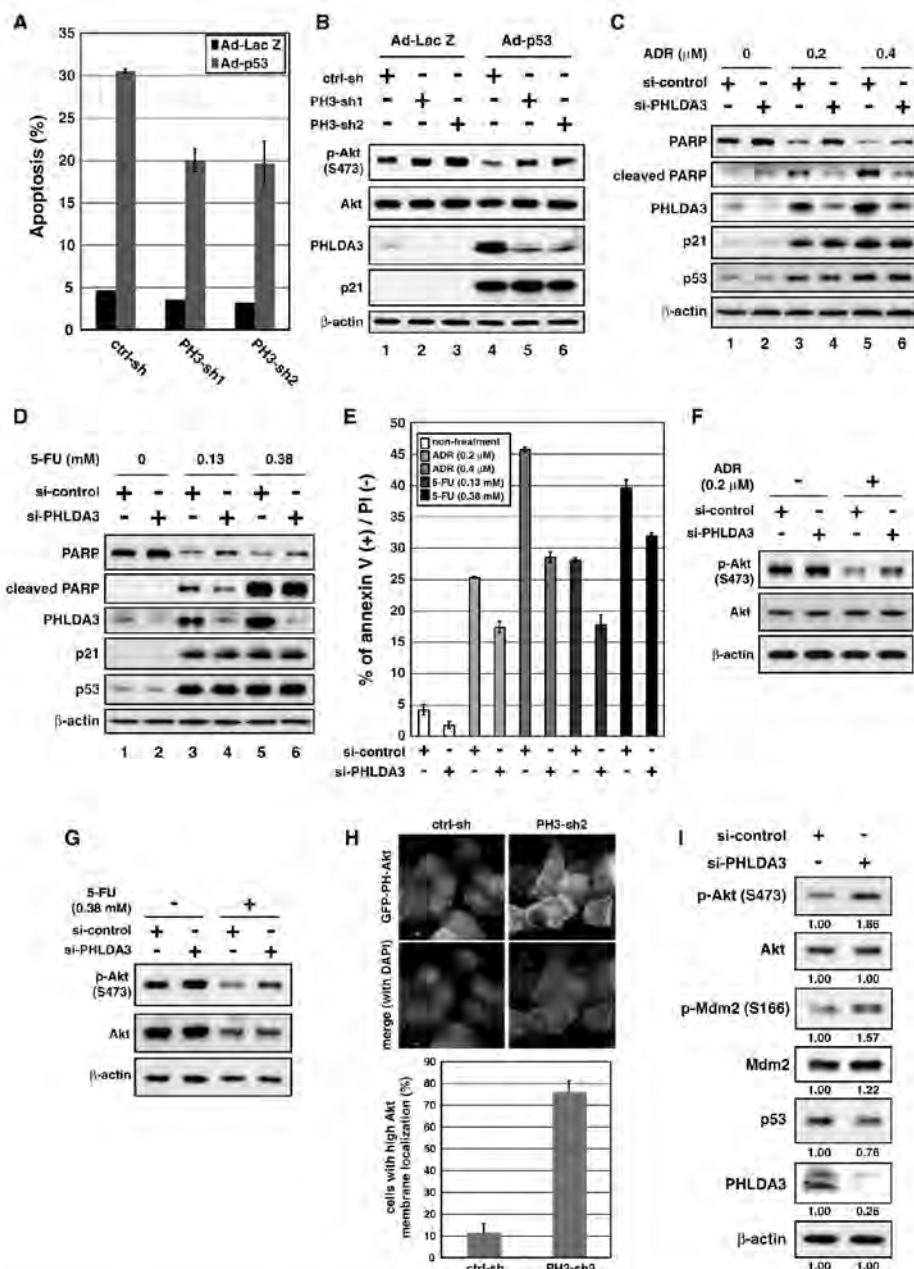


Figure 5. PHLDA3 Is Required for p53-Dependent Apoptosis

(A and B) Downregulation of PHLDA3 results in decreased p53-dependent apoptosis and elevated Akt phosphorylation. Ctrl-sh, PH3-sh1, and PH3-sh2 cells were infected with Ad-p53 at moi 3 (in A) or moi 1 (in B). Apoptotic cells as determined by cells with sub-G1 DNA content were analyzed 43 hr post-infection, and the mean \pm SD for triplicate samples is shown (A). In (B), cells were treated with z-VAD-fmk to protect Akt from p53-dependent Akt degradation. Cells were harvested 50 hr post-infection and analyzed by western blotting. (C–G) Control or PHLDA3-targeting siRNAs were introduced into LNCaP cells. Cells were treated with adriamycin or 5-FU 30 hr post-transfection. Cells were harvested 42 hr (C–E and G) or 36 hr (F) post-treatment and analyzed by western blotting (C, D, F, and G) or by FACS for annexin V-positive/PI-negative cells (E). The mean \pm SD for triplicate samples is shown.

inhibits Akt activity by affecting upstream signals of Akt. Since PI3K-produced PIP_3 is essential for Akt activation, we analyzed the amount of PIP_3 in cells expressing PHLDA3 using the PIP_3 mass strip kit. Acidic lipids were extracted from MM468 cells infected with Ad-LacZ and Ad-PHLDA3 and blotted onto a PIP_3 strip. PIP_3 was quantified by detecting membrane-blotted acidic lipids with a PIP_3 detector. As shown in Figure 4E, no difference in the amount of PIP_3 was detected between control and PHLDA3-expressing cells, while significantly reduced PIP_3 was detected in MM468 cells treated with LY294002. As PHLDA3 did not affect Akt upstream signals, we next tested whether PHLDA3 physically interacts with Akt to inhibit Akt binding to PIP. HA-tagged Akt and GFP-PHLDA3 or GFP-Akt were coexpressed and immunoprecipitated with anti-HA antibody and analyzed to identify direct interaction between the proteins (Figure S12). Although Akt homodimerization was detected, as previously reported (Franke et al., 1997), no interaction between PHLDA3 and Akt was observed. We finally performed an *in vitro* protein-lipid overlay assay to see if PHLDA3 directly interferes with Akt binding to PIP (Figure 4F). PHLDA3 and Akt were mixed in a molar ratio of 1:1 and reacted with $PI(3,4,5)P_3$ and $PI(3,4)P_2$ to test whether PHLDA3 competitively interferes with Akt binding to PIP. As shown in Figure 4F, Akt binding to PIP was significantly inhibited by PHLDA3 but not when Akt was mixed with control GST. Collectively, these results demonstrate that PHLDA3 does not change the amount of PIP_3 within the cell or interact physically with Akt but does repress Akt activity by competitively binding to PIP.

PHLDA3 Contributes to p53-Dependent Apoptosis and Repression of Akt

We next examined whether PHLDA3 contributes to p53-dependent apoptosis. We stably knocked down PHLDA3 in MM468 cells by introducing two different shRNAs (PH3-sh1 and PH3-sh2) that efficiently knocked down PHLDA3 expression (Figures S1C, S2B, and S14B). As shown in Figure S2B, induction of p21 or Noxa by p53-expressing adenovirus (Ad-p53) did not differ among ctrl-sh, PH3-sh1, and PH3-sh2 cells, showing that the p53 pathway is normal except for PHLDA3 induction in PH3-sh1 and PH3-sh2 cells. Using these cell lines, the efficacy of p53-dependent apoptosis induced by Ad-p53 infection was analyzed. Apoptosis was not observed in cells infected with control LacZ-expressing adenovirus (Ad-LacZ), whereas Ad-p53 induced apoptosis in ctrl-sh cells; however, apoptosis by Ad-p53 was significantly diminished in PH3-sh1 and 2 cells (Figure 5A).

Inhibition of the survival signaling pathway by Akt is important for p53-dependent apoptosis (Stambolic et al., 1999), and repression of Akt activity was observed upon p53 expression in MM468 cells (Figures 4A and 5B, lane 4). It has been proposed that p53-dependent inhibition of the Akt pathway is mediated by PTEN or caspase (Oren, 2003); however, as MM468 cells do not have functional PTEN and no degradation of Akt is detected, Akt

repression by p53 detected here is independent of caspase and PTEN. These results suggest a novel Akt-repressing pathway downstream of p53. We therefore analyzed whether PHLDA3 acts downstream of p53 to repress Akt. As shown in Figure 5B, in Ad-p53 infected cells, PH3-sh cells showed elevated Akt phosphorylation compared to ctrl-sh cells, demonstrating the involvement of PHLDA3 in p53-dependent repression of Akt (lanes 4–6). All cells infected with Ad-p53 showed lower Akt phosphorylation levels than equivalent cells infected with Ad-LacZ, at least partially because of residual PHLDA3 induction by p53 in PH3-sh cells. Notably, PHLDA3 expression levels had a reverse correlation with Akt phosphorylation levels. Cells with high PHLDA3 expression had very low levels of activated Akt (lane 4), cells with moderate PHLDA3 expression had medium levels (lanes 1, 5, and 6), and cells with very low PHLDA3 expression had high levels (lanes 2 and 3).

We further analyzed involvement of PHLDA3 in p53-dependent apoptosis and Akt repression induced by DNA damage. LNCaP cells were transfected with control or PHLDA3-targeting siRNAs and treated with adriamycin or 5-FU, which induces p53-dependent apoptosis (Figure S13). Upon treatment with the reagents, upregulation of p53 and p21 was observed (Figures 5C and 5D). PHLDA3 expression was effectively downregulated in cells transfected with siRNAs targeting PHLDA3 and, upon DNA damage, PARP cleavage and annexin V-positive/PI-negative cells were reduced, showing that PHLDA3 mediated DNA damage-induced apoptosis (Figures 5C–5E). Moreover, Akt activity was higher in cells with ablated PHLDA3 expression, indicating involvement of PHLDA3 in Akt repression upon DNA damage (Figures 5F and 5G). Taken together, these results demonstrate that PHLDA3 is required for p53-dependent apoptosis and Akt repression.

PHLDA3 Represses Akt under Basal Conditions

In addition to the effects of PHLDA3 knockdown upon p53 activation, we analyzed the effects under basal conditions. In PH3-sh cells infected with Ad-LacZ, elevated Akt phosphorylation was observed compared to ctrl-sh cells, showing that p53-independent basal PHLDA3 expression also inhibits Akt activation (Figure 5B, lane 1–3). Furthermore, as shown in Figure 5H, when control- and PH3-sh2 cells were transfected with GFP-PH-Akt, stronger localization of GFP-PH-Akt was observed in PH3-sh2 cells, further demonstrating the ability of PHLDA3 to inhibit Akt membrane translocation. In addition, we analyzed the effect of PHLDA3 knockdown under basal conditions in LNCaP cells (Figure 5I). It has been reported that Akt phosphorylates Mdm2 and increases Mdm2 activity to degrade p53 (Mayo and Donner, 2002). In PHLDA3 knocked-down cells, Akt and Mdm2 activities, elucidated by their phosphorylation, were increased (Figure 5I). Moreover, p53 levels were lower in these cells than control cells (Figure 5I and lanes 1–2 of Figures 5C and 5D); however, no such p53 decrease was observed when cells were treated with DNA-damaging agents, probably due to

(H) Ctrl-sh or PH3-sh2 cells were transfected with GFP-PH-Akt and treated with EGF for 5 min 24 hr post-transfection. Representative images of cells are shown in top panels. More than 150 cells were counted from three fields and classified into three groups: high, middle, or low GFP-PH-Akt at the plasma membrane. Percentage of cells with high GFP-PH-Akt localization at the membrane is shown in the bottom panel. The mean \pm SD from three fields is shown.

(I) Control or PHLDA3-targeting siRNAs were introduced into LNCaP cells. Cells were harvested 72 hr post-transfection and analyzed by western blotting.

Cell

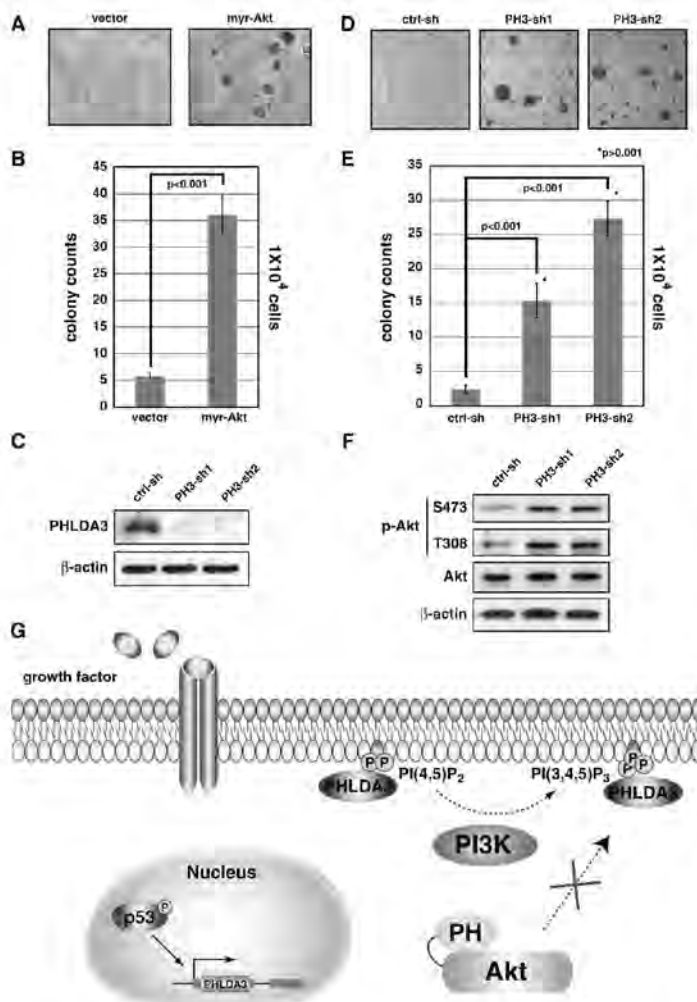


Figure 6. PHLDA3 Suppresses Anchorage-Independent Cell Growth

(A and B) Control and myr-Akt-expressing cells (1×10^4 cells) were plated in soft agar and cultured for 4 weeks. Colonies were analyzed by Image J software. Colonies were counted from three plates and the mean numbers of colonies \pm SD are shown (B).

(C–F) Ctrl-sh, PH3-sh1, and PH3-sh2 cells were plated and analyzed as described above (D and E).

(C and F) PHLDA3 knock-down efficiency and Akt activity in colonies were analyzed. Whole-cell lysate (WCL) was prepared from colonies formed in soft agar from indicated cells and analyzed for PHLDA3 expression (C) and Akt activity (F) by western blotting.

(G) Novel Akt-inhibiting pathway downstream of p53 mediated by PHLDA3.

knockdown on colony formation efficiency. PHLDA3 expression under basal conditions or in cells forming colonies was analyzed and was almost undetectable in PH3-sh cells (Figures 6C and S14B). Similar to the results obtained with cells expressing myr-Akt, cells with ablated PHLDA3 expression formed larger and more colonies than ctrl-sh cells (Figures 6D, 6E, and S14C). When Akt phosphorylation levels of cells grown in soft agar were analyzed, those of PH3-sh cells were higher than those of control cells (Figure 6F). Taken together, PHLDA3 inhibited anchorage-independent cell growth and Akt activity independent of p53, suggesting a p53-independent role of PHLDA3 in tumor suppression.

The PHLDA3 Gene Is Frequently Lost in Human Lung Endocrine Tumors

Inhibition of the Akt survival pathway is central to tumor suppression, and because PHLDA3 represses Akt in both p53-dependent and -independent manners, we considered that PHLDA3 might suppress human tumors. It has been

p53 phosphorylation protecting p53 against degradation by Mdm2 (lanes 3–6 of Figures 5C and 5D). These data demonstrate the complex mutual regulation of Akt and p53 and participation of PHLDA3 in the signaling cascade.

PHLDA3 Inhibits Anchorage-Independent Cell Growth

Since PHLDA3 mediated Akt inhibition without p53 activation, we further analyzed p53-independent function of PHLDA3. Akt is known to enhance anchorage-independent cell growth (Moore et al., 1998). We therefore analyzed whether PHLDA3 expression affects Akt-dependent colony formation in soft agar using MM468 cells without functional p53. In order to confirm Akt function in growth enhancement in soft agar, we first analyzed whether colony formation is enhanced in MM468 cells expressing myr-Akt. As shown in Figures 6A, 6B, and S14A, compared to control cells, cells expressing myr-Akt formed larger and more colonies in soft agar. We then analyzed the effect of PHLDA3

reported that PI3K/Akt pathway activation is highly important for the oncogenicity of lung tumors (Engelman and Cantley, 2006). Accordingly, we performed comprehensive copy number analysis of primary human lung tumors (158 cases), 45 adenocarcinomas, 12 bronchioalveolar carcinomas, 52 squamous cell carcinomas, 8 small cell lung carcinomas, 29 LCNECs (large-cell neuroendocrine carcinoma), and 13 carcinoids, using a custom-made array spotted with 800 BAC clones (Peng et al., 2005; Shibata et al., 2005; and T.S., unpublished data). The PHLDA3 gene is located in region 199.7 M chromosome 1, and because the most closely mapped BAC to PHLDA3 in the array is that containing PTPN7, we judged chromosomal copy number changes of PHLDA3 by copy number changes of BAC containing PTPN7 (chromosomal locations of genes, Figure 7A). Interestingly, while no chromosomal alteration at the PTPN7 locus was observed in adenocarcinoma, bronchioalveolar, squamous cell, and small-cell lung carcinoma, frequent chromosomal loss was

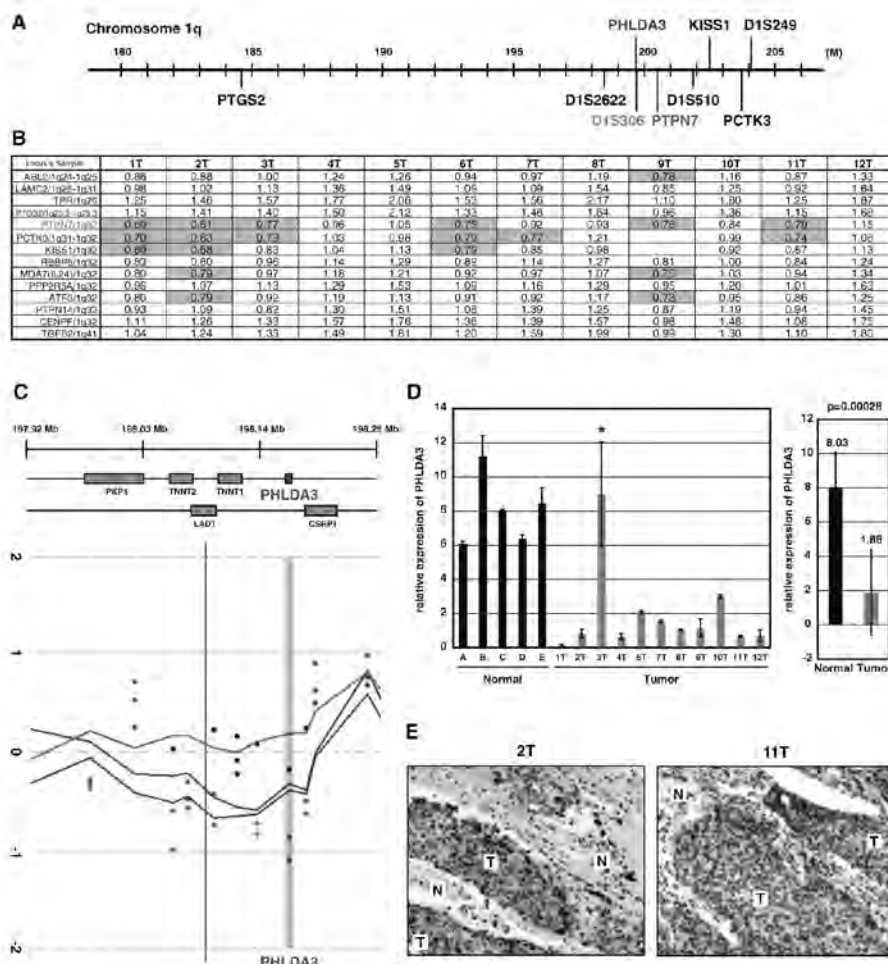


Figure 7. PHLDA3 Locus Is Lost and PHLDA3 Expression Is Downregulated in LCNECs

(A) Chromosomal locations of *PHLDA3* gene, BACs used in CGH analysis, and microsatellite markers.

(B) Chromosome copy number alterations analyzed by MCG cancer array-800 CGH. When the signal ratio (test signal/reference signal) was less than 0.8, it was defined as chromosomal loss. Signal ratios less than 0.8 are in shaded boxes.

(C) Representative results of Agilent 44K CGH analysis on the *PHLDA3* gene locus in LCNEC samples. Chromosomal copy number ratio (tumor DNA/normal DNA) converted to log2 data at each oligonucleotide probe was plotted (green, red, and black spots indicate lost, amplified, and retained signals, respectively). The location of the *PHLDA3* gene locus is shown by a shaded column. Small chromosomal deletions, including *PHLDA3* locus, were detected in two LCNEC cases (blue lines, derived from patients L2 and L5, see Figure S15B), while no copy number loss was observed in the other case (red line, patient L17). Chromosome copy numbers shown by blue and red lines were calculated by applying a weighted moving-average window of 1 Mb.

(D) Expression of *PHLDA3* was analyzed by quantitative RT-PCR. Total RNAs were prepared from normal lung tissues (derived from patients A–E) and LCNECs (derived from patients 1T–12T). *PHLDA3* mRNA levels were analyzed as in Figure 1D. In the right column, the mean expression \pm SD of *PHLDA3* expression in normal lungs and tumor samples is shown.

(E) LCNEC tumor sections were subjected to immunohistochemistry to detect activated Akt. Stronger positive brown signals were detected in tumor regions (T) compared to normal tissue regions (N).

detected in LCNEC and carcinoid samples (11/29 LCNECs and 3/13 carcinoids showed chromosome loss at the PTPN7 locus, Figures 7B and S15A). In addition, we analyzed another cohort of 17 primary LCNECs with much higher resolution using the Agilent 44K oligonucleotide array, and 5 tumor samples showed deletion of the *PHLDA3* gene locus, further demonstrating the

high frequency of chromosome loss at the *PHLDA3* locus in LCNECs (Figures 7C and S15B). To validate chromosome copy number alterations detected by comparative genomic hybridization (CGH), we next determined allelic loss in that region using microsatellite markers in 12 CGH-analyzed LCNEC samples. Five of six samples showing chromosomal loss by CGH analysis

concordantly revealed loss of heterozygosity (Figure S15C). Moreover, 3 of 6 samples showing no chromosomal loss by CGH analysis had allelic imbalance; therefore, collectively, 9 of 12 LCNECs had chromosomal abnormality at the *PHLDA3* locus.

We also analyzed p53 and PTEN status in 32 LCNEC samples (Figures S16A and S16B). The association between *PHLDA3* loss and WT genotype of PTEN was statistically insignificant ($p = 0.68$, by Fisher's exact test). *PHLDA3* and PTEN inhibit the PI3K/Akt pathway by different mechanisms and, as shown for MM468 cells lacking PTEN, loss of *PHLDA3* is additive to PTEN loss in Akt inhibition (Figures 4–6); therefore, it is reasonable that PTEN loss is not mutually exclusive to *PHLDA3* loss. On the other hand, while 63% (5/8) of tumors with WT p53 exhibited *PHLDA3* loss, only 13% (3/24) with nonfunctional p53 had *PHLDA3* loss; however, most likely due to the limited numbers of LCNEC samples, the association of *PHLDA3* loss and WT genotype of p53 was insignificant ($p = 0.088$).

Reduced *PHLDA3* Expression and Elevated Akt Activation in LCNECs

We then analyzed whether such high frequency of chromosomal loss and aberration leads to abnormal *PHLDA3* expression in tumors. As shown in Figure 7D, *PHLDA3* expression was examined in 5 normal lung tissues and 11 CGH-analyzed LCNEC samples by quantitative RT-PCR. Except for one sample, obtained from a patient receiving chemotherapy prior to surgery (3T), all samples showed significant reduction of *PHLDA3* expression. As we found no somatic mutation within the *PHLDA3* gene open reading frame in the 12 tumor samples described in Figures 7B and 7C (data not shown) and the highly reduced *PHLDA3* expression in these tumors cannot be explained solely by hemizygous chromosome loss, *PHLDA3* locus in tumors might have undergone epigenetic changes, resulting in reduced *PHLDA3* expression.

As a consequence of decreased *PHLDA3* expression, we analyzed whether Akt activation occurs in these tumors. Immunohistochemistry of 32 LCNECs, including 10 tumors analyzed for *PHLDA3* expression, revealed Akt activity levels in these tumors. Elevated phospho-Akt staining was detected in 27 tumor samples (including 9 analyzed for *PHLDA3* expression), in which phospho-Akt staining was detected on the cellular membrane, cytoplasm, and nuclei (Figures 7E and S16). Taken together, these results indicate that *PHLDA3* may exhibit a tumor-suppressing function in LCNECs through Akt inhibition.

DISCUSSION

PHLDA3 Is a PH Domain-Only Protein and an Akt Repressor

We have demonstrated that the *PHLDA3* gene is a direct target gene of p53. Although *PHLDA3* has been identified as a p53-inducible gene by several groups, this report is the first to identify *PHLDA3* as a direct target gene of p53 (Jen and Cheung, 2005; Kerley-Hamilton et al., 2005). Previously, the murine *PHLDA3* (also named *Tih1*) gene was cloned as the closest paralog of murine *lpl*, also known as *PHLDA2* (Frank et al., 1999). The *lpl* gene is expressed in the yolk sac, placenta, and fetal liver, while *PHLDA3* is expressed in multiple fetal and adult tissues,

indicating that these two genes have nonoverlapping functions in development. In agreement, *lpl* knockout mice showed placental overgrowth, confirming that at least one of *lpl*'s biological functions is to regulate placental growth, while *PHLDA3* knockout mice did not show this phenotype (Frank et al., 2002). Both *PHLDA3* and *lpl* proteins are mostly composed of the PH domain. PIP binding analysis was performed using PH domains of *PHLDA3* and *lpl* proteins, and both bound to PIP with broad specificity for PIP (Figure 3C and Saxena et al., 2002); however, their physiological function remained unclear. Here, we showed that *PHLDA3* functions as a PH domain-only protein and interferes with another PH domain-containing protein, Akt (Figure 6G).

It has been proposed that specific binding of PH domains to PIP is necessary but not sufficient to recruit the PH domain to the membrane, and alternative co-operative mechanisms are required (Lemmon and Ferguson, 2000; Maffucci and Falasca, 2001). It is also suggested that binding of PH domains to other membrane components, most probably proteins, is essential to enable specific participation in the regulation of specific signaling pathways (Varnai et al., 2005). In agreement, it has been reported that among PIP₃-binding PH domains, those of Btk, Akt, and Gab1 have Akt-inhibiting ability while those of Grp1 and ARNO do not (Ren and Wu, 2003; Varnai et al., 2005). Although it was shown that PIP₃ binding ability is required for Akt inhibition, not all PH domains that bind PIP₃ have Akt-inhibiting activity, indicating the importance of alternative co-operative mechanisms in selective functions of PH domains. *PHLDA3* and the isolated PH domain of Akt similarly inhibited the Akt pathway but had almost no effect on the Grp1-regulated pathway, showing the selective function of *PHLDA3* (Figure 3). Results by in vitro protein-lipid overlay assay demonstrated that *PHLDA3* interferes with Akt binding to PIP directly (Figure 4F); however, alternative mechanisms may cause *PHLDA3* to function specifically as a dominant-negative form of Akt, and it is an important future issue to determine whether such alternative mechanisms exist.

Functions of *PHLDA3* in Lung Endocrine Tumors

By comprehensive analysis of human lung tumors using array-based CGH analysis, we found that the *PHLDA3* genomic locus is frequently lost in LCNECs and carcinoids, both of which are lung endocrine tumors. Lung endocrine tumors store and release small peptides and biogenic amines and are divided into four subtypes: (1) LCNEC, (2) carcinoid, (3) atypical carcinoid, and (4) small-cell lung cancer (Righi et al., 2007). Although lung endocrine tumors have certain uniform features on microscopy and immunohistochemical staining, they have a distinct incidence, epidemiology, and metastatic propensity and distinct clinical characteristics; therefore, defining their molecular and cellular characteristics is essential to improving diagnosis and therapy. The high incidence of loss of the *PHLDA3* genomic locus may account for a molecular characteristic of LCNECs and carcinoids. LCNEC has aggressive clinical behavior, showing poor prognosis and high affinity for distant metastasis (Righi et al., 2007). In addition, LCNEC was recognized rather recently, and therefore no efficient therapy has been established. It has been reported that nicotine and NKK (tobacco carcinogen) bind to nicotinic acetylcholine receptor and activate the Akt pathway

and contribute to tobacco-related carcinogenesis (West et al., 2003). Since LCNEC is directly related to smoking, our findings suggest that decreased expression of PHLDA3 may play an important role in the development and malignant progression of LCNEC. Accordingly, introducing efficient therapies for Akt repression may lead to a better prognosis for LCNEC patients.

In summary, we present a novel Akt-inhibiting pathway, in which Akt activity is inhibited by a PH domain-only protein, PHLDA3. Since PHLDA3 binds to various PIP, and there are numerous PH domain-containing proteins, further investigation will clarify whether PHLDA3 targets proteins other than Akt. Moreover, further detailed analysis of PHLDA3 abnormality in human cancers and tumor formation in *PHLDA3* knockout mice is necessary to assess the involvement of PHLDA3 in tumorigenesis.

EXPERIMENTAL PROCEDURES

For further detailed experimental procedures, please see the Supplemental Experimental Procedures.

ChIP-chip Assay and ChIP Sequence Analysis

For p53 induction, cells were treated with 5-FU (0.375 mM for 9 hr) and UV (10 J, harvested 9 hr post-irradiation). ChIP sequence analysis was performed on Illumina cluster station and 1G analyzer following the manufacturer's instructions.

p53 Pull-Down Assay by Biotinylated DNA Probe

Biotinylated probes were attached to streptavidin-magnetic beads and incubated with cell lysate prepared from p53-overexpressing H1299 cells.

Protein-Lipid Overlay Assay

Various phospholipids were spotted onto nitrocellulose membranes and incubated with purified proteins. Protein binding to the phospholipids was detected by enhanced chemiluminescence.

Cell Spreading and Cell Attachment Assay

Assay was performed as described (Vamali et al., 2005). COS7 cells were transfected with the indicated constructs for 24 hr. For the cell-spreading assay, cells were then plated on fibronectin-coated chamber slides and harvested 20 min after plating. For the attachment assay, cells were divided into three aliquots, one of which was immediately harvested. The other two aliquots were plated and allowed to attach for 30 min. Attached cells were harvested and analyzed by western blotting.

Quantification of Cellular PI(3,4,5)P₃

PI(3,4,5)P₃ was quantified using a PIP₃ mass strip kit (Echelon Biosciences Inc., Salt Lake City, UT). Lipids were extracted from 3 × 10⁶ MM468 cells infected with Ad-LacZ or Ad-PHLDA3, and cells were treated with LY294002 for 12 hr.

Array-Based Comparative Genomic Hybridization Analysis

BAC CGH array hybridization was carried out as described using MCG cancer array-800 (Peng et al., 2005). For higher-density oligonucleotide array CGH, we used Human Genomic CGH microarray 44B (Agilent Technologies, Palo Alto, CA).

SUPPLEMENTAL DATA

Supplemental Data include Supplemental Experimental Procedures, Supplemental References, and 16 figures and can be found with this article online at [http://www.cell.com/supplemental/S0092-8674\(08\)01563-8](http://www.cell.com/supplemental/S0092-8674(08)01563-8).

ACKNOWLEDGMENTS

We are grateful to Atsushi Okabe for production of ChIP-chip and ChIP sequence data and Hiroko Meguro and Kaori Shiina for analysis of ChIP-chip and ChIP sequence samples. This study was supported by the program for the promotion of Fundamental Studies in Health Sciences of the Pharmaceuticals and Medical Devices Agency (to T.O. and H.I.), a Grant-in-Aid for Scientific Research and a grant of the Genome Network Project from the Ministry of Education, Culture, Sports, Science and Technology of Japan (to H.A.), a Grant-in-Aid for Scientific Research from the Ministry of Education, Culture, Sports, Science and Technology of Japan (to Y.T.), and a Grant-in-Aid for Third Term Comprehensive Control Research for Cancer from the Ministry of Health, Labor and Welfare, Japan (to T.S. and Y.T.). T.K. is a recipient of a research fellowship from the Japan Society for the Promotion of Science for Young Scientists.

Received: March 3, 2008

Revised: September 1, 2008

Accepted: December 3, 2008

Published: February 5, 2009

REFERENCES

- Bode, A.M., and Dong, Z. (2004). Post-translational modification of p53 in tumorigenesis. *Nat. Rev. Cancer* 4, 793–805.
- Brooks, C.L., and Gu, W. (2008). p53 ubiquitination: Mdm2 and beyond. *Mol. Cell* 27, 307–315.
- Cully, M., You, H., Levine, A.J., and Maki, T.W. (2006). Beyond PTEN mutations: the PI3K pathway as an integrator of multiple inputs during tumorigenesis. *Nat. Rev. Cancer* 6, 184–192.
- Engelman, J.A., and Cantley, L.C. (2006). The role of the ErbB family members in non-small cell lung cancers sensitive to epidermal growth factor receptor kinase inhibitors. *Clin. Cancer Res.* 12, 4372s–4376s.
- Frank, D., Mendelsohn, C.L., Ciccone, E., Svensson, K., Ohlsson, R., and Tycko, B. (1999). A novel pleckstrin homology-related gene family defined by *lpl/Tssc3*, *TDAG51*, and *Tih1*: tissue-specific expression, chromosomal location, and parental imprinting. *Mamm. Genome* 10, 1150–1159.
- Frank, D., Fortino, W., Clark, L., Musalo, R., Wang, W., Saxena, A., Li, C.M., Reik, W., Ludwig, T., and Tycko, B. (2002). Placental overgrowth in mice lacking the imprinted gene *lpl*. *Proc. Natl. Acad. Sci. USA* 99, 7490–7495.
- Franke, T.F., Kaplan, D.R., Cantley, L.C., and Toker, A. (1997). Direct regulation of the Akt proto-oncogene product by phosphatidylinositol-3,4-bisphosphate. *Science* 275, 665–668.
- Harnagel, J., and Bismuth, G. (2002). Imaging antigen-induced PI3K activation in T cells. *Nat. Immunol.* 3, 1090–1096.
- Harris, S.L., and Levine, A.J. (2005). The p53 pathway: positive and negative feedback loops. *Oncogene* 24, 2899–2908.
- Jen, K.Y., and Cheung, V.G. (2005). Identification of novel p53 target genes in ionizing radiation response. *Cancer Res.* 65, 7666–7673.
- Kawase, T., Ichikawa, H., Ohta, T., Nozaki, N., Tashiro, F., Ohki, R., and Taya, Y. (2008). p53 target gene AEN is an exonuclease required for p53-dependent apoptosis. *Oncogene* 27, 3797–3810.
- Kerley-Hamilton, J.S., Pike, A.M., Li, N., DiRenzo, J., and Spinella, M.J. (2005). A p53-dominant transcriptional response to cisplatin in testicular germ cell tumor-derived human embryonal carcinoma. *Oncogene* 24, 6090–6100.
- Lemmon, M.A., and Ferguson, K.M. (2000). Signal-dependent membrane targeting by pleckstrin homology (PH) domains. *Biochem. J.* 350, 1–18.
- Liu, G., and Chen, X. (2006). Regulation of the p53 transcriptional activity. *J. Cell. Biochem.* 97, 448–458.
- Lu, J., Manning, B.D., and Cantley, L.C. (2003). Targeting the PI3K-Akt pathway in human cancer: rationale and promise. *Cancer Cell* 4, 257–262.
- Maftucci, T., and Falasca, M. (2001). Specificity in pleckstrin homology (PH) domain membrane targeting: a role for a phosphoinositide-protein co-operative mechanism. *FEBS Lett.* 506, 173–179.

Cell

- Manning, B.D., and Cantley, L.C. (2007). AKT/PKB signaling: navigating downstream. *Cell* 129, 1261–1274.
- Mayo, L.D., and Donner, D.B. (2002). The PTEN, Mdm2, p53 tumor suppressor-oncoprotein network. *Trends Biochem. Sci.* 27, 462–467.
- Moore, S.M., Rintoul, R.C., Walker, T.R., Chilvers, E.R., Haslett, C., and Sethi, T. (1998). The presence of a constitutively active phosphoinositide 3-kinase in small cell lung cancer cells mediates anchorage-independent proliferation via a protein kinase B and p70s6k-dependent pathway. *Cancer Res.* 58, 5239–5247.
- Oda, E., Ohki, R., Murasawa, H., Nemoto, J., Shibue, T., Yamashita, T., Tokino, T., Taniguchi, T., and Tanaka, N. (2000). Noxa, a BH3-only member of the Bcl-2 family and candidate mediator of p53-induced apoptosis. *Science* 288, 1053–1058.
- Ohki, R., Nemoto, J., Murasawa, H., Oda, E., Inazawa, J., Tanaka, N., and Taniguchi, T. (2000). Reprimin, a new candidate mediator of the p53-mediated cell cycle arrest at the G2 phase. *J. Biol. Chem.* 275, 22627–22630.
- Ohki, R., Kawase, T., Ohta, T., Ichikawa, H., and Taya, Y. (2007). Dissecting functional roles of p53 N-terminal transactivation domains by microarray expression analysis. *Cancer Sci.* 98, 189–200.
- Oren, M. (2003). Decision making by p53: life, death and cancer. *Cell Death Differ.* 10, 431–442.
- Peng, W.X., Shibata, T., Katoh, H., Kokubu, A., Matsuno, Y., Asamura, H., Tsuchiya, R., Kanai, Y., Hosoda, F., Sakiyama, T., et al. (2005). Array-based comparative genomic hybridization analysis of high-grade neuroendocrine tumors of the lung. *Cancer Sci.* 96, 661–667.
- Ren, Y., and Wu, J. (2003). Simultaneous suppression of Erk and Akt/PKB activation by a Gab1 pleckstrin homology (PH) domain decoy. *Anticancer Res.* 23, 3231–3236.
- Righi, L., Volante, M., Rapa, I., Scagliotti, G.V., and Papotti, M. (2007). Neuroendocrine tumours of the lung. A review of relevant pathological and molecular data. *Virchows Arch.* 451, 51–59.
- Saxena, A., Morozov, P., Frank, D., Musalo, R., Lemmon, M.A., Skolnik, E.Y., and Tycko, B. (2002). Phosphoinositide binding by the pleckstrin homology domains of Ipi and Tih1. *J. Biol. Chem.* 277, 49935–49944.
- Scheid, M.P., and Woodgett, J.R. (2003). Unravelling the activation mechanisms of protein kinase B/Akt. *FEBS Lett.* 546, 108–112.
- Schneider, R., Barnister, A.J., Myers, F.A., Thorne, A.W., Crane-Robinson, C., and Kouzarides, T. (2004). Histone H3 lysine 4 methylation patterns in higher eukaryotic genes. *Nat. Cell Biol.* 6, 73–77.
- Shibata, T., Uryu, S., Kokubu, A., Hosoda, F., Ohki, M., Sakiyama, T., Matsuno, Y., Tsuchiya, R., Kanai, Y., Kondo, T., et al. (2005). Genetic classification of lung adenocarcinoma based on array-based comparative genomic hybridization analysis: its association with clinicopathologic features. *Clin. Cancer Res.* 11, 6177–6185.
- Songyang, Z., Baltimore, D., Cantley, L.C., Kaplan, D.R., and Franke, T.F. (1997). Interleukin 3-dependent survival by the Akt protein kinase. *Proc. Natl. Acad. Sci. USA* 94, 11345–11350.
- Stambolic, V., Mak, T.W., and Woodgett, J.R. (1999). Modulation of cellular apoptotic potential: contributions to oncogenesis. *Oncogene* 18, 6094–6103.
- Stokoe, D., Stephens, L.R., Copeland, T., Gaffney, P.R., Reese, C.B., Painter, G.F., Holmes, A.B., McCormick, F., and Hawkins, P.T. (1997). Dual role of phosphatidylinositol-3,4,5-trisphosphate in the activation of protein kinase B. *Science* 277, 567–570.
- Varnai, P., Bondeva, T., Tamas, P., Toth, B., Buday, L., Hunyady, L., and Balla, T. (2005). Selective cellular effects of overexpressed pleckstrin-homology domains that recognize PtdIns(3,4,5)P3 suggest their interaction with protein binding partners. *J. Cell Sci.* 118, 4879–4888.
- Vogelstein, B., Lane, D., and Levine, A.J. (2000). Surfing the p53 network. *Nature* 408, 307–310.
- Vousden, K.H., and Prives, C. (2005). p53 and prognosis: new insights and further complexity. *Cell* 120, 7–10.
- West, K.A., Brognard, J., Clark, A.S., Linnoila, J.R., Yang, X., Swain, S.M., Harris, C., Belinsky, S., and Dennis, P.A. (2003). Rapid Akt activation by nicotine and a tobacco carcinogen modulates the phenotype of normal human airway epithelial cells. *J. Clin. Invest.* 111, 81–90.

M E M O

[illegible]

分子遺伝分野

三木 義男

難治疾患研究所・遺伝疾患研究部門
遺伝子応用医学・教授



1) 研究の課題名

I. 骨腫瘍のアポトーシス誘導機構

(Induction of apoptosis in bone and soft tissue tumors)

骨腫瘍は、原発腫瘍の頻度は少ないが、転移性骨腫瘍の占める割合は高い。これまでの研究から TNF-alpha より誘導された NF-kappa B の活性はがんの骨転移の発生と進展に大きな関わりを持つことが知られている。しかし、TNF-alpha で誘導された NF-kappa B の転写活性制御は今まだ不明点が多い。Protein Kinase C-delta (PKC-delta) はがん細胞のアポトーシス、増殖阻害、細胞分化に関わる Protein Kinase として知られている。我々は TNF-alpha より誘導された NF-kappa B の活性制御に注目し、分子生物学手法で PKC-delta と NF-kappa B family の関連性を見出した。さらに免疫沈降法などにより、NF-kappa B のメインユニット RelA/p65 と PKC-delta との会合を見出し、PKC-delta が RelA/p65 の転写活性に関わっていることを明らかにした。我々は NF-kappa B の活性化制御機構の解析を進めることで、転移性骨腫瘍の発生、発展メカニズムを解明し、がんによる骨破壊を抑制することに繋がると考えている。

II. 乳がん原因遺伝子 BRCA2 と Nucleophosmin (NPM) の結合とその機能解析

(Identification of novel BRCA2-related genes: Functional analysis of Nucleophosmin (NPM))

BRCA1 と BRCA2 の変異は日本では約半数の家族性乳癌に見られている。両遺伝子産物は複合体を形成しているため、他にも相互作用する分子の存在が考えられる。このような分子は乳癌発生機構に関与していると予想されるので、質量分析法を用いて BRCA2 と相互作用する遺伝子産物の同定を試みた。得られた候補分子 NPM については哺乳動物細胞で過剰発現し免疫共沈降によって BRCA2 との相互作用を確認し、さらに、内在性の

BRCA2 との相互作用を確認した。得られた NPM は両 BRCA 遺伝子と同様に重要な中心体制御機構に関与している可能性が高いので RNAi を用いて表現型を調べる。本研究で使用する実験技術は成熟した手法であり計画の実現性は高い。

2) 研究内容の英文要約

(1) Molecular markers associated with lymph node metastasis in pancreatic ductal adenocarcinoma by genome-wide expression profiling.

Lymph node metastasis (LNM) is the most important prognostic factor in patients undergoing surgical resection of In this study, we aimed to identify molecular markers associated with LNM in pancreatic ductal adenocarcinoma (PDAC) using genome-wide expression profiling. In this study, laser microdissection and genome-wide transcriptional profiling were used to identify genes that were differentially expressed between PDAC cells with and without LNM obtained from 20 patients with PDAC. In the results, microarray profiling identified 46 genes that were differently expressed between PDAC with and without LNM with certain significance. In 63 patients with PDAC, significant LNM predictors in PDAC elucidated from multivariate analysis were low expression of activating enhancer binding protein 2 (AP2alpha) ($P = 0.012$) and high expression of mucin 17 (MUC17) ($P = 0.0192$). Furthermore, multivariate analysis revealed that AP2alpha-low expression and MUC17-high expression are independent prognostic factors for poor overall survival ($P = 0.0012$, 0.0001 , respectively).

(2) DNA damage signalling recruits RREB-1 to the p53 tumour suppressor promoter.

Transcriptional regulation of the p53 tumour suppressor gene plays an important role in the control of the expression of various target genes involved in the DNA damage response. However, the molecular basis of this regulation remains obscure. In the present study we

demonstrate that RREB-1 (Ras-responsive-element-binding protein-1) efficiently binds to the p53 promoter via the p53 core promoter element and transactivates p53 expression. Silencing of RREB-1 significantly reduces p53 expression at both the mRNA and the protein levels. Notably, disruption of RREB-1-mediated p53 transcription suppresses the expression of the p53 target genes. We also show that, upon exposure to genotoxic stress, RREB-1 controls apoptosis in a p53-dependent manner. These findings provide evidence that RREB-1 participates in modulating p53 transcription in response to DNA damage.

(3) Protein kinase Cdelta activates RelA/p65 and nuclear factor-kappaB signaling in response to tumor necrosis factor-alpha.

Nuclear factor-kappaB (NF-kappaB) is tightly modulated by IkappaB kinases and IkappaBalpha in the cytoplasm. Here, we show that protein kinase C (PKC) delta controls the main subunit of NF-kappaB, RelA/p65. The results also show that PKCdelta is targeted to the nucleus and forms a complex with RelA/p65 following TNF-alpha exposure. Importantly, kinase activity of PKCdelta is required for RelA/p65 transactivation. In concert with these results, PKCdelta activates RelA/p65 for its occupancy to target-gene promoters, including IkappaBalpha and p100/p52. Moreover, functional analyses show that inhibition of PKCdelta is associated with substantial attenuation of NF-kappaB activity in response to TNF-alpha. These findings provide evidence that PKCdelta orchestrates RelA/p65 transactivation, a requisite for NF-kappaB signaling pathway in the nucleus.

(4) Gene expression-based diagnosis of efficacy of chemotherapy for breast cancer.

Development of a clear index to select drugs, i.e., accurate prediction of drug sensitivity, is important not only to obtain the maximum therapeutic effects of drugs, but also realize personalized medicine (tailor-made medicine). With the recent advancement in genome science represented by microarrays, molecular-level elucidation of many diseases including cancers has been progressing. It has been clarified that molecular information, such as gene expression profiles of cancer cells and gene polymorphisms in individual patients, affects not only cancer development and progression, but also therapeutic and adverse effects. The establishment of a therapeutic method by clinical application of this information has been progressing, in which the therapeutic effects of drugs are accurately predicted, and the maximum effects are obtained corresponding to cancer properties and patients' characteristics.

(5) Pim-1 controls NF-kappaB signalling by stabilizing RelA/p65.

Post-translational modification and degradation of proteins by the ubiquitin-proteasome system are key regulatory mechanisms in cellular responses to various stimuli. In this study we show that phosphorylation of RelA/p65 at Ser276 prevents its degradation by ubiquitin-mediated proteolysis. In contrast, impairment of Ser276 phosphorylation affects constitutive degradation of RelA/p65. Importantly, we identify Pim-1 as a further kinase responsible for the phosphorylation of RelA/p65 at Ser276. Depletion of Pim-1 hinders not only Ser276 phosphorylation but also transactivation of RelA/p65 target genes. We also show that Pim-1 contributes to recruitment of RelA/p65 to kappaB-elements to activate NF-kappaB signalling after TNF-alpha stimulation. In concert with these results, the knockdown of Pim-1 impairs IL-6 production and augments apoptosis by interfering RelA/p65 activation.

(6) BRCA2 interacts with the cytoskeletal linker protein plectin to form a complex controlling centrosome localization.

The breast cancer susceptibility gene (BRCA2) is localized mainly in the nucleus where it plays an important role in DNA damage repair. Some BRCA2 protein is also present in the centrosome. Here, we demonstrate that BRCA2 interacts with plectin, a cytoskeletal cross-linker protein, and that this interaction controls the position of the centrosome. We induced phosphorylation of plectin in prepared fractions of HeLa cells by adding activated CDK1/CycB kinase. Consequently, there was significant dissociation of the centrosome from the nuclear membrane. Plectin has six homologous ankyrin-like repeat domains (termed PLEC M1-M6). Using a pull-down assay, we found that GST-PLEC M1 and a GST-C-terminal region fusion protein (which comprised PLEC M6, along with an adjacent vimentin site) interacted with BRCA2. In addition, when either BRCA2 or plectin was suppressed by the appropriate siRNA, a similar change in centrosomal positioning was observed. We suggest that the BRCA2-plectin interaction plays an important role in the regulation of centrosome localization and also that displacement of the centrosome may result in genomic instability and cancer development.

(7) ATM augments nuclear stabilization of DYRK2 by inhibiting MDM2 in the apoptotic response to DNA damage.

The tumor suppressor p53 is a transcription factor that regulates cell cycle, DNA repair, senescence, and apoptosis in response to DNA damage. Phosphorylation of p53 at Ser46 is indispensable for the commitment to apoptotic cell death. A previous study has shown that, upon exposure to genotoxic stress, DYRK2 translocates into the nucleus and phosphorylates p53 at Ser46, thereby inducing apoptosis. However, less is known about mechanisms responsible for

intracellular control of DYRK2. Here we show the functional nuclear localization signal at amino-terminal domain of DYRK2. Under normal conditions, nuclear and not cytoplasmic DYRK2 is ubiquitinated by MDM2, resulting in its constitutive degradation. In the presence of proteasome inhibitors, we detected a stable complex of DYRK2 with MDM2 at the nucleus. Upon exposure to genotoxic stress, ATM phosphorylates DYRK2 at Thr33 and Ser369, which enables DYRK2 to escape from degradation by dissociation from MDM2 and to induce the kinase activity toward p53 at Ser46 in the nucleus. These findings indicate that ATM controls stability and pro-apoptotic function of DYRK2 in response to DNA damage.

(8) Introduction and characterization of a polymerase-dead point mutation into the POLK gene in vertebrates.

The chicken DT40 cell line is widely used for gene knock-outs. We attempted to introduce a polymerase-dead point mutation into Polkappa, a polymerase for translesion DNA synthesis, taking advantage of the highly efficient targeted integration in DT40 cells. The resulting cells (REV3 (-/-) POLK (/) (pol-dead)) proliferated with the same kinetics as the parental REV3 (-/-) cells. Though the mock-treated REV3 (-/-) POLK (/) (mock) cells showed the same sensitivity as the parental REV3 (-/-) cells to methyl methanesulfonate, the REV3 (-/-) POLK (/) (pol-dead) cells demonstrated the same sensitivity as the REV3 (-/-) POLK (/) double knock-out cells. This implies that the presence of the polymerase-dead Polkappa does not interfere with other polymerases repairing monoalkylation damage.

3) 本事業に関連して世界的な研究拠点形成に向けて、以下の点で改善・整備等されたこと

A (研究拠点体制)

研究室におけるスペースの確保、機器の整備および補充、研究推進のためのスケジュール等を作成し研究室内部の体制を整備するとともに、整形外科、口腔外科等の臨床グループとの共同研究計画を立案し総合的に研究拠点体制の整備を進めた。

B (研究教育環境)

ジャーナルクラブ、研究進捗ミーティング、GCOEセミナー等研究教育環境の整備を進めた。

C (人材確保)

大学院生3人がGCOE研究を遂行している。

D (人材育成)

新たに入学する大学院生を含め上記体制で人材育成に努めている。

E (国際化)

GCOEプログラムの中で国際セミナーへの参加、海外招聘研究者との議論等を通して国際化を図っている。

4) GCOE事業を推進するに当たって力を入れた点

GCOE推進研究者間で共同研究計画案を立案し、特に臨床グループとの共同研究で患者臨床検体を用いたゲノム研究推進体制の構築に努力した。

5) 英文原著論文

1. Hirono, S., Yamaue, H., Hoshikawa, Y., Ina, S., Tani, M., Kawai, M., Ushijima, M., Matsuura, M., Saiki, Y., Saiura, A., Yamamoto, J., Miki, Y. and Noda, T. (2009) Molecular markers associated with lymph node metastasis in pancreatic ductal adenocarcinoma by genome-wide expression profiling. *Cancer Sci*.
2. Liu, H., Hew, H.C., Lu, Z.G., Yamaguchi, T., Miki, Y. and Yoshida, K. (2009) DNA damage signalling recruits RREB-1 to the p53 tumour suppressor promoter. *Biochem J*, 422, 543-51.
3. Lu, Z.G., Liu, H., Yamaguchi, T., Miki, Y. and Yoshida, K. (2009) Protein kinase Cdelta activates RelA/p65 and nuclear factor-kappaB signaling in response to tumor necrosis factor-alpha. *Cancer Res*, 69, 5927-35.
4. Nihira, K., Ando, Y., Yamaguchi, T., Kagami, Y., Miki, Y. and Yoshida, K. (2009) Pim-1 controls NF-kappaB signalling by stabilizing RelA/p65. *Cell Death Differ*.
5. Niwa, T., Saito, H., Imajoh-ohmi, S., Kaminishi, M., Seto, Y., Miki, Y. and Nakanishi, A. (2009) BRCA2 interacts with the cytoskeletal linker protein plectin to form a complex controlling centrosome localization. *Cancer Sci*, 100, 2115-25.
6. Taira, N., Yamamoto, H., Yamaguchi, T., Miki, Y. and Yoshida, K. (2009) ATM augments nuclear stabilization of DYRK2 by inhibiting MDM2 in the apoptotic response to DNA damage. *J Biol Chem*.
7. Takenaka, K. and Miki, Y. (2009) Introduction and characterization of a polymerase-dead point mutation into the POLK gene in vertebrates. *FEBS Lett*, 583, 661-4.
8. Tanaka, S., Mogushi, K., Yasen, M., Noguchi, N., Kudo, A., Nakamura, N., Ito, K., Miki, Y., Inazawa, J., Tanaka, H. and Arii, S. (2009) Gene-expression phenotypes for vascular invasiveness of hepatocellular carcinomas. *Surgery*.

6) 著書

1. Miki, Y. (2009) Gene expression-based diagnosis of efficacy of chemotherapy for breast cancer. *Breast Cancer*.

2. 三木義男.【臨床遺伝子学'09 がんの遺伝子学】がんマーカーとゲノム解析 乳癌のトランスクリプトーム情報による抗がん剤の効果予測. 最新医学 2009;64:2023-9.
3. 三木義男.【ゲノム研究最前線 疾患ゲノム研究の現状と展望】最新のゲノムワイド解析技術. 日本臨床 2009;67:1058-61.
4. 三木義男.【個別化医療 実現に向けた基盤整備】基礎的観点から ゲノム、トランスクリプトーム情報とがん治療. 治療学 2009;43:268-71.
5. 長崎光一, 三木義男.【乳癌治療Update 最新診療コンセンサス】最新治療トピックス 治療効果予測 遺伝子発現情報に基づいた乳癌薬物療法の有効性診断 乳癌の抗癌剤感受性予測. 医学のあゆみ 2009;230:89-93.
6. 長崎光一, 三木義男.【がん薬物療法学 基礎・臨床研究のアップデート】癌分子診断のための手法 トランスクリプトーム解析 (cDNA マイクロアレイ、DNA チップ). 日本臨床 2009;67:148-55.
7. 大石陽子, 三浦妙太, 佐原八束, 川村徹, 佐藤康, 中嶋昭, 三木義男. 乳がんにおける stmn1 高発現症例の病理学的特徴. 日本乳癌学会総会プログラム抄録集 2009;06:550.
8. 三木義男, 中西啓. Brca2 は 14-3-3 γ と結合して中心体の凝集に関与する. 家族性腫瘍 2009;9:A33.
9. 小松哲, 長崎光一, 篠原剛, 五十嵐淳, 藤森芳郎, 山岸喜代文, 西村博行, 藤森実, 三木義男. 乳癌における新規遺伝子多型の同定. 日本外科学会雑誌 2009;110:513.
10. 石井紀子, 新井正美, 三木義男. 遺伝カウンセリング後の hnpcc 患者・家族の近親者への医療機関受診勧奨支援の重要性について. 家族性腫瘍 2009;9:A45.
11. 大石陽子, 三浦妙太, 佐原八束, 川村徹, 佐藤康, 中嶋昭, 三木義男. 乳がんにおける stmn1 高発現症例の病理学的特徴. 日本乳癌学会総会プログラム抄録集 2009;06:550.

9) 外部資金の獲得状況

- ・科学研究費補助金、特定領域 (C) (2)
- 研究題目: 乳腺発がんにおける BRCA1、BRCA2 の役割
- 代表: 三木 義男
- 期間: 平成 20 年—21 年
- 研究費総額: 2,140 万円

7) 学会発表 (英文)

1. Miki Y. Molecular prediction of therapeutic response and adverse effect of chemotherapy in breast cancer. International Symposium, New Frontiers in Cancer Research, Hokkaido, Japan, March 18, 2009

8) 学会発表 (和文)

1. 吉村慶子, 長崎光一, 岩瀬拓士, 秋山太, 三木義男. 乳癌の新規予後因子の同定. 日本乳癌学会総会プログラム抄録集 2009;06:246.
2. 五木田茶舞, 阿江啓介, 下地尚, 石田剛, 松本誠一, 三木義男, 四宮謙一. 分子生物学的手法による高分化型脂肪肉腫の鑑別診断の試み. 日本整形外科学会雑誌 2009;83:S886.
3. 三木義男, 牛嶋大, 松浦正明, 長崎光一. 乳癌における治療効果予測因子の現状と今後の展望 化学療法の効果予測因子 基礎の立場から. 日本乳癌学会総会プログラム抄録集 2009;06:189.

10) 特別講演、招待講演

1. 三木義男, 長崎光一, 牛嶋大, 宮田敏, 松浦正明, 野田哲生. 分子情報を用いた個別化医療の TR. 第 68 回日本癌学会学術総会, 横浜, 2009 年 10 月

11) 自己評価

GCOE プログラムに参加し、骨軟部腫瘍 (骨肉腫、軟骨肉腫、歯肉癌など) を中心に、ゲノム科学を応用した研究を進めてきた。一方、骨肉腫におけるアポトーシス誘導メカニズムについても、生化学的に解明を進めその一部を解明することに成功した。今度は、臨床系グループとの共同研究体制を構築し臨床検体収拾システムを作製、順次癌組織の収集を促進し遺伝子発現プロファイル解析を進める。また、口腔病理学分野との共同で癌の間質における Interleukin-6 の重要性に関する論文を作成した。教育等には大きく貢献できたと判断している。

12) 教室、分野や講座の准教授、講師、助教、
特別研究員、ポスドク、指導を受けた大学
院生の名前 (AISSには○印) のリスト

准教授 吉田 清嗣

助教 竹中 克也

○ D4 Lu Zheng Guang
呂 正光

○ D4 Wang Hui Feng
王 慧峰

○ D3 木村 純子

D3 平 直江

○ D3 Hew Hoi Chin
侯 韋君

D2 高岡 美帆

D2 仁平 啓史

D2 Wali Nadila
瓦力 娜迪拉

D1 Mariku Sadiya
真利久 サディヤ

M2 工藤 卓也

Protein Kinase C δ Activates RelA/p65 and Nuclear Factor- κ B Signaling in Response to Tumor Necrosis Factor- α

Zheng-Guang Lu, Hanshao Liu, Tomoko Yamaguchi, Yoshio Miki, and Kiyotsugu Yoshida

Department of Molecular Genetics, Medical Research Institute, Tokyo Medical and Dental University, Tokyo, Japan

Abstract

Nuclear factor- κ B (NF- κ B) is tightly modulated by I κ B kinases and I κ B α in the cytoplasm. On stimulation, NF- κ B translocates into the nucleus to initiate transcription; however, regulation of its transcriptional activity remains obscure. Here, we show that protein kinase C (PKC) δ controls the main subunit of NF- κ B, RelA/p65. On exposure to tumor necrosis factor- α (TNF- α), the expression of RelA/p65 target genes such as I κ B α , RelB, and p100/p52 is up-regulated in a PKC δ -dependent manner. The results also show that PKC δ is targeted to the nucleus and forms a complex with RelA/p65 following TNF- α exposure. Importantly, kinase activity of PKC δ is required for RelA/p65 transactivation. In concert with these results, PKC δ activates RelA/p65 for its occupancy to target-gene promoters, including I κ B α and p100/p52. Moreover, functional analyses show that inhibition of PKC δ is associated with substantial attenuation of NF- κ B activity in response to TNF- α . These findings provide evidence that PKC δ orchestrates RelA/p65 transactivation, a requisite for NF- κ B signaling pathway in the nucleus. [Cancer Res 2009;69(14):5927–35]

Introduction

The protein kinase C (PKC) family represents serine and threonine kinases that are responsible for a variety of cellular responses such as growth, proliferation, transformation, and cell death (1, 2). The PKC family is subdivided into three categories: conventional, novel, and atypical PKCs (1, 2). Accumulating lines of evidence have revealed that PKC δ , a novel PKC, plays a crucial role in the cellular response to genotoxic stress (3–5). On exposure to DNA damage, PKC δ is activated and cleaved by caspase-3 to form a 40 kDa catalytically active fragment. Overexpression of the PKC δ catalytic fragment induces chromatin condensation and DNA fragmentation, which supports a role for PKC δ cleavage in the induction of apoptosis (6). Other studies have shown that PKC δ interacts with the c-Abl tyrosine kinase (7). c-Abl is a proapoptotic tyrosine kinase that targets to the nucleus following genotoxic stress (8–10). Importantly, c-Abl-mediated phosphorylation activates PKC δ and induces its translocation to the nucleus (7). Consistent with these findings, tyrosine phosphorylation of PKC δ is necessary for its nuclear translocation and subsequent caspase-dependent cleavage (2, 11, 12). Previous studies have also shown

that the nuclear complex of c-Abl and Lyn tyrosine kinases includes the protein tyrosine phosphatase SHPTP1 (13, 14) and that PKC δ phosphorylates and inactivates SHPTP1 in response to genotoxic stress (15). Another study showed that cells derived from PKC δ -null transgenic mice were defective in mitochondria-dependent apoptosis induced by DNA damage (16). We have recently shown that PKC δ phosphorylates the p53 tumor suppressor to induce apoptotic cell death (17). Furthermore, recent studies have shown that PKC δ interacts with and phosphorylates Rad9, a key factor involved in checkpoint regulation of the DNA damage responses (18, 19). Inhibition of PKC δ attenuates Rad9-mediated apoptosis. These findings collectively support an essential role for PKC δ in the induction of apoptosis in the genotoxic stress response (2). By contrast, several lines of studies showed a pivotal role for PKC δ in antiapoptotic function in response to cytokines, including tumor necrosis factor- α (TNF- α ; refs. 20–22). Expression with a PKC δ kinase-dead mutant or with a small interfering RNA (siRNA) targeting PKC δ increased the apoptotic effect of TNF-related apoptosis-inducing ligand, whereas overexpression of PKC δ decreased it (22). Intriguingly, phosphorylation of PKC δ on Tyr¹⁵⁵ was required for its cleavage in response to TNF-related apoptosis-inducing ligand. In addition, cleavage of PKC δ by caspases was essential for its protective effect because overexpression of a caspase-resistant mutant did not protect glioma cells from TNF-related apoptosis-inducing ligand-induced apoptosis (22). Another study showed that inhibition of PKC δ attenuated TNF- α -induced nuclear factor- κ B (NF- κ B) activation in human neutrophils (21). A further study suggested that PKC δ depletion by PKC δ siRNA resulted in inhibition of TNF-mediated extracellular signal-regulated kinase 1/2 activation, which is involved in an essential component of TNF- α -mediated signaling (20). These findings collectively imply a protective role for PKC δ in TNF- α -induced apoptosis. Precise mechanisms in which PKC δ controls signaling pathways to protect cells from apoptosis, however, remain obscure.

NF- κ B is an inducible transcription factor that controls the expression of several proteins involved in the regulation of cell survival and immune response (23). NF- κ B is a dimer formed from a multisubset family consisting of RelA/p65, RelB, c-Rel, p105/p50 (NF- κ B1), and p100/p52 (NF- κ B2). NF- κ B is activated by a bewildering array of stimuli, including biological agents such as TNF- α , interleukin (IL)-1, bacterial endotoxin, and phorbol esters and cytotoxic stimuli such as chemotherapeutic agents, ultraviolet light, oxidative stress, and ionizing radiation (24, 25). Activation of NF- κ B is regulated by multiple distinct signaling cascades including inhibitors of the NF- κ B (I κ B) kinase (IKK) signalosome (26, 27). IKK phosphorylates I κ B α at Ser³² and Ser³⁶ in response to a variety of stimuli, resulting in its ubiquitination and subsequent proteasomal degradation (26, 27). The released NF- κ B targets to the nucleus and thereby induces the expression of specific target genes. In addition to nuclear translocation of the NF- κ B complex, previous studies have shown that a subunit of NF- κ B, RelA/p65, is post-translationally

Note: Supplementary data for this article are available at Cancer Research Online (<http://cancerres.aacrjournals.org/>).

K. Yoshida and Y. Miki share senior authorship.

Requests for reprints: Kiyotsugu Yoshida, Department of Molecular Genetics, Medical Research Institute, Tokyo Medical and Dental University, 1-5-45 Yushima, Bunkyo-ku, Tokyo 113-8510, Japan. Phone: 81-3-5803-5826; Fax: 81-3-5803-0242; E-mail: yos.mgen@mri.tmd.ac.jp.

©2009 American Association for Cancer Research.

doi:10.1158/0008-5472.CAN-08-4786

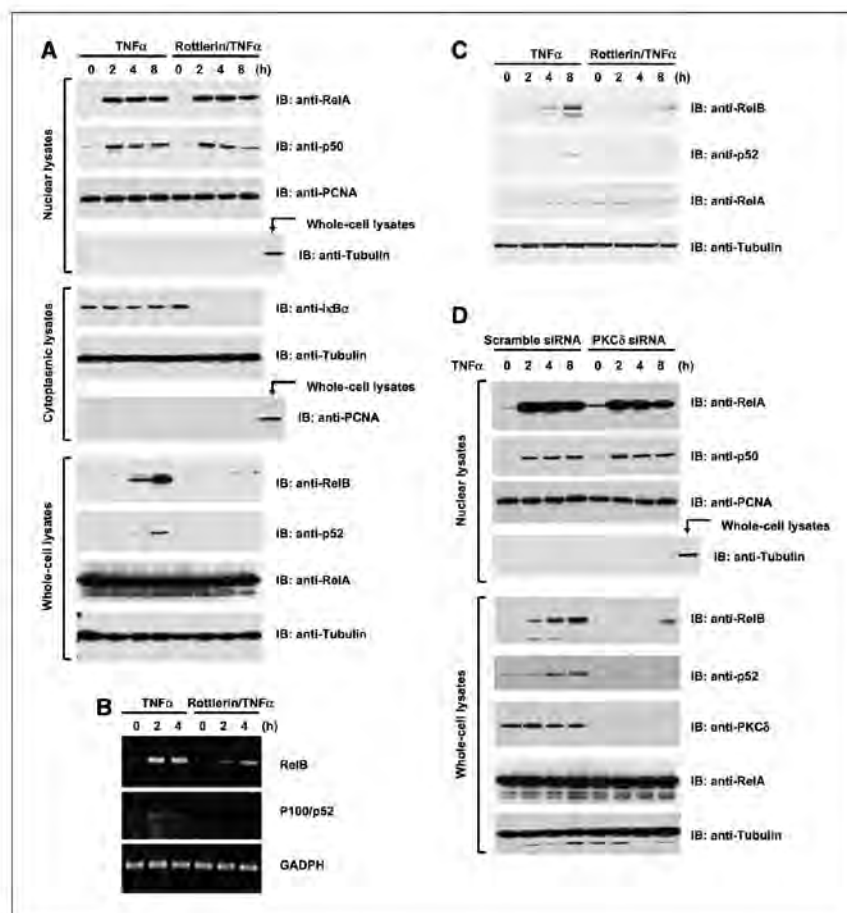


Figure 1. PKC δ is involved in RelA/p65 transactivation following TNF- α exposure. **A** and **B**, 293T cells were pretreated with or without rotterlin for 30 min followed by treatment with TNF- α for indicated times. Nuclear, cytoplasmic, and whole-cell lysates were subjected to immunoblot analysis with the indicated antibodies (**A**). Total RNA was subjected to reverse transcription-PCR analysis using primer sets for RelB (*top*), p100/p52 (*middle*), or GAPDH (*bottom*). **C**, U2OS cells were left untreated or pretreated with rotterlin followed by treatment with TNF- α . Whole-cell lysates were subjected to immunoblot analysis with the indicated antibodies. **D**, U2OS cells were transfected with the PKC δ siRNA for 48 h followed by treatment with TNF- α for indicated times. Nuclear lysates and whole-cell lysates were subjected to immunoblot analysis with the indicated antibodies.

modified such as phosphorylation or acetylation, and those changes influence its transcriptional activity. However, recent data showing a role for Ser³³⁶ phosphorylation by IKKs on RelA/p65 activation in response to TNF- α remain controversial (28–33). In this context, mechanisms for RelA/p65 transactivation following nuclear translocation are largely unclear.

In this study, we show that inhibition of PKC δ is associated with attenuation of RelA/p65 transactivation in response to TNF- α . The results show that PKC δ translocates from the cytoplasm into the nucleus after TNF- α exposure. Importantly, kinase activity of PKC δ is required for its nuclear targeting and RelA/p65 transactivation. However, phosphorylation of RelA/p65 is not involved in PKC δ -mediated activation of RelA/p65. These findings collectively support a novel mechanism in which regulation of RelA/p65 by PKC δ contributes to TNF- α -induced activation of NF- κ B signaling pathway.

Materials and Methods

Cell culture. U2OS (human osteosarcoma) cells were cultured in RPMI 1640 supplemented with 10% heat-inactivated fetal bovine serum, 100 units/mL penicillin, 100 μ g/mL streptomycin, and 2 mmol/L L-glutamine. 293T (human embryonal kidney) cells were grown in DMEM containing 10% fetal bovine serum and antibiotics. Cells were treated with

20 ng/mL TNF- α (human TNF- α ; PeproTech), 5 μ mol/L rotterlin (Sigma-Aldrich), or 100 ng/mL NF- κ B inhibitor (Santa Cruz Biotechnology).

siRNA transfection. siRNA duplexes (siRNAs) targeting for PKC δ were synthesized and purified by Invitrogen (Stealth RNAi). Transfection of siRNAs was done using Lipofectamine RNAi Max (Invitrogen) according to the manufacturer's protocol.

Immunoprecipitation and immunoblot analysis. Cell lysates were prepared as described elsewhere (14, 34). Soluble proteins were incubated with anti-PKC δ (Santa Cruz Biotechnology) or anti-RelA/p65 (Santa Cruz Biotechnology) antibodies for 2 h at 4°C followed by a 1 h incubation with protein A/G (Santa Cruz Biotechnology) Sepharose beads. Cell lysates or immunoprecipitates were separated by SDS-PAGE and transferred to nitrocellulose filters, which were then incubated with anti-I κ B α (Santa Cruz Biotechnology), anti-RelA/p65, anti-p50 (Santa Cruz Biotechnology), anti-RelB (Santa Cruz Biotechnology), anti-p52 (Santa Cruz Biotechnology), anti-PKC δ , anti-phospho-RelA/p65 (Cell Signaling), anti-PCNA (Santa Cruz Biotechnology), or anti-tubulin (Sigma-Aldrich). After washing, the membranes were incubated with anti-rabbit or anti-mouse IgG-peroxidase conjugate (Santa Cruz Biotechnology). The antigen-antibody complexes were visualized by chemiluminescence (Perkin-Elmer).

Subcellular fractionation. Subcellular fractionation was done as described previously (18, 19). Purity of the fractions was monitored by immunoblot analysis.

Immunofluorescence assay. Cells cultured in chamber slides were fixed in methanol for 5 min, permeabilized in 1% Triton X-100 for 15 min, washed

PKC δ Activates RelA/p65 by TNF- α

with PBS, and blocked with 10% goat serum in PBS for 1 h. After washing with PBS, the cells were immunostained with anti-RelA/p65 or anti-PKC δ followed by reaction with FITC- or TRITC-conjugated secondary antibodies. Nuclei were stained with 4',6-diamidino-2-phenylindole.

Electrophoretic mobility shift assay. Electrophoretic mobility shift assay was done using LightShift Chemiluminescent EMSA Kit (Pierce) according to the manufacturer's instructions. For each reaction, 1 μ g nuclear extract was incubated with biotin end-labeled κ B oligonucleotide probes. The probe sequence is as follows: 5'-AGTTGAGGGGACTTCC-CAGGC-3'.

Chromatin immunoprecipitation assay. Chromatin immunoprecipitation and re-chromatin immunoprecipitation assays were done as described previously (35). PCR amplification was done in chromatin immunoprecipitated fragments using the following oligonucleotide pairs: κ B α (5'-GACGACCCCAATTCAAATCG-3' and 5'-TCAGGCTCGGG-

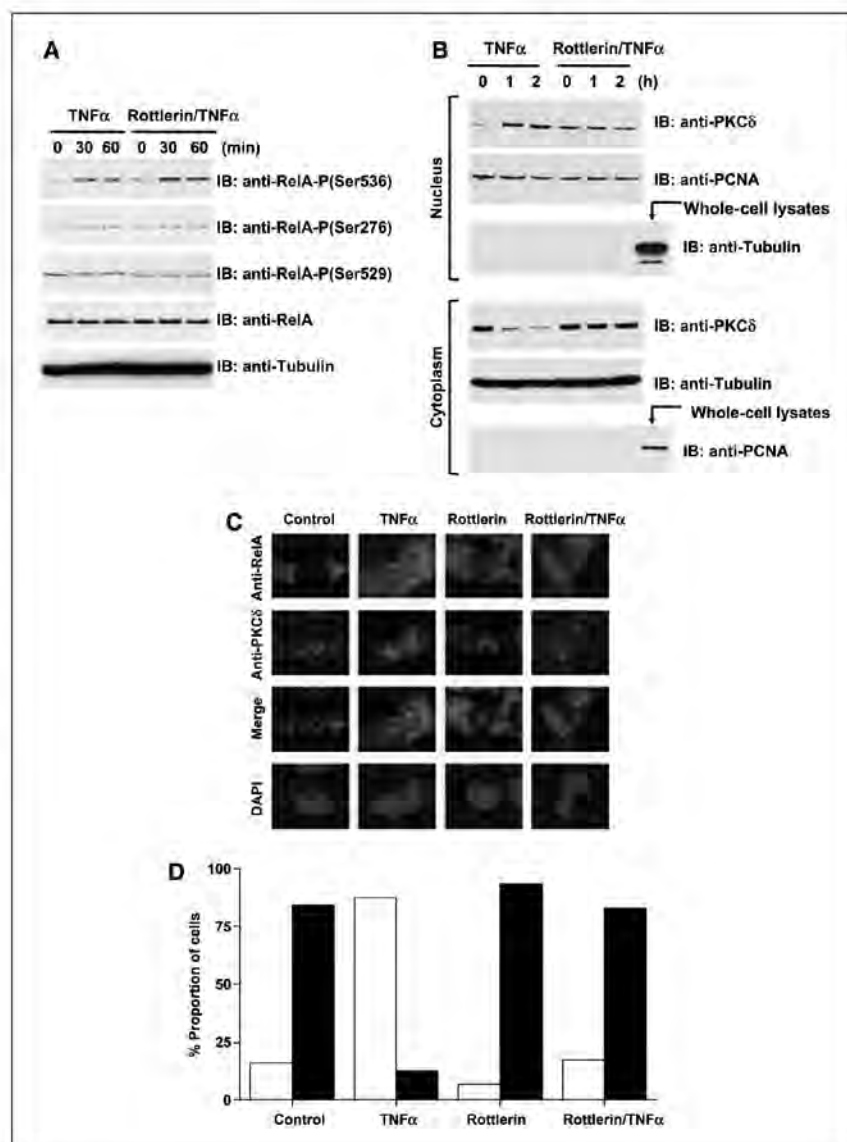
GAATTCC-3') and p100/p52 (5'-GTGAAAGACCCTCTGTCCCT-3' and 5'-GTGGAGAGCGAGATCCGGAGTT-3').

Reporter gene assays. 293 cells stably transfected with pNF- κ B-luc and pTK-hyg (Panomics) were treated with TNF- α . The luciferase activity was determined by the Bright-Glo Luciferase Assay System (Promega) according to the manufacturer's protocol. The relative fold increase in activity compared with untreated cells was determined (36). The data represent mean \pm SD from at least three to four independent experiments, each done in triplicate.

IL-6 production. Cells were plated onto 24-well plates and stimulated with TNF- α . After 24 h, the culture supernatants were assayed for IL-6 production using OptEIA human IL-6 ELISA kit II (BD Pharmingen) according to the manufacturer's instruction.

Apoptosis assay. The apoptotic effect was measured after 24 h using the DeadEnd Fluorometric TUNEL System (Promega).

Figure 2. Kinase activity is required for nuclear targeting of PKC δ in response to TNF- α . **A**, 293T cells were left untreated or pretreated with rottlerin followed by treatment with TNF- α . Cell lysates were analyzed by immunoblotting with anti-phospho-RelA/p65 or anti-tubulin. **B**, 293T cells were pretreated with or without rottlerin for 30 min followed by treatment with TNF- α for indicated times. Nuclear and cytoplasmic lysates were subjected to immunoblot analysis with the indicated antibodies. **C**, U2OS cells were left untreated or treated with TNF- α in the presence or absence of rottlerin. Cells were fixed and stained with anti-RelA/p65 or anti-PKC δ . Merged images are also shown. Nuclei were stained with 4',6-diamidino-2-phenylindole (DAPI). **D**, to estimate the staining, subcellular localization of PKC δ was scored according to whether it was higher in the nucleus (open columns) or in the cytoplasm (closed columns).



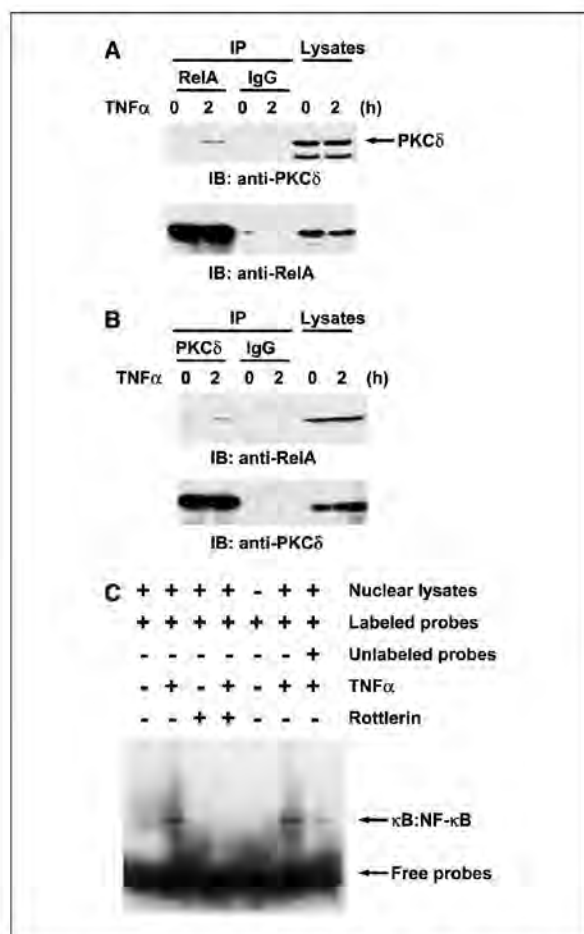


Figure 3. PKC δ interacts with RelA/p65. **A** and **B**, 293T cells were treated with TNF- α for indicated times. Cell lysates were immunoprecipitated with anti-RelA/p65 (**A**) or anti-PKC δ (**B**) followed by immunoblot analysis with anti-PKC δ or anti-RelA/p65. Immunoprecipitates with normal IgG were used as negative control. **C**, U2OS cells were left untreated or treated with TNF- α in the presence or absence of rottlerin. Twenty femtomoles of biotin-conjugated κ B-oligonucleotide probes were incubated with (lanes 1-4, 6, and 7) or without (lane 5) nuclear lysates. Additional incubation with 200-fold molar excess amount of unlabeled probes (lane 7) was included to assess specific DNA-protein interaction.

Results

PKC δ is involved in the activation of RelA/p65 transcription function in response to TNF- α . Previous studies showed that treatment of cells with TNF- α induces I κ B α degradation, resulting in nuclear translocation and activation of NF- κ B (37). To determine if PKC δ is involved in TNF- α -induced NF- κ B activation, 293T cells were treated with TNF- α in the presence or absence of the specific PKC δ inhibitor rottlerin. Subcellular fractionation assays revealed that nuclear targeting of NF- κ B including RelA/p65 and p105/p50 is independent of PKC δ activity (Figs. 1A and 4A, nuclear lysates). However, resynthesis of I κ B α after TNF- α exposure, which is transcriptionally induced by RelA/p65 (38), was diminished in rottlerin-treated cells, suggesting that PKC δ activity is associated with the activation of NF- κ B transcription function (Fig. 1A, cytoplasmic lysates). Moreover, on exposure to TNF- α , increased

expression of RelB and p100/p52, both are also the transcriptional targets of RelA/p65 (39, 40), significantly reduced in cells pretreated with rottlerin (Fig. 1, whole-cell lysates). Similar results were obtained in U2OS cells (Fig. 1C). To further define the involvement of PKC δ in transcriptional activity of RelA/p65, reverse transcription and subsequent PCR assays were done to monitor transcription of RelA/p65 target genes. The results showed that increased expression of RelB and p100/p52 attenuated in cells pretreated with rottlerin (Fig. 1B). Similar findings were obtained in U2OS cells (data not shown). To confirm the requirement of PKC δ in RelA/p65 activation, U2OS cells were transfected with scramble siRNA or PKC δ -specific siRNA followed by treatment with TNF- α . As shown for pretreatment with rottlerin (Fig. 1A-C), the status of PKC δ expression was not associated with nuclear translocation of RelA/p65 and p105/p50 (Fig. 1D, nuclear lysates). In contrast, TNF- α -induced expression of RelB and p100/p52 was markedly attenuated in cells silenced for PKC δ (Fig. 1D, whole-cell lysates). Taken together, these results show that PKC δ induces the activation of RelA/p65 transcription function in response to TNF- α .

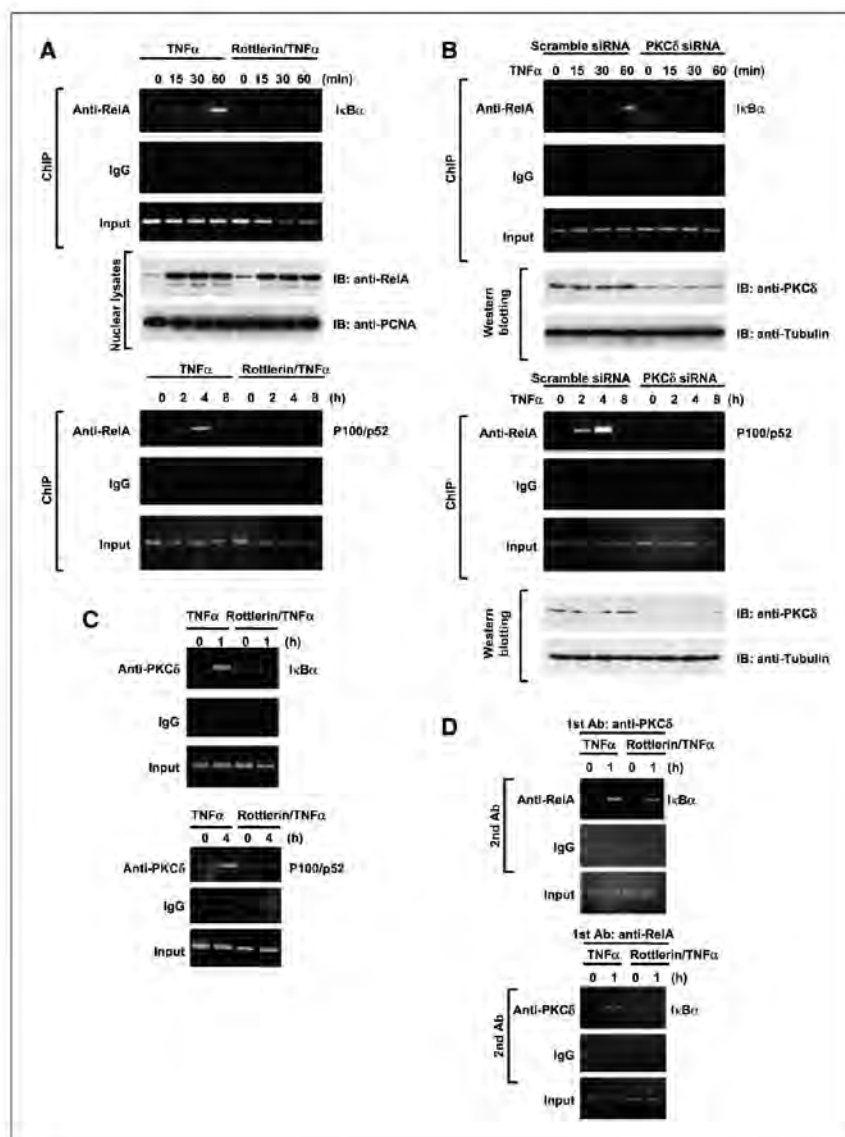
Nuclear targeting of PKC δ triggers TNF- α -induced RelA/p65 activation. To explore precise mechanisms in which PKC δ control RelA/p65, we first examined PKC δ phosphorylation of RelA/p65 because our previous study showed that PKC δ activates IKK α in response to oxidative stress (41). Other studies showed that IKK phosphorylates RelA/p65 at Ser⁵³⁶ to induce its transactivation (31-33). Hence, to assess the possibility that PKC δ activates IKKs that subsequently phosphorylate Ser⁵³⁶, 293T cells were treated with TNF- α in the presence or absence of rottlerin. Immunoblot analysis with anti-phospho-Ser⁵³⁶ showed no remarkable effect on Ser⁵³⁶ phosphorylation, indicating that IKK phosphorylation of RelA/p65 is irrelevant to PKC δ on exposure to TNF- α (Fig. 2A). Other studies have shown that phosphorylation of RelA/p65 at Ser²⁷⁶ is essential for its activity after TNF- α stimulation (29, 42). To examine the involvement of PKC δ on Ser²⁷⁶ phosphorylation, 293T cells were treated with TNF- α in the presence or absence of rottlerin. The results showed that PKC δ activity is scarcely involved in Ser²⁷⁶ phosphorylation following TNF- α exposure (Fig. 2A). Another study has shown that phosphorylation of RelA/p65 at Ser⁵²⁹ is essential for its activity after TNF- α stimulation (43). To determine if PKC δ is associated with Ser⁵²⁹ phosphorylation, 293T cells were left untreated or treated with TNF- α in the presence or absence of rottlerin. Ser⁵²⁹ was constitutively phosphorylated, and as shown for phosphorylation of Ser²⁷⁶ or Ser⁵³⁶, there was no significant difference on Ser⁵²⁹ phosphorylation with impairment of PKC δ activity after TNF- α exposure (Fig. 2A). These findings collectively indicate that PKC δ affects RelA/p65 in a phosphorylation-independent manner. Our previous studies also showed that PKC δ rapidly moves to the nucleus after genotoxic stress and this nuclear targeting depends on its kinase activity (19). These findings led us to examine whether TNF- α induces nuclear translocation of PKC δ . Subcellular fractionation assays clearly showed that cytoplasmic PKC δ immediately moved into the nucleus (Fig. 2B). Importantly, inhibition of PKC δ activity impeded its nuclear translocation following TNF- α treatment (Fig. 2B), suggesting the possibility that nuclear targeting of PKC δ affects regulation of TNF- α -induced RelA/p65 activation. To determine if nuclear targeting of PKC δ is dependent on RelA/p65, cells were pretreated with NF- κ B inhibitor followed by treatment with TNF- α . The results showed that there is little, if any, effect of NF- κ B activity on TNF- α -induced nuclear translocation of PKC δ (Supplementary Fig. S1). To convince nuclear targeting of PKC δ in response to TNF- α , we

performed immunofluorescent staining. Nuclear PKC δ was increased after TNF- α stimulation (Fig. 2C and D). Moreover, in concert with the immunoblot analysis, inhibition of PKC δ activity by rottlerin diminished its nuclear translocation in response to TNF- α , confirming that kinase activity is required for nuclear targeting of PKC δ (Fig. 2C and D). We also confirmed that TNF- α -induced nuclear translocation of RelA/p65 is independent of PKC δ activity (Fig. 2C).

PKC δ interacts with RelA/p65 after TNF- α exposure. The findings that both PKC δ and RelA/p65 move into the nucleus following TNF- α treatment provided a conceivable model in which PKC δ associates with RelA/p65. To address this possibility, 293T cells were left untreated or treated with TNF- α ; then, cell lysates were subjected to immunoprecipitation with anti-RelA/p65 and

subsequent immunoblotting with anti-PKC δ . PKC δ was coimmunoprecipitated with RelA/p65 in TNF- α -treated cells but not untreated cells (Fig. 3A). Moreover, reciprocal experiments confirmed this interaction (Fig. 3B). These findings show the inducible interaction of PKC δ with RelA/p65 after TNF- α exposure. To examine whether PKC δ affects NF- κ B activity, U2OS cells were left untreated or treated with TNF- α in the presence or absence of rottlerin. Nuclear lysates were then subjected to electrophoretic mobility shift assay analysis. A shifted band was detected when the κ B probes were incubated with nuclear lysates from TNF- α -treated cells but not control cells (Fig. 3C). Moreover, the band disappeared in the presence of rottlerin, suggesting that PKC δ activity is required for the efficient binding of NF- κ B to κ B elements in response to TNF- α .

Figure 4. PKC δ induces RelA/p65 transactivation after TNF- α exposure. **A**, 293T cells were pretreated with or without rottlerin for 30 min followed by treatment with TNF- α . Chromatin immunoprecipitation (ChIP) assays were done using primer sequences for I κ B α or p100/p52. PCR was done with chromatin fragments immunoprecipitated with anti-RelA/p65 or normal IgG. The input represents PCR amplification of total chromatin before immunoprecipitation. Nuclear lysates were subjected to immunoblot analysis with the indicated antibodies. **B**, U2OS cells were transfected with the PKC δ siRNA and then treated with TNF- α . Chromatin immunoprecipitation assay was done as described above. Cell lysates were subjected to immunoblot analysis with anti-PKC δ or anti-tubulin. **C**, 293T cells were left untreated or pretreated with rottlerin followed by treatment with TNF- α for indicated times. Chromatin fragments were immunoprecipitated with anti-PKC δ . Chromatin immunoprecipitation assays were done with primer sequences for I κ B α or p100/p52. **D**, 293T cells were treated as described above. Re-chromatin immunoprecipitation assays were done with the use of anti-PKC δ , and the eluted samples were then immunoprecipitated with anti-RelA/p65 or anti-IgG. Precipitated chromatin was analyzed by PCR using primer sequences for I κ B α (top three panels). Re-chromatin immunoprecipitation assays were also done by using anti-RelA/p65 for the first immunoprecipitation and anti-PKC δ for the second immunoprecipitation (bottom three panels).



Cancer Research

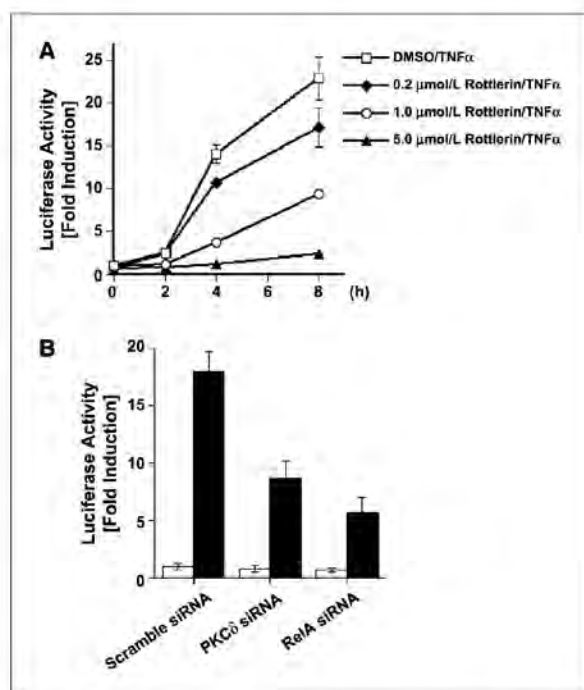


Figure 5. PKC δ is involved in NF- κ B transactivation in response to TNF- α . **A**, 293 cells expressing pNF- κ B-luc were left untreated or treated with rottlerin followed by the treatment with TNF- α for indicated times. Luciferase assays were done. Mean \pm SD from three independent experiments, each done in triplicate. **B**, 293/NF- κ B-luc cells were transfected with scramble siRNA, PKC δ siRNA, or RelA/p65 siRNA followed by the treatment with (closed columns) or without (open columns) TNF- α for 6 h. Luciferase activity was measured 48 h post-transfection. Mean \pm SD from three independent experiments, each done in triplicate.

PKC δ controls RelA/p65 occupancy to the target-gene promoters. To further define the functional interaction between PKC δ and RelA/p65, we performed chromatin immunoprecipitation assays to clarify the role for PKC δ on promoter binding of RelA/p65. 293T cells were left untreated or treated with TNF- α in the presence or absence of rottlerin. Isolated chromatin was immunoprecipitated with anti-RelA/p65 or control IgG followed by PCR analysis with primers targeted to the κ B elements of I κ B α or p100/p52 promoter. RelA/p65 occupancy to the I κ B α promoter was detectable after TNF- α exposure (Fig. 4A). Importantly, inhibition of PKC δ activity abrogated this occupancy (Fig. 4A). Similar results were obtained with the p100/p52 promoter (Fig. 4A). To establish the requirement of PKC δ on binding of RelA/p65 to the target-gene promoters, 293T cells were transfected with scramble siRNA or PKC δ -specific siRNA followed by treatment with TNF- α . As shown for rottlerin, chromatin immunoprecipitation analyses revealed that RelA/p65 occupies the κ B elements of I κ B α promoter in control cells and not PKC δ silencing cells (Fig. 4B). Similar findings were obtained with the p100/p52 promoter (Fig. 4B). Taken together, these results show that PKC δ is required for the binding of RelA/p65 to the κ B elements in response to TNF- α . The demonstration that PKC δ inducibly interacts with RelA/p65 following TNF- α exposure led us to determine if PKC δ forms a complex with RelA/p65 on the promoters. As expected, chromatin immunoprecipitation analyses with anti-PKC δ immunoprecipitates

clearly showed that, on exposure to TNF- α , PKC δ occupies the κ B elements of I κ B α promoter (Fig. 4C). More importantly, inhibition of PKC δ activity was associated with complete abrogation of its occupancy (Fig. 4C). Comparable results were obtained with the p100/p52 promoter (Fig. 4C). These findings indicate that PKC δ and RelA/p65 form a complex to occupy κ B elements on RelA/p65 target promoters in response to TNF- α . Furthermore, activation of PKC δ is necessary to induce the transcription function of RelA/p65. To determine if recruitment of PKC δ to the promoters depends on its interaction with RelA/p65, U2OS cells were transfected with scramble siRNA or RelA/p65 siRNA followed by treatment with TNF- α . Analysis of chromatin immunoprecipitation assays showed that TNF- α -induced PKC δ occupancy to the I κ B α promoter was completely abolished in cells silenced for RelA/p65 (Supplementary Fig. S2A). Similar results were obtained with the p100/p52 promoter (Supplementary Fig. S2B). These findings suggest that PKC δ binding to the promoters of the NF- κ B target genes is dependent on its interaction with RelA/p65. To address the mechanism of PKC δ -dependent recruitment of RelA/p65 to the promoters of NF- κ B genes, we have performed re-chromatin immunoprecipitation assays. Chromatin was immunoprecipitated with anti-PKC δ as the first antibody, and the eluted samples were then immunoprecipitated with anti-RelA/p65 or anti-IgG antibody. Chromatin templates containing κ B elements of I κ B α promoter, which were associated with PKC δ , were also immunoprecipitated by anti-RelA/p65 but not by anti-IgG after TNF- α exposure (Fig. 4D). More importantly, this co-occupancy was markedly diminished in the presence of rottlerin (Fig. 4D). To confirm these results, we performed reciprocal re-chromatin immunoprecipitation assays in which anti-RelA/p65 was used for the first immunoprecipitation and then anti-PKC δ for the second immunoprecipitation. As expected, the results yielded similar conclusions (Fig. 4D). These findings indicate that, on exposure to TNF- α stimulation, PKC δ may form a complex with RelA/p65 to occupy κ B elements and that this activation of PKC δ may be required for the co-occupancy to κ B elements.

PKC δ induces transcriptional activity of RelA/p65 following TNF- α exposure. To examine whether PKC δ enhances TNF- α -induced RelA/p65 activation, 293 cells stably transfected with the luciferase-reporter vector-containing κ B elements were treated with TNF- α in the presence or absence of rottlerin. Pretreatment with rottlerin significantly attenuated the NF- κ B activity in a dose-dependent manner (Fig. 5A). By sharp contrast, there was little, if any, effect on pretreatment of classic PKC inhibitor Gö6976 (data not shown). To confirm this finding, cells were transfected with scramble siRNA, PKC δ -specific siRNA, or RelA/p65-specific siRNA. As expected, silencing of RelA/p65 was associated with pronounced inhibition of NF- κ B activity in response to TNF- α (Fig. 5B). Importantly, knocking down PKC δ significantly diminished TNF- α -induced NF- κ B activation (Fig. 5B).

PKC δ affects cellular function of NF- κ B by controlling RelA/p65 in response to TNF- α . To examine the biological significance of PKC δ -dependent regulation of RelA/p65 transcriptional activity, we have investigated TNF- α -induced IL-6 production and apoptotic cell death. 293T cells were left untreated or treated with TNF- α in the presence or absence of rottlerin. As expected, TNF- α stimulation substantially imposed IL-6 production (Fig. 6A, left). In contrast, inhibition of PKC δ activity by pretreatment with rottlerin impaired production of IL-6 in response to TNF- α (Fig. 6A, left). Similar results were obtained with U2OS cells silenced for PKC δ (Fig. 6A, right). These data show that PKC δ induces transcriptional

activity of RelA/p65 to produce IL-6 in response to TNF- α . With regard to the apoptotic insults, U2OS cells were left untreated or treated with TNF- α in the presence or absence of rottlerin. Analysis of TUNEL assays revealed that apoptotic cells were slightly increased following TNF- α exposure (Fig. 6B). Importantly, TNF- α -induced apoptotic induction was significantly enhanced in the presence of rottlerin (Fig. 6B). Comparable findings were obtained with cells silenced for PKC δ (Fig. 6B). To further assess TNF- α -induced apoptosis, cells were left untreated or treated with TNF- α in the presence or absence of NF- κ B inhibitor. Analysis of TUNEL assays showed that impeding NF- κ B activity facilitates apoptotic cell death induced by TNF- α (Fig. 6B). Similar results were obtained in cells transfected with RelA/p65 siRNA (Fig. 6B). To substantiate whether the finding that inhibition of PKC δ potentiates TNF- α -induced apoptosis is dependent on NF- κ B, NF- κ B inhibitor was cotreated together with rottlerin in cells. After TNF- α stimulation, induction of apoptosis by combination of NF- κ B inhibitor and rottlerin was comparable with that by NF- κ B inhibitor or RelA/p65 siRNA alone (Fig. 6B). Consistent results were obtained with combination of NF- κ B inhibitor and PKC δ siRNA (Fig. 6B). These results show that abrogation of the PKC δ -NF- κ B signaling, at least in part, diminishes the protective effect from TNF- α -induced apoptotic cell death. As a result, cells undergoing apoptosis were significantly increased.

Taken together, these findings thus support a model in which, on exposure to TNF- α , PKC δ is targeted into the nucleus and forms a complex with RelA/p65 to activate transcription function on the promoters (Fig. 6C). More importantly, PKC δ plays a crucial role in NF- κ B activation by controlling RelA/p65 to regulate cellular function and fate in response to TNF- α .

Discussion

NF- κ B is a key transcription factor in cell survival, immunity, development, and many other important biological processes. Understanding regulation of NF- κ B thus contributes to elucidation for cellular response to the homeostasis system. Accumulating lines of evidence have revealed that NF- κ B is activated by various stimuli such as cytokines, radiation, viral infection, and reactive oxygen species (27). In this study, we have focused on TNF- α -induced NF- κ B activation. In resting cells, NF- κ B is localized in the cytoplasm tethered by I κ B α . Once IKK signalosome is activated by various stimuli, I κ B α is phosphorylated and degraded to allow nuclear translocation of dimeric NF- κ B. Numerous studies have paid much attention on regulation of nuclear targeting of NF- κ B in response to diverse stimuli. However, little is known about an activation mechanism of NF- κ B in the nucleus. In this regard, the present study shows that PKC δ is involved in RelA/p65 activation in the nucleus. We have shown previously that PKC δ translocates into the nucleus after treatment of cells with 1- β -D-arabinofuranosylcytosine (19). Moreover, pretreatment with rottlerin attenuated nuclear targeting of PKC δ (19). We also proved that PKC δ activates nuclear substrates by phosphorylation, including Rad9, topoisomerase II α , and p53, to induce apoptosis in response to DNA damage (2). These findings support a model in which, on exposure to genotoxic stress, PKC δ is targeted to the nucleus and phosphorylates several nuclear targets for induction of apoptosis. In the present study, the results indicate TNF- α -induced nuclear translocation of PKC δ and its interaction with RelA/p65. To our best knowledge, this is the first report showing nuclear translocation of PKC δ after TNF- α stimulation. Mechanisms for nuclear

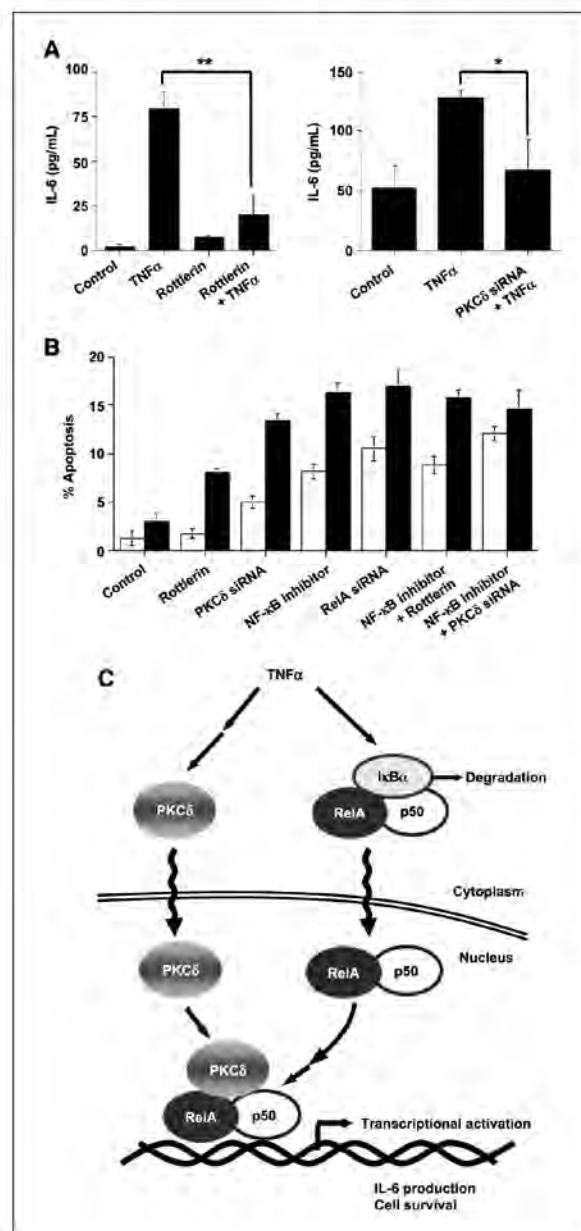


Figure 6. PKC δ affects NF- κ B to induce IL-6 and to protect apoptosis following TNF- α exposure. **A**, 293T cells were pretreated with or without rottlerin for 30 min followed by treatment with TNF- α for 24 h. The amount of secreted IL-6 production was measured by ELISA. Mean \pm SD from three independent experiments, each done in triplicate (*left*). **, $P < 0.01$. U2OS cells were transfected with the PKC δ siRNA and then treated with TNF- α . IL-6 was measured as mentioned above (*right*). *, $P < 0.05$. **B**, U2OS cells were pretreated with rottlerin or NF- κ B inhibitor and then left untreated (*open columns*) or treated with TNF- α (*closed columns*) for 24 h. Cells were transfected with the PKC δ siRNA or RelA/p65 siRNA followed by treatment with TNF- α . NF- κ B inhibitor was also incubated together with rottlerin or PKC δ siRNA in cells. TUNEL assays were done to assess apoptotic cell death. Mean \pm SD from five fields of 100 to 300 cells, each done for at least three independent experiments. **C**, a proposed model of the PKC δ -RelA/p65 pathway and NF- κ B signaling in response to TNF- α . On exposure to TNF- α , PKC δ and RelA/p65 translocate from the cytoplasm into the nucleus. PKC δ then forms a complex with RelA/p65 on the κ B elements of the promoter to facilitate transactivation of NF- κ B.

Cancer Research

targeting of PKC δ remain unclear. Nevertheless, the findings that kinase activity is required for nuclear translocation, as shown similarly in the genotoxic stress response (19), suggest a common machinery for its nuclear migration. We also found inducible interaction between PKC δ and RelA/p65 predominantly in the nucleus after TNF- α stimulation (Figs. 2C and 3A and B). In this context, at least in a physiologic condition, activation of PKC δ would be prerequisite for its nuclear targeting and subsequent binding to RelA/p65. These data thus suggest that both activity of and interaction with PKC δ could be indispensable for TNF- α -induced RelA/p65 activity. The demonstration that inhibition of PKC δ by rottlerin abrogates its interaction with RelA/p65 (data not shown) further supports the involvement for nuclear targeting of PKC δ on exposure to TNF- α . More importantly, rottlerin or siRNA blocked TNF- α -induced I κ B α or p100/p52 expression (Fig. 1), suggesting that inducible nuclear interaction between PKC δ and RelA/p65 is, at least in part, essential for activation of NF- κ B signaling pathways in response to TNF- α . In concert with these observations, chromatin immunoprecipitation assays further indicated that both PKC δ and RelA/p65 are detectable on κ B elements of I κ B α or p100/p52 promoters, and these occupancies are substantially diminished by inhibition of PKC δ activity. These findings thus indicate that PKC δ is associated with the regulation of RelA/p65 transcriptional activity elicited by TNF- α . Moreover, it is conceivable that PKC δ controls RelA/p65 by inducible interaction because PKC δ is not involved in nuclear targeting of RelA/p65 (Figs. 1A and D, 2C, and 4A). Another issue to be solved is the precise mechanism by which PKC δ regulates RelA/p65 in the nucleus. Given previous findings that PKC δ activates IKK α by oxidative stress and IKK α can phosphorylate and activate RelA/p65 at Ser³⁶, we examined whether PKC δ activates RelA/p65 by IKK α -mediated phosphorylation at Ser³⁶. The present results clearly showed that PKC δ is not involved in Ser³⁶ phosphorylation following TNF- α exposure. We also showed the dispensable role for PKC δ on Ser²⁷⁶ and Ser³²⁹ phosphorylation of RelA/p65. It also remains elusive whether PKC δ directly regulates the other NF- κ B members, such as RelB or p100/p52, in response to TNF- α . Further studies are needed to clarify this issue and this feasibility is currently under investigation.

In tumor cell lines, the role of PKC δ is a paradox. It can induce both cell survival and apoptosis depending on cell types

and its subcellular localization (2). For instance, treatment with anticancer agents resulted in a translocation of PKC δ from cytoplasm into nucleus concomitant with induction of apoptosis (12, 19, 44). Our recent studies showed PKC δ is involved in phosphorylation of p53 and potentiates p53-dependent apoptosis in response to DNA damage (17). PKC δ also induces transcription of the p53 tumor suppressor gene in the apoptotic response to DNA damage (35). These results thus indicate that PKC δ functions as a proapoptotic kinase in response to genotoxic stress (2). However, in this study, inhibition of PKC δ depressed both DNA binding of RelA/p65 and expression of the antiapoptotic proteins, RelB and p100/p52 (Fig. 1). In agreement with these results, PKC δ has been identified as a prosurvival factor in human breast tumor cell lines (45). Moreover, activation of PKC δ increased expression of the antiapoptotic proteins, FLIP (46) and cIAP-2 (47). In multiple myeloma cells, down-regulation of PKC δ resulted in apoptosis (48). These findings show a role for PKC δ on antiapoptotic regulation in some tumor cells. In this regard, previous studies also suggested an antiapoptotic role for PKC δ in response to TNF- α ; however, precise mechanisms remain unknown (20–22). Importantly, numerous studies have shown the association between constitutive NF- κ B activity in various types of cancer (49). The present study thus shows that PKC δ is a pivotal activator of NF- κ B and is essential for its nuclear function in tumors. A thorough understanding of how PKC δ /NF- κ B pathway regulates cell fate should help benefit for the cancer therapy.

Disclosure of Potential Conflicts of Interest

No potential conflicts of interest were disclosed.

Acknowledgments

Received 12/20/08; revised 4/16/09; accepted 5/4/09; published OnlineFirst 6/23/09.

Grant support: Ministry of Education, Science and Culture of Japan (K. Yoshida, and Y. Miki) and Sumitomo Foundation, Mochida Memorial Foundation for Medical and Pharmaceutical Research, Astellas Foundation for Research on Metabolic Disorders, Life Science Foundation of Japan, Uehara Memorial Foundation, Cell Science Research Foundation, and Senri Life Science Foundation (K. Yoshida).

The costs of publication of this article were defrayed in part by the payment of page charges. This article must therefore be hereby marked advertisement in accordance with 18 U.S.C. Section 1734 solely to indicate this fact.

References

- Nishizuka Y. The molecular heterogeneity of protein kinase C and its implications for cellular regulation. *Nature* 1988;334:661–5.
- Yoshida K. PKC δ signaling: mechanisms of DNA damage response and apoptosis. *Cell Signal* 2007;19:892–901.
- Kanithasamy AG, Kitazawa M, Kanithasamy A, Anantharam V. Role of proteolytic activation of protein kinase C δ in oxidative stress-induced apoptosis. *Antioxid Redox Signal* 2003;5:609–20.
- Sun X, Wu F, Datta R, Kharbanda S, Kufe D. Interaction between protein kinase C δ and the c-Abl tyrosine kinase in the cellular response to oxidative stress. *J Biol Chem* 2000;275:7470–3.
- Yoshida K, Yamaguchi T, Shinagawa H, Taira N, Nakayama KI, Miki Y. Protein kinase C δ activates topoisomerase II α to induce apoptotic cell death in response to DNA damage. *Mol Cell Biol* 2006;26:3114–31.
- Gayther T, Huggan M, Talamian RV, et al. Proteolytic activation of protein kinase C δ by an ICE/CED 3-like protease induces characteristics of apoptosis. *J Exp Med* 1996;184:2399–404.
- Yuan ZM, Utsugisawa T, Ishiko T, et al. Activation of protein kinase C δ by the c-Abl tyrosine kinase in response to ionizing radiation. *Oncogene* 1998;16:1643–8.
- Yoshida K, Miki Y. Enabling death by the Abl tyrosine kinase: mechanisms for nuclear shuttling of c-Abl in response to DNA damage. *Cell Cycle* 2005;4:777–9.
- Yoshida K, Yamaguchi T, Natsume T, Kufe D, Miki Y. JNK phosphorylation of 14-3-3 proteins regulates nuclear targeting of c-Abl in the apoptotic response to DNA damage. *Nat Cell Biol* 2005;7:278–85.
- Yuan ZM, Huang Y, Ishiko T, Kharbanda S, Weichselbaum R, Kufe D. Regulation of DNA damage-induced apoptosis by the c-Abl tyrosine kinase. *Proc Natl Acad Sci U S A* 1997;94:1437–40.
- Blass M, Kronfeld I, Kazimirovsky G, Blumberg PM, Brodie C. Tyrosine phosphorylation of protein kinase C δ is essential for its apoptotic effect in response to etoposide. *Mol Cell Biol* 2002;22:182–95.
- DeVries TA, Neville MC, Reyland ME. Nuclear import of PKC δ is required for apoptosis: identification of a novel nuclear import sequence. *EMBO J* 2002;21:6050–60.
- Kharbanda S, Bharti A, Pei D, et al. The stress response to ionizing radiation involves c-Abl-dependent phosphorylation of SHPTP1. *Proc Natl Acad Sci U S A* 1996;93:898–901.
- Yoshida K, Kharbanda S, Kufe D. Functional interaction between SHPTP1 and the Lyn tyrosine kinase in the apoptotic response to DNA damage. *J Biol Chem* 1999;274:3663–8.
- Yoshida K, Kufe D. Negative regulation of the SHPTP1 protein tyrosine phosphatase by protein kinase C δ in response to DNA damage. *Mol Pharmacol* 2001;60:1431–8.
- Leitges M, Mayr M, Braun U, et al. Exacerbated vein graft arteriosclerosis in protein kinase C δ -null mice. *J Clin Invest* 2001;108:1505–12.
- Yoshida K, Liu H, Miki Y. Protein kinase C δ regulates Ser⁷³ phosphorylation of p53 tumor suppressor in the apoptotic response to DNA damage. *J Biol Chem* 2006;281:5734–40.
- Yoshida K, Komatsu K, Wang HG, Kufe D. c-Abl tyrosine kinase regulates the human Rad9 checkpoint

- protein in response to DNA damage. *Mol Cell Biol* 2002; 22:3292–300.
19. Yoshida K, Wang HG, Miki Y, Kufe D. Protein kinase C δ is responsible for constitutive and DNA damage-induced phosphorylation of Rad9. *EMBO J* 2003;22:1431–41.
 20. Kilpatrick LE, Sun S, Mackie D, Baik F, Li H, Korchak HM. Regulation of TNF mediated antiapoptotic signaling in human neutrophils: role of δ -PKC and ERK1/2. *J Leukoc Biol* 2006;80:1512–21.
 21. Kilpatrick LE, Lee JY, Huines KM, Campbell DE, Sullivan KL, Korchak HM. A role for PKC- δ and PI 3-kinase in TNF- α -mediated antiapoptotic signaling in the human neutrophil. *Am J Physiol Cell Physiol* 2002;283:C48–57.
 22. Okhrimenko H, Lu W, Xiang C, et al. Roles of tyrosine phosphorylation and cleavage of protein kinase C δ in its protective effect against tumor necrosis factor-related apoptosis inducing ligand-induced apoptosis. *J Biol Chem* 2005;280:23643–52.
 23. Karin M, Lin A. NF- κ B at the crossroads of life and death. *Nat Immunol* 2002;3:221–7.
 24. Ghosh S, Karin M. Missing pieces in the NF- κ B puzzle. *Cell* 2002;109 Suppl:S81–96.
 25. Li Q, Verma IM. NF- κ B regulation in the immune system. *Nat Rev Immunol* 2002;2:225–34.
 26. Karin M. How NF- κ B is activated: the role of the I κ B kinase (IKK) complex. *Oncogene* 1999;18:5867–74.
 27. Hayden MS, Ghosh S. Signaling to NF- κ B. *Genes Dev* 2004;18:2195–224.
 28. Sasaki CY, Barberi TJ, Ghosh P, Longo DL. Phosphorylation of RelA/p65 on serine 536 defines an I κ B α -independent NF- κ B pathway. *J Biol Chem* 2005;280:34538–47.
 29. Okazaki T, Sakon S, Sasazuki T, et al. Phosphorylation of serine 276 is essential for p65 NF- κ B subunit-dependent cellular responses. *Biochem Biophys Res Commun* 2003;300:807–12.
 30. Buss H, Dorrie A, Schmitz ML, Hoffmann E, Resch K, Kracht M. Constitutive and interleukin-1-inducible phosphorylation of p65 NF- κ B at serine 536 is mediated by multiple protein kinases including I κ B kinase (IKK)- α , IKK β , IKK ϵ , TRAF family member-associated (TANK)-binding kinase 1 (TBK1), and an unknown kinase and couples p65 to TATA-binding protein-associated factor II31-mediated interleukin-8 transcription. *J Biol Chem* 2004;279:55633–43.
 31. Sakurai H, Chiba H, Miyoshi H, Sugita T, Toriumi W. I κ B kinases phosphorylate NF- κ B p65 subunit on serine 536 in the transactivation domain. *J Biol Chem* 1999;274:30351–6.
 32. Sakurai H, Suzuki S, Kawasaki N, et al. Tumor necrosis factor- α -induced IKK phosphorylation of NF- κ B p65 on serine 536 is mediated through the TRAF2, TRAF5, and TAK1 signaling pathway. *J Biol Chem* 2003;278:36916–23.
 33. Sizemore N, Lerner N, Dombrowski N, Sakurai H, Stark GR. Distinct roles of the I κ B kinase α and β subunits in liberating nuclear factor κ B (NF- κ B) from I κ B and in phosphorylating the p65 subunit of NF- κ B. *J Biol Chem* 2002;277:3863–9.
 34. Yoshida K, Wetzelbaum R, Kharbanda S, Kufe D. Role for Lyn tyrosine kinase as a regulator of stress-activated protein kinase activity in response to DNA damage. *Mol Cell Biol* 2000;20:5370–80.
 35. Liu H, Lu ZG, Miki Y, Yoshida K. Protein kinase C δ induces transcription of the TP53 tumor suppressor gene by controlling death-promoting factor Bif in the apoptotic response to DNA damage. *Mol Cell Biol* 2007;27:8480–91.
 36. Yamaguchi T, Kimura J, Miki Y, Yoshida K. The deubiquitinating enzyme USP11 controls an IKK α -p53 signaling pathway in response to TNF α . *J Biol Chem* 2007;282:33943–8.
 37. Baud V, Karin M. Signal transduction by tumor necrosis factor and its relatives. *Trends Cell Biol* 2001;11:372–7.
 38. Le Bail O, Schmidt-Ullrich R, Israel A. Promoter analysis of the gene encoding the I κ B- α /MAD3 inhibitor of NF- κ B: positive regulation by members of the rel/NF- κ B family. *EMBO J* 1993;12:5043–9.
 39. Bren GD, Solan NJ, Miyoshi H, Pennington KN, Pobst LJ, Paya CV. Transcription of the RelB gene is regulated by NF- κ B. *Oncogene* 2001;20:7722–33.
 40. Liptay S, Schmid RM, Nabel EG, Nabel GJ. Transcriptional regulation of NF- κ B2: evidence for κ B-mediated positive and negative autoregulation. *Mol Cell Biol* 1994;14:7695–703.
 41. Yamaguchi T, Miki Y, Yoshida K. Protein kinase C δ activates I κ B-kinase α to induce the p53 tumor suppressor in response to oxidative stress. *Cell Signal* 2007;19:2088–97.
 42. Zhong H, Voll RE, Ghosh S. Phosphorylation of NF- κ B p65 by PKA stimulates transcriptional activity by promoting a novel bivalent interaction with the coactivator CBP/p300. *Mol Cell* 1998;1:661–71.
 43. Wang D, Westerheide SD, Hanson JL, Baldwin AS, Jr. Tumor necrosis factor α -induced phosphorylation of RelA/p65 on Ser⁵³⁶ is controlled by casein kinase II. *J Biol Chem* 2000;275:32592–7.
 44. Reno EM, Haughian JM, Dimitrova IK, Jackson TA, Shroyer KR, Bradford AP. Analysis of protein kinase C δ (PKC δ) expression in endometrial tumors. *Hum Pathol* 2008;39:21–9.
 45. McCracken MA, Miraglia LJ, McKay RA, Strobl JS. Protein kinase C δ is a prosurvival factor in human breast tumor cell lines. *Mol Cancer Ther* 2003;2:273–81.
 46. Wang Q, Wang X, Zhou Y, Evers BM. PKC δ -mediated regulation of FLIP expression in human colon cancer cells. *Int J Cancer* 2006;118:326–34.
 47. Wang Q, Wang X, Evers BM. Induction of cIAP-2 in human colon cancer cells through PKC δ /NF- κ B. *J Biol Chem* 2003;278:51091–9.
 48. Ni H, Ergin M, Tibudan SS, Denning MF, Izban KE, Alkan S. Protein kinase C- δ is commonly expressed in multiple myeloma cells and its downregulation by roflumilast causes apoptosis. *Br J Haematol* 2003;121:849–56.
 49. Rayet B, Gelinas C. Aberrant rel/nfkb genes and activity in human cancer. *Oncogene* 1999;18:6938–47.

分子生物学分野

石野 史敏

難治疾患研究所・ゲノム応用医学研究部門
分子生物学・教授



1) 研究の課題名

ヒト遺伝疾患におけるジェネティックおよびエピジェネティックな原因および発症機序の解明

Genetic and epigenetic diseases: identification and elucidation of their responsible genes and underlying mechanisms

遺伝子の変異やエピジェネティックな遺伝子発現制御異常が原因となるヒト疾患における原因遺伝子の同定および疾患モデルマウスなどをもちいた発症機序の解明により、新しい診断・治療法の開発へつなげる基礎研究を推進する。

Silver-Russell 症候群 (SRS) では、成長の促進や阻害に働くインプリント遺伝子の発現制御異常によって出生前後の成長遅滞が観察される。われわれはヒト染色体7番の3カ所に、PEG1/MEST、PEG10、GRB10の原因候補遺伝子を同定してきた。実際に、Peg1/Mest および Peg10 ノックアウトマウスの解析から、これらが胎児成長および出生後の成長に重要な機能をもつ事を明らかにしている。本年度の研究では、インプリント制御を破壊し Grb10 遺伝子を過剰発現するモデルマウスの解析から、Grb10 が成長阻害に機能する事、この遺伝子のわずかな発現量の増加 (1.5~2.0 倍以内) が、胎児成長および出生後の成長に大きな影響 (30-40% の体重減) を引き起こすことを明らかにした。これにより、染色体7番短腕のトリソミーによる SRS が GRB10 遺伝子の過剰発現が原因であることを裏付けた (Hum Mol Genet 2009)。

ヒト染色体14番の父親性2倍体 (patUPD14) による新生児致死の原因が、インプリンティング制御の異常による PEG11/RTL1 の過剰発現によることをヒト患者およびノックアウトマウスをもちいた実験によりこれまで明らかにした (Nat Genet 2008a, 2008b)。ヒトでは新生児の肋骨形成異常が顕著にみられるが、その異常の

程度は PEG11/RTL1 の過剰度と比例している。PEG11/RTL1 発現量は、インプリンティング制御だけでなく母親性発現を示すアンチセンス RNA (antiPEG11/RTL1) による制御も受けている。両者を同時に欠失したマウスの解析から、antiPEG11/RTL1 には PEG11/RTL1 だけでなく他の遺伝子の制御を介した機能がある事を確かめた (未発表データ)。

生殖補助医療にもちいられる発生工学技術が個体発生に与えるエピジェネティックな影響

Epigenetic effects on fetal and postnatal development induced by artificial reproductive technologies.

新しい発生工学技術の開発やそれにより生み出されるマウスの個体発生におけるエピジェネティック制御の変動の問題をとりあげ、将来の生殖補助医療および再生医療におけるエピジェネティックな安全性の確保にむけた研究を進める。

体外受精 (IVF) や顕微授精 (ICSI) はヒトにおける生殖補助医療に利用され、その使用は増加傾向にある。しかし、これらの技術が胎児期の個体発生にどのような影響を与えるかという問題については、多くの懸念が表明されているにもかかわらず、明確な結論は得られていない。われわれは、これら発生工学技術が個体発生に与える影響を明らかにするために、理研バイオリソースセンターとの共同研究により、遺伝的に均一なマウスをもちい、すべての実験条件をそろえた条件で体系的な解析を実施した。その結果、IVF には正常の受精胚と差がみられないが、ICSI においては、少なくとも遺伝子発現の変動が新生児期まで見られる事が明らかとなった (投稿中)。

2)



Grb10-DMR KOの発育異常の図

3) 研究内容の英文要約

Spinocerebellar Ataxia Type 31 Is Associated with "Inserted" Penta-Nucleotide Repeats Containing (TGGAA) n,

Spinocerebellar ataxia type 31 (SCA31) is an adult-onset autosomal-dominant neurodegenerative disorder showing progressive cerebellar ataxia mainly affecting Purkinje cells. The SCA31 critical region was tracked down to a 900 kb interval in chromosome 16q22.1, where the disease shows a strong founder effect. By performing comprehensive Southern blot analysis and BAC- and fosmid-based sequencing, we isolated two genetic changes segregating with SCA31. One was a single-nucleotide change in an intron of the thymidine kinase 2 gene (TK2). The other was an insertion, from 2.5–3.8 kb long, consisting of complex penta-nucleotide repeats including a long (TGGAA) n stretch. The SCA31 repeat insertion's length inversely correlated with patient age of onset. The repeat insertion was located in introns of TK2 and BEAN expressed in the brain and formed RNA foci in the nuclei of patients' Purkinje cells. Because (TGGAA) n is a characteristic sequence of paracentromeric heterochromatin, we speculate that the insertion might have originated from heterochromatin. SCA31 is important because it exemplifies human diseases associated with 'inserted' microsatellite repeats that can expand through transmission. Our finding suggests that the ectopic microsatellite repeat, when transcribed, might cause a disease involving the essential splicing factors.

Efficient Production of Androgenetic Embryos by Round Spermatid Injection.

Mammalian androgenetic embryos can be produced by pronuclear exchange of fertilized oocytes or by dispermic in vitro fertilization of enucleated oocytes. Here, we report a new technique for producing mouse androgenetic embryos by injection of two round spermatid nuclei into

oocytes, followed by female chromosome removal. We found that injection of round spermatids resulted in high rates of oocyte survival (88%). Androgenetic embryos thus produced developed into mid-gestation fetuses at various rates, depending on the mouse strain used. All the fetuses examined maintained paternally specific genomic imprinting memories. This technique also enabled us to produce complete heterozygous F1 embryos by injecting two spermatids from different strains. The best rate of fetal survival (12% per embryos transferred) was obtained with C57BL/6 3 DBA/2 androgenetic embryos. We also generated embryonic stem cell lines efficiently with the genotype of *Mus musculus domesticus* and *M. m. molossinus*. Thus, injection of two round spermatid nuclei followed by maternal enucleation is an effective alternative method of producing androgenetic embryos that consistently develop into blastocysts and mid-gestation fetuses.

Paternal deletion of Meg1/Grb10 DMR causes maternalization of the Meg1/Grb10 cluster in mouse proximal Chromosome 11 leading to severe preand postnatal growth retardation

Mice with maternal duplication of proximal Chromosome 11 (MatDp (prox11)), where Meg1/Grb10 is located, exhibit pre- and postnatal growth retardation. To elucidate the responsible imprinted gene for the growth abnormality, we generated novel model mice mimicking the pattern of imprinted gene expression observed in the MatDp (prox11) by deleting differentially methylated region of Meg1/Grb10 (Meg1-DMR). We found that the mouse-specific repeat sequence consisting of several CTCF-binding motifs in the Meg1-DMR functions as a silencer, suggesting that the Meg1/Grb10 imprinted region adopted a different regulatory mechanism from the H19/Igf2 region. Paternal deletion of the Meg1-DMR caused both upregulation of the maternally expressed Meg1/Grb10 Type I in the whole body and loss of paternally expressed Meg1/Grb10 Type II, demonstrating maternalization of the entire Meg1/Grb10 imprinted region. We confirmed that the Meg1-DMR mice exhibited the same growth abnormalities as the MatDp (prox11) mice. Fetal and neonatal growth was very sensitive to the expression level of Meg1/Grb10 Type I, indicating that the 2-fold increment of the Meg1/Grb10 Type I is one of the major causes of the growth retardation observed in the MatDp (prox11) and the Meg1-DMR. This suggests that the corresponding human GRB10 Type I plays an important role in the etiology of Silver-Russell syndrome caused by partial trisomy of 7p11-p13.

4) 本事業に関連して世界的な研究拠点形成に向けて、以下の点で改善・整備等されたこと

A (研究拠点体制)

拠点内の共同研究の推進により、研究に新たな展開を盛り込む事が可能になった。

B (研究教育環境)

独立した研究者をめざす優秀なポスドク (GCOE 特任講師) が研究室において頑張っている姿をみせることは、大学院生に自分の将来を考える上で重要なロールモデルとなっている。

C (人材確保)

将来性の高い研究者を GCOE 特任講師として採用できた。研究上では直接の関係は少ないが、大学院生に良い影響をあたえている。

D (人材育成)

採用した GCOE 特任講師には、施設、機器などの利用に便宜をはかり、自身の研究に専念してもらえる環境を提供している。また、近いうちに独立して研究室を運営できるよう、現在の研究だけでなく、研究の将来構想や学生の指導法や研究室運営の仕方などについて相談にのっている。

E (国際化)

これまでも博士課程の大学院生には、共同研究で1-3ヶ月海外に滞在して研究できる機会を与えていた。また、相手国からも大学院生を受け入れていた。本拠点には外国人大学院生が多くいるため、これらが従来よりもスムーズに展開できるようになると考えている。

5) GCOE 事業を推進するに当たって力を入れた点

指導している大学院生にとって自分の将来を考える上で良い経験を得られる環境を作ること。大学院生の個別研究指導でそれぞれの個性を伸ばす指導をすることは当然として、研究者としての経歴にはいろいろな選択肢が存在することを知らせる事は重要である。本制度などで、多様なキャリアを持つ人材 (テニュアトラック (MTT) のポスドク、GCOE のポスドク、大型研究費によるポスドク) を研究室内に導入することが可能になった。自分が将来、大学の正規の助教ポストを含めこのような立場になったとき、どのように研究に打ち込むことが必要なのか?それを大学院生時代に、見知っておく事は、本人の将来設計に重要であると考えている。

6) 英文原著論文

1. Miki H, Hirose M, Ogonuki N, Inoue K, Kezuka F, Honda A, Mekada K, Hanaki K I, Iwafune H, Yoshiki A, Ishino F and Ogura A. Efficient production of androgenetic embryos by round spermatid injection. *Genesis* 47(3): 155-160, 2009
2. Shiura H, Nakamura K, Hikichi T, Hino T, Oda K, Suzuki-Migishima R, Kohda T, Kaneko-Ishino T, Ishino F. Paternal deletion of *Meg1/Grb10* DMR causes maternalization of the *Meg1/Grb10* cluster in mouse proximal Chromosome 11 leading to severe pre- and postnatal growth retardation. *Hum. Mol. Genet.* 18(8), 1424-1438, 2009
3. Sato N, Aino T, Kobayashi K, Asakawa S, Ishiguro T, Tsunemi T, Takahashi M, Matsuura T, Flanigan K M, Iwasaki I, Ishino F, Saito Y, Murayama S, Yoshida M, Hashizume Y, Takahashi Y, Tsuji S, Shimizu N, Toda T, Ishikawa K and Mizusawa H. Spinocerebellar Ataxia Type 31 Is Associated with 'Inserted' Penta-Nucleotide Repeats Containing (TGGAA)_n. *Am. J. Hum. Genet.* 85(5), 544-557, 2009

7) 著書

金児-石野知子、石野史敏 哺乳類の原点? カモノハシ—哺乳類のゲノム機能の進化を探る— 蛋白質・核酸・酵素 54 (1) : 58-64, 2009

石野史敏、金児-石野知子 ゲノム機能解析からみえてきた哺乳類の進化 *Biophilia* 5 (3) : 44-48, 2009.

金児-石野知子、石野史敏 哺乳類における胎生の進化とレトロトランスポゾン 特集 genetics/epigenetics から見えてきたゲノム機能の進化 実験医学 27 (19) : 3080-3086, 2009.

石野史敏 ゲノムインプリンティング 炎症と免疫 18 (1) :109-111, 2010.

8) 平成21年度までの自己評価

新生児における肋骨形成異常 (ベル型肋骨) に関わる PEG11/RTL1 と antiPEG11/RTL1 の2つの逆向きに重なりあう転写産物は、それ以外にも胎盤形成、生後の発達不良、精神遅滞など多くの病態に関係すると考えられる。特に antiPEG11/RTL1 は non-coding RNA でありながら

microRNA を6-7個含み、PEG11/RTL1だけでなく複数のターゲット遺伝子を持つと考えられる。MicroRNAの重要性は近年、注目を集めているが、複数（多数）の標的遺伝子を持つこのような因子の疾患における作用標的と機序を解明するためには、新しい方法論が必要とされることは明白である。現在の生物学が抱える大きなチャレンジすべき課題であり、一歩ずつ様子をみながら前進をしている状況である。

9) 学会発表（英文）

1. Fumitoshi Ishino, Ryuichi Ono, Shunsuke Suzuki, Yoichi Sekita, Mie Naruse, Takashi Kohda and Tomoko Kaneko-Ishino. Retrotransposons and Evolution of Genomic Imprinting and Placentation in Mammals. Symposium: Epigenetic impacts for differentiation and patterning. The 42nd Annual Meeting for the Japanese Society of Developmental Biologists. May 28-31, 2009 (Toki Messe, Niigata) .
2. Fumitoshi Ishino, Ryuichi Ono, Shunsuke Suzuki, Yoichi Sekita, Mie Naruse, Takashi Kohda and Tomoko Kaneko-Ishino. Contribution of Retrotransposons to the Evolution of Genomic Imprinting and Placentation in Mammals The 24th NAITO Conference on Nuclear Dynamics and RNA (II) June 23-26, 2009 (Chateraise Gateaux Kingdom, Sapporo, Hokkaido) .
3. Fumitoshi Ishino. Retrotransposons and trophoblast biology. Trophoblast Day Meeting. July 14-15, 2009 (University of Cambridge, UK) .
4. Fumitoshi Ishino. Retrotransposon-derived imprinted genes, Peg10 and Peg11/Rtl1 and their relation to the origin of viviparity in mammals. From Imprinting to the Epigenome in 25 years. September 4-6, 2009 (University of Cambridge, UK) .
5. Fumitoshi Ishino, Ryuichi Ono, Yoichi Sekita, Shunsuke Suzuki, Mie Naruse, Takashi Kohda Atsuo Ogura, Kenji Nakamura, Minesuke Yokoyama, Marilyn Renfree and Tomoko Kaneko-Ishino. Mammalian-specific genes derived from retrotransposons functioning placenta formation. The 32nd Annual Meeting of the Molelular Biology Society of Japan. Workshop: Integrative approaches towards evolutionary studies. December 9-12, 2009 (Pacifco Yokohama, Yokohama) .
6. Hisako Watanabe, Masahito Irie, Takashi Kohda, Fumitoshi Ishino and Tomoko Kaneko-Ishino. The effects of maternal undernutrition on fetal growth. The 32nd Annual Meeting of the Molelular Biology Society of Japan. December 9-12, 2009 (Pacifco Yokohama, Yokohama) .
7. Hirotaka Iwafune, Yuki Yamaguchi, Tomohiro Suzuki, Hiroyasu Furumi, Masakazu Hashimoto, Takashi Kohda, Hideaki Kaneda, Shigeharu Wakana, Toshihiko Shiroishi,

- Hiroyuki Sasaki, Fumitoshi Ishino. Analysis on mutant mice exhibiting abnormal methylation in DMR. . The 32nd Annual Meeting of the Molelular Biology Society of Japan. December 9-12, 2009 (Pacifco Yokohama, Yokohama) .
8. Daisuke Endo, Yoichi Sekita, Tomoko Kaneko-Ishino, Masayo Kagami, Ryuichi Ono, Takashi Kohda, Tsutomu Ogata, Fumitoshi Ishino. AntiPeg11/Rtl1, essential antisense RNA of retrotransposon derived gene plays two different roles in mouse development. The 32nd Annual Meeting of the Molelular Biology Society of Japan. December 9-12, 2009 (Pacifco Yokohama, Yokohama) .
 9. Masayuki, Ishii, Ryuichi Ono, Mie Naruse, Daisuke Endo, Masahito Irie, Hirotaka Iwafune, Takashi Kohda, Tomoko Kaneko-Ishino and Fumitoshi Ishino. Analysis of retrotransposon-derived genes, Sirh4, Sirh5 and Sirh6. The 32nd Annual Meeting of the Molelular Biology Society of Japan. December 9-12, 2009 (Pacifco Yokohama, Yokohama) .
 10. Sawa Iwasaki, Takashi Kohda, Tomoko Kaneko-Ishino and Fumitoshi Ishino. Verification of the imprinting status of retrotransposon-derived Pnma-family genes. The 32nd Annual Meeting of the Molelular Biology Society of Japan. December 9-12, 2009 (Pacifco Yokohama, Yokohama) .
 11. Takashi Kohda, Kimiko Inoue, Narumi Ogonuki, Sawa Iwasaki, Xijia Xia, Teruhiko Wakayama, Atsuo Ogura, Tomoko Kaneko-Ishino and Fumitoshi Ishino. The epigenetic shift and random drift of the genome induced by embryo manipulations. The 32nd Annual Meeting of the Molelular Biology Society of Japan. December 9-12, 2009 (Pacifco Yokohama, Yokohama) .
 12. Ryuichi Ono, Mie Naruse, Kenji Nakamura, Toshiaki Hino, Daisuke Endo, Masahito Irie, Hirotaka Iwafune, Masayuki Ishii, Takako Usami, Takashi Kohda, Atsuo Ogura, Minesuke Yokoyama, Tomoko Kaneko-Ishino and Fumitoshi Ishino. The function of retrotransposon-derived gene. The 32nd Annual Meeting of the Molelular Biology Society of Japan. December 9-12, 2009 (Pacifco Yokohama, Yokohama) .
 13. Mie Naruse, Ryuichi Ono, Yoichi Sekita, Daisuke Endo, Masahito Irie, Hirotaka Iwafune, Masayuki Ishii, Kenji Nakamura, Toshiaki Hino, Takashi Kohda, Minesuke Yokoyama, Tomoko Kaneko-Ishino and Fumitoshi Ishino. Retrotransposon-derived Sirh-family genes and mammalian viviparity. The 32nd Annual Meeting of the Molelular Biology Society of Japan. December 9-12, 2009 (Pacifco Yokohama, Yokohama) .

10) 学会発表（和文）

1. 石野史敏、小野竜一、関田洋一、鈴木俊介、金児—石野知子 哺乳類に特異的に存在するレトロトランスポソ

- ン由来の遺伝子と胎盤形成 第147回 日本獣医学会学術集会 ワークショップ レトロエレメントのダイナミズム 平成21年4月2日(栃木県総合文化センター、宇都宮)。
2. 石野史敏、金児—石野知子 レトロトランスポゾン はどのように哺乳類の進化に関わったか? -その Genetic な役割と Epigenetic な役割について- 第56回 日本実験動物学会総会 シンポジウム 哺乳動物の発生と進化におけるエピジェネティクスの役割 平成21年5月14日(大宮ソニックシティ、大宮)。
 3. 石野史敏 哺乳類の胎生獲得におけるレトロトランスポゾンの寄与 京都大学ウイルス研究所学術講演会 平成21年7月10日(芝蘭会館、京都大学)。
 4. 石野史敏、金児—石野知子 ゲノムインプリンティングの起源 —そのとき哺乳類ゲノムに何が起きたのか?- 第82回日本生化学会年会 シンポジウム トランスポゾンとの共生が織りなすゲノムシステムのダイナミクス 平成21年10月14日(神戸国際会議場、神戸)。
 5. 石野史敏 哺乳類の胎生とゲノムインプリンティングの進化におけるレトロトランスポゾンの役割について 北海道大学医学部セミナー 平成21年11月5日(北海道大学医学部、札幌)。

11) 外部資金の獲得状況

1. 日本学術振興会 学術創成研究
研究課題:「ゲノム刷込みに関連する哺乳類特異的遺伝子群の個体発生・系統発生における役割」
研究期間:平成18年度～平成22年度(5年間)
総額:415,090千円
2. 日本学術振興会 日豪二国間共同研究
研究課題:「有袋類におけるゲノムインプリンティングの解析」
研究期間:平成21年度～平成22年度(2年間)
平成21年度分 2,450千円

12) 特別講演、招待講演

1. 石野史敏、小野竜一、関田洋一、鈴木俊介、金児—石野知子 哺乳類に特異的に存在するレトロトランスポゾン由来の遺伝子と胎盤形成 第147回 日本獣医学会学術集会 ワークショップ レトロエレメントのダイナミズム 平成21年4月2日(栃木県総合文化センター、宇都宮)。
2. 石野史敏、金児—石野知子 レトロトランスポゾンはどのように哺乳類の進化に関わったか? -その Genetic な役割と Epigenetic な役割について- 第56

回日本実験動物学会総会 シンポジウム 哺乳動物の発生と進化におけるエピジェネティクスの役割 平成21年5月14日(大宮ソニックシティ、大宮)。

3. Fumitoshi Ishino, Ryuichi Ono, Shunsuke Suzuki, Yoichi Sekita, Mie Naruse, Takashi Kohda and Tomoko Kaneko-Ishino. Retrotransposons and Evolution of Genomic Imprinting and Placentation in Mammals. Symposium: Epigenetic impacts for differentiation and patterning. The 42nd Annual Meeting for the Japanese Society of Developmental Biologists. May 28-31, 2009 (Toki Messe, Niigata) .
4. Fumitoshi Ishino, Ryuichi Ono, Shunsuke Suzuki, Yoichi Sekita, Mie Naruse, Takashi Kohda and Tomoko Kaneko-Ishino. Contribution of Retrotransposons to the Evolution of Genomic Imprinting and Placentation in Mammals The 24th NAITO Conference on Nuclear Dynamics and RNA (II) June 23-26, 2009 (Chateraise Gateaux Kingdom, Sapporo, Hokkaido) .
5. 石野史敏 哺乳類の胎生獲得におけるレトロトランスポゾンの寄与 京都大学ウイルス研究所学術講演会 平成21年7月10日(芝蘭会館、京都大学)。
6. Fumitoshi Ishino. Retorotransposons and trophoblast biology. Trophoblast Day Meeting. July 14-15, 2009 (University of Cambridge, UK) .
7. Fumitoshi Ishino. Retorotransposon-derived imprinted genes, Peg10 and Peg11/Rtl1 and their relation to the origin of viviparity in mammals. From Imprinting to the Epigenome in 25 years. September 4-6, 2009 (University of Cambridge, UK) .
8. 石野史敏、金児—石野知子 ゲノムインプリンティングの起源 —そのとき哺乳類ゲノムに何が起きたのか?- 第82回日本生化学会年会 シンポジウム トランスポゾンとの共生が織りなすゲノムシステムのダイナミクス 平成21年10月14日(神戸国際会議場、神戸)。
9. 石野史敏 哺乳類の胎生とゲノムインプリンティングの進化におけるレトロトランスポゾンの役割について 北海道大学医学部セミナー 平成21年11月5日(北海道大学医学部、札幌)。
10. Fumitoshi Ishino, Ryuichi Ono, Yoichi Sekita, Shunsuke Suzuki, Mie Naruse, Takashi Kohda Atsuo Ogura, Kenji Nakamura, Minesuke

Yokoyama, Marylin Renfree and Tomoko Kaneko-Ishino. Mammalian-specific genes derived from retrotransposons functioning placenta formation. The 32nd Annual Meeting of the Molecular Biology Society of Japan. Workshop: Integrative approaches towards evolutionary studies. December 9-12, 2009 (Pacifico Yokohama, Yokohama) .

13) 新聞、雑誌、TV 報道

- ・NHK スペシャル「女と男」第三回 男が消える？
人類も消える？
1月18日（日）午後9時～9時58分 制作協力
- ・朝日新聞2009. 4. 7. 朝刊

14) GCOE 総合講義のサマリー

哺乳類特異的な遺伝子発現機構であるゲノムインプリンティングに起因するヒト疾患（Silver-Russell 症候群、Beckwith-Wiedmann 症候群、Prader-Wili/Angelman 症候群、UPD14 症候群など）について、その疾患の原因となるインプリント遺伝子およびその発現異常による発症機構を解説した。特にインプリント調節領域の欠失や DNA メチル化異常（エピメューテーション）がどのように疾患の発症につながるかを解説した。

また、父親・母親由来のインプリント記憶がどのように生殖細胞系列でプログラムされ次世代に伝わるかを、インプリント調節領域における DNA メチル化と脱メチル化の観点から説明した。また、なぜ哺乳類にだけこの機構が存在するのかという問題を、哺乳類を構成する3つのグループ、単孔類（卵生）、有袋類（胎生）、真獣類（胎生）および他の高等脊椎動物である鳥類、魚類（どちらも卵生）のゲノム配列比較から解説し、哺乳類ゲノムに特徴的に増加しているレトロトランスポゾン由来の配列との関連を論じた。特に、哺乳類の胎生の起源に関してはレトロトランスポゾン由来の新規獲得遺伝子が重要な位置を占めている事を紹介し、ゲノムインプリンティングの起源に関してもレトロトランスポゾンの挿入やゲノム構造の変化との関係を論じた。

15) 教室、分野や講座の准教授、講師、助教、特別研究員、ポスドク、指導を受けた大学院生の名前 (AISS には○印) のリスト

准教授 幸田 尚
助 教 小野 竜一
MTT 特任講師 小林 慎

GCOE 特任講師 李 知英
特任助教 鈴木 俊介
特任助教 志浦 寛相
特任助教 遠藤 大輔
特任助教 成瀬 美衣
大学院生 D3 ○岩船 浩孝
大学院生 D3 入江 将仁
大学院生 D3 松本 和也
大学院生 D1 岩崎 佐和
大学院生 D1 石井 雅之
大学院生 M2 山口 祐季
大学院生 M2 夏 希佳
大学院生 M1 及川 真実
大学院生 M1 高橋 沙央里

16) GCOE 活動についての感想、コメント、改善を望む点など

英語での講義が、日本人大学院生にはまだ負担になっているように思うが、英語でのプレゼンテーションの演習などが準備されたことにより、積極的に関わっている学生には良い環境が整ってきたと感じている。また、若手研究者支援として GCOE で雇用した特任講師、特任助教の将来のキャリアについては、今後充分考えて行く必要があると考えている。

Paternal deletion of *Meg1/Grb10* DMR causes maternalization of the *Meg1/Grb10* cluster in mouse proximal Chromosome 11 leading to severe pre- and postnatal growth retardation

Hirosuke Shiura¹, Kenji Nakamura², Takafusa Hikichi^{3,†}, Toshiaki Hino², Kanako Oda², Rika Suzuki-Migishima^{2,‡}, Takashi Kohda¹, Tomoko Kaneko-Ishino⁴ and Fumitoshi Ishino^{1,5,*}

¹Department of Epigenetics, Medical Research Institute, Tokyo Medical and Dental University, 1-5-45 Yushima, Bunkyo-ku, Tokyo 113-8510, Japan, ²Mitsubishi Kagaku Institute of Life Science, 11 Minamiooya, Machida, Tokyo 194-8511, Japan, ³Center for Biological Resources and Informatics, Tokyo Institute of Technology, 4259 Nagatsuta-cho, Midori-ku, Yokohama 226-8501, Japan, ⁴School of Health Sciences, Tokai University, Bohseidai, Isehara, Kanagawa 259-1193, Japan and ⁵Global Center of Excellence (GCOE) Program, International Research Center for Molecular Science in Tooth and Bone Diseases

Received November 27, 2008; Revised and Accepted January 23, 2009

Mice with maternal duplication of proximal Chromosome 11 (MatDp(prox11)), where *Meg1/Grb10* is located, exhibit pre- and postnatal growth retardation. To elucidate the responsible imprinted gene for the growth abnormality, we examined the precise structure and regulatory mechanism of this imprinted region and generated novel model mice mimicking the pattern of imprinted gene expression observed in the MatDp(prox11) by deleting differentially methylated region of *Meg1/Grb10* (*Meg1*-DMR). It was found that *Cobl* and *Ddc*, the neighboring genes of *Meg1/Grb10*, also comprise the imprinted region. We also found that the mouse-specific repeat sequence consisting of several CTCF-binding motifs in the *Meg1*-DMR functions as a silencer, suggesting that the *Meg1/Grb10* imprinted region adopted a different regulatory mechanism from the *H19/Igf2* region. Paternal deletion of the *Meg1*-DMR (+ Δ DMR) caused both upregulation of the maternally expressed *Meg1/Grb10* Type I in the whole body and *Cobl* in the yolk sac and loss of paternally expressed *Meg1/Grb10* Type II and *Ddc* in the neonatal brain and heart, respectively, demonstrating maternalization of the entire *Meg1/Grb10* imprinted region. We confirmed that the + Δ DMR mice exhibited the same growth abnormalities as the MatDp(prox11) mice. Fetal and neonatal growth was very sensitive to the expression level of *Meg1/Grb10* Type I, indicating that the 2-fold increment of the *Meg1/Grb10* Type I is one of the major causes of the growth retardation observed in the MatDp(prox11) and + Δ DMR mice. This suggests that the corresponding human *GRB10* Type I plays an important role in the etiology of Silver-Russell syndrome caused by partial trisomy of 7p11-p13.

INTRODUCTION

The mouse *Meg1/Grb10* gene was originally identified as a maternally expressed imprinted gene using a subtractive protocol between androgenetic and normal fertilized embryos (1). It exhibits maternal expression in almost all tissues and organs

while the human orthologue, *GRB10*, exhibits a biallelic expression in the corresponding regions. However, in the brain, both human *GRB10* and mouse *Meg1/Grb10* have been reported to be preferentially expressed from paternal alleles (2–6). Interestingly, these genes have two corresponding promoter regions. Type I transcripts from upstream

*To whom correspondence should be addressed. Tel: +81 358034862; Fax: +81 358034863; Email: fishino.epgn@mri.tmd.ac.jp

[†]Present address: Research Institute, International Medical Center of Japan, 1-2-21 Toyama, Shinjuku-ku, Tokyo 162-8655, Japan.

[‡]Present address: IVF Namba Clinic, 1-17-28 Minamihorie, Nishi-ku, Osaka 550-0015, Japan.

promoters display maternal and biallelic expression in mice and humans, respectively, in almost all tissues. Type II transcripts from downstream promoters display paternal expression in the brain in both species (6–9).

The DMR locating on human *GRB10* and mouse *Meg1/Grb10* region (*Meg1*-DMR, also known as *Grb10* CpG island 2 (CGI 2) DMR) overlaps the brain-specific downstream promoter in both species; it is hypermethylated on the inactive maternal allele while non-methylated on the active paternal allele, suggesting that DNA methylation directly regulates the imprinted paternal expression of *GRB10* and *Meg1/Grb10* Type II transcripts (6–8). In addition, we have also demonstrated the existence of a mouse-specific repeat (MSR) sequence in the mouse *Meg1*-DMR, where an insulator CTCF protein binds in a DNA-methylation-sensitive manner. Therefore, we have proposed a molecular mechanism model in which the CTCF binding to the MSR controls the mouse-specific maternal expression of *Meg1/Grb10* Type I transcript via an insulator function, as has been observed in the *Igf2/H19* region (6,10,11).

Until recently, there was no evidence for the existence of other imprinted genes around *Meg1/Grb10* (5). However, it has been reported that one of the promoter variants of mouse *Ddc*, which is located on the 3' side of *Meg1/Grb10*, exhibits heart-specific paternal expression (12), suggesting that the *Meg1/Grb10* region also comprises an imprinted gene cluster consisting of certain other genes where the *Meg1*-DMR regulates all the imprinted genes, as in the case of other imprinted domains. Thus, in order to elucidate the precise structure of this imprinted region, more extensive search of the imprinted genes around *Meg1/Grb10* is required.

Meg1/Grb10 encodes an adaptor protein which binds to certain tyrosine-kinase receptors, such as insulin receptor or insulin-like growth factor I receptor (13–24), suggesting that the protein is implicated in growth. It is known that the mice with maternal disomy Chromosome 11 (MatDi(11)) and maternally duplicated proximal Chromosome 11 (MatDp(prox11)), where *Meg1/Grb10* locates, exhibit pre- and postnatal growth retardation, while mice with paternal disomy of Chromosome 11 (PatDi(11)) or paternally duplicated proximal Chromosome 11 (PatDp(prox11)) exhibit pre- and postnatal promotion of growth (25–27), suggesting that imprinted *Meg1/Grb10* is a candidate gene for the growth phenotypes. However, the precise role of the *Meg1/Grb10* protein in growth remains unclear, because both positive and negative effects on the signaling pathways via those receptors have been reported *in vitro* (13,17,22–24,28–37). Then, the *in vivo* inhibitory role in growth was clearly demonstrated by *Meg1/Grb10* knockout (KO) mice that exhibited embryonal and placental overgrowth when the knockout allele was transmitted from their mother, as in the case of PatDi(11) and PatDp(prox11) mice (38).

In contrast, overproduction effects of *Meg1/Grb10* on fetal or neonatal growth have still not been successfully obtained. We previously generated *Meg1/Grb10* transgenic (*Meg1*Tg) mice in which *Meg1/Grb10* cDNA was transcribed from the chicken β -actin promoter and stimulated by the CMV enhancer (CAG vector) (39,40). Although an approximately 1.5-fold *Meg1/Grb10* expression level was observed in the *Meg1*Tg embryos compared with that of controls, embryonic growth

retardation was not observed. However, it is highly probable that the *Meg1* Tg mice did not in fact represent the precise expression profile of *Meg1/Grb10* during development, because the transgene did not have the original promoter and coupled with an external enhancer.

In this study, we analyzed the imprinted expression of the neighboring genes of *Meg1/Grb10* and demonstrated that the *Meg1/Grb10* imprinted region encompassed approximately 650 kb, including both of the neighboring *Cobl* and *Ddc* genes. *In vitro* functional assays showed that the MSR sequence in the *Meg1*-DMR can function as a silencer, suggesting that the *Meg1/Grb10* imprinted region is regulated by a different mechanism from that of the *H19/Igf2* region. Finally, we constructed a novel model mouse expressing a double dosage of the *Meg1/Grb10* Type I transcript in the correct tissues and organs by deletion of the imprinting control center, the *Meg1*-DMR. These mice exhibited the same growth retardation phenotype as the MatDi(11) and MatDp(prox11) mice, as expected. We also observed that a subtle increment of the *Meg1/Grb10* Type I expression significantly affected fetal and neonatal growth by comparing two slightly different types of mice with the *Meg1*-DMR deletion, those with and without Neo genes (neomycin-resistance genes) in the deletion construct. This indicates that the pre- and postnatal growth retardation observed in both the *Meg1*-DMR deletion mice and the MatDi(11) and MatDp(prox11) mice is mainly attributable to the double dosage of the *Meg1/Grb10* Type I transcript. Based on these results, we discuss the possibility that the corresponding *GRB10* Type I transcript expressed in the entire body could be responsible for the etiology of the human Silver-Russell syndrome (SRS) caused by partial duplication of 7p11–p13, even if it is not imprinted in humans.

RESULTS

The *Meg1/Grb10* imprinted cluster contains novel imprinted genes

Meg1/Grb10 has long been known as an isolated single imprinted gene in the mouse proximal Chromosome 11 (1,5) (Fig. 1A and B), but recently it was reported that *Ddc* transcribed from exon 1a (hereafter referred to as *Ddc*-exon1a) showed complete paternal expression only in neonatal heart, by comparing the expression profiles between mice with PatDp(prox11) and MatDp(prox11) (12). We further demonstrated that an alternative promoter variant of *Ddc* which transcribed from exon 1 (hereafter referred to as *Ddc*-exon1) and *Cobl* also showed paternally and maternally biased expression in a tissue-specific manner, respectively.

By analyzing mice produced by reciprocal crosses between C57BL/6J (B6) and JF1/Msf (JF1) (41), we examined the imprinting status of several transcripts from neighboring genes of *Meg1/Grb10*, such as *Cobl* and *Ddc* locating on the 5' and 3' sides of *Meg1/Grb10*, respectively, and *Figl1* and *Igf2*, next to *Ddc* (Fig. 1A–I). There was a slightly biased expression from paternal alleles of *Ddc*-exon1 in yolk sac and liver, but not in embryos (Fig. 1C–E). Interestingly, another transcript, *Ddc*-exon1a, did exhibit a paternally biased expression in embryos. In addition, we reconfirmed the

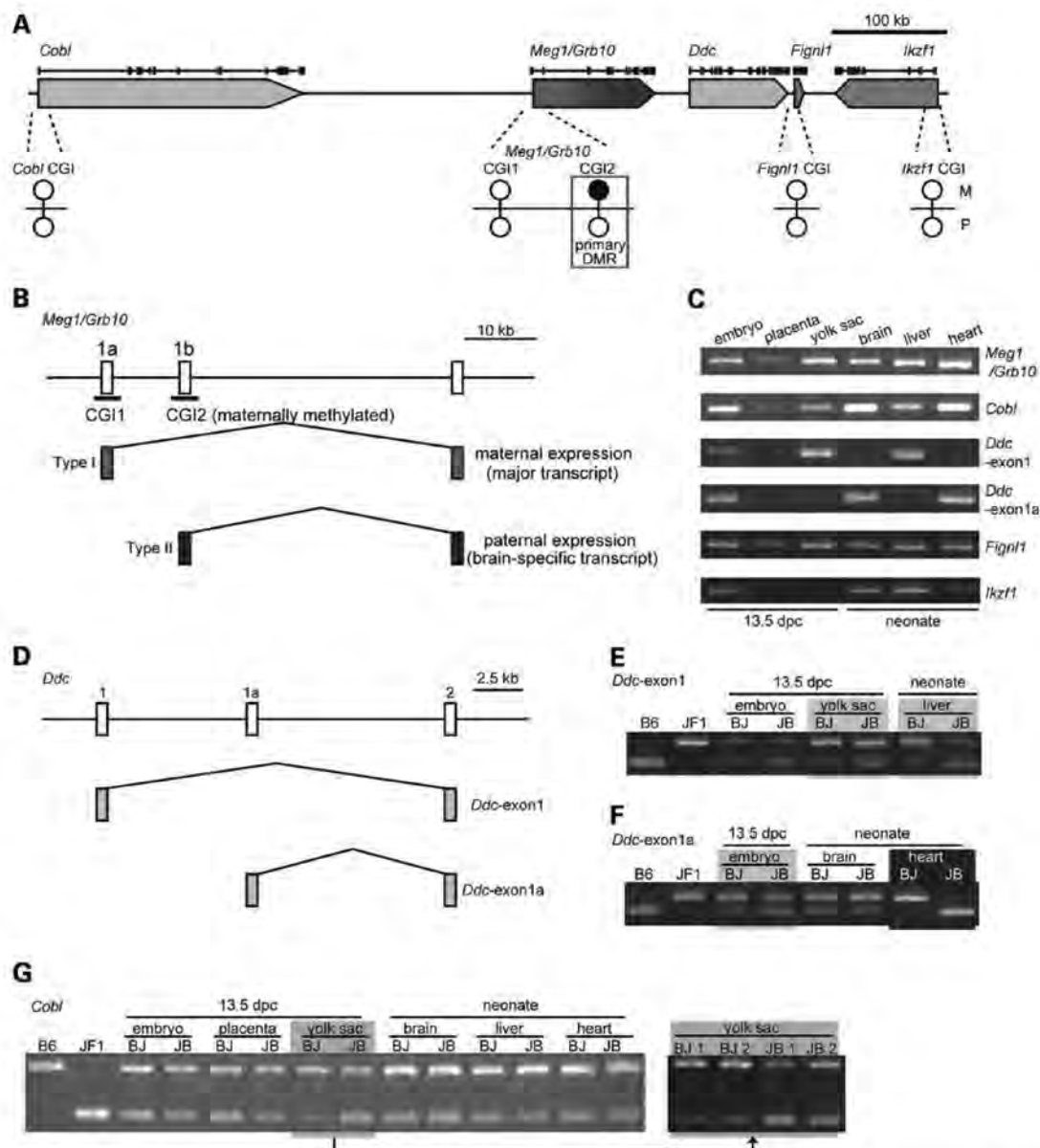


Figure 1. Allelic expression and methylation of CpG islands, with profiles of the neighboring genes of mouse *Meg1/Grb10*. (A) Physical map of the neighboring genes of *Meg1/Grb10*. The arrows show the direction of each transcription unit. Red and pink indicate the maternally and paternally biased expressed genes, respectively, and blue and light blue indicate the paternally and maternally biased expressed genes. The exon-intron structure of each gene is indicated above each arrow. DNA methylation status of CpG islands is indicated as lollipop figures. Black and white lollipops indicate hyper- and hypomethylation, respectively. M (upper side) and P (lower side) indicate maternal and paternal allele, respectively. (B) Schematic representation of the promoter-specific *Meg1/Grb10* expression patterns (presented to scale). (C) Expression profiles of *Meg1/Grb10*, *Cob1*, *Ddc*, *Fign1* and *Ikzf1* in 13.5 dpc conceptuses and neonatal tissues. (D–I) Allelic expression analysis of *Meg1/Grb10* neighboring genes using F1 mice from reciprocal crosses between C57BL/6J (B6) and JF1/MsJ (JF1). BJ and JB indicate F1 mice from B6 mother × JF1 father and JF1 mother × B6 father, respectively. B6 and JF1 expression patterns are shown as controls. In each transcript, the tissues where the transcript is expressed (shown in C) were examined. (D) Schematic representation of the *Ddc* promoter variants (presented to scale). (E and F) RFLP analysis of *Ddc-exon1* (E) and *Ddc-exon1a* (F) expression. Each promoter variant (*Ddc-exon1* and *Ddc-exon1a*) was detected by promoter-specific PCR. The light blue and blue boxes indicate paternally biased and fully paternal expression, respectively. (G) RFLP analysis of *Cob1* expression. The pink box indicates maternally biased expression. (H) Direct sequencing analysis of *Fign1* expression. Arrows indicate polymorphic sites between B6 and JF1. (I) RFLP analysis of *Ikzf1* expression. (J–L) Methylation analysis of the CpG islands implicated in *Cob1* (J), *Fign1* (K) and *Ikzf1* (L) promoter regions. Each CpG methylation was examined by sequencing bisulfite-treated genomic DNA from BJ embryo, placenta and yolk sac. Open and filled circles indicate unmethylated CpG and methylated CpG dinucleotides, respectively. In *Cob1* and *Fign1*, parental alleles were determined by polymorphism between B6 and JF1 mice. The embryo samples are shown. The same results were produced by using placenta and yolk sac samples.

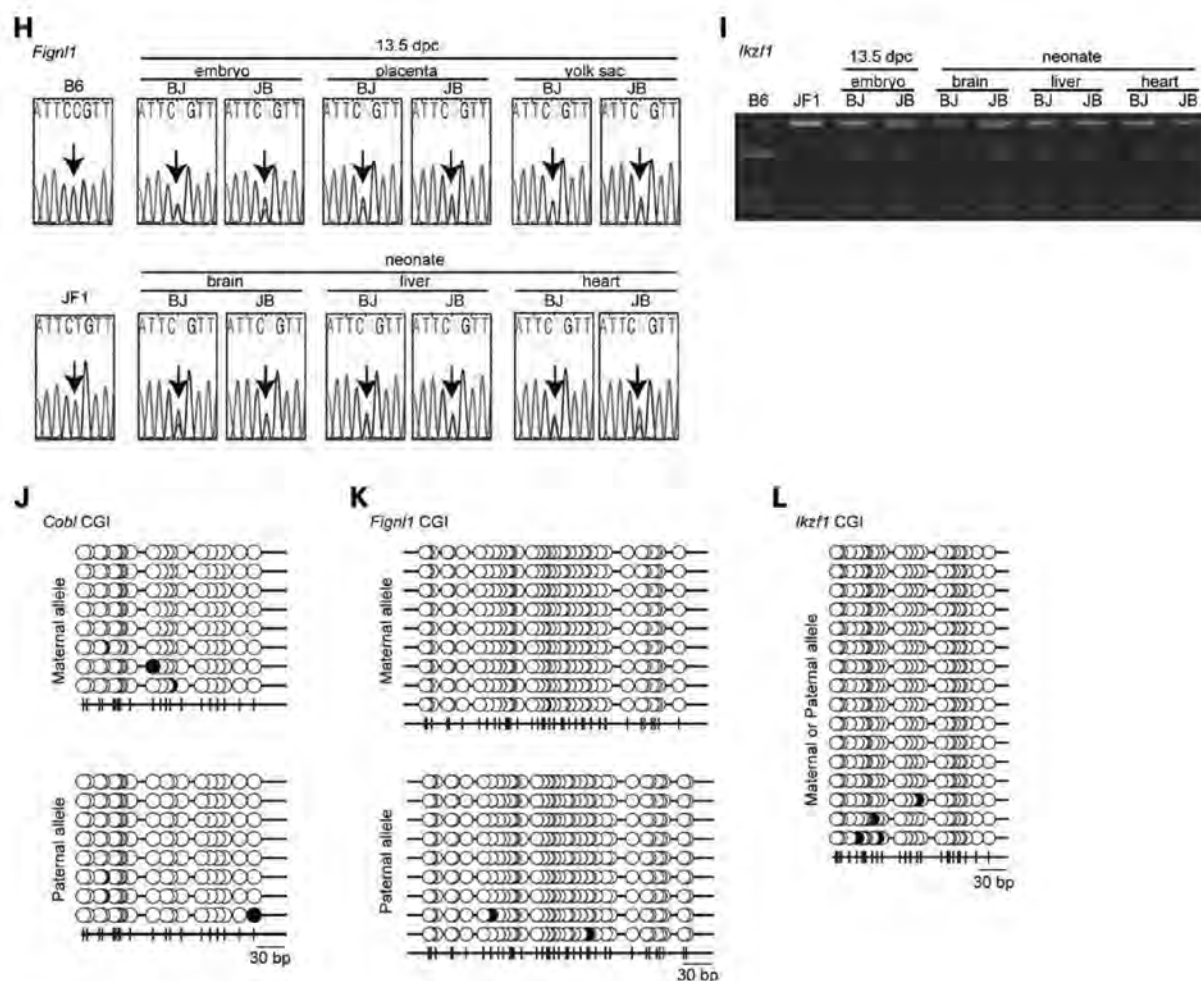


Figure 1. Continued

results that *Ddc*-exon1a exhibited heart-specific paternal expression in neonates while it was biallelically expressed in neonatal brain (Fig. 1C, D and F). *Cobl* exhibited biallelic expression in all tissues examined except yolk sac, where the expression pattern was slightly maternally biased (Fig. 1C and G). These biased expression patterns of *Ddc* and *Cobl* were confirmed by allele-specific quantitative PCR (Supplementary Material, Fig. S1). *Fignl1* and *Ikzf1* exhibited biallelic expression and no clearly biased expression in any of the tissues examined by direct sequence analysis and restriction fragment length polymorphism (RFLP), respectively (Fig. 1C, H and I). These results demonstrate that at least two neighboring genes of *Meg1/Grb10*, *Cobl* and *Ddc*, are imprinted, and that the *Meg1/Grb10* imprinted region is comprised of approximately 650 kb in the mouse proximal Chromosome 11.

As previously shown, the *Meg1*-DMR corresponding to CpG island 2 (CGI 2) of *Meg1/Grb10* is a primary DMR in this region (Fig. 1A) (6,7). Next, we examined the DNA methylation status of the other CpG islands (CGIs) in the

promoter regions of *Cobl*, *Fignl1* and *Ikzf1*. As shown in Figure 1A and J–L, we confirmed that all the CGIs examined were hypomethylated as well as CGI 1 of *Meg1/Grb10*, which locates on the promoter region of *Meg1/Grb10* Type I transcript (6,7). No CGIs and no differentially methylated CpG sites are reported in and around the *Ddc*-exon1a promoter region (12). The same was true for the *Ddc*-exon1 promoter (data not shown). Thus, the *Meg1*-DMR, the CGI 2 DMR of *Meg1/Grb10*, is the only primary DMR in this imprinted region which possibly regulates all of these imprinted genes.

The MSR sequence can function as a silencer

Next, we addressed the mechanism of imprinted regulation by *in vitro* functional assays using several vector constructs, especially the role of the MSR sequence (shown in Fig. 2A) containing several CTCF binding sites within the *Meg1*-DMR. Unexpectedly, we found that the MSR, by itself, could function as a silencer.

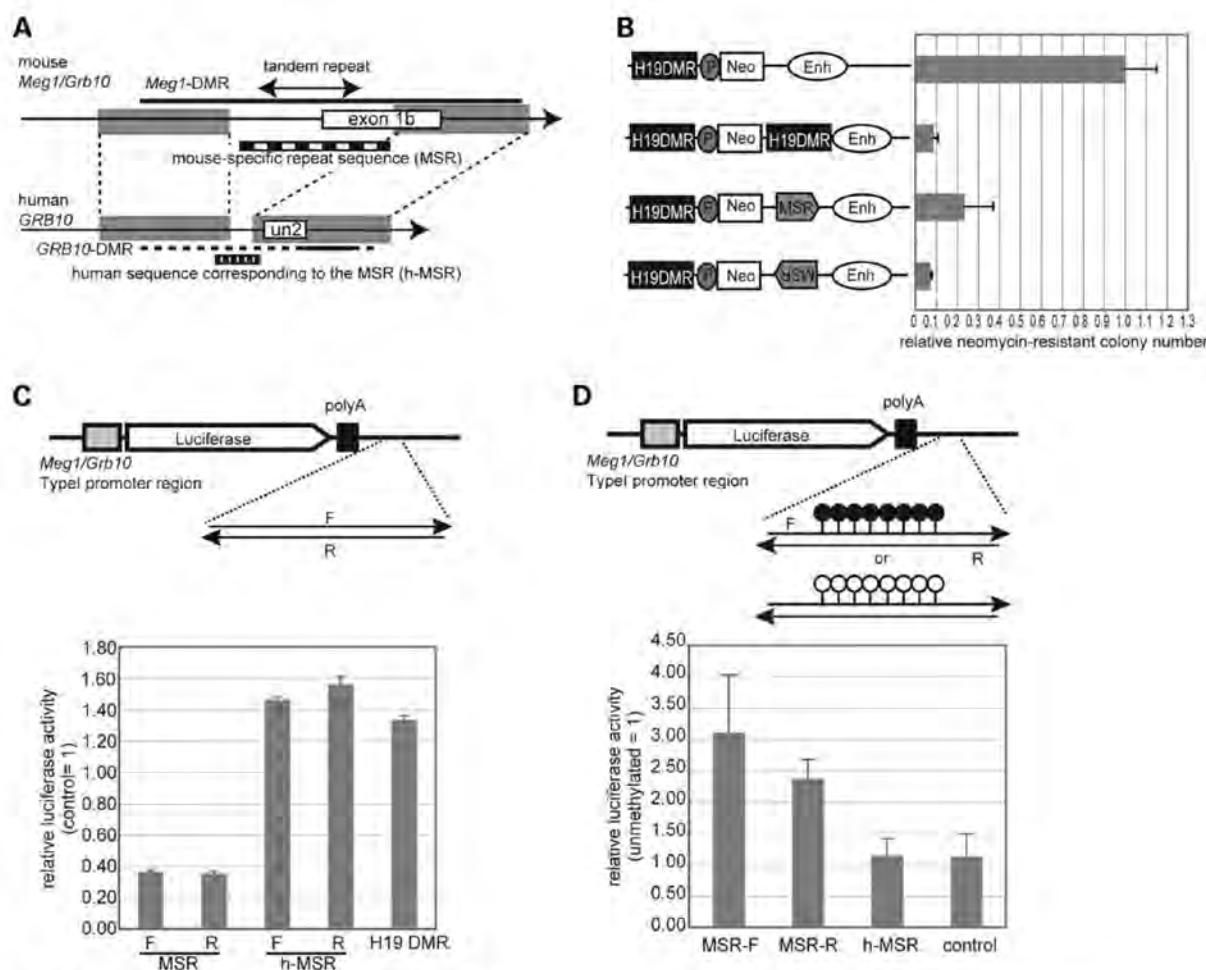


Figure 2. *In vitro* reporter assays for the *Meg1*-DMR genomic function. (A) Mouse *Meg1*-DMR and human *GRB10*-DMR regions exhibit high sequence homology with the exception of the mouse-specific sequence containing tandem repeats. DNA homology was calculated using the program VISTA (<http://genome.lbl.gov/vista/index.shtml>). Gray boxes indicate conserved regions between mouse and human. The regions with the striped bar were used as the MSR sequence and the human sequence corresponding to the MSR (h-MSR) in this study. The confirmed DMR are indicated with bold lines (6,7,67). In humans, the putative DMR, which has a high homology with mouse *Meg1*-DMR, is indicated as a bold dashed line. (B) The MSR sequence within *Meg1*-DMR has insulator or/and silencer properties. The mouse cell line 'L cells' was stably transfected with the indicated construct and grown in medium containing G418. The number of neomycin-resistant colonies obtained with a no-insertion control (top column) was set as 1. Neo, neomycin-resistance gene; P, mouse *H19* promoter; Enh, *H19* ectoderm enhancers; MSR, mouse-specific sequence within *Meg1*-DMR shown in (A). (C) The MSR sequence within *Meg1*-DMR has silencer properties. The test fragments, MSR sequence, h-MSR (human sequence corresponding to the MSR) (shown in (A)) and *H19* DMR, were inserted downstream of the polyA signal sequence of the vector including the luciferase gene derived from the mouse *Meg1/Grb10* Type 1 promoter (pGL3Mp vector). The reporter constructs were transfected into L cells and the luciferase activity of each reporter construct was measured. DNA fragments of comparable length to test fragments were chosen from the mouse genome and used as a control for each reporter construct. A value of 1 represents the activity of the control construct. (D) The silencer properties of MSR sequence within the *Meg1*-DMR is methylation-sensitive. pGL3Mp reporter constructs with methylated or unmethylated inserts were transfected into L cells, and luciferase activity of each construct was measured. The value of 1 represents the luciferase activity of the unmethylated case for each reporter construct. DNA fragments of comparable length to MSR was chosen from the mouse genome and used as a control fragments.

First, the insulator action was examined using two different assays: transient assay using luciferase vectors (data not shown) and stable assay using neomycin resistance gene (Neo) vectors (Fig. 2B) (42). In both vectors, the MSR or *H19* DMR insulator was positioned between the promoter and the enhancer. The MSR inserted in either direction significantly reduced the number of Neo-resistant colony as in the case of the control *H19* DMR, although that in the

forward direction was weaker than the reverse direction (Fig. 2B). These results indicate that the MSR within the *Meg1*-DMR had some capacity to reduce the Neo expression. However, using these kinds of assays, it is essentially impossible to discriminate insulator activity from silencer activity.

We then tested whether the MSR had silencer activity by using vector constructs without an enhancer. In these

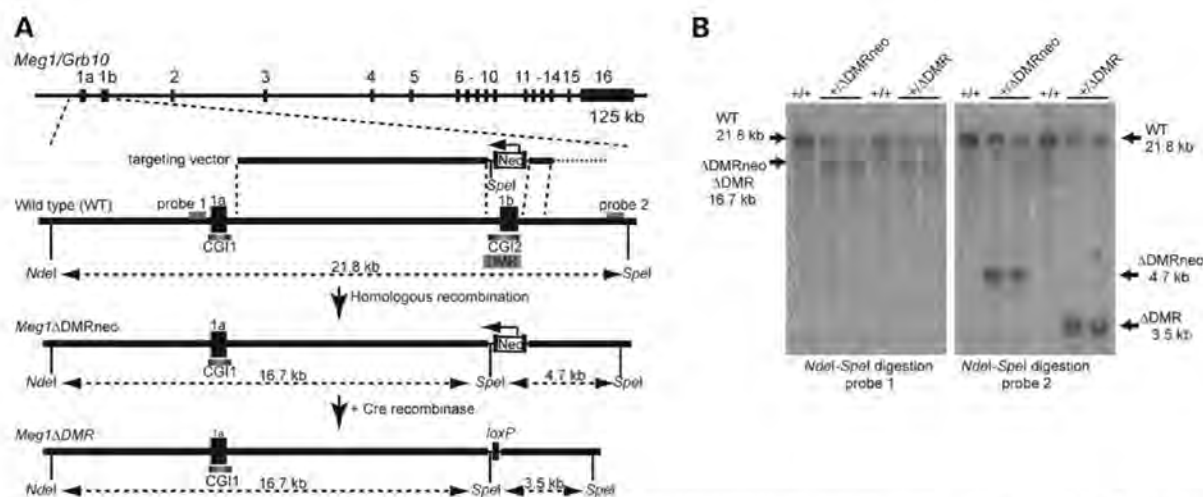


Figure 3. Targeted deletion of *Meg1*-DMR. (A) Schematic representations of mouse *Meg1/Grb10*, the targeting vector and the targeted *Meg1*-DMR. The *Meg1*ΔDMRneo allele was generated by homologous recombination of the wild-type allele with the targeting vector. In the targeted allele, all CpGs (except for one CpG on the 5' side) within the DMR were replaced by a neomycin-resistance gene (Neo). The arrow over the Neo and bold vertical bars surrounding Neo indicate the direction of Neo expression and the loxP sites, respectively. To generate the *Meg1*ΔDMR allele, the neomycin-resistance gene was eliminated using the Cre-loxP system. (B) Southern blot analysis of the *Meg1*ΔDMRneo and *Meg1*ΔDMR alleles. Genomic DNA was digested with *NdeI* and *SpeI* and hybridized with probe 1 or probe 2, as indicated in (A).

vectors, the luciferase gene was driven by the *Meg1*-Type I promoter and the MSR or the *H19* DMR was placed downstream. This experiment clearly demonstrated that the MSR in either the forward or reverse orientation could down-regulate the luciferase activity while no such effect was observed with the *H19* DMR (Fig. 2C). Importantly, its silencer function was DNA methylation sensitive because the luciferase expression increased 2–3-fold when fully methylated fragments were inserted (Fig. 2D). The human sequence corresponding to the MSR (h-MSR, shown in Fig. 2A) has no CTCF binding sites (43) and showed no silencer function (Fig. 2C), and DNA methylation did not affect the result (Fig. 2D). These results indicate that the MSR containing several CTCF-binding sites within the *Meg1*-DMR, by itself, can play a silencer role in a DNA-methylation-dependent manner. Although it is not easy to integrate the silencer function of the MSR with the regulatory mechanism of the *Meg1/Grb10* imprinted region, it is probable that the *Meg1*-DMR plays a different role from the *H19* DMR.

Paternal inheritance of the *Meg1*ΔDMR allele results in maternalization of the *Meg1/Grb10* imprinted region by disruption of imprinted regulation

We generated mice with the *Meg1*-DMR deletion (*Meg1*ΔDMR) to produce mice exhibiting biallelic expression of *Meg1/Grb10* Type I transcript during development in order to directly see the growth inhibitory effect (Fig. 3). We confirmed that mice with paternal transmission of the *Meg1*ΔDMR induced expression of the *Meg1/Grb10* Type I transcript from the paternal allele, and moreover, disrupted imprinted expression patterns of *Ddc* and *Cobl* were observed in these mice.

Parent-of-origin-specific expression of the imprinted genes was examined using two reciprocal F1 mice, one from a hetero mutant dam and JF1 sire (*ΔDMR/JF1*) and the other from a JF1 dam and hetero mutant sire (*JF1/ΔDMR*). RT-PCR analysis demonstrated that almost all of the *Meg1/Grb10* expression was due to the Type I transcript (data not shown) and exhibited maternal expression in all of the tissues examined except neonatal brain in the wild-type (*JF1/+* and *+/JF1*) mice, as previously reported. However, paternal transmission of *ΔDMR* (*JF1/ΔDMR* mice) activated expression of the paternally silenced allele, resulting in biallelic expression of the *Meg1/Grb10* Type I from the upstream promoter (Fig. 4A). This biallelic expression is different from that observed in normal neonatal brain, in which *Meg1/Grb10* exhibits biallelic expression due to a combined expression of both the maternally expressed Type I from exon 1a and the paternally expressed Type II from the brain-specific exon 1b promoter (Fig. 4A and B).

In the case of *Ddc*, RFLP analysis indicated that the expression levels of paternal *Ddc*-exon1 in yolk sac and liver, as well as those of *Ddc*-exon1a in embryos, were reduced relative to those of *JF1/+* (Fig. 4C and D). A 50 to 60% reduction was confirmed in each case by allele-specific quantitative PCR analysis (Fig. 4E–G). The paternal expression of the *Ddc*-exon1a in neonatal heart was completely repressed in *JF1/ΔDMR* (Fig. 4D). In contrast, paternal *Cobl* expression was increased in the *JF1/ΔDMR* yolk sac compared with that of *JF1/+*. Although we failed to detect any obvious alteration in expression pattern between *JF1/+* and *JF1/ΔDMR* by RFLP analysis (Fig. 4H), allele-specific quantitative PCR analysis revealed a 40% increment in paternal *Cobl* expression (Fig. 4I). These results demonstrate that the *Meg1*-DMR regulates the entire *Meg1/Grb10* imprinted region consisting of *Cobl*, *Meg1/Grb10* and *Ddc*.

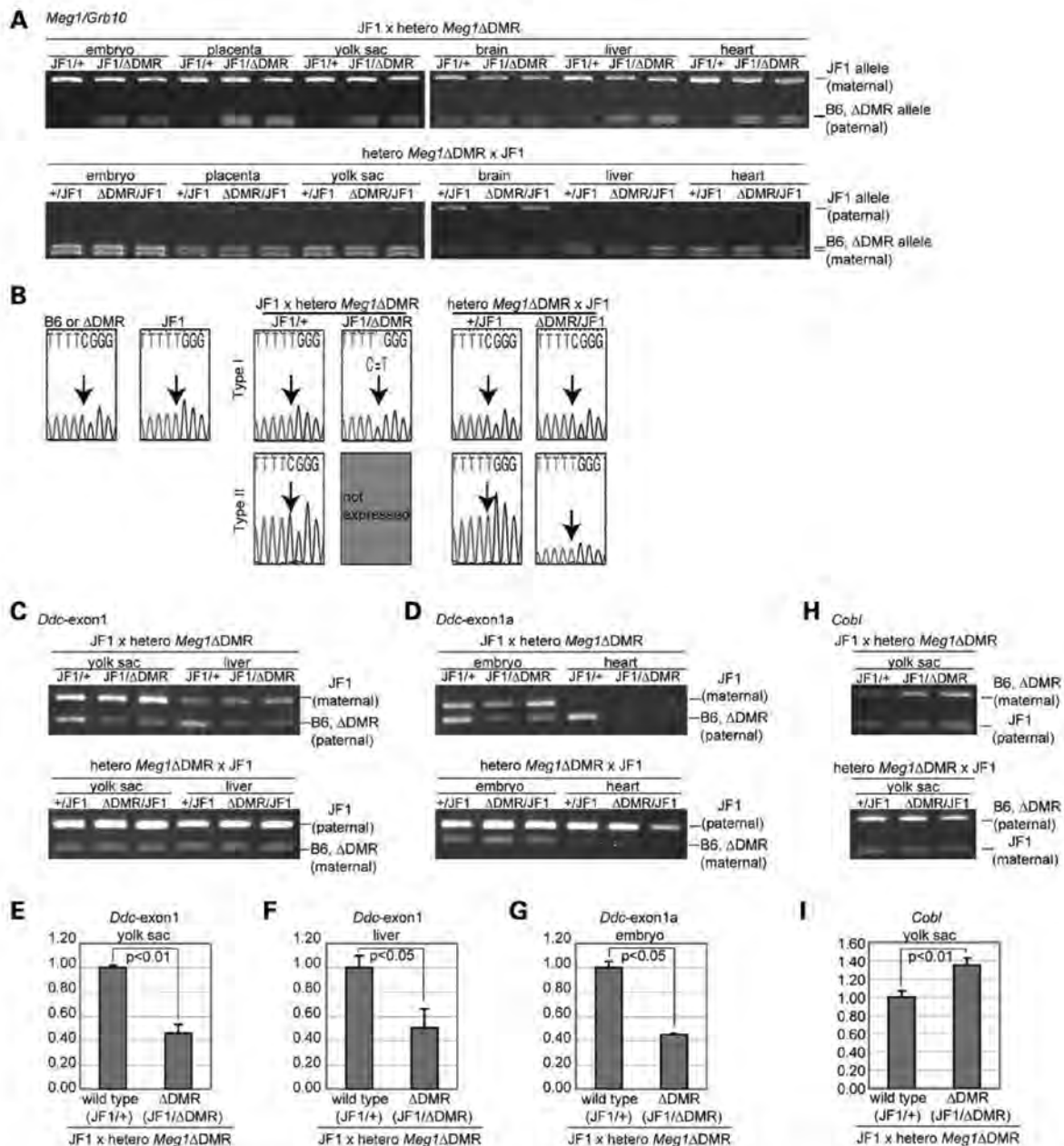


Figure 4. Analysis of imprinted genes in *Meg1ΔDMR* mice. Allelic expression of the imprinted genes in the mice with paternal and maternal *Meg1ΔDMR* deletion was examined by using 13.5 dpc conceptuses and neonatal tissues of F1 mice from JF1 and heterozygous *Meg1ΔDMR* mice. JF1/ΔDMR and ΔDMR/JF1 indicate the mice with paternal and maternal *Meg1ΔDMR* allele, respectively, and JF1/+ and +JF1 are wild-type controls for JF1/ΔDMR and ΔDMR/JF1, respectively. (A) RFLP analysis of *Meg1/Grb10* expression in *Meg1ΔDMR* mice. The upper and lower panels show the expression patterns in the mice with the paternal and maternal *Meg1ΔDMR* allele, respectively. (B) Direct sequencing analysis of *Meg1/Grb10* expression in neonatal brain. The expression patterns of the mice with the paternal (center) and maternal (right) *Meg1ΔDMR* allele are shown. B6 (or ΔDMR) and JF1 expression pattern are shown as controls (left) and arrows indicate polymorphic sites between B6 (or ΔDMR) and JF1 mice. (C and D) RFLP analysis of *Ddc-exon1* (C) and *Ddc-exon1a* (D) expression in *Meg1ΔDMR* mice. The tissues where each transcript is imprinted (shown in Fig. 1 (D)) were examined. The upper and lower panels show the expression pattern of the mice with the paternal and maternal *Meg1ΔDMR* allele, respectively. (E–G) Quantitative PCR analysis of *Ddc-exon1* expression in the yolk sac (E) and liver (F), and *Ddc-exon1a* expression in the embryo (G). The value of '1' represents the expression level in the JF1/+ paternal wild-type (B6) allele. The paternal *Meg1ΔDMR* deletion caused downregulation of imprinted expression of these transcripts in cis. (H) RFLP analysis of *Cobl* expression in *Meg1ΔDMR* mice. (I) Quantitative PCR analysis of *Cobl* expression in the yolk sac. The value of 1 represents the expression level in the JF1/+ paternal wild-type (B6) allele. The paternal *Meg1ΔDMR* deletion caused upregulation of imprinted expression of *Cobl* in cis, in contrast to *Ddc-exon1* and *Ddc-exon1a*.

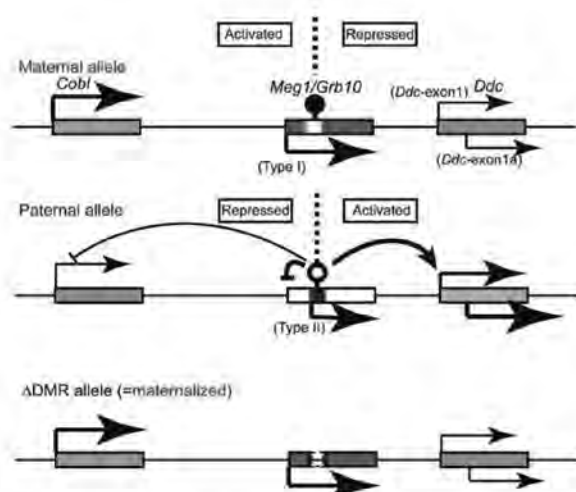


Figure 5. Imprinting regulation of the *Meg1/Grb10* region. Schematic representations of imprinted expression in the *Meg1/Grb10* imprinted region. *Meg1*-DMR seems to mark the boundary between the maternally biased and maternal transcripts (*Cob1* and *Meg1/Grb10* Type I) and the paternal and paternally biased transcripts (*Meg1/Grb10* Type II and *Ddc*). Deletion of *Meg1*-DMR is comparable to hypermethylation of *Meg1*-DMR in the maternal allele. Red and pink indicate maternal and maternally biased expression, respectively, and blue and light blue indicate paternal and paternally biased expression, respectively. Arrows indicate the direction of the expression of each transcript, and the size of the arrows reflects expression level. The filled and open lollipops indicate methylated and unmethylated *Meg1*-DMR, respectively.

In all of the transcripts examined, maternal *Meg1*ΔDMR transmission did not have any effect on imprinted expression in the region (Fig. 4A–D and H).

The *Meg1*-DMR hypermethylated in the maternal allele has both a promotional role for the maternally expressed *Meg1/Grb10* Type I and maternally biased *Cob1* and an inhibitory role for the paternally expressed *Meg1/Grb10* Type II and the paternally expressed/paternally biased *Ddc*, respectively, while the *Meg1*-DMR hypomethylated in the paternal allele acts *vice versa* (Fig. 5). Paternal deletion of the *Meg1*-DMR leads to the activation of the upstream maternally expressed genes and repression of downstream paternally expressed genes, and therefore, is comparable to the hypermethylated *Meg1*-DMR in the maternal allele (Fig. 5). Thus, it is concluded that the paternal deletion of the *Meg1*-DMR causes maternalization of the *Meg1/Grb10* imprinted region on paternal Chromosome 11.

Biallelic expression of *Meg1/Grb10* Type I in the entire body results in pre- and postnatal growth retardation

The mice with maternal deletion of the *Meg1*-DMR did not display any clear phenotypes (data not shown). However, the mice with paternal deletion of the *Meg1*-DMR (+/ΔDMR) exhibited growth retardation from 12.5 dpc (days post coitus) and an ~30% reduction of the fetal weight was evident at term. Interestingly, placental growth retardation was slightly delayed and exhibited from 13.5 dpc and its weight exhibited a 20% reduction at term, suggesting *Meg1*/

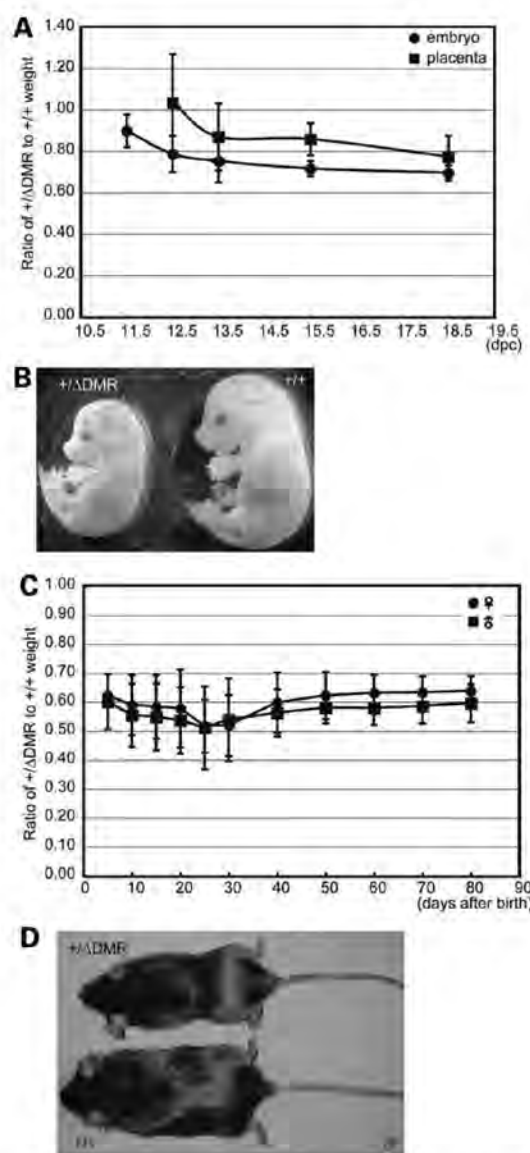


Figure 6. Pre- and postnatal growth of the mice with paternal *Meg1*-DMR deletion. (A) Growth curves of embryonic and placental weight. For each embryonic stage (11.5, 12.5, 13.5, 15.5 and 18.5 dpc), +/+ and +/ΔDMR embryos and placentas from crosses of +/+ female with hetero *Meg1*ΔDMR male mice were collected and weighed. Mean weights were calculated for each genotype within a litter. A value of 1 represents the mean weight of +/+ mice. (B) +/ΔDMR (left) and +/+ (right) embryos at 15.5 dpc. (C) Growth curves of male and female +/ΔDMR mice. Mean weights were calculated for each genotype and sex within a litter. A value of 1 represents the mean weight of +/+ mice. (D) +/ΔDMR (upper) and +/+ (lower) male littermates at the 3 months of age.

Grb10 functions primarily in embryos and secondarily in placentas (Fig. 6A and B). After birth, the growth retardation, which was ~60% of the normal weight, was maintained throughout the postnatal period to the adult stage (Fig. 6C

Table 1. Comparison of growth and expression level of *Meg1/Grb10*, *Cobl* and *Ddc* between +/ Δ DMR and +/ Δ DMRneo mice

Genotype	Weight (+/+ = 1)			mRNA level (12.5 dpc, +/+ = 1)		
	12.5 dpc	18.5 dpc	20 D (male)	<i>Meg1/Grb10</i>	<i>Cobl</i>	<i>Ddc</i>
+/ Δ DMR	0.789*	0.704**	0.566**	1.928*	1.075	0.709
+/ Δ DMRneo	0.960	0.836	0.738	1.655	1.056	0.758

D, days after birth.

* $P < 0.05$, ** $P < 0.01$.

and D), suggesting that biallelic expression of the *Meg1/Grb10* Type I in the entire body led to growth retardation in both the pre- and postnatal periods.

Negative correlation between the *Meg1/Grb10* expression level and pre- and postnatal growth was confirmed by comparing *Meg1/ΔDMR* mice and *Meg1/ΔDMRneo* mice. The *Meg1/ΔDMRneo* mice retained the neomycin resistance gene (Neo) replaced by the *Meg1*-DMR (Fig. 3). +/ Δ DMRneo mice carrying the Neo allele displayed mild growth retardation (74% of normal at 20 days after birth) compared to the +/ Δ DMR mice without the Neo allele (57% of the normal). Importantly, a significant difference in the expression level of *Meg1/Grb10* Type I was confirmed in the 12.5 dpc embryos between +/ Δ DMR and +/ Δ DMRneo mice: the expression level of *Meg1/Grb10* Type I was higher in the former fetuses (1.93-fold compared with normal), which displayed severe growth retardation compared with the latter (1.65-fold) (Table 1), while the expression levels of *Cobl* and *Ddc* did not display any significant differences between these two mice. These results indicate that fetal growth was extremely sensitive to the level of *Meg1/Grb10* Type I, and that its elevated expression is the primary cause of the pre- and postnatal growth retardation observed in +/ Δ DMR mice.

DISCUSSION

This study has demonstrated that the *Meg1/Grb10* imprinted region on the mouse proximal Chromosome 11 consists of at least five imprinted transcripts of the three genes, *Cobl*, *Meg1/Grb10* Types I and II, and *Ddc*-exon1 and -exon1a and that they are, respectively, regulated by the *Meg1*-DMR in a tissue-specific manner. It has also demonstrated that the deletion of the *Meg1*-DMR is comparable to the fully methylated status of the *Meg1*-DMR in the maternal alleles in terms of genomic imprinting regulation. Therefore, its paternal deletion maternalizes the entire *Meg1/Grb10* imprinted region.

The DMR coupled with the CTCF-binding sites is very effective for the regional control of multiple imprinted genes. The human homologous DMR region has no such CTCF-binding sequences and the *GRB10* Type I transcript exhibits biallelic expression in almost all tissues, and there have been no obvious data demonstrating the imprinting expression of *COBL* and *DDC*, although *GRB10* Type II transcript does exhibit paternal expression in the brain, as is also the case with mice (5,6,12). Therefore, the function of the CTCF-binding sequences is of considerable interest.

Previously, we reported that CTCF insulator protein bound to the mouse-specific CTCF-binding repeat sequence in the

Meg1-DMR in a methylation-sensitive manner (6). There have not been any CTCF binding sites reported in the corresponding human sequence (h-MSR) (43). We then proposed that the insulator function of the CTCF is essential for the regulation of the maternally expressed *Meg1/Grb10* Type I transcript in mice as in the case of the *Igf2/H19* region (6,10,11). In this insulator model, the paternal expression of the *Meg1/Grb10* Type II transcript is explained by the absence of DNA methylation of its promoter region within the *Meg1*-DMR, and the maternal expression of *Meg1/Grb10* Type I transcript is explained by the enhancer blocking activity of the CTCF bound to the MSR sequence within the *Meg1*-DMR (6). The maternal expression of the *Cobl* located upstream of the *Meg1*-DMR fits this model, but paternal expression of the *Ddc* that locates downstream of the *Meg1*-DMR does not. Because there are no DMRs around *Ddc*-exon1 and -exon1a (12), its maternal repression cannot thus be explained. Therefore, we investigated the mechanism of the imprinting regulation by *Meg1*-DMR using several reporter vector constructs transfected into cultured cells, and demonstrated that the MSR sequence within *Meg1*-DMR, but not its corresponding human h-MSR sequence, functioned as a silencer, although an insulator function could not be excluded. The *Meg1*-DMR seems to function as a boundary between the maternally expressed upstream and paternally expressed downstream regions (Fig. 5). As the DNA methylation-sensitive silencer is not sufficient to explain the mechanism of this imprinted region as well as the insulator model, as discussed above, the involvement of other factors is necessary. As a genome-wide interaction between cohesin and CTCF was recently demonstrated (44–47), we may account for the three-dimensional structure change induced by the cohesin-CTCF complex in the regulation of this imprinted region. Therefore, further experiments will be required to elucidate the precise regulation mechanism of the *Meg1/Grb10* imprinted region.

The reason for the biased expression of *Ddc*-exon1 in yolk sac and neonatal liver, *Ddc*-exon1a in embryo and *Cobl* in yolk sac remains unknown. It is highly possible that transcripts from some promoters have parent-of-origin-specific expressions, but other transcripts from other promoters have non-imprinted expression. Then, we may simply recognize them as biased when detecting both at the same time. However, so far, we have not detected any novel promoters of *Cobl* and *Ddc* (data not shown). Alternatively, the co-existence of several different cell types in the tissues examined also may contribute to the biased expression patterns to some extent. As described above, all of the biased expressions of these transcripts were observed to be highly tissue-specific,

Table 2. Comparison of growth among MatDi(11), MatDp(prox11) and +/ΔDMR mice

Reference	Body weight (±/±=1)		+/ΔDMR	Placenta weight (±/±=1)	
	MatDi(11) (25,26)	MatDp(prox11) (27)		MatDi(11) (26)	+/ΔDMR
Embryonic stage(dpc)					
12.5	0.778	N.D.	0.786	0.870	1.034
13.5	0.695	N.D.	0.726	0.709	0.887
15.5	0.699	N.D.	0.715	0.781	0.857
After birth					
Neonate	0.608 (2D)	0.603 (at birth)	0.642 (5D)	N.D.	N.D.
3 weeks	0.591	0.525	0.566	N.D.	N.D.

D, days after birth. N.D., no data.

such as yolk sac, embryos and neonatal heart, suggesting that the cell-type-specific monoallelic expression, such as the brain-specific paternal expression of *Meg1/Grb10* Type II, may occur in a minority of cells in these tissues using cell-type-specific transcription factors.

The +/ΔDMR mice exhibit biallelic expression of the *Meg1/Grb10* Type I transcripts, resulting in severe embryonic and placental growth retardation. It is assumed that the +/ΔDMR mice have the same expression pattern of imprinted genes in the *Meg1/Grb10* imprinted region as those of the MatDi(11) and MatDp(prox11) mice, because they have one maternal and maternalized *Meg1/Grb10* imprinted region. An essentially identical phenotype was observed between these mice, indicating that the most probable cause of the growth inhibition is the double dosage of *Meg1/Grb10* Type I (Table 2).

As shown in this study, the +/ΔDMR mice have an additional loss of the paternal expression of *Meg1/Grb10* Type II in brain and also *Ddc*-exon1a in neonatal heart. Therefore, logically, it is not possible to conclude that the double dosage of *Meg1/Grb10* Type I expression is the direct cause of such growth inhibitory effect in this and the MatDi(11) and MatDp(prox11) experiments. It is possible that a loss of the paternal expression of *Meg1/Grb10* Type II in the brain and/or *Ddc*-exon1a in the heart also contributes to or is a major cause of the phenotype. One piece of supportive evidence of *Meg1/Grb10* Type I being a major contributor comes from the experimental finding that fetal and postnatal growth was very sensitive to the expression level of the *Meg1/Grb10* Type I, which was obtained by a comparison with two mice lines, one with and one without the neomycin construct (Table 1). Our analysis of the +/ΔDMRneo mice with Neo revealed that an artificial transcript, possibly from the Neo promoter, was expressed in the anti-sense direction to *Meg1/Grb10* by accident, suggesting that the *Meg1/Grb10* Type I expression was reduced by the influence of this anti-sense RNA to some degree. Therefore, final expression level of *Meg1/Grb10* Type I only reached 1.6–1.7-fold compared to the expected value of 2-fold observed in the +/ΔDMR mice (without Neo). The +/ΔDMRneo mice also lack the paternal expression of *Meg1/Grb10* Type II in the brain and *Ddc*-exon1a in heart (data not shown), and exhibit the same level of *Cobl* and *Ddc* in whole embryo. Therefore, we can conclude that the growth inhibitory effect observed in these mice is dependent on the expression level of *Meg1/Grb10*

Type I and that a slight change (1.6–1.7- to 2.0-fold increment) of its expression level has a great impact on embryonic and postnatal growth (0.74 to 0.57-fold weight reduction of neonates).

Another piece of supportive evidence comes from the previous work on *Meg1/Grb10* knockout mice (*Meg1/Grb10* KO) (38). This report showed that maternal transmission of loss of the *Meg1/Grb10* Type I in the entire body resulted in fetal growth promotion with disproportionate liver overgrowth, demonstrating that the loss of maternally expressed *Meg1/Grb10* Type I in the entire body was responsible for the growth promotion effects observed in the PatDi(11) and PatDp(prox11) mice. However, there were not any notable growth effects observed upon its paternal transmission in the pre- and postnatal stages, so it is clear that the loss of paternal expression of *Meg1/Grb10* Type II in the brain itself does not have any growth effect. Together with their results, it is concluded that *Meg1/Grb10* Type I plays an essential role in growth regulation via its strong growth inhibitory effect *in vivo*. However, placental growth retardation in the +/ΔDMR seems milder than that in MatDi(11) (Table 2), suggesting that there is/are other imprinted gene(s) involved to placental growth in proximal Chromosome 11 other than the *Meg1/Grb10* imprinted region.

In humans, SRS is characterized by pre- and postnatal growth failure (48). In approximately 30–65% patients, hypomethylation of *H19* DMR associated with a reduced expression of *IGF2* has been observed (48–54). Maternal disomy of Chromosome 7 has also been demonstrated in ~10% of the cases (48). This suggests that at least one imprinted gene on Chromosome 7 is involved in the pathogenesis of SRS, such as the paternally expressed *PEG1/MEST* and *PEG10* that have growth promotional effects and/or putative maternally expressed genes that have inhibitory function (55,56). *Peg1/Mest* knockout mice display significant pre- and postnatal growth retardation, although no *PEG1/MEST* mutations have been identified as yet (57–59). It has recently been reported that a patient with paternal deletion of *PEG10* and the neighboring imprinted gene *SGCE* showed pre- and postnatal growth retardation due to severe placental defects like the *Peg10* knockout mice, although the mice died at an early stage of development (60,61).

GRB10 has been one of the strong candidate genes implicated in the growth retardation of SRS because its mouse ortholog *Meg1/Grb10* is maternally expressed (1). However,

it is widely accepted that human *GRB10* Type I is biallelically expressed in the majority of tissues and organs, while only paternal expression of *GRB10* Type II in brain has been confirmed (2–4). Therefore, it is not likely that *GRB10* is the gene responsible in the SRS case of maternal disomy of Chromosome 7, although we cannot rule out the possibility that *GRB10* does exhibit imprinted maternal expression in some growth affecting tissue(s). Recently, cases of SRS having duplicated 7p11–p13 including the *GRB10* gene (partial trisomy of 7p11–p13) were reported (62–64). In these cases, it is highly probable that a 50% increase in the expression of *GRB10* located on 7p11–p13 causes SRS, because we have demonstrated that subtle changes of the expression of the growth inhibitory factor *Meg1/Grb10* has significant influence on pre- and postnatal growth (Table 1). It was also reported recently that the patients with a duplication of 7p11.2–p12 not including *GRB10* showed no association with futures of SRS, including the growth retardation effect (65). Therefore, it is strongly suggested that an increased level of *GRB10* is at least one of the major causes of the growth retardation seen in SRS patients with a duplication of 7p11–p13.

MATERIALS AND METHODS

Generation of *Meg1*ΔDMR mice

To generate the *Meg1*ΔDMR targeting vector, a DNA fragment including the *Meg1*-DMR region was screened from the 129SvJ lambda genomic library (Stratagene). A 9.7 kb fragment (*SacII*-*EheI*) and a 1.0 kb fragment (*HindIII*-*EcoRI*) were ligated with loxP–neomycin resistance gene–loxP fragment. The targeting vector was linearized and electroporated into ES cells (CCE) of 129/Sv/Ev mouse origin. The cells were incubated under G418 selection for 1 week and 1382 colonies were obtained. Of them, 120 colonies were selected, and the genomic DNA were prepared and digested with *NdeI* and *SpeI* for Southern blot analysis to identify the correctly targeted cells. A 5' probe (probe 1) and 3' probe (probe 2) were used to detect a 16.7 and 4.7 kb *Meg1*ΔDMR-neo and a 16.7 and 3.5 kb *Meg1*ΔDMR fragment, respectively. The *Meg1*ΔDMRneo targeted ES cells that resulted from homologous recombination were used to generate chimeric mice by blastocyst injection. Male chimeras were bred to C57BL/6J females and their agouti progeny were genotyped by PCR amplification of tail DNA samples using the *Meg1*ΔDMRneo allele and endogenous *Meg1/Grb10* forward primers along with a common reverse primer. To generate the *Meg1*ΔDMR allele, the neomycin-resistance gene was eliminated by injection of Cre recombinase expression vector into fertilized eggs derived from hetero *Meg1*ΔDMR-neo sire and C57BL/6J dam. Tail DNA samples were used for Southern blot (described above) and PCR analysis using the *Meg1*ΔDMR allele and endogenous *Meg1/Grb10* forward primers along with a common reverse primer to identify the mice with *Meg1*ΔDMR allele. The primers used are listed below. *Meg1*ΔDMRneo allele forward primer: 5'-GGACGTAACTCCTCTTCAGACC-3', *Meg1*ΔDMR allele forward primer: 5'-GAACCTCTTCGAGGGACCTAAT-3', endogenous *Meg1/Grb10* forward primer: 5'-CTAAGGTT

GGCCTGGTCATC-3' and common reverse primer: 5'-GCTCTGTCCAGGCCTCTTATC-3'.

Polymerase chain reaction

For PCR reactions, 20 ng of genomic DNA or 5 ng of cDNA in a 50 μl reaction mixture containing 1 × ExTaq buffer (TaKaRa), 2.5 mM dNTP mixture, 0.8 μM primers and 1.25 U of ExTaq (TaKaRa) were subjected to 30–35 PCR cycles. PCR was carried out under the following conditions: 96°C for 15 s, 55–65°C for 30 s and 72°C for 30–90 s. The PCR primer sequences used in each PCR are listed in each section.

Bisulfite methylation assay

Genomic DNA from the BJ 13.5 dpc embryo, placenta and yolk sac were used and modified with sodium bisulfite as described previously. The treated DNA was amplified by PCR using the primer pairs listed below. *Cobl*: 5'-AAATATATATAAGGGTTTTATAGTAGTAT-3' and 5'-TAAATTCTAAAA-CAAAAAC-3', *Figl1*: 5'-GGATAGAAGAAAA TAAATTAAGTATA-3' and 5'-AACTAAATCTCCCTCA TAAAAAC-3', *Ikzf1*: 5'-GAGGGTGTGTTTTTTTGATT-3' and 5'-TTATTAATAATACCCTACTAAATTAAC-3'. The PCR products were subcloned into pGEM T-Easy vector (Promega) and sequenced. CpG methylation status was analyzed by the QUMA program (http://quma.cdb.riken.jp/top/quma_main_j.html) (66). In *Cobl* and *Ikzf1* analysis, the first 19 and 25 CpGs were used, respectively.

Colony assay

The reporter plasmids pHNE and pHNE (top and second column of Fig. 2B, respectively) were obtained from Dr K. Ishihara (Kumamoto University, Japan) (42). The pHNE vector consists of a neomycin-resistance (Neo) gene driven by the *H19* promoter, a 2.5 kb *NsiI*-*BglII* fragment containing the enhancers and 1.8 kb *AatII*-*HindIII* fragment containing the *H19* DMR insulator. This insulator prevents influence from the adjacent regions. The pHNE vector is composed of pHNE containing an additional *H19* DMR insulator between Neo and the enhancers. To make test vectors, the MSR sequence within *Meg1*-DMR fragments was generated by PCR and inserted into the *XhoI* site of pHNE between the Neo gene and the enhancers. For the PCR reaction, 20 ng of genomic DNA in a 50 μl reaction mixture containing 1 × buffer for KOD Dash (TOYOBO), 2.0 mM dNTP mixture, 0.8 μM primers and 1.0 U of KOD Dash (TOYOBO) were subjected to 35 PCR cycles. PCR was carried out under the following conditions: 96°C for 30 s, 68°C for 2 s and 74°C for 30 s. The primer pairs were designed with *XhoI* site on the 5'-end of each primer. The PCR product was digested with *XhoI* (TaKaRa) and ligated with the pHNE vector. The following primer sequences were used: 5'-GATGGCATTG GGGAGGCTGTGTTGC-3' and 5'-GCTCTGGAGCCTAGAGGAGCGCGG-3'. The direction of the fragments inserted into pHNE was confirmed by sequencing. The reporter constructs were linearized with *MluI* (TOYOBO), and 0.17 pmol of each construct was transfected into L cell by electroporation

using Nucleofector 1 (amaxes biosystems) with a pGL3-control vector (Promega) encoding the firefly luciferase gene. After 48 h, cells were replated and selected by G418 (400 µg/ml). Colonies were counted after 2 weeks of selection. The number of G418-resistant colonies was corrected for transfection efficiency based on the luciferase activity and normalized to that obtained with pHNE.

Luciferase assays

Test reporter constructs were co-transfected into L cells with a pMLuc2 renilla luciferase vector (Novagen) as an internal control using Lipofectamine 2000 reagent (Invitrogen) according to the manufacturer's instructions. After 24 h, cells were analyzed for luciferase activity using the Dual-Glo Luciferase Assay System (Promega) according to the manufacturer's instructions. The assays were performed in triplicate and more than three times. Luciferase activity of each sample was measured by a GENE LIGHT 55A (Microtec) and normalized to a control (renilla luciferase activity).

Silencer assays

pGL3Mp vector was generated by inserting the *Meg1/Grb10* Type I promoter region into the *BglII-HindIII* site of the pGL3-Basic vector (Promega). The *Meg1/Grb10* promoter region was PCR-amplified using the forward primer 5'-ACAATGCACACAGCACAGC-3' with *BglII* site on the 5'-end and the reverse primer 5'-ACTCCTACCTGACGTGCAGC-3' with *HindIII* site on the 5'-end. The PCR product was digested with *BglII* and *HindIII* (TaKaRa) and ligated with pGL3-Basic vector. A KOD Dash (TOYOBO) was used for the PCR. Twenty nanogram of genomic DNA in a 50 µl reaction mixture containing 1× buffer for KOD Dash (TOYOBO), 2.0 mM dNTP mixture, 0.8 µM primers, 2.5% DMSO and 1.0 U of KOD Dash (TOYOBO) were subjected to 35 PCR cycles. PCR was carried out under the following conditions: 96°C for 30 s, 64°C for 2 s and 74°C for 30 s. To generate reporter constructs, test DNA fragments (MSR, h-MSR, *H19* DMR, control for *Meg1*-DMR, control for h-MSR and control for *H19* DMR) were generated by PCR using primers designed with *BglII* and *Sall* sites at their 5'-end. For MSR, the PCR conditions and primer sequence were described above. For others, PCR was performed using ExTaq (TaKaRa), and the PCR primers were listed below. h-MSR: 5'-CGGAGGCTGAGTATTGCAG-3' and 5'-GGCGCAGAAAACCGAC-3', *H19* DMR: 5'-CTTGGACGTCTGCTGAATCAG-3' and 5'-CGTCTGCCGAGCAATATGTAGTA-3', control for MSR: 5'-ACACTCTAGCCCAGGAGCAA-3' and 5'-GAGGGCAATACACACTGCCT-3', control for h-MSR: 5'-TTTGGTGGGCTAACGATGAT-3' and 5'-ATGGACTCTCCAGCATGGAG-3', control for *H19* DMR: 5'-GAAGGCTTAGTCCCTGGGAG-3' and 5'-CTCCTTTAAATTCGTGACGACA-3'. The PCR products were digested with *BglII* and *Sall* (TaKaRa) and ligated with the pGL3Mp vector. The reporter constructs were transfected into L cells, and the luciferase activity of each construct was measured as described above.

Methylated cassette approach

pGL3Mp vectors with insertion of MSR-F/R and control for MSR were digested with *HpaI* and *Sall* (TaKaRa), and the pGL3Mp vector fragment and the insert fragments of each construct (MSR-F/R, h-MSR or control for MSR) were purified by gel extraction using the RECO CHIP (TaKaRa). The insert fragments were methylated with *SssI* methyltransferase (New England Biolabs), and the methylation status of the insert fragments was analyzed by digestion with *HpaI* for MSR and h-MSR, and with *HpyCH4IV* for control. The mock-methylated fragments were treated in the same way without the addition of *SssI*. The methylated and mock-methylated insert fragments were ligated within the pGL3Mp vector. Each ligation mix was phenol/chloroform extracted and used directly for transfection. The luciferase activity of each construct was measured as described above.

Allelic expression analysis

The allelic expression of the *Meg1/Grb10*, *Meg1/Grb10* Type I, *Meg1/Grb10* Type II, *Cobl*, *Ddc*, *Ikzf1* and *Figl1* genes between JF1 and C57BL/6J (or ΔDMR (=129/Sv/Ev)) was detected by PCR-RFLP and direct sequencing analysis. PCR were performed under the conditions described above. The following primers were used for DNA amplifications. *Meg1/Grb10*: 5'-CTTGATACCACCCAGAAAGTCTG-3' and 5'-AACCCAAAGCATTGGCAG-3', *Meg1/Grb10* Type I: 5'-CACGAAAGTTCCGCGCA-3' and 5'-AGTATCAGTATCAGACTGCATGTTG-3', *Meg1/Grb10* Type II: 5'-GCGATCATTCGTCTCTGAGC-3' and 5'-AGTATCAGTATCAGAC TGCATGTTG-3', *Cobl*: 5'-AAGTGAATGAGGACGGCG-3' and 5'-GGTGAGAAGGATTCAGGTGG-3', *Ddc*-exon1: 5'-TTCGCAGAGCTGGACAATC-3' and 5'-TGCAAGCATAGCTGGGTATG-3', *Ddc*-exon1a: 5'-CGAATAGAGAGGAGCGCAT-3' and 5'-TGCAAGCATAGCTGGGTATG-3', *Ikzf1*: 5'-CTTTCGGGATCCCTTTGAGT-3' and 5'-CCTTCAGCATATGCACAAC-3', *Figl1*: 5'-TTGTGTTCTCTTCTGGCTGTG-3' and 5'-CAGCTTCATCAATCTCTTGGG-3'. For RFLP analysis of *Meg1/Grb10*, *Cobl*, *Ddc* and *Ikzf1*, the PCR products were digested with *MspI* (TaKaRa), *BanI* (New England Biolabs), *MspI* and *MspI*, and subjected to agarose gel electrophoresis. For direct sequencing analysis of *Figl1*, the PCR products were sequenced directly.

Real-time quantitative PCR

The assays were performed in triplicate and the copy number of genes examined were calculated with a LightCycler 480 (Roche Diagnostics) by using Power SYBR Green PCR Master Mix (Applied Biosystems) for the analysis of total expression and TaqMan Gene Expression Master Mix with TaqMan MGB probes (Applied Biosystems) for the analysis of allele-specific expression. PCR was carried out under the following conditions: 96°C for 15 s, 65°C for 30 s and 72°C for 30 s for the total expression analysis, and 96°C for 15 s, 60°C for 30 s for the allele-specific analysis. For the total expression analysis, the data for each gene were normalized to an internal standard (β -actin), and for the B6 or *Meg1*ΔDMR allele-specific analysis, the expression levels

were normalized to the JF1 allele expression level. The sequences of the primers for the TaqMan probes used are listed below. For total expression analysis: for *Meg1/Grb10*, 5'-GTTTCTGAGAATTCTCTGTGGC-3' and 5'-CTGTGAGACTCCTCGCGG-3'; for *Cobl*, 5'-TCTGTGAAAGTGCCAGCATC-3' and 5'-TGTGGACAGCAGCAGGATAG-3'; for *Ddc*, 5'-TAGAATGTACGGAGTCAAGGGG-3' and 5'-AGCAGCTCTGCTTTTCAATCTTT-3'; for β -actin, 5'-AAGTGTGACGTTGACATCCG-3' and 5'-GATCCACATCTGCTGAAGG-3'. For allele-specific analysis: for *Cobl*, 5'-AAGCTATGACATGCATCAGGTT-3' and 5'-TGTTGAAATCTCAGGCTCCAT-3' with TaqMan probe 5'-CTGTGAAGGAGCCTT-3' (B6 or *Meg1* Δ DMR) or 5'-CTGTGAAAGGAGCCTT-3' (JF1); for *Ddc*-exon1, 5'-CAATGCCATCCAGATAGTCACTA-3' and 5'-AGTGGACCTGTGAAGAATCCAAA-3' with TaqMan probe 5'-TCTCCTCCGGAATT-3' (B6 or *Meg1* Δ DMR) or 5'-CTCTCCTTCGGAATT-3' (JF1); for *Ddc*-exon1a, 5'-CAATGCCATCCAGATAGTCACTA-3' and 5'-CCAGCTGCCTTTTCAACATG-3' with the same TaqMan probes as *Ddc*-exon1.

Statistical analysis

Results are presented as the means \pm standard deviation. Statistical analyses were performed using Mann-Whitney *U*-test.

SUPPLEMENTARY MATERIAL

Supplementary Material is available at *HMG* online.

ACKNOWLEDGEMENTS

We thank S. Aizawa of Center for Developmental Biology, RIKEN for providing the DT-A vector that was used for making *Meg1* Δ DMR construct, E. Robertson of University of Oxford for the CCE ES cells, Y. Nakahara and M. Takabe of the Mitsubishi Kagaku Institute of Life Sciences for animal breeding and H. Hasegawa, N. Kawabe of the Tokai University for histological analysis. The JF1/Msf mouse strain (RBRC00639) was provided by RIKEN BRC, which is participating in the National Bio-Resource Project of the MEXT, Japan. Pacific Edit reviewed the manuscript prior to submission.

Conflict of Interest statement. None declared.

FUNDING

This work was supported by grants from Creative Science Research, the research program of Japan Society for the Promotion of Science (JSPS), the Japanese Ministry of Education, Global Center of Excellence (GCOE) Program, "International Research Center for Molecular Science in Tooth and Bone Diseases", the Mitsubishi Foundation and the Ministry of Health, Labor and Welfare for Child Health and Development (17C-2) and a Grant-in-Aid for Scientific Research on Priority Areas from the Ministry of Education, Culture, Sports, Science and Technology of Japan (1508023) to F.I., and the Asahi Glass Foundation and JSPS, Grants-in Aid for Scientific Research to T.K.-L.

REFERENCES

- Miyoshi, N., Kuroiwa, Y., Kohda, T., Shitara, H., Yonekawa, H., Kawabe, T., Hasegawa, H., Barton, S.C., Surani, M.A., Kaneko-Ishino, T. *et al.* (1998) Identification of the *Meg1/Grb10* imprinted gene on mouse proximal chromosome 11, a candidate for the Silver-Russell syndrome gene. *Proc. Natl Acad. Sci. USA*, **95**, 1102–1107.
- Blagitko, N., Mergenthaler, S., Schulz, U., Wollmann, H.A., Craigen, W., Eggermann, T., Ropers, H.H. and Kalscheuer, V.M. (2000) Human *GRB10* is imprinted and expressed from the paternal and maternal allele in a highly tissue- and isoform-specific fashion. *Hum. Mol. Genet.*, **9**, 1587–1595.
- Hitchins, M.P., Monk, D., Bell, G.M., Ali, Z., Preece, M.A., Stanier, P. and Moore, G.E. (2001) Maternal repression of the human *GRB10* gene in the developing central nervous system; evaluation of the role for *GRB10* in Silver-Russell syndrome. *Eur. J. Hum. Genet.*, **9**, 82–90.
- McCann, J.A., Zheng, H., Islam, A., Goodyer, C.G. and Polychronakos, C. (2001) Evidence against *GRB10* as the gene responsible for Silver-Russell syndrome. *Biochem. Biophys. Res. Commun.*, **286**, 943–948.
- Hitchins, M.P., Bentley, L., Monk, D., Beechey, C., Peters, J., Kelsey, G., Ishino, F., Preece, M.A., Stanier, P. and Moore, G.E. (2002) DDC and COBL, flanking the imprinted *GRB10* gene on 7p12, are biallelically expressed. *Mamm. Genome*, **13**, 686–691.
- Hikichi, T., Kohda, T., Kaneko-Ishino, T. and Ishino, F. (2003) Imprinting regulation of the murine *Meg1/Grb10* and human *GRB10* genes; roles of brain-specific promoters and mouse-specific CTCF-binding sites. *Nucleic Acids Res.*, **31**, 1398–1406.
- Arnaud, P., Monk, D., Hitchins, M., Gordon, E., Dean, W., Beechey, C.V., Peters, J., Craigen, W., Preece, M., Stanier, P. *et al.* (2003) Conserved methylation imprints in the human and mouse *GRB10* genes with divergent allelic expression suggests differential reading of the same mark. *Hum. Mol. Genet.*, **12**, 1005–1019.
- Yamasaki-Ishizaki, Y., Kayashima, T., Mapendano, C.K., Soejima, H., Ohta, T., Masuzaki, H., Kinoshita, A., Urano, T., Yoshiura, K., Matsumoto, N. *et al.* (2007) Role of DNA methylation and histone h3 lysine 27 methylation in tissue-specific imprinting of mouse *grb10*. *Mol. Cell. Biol.*, **27**, 732–742.
- Sanz, L.A., Chamberlain, S., Sabourin, J.C., Henckel, A., Magnuson, T., Hugnot, J.P., Feil, R. and Arnaud, P. (2008) A mono-allelic bivalent chromatin domain controls tissue-specific imprinting at *Grb10*. *EMBO J.*, **27**, 2523–2532.
- Bell, A.C. and Felsenfeld, G. (2000) Methylation of a CTCF-dependent boundary controls imprinted expression of the *Igf2* gene. *Nature*, **405**, 482–485.
- Hark, A.T., Schoenherr, C.J., Katz, D.J., Ingram, R.S., Levorse, J.M. and Tilghman, S.M. (2000) CTCF mediates methylation-sensitive enhancer-blocking activity at the *H19/Igf2* locus. *Nature*, **405**, 486–489.
- Menheniott, T.R., Woodfine, K., Schulz, R., Wood, A.J., Monk, D., Giraud, A.S., Baldwin, H.S., Moore, G.E. and Oakey, R.J. (2008) Genomic imprinting of dopa decarboxylase in heart and reciprocal allelic expression with neighboring *Grb10*. *Mol. Cell. Biol.*, **28**, 386–396.
- Liu, F. and Roth, R.A. (1995) Grb-IR: a SH2-domain-containing protein that binds to the insulin receptor and inhibits its function. *Proc. Natl Acad. Sci. USA*, **92**, 10287–10291.
- Dey, B.R., Frick, K., Lopaczynski, W., Nissley, S.P. and Furlanetto, R.W. (1996) Evidence for the direct interaction of the insulin-like growth factor I receptor with IRS-1, Shc, and Grb10. *Mol. Endocrinol.*, **10**, 631–641.
- Hansen, H., Svensson, U., Zhu, J., Laviola, L., Giorgino, F., Wolf, G., Smith, R.J. and Riedel, H. (1996) Interaction between the *Grb10* SH2 domain and the insulin receptor carboxyl terminus. *J. Biol. Chem.*, **271**, 8882–8886.
- Morrione, A., Valentinis, B., Li, S., Ooi, J.Y., Margolis, B. and Baserga, R. (1996) Grb10: A new substrate of the insulin-like growth factor I receptor. *Cancer Res.*, **56**, 3165–3167.
- O'Neill, T.J., Rose, D.W., Pillay, T.S., Hotta, K., Olefsky, J.M. and Gustafson, T.A. (1996) Interaction of a GRB-IR splice variant (a human *GRB10* homolog) with the insulin and insulin-like growth factor I receptors. Evidence for a role in mitogenic signaling. *J. Biol. Chem.*, **271**, 22506–22513.
- Dong, L.Q., Du, H., Porter, S.G., Kolakowski, L.F., Lee, A.V., Mandarino, L.J., Fan, J., Yee D. and Liu F. (1997) Cloning, chromosome localization, expression, and characterization of an Src homology 2 and pleckstrin

- homology domain-containing insulin receptor binding protein hGrb10gamma. *J. Biol. Chem.*, **272**, 29104–29112.
19. Dong, L.Q., Farris, S., Christal, J. and Liu, F. (1997) Site-directed mutagenesis and yeast two-hybrid studies of the insulin and insulin-like growth factor-1 receptors: the Src homology-2 domain-containing protein hGrb10 binds to the autophosphorylated tyrosine residues in the kinase domain of the insulin receptor. *Mol. Endocrinol.*, **11**, 1757–1765.
 20. Frantz, J.D., Giorgetti-Peraldi, S., Orlinger, E.A. and Shoelson, S.E. (1997) Human GRB-IRbeta/GRB10. Splice variants of an insulin and growth factor receptor-binding protein with PH and SH2 domains. *J. Biol. Chem.*, **272**, 2659–2667.
 21. Laviola, L., Giorgino, F., Chow, J.C., Baquero, J.A., Hansen, H., Ooi, J., Zhu, J., Riedel, H. and Smith, R.J. (1997) The adapter protein Grb10 associates preferentially with the insulin receptor as compared with the IGF-1 receptor in mouse fibroblasts. *J. Clin. Invest.*, **99**, 830–837.
 22. Morriene, A., Valentinis, B., Resnicoff, M., Xu, S. and Baserga, R. (1997) The role of mGrb10alpha in insulin-like growth factor I-mediated growth. *J. Biol. Chem.*, **272**, 26382–26387.
 23. He, W., Rose, D.W., Olefsky, J.M. and Gustafson, T.A. (1998) Grb10 interacts differentially with the insulin receptor, insulin-like growth factor I receptor, and epidermal growth factor receptor via the Grb10 Src homology 2 (SH2) domain and a second novel domain located between the pleckstrin homology and SH2 domains. *J. Biol. Chem.*, **273**, 6860–6867.
 24. Wang, J., Dai, H., Yousaf, N., Moussaif, M., Deng, Y., Boufelliga, A., Swamy, O.R., Leone, M.E. and Riedel, H. (1999) Grb10, a positive, stimulatory signaling adapter in platelet-derived growth factor BB-, insulin-like growth factor I-, and insulin-mediated mitogenesis. *Mol. Cell. Biol.*, **19**, 6217–6228.
 25. Cattanach, B.M. and Kirk, M. (1985) Differential activity of maternally and paternally derived chromosome regions in mice. *Nature*, **315**, 496–498.
 26. Cattanach, B.M., Beechey, C.V., Rasberry, C., Jones, J. and Papworth, D. (1996) Time of initiation and site of action of the mouse chromosome 11 imprinting effects. *Genet. Res.*, **68**, 35–44.
 27. Cattanach, B.M., Shibata, H., Hayashizaki, Y., Townsend, K.M., Ball, S. and Beechey, C.V. (1998) Association of a redefined proximal mouse chromosome 11 imprinting region and U2afp-rs/U2af1-rs1 expression. *Cytogenet. Cell Genet.*, **80**, 41–47.
 28. Stein, E.G., Gustafson, T.A. and Hubbard, S.R. (2001) The BPS domain of Grb10 inhibits the catalytic activity of the insulin and IGF1 receptors. *FEBS Lett.*, **493**, 106–111.
 29. Deng, Y., Bhattacharya, S., Swamy, O.R., Tandon, R., Wang, Y., Janda, R. and Riedel, H. (2003) Growth factor receptor-binding protein 10 (Grb10) as a partner of phosphatidylinositol 3-kinase in metabolic insulin action. *J. Biol. Chem.*, **278**, 39311–39322.
 30. Vecchione, A., Marchese, A., Henry, P., Rotin, D. and Morriene, A. (2003) The Grb10/Nedd4 complex regulates ligand-induced ubiquitination and stability of the insulin-like growth factor I receptor. *Mol. Cell. Biol.*, **23**, 3363–3372.
 31. Wick, K.R., Werner, E.D., Langlais, P., Ramos, F.J., Dong, L.Q., Shoelson, S.E. and Liu, F. (2003) Grb10 inhibits insulin-stimulated insulin receptor substrate (IRS)-phosphatidylinositol 3-kinase/Akt signaling pathway by disrupting the association of IRS-1/IRS-2 with the insulin receptor. *J. Biol. Chem.*, **278**, 8460–8467.
 32. Langlais, P., Dong, L.Q., Ramos, F.J., Hu, D., Li, Y., Quon, M.J. and Liu, F. (2004) Negative regulation of insulin-stimulated mitogen-activated protein kinase signaling by Grb10. *Mol. Endocrinol.*, **18**, 350–358.
 33. Dufresne, A.M. and Smith, R.J. (2005) The Adapter Protein GRB10 Is an Endogenous Negative Regulator of Insulin-Like Growth Factor Signaling. *Endocrinology*, **146**, 4399–4409.
 34. Mori, K., Giovannone, B. and Smith, R.J. (2005) Distinct Grb10 domain requirements for effects on glucose uptake and insulin signaling. *Mol. Cell. Endocrinol.*, **230**, 39–50.
 35. Ramos, F.J., Langlais, P.R., Hu, D., Dong, L.Q. and Liu, F. (2006) Grb10 mediates insulin-stimulated degradation of the insulin receptor: a mechanism of negative regulation. *Am. J. Physiol. Endocrinol. Metab.*, **290**, E1262–E1266.
 36. Deng, Y., Zhang, M. and Riedel, H. (2008) Mitogenic roles of Gab1 and Grb10 as direct cellular partners in the regulation of MAP kinase signaling. *J. Cell. Biochem.*, **105**, 1172–1182.
 37. Monami, G., Emiliozzi, V. and Morriene, A. (2008) Grb10/Nedd4-mediated multiubiquitination of the insulin-like growth factor receptor regulates receptor internalization. *J. Cell. Physiol.*, **216**, 426–437.
 38. Charalambous, M., Smith, F.M., Bennett, W.R., Crew, T.E., Mackenzie, F. and Ward, A. (2003) Disruption of the imprinted Grb10 gene leads to disproportionate overgrowth by an Igf2-independent mechanism. *Proc. Natl Acad. Sci. USA*, **100**, 8292–8297.
 39. Shiura, H., Miyoshi, N., Konishi, A., Wakasaka-Saito, N., Suzuki, R., Muguruma, K., Kohda, T., Wakana, S., Yokoyama, M., Ishino, F. *et al.* (2005) Meg1/Grb10 overexpression causes postnatal growth retardation and insulin resistance via negative modulation of the IGF1R and IR cascades. *Biochem. Biophys. Res. Commun.*, **329**, 909–916.
 40. Yamamoto, Y., Ishino, F., Kaneko-Ishino, T., Shiura, H., Uchio-Yamada, K., Matsuda, J., Suzuki, O. and Sato, K. (2008) Type 2 diabetes mellitus in a non-obese mouse model induced by Meg1/Grb10 overexpression. *Exp. Anim.*, **57**, 385–395.
 41. Koide, T., Moriawaki, K., Uchida, K., Mita, A., Sagai, T., Yonekawa, H., Katoh, H., Miyashita, N., Tsuchiya, K., Nielsen, T.J. *et al.* (1998) A new inbred strain JF1 established from Japanese fancy mouse carrying the classic piebald allele. *Mamm. Genome*, **9**, 15–19.
 42. Ishihara, K. and Sasaki, H. (2002) An evolutionarily conserved putative insulator element near the 3' boundary of the imprinted Igf2/H19 domain. *Hum. Mol. Genet.*, **11**, 1627–1636.
 43. Barski, A., Cuddapah, S., Cui, K., Roh, T.Y., Schones, D.E., Wang, Z., Wei, G., Chepelev, I. and Zhao, K. (2007) High-resolution profiling of histone methylations in the human genome. *Cell*, **129**, 823–837.
 44. Partho, V., Hadjir, S., Spivakov, M., Leleu, M., Sauer, S., Gregson, H.C., Jarmuz, A., Canzonetta, C., Webster, Z., Nesterova, T. *et al.* (2008) Cohesins functionally associate with CTCF on mammalian chromosome arms. *Cell*, **132**, 422–433.
 45. Rubio, E.D., Reiss, D.J., Welesch, P.L., Distche, C.M., Filipova, G.N., Baliga, N.S., Aebersold, R., Ranish, J.A. and Krumm, A. (2008) CTCF physically links cohesin to chromatin. *Proc. Natl Acad. Sci. USA*, **105**, 8309–8314.
 46. Stedman, W., Kang, H., Lin, S., Kissil, J.L., Bartolomei, M.S. and Lieberman, P.M. (2008) Cohesins localize with CTCF at the KSHV latency control region and at cellular c-myc and H19/Igf2 insulators. *EMBO J.*, **27**, 654–666.
 47. Wendt, K.S., Yoshida, K., Itoh, T., Bando, M., Koch, B., Schirghuber, E., Tsutsumi, S., Nagae, G., Ishihara, K., Mishiro, T. *et al.* (2008) Cohesin mediates transcriptional insulation by CCCTC-binding factor. *Nature*, **451**, 796–801.
 48. Abu-Amero, S., Monk, D., Frost, J., Preece, M., Stanier, P. and Moore, G.E. (2008) The genetic aetiology of Silver-Russell syndrome. *J. Med. Genet.*, **45**, 193–199.
 49. Gicquel, C., Rossignol, S., Cabrol, S., Houang, M., Steunou, V., Barbu, V., Danton, F., Thibaud, N., Le Merrer, M., Burglen, L. *et al.* (2005) Epimutation of the telomeric imprinting center region on chromosome 11p15 in Silver-Russell syndrome. *Nat. Genet.*, **37**, 1003–1007.
 50. Blek, J., Terhal, P., van den Bogaard, M.J., Maas, S., Hamel, B., Salieb-Beugelaar, G., Simon, M., Letreboer, T., van der Smagt, J., Kroes, H. *et al.* (2006) Hypomethylation of the H19 gene causes not only Silver-Russell syndrome (SRS) but also isolated asymmetry or an SRS-like phenotype. *Am. J. Hum. Genet.*, **78**, 604–614.
 51. Eggermann, T., Schonherr, N., Meyer, E., Obermann, C., Mavany, M., Eggermann, K., Ranke, M.B. and Wollmann, H.A. (2006) Epigenetic mutations in 11p15 in Silver-Russell syndrome are restricted to the telomeric imprinting domain. *J. Med. Genet.*, **43**, 615–616.
 52. Netchine, I., Rossignol, S., Dufourg, M.N., Azzi, S., Rousseau, A., Perin, L., Houang, M., Steunou, V., Esteve, B., Thibaud, N. *et al.* (2007) 11p15 imprinting center region 1 loss of methylation is a common and specific cause of typical Russell-Silver syndrome: clinical scoring system and epigenetic-phenotypic correlations. *J. Clin. Endocrinol. Metab.*, **92**, 3148–3154.
 53. Binder, G., Seidel, A.K., Martin, D.D., Schweizer, R., Schwarze, C.P., Wollmann, H.A., Eggermann, T. and Ranke, M.B. (2008) The endocrine phenotype in Silver-Russell syndrome is defined by the underlying epigenetic alteration. *J. Clin. Endocrinol. Metab.*, **93**, 1402–1407.
 54. Yamazawa, K., Kagami, M., Nagai, T., Kondoh, T., Onigata, K., Maeyama, K., Hasegawa, T., Hasegawa, Y., Yamazaki, T., Mizuno, S. *et al.* (2008) Molecular and clinical findings and their correlations in Silver-Russell syndrome: implications for a positive role of IGF2 in growth determination and differential imprinting regulation of the IGF2-H19 domain in bodies and placentas. *J. Mol. Med.*, **86**, 1171–1181.

1438 Human Molecular Genetics, 2009, Vol. 18, No. 8

55. Kobayashi, S., Kohda, T., Miyoshi, N., Kuroiwa, Y., Aisaka, K., Tsutsumi, O., Kaneko-Ishino, T. and Ishino, F. (1997) Human PEG1/MEST, an imprinted gene on chromosome 7. *Hum. Mol. Genet.*, **6**, 781–786.
56. Ono, R., Kobayashi, S., Wagatsuma, H., Aisaka, K., Kohda, T., Kaneko-Ishino, T. and Ishino, F. (2001) A retrotransposon-derived gene, PEG10, is a novel imprinted gene located on human chromosome 7q21. *Genomics*, **73**, 232–237.
57. Lefebvre, L., Viville, S., Barton, S.C., Ishino, F., Keverne, E.B. and Surani, M.A. (1998) Abnormal maternal behaviour and growth retardation associated with loss of the imprinted gene Mest. *Nat. Genet.*, **20**, 163–169.
58. Riesewijk, A.M., Blagitko, N., Schinzel, A.A., Hu, L., Schulz, U., Hamel, B.C., Ropers, H.H. and Kalscheuer, V.M. (1998) Evidence against a major role of PEG1/MEST in Silver-Russell syndrome. *Eur. J. Hum. Genet.*, **6**, 114–120.
59. Kobayashi, S., Uemura, H., Kohda, T., Nagai, T., Chinen, Y., Naritomi, K., Kinoshita, E.J., Ohashi, H., Imaizumi, K., Tsukahara, M. *et al.* (2001) No evidence of PEG1/MEST gene mutations in Silver-Russell syndrome patients. *Am. J. Med. Genet.*, **104**, 225–231.
60. Ono, R., Nakamura, K., Inoue, K., Naruse, M., Usami, T., Wakisaka-Saito, N., Hino, T., Suzuki-Migishiina, R., Ogonuki, N., Miki, H. *et al.* (2006) Deletion of Peg10, an imprinted gene acquired from a retrotransposon, causes early embryonic lethality. *Nat. Genet.*, **38**, 101–106.
61. Bonnet, C., Gregoire, M.J., Vibert, M., Raffo, E., Leheup, B. and Jonveaux, P. (2008) Cryptic 7q21 and 9p23 deletions in a patient with apparently balanced de novo reciprocal translocation t(7;9)(q21;p23) associated with a dystonia-plus syndrome: paternal deletion of the epsilon-sarcoglycan (SGCE) gene. *J. Hum. Genet.*, **53**, 876–885.
62. Joyce, C.A., Sharp, A., Walker, J.M., Bullman, H. and Temple, I.K. (1999) Duplication of 7p12.1-p13, including GRB10 and IGFBP1, in a mother and daughter with features of Silver-Russell syndrome. *Hum. Genet.*, **105**, 273–280.
63. Monk, D., Wakeling, E.L., Proud, V., Hitchins, M., Abu-Amro, S.N., Stanier, P., Preece, M.A. and Moore, G.E. (2000) Duplication of 7p11.2-p13, including GRB10, in Silver-Russell syndrome. *Am. J. Hum. Genet.*, **66**, 36–46.
64. Monk, D., Bentley, L., Hitchins, M., Myler, R.A., Clayton-Smith, J., Ismail, S., Price, S.M., Preece, M.A., Stanier, P. and Moore, G.E. (2002) Chromosome 7p disruptions in Silver Russell syndrome: delineating an imprinted candidate gene region. *Hum. Genet.*, **111**, 376–387.
65. Leach, N.T., Chudoba, I., Stewart, T.V., Holmes, L.B. and Weremowicz, S. (2007) Maternally inherited duplication of chromosome 7, dup(7)(p11.2p12), associated with mild cognitive deficit without features of Silver-Russell syndrome. *Am. J. Med. Genet. A*, **143**, 1489–1493.
66. Kumaki, Y., Oda, M. and Okano, M. (2008) QUMA: quantification tool for methylation analysis. *Nucleic Acids Res.*, **36**, W170–W175.
67. Kobayashi, H., Suda, C., Abe, T., Kohara, Y., Ikemura, T. and Sasaki, H. (2006) Bisulfite sequencing and dinucleotide content analysis of 15 imprinted mouse differentially methylated regions (DMRs): paternally methylated DMRs contain less CpGs than maternally methylated DMRs. *Cytogenet. Genome Res.*, **113**, 130–137.

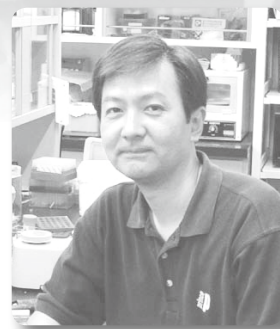
M E M O

[illegible]

分子細胞生物学分野

澁谷 浩司

医歯学総合研究科・器官システム制御学系専攻
細胞機能調節学・教授



1) 研究の課題名

p38-NLK経路による前頭部形成制御

NLK, an essential effector for of anterior formation,
functions downstream of p38 MAP kinase

研究内容

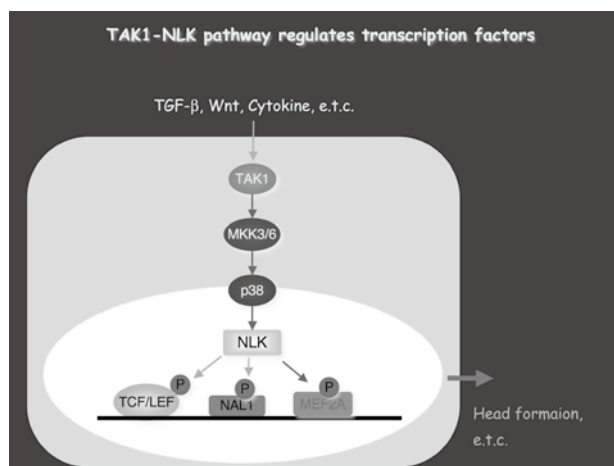
Nemo-like kinase (NLK) は、Drosophila の複眼の細胞極性、翅の形態形成、表皮のパターニングを担うNemoの相同遺伝子として単離されたMAPキナーゼファミリー・スレオニンキナーゼである。前頭部形成におけるNLKの機能を検討するために、NLKと相互作用する分子群を網羅的に検索したところ、MAPキナーゼファミリーの一つであるp38が単離された。NLKがキナーゼとして機能を発揮するためには特定の部位のリン酸化修飾が必要であり、NLKはp38によるリン酸化を介して頭部形成を制御しているのではないかと考え検討した結果、下記のような新たな知見を得ることができた。

- 1) NLKとp38との会合は、培養細胞系を用いた共発現系および内在的にNLKとp38が発現している培養細胞系において免疫沈降実験により確認された。
- 2) 大腸菌から調整したGST-NLK融合タンパクを基質としてin vitro キナーゼアッセイを実施したところ、p38はNLKの特定のセリン残基を直接リン酸化することが明らかとなった。また、分化誘導された神経細胞株Neuro2Aにおいて内在性p38の機能をsiRNAにより消失させるとNLKのリン酸化レベルが低下した。
- 3) ツメガエル初期胚において特異的なMOを用いてp38の機能を消失させると、NLKの機能消失の時と同様に、頭部前方領域の形成不全と各種前方神経マーカーの発現低下が観察された。p38の機能消失による表現型は、野生型NLKの強制発現では回復されたが、p38によるリン酸化部位をアラニンに置換した変異型NLKでは回復されなかった。

今回得られた新たな知見より、ツメガエルにおける頭

部前方領域の形成過程にp38-NLK経路が関与する可能性を示唆するものであり、このときp38はリン酸化修飾を介してNLKの機能を制御しているものと考えられた。

2)



3) 研究内容の英文要約

DNA demethylation in hormone-induced transcriptional derepression.

Epigenetic modifications at the histone level affect gene regulation in response to extracellular signals. However, regulated epigenetic modifications at the DNA level, especially active DNA demethylation, in gene activation are not well understood. Here we report that DNA methylation/demethylation is hormonally switched to control transcription of the cytochrome p450 27B1 (CYP27B1) gene. Reflecting vitamin-D-mediated transrepression of the CYP27B1 gene by the negative vitamin D response element (nVDRE), methylation of CpG sites ((5m) CpG) is induced by vitamin D in this gene promoter. Conversely, treatment with parathyroid hormone, a hormone known to activate the CYP27B1 gene, induces active demethylation of the (5m) CpG sites in this promoter. Biochemical purification of a complex associated

with the nVDRE-binding protein (VDIR, also known as TCF3) identified two DNA methyltransferases, DNMT1 and DNMT3B, for methylation of CpG sites, as well as a DNA glycosylase, MBD4 (ref. 10). Protein-kinase-C-phosphorylated MBD4 by parathyroid hormone stimulation promotes incision of methylated DNA through glycosylase activity, and a base-excision repair process seems to complete DNA demethylation in the MBD4-bound promoter. Such parathyroid-hormone-induced DNA demethylation and subsequent transcriptional derepression are impaired in Mbd4 (-/-) mice. Thus, the present findings suggest that methylation switching at the DNA level contributes to the hormonal control of transcription.

TMEPAI, a transmembrane TGF- β -inducible protein, sequesters Smad proteins from active participation in TGF- β signaling

Transforming growth factor- β (TGF- β) is a multifunctional cytokine of key importance for controlling embryogenesis and tissue homeostasis. How TGF- β signals are attenuated and terminated is not well understood. Here, we show that TMEPAI, a direct target gene of TGF- β signaling, antagonizes TGF- β signaling by interfering with TGF- β type I receptor (T β RI)-induced R-Smad phosphorylation. TMEPAI can directly interact with R-Smads via a Smad interaction motif (SIM). TMEPAI competes with Smad anchor for receptor activation (SARA) for R-Smad binding, thereby sequestering R-Smads from T β RI kinase activation. In mammalian cells, ectopic expression of TMEPAI inhibited TGF- β -dependent regulation of plasminogen activator inhibitor (PAI)-1, JunB, cyclin-dependent kinase (cdk) inhibitors and c-myc expression, whereas specific siRNA-mediated knockdown of TMEPAI expression prolonged duration of TGF- β -induced Smad2 and Smad3 phosphorylation and concomitantly potentiated cellular responsiveness to TGF- β . Consistently, TMEPAI inhibits activin-mediated mesoderm formation in *Xenopus* embryos. Taken together, TMEPAI participates in a negative feedback loop to control the duration and intensity of TGF- β /Smad signaling.

NLK, an essential effector for of anterior formation, functions downstream of p38 MAP kinase

Nemo-like kinase (NLK) is known to function as a mitogen-activated protein kinase (MAPK)-like kinase. However, the upstream molecules and the molecular events mechanisms to that regulate the NLK activity remain unclear. In the present study, we identified p38 MAPK as an upstream kinase and activator for of NLK. p38 regulates the function of NLK via phosphorylation, and this modification can be abrogated by depletion of endogenous p38. In *Xenopus* embryos, depletion of either p38 β or NLK by antisense morpholino oligonucleotides

results in a severe defect in anterior development and impaired expression of endogenous anterior markers. It is notably notable that morphants of *Xenopus* p38 α , another isoform of the p38 MAPK family, exhibited no obvious defects in anterior development. Defects in head formation or expression of the anterior marker genes caused by deprivation of suppression of endogenous p38 β expression could be rescued by expression of wild-type NLK, but not mutant NLK containing a mutated lacking the p38 β phosphorylation site. On the contrary In contrast, the defects in head formation or expression of the anterior marker genes caused by deprivation suppression of endogenous NLK expression could not be rescued by expression of p38. These results provide the first evidence that p38 specifically regulates NLK function required for the anterior formation in *Xenopus* development.

4) 本事業に関連して世界的な研究拠点形成に向けて、以下の点で改善・整備等されたこと

A (研究拠点体制)

国際研究推進部先端拠点研究推進のための”歯と骨のグローバルCOE拠点内における異なる分野のInnovationを確立する研究提案”として口腔病理学分野(山口朗教授、飯村忠浩国際PIシャペロン特任准教授)との共同研究を推進した。

D (人材育成)

国際PIシャペロン教員である後藤利保を分野准教授として採用した。

E (国際化)

分野内でのセミナーを英語で実施している。

5) GCOE事業を推進するに当たって力を入れた点

将来の優秀な研究者に成るべく大学院生の育成

6) 英文原著論文

1. Kim, M., Kondo, T., Takada, I., Youn, M.-Y., Yamamoto, Y., Takahashi, S., Matsumoto, T., Fujiyama, S., Shirode, Y., Yamaoka, I., Kitagawa, H., Takeyama, K., Shibuya, H., Ohtake, F. and Kato, S. (2009). DNA demethylation in hormone-induced transcriptional derepression. *Nature* 461, 1007-1012.
2. Watanabe, Y., Itoh, S., Goto, T., Ohnishi, E., Inamitsu, M., Itoh, F., Satoh, K., Wiercinska, E., Yang, W., Shi, L., Tanaka, A., Nakano, N., Mommaas, A. M., Shibuya, H., ten Dijke, P. and Kato, M. TMEPAI, a transmembrane TGF- β -inducible protein, sequesters Smad proteins from active participation in TGF- β signaling. *Mol. Cell*.
3. Ohnishi, E., Goto, T., Sato, A., Kim, M., Iemura, S., Ishitani,

T., Natsume, T., Ohnishi, J. and Shibuya, H. NLK, an essential effector of anterior formation, functions downstream of p38 MAP kinase. Mol. Cell. Biol. .

7) 平成21年度までの自己評価

やや停滞気味ながら着実に研究が進行し、論文としてまとまりつつある状況である。また、本GCOE国際PIシャペロン教員であった後藤利保を准教授に迎え、研究の質も向上し、今後、数年以内で良い研究成果が得られるものと思われる。

8) 学会発表（和文）

小川 靖、吉田 実代、大西 英理子、平松 俊行、小野木 博、澁谷 浩司、細谷 孝充、萩原正敏 リン酸化阻害剤によるダウン症治療薬開発アプローチ 第82回日本薬理学会年会、2009年3月16-18日、横浜。

後藤利保、大西英理子、佐藤淳、金美善、家村俊一郎、石谷太、夏目徹、大西淳之、澁谷浩司 NLK, an essential effector for of anterior formation, functions downstream of p38 MAP kinase. 第32回日本分子生物学会年会、2009年12月11日、横浜。

9) 外部資金の獲得状況

科学研究費補助金、特定領域研究

「発生分化を制御するDECODE回路の解明」

代表:澁谷浩司

期間:平成17-21年度

研究費総額:9000万円

10) 教室、分野や講座の准教授、講師、助教、特別研究員、ポスドク、指導を受けた大学院生の名前（AISSには○印）のリスト

准教授 後藤利保

MTT 特任助教 佐藤淳

大学院生 清水幹容、田雅文

11) GCOE 活動についての感想、コメント、改善を望む点など自由形式で記載

総合プレゼンテーションの廃止を強く望みます。

Nemo-Like Kinase, an Essential Effector of Anterior Formation, Functions Downstream of p38 Mitogen-Activated Protein Kinase^{▽†}

Eriko Ohnishi,^{1‡} Toshiyasu Goto,^{1,2‡} Atsushi Sato,^{1,3‡} Mi-sun Kim,¹ Shun-ichiro Iemura,⁴ Tohru Ishitani,⁵ Tohru Natsume,⁴ Junji Ohnishi,¹ and Hiroshi Shibuya^{1,2*}

Department of Molecular Cell Biology, Medical Research Institute and School of Biomedical Science,¹ Global Center of Excellence Program, International Research Center for Molecular Science in Tooth and Bone Diseases,² and Medical Top Track Program, Medical Research Institute,³ Tokyo Medical and Dental University, Bunkyo-ku, Tokyo 113-8510, National Institutes of Advanced Industrial Science and Technology, Biological Information Research Center (IBIRC), Kokubun-ku, Tokyo 135-0064,⁴ and Division of Cell Regulation Systems, Post-Genome Science Center, Medical Institute of Bioregulation, Kyushu University, Maidashi, Higashi-ku, Fukuoka 812-8582,⁵ Japan

Received 2 May 2009/Returned for modification 22 June 2009/Accepted 10 November 2009

Nemo-like kinase (NLK) is known to function as a mitogen-activated protein kinase (MAPK)-like kinase. However, the upstream molecules and molecular mechanisms that regulate NLK activity remain unclear. In the present study, we identified p38 MAPK as an upstream kinase and activator of NLK. p38 regulates the function of NLK via phosphorylation, and this modification can be abrogated by depletion of endogenous p38. In *Xenopus laevis* embryos, depletion of either p38 β or NLK by antisense morpholino oligonucleotides results in a severe defect in anterior development and impaired expression of endogenous anterior markers. It is notable that morphants of *Xenopus* p38 α , another isoform of the p38 MAPK family, exhibited no obvious defects in anterior development. Defects in head formation or in the expression of anterior marker genes caused by suppression of endogenous p38 β expression could be rescued by expression of wild-type NLK but not by expression of mutant NLK lacking the p38 β phosphorylation site. In contrast, defects in head formation or in the expression of anterior marker genes caused by suppression of endogenous NLK expression could not be rescued by expression of p38. These results provide the first evidence that p38 specifically regulates NLK function, which is required for anterior formation in *Xenopus* development.

Nemo-like kinase (NLK) is an evolutionarily conserved serine-threonine protein kinase that was originally isolated as a murine orthologue of *Drosophila melanogaster* Nemo, which is involved in diverse signaling processes (3). Studies of Nemo-null mutants in *Drosophila* revealed that Nemo plays a role in head development and in the pathway governing epithelial planar cell polarity during eye development by controlling programmed cell death (19). In our previous studies, we demonstrated that NLK is involved in the suppression of the Wnt/ β -catenin signaling pathways. NLK inactivates a transcriptional unit composed of β -catenin/T-cell factor (TCF)/lymphoid enhancer-binding factor (LEF) by phosphorylation of TCF/LEF, which inhibits the binding of this complex to its target gene sequences (10, 28). NLK functions downstream of transforming growth factor β -activated kinase 1 (TAK1), a member of the mitogen-activated protein kinase kinase kinase (MAPKKK or MAP3K) family (10, 22). Wnt1 (9), and Wnt5a (8). Loss of NLK/Nemo function results in an embryonic lethal phenotype

in *Drosophila* (19), *Caenorhabditis elegans* (24), and mice (15), strongly implicating NLK/Nemo as a very important regulator of cell growth, patterning, and death. We previously demonstrated that in *Xenopus laevis* embryos, expression of NLK is restricted to the central nervous system, eye field, and anterior neural crest cell populations. *Xenopus* NLK is involved in anterior formation and the expression of anterior neural marker genes (6). Our recent data indicate that, in addition to TCF/LEF, NLK associates with and modulates the activities of other transcription factors, including xSox11, STAT3 (22), HMG2L1 (27), and MEF2A (26). This suggests that NLK contributes to various signaling pathways via its ability to interact with a diverse collection of transcription factors.

The activation of p38 in response to a wide range of extracellular stimuli is reflected in the diverse range of MAP3Ks (TAK1, ASK1, DLK, and MEKK4, etc.) that participate in p38 activation, illustrating the complexity of this signaling pathway (16, 17). The MAP3Ks phosphorylate and activate the MAPK kinases (MAP2Ks) MKK6 and MKK3, which in turn phosphorylate the p38 MAPKs. In vertebrates, there are four isoforms of p38: p38 α , p38 β , p38 γ , and p38 δ . These isoforms are characterized by a Thr-Gly-Tyr (TGY) dual-phosphorylation motif (11). Once activated, p38s phosphorylate their substrates on serine/threonine residues. The list of reported downstream substrates of p38 continues to expand and includes other protein kinases and many transcription factors, suggesting its pos-

* Corresponding author. Mailing address: Department of Molecular Cell Biology, Medical Research Institute, Tokyo Medical and Dental University, Bunkyo-ku, Tokyo 113-8510, Japan. Phone and fax: 81-3-5803-4901. E-mail: shibuya.mcb@mri.tmd.ac.jp.

† Supplemental material for this article may be found at <http://mcb.asm.org/>.

‡ E.O., T.G., and A.S. contributed equally to this work.

Published ahead of print on 23 November 2009.

sible role in regulating gene expression at the transcriptional level. Analysis of several of the downstream targets of p38 that are lineage specific or that play an essential role in development have indicated a central role of the p38 pathway in various developmental and differentiation processes (21).

In the present study, we report the novel finding that the p38 β isoform is a functional partner of NLK. NLK was found to associate with, and to be specifically phosphorylated by, p38 β . Depletion of either *Xenopus* p38 β (xp38 β) or xNLK resulted in defects in anterior neural development in *Xenopus* embryos, including the loss of eye and head structures. The phenotypes induced by depletion of endogenous xp38 β were rescued by overexpression of wild-type xNLK but not by a nonphosphorylatable mutant of xNLK. These results reveal a new role of p38 β in the phosphorylation and regulation of NLK function during anterior formation.

MATERIALS AND METHODS

Plasmid construction. The *Xenopus* and human p38 α and β MAPK isoforms were amplified by reverse transcription-PCR (RT-PCR) from cDNA templates prepared from *Xenopus* embryos and 293 cells, respectively, and were subcloned into the pCS2+ and pRK5 vectors. Each kinase-negative (KN) mutant was constructed by replacing the lysine residue with methionine: K53M in xp38 β , K155M in murine NLK (mNLK), K89M in xNLK1, and K173M in xNLK2.

Embryo handling and morpholino oligonucleotides. Capped mRNAs were synthesized from linearized vectors using the mMessage Machine kit (Ambion). The morpholino oligonucleotides (MOs) (Gene Tools, LLC) used here were 5'-GCCCTTCCCTACACGGATGTCCTCC-3' (xNLK1-MO) (22), 5'-GTAGA TGTGCCGCAAGAGACATTC-3' (xNLK2-MO), 5'-CGCCCGCTCATCTT GCCCGACCGG-3' (xp38 β -MO), and 5'-GACGTAAGATTGATTGGATGA CATA-3' (xp38 α -MO). MOs and mRNAs were then injected into two animal blastomeres at the 2-cell stage for dissection of animal caps or into two animal dorsal blastomeres at the 8-cell stage for RT-PCR analysis and observation of embryo phenotypes. Animal cap explants or head regions of the injected embryos were dissected at the late blastula stage (stage [st.] 9) or tailbud stage (st. 25), respectively. The specificities of xp38 β -MO, xp38 α -MO, and xNLK2-MO were confirmed by their abilities to inhibit the translation of FLAG-tagged mRNAs (see Fig. S1 in the supplemental material).

RT-PCR analysis. Total RNA was prepared using TRIzol (Invitrogen). cDNA synthesis was carried out using Moloney murine leukemia virus reverse transcriptase (Invitrogen). The sequences of the primer pairs have been described previously (6, 26) and are as follows: xp38 β , 5'-GACAGCAGCATCACCTCC TCA-3' and 5'-TATCTGCTATGTCCTGCTCCCTTTTC-3'; xp38 α , 5'-CAT GCGACTGACGGGGACTC-3' and 5'-GCTATCGGCTCATCATCAGG-3'; xNLK1, 5'-ATGCTGCTGTTTGACCCGCTGAAGCG-3' and 5'-AGGGCACT CATGCGAGAAGGTT-3'; xNLK2, 5'-GCTGTGCAAGTTGGCGAGGGATT G-3' and 5'-GCGGCGGAGCTGAAGAGGAA-3'. *Xenopus* embryonic ornithine decarboxylase (ODC) or histone H4 (H4) was used for normalization of cDNA samples.

Antibodies and cell lines. The following antibodies were used for immunoprecipitation and/or Western blot analysis: horseradish peroxidase conjugated anti-mouse IgG (GE), horseradish peroxidase conjugated anti-rabbit IgG (GE), horseradish peroxidase conjugated anti-rat IgG (GE), anti-T7 (Novagen), anti-hemagglutinin (anti-HA) (3F10; Roche), anti-FLAG (M2; Sigma), anti-p38 β 2 (Zymed), anti-p38 α (Cell Signaling), anti-NLK (8), anti-p38 (Cell Signaling), anti-ph-p38 (Cell Signaling), and anti-ph-mNLK-S510 (Sigma). Also, we used following cell lines: HEK 293 cells, Neuro2A cells, PC12 cells, COS1 cells, and C2C12 cells. The growth medium of each cell is described by the American Type Culture Collection and Evangelopoulos et al. (4).

Protein identification by LC-MS/MS analysis. FLAG-mouse NLK was expressed in 293 cells, and NLK and associated proteins were recovered from cell extracts by immunoprecipitation with an anti-FLAG antibody. The NLK-associated complexes were digested with *Achromobacter* protease I (Takara), and the resulting peptides were analyzed using a nanoscale liquid chromatography-tandem mass spectrometry (LC-MS/MS) system, as described previously (20).

In vitro kinase assay. 293 cells, COS-1 cells, or PC12 cells were transfected with the FLAG-NLK or FLAG-p38 expression plasmid. The lysates were prepared from the transfected cells using lysis buffer and were immunoprecipitated

with anti-FLAG antibody M2. Immunoprecipitates were incubated with bacterially expressed glutathione S-transferase (GST) fusion proteins in 30 μ l kinase buffer containing 10 mM HEPES (pH 7.4), 1 mM dithiothreitol (DTT), 5 mM MgCl₂, and 5 μ Ci of [γ -³²P]ATP at 30°C for 15 to 30 min. Phosphorylated substrates were subjected to SDS-PAGE and quantitated using a BAS 2500 image analyzer (Fujifilm).

RNA interference. For differentiation experiments, PC12 cells were subjected to 50 ng/ml nerve growth factor (NGF) treatment with fresh serum-free Dulbecco's modified Eagle medium (DMEM) and were further incubated for 20 min. We designed small interfering RNAs (siRNAs) against mouse p38 α (sense, 5'-GAAUAUCCGCUAAGGAUGC-3') and p38 β (sense, 5'-GCACGAGAAC GUCAUAGGA-3') mRNAs along with their corresponding antisense RNA oligonucleotides with two thymidine residues (dTdT) at the 3' end of the sequence (Dharmacon). A commercial control siRNA (siCONTROL Non-Targeting siRNA #2; Dharmacon) was used for the negative-control siRNA. These siRNAs were transfected into PC12 cells using Lipofectamine 2000 (Invitrogen) according to the manufacturer's instructions. After 48 h posttransfection, the medium was replaced with fresh serum-free DMEM to induce the differentiation of PC12 cells.

Whole-mount *in situ* hybridization. pBluescript vectors containing a cDNA fragment of xNLK1 encoding the C-terminal region (nucleotides 780 to 1344; GenBank accession no. AB071285), xNLK2 encoding the C-terminal region (nucleotides 2437 to 3280; GenBank accession no. AB490416), xp38 β encoding the 3' untranslated region (nucleotides 2275 to 2864; GenBank accession no. AB490414), or xp38 α encoding the 3' untranslated region (nucleotides 1257 to 1816; GenBank accession no. AB490415) were used as templates to generate digoxigenin (DIG)-labeled RNA probes using a DIG RNA labeling kit (Roche) according to the manufacturer's protocol. Whole-mount *in situ* hybridization with digoxigenin-labeled RNA probes was performed on staged embryos essentially as described by Hemmati-Brivanlou et al. (5) with the following modifications. After manual removal of the vitelline membranes, embryos were fixed in 4% paraformaldehyde (PFA) in phosphate-buffered saline (PBS), followed by dehydration by gradual methanol washing. Embryos were rehydrated with PBS containing 0.01% Triton X-100 and were then treated with proteinase K (2 μ g/ml) for 10 min at ambient temperature, followed by postfixation with 4% PFA for 20 min. Hybridization was performed at 68°C with 50% formamide, 5 \times SSC (1 \times SSC is 0.15 M NaCl plus 0.015 M sodium citrate), 2 \times Denhardt's solution, 200 μ g/ml tRNA, 0.01% Triton X-100, and 0.1% 3-(3-cholamidopropyl)-dimethylammonio]-1-propanesulfonate (CHAPS), containing 200 ng/ml of the digoxigenin-labeled RNA probe. Color detection was carried out with BM purple (Roche).

RESULTS

p38 β MAPK associates with NLK. Our previous studies have shown that NLK is involved in forebrain development and neural differentiation in *Xenopus* (6, 26). However, there is no information about direct upstream regulators of NLK that may function in these processes. To explore potential regulators of NLK function, we initially performed a high-throughput analysis of proteins that coimmunoprecipitated with FLAG-tagged NLK in 293 cells using direct nanoflow liquid chromatography-coupled tandem MS (20). We identified the p38 β MAPK isoform as a candidate protein that may physically interact with NLK (data not shown). Both p38 β and NLK belong to the MAPK family; however, we have found no reports of direct regulation of a MAPK by another MAPK family member. The interaction between ectopically expressed p38 β and NLK was confirmed in 293 cells (Fig. 1A and B). p38 β could also be coimmunoprecipitated with a kinase-negative mutant of NLK, NLK-KN (Fig. 1C). This indicates that the association between NLK and p38 β does not require NLK kinase activity. Immunoprecipitation analysis using an anti-NLK antibody confirmed the existence of an endogenous NLK and p38 β complex in the mouse neuroblastoma cell line Neuro2A (Fig. 1D). Moreover, analysis of both ectopically expressed and endogenous molecules showed that p38 α also

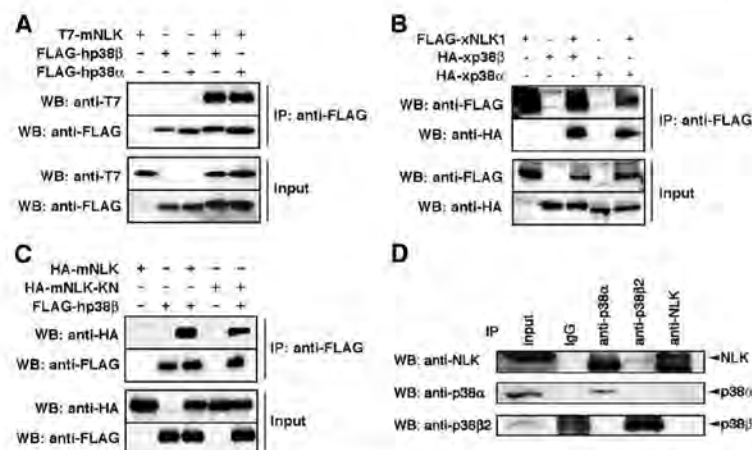


FIG. 1. p38 MAPK associates with NLK. (A to C) Interactions among ectopically expressed genes. 293 cells were transfected as indicated. Immunoprecipitates (IP) obtained using an anti-FLAG antibody were subjected to Western blotting (WB) with the indicated antibodies. +, present; -, absent. (A) Interaction between mNLK and human p38 (hp38β or hp38α). (B) Interaction between xNLK1 and xp38 (xp38β or xp38α). (C) Interaction between xp38 and kinase-negative mNLK (mNLK-KN). (D) Interactions among endogenous genes. Immunoprecipitates obtained from mouse neuroblastoma Neuro2A cells using the indicated antibodies were subjected to Western blotting with the indicated antibodies. Each specific antibody detected the respective endogenous protein, and the anti-NLK antibody detected NLK protein in immunoprecipitates using anti-p38β and anti-p38α.

associates with NLK (Fig. 1A, B, and D). Thus, these results suggest that p38α and β indistinguishably associate with NLK.

p38 phosphorylates a specific site in NLK. To examine whether p38 phosphorylates NLK or vice versa, we performed *in vitro* kinase assays using a catalytically inactive mutant of NLK-KN as a substrate. Figure 2A shows that p38β was barely phosphorylated by NLK. On the other hand, good phosphorylation of NLK by p38β was obtained in a kinase activity-dependent manner (Fig. 2C, lanes 1 to 4). There are two NLK species in *Xenopus* and zebrafish: NLK1 and NLK2 (6). Three of four putative p38 phosphorylation motifs, Ser-Pro or Thr-Pro, are conserved between these two NLKs. The putative phosphorylation site of NLK2 in the C terminus is conserved among many different species, including mice and humans (Fig. 2B; see also Fig. S2 in the supplemental material). We thus tested whether p38β phosphorylates either of these putative phosphorylation residues using NLK S/A or T/A mutants, in which the serine or threonine residues are replaced with alanine. A single amino acid replacement of Ser⁴² in xNLK1 with alanine (S42A) significantly abrogated phosphorylation of xNLK1 (Fig. 2D, lanes 5 to 8) *in vitro*, indicating that Ser⁴² is the specific site of xNLK1 phosphorylation by p38β. On the other hand, replacement of Ser⁵¹⁰ of mNLK with alanine (GST-mNLK S510A) also caused a reduction in NLK phosphorylation by p38β (Fig. 2C). Moreover, Ser⁵²⁸ of xNLK2 was also specifically phosphorylated by p38β. (Fig. 2E). We confirmed that the same Ser residues were phosphorylated by p38α (Fig. 2F). These results indicate that the phosphorylation of the conserved Ser residue in different species is involved in the p38-mediated reaction.

We then asked whether NLK is activated by p38. Flag-mNLK was coexpressed in COS1 cells together with increasing amounts of TAK1/TAB1, an upstream MAPKKK of NLK (10, 18), or together with the constitutively active MKK6

(MKK6EE), an upstream MAPKK of p38 (1, 7). Flag-mNLK protein was immunoprecipitated from the cell lysates with an anti-Flag antibody, and kinase activities in the immunoprecipitates were measured. The NLK immunoprecipitates were assayed using bacterially expressed GST-LEF-1, which is a specific substrate for NLK (9). Both TAK1/TAB1 and MKK6EE enhanced NLK-mediated phosphorylation of GST-LEF-1 in a dose-dependent manner (Fig. 2G). When *in vitro* kinase assays were performed in the presence of SB203580 or SB20219, specific inhibitors of p38 (7), phosphorylation of GST-Lef1 by NLK was weak (Fig. 2H), suggesting that p38 is required for the observed activation of NLK. To evaluate the physiological relevance of p38 to activate NLK in the signaling pathway, we used siRNA to suppress expression of the endogenous p38 proteins in PC12 cells treated with NGF. We examined the effect of p38 siRNA on the phosphorylation level of STAT3, another substrate of NLK (22). As shown in Fig. 3A (left panels), NGF treatment enhanced the phosphorylation of STAT3. When endogenous p38 expression was suppressed with a p38 siRNA (sip38), NGF-induced phosphorylation of STAT3 was reduced compared with that in the control (si-Control) (Fig. 3A, right panels). We also confirmed that endogenous NLK expression was not affected with or without the p38 siRNA pretreatment (Fig. 3B). These data suggest that p38 is physiologically required for the activation of NLK.

p38β functions in anterior neural development. To assess the possible involvement of p38 in *Xenopus* embryonic development, we first examined the temporal and spatial expression patterns of xp38α, xp38β, xNLK1, and xNLK2 by RT-PCR analysis and whole-mount *in situ* hybridization (Fig. 4A and B; see also Fig. S3 in the supplemental material). We found that the expression of both xp38α and xNLK1 was relatively constant level throughout embryogenesis. On the other hand, xp38β was expressed from maternally deposited mRNA, and

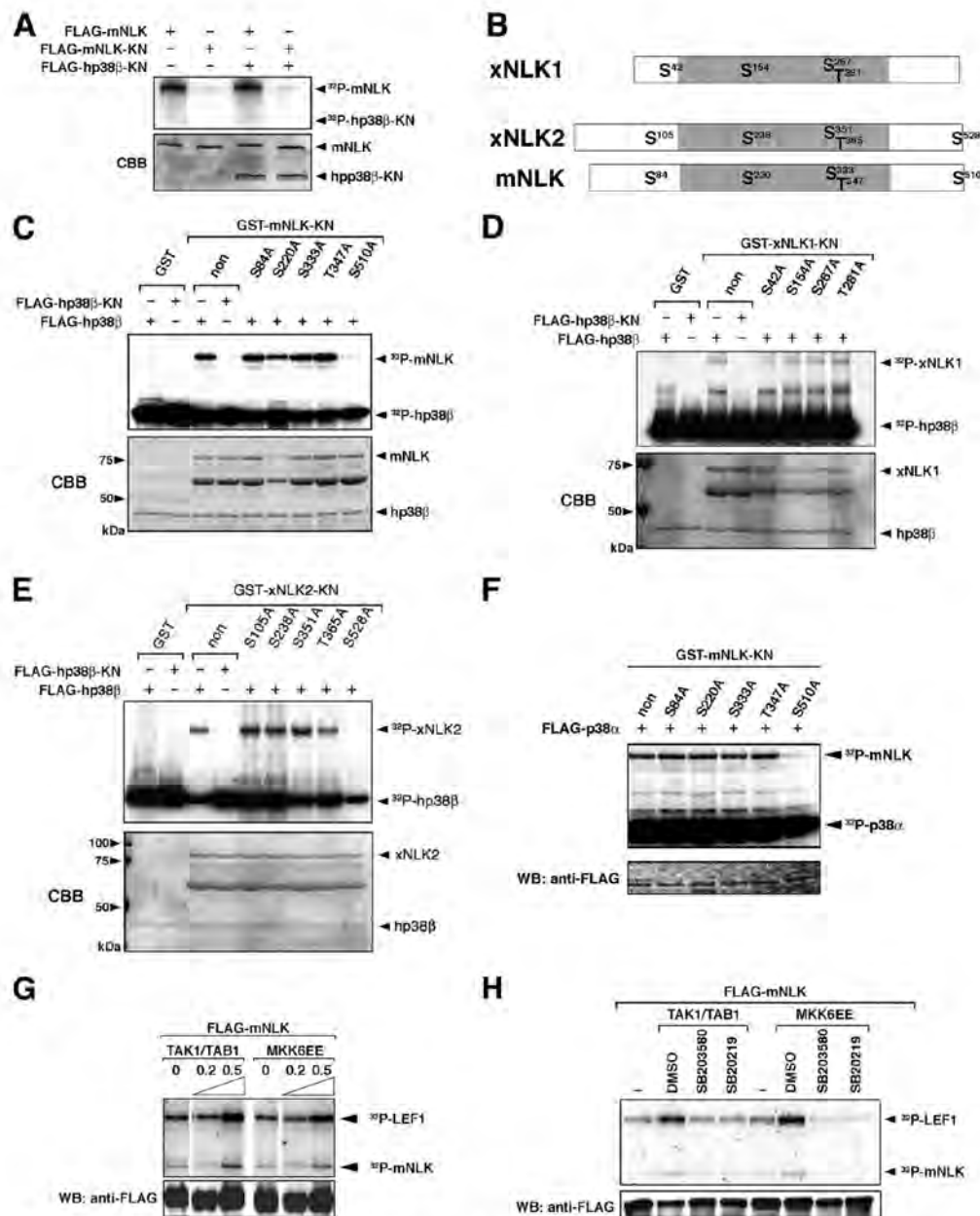


FIG. 2. p38β phosphorylates a specific site in NLK. (A) Phosphorylation of p38 by NLK. 293 cells were transfected with Flag-tagged genes and a constitutively active form of MKK6 (MKK6EE). Immunoprecipitates obtained with an anti-FLAG antibody were incubated with [γ -³²P]ATP. (B) Schematic of NLK genes. The putative p38 phosphorylation motifs are indicated as S and T. The kinase domain is shaded. (C to E) Phosphorylation of NLK by p38β. 293 cells were transfected with FLAG-tagged hp38β or hp38β-KN, together with MKK6EE. Immunoprecipitates obtained with an anti-FLAG antibody were incubated with [γ -³²P]ATP and bacterially expressed mNLK-KN and its mutants (C), xNLK1-KN and its mutants (D), or xNLK2-KN and its mutants (E). Phosphorylation and Coomassie brilliant blue (CBB) staining of each protein are indicated by arrowheads. (F) Phosphorylation of NLK by p38α. 293 cells were transfected with FLAG-tagged p38α. Immunoprecipitates obtained with an anti-FLAG antibody were incubated with [γ -³²P]ATP and bacterially expressed mNLK-KN and its mutants. The phosphorylation of mNLK and p38α is indicated by arrowheads. (G and H) COS1 cells were transfected with FLAG-tagged mNLK, together with TAK1/TAB1 or MKK6EE. Immunoprecipitates obtained with an anti-FLAG antibody were incubated with [γ -³²P]ATP and bacterially expressed LEF1 as a substrate. (G) Enhancement of phosphorylation by TAK1/TAB1 or MKK6 (MKK6EE). Numbers indicate amounts of transfected genes (μg). (H) Preincubation with SB203580 and SB20219, specific inhibitors of p38 activity, reduced phosphorylation of LEF1.

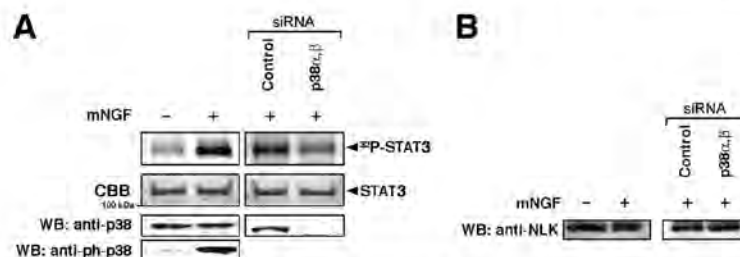


FIG. 3. p38 is required for the activation of NLK. (A) PC12 cells were treated with 50 ng/ml mNGF. Immunoprecipitates obtained with an anti-NLK antibody were incubated with $[\gamma\text{-}^{32}\text{P}]\text{ATP}$ and bacterially expressed STAT3 as a substrate of NLK. anti-ph-p38, anti-phospho-antibody for p38. (Left lanes) Phosphorylation of STAT3 and endogenous p38 following NGF treatment. (Right lanes) PC12 cells were pretreated with the control siRNA or a p38 α , β siRNA. Phosphorylation and Coomassie brilliant blue (CBB) staining of STAT3 are indicated by arrowheads. (B) Effects of p38 siRNAs on NLK expression. p38-siRNAs did not alter NLK expression.

its zygotic expression was induced after the neurula stage, especially in the head region of the embryo. The expression of xNLK2 was relatively weak compared to the expression of xNLK1. As shown in Fig. 4B, symmetrical expression of these genes was detected in both the anterior and posterior neural tubes (two stripes along the lateral neural plate, two eye primordial, forebrain, cement gland, and posterior neural tubes) at the late neural stage (stage 19). To address the physiological relationship between NLK and p38, we synthesized antisense morpholino oligonucleotides (MOs) against xNLK1, xNLK2, xp38 β , and xp38 α (see Materials and Methods). By Western blot analysis, we confirmed that injection of the xNLK1-, xNLK2-, xp38 β - and xp38 α -MOs specifically reduced the expression of these proteins (22) (see Fig. S1 in the supplemental material). When xp38 β -MO was injected into the anterior region, which develops mainly into neuroectodermal tissues and head structure, the resulting phenotype was similar to that resulting from injection of the xNLK1- or xNLK2-MO, namely, incomplete formation of the eyes (Fig. 4C; see also Fig. S4 and S5 in the supplemental material) and reduced expression of anterior markers such as Otx2, Pax6, Lhx2, Rx, and Six3 (Fig. 4D; see also Fig. S4 and S5 in the supplemental material). On the other hand, no apparent phenotype was detected following injection of as much as 20 ng of xp38 α -MO or a control MO. The anterior defects induced by xp38 β -MO were rescued by coinjection of wild-type xp38 β mRNA, but not by kinase-inactive or wild-type xp38 α mRNA (Fig. 5). These results suggest that xp38 β is specifically involved in anterior formation in *Xenopus* embryos.

p38 regulates NLK function through Ser phosphorylation.

To further examine the phosphorylation of specific Ser residues in NLK by p38, we generated polyclonal antibodies against mouse NLK phospho-Ser⁵¹⁰. Wild-type mNLK or mutant mNLK-S510A was expressed in C2C12 cells together with p38 β and the constitutively active MKK6 (MKK6EE), and cell lysates were subjected to immunoblot analysis using anti-phospho-Ser⁵¹⁰. A band corresponding to wild-type mNLK could be detected in cells expressing wild-type mNLK, but not in those expressing mNLK-S510A (Fig. 6A). Significantly smaller amounts of phospho-Ser⁵¹⁰ mNLK were detected in *Xenopus* embryos treated with xp38 β -MO, whereas phospho-Ser⁵¹⁰ mNLK amounts were unaffected in embryos treated with xp38 α -MO or a control MO (Fig. 6B). These results demon-

strate that endogenous p38 β phosphorylates the specific Ser residue of NLK.

We next examined whether xp38 β functions upstream of xNLK. We found that anterior defects induced by xp38 β -MO could be rescued by coinjection with wild-type xNLK1 or xNLK2 mRNA (Fig. 7A, lanes 3 and 5), but not with mRNA encoding nonphosphorylatable mutants (xNLK1-S42A or xNLK2-S528A) (Fig. 7A, lanes 4 and 6), indicating that anterior formation depends on the phosphorylation of xNLK. In addition, anterior defects induced by xNLK1- or xNLK2-MO were not rescued by either nonphosphorylatable xNLK-SA mutant (Fig. 7B, lanes 4 and 9). In contrast, coinjection with xp38 β mRNA failed to rescue the defects in anterior formation caused by depletion of xNLK1 but could rescue those caused by depletion of xNLK2 (Fig. 7B, lanes 5 and 10). We also confirmed that the anterior defect caused by xNLK1- or xNLK2-MO was redundantly rescued by xNLK2 or xNLK1 mRNA, respectively (Fig. 7C, lanes 3 and 5). These results suggest that xNLK1 is necessary for inducing anterior formation downstream of xp38 β signaling in *Xenopus*. We examined this further using the xNLK1-S42D, xNLK2-S528D, and mNLK-S510D mutants, in which the Ser residues of NLK were replaced with an aspartic acid, mimicking the phosphorylated serine. We found that the anterior defects induced by xNLK1-MO or xNLK2-MO could be rescued by coinjection with small amounts of xNLK1-S42D or xNLK2-S528D mRNA, respectively, but not by coinjection with wild-type NLK mRNA (Fig. 7D, lanes 2 to 7). The anterior defects caused by xp38 β -MO were also rescued by coinjection with NLK SD mutant mRNA (Fig. 7D, lanes 8 to 12). It is noteworthy that mutation of each phosphorylation site in mNLK and xNLK1 to Ala resulted in reduced kinase activity in the cultured cells (Fig. 7E). These results suggest that the sites of p38 phosphorylation in NLK are essential for its function and catalytic activity.

DISCUSSION

Our previous studies have shown that NLK induces the expression of anterior neural markers in animal pole explants (6). In the present study, we identified the MAPK family member p38 as a novel activator of the serine/threonine kinase NLK, and we show that p38-NLK signaling controls anterior

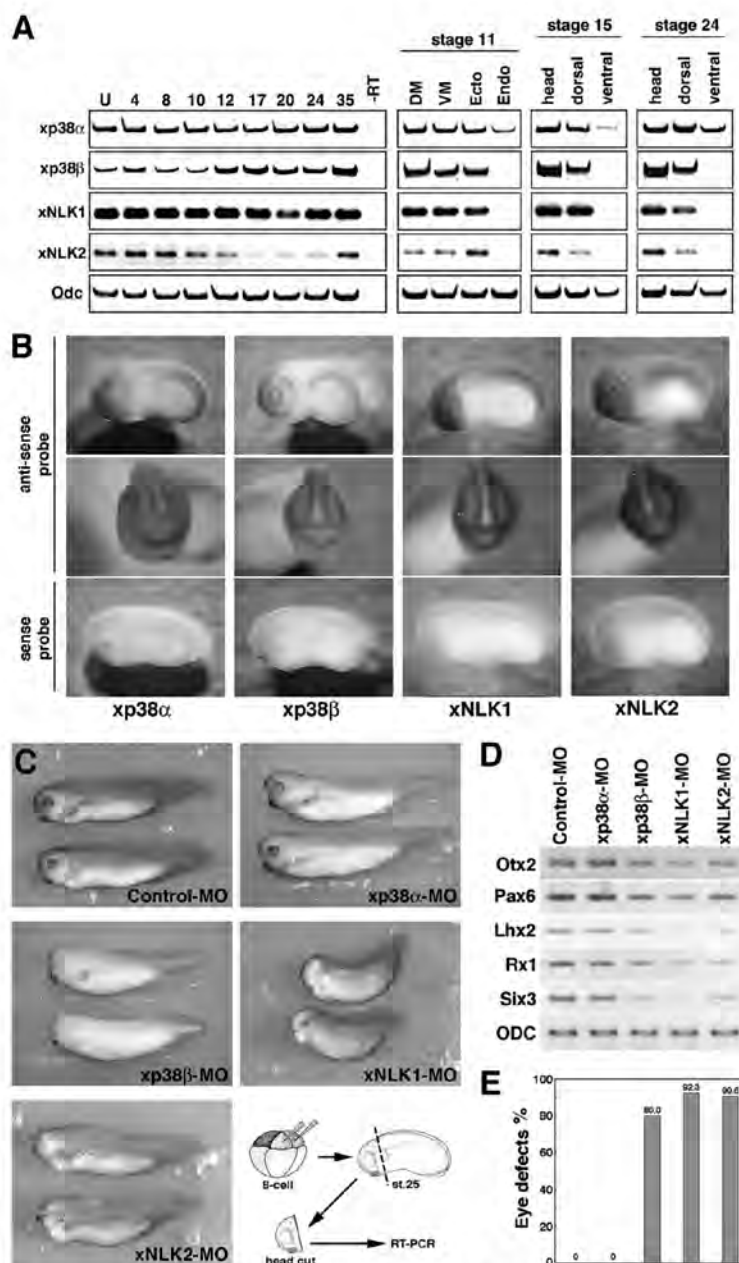


FIG. 4. p38β functions in anterior neural development. (A) RT-PCR revealed temporal expression of xp38α, xp38β, xNLK1, and xNLK2. Numbers above lanes indicate developmental stages; U, unfertilized eggs. Semiquantitative RT-PCR to determine spatial expression was also performed using different dissections of embryos at several stages (stages 11, 15, and 24). DM, dorsal marginal zone; VM, ventral marginal zone; Ecto, ectoderm; Endo, endoderm. (B) Whole-mount *in situ* hybridization showed that these genes are similarly expressed in the head and on the dorsal side (stage 19). The sense RNA probe for each gene was used as a negative control (bottom panels). Images are lateral views, with the anterior ends toward the left (top and bottom panels), and front views (center panels) of head regions. (C to E) Characterization of each morphant. A control morpholino oligonucleotide (Control-MO) (20 ng), xp38α-MO (20 ng), xp38β-MO (20 ng), xNLK1-MO (10 ng), and xNLK2-MO (40 ng) were injected into two animal dorsal blastomeres of 8-cell-stage embryos. (C) Phenotypes of injected embryos at stage 35. Methods for RT-PCR analysis of anterior neural marker genes are indicated in the bottom right panel. (D) Expression of anterior neural marker genes Otx2, Pax6, Lhx2, Rx1, and Six3 in each morphant. ODC (ornithine decarboxylase) was used as a loading control. Total RNAs from the heads of the injected embryos at stage 25 were prepared. (E) Proportion of embryos with eye defects for each morphant in panel C. Each bar corresponds to the lane in panel D with which it is lined up.

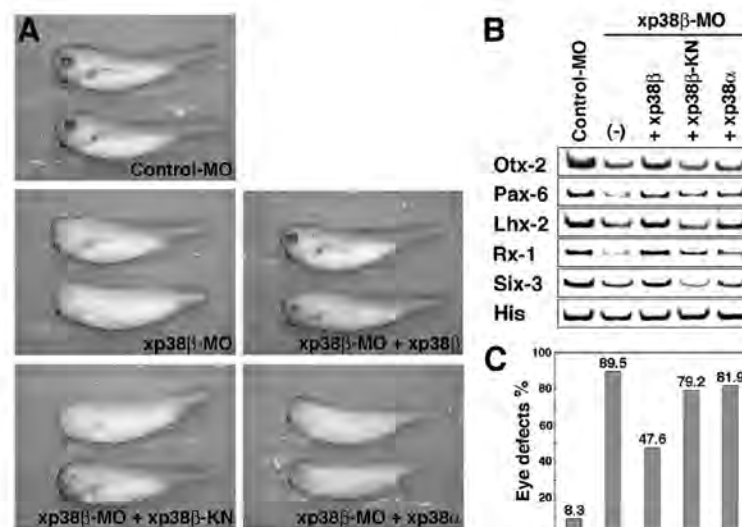


FIG. 5. p38 β and its kinase activity are necessary for anterior development. A control MO (20 ng) or xp38 β -MO (20 ng) was coinjected with xp38 β (500 pg), xp38 β -KN (500 pg), or xp38 α (500 pg) mRNA. (A) Phenotypes of injected embryos at stage 35. (B) RT-PCR analysis of anterior neural marker genes. His (histone H4) was used as a loading control. (C) Proportion of embryos with eye defects for each morphant in panel A. Each bar corresponds to the lane in panel B with which it is lined up.

neural development in *Xenopus*. Depletion of xNLK1, xNLK2, or xp38 β resulted in severe defects in anterior neural development, including loss of eye formation. The defects induced by depletion of xp38 β were rescued by expression of wild-type xNLK1 or xNLK2, but not by either of two nonphosphorylatable mutants (xNLK1-S42A or xNLK2-S528A). Interestingly, coinjection with xp38 β mRNA failed to rescue the defects in anterior formation caused by depletion of xNLK1 but could rescue those caused by depletion of xNLK2 (Fig. 7B). Our studies demonstrated that the expression of xNLK2 was considerably weaker than that of xNLK1 (Fig. 4A). Moreover,

xNLK1 and xNLK2 function redundantly in anterior formation, such that when xNLK2 is depleted, the xNLK1 signal mediated by p38 β can compensate (Fig. 7C). Thus, these results indicate that xp38 β functions upstream of xNLK in the development of anterior neural structures. Our results demonstrate the existence of a new molecular mechanism involving p38-NLK signaling in the regulation of endogenous anterior tissue development, including eye formation, in *Xenopus*.

We identified the p38 β MAPK isoform as a protein that physically interacts with NLK. In *Xenopus*, three isoforms of the p38 family have been identified: xp38 α , xp38 β , and xp38 γ (23, 25). Studies of mammalian p38 α and p38 β molecules suggest that these isoforms may overlap in their biological functions (16, 17). On the other hand, it is well known that the function of p38 γ is different from those of p38 α and p38 β (16, 17). Indeed, a previous report indicates that xp38 γ , but not xp38 α or xp38 β , promotes the meiotic G₂/M transition in *Xenopus* (23). Therefore, we focused on the function of xp38 α and xp38 β in *Xenopus* development. Interestingly, we found that depletion of xp38 α did not affect anterior formation or the expression of any anterior marker genes, whereas depletion of endogenous xp38 β blocked both anterior formation and the induction of these markers (Fig. 4). Thus, xp38 β appears to be selectively responsible for regulating certain aspects of anterior formation via the activation of xNLK. Recently, Keren et al. reported that p38 α regulates the expression of xMyf5 during *Xenopus* development (13). Depletion of xp38 α by an MO was not reported to have any effect on anterior formation, but this may be due to the limited function of xp38 α in *Xenopus*. On the other hand, Beardmore et al. reported that p38 β knockout mice are viable, with no obvious health problems (2). They speculate that the reason for this mild phenotype could be compensation between p38 α and p38 β isoforms. Although there are discrepancies in that p38 α could not compensate for the

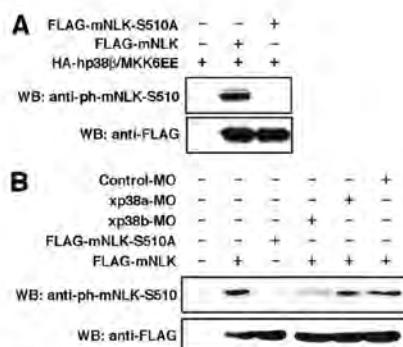


FIG. 6. p38 regulates NLK function through Ser phosphorylation. (A) C2C12 cells were transfected as indicated. anti-ph-mNLK-S510 is the anti-phospho-antibody for mNLK-S510. Whole-cell lysates were subjected to Western blotting using the indicated antibodies. (B) A control MO (20 ng), xp38 α -MO (20 ng), or xp38 β -MO (20 ng) was coinjected with FLAG-tagged mNLK (50 pg) or mNLK-S510A (50 pg) mRNA as described in Materials and Methods. Lysates from the heads of the injected embryos at stage 25 were subjected to Western blotting using the indicated antibodies.

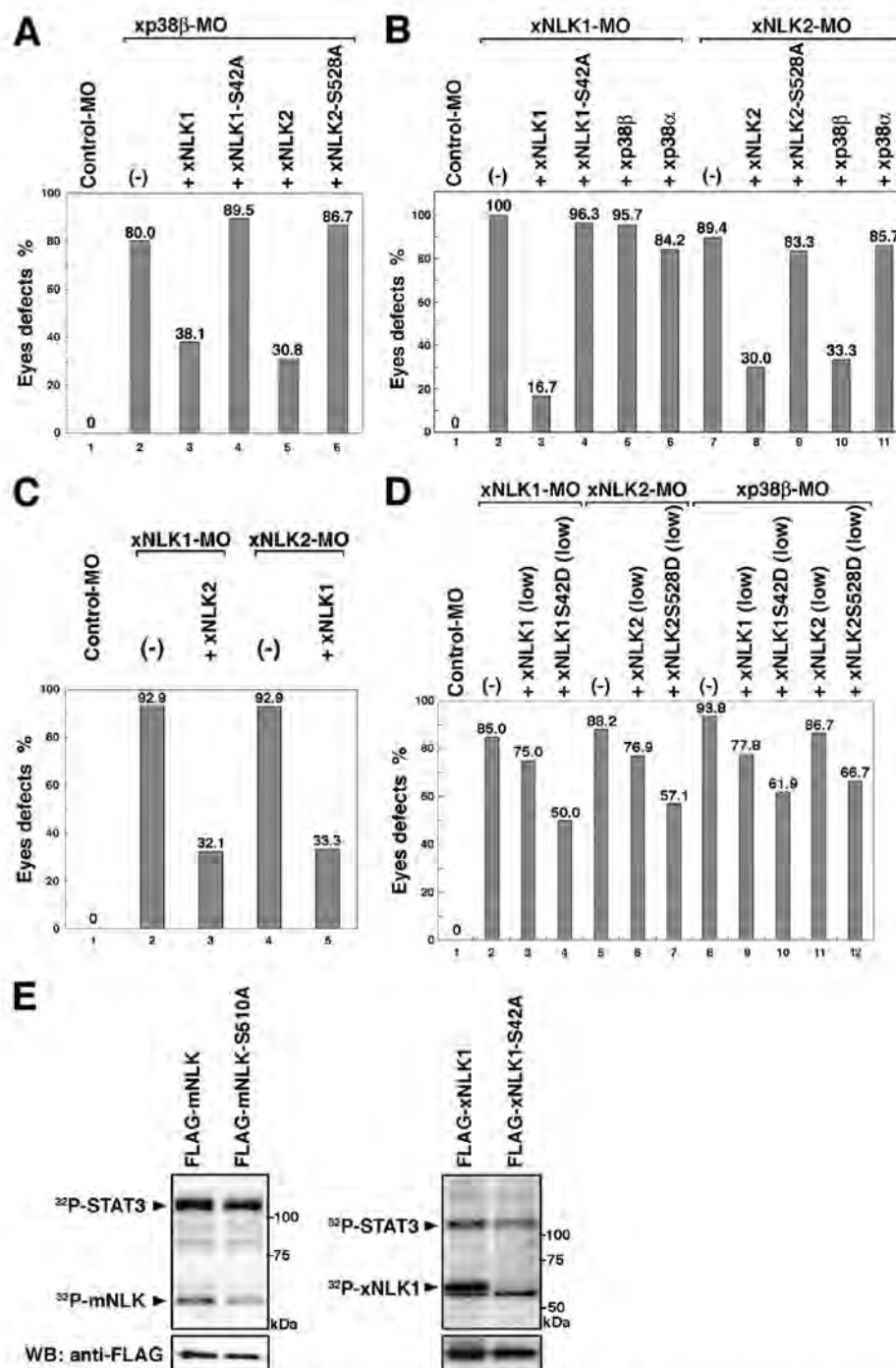


FIG. 7. The Ser phosphorylation of NLK by p38 is essential for anterior formation. (A to D) Phenotypes of injected embryos were observed at stage 35. Each graph shows the proportion of embryos with eye defects for each morphant. Each MO or mRNA was injected as described in Materials and Methods. (A) A control MO (20 ng) or xp38 β -MO (20 ng) was coinjected with xNLK1 (62.5 pg), xNLK2 (50 pg), xNLK1-S42A (62.5 pg), or xNLK2-S528A (50 pg) mRNA. (B) A control MO (20 ng), xNLK1-MO (10 ng), or xNLK2-MO (20 ng) was coinjected with xNLK1 (62.5 pg), xNLK2 (50 pg), xNLK1-S42A (62.5 pg), xNLK2-S528A (50 pg), xp38 β (500 pg), or xp38 α (500 pg) mRNA. (C) A control MO (20 ng), xNLK1-MO (10 ng), or xNLK2-MO (40 ng) was coinjected with xNLK1 (62.5 pg) or xNLK2 (50 pg) mRNA. (D) A control MO (20 ng), xp38 β -MO (20 ng), xNLK1-MO (10 ng), or xNLK2-MO (20 ng) was coinjected with low-dose xNLK1 (10 pg), xNLK1-S42D (10 pg), xNLK2 (10 pg), or xNLK2-S528D (10 pg) mRNA. (E) 293 cells were transfected with Flag-tagged NLKs and SA mutants (left panels for mNLK, right panels for xNLK1). Immunoprecipitates obtained with an anti-FLAG antibody were incubated with [γ - 32 P]ATP and bacterially expressed STAT3 as a substrate of NLK. The phosphorylation of STAT3 and NLK itself is indicated by arrowheads.

function of p38 β in *Xenopus* anterior formation in contrast to the function in mice, our studies of *Xenopus* may provide the first indication of p38 β function in embryogenesis, and they provide the first evidence of isoform-specific functional differences between p38 α and p38 β family members. However, the details of how p38 β specifically contributes to early developmental processes in *Xenopus* embryos remain to be determined and will require additional study.

We have previously demonstrated that the MAP3K TAK1 activates the MAPK-like kinase NLK in a signaling pathway (9, 18). Since TAK1 does not directly interact with NLK, it was assumed that a known molecule, such as a MAPKK, may function upstream of NLK in this pathway. Kanei-Ishii et al. reported that HIPK2 could bind to and activate NLK in the TAK1 signaling pathway (12). However, they failed to detect activation of HIPK2 kinase activity by TAK1. In this study, we demonstrated that p38 MAPK directly interacts with NLK and regulates its kinase activity. Moreover, it is well known that p38 MAPK is activated by MAP3K TAK1 (14). Actually, we found that NLK was activated by activated TAK1 and MKK6 (Fig. 2G) and that this activation was inhibited in the presence of p38-specific inhibitors (Fig. 2H). Taken together, these findings provide the first evidence that NLK functions as a downstream kinase of a MAPK rather than as a MAPK-like kinase.

We demonstrated that p38 directly phosphorylates NLKs at specific sites and that this leads to their activation. We found that NLK1, a gene conserved in *Xenopus* and zebrafish, and NLK2, a gene conserved among many species, are each phosphorylated on different sites by p38. We also found that each p38 phosphorylation site is similarly required for activation of NLK. Interestingly, the p38 phosphorylation sites in the two NLK molecules are localized to the N-terminal or C-terminal region. This suggests that the position of the p38 phosphorylation site in the NLK molecule is structurally critical. It is likely that the specific site in NLK is phosphorylated by p38 and that phosphorylation at the terminal region of the molecule may suffice to induce its activation. However, further study will be required to understand the precise molecular mechanisms by which p38 regulates the activities of NLK1 and NLK2.

ACKNOWLEDGMENTS

We thank K. Matsumoto for valuable discussions, H. Nishitoh and T. Maruyama for technical advice, and M. Lamphier for critical reading of the manuscript.

This work was supported by Grants-in-Aid for scientific research from the Ministry of Education, Science, Sports, and Culture of Japan.

REFERENCES

- Alonso, G., C. Ambrosino, M. Jones, and A. R. Nebreda. 2000. Differential activation of p38 mitogen-activated protein kinase isoforms depending on signal strength. *J. Biol. Chem.* 275:40641–40648.
- Beardmore, V. A., H. J. Hinton, C. Eftychi, M. Apostolaki, M. Armaka, J. Durragh, J. McIlrath, J. M. Carr, L. J. Armit, C. Clacher, L. Malone, G. Kollias, and J. S. C. Arthur. 2005. Generation and characterization of p38 β (MAPK11) gene-targeted mice. *Mol. Cell. Biol.* 25:10454–10464.
- Brott, B. K., B. A. Pinsky, and R. L. Erikson. 1998. Nlk is a murine protein kinase related to Erk/MAP kinases and localized in the nucleus. *Proc. Natl. Acad. Sci. U. S. A.* 95:963–968.
- Evangelopoulos, M. E., J. Weis, and A. Krutigen. 2005. Signalling pathways leading to neuroblastoma differentiation after serum withdrawal: HDL blocks neuroblastoma differentiation by inhibition of EGFR. *Oncogene* 24: 3309–3318.
- Hemmati-Brivanlou, A., D. Frank, M. E. Bolce, B. D. Brown, H. L. Sive, and R. M. Harland. 1990. Localization of specific mRNAs in *Xenopus* embryos by whole-mount in situ hybridization. *Development* 110:325–330.
- Hyodo-Miura, J., S. Urushiyama, S. Nagai, M. Nishita, N. Ueno, and H. Shibuya. 2002. Involvement of NLK and Sox11 in neural induction in *Xenopus* development. *Genes Cells* 7:487–496.
- Inoue, T., D. Hammaker, D. L. Boyle, and G. S. Firestein. 2005. Regulation of p38 MAPK by MAPK kinases 3 and 6 in fibroblast-like synoviocytes. *J. Immunol.* 174:4301–4306.
- Ishitani, T., S. Kishida, J. Hyodo-Miura, N. Ueno, J. Yasuda, M. Waterman, H. Shibuya, R. T. Moon, J. Ninomiya-Tsuji, and K. Matsumoto. 2003. The TAK1-NLK mitogen-activated protein kinase cascade functions in the Wnt-5a/Ca(2+) pathway to antagonize Wnt/beta-catenin signaling. *Mol. Cell. Biol.* 23:131–139.
- Ishitani, T., J. Ninomiya-Tsuji, and K. Matsumoto. 2003. Regulation of lymphoid enhancer factor 1/T-cell factor by mitogen-activated protein kinase-related Nemo-like kinase-dependent phosphorylation in Wnt/beta-catenin signaling. *Mol. Cell. Biol.* 23:1379–1389.
- Ishitani, T., J. Ninomiya-Tsuji, S. Nagai, M. Nishita, M. Meneghini, N. Barker, M. Waterman, B. Bowerman, H. Clevers, H. Shibuya, and K. Matsumoto. 1999. The TAK1-NLK-MAPK-related pathway antagonizes signaling between beta-catenin and transcription factor TCF. *Nature* 399:798–802.
- Jiang, Y., H. Gram, M. Zhao, L. New, J. Gu, L. Feng, F. Di Padova, R. J. Ulevitch, and J. Han. 1997. Characterization of the structure and function of the fourth member of p38 group mitogen-activated protein kinases, p38delta. *J. Biol. Chem.* 272:30122–30128.
- Kanei-Ishii, C., J. Ninomiya-Tsuji, J. Tanikawa, T. Nomura, T. Ishitani, S. Kishida, K. Kokura, T. Kurahashi, E. Ichikawa-Iwata, Y. Kim, K. Matsumoto, and S. Ishii. 2004. Wnt-1 signal induces phosphorylation and degradation of c-Myc protein via TAK1, HIPK2, and NLK. *Genes Dev.* 18:816–829.
- Keren, A., E. Bengal, and D. Frank. 2005. p38 MAP kinase regulates the expression of XMyf5 and affects distinct myogenic programs during *Xenopus* development. *Dev. Biol.* 288:73–86.
- Keren, A., Y. Tamir, and E. Bengal. 2006. The p38 MAPK signaling pathway: a major regulator of skeletal muscle development. *Mol. Cell Endocrinol.* 252:224–230.
- Kortenjann, M., M. Nehls, A. J. Smith, R. Carsetti, J. Schuler, G. Kohler, and T. Boehm. 2001. Abnormal bone marrow stroma in mice deficient for Nemo-like kinase, Nlk. *Eur. J. Immunol.* 31:3580–3587.
- Kumar, S., J. Boehm, and J. C. Lee. 2003. p38 MAP kinases: key signalling molecules as therapeutic targets for inflammatory diseases. *Nat. Rev. Drug Discov.* 2:717–726.
- Kyriakis, J. M., and J. Avruch. 2001. Mammalian mitogen-activated protein kinase signal transduction pathways activated by stress and inflammation. *Physiol. Rev.* 81:807–869.
- Meneghini, M. D., T. Ishitani, J. C. Carter, N. Hisamoto, J. Ninomiya-Tsuji, C. J. Thorpe, D. R. Hamill, K. Matsumoto, and B. Bowerman. 1999. MAP kinase and Wnt pathways converge to downregulate an HMG-domain repressor in *Caenorhabditis elegans*. *Nature* 399:793–797.
- Mirkovic, L., K. Charish, S. M. Gorski, K. McKnight, and E. M. Verheyen. 2002. *Drosophila nemo* is an essential gene involved in the regulation of programmed cell death. *Mech. Dev.* 119:9–20.
- Natsume, T., Y. Yamauchi, H. Nakayama, T. Shinkawa, M. Yanagida, N. Takahashi, and T. Isobe. 2002. A direct nanoflow liquid chromatography-tandem mass spectrometry system for interaction proteomics. *Anal. Chem.* 74:4725–4733.
- Nebreda, A. R., and A. Porras. 2000. p38 MAP kinases: beyond the stress response. *Trends Biochem. Sci.* 25:257–260.
- Ohkawara, B., K. Shirakabe, J. Hyodo-Miura, R. Matsuo, N. Ueno, K. Matsumoto, and H. Shibuya. 2004. Role of the TAK1-NLK-STAT3 pathway in TGF-beta-mediated mesoderm induction. *Genes Dev.* 18:381–386.
- Perdiguerro, E., M. J. Pillaire, J. F. Bodart, F. Hennesdorf, M. Frodin, N. S. Duesbery, G. Alonso, and A. R. Nebreda. 2003. Xp38gamma/SAPK3 promotes meiotic G(2)/M transition in *Xenopus* oocytes and activates Cdc25C. *EMBO J.* 22:5746–5756.
- Rocheleau, C. E., J. Yasuda, T. H. Shin, R. Lin, H. Sawa, H. Okano, J. R. Priess, R. J. Davis, and C. C. Mello. 1999. WRM-1 activates the LIT-1 protein kinase to transduce anterior/posterior polarity signals in *C. elegans*. *Cell* 97:717–726.
- Rouse, J., P. Cohen, S. Trigon, M. Morange, A. Alonso-Llamazares, D. Zamanillo, T. Hunt, and A. R. Nebreda. 1994. A novel kinase cascade triggered by stress and heat shock that stimulates MAPKAP kinase-2 and phosphorylation of the small heat shock proteins. *Cell* 78:1027–1037.
- Satoh, K., J. Ohnishi, A. Sato, M. Takeyama, S. Iemura, T. Natsume, and H. Shibuya. 2007. Nemo-like kinase-myocyte enhancer factor 2A signaling regulates anterior formation in *Xenopus* development. *Mol. Cell. Biol.* 27:7623–7630.
- Yamada, M., B. Ohkawara, N. Ichimura, J. Hyodo-Miura, S. Urushiyama, K. Shirakabe, and H. Shibuya. 2003. Negative regulation of Wnt signalling by HMGL1, a novel NLK-binding protein. *Genes Cells* 8:677–684.
- Yamada, M., J. Ohnishi, B. Ohkawara, S. Iemura, K. Satoh, J. Hyodo-Miura, K. Kawachi, T. Natsume, and H. Shibuya. 2006. NARF, an nemo-like kinase (NLK)-associated ring finger protein regulates the ubiquitylation and degradation of T cell factor/lymphoid enhancer factor (TCF/LEF). *J. Biol. Chem.* 281:20749–20760.

LETTERS

DNA demethylation in hormone-induced transcriptional derepression

Mi-Sun Kim^{1,2,3}, Takeshi Kondo², Ichiro Takada², Min-Young Youn², Yoko Yamamoto², Sayuri Takahashi², Takahiro Matsumoto^{1,2}, Sally Fujiyama^{1,2}, Yuko Shiode^{1,2}, Ikuko Yamaoka^{1,2}, Hirochika Kitagawa², Ken-Ichi Takeyama², Hiroshi Shibuya³, Fumiaki Ohtake^{1,2} & Shigeaki Kato^{1,2}

Epigenetic modifications at the histone level affect gene regulation in response to extracellular signals^{1,2}. However, regulated epigenetic modifications at the DNA level, especially active DNA demethylation, in gene activation are not well understood^{3–5}. Here we report that DNA methylation/demethylation is hormonally switched to control transcription of the cytochrome p450 27B1 (*CYP27B1*) gene. Reflecting vitamin-D-mediated transrepression of the *CYP27B1* gene by the negative vitamin D response element (nVDRE)^{6,7}, methylation of CpG sites (^{5m}CpG) is induced by vitamin D in this gene promoter. Conversely, treatment with parathyroid hormone, a hormone known to activate the *CYP27B1* gene⁸, induces active demethylation of the ^{5m}CpG sites in this promoter. Biochemical purification of a complex associated with the nVDRE-binding protein (VDIR, also known as TCF3)^{6,7} identified two DNA methyltransferases, DNMT1 and DNMT3B, for methylation of CpG sites⁹, as well as a DNA glycosylase, MBD4 (ref. 10). Protein-kinase-C-phosphorylated MBD4 by parathyroid hormone stimulation promotes incision of methylated DNA through glycosylase activity¹¹, and a base-excision repair process seems to complete DNA demethylation in the MBD4-bound promoter. Such parathyroid-hormone-induced DNA demethylation and subsequent transcriptional derepression are impaired in *Mbd4*^{-/-} mice¹². Thus, the present findings suggest that methylation switching at the DNA level contributes to the hormonal control of transcription.

CYP27B1 is the final enzyme in vitamin D biosynthesis, and it is primarily expressed in the renal proximal tubule¹³. Two calcemic hormones strictly regulate *CYP27B1* gene transcription¹⁴. Parathyroid hormone (PTH) induces *CYP27B1* expression by activating protein kinase A and C (PKA and PKC, respectively)^{15,16}. 1 α ,25-dihydroxyvitamin D₃ (1 α ,25(OH)₂D₃), a hormonally active form of vitamin D₃, is a repressive signal that binds to and activates the nuclear vitamin D receptor (VDR)^{14–16}. A basic helix–loop–helix transcriptional activator (VDR interacting repressor, VDIR) regulates the transcription of *CYP27B1* by the negative vitamin D response element (nVDRE)^{6,7}. Heterodimers of vitamin-D-bound VDR and retinoid X receptor (RXR) repress the activation of VDIR that is bound upon the nVDRE by means of the histone deacetylase (HDAC) co-repressor complex⁸.

We found that the HDAC inhibitor trichostatin A (TSA) did not fully abrogate vitamin-D-induced transrepression in either 293F cells or mouse cortical tubular (MCT) cells (Supplementary Fig. 2). Using newly established stable 293F and MCT transformants expressing Flag–VDIR, we tested for other factor(s)/complex(es) that co-repressed transcription^{17,18} (Supplementary Fig. 3a). The VDIR and VDR interactants consisted of several complexes when fractionated

on an ion-exchange column (Supplementary Fig. 3b) and a glycerol gradient (data not shown)^{17,18}. We identified DNA methyltransferases 1 and 3B (DNMT1 and DNMT3B)⁹ as VDIR and VDR interactants (Fig. 1a) with DNMT activity (Fig. 1g). Generally, DNMT family members methylate cytosines at specific DNA sequences to repress gene expression¹⁹. In a luciferase assay in 293F cells, both DNMT1 and DNMT3B acted as co-repressors for vitamin-D-induced transrepression of the *CYP27B1* promoter (Supplementary Fig. 5). Vitamin-D-induced DNA methylation of cytosines (^{5m}C) was found in the CpG regions of the promoter in 293F cells (see Fig. 1b) and MCT cells (data not shown), as assessed by bisulphite sequencing (Fig. 1c and Supplementary Fig. 6), methylation-specific PCR (Supplementary Fig. 7), and chromatin immunoprecipitation and quantitative PCR (ChIP-qPCR) with an anti-^{5m}C antibody (Fig. 1d). This methylation step required DNMT1 and DNMT3B (Fig. 1d and Supplementary Fig. 8) based on knockdown assays (Supplementary Fig. 4). The knockdown of DNMTs abrogated vitamin-D-induced transrepression of endogenous *CYP27B1* (Fig. 1e), and a DNMT inhibitor, 5-azacytidine, plus TSA, abolished vitamin-D-induced transrepression (Supplementary Fig. 2). Vitamin-D-induced recruitment of DNMT1 and DNMT3B was detected at the *CYP27B1* promoter by ChIP analysis (Fig. 1f and Supplementary Fig. 9), presumably as direct VDR interactants as observed in an *in vitro* glutathione S-transferase (GST)–pull-down assay (Supplementary Fig. 10). DNA methylation of the CpG sites in the promoter and coding regions (Fig. 1c, d), as well as histone deacetylation (Fig. 1d, f), were induced by vitamin D, but a heterochromatin marker, HP1 α ^{18,20}, was not detected (Supplementary Fig. 11). Upregulation of DNMT activity of the VDIR immunocomplex by vitamin D was reduced in the presence of PTH (Fig. 1g). Continued PTH treatment of cells that had been pre-incubated with vitamin D induced demethylation of the ^{5m}CpGs (Figs 1c, 2d and Supplementary Fig. 7).

Next, we assayed for a PTH effect in DNA replication. In proximal renal tubule cells expressing the *Cyp27b1* gene in mice, bromodeoxyuridine (BrdU) incorporation (Supplementary Fig. 12a)²⁰ was not affected by either 48 h PTH treatment or VDR deficiency (*Vdr*^{-/-})²¹ (Fig. 2a). Likewise, PTH-induced DNA demethylation of the *CYP27B1* promoter in 293F cells was detected despite 24 h arrest of the cell cycle after serum depletion or treatment with aphidicolin²² (Fig. 2b and Supplementary Fig. 12b, c). It was thus unlikely that ^{5m}C replaces C in the newly synthesized DNA during DNA replication.

We characterized MBD4 (refs 10, 12) further because MBD4 recruitment to the promoter coincided with the state of DNA methylation (Fig. 2c, d and Supplementary Fig. 13). MBD4 belongs to the 5-methyl-CpG binding domain (MBD) family, which is implicated in

¹ERATO, Japan Science and Technology Agency, 4-1-8 Honcho, Kawaguchi, Saitama 332-0012, Japan. ²Institute of Molecular and Cellular Biosciences, University of Tokyo, 1-1-1 Yayoi, Bunkyo-ku, Tokyo 113-0032, Japan. ³Department of Molecular Cell Biology, Medical Research Institute and School of Biomedical Science, Tokyo Medical and Dental University, Yushima, Bunkyo-ku, Tokyo 113-8510, Japan.

LETTERS

NATURE | Vol 461 | 15 October 2009

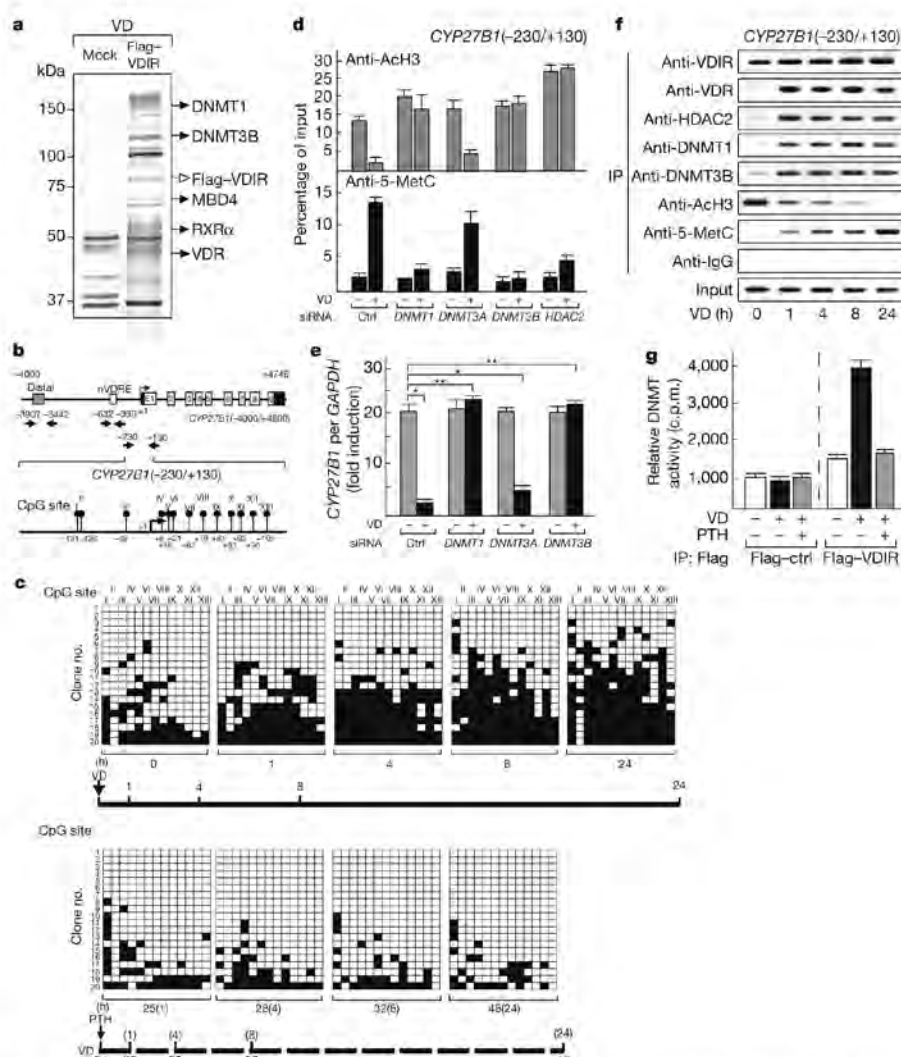


Figure 1 | Hormonal control of DNA methylation/demethylation of the *CYP27B1* gene promoter. **a**, Silver staining of anti-Flag affinity purification, followed by anion-exchange column chromatography using vitamin D (VD; 100 nM)-treated MCT cells expressing Flag-VDIR. **b**, Schematic representation of the CpG sites in the *CYP27B1* promoter and coding region. Black filled circles indicate CpG sites. **c**, Time course of DNA methylation/demethylation in *CYP27B1* (-230/+130) region. Bisulphite sequencing was performed using vehicle-treated, vitamin D (100 nM)-treated and vitamin D/PTH (1 μM)-treated 293F cells for the indicated time. Numbers in parentheses denote time after PTH treatment. White and black squares indicate unmethylated and methylated CpGs, respectively. **d**, **e**, ChIP-qPCR

analyses of 293F cells transfected with indicated short interfering RNAs (siRNAs), treated with vitamin D (100 nM) for 24 h (means ± s.d., n = 3) (**d**) and qPCR (means ± s.d., n = 3, *P < 0.005, **P > 0.2) (**e**). Ctrl, control. **f**, Time-dependent ChIP analyses using 293F cells with vitamin D (100 nM) treatments for the indicated times. **g**, DNMT activity using Flag-VDIR immunoprecipitants (IP) in vitamin D/PTH-treated 293F cells. Activity (means ± s.d., n = 3) is shown as c.p.m. of S-adenosyl-L-[methyl-³H]-methionine incorporated into oligonucleotide substrate. Background activity was measured in the control experiments performed with Flag-alone immunoprecipitants.

transcriptional repression²³. Unlike other MBD family members, MBD4 functions in DNA repair as a thymine glycosylase to remove T/G mismatches generated after the deamination of 5mC (refs 10, 24). ChIP analyses showed that MBD4 was the only MBD protein identified at the *CYP27B1* promoter (Fig. 2c). MBD4 was co-immunoprecipitated with VDIR in the presence of vitamin D, and remained associated after co-treatment of vitamin D with PTH independent of the dissociation of DNMTs from VDIR (Fig. 2e). These hormonal effects were not seen in the reported MBD4-binding 5mCpG sites in the multidrug resistance (*MDR*, also known as *ABCB1*) gene promoter²⁵ (Supplementary Fig. 14). VDIR seemed to be indispensable for MBD4 recruitment to the promoter (Fig. 2f and Supplementary Fig. 15), presumably through

physical interaction (Supplementary Fig. 16). It was recently reported that in transcriptionally active promoters, demethylation of 5mCpGs requires DNMT3A/B for deamination of 5mCpGs for further T/G mismatch repair²⁶. However, in 293F cells pretreated with vitamin D for 24 h, DNMT1, DNMT3B or thymine-DNA glycosylase (TDG) was dispensable for PTH-induced demethylation of 5mCpGs within the *CYP27B1* promoter (Fig. 2g). Knockdown of *MBD4*, but not *MBD2*, blocked PTH-induced demethylation of 5mCpGs (Fig. 2h, i and Supplementary Fig. 17). Given the efficient binding of MBD4 to 5mCpG (ref. 10), we proposed that the DNA glycosylase activity of MBD4 induced active DNA demethylation of the 5mCpG sites. We tested this idea with an MBD4 mutant with a deletion in the putative

1008

©2009 Macmillan Publishers Limited. All rights reserved

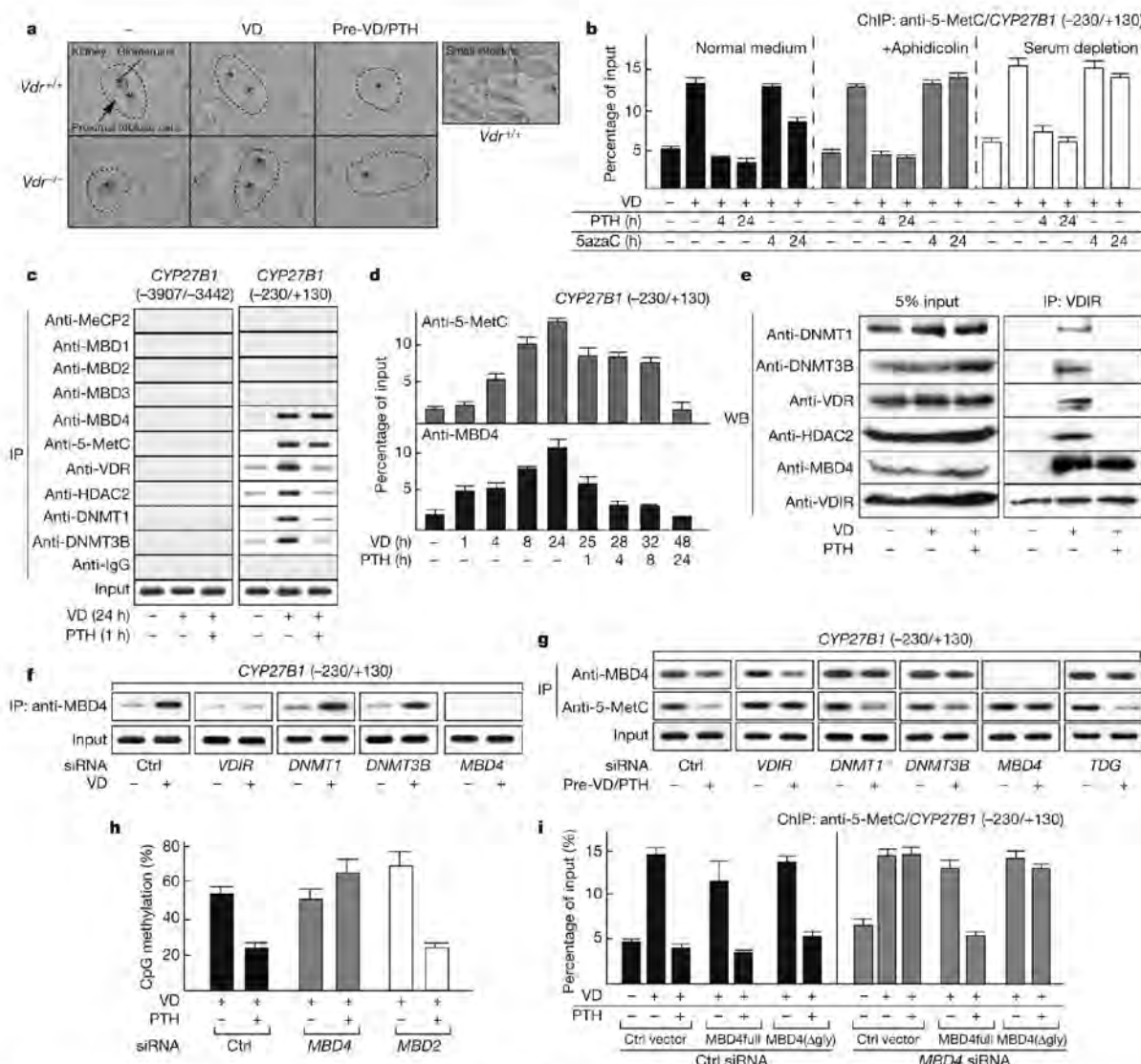


Figure 2 | MBD4 is indispensable for PTH-induced DNA demethylation in the *CYP27B1* promoter. **a**, *In vivo* BrdU incorporation in the kidney and small intestine (control) of mice with indicated genotypes. Proximal tubular cells surrounding the glomerulus (asterisk) are circled by a dashed line. Original magnification, $\times 200$. Experimental details are presented in Supplementary Fig. 11a. **b**, ChIP-qPCR analyses using 293F cells treated with aphidicolin (5 μ M) or cultured with serum-free DMEM (means \pm s.d., $n = 3$). 5-azaC, 5-azacytidine. **c**, **d**, ChIP analyses (**c**) and ChIP-qPCR analyses (means \pm s.d., $n = 3$) (**d**) using vitamin D/PTH-treated 293F cells. **e**, Western blotting (WB) using immunoprecipitates with anti-VDIR antibody in vitamin D/PTH-treated MCT cells. **f**, ChIP analyses using 293F

glycosylase catalytic domain (Δ gly) (Supplementary Figs 19a and 21a). This mutant was defective in PTH-induced DNA demethylation in cells deficient of endogenous MBD4 (Fig. 2i and Supplementary Fig. 18).

To test the idea that downstream signalling of PTH activates MBD4-mediated DNA demethylation, phosphorylation of putative sites on MBD4 by PKA and PKC (downstream signalling factors of PTH)¹³ was measured with recombinant proteins (Supplementary Fig. 19). MBD4 was phosphorylated by PKC *in vitro* (Fig. 3a) and in 293F cells (Fig. 3b and Supplementary Fig. 20). With MBD4 recombinant mutants, serine residues (165 and 262) were mapped as PKC-phosphorylation sites

(Fig. 3c). We addressed whether MBD4 has DNA glycosylase activity with mismatched and methylated CpG oligonucleotides, using TDG as a control, in *in vitro* assays^{23,26}. Strand incisions by unphosphorylated MBD4 were clearly seen in T/G mismatched oligonucleotides, confirming the reported glycosylase activity of MBD4 for T/G mismatch (Fig. 3d, e and Supplementary Fig. 21)^{10,26}. Although the direct DNA binding of MBD4 to both oligonucleotides was detected on electrophoretic mobility shift assays (EMSA) (Supplementary Fig. 22), strand incision of the methylated CpG oligonucleotides was less pronounced. However, strand incision of methylated CpG oligonucleotides was

cells transfected with indicated siRNAs for 24 h, and then treated with vitamin D (24 h). **g**, ChIP analyses using vitamin-D-treated 293F cells transfected with indicated siRNAs for 24 h, then further treated with PTH (24 h). **h**, Bisulphite sequencing using 293F cells transfected with indicated siRNAs for 24 h, then further treated with vitamin D and PTH (24 h) (means \pm s.d., three independent experiments, $n = 15$). **i**, ChIP-qPCR analyses of vitamin D/PTH-treated 293F cells transfected with siRNAs and rescue vectors containing wild-type MBD4 (MBD4full) or a MBD4(Δ gly) for 48 h in the presence or absence of vitamin D (48 h) and/or PTH (24 h) (means \pm s.d., $n = 3$).

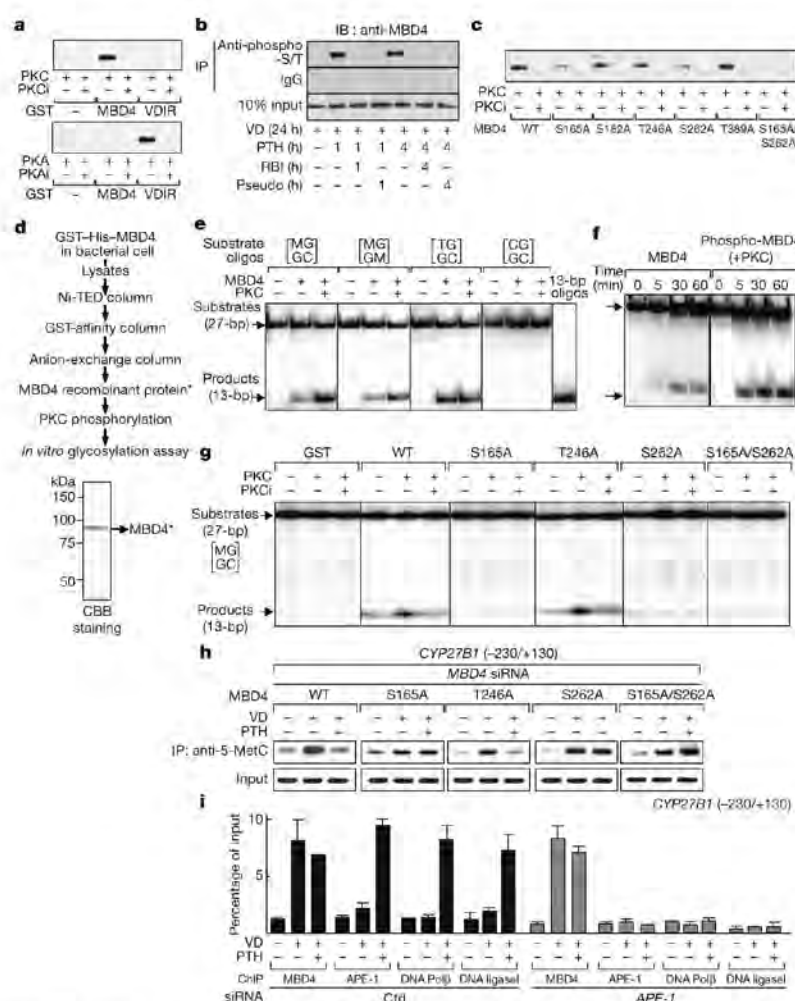


Figure 3 | The DNA glycosylase activity of MBD4 is potentiated by PKC-phosphorylation. **a**, In vitro kinase assay using GST-MBD4 and GST-VDIR with recombinant PKC or PKA. PKC inhibitors (PKCi; RBI and PKC pseudosubstrate) or a PKA inhibitor (H89) were added to the reactions as indicated. **b**, Western blotting with anti-MBD4 using immunoprecipitants with anti-phospho-S/T antibody on the treatments as indicated. **c**, In vitro kinase assay using recombinant MBD4 mutants, in which alanine replacements were introduced into the serine or threonine residues. **d**, In vitro glycosylation assay protocol (top) and CBB staining of human recombinant MBD4 (bottom). Experimental details of recombinant MBD4 preparations are presented in Supplementary Fig. 21. **e**, In vitro

glycosylation assay with 0.5 µg of recombinant MBD4 and 5 nM of indicated oligonucleotides: hemi-methylated CpG [MG/GC], symmetrical methylated CpG [MG/GM], mismatched [TG/GC] and unmethylated CpG [CG/GC]. The top arrow indicates substrates (27-base pair (bp) oligonucleotides) and the bottom arrow indicates breakage products (13-bp oligonucleotides). **f**, The kinetics of the PKC-mediated ³H-CpG glycosylation activity of MBD4 with MG/GC. **g**, In vitro glycosylation assay using phosphorylation-defective MBD4 mutants. **h**, ChIP analyses of 293F cells transfected with MBD4 siRNA and rescue vectors containing indicated MBD4 derivatives. **i**, ChIP-qPCR analyses of vitamin D/PTH-treated 293F cells transfected with APE-1 siRNAs (means ± s.d., n = 3).

significant when MBD4 was phosphorylated by PKC²² (Fig. 3e, f and Supplementary Fig. 23). A PKC inhibitor attenuated the enzymatic activity of MBD4 (Fig. 3g). Consistent with this, phosphorylation mutants attenuated PTH-induced DNA demethylation in 293F cells deficient in endogenous MBD4 (Fig. 3h), although their DNA-binding activities were retained (Supplementary Fig. 24). We then evaluated whether major factors responsible for DNA repair were involved in this mechanism^{11,26,27}. ChIP analyses showed that apurinic/apyrimidinic (AP) endonuclease-1 (APE-1, also known as APEX1), DNA ligase I and polymerase (Pol) β—components of the base-excision repair process—were recruited simultaneously to the promoter together with MBD4 (Fig. 3i and Supplementary Fig. 25). APE-1 was pivotal in the recruitment of these DNA repair factors (Fig. 3i). These data indicate that DNA demethylation is completed through a base-excision repair

process after glycosylation by MBD4. Consistent with the role of MBD4 in PTH-induced DNA demethylation, MBD4 knockdown reversed the effects of PTH on the *CYP27B1* promoter (Fig. 4a) and endogenous gene expression (Supplementary Fig. 26). Neither the MBD4 phosphorylation mutants nor the catalytic domain deletion mutant (Δgly) conferred a response to PTH (Fig. 4b and Supplementary Fig. 27). In ChIP analyses of the *CYP27B1* promoter, PTH-induced DNA demethylation was coupled to histone acetylation, H3K4 methylation and Ser-5-phosphorylated RNA Pol II recruitment⁷ (Fig. 4c and Supplementary Fig. 28). Such PTH-induced alterations were abolished by depletion of MBD4 (Fig. 4c).

Finally, the physiological role of MBD4 in PTH-induced derepression was tested in *Mbd4*^{-/-} mice. Vitamin D treatment for 3 days effectively suppressed endogenous *Cyp27b1* gene expression (Fig. 4d,

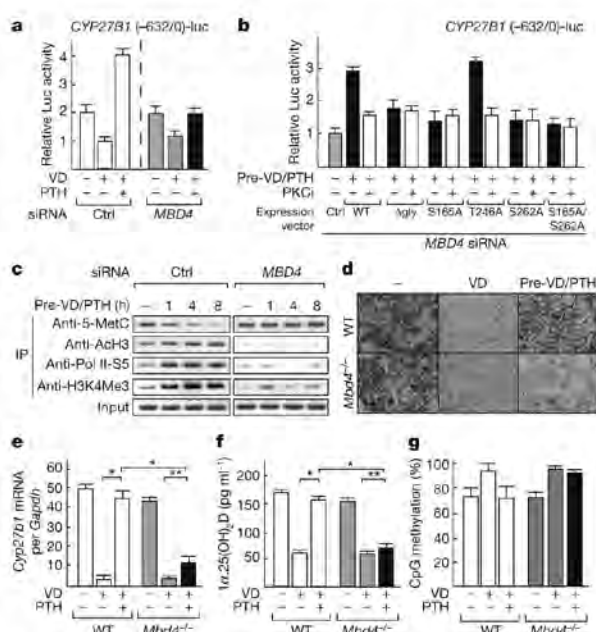


Figure 4 | MBD4-mediated DNA demethylation derepresses transcription of the vitamin D-transrepressed *CYP27B1* gene. **a**, Luciferase assay using 293F cells. The cells were transfected with MBD4 siRNA for 24 h, and luciferase reporter containing the *CYP27B1* (-632/0) promoter, in the presence or absence of vitamin D (48 h) and/or PTH (last 24 h) (means \pm s.d., $n = 3$). **b**, Luciferase assay using MBD4-knockdown 293F cells, transfected with phosphorylation-defective MBD4 mutants. **c**, ChIP analyses of vitamin D/PTH-treated 293F cells transfected with indicated siRNAs. **d**, *In situ* hybridization analysis of murine kidneys using antisense riboprobe for *Cyp27b1*. The *Cyp27b1* mRNAs (dark blue) are broadly localized in the uriniferous tubule cells. Original magnification, $\times 200$. **e**, **f**, qPCR from total RNAs isolated from murine kidneys (**e**) and serum levels of $1,25(\text{OH})_2\text{D}$ (**f**) with the indicated genotypes (wild type, *Mbd4*^{-/-} medium-chain triglyceride vehicle-treated group, $n = 4$; wild type, *Mbd4*^{-/-} vitamin-D-treated group, $n = 3$; wild type, *Mbd4*^{-/-} pre-vitamin-D-PTH-treated group, $n = 7$) (means \pm s.d., * $P < 0.001$, ** $P > 0.2$). **g**, Bisulphite sequencing using whole murine kidneys (means \pm s.d., three independent experiments, $n = 30$).

e) and induced DNA methylation in the kidneys of wild-type and *Mbd4*^{-/-} mice (Fig. 4g and Supplementary Fig. 29). Administration of PTH to vitamin-D-pretreated, wild-type mice derepressed *Cyp27b1*, as determined by qPCR with reverse transcription (qRT-PCR; Fig. 4e) and *in situ* hybridization (Fig. 4d). The recovery of serum $1,25(\text{OH})_2\text{D}$ levels (Fig. 4f) as well as DNA demethylation (Fig. 4g) were consistently seen. In *Mbd4*^{-/-} mice, PTH effects were significantly impaired (Fig. 4d–g), confirming the *in vitro* observations.

Active DNA demethylation has been implicated in the derepression of silenced gene promoters during early development^{2–3}. The involvement of active DNA demethylation of gene promoters for regulated transcription is, however, largely unknown. Here we found that DNA methylation/demethylation that determined the function of the *CYP27B1* gene promoter was regulated by hormonal switching (see Supplementary Fig. 1). Transcriptional derepression of the *CYP27B1* gene by active DNA demethylation was hormonally inducible. Thus, epigenetic switching at the DNA level reflects, at least in part, well-established hormonal actions on gene regulation.

Hormonally regulated DNA demethylation of the *CYP27B1* gene promoter is mediated by glycosylase activity of MBD4 by PKC-mediated phosphorylation. Although MBD4 is involved in repairing mismatched T/G, structural alteration of MBD4 caused by phosphorylation may shift its substrate specificity. Considering the association

of base-excision repair factors with MBD4 on 5mCpG sites in the *CYP27B1* gene promoter, it is likely that this form of active DNA demethylation involves a base-excision repair process. The dissociation of DNMTs from VDIR and MBD4 in the presence of PTH seems to preclude re-methylation of the repaired cytosine. Thus, DNA repair-mediated DNA demethylation in metazoans is probably accomplished by diverse processes that are dependent on the epigenetic context^{25,28–30}.

METHODS SUMMARY

Biochemical purification of VDIR-associated proteins. Preparation of the nuclear extracts, anti-Flag affinity purification, and mass spectrometry were performed as previously described¹⁷. Details are provided in Supplementary Methods.

***In vitro* glycosylation assay.** *In vitro* glycosylation assays were performed essentially as previously described^{10,25,26}. Recombinant GST-MBD4 and its derivatives were purified from *Escherichia coli*, and subjected to a phosphorylation reaction by PKC. 5'-end [γ -³²P]-ATP-labelled DNA substrates were incubated with phosphorylated or non-phosphorylated GST-MBD4 as detailed in the Supplementary Methods.

Bisulphite sequencing and methyl-specific PCR. Genomic DNA was isolated from cell lines and wild-type or *Mbd4*-deficient mice, treated with vehicle, vitamin D or PTH as indicated. Bisulphite treatment and sequencing were performed as described. Results are representative of at least three independent experiments. Details are provided in Supplementary Methods.

DNMT assay. The VDIR complex was purified by immunoprecipitation. 293F cells were transfected as indicated with Flag-tagged VDIR, and cultured in the presence or absence of vitamin D for 24 h, and then PTH for 24 h. After 48 h, the cells were collected, and the Flag-tagged VDIR complex was purified by Flag M2 agarose (Sigma). DNA methyltransferase activity was found in the VDIR immunoprecipitates from the 293F cells only after treatment with vitamin D. Activity is displayed as counts per minute (c.p.m.) of S-adenosyl-L-[methyl-³H]-methionine incorporated into an oligonucleotide substrate.

Received 18 August 2008; accepted 24 August 2009.

- Goldberg, A. D., Allis, C. D. & Bernstein, E. Epigenetics: a landscape takes shape. *Cell* **128**, 635–638 (2007).
- Trojer, P. & Reinberg, D. Histone lysine demethylases and their impact on epigenetics. *Cell* **125**, 213–217 (2006).
- Reik, W. Stability and flexibility of epigenetic gene regulation in mammalian development. *Nature* **447**, 425–432 (2007).
- Bird, A. Perceptions of epigenetics. *Nature* **447**, 396–398 (2007).
- Egger, G., Liang, G., Aparicio, A. & Jones, P. A. Epigenetics in human disease and prospects for epigenetic therapy. *Nature* **429**, 457–463 (2004).
- Murayama, A. et al. The promoter of the human 25-hydroxyvitamin D₃ 1 α -hydroxylase gene confers positive and negative responsiveness to PTH, calcitonin, and $1,25(\text{OH})_2\text{D}_3$. *Biochem. Biophys. Res. Commun.* **249**, 11–16 (1998).
- Murayama, A. et al. Transrepression by a liganded nuclear receptor via a bHLH activator through co-regulator switching. *EMBO J.* **23**, 1598–1608 (2004).
- Brenza, H. L. et al. Parathyroid hormone activation of the 25-hydroxyvitamin D₃ 1 α -hydroxylase gene promoter. *Proc. Natl. Acad. Sci. USA* **95**, 1387–1391 (1998).
- Rhee, I. et al. DNMT1 and DNMT3b cooperate to silence genes in human cancer cells. *Nature* **416**, 552–556 (2002).
- Hendrich, B. et al. The thymine glycosylase MBD4 can bind to the product of deamination at methylated CpG sites. *Nature* **401**, 301–304 (1999).
- Jiricny, J. & Menigatti, M. DNA cytosine demethylation: are we getting close? *Cell* **135**, 1167–1169 (2008).
- Millar, C. B. et al. Enhanced CpG mutability and tumorigenesis in MBD4-deficient mice. *Science* **297**, 403–405 (2002).
- Potts, J. T. & Gardella, T. J. Progress, paradox, and potential: parathyroid hormone research over five decades. *Ann. NY Acad. Sci.* **1117**, 196–208 (2007).
- Chambon, P. A decade of molecular biology of retinoic acid receptors. *FASEB J.* **10**, 940–954 (1996).
- Hausler, M. R. et al. The nuclear vitamin D receptor: biological and molecular regulatory properties revealed. *J. Bone Miner. Res.* **13**, 325–349 (1998).
- McKenna, N. J. & O'Malley, B. W. Combinatorial control of gene expression by nuclear receptors and coregulators. *Cell* **108**, 465–474 (2002).
- Ohtake, F. et al. Dioxin receptor is a ligand-dependent E3 ubiquitin ligase. *Nature* **446**, 562–566 (2007).
- Fuks, F. et al. DNA methyltransferase Dnmt1 associates with histone deacetylase activity. *Nature Genet.* **24**, 88–91 (2000).
- Maison, C. & Almouzni, G. HPI and the dynamics of heterochromatin maintenance. *Nature Rev. Mol. Cell Biol.* **5**, 296–305 (2004).
- Yoshizawa, T. et al. Mice lacking the vitamin D receptor exhibit impaired bone formation, uterine hypoplasia and growth retardation after weaning. *Nature Genet.* **16**, 391–396 (1997).

LETTERS

NATURE | Vol 461 | 15 October 2009

21. Takezawa, S. *et al.* A cell cycle-dependent co-repressor mediates photoreceptor cell-specific nuclear receptor function. *EMBO J.* **26**, 764–774 (2007).
22. Ballestar, E. & Wolffe, A. P. Methyl-CpG-binding proteins. Targeting specific gene repression. *Eur. J. Biochem.* **268**, 1–6 (2001).
23. Zhu, B. *et al.* 5-Methylcytosine DNA glycosylase activity is also present in the human MBD4 (G/T mismatch glycosylase) and in a related avian sequence. *Nucleic Acids Res.* **28**, 4157–4165 (2000).
24. El-Osta, A., Kantharidis, P., Zalcberg, J. R. & Wolffe, A. P. Precipitous release of methyl-CpG binding protein 2 and histone deacetylase 1 from the methylated human multidrug resistance gene (*MDR1*) on activation. *Mol. Cell. Biol.* **22**, 1844–1857 (2002).
25. Métiévier, R. *et al.* Cyclical DNA methylation of a transcriptionally active promoter. *Nature* **452**, 45–50 (2008).
26. Waters, T. R., Gallinari, P., Jiricny, J. & Swann, P. F. Human thymine DNA glycosylase binds to apurinic sites in DNA but is displaced by human apurinic endonuclease 1. *J. Biol. Chem.* **274**, 67–74 (1999).
27. Tini, M. *et al.* Association of CBP/p300 acetylase and thymine DNA glycosylase links DNA repair and transcription. *Mol. Cell* **9**, 265–277 (2002).
28. Gehring, M. *et al.* DEMETER DNA glycosylase establishes MEDEA polycomb gene self-imprinting by allele-specific demethylation. *Cell* **124**, 495–506 (2006).

29. Barreto, G. *et al.* *Gadd45a* promotes epigenetic gene activation by repair-mediated DNA demethylation. *Nature* **445**, 671–675 (2007).
30. Kangaspeka, S. *et al.* Transient cyclical methylation of promoter DNA. *Nature* **452**, 112–115 (2008).

Supplementary Information is linked to the online version of the paper at www.nature.com/nature.

Acknowledgements We thank A. Murayama, K. Saito and A. Matsukage for discussions, Y. Imai and R. Fujiki for technical assistance, K. Sugawara for plasmids, and M. Yamaki and H. Yamazaki for preparing the manuscript. This work was supported in part by priority areas from the Ministry of Education, Culture, Sports, Science and Technology (to F.O. and S.K.).

Author Contributions M.-S.K., F.O. and S.K. designed the experiments. M.-S.K., S.F. and F.O. performed biochemical assays. M.-S.K., M.-Y.Y., Y.Y., Y.S. and I.Y. conducted the promoter analysis. T.K., S.T. and T.M. carried out the animal study. M.-S.K. and K.-I.T. were responsible for the data interpretation. M.-S.K. and S.K. wrote the manuscript. All authors discussed the results and commented on the manuscript.

Author Information Reprints and permissions information is available at www.nature.com/reprints. Correspondence and requests for materials should be addressed to S.K. (uskato@mail.ecc.u-tokyo.ac.jp).

分子代謝学分野

小川 佳宏

医歯学総合研究科・器官システム制御学系専攻
内分泌学・教授



1) 研究の課題名

1) 脂肪細胞とマクロファージの相互作用における転写因子ATF3の病態生理的意義に関する研究

近年、動脈硬化と同様に、肥満の脂肪組織においてもマクロファージの浸潤が増加することが明らかになり、マクロファージがメタボリックシンドロームの発症および進展の重要な担い手であると想定されている。我々は既に、脂肪細胞に由来する飽和脂肪酸が自然免疫反応に中心的な役割を果たす4型Toll様受容体（TLR4）の内在性リガンドとしてマクロファージを活性化することを証明し、メタボリックシンドロームの病態形成に関与することを見出した。更に、マクロファージにおける飽和脂肪酸の標的分子としてATF3を同定し、ATF3が肥満の脂肪組織に浸潤するマクロファージに高発現することを明らかにした。培養マクロファージを用いた検討により、ATF3は飽和脂肪酸/TLR4/NF- κ B経路の負の制御因子として作用することが明らかになった。実際、マクロファージ特異的にATF3を過剰発現するトランスジェニックマウスでは、肥満に伴うマクロファージの活性化が減弱しており、ATF3が慢性炎症を基盤とするメタボリックシンドロームの新しい創薬ターゲットとなる可能性が示唆された（Circ. Res. 105:25-32, 2009）。

2) 腎臓障害におけるレプチンの単球/マクロファージ機能調節作用に関する研究

レプチンは脂肪組織に由来する代表的なアディポサイトカインであり、主に視床下部を介して強力に摂食量の減少とエネルギー代謝の亢進をもたらす。肥満と体重増加を制御する。本研究では、一側尿管結紮（Unilateral Ureteral Obstruction; UUO）によるマウス腎臓細管間質障害モデルを用いて、単球/マクロファージ機能調節におけるレプチンの病態生理的意義を検討した。遺伝的にレプチンを欠損するob/obマウスでは、野生型マウス

と比較して、UUOによるマクロファージ浸潤が著しく抑制されていた。レプチン受容体遺伝子に変異を有するdb/dbマウスにおいてもob/obマウスと同様に腎臓障害の明らかな抑制が認められた。浸透圧ミニポンプによるレプチンの皮下投与によりob/obマウスにおいて観察されたマクロファージ浸潤の抑制が消失した。この時、ob/obマウスにレプチンを脳室内投与すると、皮下投与の場合と同様に腎臓へのマクロファージ浸潤が増加し、その効果はメラノコルチン3型および4型受容体のアンタゴニスト（SHU9119）の同時投与によりほぼ完全に遮断された。腎臓細管間質障害モデルにおいて、レプチン欠損は腎臓マクロファージ浸潤に対して抑制的に作用することが明らかとなり、視床下部メラノコルチン系の関与が示唆された（Endocr. J. 2009 Oct 23. [Epub ahead of print]）。

3) 肥満の脂肪組織におけるDNAメチル化酵素に関する研究

これまで遺伝素因によるところが大きいと考えられてきた「太りやすい」体質の原因に、栄養環境を含めた環境因子が少なからず影響を与えていることが明らかとなりつつある。従来、DNAのメチル化は、個体発生の時期や癌形成の過程を除いて、一生のうちに変化することは殆どないと考えられてきた。しかしながら、最近では、環境因子によるDNAメチル化状態の変化が指摘されている。我々は、肥満の脂肪組織ではDNAメチル化酵素のうちde novo（新規）DNAメチル化酵素（Dnmt3a）の遺伝子発現が増加することを見出し、DNAメチル化のダイナミックな変化を想定した。肝臓や筋肉等他の臓器では変化せず、他のDnmtsの中で唯一Dnmt3aだけが増加した。そこで、脂肪組織でDnmt3aを特異的に過剰発現するトランスジェニックマウスを作成した。Dnmt3aの過剰発現により我々はがん抑制遺伝子SFRP1

遺伝子のプロモーターのDNAメチル化のわずかな増加と、その遺伝子発現のわずかな抑制を観察した。一般的にDNAメチル化は遺伝子発現抑制に働くことが知られる。肥満により発現が減少する遺伝子が多い。このようなdown-regulateのメカニズムの一部にDnmt3aを介したDNAメチル化が機能するかもしれない。一方、Dnmt3aマウスでIRF9の遺伝子発現増加が観察された。IRF9はインターフェロン α/β シグナリングの下流の転写因子である。また、普通食を与えた場合に比べ、高脂肪食を与えたDnmt3aマウスの脂肪組織では炎症性遺伝子TNF α やMCP1の遺伝子発現の増加が観察された (Obesity 2009 Aug 13. [Epub ahead of print])。

4) 骨格筋萎縮における転写因子FOXO1の標的遺伝子の探索

骨格筋はヒトの体重の約40%の重量を占め、インスリンの標的組織として糖代謝に重要な役割を果たしており、適度な運動による骨格筋機能の活性化は、糖尿病の予防および病態の改善に有効であること、糖尿病患者の骨格筋では豊富にミトコンドリアを含有する赤筋の割合が減少することが知られている。以上より、骨格筋量の調節機構を解明し、糖尿病における骨格筋減少の予防法を開発することは臨床的に極めて重要である。我々は既に、ストレプトゾトシン負荷によるインスリン分泌低下型糖尿病や絶食時のマウスの骨格筋において、フォークヘッド型転写調節因子であるFOXO1が著しく増加すること、これが骨格筋、特に赤筋線維萎縮を誘導することを証明した。従来、FOXO1はインスリンシグナルに拮抗すること知られているが、骨格筋萎縮におけるFOXO1の病態生理的意義については不明な点が多い。

本研究では、骨格筋におけるFOXO1の標的遺伝子の探索をおこなっている。骨格筋におけるFOXO1の標的遺伝子の同定とその発現調節が明らかになるため、FOXO1を起点とした骨格筋萎縮の分子機構の全貌が明らかになる。例えば、我々は、蛋白質分解酵素であるカテプシンL遺伝子がFOXO1の標的遺伝子であることを予備的に確認しており、この機能的意義を検証する。本研究により、FOXO1の標的遺伝子をターゲットとした新しい抗骨格筋萎縮創薬と新しい骨格筋萎縮抑制作用を有する薬剤の探索系が確立される。本研究により、糖尿病におけるインスリン作用障害の分子機構の解明と骨格筋萎縮を標的とした新しい糖尿病の治療法の確立および糖尿病患者のQOLの向上が期待される。

5) 血管線維化病変形成におけるcGMPキナーゼ (cGK) およびcGKによるRhoASer188リン酸化の意義に関する研究

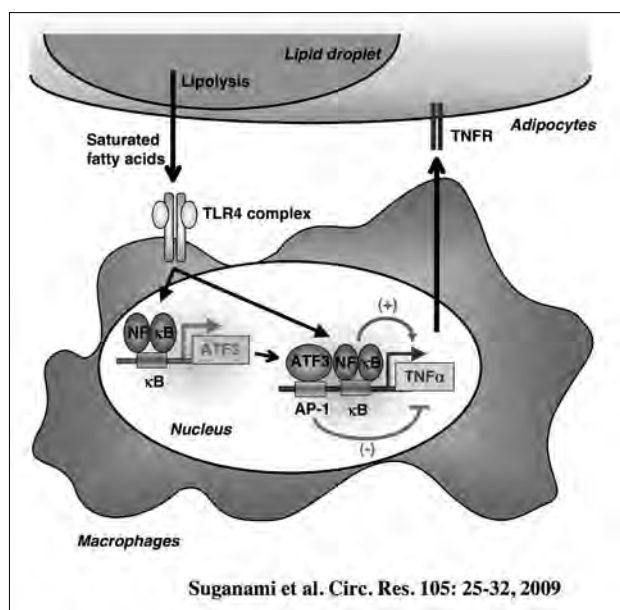
高血圧症・動脈硬化症に随伴する血管周囲線維化は、虚血性脳心疾患の重要な基盤病態であるにもかかわらず、いまだ有効な治療法が確立されていない。線維化の促進および抑制に与る複数の細胞内経路がこれまでに同定されているが、これらシグナル間の協調・拮抗の統御機構は不明であり、その解明により有効な抗線維化療法の開発へ寄与することが期待される。ナトリウム利尿ペプチド (NPs) は血管平滑筋 (VSMCs) における肥大や線維化形成を著明に抑制する。我々は、NPsの下流エフェクターであるI型cGK (cGK I) のヘテロ欠損マウスを用いた検討により、内因性cGK I活性の抑制により低分子量G蛋白RhoA-Rhoキナーゼ経路の活性化を介して線維化病変が誘導されることを見いだした。さらに我々が以前報告したcGK IによるRhoAのリン酸化部位Ser188をAla188に置換した変異体RhoAをVSMCに発現するマウスの作成および解析を通じて、NPs-cGK系による血管線維化抑制作用は、cGK IによるRhoAのリン酸化・機能抑制を介していることを明らかにした。本研究により、線維化促進経路であるRhoA-Rhoキナーゼ系と線維化抑制経路であるNPs-cGK I系は、cGK IによるRhoAのリン酸化を介してクロストークすることが明らかにされた (Mol. Cell Biol. 29:6018-6032, 2009)。

6) 血管内皮Rac1による脳神経細胞保護作用の研究

外因性神経栄養因子による脳神経疾患治療が従来試みられてきたが、血液脳関門が障害となり脳組織への十分な浸透を達成できず臨床応用が困難であった。最近、血管が隣接神経細胞と相互作用して神経の保護・機能調節に与ることが注目されている (神経-血管ユニット; Neurovascular unit) が、その分子機序は未解明である。我々は血管内皮機能制御における中心的メディエータとして低分子量G蛋白Rac1に注目している。血管内皮特異的Rac1ヘテロノックアウトマウスを用いて、脳梗塞モデル (中大脳動脈一過性閉塞) を作成したところ、対照に比して梗塞サイズおよび脳浮腫が著明に減少した。Rac1^{+/-}およびRac1^{+/+}マウス内皮間でマイクロアレイ解析を施行したところ、Rac1^{+/-}内皮で神経・血管保護に関わる3つの遺伝子カテゴリー、すなわち1.ストレス応答因子、2.血管基底膜構成因子、3.神経栄養因子、の発現上昇が認められた。Rac1^{+/-}内皮細胞では、低酸素負荷下の生存性上昇および透過性の減少、さらに単層形

成後の酵素消化耐性の上昇が認められ、遺伝子発現プロファイルに合致するフェノタイプと考えられた。さらに、Rac1+/-内皮細胞と大脳皮質神経細胞の共培養下において、酸素糖除去刺激で誘導される神経細胞死が減弱した。Rac1+/-内皮細胞において artemin を含む神経栄養因子の分泌が上昇しており、パラクライン機序による内皮由来神経保護活性の上昇が明らかになった (Expert. Rev. Neurother. 9:1171-1186, 2009)。

2)



3) 研究内容の英文要約

1) Activating Transcription Factor 3 Constitutes a Negative Feedback Mechanism that Attenuates Saturated Fatty Acid/Toll-like Receptor 4 Signaling and Macrophage Activation in Obese Adipose Tissue

Obese adipose tissue is markedly infiltrated by macrophages, suggesting that they may participate in the inflammatory pathways that are activated in obese adipose tissue. Evidence has suggested that saturated fatty acids released via adipocyte lipolysis serve as a naturally occurring ligand that stimulates TLR4 signaling, thereby inducing the inflammatory responses in macrophages in obese adipose tissue. Through a combination of cDNA microarray analyses of saturated fatty acid-stimulated macrophages in vitro and obese adipose tissue in vivo, here we identified ATF3, a member of the ATF/cAMP response element-binding protein family of basic leucine zipper-type transcription factors, as a target gene of saturated fatty acids/TLR4 signaling in macrophages in obese adipose tissue. Importantly, ATF3, when induced by saturated fatty acids, can transcriptionally repress

TNF α production in macrophages in vitro. Furthermore, transgenic overexpression of ATF3 specifically in macrophages results in the marked attenuation of pro-inflammatory M1 macrophage activation in the adipose tissue from genetically obese KKA^y mice fed high-fat diet. This study provides evidence that ATF3, which is induced in obese adipose tissue, acts as a transcriptional repressor of saturated fatty acids/TLR4 signaling, thereby revealing the negative feedback mechanism that attenuates obesity-induced macrophage activation. Our data also suggest that activation of ATF3 in macrophages offers a novel therapeutic strategy to prevent or treat obesity-induced adipose tissue inflammation (Circ. Res. 105: 25-32, 2009)

2) Role of central leptin signaling in renal macrophage infiltration

Monocytes/macrophages are key mediators of wound repair, tissue remodeling, and inflammation. However, the molecular mechanisms underlying macrophage recruitment to the site of inflammation is not fully understood. Leptin acts directly on the hypothalamus, thereby regulating food intake and energy expenditure. The leptin receptor, a single transmembrane protein that belongs to the gp130 family of cytokine receptor superfamily, is expressed not only in the hypothalamus but in a variety of peripheral tissues, suggesting the role of leptin as a pro-inflammatory adipocytokine in peripheral tissues. Here, we show that deficiency of leptin signaling reduces renal macrophage infiltration after UUO. Bone marrow transplantation studies using leptin signaling-deficient db/db mice revealed that leptin signaling in bone marrow cells may not play a major role in the UUO-induced renal macrophage infiltration. Interestingly, central leptin administration reverses the otherwise reduced UUO-induced renal macrophage infiltration in leptin-deficient ob/ob mice. This is effectively abolished by central co-administration of SHU9119, a melanocortin-3 receptor/melanocortin-4 receptor antagonist. This study demonstrates that central leptin administration in ob/ob mice accelerates renal macrophage infiltration through the melanocortin system, thereby suggesting that the central nervous system, which is inherent to integrate information from throughout the organism, is able to control peripheral inflammation (Endocr. J. 2009 Oct 23. [Epub ahead of print]) .

3) Increased expression of DNA methyltransferase 3a in obese adipose tissue: studies with transgenic mice overexpressing Dnmt3a

Obesity arises from a complex interaction between genetic and environmental factors, but the molecular basis of the interaction is poorly understood. Epigenetic mechanisms are likely to be involved in the development of obesity. DNA methylation is a key epigenetic contributor to the

maintenance of gene silencing. In mammals, three CpG DNA methyltransferases, Dnmt1, Dnmt3a and Dnmt3b, coordinately regulate the methylation of DNA in the genome. Studies with Dnmts have focused mainly on development and cancer. However, their role in normal adult tissues, including the adipose tissue, remains largely unclear. Here, we show that Dnmt3a mRNA expression is markedly increased in obese adipose tissue. The data of this study also demonstrates that transgenic overexpression of Dnmt3a in the adipose tissue increases expression of some proinflammatory genes during a high-fat diet. This study highlights the potential role of Dnmt3a in the adult tissue as well as in the developing embryo and cancer (Obesity 2009 Aug 13. [Epub ahead of print]) .

4) Molecular target of skeletal muscle atrophy, focusing on a forkhead-transcription factor, FOXO1

Skeletal muscle is the largest organ in the human body, comprising about 40% of body weight. Skeletal muscle accounts for the majority of insulin-stimulated glucose uptake in the body. It is well known that exercise training, such as walking, improves skeletal muscle activity and decreases the incident rate of diabetes. The number of type I muscle fibers (mitochondria rich, red fibers) is reduced in diabetic subjects compared with controls. Muscle atrophy is caused by various diseases, including diabetes, and severely decreases the quality of life. Detailed molecular mechanisms on this process need to be understood. Previously, we found that a transcription factor FOXO1 is markedly up-regulated in skeletal muscle during muscle atrophy (streptozotocin-induced diabetes and starvation) . Moreover, we established transgenic mice specifically overexpressing FOXO1 in their skeletal muscle. Interestingly, these mice showed reduced skeletal muscle mass with suppressed type I fiber gene expression. FOXO1 acts negatively as a downstream player in insulin signaling. However, the pathophysiological role of FOXO1 in skeletal muscle atrophy is still unclear. The present research investigates their detailed mechanisms, in vivo and in vitro, focusing on FOXO1. In this study, we are examining the gene expression events during muscle atrophy. We showed that FOXO1 enhanced expression of cathepsin L gene, which is involved in lysosomal proteolysis. Our working hypothesis is that cathepsin L is a direct target of FOXO1 in the skeletal muscle, and having a role of the FOXO1/cathepsin L pathway in diabetes-induced skeletal muscle metabolic change and atrophy. The results of this study are expected to provide further insight into the molecular basis of insulin resistance and possibilities for new treatments of diabetes-induced atrophy and other types of skeletal muscle atrophy, and possibly increase the quality of life.

5) cGMP kinase and RhoA Ser188 phosphorylation integrate pro- and anti-fibrotic signals in blood vessels

Vascular fibrosis is a major complication of hypertension and atherosclerosis, yet it is largely untreatable. Natriuretic peptides (NPs) repress fibrogenic activation of vascular smooth muscle cells (VSMCs) , but the intracellular mechanism mediating this effect remains undetermined. Here we show that inhibition of RhoA through phosphorylation at Ser188, the site targeted by the NP effector cyclic GMP (cGMP) -dependent protein kinase I (cGK I) , is critical to fully exert antifibrotic potential. cGK I^{+/-} mouse blood vessels exhibited an attenuated P-RhoA level and concurrently increased RhoA/ROCK signaling. Importantly, cGK I insufficiency caused dynamic recruitment of ROCK into the fibrogenic programs, thereby eliciting exaggerated vascular hypertrophy and fibrosis. Transgenic expression of cGK I-unphosphorylatable RhoA^{A188} in VSMCs augmented ROCK activity, vascular hypertrophy, and fibrosis more prominently than did that of wild-type RhoA, consistent with the notion that RhoA^{A188} escapes the intrinsic inhibition by cGK I. Additionally, VSMCs expressing RhoAA188 became refractory to the antifibrotic effects of NPs. Our results identify cGK I-mediated Ser188 phosphorylation of RhoA as a converging node for pro- and antifibrotic signals and may explain how diminished cGMP signaling, commonly associated with vascular malfunction, predisposes individuals to vascular fibrosis.

6) Targeting eNOS and beyond: Emerging heterogeneity of the role of endothelial Rho proteins in stroke protection

Currently available modalities for the treatment of acute ischemic stroke are aimed to preserve or augment cerebral blood flow (CBF) . Experimental evidence suggests that statins, which show 25-30% reduction of stroke incidence in clinical trials, confer stroke protection by upregulation of eNOS and increasing CBF. The upregulation of eNOS by statins is mediated by inhibition of small GTP-binding protein RhoA. Our recent study uncovered a unique role for a Rho-family member Rac1 in stroke protection. Rac1 in endothelium does not affect CBF. Instead, inhibition of endothelial Rac1 leads to broad upregulation of genes relevant to neurovascular protection. Intriguingly, inhibition of endothelial Rac1 enhances neuronal cell survival through endothelium-derived neurotrophic factors including artemin. This review discusses the emerging therapeutic opportunities to target the neurovascular signaling beyond the blood-brain barrier, with special emphasis on the novel role of endothelial Rac1 in stroke protection (Expert. Rev. Neurother. 9:1171-1186, 2009) .

4) 本事業に関連して世界的な研究拠点形成に向けて、以下の点で改善・整備等されたこと

C (人材確保)

ハーバード大学より国際PIシャペロンとして澤田直樹博士が帰国した。

D (人材育成)

本事業に先立つ21世紀COE事業にて支援を受けた大学院生(SS学生)が本年11月よりカリフォルニア州立大学ロサンゼルス校・HHMI (Peter Tontonoz研究室) に留学した。

E (国際化)

国際PIシャペロン(澤田直樹)がハーバード大学(Beth Israel Deaconess Medical Center: Zoltan Arany研究室)と共同研究を展開した。

5) GCOE事業を推進するに当たって力を入れた点

国際PIシャペロン(澤田直樹)による国際共同研究の推進

6) 英文原著論文

1. T. Suganami, X. Yuan, Y. Shimoda, K. Uchio-Yamada, N. Nakagawa, I. Shirakawa, T. Usami, T. Tsukahara, K. Nakayama, Y. Miyamoto, K. Yasuda, J. Matsuda, Y. Kamei, S. Kitajima, Y. Ogawa. Activating transcription factor 3 constitutes a negative feedback mechanism that attenuates saturated fatty acid/Toll-like receptor 4 signaling and macrophage activation in obese adipose tissue. *Circ. Res.* 105:25-32, 2009.
2. Y. Kamei, T. Suganami, T. Ehara, S. Kanai, K. Hayashi, Y. Yamamoto, S. Miura, O. Ezaki, M. Okano, Y. Ogawa. Increased expression of DNA methyltransferase 3a in obese adipose tissue: studies with transgenic mice. *Obesity* 2009 Aug 13.
3. N. Satoh, A. Shimatsu, K. Kotani, A. Himeno, H. Yamakage, T. Majima, K. Yamada, T. Suganami, Y. Ogawa. Highly purified eicosapentaenoic acid reduces cardio-ankle vascular index in association with decrease in serum amyloid A-LDL in metabolic syndrome. *Hypertens. Res.* 32:1004-1008, 2009.
4. M. Tanaka, T. Suganami, S. Sugita, Y. Shimoda, M. Kasahara, S. Aoe, M. Takeya, S. Takeda, Y. Kamei, Y. Ogawa. Role of central leptin signaling in renal macrophage infiltration under unilateral ureteral obstruction. *Endocr. J.* 2009 Oct 23.
5. N. Satoh, A. Shimatsu, A. Himeno, Y. Sasaki, H. Yamakage, K. Yamada, T. Suganami, Y. Ogawa. Unbalanced M1/M2 phenotype of peripheral blood

monocytes in obese diabetic patients: effect of pioglitazone. *Diabetes Care* .

6. N. Sawada, H. Itoh, K. Miyashita, H. Tsujimoto, M. Sone, K. Yamahara, Z.P. Arany, F. Hofmann, K. Nakao. cGMP kinase and RhoA Ser188 phosphorylation integrate pro- and anti-fibrotic signals in blood vessels. *Mol. Cell Biol.* 29:6018-6032, 2009.
7. N. Sawada, J.K. Liao. Targeting eNOS and beyond: emerging heterogeneity of the role of endothelial Rho proteins in stroke protection. *Expert. Rev. Neurother.* 9:1171-1186, 2009.

7) 平成21年度までの自己評価

過去数年間進めてきた研究テーマはそれぞれがまとまってきたが、今後、研究テーマの選択と集中を通して、よりスケールの大きな研究を推進したい。関連領域の若手の人材育成は順調に進んでいると考えている。

8) 学会発表 (英文)

© N. Sawada, Y. Ogawa, J. K. Liao: Rac1 GTPase is a critical mediator of endothelium-derived neurotrophic activity. *Keystone Symposia 2010*. 示説 Keystone, Colorado, USA. February 28-March 5, 2010.

© T. Suganami, Y. Ogawa: Role of saturated fatty acid/TLR4 signaling in macrophages in obesity-induced adipose tissue inflammation. *The 17th International Symposium on Molecular Cell Biology of Macrophages 2009*. 口頭 Kanazawa, Japan. Jul.3-4, 2009.

© T. Suganami, X. Yuan, N. Nakagawa, I. Shirakawa, Y. Kamei, Y. Ogawa: Activating transcription factor 3 constitutes a negative feedback mechanism that attenuates saturated fatty acid/TLR4 signaling and macrophage activation in obese adipose tissue. *Keystone Symposia 2010*. 示説 Banff, Canada. February 12-17, 2010.

9) 学会発表 (和文)

1. 小川佳宏:「TLR4の内因性リガンドとしての飽和脂肪酸」:日本薬学会第129年会,2009.3.26-28,京都
2. 伊藤綾香、菅波孝祥、山内明、山内三爵子、神山隆治、喜田中都、平田結緒、金ヶ寄史朗、亀井康富、小川佳宏:「肥満の脂肪組織におけるマクロファージ浸潤の分子機構」:第46回日本臨床分子医学会学術集会,2009.4.12-13,東京
3. 菅波孝祥、小川佳宏:「肥満細胞組織の炎症性変化における脂肪組織とマクロファージの相互作用の意義」:第82回日本内分泌学会学術総会,2009.4.23-25,群馬
4. 田中都、菅波孝祥、杉田聡、竹屋元裕、笠原正登、

- 竹田秀、小川佳宏:「中枢神経系を介するレプチンの炎症調節作用」:第82回日本内分泌学会学術総会,2009.4.23-25,群馬
5. 小川佳宏、菅波孝祥:「脂肪細胞リモデリング」:第52回日本糖尿病学会年次学術集会,2009.5.21-24,大阪
6. 小川佳宏、亀井康富:「メタボリックシンドロームのエピジェネティクス制御」:第9回日本抗加齢医学会総会,2009.5.28-29,東京
7. 小川佳宏、菅波孝祥:「発生工学的手法によるメタボリックシンドローム関連遺伝子の機能解析」:第45回高血圧関連疾患モデル学会学術総会,2009.9.4-5,東京
8. 菅波孝祥、小川佳宏:「肥満の脂肪組織炎症における脂肪細胞とマクロファージの相互作用」:第30回日本肥満学会,2009.10.9-10,静岡
9. 伊藤綾香、菅波孝祥、袁勲梅、宇佐美貴子、亀井康富、小川佳宏:「脂肪細胞特異的MKP-1過剰発現トランスジェニックマウスの作製と表現型の解析」:第30回日本肥満学会,2009.10.9-10,静岡
10. 杉田聡、亀井康富、赤池史子、菅波孝祥、金井紗綾香、三浦進司、江崎治、小川佳宏:「骨格筋特異的RXR γ 過剰発現マウスは糖代謝改善作用を示す」:第30回日本肥満学会,2009.10.9-10,静岡
11. 田中都、菅波孝祥、杉田聡、青江誠一郎、亀井康富、小川佳宏:「中枢神経系を介するレプチンの炎症・免疫調節作用」:第30回日本肥満学会,2009.10.9-10,静岡
12. 亀井康富、菅波孝祥、江原達弥、金井紗綾香、三浦進司、江崎治、小川佳宏:「肥満とDNAメチル化:DNAメチル化酵素遺伝子改変マウスとメチル化促進飼料による検討」:第30回日本肥満学会,2009.10.9-10,静岡
13. 中川信貴、菅波孝祥、袁勲梅、白川伊吹、亀井康富、岡淳一郎、小川佳宏:「脂肪組織マクロファージにおける新規炎症抑制性転写因子ATF3の機能的意義の検討」:第30回日本肥満学会,2009.10.9-10,静岡
14. 山崎芳浩、亀井康富、三浦進司、杉田聡、赤池史子、金井紗綾香、平田結喜緒、江崎治、菅波孝祥、小川佳宏:「骨格筋におけるFOXO1によるタンパク分解酵素カテプシンL遺伝子の転写調節」:第30回日本肥満学会,2009.10.9-10,静岡
15. 伊藤美智子、中川信貴、菅波孝祥、亀井康富、小川佳宏:「ヒトNASH様病変を呈する新しいマウスモデルの確立-MC4R欠損マウスの解析-」:第30回日本肥満学会,2009.10.9-10,静岡
16. 小川佳宏:「メタボリックシンドロームと自然炎症」:

第82回日本生化学会大会,2009.10.21-24,神戸

17. 小川佳宏:「メタボリックシンドロームの基盤病態としての慢性炎症:脂肪組織リモデリングに焦点を当てて」:第32回日本分子生物学会年会,2009.12.9-12,横浜

10) 受賞

澤田直樹

First-place winner, 2009 Young Investigator's Award in Physiology, Pharmacology and Pathology. The American College of Cardiology.

菅波孝祥

平成21年 第24回 岡本研究奨励賞

田中都

第30回日本肥満学会 若手研究奨励賞

11) 外部資金の獲得状況

- ・科学研究費補助金、新学術領域
研究題目:メタボリックシンドロームにおける内因性リガンドと病原体センサーの機能的意義の解明
代表:小川佳宏
期間:平成21年-平成25年
研究費総額:4,160万円(本人分:2,560万円)
- ・科学研究費補助金、基盤B
研究題目:脂肪組織リモデリングと脂肪毒性の分子機構の解明
代表:小川佳宏
期間:平成20年-平成22年
研究費総額:410万円
- ・科学研究費補助金、挑戦的萌芽
研究題目:肥満に関連するDNAメチル化標的遺伝子の同定と機能解析
代表:小川佳宏
期間:平成20年-平成21年
研究費総額:140万円
- ・文科省JST橋渡し研究支援推進プログラム
研究題目:骨髄由来liver repair cell(LR細胞)の開発
代表:坂井田功
期間:平成21年
研究費総額:2,000万円(本人分:260万円)
- ・厚労省科学研究費補助金、難治性疾患克服研究事業
研究題目:中枢性摂食異常症に関する調査研究
代表:小川佳宏
期間:平成20年-平成25年
研究費総額:1,700万円(本人分:350万円)

- ・厚労省科学研究費補助金、地球規模保健課題推進研究事業

研究題目:肥満関連疾患のアジアと米国における遺伝疫学的検討とその対策に関する研究

代表:川上正舒

期間:平成21年

研究費総額:1,462万円(本人分:50万円)

- ・財団法人武田科学振興財団 2009年度特定研究助成金

研究題目:慢性炎症を基盤病態とする生活習慣病・癌に関する臓器横断的研究と医学応用

代表:小川佳宏

期間:平成21年

研究費総額:5,000万円(本人分:2,000万円)

- ・内藤記念科学奨励金(研究助成)

研究題目:メタボリックシンドロームにおける慢性炎症の病態生理的意義の解明と医学応用

代表:小川佳宏

期間:平成21年

研究費総額:300万円

12) 特別講演、招待講演

Y. Ogawa. Adipose tissue remodeling. The 2009 Pennington Scientific Symposia Series. US-Japan Nutrition and Metabolism Panel Annual Symposium. Emerging Issues in Energy Balance, Adipocyte Biology & Developmental Origins of Chronic Disease. 口頭 Baton Rouge, November 8-10, 2009.

13) 新聞、雑誌、TV報道

朝日新聞 2009年9月29日

毎日新聞 2009年11月13日

14) GCOE 総合講義サマリー

Obese adipose tissue is characterized by adipocyte hypertrophy, followed by increases in angiogenesis, macrophage infiltration, and pro-inflammatory adipocytokine production, suggesting the previously unrecognized dynamic changes, which may be referred to as "adipose tissue remodeling". Using an in vitro co-culture system composed of 3T3-L1 adipocytes and RAW264 macrophages, we have provided evidence that a paracrine loop involving saturated fatty acids and TNF α derived from adipocytes and macrophages, respectively, establishes a vicious cycle that aggravates inflammatory changes in obese adipose tissue. Interestingly, saturated fatty acids, which are released in large quantities from hypertrophied adipocytes via the macrophage-induced adipocyte lipolysis, serve as a

naturally occurring ligand for TLR4, thereby inducing the inflammatory changes in obese adipose tissue. Our data help elucidate the molecular mechanism of "adipose tissue remodeling" or obesity-induced adipose tissue inflammation.

15) 教室、分野や講座の准教授、講師、助教、特別研究員、ポスドク、指導を受けた大学院生の名前(AISSには○印)のリスト

亀井康富(准教授)

山本幸男(特任講師)、澤田直樹(特任講師)

菅波孝祥(助教)

伊藤綾香(ポスドク)、袁勲梅(ポスドク)

白川伊吹(ポスドク)、田中都(ポスドク)

樋口恵子(ポスドク)

伊藤美智子(学振特別研究員)

蜂屋瑠見(学振特別研究員)

山本貴信(大学院生)

山城健二(東京慈恵会医科大学:博士課程大学院生)

○山崎芳浩(大学院生)

杉田聡(学振特別研究員)

市岡誠之(社会人大学院生)

津田直人(社会人大学院生)

江原達弥(社会人大学院生)


南部宏英(社会人大学院生)

中川信貴(東京理科大学:修士課程大学院生)

服部真季(東京理科大学:卒業研究生)

Circulation Research

JOURNAL OF THE AMERICAN HEART ASSOCIATION

American Heart Association® 
Learn and LiveSM

Activating Transcription Factor 3 Constitutes a Negative Feedback Mechanism That Attenuates Saturated Fatty Acid/Toll-Like Receptor 4 Signaling and Macrophage Activation in Obese Adipose Tissue

Takayoshi Suganami, Xunmei Yuan, Yuri Shimoda, Kozue Uchio-Yamada, Nobutaka Nakagawa, Ibuki Shirakawa, Takako Usami, Takamitsu Tsukahara, Keizo Nakayama, Yoshihiro Miyamoto, Kazuki Yasuda, Junichiro Matsuda, Yasutomi Kamei, Shigetaka Kitajima and Yoshihiro Ogawa

Circ. Res. 2009;105:25-32; originally published online May 28, 2009;

DOI: 10.1161/CIRCRESAHA.109.196261

Circulation Research is published by the American Heart Association, 7272 Greenville Avenue, Dallas, TX 75214

Copyright © 2009 American Heart Association. All rights reserved. Print ISSN: 0009-7330. Online ISSN: 1524-4571

The online version of this article, along with updated information and services, is located on the World Wide Web at:

<http://circres.ahajournals.org/cgi/content/full/105/1/25>

Data Supplement (unedited) at:

<http://circres.ahajournals.org/cgi/content/full/CIRCRESAHA.109.196261/DC1>

Subscriptions: Information about subscribing to Circulation Research is online at <http://circres.ahajournals.org/subscriptions/>

Permissions: Permissions & Rights Desk, Lippincott Williams & Wilkins, a division of Wolters Kluwer Health, 351 West Camden Street, Baltimore, MD 21202-2436. Phone: 410-528-4050. Fax: 410-528-8550. E-mail: journalpermissions@lww.com

Reprints: Information about reprints can be found online at <http://www.lww.com/reprints>

Activating Transcription Factor 3 Constitutes a Negative Feedback Mechanism That Attenuates Saturated Fatty Acid/Toll-Like Receptor 4 Signaling and Macrophage Activation in Obese Adipose Tissue

Takayoshi Suganami, Xunmei Yuan, Yuri Shimoda, Kozue Uchio-Yamada, Nobutaka Nakagawa, Iibuki Shirakawa, Takako Usami, Takamitsu Tsukahara, Keizo Nakayama, Yoshihiro Miyamoto, Kazuki Yasuda, Junichiro Matsuda, Yasutomi Kamei, Shigetaka Kitajima, Yoshihiro Ogawa

Abstract—Obese adipose tissue is markedly infiltrated by macrophages, suggesting that they may participate in the inflammatory pathways that are activated in obese adipose tissue. Evidence has suggested that saturated fatty acids released via adipocyte lipolysis serve as a naturally occurring ligand that stimulates Toll-like receptor (TLR)4 signaling, thereby inducing the inflammatory responses in macrophages in obese adipose tissue. Through a combination of cDNA microarray analyses of saturated fatty acid-stimulated macrophages in vitro and obese adipose tissue in vivo, here we identified activating transcription factor (ATF)3, a member of the ATF/cAMP response element-binding protein family of basic leucine zipper-type transcription factors, as a target gene of saturated fatty acids/TLR4 signaling in macrophages in obese adipose tissue. Importantly, ATF3, when induced by saturated fatty acids, can transcriptionally repress tumor necrosis factor- α production in macrophages in vitro. Chromatin immunoprecipitation assay revealed that ATF3 is recruited to the region containing the activator protein-1 site of the endogenous tumor necrosis factor- α promoter. Furthermore, transgenic overexpression of ATF3 specifically in macrophages results in the marked attenuation of proinflammatory M1 macrophage activation in the adipose tissue from genetically obese KKA^y mice fed high-fat diet. This study provides evidence that ATF3, which is induced in obese adipose tissue, acts as a transcriptional repressor of saturated fatty acids/TLR4 signaling, thereby revealing the negative feedback mechanism that attenuates obesity-induced macrophage activation. Our data also suggest that activation of ATF3 in macrophages offers a novel therapeutic strategy to prevent or treat obesity-induced adipose tissue inflammation. (*Circ Res.* 2009;105:25-32.)

Key Words: adipocytes ■ ATF3 ■ fatty acids ■ inflammation ■ macrophages ■ TLR4

Known as the metabolic syndrome, the cluster of well-established risk factors for cardiovascular disease (visceral fat obesity, impaired glucose metabolism, atherogenic dyslipidemia, and blood pressure elevation), is an increasing health problem worldwide.¹⁻³ The pathophysiology underlying the metabolic syndrome is not fully understood and visceral fat obesity appears to be an important component.⁴ There is considerable evidence that obesity is a state of chronic low-grade inflammation, which may play a critical role in the pathophysiology of the metabolic syndrome.¹⁻³

Obese adipose tissue is markedly infiltrated by macrophages, suggesting that they may participate in the inflammatory pathways that are activated in obese adipose tissue.⁵

Using an in vitro coculture system composed of adipocytes and macrophages, we have provided evidence that a paracrine loop involving saturated fatty acids and tumor necrosis factor (TNF) α derived from adipocytes and macrophages, respectively, establishes a vicious cycle that augments the inflammatory change in obese adipose tissue.⁶ Recent studies have also pointed to the heterogeneity of macrophages infiltrated into obese adipose tissue, ie, they follow 2 different polarization states: M1, or "classically activated" (proinflammatory) macrophages, which are induced by proinflammatory mediators such as lipopolysaccharide (LPS) and Th1 cytokine interferon- γ ; and M2, or "alternatively activated" (antiinflammatory) macrophages, which are generated in vitro by expo-

Original received February 23, 2009; revision received May 11, 2009; accepted May 20, 2009.

From the Department of Molecular Medicine and Metabolism (T.S., X.Y., Y.S., N.N., I.S., Y.K., Y.O.), Department of Biochemical Genetics (S.K.), Global Center of Excellence Program (Y.O.); and International Research Center for Molecular Science in Tooth and Bone Diseases, Laboratory of Recombinant Animals (T.U.), Medical Research Institute, Tokyo Medical and Dental University, Tokyo; Division of Biomedical Research Resources (K.U.-Y., J.M.), National Institute of Biomedical Innovation, Osaka; Kyoto Institute of Nutrition and Pathology (T.T., K.N.); Department of Medicine (Y.M.), Division of Atherosclerosis and Diabetes, National Cardiovascular Center Hospital, Osaka; and Department of Metabolic Disorder (K.Y.), Research Institute, International Medical Center of Japan, Tokyo, Japan.

Correspondence to Yoshihiro Ogawa, Department of Molecular Medicine and Metabolism, Medical Research Institute, Tokyo Medical and Dental University, 1-5-45 Yushima, Bunkyo-ku, Tokyo 113-8510, Japan. E-mail ogawa.mmm@mri.tmd.ac.jp

© 2009 American Heart Association, Inc.

Circulation Research is available at <http://circres.ahajournals.org>

DOI: 10.1161/CIRCRESAHA.109.196261

Downloaded from circres.ahajournals.org at NANKODO CO LTD on February 8, 2010

sure to Th2 cytokines such as interleukin (IL)-4 and IL-13.⁷⁻⁹ Evidence has accumulated indicating that macrophages, which are infiltrated into obese adipose tissue, exhibit the phenotypic change from M2 to M1 polarization.⁷⁻⁹ Recent evidence also showed that the nuclear receptor peroxisome proliferator-activated receptor- γ or - δ regulates M2 polarization of adipose tissue macrophages and thus systemic insulin sensitivity.^{8,9} It is, therefore, conceivable that M1 macrophages induce the release of saturated fatty acids from hypertrophied adipocytes via lipolysis, which, in turn, may serve as a proinflammatory adipocytokine locally in the adipose tissue.

Free fatty acids represent an important energy source mobilized from triglycerides stored in the adipose tissue, particularly during periods of starvation, but recent evidence has suggested the pathophysiologic roles other than the supply of nutrients in times of fasting or increased energy demand.¹⁰ For instance, elevated levels of circulating free fatty acids, which are often associated with visceral fat obesity, increase fat accumulation in insulin target tissues such as the skeletal muscle and liver and contribute to insulin resistance.¹¹ We and others have reported that saturated fatty acids, which are released from adipocytes via the macrophage-induced lipolysis, serve as a naturally occurring ligand for Toll-like receptor (TLR)4 complex, which is essential for the recognition of LPS, to induce nuclear factor (NF)- κ B activation in macrophages.¹²⁻¹⁴ Evidence has also suggested that TLR4 plays an important role in adipose tissue inflammation.¹⁴⁻¹⁷ Because macrophages in obese adipose tissue are exposed to saturated fatty acids released in large quantities from hypertrophied adipocytes, there might be negative regulatory mechanisms, whereby macrophages are protected against the saturated fatty acid-induced inflammatory response in obese adipose tissue.

Through a combination of cDNA microarray analyses of saturated fatty acid-stimulated macrophages *in vitro* and obese adipose tissue *in vivo*, we identified activating transcription factor (ATF)3, a member of the ATF/cAMP response element-binding protein (CREB) family of basic leucine zipper-type transcription factors^{18,19} that is markedly induced in macrophages through TLR4 in response to saturated fatty acids *in vitro* and in obese adipose tissue *in vivo*. This study provides evidence that ATF3 acts as a transcriptional repressor of saturated fatty acids/TLR4 signaling in macrophages, thereby revealing the negative feedback mechanism that attenuates obesity-induced macrophage activation in obese adipose tissue. Our data also suggest that activation of ATF3 in macrophages offers a novel therapeutic strategy to prevent or treat obesity-induced inflammation and thus the metabolic syndrome associated with excess adiposity.

Materials and Methods

An expanded Materials and Methods section is available in the Online Data Supplement at <http://circres.ahajournals.org>.

Materials and Antibodies

Details are provided in the Online Data Supplement.

Animals

Six-week-old male C3H/HeJ mice, which have defective LPS signaling attributable to a missense mutation in the TLR4 gene,²⁰ and control C3H/HeN mice were purchased from CLEA Japan (Tokyo, Japan). Genetically obese *ob/ob*, *db/db*, and *KKA^y* mice were purchased from CLEA Japan and Charles River Japan (Tokyo, Japan). Details on experimental conditions are provided in the Online Data Supplement. All animal experiments were conducted in accordance to the guidelines of Tokyo Medical and Dental University Committee on Animal Research (No. 0090058).

Generation of Transgenic Mice Overexpressing ATF3 in Macrophages

Details are provided in the Online Data Supplement.

Cell Culture

RAW264 macrophage cell line (RIKEN BioResource Center, Tsukuba, Japan), 3T3-L1 preadipocytes, and HEK293 (American Type Culture Collection, Manassas, Va) were maintained in DMEM (Nacalai Tesque, Kyoto, Japan) containing 10% FBS (BioWest, Miami, Fla). Differentiation of 3T3-L1 preadipocytes to mature adipocytes was performed as previously described^{6,12} and used as differentiated 3T3-L1 adipocytes at days 8 to 10 after the induction of differentiation. Murine peritoneal macrophages and bone marrow-derived macrophages were prepared as described.¹²

Chromatin Immunoprecipitation Assay

Details are provided in the Online Data Supplement.

Retrovirus-Mediated Overexpression and Knockdown of ATF3 in Macrophages

Retrovirus-mediated overexpression of the full-length mouse ATF3 cDNA and knockdown of endogenous ATF3 were performed in RAW264 macrophages as described in the Online Data Supplement.

Quantitative Real-Time PCR

Total RNA was extracted from cultured cells using Sepazol reagent (Nacalai Tesque) and quantitative real-time PCR was performed with an ABI Prism 7000 Sequence Detection System using PCR Master Mix Reagent (Applied Biosystems, Foster City, Calif).^{6,12} Primers used in this study are described in Online Table I. Levels of mRNA were normalized to those of 36B4 mRNA.

Histological Analysis

Histological analysis was performed as previously described using the paraffin-embedded sections of the epididymal white adipose tissue.¹⁵ In brief, hematoxylin/eosin staining was used to compare the adipocyte cell size with the software Win Roof (Mitani, Chiba, Japan).¹⁵ The presence of F4/80-positive macrophages in the adipose tissue was detected immunohistochemically using the rat monoclonal antimouse F4/80 antibody²¹ as described previously.¹⁵ The number of F4/80-positive cells was counted in more than 10 mm² area of each section and expressed as the mean number/mm².

Western Blotting of ATF3

Whole cell lysates were prepared as previously described.⁶ Samples (20 μ g protein per lane) were separated by 12.5% SDS-PAGE and Western blotting was performed using antibodies against ATF3 (Santa Cruz Biotechnology).

Measurement of TNF α Levels in Culture Media

The TNF α levels in culture supernatants were determined by a commercially available ELISA kit (R&D systems, Minneapolis, Minn).⁶

Transient Transfection and Luciferase Assay

Details are provided in the Online Data Supplement.

Statistical Analysis

Data were expressed as the means \pm SE. Statistical analysis was performed using ANOVA, followed by Scheffé's test unless otherwise described. $P < 0.05$ was considered to be statistically significant.

Results and Discussion

Identification of ATF3 As a Target Gene of Saturated Fatty Acids in Macrophages in Obese Adipose Tissue

We have provided *in vitro* evidence that saturated fatty acids, which are released from adipocytes via the macrophage-induced lipolysis, serves as a naturally occurring ligand that stimulates TLR4 signaling in macrophages.¹² To search for target gene(s) of saturated fatty acids in macrophages in obese adipose tissue, we performed cDNA microarray analysis of obese adipose tissue from *ob/ob* mice and palmitate-stimulated RAW264 macrophages (Online Figure 1, a). Up-regulated genes under both conditions included chemokines, proinflammatory cytokines, acute phase reactants, and ATF3 (Online Table II), whereas 5 genes were downregulated (Online Table III). ATF3 is a member of the ATF/CREB family of transcription factors.^{18,19} ATF3 is rapidly induced in response to several stimuli and insults, such as chemicals, irradiation, and oxidative stress, and, in turn, negatively regulates target genes as a transcriptional repressor.^{18,19} Although ATF3 plays a role in apoptosis and cell cycle,^{18,19,22} the role of ATF3 in obesity is largely unknown. We, therefore, investigated the tissue distribution of ATF3 in obese and lean mice. Similar to macrophage marker F4/80, ATF3 mRNA expression was markedly increased in the adipose tissue from *db/db* mice relative to wild-type mice (Online Figure 1, b). In this study, there was a significant increase in ATF3 mRNA expression in the liver from *db/db* mice relative to wild-type mice ($P < 0.01$).

We confirmed our cDNA microarray data by real-time PCR and immunostaining. Expression of ATF3 and F4/80 mRNAs was increased in the adipose tissue during the course of diet-induced obesity (Figure 1A). We also observed upregulation of ATF3 and F4/80 in the adipose tissue from *ob/ob* mice (Figure 1B). Collagenase digestion of the adipose tissue, which is validated by F4/80 and adiponectin mRNA expression, revealed that ATF3 is expressed predominantly in stromal-vascular fraction in the adipose tissue (Figure 1C). Furthermore, ATF3 mRNA expression was increased significantly in *ob/ob* mice fed high-fat diet relative to wild-type mice fed standard diet ($P < 0.01$) (Figure 1C). We also confirmed by immunostaining of ATF3 and F4/80 using serial sections of obese adipose tissue that most ATF3-positive cells are stained with F4/80 (Figure 1D). These observations indicate that ATF3 is markedly upregulated in obese adipose tissue, especially in infiltrated macrophages.

Saturated Fatty Acids Induce ATF3 via TLR4 in Macrophages In Vitro and In Vivo

We next examined the involvement of TLR4 in the saturated fatty acid-induced ATF3 mRNA and protein expression in macrophages *in vitro*. Saturated fatty acids, such as palmitate and stearate, and LPS increased significantly ATF3 mRNA and protein expression in RAW264 macrophages ($P < 0.05$

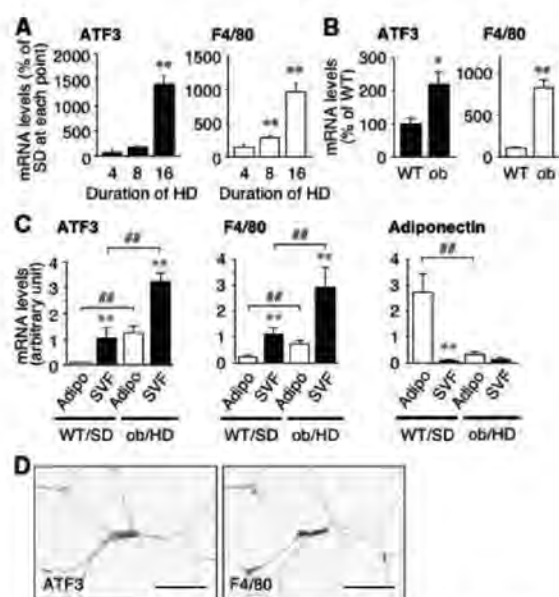


Figure 1. ATF3 expression in obese adipose tissue. ATF3 and F4/80 mRNA expression in the epididymal adipose tissue from high-fat diet (HD)-fed obese mice for up to 16 weeks (A) and genetically obese *ob/ob* mice at 15 weeks of age (*ob*) (B). * $P < 0.05$, ** $P < 0.01$ vs standard diet (SD) or wild-type mice (WT) ($n = 6$ to 10). C, ATF3, F4/80, and adiponectin mRNA expression in mature adipocytes (Adipo) and stromal-vascular fraction (SVF) in the epididymal adipose tissue from SD-fed WT and HD-fed *ob/ob*. ** $P < 0.01$ vs the respective Adipo, ### $P < 0.01$ ($n = 4$ to 5). D, ATF3 and F4/80 immunostaining in the epididymal adipose tissue from HD-fed *ob/ob*. Original magnification, $\times 400$. Scale bars = 100 μm .

versus vehicle) (Figure 2A through 2D). Interestingly, unsaturated fatty acids, such as oleate and eicosapentaenoic acid, did not affect ATF3 mRNA expression (Figure 2C and 2D and data not shown), suggesting the structure-specific effect of free fatty acids. We found that palmitate fails to increase ATF3 mRNA expression in peritoneal macrophages from C3H/HeJ mice with defective TLR4 signaling (Figure 2E). We also observed that BAY11-7085, an NF- κ B inhibitor, markedly inhibits the palmitate-induced ATF3 mRNA expression in RAW264 macrophages (Figure 2F). The data were confirmed using RAW264 macrophages overexpressing a super-repressor form of I κ B α (SR-I κ B α) (Figure 2G). Furthermore, selective NF- κ B activation by transient overexpression of p50 and p65 subunits of NF- κ B increased significantly the ATF3 promoter activity in HEK293 cells ($P < 0.01$) (Figure 2H). In this setting, the changes in ATF3 mRNA expression were almost parallel to those in TNF α mRNA expression (Figure 2E and 2F and data not shown). These observations indicate that TLR4/NF- κ B pathway plays an important role in saturated fatty acid-induced ATF3 and TNF α expression in macrophages. On the other hand, palmitate and stearate, but not unsaturated fatty acids, are known to serve as precursors for *de novo* ceramide synthesis, thereby inducing inflammatory changes in certain cells.^{23,24} However, we observed that pharmacological inhibition of ceramide synthesis slightly inhibits the palmitate-induced ATF3

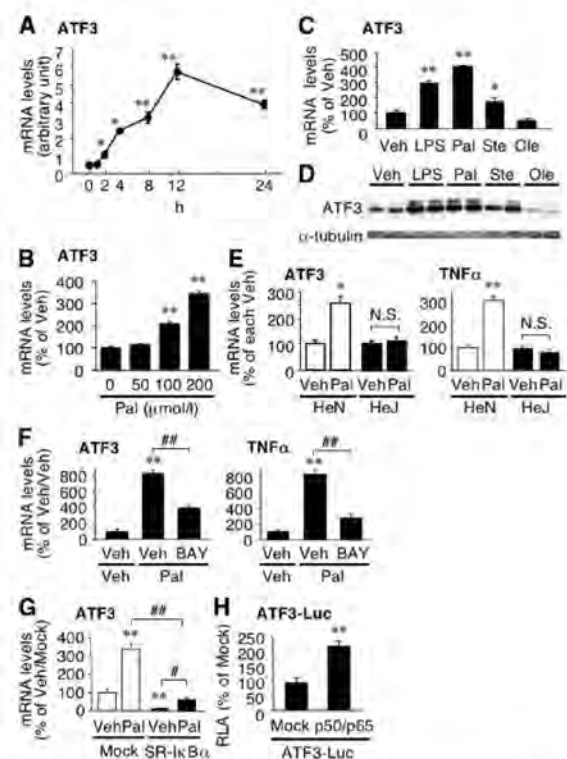


Figure 2. Saturated fatty acid-induced ATF3 expression in cultured macrophages. **A**, Time course of palmitate-induced ATF3 mRNA expression in RAW264 macrophages. Pal indicates palmitate 200 $\mu\text{mol/L}$. * $P < 0.05$ vs 0 hour. **B**, Dose-dependent effect of palmitate on ATF3 mRNA expression in RAW264 macrophages. Veh indicates vehicle; LPS, LPS 10 ng/mL; Pal, palmitate 200 $\mu\text{mol/L}$; Ste, stearate 200 $\mu\text{mol/L}$; Ole, oleate 200 $\mu\text{mol/L}$. * $P < 0.05$, ** $P < 0.01$ vs Veh. **C**, Effect of saturated and unsaturated fatty acids (FAs) on ATF3 mRNA (C) and protein (D) expression in RAW264 macrophages. Veh indicates vehicle; LPS, LPS 10 ng/mL; Pal, palmitate 200 $\mu\text{mol/L}$; Ste, stearate 200 $\mu\text{mol/L}$; Ole, oleate 200 $\mu\text{mol/L}$. * $P < 0.05$, ** $P < 0.01$ vs Veh. **E**, Role of TLR4 in the palmitate-induced ATF3 and TNF α mRNA expression in peritoneal macrophages. HeN and HeJ indicate peritoneal macrophages from wild-type C3H/HeN and TLR4 mutant C3H/HeJ mice, respectively. * $P < 0.05$, ** $P < 0.01$ vs Veh/HeN. **F**, Effect of NF- κB inhibitor BAY11-7085 (BAY, 10 $\mu\text{mol/L}$) on the palmitate-induced ATF3 and TNF α mRNA expression in RAW264 macrophages. ** $P < 0.01$ vs Veh/Veh, ## $P < 0.01$. **G**, Effect of super-repressor I $\kappa\text{B}\alpha$ (SR-I $\kappa\text{B}\alpha$) on the palmitate-induced ATF3 and TNF α mRNA expression in RAW264 macrophages. Mock and SR-I $\kappa\text{B}\alpha$, stably mock-, and SR-I $\kappa\text{B}\alpha$ -expressing RAW264 macrophages, respectively. ** $P < 0.01$ vs Veh/mock; # $P < 0.05$, ## $P < 0.01$. **H**, Effect of NF- κB activation on ATF3 promoter activity. The luciferase reporter containing a 1.8-kb human ATF3 promoter fragment (ATF3-Luc) with p50 and p65 subunits of NF- κB or mock was transiently transfected in RAW264 macrophages. ** $P < 0.01$ vs mock ($n = 4$ to 6).

mRNA expression in RAW264 macrophages (T. Suganami, I. Shirakawa, Y. Ogawa, unpublished data, 2009). These observations, taken together, suggest that saturated fatty acid-induced ATF3 expression is mediated mostly through the TLR4/NF- κB pathway.

We next examined the role of TLR4 in ATF3 expression in the interaction between adipocytes and macrophages. We have established an in vitro coculture system composed of adipocytes and macrophages and found that saturated fatty acids, which are released from adipocytes via the macro-

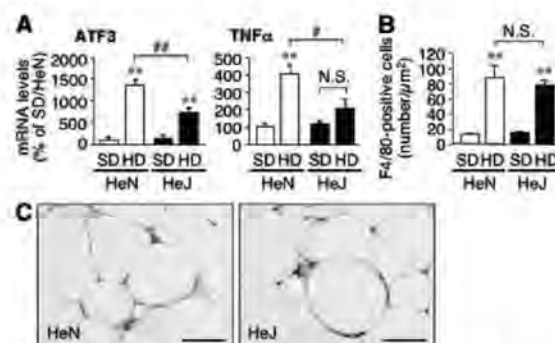


Figure 3. Role of TLR4 in obesity-induced ATF3 mRNA expression in adipose tissue macrophages. ATF3 and TNF α mRNA expression (A) and macrophage infiltration (B) in the adipose tissue from mice fed high-fat diet (HD) or standard diet (SD). ** $P < 0.01$ vs the respective SD; # $P < 0.05$, ## $P < 0.01$ ($n = 6$ to 10). C, Immunostaining for ATF3 in the adipose tissue from HD-fed HeN and HeJ. Original magnification, $\times 400$. Scale bars = 100 μm .

phage-induced lipolysis, are capable of activating the TLR4/NF- κB signaling.^{6,12} Coculture of 3T3-L1 adipocytes with peritoneal macrophages from C3H/HeN mice resulted in the upregulation of ATF3 and TNF α mRNAs, which was significantly inhibited in the coculture with peritoneal macrophages from C3H/HeJ mice ($P < 0.05$) (Online Figure II, a). We found that BAY11-7085 effectively inhibits the upregulation of ATF3 and TNF α mRNA expression in the coculture system (Online Figure II, b).

Using C3H/HeJ and C3H/HeN mice fed high-fat diet, we also examined the involvement of TLR4 in obesity-induced ATF3 expression in the adipose tissue. There were no significant differences in body weight and adipose tissue weight between high-fat diet-fed C3H/HeN and C3H/HeJ mice (Online Table IV). Similar to our previous data on TNF α ,¹⁵ the high-fat diet-induced increase in ATF3 mRNA expression was significantly attenuated in the adipose tissue from C3H/HeJ mice relative to C3H/HeN mice ($P < 0.01$) (Figure 3A). Importantly, there was no significant change in the number of macrophages infiltrated into the adipose tissue, as assessed by F4/80 immunostaining (Figure 3B), suggesting the attenuation of macrophage activation in C3H/HeJ mice. Immunohistochemical analysis also confirmed the marked reduction of ATF3 staining in C3H/HeJ mice relative to C3H/HeN mice during the high-fat diet (Figure 3C). Collectively, these observations suggest that the saturated fatty acid-induced ATF3 expression in macrophages is mediated via TLR4 in vitro and in vivo.

ATF3 Reduces Saturated Fatty Acid-Induced TNF α Production in Macrophages

To elucidate the functional role of ATF3 in macrophages, we examined the effect of ATF3 overexpression on proinflammatory cytokine production in macrophages in vitro. A full-length mouse ATF3 cDNA was stably overexpressed in RAW264 macrophages by retroviral transduction, which was confirmed by real-time PCR and Western blotting (Figure 4A). In RAW264 macrophages overexpressing ATF3 (ATF3-RAW264), the palmitate- and LPS-induced increase in TNF α

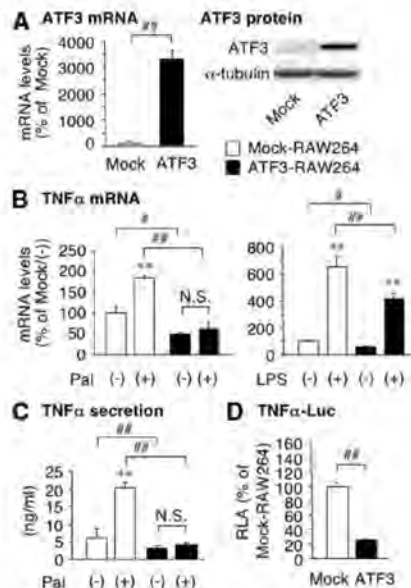


Figure 4. Effect of ATF3 overexpression on saturated fatty acid-induced TNF α production in cultured macrophages. A, Retrovirus-mediated stable overexpression of a full-length mouse ATF3 cDNA in RAW264 macrophages (ATF3-RAW264) and control RAW264 macrophages (Mock-RAW264). Effect of ATF3 overexpression on the palmitate- and LPS-induced TNF α mRNA expression (B) and secretion (C). D, Effect of ATF3 overexpression on the TNF α promoter activity. Pal indicates palmitate 200 μ M/L; LPS, LPS 10 ng/mL. ** P <0.01 vs the respective control; # P <0.05, ## P <0.01 (n =4).

mRNA expression was significantly reduced relative to control RAW264 macrophages (Mock-RAW264) (P <0.01) (Figure 4B). We confirmed that the palmitate- and LPS-induced increase in TNF α secretion in the ATF3-RAW264 culture media is significantly reduced relative to Mock-RAW264 (P <0.01) (Figure 4C). We also observed with a luciferase reporter assay that TNF α promoter activity is markedly inhibited in ATF3-RAW264 relative to Mock-RAW264 (Figure 4D). Similarly, the palmitate-induced increase in IL-6 and inducible nitric oxide synthase was significantly reduced in ATF3-RAW264 relative to Mock-RAW264 (Online Figure III. a). These observations indicate that overexpression of ATF3 is capable of reducing the saturated fatty acid-induced proinflammatory cytokine production in macrophages.

We next examined the effect of knockdown of endogenous ATF3 gene expression in RAW264 macrophages. Stable knockdown of ATF3 using 2 independent short hairpin loop RNAs (shATF3#1 and shATF3#3) was confirmed by Western blotting (Figure 5A). The ATF3-knockdown RAW264 macrophages (shATF3#1-RAW264 and shATF3#3-RAW264) exhibited significant enhancement of the palmitate-induced TNF α mRNA expression relative to control RAW264 macrophages (shGFP-RAW264) (P <0.01) (Figure 5B). The effect of ATF3 knockdown on TNF α mRNA expression persisted until 24 hours after stimulation with LPS (Figure 5C). Knockdown of ATF3 also significantly increased TNF α secretion in the culture media (P <0.01) (Figure 5D). Furthermore, we observed that the TNF α promoter activity is

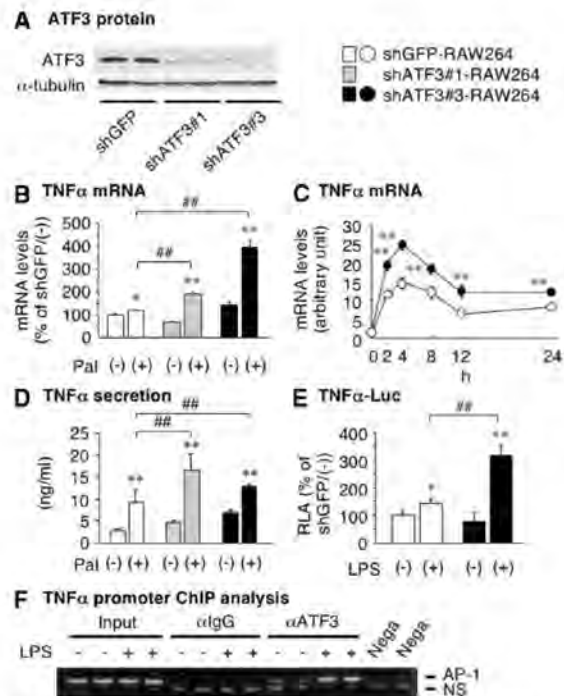


Figure 5. Effect of ATF3 knockdown on saturated fatty acid-induced TNF α production in cultured macrophages. A, Retrovirus-mediated ATF3 knockdown in RAW264 macrophages. Two short hairpin loop RNAs (shATF3#1 and shATF3#3) designed to target different sequences within ATF3 mRNA effectively knocked down endogenous ATF3 in RAW264 macrophages. B, Effect of ATF3 knockdown on the palmitate-induced TNF α mRNA expression. C, Time course of the LPS-induced TNF α mRNA expression in RAW264 macrophages. D, Effect of ATF3 knockdown on the palmitate-induced TNF α secretion. E, Effect of ATF3 knockdown on the TNF α promoter activity. shATF3#1-RAW264 and shATF3#3-RAW264 indicate ATF3-knockdown RAW264 macrophages; shGFP-RAW264, control RAW264 macrophages; Pal, palmitate 200 μ M/L; LPS, LPS 10 ng/mL. ** P <0.01 vs the respective control; # P <0.05, ## P <0.01 (n =4). F, TNF α promoter chromatin immunoprecipitation analysis with chromatin extracts prepared from RAW264 macrophages treated with or without LPS (100 ng/mL) for 6 hours. α ATF3 indicates anti-ATF3 antibody; α IGG, normal rabbit IgG; Nega, negative control without template; NS, nonspecific band.

significantly increased in shATF3#3-RAW264 relative to shGFP-RAW264 (P <0.01) (Figure 5E). These observations suggest that once induced by the saturated fatty acids/TLR4 signaling, ATF3 attenuates the saturated fatty acid-induced TNF α production in macrophages, thereby constitute a negative feedback mechanism to reduce the TLR4 signaling induction of proinflammatory cytokine production. This notion is consistent with a recent report by Gilchrist et al that ATF3 acts as a negative regulator of the LPS-induced TLR4 signaling.²⁵

In the proximal region of the IL-6 and IL-12b promoters, ATF3-binding ATF/CREB sites are located close to NF- κ B binding sites.²⁵ NF- κ B and ATF3, both of which are activated by saturated fatty acids/TLR4 signaling, can positively and negatively regulate their target proinflammatory cytokines, respectively.²⁵ However, there are no consensus sequences

corresponding to the ATF/CREB site close to the NF- κ B-binding site (–534 bp) in the proximal region of TNF α promoter. In this study, we performed chromatin immunoprecipitation analysis with RAW264 macrophages and found that ATF3 is recruited to the region containing the activator protein (AP)-1 site (–926 bp) of the endogenous TNF α promoter (Figure 5F). This observation is consistent with a previous report that ATF3 binds to the AP-1 site.²⁶ It is, therefore, interesting to know how ATF3 negatively regulates TNF α and IL-6 production via its distinct binding sites; the AP-1 and ATF/CREB sites, respectively. In addition, histone deacetylase and heat shock transcription factor 1 are required for the action of ATF3 on the IL-6 promoter.^{25,27} It is, therefore, important to identify ATF3-interacting proteins on the TNF α promoter.

Distinct Intracellular Signaling Pathways Plays a Role in the Palmitate- and LPS-Induced ATF3 Expression

In this study, we demonstrated that saturated fatty acids induce ATF3 expression in macrophages through the TLR4/NF- κ B pathway, which is consistent with the previous report on LPS.²⁵ Besides NF- κ B, mitogen-activated protein kinases (MAPKs) are an important intracellular signaling pathway downstream of TLR4,²⁸ and c-Jun N-terminal kinase (JNK) and p38 MAPK have been reported to play a role in ATF3 expression in certain cell types.^{29,30} We, therefore, examined the involvement of MAPKs in the saturated fatty acid- and LPS-induced ATF3 mRNA expression and found that SB20358038, a p38 MAPK inhibitor, inhibits significantly the palmitate-induced ATF3 mRNA expression ($P<0.01$) (Online Figure IV). On the other hand, SP600125, a JNK inhibitor, inhibited most effectively the LPS-induced ATF3 mRNA expression ($P<0.01$) (Online Figure IV). Moreover, we found that ERK plays a major role in the palmitate-induced TNF α mRNA expression, whereas other MAPKs may also contribute to the LPS-induced TNF α mRNA expression (Online Figure IV). These observations, taken together, suggest that distinct intracellular signaling pathways may mediate the saturated fatty acid- and LPS-induced ATF3 mRNA expression through TLR4. It is interesting to know how endogenous and exogenous TLR4 ligands such as saturated fatty acids, oxidized phospholipids, and cytosolic and nuclear proteins, and LPS,^{12,28,31} exert their effects through the unique signaling pathways, thereby leading to a variety of cellular responses.

Transgenic Overexpression of ATF3 Attenuates Macrophage Activation in Obese Adipose Tissue

To elucidate the role of ATF3 in macrophages infiltrated into obese adipose tissue, we developed transgenic mice overexpressing human ATF3 in macrophages under the control of SR-A promoter (ATF3 Tg) (Online Figure V, a).³² Genomic Southern blot analysis identified 9 (line 2), 13 (line 25), and 20 (line 35) transgene copies in independent founder lines (data not shown). Western blot analysis of ATF3 revealed 3-fold and 2-fold increase in ATF3 protein levels in bone marrow-derived macrophages from lines 25 and 35, respectively, relative to wild-type mice (Online Figure V, b). In this

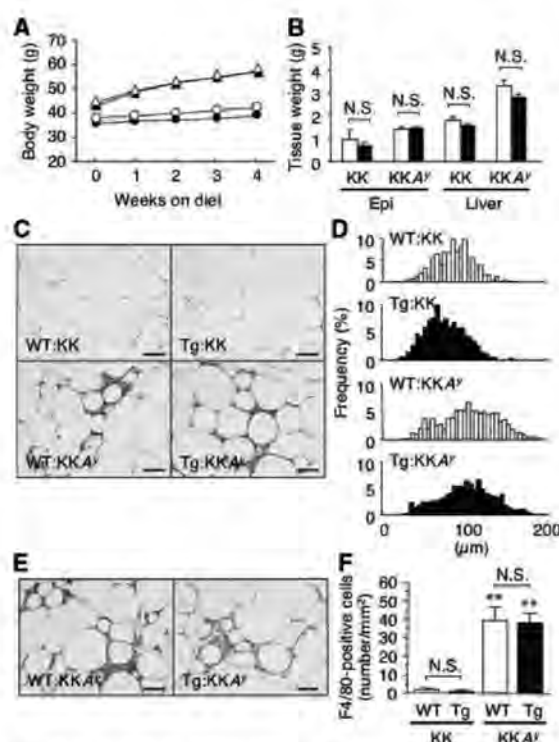


Figure 6. Adipocyte hypertrophy and macrophage infiltration in the adipose tissue from transgenic mice with macrophage-specific ATF3 overexpression. **A**, Time course of body weight. \circ , WT:KK; \bullet , transgenic (Tg):KK; \triangle , WT:KKA^y; \blacktriangle , Tg:KKA^y. **B**, The epididymal adipose tissue (Epi) and liver weights. Open bar, WT; closed bar, Tg. **C**, Hematoxylin/eosin staining of the epididymal adipose tissue. **D**, Histogram of diameters of adipocytes in the epididymal adipose tissue. **E**, F4/80 immunostaining of the epididymal adipose tissue. **F**, Cell count of F4/80-positive cells in the epididymal adipose tissue. ** $P<0.01$ vs the respective KK background ($n=6$ to 13).

study, there was no significant increase in ATF3 levels in line 2 macrophages (Online Figure V, b). We observed essentially the same data using peritoneal macrophages from 3 independent transgenic lines (Online Figure V, b).

We crossed ATF3 Tg (line 35) with genetically obese KKA^y mice and obtained 4 genotypes as the F1 generation (wild-type on the KK background [WT:KK], ATF3 Tg on the KK background [ATF3 Tg:KK], wild-type on the KKA^y background [WT:KKA^y], and ATF3 Tg on the KKA^y background [ATF3 Tg:KKA^y]) at a Mendelian ratio (data not shown). In this study, WT:KK and ATF3 Tg:KK were fed standard diet and WT:KKA^y and ATF3 Tg:KKA^y were fed high-fat diet for 4 weeks. During the course of high-fat diet feeding, transgenic overexpression of ATF3 in macrophages did not affect significantly body weight and epididymal fat weight on KK and KKA^y backgrounds (Figure 6A and 6B). The liver weight tended to be decreased in ATF3 Tg:KKA^y relative to WT:KKA^y, but the difference did not reach statistical significance (Figure 6B). Histological analysis showed no apparent difference in adipocyte cell size between genotypes (Figure 6C and 6D). There was no significant difference in obesity-induced macrophage infiltration be-

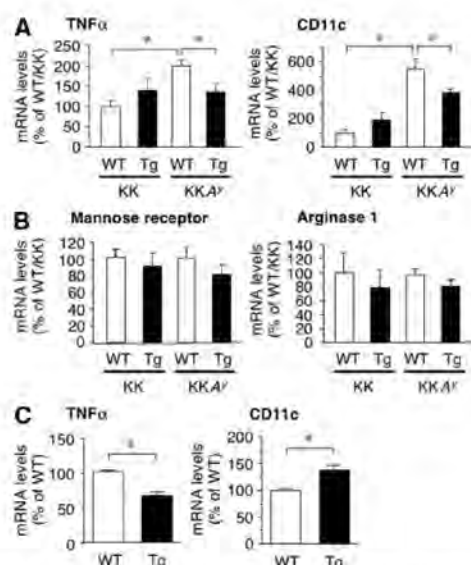


Figure 7. Effect of ATF3 on activation and polarization of adipose tissue macrophages and peritoneal macrophages from macrophage-specific ATF3 transgenic mice. A and B, mRNA expression of M1 markers (TNF α and CD11c) (A) and M2 markers (mannose receptor and arginase 1) (B) in the epididymal adipose tissue from WT:KK, Tg:KK, WT:KKA^y, and Tg:KKA^y mice. C, mRNA expression of M1 markers (TNF α and CD11c) in peritoneal macrophages from WT and Tg on the C57BL/6J background. * $P < 0.05$ ($n = 6$ to 13).

tween WT:KKA^y and ATF3 Tg:KKA^y (Figure 6E and 6F). These observations suggest that transgenic overexpression of ATF3 in macrophages does not affect adipocyte hypertrophy and macrophage infiltration in obese adipose tissue.

We also examined the effect of ATF3 on macrophage activation and polarization in the adipose tissue from transgenic mice with macrophage-specific overexpression of ATF3. We observed a marked increase in TNF α mRNA expression in the adipose tissue from WT:KKA^y relative to WT:KK, which was significantly attenuated in ATF3 Tg:KKA^y ($P < 0.05$) (Figure 7A). In this study, M1 macrophage marker CD11c was also increased in the adipose tissue from WT:KKA^y relative to WT:KK (Figure 7B), which was effectively inhibited in ATF3 Tg:KKA^y ($P < 0.05$) (Figure 7A). Moreover, IL-6 mRNA expression tended to be decreased in the adipose tissue from ATF3 Tg:KKA^y mice relative to WT:KKA^y (Online Figure III, b). By contrast, we found no significant difference in mRNA expression of M2 macrophage markers, mannose receptor and arginase 1, among genotypes (Figure 7B). These observations suggest that overexpression of ATF3 in macrophages is capable of inhibiting macrophage activation and M1 polarization in the adipose tissue in vivo (Figure 8).

We next examined TNF α and CD11c mRNA expression in peritoneal macrophages prepared from ATF3 Tg and WT on the C57BL/6J background. Similar to the data on the adipose tissue (Figure 7A), TNF α mRNA expression was significantly suppressed in peritoneal macrophages from ATF3 Tg relative to WT ($P < 0.05$) (Figure 7C). Interestingly, CD11c mRNA expression in peritoneal macrophages was rather

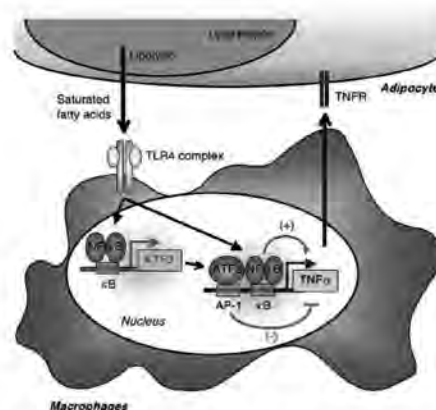


Figure 8. Negative feedback mechanism involving ATF3 as a transcriptional repressor of saturated fatty acid/TLR4 signaling in macrophages in obese adipose tissue. In the interaction between adipocytes and macrophages, ATF3 is upregulated in macrophages through the saturated fatty acids/TLR4/NF- κ B signaling. Once induced, ATF3 can transcriptionally reduce the saturated fatty acids/TLR4 signaling-induced proinflammatory cytokine production. Our data have identified ATF3 as a transcriptional repressor of saturated fatty acid/TLR4 signaling, thereby revealing the negative feedback mechanism that attenuates macrophage activation in obese adipose tissue. TNFR indicates TNF α receptor; AP-1 and κ B, AP-1- and NF- κ B-binding elements, respectively.

higher in ATF3 Tg than in WT ($P < 0.05$) (Figure 7C). In this regard, using ATF3-RAW264 and shATF3-RAW264, we did not observe that ATF3 has impact on CD11c mRNA expression in vitro (data not shown), suggesting that CD11c may not be a transcriptional target of ATF3 in macrophages. Further studies are needed to elucidate the role of ATF3 in obesity-induced M1 polarization of adipose tissue macrophages. Global ATF3-deficient mice are viable,^{19,25} but the role of ATF3 in glucose/lipid metabolism has not been elucidated. Because activation and polarization of adipose tissue macrophages play an important role in the metabolic status,⁷⁻⁹ studies with ATF3 Tg and macrophage-specific ATF3-deficient mice would help elucidate the pathophysiologic role of ATF3 in macrophages in adipose tissue inflammation and systemic glucose/lipid metabolism.

In conclusion, ATF3 is upregulated in macrophages in the interaction between adipocytes and macrophages through the saturated fatty acids/TLR4/NF- κ B signaling. Once induced, ATF3 can transcriptionally reduce the saturated fatty acids/TLR4 signaling induction of proinflammatory cytokine production. Among known negative regulators of TLR4 signaling,²⁸ ATF3 is unique in that it represses the TLR4 target genes via a transcriptional mechanism. This study provides evidence that ATF3 acts as a transcriptional repressor of saturated fatty acids/TLR4 signaling, thereby revealing the negative feedback mechanism that attenuates macrophage activation in obese adipose tissue (Figure 8). Our data also suggest that activation of ATF3 in macrophages may offer a novel therapeutic strategy to prevent or treat obesity-induced adipose tissue inflammation.

Acknowledgments

We thank Ai Togo for secretarial assistance and Takanori Kunieda and Tae Mieda for technical assistance. We are also grateful to the members of the Ogawa laboratory for discussions.

Sources of Funding

This work was supported in part by a Grant-in-Aid for Scientific Research from the Ministry of Education, Culture, Sports, Science and Technology of Japan and Ministry of Health, Labor and Welfare of Japan and research grants from Takeda Science Foundation and Takeda Medical Research Foundation.

Disclosures

None.

References

- Grundy SM, Brewer HB, Jr, Cleeman Jr, Smith SC Jr, Lenfant C. Definition of metabolic syndrome: report of the National Heart, Lung, and Blood Institute/American Heart Association conference on scientific issues related to definition. *Circulation*. 2004;109:433–438.
- Hotamisligil GS. Inflammation and metabolic disorders. *Nature*. 2006;444:860–867.
- Berg AH, Scherer PE. Adipose tissue, inflammation, and cardiovascular disease. *Circ Res*. 2005;96:939–949.
- Matsuzawa Y, Funahashi T, Nakamura T. Molecular mechanism of metabolic syndrome X: contribution of adipocytokines adipocyte-derived bioactive substances. *Ann N Y Acad Sci*. 1999;892:146–154.
- Weisberg SP, McCann D, Desai M, Rosenbaum M, Leibel RL, Ferrante AW Jr. Obesity is associated with macrophage accumulation in adipose tissue. *J Clin Invest*. 2003;112:1796–1808.
- Suganami T, Nishida J, Ogawa Y. A paracrine loop between adipocytes and macrophages aggravates inflammatory changes: role of free fatty acids and tumor necrosis factor α . *Arterioscler Thromb Vasc Biol*. 2005;25:2062–2068.
- Lumeng CN, Bodzin JL, Saltiel AR. Obesity induces a phenotypic switch in adipose tissue macrophage polarization. *J Clin Invest*. 2007;117:175–184.
- Kang K, Reilly SM, Karabacak V, Gangl MR, Fitzgerald K, Hatano B, Lee CH. Adipocyte-derived Th2 cytokines and myeloid PPAR δ regulate macrophage polarization and insulin sensitivity. *Cell Metab*. 2008;7:485–495.
- Odegaard JI, Ricardo-Gonzalez RR, Red Eagle A, Vats D, Morel CR, Goforth MH, Subramanian V, Mukundan L, Ferrante AW, Chawla A. Alternative M2 activation of Kupffer cells by PPAR δ ameliorates obesity-induced insulin resistance. *Cell Metab*. 2008;7:496–507.
- Cao H, Gerhold K, Mayers JR, Wiest MM, Watkins SM, Hotamisligil GS. Identification of a lipokine, a lipid hormone linking adipose tissue to systemic metabolism. *Cell*. 2008;134:933–944.
- Unger RH. Lipotoxicity in the pathogenesis of obesity-dependent NIDDM. Genetic and clinical implications. *Diabetes*. 1995;44:863–870.
- Suganami T, Tanimoto-Koyama K, Nishida J, Itoh M, Yuan X, Mizuarai S, Kotani H, Yamaoka S, Miyake K, Aoe S, Kamei Y, Ogawa Y. Role of the Toll-like receptor 4/NF- κ B pathway in saturated fatty acid-induced inflammatory changes in the interaction between adipocytes and macrophages. *Arterioscler Thromb Vasc Biol*. 2007;27:84–91.
- Lee JY, Sohn KH, Rhee SH, Hwang D. Saturated fatty acids, but not unsaturated fatty acids, induce the expression of cyclooxygenase-2 mediated through Toll-like receptor 4. *J Biol Chem*. 2001;276:16683–16689.
- Shi H, Kokoeva MV, Inouye K, Tzameli I, Yin H, Flier JS. TLR4 links innate immunity and fatty acid-induced insulin resistance. *J Clin Invest*. 2006;116:3015–3025.
- Suganami T, Mieda T, Itoh M, Shimoda Y, Kamei Y, Ogawa Y. Attenuation of obesity-induced adipose tissue inflammation in C3H/HeJ mice carrying a Toll-like receptor 4 mutation. *Biochem Biophys Res Commun*. 2007;354:45–49.
- Poggi M, Bastelica D, Gual P, Iglesias MA, Gremeaux T, Knauf C, Peiretti F, Verdier M, Johan-Vague I, Tanti JP, Burcelin R, Alessi MC. C3H/HeJ mice carrying a Toll-like receptor 4 mutation are protected against the development of insulin resistance in white adipose tissue in response to a high-fat diet. *Diabetologia*. 2007;50:1267–1276.
- Tsukumo DM, Carvalho-Filho MA, Carvalheira JB, Prada PO, Hirabara SM, Schenka AA, Araujo EP, Vassallo J, Curi R, Velloso LA, Saad MJ. Loss-of-function mutation in Toll-like receptor 4 prevents diet-induced obesity and insulin resistance. *Diabetes*. 2007;56:1986–1998.
- Cai Y, Zhang C, Nawa T, Aso T, Tanaka M, Oshiro S, Ichijo H, Kitajima S. Homocysteine-responsive ATF3 gene expression in human vascular endothelial cells: activation of c-Jun NH $_2$ -terminal kinase and promoter response element. *Blood*. 2000;96:2140–2148.
- Hartman MG, Lu D, Kim ML, Kociba GJ, Shukri T, Buteau J, Wang X, Frankel WL, Guiridge D, Prentki M, Grey ST, Ron D, Hai T. Role for activating transcription factor 3 in stress-induced beta-cell apoptosis. *Mol Cell Biol*. 2004;24:5721–5732.
- Poltorak A, He X, Smirnova I, Liu MY, Van Huffel C, Du X, Birdwell D, Alejos E, Silva M, Galanos C, Freudenberg M, Ricciardi-Castagnoli P, Layton B, Beutler B. Defective LPS signaling in C3H/HeJ and C57BL/10ScCr mice: mutations in TLR4 gene. *Science*. 1998;282:2085–2088.
- Kitagawa K, Wada T, Furuichi K, Hashimoto H, Ishiwata Y, Asano M, Takeya M, Kuziel WA, Matsushima K, Mukaida N, Yokoyama H. Blockade of CCR2 ameliorates progressive fibrosis in kidney. *Am J Pathol*. 2004;165:237–246.
- Tamura K, Hua B, Adachi S, Guney I, Kawachi J, Morioka M, Tamamori-Adachi M, Tanaka Y, Nakabeppu Y, Sunamori M, Sedivy JM, Kitajima S. Stress response gene ATF3 is a target of c-myc in serum-induced cell proliferation. *EMBO J*. 2005;24:2590–2601.
- Shulman GI. Cellular mechanisms of insulin resistance. *J Clin Invest*. 2000;106:171–176.
- Havens L, Danielsson KN, Fogelstrand L, Wiklund O. Induction of proinflammatory cytokines by long-chain saturated fatty acids in human macrophages. *Atherosclerosis*. 2009;202:382–393.
- Gilchrist M, Thorsson V, Li B, Rust AG, Korb M, Roach JC, Kennedy K, Hai T, Bolouri H, Aderem A. Systems biology approaches identify ATF3 as a negative regulator of Toll-like receptor 4. *Nature*. 2006;441:173–178.
- Kim HB, Kong M, Kim TM, Suh YH, Kim WH, Lim JH, Song JH, Jung MH. NFATc4 and ATF3 negatively regulate adiponectin gene expression in 3T3-L1 adipocytes. *Diabetes*. 2006;55:1342–1352.
- Inouye S, Fujimoto M, Nakamura T, Takaki E, Hayashida N, Hai T, Nakai A. Heat shock transcription factor 1 opens chromatin structure of interleukin-6 promoter to facilitate binding of an activator or a repressor. *J Biol Chem*. 2007;282:33210–33217.
- Akira S, Takeda K. Toll-like receptor signalling. *Nat Rev Immunol*. 2004;4:499–511.
- Lim JH, Lee JI, Suh YH, Kim W, Song JH, Jung MH. Mitochondrial dysfunction induces aberrant insulin signalling and glucose utilisation in murine C2C12 myotube cells. *Diabetologia*. 2006;49:1924–1936.
- Lu D, Chen J, Hai T. The regulation of ATF3 gene expression by mitogen-activated protein kinases. *Biochem J*. 2007;401:559–567.
- Imai Y, Kuba K, Neely GG, Yaghubian-Malhami R, Perkmann T, van Loo G, Ermolaeva M, Veldhuizen R, Leung YH, Wang H, Liu H, Sun Y, Pasparakis M, Kopf M, Mech C, Bavari S, Peiris JS, Slutsky AS, Akira S, Hultqvist M, Holmdahl R, Nicholls J, Jiang C, Binder CJ, Penninger JM. Identification of oxidative stress and Toll-like receptor 4 signaling as a key pathway of acute lung injury. *Cell*. 2008;133:235–249.
- Horvai A, Palinski W, Wu H, Moulton KS, Kalla K, Glass CK. Scavenger receptor A gene regulatory elements target gene expression to macrophages and to foam cells of atherosclerotic lesions. *Proc Natl Acad Sci U S A*. 1995;92:5391–5395.

Expanded Materials and Methods

Materials and Antibodies

NF- κ B inhibitor BAY11-7085, p38 MAPK inhibitor SB203580, and JNK inhibitor SP600125 were purchased from Merck (San Diego, CA). MEK inhibitor U0126 was purchased from Cell Signaling Technology (Danvers, MA). The pEF-p50-NHA and pEF-p60 plasmids which express p50 and p65 subunits of NF- κ B, respectively, and the pMRX-SR-I κ B α plasmid which expresses a super-repressor form of I κ B α (SR-I κ B α ; a degradation-resistant mutant of I κ B α) are described elsewhere.^{1,2} LPS (from *Escherichia coli* O111: B4) and anti- α -tubulin antibody were purchased from Sigma (San Diego, CA). Palmitate, stearate, and oleate were purchased from Sigma, solubilized in ethanol, and conjugated with fatty acids- and immunoglobulin-free bovine serum albumin (Sigma) at a molar ratio of 10: 1 (fatty acid: albumin) in low serum medium as previously described.³ The concentrations of palmitate used in this study ($< 200 \mu\text{mol/l}$) are within the physiologic levels. Antibody against ATF3 was purchased from Santa Cruz (sc-188, Santa Cruz, CA). All other reagents were purchased from Sigma or Nacalai Tesque (Kyoto, Japan) unless otherwise described.

cDNA Microarray Analysis

Serum starved RAW264 macrophages were treated with palmitate ($200 \mu\text{mol/l}$) or vehicle for 5 h. The epididymal adipose tissue was prepared from 12-week-old male *ob/ob* and wild-type mice. DNA microarray analysis was performed as previously described.⁴ In brief, total RNA was extracted using TRIzol reagent (Invitrogen, Carlsbad, CA) and repurified with an RNeasy purification kit (Qiagen, Hilden, Germany). Ten μg of RNA was applied for microarray analysis (Mouse Genome 430A 2.0; Affymetrix, Santa Clara, CA) and GeneChip software (Affymetrix) was utilized for analysis of microarray data.

Co-culture of Adipocytes and Macrophages

Co-culture of adipocytes and macrophages was performed as described.^{1,4} In brief, serum starved differentiated 3T3-L1 adipocytes ($\sim 0.5 \times 10^6$ cells) were cultured in a 35-mm dish and

macrophages (1.0×10^5 cells of RAW264 macrophages or peritoneal macrophages) were plated onto 3T3-L1 adipocytes. The cells were cultured for 24 h with contact each other and harvested. As a control, adipocytes and macrophages, the numbers of which were equal to those in the co-culture, were cultured separately and mixed after harvest.

Animals

Six-week-old male C3H/HeJ mice which have defective LPS signaling due to a missense mutation in the TLR4 gene⁵ and control C3H/HeN mice were purchased from CLEA Japan (Tokyo, Japan). Genetically obese *ob/ob*, *db/db*, and *KKA^y* mice were purchased from CLEA Japan and Charles River Japan (Tokyo, Japan). The animals were housed in individual cages in a temperature-, humidity-, and light-controlled room (12-h light and 12-h dark cycle) and allowed free access to water and standard chow (Oriental MF; 362 kcal/100 g, 5.4% energy as fat) (Oriental Yeast, Tokyo, Japan), when otherwise noted. In the high-fat feeding experiments, male mice at 10 weeks of age were given free access to water and either the standard chow or high-fat diet (D12492; 556 kcal/100g, 60% energy as fat; Research Diets, New Brunswick, NJ) for 4 weeks.⁶ At the end of the experiments, mice were sacrificed after a 1-h fast under intraperitoneal pentobarbital anesthesia (30 mg/kg). All animal experiments were conducted in accordance to the guidelines of Tokyo Medical and Dental University Committee on Animal Research (No. 0090058).

Generation of Transgenic Mice Overexpressing ATF3 in Macrophages

The 4.96-kb enhancer/promoter of the human scavenger receptor-A (SR-A) gene capable of macrophage-specific expression was kindly provided by Dr. Christopher K. Glass (University of California, San Diego, CA).⁷ A full-length human ATF3 cDNA was fused with SR-A enhancer/promoter and a human growth hormone polyadenylation site. The transgene (Online Figure Va) was linearized and microinjected into the pronuclei of C57BL/6J mouse fertilized eggs. To identify founder mouse lines that carried the SR-A enhancer/promoter-ATF3 transgene, Southern blot analysis was performed using tail tissue DNA. Expression of ATF3

mRNA and protein in peritoneal and bone marrow-derived macrophages was evaluated by real-time PCR and Western blotting, respectively.

Chromatin Immunoprecipitation (ChIP) Assay

To assess ATF3 binding to the TNF α promoter, ChIP assay was performed using the ChIP assay kit (Upstate Biotechnology, CA) according to the manufacture's instruction⁸. After stimulation with LPS, cells were fixed in 1% formaldehyde for 15 min at 37°C to cross-link DNA and proteins, lysed, and sheared with a handy sonicator (Tomy Seiko, Tokyo, Japan) to generate DNA ranging in size from 200 to 1000 bp. The lysates were pre-cleared with protein A-agarose and immunoprecipitated by incubating overnight at 4°C with anti-ATF3 antibody (Sant Cruz) or normal rabbit IgG as a negative control. Before immunoprecipitation, "input" samples were removed from the lysates. After immunoprecipitation, protein-DNA complexes were eluted in a buffer containing 1% SDS and 0.1 M NaHCO₃, and the cross-links were reversed. The resulting DNA was purified by phenol/chloroform extraction and ethanol precipitation, and subjected to semiquantitative PCR analysis.

The primers used for PCR were designed to amplify the proximal sequence of the mouse TNF α promoter containing the AP-1 site at -926 bp relative to the transcription start site (NM_013693): forward (5'-CAGAGACATGGTGGATTACG-3') and reverse (5'-GCCCTGCTTCCAGGATTCTC-3').

Retrovirus-mediated Overexpression and Knockdown of ATF3 in Macrophages

A full-length mouse ATF3 cDNA, consisting of 543 bp encoding 181 amino acid residues, was amplified by PCR with a pair of primers, one with a BamHI site and the other with an EcoRI site at the terminus. The PCR product was inserted into the BamHI/EcoRI cloning sites of the pMRX retroviral vector.⁹ The retroviral expression vector (pMRX-mATF3) capable of expressing mouse ATF3 ORF was transfected into Plat-E packaging cells^{9, 10} and the retrovirus was harvested 48 h to 72 h after transfection.¹¹ RAW264 cells were infected with the viral supernatant for 4 h and then cultured in medium supplemented with 10% fetal bovine

serum before selection. Puromycin (5 μ g/ml) was added to the medium 2 days after the initial infection and the selection was continued for 2 weeks. Stable ATF3-RAW264 cell line was obtained after evaluating the expression levels of ATF3 protein by Western blotting.

pSINsi-hU6 DNA (Code 3661, Takara Bio, Otsu, Japan) for the synthesis of siRNA under the control of the human U6 promoter was used to generate pshATF3 plasmids expressing hairpin RNAs of ATF3 target sequences. The resulting pshATF3#1 and pshATF3#3, synthesizing sequences corresponding to nt 745-763 (5'-GGAACCTCTTTATCCAACA-3') and nt 989-1007 (5'-GCATCCTTTGTCTCACCAA-3'), respectively, of mouse ATF3 mRNA (NM_007498) were used for knockdown of endogenous ATF3. As a control, pshGFP was constructed in the same way and the sequence used to target the GFP gene was as described elsewhere.¹² Retrovirus preparation and RAW264 cell infection are the same as described above except that the selection is under G418 (400 μ g/ml, Invitrogen, Carlsbad, CA). Stable shATF3-Raw264 cell line was verified for the knockdown efficiency by Western blotting.

Transient Transfection and Luciferase Assay

A luciferase reporter assay was performed as previously described⁴ using the luciferase reporter constructs for ATF3 and TNF α promoters.¹³ The luciferase reporter construct with no cis-acting DNA elements was used as a negative control. In brief, RAW264 macrophages or HEK293 cells were transiently transfected by electroporation (Nucleofector system; Amaxa, Gaithersburg, MD) or lipofectamine 2000 (Invitrogen), with a luciferase reporter vector and pRL-TK vector (Promega, Madison, WI) as an internal control for transfection efficiency. The luciferase activity was determined using the Dual-Luciferase Reporter Assay System (Promega).

References

1. Tomita S, Fujita T, Kirino Y, Suzuki T. PDZ domain-dependent suppression of NF- κ B/p65-induced A β 42 production by a neuron-specific X11-like protein. *J Biol Chem*. 2000;275:13056-13060.
2. Hironaka N, Mochida K, Mori N, Maeda M, Yamamoto N, Yamaoka S. Tax-independent constitutive I κ B kinase activation in adult T-cell leukemia cells. *Neoplasia*. 2004;6:266-278.
3. Suganami T, Nishida J, Ogawa Y. A paracrine loop between adipocytes and macrophages aggravates inflammatory changes: role of free fatty acids and tumor necrosis factor α . *Arterioscler Thromb Vasc Biol*. 2005;25:2062-2068.
4. Suganami T, Tanimoto-Koyama K, Nishida J, Itoh M, Yuan X, Mizuarai S, Kotani H, Yamaoka S, Miyake K, Aoe S, Kamei Y, Ogawa Y. Role of the Toll-like receptor 4/NF- κ B pathway in saturated fatty acid-induced inflammatory changes in the interaction between adipocytes and macrophages. *Arterioscler Thromb Vasc Biol*. 2007;27:84-91.
5. Poltorak A, He X, Smirnova I, Liu MY, Van Huffel C, Du X, Birdwell D, Alejos E, Silva M, Galanos C, Freudenberg M, Ricciardi-Castagnoli P, Layton B, Beutler B. Defective LPS signaling in C3H/HeJ and C57BL/10ScCr mice: mutations in TLR4 gene. *Science*. 1998;282:2085-2088.
6. Suganami T, Mieda T, Itoh M, Shimoda Y, Kamei Y, Ogawa Y. Attenuation of obesity-induced adipose tissue inflammation in C3H/HeJ mice carrying a Toll-like receptor 4 mutation. *Biochem Biophys Res Commun*. 2007;354:45-49.
7. Horvai A, Palinski W, Wu H, Moulton KS, Kalla K, Glass CK. Scavenger receptor A gene regulatory elements target gene expression to macrophages and to foam cells of atherosclerotic lesions. *Proc Natl Acad Sci U S A*. 1995;92:5391-5395.
8. Kamei Y, Miura S, Suganami T, Akaike F, Kanai S, Sugita S, Katsumata A, Aburatani H, Unterman TG, Ezaki O, Ogawa Y. Regulation of SREBP1c gene expression in skeletal

Online Supplement CIRCRESAHA/2009/196261/R1 6

- muscle: role of retinoid X receptor/liver X receptor and forkhead-O1 transcription factor. *Endocrinology*. 2008;149:2293-2305.
9. Saitoh T, Nakayama M, Nakano H, Yagita H, Yamamoto N, Yamaoka S. TWEAK induces NF- κ B p100 processing and long lasting NF- κ B activation. *J Biol Chem*. 2003;278:36005-36012.
 10. Morita S, Kojima T, Kitamura T. Plat-E: an efficient and stable system for transient packaging of retroviruses. *Gene Ther*. 2000;7:1063-1066.
 11. Ito A, Suganami T, Miyamoto Y, Yoshimasa Y, Takeya M, Kamei Y, Ogawa Y. Role of MAPK phosphatase-1 in the induction of monocyte chemoattractant protein-1 during the course of adipocyte hypertrophy. *J Biol Chem*. 2007;282:25445-25452.
 12. Caplen NJ, Parrish S, Imani F, Fire A, Morgan RA. Specific inhibition of gene expression by small double-stranded RNAs in invertebrate and vertebrate systems. *Proc Natl Acad Sci U S A*. 2001;98:9742-9747.
 13. Cai Y, Zhang C, Nawa T, Aso T, Tanaka M, Oshiro S, Ichijo H, Kitajima S. Homocysteine-responsive ATF3 gene expression in human vascular endothelial cells: activation of c-Jun NH₂-terminal kinase and promoter response element. *Blood*. 2000;96:2140-2148.

Online Figure Legends**Online Figure I. Identification of ATF3 as a Target Gene of Saturated Fatty Acid in Obese Adipose Tissue.**

(a) cDNA microarray analysis screening for a target of saturated fatty acid/TLR4 signaling in obese adipose tissue. RAW264 macrophages were treated with either palmitate (200 $\mu\text{mol/l}$) or vehicle for 5 h. The epididymal adipose tissue was prepared from 12-week-old male *ob/ob* or wild-type mice. (b) Tissue distribution of ATF3 and F4/80 mRNAs in mice. WAT, white adipose tissue. Open and closed bars indicate wild-type mice fed standard diet and *db/db* mice fed high-fat diet, respectively. * $P < 0.01$ vs. wild-type mice fed standard diet. $n = 4-6$.

Online Figure II. Role of the TLR4/NF- κ B Signaling in ATF3 mRNA Expression in the Interaction between Adipocytes and Macrophages.

(a) ATF3 and TNF α mRNA expression in the co-culture between 3T3-L1 adipocytes and peritoneal macrophages obtained from C3H/HeN mice (HeN) or C3H/HeJ mice (HeJ). ct, control culture; co, co-culture. * $P < 0.05$, ** $P < 0.01$ vs. the respective ct; # $P < 0.05$. $n = 4$. (b) Role of NF- κ B in the co-culture-induced ATF3 and TNF α mRNA expression. Co-culture was performed using 3T3-L1 adipocytes and RAW264 macrophages. BAY, BAY11-7085 10 $\mu\text{mol/l}$. * $P < 0.05$, ** $P < 0.01$ vs. Veh/ct; # $P < 0.05$, ## $P < 0.01$. $n = 4$.

Online Figure III. Effect of ATF3 Overexpression on IL-6 and iNOS mRNA Expression *in vitro* and *in vivo*.

(a) Effect of ATF3 on the palmitate-induced IL-6 and iNOS mRNA expression in RAW264 macrophages overexpressing ATF3 (ATF3) and control RAW264 macrophages (Mock). (b) IL-6 and iNOS mRNA expression in the adipose tissue from WT:KK, Tg:KK, WT:KK A^y , and Tg:KK A^y mice. Veh, vehicle; Pal, palmitate 200 $\mu\text{mol/l}$; WT, wild-type; Tg, ATF3 transgenic mice. ** $P < 0.01$ vs. Veh/Mock; ## $P < 0.01$. $n = 4$.

Online Figure IV. Effect of MAPK Inhibitors on Palmitate- and LPS-induced ATF3 and TNF α mRNA Expression in RAW264 Macrophages.

Veh, vehicle; Pal, palmitate

Online Supplement CIRCRESAHA/2009/196261/R1 8

100 $\mu\text{mol/l}$; LPS, LPS 10 ng/ml; U, U0126 5 $\mu\text{mol/l}$; SP, SP600125 10 $\mu\text{mol/l}$; SB, SB203580 10 $\mu\text{mol/l}$. $**P < 0.01$ vs. Veh/Veh, $##P < 0.01$. $n = 4$.

Online Figure V. Generation of Transgenic Mice Overexpressing ATF3 in Macrophages. (a) Schematic representation of the mouse SR-A promoter/human ATF3 fusion gene. (b) Western blot analysis of ATF3 protein expression in peritoneal macrophages and bone marrow-derived macrophages obtained from three independent transgenic lines (#2, #25, #35) and wild-type mice.

Online Table 1. Primers used in this study.

Genes	Primers
Adiponectin	Fw: 5'-ATGGCAGAGATGGCACTCCT-3' Rv: 5'-CCTTCAGCTCCTGTCATTCCA-3'
Arginase 1	Fw: 5'-CTCCAAGCCAAAGTCCTTAGAG-3' Rv: 5'-AGGAGCTGTCAATTAGGGACATC-3'
ATF3	Fw: 5'-TGCCTGCAGAAAGAGTCAGAGA-3' Rv: 5'-AGCTCCTCGATCTGGGCC-3'
CD11c	Fw: 5'-CTGGATAGCCTTTCTTCTGCTG-3' Rv: 5'-GCACACTGTGTCCGAACTC-3'
F4/80	Fw: 5'-CTTTGGCTATGGGCTTCCAGTC-3' Rv: 5'-GCAAGGAGGACAGAGTTTATCGTG-3'
IL-6	Fw: 5'-ACAACCACGGCCTTCCCTACTT-3' Rv: 5'-CACGATTTCCCAGAGAACATGTG-3'
iNOS	Fw: 5'-CCAAGCCCTCACCTACTTCC-3' Rv: 5'-CTCTGAGGGCTGACACAAGG-3'
Mannose receptor	Fw: 5'-CGGTGAACCAAATAATTACCAAAAT-3' Rv: 5'-GTGGAGCAGGTGTGGGCT-3'
TNF α	Fw: 5'-ACCCTCACACTCAGATCATCTTC-3' Rv: 5'-TGGTGGTTTGCTACGACGT-3'
36B4	Fw: 5'-GGCCCTGCACTCTCGCTTTC-3' Rv: 5'-TGCCAGGACGCGCTTGT-3'

Online Table II. Up-regulated genes both in obese adipose tissue and saturated fatty acid-stimulated macrophages.

Accession ID	Gene Symbol	Gene Title	Adipose tissue (<i>ob/ob</i> vs. WT)	RAW264 (Pal vs. Veh)
NM_031167	Il1rn	interleukin 1 receptor antagonist	15.0	2.6
NM_015811	Rgs1	regulator of G-protein signaling 1	14.8	2.8
NM_010442	Hmox1	heme oxygenase (decycling) 1	8.6	3.5
M57525	Il1rn	interleukin 1 receptor antagonist	8.6	2.1
NM_023044	Slc15a3	solute carrier family 15, member 3	8.6	3.7
BC022752	Slc37a2	solute carrier family 37 (glycerol-3-phosphate transporter), member 2	8.6	2.3
AF065933	Ccl2	chemokine (C-C motif) ligand 2	7.8	3.2
BC019946	Atf3	activating transcription factor 3	5.2	4.3
AV026617	Fos	FBJ osteosarcoma oncogene	5.2	4.3
NM_011315	Saa3	serum amyloid A 3	4.9	2.0
NM_008871	Serpine1	serine (or cysteine) proteinase inhibitor, clade E, member 1	4.7	17.1
BM210600	Npn3	neoplastic progression 3	4.4	2.3
AK011545	Baspl	brain abundant, membrane attached signal protein 1	4.4	2.6
NM_138648	unknown	unknown	4.3	2.1
NM_013612	Slc11a1	solute carrier family 11 (proton-coupled divalent metal ion transporters), member 1	4.1	2.0
BC011325	Npn3	neoplastic progression 3	3.7	2.6
AF128193	Ccl7	chemokine (C-C motif) ligand 7	3.2	3.0
NM_008129	Gclm	glutamate-cysteine ligase, modifier subunit	2.6	2.8
NM_016903	Esd	esterase D/formylglutathione hydrolase	2.4	2.3
M57525	Il1rn	interleukin 1 receptor antagonist	2.3	2.1

ob/ob and WT, 12-week-old male *ob/ob* and wild-type mice, respectively. Pal, palmitate 200 μ mol/l; Veh, vehicle.

Downloaded from circres.ahajournals.org at NANKODO CO LTD on February 8, 2010

Online Table III. Down-regulated genes both in obese adipose tissue and saturated fatty acid-stimulated macrophages.

Accession ID	Gene Symbol	Gene Title	Adipose tissue (<i>ob/ob</i> vs. WT)	RAW264 (Pal vs. Veh)
NM_026713	Mogat1	monoacylglycerol O-acyltransferase 1	-5.9	-2.0
BB560574	Cd24a	CD24a antigen	-3.9	-3.2
NM_007446	Amy1	amylase 1, salivary	-3.0	-2.5
BI686700	LOC216024	Similar to heterogeneous nuclear ribonucleoprotein H3, isoform a	-2.5	-2.3
BG074158	2610001E17Rik	RIKEN cDNA 2610001E17 gene	-2.4	-2.3

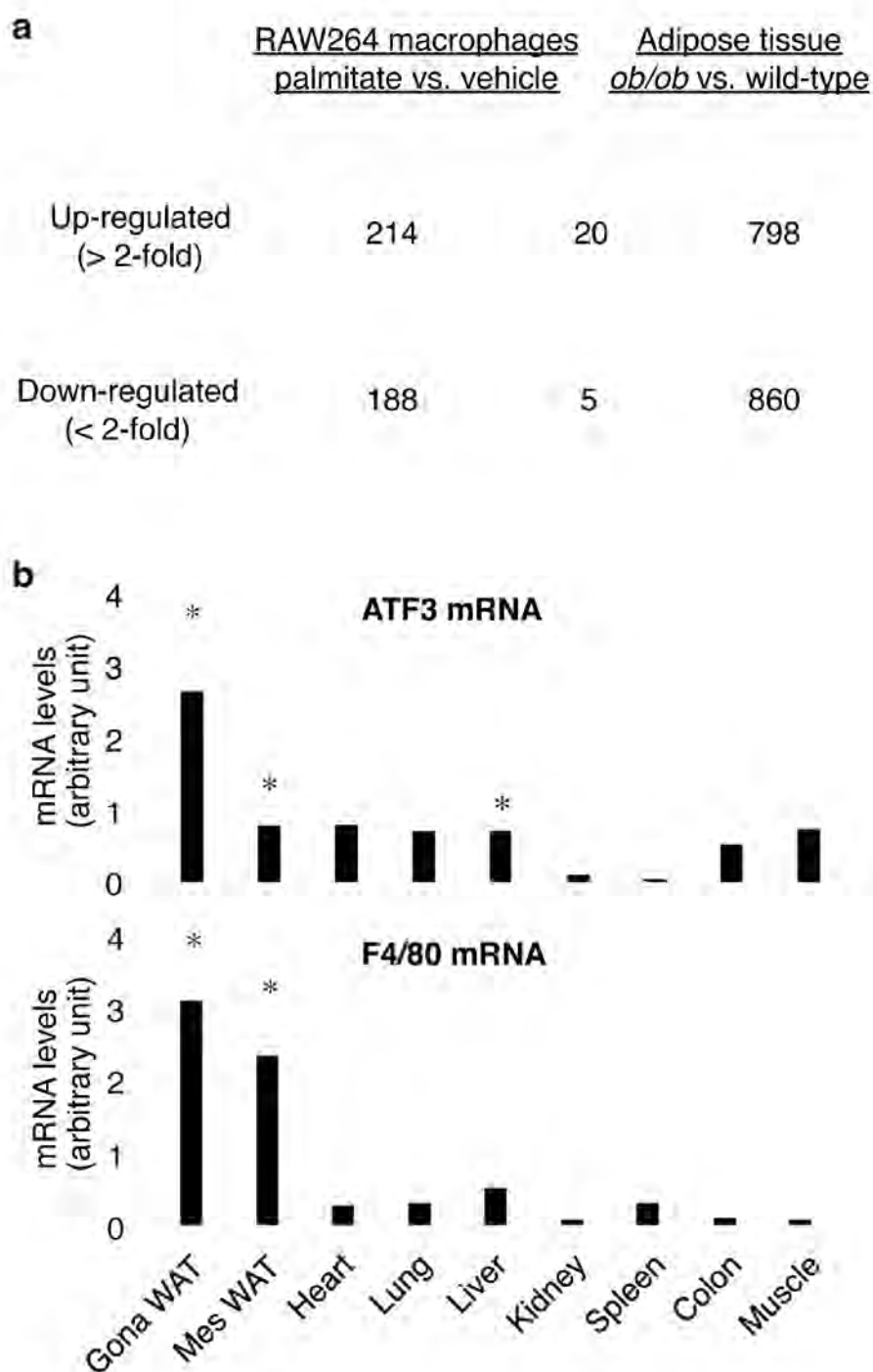
ob/ob and WT, 12-week-old male *ob/ob* and wild-type mice, respectively. Pal, palmitate 200 μ mol/l; Veh, vehicle.

Downloaded from circres.ahajournals.org at NANKODO CO LTD on February 8, 2010

Online Table IV. Body weight and adipose tissue weight of C3H/HeJ and C3H/HeN mice on a standard or high-fat diet for 16 weeks.

	body weight (g)	epididymal WAT weight (g)	mesenteric WAT weight (g)
SD-fed HeN	27.1 ± 0.8	0.21 ± 0.03	0.17 ± 0.03
HD-fed HeN	39.3 ± 0.8*	0.54 ± 0.04**	0.47 ± 0.02**
SD-fed HeJ	31.2 ± 1.0	0.31 ± 0.07	0.18 ± 0.05
HD-fed HeJ	41.0 ± 0.8 ^{##}	0.61 ± 0.03 ^{##}	0.43 ± 0.03 ^{##}

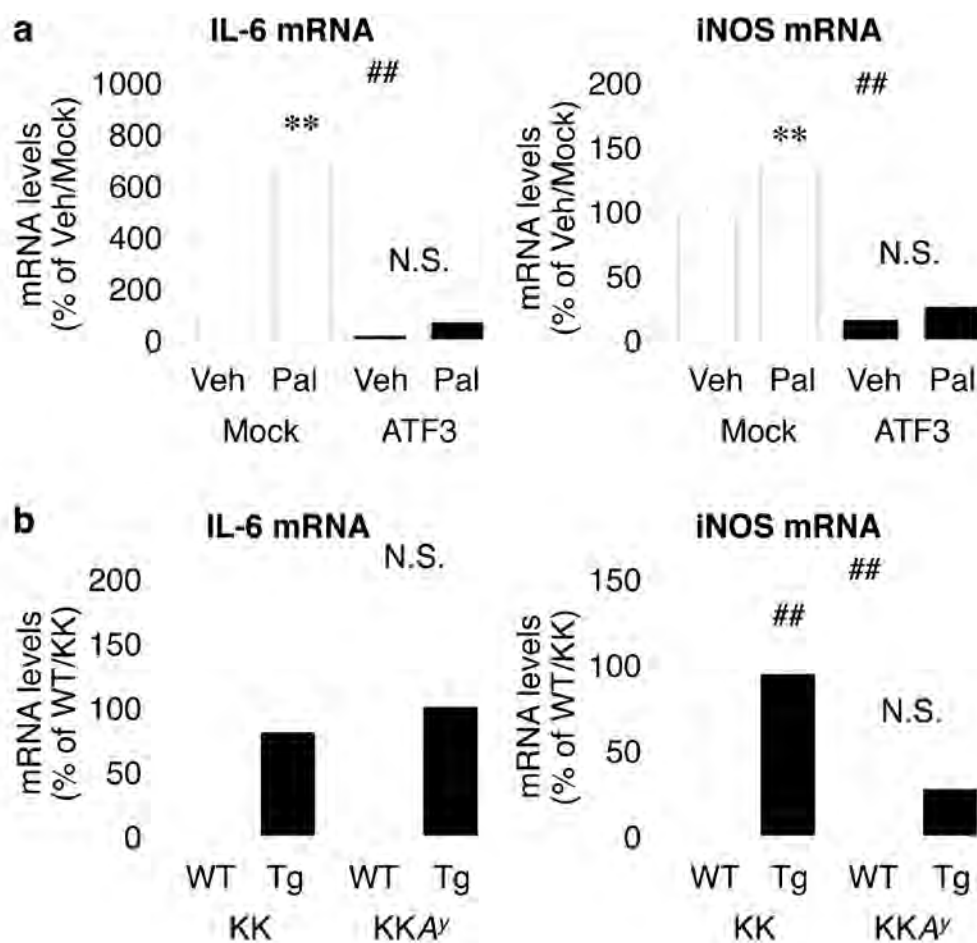
SD, standard diet; HD, high-fat diet; HeN, C3H/HeN; HeJ, C3H/HeJ; WAT, white adipose tissue. * $P < 0.05$, ** $P < 0.01$ vs. SD-fed HeN, ^{##} $P < 0.01$ vs. SD-fed HeJ, $n = 6-10$.



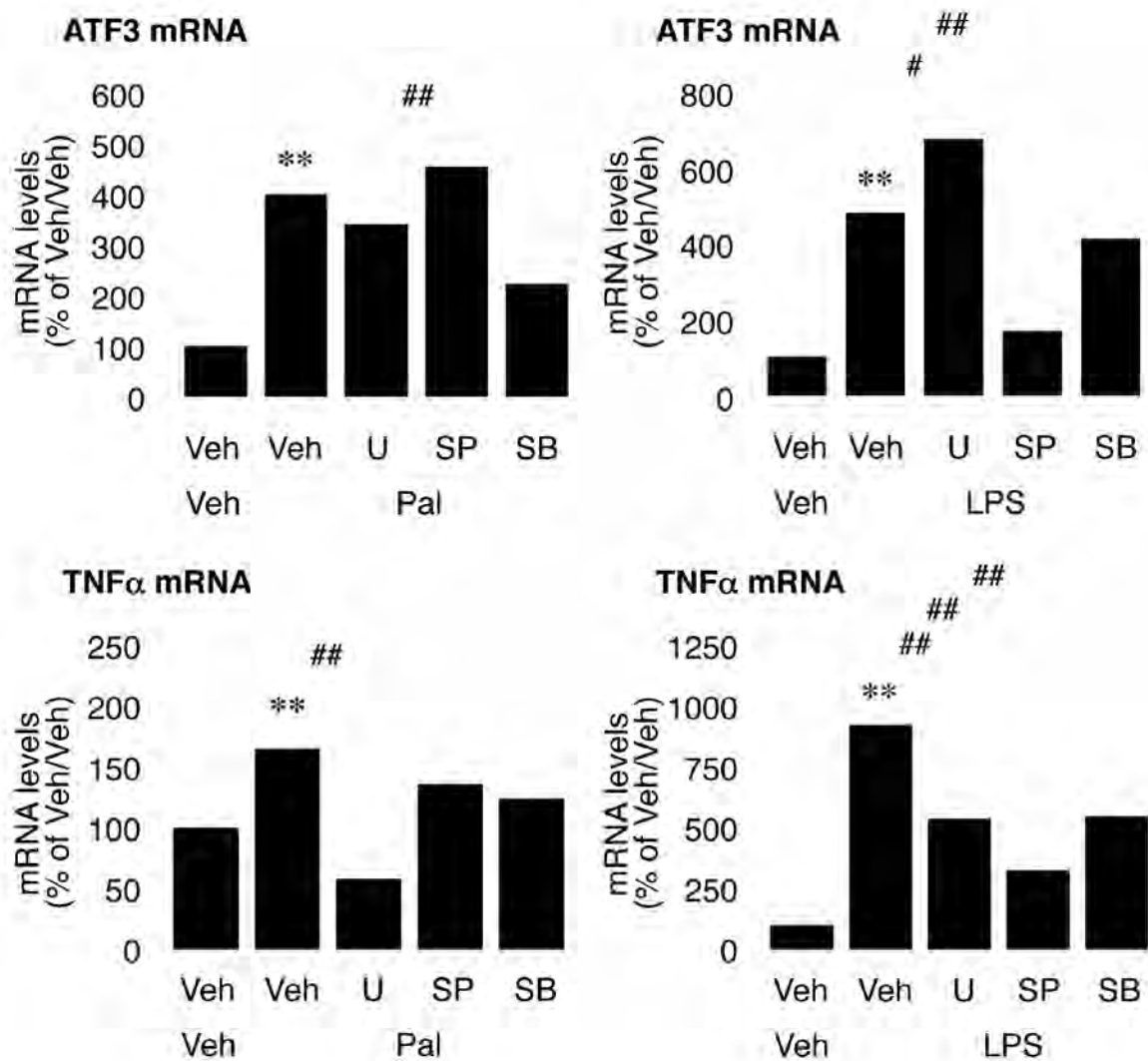
Online Figure I



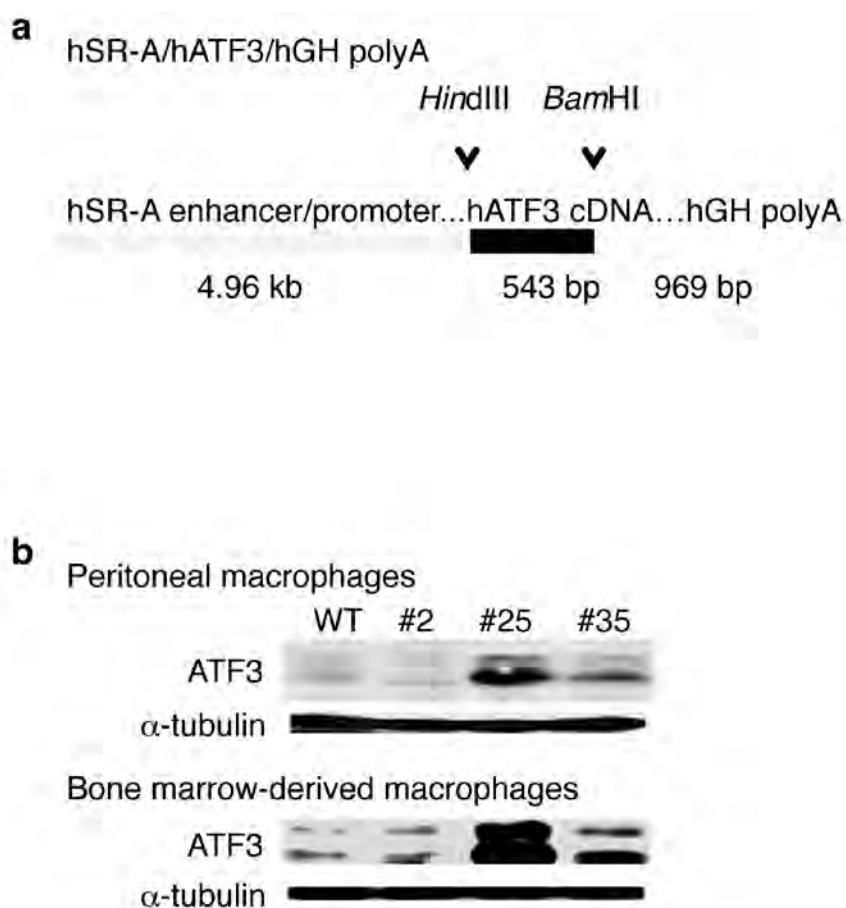
Downloaded from circres.ahajournals.org at NANKODO CO LTD on February 8, 2010



Online Figure III



Online Figure IV



Online Figure V

Downloaded from circres.ahajournals.org at NANKODO CO LTD on February 8, 2010

形質発現分野

萩原 正敏

疾患生命科学研究部・高次生命制御研究部門
形質発現制御学・教授



1) 研究の課題名

mRNA スプライシングと遺伝子発現諸過程との連携の解析

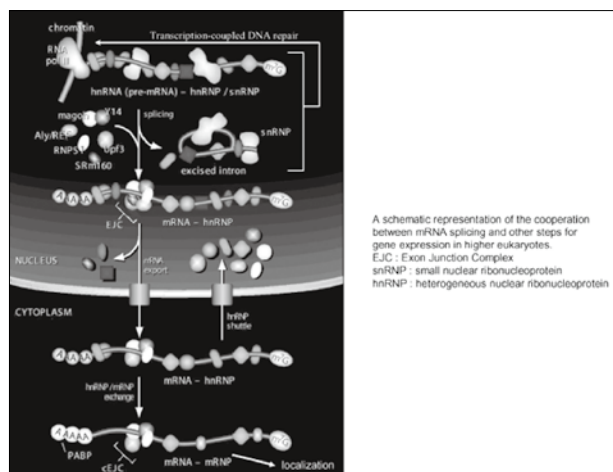
高等真核生物では、核にコードされる遺伝子の多くはイントロンによって分断化されている。さらにヒトでは、RNA ポリメラーゼ II によって転写される一次転写産物のうち実に95%以上がイントロンである。これらのことは、イントロンを除く反応、すなわち mRNA スプライシングが遺伝子発現には必須であり、除去されたイントロンが核内できちんと代謝されることが必要であることを示している。このイントロン代謝過程を明らかにしたいと考えている。また、mRNA スプライシングは単にイントロンを除去するだけの反応ではなく、エクソンとエクソンとの連結部近傍に、EJC という特異的な複合体を付加し、mRNA スプライシングと他の細胞内遺伝子発現過程との連携を行う過程であることが明らかになってきた。中でも神経細胞における細胞内 mRNA 局在、転写と共役した DNA 修復 (TCR) との連携を示唆するデータを得ており、mRNA スプライシングとこれらの過程の新たな連携を明らかにしていきたいと考えている。

・ Molecular links of mRNA splicing with Transcription coupled DNA repair and mRNA Localization in the cytoplasm

In higher eukaryotes, most genes in the nucleus are separated by introns. Furthermore, more than 95% region of the primary transcripts produced by RNA polymerase II is intronic sequence in human. These results indicate that mRNA splicing is an essential step for gene expression in eukaryotes, and also imply that post splicing turnover of excised introns in the nucleus is important for higher eukaryotes. We would like to understand this step comprehensively including the factors involved. Recently it has been shown that mRNA splicing is a step not only to remove introns but also to make a link with other gene

expression steps by depositing Exon Junction Complex near exon-exon junctions. The results we obtained so far suggest that mRNA splicing affects transcription coupled DNA repair and mRNA localization in the cytoplasm of neuronal cells. We would like to uncover new links between mRNA splicing and those steps.

2)



3) 研究内容の英文要約

1. VEGF is produced either as pro-angiogenic or anti-angiogenic proteins depending upon splice site choice in the terminal, eighth exon. Proximal splice site selection (PSS) in exon 8 generates pro-angiogenic isoforms such as VEGF165, and distal splice site selection (DSS) results in anti-angiogenic isoforms such as VEGF165b. Cellular decisions on splice site selection depend upon the activity of RNA binding splice factors, such as ASF/SF2, which have previously been shown to regulate VEGF splice site choice. To determine the mechanism by which the pro-angiogenic splice site choice is mediated, we investigated the effect of inhibition of ASF/SF2 phosphorylation by SR protein kinases (SRPK1/2) on splice site choice in epithelial cells and

- in in vivo angiogenesis models. Epithelial cells treated with insulin like growth factor-1 (IGF-1) increased PSS and produced more VEGF165 and less VEGF165b. This down-regulation of DSS and increased PSS was blocked by protein kinase C inhibition and SRPK1/2 inhibition. IGF-1 treatment resulted in nuclear localisation of ASF/SF2, which was blocked by SPRK1/2 inhibition. Pull down assay and RNA immunoprecipitation using VEGF mRNA sequences identified an 11 nucleotide sequence required for ASF/SF2 binding. Injection of an SRPK1/2 inhibitor reduced angiogenesis in a mouse model of retinal neovascularisation, suggesting that regulation of alternative splicing could be a potential therapeutic strategy in angiogenic pathologies.
2. Viruses use alternative splicing to produce a broad series of proteins from small genomes by utilizing the cellular splicing machinery. Since viruses use cellular RNA binding proteins for viral RNA processing, it is presumable that the splicing of cellular pre-mRNAs is affected by viral infection. Here, we showed that herpes simplex virus type 2 (HSV-2) modifies the expression of promyelocytic leukemia (PML) isoforms by altering pre-mRNA splicing. Using a newly developed virus-sensitive splicing reporter, we identified the viral protein ICP27 as an alternative splicing regulator of PML isoforms. ICP27 was found to bind preferentially to PML pre-mRNA and directly inhibit the removal of PML intron 7a in vitro. Moreover, we demonstrated that ICP27 functions as a splicing silencer at the 3' splice site of the PML intron 7a. The switching of PML isoform from PML-II to PML-V as induced by ICP27 affected HSV-2 replication, suggesting that the viral protein modulates the splicing code of cellular pre-mRNA (s) governing virus propagation.
 3. Serine/arginine-rich (SR) proteins play essential roles in the constitutive and regulated splicing of precursor mRNAs. Phosphorylation of the arginine/serine dipeptide-rich (RS) domain by SR protein kinases such as Cdc2-like kinases (Clk/Sty) modulates their subcellular localization and activation. However, it remains unclear how these kinases and their target SR proteins are regulated by extracellular signals. Regulation of protein kinase C betaII (PKCbetaII) pre-mRNA alternative splicing via exon inclusion by Akt2, a central kinase in insulin action, involves phosphorylation of SR proteins. Here we showed that Akt2, in response to insulin, resulted in phosphorylation of Clk/Sty, which then altered SR protein phosphorylation in concert with Akt2. Insulin-stimulated PKCbetaII pre-mRNA splicing was blocked by Clk/Sty and phosphatidylinositol-3-kinase inhibitors, and diabetic Akt2-null mouse tissues had impaired phospho-Clk/Sty, SR protein phosphorylation, and PKCbetaII expression. Furthermore, we observed that Akt2 phosphorylated several SR proteins distinct from Clk/Sty in response to insulin. Akt2-catalyzed phosphorylation of Clk/Sty and SR proteins revealed a role for both kinases in splicing regulation indicating dual functions for Akt2 in response to insulin in this pathway.
 4. SR proteins are non-snRNP splicing factors harbouring a domain rich in Arg-Ser repeats, which are extensively phosphorylated by several kinases. We performed a comparative study of different SR kinases, including SRPK, Clk, PRP4 and DYRK, and found that only Clks efficiently altered 5' splice site selection of Adenovirus E1A. The phosphorylation state of SR proteins was examined using a phospho-SR specific antibody mAb1H4 and a 75 kDa protein was most evidently hyperphosphorylated by Clks. Administration of TG003, a specific inhibitor for the Clk family members, specifically and rapidly induced dephosphorylation of 75 kDa SR protein. Imaging with mRFP-SRp75 in living cells revealed that its nuclear distribution was rapidly altered upon inhibition of the Clk activity by TG003. Co-transfection experiments demonstrated that HA-tagged SRp75 was hyperphosphorylated by Clk family members, but not by other SR kinases. These results indicate that Clks specifically hyperphosphorylate SRp75. Furthermore, SRp75 over-expression promoted the selection of 12S 5' splice site in E1A pre-mRNA, which is stimulated by co-expression of Clks. These results suggest that the specific combination of SR protein and SR kinase plays a distinct role in alternative splicing through dynamic balance of phosphorylation.
 5. Alternative splicing of pre-mRNAs greatly contributes to the spatiotemporal diversity of gene expression in metazoans. However, the molecular basis of developmental regulation and the precise sequence of alternative pre-mRNA processing in vivo are poorly understood. In the present study, we focus on the developmental switching of the mutually exclusive alternative splicing of the *let-2* gene of *Caenorhabditis elegans* from the exon 9 form in embryos to the exon 10 form in adults. By visualizing the usage of the *let-2* mutually exclusive exons through differential expression of green fluorescent protein (GFP) and red fluorescent protein (RFP), we isolated several switching-defective mutants and identified the alternative splicing defective-2 (*asd-2*) gene, encoding a novel member of the evolutionarily conserved STAR (signal transduction activators of RNA) family of RNA-binding proteins. Comparison of the amounts of partially spliced *let-2* RNAs in synchronized wild-type and *asd-2* mutant worms suggested that either of the introns downstream from the *let-2* mutually exclusive exons is removed prior to the removal of the upstream ones, and that *asd-2* promotes biased excision of intron 10 in the late larval stages. We propose that the developmental switching

between alternative sequences of intron removal determines the ratio between the mature let-2 mRNA isoforms.

4) GCOE事業を推進するに当たって力を入れた点

大学院生に Scientistとしての理想を醸成し、実践的研究能力を身に付けさせるべく、活発な双方向的 discussionを心がけた。

5) 英文原著論文

1. Nowak DG, Amin EM, Rennel ES, Hoareau-Aveilla C, Gammons M, Damodoran G, Hagiwara M, Harper SJ, Woolard J, Lodomery MR, Bates DO.(2009) Regulation of vascular endothelial growth factor (VEGF) splicing from pro-angiogenic to anti-angiogenic isoforms - a novel therapeutic strategy for angiogenesis, J. Biol. Chem. Nov 11
2. Nojima T, Oshiro-Ideue T, Nakanoya H, Kawamura H, Morimoto M, Kawaguchi Y, Kataoka N and Hagiwara M (2009) Herpesvirus protein ICP27 switches PML isoform by altering mRNA splicing Nucleic. Acids Res. Oct;37(19):6515-27
3. Jiang K, Patel NA, Watson JE, Apostolatos H, Kleiman E, Hanson O, Hagiwara M, Cooper DR. (2009) Akt2 regulation of Cdc2-like kinases (Clk/Sty), serine/arginine-rich (SR) protein phosphorylation, and insulin-induced alternative splicing of PKC δ mRNA. Endocrinology 2009 May;150(5):2087-97
4. Yomoda, J., Muraki, M., Kataoka, N., Hosoya, T., Suzuki, M., Hagiwara, M. and Kimura, H. (2008) Combination of Clk family kinase and SRp75 modulates alternative splicing of Adenovirus E1A. Genes Cells, 13, 233-244.
5. Ohno, G., Hagiwara, M. and Kuroyanagi, H. (2008) STAR family RNA-binding protein ASD-2 regulates developmental switching of mutually exclusive alternative splicing in vivo. Genes & Dev., 22,360-374.

6) 著書

萩原正敏 mRNA スプライシング制御から難治疾患の治療へ (2009) 実験医学 Vol.27 No.17 190-195

萩原正敏 タンパク質リン酸化酵素を標的とした創薬 (2009) 現代化学 11月 63-67

萩原正敏 リン酸化依存的スプライシング制御機構 蛋白質 核酸 酵素 増刊『mRNA プログラム』(印刷中)
野島孝之、萩原正敏 ウイルスによるスプライシング暗号の利用と攪乱 (2009) 実験医学 Vol.27, No.10, 1482-1487.

萩原正敏 リン酸化酵素阻害剤のケミカルバイオロジー (2008)「新規素材探索－医薬品リード化合物・食品素材を求めて－」129-135 (CMC 出版)

萩原正敏 ケミカルバイオロジー概論 (2008) 日薬理誌 132, 4-6.

萩原正敏 リン酸化酵素阻害薬によるケミカルバイオロジー研究の展開 (2008) 日薬理誌 132, 22-25.

7) 特許取得、特許申請

- 1) 発明の名称:蛋白質のリン酸化を測定するためのモニター蛋白質
①発明者:萩原正敏、井上敏、永井康雄
②出願日:1999年9月2日 (PCT/JP99/04769)
③出願人:国立大学法人東京医科歯科大学
④発明の内容の概略:蛋白のリン酸化による構造変化を FRET によって可視化することに成功し、生きた細胞内のリン酸化反応を計時的にモニターし定量化できるモニター蛋白質 ART を開発した。
- 2) 発明の名称:異常スプライシング関連疾患の治療薬候補物質
①発明者:萩原正敏、鈴木正昭
②出願日:2005年1月6日 (US 11/029/470)
2005年1月7日 (AU 2005200040)
③出願人:国立大学法人東京医科歯科大学
④発明の内容の概略:Clk 阻害により異常スプライシングを是正する化合物に関する特許。
- 3) 発明の名称:SR 蛋白質のリン酸化制御方法、および SR 蛋白質の活性制御剤を有効成分とする抗ウイルス剤
①発明者:萩原正敏、福原武志、鈴木正昭、細谷孝充
②基礎出願日:2003年12月26日 (特願 2003-435085)
PCT 出願日:2004年12月24日 (PCT/JP2004/19393)
③出願人:萩原 正敏
④発明の内容の概略:新規 SR タンパク質リン酸化酵素阻害剤のウイルス増殖抑制に関する特許。
- 4) 発明の名称:生体内における選択的スプライシングレポーター系
①発明者:萩原正敏、黒柳秀人
②米国 出願日:2006年9月26日 (US .11/904, 094)
③出願人:国立大学法人東京医科歯科大学

- ④発明の内容の概略:線虫で選択的スプライシングを可視化し、制御因子や制御化合物を同定する方法に関する特許。
- 5) 発明の名称:抗DNAウイルス作用を有するアニリン誘導体
- ①発明者:萩原正敏、小野木博、細谷孝充、山本誠、野中洋介、平松俊行
- ②基礎出願日:2007年8月3日 (特願 2007-203356)
PCT 出 願 日:2008年8月1日 (PCT / JP2008 / 064267)
- ③出願人:株式会社 キノファーマ
- ④発明の内容の概略:DNAウイルスに対して抗ウイルス作用を有するアニリン誘導体に関する特許。
- 6) 発明の名称:発光タンパク質を用いたリン酸化酵素阻害物質のスクリーニング方法
- ①発明者:萩原正敏、野村奈美子、木村広、野崎直仁
- ②基礎出願日:2008年3月4日 (特願 2008-053502)
日本 本 出 願 日:2009年3月3日 (特 願 2009-049763)
- ③出願人:株式会社キノファーマ
- ④発明の内容の概略:発光タンパク質エクオリンを用いて、non-RIで高感度かつ簡便にリン酸化酵素阻害物質をスクリーニングする技術に関する特許。
- 7) 発明の名称:抗RNAウイルス作用を有するアニリン誘導体
- ①発明者:萩原正敏、小野木博、鈴木正昭、古山浩子、細谷孝充、平松俊行
- ②基礎出願日:2008年3月25日 (特願 2008-078728)
PCT 出 願 日:2009年2月4日 (JP2009 / 052253)
- ③出願人:株式会社 キノファーマ
- ④発明の内容の概略:RNAウイルスに対して抗ウイルス作用を有するアニリン誘導体に関する特許。
- 8) 発明の名称:DYRKを阻害するベンゾチアゾール誘導体を含有する医薬組成物
- ①発明者:萩原正敏、澁谷浩司、大西英理子、小川靖、細谷孝充、平松俊行、吉田実代
- ②基礎出願日:2008年7月23日 (特願 2008-190277)
韓 国 出 願 日:2008年12月31日 (KR 10-2008-0138074)
- ③出願人:株式会社 キノファーマ

④発明の内容の概略: DYRK 阻害能を有するベンゾチアゾール誘導体に関する特許。

9) 発明の名称:DYRKを阻害するピチアゾール誘導体を含有する医薬組成物

①発明者:萩原正敏、野中洋介、土橋圭子、吉田実代、平松俊行

②基礎出願日:2009年2月20日 (特願 2009-038327)

③出願人:株式会社 キノファーマ

④発明の内容の概略: DYRK 阻害能を有するピチアゾール誘導体に関する特許。

8) 学会発表 (英文)

萩原正敏:Visualization and manipulation of alternative splicing 日本分子生物学会、神戸、2008年12月

萩原正敏:Deciphering of splicing codes 大学院医歯学総合研究科「医歯学先端研究特論」第17~18回 GCOE 総合国際プレゼンテーション 平成21年3月23日 (月) 12:30~14:00 場所:歯学部4階 特別講堂

萩原正敏:Visualization of mRNA splicing by GFP and its chemical manipulation. (蛍光タンパク質による mRNA スプライシングの可視化とその制御) 2009日本化学会ノーベル賞記念シンポジウム 2009年3月25日

9) 学会発表 (和文)

萩原正敏:ダウン症治療薬の創製 第45回日本臨床分子医学会学術集会 2008/7/25

萩原正敏:Pre-mRNA の選択的スプライシング制御機構とその異常に起因する疾患 東京大学 2008年9月

萩原正敏:Pre-mRNA の選択的スプライシング制御機構とその医学的意義について 成育医療センター 2008年9月

萩原正敏:新しい創薬標的:Pre-mRNA スプライシング制御機構とその医学的意義について 三重大学 2008年12月

萩原正敏:mRNA スプライシングの分子イメージングと医療分野への展開 第19回大学院セミナー 2009年1月26日

萩原正敏:蛋白リン酸化酵素を標的とする創薬戦略 エーザイ 2008年2月

萩原正敏:リン酸化酵素阻害剤をプローブとした生命現象の解明と新しい創薬標的の発見 日本化学会 2009年3月

萩原正敏:RNA結合蛋白リン酸化酵素を標的とする創薬戦略 大学教育支援プログラム(大学院GP)「創薬に向けた医薬科学を先導する人材の要請」慶応大学 北里講堂 2009年3月

10) 外部資金の獲得状況

萩原正敏(代表) 文部科学省 特定領域研究「ヘルペスウイルスRNAの核外輸送制御機構の解明」

萩原正敏(代表) 独立行政法人 医薬基盤研究所 保健医療分野における基礎研究推進事業「RNA結合蛋白を標的とする革新的抗ウイルス剤の開発」

萩原正敏(代表) 日本学術振興会 基盤研究B(一般)「イントロンレスRNAの核外輸送の分子メカニズム」

萩原正敏(代表) 独立行政法人 新エネルギー・産業技術総合開発機構(NEDO)「分子イメージング機器研究開発プロジェクト/新規悪性腫瘍分子プローブの基盤技術開発」

萩原正敏(代表) 文部科学省 受託研究「難治感染症に対する新規治療薬開発のためのイメージング研究」

萩原正敏(代表) 財団法人 内藤記念科学振興財団 医学研究助成「神経細胞におけるmRNA前駆体上に隠されたスプライシング暗号の解読」

萩原正敏(代表) 財団法人 武田科学振興財団 生命科学的研究助成「遺伝子発現パターンの可視化によるスプライシング暗号の解明」

萩原正敏(代表) 財団法人 上原記念生命科学財団 特別研究助成「リン酸化酵素阻害剤によるウイルス増殖阻害」

11) 特別講演、招待講演(学会名、日時、場所)

国際学会招待講演

萩原正敏:Mechanism of Herpesvirus-induced Alternative Splicing of Cellular Genes, Gordon Research Conference、アメリカ、2008年7月

黒柳秀人:日英先端科学シンポジウム、神奈川、2008年10月

萩原正敏:Visualization and manipulation of alternative pre-mRNA splicing. 研究所ネットワーク国際シンポジウム 2008年11月

萩原正敏:Visualization and manipulation of mRNA splicing. 中国医科大学国際シンポジウム、瀋陽 2008年11月

萩原正敏:Visualization and manipulation of alternative pre-mRNA splicing 病態発現機構国際シンポジウム、東京、2008年12月

萩原正敏:New Visualization System to Decipher Splicing Codes Hidden in the Pre-mRNAs, Duke大学、アメリカ、2008年6月

萩原正敏:Development of New Protein Kinase Inhibitors and Their Antiviral Effects ハノイ医科大学、ベトナム 2008年9月

12) 主催学会

シンポジウム主催

1. 日本分子生物学会、神戸、2008年12月
2. The Expanding World of Post-transcriptional Regulation on Gene Expression 病態発現機構国際シンポジウム 東京、2008年12月

13) 新聞、雑誌、TV報道

日経産業新聞

H20.5.29 先端技術 「リン酸化酵素」

Published online 3 September 2009

Nucleic Acids Research, 2009, Vol. 37, No. 19 6515–6527
doi:10.1093/nar/gkp633

Herpesvirus protein ICP27 switches PML isoform by altering mRNA splicing

Takayuki Nojima^{1,2}, Takako Oshiro-Ideue¹, Hiroto Nakanoya¹, Hidenobu Kawamura¹, Tomomi Morimoto³, Yasushi Kawaguchi³, Naoyuki Kataoka⁴ and Masatoshi Hagiwara^{1,2,*}

¹Laboratory of Gene Expression, School of Biomedical Science, ²Department of Functional Genomics, Tokyo Medical and Dental University, Yushima 1-5-45, Bunkyo-ku, Tokyo 113-8510, ³Department of Infectious Disease Control, International Research Center for Infectious Diseases, The Institute of Medical Science, The University of Tokyo, Shirokanedai 4-6-1, Minato-ku, Tokyo 108-8639, Japan and ⁴Medical Top Track (MTT) Program, Medical Research Institute, Tokyo Medical and Dental University, Yushima 1-5-45, Bunkyo-ku, Tokyo 113-8510

Received April 30, 2009; Revised July 6, 2009; Accepted July 16, 2009

ABSTRACT

Viruses use alternative splicing to produce a broad series of proteins from small genomes by utilizing the cellular splicing machinery. Since viruses use cellular RNA binding proteins for viral RNA processing, it is presumable that the splicing of cellular pre-mRNAs is affected by viral infection. Here, we showed that herpes simplex virus type 2 (HSV-2) modifies the expression of promyelocytic leukemia (PML) isoforms by altering pre-mRNA splicing. Using a newly developed virus-sensitive splicing reporter, we identified the viral protein ICP27 as an alternative splicing regulator of PML isoforms. ICP27 was found to bind preferentially to PML pre-mRNA and directly inhibit the removal of PML intron 7a *in vitro*. Moreover, we demonstrated that ICP27 functions as a splicing silencer at the 3' splice site of the PML intron 7a. The switching of PML isoform from PML-II to PML-V as induced by ICP27 affected HSV-2 replication, suggesting that the viral protein modulates the splicing code of cellular pre-mRNA(s) governing virus propagation.

INTRODUCTION

As many as two-third of human genes produce two or more isoforms from one gene by alternative pre-mRNA splicing (1,2). Alternative splicing is strictly regulated across cell and tissue types, sex determinations, signal-regulated changes and developmental stages to provide a variety of gene functions depending on the situation (3,4). Alternative splicing also contributes to viral proteomic diversity (5). In the case of human immunodeficiency

virus type 1, primary RNA transcripts are alternatively spliced to generate more than 40 different mRNAs (6). As viral RNA processing is often catalyzed by cellular RNA-binding proteins such as serine-arginine rich (SR) proteins (7,8), virus infection sometimes affects the host RNA processing factor (9,10). However, the effects of viral proteins on cellular mRNA splicing have poorly been investigated.

Herpes simplex virus type 2 (HSV-2) is a nuclear replicating DNA virus and a highly adapted human pathogen with rapid lytic replication cycle. When the viral capsid makes its entry into the host cell nucleus, HSV-2 genome DNA localizes to discrete nuclear foci called promyelocytic leukemia nuclear bodies (PML-NBs), also known as nuclear domain 10 (ND10) or PML oncogenic domain (POD) (11). PML was originally characterized as part of a fusion protein with RAR α cloned from acute PML patients (12–14). PML is expressed in all normal tissues as well as tumor cell lines; however, its expression is reduced in some progressed tumors (15). The size of PML-NBs varies from 0.2 to 1 μ m, and their frequency depends on cell type, cycle, and status (16–19). PML-NBs consist of many kinds of proteins involved in various functions (20,21), and are implicated in various cell processes, including apoptosis, DNA repair, transcription, senescence, cell proliferation, signal transduction and viral pathogenicity (19,20,22–29). PML-NBs have been thought to contribute to intrinsic antiviral defense on the interferon pathway (30). However, recent reports have indicated that PML-NBs provide scaffolds for DNA viruses and promote efficient viral propagation (11,24,31). Thus, a simple model is not sufficient to accommodate all accumulated evidence.

The human *PML* gene consists of nine major exons, and several alternatively spliced PML transcripts lead to

*To whom correspondence should be addressed. Tel: +81 3 5803 5836; Fax: +81 3 5803 5853; Email: m.hagiwara.end@mri.tmd.ac.jp

© The Author(s) 2009. Published by Oxford University Press.

This is an Open Access article distributed under the terms of the Creative Commons Attribution Non-Commercial License (<http://creativecommons.org/licenses/by-nc/2.5/uk/>) which permits unrestricted non-commercial use, distribution, and reproduction in any medium, provided the original work is properly cited.

6516 *Nucleic Acids Research*, 2009, Vol. 37, No. 19

the expression of a multitude of different PML isoforms (32,33), as shown in Figure 1A. PML exon 1 to exon 4, which are common to all isoforms, are translated into the tripartite motif (TRIM) including the RING finger, B-box and coiled-coil domain. On the other hand, PML exon 5 to exon 9 can be alternatively spliced, generating multiple PML isoforms such as PML-I containing the putative exonuclease III domain (34). Furthermore, PML exon 6 contains the nuclear localization signal, and can be excluded for the expression of the cytoplasmic PML-VII isoform, which is essential for TGF- β signaling (27,33). Thus, the *PML* gene utilizes alternative pre-mRNA splicing for the functional diversity of its own protein products.

In this study, we hypothesized that the conflicting host-virus interactions at PML-NBs may reflect the differential functions of PML isoforms. Consequently, we found that the expression of PML splicing isoforms was switched during HSV-2 infection by alternative splicing. Our group has recently developed a splicing reporter capable of visualization of alternative splicing events *in vivo* and has also identified novel *trans*-acting factors (35,36). Here, we newly developed a virus-sensitive splicing reporter whose fluorescent protein expression is changed in HSV-2-infected cells, and we identified infected cell protein 27 (ICP27) as an alternative splicing regulator. ICP27 preferentially interacted with PML pre-mRNA and suppressed intron 7a removal presumably by modulating 3' splice site (ss) recognition of the cellular *trans*-acting factor.

MATERIALS AND METHODS

Construction of plasmids

We constructed the reporter minigene PML E6-7b by amplifying the *PML* genomic DNA fragments spanning from exon 6 to exon 7b and cloning to a pcDNA3 vector (Invitrogen). Constructs expressing myc-tagged HSV-2 cDNAs and Flag-tagged ICP27 were prepared by inserting PCR products from the cDNA of HSV-2-infected HEK293 cells into the pcDNA3 vector. A construct for the preparation of the T-REx293/Flag-ICP27 stable cell line was prepared by inserting PCR products from the cDNA of HSV-2-infected HEK293 cells into the pcDNA5/FRT vector in accordance with the manufacturer's protocol (Invitrogen). Constructs expressing RFP-PML-II and RFP-PML-V were prepared by inserting PCR products from the cDNA of HEK293 cells into the pmRFP-C1 vector (Clontech). The constructs of ICP27 mutant M15, PML-small interference (siRNA)-resistant mutants, PML intron 7a-deletion mutant d1 and PML 3' ss mutants m1-m4 were made using a QuikChange II XL kit (Stratagene). The cloning primers are shown in Supplementary Table S1.

RT-PCR

RNA was isolated from intact, HSV-2-infected cells, and transfected cells with sepaSol RNA I (Nacalai). For reverse transcription, 500 ng of total RNA from each sample was incubated with oligo (dT)₂₀ and Superscript II reverse transcriptase (Invitrogen). PCR products were

analyzed by 2% agarose gel electrophoresis, followed by ethidium bromide staining. As shown in Figure 1C, semi-quantitative PCR products were analyzed using the 2100 Bioanalyzer (Agilent Technologies) following the protocol stated in the manuals. The PCR primers are shown in Supplementary Table S2.

Viruses and antibodies

HSV-2 strain G [HSV-2 (G)] and Venus-HSV-2 strain YK381 were used at multiplicities of infection (MOI) based on their plaque-forming unit titers in Vero cells. Anti-Flag M2 antibody, anti-c-myc antibody, anti-ICP27 (8.F.137B) and Pan-PML antibody (H-238) were purchased from Sigma, Nacalai, Abcam and Santa Cruz, respectively. PML-II- and PML-V-specific sera were a kind gift from H. de The (18).

Construction of YK381 expressing Venus fluorescent protein

In pRB5198 (37), a region containing the bidirectional polyadenylation [poly(A)] signals of HSV-1(F) UL21 and UL22 was cloned into pBluescript II KS(+) (Stratagene). To construct p26.5-Venus, a SacI-BstEII fragment of pRB4090 (a kind gift from Dr Bernard Roizman) containing the promoter region of HSV-1(F) UL26.5 and a BamHI-EcoRI fragment of Venus/pCS2 (38) containing the entire open reading frame of Venus were subsequently cloned into pRB5198. The resultant plasmid contains a Venus expression cassette driven by the UL26.5 promoter. The BamHI fragment, 8.2 kb, encoding UL1 to a part of UL5 of the HSV-2 186 viral genome was cloned into pBluescript II KS(+) to yield p2UL3-4. p2UL3-4pac, in which the PacI site was introduced into the region between poly (A) signals for HSV-2 186 UL3 and UL4 genes, was generated by site-specific mutagenesis. p26.5-Venus in 2UL3-4 was constructed by cloning the SacI-KpnI fragment of p26.5-Venus containing the Venus expression cassette into the PacI site of p2UL3-4pac and used as a transfer plasmid for the generation of a recombinant virus YK381 expressing Venus fluorescent protein driven by the UL26.5 promoter, as described previously (38). YK381 exhibits an identical phenotype to wild-type HSV-2 186 in cell cultures and mouse models (T.M. and Y.K., unpublished observation).

Virus infection

HeLa and HEK293 cells were seeded into 6-well plates, and cells reaching 100% confluence were infected with HSV-2(G), as stated in the relevant figure legend. To examine the role of PML in HSV-2 replication, HeLa cells were transfected with PML siRNA for 48 h before the viral infection. For the PML splicing isoform rescue experiments shown in Figure 8F, HeLa cells were transfected with PML siRNA and then with plasmids containing either the siRNA-resistant RFP-PML-II mutant or RFP-PML-V mutant on the next day. HeLa cells were infected with HSV-2(G) for 24 h after plasmid transfection. The production of infectious HSV-2 was assessed by plaque assay in Vero cells (39). Vero cells

grown in 6-well plates to nearly 100% confluency were infected with a diluted whole-cell extract of HSV-2(G)-infected cells. The whole cell extract was prepared by three repeats of freeze-thaw disruption of HSV-2(G)-infected cells. After 1 h adsorption, the inoculum was removed and the cell monolayer was overlaid with Dulbecco's modified Eagle medium (DMEM) containing 1% fetal calf serum (FCS) and 0.16 mg/ml pooled human immunoglobulin (Sigma). The overlaid medium was removed after 2 days of infection, and the infected cell monolayer was fixed and stained with methanol and 0.1% crystal violet, respectively.

Confocal immunofluorescence microscopy

Twenty-four hours after the transfection, cells on 15-mm glass coverslips were fixed with 4% paraformaldehyde for 10 min, permeabilized with 0.5% Triton X-100 for 20 min, blocked with the blocking solution (0.2% Gelatin, 1% BSA, 0.05% Tween 20 in PBS) for 30 min and reacted with a diluted primary antibody in the blocking solution for 12 h at 4°C. After incubation, cells were washed extensively with a washing solution [0.05% Tween 20 in PBS (pH 8.0)], incubated for 2 h at room temperature with the appropriate secondary antibody diluted in the blocking solution, and then washed three times with the washing solution. The cells were analyzed under a confocal microscope (Olympus; FV1000; confocal aperture, 300 µm) through a PLAPO 60× NA:1.40 objective lens. ICP27 and PML-NB signals were collected sequentially by excitation with a 488 nm laser and a 543 nm laser, respectively.

Transfection of plasmids and siRNAs

HeLa, HEK293, and Vero cells were grown in DMEM (Nacalai) supplemented with 10% heat-inactivated FCS, and then maintained by the standard protocol. HeLa and HEK293 cells were transfected with GeneJuice (Roche) or Lipofectamine 2000 (Invitrogen) and TransIT293 (Mirus), respectively. All plasmids used for transfection were prepared using a Maxiprep kit (Biogene). HEK293 cells were grown in a monolayer in 6-well plates, and then co-transfected with 500 ng per well of a reporter plasmid and 500 ng of either myc-vector or plasmids expressing myc-tagged HSV-2 proteins.

siRNA transfection was performed in 12-well plates by transfecting HeLa cells with 20 pmol per well of siRNAs against either the *LacZ* reporter (Invitrogen) or *PML* (Invitrogen, UCUUGGAUACAGCUGCAUCUUUC CC), using Lipofectamine RNAiMAX (Invitrogen).

In vitro splicing reaction

The PCR products of human T7-PML wt (exon 7, 53 nt; intron 7a, 641 nt; and exon 7b, 213 nt) and T7-PML d1 (exon 7, 53 nt; intron 7a, 257 nt; and exon 7b, 213 nt) were used as the DNA template for T7 transcription. Pre-mRNA substrates were m7GpppG-capped and ³²P-labeled by *in vitro* transcription. *In vitro* splicing reactions were performed in 20 µl volumes at 30°C under the conditions described by Krainer *et al.* (40). As shown in Figure 6E, highly purified Flag-ICP27 was added in the reaction system. After the reaction,

RNA was subjected to denaturing PAGE analysis and autoradiography.

RNA immunoprecipitation

Nuclear extracts were prepared from HEK293 cells transfected with plasmids expressing Flag alone, Flag-ICP27 wild-type and M15. ³²P-labeled PML exon 7-7b, β-globin and δ-crystallin RNA were prepared by *in vitro* transcription with [α -³²P]UTP and T7 RNA polymerase (Takara). Gel purified RNA was incubated for 30 min at 30°C with each nuclear extract in 20 µl of RNA binding buffer [20 mM HEPES-KOH (pH 7.9), 100 mM KCl, 5% Glycerol, 1% Triton X-100, 2 mM DTT and 0.2 mM PMSF] supplemented with 0.4 U of an RNase inhibitor (Promega), and immunoprecipitation was then performed with Flag-M2 antibody. Each RNA was purified by the protein removal and ethanol precipitation. The purified RNAs were analyzed by denaturing PAGE and imaging using a phosphorimager (FLA-3000G; FUJIFILM).

Preparation of stable transfected T-Rex293 cells

T-Rex293 cells (the HEK293 cell line expressing a tetracycline repressor obtained from Invitrogen) were grown following the manufacturer's protocol in DMEM (Nacalai) containing 10% heat-inactivated FCS and 10 mg/ml blasticidin (Invitrogen). To generate stably transfected tetracycline inducible cell lines, T-Rex293 cells were co-transfected with either pcDNA5-Flag or pcDNA5-Flag-ICP27. After 48 h post-transfection, these transfected cells were grown in the presence of 0.1 mg/ml hygromycin B following the manufacturer's protocol to select stable transfected clones.

RESULTS

HSV-2 infection switches the expression pattern of PML isoforms

We first compared the splicing patterns of PML transcripts from HeLa cells, with and without HSV-2 infection. Total RNAs of HeLa cells were collected immediately (0 h post-infection, 0 hpi) and 3 h post-infection (3 hpi). The RT-PCR analysis, using the primer sets indicated in Figure 1A, showed that the amounts of mRNAs containing PML-I-specific exon 8-9 and PML-II-specific exon 6-7b were reduced in the HSV-2-infected HeLa cells (Supplementary Figure S1A and Figure 1B, top, lane 4), whereas the amounts of PML mRNA containing constitutive exon 1-4 (Supplementary Figure S1A) and exon 6-7 (Figure 1B, middle, lane 4), and GAPDH mRNA were much less reduced (Figure 1B, bottom, lane 4 and Supplementary Figure S1A).

Moreover, we examined other cellular mRNAs containing constitutive introns (Aly/REF intron 4, Lamin A/C intron 6), alternative introns (Lamin A/C introns 9 and 10) and minor introns (PI20 intron 6, HPS1 intron 16) by RT-PCR analysis. The expression levels and splicing patterns of the mRNAs containing these introns were not significantly changed (Supplementary

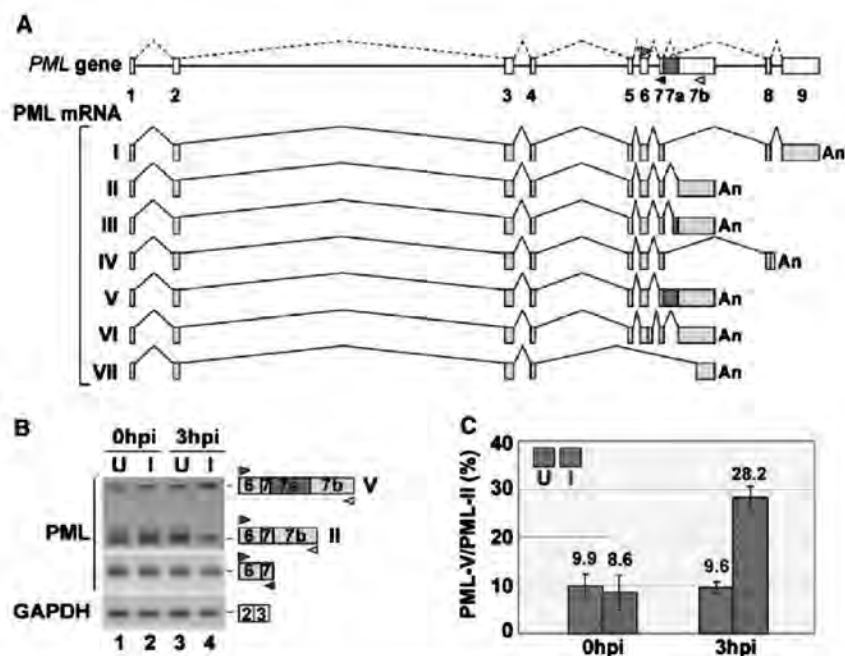


Figure 1. Modulation of PML expression by HSV-2 infection. (A) Schematic representation of the *PML* gene and mRNA species generated by alternative splicing. The positions of different primer sets used for RT-PCR are indicated by colored arrow heads. (B) RT-PCR analysis (28 cycles) of uninfected (U; lanes 1 and 3) and HSV-2-infected (I; lanes 2 and 4) HeLa cells at MOI 1 (0 hpi and 3 hpi). GAPDH primers were used as a control. (C) Graphic representation of the splicing ratios PML-V/PML-II. Green and red box indicate the splicing ratio in HSV-2-infected (I) and uninfected (U) cells, respectively ($n = 3$).

Figure S1B). Interestingly, the amount of mRNA containing PML-V-specific exon 7a-7b was increased in the HSV-2-infected cells (Figure 1B, top). The quantitative analysis also showed that the ratio of PML splicing isoforms (PML-V/PML-II) was enhanced by HSV-2 infection (Figure 1C, 2.9-fold in 3 hpi). Consistent with the reduction in PML-II-specific exon 7b, PML-II foci recognized by PML-II-specific antibody were reduced in the HSV-2-infected cells (Supplementary Figure S2). These observations indicate that HSV-2 infection changes the alternative splicing of PML pre-mRNA.

The splicing reporter of PML gene is sensitive to HSV-2 infection

We have recently succeeded in visualizing the tissue-specific regulation of alternative pre-mRNA splicing in live nematodes by developing a transgenic reporter system with fluorescent proteins (35). Using this system, we have identified three genes as alternative splicing regulators (35,36). To clarify the HSV-2-mediated regulatory mechanism of alternative splicing of the PML pre-mRNA, we prepared splicing reporter minigene constructs containing the region from exon 6 to exon 7b of the PML gene without or with the red fluorescent protein (RFP) coding region, and named them E6-7b and E6-7b-RFP, respectively (Figure 2A). The splicing reporter E6-7b-RFP can express RFP only when intron 7a is spliced out and the PML-II form is produced. Notably, when we transfected E6-7b-RFP into HeLa cells, RFP was detected

in the transfected cells. To examine whether or not we can use E6-7b-RFP as a screening tool of viral splicing regulators, we observed RFP expression in Venus-HSV-2-infected cells. As we initially assumed, the RFP expression was reduced in the Venus-HSV-2-infected cells in a viral titer-dependent manner (Figure 2B and Supplementary Figure S3), suggesting that the minigene reporter reflects the splicing alteration induced by HSV-2 infection. To examine whether or not the reduction of RFP expression was caused by HSV-2 regulated-pre-mRNA splicing, we performed RT-PCR analysis of HeLa cells transfected with the E6-7b (Figure 2C, lanes 1 and 2) or E6-7b-RFP (Figure 2C, lanes 3 and 4) reporter and then infected with HSV-2 at MOI 10 for 3 hours (Figure 2C, lanes 2 and 4). Regardless of the additional RFP coding region, the promotion of intron 7a retention in the HSV-2-infected HEK293 cells was confirmed by RT-PCR (Figure 2C, lanes 3 and 4). The incomplete retention of intron 7a by HSV-2 infection might be caused by the remaining uninfected cells under the experimental condition, as shown in Figure 1B, lanes 4. These observations indicate that the E6-7b-RFP reporter can be used as a screening tool of viral splicing regulators.

The viral protein ICP27 switches the splicing pattern of PML pre-mRNA

To identify viral splicing regulator(s), HSV-2 cDNAs coding 26 viral nuclear proteins of HSV-2 were co-transfected with PML E6-7b-RFP into HeLa cells,

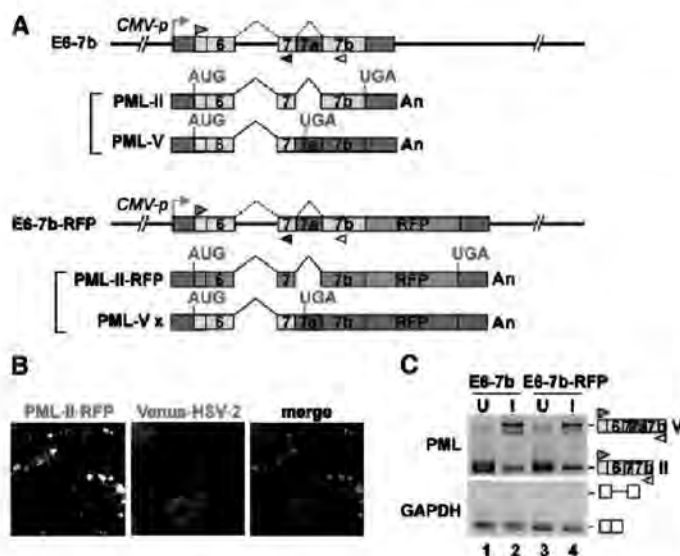


Figure 2. Visualization of virus-sensitive splicing reporter of the *PML* gene. (A) Schematic representation of two splicing reporters. The splicing reporter involving the *PML* gene from exon 6 to exon 7b with (E6-7b-RFP) or without (E6-7b) the RFP coding region, and mRNAs derived from the reporter. Predicted ORFs are indicated in red (PML-II-RFP) or gray (PML-V x), and UTRs in dark gray. The positions of different primer sets used for RT-PCR are indicated. This reporter is driven by the CMV promoter. (B) Microscopy analysis of Venus-HSV-2-infected cells. HeLa cells were infected with Venus-HSV-2 at MOI 0.01. After 3 h infection, E6-7b-RFP was transfected into the cells. After 24 h infection, RFP expression was reduced particularly in Venus-HSV-2 infected cells, although RFP was well detected in uninfected cells. Venus-HSV-2 is indicated in green. (C) RT-PCR analysis of uninfected (U) and infected (I) HeLa cells at MOI 10 (3hpi), into which either E6-7b or E6-7b-RFP constructs were transfected.

and it was demonstrated that RFP expression was lost only in the cells transfected with the ICP27 or UL41 expression vector (Figure 3A, panels 3 and 22). Furthermore, the reduction of RFP expression was also checked by western blot (Supplementary Figure S4). ICP27 overexpression dramatically switched the mRNA expression pattern of the *PML* E6-7b reporter from the PML-II-specific exon 7-7b form to the PML-V-specific exon 7-7a-7b form (Figure 3B, top, lane 3), whereas other viral nuclear proteins such as ICP22 or ICP0 did not affect the splicing (Figure 3B, top, lanes 4 and 5). Also, the amounts of expressed viral proteins were almost the same (Figure 3B, bottom). In contrast to ICP27, the overexpression of UL41 encoding a viral nuclease (41) suppressed PML-II-RFP expression owing to the promotion of PML-II-RFP RNA degradation (data not shown). To investigate whether ICP27 can induce switching of the endogenous *PML* splicing isoform, we transfected myc-tagged ICP27 cDNA and then checked for endogenous *PML* transcripts by RT-PCR analysis using a combination of exon 6-forward and exon 7b-reverse primers. The results showed that the intron 7a retention of endogenous *PML* transcripts was promoted in proportion to the amount of transfected ICP27 cDNA (Figure 3C, top and bottom); however, ICP27 did not inhibit the removal of other introns in *PML* pre-mRNA (Figure 3C, upper middle) or actin pre-mRNA (Figure 3C, lower middle). The foci in myc-tagged ICP27-expressing cells that were recognized by

anti-PML-II antibody were decreased (Figure 3D, center), whereas those recognized by anti-PML-V sera were increased (Figure 3D, right) compared with untransfected HeLa cells. Moreover, the endogenous PML-II mRNA was switched to PML-V mRNA in a Flag-tagged ICP27 stable expressing cell line (T-Rex293/Flag-ICP27), whose transcription was regulated by tetracycline addition (Figure 3E). However, as far as we have checked, the removal of the other introns containing the constitutive introns, alternative intron and minor introns was not affected by Flag-ICP27 (Supplementary Figure S1C). These observations indicate that ICP27 preferentially switches the expression of *PML* isoforms from PML-II to PML-V.

Interestingly, the foci recognized by anti-Pan-PML antibody were unchanged or only slightly decreased (Figure 3D, left). Although PML-I-specific exon 8-9 transcripts were decreased in HSV-2-infected cells, they were not changed in ICP27-expressing cells (Supplementary Figure S1A). These results suggest that PML-I mRNA expression is regulated by other viral factors other than ICP27 or cellular signal induced proteins (e.g. interferon stimulating factors) in HSV-2-infected cells.

KH3 domain of ICP27 is required to switch the *PML* isoform

As shown in Figure 4A, ICP27 contains defined functional domains, including a nuclear export signal (NES), the arginine- and glycine-rich motif (RGG box), the

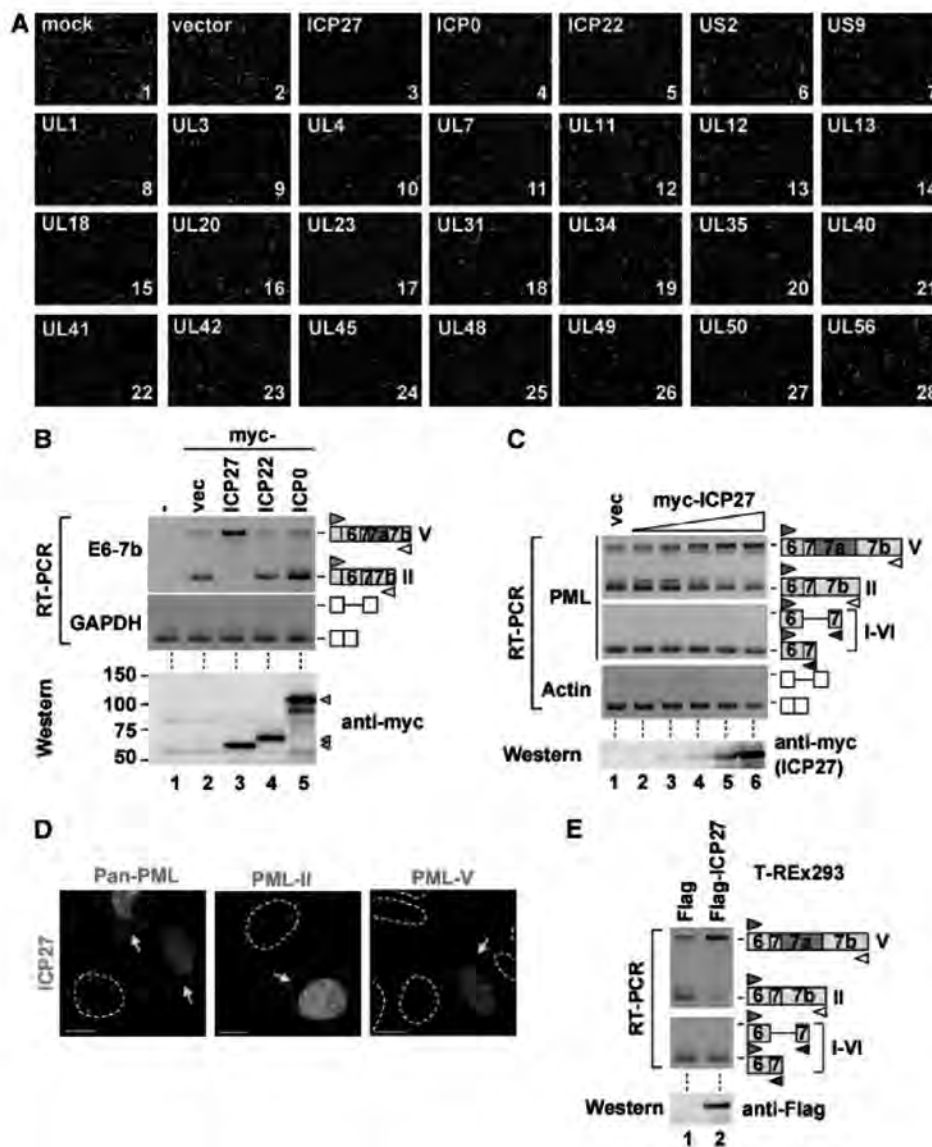
6520 *Nucleic Acids Research*, 2009, Vol. 37, No. 19

Figure 3. Retention of PML intron 7a by ICP27. (A) Microscopy analysis of HeLa cells transfected with the combinations of the E6-7b-RFP construct and each HSV-2 cDNA performed by detecting RFP signaling (red). DNAs were stained with DAPI (blue). (B) RT-PCR analysis of HEK293 cells transfected with the combinations of E6-7b constructs and plasmids containing myc-tagged HSV-2 cDNA (B, upper panels). Whole-cell extracts of HEK293 cells transfected with these plasmids were subjected to western blot analysis for myc-tag (B, bottom). (C) RT-PCR, using the primers shown in Figure 1A, and western blot analysis of HEK293 cells transfected with 2-fold dilution series of myc-tagged ICP27. (D) Immunofluorescence of HeLa cells transfected with myc-tagged ICP27. PML-NBs were stained with anti-Pan-PML (left), PML-II specific (center) and PML-V specific (right) sera. Scale bar, 10 μ m. Yellow arrows indicate ICP27-transfected cells. (E) RT-PCR analysis, using the primers shown in Figure 1A, and western blot analysis for Flag-tag of T-REx293 expressing Flag-tag peptides and Flag-ICP27.

RGG box with nearby sequence (R2) and 3 KH domains. To identify the ICP27 region required to promote retention of intron 7a of PML, we prepared a series of ICP27 mutants lacking NES (d1-2), the RGG box (Δ RGG), and the RGG box plus R2 (Δ RR2) (Figure 4A). Overexpression of the deletion mutants of ICP27 retained the promotion activity for intron 7a retention (Figure 4B,

top, lanes 4–6), whereas ICP27 mutant M15 containing altered residues at 465 and 466 (P465L/G466E) in the KH3 domain (42) failed to switch the alternative splicing of PML pre-mRNA (Figure 4B, top, lane 7). Wild-type ICP27 and the mutants were equally expressed in individual transfected cells (Figure 4B, bottom), and the foci of PML-II were unaffected by M15 expression (Figure 4C,

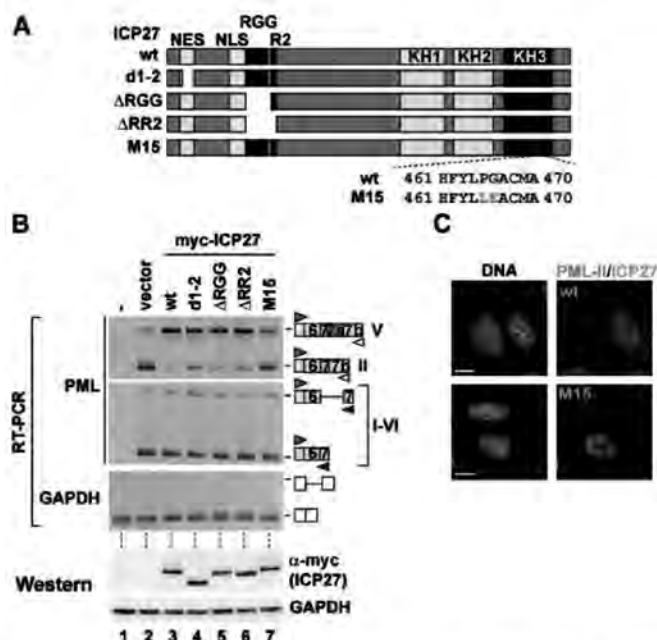


Figure 4. Effects of ICP27 mutants on PML RNA splicing. (A) Schematic representation of the structure of ICP27 mutants. (B) RT-PCR and western blot analysis of HEK293 cells transfected with either myc-tagged ICP27 wild-type or mutant plasmids. (C) Immunofluorescence of HeLa cells transfected with either myc-tagged ICP27 wild-type or the M15 plasmid, stained with anti-myc antibody and PML-II specific sera.

lower panels). These results indicate that the KH3 domain of ICP27 is critical for the switching of the PML isoform from PML-II to PML-V.

Since the ICP27 protein of HSV-1 is highly homologous to that of HSV-2, which we used, we next tested whether HSV-1 ICP27 protein could also affect the PML splicing or not. The ICP27 of HSV-1 also promoted the intron retention of PML splicing (Supplementary Figure S5A, lane 4). The *ICP27* gene is conserved in all members of the herpesvirus family. The *UL69* gene (cytomegalovirus; CMV), *EB2* (or *SM*) gene (Epstein-Barr virus; EBV) and *ORF57* gene (Kaposi's sarcoma-associated herpesvirus; KSHV and the herpesvirus saimiri; HVS) are homologues of the *ICP27* gene of each virus. In addition, the amino acids PG at 465 and 466 in the KH3 domain of ICP27, which are essential for splicing regulation of PML pre-mRNA (Figure 4B), are conserved within herpesviridae (Supplementary Figure S5B) (43). Furthermore, ICP27 and ORF57 reportedly promote intron retention of viral RNA (44,45). Taken together, these observations strongly suggest that ICP27-mediated alternative splicing of PML pre-mRNA is a common feature in the herpesvirus family.

ICP27 is specifically associated with PML pre-mRNA

To examine whether or not ICP27 preferentially associates with PML pre-mRNA, we performed RNA immunoprecipitation assay. Three pre-mRNAs containing human PML exon 7 to exon 7b, human β -globin exon 1 to exon 2 and chicken δ -crystallin exon 14 to exon 15, which were synthesized by *in vitro* transcription and labeled

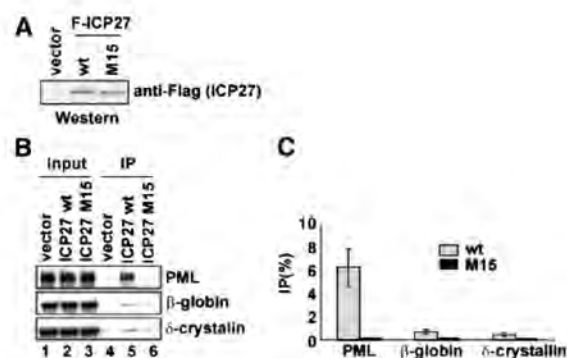


Figure 5. RNA binding specificity of ICP27. (A) Western blot analysis, using anti-Flag antibody, of nuclear extract from HEK293 cells transfected with Flag-vector and Flag-ICP27 wild-type (wt) and M15 expression plasmids. (B) RNA immunoprecipitation. Each 32 P-labeled *in vitro* transcript was incubated with the nuclear extracts from HEK293 cells expressing Flag-tag or Flag-tagged ICP27, and then immunoprecipitated with anti-Flag antibody. (C) Quantitation of three independent experiments is shown. Error bars represent SDs ($n = 3$).

with [α - 32 P] UTP, were mixed with the nuclear extract from HEK293 cells expressing Flag-tagged ICP27 (Figure 5A). Following incubation, RNAs were immunoprecipitated with anti-Flag antibody. The results showed that Flag-ICP27 was co-immunoprecipitated with PML pre-mRNA more efficiently (9.3- to 14.0-fold) than β -globin and δ -crystallin pre-mRNAs (Figure 5B, lane 5

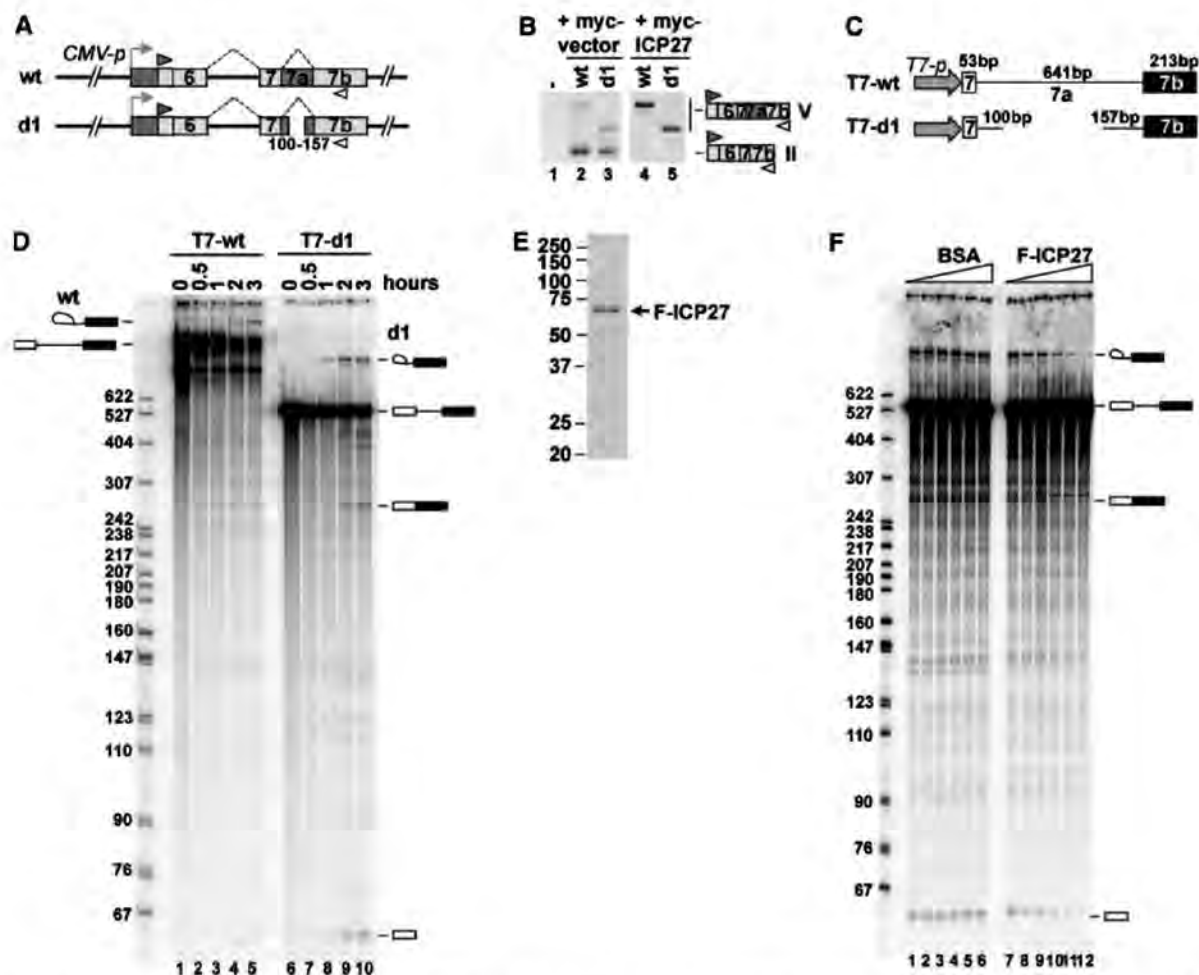
6522 *Nucleic Acids Research*, 2009, Vol. 37, No. 19

Figure 6. Inhibition of PML pre-mRNA splicing by ICP27. (A) Schematic representation of E6-7b wt and deletion-mutant splicing reporters, d1. The reporter E6-7b d1 contains a 100-bp fragment downstream of the 5' splice site and a 157-bp fragment upstream of the 3' splice site of intron 7a. (B) RT-PCR analysis of HEK293 cells transfected with Flag-vector (lane 1), and the combination of either E6-7b wt (lanes 2 and 4) or d1 (lanes 3 and 5) with either myc-vector (lanes 2 and 3) or myc-ICP27 (lanes 4 and 5). (C) Schematic representation of three E7-7b DNA templates, T7-wt (exon 7: 53 bp; intron 7a: 641 bp; exon 7b: 213 bp) and T7-d1 (exon 7: 53 bp; intron 7a: 257 bp; exon 7b: 213 bp), which are driven by the T7 promoter. (D) *In vitro* splicing of T7-wt (lanes 1–5) and T7-d1 (lanes 6–10) for the indicated time. The size of the pBR322 MspI-digested DNA marker is indicated on the right side of the panel. The pre-mRNA, mature mRNA and splicing intermediates are described on both sides of the panel. (E) A 10% SDS-PAGE and Coomassie Brilliant Blue (CBB) staining of the purified Flag-ICP27 from the nuclear extract of T-Rex 293 cells expressing Flag-ICP27. (F) Effects of ICP27 on T7-d1 splicing *in vitro*. Two-fold dilution series (0, 25, 50, 100, 200 and 400 ng) of BSA (lanes 1–6) and highly purified Flag-ICP27 (lanes 7–12) were added to the *in vitro* splicing reaction.

and 5C, gray bars). Further, RNA immunoprecipitation experiment using the nuclear extract from HEK293 cells expressing Flag-ICP27 mutant M15 demonstrated that Flag-ICP27 mutant M15 was not co-immunoprecipitated with these pre-mRNAs (Figure 5B, lane 6 and 5C, black bars). Moreover, the amounts of Flag-ICP27 wild-type and M15 proteins were almost equally expressed (Figure 5A), indicating that ICP27 specifically associated with PML pre-mRNA, at least among cellular pre-mRNAs, and that the associations depended on the KH domains, which were presumably the RNA binding sites.

ICP27 directly inhibits the removal of PML intron 7a

To examine whether or not ICP27 directly inhibits PML pre-mRNA splicing, we performed an *in vitro* splicing reaction. The DNA template T7-wt containing a T7 promoter and PML exon 7 to exon 7b was prepared by PCR and used for T7 transcription (Figure 6C). The *in vitro* splicing reaction resulted in the T7-wt transcript slightly generating splicing intermediates (Figure 6D, lanes 1–5), which led us to modify the T7-wt DNA template. We prepared the mutant d1 which has deletion in intron 7a, as described in Figure 6A. Transfection of the d1 construct showed that the PML d1 transcript was efficiently

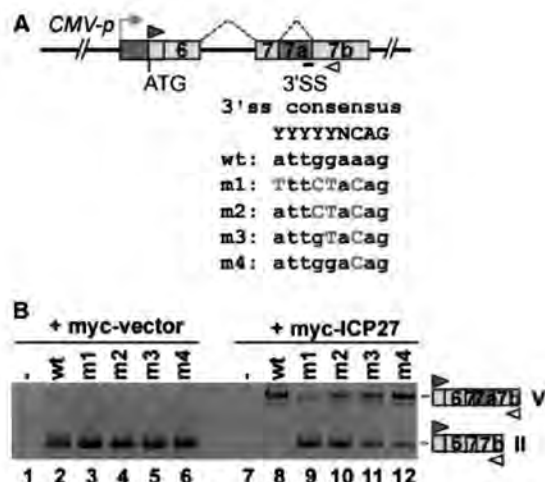


Figure 7. The weak 3' ss essential for ICP27-mediated alternative splicing of PML pre-mRNA. (A) Scheme of the E6-7b construct wild-type and a series of point mutations at the 3' ss in PML intron 7a. (B) Results of RT-PCR analysis of HeLa cells transfected with each E6-7b *cis*-mutant and myc-tagged ICP27.

removed from intron 7a and that intron 7a of d1 RNA was retained by myc-ICP27, as well as the PML wt transcript (Figure 6B, lanes 3 and 5). These results indicate that the PML d1 mutant can be useful for *in vitro* splicing reactions. The *in vitro* splicing of the T7-d1 transcript showed that it was more efficiently spliced than the T7-wt transcript (Figure 6D, lanes 6–10). Next, we examined the effects of ICP27 on PML splicing. Flag-ICP27 was purified from T-REx293 cells expressing Flag-ICP27, and then the highly purified Flag-ICP27 was added to the *in vitro* splicing reaction using d1 mutant RNA. The results showed that the productions of T7-d1 spliced mRNA and intermediates were inhibited by the addition of purified Flag-ICP27 in a dose-dependent manner (Figure 6F, lanes 7–12), but not by BSA (Figure 6F, lanes 1–6). These results indicate that ICP27 directly inhibits PML pre-mRNA splicing.

3' Splice site of intron 7a of PML pre-mRNA is critical for ICP27-mediated switching

The alternative splicing depends on the utilization of the 5' ss and 3' ss at the end of introns (3). The 5' ss includes a GU dinucleotide at the intron end encompassed within a less conserved consensus sequence. At the other end of the intron, the 3' ss region has conserved a polypyrimidine tract capable of associating with U2AF65/35, followed by a terminal AG at the extreme 3'-end of the intron (YYYYYNACAG) (46). In contrast, the 3' ss sequence of PML intron 7a is a purine-rich sequence (ATTGGAAAG). To evaluate the involvement of the atypical 3' ss of intron 7a for the ICP27-mediated switching from PML-II to PML-V, we mutated the 3' ss region of intron 7a in the PML E6-7b reporter to match with the 3' ss consensus sequence (Figure 7A, m1–m4). RT-PCR analysis showed that the ICP27-induced retention of PML intron 7a was

diminished in proportion to the number of mutated nucleotides at the 3' ss (Figure 7B, lanes 8–12).

PML splicing isoform II contributes to production of infectious HSV-2

To examine the differential roles of PML isoforms in host-virus interactions, we attempted rescue experiments with a siRNA-resistant PML isoform in PML pre-knocked down HeLa cells. We first efficiently knocked down all PML isoforms from HeLa cells with siRNA (siPML4) against PML exon 4. Following 48 h of siRNA transfection, HSV-2 was infected and then HSV-2 titer was measured by plaque assay (Figure 8A). siPML4 efficiently knocked down endogenous PML isoforms (Figure 8B, lane 2), whereas control siRNA (siLacZ) did not knock down any of them (Figure 8B, lane 1). Plaque assay revealed that HSV-2 replication was suppressed by ~80% in the PML-knocked-down HeLa cells (Figure 8C), consistent with the results of the immunofluorescence analysis (Supplementary Figure S6). We then transfected these cells with a plasmid encoding either RFP, RFP-PML-II or RFP-PML-V with a silent mutation that makes the PML isoform resistant to siPML4, and thereafter evaluated the plaque-forming activity of the virus (Figure 8D). The rescue experiment showed that RFP-PML-II increased the HSV-2 plaque number (~1.6-fold RFP), but RFP-PML-V did not (Figure 8F), although the expression levels of the RFP-PML-II and RFP-PML-V mRNAs were similar (Figure 8E, lanes 2 and 3). The result showed that the difference in the rescue experiments between only RFP and RFP-PML-II appeared smaller than the reduction of HSV-2 replication by the knock-down of all PML isoforms. One possible explanation is the transfection efficiencies of RFP (43%), RFP-PML-II (33%) and RFP-PML-V (34%) (Supplementary Figure S7). These observations suggest that the difference in HSV-2 plaque number may become larger if all cells expressed siRNA-resistant PML isoforms, suggesting that PML-II plays a specific role in efficient HSV-2 replication.

DISCUSSION

In this study, we identified ICP27 as a splicing regulator of PML pre-mRNA, showing the possibility that the viral protein switches alternative splicing of specific cellular RNA in association with functional alteration.

Selective splicing regulation by ICP27

HSV ICP27 is one of the immediate early (IE) proteins of HSV and plays an essential role in the expression of viral late genes (47,48). ICP27 interacts and co-localizes with cellular splicing factors, such as small nuclear ribonucleoproteins (snRNPs) (49), SR proteins, SR protein kinase 1 (SRPK1) (50) and spliceosome-associated protein 145 (SAP145) (51), and is suggested to inhibit the splicing of cellular pre-mRNAs by impairing spliceosomal assembly (50). However, considering that some essential viral pre-mRNAs such as ICP0 have introns and require splicing, it is less likely that HSV suppresses constitutive

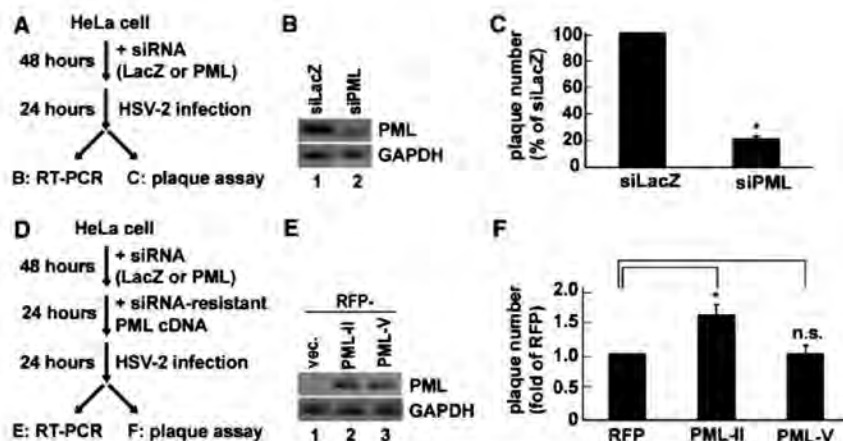
6524 *Nucleic Acids Research*, 2009, Vol. 37, No. 19

Figure 8. Differential function of PML isoforms in relation to HSV-2 infection. (A) Experimental procedure for examining the role of PML in HSV-2 viral production. Knockdown of all endogenous PML splicing variants in HeLa cells was performed using siRNA against PML (siPML4). After 48 h of incubation, HeLa cells were infected with HSV-2 at MOI 0.01 for 24 h. RT-PCR analysis (B) and plaque assay (C) were performed to determine knockdown efficiency and viral titer, respectively. (B) RT-PCR analysis, using PML ex3-ex4 primers, of siLacZ- or siPML4-treated HeLa cells. (C) Production of infectious HSV-2 in either siLacZ- or siPML4-treated HeLa cells as assessed by plaque assay ($n = 4$). (D) Experimental procedure for the rescue assay of PML splicing variants. After 48 h of siRNA treatment, the expression plasmids of either RFP or siRNA-resistant PML II or PML-V were transfected for 24 h. Following 24 h of infection with HSV-2 at MOI 0.01, RT-PCR analysis (E) and plaque assay (F) were performed. (E) RT-PCR analysis of siPML4-treated HeLa cells transfected with the RFP vector, RFP-PML-II siRNA resistant (siR), or RFP-PML-V siR expression plasmids. Details are described in 'Materials and Methods' section. (F) Production of infectious HSV-2 in HeLa cells siPML4-treated and then transfected with each PML plasmid as assessed by plaque assay ($n = 4$). * $P < 0.001$; n.s., not significant.

pre-mRNA splicing. Interestingly, we observed that ICP27 specifically bound to PML pre-mRNA (Figure 5B, lane 5) and selectively switched the isoform from PML-II to PML-V by promoting the retention of PML intron 7a (Figure 3E). Our results indicate that ICP27 is an alternative splicing factor, although it does not inhibit all constitutive splicing. Moreover, the observed *in vitro* splicing suggested that ICP27 directly suppressed the early stage of spliceosome assembly on PML intron 7a, because splicing intermediates (5' exon and lariat-3' exon) were reduced by ICP27 addition (Figure 6F).

The selectivity of ICP27-dependent regulation may be related to the relative weakness of the 3' ss of PML intron 7a. PML intron 7a was not retained even in the presence of ICP27 when we mutated the 3' ss to the consensus sequence for U2AF65/35 (Figure 7B). Therefore, it is also relevant to examine whether ICP27 selectively binds to the 3' ss of PML intron 7a by competing with U2AF65/35. Sokolowski *et al.* (52) showed that ICP27 binds to many different viral sequences by yeast three-hybrid screening of an HSV-1 genomic library; however, the target RNA sequence of ICP27 remains to be elucidated. Since the ICP27 homolog contains more cellular targets than PML pre-mRNA (53), *in vitro* systematic evolution of ligands by exponential enrichment (SELEX) and *in vivo* UV cross-linking immunoprecipitation (CLIP) are currently under way in our laboratory to determine the consensus target sequence of ICP27.

A possible role of ICP27-mediated mRNA export on alternative splicing

Transfection experiments revealed that ICP27 promoted the intron 7a retention (Figure 3B, lane 3). Although our

results showed that ICP27 directly inhibited the splicing of PML intron 7a *in vitro* (Figure 6F), ICP27-mediated alternative splicing modulation is still possible to be explained by another mechanism, a promotion of pre-mRNA export by ICP27. It has been shown that ICP27 shuttles between the nucleus and the cytoplasm in host cells (54,55), and that ICP27 homologues stimulate the export of viral mRNAs by interacting with the mRNA export adaptor REF (56–61). The splicing reaction at the weak ss of PML intron 7a may take longer time than that at the consensus ss, and the accelerated mRNA export induced by ICP27 does not provide sufficient time for PML pre-mRNA to be spliced in the nucleus. These two possibilities are not mutually exclusive. It will be of interest to investigate if ICP27 promotes export of pre-mRNAs that harbor introns with weak 3' ss, such as PML.

The role of ICP27 KH domain on PML alternative splicing

ICP27 M15 mutant failed to alter the expression of PML splicing isoform (Figure 4B, lane 7), suggesting that the KH3 domain is critical for the regulation of splicing. Therefore, we checked whether other KH domains are also essential for splicing regulation or not. RT-PCR analyses indicate that the mutants lacking either the KH2 domain or the KH3 domain were not able to completely switch PML splicing isoforms (data not shown). These results suggest that both the KH2 and the KH3 domains are required for altering the splicing. Unfortunately, the mutant lacking the KH1 domain was not expressed enough for the splicing experiment. It is highly likely that all of three KH domains are required for the regulation of the splicing.

Differential roles of PML isoform

PML isoforms have differential localizations and functions (32–34). For example, p53 interacts with PML-IV, but not with PML-III, and thus it was speculated that p53-PML-IV interaction was required for p53 recruitment into PML-NBs to modulate cell survival (62). Moreover, retinoblastoma protein (pRB) interacts more efficiently with PML-IV than with PML-II, suggesting that pRB-PML-IV interaction plays an important role in the regulation of cell differentiation and proliferation (63). In the present study, we showed that PML-II can enhance HSV-2 proliferation in HeLa cells (Figure 8F). In addition to HSV-2, adenovirus type 5 E4-ORF3 protein reportedly rearranges PML-NBs to a track-like structure by specifically interacting with PML-II (64,65), suggesting that PML-II may function as a modulator of the viral environment. However, as shown in the present study, HSV-2 infection switches the PML isoform from PML-II to PML-V. Apparently, this switching reduces the efficiency of viral replication (Figure 8F) and is thus not favorable to the virus, although it may also contribute to persistent viral infection by controlling viral replication rate through a negative feedback mechanism. Another possibility is that this switching is relevant to host defense to virus production. Because ICP27 is expressed at early stage of virus infection, the infected cell may utilize ICP27 as virus antigen to monitor virus infection and then the cells may try to reduce virus replication rate by producing PML-V, which results in delay of the expansion of virus infection to surrounding cells.

The expression of PML isoforms differs in various cell lines or tissues. For example, PML-I is the dominant form expressed in the brain but not in the liver (18). However, the regulation mechanisms of the cell type- or tissue-specific alternative splicing of PML pre-mRNA have not been clarified to date. In this study, using our original splicing reporter with RFP, we demonstrated that the viral protein ICP27 regulates the switching of the PML isoform from PML-II to PML-V by promoting the retention of PML intron 7a; PML-I, however, was not affected by ICP27 (Supplementary Figure S1A). The mechanism underlying the HSV-induced decrease in PML-I remains to be elucidated. The splicing reporter system used in the present study may pave the way for identifying the cellular regulators of PML alternative splicing, along with viral regulatory proteins.

SUPPLEMENTARY DATA

Supplementary Data are available at NAR Online.

ACKNOWLEDGEMENTS

We are grateful to H. de Thè for providing the anti-PML-II and PML-V specific sera. We thank A. Hiraishi and C. Parlayan for critically reading the article; and members of M.H.'s Laboratory for helpful comments.

FUNDING

Grants-in-Aid (to M.H.) from the Ministry of Education, Culture, Sports, Science, and Technology (MEXT) of Japan; the National Institute of Biomedical Innovation (NIBI); Japanese Ministry of Education, Global Center of Excellence (GCOE) Program; International Research Center for Molecular Science in Tooth and Bone Diseases; Program for Improvement of Research Environment for Young Researchers from Special Coordination Funds for Promoting Science and Technology (SCF) commissioned by MEXT of Japan (to N.K.). Funding for open access charge: [Ministry of Education, Culture, Sports, Science, and Technology of Japan (to T.N.)].

Conflict of interest statement. None declared.

REFERENCES

1. Johnson, J.M., Castle, J., Garrett-Engle, P., Kan, Z., Loerch, P.M., Armour, C.D., Santos, R., Schadt, E.E., Stoughton, R. and Shoemaker, D.D. (2003) Genome-wide survey of human alternative pre-mRNA splicing with exon junction microarrays. *Science*, **302**, 2141–2144.
2. Blencowe, B.J. (2006) Alternative splicing: new insights from global analyses. *Cell*, **126**, 37–47.
3. Black, D.L. (2003) Mechanisms of alternative pre-messenger RNA splicing. *Annu. Rev. Biochem.*, **72**, 291–336.
4. Matlin, A.J., Clark, F. and Smith, C.W. (2005) Understanding alternative splicing: towards a cellular code. *Nat. Rev. Mol. Cell Biol.*, **6**, 386–398.
5. Schwartz, S., Felber, B.K., Fenyo, E.M. and Pavlakis, G.N. (1990) Env and Vpu proteins of human immunodeficiency virus type 1 are produced from multiple bicistronic mRNAs. *J. Virol.*, **64**, 5448–5456.
6. Stoltzfus, C.M. and Madsen, J.M. (2006) Role of viral splicing elements and cellular RNA binding proteins in regulation of HIV-1 alternative RNA splicing. *Curr. HIV Res.*, **4**, 43–55.
7. Long, J.C. and Cáceres, J.F. (2009) The SR protein family of splicing factors: master regulators of gene expression. *Biochem. J.*, **417**, 15–27.
8. Lin, S. and Fu, X.D. (2007) SR proteins and related factors in alternative splicing. *Adv. Exp. Med. Biol.*, **623**, 107–122.
9. Kanopka, A., Muhlemann, O., Petersen-Mahrt, S., Estmer, C., Ohmalm, C. and Akusjarvi, G. (1998) Regulation of adenovirus alternative RNA splicing by dephosphorylation of SR proteins. *Nature*, **393**, 185–187.
10. Fukuhara, T., Hosoya, T., Shimizu, S., Sumi, K., Oshiro, T., Yoshinaka, Y., Suzuki, M., Yamamoto, N., Herzenberg, L.A., Herzenberg, L.A. et al. (2006) Utilization of host SR protein kinases and RNA-splicing machinery during viral replication. *Proc. Natl Acad. Sci. USA*, **103**, 11329–11333.
11. Ishov, A.M. and Maul, G.G. (1996) The periphery of nuclear domain 10 (ND10) as site of DNA virus deposition. *J. Cell Biol.*, **134**, 815–826.
12. de Thé, H., Lavau, C., Marchio, A., Chomienne, C., Degos, L. and Dejean, A. (1991) The PML-RAR alpha fusion mRNA generated by the t(15;17) translocation in acute promyelocytic leukemia encodes a functionally altered RAR. *Cell*, **66**, 675–684.
13. Kakizuka, A., Miller, W.H. Jr., Umesono, K., Warrell, R.P. Jr., Frankel, S.R., Murty, V.V., Dmitrov, S.E. and Evans, R.M. (1991) Chromosomal translocation t(15;17) in human acute promyelocytic leukemia fuses RAR alpha with a novel putative transcription factor, PML. *Cell*, **66**, 663–674.
14. Goddard, A.D., Borrow, J., Freemont, P.S. and Solomon, E. (1991) Characterization of a zinc finger gene disrupted by the t(15;17) in acute promyelocytic leukemia. *Science*, **254**, 1371–1374.
15. Gurrieri, C., Capodice, P., Bernardi, R., Scaglioni, P.P., Nafa, K., Rush, L.J., Verbel, D.A., Cordon-Cardo, C. and Pandolfi, P.P. (2004)

- Loss of the tumor suppressor PML in human cancers of multiple histologic origins. *J. Natl Cancer Inst.*, **96**, 269–279.
16. Terris, B., Baldin, V., Dubois, S., Degott, C., Flejou, J.F., Henin, D. and Dejean, A. (1995) PML nuclear bodies are general targets for inflammation and cell proliferation. *Cancer Res.*, **55**, 1590–1597.
 17. Koken, M.H., Linares-Cruz, G., Quignon, F., Viron, A., Chelbi-Alix, M.K., Sobczak-Thépot, J., Juhlin, L., Degos, L., Calvo, F. and de Thé, H. (1995) The PML growth-suppressor has an altered expression in human oncogenesis. *Oncogene*, **10**, 1315–1324.
 18. Condemine, W., Takahashi, Y., Zhu, J., Puvion-Dutilleul, F., Guégan, S., Janin, A. and de Thé, H. (2006) Characterization of endogenous human promyelocytic leukemia isoforms. *Cancer Res.*, **66**, 6192–6198.
 19. Salomoni, P. and Pandolfi, P.P. (2002) The role of PML in tumor suppression. *Cell*, **108**, 165–170.
 20. Zhong, S., Salomoni, P. and Pandolfi, P.P. (2000) The transcriptional role of PML and the nuclear body. *Nat. Cell Biol.*, **2**, E85–E90.
 21. Hofmann, T.G. and Will, H. (2003) Body language: the function of PML nuclear bodies in apoptosis regulation. *Cell Death Differ.*, **10**, 1290–1299.
 22. Guo, A., Salomoni, P., Luo, J., Shih, A., Zhong, S., Gu, W. and Pandolfi, P.P. (2000) The function of PML in p53-dependent apoptosis. *Nat. Cell Biol.*, **2**, 730–736.
 23. Dellaire, G. and Bazett-Jones, D.P. (2004) PML nuclear bodies: dynamic sensors of DNA damage and cellular stress. *Bioessays*, **26**, 963–977.
 24. Ching, R.W., Dellaire, G., Eskiw, C.H. and Bazett-Jones, D.P. (2005) PML bodies: a meeting place for genomic loci? *J. Cell Sci.*, **118**, 847–854.
 25. Pearson, M., Carbone, R., Sebastiani, C., Cioce, M., Fagioli, M., Saito, S., Higashimoto, Y., Appella, E., Minucci, S., Pandolfi, P.P. et al. (2000) PML regulates p53 acetylation and premature senescence induced by oncogenic Ras. *Nature*, **406**, 207–210.
 26. Wang, Z.G., Delva, L., Gaboli, M., Rivi, R., Giorgio, M., Cordon-Cardo, C., Grosveld, F. and Pandolfi, P.P. (1998) Role of PML in cell growth and the retinoic acid pathway. *Science*, **279**, 1547–1551.
 27. Lin, H.K., Bergmann, S. and Pandolfi, P.P. (2004) Cytoplasmic PML function in TGF- β signalling. *Nature*, **431**, 205–211.
 28. Everett, R.D. (2001) DNA viruses and viral proteins that interact with PML nuclear bodies. *Oncogene*, **20**, 7266–7273.
 29. Regad, T. and Chelbi-Alix, M.K. (2001) Role and fate of PML nuclear bodies in response to interferon and viral infections. *Oncogene*, **20**, 7274–7286.
 30. Chée, A.V., Lopez, P., Pandolfi, P.P. and Roizman, B. (2003) Promyelocytic leukemia protein mediates interferon-based anti-herpes simplex virus 1 effects. *J. Virol.*, **77**, 7101–7105.
 31. Maul, G.G., Ishov, A.M. and Everett, R.D. (1996) Nuclear domain 10 as preexisting potential replication start sites of herpes simplex virus type-1. *Virology*, **217**, 67–75.
 32. Jensen, K., Shiels, C. and Freemont, P.S. (2001) PML protein isoforms and the RBCC/TRIM motif. *Oncogene*, **20**, 7223–7233.
 33. Nisole, S., Stoye, J.P. and Saib, A. (2005) TRIM family proteins: retroviral restriction and antiviral defence. *Nat. Rev.*, **3**, 799–808.
 34. Condemine, W., Takahashi, Y., Le Bras, M. and de Thé, H. (2007) A nucleolar targeting signal in PML-1 addresses PML to nucleolar caps in stressed or senescent cells. *J. Cell Sci.*, **120**, 3219–3227.
 35. Kuroyanagi, H., Kobayashi, T., Mitani, S. and Hagiwara, M. (2006) Transgenic alternative-splicing reporters reveal tissue-specific expression profiles and regulation mechanisms in vivo. *Nat. Methods*, **3**, 909–915.
 36. Ohno, G., Hagiwara, M. and Kuroyanagi, H. (2008) STAR family RNA-binding protein ASD-2 regulates developmental switching of mutually exclusive alternative splicing in vivo. *Genes Dev.*, **22**, 360–374.
 37. Tanaka, M., Kagawa, H., Yamanashi, Y., Sata, T. and Kawaguchi, Y. (2003) Construction of an excisable bacterial artificial chromosome containing a full-length infectious clone of herpes simplex virus type 1: viruses reconstituted from the clone exhibit wild-type properties in vitro and in vivo. *J. Virol.*, **77**, 1382–1391.
 38. Sugimoto, K., Uema, M., Sagara, H., Tanaka, M., Sata, T., Hashimoto, Y. and Kawaguchi, Y. (2008) Simultaneous tracking of capsid, tegument, and envelope protein localization in living cells infected with triply fluorescent herpes simplex virus 1. *J. Virol.*, **82**, 5198–5211.
 39. Tanaka, M., Kodaira, H., Nishiyama, Y., Sata, T. and Kawaguchi, Y. (2004) Construction of recombinant herpes simplex virus type 1 expressing green fluorescent protein without loss of any viral genes. *Microbes Infect./Institut Pasteur*, **6**, 485–493.
 40. Krainer, A.R., Maniatis, T., Ruskin, B. and Green, M.R. (1984) Normal and mutant human beta-globin pre-mRNAs are faithfully and efficiently spliced in vitro. *Cell*, **36**, 993–1005.
 41. Strom, T. and Frenkel, N. (1987) Effects of herpes simplex virus on mRNA stability. *J. Virol.*, **61**, 2198–2207.
 42. Rice, S.A. and Lam, V. (1994) Amino acid substitution mutations in the herpes simplex virus ICP27 protein define an essential gene regulation function. *J. Virol.*, **68**, 823–833.
 43. Soliman, T.M. and Silverstein, S.J. (2000) Herpesvirus mRNAs are sorted for export via Crm1-dependent and -independent pathways. *J. Virol.*, **74**, 2814–2825.
 44. Sedlackova, L., Perkins, K.D., Lengyel, J., Strain, A.K., van Santen, V.L. and Rice, S.A. (2008) Herpes simplex virus type 1 ICP27 regulates expression of a variant, secreted form of glycoprotein C by an intron retention mechanism. *J. Virol.*, **82**, 7443–7455.
 45. Majerciak, V., Yamanegi, K., Allemand, E., Krulik, M., Krainer, A.R. and Zheng, Z.M. (2008) Kaposi's sarcoma-associated herpesvirus ORF57 functions as a viral splicing factor and promotes expression of intron-containing viral lytic genes in spliceosome-mediated RNA splicing. *J. Virol.*, **82**, 2792–2801.
 46. Wu, S., Romfo, C.M., Nilsen, T.W. and Green, M.R. (1999) Functional recognition of the 3' splice site AG by the splicing factor U2AF35. *Nature*, **402**, 832–835.
 47. Sacks, W.R., Greene, C.C., Aschman, D.P. and Schaffer, P.A. (1985) Herpes simplex virus type 1 ICP27 is an essential regulatory protein. *J. Virol.*, **55**, 796–805.
 48. Rice, S.A. and Knipe, D.M. (1988) Gene-specific transactivation by herpes simplex virus type 1 alpha protein ICP27. *J. Virol.*, **62**, 3814–3823.
 49. Sandri-Goldin, R.M. and Hibbard, M.K. (1996) The herpes simplex virus type 1 regulatory protein ICP27 coimmunoprecipitates with anti-Sm antiserum, and the C terminus appears to be required for this interaction. *J. Virol.*, **70**, 108–118.
 50. Sciabica, K.S., Dai, Q.J. and Sandri-Goldin, R.M. (2003) ICP27 interacts with SRPK1 to mediate HSV splicing inhibition by altering SR protein phosphorylation. *EMBO J.*, **22**, 1608–1619.
 51. Bryant, H.E., Wadd, S.E., Lamond, A.J., Silverstein, S.J. and Clements, J.B. (2001) Herpes simplex virus IE63 (ICP27) protein interacts with spliceosome-associated protein 145 and inhibits splicing prior to the first catalytic step. *J. Virol.*, **75**, 4376–4385.
 52. Sokolowski, M., Scott, J.E., Heaney, R.P., Patel, A.H. and Clements, J.B. (2003) Identification of herpes simplex virus RNAs that interact specifically with regulatory protein ICP27 in vivo. *J. Biol. Chem.*, **278**, 33540–33549.
 53. Verma, D. and Swaminathan, S. (2008) Epstein-Barr virus SM protein functions as an alternative splicing factor. *J. Virol.*, **82**, 7180–7188.
 54. Phelan, A. and Clements, J.B. (1997) Herpes simplex virus type 1 immediate early protein IE63 shuttles between nuclear compartments and the cytoplasm. *J. Gen. Virol.*, **78**(Pt 12), 3327–3331.
 55. Mears, W.E. and Rice, S.A. (1998) The herpes simplex virus immediate-early protein ICP27 shuttles between nucleus and cytoplasm. *Virology*, **242**, 128–137.
 56. Hiriart, E., Farjat, G., Gruffat, H., Nguyen, M.V., Sergeant, A. and Manet, E. (2003) A novel nuclear export signal and a REF interaction domain both promote mRNA export by the Epstein-Barr virus EB2 protein. *J. Biol. Chem.*, **278**, 335–342.
 57. Malik, P., Blackburn, D.J. and Clements, J.B. (2004) The evolutionarily conserved Kaposi's sarcoma-associated herpesvirus ORF57 protein interacts with REF protein and acts as an RNA export factor. *J. Biol. Chem.*, **279**, 33001–33011.
 58. Williams, B.J., Boyne, J.R., Goodwin, D.J., Roaden, L., Hautbergue, G.M., Wilson, S.A. and Whitehouse, A. (2005) The prototype gamma-2 herpesvirus nucleocytoplasmic shuttling protein, ORF 57, transports viral RNA through the cellular mRNA export pathway. *Biochem. J.*, **387**, 295–308.

59. Lischka, P., Toth, Z., Thomas, M., Mueller, R. and Stamminger, T. (2006) The UL69 transactivator protein of human cytomegalovirus interacts with DEXD/H-Box RNA helicase UAP56 to promote cytoplasmic accumulation of unspliced RNA. *Mol. Cell Biol.*, **26**, 1631–1643.
60. Soliman, T.M., Sandri-Goldin, R.M. and Silverstein, S.J. (1997) Shuttling of the herpes simplex virus type 1 regulatory protein ICP27 between the nucleus and cytoplasm mediates the expression of late proteins. *J. Virol.*, **71**, 9188–9197.
61. Koffa, M.D., Clements, J.B., Izaurralde, E., Wadd, S., Wilson, S.A., Mattaj, J.W. and Kuersten, S. (2001) Herpes simplex virus ICP27 protein provides viral mRNAs with access to the cellular mRNA export pathway. *EMBO J.*, **20**, 5769–5778.
62. Fogal, V., Gostissa, M., Sandy, P., Zacchi, P., Sternsdorf, T., Jensen, K., Pandolfi, P.P., Will, H., Schneider, C. and Del Sal, G. (2000) Regulation of p53 activity in nuclear bodies by a specific PML isoform. *EMBO J.*, **19**, 6185–6195.
63. Alcalay, M., Tomassoni, L., Colombo, E., Stoldt, S., Grignani, F., Fagioli, M., Szekely, L., Helin, K. and Pelicci, P.G. (1998) The promyelocytic leukemia gene product (PML) forms stable complexes with the retinoblastoma protein. *Mol. Cell Biol.*, **18**, 1084–1093.
64. Doucas, V., Ishov, A.M., Romo, A., Juguilon, H., Weitzman, M.D., Evans, R.M. and Maul, G.G. (1996) Adenovirus replication is coupled with the dynamic properties of the PML nuclear structure. *Genes Dev.*, **10**, 196–207.
65. Hoppe, A., Beech, S.J., Dimmock, J. and Leppard, K.N. (2006) Interaction of the adenovirus type 5 E4 Orf3 protein with promyelocytic leukemia protein isoform II is required for ND10 disruption. *J. Virol.*, **80**, 3042–3049.